Energy Research and Development Division
FINAL PROJECT REPORT

TRANSMISSION GRID RESEARCH

Appendices A-B

Prepared for: California Energy Commission
Prepared by: California Institute for Energy and Environment

University of California
ciee

FEBRUARY 2012
CEC-500-2013-098-APA-B

PREPARED BY:

Primary Authors:
Merwin Brown
Larry Miller
Lloyd Cibulka
Alexandra Von Meier
Lorraine Hwang

California Institute for Energy & Environment
University of California
2087 Addison Street, Second Floor
Berkeley, CA 94704
510 643-0038
www.uc-ciee.org

Contract Number: 500-07-037

Prepared for:

California Energy Commission

Jamie Patterson
Contract Manager

Fernando Piña
Office Manager
Energy Systems Research Office

Laurie ten Hope
Deputy Director
Energy Research and Development Division

Robert P. Oglesby
Executive Director

DISCLAIMER

This report was prepared as the result of work sponsored by the California Energy Commission. It does not necessarily represent the views of the Energy Commission, its employees or the State of California. The Energy Commission, the State of California, its employees, contractors and subcontractors make no warranty, express or implied, and assume no legal liability for the information in this report; nor does any party represent that the uses of this information will not infringe upon privately owned rights. This report has not been approved or disapproved by the California Energy Commission nor has the California Energy Commission passed upon the accuracy or adequacy of the information in this report.

ACKNOWLEDGEMENTS

The CIEE Electric Grid Research team - Merwin Brown, Lloyd Cibulka, Jim Cole, Gilda Garcia, Lorraine Hwang, Larry Miller, and Sascha von Meir - is grateful to the other researchers and their institutions – MCEER, Pacific Earthquake Engineering Research Center, Pacific Northwest National Laboratory, and Virginia Tech – for their expertise and dedication in conducting the research and development accomplished in this effort. The team also wants to thank the many advisors, especially Policy Advisory Committee (PAC) and the Technical Advisory Committees (TAC) which support it. Committee membership was composed primarily of personnel from the 3 major investor owned utilities (IOU) in California – Pacific Gas and Electric (PG&E), San Diego Gas and Electric (SDG&E), and Southern California Edison (SCE)–and the California ISO (CAISO,) and chaired by an Energy Commission commissioner. Additional participants were often included to share knowledge on the meeting's focus including the Assistant Secretary of the Office of Electricity for the U.S. Department of Energy, a representative of the Bonneville Power Association, and the Utility Variable-Generation Integration Group.

This work was funded by the California Energy Commission PIER program under Contract 500-07-037. CIEE is especially grateful for this financial support which has made a significant contribution to advancing the technology needed for the modernization of California's electric grid for meeting California's energy policy goals. Electric Grid Research at CIEE is creating technologies for new tools to modernize the grid and maximize its ability to meet customer needs and California's aggressive energy-policy goals. The vision is a smarter, more responsive, more robust grid — the heart of California's quest to reduce greenhouse gases, improve energy efficiency, and deploy more renewable energy, all while satisfying the new and growing ways customers use electricity. With funding and direction from the California Energy Commission's Public Interest Energy Research (PIER) program, CIEE has worked, and is prepare to continue working, to make these new technologies reality through research. This report was prepared by the CIEE. CIEE makes no warranties as to the suitability of this product for any particular purpose.

PREFACE

The California Energy Commission Energy Research and Development Division supports public interest energy research and development that will help improve the quality of life in California by bringing environmentally safe, affordable, and reliable energy services and products to the marketplace.

The Energy Research and Development Division conducts public interest research, development, and demonstration (RD&D) projects to benefit California.

The Energy Research and Development Division strives to conduct the most promising public interest energy research by partnering with RD&D entities, including individuals, businesses, utilities, and public or private research institutions.

Energy Research and Development Division funding efforts are focused on the following RD&D program areas:

- Buildings End-Use Energy Efficiency
- Energy Innovations Small Grants
- Energy-Related Environmental Research
- Energy Systems Integration
- Environmentally Preferred Advanced Generation
- Industrial/Agricultural/Water End-Use Energy Efficiency
- Renewable Energy Technologies
- Transportation

Transmission Grid Research is the final report for the Transmission Grid Research project (Contract Number 500-07-037) conducted by the California Institute for Energy and Environment. The information from this project contributes to the Energy Research and Development Division's Energy-Related Environmental Research Program.

For more information about the Energy Research and Development Division, please visit the Energy Commission's website at www.energy.ca.gov/research/ or contact the Energy Commission at 916-327-1551.

ABSTRACT

This report presents results from 11 public interest research projects that advance science and technologies related to the electric power transmission grid. These projects fall within three focus areas: infrastructure, real-time operations, and planning and environmental activities. Three projects summarized current status, research gaps, and recommended research for each focus area. In the infrastructure area, two projects evaluated the seismic issues associated with transformer bushings and substation insulators and made recommendations for adoption by the Institute for Electrical and Electronics Engineers Standard 693, which specifies testing of these components. Three projects focused on real-time operations. The wide area energy management storage systems project analyzed the combination of fast and slow storage over two balancing areas. A project on oscillation detection developed new algorithms for measuring oscillations in real time. The project on modal analysis for grid operation on the Western Interconnection developed a decision support tool to suggest mitigation steps for poorly damped wide area oscillations. In the planning and environmental areas, two projects were completed. The adaptive relay project studied four different applications of the use of synchrophasor data to improve protective systems. The online tools for wind and solar project developed tools for use by the California Independent System Operator to forecast system demands for ramping and regulation and possible congestion over the following 24-hour period. Finally, the technology transfer research project focused on disseminating research results and encouraging further commercialization of the research.

Keywords: electric transmission, renewables, renewable energy integration, greenhouse gases (GHG), emissions, reliability, renewable penetration, energy efficiency, electric power system, Smart Grid, infrastructure, renewable portfolio standard (RPS), transmission and distribution (T&D), transmission planning, transmission operations, transmission infrastructure, once though cooling, technology transfer

Please use the following citation for this report:

Brown, Merwin; Miller, Larry; Cibulka, Lloyd; Von Meier, Alexandra; Hwang, Lorraine. (California Institute for Energy and Environment). 2012. ***Transmission Grid Research,*** California Energy Commission. Publication Number: CEC-500-2013-098-APA-B

TABLE OF CONTENTS

Acknowledgements i

PREFACE ii

ABSTRACT iii

TABLE OF CONTENTS iv

APPENDIX A: Transmission Grid Infrastructure Final Report A-1

APPENDIX B: Seismic Bushing Analysis Final Report B-1

APPENDIX A:
Transmission Grid Infrastructure Final Report

Arnold Schwarzenegger
Governor

FUTURE TRANSMISSION GRID INFRASTRUCTURE RESEARCH REPORT

PIER FINAL PROJECT REPORT

Prepared For:
California Energy Commission
Public Interest Energy Research Program

Prepared By:
California Institute for Energy and Environment

July 2009

Prepared By:
California Institute for Energy and the Environment
Project Manager: Merwin Brown
Authors: Lloyd Cibulka, Merwin Brown
Sacramento, CA 95814
Commission Contract No. 500-07-037

Prepared For:
Public Interest Energy Research (PIER)
California Energy Commission

Jamie Patterson
Contract Manager

Pedro Gomez
Program Area Lead
Energy Systems Integration

Mike Gravely
Office Manager
Energy Systems Research

Thom Kelly, Ph.D.
Deputy Director
ENERGY RESEARCH AND DEVELOPMENT DIVISION

Melissa Jones
Executive Director

DISCLAIMER

This report was prepared as the result of work sponsored by the California Energy Commission. It does not necessarily represent the views of the Energy Commission, its employees or the State of California. The Energy Commission, the State of California, its employees, contractors and subcontractors make no warrant, express or implied, and assume no legal liability for the information in this report; nor does any party represent that the uses of this information will not infringe upon privately owned rights. This report has not been approved or disapproved by the California Energy Commission nor has the California Energy Commission passed upon the accuracy or adequacy of the information in this report.

Preface

The California Energy Commission's Public Interest Energy Research (PIER) Program supports public interest energy research and development that will help improve the quality of life in California by bringing environmentally safe, affordable, and reliable energy services and products to the marketplace.

The PIER Program conducts public interest research, development, and demonstration (RD&D) projects to benefit California.

The PIER Program strives to conduct the most promising public interest energy research by partnering with RD&D entities, including individuals, businesses, utilities, and public or private research institutions.

- PIER funding efforts are focused on the following RD&D program areas:
- Buildings End–Use Energy Efficiency
- Energy Innovations Small Grants
- Energy–Related Environmental Research
- Energy Systems Integration
- Environmentally Preferred Advanced Generation
- Industrial/Agricultural/Water End–Use Energy Efficiency
- Renewable Energy Technologies
- Transportation

Future Transmission Grid Infrastructure Research Report is the Task 2.0 final report for the contract number 500-07-037 conducted by California Institute for Energy and Environment (CIEE). The information from this project contributes to PIER's Energy Systems Integration Program.

For more information about the PIER Program, please visit the Energy Commission's website at www.energy.ca.gov/research/ or contact the Energy Commission at 916-654-4878.

Please cite this report as follows:

Cibulka, Lloyd, and Merwin Brown. 2009. *Future Transmission Grid Infrastructure Research Report,* California Energy Commission, PIER Energy Systems Integration Program.

Table of Contents

Preface iii
Table of Contents iv
Abstract v
Executive Summary 1
1.0 Purpose 7
2.0 Introduction and Process 8
3.0 Engagements with Stakeholders, Researchers and Technology Developers 10
4.0 Problem Statement 13
5.0 Initial Transmission Infrastructure Research Candidates 18
5.1. Real-time Rating (RTR) Technologies 18
5.2. Advanced Overhead AC Transmission Systems 18
5.3. Underground AC Transmission Systems 18
5.4. High Voltage Direct Current (HVDC) Transmission Systems 19
5.5. Voltage Source Converter (VSC) HVDC Technology 19
5.6. Conversion of AC lines to DC 20
5.7. Energy Storage Technologies 20
5.8. Power Flow Control Technologies 21
5.9. Intelligent Protection Systems Using Adaptive Relays Controlled by Wide Area Synchrophasors Demonstration 22
5.10. Superconducting Technologies 22
6.0 References 23
7.0 Glossary 24

Abstract

California has adopted aggressive energy policy goals to significantly reduce greenhouse gases, improve energy efficiencies and deploy increased penetrations of renewable energy generation. Substantial increases in the generation of electricity from renewable resources that are located remote from customers will be necessary to achieve the RPS goals, and must rely on adequate, economical and reliable transmission for delivering renewable electricity to consumers. The current system will be challenged in performing its roles in meeting these goals. New transmission technologies offer the prospect of providing a substantial portion of the new or expanded capabilities to supplement traditional solutions.

This report contains the approach, framework and initial plan for achieving the goal for Task 2.0, "Future Transmission Grid Infrastructure Research Plan," of Contract 500-07-037, which is to identify new or expanded transmission infrastructure research activities that

- Increase the transmission of electricity from renewable resources,
- Increase the efficiency of the transmission system, and
- Reduce the emissions of greenhouse gases (GHG) that are associated with the transmission system.

The report addresses but is not limited to research activities related to real time system operations in the following areas:

- Integration of renewables
- Smart Grid technologies
- Transmission system efficiency and associated reductions in greenhouse gas emissions

Keywords: electric transmission, renewables, renewable energy integration, greenhouse gases (GHG), emissions, reliability, renewable penetration, energy efficiency, electric power system, Smart Grid, infrastructure, renewable portfolio standard (RPS), transmission and distribution (T&D), transmission planning, transmission operations

Executive Summary

Purpose

This report contains the approach, framework and initial plan for Task 2.0, "Future Transmission Grid Infrastructure Research Plan," of the California Energy Commission Contract 500-07-037, which is to identify new or expanded transmission infrastructure research activities that:

1. Increase the transmission of electricity from renewable resources,
2. Increase the efficiency of the transmission system, and
3. Reduce the emissions of greenhouse gases (GHG) that are associated with the transmission system.

The report addresses, but is not limited to, a description of what future transmission infrastructure research activities could be conducted in the context of the following:

- Research into equipment and devices to provide direct improvements to the transmission infrastructure for the integration of renewable energy resources.
- Research SmartGrid technologies for their application to improve the transmission infrastructure to increase the transmission of electricity from renewable resources.
- Research equipment and devices that increase the efficiency of the transmission infrastructure and reduce emission of GHG that are directly associated with the transmission infrastructure.

This report incorporates research activities identified to date for this research area.

Introduction

California has adopted aggressive energy policy goals to significantly reduce greenhouse gases, improve energy efficiencies and increase penetration of renewable energy generation. The electric transmission and distribution (T&D) system in California is a factor in being able to meet each of these goals. Although fractionally small, there are substantial energy losses in transporting electricity, which could be reduced with efficiency improvements. While T&D *per se* directly contributes relatively little to increasing GHG on a sustained basis, there are opportunities to reduce GHG emissions in design, construction, operations and maintenance. Perhaps most significantly, however, T&D is absolutely essential to meet the state's renewable portfolio standard (RPS) goals. Substantial increases in the generation of electricity from renewable resources in remote locations will be necessary to achieve the RPS goals, and must rely on adequate, economical and reliable T&D for delivering renewable electricity to consumers. The current T&D system will be challenged in performing its roles in meeting these goals.

Meeting these challenges will require new or expanded capabilities for the grid. New transmission technologies offer the prospect of providing a substantial portion of the new or

expanded capabilities to supplement traditional solutions. These technologies can be classified among three broad categories: a) infrastructure, b) real time systems operation, and c) transmission planning, uncertainty analysis and environmental research. This *Future Transmission Grid Infrastructure Research* report addresses the first of these.

Many of these new technologies will require additional development before they can be commercially or routinely deployed. The process for identifying the research activities of most value starts with identifying the most critical issues facing the electric industry community, and matching new technologies to address those issues. However there are often gaps between the current and desired status of each technology. These gaps have been identified along with the research, development and demonstration to work toward closing the gaps. The degree of success of this process depends largely on obtaining the best and latest policy, industry and technology knowledge by engaging public and private stakeholders and technology developers.

Stakeholder Engagement

A significant amount of situational analysis, technology identification, and evaluation of research and development needs, have been, and will be, accomplished by means of meetings that include representatives of key public and private stakeholders, and research and technology developer organizations. CIEE has found that the most effective means to obtain comprehensive and meaningful information about promising new research avenues is to meet at stakeholder and researcher sites so as to be accessible to a wide array of scientific, engineering, and business personnel to solicit their viewpoints and ideas. Where feasible, this is the preferred approach. It will be augmented by telephone conversations and interviews; participation in industry conferences, symposia and workshops; and other means as appropriate and feasible.

In addition, CIEE also holds Technical Advisory Committee meetings, typically "brainstorming" types of meetings to discuss stakeholder and CIEE perspectives on new technology, planning, operations and environmental needs. Follow-up meetings are sometimes warranted to discuss draft versions of the major findings.

The following are organizations which hold meetings that could contribute to the development of the technical information described in this report. This is not an exclusive list; indeed, many additional, unanticipated meeting and conference opportunities are expected to arise, some on relatively short notice.

- **IEEE Power Engineering Society (PES) General Meeting**

  The IEEE/PES General Meeting is the premier annual conference for the electric power industry; CIEE may be invited to participate as a presenter, panelist or session chair. It is a valuable opportunity to gather intelligence on electric power technologies developments and to network with other utilities, researchers, manufacturers, consultants and engineers.

- **IEEE/CIGRE Joint International Symposium on Integration of Renewables**

CIGRE is the European research organization that is concerned with power system technology issues. In 2009 IEEE and CIGRE are holding a Joint Symposium on the topic of "Integration of Wide-Scale Renewable Resources into the Power Delivery System." Participation in CIGRE activities such as this one would provide significant additional information on international technology developments in power systems.

- **Electric Power Research Institute (EPRI) Workshops**

  EPRI has a number of research program areas that directly relate to the infrastructure research activities of PIER TRP. The CIEE TRP has participated in EPRI Working Groups, Task Forces, and Project Advisory Groups, and will continue to do so, as it is advantageous to leverage EPRI's activities with PIER TRP's.

- **HVDC Technologies Workshop**

  HVDC Technologies have been identified as a key technology that can potentially provide near-term benefits to the California transmission system, particularly in terms of renewable integration. CIEE TRP is in the planning stages of hosting a Workshop to assist in developing recommended new avenues of research.

- **Underground Transmission Technologies Workshop**

  Underground Transmission Technologies have been identified as another key technology and are particularly relevant to efforts to facilitate the siting and approval of new transmission lines. CIEE TRP is in the planning stages of hosting a Workshop to assist in developing recommended new avenues of research.

- **Energy Storage Technologies Workshops and Conferences**

  The storage of electric energy has been identified as a key enabling technology. Electric storage is a wide and diverse field of technology development, and there will be numerous conferences, workshops, meetings and tutorials that will be held, so CIEE TRP will look for opportunities to participate in high-value events.

- **Meetings with IOUs and the CAISO**

  In general, CIEE TRP will schedule meetings with these entities on an ad-hoc basis, as needed to meet with key engineers and researchers at stakeholder sites, to develop the information necessary for defining the needed research in transmission infrastructure technologies.

Problem Statement

Renewable resources within California are extensive and varied, and California has established aggressive RPS goals to increase the fraction of electricity made from renewable energy resources and to decrease greenhouse gas emissions under AB 32. By 2010, 20% of California's electricity is to come from renewables, and by 2020, perhaps 33%. Most of the new sources are expected to connect to the transmission system in remote locations and to exhibit properties quite different from traditional generation and loads, posing special challenges for providing timely adequate grid delivery capacity, maintaining reliability, and avoiding economic inefficiencies. We refer collectively to these challenges as the problem of Renewables Integration

(RI), and it is often cited as the major barrier to achieving the renewable goals of the state. New technologies will be required to provide the functional capabilities required for success.

These new technologies can be applied in the context of providing three new or expanded broad capabilities: (1) Provide physical access for each new power plant, (2) Reliably accommodate any unique renewable generator behaviors, and (3) Increase the grid's power carrying capacity to handle the additional electric power flows. As solutions are developed through research to address the issues raised in meeting these three main state policy goals of renewable generation deployment, GHG reduction and energy efficiency improvements, the transmission community must continue to ensure that transmission meets the critical requirements for adequacy, reliability, affordability, security, safety, and environmental protection.

Initial Transmission infrastructure Research Candidates

Examples of the types of technologies and technology platforms that would qualify for examination include (but are not limited to) the following:

- **Real-time Rating (RTR) Technologies**

  Combinations of hardware and software that use real-time information about the physical condition of the transmission system and its environment to provide capacity ratings that are closer to the actual physical thermal limits of the system, compared to the generally more conservative "static" ratings typically used. With this real-time information, transmission system operators can make better-informed decisions about generation dispatch and other operating issues, and system planners can have another tool to deal with transmission capacity expansion planning.

- **Advanced Overhead AC Transmission Systems**

  Defined as alternatives to the typical single-circuit lattice tower designs, this category includes voltage uprating, reconductoring, bundled conductors, high-temperature/low-sag (HTLS) conductors, and high phase order designs.

- **Underground AC Transmission Systems**

  The lack of visual impacts is desirable from a public and permitting point of view, especially as compared to overhead lines, but underground lines have construction and cost issues. Still, recent advances in underground technologies, materials and construction methods may provide opportunities for cost-effective and timely implementation of new transmission lines, or conversion of older lines, particularly where access to new renewable generation is concerned.

- **High Voltage Direct Current (HVDC) Transmission Systems**

  HVDC lines can be more compact and less expensive than AC lines of the same capacity. However, HVDC converter terminals are very expensive, being based on high-voltage solid-state electronics and requiring large amounts of AC capacitors at both ends to provide reactive support. Thus, the choice of AC vs. DC depends on the distance and the need for intermediate converter stations, with DC being generally more economical for

single lines over about 400 miles. While HVDC technology is basically very mature, at the very least an updated analysis of the costs vs. the benefits for the California market may be called for.

- **Voltage Source Converter (VSC) HVDC**

  VSCs are less expensive and have more operational flexibility than the conventional current-controlled thyristor HVDC technology, and do not require reactive compensation. Currently demonstrated at voltages up to 300 kV DC, and several hundred MW of power transfer, this type of HVDC technology typically uses direct-buried solid-dielectric cables, rather than pipe-type cables or an overhead line, for the conductors. Also, a VSC HVDC line can be trenched in the right-of-way underneath an existing overhead AC line, adding corridor capacity without modifying the existing overhead AC line in any way, and without any additional visual impacts.

- **Conversion of AC lines to DC**

  An existing AC line, whether it is overhead or underground, can be converted to HVDC or VSC DC without modifying the line conductors, towers and insulators in any way; only the terminals need to be modified, with HVDC converters installed at the substations in place of AC transformers. Such a conversion can increase the power capability of an existing line by a factor of at least 2 or 3, with reduced transmission losses.

- **Energy Storage Technologies**

  Storage has a number of potentially beneficial applications in the electric system, essentially involving a temporal shift between the generation of electric energy and its consumption. Storage has taken on added importance with the increase of renewables plants, given that the intermittency and variability of some renewables increases the complexity of the system operator's job; storage systems can provide the needed response to mitigate these characteristics of renewables. Storage can also be used to provide ancillary services to the system operator, such as voltage support, peaking power, and regulation, which would otherwise be supplied by fossil-fuel power plants.

- **Power Flow Control Technologies**

  The AC electric power system, by its nature, does not have a high degree of controllability in terms of system operators being able to direct power to particular transmission lines or paths. This results in inefficient use of transmission assets, congestion, and relative uneconomic operation. The limited array of tools available to system operators includes generators under their direct control, series and shunt capacitors, phase-shifting transformers, synchronous condensers, switches, and power electronics based devices, including FACTS HVDC systems, and power conversion devices used to interface distributed renewable resources.

- **Intelligent Protection Systems Using Adaptive Relays Controlled by Wide Area Synchrophasors Demonstration**

The wide area, synchrophasor-based monitoring, data analysis, diagnosis, communications and control technology platform provides a foundation to monitor, supervise, and modify the operation of adaptive relay protection systems in real-time based on a diagnostic analysis of the state of the power system. Fundamental research and application development research is underway, funded by PIER and Virginia Tech. The next step is the demonstration of the use of wide area synchrophasor data to reduce the likelihood of false triggering by protective relays.

- **Superconducting Technologies**

  This class of equipment includes transformers, generators, motors, cables, storage systems, and control devices that use superconducting wire in place of copper or aluminum conductors. Superconducting electrical equipment has the advantages of much lower losses, reduced size and significant increases in power-carrying capacity over conventional AC equipment. Second-generation (2G) superconducting wire uses liquid nitrogen rather than liquid helium as a refrigerant, making today's superconducting devices much more cost-effective than previous designs.

Benefits to California

This work benefits California by addressing how new technologies can be developed for helping the electric transmission and distribution system (T&D) perform its role in meeting the three main state policy goals of renewable generation deployment, GHG reduction and energy efficiency improvements, while continuing to assure that transmission meets the critical requirements for adequacy, reliability, affordability, security, safety, and environmental protection. California has adopted aggressive energy policy goals to significantly reduce greenhouse gases, improve energy efficiencies and increase penetration of renewable energy generation. The electric T&D system in California is a factor in being able to meet each of these goals, but currently faces many challenges in performing its roles in achieving them. Meeting these challenges will require new or expanded capabilities for the grid, and new transmission technologies offer the prospect of providing a substantial portion of the new or expanded capabilities to supplement traditional solutions. This report identifies the drivers and rationales that create the needs for new technologies, and describes the most promising new technologies and the research activities needed to help bring them to productive deployment and commercial reality in a manner that meets California needs in a timely fashion.

1.0 Purpose

This report contains the approach, framework and initial plan for achieving the goal for Task 2.0, "Transmission Grid Infrastructure Research," of Contract 500-07-037, which is to identify new or expanded transmission infrastructure research activities that:

1. Improve the transmission infrastructure to increase the transmission of electricity from renewable resources,
2. Improve the efficiency of the transmission infrastructure, and
3. Reduce the emissions of greenhouse gases (GHG) that are associated with the transmission infrastructure.

The report addresses, but is not limited to, a description of what future transmission system infrastructure research activities could be conducted in the context of the following:

- Research into equipment and devices to provide direct improvements to the transmission infrastructure for the integration of renewable energy resources.
- Research SmartGrid technologies for their application to improve the transmission infrastructure to increase the transmission of electricity from renewable resources.
- Research equipment and devices that increase the efficiency of the transmission infrastructure and reduce emission of GHG that are directly associated with the transmission infrastructure.

This report incorporates research activities identified to date for this research area.

2.0 Introduction and Process

California has adopted aggressive energy policy goals to significantly reduce greenhouse gases (GHG), improve energy efficiencies and deploy increased penetrations of renewable energy generation. The electric transmission and distribution (T&D) system in California is a factor, in varying degrees, in being able to meet each of these goals. Although fractionally small, there are substantial energy losses in transporting electricity, which, with efficiency improvements, could be reduced. While T&D *per se* directly contributes relatively little to increasing GHG on a sustained basis, there are some opportunities to reduce emissions in design, construction, operations and maintenance. Perhaps most significantly, however, T&D is absolutely essential for meeting the state's renewable portfolio standard (RPS) goals. Substantial increases in the generation of electricity from renewable resources that are located remote from customers will be necessary to achieve the RPS goals, and must rely on adequate, economical and reliable T&D for delivering renewable electricity to consumers. The current T&D system will be challenged in performing its roles in meeting these goals.

Meeting these challenges will require new or expanded capabilities for the grid. For example, at higher RPS levels, the conventional "build" solutions, namely extending new lines or expanding the capacity of existing transmission gateways to load centers using traditional technologies, and building conventional power plants for support, will prove inadequate by themselves, either because they are not the most cost effective, or obtaining the necessary permits will be very difficult. New transmission technologies offer the prospect of providing a substantial portion of the new or expanded capabilities to supplement these traditional solutions. These technologies can be classified among three broad categories: infrastructure real time systems operation and transmission planning, uncertainty analysis and environmental research. This *Future Transmission Infrastructure Research Report* addresses the first of these, including physical equipment and components of the transmission system: transmission lines, transformers, substations, and other apparatus.

Many of these new technologies are at an immature stage of development, and will require additional development before they can be commercially or routinely deployed to provide their benefits to the grid. The process for identifying the research activities of most value starts with identifying the most critical issues facing the electric industry community, and matching new technologies that enable enhanced or new capabilities to address those issues. However, there are often gaps between the current and desired status of each technology. These development gaps are barriers to achieving the needed transmission capabilities, and are often the result of deficiencies in materials; mathematical, scientific, engineering or process knowledge; system design and integration; standards setting and performance verification; scale; user confidence; and other factors. The final step is to identify what research, development and demonstration efforts are needed in each case to work toward closing the gaps. The degree of success of this process depends largely on obtaining the best and latest policy, industry and technology knowledge by engaging public and private stakeholders and technology developers.

Section 3, "Engagements with Stakeholders, Researchers and Technology Developers," provides examples of planned engagements with stakeholders, researchers and technology developers

who can contribute the most to updating and identifying new issues, technologies and research needed and its importance. These engagements often take the form of targeted meetings with several representatives of key stakeholders, researchers and technology developers, technical advisory committee and R&D scoping meetings, and T&D industry, government, and university workshops and conferences attended by leading researchers, technology developers and stakeholder representatives. While some of these meetings can be conducted or attended via telecommunications media when practical, it is expected that other meetings, e.g., interactive meetings using "flipcharts and white board" discussions, viewing transmission system equipment and facilities, or involving complex technical discussions, will require participation on location in order to achieve mutual understanding in a time effective manner resulting in an acceptable outcome.

Section 4, "Problem Statement," is a situational analysis that provides the starting point context for engaging stakeholders and technology developers in identifying changes in market, policy and technology drivers that create, or will create, T&D issues that might be addressed through development and application of new technologies.

Section 5, "Current Technology Candidates and Research Activities," lists the most current technology candidates and research activities which will make significant contributions to achieving the grid functionality for achieving California's energy policy goals. This list reflects the latest knowledge obtained in the process described above, as well that built on the understanding and experience acquired from CIEE participation in the existing PIER Transmission and related R&D programs. It will be amended as warranted following the engagements with stakeholders and technology developers and analysis of findings.

3.0 Engagements with Stakeholders, Researchers and Technology Developers

A significant amount of situational analysis, technology identification, and evaluation of research and development needs will be done by means of meetings (by telecommunications or onsite) that include representatives of key public and private stakeholders, and research and technology developer organizations. Candidates usually include, but are not limited to, the organizations represented on the TRP Policy Advisory Committee (PAC): CAISO, SCE, PG&E, SDG&E, BPA and UWIG; selected research organizations such as EPRI, CERTS, PSERC, DOE, and the National Laboratories; the IEEE, particularly its Power Engineering Society T&D Committee; utility regulatory bodies such as the Energy Commission and the Public Utilities Commission; consultants and independent experts; and leading universities involved in electric systems research. CIEE has found that the most effective means to obtain comprehensive and meaningful information about promising new research avenues for transmission planning and environment of interest to stakeholders is to meet at stakeholder and researcher sites so as to be accessible to a wide array of scientific, engineering, and business personnel to solicit their viewpoints and ideas. Where economically warranted and feasible, this approach will be the preferred approach with selected candidates. It will be augmented by telephone conversations and interviews; participation in industry conferences, symposia and workshops; and other means as appropriate and feasible.

In addition, CIEE also holds Technical Advisory Committee meetings, typically "brainstorming" types of meetings, to discuss stakeholder and CIEE perspectives on new technology, planning, operations and environmental needs. Follow-up meetings are sometimes warranted to discuss draft versions of the major findings.

The following are organizations which hold meetings that could contribute to the development of the technical information described in this report, and therefore are under consideration for attendance by CIEE personnel, and potential workshops and other activities under consideration by the TRP for this purpose. This is not an exclusive list; indeed, many additional, unanticipated meeting and conference opportunities are expected to arise, some on relatively short notice.

- **IEEE Power Engineering Society (PES) General Meeting**

  The IEEE/PES General Meeting is held annually in mid-summer at various locations, usually in the United States, but sometimes in other countries. It is the premier conference for the electric power industry; covering more than four days, it comprises working group and committee meetings, technical paper presentations, panel discussions, technical tours and workshops covering the entire range of electric power system technology topics. CIEE may be invited to participate as a presenter, panelist or session chair. It is also a valuable opportunity to gather intelligence on electric power technologies developments and to network with other utilities, researchers, manufacturers consultants and engineers.

- **IEEE/CIGRE Joint International Symposium on Integration of Renewables**

  CIGRE is the European research organization that is concerned with technology issues related to planning, operation, design, construction, and maintenance of power systems, as well as protection of power systems, system control, telecommunication equipment and information systems. CIGRE's General Session meeting is held in even-numbered years in August, and CIGRE sponsors numerous Regional Meetings and Colloquia every year. In 2009 IEEE and CIGRE are holding a Joint Symposium on the topic of "Integration of Wide-Scale Renewable Resources into the Power Delivery System." Participation in CIGRE activities would provide significant additional information on international technology developments in power systems.

- **Electric Power Research Institute (EPRI) Workshops**

  EPRI has a number of research program areas that directly relate to the infrastructure research activities of PIER TRP, including:

  - Increased Transmission Capacity (ITC) Program
  - Increased Power Flow (IPF) Program
  - Substation Automation Program
  - High-Voltage Transmission Systems
  - Underground Transmission Systems
  - Transmission Substations

  The CIEE TRP has participated in EPRI Working Groups, Task Forces, and Project Advisory Groups, and will continue to do so, as it is advantageous to leverage EPRI's activities with PIER TRP's. Some of these meetings will be local, i.e., requiring travel to Palo Alto or other in-state locations. Others will be out-of-state, and in rare cases will be held at international venues.

- **HVDC Technologies Workshop**

  HVDC Technologies have been identified as a key technology that can potentially provide near-term benefits to the California transmission system, particularly in terms of renewable integration, with the application of some technology assessment and demonstration projects and related research activities. CIEE TRP is in the planning stages of hosting a Workshop, either in Sacramento or the Bay Area, with utilities, technology developers, researchers and other industry stakeholders. The purpose of this workshop will be to gain better definition of the benefits, costs and implementation barriers to wider use of HVDC technology in California, and develop recommended new avenues of research as indicated.

- **Underground Transmission Technologies Workshop**

  Underground Transmission Technologies have been identified as another key technology that can potentially provide near-term benefits to the California transmission system, and are particularly relevant to efforts to facilitate the siting and approval of new transmission lines, such as those contemplated for new, central station power

plants. CIEE TRP is in the planning stages of hosting a Workshop, either in Sacramento or the Bay Area, with utilities, technology developers, researchers and other industry stakeholders. The purpose of this workshop will be to gain better definition of the benefits, costs and implementation barriers to wider use of underground transmission in California, and develop recommended new avenues of research as indicated.

- **Energy Storage Technologies Workshops and Conferences**

  The storage of electric energy has been identified as a key enabling technology that can potentially provide near-term benefits to the California transmission system, and is especially relevant to addressing the issues of peak loading, transmission congestion, volt/VAR support, ancillary services, and the mitigation of intermittency and variability characteristics exhibited by some renewable generation plants. Electric storage is a wide and diverse field of technology development, and there will be numerous conferences, workshops, meetings and tutorials that will be held, so CIEE TRP will look for opportunities to participate in high-value events. One possibility is the Storage Week Summit, to be held in La Jolla, CA, July 13-14, 2009.

- **Meetings with IOUs and the CAISO**

  In general, CIEE TRP will schedule meetings with these entities on an ad-hoc basis, as needed to meet with key engineers and researchers at stakeholder sites, to develop the information necessary for defining the needed research in transmission infrastructure technologies. It is anticipated that most of these meetings will be in-state, requiring only local travel and a minimum of hotel stays.

4.0 Problem Statement

Renewable resources within California are extensive and varied, and California has established aggressive RPS goals to increase the fraction of electricity made from renewable energy resources and to decrease greenhouse gas emissions under AB 32. By 2010, 20% of California's electricity is to come from renewables, and by 2020, perhaps 33%. This new generation will be integrated into the electric grid at both the transmission and distribution levels, but most of it is expected to connect to the transmission system in remote locations. Some of this renewable generation will exhibit properties quite different from traditional generation and loads, which poses special challenges for providing timely adequate grid delivery capacity, maintaining reliability, and avoiding economic inefficiencies. We refer collectively to these challenges as the problem of Renewables Integration (RI), and it is often cited as the major barrier to achieving the renewable goals of the state.

The renewable resources for larger, central station renewable power plants tend to be located remote from load centers and other generation resources, and therefore are remote from the existing electric transmission lines. Extension of new transmission capacity is expensive and often takes many years getting siting approved. Given the relatively short construction times for many types of renewable generation, having transmission available when the power plant is ready to make its contribution toward meeting the renewable goals is problematic and threatens the ability to meet the RPS goals. Furthermore, adding new generation without upgrading existing transmission capacity or adding new capacity can result in more economic inefficiencies such as higher congestion costs for consumers.

At the other extreme, some of these renewable generators will be located, and integrated into the grid, near or at the electric loads. Prime examples are photovoltaic panels mounted on building roof-tops, and small biomass-fueled generators located at the community level. These "distributed" generators, in contrast to "central station," are usually connected at the distribution level, which in general was not designed to connect generation resources of any kind, and can cause some safety and operational issues. And while some of the power from a distributed generator might be fed to a neighboring load by the grid, some, if not most, of the power will be consumed locally, creating an ambiguous role as a new kind of generator acting as a negative load, at least from a transmission perspective.

From a transmission operational dynamics perspective, geothermal and biomass energy are similar to traditional power generators, especially base-load, and therefore do not pose much concern about their operational behavior within the power grid, though some biomass resources vary seasonally. Some types of renewable generation, however, are "fueled" by variable, or intermittent, energy sources like wind and sunshine, i.e., insolation, which are controlled by weather and rotation of the earth. These intermittent renewables can create renewable energy power plant behaviors for which the grid was not designed and that are quite unfamiliar to grid operators and outside their control. Relatively small penetrations of intermittent renewables are expected to have "operational implications significant but manageable" ("California Independent System Operator Integration of Renewable Resources," David Hawkins & Clyde Loutan, CAISO, November 2007). For greater penetration levels,

however, transmission infrastructure expansion, improved wind and solar forecasting, increased ancillary services for the grid, and new technologies for a smarter, more flexible grid will be required.

Not all the news associated with increased use of renewable generation integrated into the grid is negative. In addition to the obvious reduction in greenhouse gas reductions, inherent in renewable generation is a hedge against volatility in fuel prices and reliance on imported fossil fuels. Certain renewable resources, such as solar, have a reasonably strong correlation with load temporal profiles in California, and therefore might help with meeting peak load demands, and, especially for distributed forms, reducing congestion costs, deferring grid infrastructure investment and perhaps providing local voltage support. The non-intermittent renewable resources, such as geothermal and biomass, of course can add to a growing need for baseload generation capacity. Proper integration among renewable resource types and across geographical regions might further enhance renewables' contribution to a stable, reliable and affordable grid.

The successful integration into the electric grid of the renewable generation required to meet state RPS goals needs coordination among many public and private sector stakeholders in the renewable and electric grid communities. But new technologies will also be required to provide the functional capabilities required for success.

These new technologies can be applied in the context of providing three new or expanded broad capabilities: (1) Provide physical access for each new power plant, (2) Reliably accommodate any unique renewable generator behaviors, and (3) Increase the grid's power carrying capacity to handle the additional electric power flows.

New technologies to provide faster access for new renewable plants will, in general, need to put new transmission lines in a better light. One aspect of this capability is to use new technologies, such as underground cables, to reduce the visibility of transmission infrastructure, since that issue seems to be a major barrier for gaining public acceptance of new transmission expansions. The other aspect is to enhance the understanding by all interested parties of the need for, and relative economic and strategic value of, new transmission infrastructure through interactive planning and advanced analysis tools, so that siting and permitting decisions can be made on a fully-informed, objective and inclusive technical basis.

New technologies to accommodate the unique renewable generator behaviors will, in general, need to enable a smarter and more flexible and fast-acting grid to handle such behaviors as ramp following and intermittency. This "Smart Grid" capability needs to span timeframes ranging from milliseconds for automated operations, to seconds to hours for manual operations, to days for markets and short-term planning; and it must span the topology of the whole interconnection, from generators – central and distributed – to the customers' electric meters, and their appliances and equipment.

In a similar fashion, new technologies can increase transmission capacity by optimizing the grid for greater power flow. Because of operational uncertainties regarding stability and thermal limits, the grid power flow limits are conservatively set, leaving considerable transmission

capacity "on the table." Various new Smart Grid technologies can be developed and deployed to provide more accurate real-time measured and predicted grid status conditions and margins over a wide area that could potentially be used to relax some of these constraints and free up additional transmission capacity in the existing system. Other technologies can provide the capability to control the grid better and faster allowing it to be operated closer to the real margins without jeopardizing reliability, again freeing up additional transmission capacity in the existing system. Other technologies, especially new technologies, can upgrade the existing infrastructure to handle higher power flows in the same pathway. Finally long range system planning tools that consider congestion management many years into the future can increase the capacity of new system expansions.

New planning technologies, such as statistical and probabilistic analysis and planning tools, are particularly well suited to the needs of the T&D system under growing uncertainty. Changes in generation and loads require new data and modeling capabilities. Also, new web-based tools can enable enhanced communication and interactive planning within the transmission community and the public. The enhanced or new transmission capabilities that may be achieved with these new technologies represent feasible and potentially cost-effective solutions to the challenges of transmission capacity and controllability resulting from renewable deployment, and reduction of electric losses and GHG.

While the transmission system's largest impact on the reduction of GHGs is its ability to integrate renewables, there are some other aspects to consider such as GHGs produced in construction activities, operations and maintenance. The release of SF_6, a GHG that is about 20,000 times more potent than CO_2, from various electric components is one example. The CO_2 released by transportation and earthmoving equipment during construction is another. Likewise, electricity delivery losses, e.g., those resulting from Ohm's Law effects, will decrease the amount of renewable energy delivered to the customer by approximately 10%, and will correspondingly increase the amount of fossil fuel burned to deliver a given amount of electricity to a customer. Some new infrastructure technologies and improved operations and long range planning have the potential to reclaim some of these electrical energy losses.

Of the total amount of energy generated in the grid, approximately 7–10% is lost as heat due to resistance in transmission lines, transformers and other equipment. A comparable amount of energy (approx. 5–10%) is lost in the distribution system. Reducing system losses translates into energy production cost savings and reduced GHG. Methods for optimum real-time configuration and operation of the grid will likely produce a much greater percentage efficiency improvement than is attainable from focusing on resistive losses, especially on a per dollar invested basis.

In power system planning, utility engineers are very much aware that transmission system inefficiency is correlated with low system voltages, congestion or overloading, lack of operating flexibility, or other negative impacts. Proper planning and design generally tend to result in a more efficient system, both in the physical system and how it is operated. The optimal power flow, which is widely used, basically allows planners and operators to design and operate the transmission system with the highest efficiency.

However, from an overall system perspective, because losses can't be directly measured, only calculated as the total system generation minus net delivered load, and will vary as line loadings change, it has historically been very difficult to pinpoint specific lines as candidates for economic upgrade based on losses alone.

Principal drivers for transmission system efficiency are:

- Enable renewable generation to meet RPS goals.
- Reduce the use of fossil fuels.
- Reduce greenhouse gas (GHG) production.
- Reduce costs to ratepayers.
- Maintain overall system reliability.
- Enable efficient energy markets.

There are two major areas regarding transmission efficiency:

- Resistive and inductive losses, primarily in lines and transformers (physical efficiency).
- Optimal configuration and operation of the grid (operational efficiency).

Resistive/inductive losses can be reduced by:

- Using larger diameter conductors
- Adding/bundling conductors
- Using advanced low-loss conductors
- Using low-loss transformers
- Installing series capacitors in lines (reduces line inductance, and current magnitude)
- Installing shunt and series capacitors to optimize voltage profiles
- Optimizing generation dispatch to minimize peak loading on lines
- Uprating line voltages, e.g., converting a 115kV line to 230kV
- Installing storage at strategic locations to minimize congestion and peak line loading, optimize voltages, etc.
- Using HVDC lines instead of AC lines

These measures may or may not be cost-effective solely on the basis of reducing losses, but loss reduction is normally a factor that is taken into account when designing and planning transmission systems.

Operational methods to increase transmission system efficiency are:

- Intelligent management systems, e.g., Smart Grid
- Optimal power flow applications

Finally, as solutions are developed through research to address the issues raised in meeting these three main state policy goals of renewable generation deployment, GHG reduction and energy efficiency improvements, the transmission community must continue to ensure that

transmission meets the critical requirements for adequacy, reliability, affordability, security, safety, and environmental protection.

5.0 Initial Transmission Infrastructure Research Candidates

Examples of the types of technologies and technology platforms that would qualify for examination include (but are not limited to) the following:

5.1. Real-time Rating (RTR) Technologies

Combinations of hardware (sensors, data acquisition systems, and communications systems) and software that use real-time information about the physical condition of the transmission system and its environment to provide capacity ratings that are closer to the actual physical thermal limits of the system, compared to the generally more conservative "static" ratings typically used. With this real-time information, transmission system operators can make better-informed decisions about generation dispatch and other operating issues, and system planners can have another tool to deal with transmission capacity expansion planning.

- Major Goals Addressed: Increase use of renewable generation.
- Major Issues Addressed: Increase capacity, maintain reliability, improve safety, increase asset utilization.
- Major Developmental Gap(s): Applications/visualization; user confidence.
- Major Proposed R&D Activity: RTR Use Case Study: Conduct review of current technologies and their use, identification of user needs and range of applications, an assessment of benefits vs. costs, and identification of barriers to wider use; and development of proposed next steps.

5.2. Advanced Overhead AC Transmission Systems

Define as alternatives to the typical single-circuit lattice tower designs, this category includes voltage uprating, reconductoring, bundled conductors, high-temperature/low-sag (HTLS) conductors, and high phase order designs.

- Major Goals Addressed: Increase use of renewable generation, improve the efficiency of the transmission infrastructure.
- Major Issues Addressed: Accelerate siting, increase capacity
- Major Developmental Gap(s): Cost-effectiveness; maintenance and personnel training issues.
- Major Proposed R&D Activity: Use Case Study: Conduct review of current technologies and applications, identification of user needs and range of applications, assessment of benefits vs. costs, identification of barriers to use, and recommended next steps. Follow-on project to the High-Temperature, Low-Sag Conductors project, looking at connectors, stringing techniques, and other issues identified in the first project.

5.3. Underground AC Transmission Systems

Their lack of visual impacts is desirable from a public and permitting point of view, especially as compared to overhead lines, but underground lines have construction and cost issues. Still, recent advances in underground technologies, materials and construction methods may provide

opportunities for cost-effective and timely implementation of new transmission lines, or conversion of older lines, particularly where access to new renewable generation is concerned.

- Major Goals Addressed: Increase use of renewable generation, improve the efficiency of the transmission infrastructure.
- Major Issues Addressed: Accelerate siting, increase capacity, enhance security from wildfires, improve public safety.
- Major Developmental Gap(s): User confidence, costs, applications, construction issues, maintenance.
- Major Proposed R&D Activity: Underground Transmission Technology Solutions for Renewable Generation Transmission Integration and Protection from Natural Disasters. This proposed project will identify promising existing and emerging underground transmission technologies, evaluate generic cost/benefits, identify deployment issues/barriers and technology gaps, and recommend research required to help ensure and accelerate increased availability of underground transmission technologies ($200K).

5.4. High Voltage Direct Current (HVDC) Transmission Systems

HVDC lines can be more compact and less expensive than AC lines of the same capacity. However, HVDC converter terminals are very expensive, being based on high-voltage solid-state electronics and requiring large amounts of AC capacitors at both ends to provide reactive support. Thus, the choice of AC vs. DC depends on the distance and the need for intermediate converter stations, with DC being generally more economical for single lines over about 400 miles. While HVDC technology is basically very mature, at the very least an updated analysis of the costs vs. the benefits for the California market may be called for.

- Major Goals Addressed: Increase use of renewable generation, improve the efficiency of the transmission infrastructure.
- Major Issues Addressed: Accelerate siting, increase capacity, enhance security from wildfires, improve public safety.
- Major Developmental Gap(s): User confidence, costs, applications, construction issues, maintenance.
- Major Proposed R&D Activity: Stakeholder workshop to explore issues around greater acceptance of HVDC technologies by California utilities. Use information from workshop to perform a Use Case Study of HVDC technologies to identify promising technologies, applications and host utility sites.

5.5. Voltage Source Converter (VSC) HVDC Technology

VSCs are less expensive and have more operational flexibility than the conventional current-controlled thyristor HVDC technology, and do not require reactive compensation on the AC side. Currently demonstrated at voltages up to 300kV DC and power transfer levels of several hundred MW, this type of HVDC technology typically uses direct-buried solid-dielectric cables, rather than pipe-type cables or an overhead line, for the conductors. Also, a VSC HVDC line can

be trenched in the right-of-way underneath an existing overhead AC line, adding corridor capacity without modifying the existing overhead AC line in any way, and without any additional visual impacts.

- Major Goals Addressed: Increase use of renewable generation, improve the efficiency of the transmission infrastructure.
- Major Issues Addressed: Accelerate siting, increase capacity, enhance security from wildfires, improve public safety.
- Major Developmental Gap(s): User confidence, costs, applications, construction issues, maintenance.
- Major Proposed R&D Activity: Stakeholder workshop to explore issues around greater acceptance of VSC-based HVDC technologies by California utilities (include in scope of aforementioned HVDC workshop). Use information from workshop to perform a Use Case Study of VSC HVDC technologies to identify promising technologies, applications and host utility sites.

5.6. Conversion of AC lines to DC

An existing AC line, whether it is overhead or underground, can be converted to HVDC or VSC DC without modifying the line conductors, towers and insulators in any way; only the terminals need to be modified, with HVDC converters installed at the substations in place of AC transformers. Such a conversion can increase the power capability of an existing line by a factor of at least 2 or 3, with reduced transmission losses.

- Major Goals Addressed: Increase use of renewable generation, improve the efficiency of the transmission infrastructure.
- Major Issues Addressed: Accelerated siting, increased capacity.
- Major Developmental Gap(s): User confidence, costs, applications.
- Major Proposed R&D Activity: Stakeholder workshop to explore and identify promising technologies, applications and host utility sites. Follow-on work could include a cost-benefit study or a Use Case Study to identify which California transmission lines are potential candidates for conversion.

5.7. Energy Storage Technologies

Storage has a number of potentially beneficial applications in the electric system, essentially involving a temporal shift between the generation of electric energy and its consumption. Storage has taken on added importance with the increase of renewables plants, given that the intermittency and variability of some renewables increases the complexity of the system operator's job; storage systems can provide the needed response to mitigate these characteristics of renewables. Storage can also be used to provide ancillary services to the system operator, such as voltage support, peaking power, and regulation, which would otherwise be supplied by fossil-fuel power plants.

- Major Goals Addressed: Increase use of renewable generation, improve the efficiency of the transmission infrastructure.
- Major Issues Addressed: Enhanced operational flexibility, improve system control, reduce the need for new transmission infrastructure.
- Major Developmental Gap(s): Costs, applications, size, speed of response, integration with system control methodologies.
- Major Proposed R&D Activity: Monitor technology developments, demonstration projects and industry trends. Support efforts by utilities to identify promising and cost-effective applications.

5.8. Power Flow Control Technologies

The AC electric power system, by its nature, does not have a high degree of controllability in terms of system operators being able to direct power to particular transmission lines or paths. This frequently results in inefficient use of transmission assets, congestion, and uneconomic operation. The limited array of tools available to system operators includes generators under their direct control; series and shunt capacitors; phase-shifting transformers; synchronous condensers; switches; power electronics based devices including FACTS and HVDC systems; and power conversion devices used to interface distributed renewable resources.

- Major Goals Addressed: Increase use of renewable generation, improve the efficiency of the transmission infrastructure.
- Major Issues Addressed: Increase capacity, maintain/improve system reliability.
- Major Developmental Gap(s): User confidence, costs, applications, integration with intelligent controls and operating systems.
- Major Proposed R&D Activity:
    - SmartWire Industry Demonstration in California: Install 5 - 10 SmartWire units and run tests for power flow control. Follow-on to current CIEE TRP project with Georgia Tech consortium to develop smart grid variable impendence power flow control technology ($500K).
    - Power Flow Control Technologies for Increased Renewable Imports into California: Analyze the technical performance, costs and benefits derived by electricity consumers and transmission owners of various promising advanced power flow control technologies (e.g. FACTS, DC transmission), energy storage, demand side options, and transmission capacity additions for increasing the import of renewable energy resources into California, including consideration of benefits of these technologies in mitigating the impact of retirements of thermal power plants in reducing critically important inertia, voltage and dynamic characteristics of the California electric system. (Note: This project is similar to objective and scope to Steve Lee's Network Control for Wind Energy Integration for California project submitted previously) ($350K).

- Development of Fault Current Controller Technology, Phase II: Field test a second-generation high-temperature superconducting fault current controller technology. DOE has allocated $12.7 million in cost sharing to this $25 million project to the team of American Superconductor, Siemens AG (Germany), Nexans (France), the University of Houston, Los Alamos National Laboratory, SCE and TRP.

5.9. Intelligent Protection Systems Using Adaptive Relays Controlled by Wide Area Synchrophasors Demonstration

The wide-area synchrophasor-based monitoring, data analysis, diagnosis, communications and control technology platform provides a foundation to monitor, supervise, and modify the operation of adaptive relay protection systems in real time based on a diagnostic analysis of the state of the power system. Fundamental research and application development research is underway, funded by PIER and Virginia Tech. The next step is the demonstration of the use of wide-area synchrophasor data to reduce the likelihood of false triggering by protective relays.

- Major Goals Addressed: Increase use of renewable generation.
- Major Issues Addressed: Increase capacity, maintain/improve system reliability.
- Major Developmental Gap(s): User confidence, costs, field tests.
- Major Proposed R&D Activity: Conduct field demonstrations in California of the applications being developed in the ongoing PIER-funded efforts.

5.10. Superconducting Technologies

This class of equipment includes transformers, generators, motors, cables, storage systems, and control devices that use superconducting wire in place of copper or aluminum conductors. Superconducting electrical equipment has the advantages of much lower losses, reduced size and significant increases in power-carrying capacity over conventional AC equipment. Second-generation (2G) superconducting wire uses liquid nitrogen rather than liquid helium as a refrigerant, making today's superconducting devices much more cost-effective than previous designs.

- Major Goals Addressed: Increase use of renewable generation, improve the efficiency of the transmission infrastructure.
- Major Issues Addressed: Increase capacity, maintain/improve system reliability.
- Major Developmental Gap(s): Costs, maintenance, longevity, reliability, user confidence.
- Major Proposed R&D Activity: Monitor technology developments, demonstration projects and industry trends. Support efforts by utilities to identify promising and cost-effective applications, and seek opportunities for cost-sharing for demonstrations of high-value deployments. See also Development of Fault Current Controller Technology, Phase II, under Power Flow Control Technologies, above.

6.0 References

Brown, Merwin, et al, 2008. *Transmission Technology Research for Renewable Integration*, California Energy Commission, PIER Program Energy Commission-500-99-013.

California Renewable Portfolio Standard (RPS): cf. Senate Bill 1078 (2002), Assembly Bill 32 (2006), Senate Bill 107 (2006), and Governor's Executive Order S-14-08 (November 17, 2008).

California Energy Commission, 2008. *2008 Integrated Energy Policy Report Update*, Sacramento: California Energy Commission.

7.0 Glossary

BPA	Bonneville Power Administration
CAISO	California Independent System Operator
CIEE	California Institute for Energy and the Environment
CERTS	Consortium for Electric Reliability Technology Solutions
DOE	Department of Energy
EPRI	Electric Power Research Institute
FACTS	Flexible Alternating Current Transmission Systems
GHG	Greenhouse Gas
HTLS	High Temperature, Low Sag
HVDC	High Voltage Direct Current
IOU	Investor Owned Utility
IEEE	Institute of Electrical and Electronics Engineers
CIGRÈ	Conférence Internationale des Grands Réseaux Electriques (International Council on Large Electric Systems)
NASPI	North American Synchrophasor Initiative
PG&E	Pacific Gas and Electric
PNNL	Pacific Northwest National Laboratory
PES	Power Engineering Society
PSERC	Power Systems Engineering Research Center
PIER	Public Interest Energy Research
PAC	Policy Advisory Committee
RTR	Real Time Ratings
RI	Renewable Integration
RPS	Renewables Portfolio Standard
R&D	Research and Development
RD&D	Research, Development, and Demonstration
SDG&E	San Diego Gas and Electric

SCE	Southern California Edison
STATCOM	Static Synchronous Compensator
SVC	Static VAR Compensator
T&D	Transmission and Distribution
TRP	Transmission Research Program
UWIG	Utility Wind Integration Group
VSC	Voltage Source Converter
WECC	Western Electricity Coordinating Council

APPENDIX B:
Seismic Bushing Analysis Final Report

Public Interest Energy Research (PIER) Program

FINAL PROJECT REPORT

EVALUATION OF THE SEISMIC PERFORMANCE OF HIGH-VOLTAGE TRANSFORMER BUSHINGS

Prepared for: California Energy Commission

Prepared by: University at Buffalo – The State University of New York

MARCH 2012

Prepared by:

Reinhorn, Andrei M., Ph.D, PE
Filiatrault, Andre R., Ph.D, PEng
Muhammad, Fahad, Ph.D Candidate
Kong, Dohwan, Ph.D, PE
Koliou, Maria, Ph.D Candidate
Oikonomou, Konstantinos, Ph.D Candidate
Nicholas Oliveto, Ph.D Candidate
University at Buffalo, the State University of New York
Buffalo, NY 14260, USA

Schiff, Anshel, Ph.D
Precision Measurement Instruments
Los Altos Hills, CA 94022

Contract Number: 500-03-037
Work Authorization: TRP-08-03

Prepared for:

California Energy Commission

Jamie Patterson
Contract Manager

Fernando Pina
Office Manager
Energy Systems Research Office

Mike Gravely
Deputy Division Chief
Energy Research & Development Division

Laurie ten Hope
Deputy Director
Energy Research & Development Division

Robert P. Oglesby
Executive Director

DISCLAIMER

This report was prepared as the result of work sponsored by the California Energy Commission. It does not necessarily represent the views of the Energy Commission, its employees or the State of California. The Energy Commission, the State of California, its employees, contractors and subcontractors make no warrant, express or implied, and assume no legal liability for the information in this report; nor does any party represent that the uses of this information will not infringe upon privately owned rights. This report has not been approved or disapproved by the California Energy Commission nor has the California Energy Commission passed upon the accuracy or adequacy of the information in this report.

ACKNOWLEDGEMENTS

This research project was sponsored by the California Energy Commission with the support of the California Institute for Energy and Environment at the University of California–Berkeley, the Multidisciplinary Center for Earthquake Engineering Research (MCEER) at SUNY-Buffalo, and by the Bonneville Power Administration. Their support is gratefully acknowledged.

This report is the result of the research efforts and contributions of multiple individuals who performed side investigations and experiments that shaped the current material.

Particular acknowledgement is due to Dr. Leon Kempner of Bonneville Power Administration (BPA), and to the Bonneville Power Administration for supporting complementary investigations on the analysis of transformers with bushings. Their financial contribution and guidance are gratefully acknowledged.

The authors are in debt to Mr. Mark Pitman, Technical Services Manager, Mr. Scot Weinreber, Mr. Chris Zwirlein, Mr. Chris Budden, Mr. Duane Koslowski, Mr. Robert Staniszewski, and Mr. Lou Moretta, the technical staff of the Structural Engineering and Earthquake Simulation Laboratory (SEESL), who skillfully conducted experiments on full-size electrical components, particularly transformer bushings, that were critical to this effort.

Last but not least, the authors thank the advisory committee, led by Mr. Eric Fujisaki of PG&E, and chair of the IEEE 693 Working Group, for their comments and guidance throughout this research project.

PREFACE

The California Energy Commission Public Interest Energy Research (PIER) Program supports public interest energy research and development that will help improve the quality of life in California by bringing environmentally safe, affordable, and reliable energy services and products to the marketplace.

The PIER Program conducts public interest research, development, and demonstration (RD&D) projects to benefit California.

The PIER Program strives to conduct the most promising public interest energy research by partnering with RD&D entities, including individuals, businesses, utilities, and public or private research institutions.

PIER funding efforts are focused on the following RD&D program areas:

- Buildings End-Use Energy Efficiency
- Energy Innovations Small Grants
- Energy-Related Environmental Research
- Energy Systems Integration
- Environmentally Preferred Advanced Generation
- Industrial/Agricultural/Water End-Use Energy Efficiency
- Renewable Energy Technologies
- Transportation

Evaluation of the Seismic Performance of High-voltage Transformer Bushings is the final report for the CEC/PIER project "Analysis of the Seismic Performance of Transformer Bushings" (contract number 500-07-037, work authorization number TRP-08-03), conducted by Research Foundation of the State University of New York, on behalf of the Multidisciplinary Center for Earthquake Engineering Research MCEER). The information from this project contributes to PIER's Energy Systems Integration Program.

For more information about the PIER Program, please visit the Energy Commission's website at www.energy.ca.gov/research/ or contact the Energy Commission at 916-654-4878.

ABSTRACT

High-voltage transformers are essential parts of power grids. However, components of transformers, such as the bushings and surge arresters, are vulnerable to excessive vibrations caused by earthquakes. When such components fail in earthquakes, or their oil contents catch fire in the aftermath of an earthquake, there is a danger that the entire grid might be affected leading to power interruptions and losses to utility customers. Experience from laboratory tests and earthquake damage indicates that the current industry procedures for seismic qualifying of transformer bushings are not adequate for the purpose of certifying the performance of transformer bushings in response to seismic events.

The seismic qualification procedures introduced to account for mounting conditions of bushings on transformers misses and confuses the amplification of the motion of the transformer tank and components on one hand, and the influence of the dynamics of the as-installed bushing on the other. This research project develops experimentation techniques to determine the capacity of bushings, and using advanced modeling of bushings and transformers with frequency-based signal processing, derives mechanical models to enable better evaluation of seismic demands and adequacy. The research also characterizes the ability of simplified procedures to consider the significant interactions among the assemblies and the structure of the entire transformer in the qualification procedures. The resulting development is submitted to the IEEE 693 Standard Working Group for consideration in future revisions of the standard.

Nine full-scale transformer bushings installed in a generic testing rig simulating the transformer tank cover, and using a seismic simulator (shake table) to verify current and proposed standards, were tested. Finite element models and simplified mechanical models for several significant bushing/transformer assemblies were developed, and integrated procedures for qualification and design of those assemblies were developed. The research identified weaknesses of the current qualification procedures that do not consider the as-installed conditions, and which also do not fully address the importance of strength capacity-demand issues. The quantitative data from this study provide guidance for improved measurements and testing protocols, for more accurate qualification of bushings to predefined seismic requirements.

Keywords:

Transmission, high-voltage bushings, transformers, seismic, qualifications, testing, calculations, strength capacity, seismic demand, as-installed systems

Please use the following citation for this report:

Reinhorn, Andrei M.; Filiatrault, Andre R.; Fahad, Muhammad; Kong, Dohwan; Koliou, Maria; Oikonomou, Konstantinos; Oliveto, Nicholas; and Schiff, Anshel. 2011. ***Evaluation of the Seismic Performance of High-voltage Transformer Bushings.*** California Energy

TABLE OF CONTENTS

PREFACE ..... **ii**

ABSTRACT ..... **iii**

TABLE OF CONTENTS ..... **iv**

LIST OF FIGURES ..... **vi**

LIST OF TABLES ..... **xi**

EXECUTIVE SUMMARY **1**

Introduction 1

Purpose 1

Goals and Objectives 2

Conclusions and Recommendations 2

CHAPTER 1: Introduction **4**

Description of Electrical Substation Equipment 5

Seismic Vulnerability of Transformer Bushing Systems 9

Seismic Qualification of Transformers and Bushings 16

CHAPTER 2: Analytical Evaluation of Motions Affecting Transformer Bushings **25**

Numerical Investigation of Seismic Response of Transformer-Bushing Systems 25

Dynamic Analysis of Transformer Bushings 33

Lateral Motion Amplification at the Transformer Cover 51

Rotational Effects of a 230 kV Transformer Cover 60

Vertical Amplifications Due to Flexibility of Transformer Cover 60

Summary and Conclusions of Numerical Study 65

CHAPTER 3: Experimental Study of Transformer Bushings **70**

Testing Specimens 70

Testing Setups 72

Testing Methods 90

Instrumentation 117

Test Protocols and Sequences 123

Results of Bushing Tests 130
Analytical Modeling of Installed Bushings 140
CHAPTER 4: Effects of Dynamic Response of Installed Bushings 141
Response of Bushings Installed on Flexible Cover Versus Installed on Rigid Cover 141
Effects of Location of Bushings on Transformer Cover 149
Forces at Bushings' Connections 154
Effects of Rotating Transformer Cover 165
Summary of Effects of Dynamic Response of Installed Bushings 168
CHAPTER 5: Critical Evaluation of Current Qualification Standards 169
CHAPTER 6: Conclusions and Recommendations 172
GLOSSARY 175
REFERENCES 178
APPENDIX A: TEST PROTOCOLS AND SEQUENCES 184
APPENDIX B: INSTRUMENTATION OF BUSHINGS 218
APPENDIX C: INPUT HISTORY AND SPECTRA 272
APPENDIX D: BUSHING TEST RESULTS 315
APPENDIX E: DEVELOPMENT OF BUSHING MODELS 536

LIST OF FIGURES

Figure 1: Typical Electrical Substation 4

Figure 2: Typical Transformer Installation in Electrical Substation 5

Figure 3: Typical Power Transformer and Its Components 6

Figure 4: High-voltage Electrical Transformer 7

Figure 5: Typical 230 kV Transformer Bushing and Its Components 8

Figure 6: Typical 550 kV High-Voltage Bushing and Its Components 9

Figure 7: Damage to Transformer Due to Inadequate Anchorage (Izmit, Turkey, 1999) 11

Figure 8: Transformer Overturned Due to Anchorage Failure (Turkey, 1999) 11

Figure 9: Permanent Offset (left) and Overturning (right) of Rail-mounted Transformers Due to Seismic Events 12

Figure 10: Substation Buswork Damage, Taiwan, 1999 12

Figure 11: Main Failure Modes of Porcelain Bushings 13

Figure 12: Porcelain Slippage 14

Figure 13: Gasket Failure at Bushing Flange Due to Porcelain Slip 15

Figure 14: Failed Composite Bushings 16

Figure 15: Fractured Composite Bushings 17

Figure 16: Rigid Support Structure for Shake Table Testing (Steel Frame Assembly) 21

Figure 17: Rigid Support Structure for Shake Table Testing 22

Figure 18: Transformer Models Considered 26

Figure 19: Deformed Shape of High-voltage Bushing Models 32

Figure 20: Scaling of California Region Ground Motion – Ensemble 1 38

Figure 21: Scaling of FEMA P695 Ground Motion – Ensemble 2 39

Figure 22: CDF for Maximum Bending Moments for Westinghouse 525 kV Transformer-Bushing Model – Ensemble 1 42

Figure 23: CDF for Maximum Bending Moments for Westinghouse 525 kV Transformer-Bushing Model – Ensemble 2 (1D) 42

Figure 24: CDF for Maximum Bending Moments for Westinghouse 525 kV Transformer-Bushing Model – Ensemble 2 (2D) 43

Figure 25: CDF for Maximum Bending Moments for Siemens 230 kV Transformer-Bushing Model – Ensemble 1 43

Figure 26: CDF for Maximum Bending Moments for Siemens 230 kV Transformer-Bushing Model – Ensemble 2 (1D) 44

Figure 27: CDF for Maximum Bending Moments for Siemens 230 kV Transformer-Bushing Model – Ensemble 2 (2D) 44

Figure 28: CDF for Maximum Bending Moments for Siemens 500 kV Transformer-Bushing Model – Ensemble 1 45

Figure 29: CDF for Maximum Bending Moments for Siemens 500 kV Transformer-Bushing Model – Ensemble 2 (1D) 45

Figure 30: CDF for Maximum Bending Moments for Siemens 500 kV Transformer-Bushing Model – Ensemble 2 (2D) 46

Figure 31: CDF for Maximum Bending Moments for Ferranti-Packard 230 kV Transformer-Bushing Model – Ensemble 1 46

Figure 32: CDF for Maximum Bending Moments for Ferranti-Packard 230 kV Transformer-Bushing Model – Ensemble 2 (1D) 47

Figure 33: CDF for Maximum Bending Moments for Ferranti-Packard 230 kV Transformer-Bushing Model – Ensemble 2 (2D) 47

Figure 34: CDF for Moment Amplification Factors for Ensemble 1 48

Figure 35: CDF for Moment Amplification Factors for Ensemble 2 (1D) 48

Figure 36: CDF for Moment Amplification Factors for Ensemble 2 (2D) 49

Figure 37: Median Values of Moment Amplification Factor for all Four Transformer-Bushing Models – Ensemble 1 49

Figure 38: Median Values of Moment Amplification Factor for all Four Transformer-Bushing Models – Ensemble 2 (1D) 50

Figure 39: Median Values of Moment Amplification Factor for all Four Transformer-Bushing Models – Ensemble 2 (2D) 50

Figure 40: Acceleration Spectra for 500 kV Transformer at Bottom LV Bushing 52

Figure 41: Acceleration Spectra for 500 kV Transformer at Bottom HV Bushing 53

Figure 42: Acceleration Spectra for 500 kV Transformer at Bottom LV Bushing 54

Figure 43: Spectral Amplification for 500 kV Transformer at Bottom HV Bushing 55

Figure 44: Spectral Amplification for 230 kV Transformer at Bottom HV Bushing 56

Figure 45: Rotation of Cover at Bushing Mount 60

Figure 46: Vertical Vibration of Cover at Bushing Mount 65

Figure 47: Spectral Amplification of Cover in Vertical Direction at the Bushing Base – Flexible Connection 67

Figure 48: Vertical Frequencies of Transformer Cover with Mounted Bushing 68

Figure 49: Amplification of Accelerations of 230 kV Transformer Cover in Vertical Direction ... 69
Figure 50: 550 kV Porcelain Bushing Manufactured by GE (Bushing #1) ... 73
Figure 51: Schematic of 550 kV Porcelain Bushing Manufactured by GE (Bushing #1) ... 74
Figure 52: 550 kV Porcelain Bushing Manufactured by GE (Bushings #2 and #3) ... 75
Figure 53: 230 kV Porcelain Bushing Manufactured by ABB Inc. (Bushing #6) ... 76
Figure 54: 550 kV Porcelain Bushing Manufactured by ABB (Bushing #7) ... 77
Figure 55: 550 kV Porcelain Bushing Manufactured by ABB (Bushing #8) ... 78
Figure 56: 230 kV Composite Bushing Manufactured by HSP (Bushing #4A) ... 79
Figure 57: 230 kV Composite Bushing Manufactured by HSP (Bushing #4B) ... 80
Figure 58: 500 kV Composite Bushing Manufactured by Trench Ltd. (Bushing #5) ... 81
Figure 59: Conductor Simulation with Weights on Bushings ... 82
Figure 60: Fixed-base Testing of Bushings: Instrumentation Sketch of Specimen in the Lab ... 85
Figure 61: Top View of the Concrete Slab ... 85
Figure 62: Concrete Block for Fixed-base Testing of Bushings ... 86
Figure 63: Base Plate Interfacing Support Structure to the Shake Table ... 86
Figure 64: Flexible Support Structure for Shake Table Testing ... 87
Figure 65: Front Schematic of the Flexible Support Structure ... 88
Figure 66: Re-locatable Top Plate ... 89
Figure 67: Schematic of the Re-locatable Top Plate ... 91
Figure 68: Bushing Adapter Plate ... 91
Figure 69: Turret for Flexible Frame ... 92
Figure 70: Stiffeners Mounted on Re-locatable Top Plate ... 93
Figure 71: General Test Setup for a Pull Test ... 95
Figure 72: Load Function for the Pull Test ... 96
Figure 73: Non-Structural Component Simulator (NCS) Used to Pull the Top of the Bushing ... 96
Figure 74: Quick-release Test Performed on Fixed Base ... 97
Figure 75: Impact Hammer Test ... 98
Figure 76: Typical Acceleration Response and Power Spectral Density (Bushing #5) ... 99
Figure 77: Typical White Noise Acceleration History Record (Bushing #8) ... 100
Figure 78: Magnitudes of Transfer Functions in Various Channels (Bushing #5) ... 101

Figure 79: Smooth Table Impulse 102
Figure 80: Operational Movement of the Table Impulse..... 102
Figure 81: Typical Power Spectral Densities from Table Impulse Test (Bushing #5) 103
Figure 82: Sine Sweep Wave of Uniform Amplitude..... 105
Figure 83: Required Response Spectrum for 0.5 g ZPA..... 106
Figure 84: Typical Test Accelerograms for Compatibility to 0.5 g ZPA RRS (Bushing #4B) 107
Figure 85: Calculating the Factor at the Center Frequency 108
Figure 86: Acceleration History and Spectrum Before and After Trials 109
Figure 87: Typical Sine Beat Record 110
Figure 88: Response to Resonant Sine Wave..... 111
Figure 89: Matching a Sine Sweep to RRS Using the RS Matching Method..... 114
Figure 90: Matching a Sine Sweep to RRS Using RS and FFT Method 115
Figure 91: Example of Sine-sweep Time Domain Matching to RRS at High Seismic Level (HSL)..... 116
Figure 92: Setup for Liquid Damping Test 118
Figure 93: Field of View and Mounting of Krypton™ Camera 120
Figure 94: Pull Test Performed on Porcelain Bushing to Calibrate Strain Gauges 121
Figure 95: Benchmark Points in Calibration of Gauges..... 123
Figure 96: Instrumentation Sketch for Bushing #8 – Laboratory Floor 125
Figure 97: Instrumentation Sketch for Bushing #8 – Shake Table..... 126
Figure 98: Instrumentation Sketch for Bushing #8 – LEDs for Krypton™ Camera 127
Figure 99: Results of Pull Tests for Bushing #4A 133
Figure 100: Quick Release Test Response – Bushing #4A 135
Figure 101: Impact Hammer Test Response – Bushing #4A..... 136
Figure 102: Transfer Functions – Bushing #4A..... 137
Figure 103: Table Impulse Test Response – Bushing #4A..... 138
Figure 104: Acceleration Profile Along the Height of Bushing #4A – Rigid Frame 138
Figure 105: Acceleration Spectra for 230 kV Transformer at HV Bushing..... 143
Figure 106: Acceleration Spectra for 230 kV Transformer at HV Bushing (cont'd.)..... 144
Figure 107: Acceleration Spectra for 500 kV Transformer at Bottom of HV Bushing 145
Figure 108: Spectral Amplification for 230 kV Transformer at Bottom of HV Bushing..... 146

Figure 109: Acceleration Spectra and Expected Response of Bushings 147
Figure 110: Acceleration Spectra and Expected Response of Bushings (cont'd.)..... 148
Figure 111: Frequency Dependence on Bushing Location – No Turret 152
Figure 112: Frequency Dependence on Bushing Location – Tilted Turret..... 153

LIST OF TABLES

Table 1: Earthquake Events with Severe Damage to Electrical Equipment 10

Table 2: Seismic Qualification Levels According to IEEE Standard 693-2005 20

Table 3: Dimensions of Transformer Models Considered 27

Table 4: Fundamental Periods and Natural Frequencies of High-voltage Bushings on Rigid Base 27

Table 5: Periods and Natural Frequencies of Westinghouse 525 kV Transformer-Bushing Model 28

Table 6: Periods and Natural Frequencies of Siemens 230 kV Transformer-Bushing Model 28

Table 7: Periods and Natural Frequencies of Siemens 500 kV Transformer-Bushing Model 30

Table 8: Periods and Natural Frequencies of Ferranti-Packard 230 kV Transformer-Bushing Model 31

Table 9: Comparison of High-voltage Bushings on Rigid Base vs. "As-installed" 33

Table 10: California Region Earthquake Ground Motion – Ensemble 1 34

Table 11: FEMA P695 Earthquake Ground Motion – Ensemble 2 36

Table 12: Dynamic Analysis Cases 39

Table 13: Maximum Amplifications at Turret Base of Bushings* for the 500 kV Transformer Models 57

Table 14: Amplifications at Turret Base of Bushings for the 230 kV Transformer Models 58

Table 15: Maximum Amplifications at Turret Base of Bushings for the 500 kV Transformer Models 59

Table 16: Peak Accelerations and Moments of the Bushing Closest to the Conservator 62

Table 17: Peak Accelerations and Moments of the Central Bushing 63

Table 18: Peak Accelerations and Moments of the Bushing Farthest from the Conservator 64

Table 19: Summary of Data for Bushings Used in the Experimental Study 84

Table 20: Location of Bushing with and without Turret 92

Table 21: Location of Bushing and Stiffeners 93

Table 22: Krypton™ K600 Camera Accuracy 120

Table 23: Example Instrumentation List for ABB 550 kV Porcelain Bushing (Bushing #8) 124

Table 24: First Part of Test Protocol – Static Testing (Bushing #5) 128

Table 25: Second Part of Test Protocol – Dynamic Testing (Bushing #5) 129

Table 26: Third Part of Test Protocol – Bushing #5 129

Table 27: Summary of Tests for Bushing #4A 132
Table 28: Results of Pull Tests for Bushing #4A 133
Table 29: Acceleration Distribution from Simulated Seismic Motion – Bushing #4A 139
Table 30: Frequency (Hz) of Bushings in Analytical and Experimental Studies 148
Table 31: Bushing Locations and Connection Interfaces on Flexible Transformer Cover 150
Table 32: As-Installed Frequencies of Different Bushings in Different Mounting Locations..... 151
Table 33: Acceleration and Strain Gauge Measurements of Bushing #4A 157
Table 34: Acceleration and Strain Gage Measurements of Bushing #4B 158
Table 35: Acceleration and Strain Gauge Measurements of Bushing #5 159
Table 36: Acceleration and Strain Gauge Measurements of Bushing #6 160
Table 37: Acceleration and Strain Gauge Measurements of Bushing #6 (cont'd.)..... 161
Table 38: Acceleration and Strain Gauge Measurements of Bushing #7 162
Table 39: Moment-to-Shear Force Ratios and Elevation of the Inertia Centroid for Bushing #6 163
Table 40: Moment-to-Shear Force Ratios for Bushing #6 164
Table 41: Displacements Due to Bending and Rigid Body Rotations 166
Table 42: Accelerations Due to Bending and Rigid Body Rotations 167
Table 43: Glossary of Terms and Acronyms 175

EXECUTIVE SUMMARY

Introduction

Earthquakes are a significant threat to the integrity of the California electric transmission system; prolonged, widespread electric outages can cause significant hardships and economic losses to many Californians, and degrade public safety. Much of the California electric system is in highly active seismic regions, including most of the large urban areas. Previous research studies, many funded by PIER, have resulted in significant knowledge of electric system seismic behavior and have led to substantial improvements in key areas; they have also identified remaining vulnerabilities in the electric system, and several areas of high-value seismic research that can lead to a more reliable, robust and resilient electric system.

One of the least understood seismic behaviors in the electric system is the interaction between the high voltage transformer and other electrical and mechanical equipment mounted on it or connected to it. Components of transformers, such as the bushings and surge arresters, are vulnerable to excessive vibrations caused by earthquakes. When such components fail in earthquakes, or their oil content catches fire in the aftermath of an earthquake, there is a danger that the entire grid might be affected, leading to power interruptions and losses to industry.

Experience from laboratory tests and examination of post-earthquake damage indicate that the procedures for seismic qualifying of transformer bushings are not entirely valid: equipment, such as bushings, that have been successfully qualified via the currently accepted standards and certification procedures, have been known to fail from seismic events that are supposedly less severe than the standards. The working hypothesis for this study is that the currently accepted seismic qualification procedures that were intended to account for the mounting conditions of the bushing on the transformer do not adequately account for the interactions of the transformer tank and its components, nor the influence of the dynamics of the as-installed bushing itself. Research focused on these phenomena is needed, in order to revise the qualification standards.

Purpose

Current evaluations and qualification procedures, based on the protocols of IEEE Standard 693-2005: Recommended Practices for Seismic Design of Substations, consider both the bushing and the transformer in isolation from the other, and therefore fail to explicitly recognize the influence of bushing installation on, and interaction with, the transformer in actual in-service conditions. Such interactions include the flexibility of the transformer tank walls and roof on the dynamics of the bushing; the effect of the use of a turret between the tank roof or cover and the bushing flange; and the effect of bus connections (electrical conductors and associated hardware) at the top of the bushings, among others.

The primary purpose of this project is to perform focused research that will provide the scientific data necessary for the determination of the true seismic response of combined transformer-bushing systems. It is intended that the results of this project will be used by the IEEE 693 Standard Working Group to produce an updated 693 Standard. An improved Standard will enable more accurate analysis and seismic qualification of transformer bushings, and will enable bushing and transformer manufacturers to improve the seismic performance of their equipment. The end result will be a more seismically reliable and safe electric delivery system for the people of California.

Goals and Objectives

The objectives of this project are to develop experimentation techniques to determine the true strength capacity of bushings, perform laboratory testing of bushing-transformer systems using those techniques, derive mechanical models of bushings that enable better evaluation of seismic demands and adequacy, and develop recommended revisions to IEEE Standard 693 so that manufacturers can improve their products and utilities can design and operate a more seismically reliable electric system. Moreover, since the issues are practice oriented, the project is set to develop and explore the ability of simplified procedures to consider the significant interactions among the assemblies and the structure of the entire transformer in the qualification procedures.

The primary goal of this project is to determine the seismic response of the combined transformer-bushing interaction, which will determine the true strength capacity of the combined transformer-bushing system. These results will be used in recommended revisions to the IEEE Standard, thereby enabling improved seismic analysis and qualification of transformer bushings.

Conclusions and Recommendations

The research plan was based on a sequence of technical tasks: (i) evaluating the current state of the art on vulnerability and qualification testing of bushings; (ii) analytical modeling and evaluation of motions affecting the bushings mounted on transformers; (iii) laboratory testing, using a large seismic simulator (shake table) to test nine full-scale bushings installed in a newly designed generic testing rig simulating the transformer tank cover, to examine the transformer-bushing interactions and measure strength capacity; (iv) mathematical modeling of bushings using finite element analysis and simplified practical models; (v) evaluation and verification of current and proposed standards based on the modeling and experimental results ; (vi) development of recommended integrated procedures for qualification and design of transformer bushings, for inclusion in future revisions of IEEE Standard 693.

The research identified weaknesses of the current qualification procedures that do not adequately account for the as-installed conditions when mounting bushings on transformers, and that also do not fully address the important issues of strength capacity of bushings versus the seismic demands (physical forces) imposed upon them in service. Through comprehensive

quantification based on analytical and empirical study, this project has developed recommended measurement methods and test protocol requirements for improved qualification procedures for bushings, so that electrical equipment can be more accurately specified and relied upon to withstand the expected seismic events.

The recommended requirements for qualification of bushings are as follows:

1. Develop procedures for qualification that compare the strength demands to strength capacities in mechanical terms.
2. Manufacturers of bushings should determine and specify the strength capacity of bushings either by testing them to failure (whether by static or dynamic tests), or by computations using established and accepted strength models.
3. Testing of bushings to generate seismic strength demand using seismic simulators (shake tables) according to a desired severity (qualification level).
4. Determine the desired severity including identified dynamic properties of bushings and mounting conditions, though interaction factors or simplified analytical models.
5. Modify the design requirements for the covers of transformer tanks to reduce, or eliminate, the interaction issues with the bushings.
6. Further develop methods of reducing seismic demands on all components of transformers by using protective equipment or systems, or other mitigation techniques.

Recommendations 4 – 6 will require further development and basic research, to convert the findings from this project to specifications for the manufacturers, utilities and regulatory bodies.

These recommendations have been submitted to the IEEE 693 Standard Working Group. At the time of this writing, the Working Group has taken these recommendations into consideration, and is developing suggested changes to the qualification procedures in the Standard to be considered by the Working Group in future revisions to the Standard.

CHAPTER 1:
Introduction

The transmission of electrical power from the generating station to the site of distribution is a multi-phased procedure. From the moment electricity is produced until it is provided to the consumers, its voltage needs to be transformed at various points. This function is performed by a power transformer, and the bushings represent the points at which electrical conductors are connected to the power transformers.

In most cases when the power plant is located a long distance from the load, it is desirable that electricity is transmitted with minimal losses. In electrical engineering terms, for a given power level and conductor diameter, higher voltage results in lower current transfer. The power lost is proportional to the square of the current; it is therefore preferable to use a high voltage electric power transmission system. The electric power network is a vital component for the everyday life in modern societies. Electrical substations are critical components of the electric power network that supplies power for industrial, business and residential use, and they are susceptible to significant damage under strong seismic excitation. Rehabilitation of existing substations and proper design of new systems will reduce the possible post-earthquake effects and damage. A typical electrical substation is shown in Figure 1.

Figure 1: Typical Electrical Substation

Photo Credit: David Neale, Internet

The substation contains an ensemble of electrical equipment serving to step the voltage down and transfer the power to the external distribution system. Among this equipment, the electrical transformer is probably the most crucial component for the operation of the substation. In Figure 2, the transformer is the large gray structure in the center of the picture, with external cooling fans on the side; the bushings are the white components with red tops affixed vertically to the top of the transformer. The transformer is surrounded by other substation equipment including post insulators supporting bus connections, instrumentation (voltage and current transducers), surge arrestors, etc.

Figure 2: Typical Transformer Installation in Electrical Substation

Photo Credit: Ashrafi et al., 2008

Description of Electrical Substation Equipment

The electrical substation, also called the subsidiary station, serves several functions, starting with the protection of the transmission and distribution lines as well as the equipment within the substation by using sensors that detect abnormal system operating conditions and that trigger devices which isolate these lines and equipment. Most substations operate as a means of transferring power between different voltage levels by utilizing power transformers and as a means of reconfiguration of the power network by opening transmission lines or partitioning multi-section buses (Kempner, 2007; Schiff, 1999).

One of the essential pieces of equipment in any electrical substation is the power transformer. The power transformer is a device, without any moving parts, which transfers the electric power from one circuit to another by electromagnetic means. The basic components of this

device are the coils, steel core, oil, tank and bushings. A typical power transformer and its internal components are shown in Figure 3, and a typical transformer installed at a substation is shown in Figure 4.

The basic function of a transformer is to transform voltage from one level to another. Before the transfer through the high voltage lines is realized, a transformer installed at the production site is used to amplify the voltage of the current produced at the power plant. Accordingly, at the load end, a transformer is used as well to step the voltage down to acceptable levels prior to the distribution through the local transmission lines.

The basic parts of the transformer are: the tank (filled with oil), the bushings, the conservator, the radiators, the core and the coils. The core and coil assembly, through which the transformation of the electrical power is achieved, are located inside the oil-filled tank for insulation purposes and for protection from the elements. The oil serves as a means of cooling for the core, which is heated appreciably during the process of transformation. The oil also provides electrical insulation between the internal components. It is necessary that the oil remain stable at high temperatures for an extended period.

Figure 3: Typical Power Transformer and Its Components

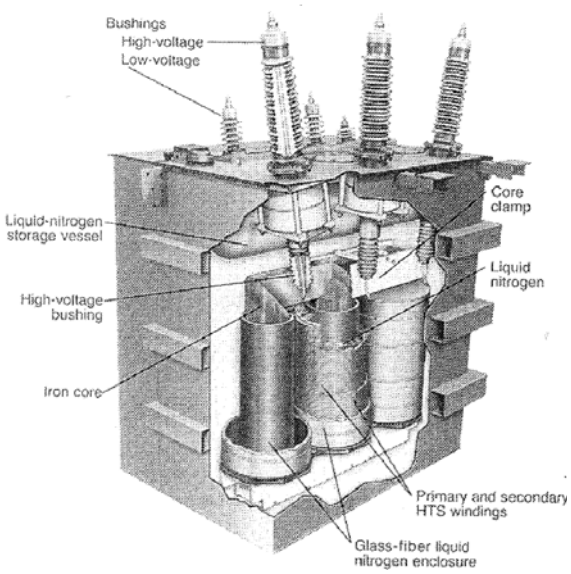

Source: Pansini, 1999

Figure 4: High-voltage Electrical Transformer

Photo Credit: Electrical Technologies Company

To enhance the procedure of cooling through convection, the heated oil is circulated through external radiators, usually attached to the side of the tank. The conservator is an external reservoir tank located above the transformer and connected to the main tank so that the oil in the main tank is free to expand at high temperatures.

Bushings are insulated conductors providing electrical connections between high voltage lines and oil-filled transformers, and are typically mounted on the top of a transformer or on a turret attached to the transformer. They serve to connect the high voltage power lines while at the same time insulating them from the metallic, conductible walls of the tank. To prevent a flashover the surrounding porcelain is designed with external sheds to provide a relatively long electrical distance between the power cables and the coils. Bushings are typically composed of a flange plate by which the bushing is attached to the turret, porcelain units (above the flange plate) and a metallic dome at the top. A typical 230 kV bushing and its components are presented in Figure 5 (Gilani, Whittaker & Fenves, 2001) .

Figure 5: Typical 230 kV Transformer Bushing and Its Components

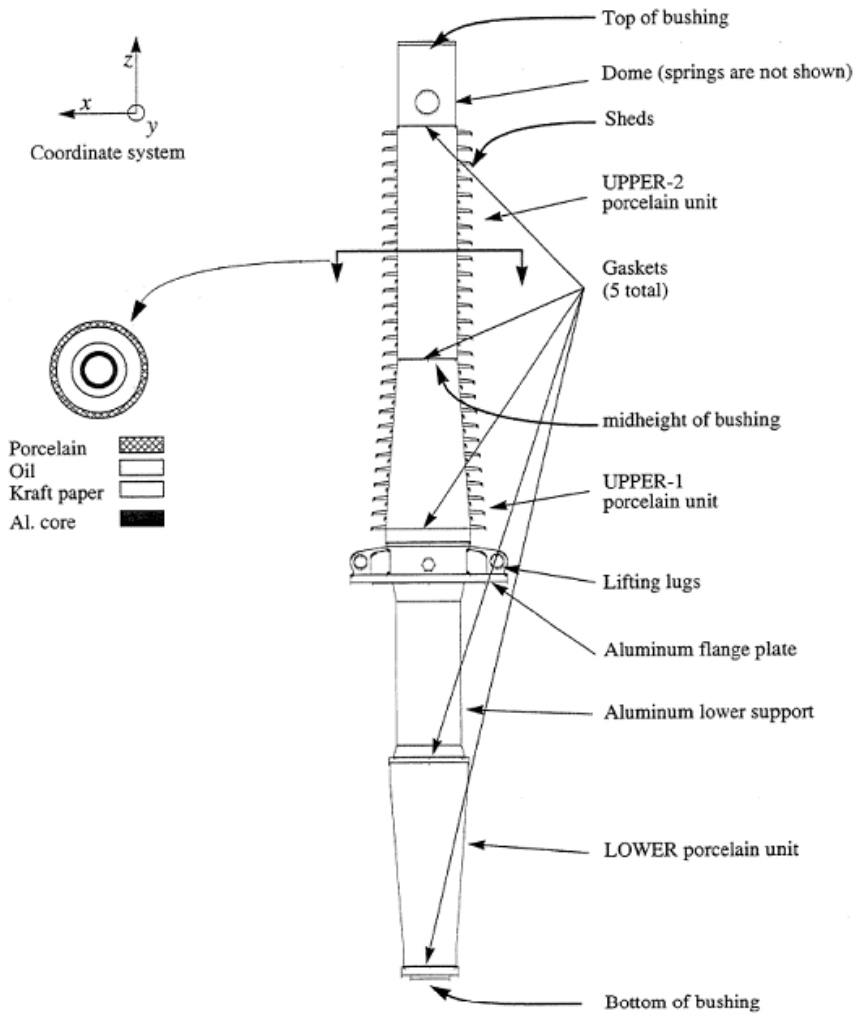

Source: Gilani, Whittaker & Fenves, 2001

The insulation is typically achieved by placing the conductor inside a case usually made of porcelain. The external part of a bushing is composed of annular porcelain segments stacked upon one another and held in place (post-tensioned) by the conductor itself. The remaining space between the conductor and the porcelain is filled with kraft paper and oil for more adequate insulation. In cross section, the bushing is composed of a central core that provides electrical connectivity, a condenser that wraps the core, perimeter annular porcelain (or composite material) units, and oil that fills the gaps between the condenser and the porcelain unit (composite units will have polymer resin fill, rather than oil). A typical 550 kV bushing and its components is depicted in Figure 6.

Figure 6: Typical 550 kV High-Voltage Bushing and Its Components

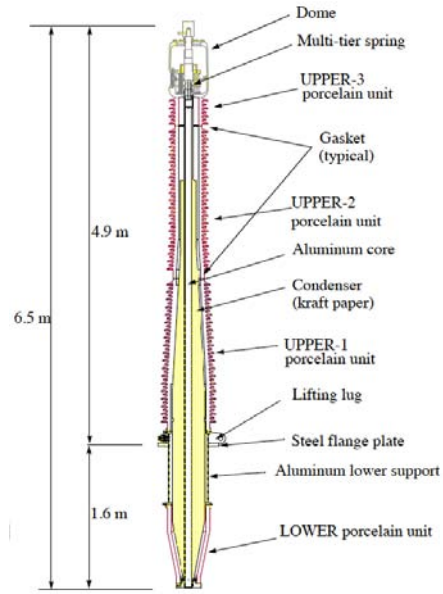

Photo Credit: State University of New York – Buffalo

Source: Gilani et al., 1999

Seismic Vulnerability of Transformer Bushing Systems

Electrical substation equipment has demonstrated vulnerable behavior under strong seismic excitation, resulting in severe damage to electric power networks. Observations from both moderate and severe ground shaking events have shown that the performance of electrical equipment, and particularly transformers, was unsatisfactory in many cases. However, the overall earthquake performance of the substations and their equipment varies. It has been observed that the equipment in substations operating at or below 115 kV (low voltage) performs well when properly anchored, while the performance of equipment operating at or above 220 kV (high voltage) depends on the specific equipment at the substations and their installation practices (Schiff, 1999).

Examples of earthquake events in which extensive damage was observed include, among others (see Table 1): Loma Prieta (Northern California), 1989; Northridge (Southern California), 1994 (Schiff & Ostrom, 1995); Kobe, Japan, 1995 (Schiff, 1998); Izmit, Turkey, 1999; Chi-Chi, Taiwan, 1999 (Schiff & Tang, 2000); Baja California, 2010 (Schiff, 2010); and Concepcion, Chile, 2010. The estimated immediate cost in terms of widespread damage was in the range of hundreds of millions of dollars for each of these events. Additional costs related to the electrical system included clearance and replacement costs of the damaged electrical equipment, expenses for the restoration of normal network operation, and daily revenue losses due to the disruption of electrical service to customers. Apart from the direct impact on the local economy, the restoration of network operations was also significantly impeded by the loss of power itself, in the cases where the seismic event caused a widespread blackout.

Table 1: Earthquake Events with Severe Damage to Electrical Equipment

Earthquake Event	Year	Magnitude (M_w)
San Fernando, USA	1971	6.6
Managua, Nicaragua	1972	7.5
Loma Prieta, USA	1989	6.9
Northridge, USA	1994	6.7
Kobe, Japan	1995	6.9
Chi-Chi, Taiwan	1999	7.6
Izmit, Turkey	1999	7.4
Conception, Chile	2010	9.1
Baja California, USA	2010	7.2

Evaluation of the damage observed in electrical transformers allows the types of failures to be classified as either global, when the damage inflicted pertains to the stability of the transformer as a whole; or local, when a component of the transformer fails.

Global Damage to Transformers

The most severe impacts to electrical substation equipment from earthquake events can be categorized into damage to the power transformers and damage to the transformer bushings. The observed failure types of power transformers are: (i) failure of unrestrained transformer, (ii) anchorage failure, (iii) conservator failure, (iv) foundation failure, and (v) damage to control boxes.

The first two types of global failures are the most common, despite the fact that it is a simple procedure to fix the transformer base to the foundation either by anchor bolts or welds. Among the global modes of failure, the most commonly encountered are the anchorage failure and the failure of unrestrained transformers. The anchorage is generally achieved by fixing the tank to the foundation with anchor bolts or by welding. There are cases in which the anchorage has failed, causing ripping in the tank and oil leakage.

There are also cases where the foundation was inadequately designed for the seismic overturning moments and failed, causing the transformer to rock and tilt. Characteristic damage due to foundation failure and an overturned transformer from the 1999 Izmit, Turkey earthquake are shown in Figure 7 and Figure 8, respectively.

Unrestrained transformers, such as rail-mounted transformers and transformers simply mounted on top of a foundation pad, experience the most common failures suffering permanent

displacements and even overturning when the ground shaking is significant, as shown in Figures 8 and 9.

Figure 7: Damage to Transformer Due to Inadequate Anchorage (Izmit, Turkey, 1999)

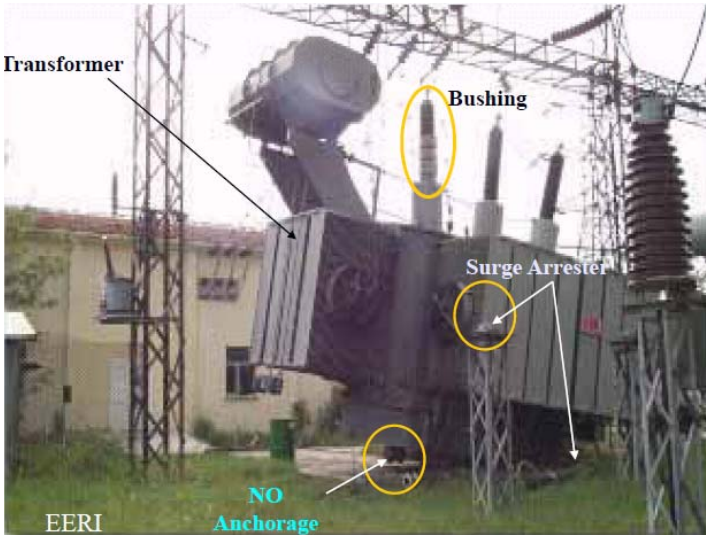

Photo Credit: Wang & Gonzales, 2008

Figure 8: Transformer Overturned Due to Anchorage Failure (Turkey, 1999)

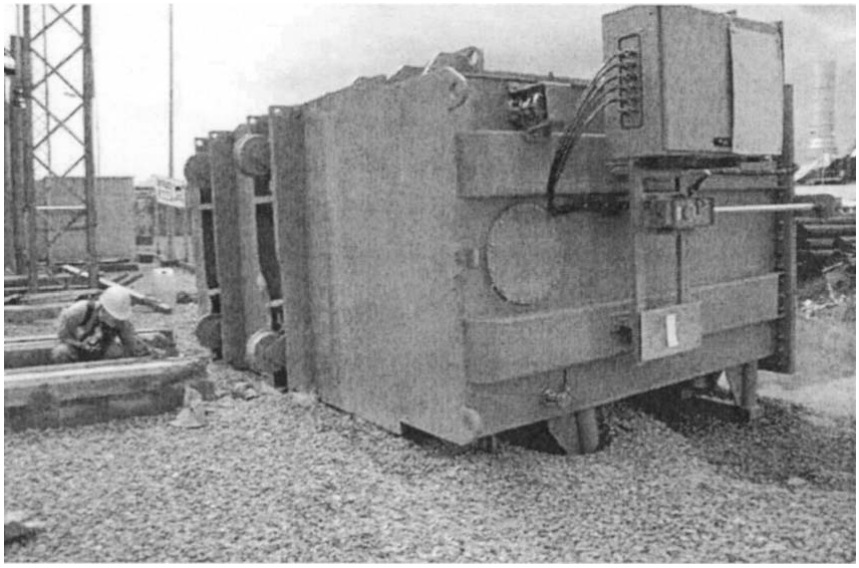

Photo Credit: Sezen & Whittaker, 2006

Figure 9: Permanent Offset (left) and Overturning (right) of Rail-mounted Transformers Due to Seismic Events

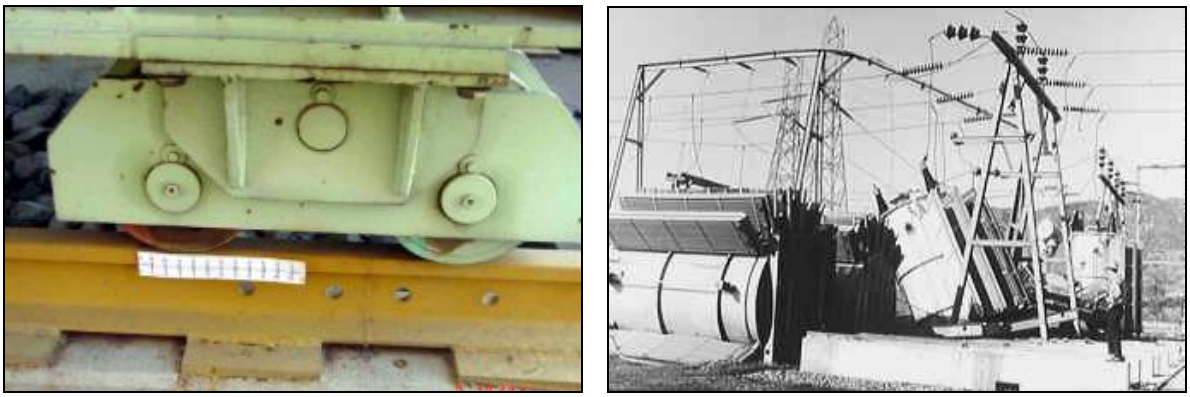

Photo Credits: Anshel Schiff, PMI

Substation Bus Structures

Transformers and their bushings are electrically and physically connected to other equipment in the substation, such as bus structures that are insulated from the ground by post insulators. This equipment is subject to shaking from seismic ground motion, and may fail, causing outages of the transformers they are connected to, as well as outages of other substation equipment (see Figure 10). Buswork and electrical connectors can also impart motions and stresses to the top of the transformer bushing.

Figure 10: Substation Buswork Damage, Taiwan, 1999

Photo Credit: Wang & Gonzales, 2008

Local Damage to Bushings

Based on the experience of past earthquakes, bushings have proven to be the most vulnerable of the components comprising the transformer system, and, almost invariably, the loss of a bushing or bushings leads to the loss of function of the transformer. A bushing loses its functionality when the oil escapes from the bushing, compromising the insulation system, in case of either physical shifting at the base, or breakage of the porcelain or composite materials. Four possible failure modes, mostly in porcelain bushings, and which were generally observed from the damage investigations into past earthquake events, are illustrated in Figure 11. These potential modes of failure are: a) porcelain unit slippage, b) oil leakage between components, c) rubber gasket extrusion, and d) porcelain unit fracture (Schiff, 1977). While each of these failure modes can occur individually, it has been found from recent post-seismic investigations that bushing failures frequently exhibit more than one of these failure modes simultaneously.

Figure 11: Main Failure Modes of Porcelain Bushings

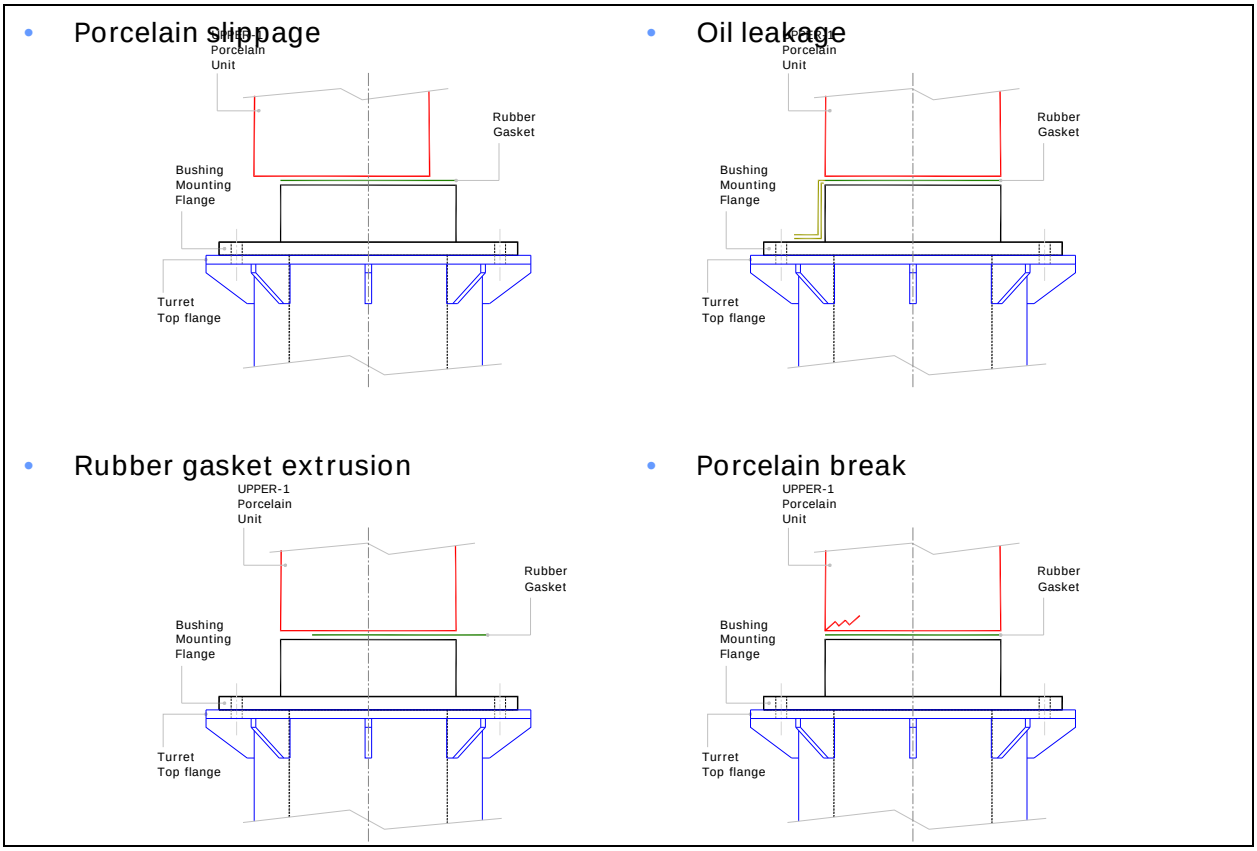

Source: Kong, 2010

Porcelain Slippage

Seismic motion will cause the bushing to shake, bend, or oscillate in various ways, and the physical stresses created by these motions may cause slippage or displacement at the base of the

bushing in the area of the mounting flange (see Figure 12). Any gap that occurs in this location will allow oil to escape, and the resulting loss of insulating capability can cause the bushing to fail.

Figure 12: Porcelain Slippage

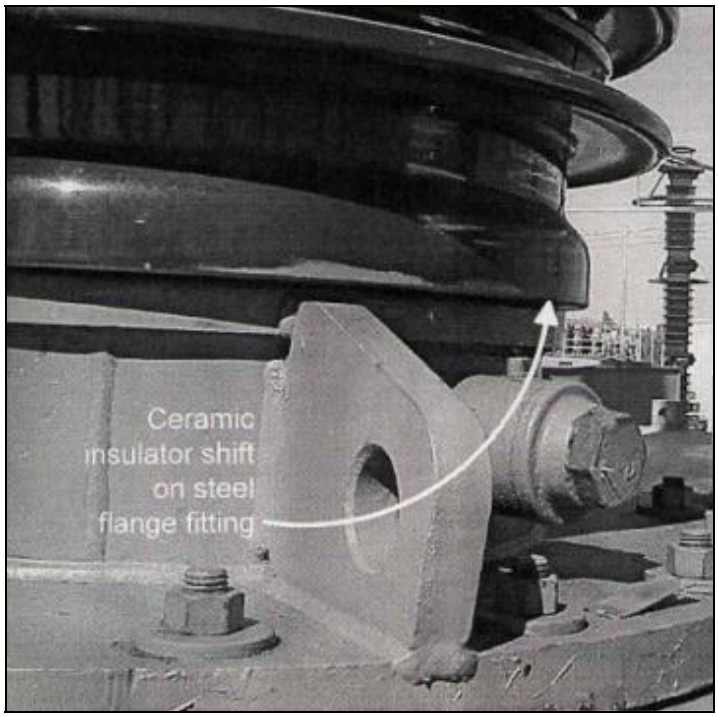

Photo Credit: Anshel Schiff, PMI

Oil Leakage

Typically, an annular-shaped rubber gasket is installed between the porcelain unit and the metal mounting flange at the base of the bushing, and is pre-stressed as a barrier against oil leakage. When lateral forces above the gasket connection due to seismic shaking are great enough, the porcelain unit may lift up at the base, opening a gap at the flange and allowing oil to escape. Even if the bushing mounting settles back to an intact state, some oil may still be lost, leading to possible eventual failure of the bushing.

Gasket Extrusion

A gasket is generally seated in a bushing flange groove or pocket so that the extrusion of the gasket from the groove will not occur easily under the application of lateral loading. However, once a porcelain unit slips or uplifts over the gasket connection, it can bear down unevenly on the gasket and force the gasket partially out of the flange groove. This can happen more easily in the case of a bushing with no grooving for the gasket. Figure 13 shows a gasket that failed due to extrusion; note also the simultaneous porcelain slippage.

Porcelain and Unit Fracture

With standard design, there is normally no direct contact between porcelain units or between a metal flange and a porcelain unit (refer again to Figure 6), resulting in very little stress concentration (Gilani, 1999). This means that the porcelain unit will be under nearly uniform compression forces from post-tensioning of the inner core. However, when a porcelain unit slips or uplifts over the gasket connection due to the lateral forces, direct contact between porcelain units or between the metal flange and the porcelain unit may occur. This will cause concentrated compression stress and may result in the fracture in the porcelain. It has been observed that the lack of slack in the connecting cable between the bushing and the connecting buswork can lead to fracture of the porcelain or composite body material at the location shown in Figure 11 (lower right illustration).

Figure 13: Gasket Failure at Bushing Flange Due to Porcelain Slip

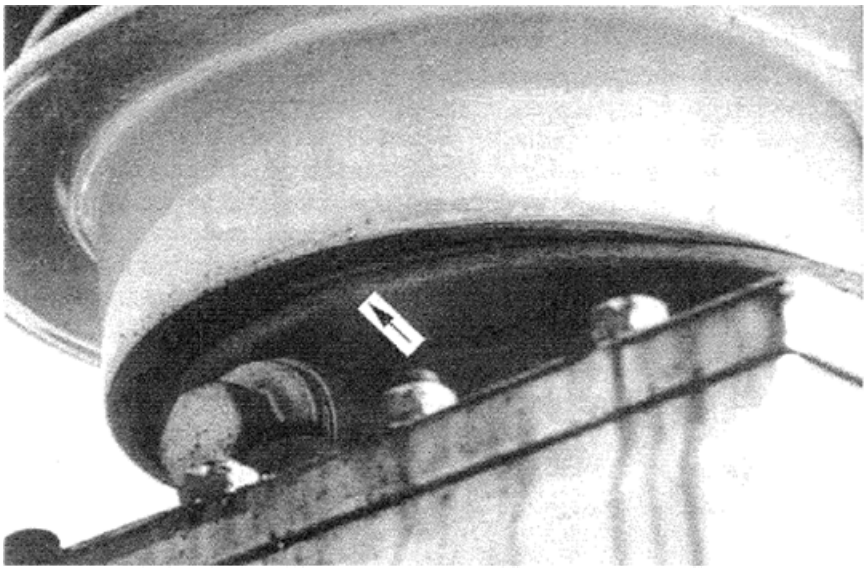

Photo Credit: Ashrafi et al., 2008

This type of damage is closely associated with the nature of bushing design. Bushings are relatively long and narrow in general shape, and thus tend to accumulate large moments and stresses close to the base. The problem is aggravated because of the low-strength and inherently brittle properties of the porcelain material. Therefore, bushings will tend to slip and fracture at the base. Other types of bushings, notably those using composite materials, made with silicone rubber sheds over hollow-core or solid-core fiberglass rods, are more flexible than porcelain and develop different failure modes. Some fracture due to excessive bending and some disconnect from their connecting flanges, due to loss of bond slip (see Figures 14 and 15).

Finally, apart from bushings, in which the damage inflicted is usually the most catastrophic for the operation of the transformer, failure has also been observed in various other ancillary

transformer components, such as radiators, conservators and surge arresters, as occurred for example in the Baja Earthquake (Schiff, 2010).

Moreover, as previously noted, other equipment connected to the transformer or nearby, whether supported directly on the ground or mounted on rigid support structures, has also been known to suffer substantial damage from seismic events and thereby directly contribute to bushing/transformer failure (see Figure 10).

An extensive list of failures of porcelain bushings and other auxiliary components is presented in Schiff, 2007.

Figure 14: Failed Composite Bushings

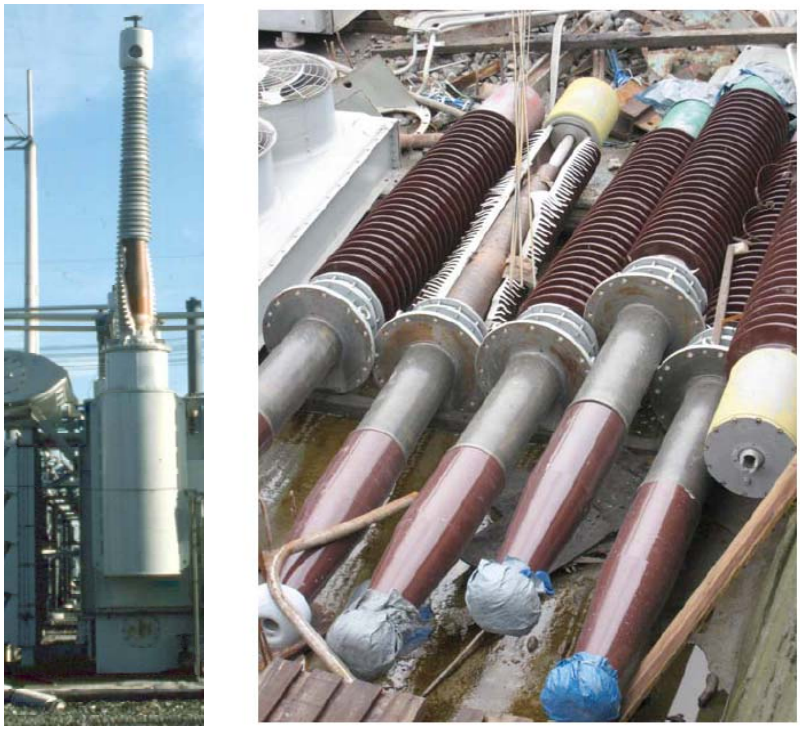

Photo Credits: Schiff, 2010

Seismic Qualification of Transformers and Bushings

It is difficult to separate the bushings from the transformers in terms of studying their seismic behavior, since the two components become an integrated system when installed in service, and act together during seismic events. Despite such inseparable function, these two components are designed and manufactured as separate entities sharing a common interface (the mounting flange), and not as an integrated system. Given the multiplicity of transformer and bushing

types and designs, this is understandable, but the mating of a specific model of transformer with a specific model of bushing creates a unique combination with unique mechanical properties. The issue becomes: How to specify seismic qualification procedures for bushings so that manufacturers and utilities can be reasonably certain that the transformer/bushing combination will perform as expected in seismic events?

Current practice is to design typical bushings and then check their suitability to resist vibrations and other forces, while comparing the performance with an acceptability criterion (Kempner, 2002, 2007). A transformer manufacturer will then use a prequalified bushing, expecting to obtain good performance during both electrical operations and also during severe seismic events.

The current practice is regulated by standards of testing and acceptance, such as IEEE Standard 693-2005: Recommended Practice for Seismic Design of Substations (IEEE, 2005) in the US and other parts of the American continent, except for Canada, which uses a generic protocol. According to a white paper (Schiff, 2007), although the transformer bushings are designed to fit almost any transformer (matching the electrical sizes and demands) and then are qualified by testing in a laboratory or by analysis according to testing standards such as IEEE 693, damage may still occur in some bushings during severe earthquakes. The author goes further and indicates that there are probably inadequate or insufficient requirements in the current standard to ensure the prevention of such damage.

Figure 15: Fractured Composite Bushings

Based on observations (Schiff, 2007 and Elder, 2008), the following description is a brief listing of key requirements in IEEE Standard 693-2005 (Annex D) for qualifying transformers to the Seismic Qualification Levels (levels described in Appendix A and in Appendix D.1.1 to D.1.3) for operation at 161 kV and above. As indicated previously, the disparate requirements for qualifying transformers and bushings are largely unrelated at present. Below are comments developed for this project by Reinhorn et al., 2011.

Recommended Practice per IEEE Standard 693-2005

IEEE Standard 693-2005 (IEEE, 2005), sometimes simply referred to as "IEEE 693," may be applied to all types of substation equipment, including transformer bushings. The method of qualification used for a transformer bushing depends upon the voltage classification of the bushing, with the methods being prescribed in Annex D, "Transformers and Liquid-filled Reactors." The qualification method for high voltage bushings is covered in section D.4.4, "Qualification of Bushings of 161 kV and Above," which specifies that the bushing is to be shake-table tested, using the time history method. The bushing must remain undamaged in such testing, while more detailed acceptance criteria are specified in section D.5, "Acceptance Criteria."

The acceptance criteria require that there shall be no slippage, visible oil leaks, or broken support flanges. The qualification criteria require stresses to be monitored in the porcelain near the flange to determine the integrity of the base. Moreover, the criteria require monitoring accelerations, relative displacements, and stresses in flanges and bolts, either by direct measurements, or by calculation from related instruments. When the qualification is done at the performance level, only the integrity of the bushing is monitored without direct measurements.

Grouping of Equipment

Because it is not practical to test every individual design, similar equipment may be grouped together for the purpose of qualification, with the most seismically vulnerable piece of equipment being tested, as described in IEEE 693, section 4.7, "Qualifying Equipment by Group." Additional equipment may be added to the grouping if it can be demonstrated that it is less seismically vulnerable than the equipment originally tested. The exact method for grouping is left to mutual agreement between the supplier and the user.

Testing of the Reference Bushing and Approval of Candidate Bushings

Tests of a "reference" bushing should be performed by qualified laboratories[1]. A bushing for which approval is sought is referred to as the "candidate bushing." The calculations should

[1] Some of the available laboratories with some experience of testing reference bushings are the Earthquake Engineering Research center (EERC) at UC/Berkeley, the Structural Engineering and Earthquake Simulation Laboratory (SEESL) at University at Buffalo, the US Army Corps of Engineers' Construction Engineering Research Laboratory (CERL) at Champaign, IL, the Structural Laboratory at Portland State University, or the Shake Table Laboratory at UC/Irvine, among others.

demonstrate that the candidate bushing is less vulnerable, seismically, than the reference bushing, and can therefore be grouped with it for the purpose of qualification. The definitions of reference bushing and candidate bushing are as defined by Elder, 2008.

Required Excitations for Qualifications

According to the current Standard, bushings are to be qualified by shake-table acceleration-history testing to withstand a "Performance Level" defined as twice the magnitude of the spectrum for the High Required Response Spectrum (RRS). The spectral acceleration is calculated using the formulas shown in Figure A.1 of IEEE 693. The zero period acceleration (ZPA) comes from the definition of the performance levels in IEEE 693, Section 8: “Seismic Performance Criteria for Electrical Substation Equipment,” with detailed description of seismic qualification levels (subsection 8.3) and projected performance requirements (subsection 8.4). The performance requirements for electrical equipment are summarized in. These requirements apply to equipment mounted on the ground or on support structures or on other equipment. Specific requirements distinguish between the cases. While transformers are mounted on the ground, the transformer bushings are usually mounted on transformer covers, and therefore subjected to generally different requirements.

For the shake-table testing mentioned above, the bushing is mounted on a rigid stand (see for example Figures 16 and 17) and the bushing flange is subjected to the excitation corresponding to the "Performance Level" (twice the RRS) amplified by an additional factor of 2, to account for the amplification that the transformer will produce at its roof or cover versus its base. Therefore, the bushing will be excited with a motion proportional to the Required Response Spectrum (RRS), but 4 times stronger.

Table 2: Seismic Qualification Levels According to IEEE Standard 693-2005[2]

Qualification Scale		ZPA* for Qualification to Seismic Levels (SQL)				ZPA* for Qualification to Performance Levels[3] (PQL)			
Levels	Equipment mounted on:	Ground	Support (or Equipment) Structure[4]			Ground	Support (or Equipment) Structure[5]		
	Properties of support structure:		Known	Not Known	Transformer Bushings		Known	Not Known	Transformer Bushings
	IEEE 693-2005 Reference Sections:	**8.3**	**8.3 + 5.5.3**	**8.3 + 5.5.4**	**8.3 + D.4.4**	**8.3**	**8.4+ 5.5.3**	**8.4 + 5.5.4**	**8.4 + D.4.4**
(1)		(2)	(3)	(4)	(5)	(6)	(7)	(8)	(9)
High		0.50	0.50 x AMP[5]	1.25	1.00	1.00	1.00 x AMP[4]	2.50	2.00
Moderate		0.25	0.25 x AMP[4]	0.63	0.50	0.50	0.50 x AMP[4]	1.25	1.00
LOW[6]		~ 0.05	~ 0.05 x AMP[4]	~ 0.13	~ 0.10	~ 0.10	~ 0.11 AMP[4]	~0.20	~0.20

*Minimum ZPA (g) x Required Response Spectrum (RRS) to be resisted by electrical equipment

---

[2] Equipment can be qualified for either: (i) "Seismic Qualification Level"(SQL) or (ii) "Performance Qualification Level" (PQL).

[3] *Qualification to Performance Levels* can be obtained by *direct testing* to minimum ZPA specified in the table. The equipment is expected to perform at the performance level, if tested to *Seismic Levels,* provided that doubling the *demand* obtained in testing is below *50% of capacity* of equipment.

[4] When the equipment is mounted directly on shake table without the support structure, the factor AMP should be multiplied by an additional factor of 1.1.

[5] AMP is the "dynamic amplification factor" at top of support structure with respect to the base.

[6] Does not require testing; design is prepared qualitatively. All values (in the colored boxes) are approximate values for design guidance.

Figure 16: Rigid Support Structure for Shake Table Testing (Steel Frame Assembly)

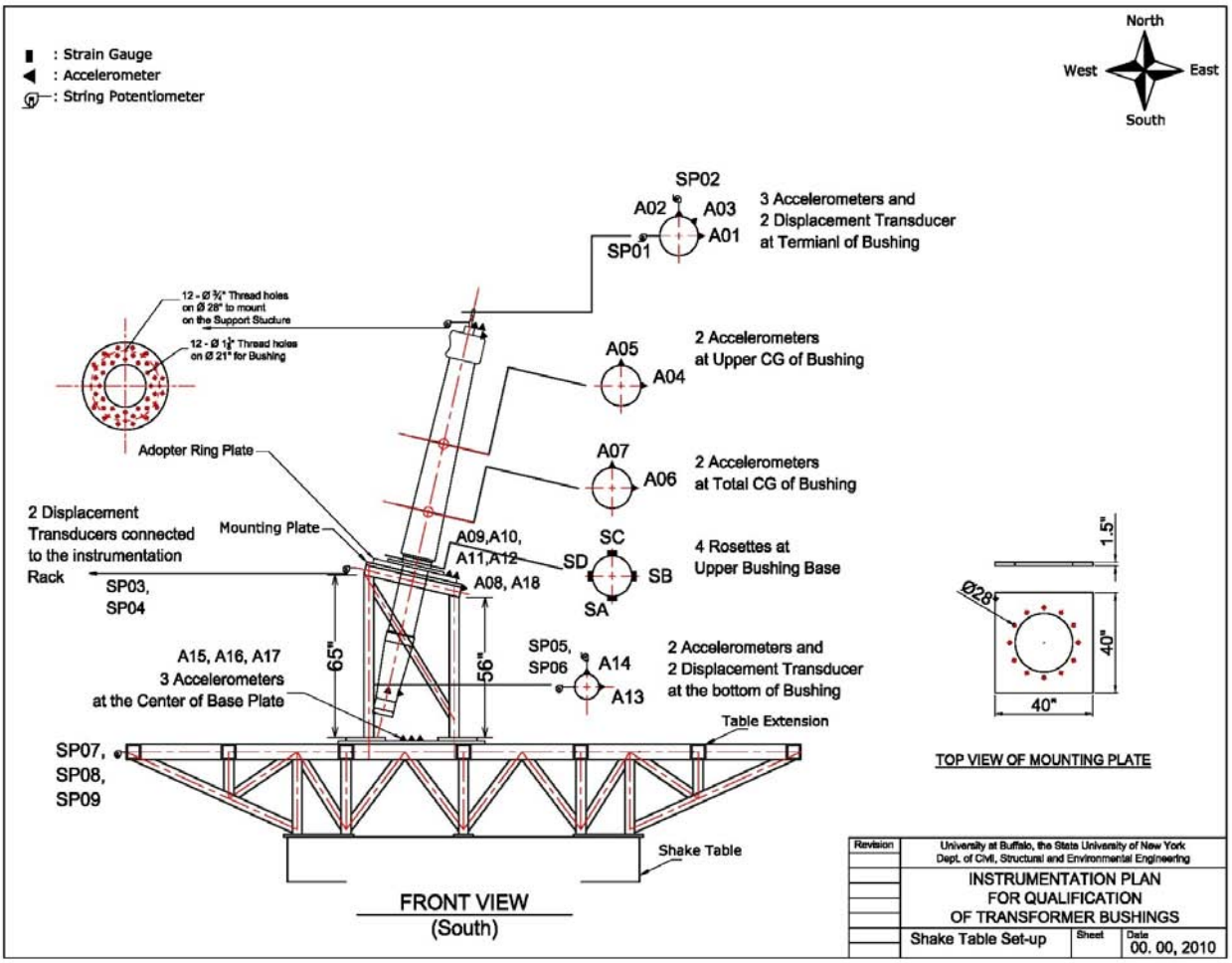

Source: State University of New York – Buffalo

Required Accounting for Service Conditions

IEEE 693 requires that during the qualification analysis or testing, for center-clamped, non-cemented bushings, the effect of changes in temperature and relative coefficients of thermal expansion of bushing components must be considered; such changes depend on the axial clamping forces applied to the central conductor to hold them together. This generally requires that the clamping force used during the testing be reduced from its nominal setting at ambient temperature. The reduction will apply to other bushings dependent on the center clamp for their resistance. The Standard recommends as best practice to report the actual level of the reduced clamping force to account for such effect.

Bushings and other equipment are to be qualified with a weight attached to the conductor terminal pad. The weight specified for 230 kV equipment is 15 lb; for 500 kV equipment it is 25 lb.

In the current practice, the resistance level is described in terms of ZPA (base accelerations) or accelerations measured or computed at the top of the bushing or at its center of gravity (either global or local), above the connection level; also defined as the "fulcrum" in Elder, 2008. Forces, moments and stresses in the connectors or in the critical sections are determined by multiplying the weights (or corresponding masses) by the above accelerations applied in the respective centers.

Figure 17: Rigid Support Structure for Shake Table Testing

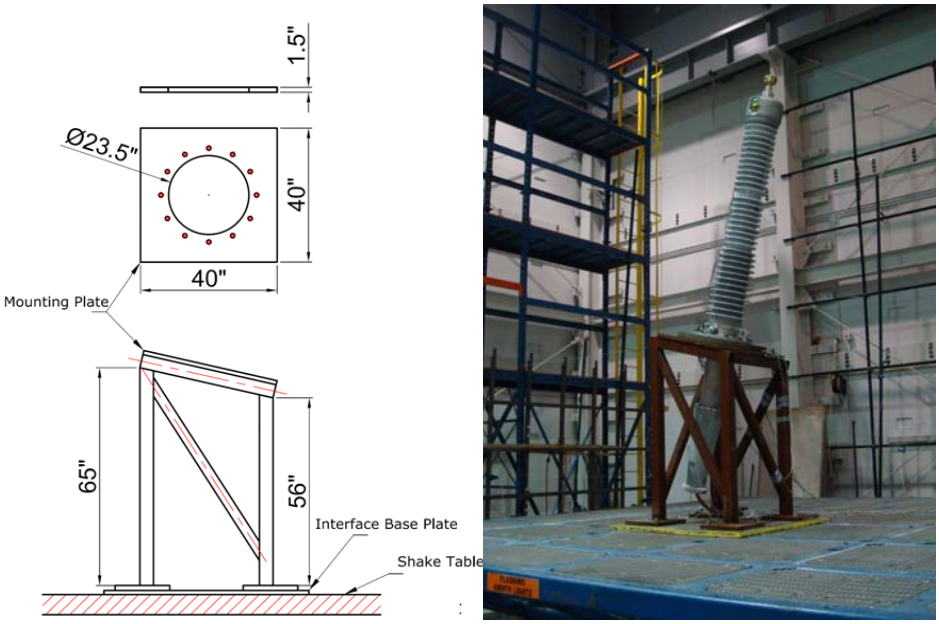

Source and Photo Credits: State University of New York – Buffalo

Comments on the Seismic Qualification of Transformers and Their Acceptability Criteria

According to IEEE 693 criteria, transformers shall be undamaged and function immediately after an earthquake that has response spectra that are as large as the High Required Response Spectra.

Tank, core and anchorage shall be qualified via static analysis, which shall include an evaluation of the load path of the core, coils, tank and base to the anchorage. The design shall ensure that load path components are sufficiently rigid that parts do not shift. Load path components will be identified.

The external components of the transformer, radiators, conservators and control cabinets should be qualified by static analysis, without consideration of the dynamic effects.

According to the Standard, the transformers should be welded to plates or beams embedded in the foundation pad. Other types of connections to the base pad do not seem to be allowed.

Comment 1: It should be noted that the functionality requirement is related to the initial momentary operations, but does not make any reference to the long-term functionality that is often lost months after the earthquake.

Comment 2: Schiff, 2007 notes that IEEE 693 does not address the dynamics of the anchoring system, which has limited stiffness and may influence the dynamic response of the tank, core, coil and tank cover on which the bushing is resting. Although the Standard notes the importance of stiffness, it does not make any recommendation on how to address it.

Comment 3: The tank is considered to be completely independent of the other auxiliary components, which in turn are influenced by its construction. In particular, the tank can modify the dynamic vibration range and transfer of vibrations to the auxiliary components depending on its stiffness, while the components may exercise amplified forces greater than the influence of their gravity.

Comments on the Seismic Qualification of Bushings and Their Acceptability Criteria

According to the current Standard, bushings are to be qualified by shake-table acceleration-history testing to withstand a "Performance Level" defined as twice the magnitude of the spectrum for the High Required Response Spectra (RRS).

The acceptance criteria require that there shall be no slippage, visible oil leaks, or broken support flanges, in visual observations.

The qualification criteria require that stresses in the flange be monitored to determine the integrity of the flange.

Comment 1: There is no provision to account for the effects of the flexibility of the tank and of the top of the transformer, to which the bushing is attached.

Comment 2: The amplification factor of 2 reflects the peak in the transfer function between the ground and the top of the transformer where the bushing or turret would be mounted. This factor of 2 must account for the amplification of the motion of the body of the transformer, and this can be due to flexibility of the transformer case, flexibility of the anchorage, and motion of the transformer and its foundation pad caused by soil-structure interaction. While this has support from analytical studies, some of the transformers develop larger amplifications (Matt and Filiatrault, 2006; Reinhorn et al., 2011).

Comment 3: When bushings are mounted on a flexible cover, their connection base will be excited not only by a translational horizontal and vertical movement, but also by a rotational component due to the cover distortion. Such excitation might be predominant in case of extremely rigid bushings.

Comment 4: The Standard does not consider the important fact that a rigid transformer bushing mounted on a rigid frame does not develop the dynamic characteristics that would be developed when it is mounted on a flexible cover. As a result, the dynamics and the amplifications during the qualification testing are inadequate compared to the "as-installed" conditions.

Comment 5: The Standard requires the clamping force to be reduced only for bushings where resistance to lateral loads is provided by the clamping force. The clamping force also resists rocking at the flange and thus reduces the loads that must be resisted by a cemented flange. It also seems that all center-clamped bushings should have clamping loads reduced for temperature effects.

Comment 6: The external added weight is meant to account for the weight of the conductor terminal hardware and does not include a significant amount of the weight of the conductor itself, the possible effects of the dynamic response of the conductor, or interaction loads due to inadequate slack in the conductor connection to adjacent equipment. Moreover, other parts of the Standard address the slack interaction loads.

Comment 7: Slippage, oil leaks and broken support flanges are failure modes that define the strength capacity of the bushing. The force level for which these occur could be measured from static tests. The sequence of these failure modes may be dictated by the respective forcing functions (or moments). The failure modes may be delayed such that the lower failure mode will still provide continuous operation (for example, it may allow slippage without oil leak).

Comment 8: The strain measurements are not directly useful unless target force or moment levels can be derived and used to monitor force demands versus force strength capacity.

CHAPTER 2:
Analytical Evaluation of Motions Affecting Transformer Bushings

Numerical Investigation of Seismic Response of Transformer-Bushing Systems

This section presents a numerical investigation of the seismic response of transformer bushings, with the objective of providing an understanding of the influences of transformer components on the bushings and its connections. The methodology was developed in Koliou (2010) and the testing procedures presented in detail in Koliou et al. (2011).

Introduction

In this section a numerical investigation on the seismic response of bushings mounted on transformer tank bases ("as installed") and on rigid bases is presented. Four different finite element models of transformer bushing systems were used for performing modal and linear dynamic time history analyses using the commercial structural analysis program *SAP2000 Advanced V.14.1.0* (Computers and Structures, 2009).

Description of Transformer Models Considered

Four different types of transformer bushing systems of various sizes, geometries and voltages, as shown in Figure 18, were considered for analysis in this research project. Table 3 presents details on the dimensions and weight of each transformer model (Filiatrault & Matt, 2006; Oikonomou, 2010).

Each three-dimensional finite element model was built in the commercial structural analysis program SAP2000 Advanced V.14.1.0 (Computers and Structures, 2009). The transformer frames were modeled as shell elements with the appropriate thickness and mass allowing for in-plane deformation and out-of-plane bending, while the transformer tank was considered to be full of oil. Beam elements as well as appropriate shell elements were used for modeling the stiffeners attached to the tank sides (Filiatrault & Matt, 2006). The high-voltage bushings were mounted on the cover plate of the transformer tank and each bushing, which was modeled as multiple beam elements in series with the appropriate geometry, stiffness and mass, consisted of three parts: (i) the upper part represented the actual high-voltage bushing, (ii) the central part was a radial array of rigid elements connected to the turret, which represented the bushing flange, and (iii) the lower part in the assembly was the turret, which was modeled as a polyhedron of the same number of surfaces as the number of the radial rigid elements. The radiators were represented by vertical elements of rectangular cross section, while the high-voltage surge arrestors were modeled as vertical beams with circular cross-section (Reinhorn et al., 2011). The oil conservator of the 230 kV Ferranti-Packard transformer model, which was represented by a cylindrical tank made up of shell elements, was considered to be full of oil and the oil was distributed uniformly on the walls as vertical loading. The tank was supported by two horizontal and two diagonal beams fixed to the tank wall (Reinhorn et al., 2011; Reinhorn et al., 2010).

Finally, it should be mentioned that the geometry, thickness and locations of all walls, plates and beams were obtained from manufacturer's structural drawings.

Figure 18: Transformer Models Considered

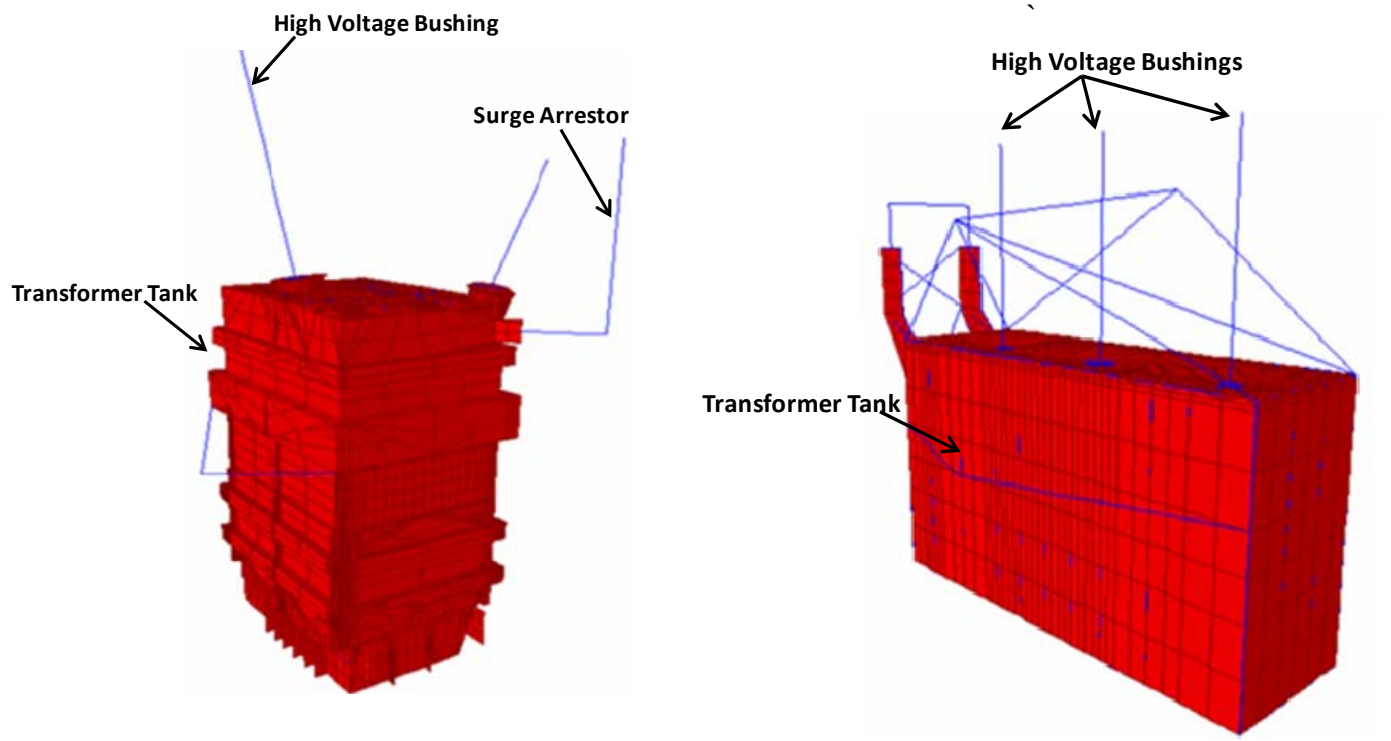

a. Westinghouse 525 kV Transformer Model

b. Siemens 230 kV Transformer Model

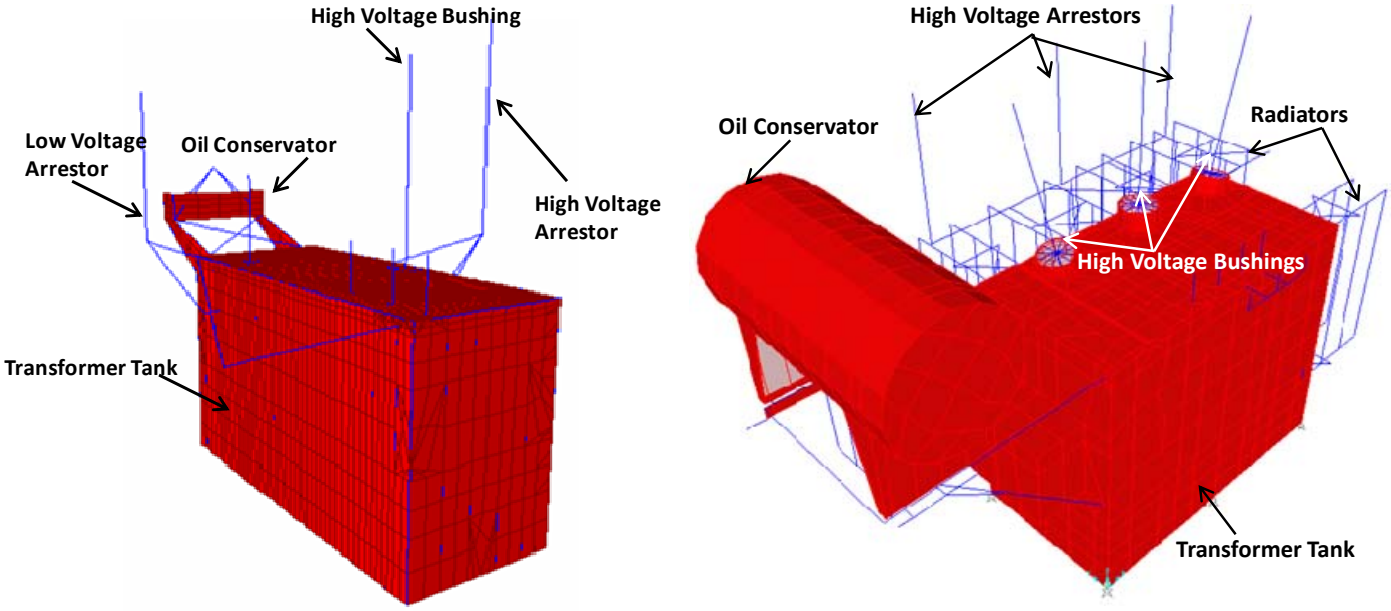

c. Siemens 500 kV Transformer Model d. Ferranti-Packard 230 kV Transformer Model

Source: Koliou et al., 2011

Table 3: Dimensions of Transformer Models Considered

Transformer Model	Dimensions (ft)			Weight** (kips)
	Length	Width	Height	
Westinghouse 525 kV	8.8	9.9	22.8	463
Siemens 230 kV	10.0	24.2	14.4	478
Siemens 500 kV	10.8	26.0	16.8	673
Ferranti-Packard 230 kV	8.3	26.0	13.0	266

**Including oil

Modal Analysis of High-voltage Transformer-Bushing Systems

Modal Analysis of High-voltage Bushings on Rigid Base

In order to conduct the modal analysis of bushing systems installed on a rigid base, the dynamic properties of the transformer bushing models were modified. More specifically, two different procedures were followed to create a rigid base for the high voltage bushings. The first approach focused on the restraint of all the degrees of freedom of the initial model, except for those of the bushing, resulting in bushing on rigid foundations. For the second approach, all the elements of the initial model, except for the bushing, were deleted and the bushing itself is restrained at its base.

Note that in both procedures used to represent the rigid base the results of the modal analysis were identical. Moreover, the period obtained for the Ferranti-Packard 230 kV model was almost equal to the period computed for the Siemens 230 kV model, as shown in Table 4, which indicates that the frequency of the 230 kV bushing on a rigid base is independent of the manufacturer.

Table 4: Fundamental Periods and Natural Frequencies of High-voltage Bushings on Rigid Base

Transformer Model	Period (sec.)	Frequency (Hz)
Westinghouse 525 kV – mode 1	0.108	9.27
Siemens 230 kV – mode 1	0.059	16.85
Siemens 500 kV – mode 1	0.114	8.75
Ferranti-Packard 230kV – mode 1	0.060	16.80

Modal Analysis of High-voltage Bushings on Transformer Tank ("As-installed" Conditions)

For each one of the transformer bushing models, a modal analysis was performed and the natural frequencies for all the modes were obtained. Note that for the Westinghouse 525 kV, Siemens 230 kV and Siemens 500 kV transformers, the number of modes considered are greatly reduced due to the complexity of the finite element models (Filiatrault & Matt, 2006), while for the Ferranti-Packard 230 kV transformer model more than 200 modes were considered. At least 90% of the total mass participation was accounted for in the two principal directions of each model. The frequency of each mode is presented in Tables 5–7 for the Westinghouse 525 kV, Siemens 230 kV and Siemens 500 kV transformers, respectively, while the first 40 modes of the Ferranti-Packard 230 kV transformer are shown in Table 8. The deformation of the first mode of each bushing system is presented in Figure 19.

Table 5: Periods and Natural Frequencies of Westinghouse 525 kV Transformer-Bushing Model

Mode	Mode Description	Period (sec.)	Frequency (Hz)
1	Surge Arrestor (1st mode)	0.377	2.65
2	High-voltage Bushing (1st mode)	0.342	2.92
3	Surge Arrestor (2nd mode)	0.328	3.05
4	High-voltage Bushing (2nd mode)	0.292	3.42
5	Transformer Frame (1st mode, Transverse)	0.119	8.38
6	Transformer Frame (1st mode, Longitudinal)	0.088	11.37
7	High-voltage Bushing (3rd mode)	0.076	13.15
8	Surge Arrestor (3rd mode)	0.069	14.58
9	Surge Arrestor (4th mode)	0.065	15.31
10	Transformer Frame (2nd mode, Transverse)	0.049	20.16
11	Transformer Shell (1st mode, Out-of-plane Bending)	0.040	24.81
12	Transformer Frame (2nd mode, Longitudinal)	0.029	33.90
13	Transformer Frame Torsion (1st mode)	0.023	42.79
14	Transformer Shell (2nd mode, Out-of-plane Bending)	0.019	50.71

Table 6: Periods and Natural Frequencies of Siemens 230 kV Transformer-Bushing Model

Mode	Mode Description	Period (sec.)	Frequency (Hz)
1	High-voltage Bushings (1st mode)	0.109	9.14
2	High-voltage Bushings (2nd mode)	0.097	10.26
3	Transformer Frame (1st mode, Transverse)	0.093	10.76
4	Transformer Frame & Bushings (2nd mode,	0.086	11.57
5	Oil Conservator Tank (1st mode, Longitudinal)	0.083	12.03
6	High-voltage Bushings (3rd mode)	0.076	13.23

7	High-voltage Bushings (4th mode)	0.074	13.51
8	Transformer Frame (2nd mode, Transverse)	0.059	16.88
9	Transformer Shell (1st mode, Out-of-plane Bending)	0.052	19.17
10	Transformer Frame (1st mode, Longitudinal)	0.039	25.05
11	Transformer Frame (4th mode, Transverse)	0.039	25.95
12	Transformer Shell (2nd mode, Out-of-plane Bending)	0.027	37.19
13	Transformer Frame (2nd mode, Longitudinal)	0.026	37.89
14	Transformer Shell (3rd mode, Out-of-plane Bending)	0.024	41.32

Table 7: Periods and Natural Frequencies of Siemens 500 kV Transformer-Bushing Model

Mode	Mode Description	Period (sec.)	Frequency (Hz)
1	High Voltage Arrestor (1st mode)	0.369	2.71
2	High Voltage Arrestor (2nd mode)	0.340	2.94
3	High Voltage Bushing (1st mode, Transverse)	0.292	3.42
4	Oil Conservator (1st mode)	0.158	6.35
5	Oil Conservator (2nd mode)	0.143	6.99
6	Low Voltage Arrestor (1st mode)	0.134	7.45
7	Low Voltage Arrestor (2nd mode)	0.123	8.13
8	High Voltage Bushing (2nd mode, Longitudinal)	0.119	8.38
9	High Voltage Bushing (3rd mode)	0.118	8.44
10	Oil Conservator & Low Voltage Bushing (1st mode)	0.101	9.89
11	Transformer Frame (1st mode, Transverse)	0.095	10.51
12	High Voltage Arrestor (3rd mode)	0.091	11.01
13	Low Voltage Bushing(1st mode)	0.080	12.46
14	Low Voltage Arrestor (3rd mode)	0.067	14.90
15	Transformer Frame (2nd mode, Transverse)	0.063	15.84
16	Transformer Shell (1st mode, Out-of-plane Bending)	0.057	17.61
17	High Voltage & Low Voltage Bushings and Arrestors (4th mode)	0.050	19.85
18	Transformer Frame (1st mode, Longitudinal)	0.048	20.85
19	Transformer Frame (2nd mode, Longitudinal)	0.046	21.93
20	Transformer Frame (2nd mode, Longitudinal)	0.044	22.73
21	Transformer Shell (2nd mode, Out-of-plane Bending)	0.035	28.73
22	Oil Conservator (2nd mode)	0.026	37.81
23	Transformer Shell (3rd mode, Out-of-plane Bending)	0.022	44.86
24	Transformer Shell and Oil Conservator (1st mode)	0.021	47.94

Table 8: Periods and Natural Frequencies of Ferranti-Packard 230 kV Transformer-Bushing Model

Mode	Mode Description	Period (sec.)	Frequency (Hz)
1	High-voltage Arrestor Closest to Conservator	0.596	1.68
2	High-voltage Arrestor Furthest from Conservator	0.595	1.68
3	Radiator	0.370	2.70
4	Conservator/Radiator	0.368	2.72
5	High-voltage Arrester Middle Unit	0.345	2.90
6	High-voltage Arrestor Support with Bushing Movement	0.243	4.12
7	High-voltage Bushing Center unit	0.210	4.76
8	Radiator with High-voltage Bushing Movement	0.192	5.20
9	Radiator with High-voltage Bushing Movement	0.186	5.39
10	Radiator with High-voltage Bushing Movement	0.183	5.46
11	High-voltage Bushings Outer Units	0.179	5.59
12	Radiator-Conservator w. High-voltage Bushing Movement	0.170	5.89
13	Radiator-Conservator w. High-voltage Bushing Movement	0.164	6.09
14	High-voltage Bushings Outer Units	0.159	6.30
15	High-voltage Bushings Outer Units	0.158	6.31
16	Larger Radiator	0.149	6.72
17	High-voltage Bushings Large Movement	0.142	7.05
18	Radiators	0.139	7.21
19	High-voltage Bushing Center Unit	0.131	7.64
20	High-voltage Bushing Center Unit	0.128	7.81
21	Radiators	0.124	8.08
22	Radiators	0.117	8.56
23	High-voltage Arrestor Support, Vertical Movement	0.115	8.72
24	High-voltage Arrestor Support, Vertical Movement	0.111	9.01
25	Radiator	0.102	9.79
26	Radiator	0.094	10.68
27	Radiator, Conservator, and Low-voltage Arrestor Support	0.090	11.07
28	Radiator and Conservator	0.087	11.55
29	Radiator	0.077	12.97
30	Low Voltage Arrestor Support	0.073	13.63
31	Radiator, Conservator, and Low-voltage Arrestor Support	0.069	14.40
32	Low-voltage Bushings and Arrestor Support	0.061	16.35
33	Low-voltage Bushings and Arrestor Support	0.056	17.80
34	Radiator, Conservator, and Low-voltage Arrestor Support	0.049	20.35
35	Transformer Tank	0.040	25.10
36	Transformer Tank, Top Plate Vertical Movement	0.035	28.35
37	Transformer Tank	0.033	29.96
38	Transformer Tank	0.018	54.51
39	Transformer Tank	0.018	55.74
40	Transformer Tank, Vertical Movement	0.017	60.39

Figure 19: Deformed Shape of High-voltage Bushing Models

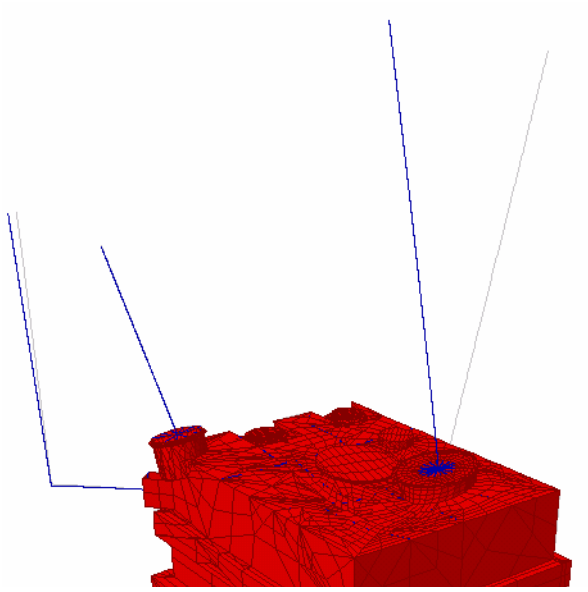

a.

Westinghouse 525 kV Transformer Model (1st mode – Longitudinal)

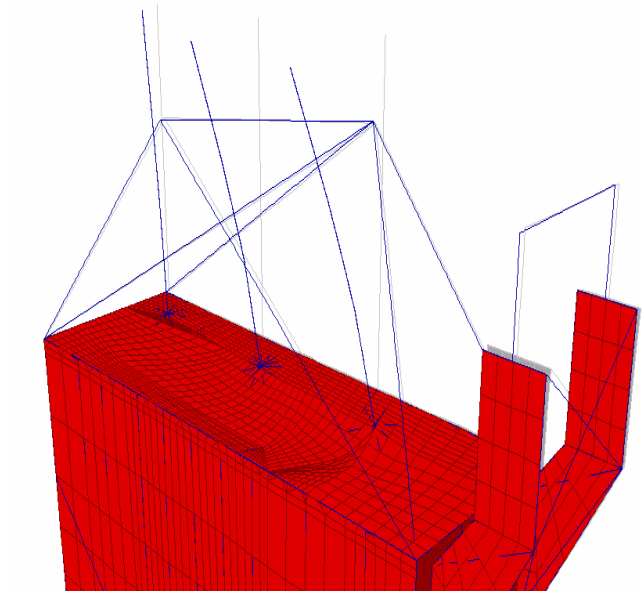

b.

Siemens 230 kV Transformer Model (1st mode – Transverse)

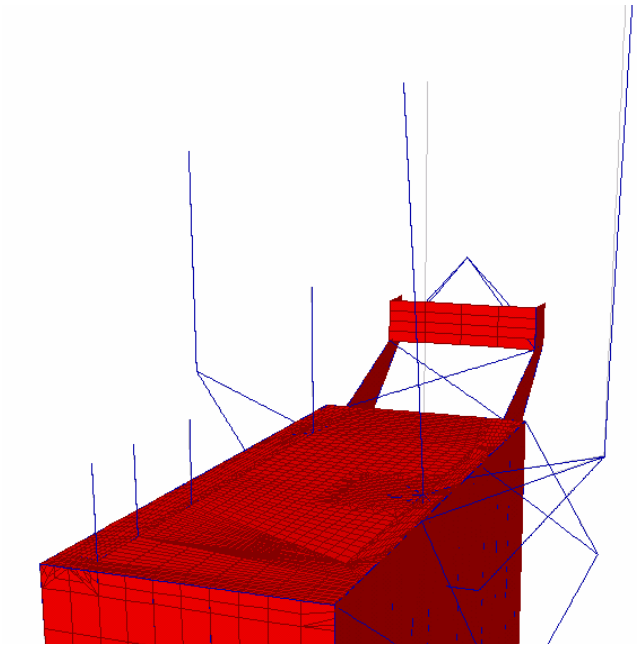

c.

Siemens 500 kV Transformer Model (1st mode – Transverse)

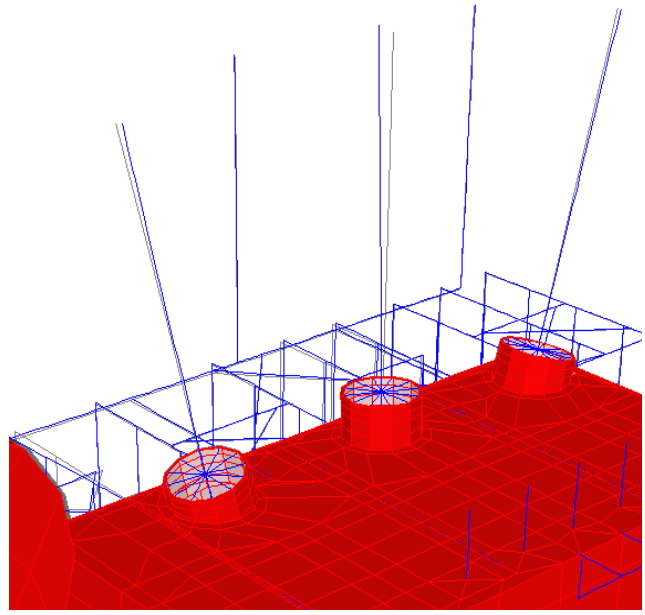

d.

Ferranti-Packard 230 kV Transformer Model (1st mode – Transverse)

Comparing the results obtained from the modal analyses of bushings installed on transformer tanks ("as-installed conditions") and on a rigid base, it can be concluded that the transformer tanks are very flexible compared to the rigid base in all the four cases of the high voltage transformer/bushing models. As a result, the fundamental frequencies of bushings mounted on a rigid base are more than 2 times the frequencies of bushings mounted on the flexible tank cover, as shown in Table 9.

Table 9: Comparison of High-voltage Bushings on Rigid Base vs. "As-installed"

Transformer Model	Support	Frequency (Hz)
Westinghouse 525 kV – mode 1	"As installed"	2.92
	Rigid Base	9.27
Siemens 230 kV – mode 1	"As installed"	9.14
	Rigid Base	16.85
Siemens 500 kV – mode 1	"As installed"	3.42
	Rigid Base	8.75
Ferranti-Packard 230 kV – mode1	"As installed"	4.76
	Rigid Base	16.80

Dynamic Analysis of Transformer Bushings

Earthquake Ground Motions Considered

Two ground motion ensembles were selected for performing linear dynamic time history analyses of the transformer-bushing models. The first ensemble consisted of 20 ground motions recorded within the California region selected such that the location of the measurement was far enough from the fault rupture to be free of any near-fault directivity pulses (Filiatrault & Matt, 2006). The second ensemble selected in this study was the un-normalized (original) motions of the FEMA P695 Far Field Ground Motion Set (FEMA P695, 2009), which contains 22 historical ground motions from all over the world with two horizontal components each, recorded at the same station. This ground motion ensemble is considered to be representative of the seismicity in the Western United States. Further information about the earthquake events is presented in Table 10 (California region) and Table 11 for ensemble 1 and ensemble 2, respectively.

Scaling Procedure

The geometric mean spectrum of each ensemble was scaled to match the IEEE 693, 2% damped, high required response spectrum (RSS) in a range of frequencies between 2.0 and 30.0 Hz. This

range was selected since the fundamental frequencies of the bushing structures vary from 2.5 Hz ("as-installed") and 25 Hz (rigid base) for the different types of bushings (Filiatrault & Matt, 2006; Reinhorn et al., 2011).

Table 10: California Region Earthquake Ground Motion – Ensemble 1

EQ. Index	Earthquake Event			Recording Station	PGA (g)
	Name	Year	M_w		
1	Superstition Hills	1987	6.7	Brawley	0.12
2	Superstition Hills	1987	6.7	El Centro Imp. Co. Cent.	0.26
3	Superstition Hills	1987	6.7	Plaster City	0.19
4	Northridge	1994	6.7	Beverly Hills 14145 Mulholland	0.42
5	Northridge	1994	6.7	Canoga Park – Topanga Can.	0.36
6	Northridge	1994	6.7	Glendale – Las Palmas	0.36
7	Northridge	1994	6.7	LA – Hollywood Stor FF#	0.23
8	Northridge	1994	6.7	LA – N Faring Rd	0.27
9	Northridge	1994	6.7	N. Hollywood – Coldwater Can.	0.27
10	Northridge	1994	6.7	Sunland – Mt. Gleason Ave.	0.16
11	Loma Prieta	1989	6.9	Capitola	0.53
12	Loma Prieta	1989	6.9	Gilroy Array #3	0.56
13	Loma Prieta	1989	6.9	Gilroy Array #4	0.42
14	Loma Prieta	1989	6.9	Gilroy Array #7	0.23
15	Loma Prieta	1989	6.9	Hollister Diff. Array	0.28
16	Loma Prieta	1989	6.9	Saratoga – W. Valley College	0.33
17	Cape Mendocino	1992	7.1	Fortuna – Fortuna Blvd#	0.12
18	Cape Mendocino	1992	7.1	Rio Dell Overpass – FF#	0.39
19	Landers	1992	7.3	Desert Hot Springs#	0.15
20	Landers	1992	7.3	Yermo Fire Station#	0.15

Despite being a popular measure in the investigation of ground motions, the median was rejected as a scaling parameter in this study, since it is not defined by an analytical mathematical equation. In fact, the *median* is described as the number separating the higher half of a sample/population from its lower half, and is computed by arranging all the values of that sample in ascending/descending order and picking the middle one (or the arithmentic mean of the two middle ones). On the other hand, the *geometric mean*, which indicates the central tendency or typical value of a set of numbers, is a more accurate measure; it is calculated by the following equation:

$$S_{ageomean}(f) = \left(\prod_{i=1}^{N} S_{ai}(f) \right)^{1/N} \tag{1}$$

where $S_{ageomean}\left(f\right)$ is the geometric mean of the spectral acceleration at a number of prescribed frequencies and $S_{ai}(f)$ is the spectral acceleration at the prescribed frequencies.

Table 11: FEMA P695 Earthquake Ground Motion – Ensemble 2

EQ. Index	Earthquake Event				Recording Station	PGA (g)*
	Name		Year	M_w		
	EQ_ID.	Earthquake				
1	12011	Northridge	1994	6.7	Beverly Hills – Mulhol	0.52
2	12012	Northridge	1994	6.7	Canyon Country–WLC	0.48
3	12041	Duzce, Turkey	1999	7.1	Bolu	0.82
4	12052	Hector Mine	1999	7.1	Hector	0.34
5	12061	Imperial Valley	1979	6.5	Delta	0.35
6	12062	Imperial Valley	1979	6.5	El Centro Array#11	0.38
7	12071	Kobe, Japan	1995	6.9	Nishi – Akashi	0.51
8	12072	Kobe, Japan	1995	6.9	Shin – Osaka	0.24
9	12081	Kocaeli, Turkey	1999	7.5	Duzce	0.36
10	12082	Kocaeli, Turkey	1999	7.5	Arcelik	0.22
11	12091	Landers	1992	7.3	Yermo Fire Station	0.24
12	12092	Landers	1992	7.3	Coolwater	0.42
13	12101	Loma Prieta	1989	6.9	Capitola	0.53
14	12102	Loma Prieta	1989	6.9	Gilroy Array#3	0.56
15	12111	Manjil, Iran	1990	7.4	Abbar	0.51
16	12121	Superstition Hills	1987	6.5	El Centro Imp. Co.	0.36
17	12122	Superstition Hills	1987	6.5	Poe Road (temp)	0.45
18	12132	Cape Mendocino	1992	7.0	Rio Dell Overpass	0.55
19	12141	Chi-Chi, Taiwan	1999	7.6	CHY 101	0.44
20	12142	Chi-Chi, Taiwan	1999	7.6	TCU045	0.51
21	12151	San Fernando	1971	6.6	LA – Hollywood Stor.	0.21
22	12171	Friuli, Italy	1976	6.5	Tolmezzo	0.35

*Larger component

The scaling of both ground motion ensembles was performed using the "Weighted Scaling Procedure." This method, which utilizes information on spectral acceleration at a number of frequencies, is more complex to apply but should, in principle, result in better matching of the target spectra.

The main target of this procedure was that each ensemble of ground motions J ($J = 1$ to 2) must be scaled only in amplitude by a factor F_J in order to minimize the error between the scaled motion spectrum and the target IEEE 693 spectrum at a number of prescribed frequencies. The minimized error E_J was obtained as a weighted average of the errors at the prescribed frequencies:

$$E_J = \sum_k w_k \left(S_{IEEE}(f_k) - F_J S_{ageomean}(f_k) \right)^2 , \quad (2)$$

where: E_J is the weighted average of the errors at the prescribed frequencies, w_k is the weight factor considered at a number of prescribed frequencies, $S_{IEEE}\left(f_k\right)$ is the target IEEE 693 spectrum at a number of prescribed frequencies, $S_{ageomean}\left(f\right)$ is the geometric mean of the spectral acceleration at a number of prescribed frequencies and F_J is the scale factor in amplitude.

In order to find a minimum of the error function in Equation 2, its derivative with respect to F_J was set equal to zero. Furthermore, to confirm that the obtained solution represented a minimum (and not a maximum) the second derivative was calculated and was found to be positive. This means that the obtained solution represented the minimum error, which was found to be:

$$F_J = \frac{\sum w_k S_{IEEE}(f_k) S_{ageomean}(f_k)}{\sum w_k S^2_{ageomean}(f_k)} \quad (3)$$

where F_J is the scale factor in amplitude, w_k is the weight factor considered at a number of prescribed frequencies, $S_{IEEE}\left(f_k\right)$ is the target IEEE 693 spectrum at a number of prescribed frequencies and $S_{ageomean}\left(f\right)$ is the geometric mean of the spectral acceleration at a number of prescribed frequencies.

Considering that F_J referred to the geometric mean of the Jth ensemble, it was straightforward to show from Equation 3 that the scale factor for each ground motion could be assumed equal to F_J. The scale factor F_J was computed, based on the procedure described above, to be equal to *2.20* for ensemble 1 and *1.74* for ensemble 2. The scaling results of both ensembles using both the geometric mean and the median spectra are presented in Figures 20 and 21 for ensemble 1 and ensemble 2, respectively.

Figure 20: Scaling of California Region Ground Motion – Ensemble 1

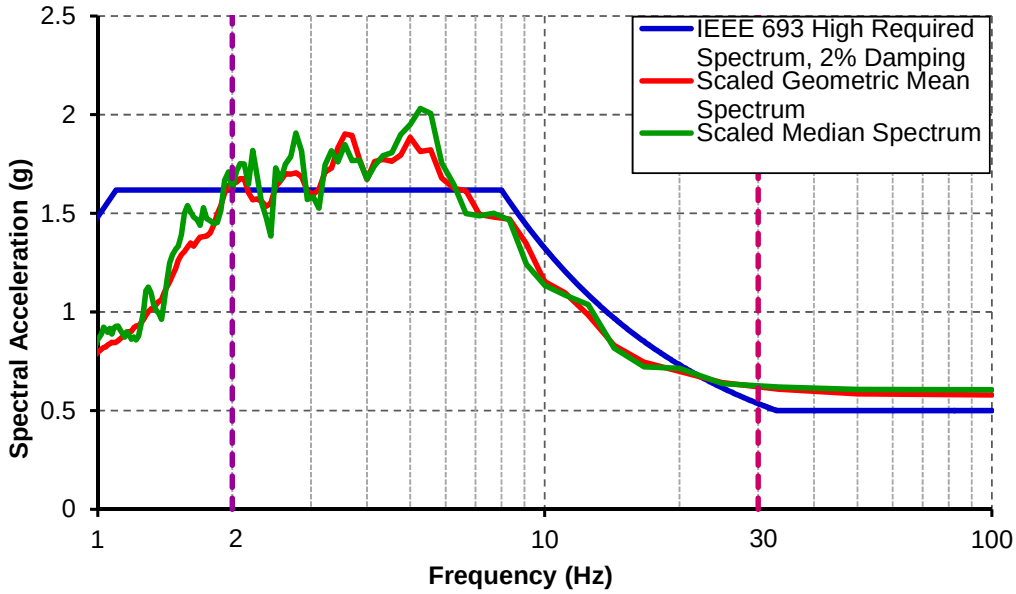

Figure 21: Scaling of FEMA P695 Ground Motion – Ensemble 2

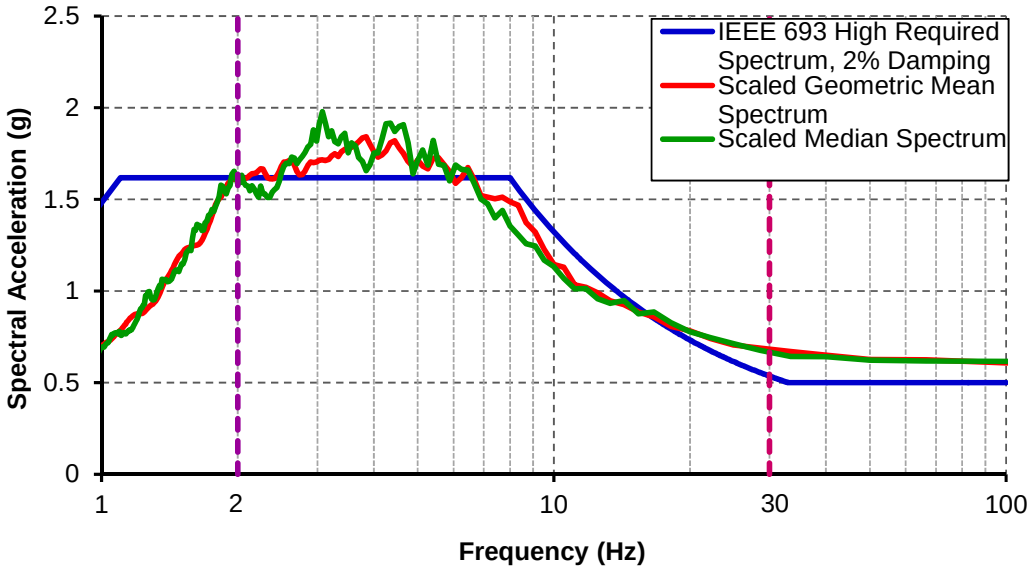

Dynamic Analysis Procedure

For all the transformer-bushings models, linear dynamic time history analyses were performed using both the ground motion ensembles 1 and 2 scaled as described in the previous section. The models were analyzed in the transverse and the longitudinal direction in all cases. All the analyses performed are summarized in Table 12.

Table 12: Dynamic Analysis Cases

Direction of motion	Ensemble 1	Ensemble 2 (FEMA P695 – 1D)	Ensemble 2 (FEMA P695 – 2D)
Longitudinal	✓	✓	✓
Transverse	✓	✓	

According to Table 12, the second ensemble was analyzed in one dimension (1D) and two dimensions (2D). The 1D analysis included all the 44 components analyzed in both transverse and longitudinal directions separately, while the 2D analysis included the 22 ground motions combining the two components in longitudinal and transverse directions, respectively. Two cases were considered for the 2D analysis: "Case 1" applied the component 1 in the longitudinal direction and the component 2 in the transverse, whereas for "Case 2" the directions of the ground motion components were rotated by 90 degrees compared to "Case 1." Note that the effects of vertical ground motions were not considered in this study.

From each analysis, the bending moment at the base of the bushing was obtained in its horizontal axes as a function of time. The maximum bending moment at a given time instant *t* was calculated as:

$$M^{*}_{\max}(t) = \max_{t}\left(\sqrt{M_x^2(t) + M_y^2(t)}\right) \tag{4}$$

where $M_x(t)$ and $M_y(t)$ are the moments at the base of the bushing at time *t* and with respect to the longitudinal and transverse axis of the transformer tank, respectively, and *max* () is the maximum absolute value over the time-history response.

Based on the results of all analyses, cumulative distribution functions (CDF) associated with the probability of non-exceeding (PoNE) a prescribed maximum moment at the base of the bushing under the two ensembles of ground motions were calculated. The PoNE was estimated by counting the number of ground motion records causing a prescribed value of the maximum bending moment at the bushing base not to be exceeded and dividing this number by the total number of records considered in the analyses. A log-normal cumulative distribution function was then fitted to the empirical data. The log-normal CDF was defined by the median value (PoNE = 50%) of the maximum bending moment and by the dispersion parameter ®, expressed as the standard deviation of the log of the values of M_{max}.

Dynamic Analysis Results

Linear dynamic time history analyses were conducted for all the analysis cases described in Table 12 and the maximum bending moment at the base of the bushing for each of the transformer models was computed according to equations (2-4). Based on the log-normal CDFs shown in Figures 22–33, it can be observed that for all transformer cases the bushing mounted on the transformer tank is very flexible compared to the bushing mounted on a rigid base. This fact can be easily identified for the maximum moment values of 50% probability of non-exceedance that are marked in each lognormal CDF.

A Moment Amplification Factor (MAF), defined as the ratio of the maximum bending moment at the base of the bushing mounted on the cover plate of the transformer ("as-installed" conditions) to the maximum bending moment obtained for the same bushing mounted on a rigid base (see equation (5)), was computed for all analysis cases and compared to the amplification factor of two defined by IEEE 693:

$$\textit{Moment Amplification Factor} = \frac{\textit{Moment when Bushing as Installed}}{\textit{Moment when Bushing Mounted on Rigid Base}} \tag{5}$$

Figures 34–36 present the MAF in the form of empirical and log-normal CDFs, while Figures 37–39 compare the median values of the MAF CDFs with the frequency-independent amplification factor of 2 recommended by IEEE 693, showing that the recommended amplification factor is non-conservative for all the transformer bushing systems. Although not much higher than the proposed amplification factor, the value of that factor computed for all the transformer models appeared to be around three, apart from the Siemens 230 kV transformer model. The Siemens 230 kV model appeared to be the most flexible transformer

(especially in the longitudinal direction) since the peak bending moment at the base of the "as-installed" bushing was more than 10 times larger than if it was rigidly mounted.

Tables 13–15 summarize the results of the analysis: maximum amplifications at the turret base for 500 kV and 230 kV bushings, and maximum amplification with corresponding frequency of motion for 500 kV bushings, respectively.

Figure 22: CDF for Maximum Bending Moments for Westinghouse 525 kV Transformer-Bushing Model – Ensemble 1

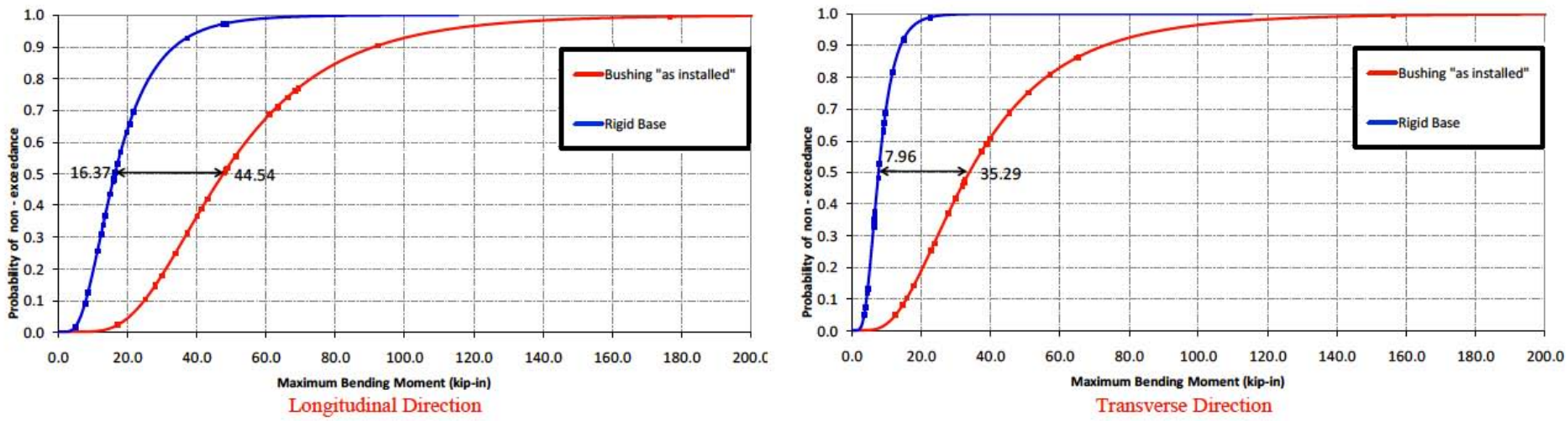

Figure 23: CDF for Maximum Bending Moments for Westinghouse 525 kV Transformer-Bushing Model – Ensemble 2 (1D)

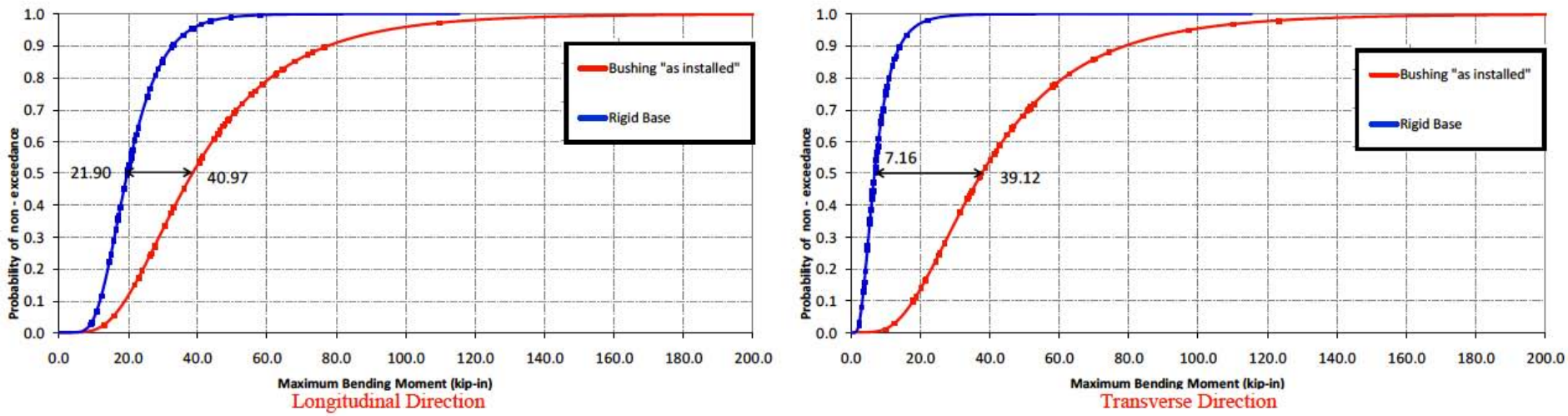

Figure 24: CDF for Maximum Bending Moments for Westinghouse 525 kV Transformer-Bushing Model – Ensemble 2 (2D)

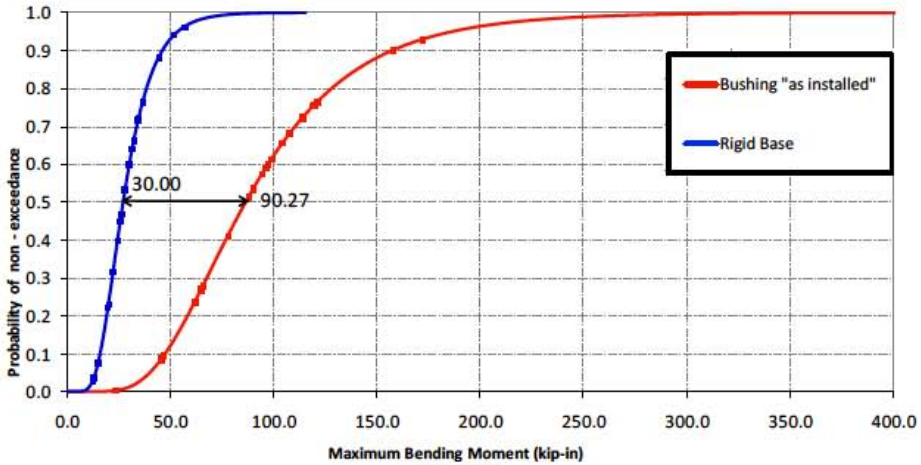

Case 1

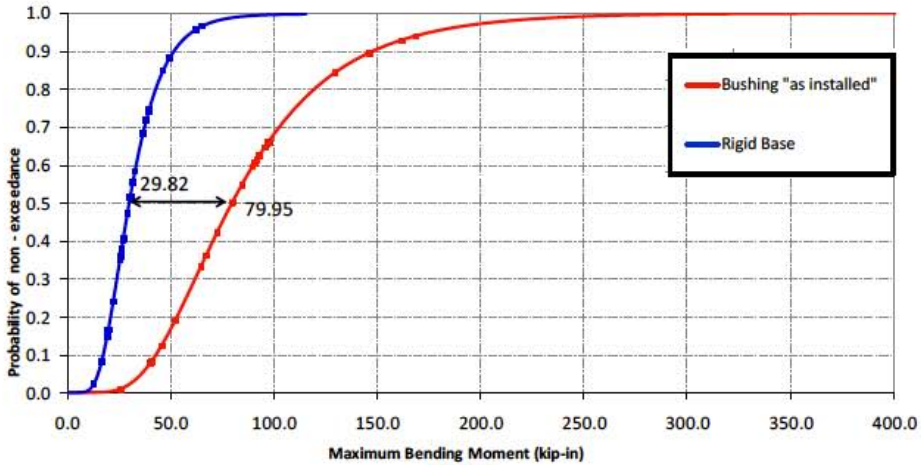

Case 2

Figure 25: CDF for Maximum Bending Moments for Siemens 230 kV Transformer-Bushing Model – Ensemble 1

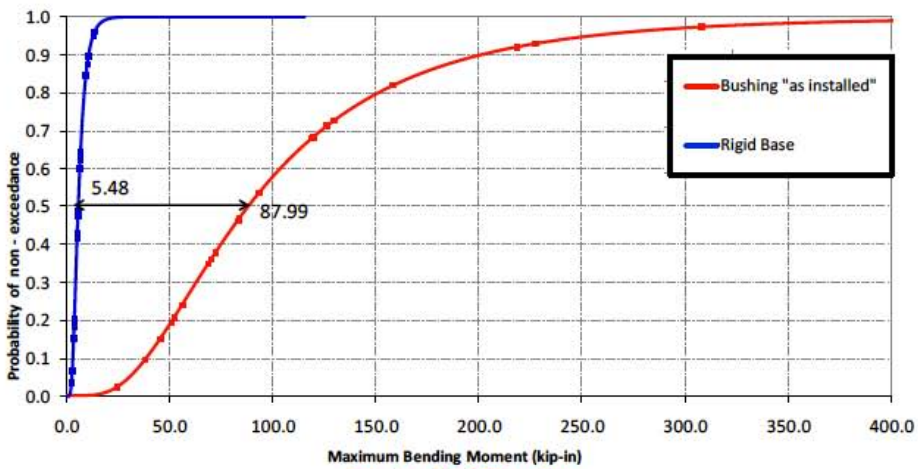

Longitudinal Direction

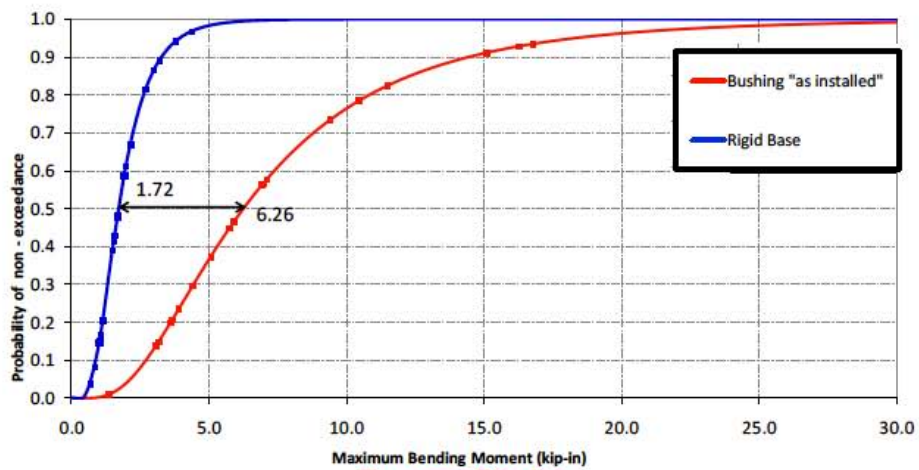

Transverse Direction

Figure 26: CDF for Maximum Bending Moments for Siemens 230 kV Transformer-Bushing Model – Ensemble 2 (1D)

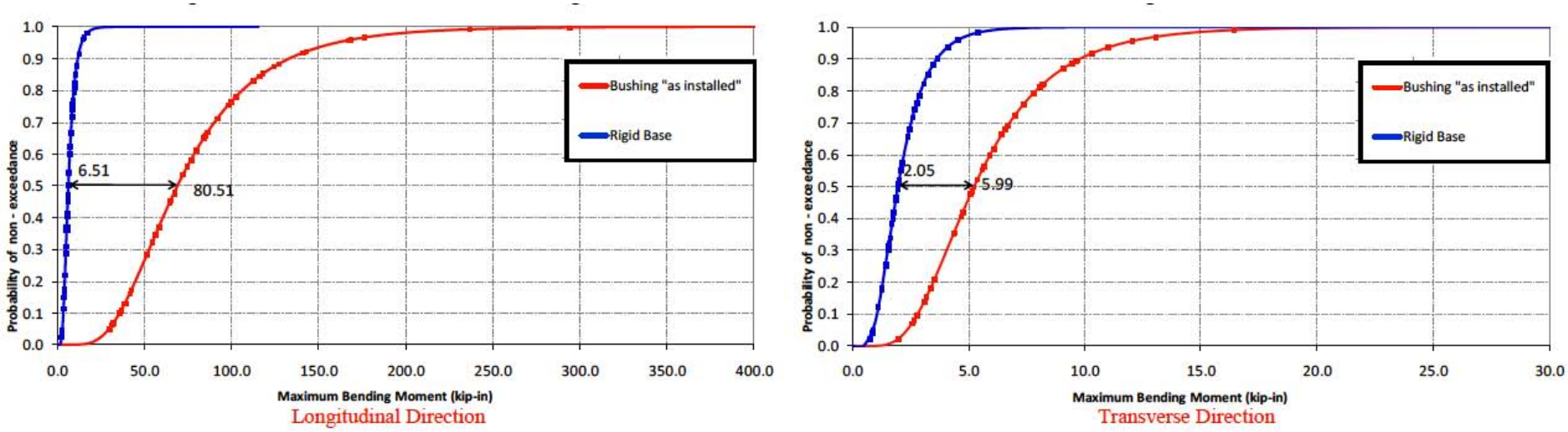

Figure 27: CDF for Maximum Bending Moments for Siemens 230 kV Transformer-Bushing Model – Ensemble 2 (2D)

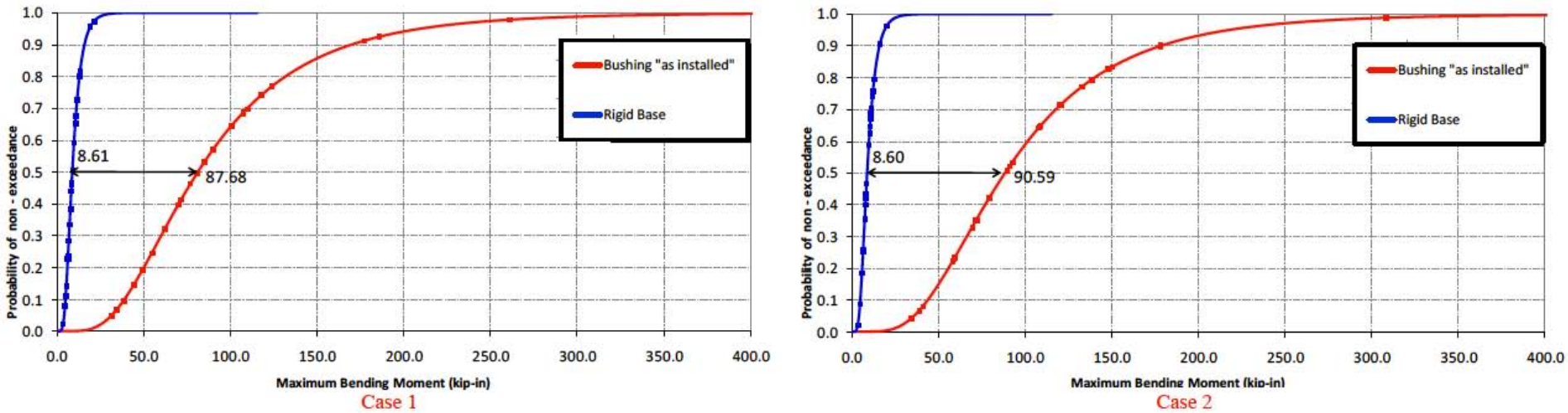

Figure 28: CDF for Maximum Bending Moments for Siemens 500 kV Transformer-Bushing Model – Ensemble 1

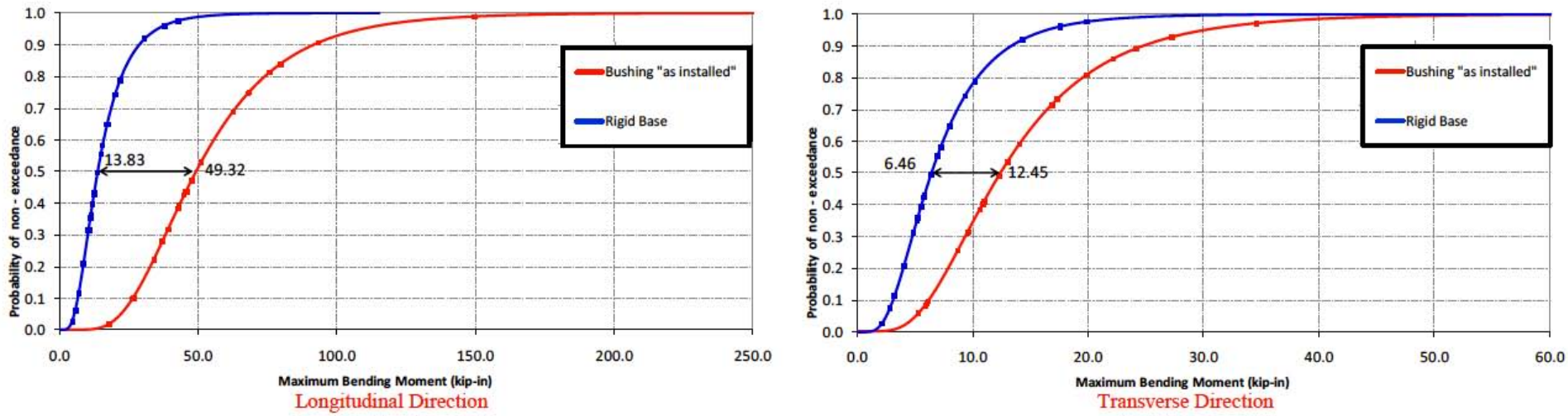

Figure 29: CDF for Maximum Bending Moments for Siemens 500 kV Transformer-Bushing Model – Ensemble 2 (1D)

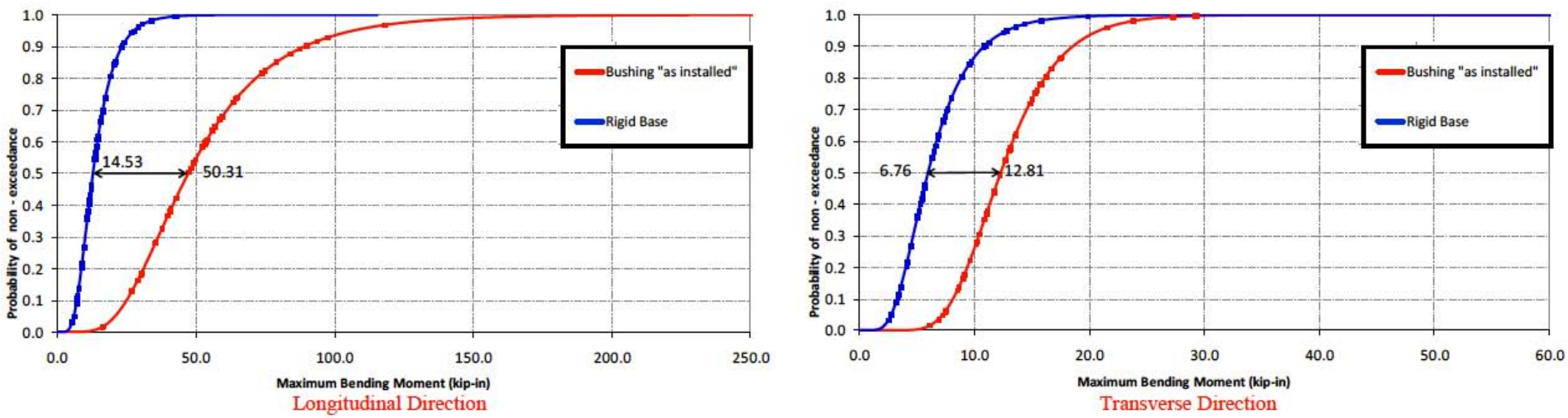

Figure 30: CDF for Maximum Bending Moments for Siemens 500 kV Transformer-Bushing Model – Ensemble 2 (2D)

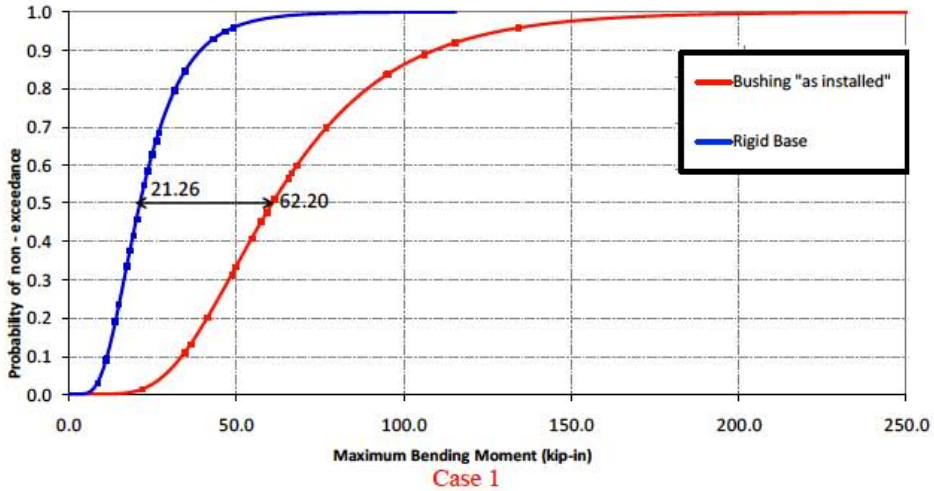

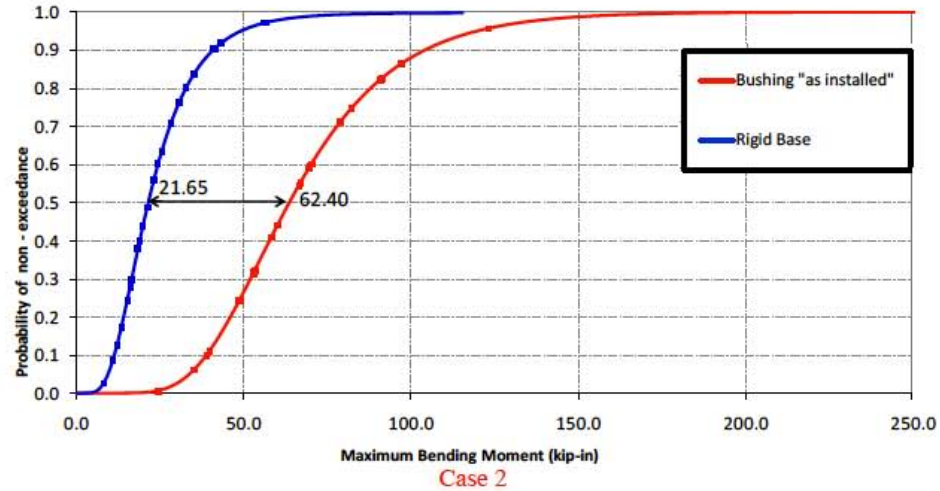

Figure 31: CDF for Maximum Bending Moments for Ferranti-Packard 230 kV Transformer-Bushing Model – Ensemble 1

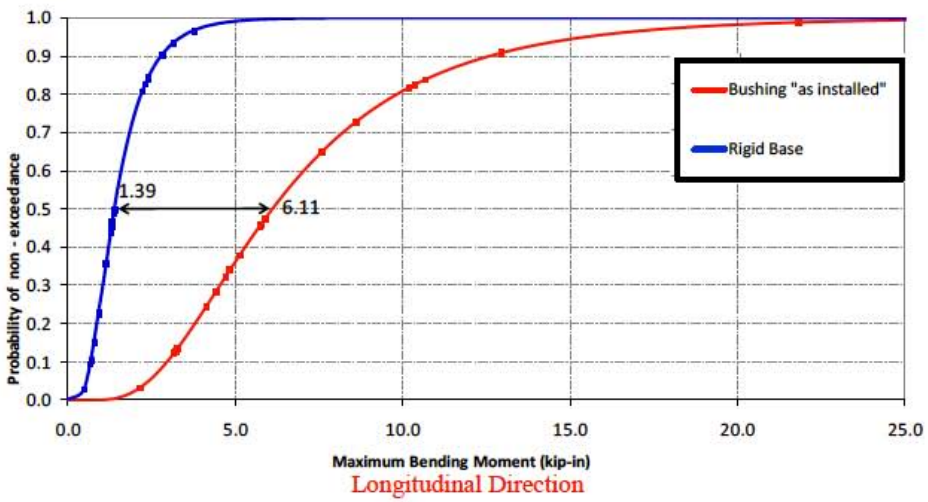

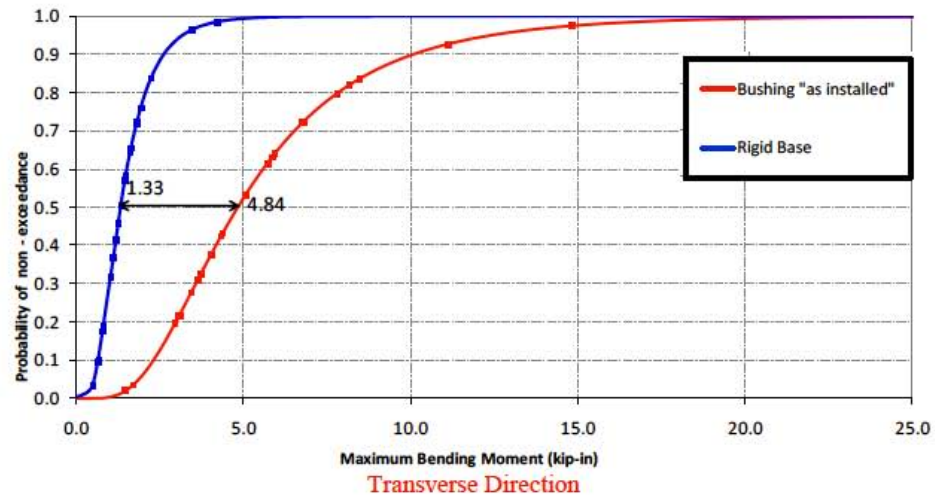

Figure 32: CDF for Maximum Bending Moments for Ferranti-Packard 230 kV Transformer-Bushing Model – Ensemble 2 (1D)

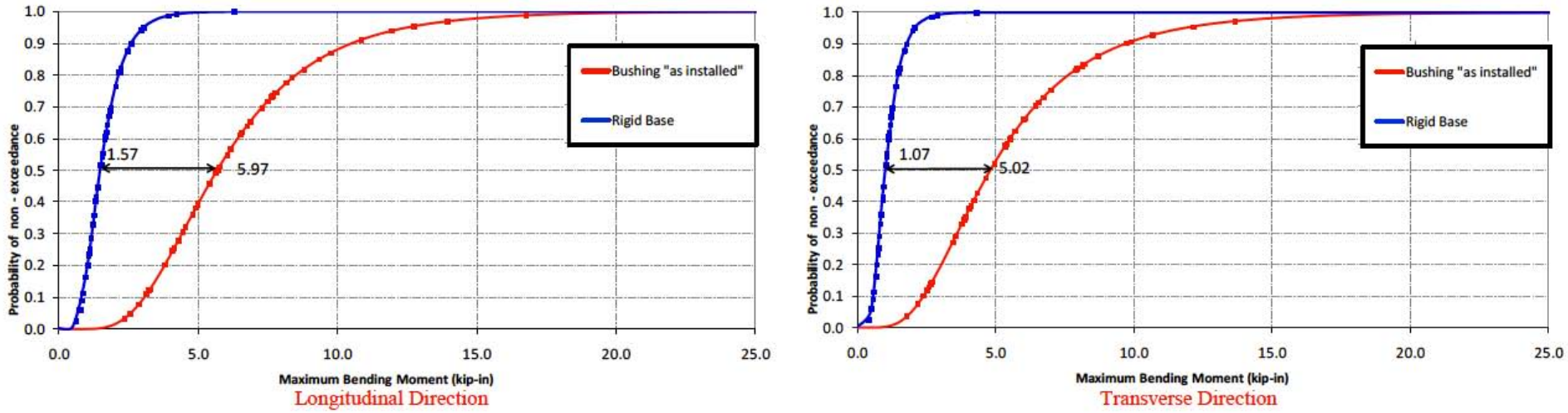

Figure 33: CDF for Maximum Bending Moments for Ferranti-Packard 230 kV Transformer-Bushing Model – Ensemble 2 (2D)

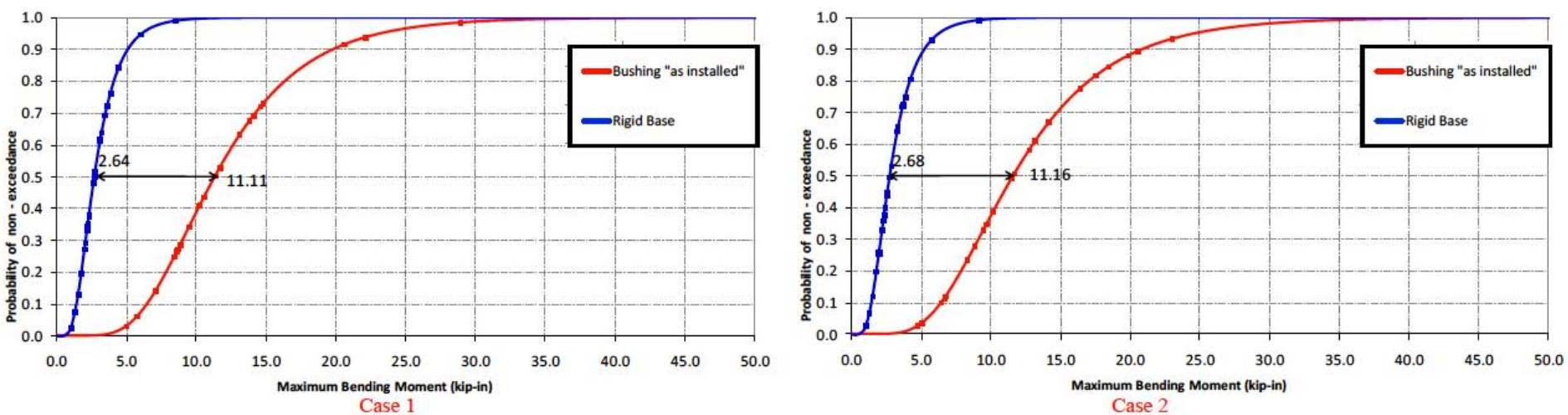

Figure 34: CDF for Moment Amplification Factors for Ensemble 1

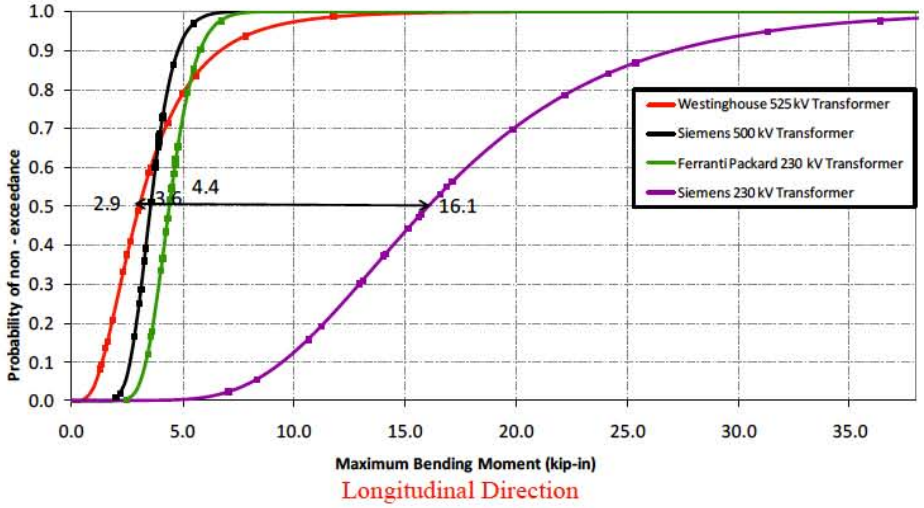

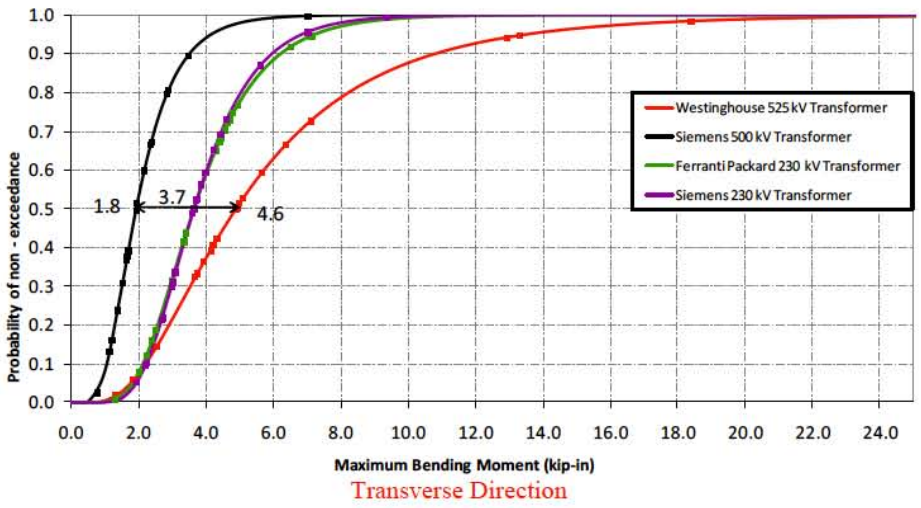

Figure 35: CDF for Moment Amplification Factors for Ensemble 2 (1D)

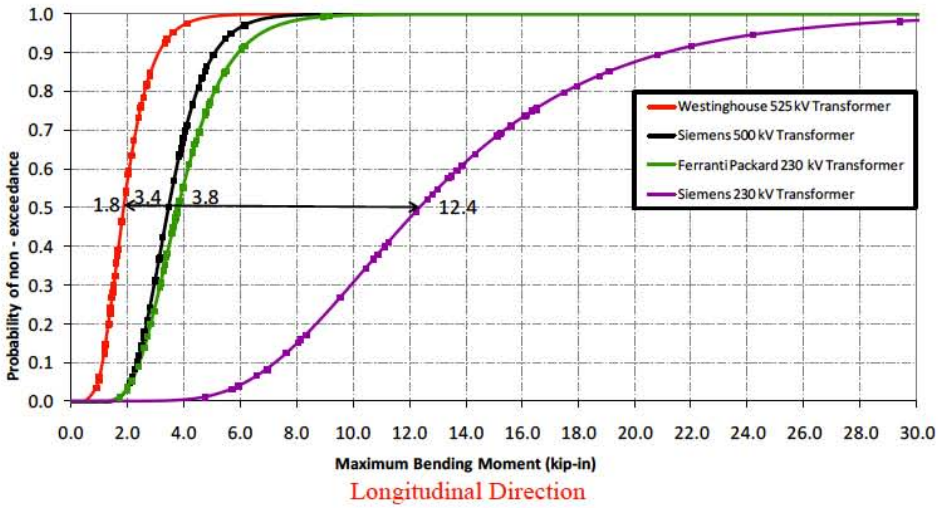

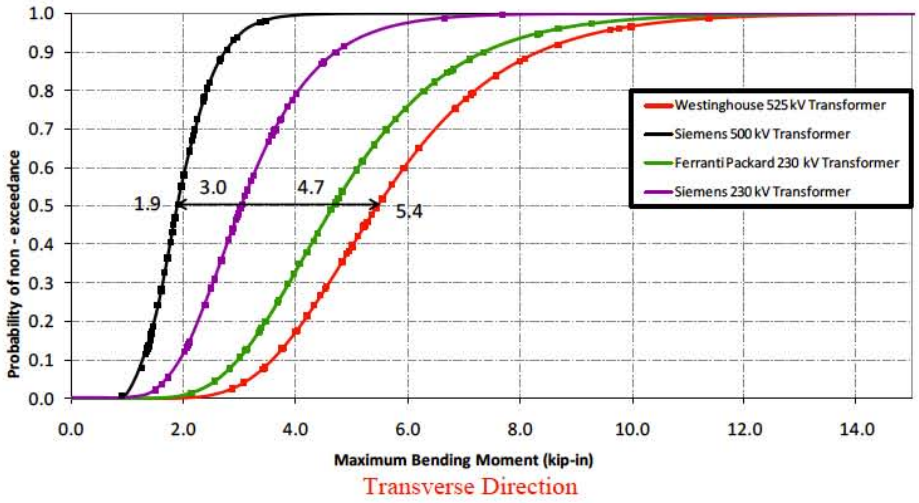

Figure 36: CDF for Moment Amplification Factors for Ensemble 2 (2D)

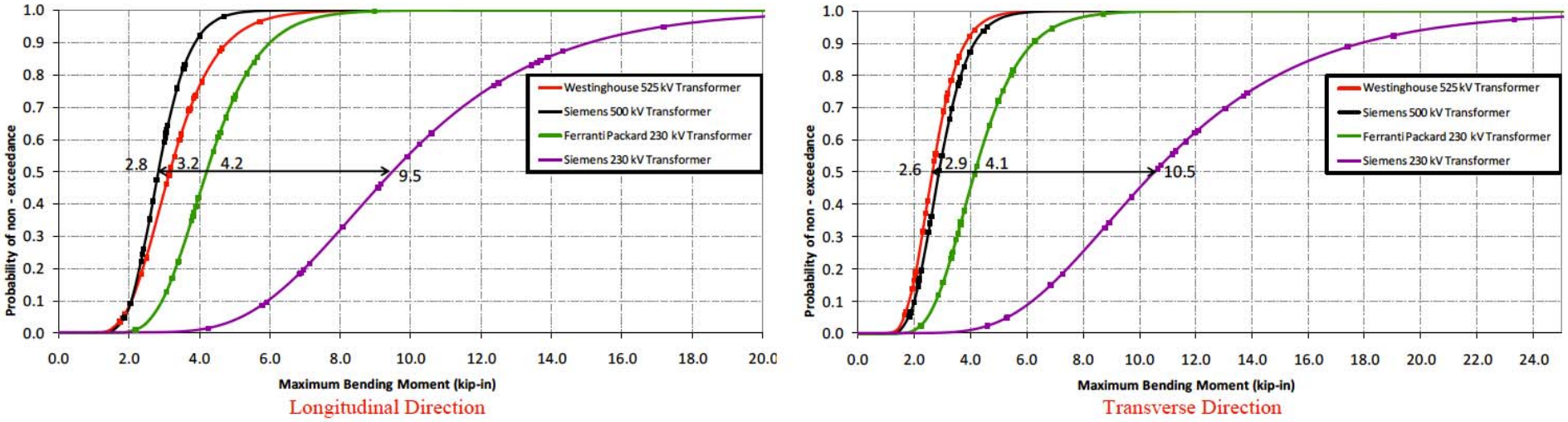

Figure 37: Median Values of Moment Amplification Factor for all Four Transformer-Bushing Models – Ensemble 1

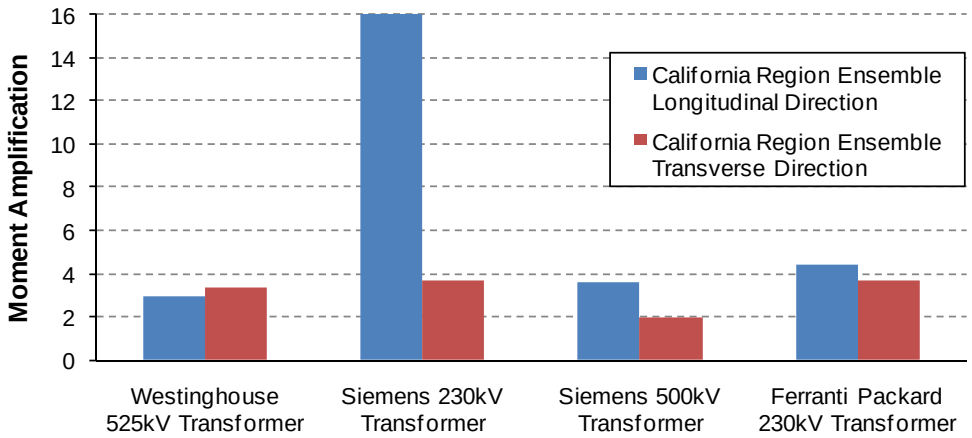

Figure 38: Median Values of Moment Amplification Factor for all Four Transformer-Bushing Models – Ensemble 2 (1D)

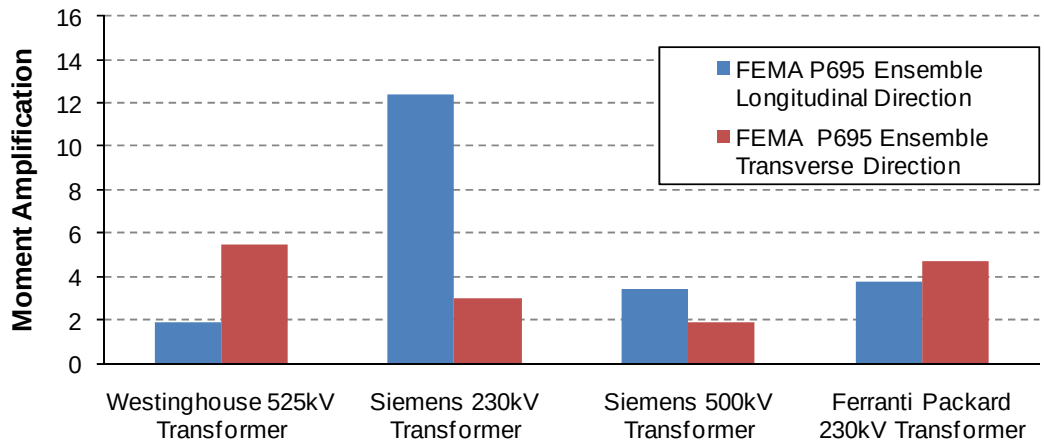

Figure 39: Median Values of Moment Amplification Factor for all Four Transformer-Bushing Models – Ensemble 2 (2D)

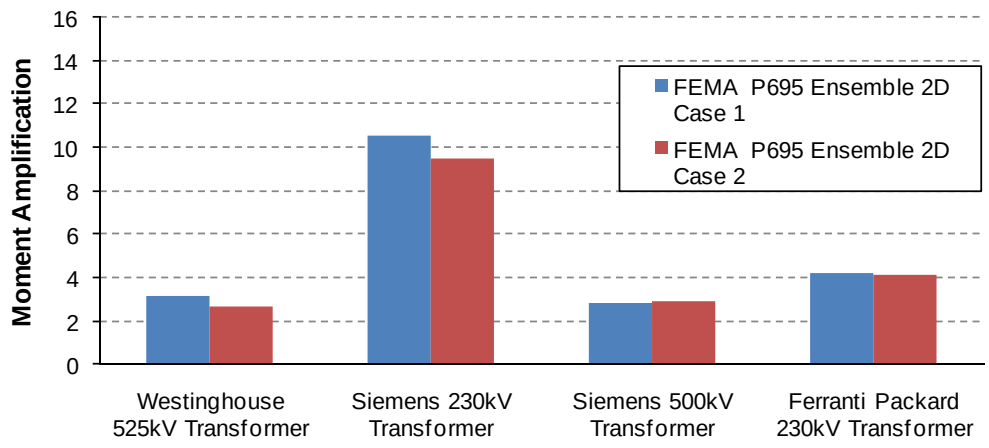

Lateral Motion Amplification at the Transformer Cover

As indicated in the previous section, when bushings are mounted on flexible transformer covers, the forces developed at the base are substantially different from the case where bushings are mounted on fixed or rigid covers. One of the sources of discrepancies is the amplification of motion at the mounting surfaces, which displays different intensities and dynamics compared to those developed at the foundation level.

This section explores the lateral motion amplifications at the transformer cover and the expected effects on the bushing responses, based on analysis of the 230 kV Ferranti-Packard transformer with various bushings and with various structural modifications to obtain the response of a family of transformers having various parameters. A detailed description of those parameters and their variations are presented by Reinhorn et al., 2011. In addition, another family of transformers based on the Siemens 500 kV transformer model was analyzed, in order to determine the effects of amplifications of motions of the tank cover plate that supports the transformer bushings.

In the analyses of the effects of the covers, the transformers were subjected to simulated accelerograms compatible with IEEE 693 (see Section 3 - Experimental Study) and to modulated natural earthquake accelerograms CEERL and LANDERS, adjusted to match IEEE 693 (See description in Section 3 and in Reinhorn et al., 2011).

The spectra of the ground motions as shown in Figures 40–44 are amplified by the transformers at various frequency ranges that are dependent on the transformer construction. These amplifications are larger than 2 (as recommended by the codes of practice) and may reach values of 3 to 4.5. The amplifications presented above are for 230 kV and 500 kV transformers that were equipped with specific bushings shown in the figures. The blue lines indicate the range of frequencies of the fixed base bushing (f_{FB}), while the orange lines indicate the range of frequencies of bushings "as-installed" (f_{AI}). Although the bushings mounted on the equipment do not have their frequencies in the range of maximum amplifications, other bushings of the same size could have frequencies in the range of maximum amplification (see Appendix E and Chapter 5).

The response spectra clearly show the influence of the response magnification when the bushing is installed on the flexible tank cover versus being installed on a rigid base.

Figure 40: Acceleration Spectra for 500 kV Transformer at Bottom LV Bushing

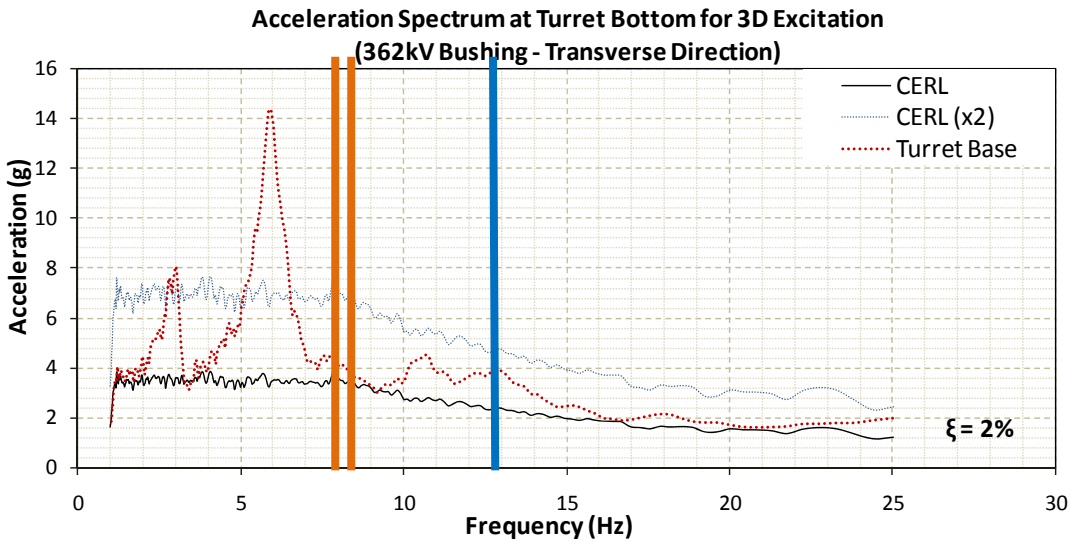

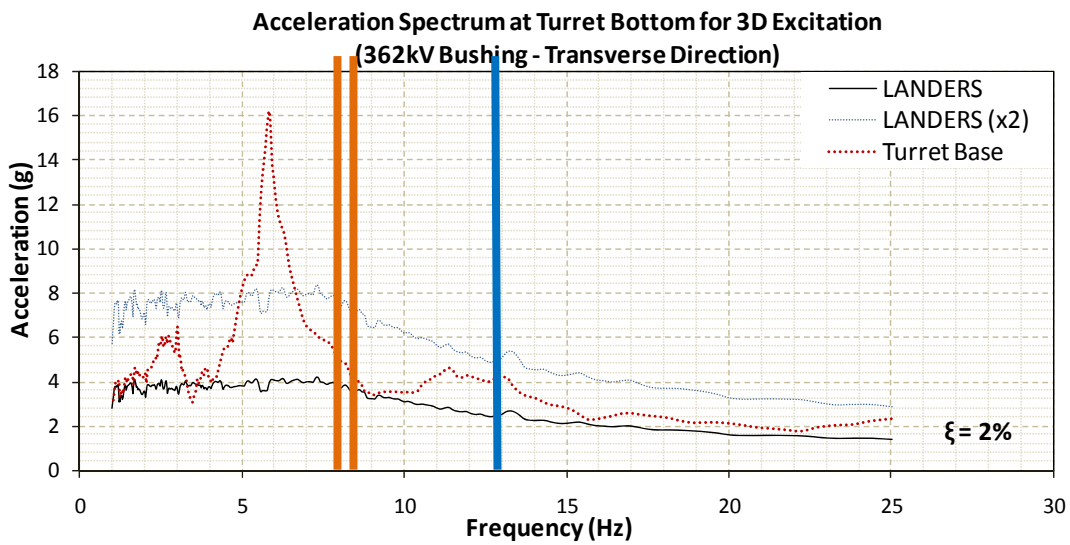

f_{AI} = 7.5–8.0 Hz , f_{FB} = 13.0 Hz

Figure 41: Acceleration Spectra for 500 kV Transformer at Bottom HV Bushing

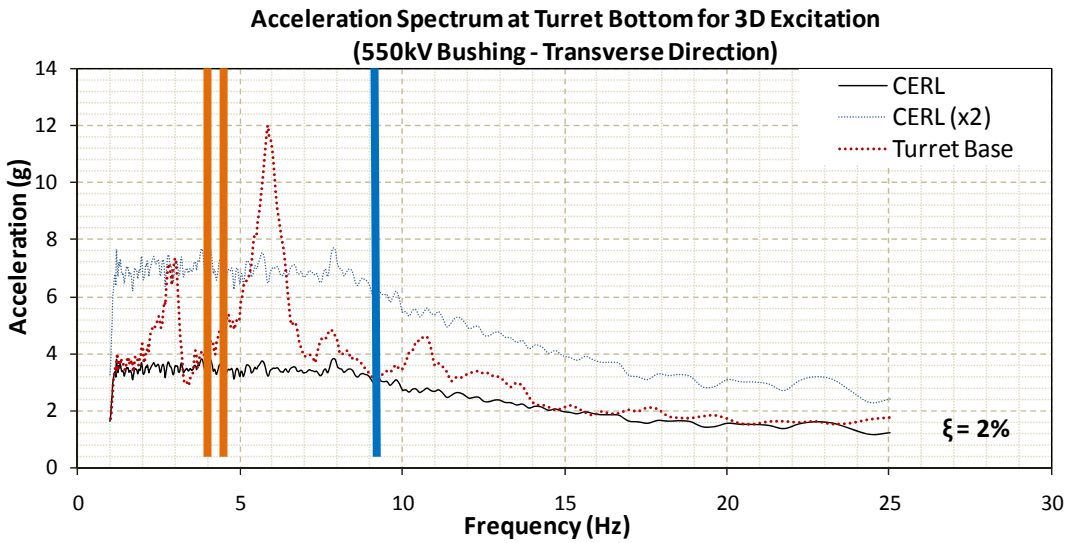

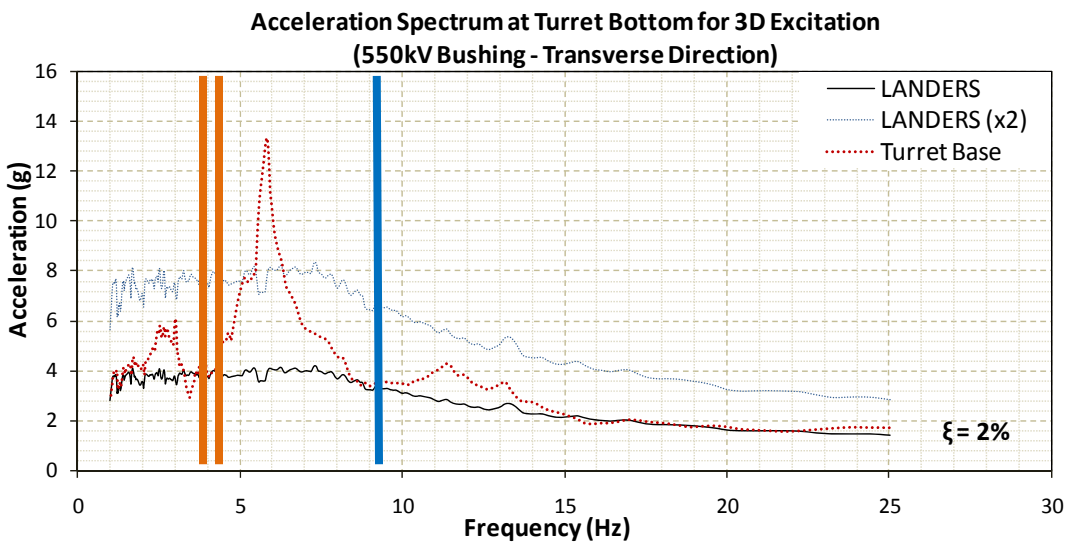

f_{AI} = 3.9–4.0 Hz, f_{FB} = 9.37 Hz

Figure 42: Acceleration Spectra for 500 kV Transformer at Bottom LV Bushing

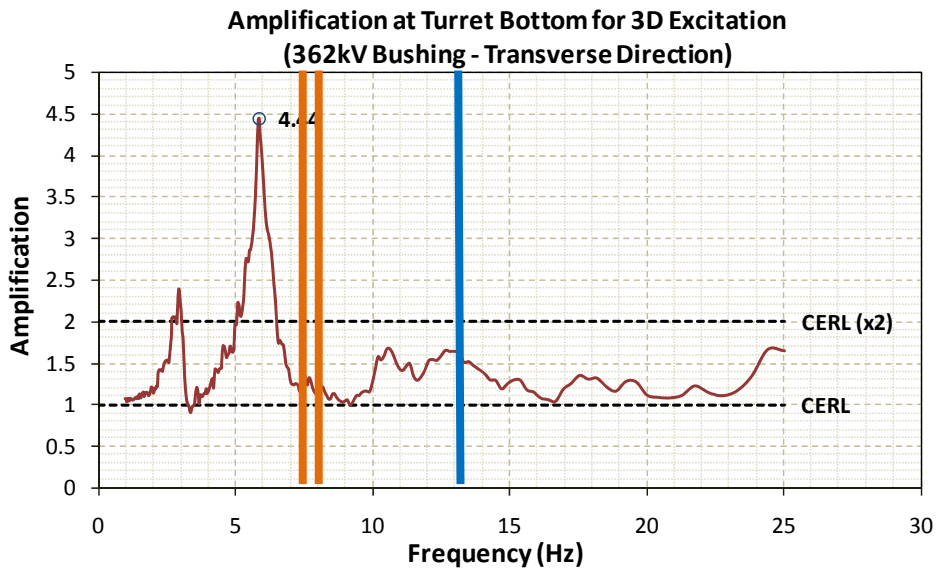

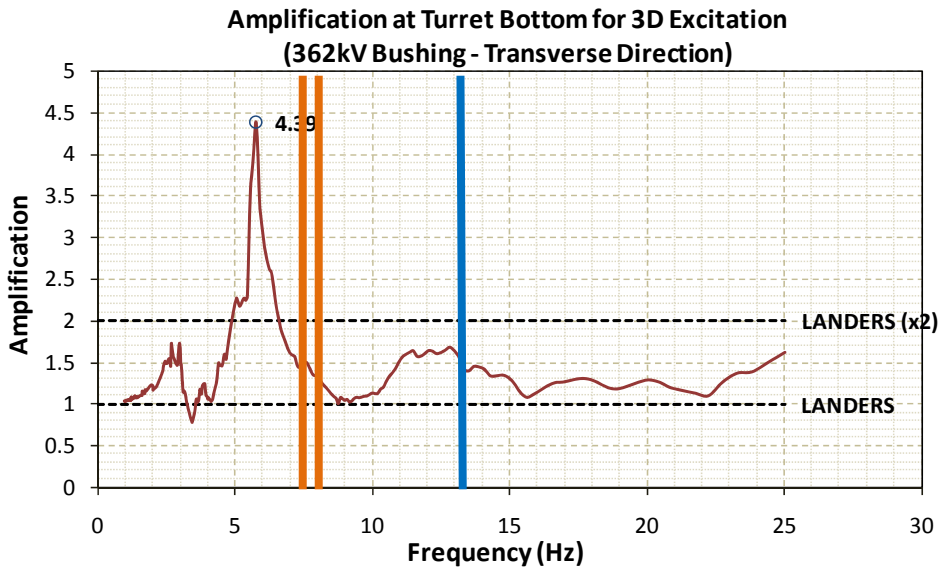

f_{AI} = 7.5–8.0 Hz, f_{FB} = 13.0 Hz

Figure 43: Spectral Amplification for 500 kV Transformer at Bottom HV Bushing

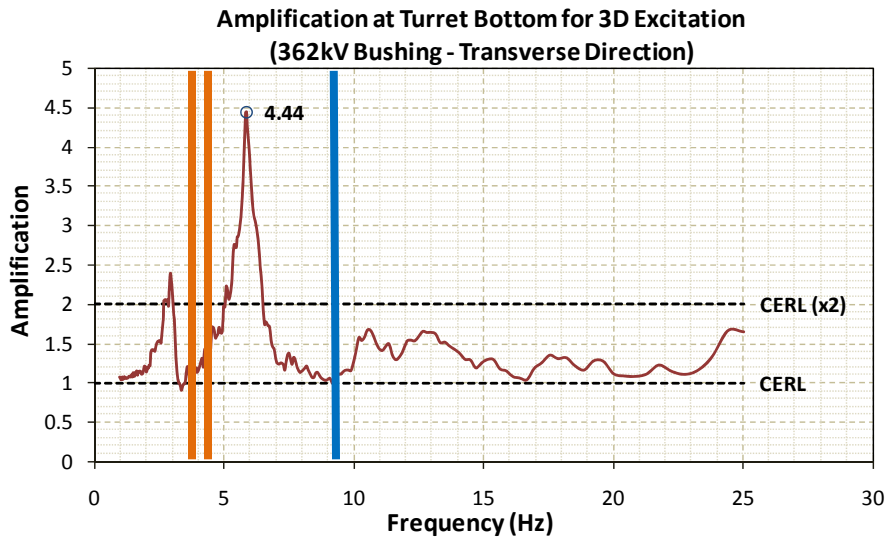

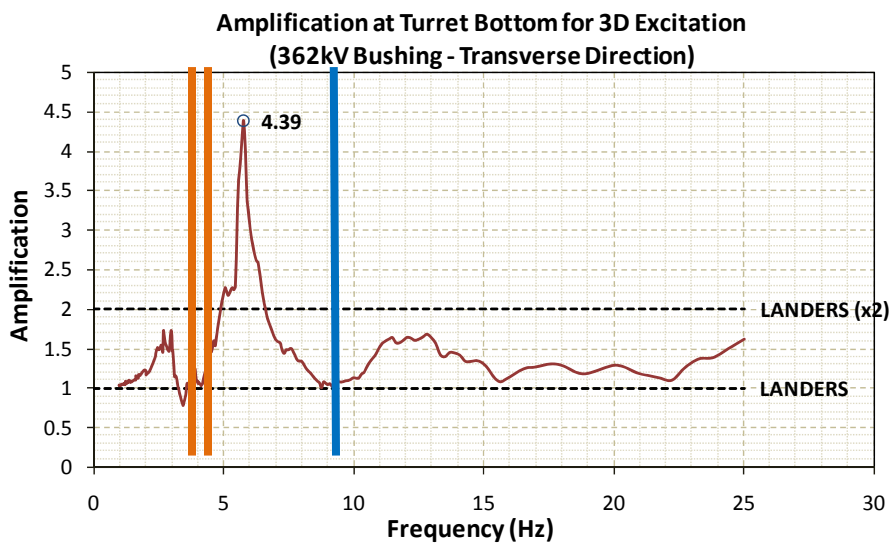

f_{AI} = 3.9–4.0 Hz, f_{FB} = 9.37 Hz

Figure 44: Spectral Amplification for 230 kV Transformer at Bottom HV Bushing

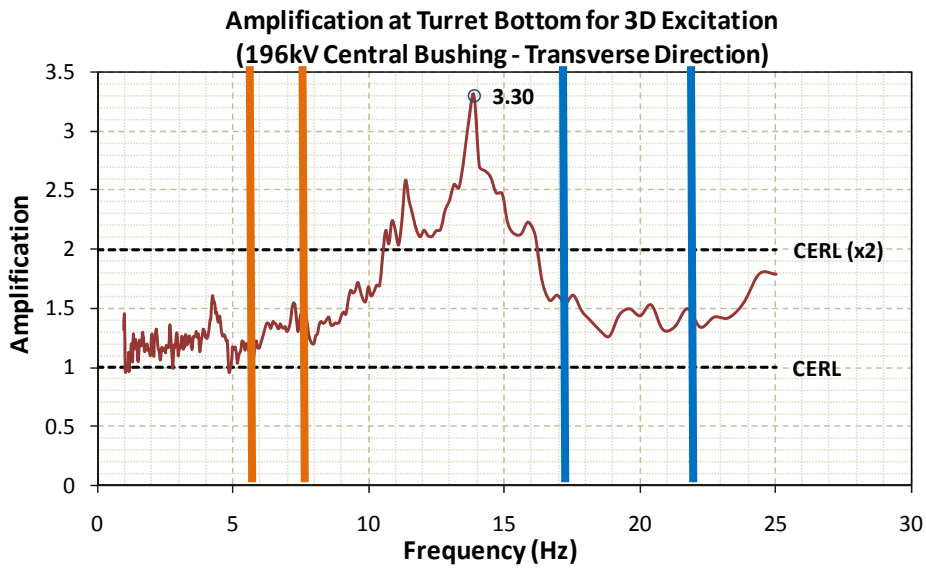

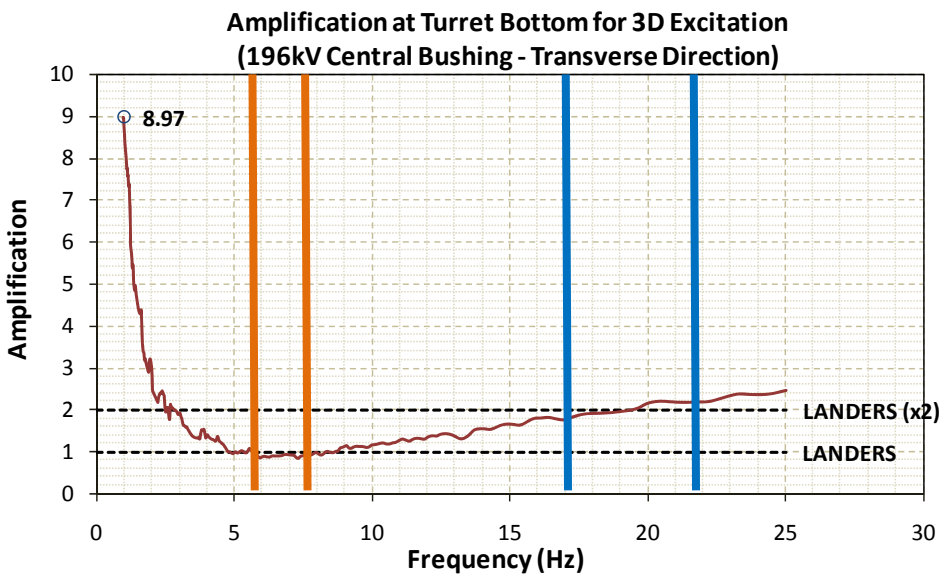

f_{AI} = 5.6–7.6 Hz, f_{FB} = 17–22 Hz

Table 13: Maximum Amplifications at Turret Base of Bushings* for the 500 kV Transformer Models

Accelerograms	500 kV Transformer (Best Modeling Possible)				500 kV Transformer (Core Connected to Cover and Side Walls)				500 kV Transformer (Core & 550 kV Frequency Close - Core Connected to Side Walls)			
	LV Bushing		HV Bushing		LV Bushing		HV Bushing		LV Bushing		HV Bushing	
	Max	Freq (Hz)	Max	Freq (Hz)	Max	Freq (Hz)	Max	Freq (Hz)	Max	Freq (Hz)	Max	Freq (Hz)
	(1)	(2)	(3)	(4)	(5)	(6)	(7)	(8)	(9)	(10)	(11)	(12)
CERL 1D (longitudinal response)	1.58	4.8	1.57	4.8	1.82	23.8	1.85	23.8	1.46	4.8	1.46	4.8
CERL 2D (longitudinal response)	1.60	4.8	1.60	4.8	3.71	24.4	3.64	24.4	1.43	4.8	1.43	4.8
CERL 2D (transverse response)	4.44	5.8	3.72	5.8	8.06	25.0	5.43	24.4	4.82	4.2	4.22	4.2
CERL 3D (longitudinal response)	1.52	4.6	1.52	4.6	7.48	25.0	7.92	25.0	1.60	4.6	1.63	4.6
CERL 3D (transverse response)	4.44	5.9	3.72	5.8	8.34	25.0	6.21	24.4	3.85	4.2	3.48	3.7
CERL 3D (vertical response)	3.34	7.9	7.45	18.9	16.95	25.0	16.50	25.0	3.27	7.4	7.41	19.2
LANDERS 1D (longitudinal response)	1.32	4.3	1.31	4.3	1.55	24.4	1.56	24.4	1.35	4.8	1.34	4.8
LANDERS 2D (longitudinal response)	1.31	4.3	1.31	4.3	1.58	25.0	1.60	25.0	1.30	4.1	1.30	4.3
LANDERS 2D (transverse response)	4.47	5.8	3.74	5.8	6.75	5.8	5.58	5.8	4.44	4.0	3.98	3.9
LANDERS 3D (longitudinal response)	1.36	4.3	1.36	4.3	3.02	25.0	2.78	25.0	1.32	4.3	1.34	4.3
LANDERS 3D (transverse response)	4.39	5.8	3.66	5.8	7.06	5.8	5.77	5.8	4.60	3.9	4.19	3.9
LANDERS 3D (vertical response)	2.30	7.8	8.83	18.5	7.82	25.0	6.86	25.0	2.50	7.8	8.08	18.2

*LV: Low-voltage Bushing – 362 kV; HV: High-voltage Bushing – 500 kV.

Table 14: Amplifications at Turret Base of Bushings for the 230 kV Transformer Models

Accelerograms	230 kV Transformer (Best Modeling Possible – MI Model)						230 kV Transformer (Seismic Bracing Provision – MII Model)					
	196 kV Bushing (Close to Conservator)		196 kV Bushing (Central)		196 kV Bushing (Far from Conservator)		196 kV Bushing (Close to Conservator)		196 kV Bushing (Central)		196 kV Bushing (Far from Conservator)	
	Max Value	Freq (Hz)	Max Value	Freq (Hz)	Max Value	Freq (Hz)	Max Value	Freq (Hz)	Max Value	Freq (Hz)	Max Value	Freq (Hz)
	(1)	(2)	(3)	(4)	(5)	(6)	(7)	(8)	(9)	(10)	(11)	(12)
CERL 1D (longitudinal response)	2.20	15.9	1.98	15.9	1.98	15.9	1.95	17.2	1.95	17.2	1.95	17.2
CERL 2D (longitudinal response)	2.46	15.9	2.15	15.9	2.15	15.9	2.33	16.4	2.33	16.4	2.34	16.4
CERL 2D (transverse response)	3.15	13.9	2.99	13.9	2.88	13.9	4.33	12.5	4.51	12.5	4.21	12.5
CERL 3D (longitudinal response)	2.46	13.9	2.22	13.9	2.19	15.9	2.50	17.2	2.50	17.2	2.51	17.2
CERL 3D (transverse response)	3.48	13.9	3.30	13.9	3.16	13.9	4.44	12.5	4.64	12.5	4.34	12.5
CERL 3D (vertical response)	5.33	25.0	11.87	16.1	6.21	15.6	4.69	25.0	10.63	20.4	5.86	24.4
LANDERS 1D (longitudinal response)	8.73	1.0	8.74	1.0	8.74	1.0	1.99	16.9	1.99	16.9	1.99	16.9
LANDERS 2D (longitudinal response)	8.74	1.0	8.75	1.0	8.75	1.0	1.71	16.9	1.99	16.9	1.70	16.9
LANDERS 2D (transverse response)	8.95	1.0	8.97	1.0	8.96	1.0	2.94	12.2	3.11	12.3	2.95	12.3
LANDERS 3D (longitudinal response)	8.74	1.0	8.75	1.0	8.75	1.0	1.87	16.9	1.86	16.9	1.86	16.9
LANDERS 3D (transverse response)	8.95	1.0	8.97	1.0	8.97	1.0	3.02	12.2	3.14	12.2	2.94	12.2
LANDERS 3D (vertical response)	7.14	1.1	7.22	1.1	7.10	1.0	5.25	1.0	8.23	20.8	6.21	23.3

Table 15: Maximum Amplifications at Turret Base of Bushings for the 500 kV Transformer Models

Accelerograms	500 kV Transformer (Core Connected to Side Walls – No Gaps – Core Tuned to 550 kV Bushing Frequency)				500 kV Transformer (Core Connected to Cover – No Gaps – Core Tuned to 550 kV Bushing Frequency)			
	LV Bushing		HV Bushing		LV Bushing		HV Bushing	
	Max	Freq (Hz)	Max	Freq (Hz)	Max	Freq (Hz)	Max	Freq (Hz)
	(1)	(2)	(3)	(4)	(5)	(6)	(7)	(8)
LANDERS 3D (longitudinal response)	1.34	4.9	1.35	4.9	1.29	4.3	1.31	4.3
LANDERS 3D (transverse response)	4.00	4.0	3.47	4.0	4.81	4.4	4.07	4.4
LANDERS 3D (vertical response)	1.71	7.2	7.08	18.2	1.62	22.7	7.01	18.2

Rotational Effects of a 230 kV Transformer Cover

In addition to the lateral movements of the whole transformer cover, there are substantial rotations in the plate at the base of the bushings that rotate the whole bushing, leading to additional accelerations and mounting forces. The following is an analysis of transformer bushings and evaluation of rotations at the base of bushings and their contribution to the accelerations in the top or center of gravity (CG) of bushings (Reinhorn et al., 2011).

When the bushing is mounted on the transformer cover acting like a supporting flexible plate, the bushing rotates the support plate at the connection in an anticlastic motion, i.e., resembling one cycle of a sinusoidal function (see Figure 45). If the bushing is mounted in the center, there is an antisymmetric deflection and a simple large rotation in the center. If the bushing is mounted in a location near the edge of the cover, the deflection of the whole plate tends to have a simple half sine-wave deflection, with a direct rotation at the edge.

Figure 45: Rotation of Cover at Bushing Mount

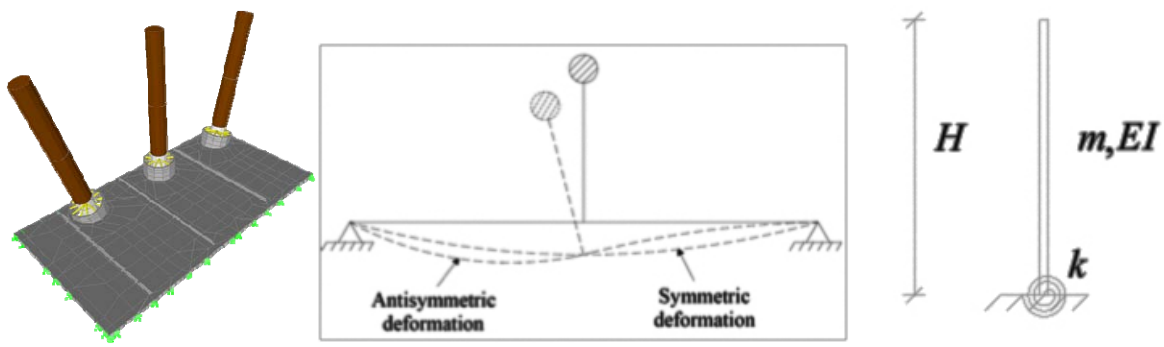

(a) Bushings on cover (b) Rotation at base mount (c) Model of bushing

The rotation is a function of the stiffness of the plate and is dynamically dependent on the weight and height of the bushing. Tables 16–18 show the rotations in rad/sec^2 of the transformer cover at the base of the bushings in a 230 kV transformer. For example, for a rigid 120″ bushing in a central location, the bushing will have 0.1 g to 0.4 g added to the translational acceleration response.

Vertical Amplifications Due to Flexibility of Transformer Cover

When the bushing is located in the center of a flexible cover, which can be modeled as a simply supported beam excited by the supports in the vertical direction as in Figure 46, then the bushing, which is very stiff vertically but has a substantial mass (weight), will vibrate vertically

with the support cover. The frequency of such vibration is entirely dependent on the weight (mass) of the bushing, the stiffness of the plate (thickness, material, structure, etc.), and the location of the bushing (if not in the center).

Table 16: Peak Accelerations and Moments of the Bushing Closest to the Conservator

#	Model	Peak Acceleration (g)											Moment (kip*in)	
		Corner 1			Bushing 1 Turret Base*						Bushing 1		Bushing 1 Base	
		L	T	V	L	T	V	RL	RT	RV	P	T	P	T
		(1)	(2)	(3)	(4)	(5)	(6)	(7)	(8)	(9)	(10)	(11)	(12)	(13)
1	**MI (Basis)**	**1.1**	**1.3**	**0.9**	**1.1**	**1.4**	**1.6**	**0.052**	**0.035**	**0.0015**	**4.2**	**2.5**	**115.8**	**68.8**
2	MI-a	1.1	1.3	0.9	1.1	1.4	1.7	0.057	0.028	0.0021	4.4	2.4	122.0	66.1
3	MI-b	1.1	1.4	0.8	1.1	1.4	1.8	0.049	0.032	0.0019	4.4	2.8	123.3	78.8
4	MI-c	1.1	1.5	0.9	1.1	1.5	1.7	0.038	0.026	0.0022	3.2	2.7	89.1	74.8
5	**MII (Basis)**	**1.1**	**1.4**	**0.9**	**1.1**	**1.3**	**1.7**	**0.057**	**0.028**	**0.0023**	**4.3**	**2.4**	**120.5**	**66.3**
6	MII-a1	1.1	1.8	0.9	1.0	1.7	1.8	0.058	0.032	0.0033	4.8	3.0	132.3	82.3
7	MII-a1i	1.1	1.8	0.9	1.1	1.7	1.8	0.062	0.033	0.0031	5.1	3.1	141.0	87.2
8	MII-a2	1.0	1.6	0.9	1.1	1.5	2.4	0.063	0.079	0.0040	4.6	3.9	127.0	109.1
9	MII-a2i	1.6	1.6	0.9	1.3	1.7	3.4	0.096	0.201	0.0082	5.4	4.3	149.8	120.5
10	MII-a2ii	1.6	1.6	0.9	1.3	1.7	2.8	0.104	0.209	0.0067	5.7	4.2	157.5	115.9
11	MII-a2iii	2.0	1.9	1.0	1.7	2.8	3.9	0.127	0.328	0.0155	7.6	5.0	210.5	137.7
12	MII-a3	1.1	1.3	0.9	1.1	1.4	1.7	0.061	0.031	0.0022	4.7	2.8	131.7	79.0
13	MII-b1	1.1	1.4	0.9	1.1	1.3	1.7	0.017	0.030	0.0023	-		-	
14	MII-b2	1.1	1.3	0.9	1.1	1.3	1.7	0.056	0.028	0.0022	4.3	2.3	119.6	63.1
15	MII-b3	1.1	1.4	0.9	1.1	1.3	1.9	0.047	0.027	0.0023	3.9	3.5	107.9	98.3
16	MII-c1	1.1	1.4	0.9	1.1	1.3	1.7	0.043	0.029	0.0023	3.6	3.0	101.0	82.5
17	MII-c1i	1.1	1.4	0.9	1.1	1.3	1.7	0.031	0.022	0.0023	2.5	3.2	70.3	87.8
18	MII-c2	1.1	1.4	0.9	1.1	1.3	1.6	0.059	0.028	0.0023	4.6	2.5	126.6	69.0
19	MII-c2i	1.2	1.5	0.9	1.1	1.5	1.9	0.046	0.031	0.0020	3.6	3.9	101.0	107.2
20	MII-c2ii	1.1	1.4	0.9	1.1	1.4	1.7	0.046	0.029	0.0021	3.4	3.3	94.7	90.7
21	MII-c3	1.1	1.4	0.9	1.1	1.3	1.7	0.045	0.033	0.0022	3.3	3.3	92.3	92.2
22	MII-d	1.1	1.4	0.9	1.1	1.3	1.9	0.052	0.030	0.0024	3.9	3.7	75.3	71.2
23	MII-e	1.1	1.5	0.9	1.1	1.5	1.7	0.045	0.028	0.0020	3.8	2.4	106.1	66.8

Rotations in rad/sec^2

IEEE Ground Motion (g)		
L	T	V
1.0	1.0	0.9

*Highlighted cells: base rotations

Table 17: Peak Accelerations and Moments of the Central Bushing

#	Model	Peak Acceleration (g)										Moment (kip*in)
		Corner 1			Bushing 2 Turret Base*						Bushing 2	Bushing 2 Base
		L	T	V	L	T	V	RL	RT	RV	Vector Sum	Vector Sum
		(1)	(2)	(3)	(4)	(5)	(6)	(7)	(8)	(9)	(10)	(11)
1	**MI (Basis)**	**1.1**	**1.3**	**0.9**	**1.1**	**1.4**	**2.4**	**0.038**	**0.057**	**0.0009**	**4.0**	**112.0**
2	MI-a	1.1	1.3	0.9	1.1	1.4	2.0	0.039	0.067	0.0021	3.6	99.5
3	MI-b	1.1	1.4	0.8	1.1	1.4	2.5	0.039	0.053	0.0013	4.1	114.5
4	MI-c	1.1	1.5	0.9	1.1	1.5	2.3	0.035	0.067	0.0014	3.3	92.3
5	**MII (Basis)**	**1.1**	**1.4**	**0.9**	**1.1**	**1.4**	**2.1**	**0.039**	**0.066**	**0.0019**	**3.6**	**99.3**
6	MII-a1	1.1	1.8	0.9	1.0	1.8	3.3	0.039	0.067	0.0029	3.8	105.2
7	MII-a1i	1.1	1.8	0.9	1.1	1.8	3.3	0.039	0.072	0.0029	3.8	105.3
8	MII-a2	1.0	1.6	0.9	1.1	1.6	2.8	0.035	0.128	0.0037	4.8	134.3
9	MII-a2i	1.6	1.6	0.9	1.3	1.7	4.3	0.041	0.443	0.0086	7.7	214.5
10	MII-a2ii	1.6	1.6	0.9	1.3	1.7	4.6	0.042	0.382	0.0076	8.4	233.6
11	MII-a2iii	2.0	1.9	1.0	1.4	2.4	5.4	0.051	0.837	0.0154	10.5	291.1
12	MII-a3	1.1	1.3	0.9	1.1	1.4	2.3	0.040	0.070	0.0019	3.5	96.5
13	MII-b1	1.1	1.4	0.9	1.1	1.4	2.1	0.040	0.064	0.0019	3.7	103.3
14	MII-b2	1.1	1.3	0.9	1.1	1.4	3.8	0.032	0.056	0.0019	-	-
15	MII-b3	1.1	1.4	0.9	1.1	1.4	2.1	0.040	0.067	0.0019	3.9	107.5
16	MII-c1	1.1	1.4	0.9	1.1	1.4	2.0	0.047	0.060	0.0019	4.3	119.8
17	MII-c1i	1.1	1.4	0.9	1.1	1.4	2.1	0.044	0.065	0.0019	4.2	115.6
18	MII-c2	1.1	1.4	0.9	1.1	1.4	2.3	0.040	0.068	0.0020	4.1	114.8
19	MII-c2i	1.2	1.5	0.9	1.1	1.6	2.1	0.042	0.058	0.0021	4.0	110.4
20	MII-c2ii	1.1	1.4	0.9	1.1	1.4	2.1	0.038	0.076	0.0018	3.8	105.6
21	MII-c3	1.1	1.4	0.9	1.1	1.4	2.0	0.041	0.067	0.0019	3.7	103.1
22	MII-d	1.1	1.4	0.9	1.1	1.3	2.4	0.042	0.072	0.0019	4.2	81.2
23	MII-e	1.1	1.5	0.9	1.1	1.5	2.4	0.038	0.068	0.0014	3.6	99.2
										IEEE Ground Motion (g)		
										L	T	V
										1.0	1.0	0.9

*Highlighted cells: base rotations

Table 18: Peak Accelerations and Moments of the Bushing Farthest from the Conservator

No	Model	Peak Acceleration (g)											Moment (kip*in)	
		Corner 1			Bushing 3 Turret Base*						Bushing 3		Bushing 3 Base	
		L	T	V	L	T	V	RL	RT	RV	P	T	P	T
		(1)	(2)	(3)	(4)	(5)	(6)	(7)	(8)	(9)	(10)	(11)	(12)	(13)
1	**MI (Basis)**	**1.1**	**1.3**	**0.9**	**1.1**	**1.3**	**1.7**	**0.046**	**0.051**	**0.0023**	**1.9**	**3.5**	**53.8**	**96.5**
2	MI-a	1.1	1.3	0.9	1.1	1.4	2.0	0.048	0.057	0.0029	2.7	3.7	74.0	102.3
3	MI-b	1.1	1.4	0.8	1.1	1.3	1.7	0.039	0.052	0.0021	2.2	4.4	61.1	120.8
4	MI-c	1.1	1.5	0.9	1.1	1.5	1.6	0.044	0.041	0.0022	2.3	3.3	64.3	91.1
5	**MII (Basis)**	**1.1**	**1.4**	**0.9**	**1.1**	**1.3**	**2.1**	**0.047**	**0.044**	**0.0027**	**2.8**	**3.6**	**77.2**	**99.7**
6	MII-a1	1.1	1.8	0.9	1.0	1.7	2.1	0.047	0.045	0.0035	2.8	4.4	76.9	120.9
7	MII-a1i	1.1	1.8	0.9	1.1	1.8	2.1	0.048	0.047	0.0034	2.3	5.1	63.9	141.0
8	MII-a2	1.0	1.6	0.9	1.1	1.6	2.3	0.065	0.091	0.0051	2.7	4.1	76.0	114.6
9	MII-a2i	1.6	1.6	0.9	1.5	1.6	3.1	0.109	0.275	0.0086	3.5	5.1	96.5	142.3
10	MII-a2ii	1.6	1.6	0.9	1.4	1.7	2.8	0.105	0.227	0.0105	2.9	4.9	79.2	134.9
11	MII-a2iii	2.0	1.9	1.0	1.9	2.5	3.6	0.141	0.436	0.0157	5.0	6.4	137.7	176.4
12	MII-a3	1.1	1.3	0.9	1.1	1.3	1.9	0.044	0.036	0.0025	2.7	3.9	74.8	107.4
13	MII-b1	1.1	1.4	0.9	1.1	1.3	1.9	0.055	0.040	0.0031	2.9	3.5	79.7	97.8
14	MII-b2	1.1	1.3	0.9	1.1	1.4	2.1	0.050	0.051	0.0029	2.8	3.5	77.1	97.7
15	MII-b3	1.1	1.4	0.9	1.1	1.3	1.4	0.041	0.040	0.0028	-		-	
16	MII-c1	1.1	1.4	0.9	1.1	1.3	1.9	0.056	0.047	0.0029	3.0	3.9	83.8	109.2
17	MII-c1i	1.1	1.4	0.9	1.1	1.3	2.0	0.049	0.040	0.0032	2.8	3.8	78.2	106.3
18	MII-c2	1.1	1.4	0.9	1.1	1.3	2.1	0.061	0.043	0.0034	2.8	4.4	77.9	123.1
19	MII-c2i	1.2	1.5	0.9	1.1	1.5	1.8	0.054	0.054	0.0033	2.3	4.0	65.1	112.3
20	MII-c2ii	1.1	1.4	0.9	1.1	1.3	2.0	0.067	0.048	0.0028	3.0	4.6	82.1	127.5
21	MII-c3	1.1	1.4	0.9	1.1	1.3	2.0	0.050	0.053	0.0037	3.0	3.8	83.8	104.7
22	MII-d	1.1	1.4	0.9	1.1	1.3	2.7	0.072	0.047	0.0026	2.9	6.2	57.0	120.1
23	MII-e	1.1	1.5	0.9	1.1	1.5	1.7	0.040	0.038	0.0038	2.2	3.7	61.6	102.8

IEEE Ground Motion (g)		
L	T	V
1.0	1.0	0.9

*Highlighted cells: base rotations

Figure 46: Vertical Vibration of Cover at Bushing Mount

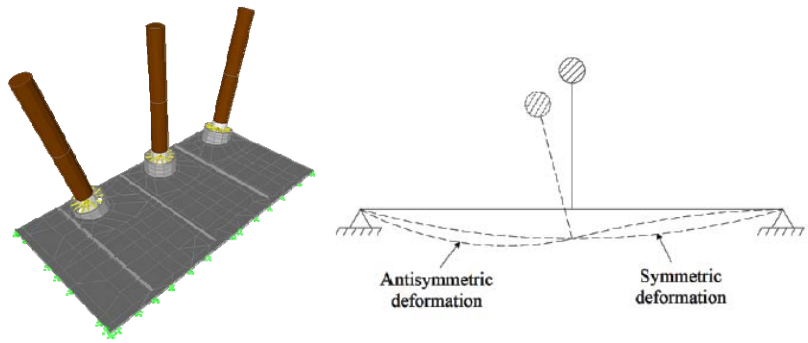

(a) Bushings on cover (b) vertical vibration – symmetric deformation

The support motion (acceleration) can be substantially amplified or reduced, depending on the match or mismatch of frequencies of the bushing cover and motions of the top of the transformer's walls, according to Equation (6):

$$AMPL_v = \frac{\ddot{u}_{bv}}{\ddot{u}_c}\sqrt{\frac{1+\left[2\xi(f/f_{bc})^2\right]}{\left[1-(f/f_{bc})^2\right]^2+\left[2\xi(f/f_{bc})^2\right]^2}} \qquad (6)$$

where f_{bc} is the as-mounted frequency of the bushing cover. For a very stiff cover the frequency tends to infinity and the amplification reduces to unity. Inherent damping plays a role, but this damping is usually limited to low values (1–3%).

As a result, the frequencies and amplification ratios based on the transfer functions shown in Figures 47 and 48 are strongly influenced by mounting location and whether the bushing is outfitted with or without a turret. Figure 49 shows the spectral response in the vertical direction with respect to the requirements of IEEE 693-compatible motions, where the frequencies show distinct changes and magnifications influenced by location on the cover, with largest amplifications in the center. The accelerations reach spectral values of up to 20 g with amplifications of up to 5 over the requirements of the standards. Particular attention is to be paid to the coupling effects at corners and edge bushings mounted in inclined positions.

Summary and Conclusions of Numerical Study

In this section a preliminary numerical investigation of the seismic response of the bushings mounted on a rigid structure (defined also as a fixed base) and mounted on a flexible transformer's cover ("as-installed") was conducted by performing modal and dynamic time analyses. The results indicate that the "as-installed" bushing is more vulnerable to seismic loading than similar bushings mounted on a rigid base.

It is clear that bushing mountings on transformer tanks have to be stiffened in such a way that the bushing response to seismic motion moves closer to the response of the rigid base analysis

and therefore the system becomes adequately resistant against intense ground shaking. In order to achieve results close to that of the rigid base analysis, researchers have investigated various stiffening approaches (Koliou et al., 2011).

The forces and moments developed at the base of the bushing as installed in the field on a flexible cover are larger in general than the same forces that will develop in a bushing supported by a rigid mount. This was shown through seismic simulations including substantial measures of uncertainties.

Moreover, this study showed that the motions that appear at the base of the bushing at the mounting connections are greater than considered by the current standards, due to several factors:

1) The lateral motion at selected frequencies of the transformer is often amplified beyond the factor of 2 specified by the codes.
2) Rotational motions resulting from bending of the cover (not addressed entirely by the current standards) exacerbate the lateral response of bushings.
3) Vertical vibrations due to cover flexibility and mass of the bushings produce excitations which influence the base motions vertically, with possible stronger effects in tilted bushings.

The above observations are also verified in the investigations chronicled in the subsequent Chapters.

Figure 47: Spectral Amplification of Cover in Vertical Direction at the Bushing Base – Flexible Connection

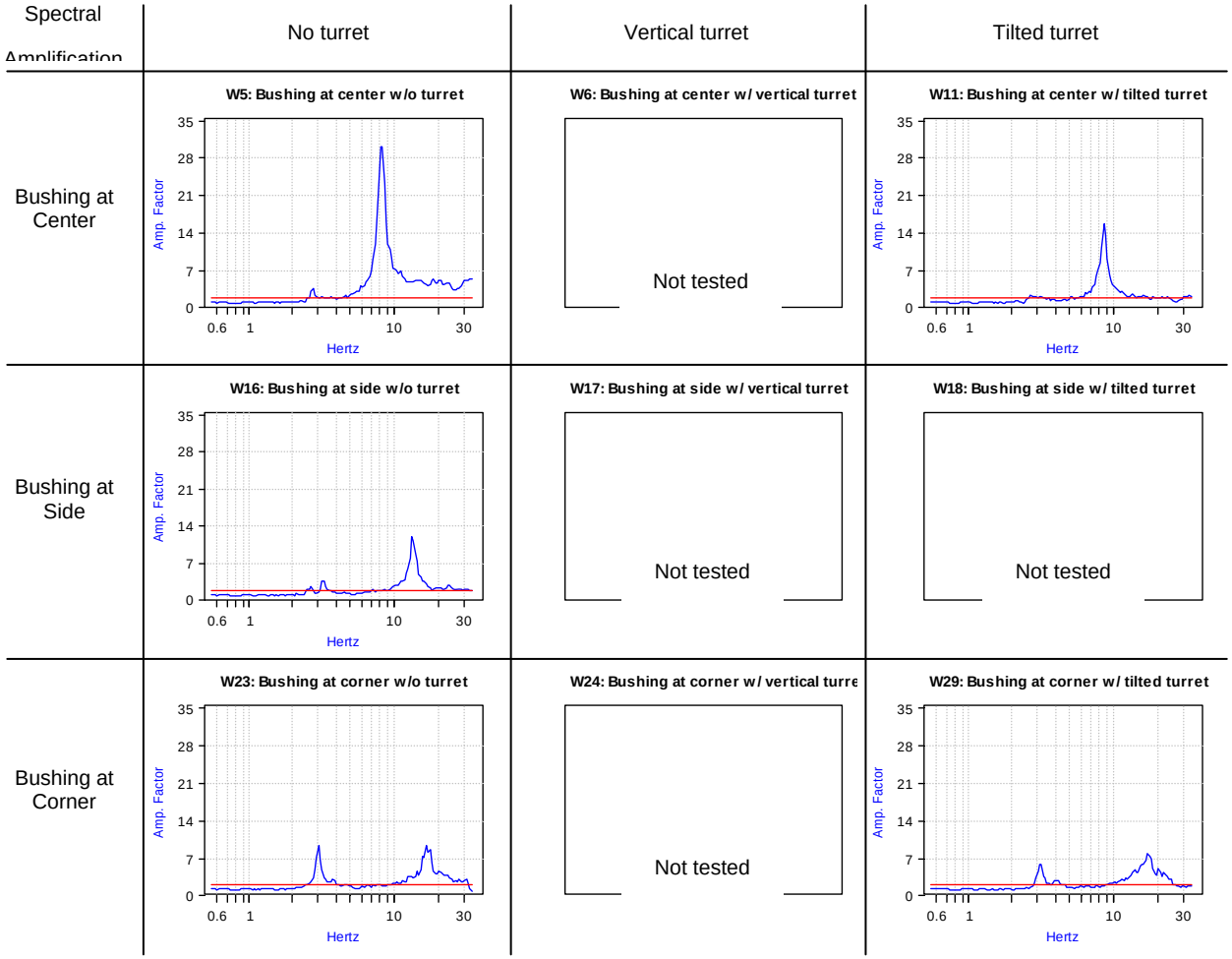

Source: Kong, 2010

Figure 48: Vertical Frequencies of Transformer Cover with Mounted Bushing

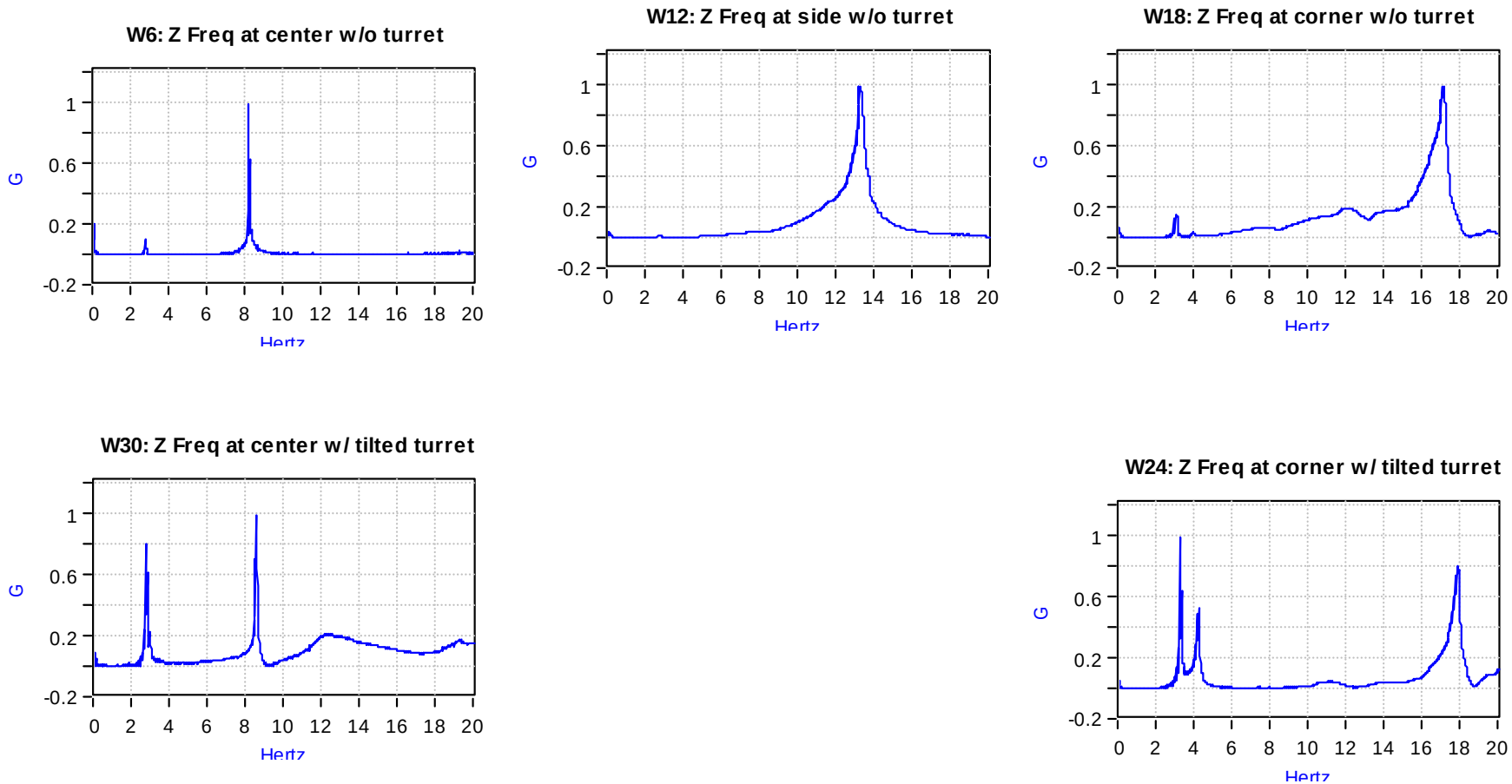

Top line: Bushing without turret. Lower line: Bushing with tilted turret.

Source: Kong, 2010

Figure 49: Amplification of Accelerations of 230 kV Transformer Cover in Vertical Direction

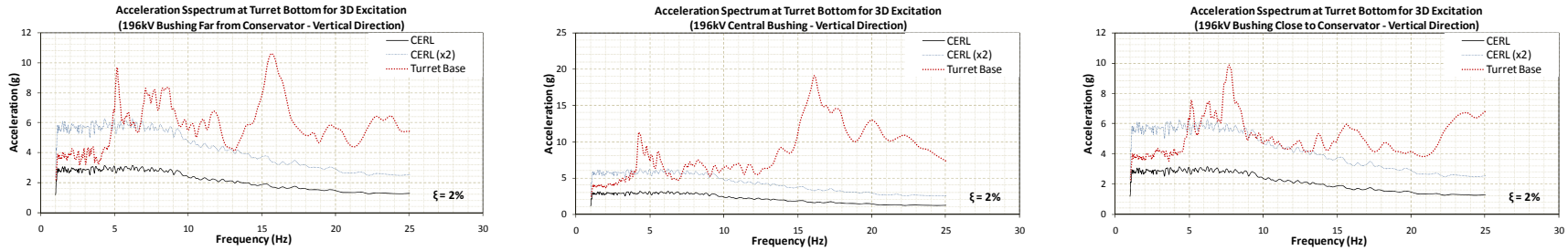

(a) Acceleration Spectrum at Base of Bushings: Three Phases

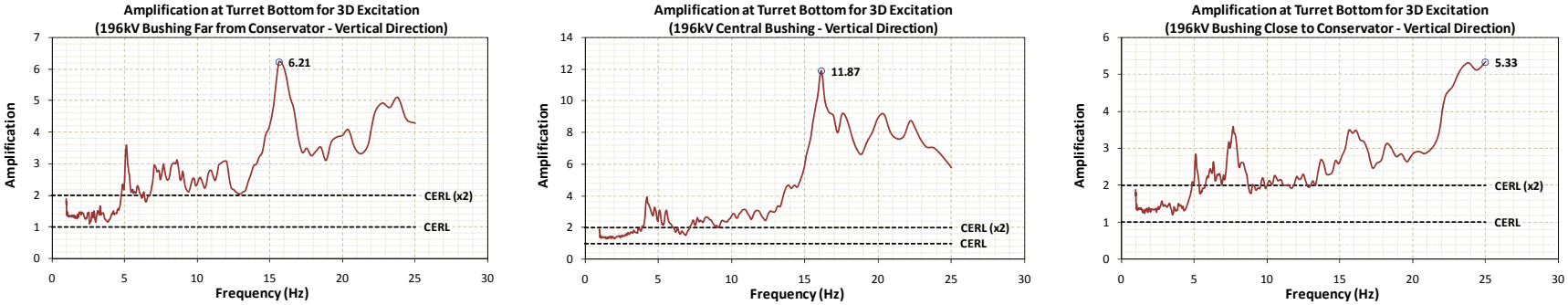

(b) Spectral Amplifications in Respect to RRS: Three Phases

Source: Reinhorn et al., 2010

CHAPTER 3:
Experimental Study of Transformer Bushings

This section describes the results of laboratory tests that were performed on transformer bushings. The objective of these tests was to develop comprehensive data on the performance of the bushings in response to simulated earthquake-induced motions and other behavioral characteristics. The primary hypothesis of this research effort is that current understanding of transformer/bushing systems in actual service is imperfect, and not based on complete knowledge of as-installed conditions and performance. Analysis of the data developed herein will be used for the formulation of suggested changes to the qualification procedures and standards relating to in-service bushing performance.

Testing Specimens

For this study nine different bushings were acquired from different sources. Three of them were manufactured by General Electric (GE), two from Hochspannungsgerate (HSP), one from Trench and three from ASEA Brown Boveri (ABB). The bushing materials also varied: six of the nine bushings were made of porcelain and three were made of composite materials (fiber-reinforced resins).

Porcelain Bushings

Generally, porcelain bushings are tapered with their maximum diameter near the mounting flange and reduced diameter toward the top (refer to Figure 6). This tapered section lowers the static CG of the section. Porcelain bushings are manufactured from several bushing segments. The conductor passing through these bushing segments is anchored at the top and the bottom. The conductor rod is pre-stressed in order to hold the porcelain components of bushings together. The force applied to the contact surfaces by the conductor is defined as the hold down load. The interface between two adjacent porcelain components and the interface between the bushing mounting flange and the bushing have “O” gaskets. These gaskets prevent oil leakage and at the same time provide a soft interface to help reduce cracking and crushing of the porcelain.

There were six porcelain bushings that were tested in SEESL. Three of these bushings were manufactured by GE: one was provided to SEESL by LADWP and two by CERL. The remaining three bushings were manufactured and provided by ABB.

The first bushing, designated as Bushing #1, is a 550 kV rated unit manufactured by GE and provided by LADWP. The total weight of this bushing was 4000 lb. and the center of gravity (CG) is located at 57.5 inches from the mounting flange. Figure 50 shows the bushing in the lab along with the manufacturer’s specifications sheet. Figure 51 shows a schematic of this bushing.

Next are the two 550 kV-rated bushings manufactured by GE and provided by CERL. The center of gravity of these bushings was located at 57.5 inches from the mounting flange. The only difference was the total weight of the bushing. The first of these two bushings, designated as Bushing #2 for this study, weighs 2800 lb.; the second, Bushing #3, is slightly heavier with a total weight of 2810 lb. Figure 52 is a schematic applicable to both bushings. Porcelain bushings are usually filled with oil when installed in service, but these two bushings were delivered empty;

they were filled with water in the lab to replicate as-installed conditions. Although there is a difference between the densities of oil and water, it was assumed that the weight difference due to water was small compared to the structural mass of the bushing. It was noted that the center of gravity did not change before and after the addition of water.

The next three porcelain bushings, one 230 kV and two 550 kV units, were manufactured and provided by ABB, and were delivered filled with oil to the recommended level. The 230 kV porcelain bushing is designated as Bushing #6 and is shown in Figure 53. The total weight of this bushing was 840 lb. and the CG was located 14 inches from the mounting flange. The two 550 kV porcelain bushings were different in size and weight. Bushing #7 (see Figure 54) was heavier at 4440 lb., with its CG at 47 inches from the mounting flange. Bushing #8 (Figure 55) was lighter at 2180 lb. with its CG at 54.8 inches from the mounting flange.

Composite Bushings

Composite bushings are significantly more flexible and lighter weight, compared to porcelain bushings of similar physical size and electrical capacity. They are usually manufactured in one piece, cast to shape, with a center hole for the conductor, which may or may not be pre-stressed (pre-stressing is sometimes necessary for porcelain bushings to assist in holding the porcelain segments together, but as composites are cast in one piece this is not always necessary). The conductor is encapsulated in a polymer-resin bonding compound to bind the conductor rod to the body of the bushing.

The composite bushings used in this study are further classified according to the voltage capacity. Two bushings manufactured by HSP and provided by LADWP are designed for 230 kV applications and were electrically and mechanically the same, differing only in total weight. The weight of one bushing was 510 lb. and is henceforth referred to as Bushing #4A (see Figure 56). The center of gravity (CG) of Bushing #4A lies 17 inches from the mounting flange. The second bushing is lighter at 385 lb. and is referred to as Bushing #4B (see Figure 57). The center of gravity of this bushing was also 17 inches from the mounting flange. The upper section was quite uniform in size while the lower section was tapered for mounting purposes. Figure 58 shows the 500 kV composite bushing manufactured by Trench (Bushing #5). The total weight, center of gravity and other properties were measured at SEESL.

Conductor Simulation

In service, a conductor is mounted at the top of a bushing for transmitting electricity to and from the transformer. During extreme events this conductor induces inertial forces on the bushing, which were simulated in the laboratory by adding a weight to the top of the bushings. It should be noted that the mass added for conductor simulation depends on the voltage capacity of the bushing, per recommendations of IEEE 693. The 230 kV bushings were mounted with a 15 lb. weight and the 500 kV bushings were mounted with a 25 lb. weight at the top of bushing, as shown in Figure 59. Table 19 presents a summary of the bushings' properties. The letters in bold, e.g., the total weight, location of center of gravity, etc., were measured in the SEESL Laboratory.

Testing Setups

Fixed-base Testing Setup

In order to find the fixed-base properties of bushings, a rigid base was designed and built at University at Buffalo SEESL for this project. The main dimensions of this support structure are 8′x8′x1′. The support block structure is made of normal strength concrete reinforced by deformed GR 60 steel. A total of six bushings were tested on this support structure, and some of them had different mounting bolt configuration. To ensure that all the bushings could be accommodated, a 2″-thick steel adapter plate was used. The steel plate had tap holes to mount the bushings rigidly. A 12″-thick concrete slab was anchored to the concrete cover of a trench that attaches to the relocatable shake tables in the SEESL. This configuration accommodates various lengths of the lower part of the bushings that extrude to almost 6 ft. (in one case); this space also allowed access to install accelerometers and displacement potentiometers. Figures 60 and 61 show detailed sketches of the concrete plate and the mounting configurations, respectively. Figure 62 shows a bushing installed on the rigid base and instrumented for testing.

Figure 50: 550 kV Porcelain Bushing Manufactured by GE (Bushing #1)

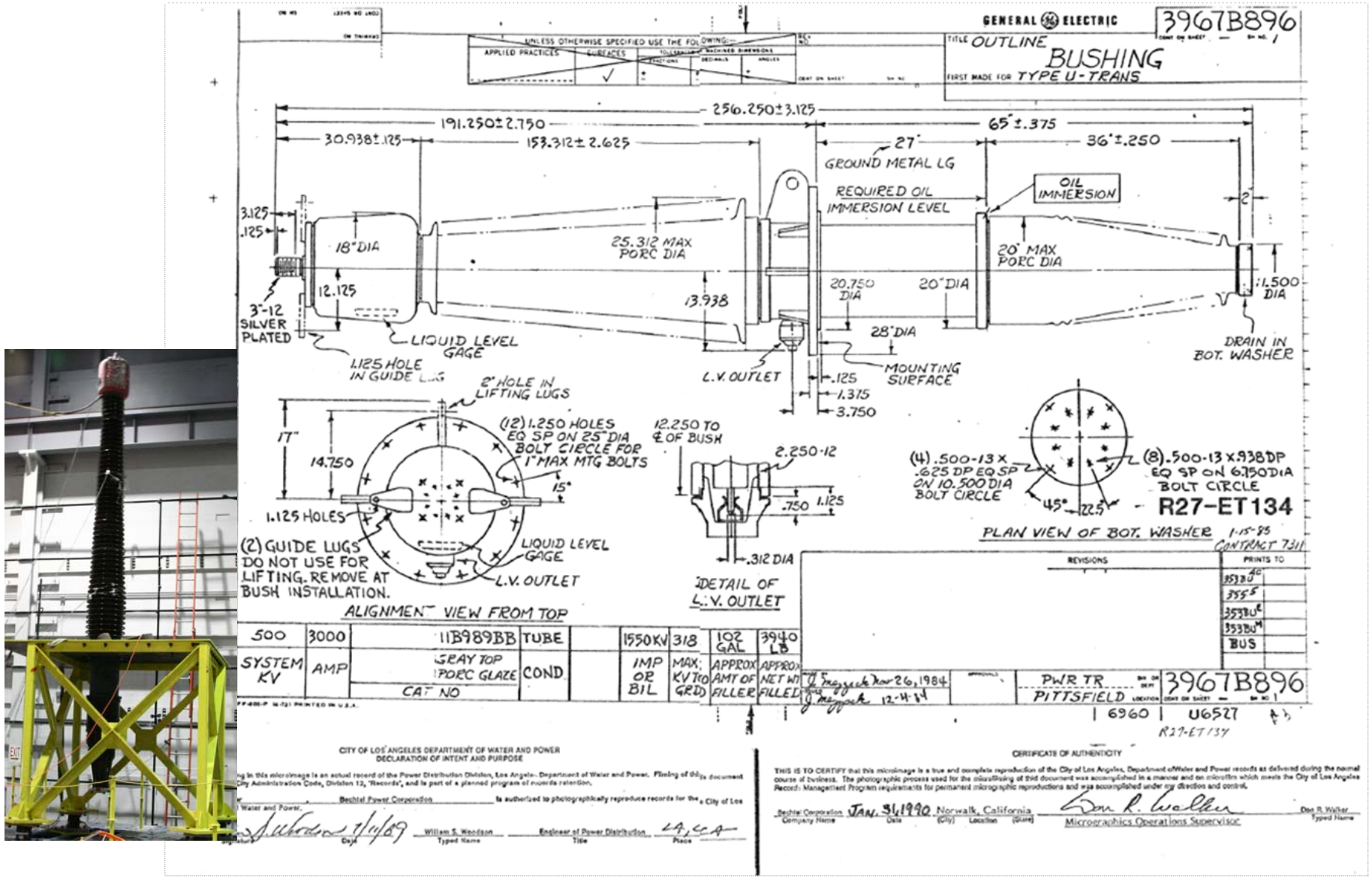

Photo Credit: SUNY-Buffalo. Schematic courtesy of General Electric Co.

Figure 51: Schematic of 550 kV Porcelain Bushing Manufactured by GE (Bushing #1)

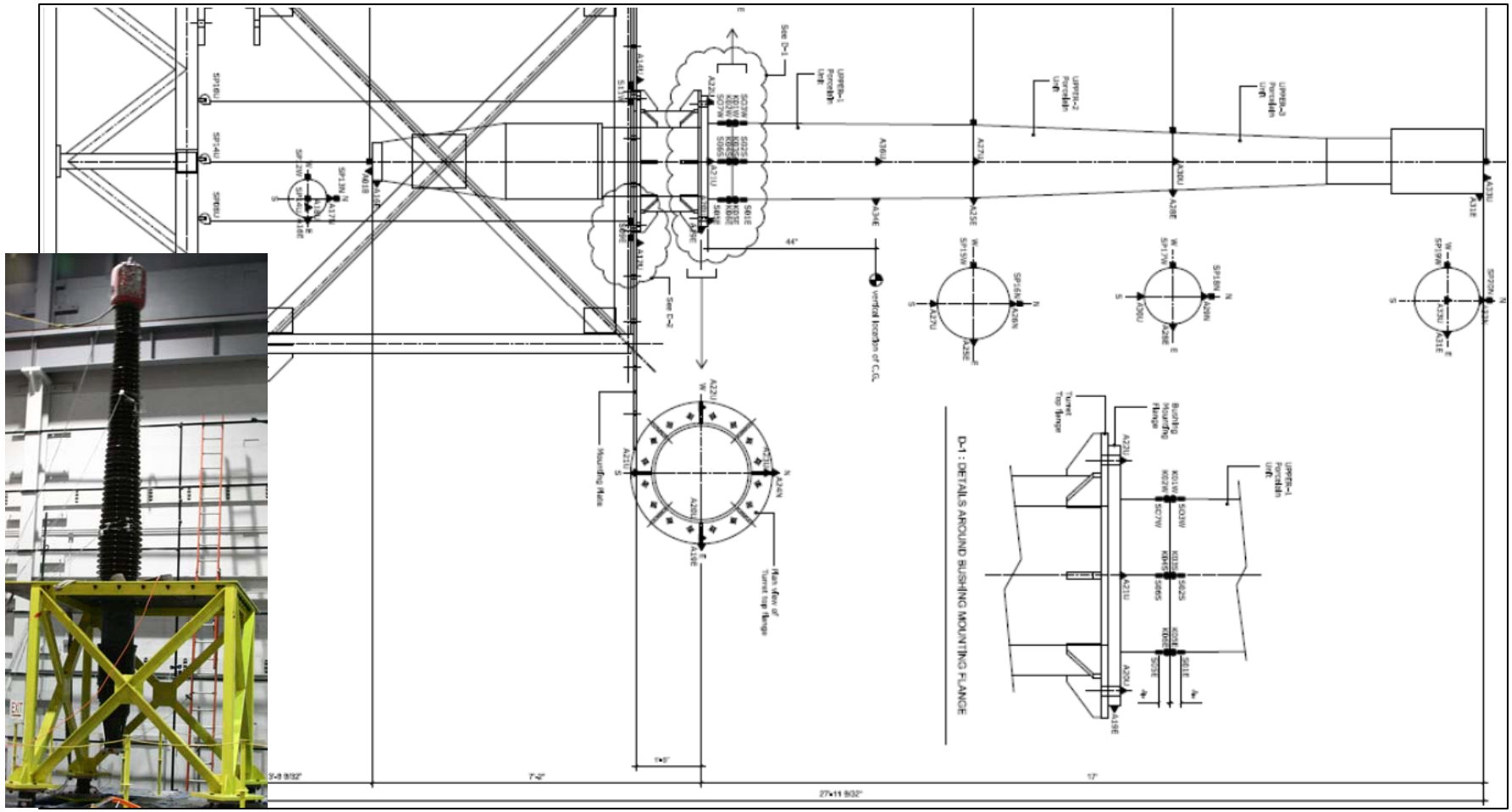

Photo Credit: SUNY-Buffalo. Schematic courtesy of General Electric Co.

Figure 52: 550 kV Porcelain Bushing Manufactured by GE (Bushings #2 and #3)

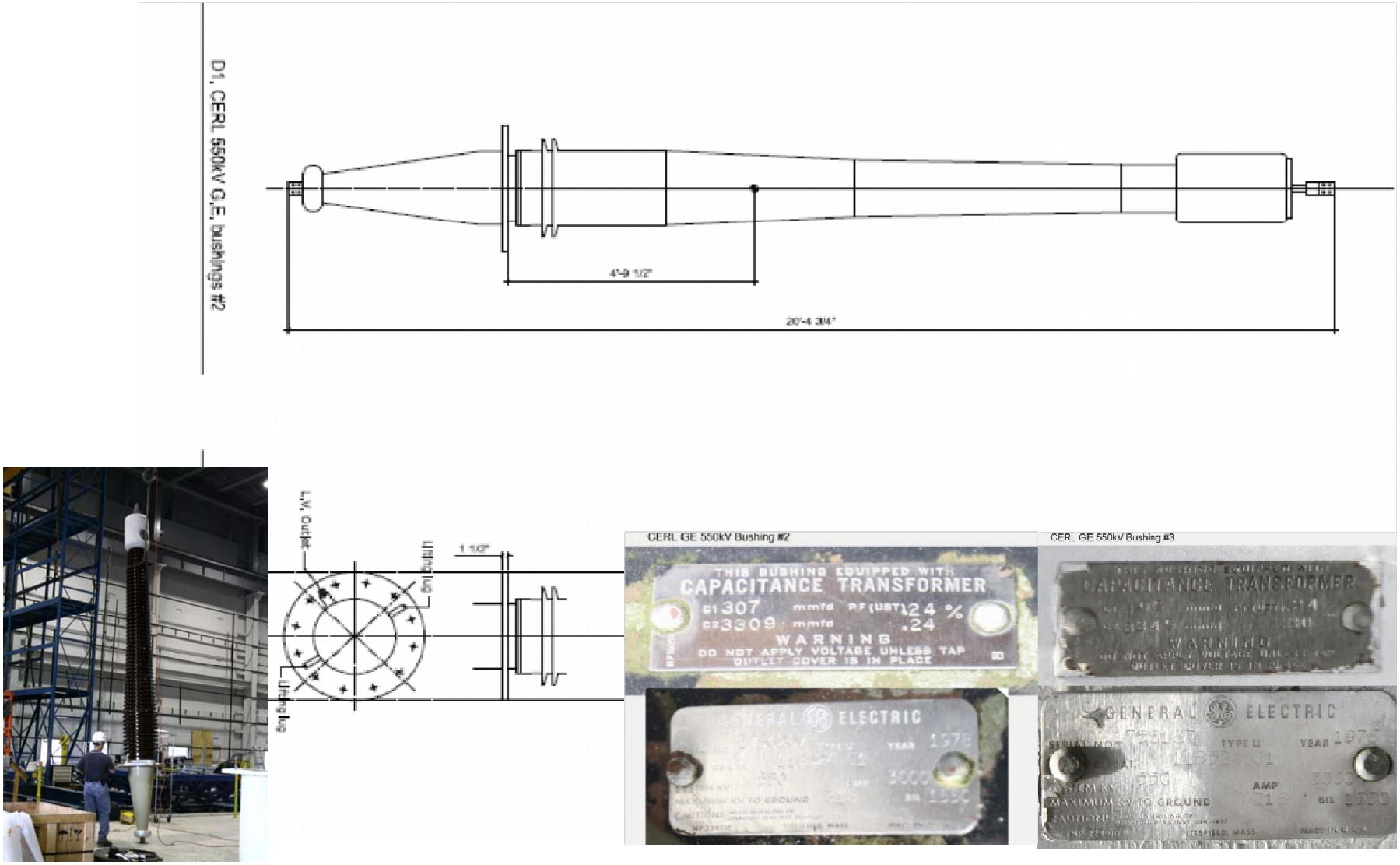

Photo Credit: SUNY-Buffalo. Schematic courtesy of General Electric Co.

Figure 53: 230 kV Porcelain Bushing Manufactured by ABB Inc. (Bushing #6)

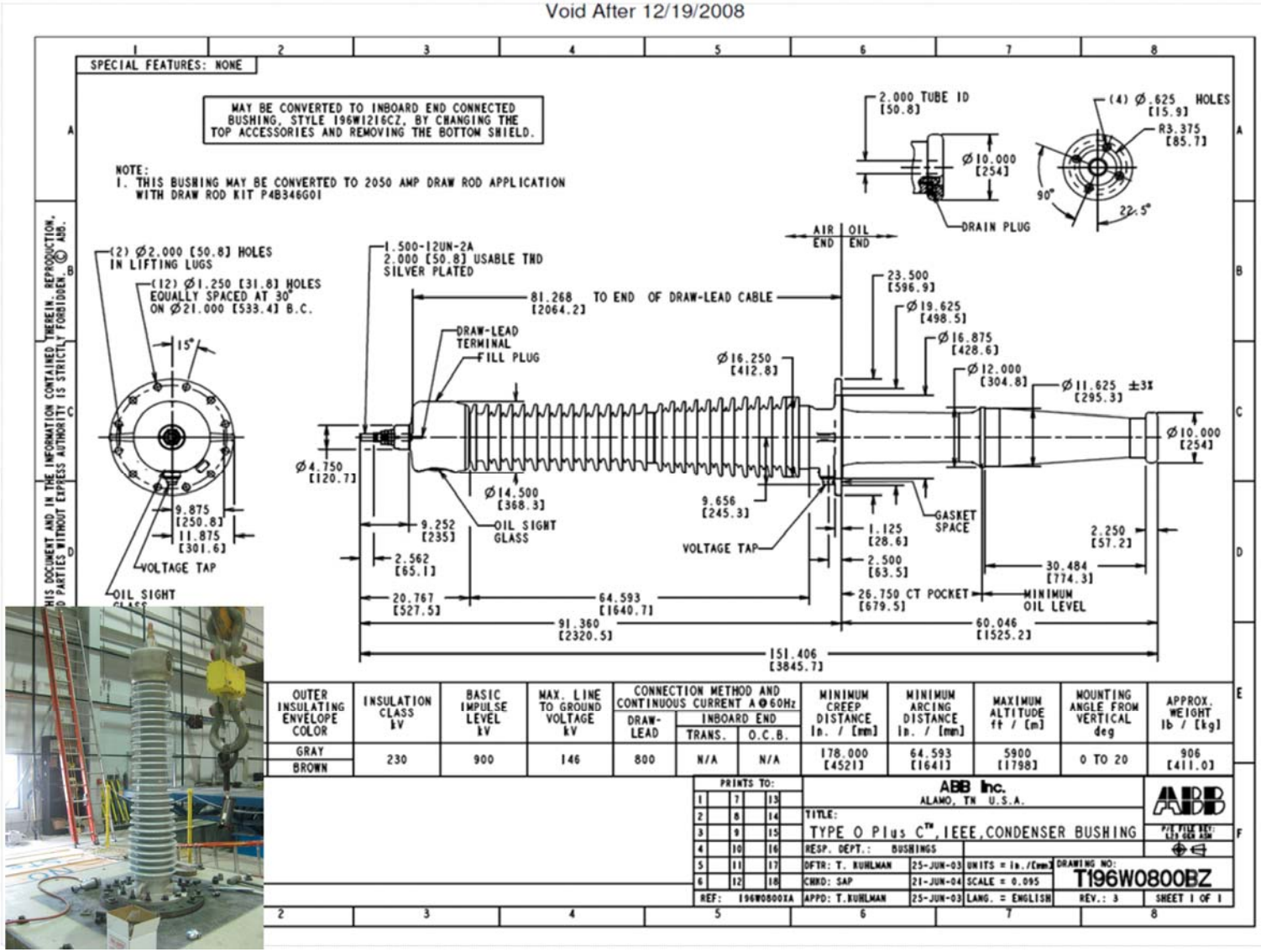

Photo Credit: SUNY-Buffalo. Schematic courtesy of ASEA Brown Boveri (ABB) Inc.

Figure 54: 550 kV Porcelain Bushing Manufactured by ABB (Bushing #7)

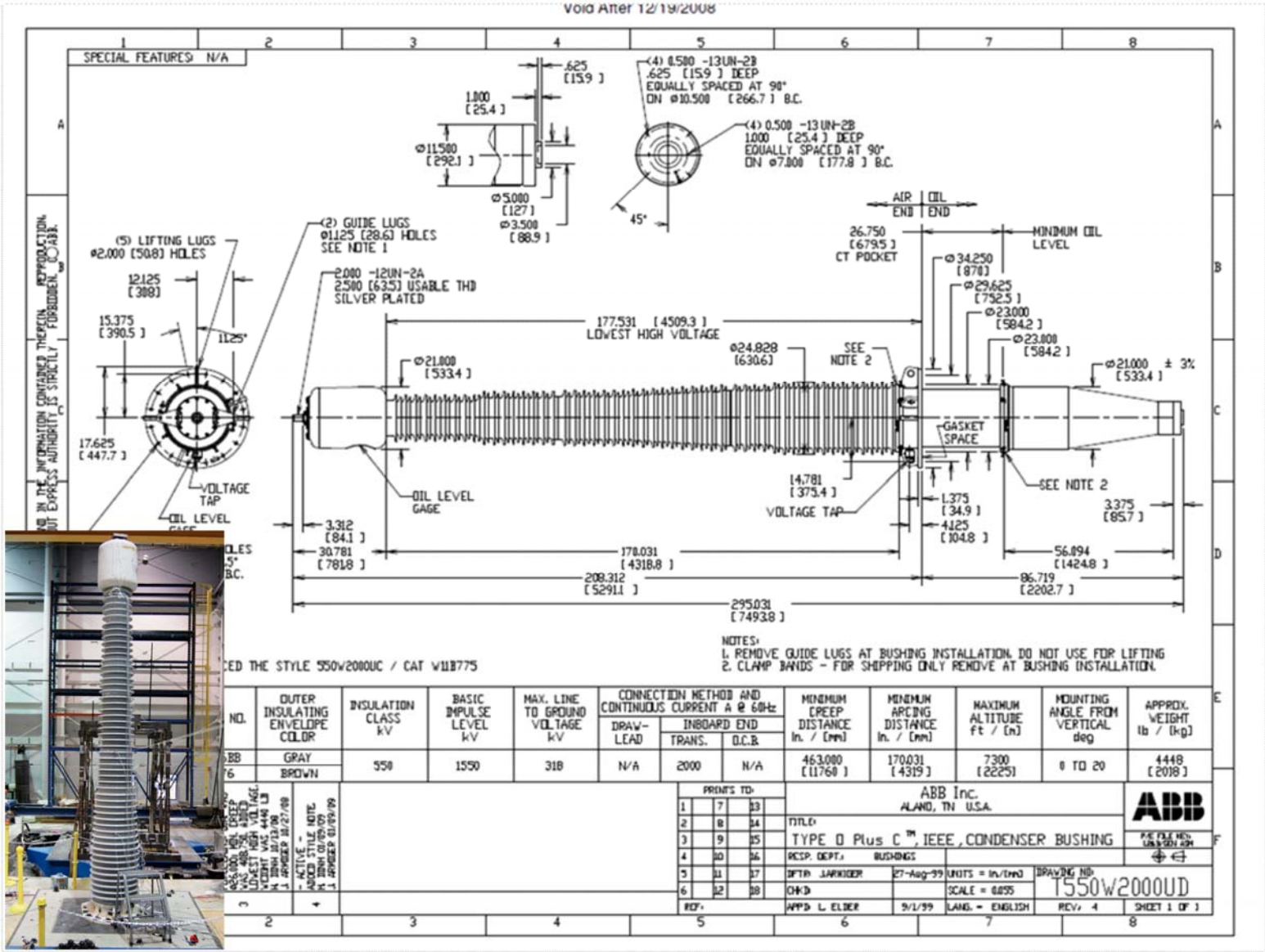

Photo Credit: SUNY-Buffalo. Schematic courtesy of ASEA Brown Boveri (ABB) Inc.

Figure 55: 550 kV Porcelain Bushing Manufactured by ABB (Bushing #8)

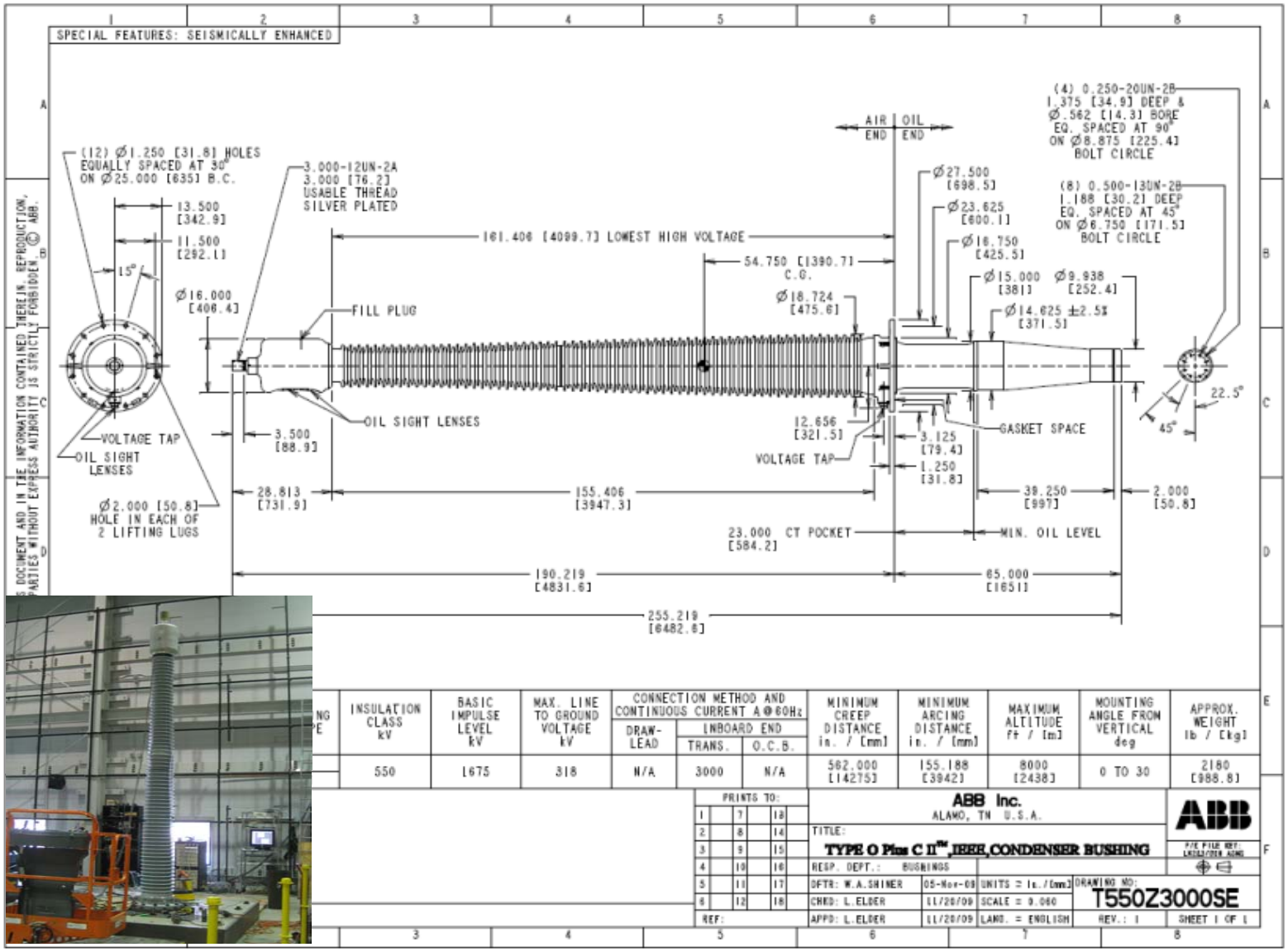

Photo Credit: SUNY-Buffalo. Schematic courtesy of ASEA Brown Boveri (ABB) Inc.

Figure 56: 230 kV Composite Bushing Manufactured by HSP (Bushing #4A)

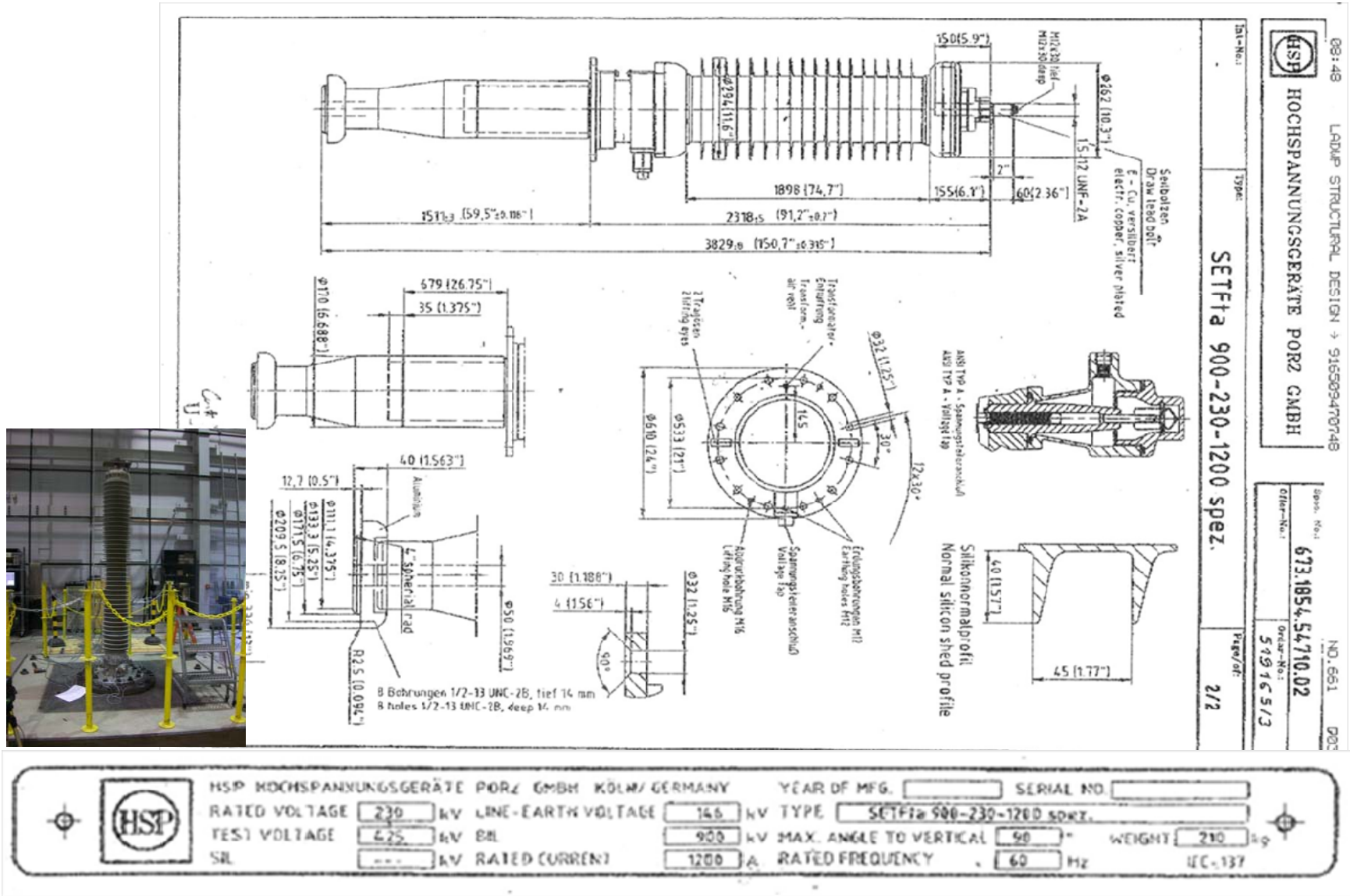

Photo Credit: SUNY-Buffalo. Schematic courtesy of Hochspannungsgerate Gmbh.

Figure 57: 230 kV Composite Bushing Manufactured by HSP (Bushing #4B)

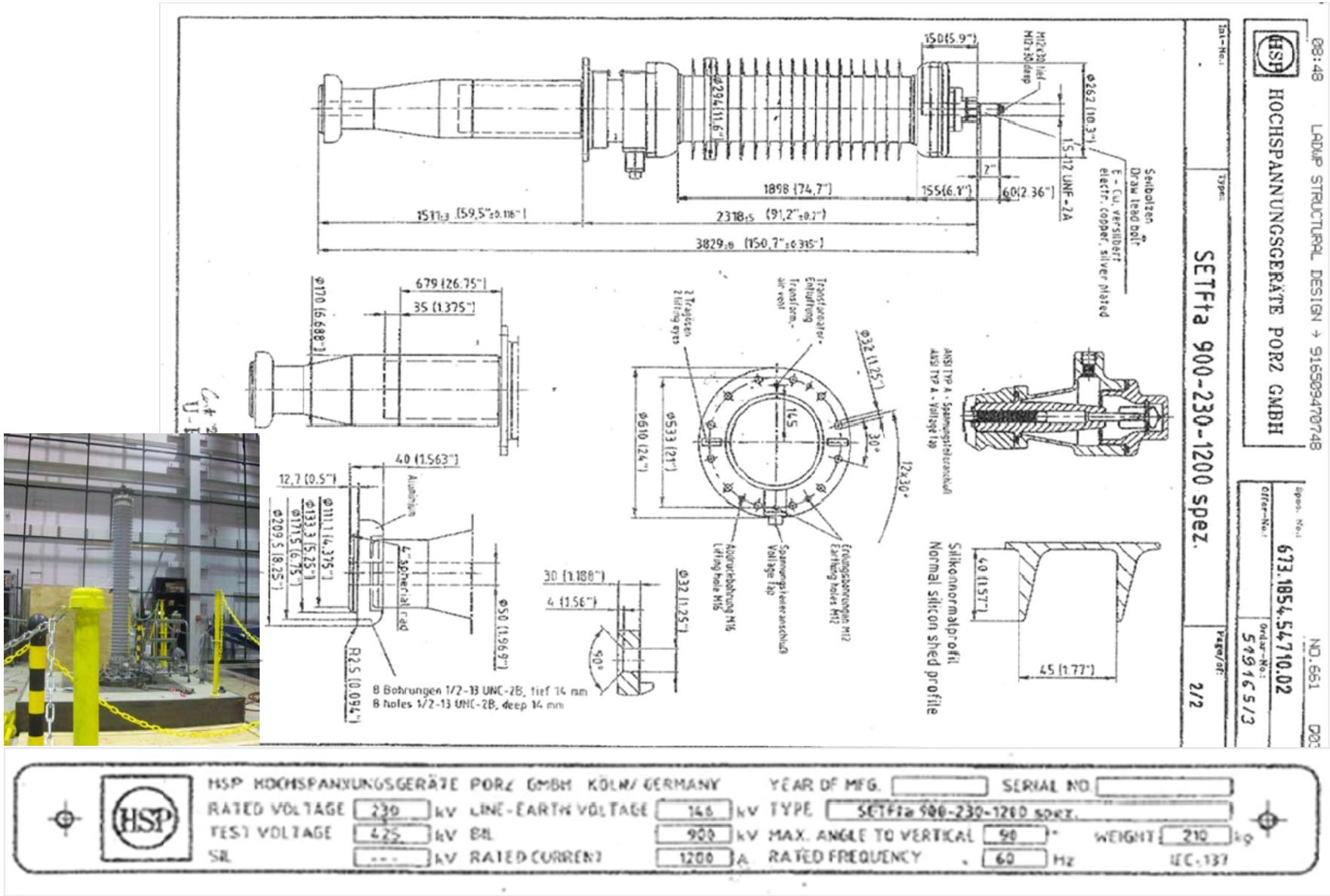

Photo Credit: SUNY-Buffalo. Schematic courtesy of Hochspannungsgerate Gmbh.

Figure 58: 500 kV Composite Bushing Manufactured by Trench Ltd. (Bushing #5)

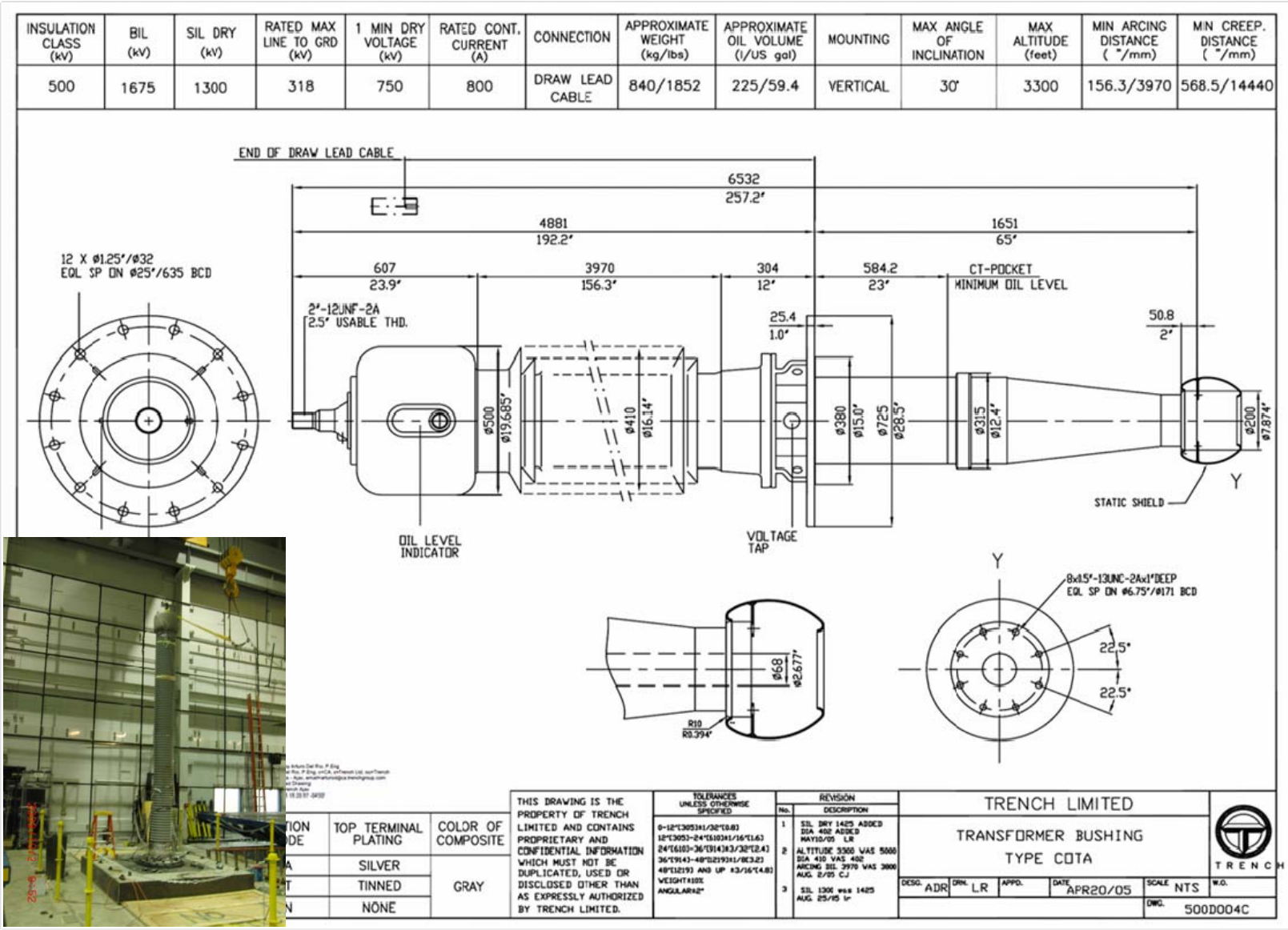

INSULATION CLASS (kV)	BIL (kV)	SIL DRY (kV)	RATED MAX LINE TO GRD (kV)	1 MIN DRY VOLTAGE (kV)	RATED CONT. CURRENT (A)	CONNECTION	APPROXIMATE WEIGHT (kg/lbs)	APPROXIMATE OIL VOLUME (l/US gal)	MOUNTING	MAX ANGLE OF INCLINATION	MAX ALTITUDE (feet)	MIN ARCING DISTANCE ("/mm)	MIN CREEP. DISTANCE ("/mm)
500	1675	1300	318	750	800	DRAW LEAD CABLE	840/1852	225/59.4	VERTICAL	30°	3300	156.3/3970	568.5/14440

Photo Credit: SUNY-Buffalo. Schematic courtesy of Trench, Ltd.

Figure 59: Conductor Simulation with Weights on Bushings

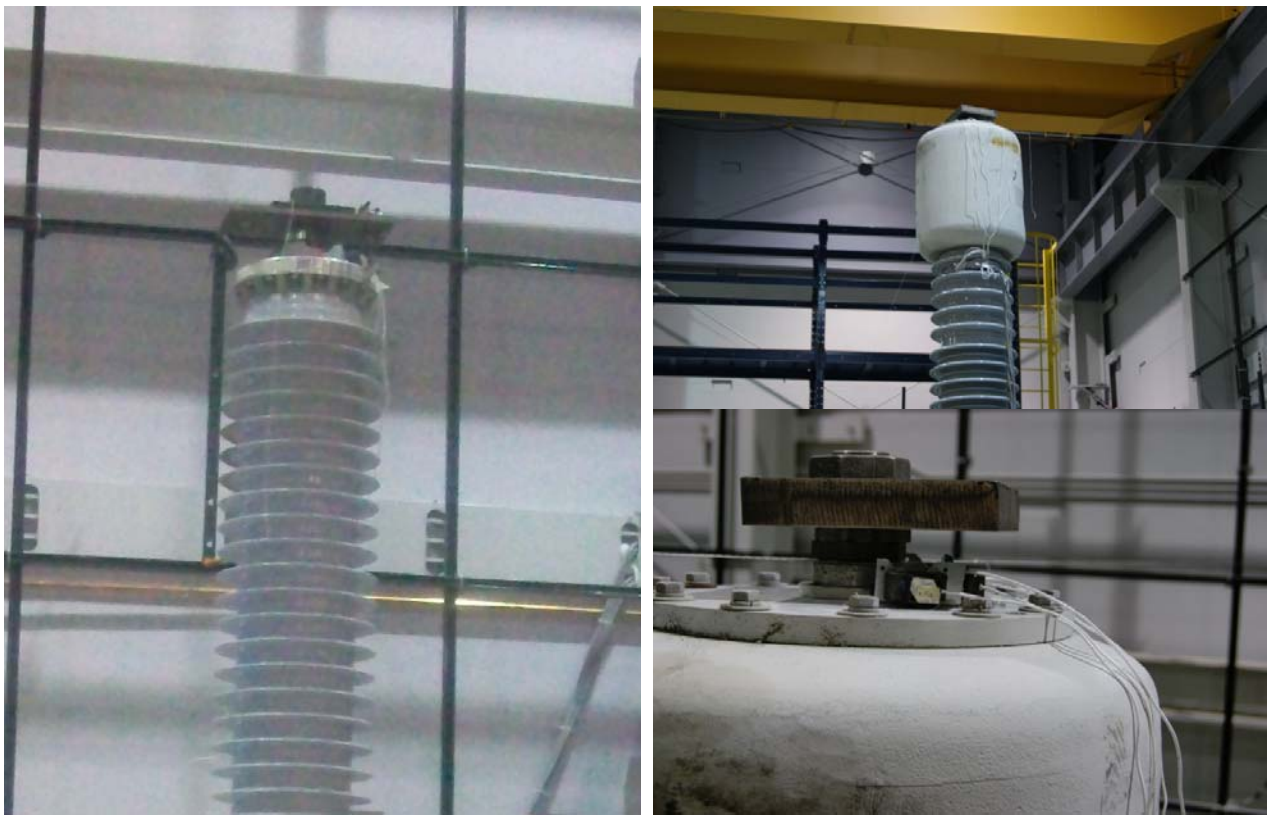

15 lb. Mass on 230 kV Bushing (left) and 25 lb. Mass on 500 kV Bushing (right)

Photo Credits: SUNY-Buffalo

Shake Table Test Setup – Rigid Frame for Tilted Bushing

The rigid frame was built per the requirements of IEEE Standard 693-2005. As previously shown in Figure 17, the frame has the top plate dimensions of 40″x40″. The height of the 4″x4″-square tubing posts is such that the top (mounting) plate is sloped 15º from the horizontal. The height on the high side is 65″ and on the shorter side it is 56″. The inclination to the top plate where bushings are mounted is therefore 9″/38″ = ~15º. The top plate has a thickness of 1.5″ and is welded on all sides with 4″x 4″ tubing beams. Similar sections are used as braces, which results in this support structure being extremely rigid for all directions of motion. The support structure is also vertically rigid and restricts the rotational motions. The bolt patern on this frame was such that it could not be accomodated directly on the shake table. For this purpose, an interface base plate of dimensions 60″x60″x2″ (see Figure 63) was placed between the support structure and the shake table extension.

Shake Table Test Setup – Flexible Frame (Straight and Tilted)

A special frame structure (see Figures 64 and 65) was developed at SUNY-Buffalo to enable testing of bushings in mounted conditions similar to those found in the field. The frame was designed to accommodate a flexible top plate (see Figure 66) simulating the cover of transformer tanks and to have very rigid frame walls to allow smooth transfer of horizontal and vertical motions from the

shake table. The main frame of the support structure has the dimensions of 8′x8′x8′, center to center between members. Steel square tubing of 5″x5″x½“ is used for the four vertical columns at corners. The tops of the columns are connected by L-shaped 5″x5″x¾“ angle braces. All four side walls of the frame are cross-braced using the same type of angle braces.

Table 19: Summary of Data for Bushings Used in the Experimental Study

Property	Units	Bushing#1	Bushing#2	Bushing#3	Bushing#4a	Bushing#4b	Bushing#5	Bushing#6	Bushing#7	Bushing#8
(1)	(2)	(3)	(4)	(5)	(6)	(7)	(8)	(9)	(10)	(11)
Manufacturer		G.E.	G.E.	G.E.	HSP	HSP	Trench	ABB	ABB	ABB
Provider		CERL	CERL	CERL	LADWP	LADWP	Trench	ABB	ABB	ABB
Material of Insulator		Porcelain	Porcelain	Porcelain	Composite	Composite	Composite	Porcelain	Porcelain	Porcelain
Voltage Capacity (kV)		500	550	550	230	230	500	196/230	550	550
Designation		GE-500 -TypeU	GE-500 -TypeU	GE-500 -TypeU	HSP-230-1200	HSP-230-1200	500D004C_3	196w0800bz	T550W2000UD	T550Z3000SE
Total Height (in)	in	290.0	244.8	244.8	150.7	150.7	257.2	151.4	295.0	255.2
Length over mounting Flange	in	204.0	194.8	194.8	91.2	91.2	192.2	91.4	208.3	190.2
Length below mounting flange	in	86.0	50.0	50.0	59.5	59.5	65.0	60.0	86.7	65.0
Max Dia. Over mounting flange	in	20.0	25.0	25.0	11.6	11.6	19.8	11.8	23.0	18.7
Max Dia. Below Mounting flange	in	20.0	18.8	18.8	8.3	8.3	12.4	10.0	23.0	16.8
Diameter of mounting flange	in	35.0	33.0	33.0	24.0	24.0	28.5	24.0	34.2	27.0
Bolt Pattern of Mounting flange	in	16-Φ 1 1/8 / Φ31	12-Φ 3/4 / Φ28	12-Φ 3/4 / Φ28	12-Φ 1 1/4 / Φ21	12-Φ 1 1/4 / Φ21	12-Φ 1 1/4 / Φ32	12-Φ 1 1/4 / Φ21	12-Φ 1 1/4 / Φ32	12-Φ 1 1/4 / Φ23
Total Weight	lbs	4000	2800	2810	510	385	1850	840	4330	2180
Location of CG (above flange)	in	57.5	57.5	57.5	17.0	17.0	65.5	14.0	47.0	54.8
Upper Bushing Weight	lbs	2744	2148	2156	248	172	1307	447	3012	1570
Location of Upper Bushing CG	in	n/a	n/a	n/a	45.0	45.0	96.0	34.0	90.0	85.2
Lower Bushing Weight	lbs	1156	552	554	162	113	443	293	1218	510
Location of Lower Bushing CG	in	n/a	n/a	n/a	27.0	27.0	24.5	28.0	59.0	39.0
Connection Housing Weight	lbs	100	100	100	100	100	100	100	100	100
Weight per unit length	lbs/in	13.45	11.03	11.07	2.72	1.89	6.80	4.89	14.34	8.15
Max. Pull Load - Fixed Base	lbs	n/a	n/a	n/a	287.1	200.0	295.7	383.0	310.0	306.5
Max. Displacement - Fixed Base	in	n/a	n/a	n/a	0.43	0.26	0.42	0.11	0.08	0.12
Stiffness Fixed Base	lbs/in	n/a	n/a	n/a	667.6	769.2	704.0	3419.6	4100.5	2554.2
Fixed Base Frequency *	Hz	**n/a**	**n/a**	**n/a**	**8.26 - 8.85**	**7.35 - 8.00**	**5.08 - 5.25**	**23.63 - 25.97**	**8.74 - 9.48**	**9.35**
As-installed Frequency **	Hz	**3.30 - 3.90**	**4.20**	**4.25**	**7.25 - 7.80**	**5.87 - 6.75**	**3.00 - 3.50**	**10.85 - 11.50**	**2.47 - 2.56**	**7.70**

Note: the Upper\Lower Bushing weight is calcualted per unit length
the numbers in bold face were measured in the lab
* Range provided when multiple installations were tested; ** Frequencies provided for center mount

Figure 60: Fixed-base Testing of Bushings: Instrumentation Sketch of Specimen in the Lab

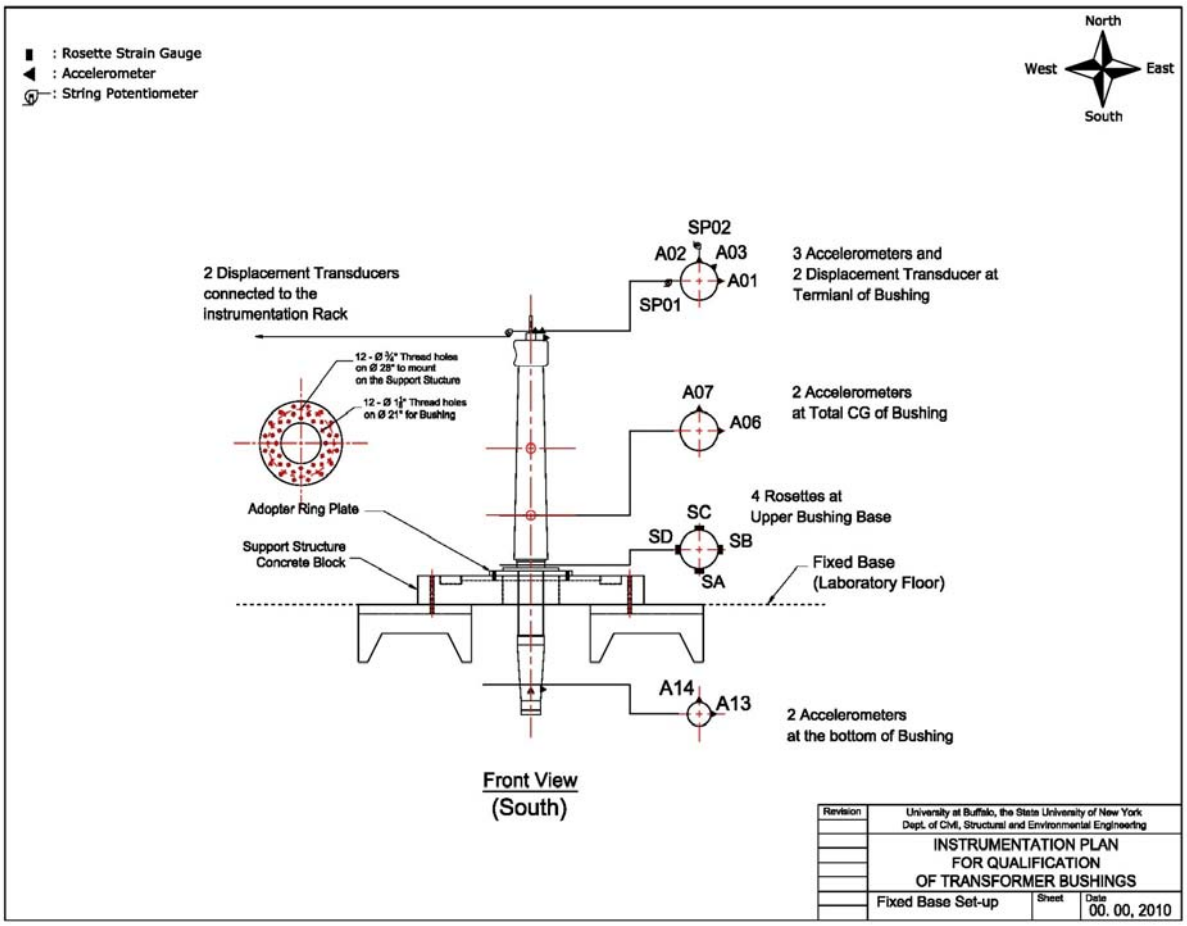

Figure 61: Top View of the Concrete Slab

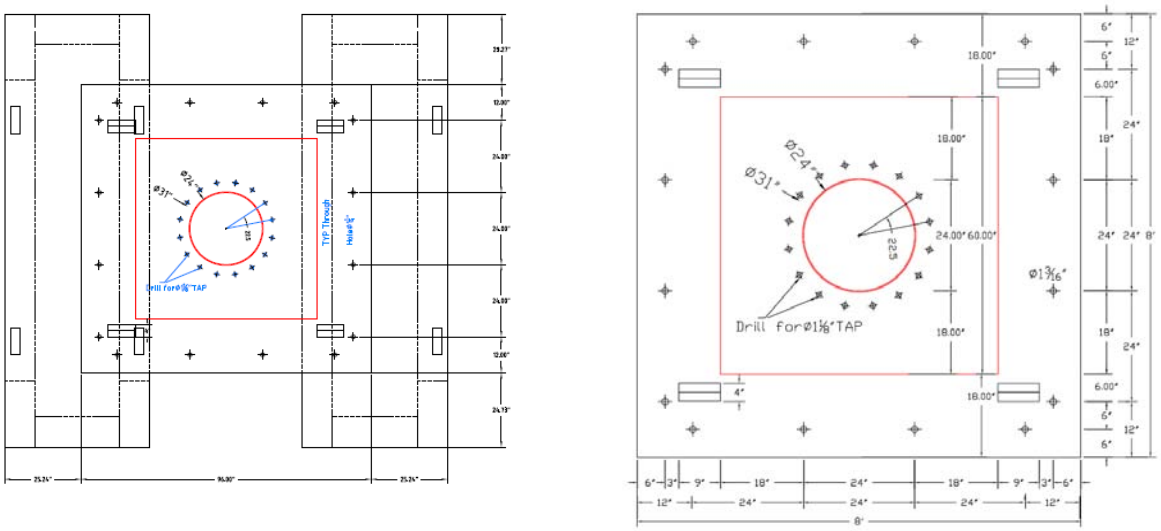

Figure 62: Concrete Block for Fixed-base Testing of Bushings

Figure 63: Base Plate Interfacing Support Structure to the Shake Table

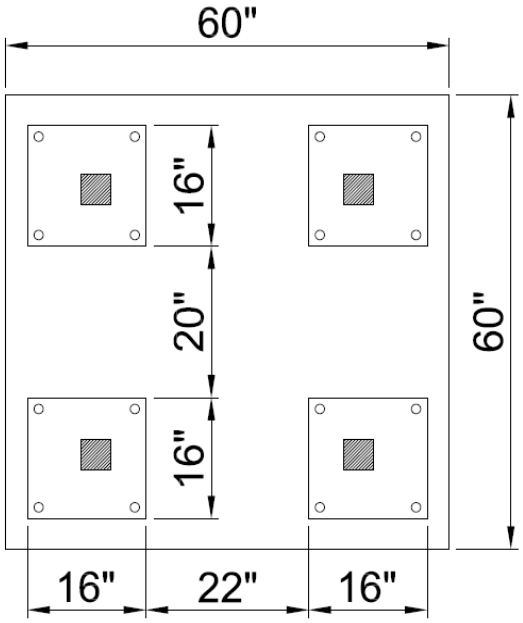

Figure 64: Flexible Support Structure for Shake Table Testing

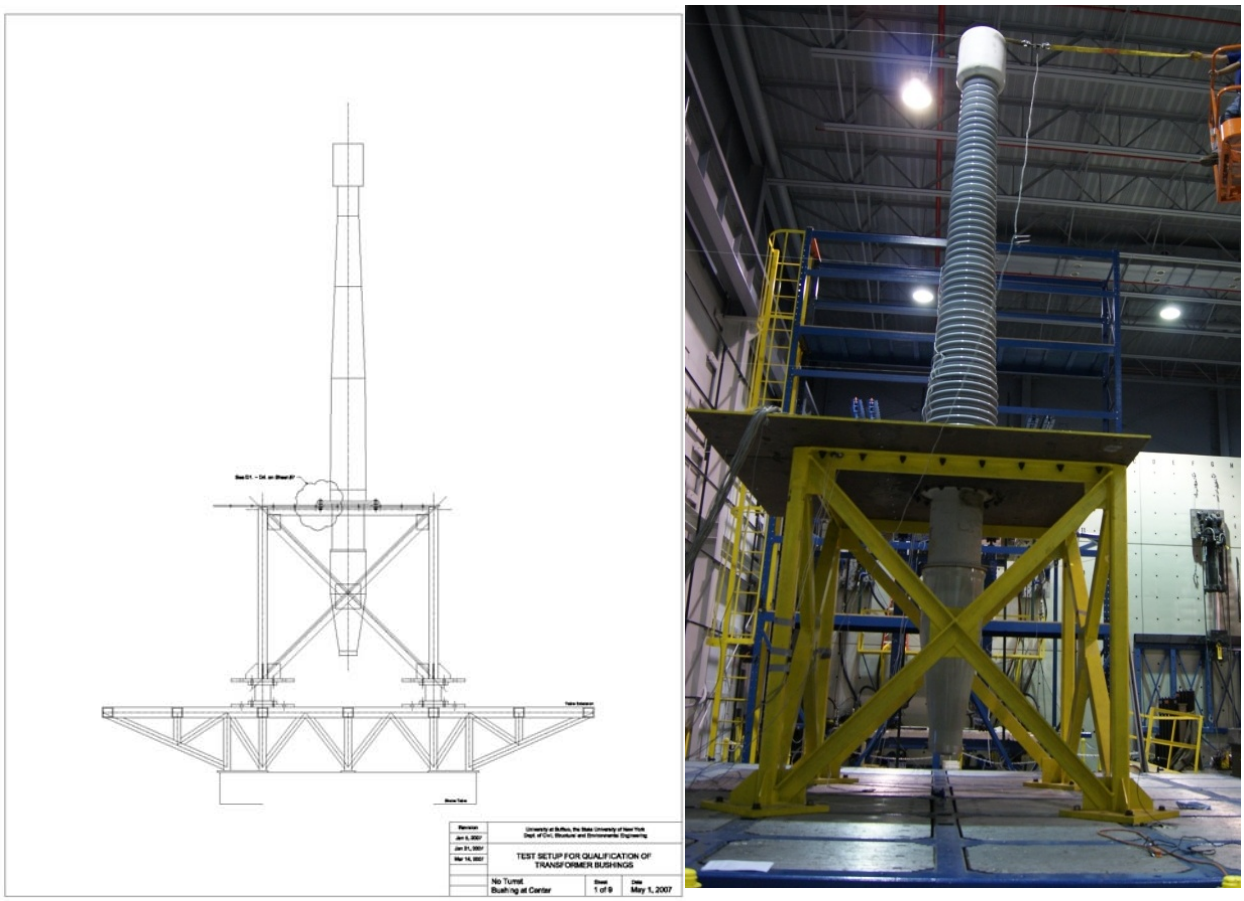

Flexible Cover Plate

The top plate is 24 inches longer and wider than the top plan of the support frame, as shown in Figure 67. It enables relocation of the bushing in the support frame by shifting the plate with respect to the sides of the frame. The top plate has additional bolt holes so that it will be firmly connected to the support frame for all cases of bushing relocation. By relocating the plate with respect to the support frame (legs) the hole can be placed alternatively in the center of the frame, at the middle, or in the corner. The alternative 1-inch or ¾-inch plates were analyzed prior to construction. From repeated analyses to find a proper thickness of the top plate, it was found that the ¾-inch thickness can cause a rocking motion or a vertical motion of the bushing while remaining in the elastic stress range. The top plate has a bushing mounting hole of 26.5″ diameter with two sets of bolt holes: a circle of 16 1-¼″ bolt holes on a 31″ diameter circle, for the direct mount of Bushings #1, #5, and #7, and a second circle of 16 1-¼″ bolt holes on a 33″ diameter for the turret mount. In any future research, the top plate can be replaced by a plate of other thickness if necessary.

Adaptor – Interface Plate

The bolt holes on the top plate and on the top flange of the turrets will fit only limited types of bushings (such as Bushings #1, #5 and #7). Other bushings have different bolt-hole patterns, so an

annular-shaped adapter plate was designed. This plate is shown in Figure 68. The inner diameter of the adapter plate is 17 in. and its thickness is 2 in. The adapter plate has four different bolt-hole patterns. The adapter plate should be installed on the top plate below the bushing mount flange.

Figure 65: Front Schematic of the Flexible Support Structure

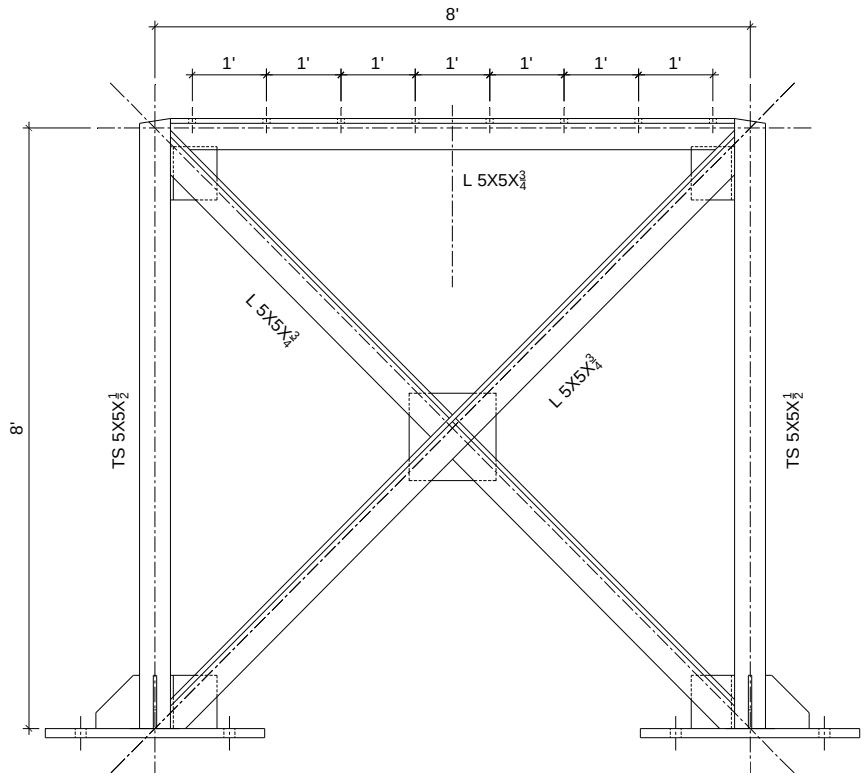

Figure 66: Re-locatable Top Plate

Turrets

Turrets are generally used to lift the mount of the bushing so that the bushing's immersed length in oil in the transformer tank can be reduced. Using a tilted turret can increase the physical separation between the heads of adjacent bushings to minimize the risk of arcing between conductors (flashover). Schematics of a vertical turret and a tilted turret, respectively, are shown in Figure 69. The height of both turrets is 17 in. at their center and the tilted turret is inclined by 20°. The turret cylinders are fabricated from ¾"-thick steel plate and their inner diameters are 25 in. The top and bottom flanges made from 1"-thick plate are welded to the cylinders and each flange is reinforced by 8-¾"-thick stiffeners. The bottom flanges of the two turrets have two circles of bolt holes on 31" and 33" diameters to accommodate the different sizes of bushings. Table 20 shows the different configurations of mounted bushings, with and without turrets.

Stiffening the Plate Cover

The top re-locatable plate is designed to be flexible. The flexibility of the plate amplifies the bushings' support motion. IEEE 693-2005 suggests that all qualification testing should be performed using rigid frames. In order to incorporate the flexibility of the transformer tank, a factor of 2 is introduced in the code to amplify the ground motions horizontally and vertically to simulate the tank amplifications; however this does not consider effects of cover plate flexibility. A series of tests was performed to investigate the difference in response between the rigid and flexible cover. In addition, a testing set-up was developed to check the effect of stiffening the cover plate. The re-locatable top plate has holes along the length and width of the plate on which stiffeners could be bolted. In the first study L6x4x½ sections were used, as shown in Figure 70. In a subsequent study using Bushing #6, the bushing was mounted at different locations with various stiffeners as shown in Table 21. Note that more bolt holes were necessary than those originally needed for this study, which were added to be able to mount stiffeners. Steel angle sections were

used to stiffen the plate. Two stiffeners (L8x6x½) were mounted on top of the plate, while smaller (L6x4x½) sections were mounted in a perpendicular direction under the plate. Stiffeners were installed in the two principal orthogonal directions to reduce the plate rotations and flexibility.

Testing Methods

Various testing techniques were used in this study in order to determine the structural and dynamic properties of the bushings and their response to dynamic conditions, as follows:

1) Identification of structural properties
   a) Pull test
2) Dynamic frequency searches
   a) Pull and quick release test
   b) Impact hammer testing
   c) Banded white noise test
   d) Sine sweep test
   e) Shake table impulse test
3) Dynamic Performance testing
   a) Random motion spectrum compatible
   b) Alternative motions spectrum compatible
   c) Historical ground motions – amplified
   d) Sine beat
   e) Sine resonant
   f) Spectrum compatible modulated sine sweep
4) Damping influences

Figure 67: Schematic of the Re-locatable Top Plate

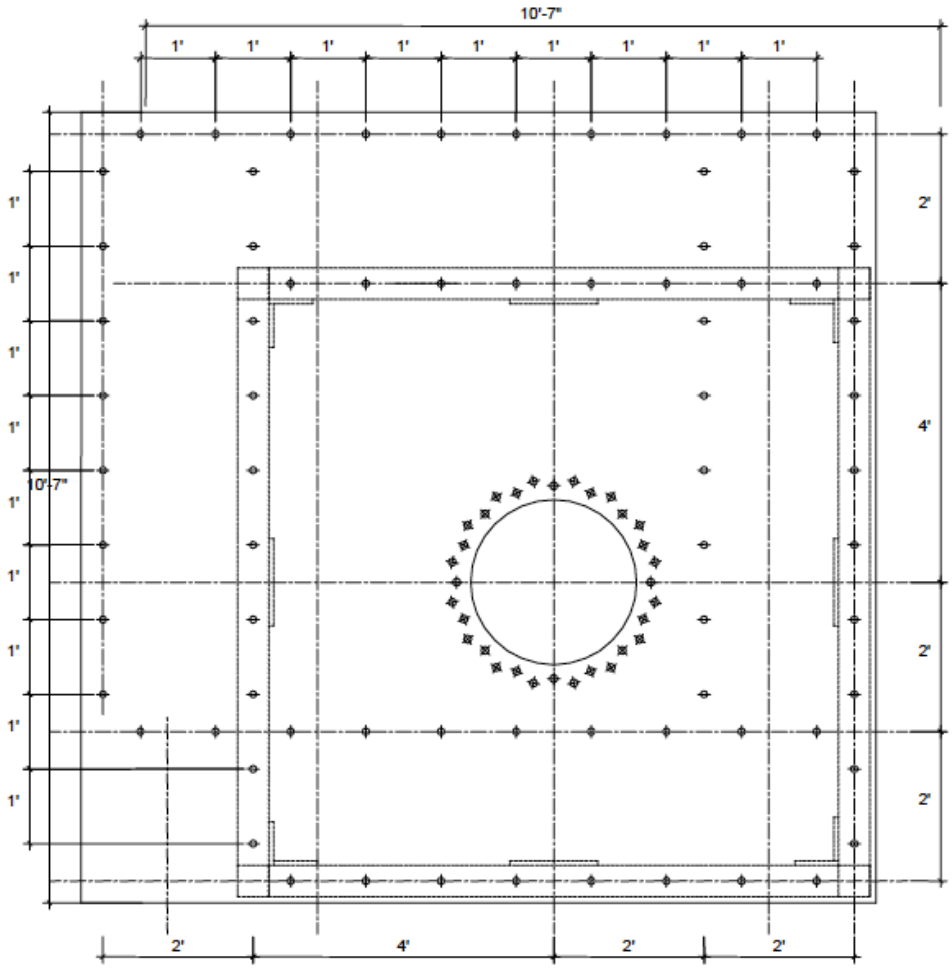

Figure 68: Bushing Adapter Plate

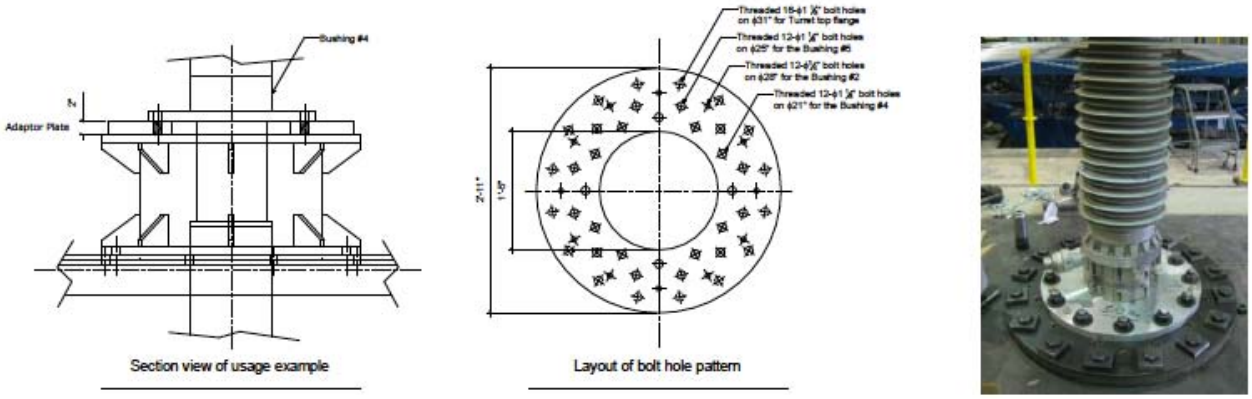

Figure 69: Turret for Flexible Frame

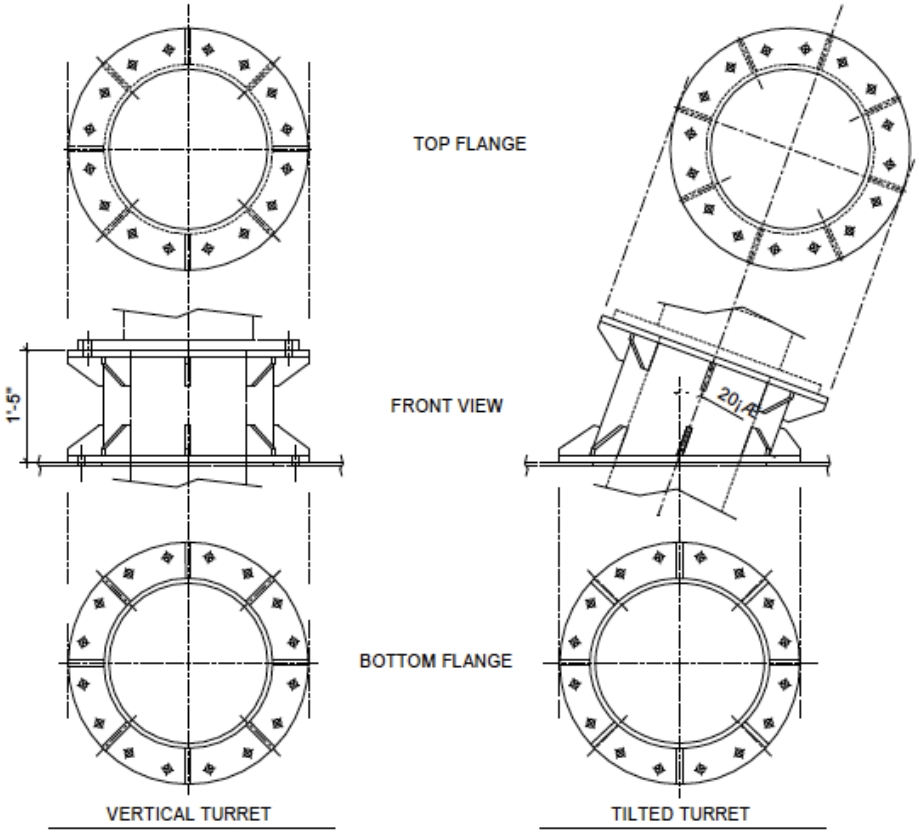

Table 20: Location of Bushing with and without Turret

	No Turret	Vertical Turret	Tilted Turret
Bushing at Center	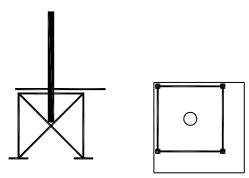	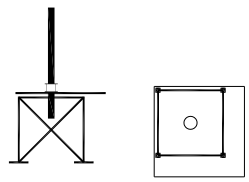	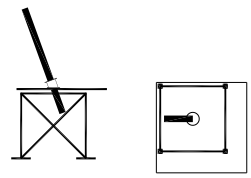
Bushing at Side	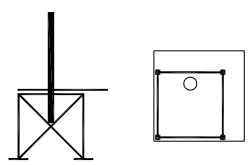	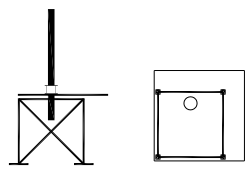	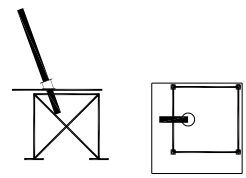
Bushing at Corner	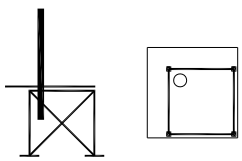	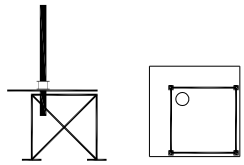	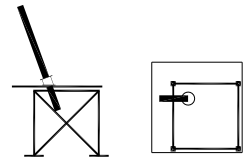

Figure 70: Stiffeners Mounted on Re-locatable Top Plate

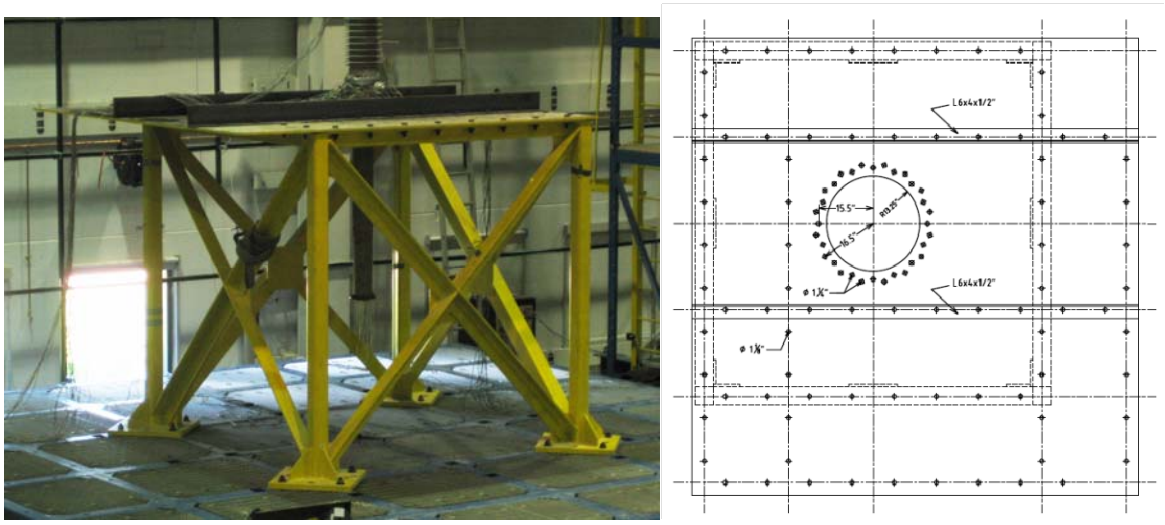

Table 21: Location of Bushing and Stiffeners

	Center	Side	Corner
No Stiffener	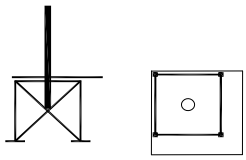	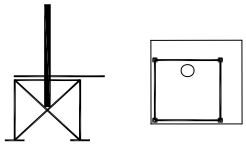	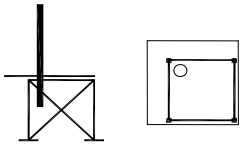
One Stiffener			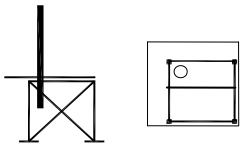
Two Stiffeners		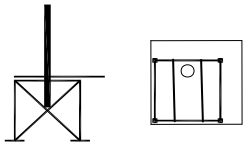	
Four Stiffeners	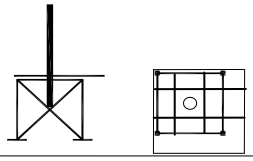		

Source: Koliou et al., 2010

Identification of Structural Properties – Pull Testing

The pull test is used to identify the structural characteristics of a test specimen: strength limits, flexibility/stiffness and rate of degradation. The tests that were performed also included sudden release of forces to determine the free vibration response of the bushings. This test provided the necessary information about the fixed base frequency and damping ratio of the bushings.

The pull test can be done within the elastic or plastic (piece-wise elastic) behavior of the bushings. If the elasticity of the structure is exceeded then the yield strength of the structure can be determined, but the deformation created cannot be recovered. Once the yield strength is exceeded, then that level should be used to determine the ultimate strength of the specimen.

The test set up is straightforward: The bushing is attached to the rigid concrete base, instrumented with accelerometers and displacement transducers attached to the structure, and then loaded applying a horizontal force to the structure, inducing a horizontal displacement (see Figure 71).

Controlled Pull Testing (Rate Loading)

The rate controlled pull testing is performed to observe the stiffness, the strength, and the energy dissipation in the bushings. The controlled pull testing was performed both in elastic and in plastic range (beyond the elastic range), up to failure.

The test setup consisted of a bushing attached to a rigid concrete block, instrumented with potentiometers and accelerometers attached to the bushing and pulled using a tensioning device or the actuators of the adjacent shake table (through the rigid frame attached to shake table). The shake table actuators or the pull actuators are programmed to produce a modified half sine wave of varying magnitude. A one-cycle cosine wave deflection (pull test) is to be applied to a stiffly supported cantilever specimen. The duration of the applied deflection should be determined depending on the material (e.g., for composites used in the electrical industry, the duration is about 5 seconds). The normalized shape of the load function applied with the actuator is shown in Figure 72.

The analytical expression for the load function is given by the following equation:

$$F = \frac{1}{2}\left(1 - \cos\left(\frac{2\pi}{AQR} T_n\right)\right) \tag{7}$$

where AQR = acquisition rate, and T_n = duration of applied function.

Depending on the height of the bushings, either the Non-structural Component Simulator (NCS) or the rigid frame mounted on shake table can be used to perform the controlled pull test. Figure 73 shows the NCS pulling the top of the bushing in the east-west (EW) direction.

Dynamic Frequency Searches

Pull and Quick-release Test

Following a pull test, a simple test called the Quick-release Test can be performed, by suddenly releasing the tension applied on the bushing by the pull test. The quick release induces free vibrations that can be used for identification of the frequencies and inherent damping of the

bushing/transformer system. Accelerometers and potentiometers are attached at the top of the bushing, at the point of interest. The acceleration is used to determine the time domain response of the bushings. The quick-release tests in this project were done in conjunction with the pull tests described above. For this test, the bushings were mounted on the rigid concrete slab. Figure 74 shows a quick release test being performed.

Figure 71: General Test Setup for a Pull Test

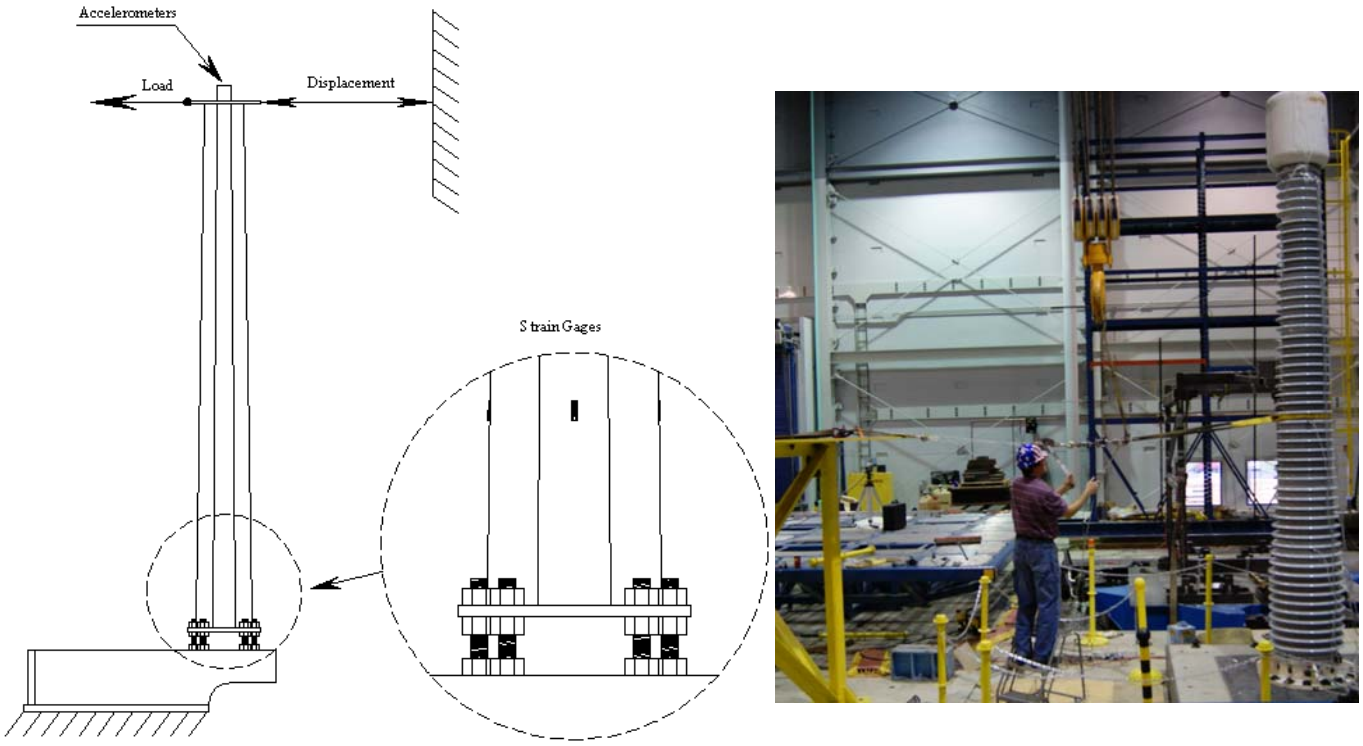

Figure 72: Load Function for the Pull Test

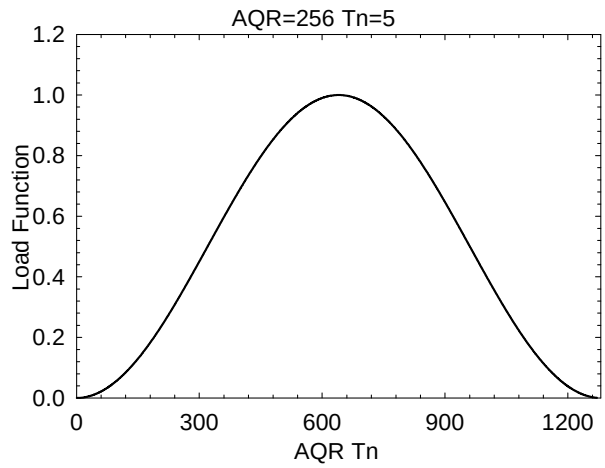

Figure 73: Non-Structural Component Simulator (NCS) Used to Pull the Top of the Bushing

Impact Hammer Testing

In this test, the bushings are gently hit with a hammer, which imposes an impulse leading to free vibrations, from which the dynamic properties of the bushing are derived. The testing procedure for an impact hammer test uses an instrumented bushing with an accelerometer at a high location. In the tests performed in this study, the accelerometers were placed at the terminal points of the bushings. A typical setup for the impact hammer test is shown in Figure 75. The impact hammer test usually excites all the dominant modes and hence gives very good estimates of the bushing frequencies.

The specimen (with the load cell attached) is struck with the hammer, and the accelerometer measures the acceleration response of the specimen. This step is repeated several times and the average of the tests is taken as the result. This repetition in steps is to allow for variations in the force of the various strikes. An example of the impact force and specimen response is shown in the top graph of Figure 76, which indicates the frequency of the bushing and shows the damping of the excited frequencies, i.e., the rate at which the bushing response is attenuated over time. The bottom graph shows the Power Spectral Density (PSD) of the bushing response. In this example, the 2nd mode, at a frequency of about 29 Hz, is more pronounced than the 1st mode at about 5 Hz. Half-power bandwidth was used to estimate the damping of bushings.

Banded White Noise

The frequencies can be obtained by applying a base motion containing significant input within a frequency bandwidth. In the beginning of the test sequence one test was always run to determine the natural frequencies and damping ratios while at the end of each series another test was conducted to see if there was any damage to the bushings. Any shift in the frequency was a proof of stiffness reduction potential damage to the bushing, without identifying its source or reason. The frequencies and the damping ratios were determined from transfer functions calculated following the testing.

Figure 74: Quick-release Test Performed on Fixed Base

Figure 75: Impact Hammer Test

Figure 76: Typical Acceleration Response and Power Spectral Density (Bushing #5)

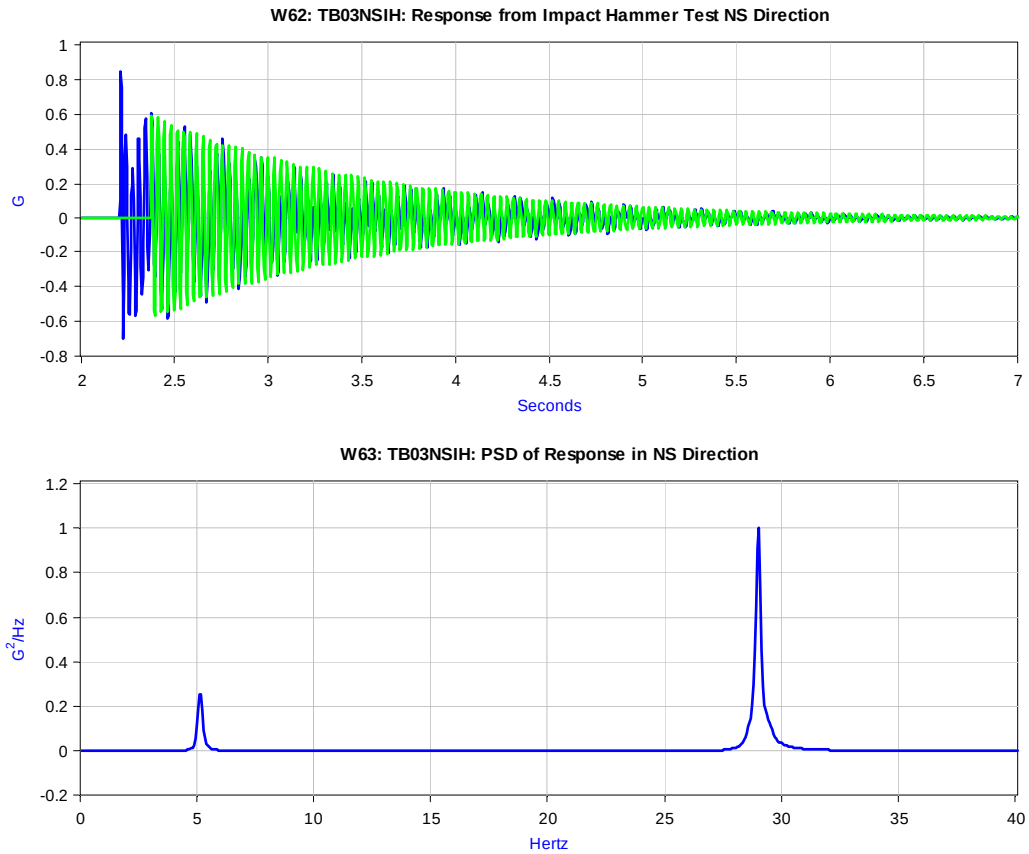

Resonance Search Tests

Resonance search tests consisting of an acceleration-controlled, low-level (0.1 g peak nominal or sometime smaller due to the sensitivity of the equipment) white noise excitation were used to characterize each bushing's natural frequencies and damping characteristics. The white noise consisted of frequency content from 1 Hz to 50 Hz with 80 sec. duration. Both longitudinal and transverse directions were tested individually. In order to avoid any damage to the test unit, peak acceleration and duration of white noise test was determined. A plot of a white noise time history test is shown in Figure 77 for Bushing #8.

A banded white noise has all the required frequency content such that the power of each frequency in the band is the same. The auto-correlation function of white noise is a Dirac Delta function, meaning the signal is uncorrelated in time. By definition the white noise must have a flat spectrum. To find the frequency and damping ratio, a transfer function was derived from the shake table to the top of the bushing. The horizontal axis of the peak indicates the dominant frequency of the bushing-support setup and the spread of this figure shows the damping ratio. A half-band method was used to estimate the damping ratio. Figure 78 shows the transfer functions for Bushing #5 in the north-south (NS) direction.

Table Impulse (New) – Shake Table with Controlled Motion

A better identification is obtained by applying a short half harmonic at or near a characteristic frequency of the bushing. Experience has shown that applying a short harmonic pulse at 0.5 Hz or 1.0 Hz below the searched frequency obtains a good resolution of dynamic response at the resonant frequency. The impulse is a table displacement as shown in Figure 79. A series of such pulses was generated by using a smooth impulse procedure developed at the University at Buffalo (SEESL) (Kong, 2010).

Figure 77: Typical White Noise Acceleration History Record (Bushing #8)

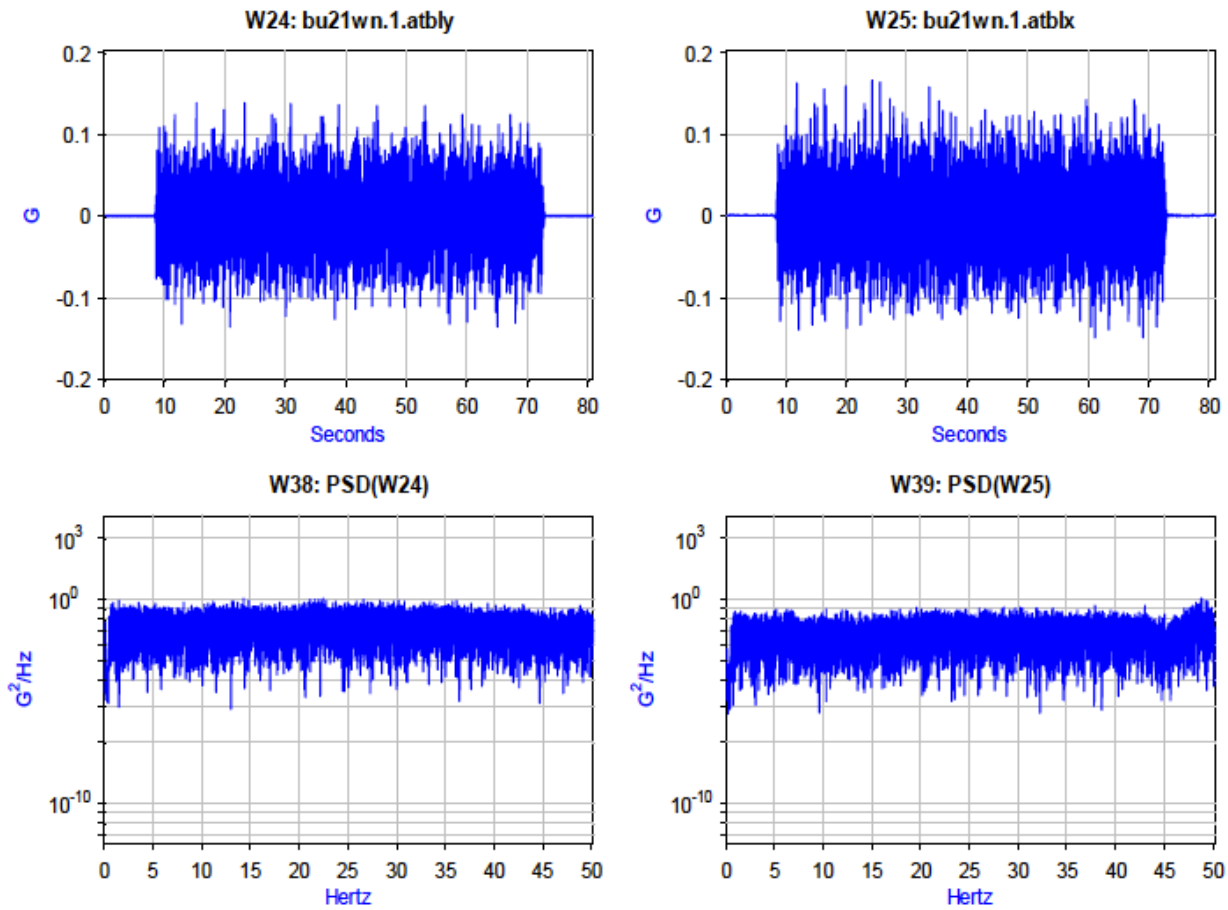

The smooth table acceleration impulse was generated by the double differentiations of the displacement impulse shown in Figure 79 and further shown in Figure 80. Several response power spectral densities (PSD) are presented in Figure 81. The figure indicates the frequency and damping ratios.

Sine Sweep for Frequency Search

Usually sine sweep is used for tracking dynamic properties of structures. A sine sweep is a continuous sinusoidal curve with a continuously varying frequency. Equation (8) shows a

fundamental equation of a sine sweep function with unit amplitude of 1 (Reinhorn and Oikonomou, 2010).

$$S(t) = \left[\sin\left\{ 2\pi f_0 * \frac{t_0}{\log 2} * \left(2^{\frac{t}{t_0}} - 1 \right) \right\} \right]_{t=0}^{t=t_1} \tag{8}$$

where: f_0 = starting frequency (Hz); $f_1 = f_0 * 2^{(N_O ct)}$: end frequency (Hz); $N_{Oct} = t_1 / t_0$: number of octaves; t_0 = sweeping rate (seconds per octave); and t_1 = end time (seconds).

Figure 78: Magnitudes of Transfer Functions in Various Channels (Bushing #5)

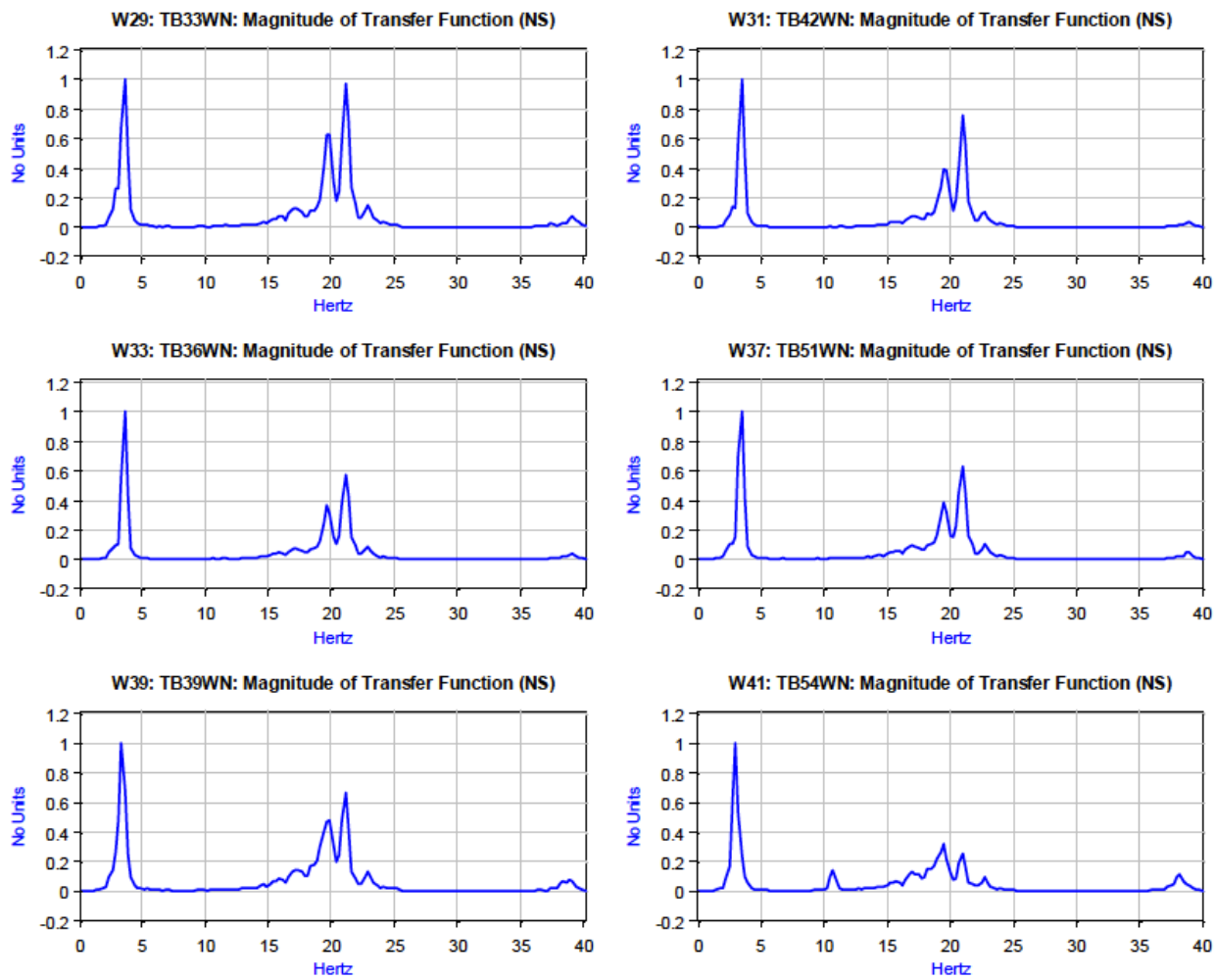

Figure 82 shows a sample of sine sweeps generated using the following parameters. The frequency axis is shown below the time axis. The starting frequency is 0.55 Hz and the center frequency doubles every 10 seconds, which is the sweeping rate. (Note that the range in which the frequency doubles is called an octave; therefore the sweeping rate is better defined in terms of time to sweep

an octave, i.e., seconds per octave). N_{oct} = 6 = number of octaves; t_0 =10 = sweeping rate (seconds per octave); f_0 = 0.55 = starting frequency (Hz); $f_1 = f_0 * 2^{N_{oct}}$ = 35.2Hz = end frequency (Hz); sampling rate = 256 Hz.

Figure 79: Smooth Table Impulse

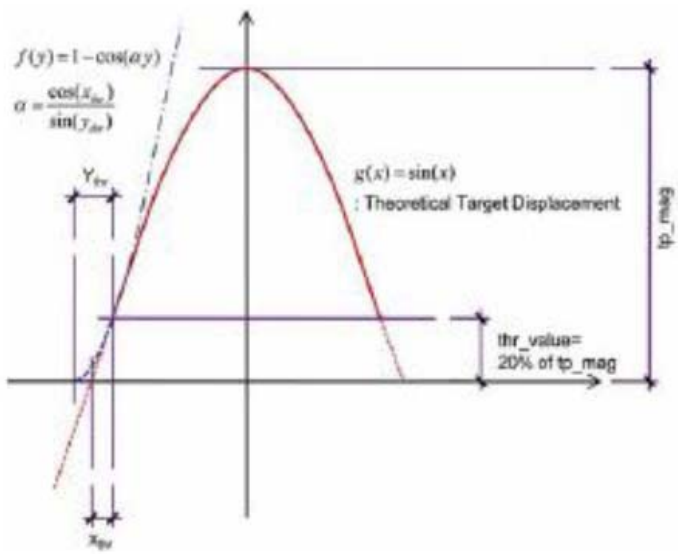

Figure 80: Operational Movement of the Table Impulse

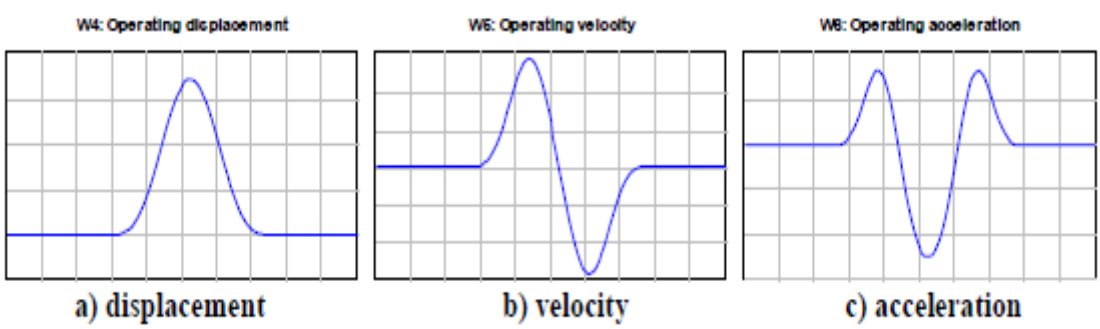

The time axis and the corresponding frequency axis have the following relation:

$$\log f_i = \log f_0 + \frac{\log 2 * t_0}{60} t_i \tag{9}$$

where: f_0 = starting frequency of the sine-sweep function (Hz), f_i = frequency corresponding to t_i (Hz), t_0 = sweeping rate (seconds per octave).

Figure 81: Typical Power Spectral Densities from Table Impulse Test (Bushing #5)

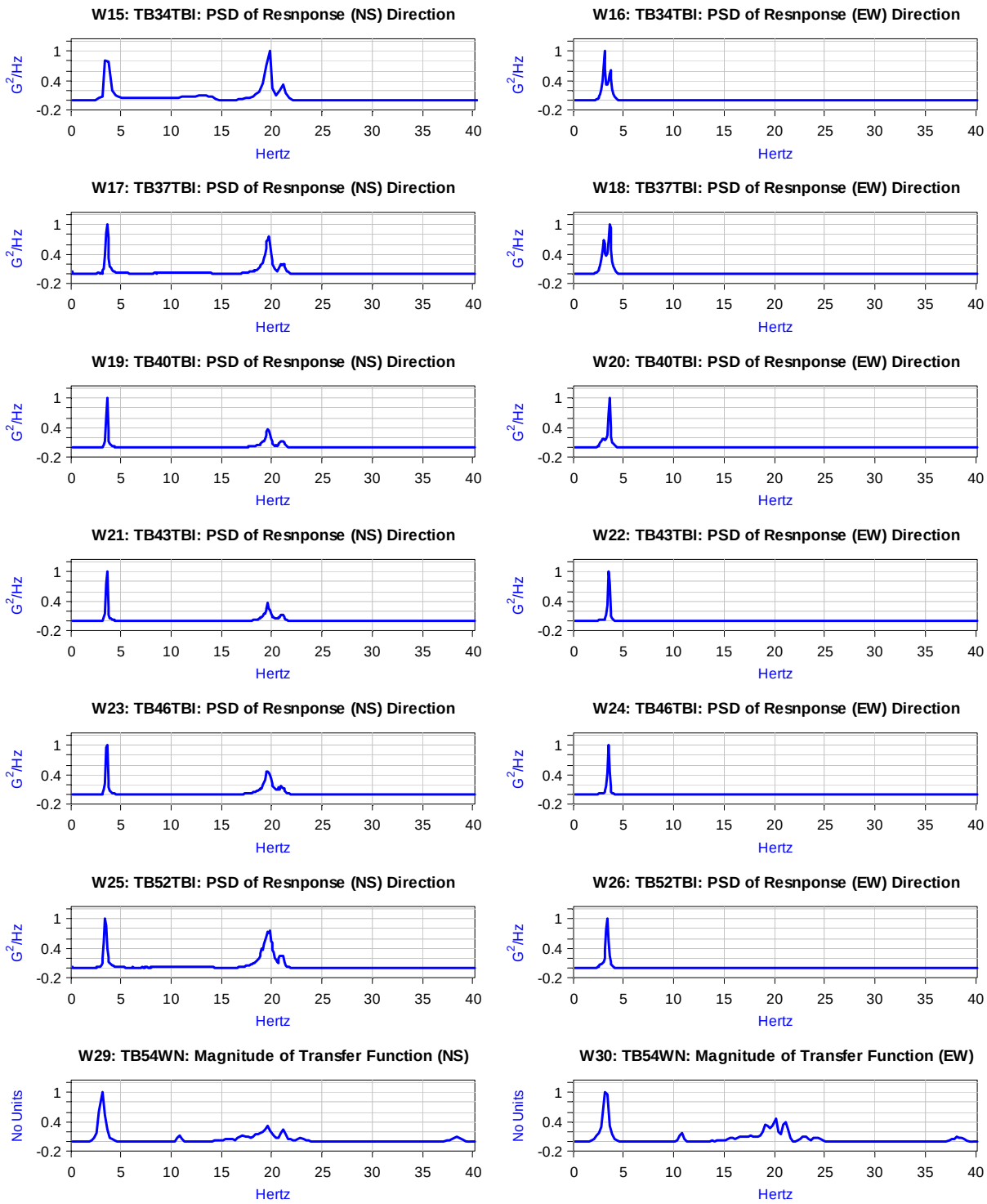

Figure 82: Sine Sweep Wave of Uniform Amplitude

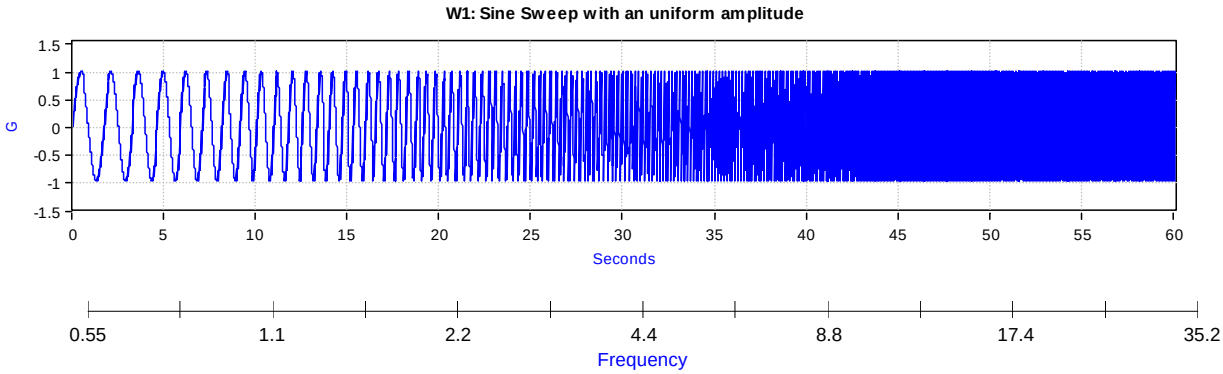

Dynamic Performance Testing – Simulated Earthquakes

Simulated earthquake ground motions were used to study the seismic performance of the transformer bushings. The following sections describe the procedure to develop earthquake histories and laboratory testing. The motions used in testing are either (1) prerecorded accelerograms from earthquake motions, (2) simulated accelerograms compatible to the spectral requirements of IEEE 693, (3) accelerograms of real earthquakes modified to fit the spectral requirements of the Standard, or (4) modulated sine sweep motions to fit the spectral requirements of the Standard.

Requirements for Input Acceleration History

IEEE 693 recommends, "The input motions shall have duration of at least 20 seconds of strong motion. The acceleration ramp-up time and decay time shall not be included in the 20 seconds of strong motion." The filtered theoretical input motion should be within tolerance limits of –5%/+30% of a required response spectrum (RRS). The RRS is generated using the following equations:

$$S_a = 1.144\beta f \qquad 0.0 \le f \le 1.1$$

$$S_a = 1.25\beta \qquad 1.1 \le f \le 8.0$$

$$S_a = \frac{(13.2\beta - 5.28)}{f} - 0.4\beta + 0.66 \qquad 8.0 \le f \le 33.0 \tag{10}$$

$$S_a = 0.5 \qquad f > 33$$

where: $\beta = \dfrac{(3.21 - 0.68\ln(d))}{2.1156}$, and d is the percentage of damping, with the limit $d \le 20\%$.

A typical RRS for zero period acceleration (ZPA) of 0.5 g, as required by IEEE 693, is shown in Figure 83.

Figure 83: Required Response Spectrum for 0.5 g ZPA

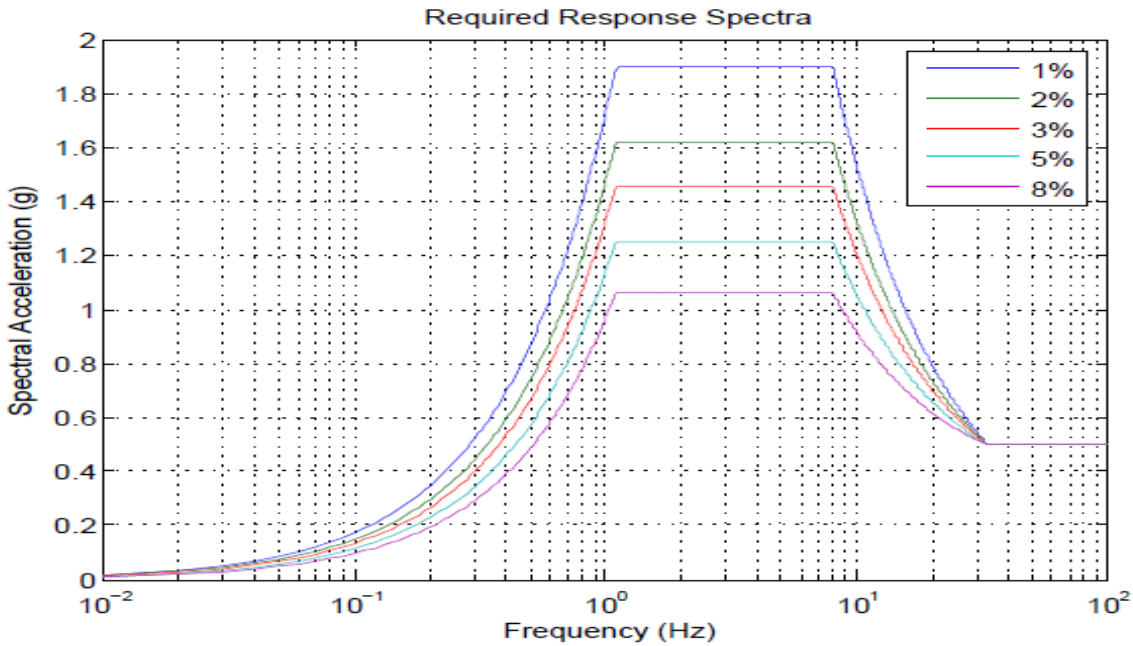

Spectrum-compatible Accelerograms

Input motion is generated using MTS Systems' Seismic Test Execution (STEX) software, which manages signal generation, data acquisition, data analysis, data files, and test operation of MTS earthquake simulators. Earthquake signals may be modified from a menu of filters with various editing and scaling functions. Earthquake signals can be modified to conform to a target response spectrum by iterative scaling of the Power Spectrum Density using traditional simulation software similar to SIMKQE (Gasparini and Vanmarcke, 1976). The earthquake and target response spectra are compared and the differences used to determine the scaling of the Power Spectral Density. This method results in stationary waves being scaled, added and subtracted to the original signal. Alternative procedures are developed similarly to these, as indicated below.

Developments in recent years of high-speed digital processors have resulted in large advances in the use of digital control for improved performance in earthquake simulators. MTS has used adaptive inverse control and online iteration methods to improve the responses of both new and old earthquake simulators. While the adaptive techniques are superior to older methods, they also produce reference accelerograms operated in open-loop mode that are only approximations of the desired signals.

Typical accelerograms obtained using STEX are shown in Figure 84 along with the TRS and the RRS. Note the fitting of TRS within the limits applied to the RRS. Note also that the accelerations are multiplied by a factor of 2 as required for the simulation of the tank cover accelerations. The acceleration histories, and corresponding TRS compared to the RRS, for all tests and all bushings, are provided in Appendix A.

Figure 84: Typical Test Accelerograms for Compatibility to 0.5 g ZPA RRS (Bushing #4B)

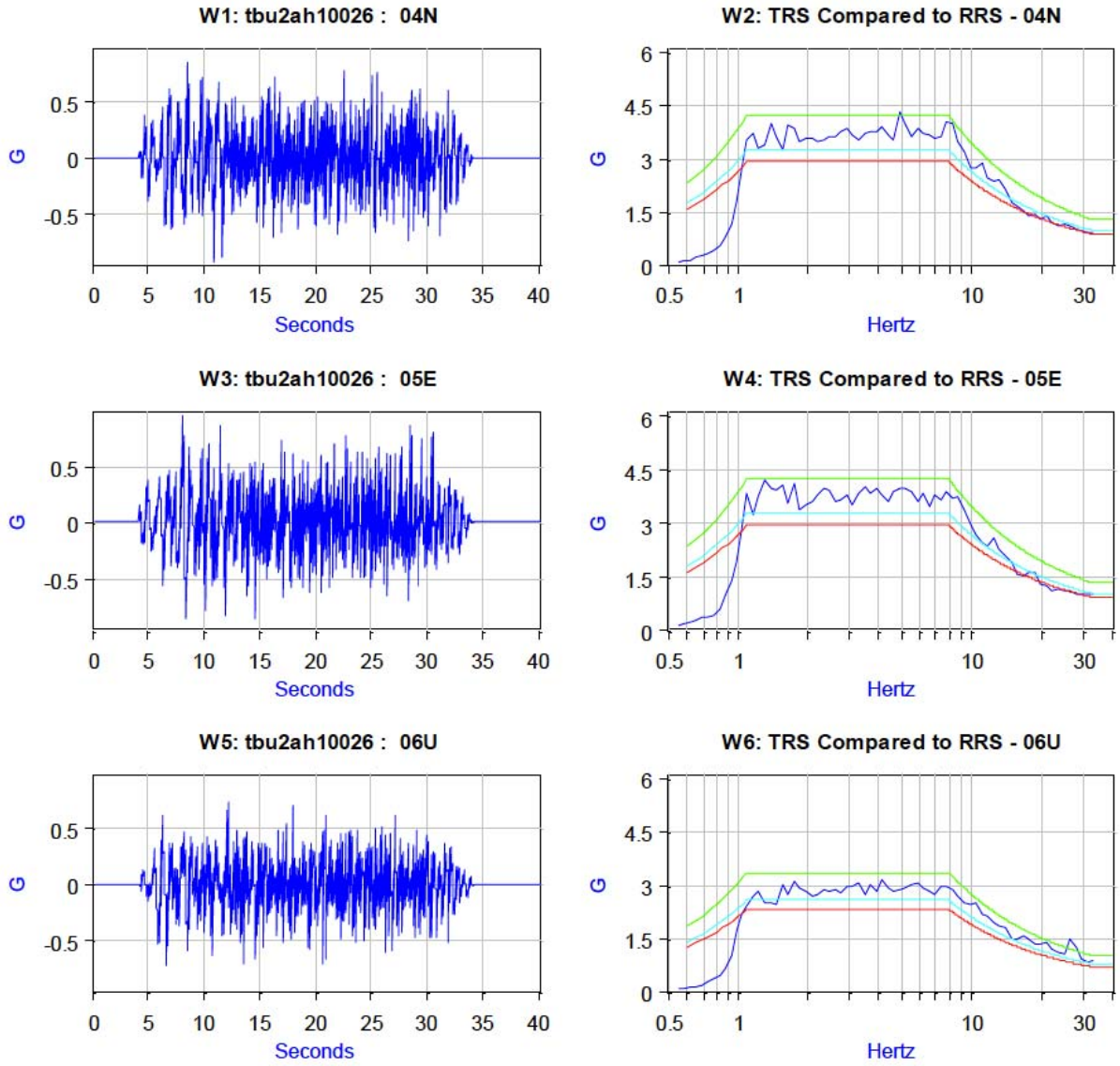

Alternative Procedure for Spectrum-compatible Accelerograms

An alternative procedure of matching an existing accelerograms (input motion) to a desired RRS consists of adapting the response spectrum using "notch filters" to correct specific frequencies, iteratively. The procedure consists on picking up the frequency at the peak point to be scaled to RRS. To reduce the peak a notch filtering function in the frequency domain is calculated with center frequency of the peak point. Then the factor of the notch function to RRS at the center frequency is calculated (see Figure 85), which is 1.62/2.52 = 0.625.

Figure 85: Calculating the Factor at the Center Frequency

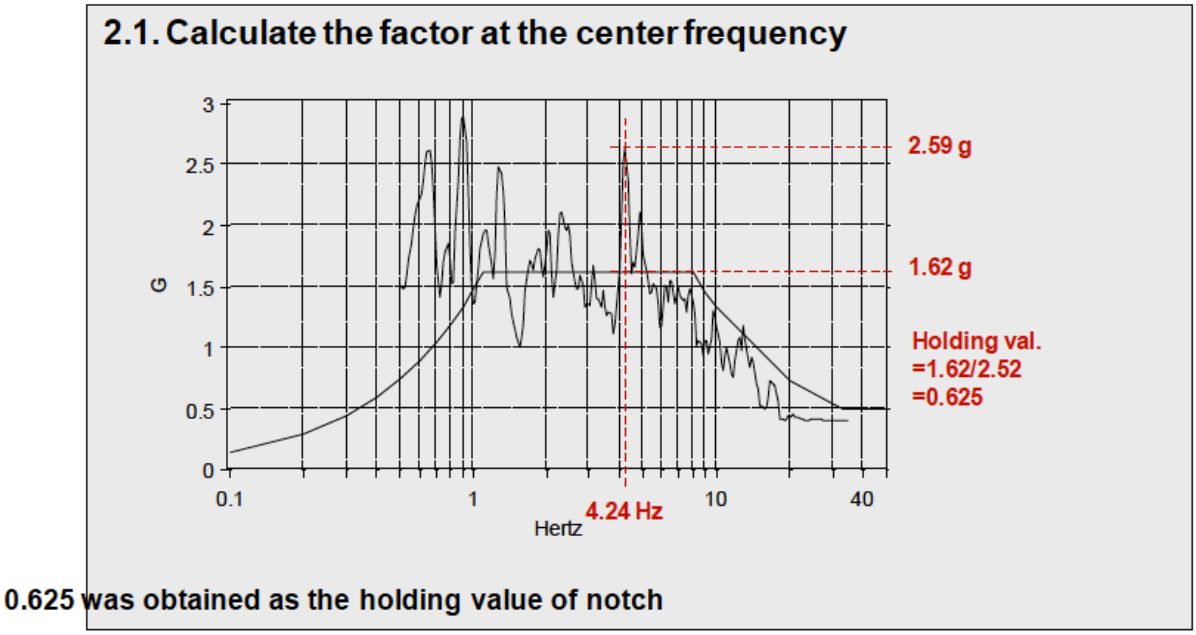

Source: Kong, 2010

A notch filtering function is developed (in frequency domain) and is multiplied with the acceleration records. The motions are then re-scaled. The process is repeated until spectrum compatible acceleration history is achieved. A spectrum fitting the desired 0.5 g RRS obtained according to this procedure is shown in Figure 86.

Historical Ground Motion Ensembles

In addition to the spectrum-compatible accelerograms, several tests were performed with Bushing #6 using past accelerograms bundled in two ensembles. The two ground motion ensembles were selected for performing linear dynamic time analyses of the transformer models in order to determine the motion on the tank cover required for the evaluation of the bushings.

The same motions used in the numerical study were also used in the experimental study after further scaling. The first ensemble contains 20 ground motions that were recorded within the California region (Filiatrault and Matt, 2005). All ground motions are such that the location of the measurement was far enough from the fault rupture to be free of any near-fault directivity pulses. The second ensemble selected in this study is the unscaled (original) motions of the FEMA P695 Far Field Ground Motion Set (FEMA P695, 2009), which contains 22 ground motions with two horizontal components each, recorded at the same station. Information about the earthquake events was described in Chapter 2 and is presented in Tables 10 and 11 for Ensemble 1 and Ensemble 2, respectively; and Figures 20 and 21 showed the IEEE 693 Spectrum with 2% damping, with overplots of scaled median and geometric mean spectra of Ensemble 1 and Ensemble 2, respectively.

Figure 86: Acceleration History and Spectrum Before and After Trials

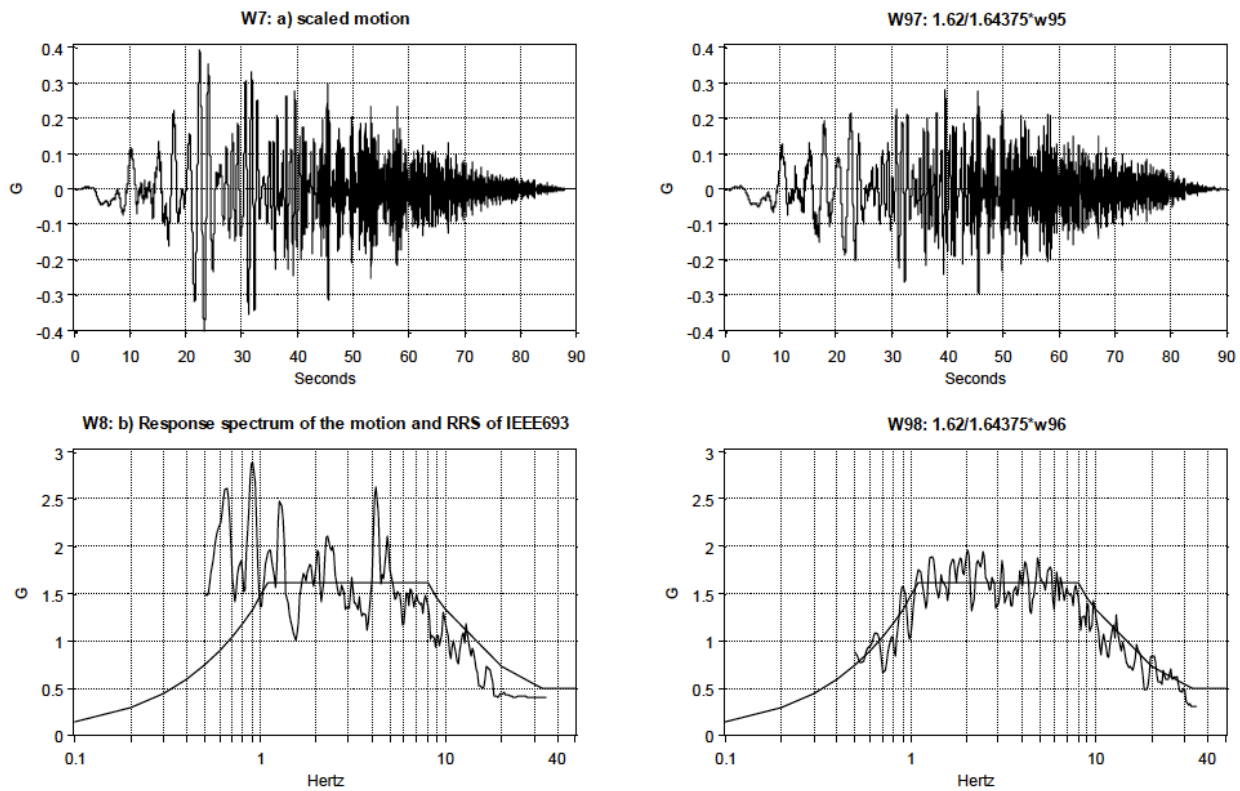

Source: Kong, 2010

Sine Beat

According to IEEE 693, "A sine beat motion consisting of a sinusoid of the equipment resonant frequencies modulated by a lower frequency sinusoid that provides at least 10 cycles of resonant frequency per beat shall be applied to the equipment and supports. There shall be a minimum of five such beats of the resonant frequency, with a pause between bursts long enough so that there will be no significant superposition of motion. The 10-cycle sine beat test shall be performed at the predominant resonant frequencies found in white noise test, once in each of the three orthogonal axes. Sine beat testing shall be run at the specific input value in the horizontal axes, each simultaneously and in phase with 80% of the specified value in the vertical axes at the predominant frequencies found in the horizontal directions. Sine beat tests should also be run at 80% of the specified value in the vertical axis at the predominant frequencies found in the vertical axis. If no predominant frequencies are found in the vertical axis below 34 Hz, then no test will be required for the vertical direction."

A typical sine beat graph is shown in Figure 87. Actual input will have some time delay between two consecutive beats so that any residual vibration may damp out.

The sine beat was generated with the following relation:

$$sin_{beat} = A_o \sin(2\pi ft) \times \sin(0.1\pi ft) \tag{11}$$

where A_o is the peak acceleration and f is the predominant frequency tested.

Figure 87: Typical Sine Beat Record

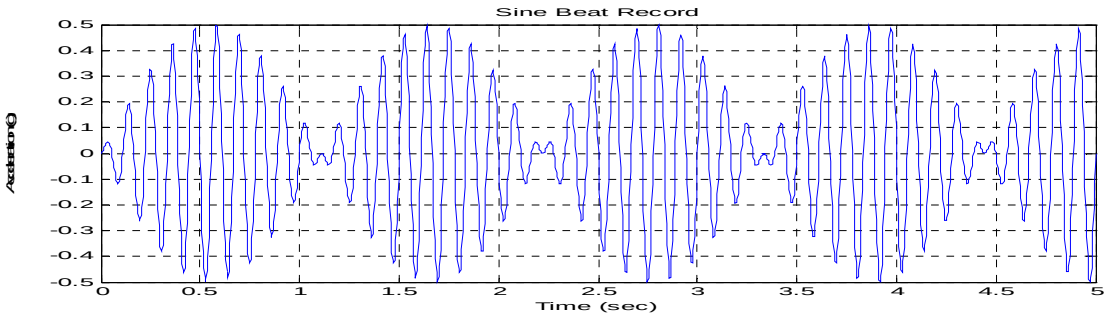

The second term in the above equation ensures that there are 10 cycles in each beat, and A_0 is the magnitude of the signal, which may vary from 0.25 g (low seismic level, LSL), 0.5 g (medium seismic level, MSL) to 1.0 g (high seismic level, HSL).

Sine-resonant

At low frequencies it is very difficult to meet the requirements of the IEEE spectra, due to excessive displacement requirements from the testing equipment. A procedure was developed to perform resonant cyclic tests to meet the IEEE 693-2005 Standard at discrete low frequencies. The electrical equipment was then tested to one cyclic (sine) test in each of the horizontal directions for the resonant frequency.

A displacement history record for the resonance tests was generated at SEESL at the University at Buffalo. The test motion record can be generated based on the expected displacement response for a resonant excitation (see Figure 88):

$$\frac{u(t)}{u_{so}} = \frac{1}{2\xi}\left(e^{\xi\omega t} - 1\right)\cos(\omega t) \quad , \tag{12}$$

where u_{so} is the input amplitude, ω is the resonant frequency and ξ is the expected damping ratio. The expected acceleration and velocity are calculated by taking derivatives of the displacement. The velocity is therefore:

$$\frac{\dot{u}(t)}{\omega u_{so}} = \frac{1}{2\xi}\left[e^{-\xi\omega t}\left[-\xi\omega\cos(\omega t) - \omega\sin(\omega t)\right] + \omega\sin(\omega t)\right] \tag{13}$$

and the acceleration is:

$$\frac{\ddot{u}(t)}{\omega^2 u_{so}} = \frac{1}{2\xi}\left[e^{-\xi\omega t}\left[(\xi^2\omega^2 - \omega^2)\cos(\omega t) + 2\xi\omega^2\sin(\omega t)\right] - \omega^2\cos(\omega t)\right] \tag{14}$$

Figure 88 shows the amplitude of the resonant acceleration for this unit. The required amplification was also based directly on the above calculations, such that sufficient acceleration is

developed to match the RRS at the resonant frequency. The number of cycles required to reach (or exceed) the desired amplification are determined from the plot.

Modulated Sine Sweep Function

Usually the sine sweep is used for tracking dynamic properties of structures. In this work a sine sweep was modulated to match an arbitrary required response spectrum (RRS) for electrical equipment (such as required by IEEE 693). Subsequently, several methods of matching were proposed, developed and investigated: (i) a direct Response Spectrum (RS) matching, (ii) a Power Spectrum Density (PSD) matching, (iii) Fast Fourier Transform (FFT) matching, (iv) a Time Domain Modulation, and (v) a Multiple Gradients Time Domain Modulation. These methods are intended to provide adequate performance and ease of simulation in a variety of laboratory settings.

Figure 88: Response to Resonant Sine Wave

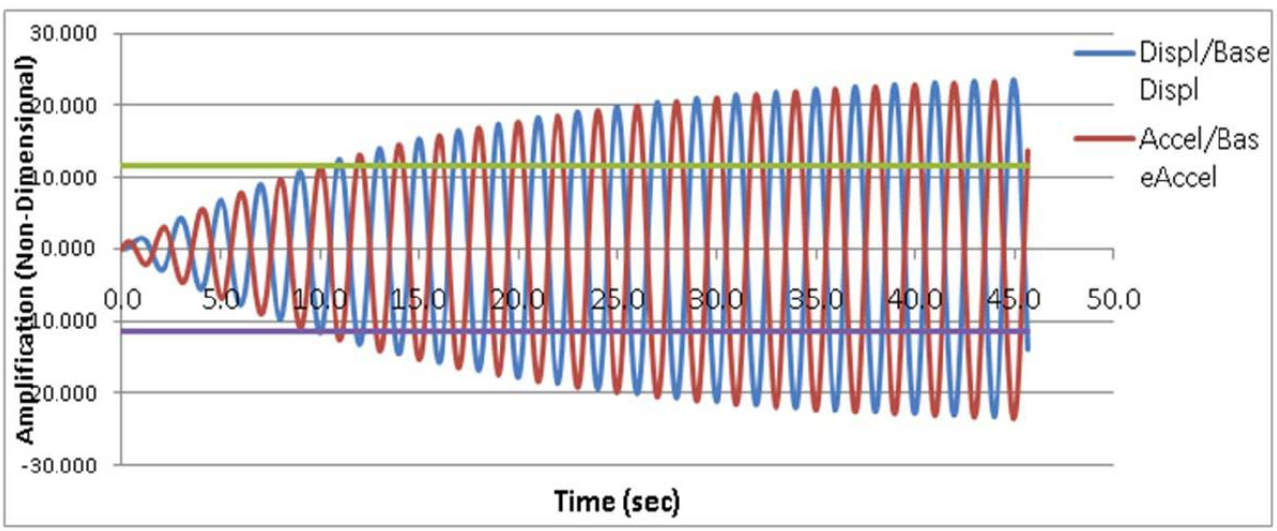

A series of sine-sweep functions with varying sweeping rates was generated to envelop a required response spectrum by the new method developed for this study. The effects of the sine sweep functions used as input ground motions in numerical analyses were compared with the effects of 20 random acceleration histories used also as input ground motions in the analyses. Several alternative shapes of sine sweep are developed herein and used as input ground motions for numerical analysis.

Matching Sine Sweep to a Required Response Spectrum

The procedure of modulating the random amplitude generating a response spectrum enveloping the required response spectrum is described as follows.

Modulation of the sine sweep is obtained by changing the amplitude at various times to fit the modulation function. The equation for a sine sweep with random amplitude is basically the same as Eq. (8), except for the modulation function, $A(t)$:

$$S(t) = A(t) * \sin\left\{2\pi f_0 * \frac{t_0}{\log 2} * \left(2^{\frac{t}{t_0}} - 1\right)\right\} \tag{15}$$

Response Spectrum (RS) Matching

An alternative method to modulate the amplitude function is using the ratio of the response spectrum of the sine sweep to the RRS in an iterative procedure. This is referred to as the Response Spectrum Matching (RS matching). Basically, the matching function needs iterations to obtain adequate results. Eq. (16) shows the basic formulation used in the iterations. In the RS matching, an (i+1)th sine-sweep function is obtained by multiplying the ith sine-sweep function with the modulation function, defined as the ratio of the RRS to the response spectrum of the ith sine-sweep function:

$$SW_{i+1}(t) = \frac{RRS}{RS_{SW_i}} * SW_i(t) \tag{16}$$

where, RRS = Required Response Spectrum (RRS), SW_i = sine-sweep obtained in ith iteration, and $RS_{SW\mathrm{i}}$ = response spectrum of the ith sine-sweep function. An example of this method is shown in Figure 89.

It is observed that the response spectrum of the sine sweep, after each iteration, is continuously diverging from the desired RRS, as the iteration to find new sine sweeps is repeated. Moreover, although the sine sweep (SW_1) after the first application of the RS matching has continuous sinusoidal curves over all time ranges, the last sine sweep (SW_5) has almost zero acceleration around certain time ranges, such as around 12, 21, 32 and 51 seconds. Although the method of response spectrum match shows very quick convergence onto the desired RRS, the repeated application also causes divergence from the desired RRS.

Matching Using Combination of RS and FFT

The RS matching, the PSD matching and the FFT matching were all evaluated, but none of them individually is adequate to match the RRS effectively. Thus, a combined method using the RS and the FFT matching was developed and evaluated. This idea comes from the characteristics of each method, that is, (i) the first iteration of the RS matching can match the RRS very quickly, but leads to errors slightly over acceptable tolerances e.g., -5%/-30% as recommended by IEEE 693-2005; and (ii) the FFT matching shows very slow convergence to the given RRS but a better match. Eq. (17) and (18) are therefore combined and used for the combined matching, in which the RS matching is applied only once on the initial sine sweep, then the FFT matching is applied repeatedly until it envelops the RRS within the tolerance allowed.

$$SW_1(t) = \frac{RRS}{RS_{SW_0}} * SW_0(t) \tag{17}$$

$$SW_{\mathrm{i}+1} = IFFT\left(\mathrm{FFT}\left(\mathrm{SW_i}\right) * \frac{RRS}{RS_{SW_i}}\right) \tag{18}$$

where: *RRS* = Required Response Spectrum (RRS); SW_0 = initial sine sweep; SW_i = sine sweep obtained in the i-th iteration; RS_{SWO} = response spectrum of the initial sine-sweep function; RS_{SWi} = response spectrum of the ith sine-sweep function; FFT(SW_i) = fast Fourier transform of SW_i; *IFFT* = inverse fast Fourier transform. The algorithm of applying the combined matching of RS and FFT matching on a sine weep is shown in the example of Figure 90.

Time Domain RRS Matching

A new method to simultaneously generate and match a desired sine sweep without iteration is developed. Eq. (19) uses the basic sine sweep equation, Eq. (15), and adds a modulation function. The sine sweep function matched to the RRS will be obtained by multiplying the uniform amplitude sweep *S(t)* with the modulation function ($TargetRS / RS_{S(t)}$), the ratio of the target response spectrum to the response spectrum of the uniform amplitude sine-sweep function. In the uniform amplitude sine-sweep function, a certain frequency component will be located only at the time corresponding to the frequency, so that applying this method only once will produce the sine-sweep matching the target response spectrum (see Figure 91).

$$SW(t) = \frac{TargetRS}{RS_{S(t)}} * S(t) \tag{19}$$

Figure 89: Matching a Sine Sweep to RRS Using the RS Matching Method

a) Initial sine-sweep (SW_0) and its response spectrum:

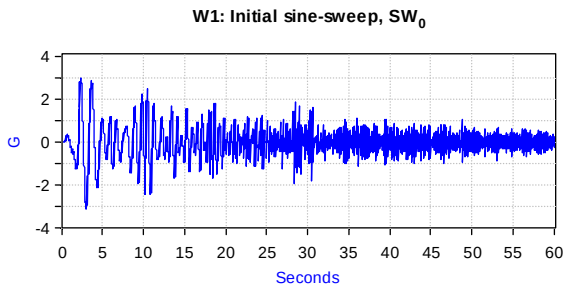

$$SW_0$$

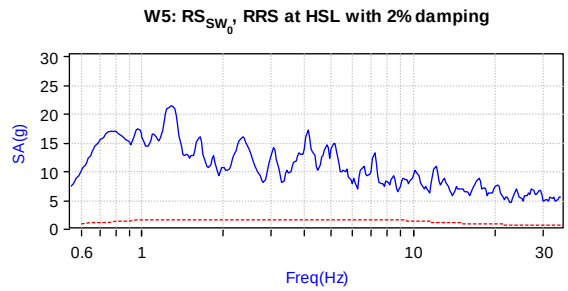

$$RS_{SW_0}$$

b) Ratio of the response spectrum to the IEEE 693 RRS at the High Seismic Level:

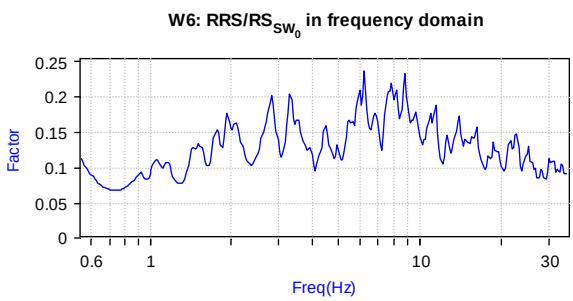

$$\frac{RRS}{RS_{SW_0}}$$

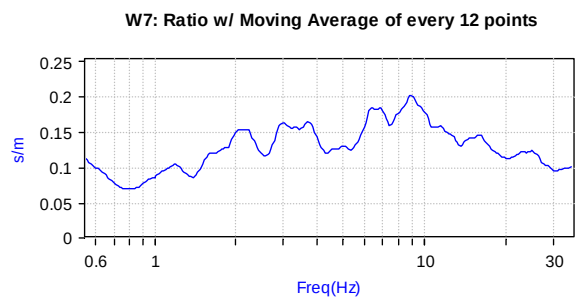

$$movavg\left(\frac{RRS}{RS_{SW_0}}, 12\right)$$

c) Final sine sweep (SW_5) obtained using RS matching:

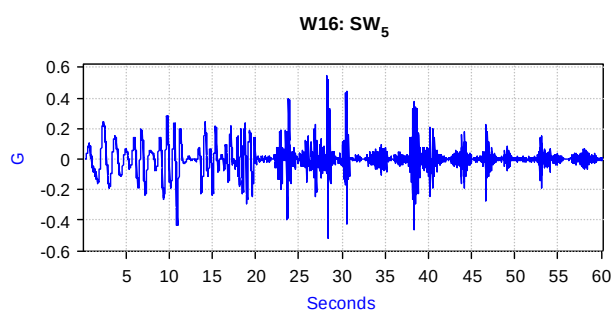

$$SW_5 = SW_4 * \frac{RRS}{RS_{SW_4}}$$

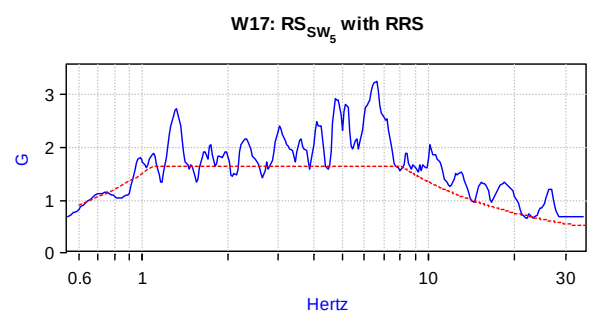

$$RS_{SW_4}$$

Figure 90: Matching a Sine Sweep to RRS Using RS and FFT Method

a) Initial sine-sweep (SW_0) and its response spectrum:

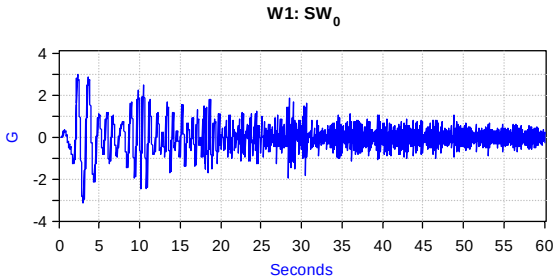

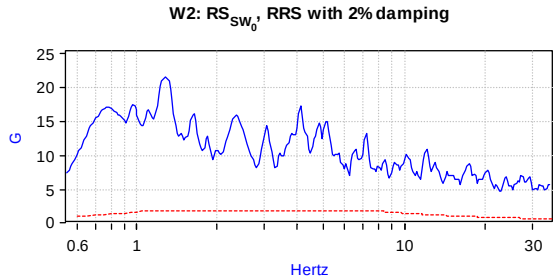

SW_0 $\qquad$ RS_{SW_0}

b) Sine-sweep (SW_1) obtained using RS matching and its response spectrum:

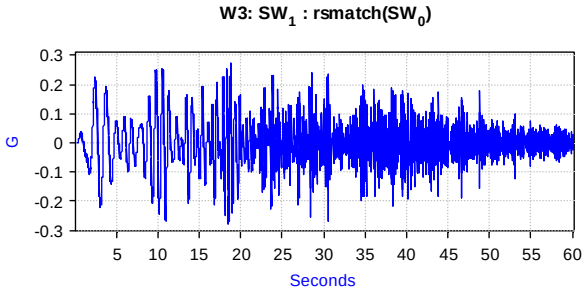

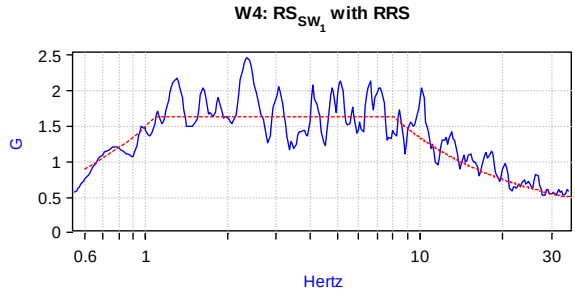

$\dfrac{RRS}{RS_{SW_0}}$ $\qquad$ RS_{SW_1}

c) Sine-sweep (SW_6) obtained using FFT matching with 5 sec. ramp up/down, and its response spectrum:

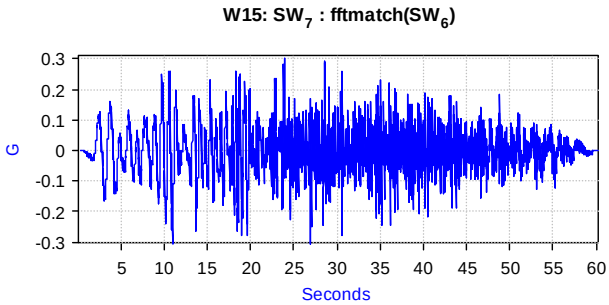

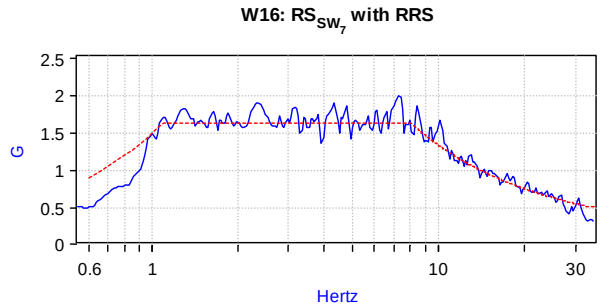

$SW_7 = fftmatch(SW_6)$ $\qquad$ RS_{SW_7}

Figure 91: Example of Sine-sweep Time Domain Matching to RRS at High Seismic Level (HSL)

a) Sine-sweep with constant amplitude, $\boldsymbol{SW}_0$

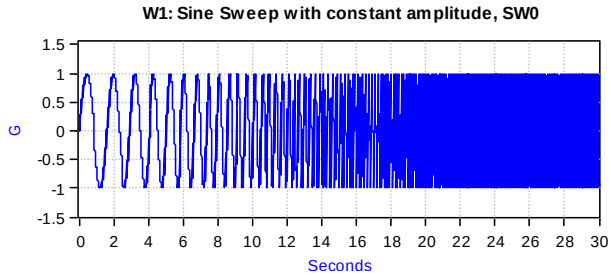

$$SW_0(t) = \sin\left\{2\pi f_0 * \frac{t_0}{\log 2} * \left(2^{\frac{t}{t_0}} - 1\right)\right\}$$

b) Response spectrum of $\boldsymbol{RS}_{SW_0}$

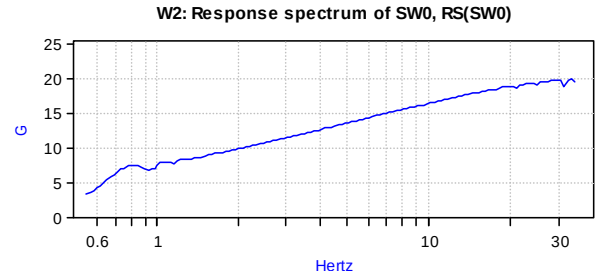

RS_{SW_0}

c) Target Response Spectrum

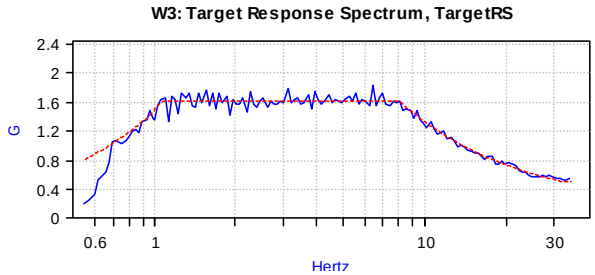

TargetRS

d) Ratio of $\boldsymbol{RS}_{SW_0}$ to $\boldsymbol{TargetRS}$

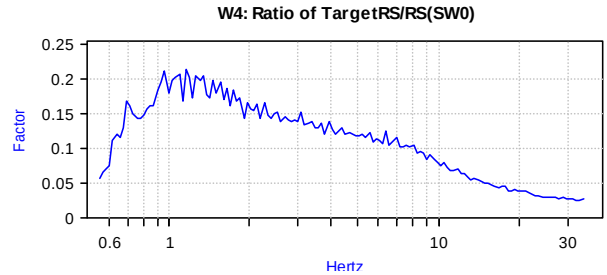

$TargetRS\ /\ RS_{SW_0}$

e) Expansion of d) to $\boldsymbol{SW}_0$

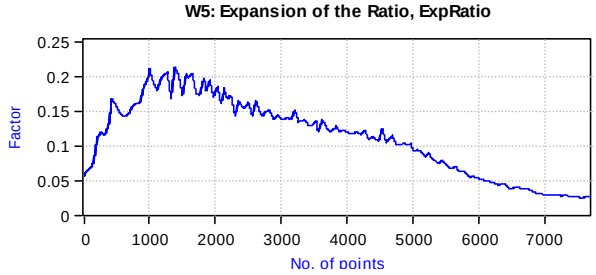

f) Multiplying e) by $\boldsymbol{SW}_0$

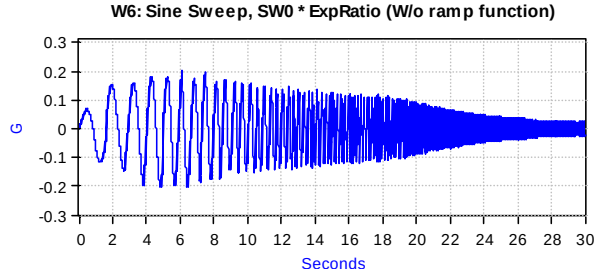

g) Applying a ramp up-down function

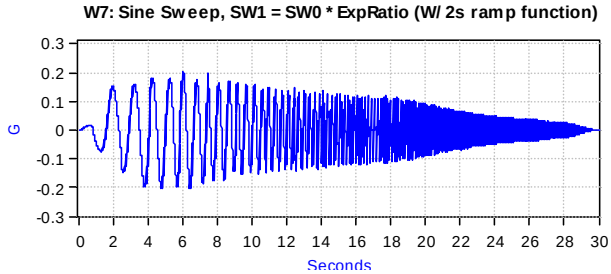

h) Response spectrum of g)

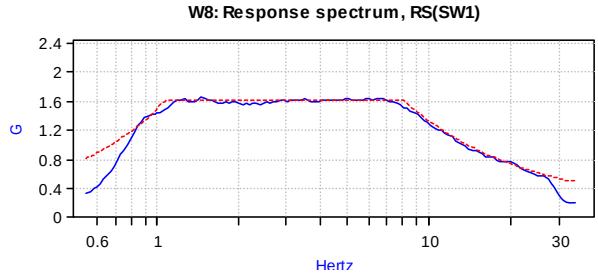

In Equation 19, $TargetRS$ = Target Response Spectrum whose shape envelops the RRS, or the RRS itself; $S(t)$ = the uniform amplitude sine sweep; and $RS_{S(t)}$ = response spectrum of the uniform amplitude sine sweep. The algorithm is presented in Figure 91 for $N_{Oct} = 6$ = number of octaves; $t_0 = 5$ = sweeping rate (seconds); $f_0 = 0.55$ = starting frequency (Hz); $f_1 = f_0 * 2^{N_{Oct}} = 35.2 Hz$ = ending frequency (Hz).

Note that a ramp is used in the lowest frequency and highest frequency ranges to achieve smooth starting and stopping of the shaking equipment. This may introduce some distortions in the lowest and highest frequencies. The sine sweep finally obtained was evaluated by shake table testing and compared with the test results using an acceleration history matching the same RRS.

Evaluation of Inherent Damping Due to Transformer Oil

The inherent damping of bushing motions can come from many potential sources: aerodynamic friction, movement in loosened parts of the mounting, movement of the conductor in oil, movement of the bushing in the oil tank, etc. Porcelain bushings are filled with oil to provide the required electrical insulation (dielectric) properties, and the oil also acts to conduct heat away from the interior of the bushing. This oil can also provide some level of damping in the bushings. Also, the transformer tank is usually filled with oil, and since the lower part of the bushing extends into the transformer, the oil inside the transformer provides some damping effect. A very small portion of damping comes from the vibration of the bushing in air. Other sources of damping can derive from loose nuts and bolts, poor connections, and opening and closing of cracks in the joints between porcelain segments.

Tests were performed on Bushing #4B to see the effect of damping. The frame was mounted securely to the floor and the bushing was mounted in the center of the frame. The bushing was pulled first in the EW direction and then the NS direction. The lower part of the bushing was immersed in a container designed at SEESL for the testing of the bushing in varying conditions of damping. The height of this container was about 92 in., and it was ensured that the mounting plate did not touch the top of the container. Figure 92 shows the test configuration.

During the first series of tests, the container was empty and a pull-release test was performed. Then the container was filled with oil and the pull-release test was performed again.

Instrumentation

Instrumentation Types

This section discusses the typical instruments used in this study. The exact configuration for each of the bushings is presented in Appendix B.

Motion Instrumentation

Critical points on the transformer bushings were identified and their motions, i.e., accelerations and displacements, were monitored. Accelerometers were also installed on the support structures and on the shake table. The accelerometers on the shake table and on top of the bushings were used to calculate the transfer functions, which were used to estimate the system frequency and damping ratio. The potentiometers were used to determine the relative motion of the bushings.

The following is a brief description of the instruments used.

Accelerometers

Piezoresistive accelerometers (Sensotek and Enedvco) were used in the laboratory for acceleration measurement. This type of accelerometer, also known as a strain gage accelerometer, is similar in principle to a piezoelectric accelerometer except it is equipped with a built-in resistor, which allows it to be used with a standard signal conditioner. There are two different types of piezoresistive accelerometers in the laboratory, details of which are provided below. These accelerometers are very stable and capable of recording high acceleration values. In this project the nominal sensitivity was around 3.8 mV/g, and the usable frequency range was from 0 to 400 Hz. The accelerometer was exceptionally stable in this range because its resonant frequency was well outside it, at around 1,000 Hz. The damping ratio was 70% of the critical which reduces the delay of recording the actual acceleration. The accelerometer had 5% maximum transverse sensitivity, which means that it is a linear accelerometer, and records the acceleration in one direction only.

Figure 92: Setup for Liquid Damping Test

(a) Container filled with water

(b) Pull test with container

Displacement

The laboratory uses many different types of displacement transducers that each have various attributes and limitations which determine their suitability for different applications. The following is a list of each different displacement transducer and a brief summary of its mechanics.

Linear Potentiometers

The most readily available and simplest position transducer is a linear potentiometer excited by a DC source such as a battery. It may be hooked up to deliver an output voltage that is essentially proportional to a straight-line position varying between zero and a maximum. Alternatively, a potentiometer may be hooked up to deliver an output varying between a negative and positive

voltage in proportion to a mechanical displacement that also varies between a maximum negative and a maximum positive value relative to a defined null position.

Linear Variable Differential Transformer (LVDT)

The word "linear" in the name of the LVDT refers to straight-line motion that is measured, rather than a linear relationship between input and output of the device. Three coils of electrically conducting wire are wound on an insulating form. By the principle of mutual inductance, an AC voltage across the terminals of the primary coil induces a voltage of the same frequency in each of the two secondary coils. If the moveable ferromagnetic core is centered, the two secondary voltages are of the same amplitude. For a positive displacement of the core, the voltage appearing across the number 1 secondary coil is greater in amplitude than at the null condition, while the amplitude across the number 2 secondary coil is lower.

MTS Temposonic Displacement Transducer

Initially a current pulse is applied to the conductor within the waveguide over its entire length. There is another magnetic field generated by the permanent magnet that exists only where the magnet is located. This field has a longitudinal component. These two fields join vectorially to form a helical field near the magnet, which in turn causes the waveguide to experience a minute torsional strain or twist only at the location of the magnet. This torsional strain pulse propagates along the waveguide at the speed of sound in this material. When the pulse arrives at the tapes in the head it is converted into a dynamic longitudinal pulse injected into the tapes. The longitudinal pulses cause the tapes to experience a momentary change in reluctance. Two coils coupling these tapes mounted in the field of two bias magnets will generate a momentary electrical pulse caused by the change in reluctance in the tapes. In order to extract the useful position information, the time difference between the launch of the initial current pulse and receipt of the signal from the output coils is measured. This time is a very precise function of the position of the moving magnet.

Strain and Force Gauges

While there are several methods of measuring strain, the most common is with a strain gauge, a device whose electrical resistance varies in proportion to the amount of strain in the device. The most widely used gauge is the bonded metallic strain gauge, which consists of a very fine wire or, more commonly, metallic foil arranged in a grid pattern. The grid pattern maximizes the amount of metallic wire or foil subject to strain in the parallel direction. The cross sectional area of the grid is minimized to reduce the effect of shear strain and Poisson ratio. The grid is bonded to a thin backing, called the carrier, which is attached directly to the test specimen. Therefore, the strain experienced by the test specimen is transferred directly to the strain gauge, which responds with a linear change in electrical resistance. Strain gauges are available commercially with nominal resistance values from 30 to 3000 Ohms (Ω), with 120, 350, and 1000 Ω being the most common values.

It is very important that the strain gauge be properly mounted onto the test specimen so that the strain is accurately transferred from the test specimen through the adhesive and strain gauge backing to the foil itself. In these tests, strain gauges were mounted on the porcelain bushing and on the metal casing of the flange. The strain gauge's sensitivity is expressed quantitatively as the gauge factor (GF), defined as the ratio of fractional change in electrical resistance to the fractional change in length: $GF = [(\Delta R/R)/(\Delta L/L)]$. The gauge factors for metallic strain gauges used in these tests are typically around 2.0.

Image-coordinate Tracking

Image-coordinate tracking is achieved with a Krypton™ K600 Portable CMM System. The K600 is a new generation of high-performance dynamic mobile coordinate measurement machine. The system combines high accuracy, large measurement volume, full freedom of space probe manipulation, and high reliability. The basic concept used for tracking the coordinates of the structure is very simple. An LED is attached to the point of interest and a three-camera system is used to locate the LED through triangulation. If only one LED is attached, the system will measure deformation in 3D. If three or more LEDs are used, then the same camera can be used to detect six degrees of freedom (DOF). The sample rate of the Krypton™ is 3000 divided by the number of LEDs. For example, if 20 active LEDs are used, the sample rate will be 150 samples per second. In this study the sample rate was restricted to 256 samples per second, to coincide with the accelerometers and displacement transducers used. Figure 93 shows a typical Krypton™ camera and its view.

The accuracy of the Krypton™ camera decreases with distance, as shown in Table 22.

Real-time Video

SEESL is equipped with three high-definition camcorders, 12 pan/tilt/zoom (PTZ) cameras and 10 charged-coupled device (CCD) cameras with integrated microphones. Each test required a different number and arrangement of video recorders, depending on the sensitivity of the tests and the number of sensitive points to be monitored. In most cases, the interface between the bushing and the bushing flange was monitored for any suspected high relative motion.

Figure 93: Field of View and Mounting of Krypton™ Camera

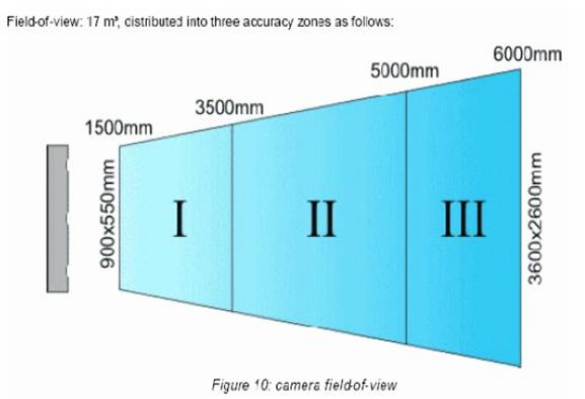

Table 22: Krypton™ K600 Camera Accuracy

Zone	Volumetric Accuracy (±2σ)	Single point Accuracy (±2σ)
I	90 µm+10 µm/m	60 µm+7 µm/m

II	90 µm+25 µm/m	60 µm+17 µm/m
III	190 µm+25 µm/m	130 µm+17 µm/m

Calibration Procedures and Data

All instruments were calibrated before use to ensure accurate data, as follows.

Accelerometers

The accelerometers were calibrated by holding them vertically, and calibrating the device to a reading of 1.0 g. When turned over suddenly, the accelerometer reading should be 2.0 g.

(b) Strain Gauge

In this study the strain gauges were directly calibrated using calibrated loads. An accurately known load was applied to the bushings and readings from the strain gauges were taken. The load cells used in the process impart some small degree of randomness since the load cell will provide values with some offset or residual error. The second type of calibration is shunt calibration using the Wheatstone bridge circuit, which is widely used in the absence of direct calibration. The critical section of the transformer bushings was at the interface of the porcelain insulator and steel mounting flange assembly. The mounting flange is the part where the maximum stresses are produced by dynamic testing of the bushing. The testing required measurements of moments and shear force at the base mounting. The strain gauges were calibrated to measure the shear forces and the bending moments directly. For the purpose of calibration the bushing was pulled at its top as shown in Figure 94.

Figure 94: Pull Test Performed on Porcelain Bushing to Calibrate Strain Gauges

The pulling force produces compression and tension strains in various directions. The elastic properties of the section, which is the effective area in compression, the effective moment of inertia in moment and modulus of elasticity of the setup is not known properly, so a combination of strain gauges is used to calculate these parameters.

The calibration procedure is as follows (see Figure 95): (a) A horizontal pull of force "F" (kips) is applied at the top of the bushing. (b) The distance between the applied force and the center of the strain gauge is given by "h." (c) The strain on the tension side "εt" and the strain on the compression side "εc," in the plane of force, are measured. (d) The total strain εt-εc is calculated, and the calibration factor is obtained as (εt-εc)/(F*h), in units of μ-strain/kip-in. (e) To find the bending moment from actual measurements, values of (εt-εc) in the plane of interest are obtained from experiments and divided by the calibration factor.

Potentiometer Calibration

Linear potentiometers with a long stroke were used to measure displacements. The potentiometers were calibrated with a standard reference meter rod.

Typical Instrumentation Lists and Locations

Instruments discussed in the above section were used for this project to observe the physical characteristics of bushings. First the bushing was mounted on a fixed base and instrumented, followed by dynamic testing on a shake table. A typical instrumentation list is shown in Table 23, indicating all types of instruments, nomenclature and positive directions. In addition, drawings showing the locations of instruments are shown in Figures 96–98. Complete instrumentation lists and location drawings for all bushings are provided in Appendix B.

Figure 95: Benchmark Points in Calibration of Gauges

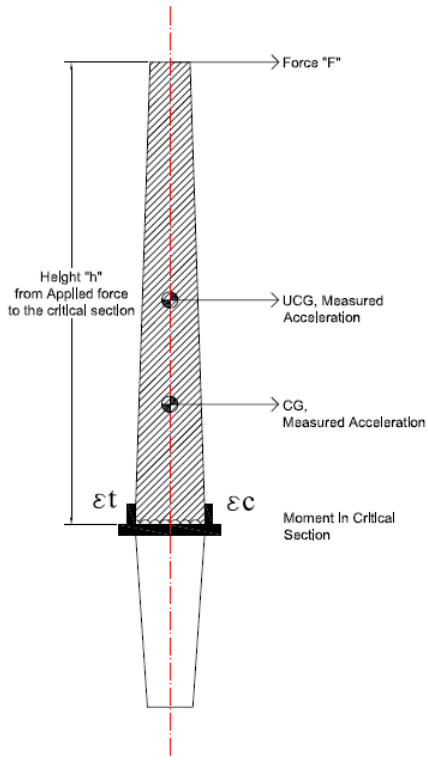

Test Protocols and Sequences

The test protocol is a test plan that lists all test sequences, types of motion to be used in testing, and special requirements during the testing. At the end of the testing, the test protocols become a logged list of the tests completed, the location of the data and its nomenclature, and observations from the testing. This section presents a typical test protocol using Bushing #5 as an example; all protocols and sequences for all bushings in this experimental study are presented in Appendix A.

Typical Testing Protocol

The test protocol usually had three components in this study. In the first part of the testing, the bushing was installed on the rigid base, and static testing (impact hammer, pull and sudden-release tests) was performed. A sample of this first part of the test protocol is presented in Table 24. During the second part of the testing, the bushings were mounted on the flexible or rigid frame, and then mounted on the shake table. During this sequence the bushing was subjected to a series of dynamic tests that included white noise, acceleration history, and table impulse tests. A sample of this second part of the test protocol for Bushing #5 is presented in Table 25. In the third and last sequence (see Table 26), the bushing was once again installed on the fixed base and was tested either with the impact hammer and simple pull tests, or pulled to failure to measure the capacity of the bushing. The tests were stopped after every series of these three tests to perform a visual inspection of the bushing.

Table 23: Example Instrumentation List for ABB 550 kV Porcelain Bushing (Bushing #8)

Instrumentation List for ABB 550Z3000SE BUSHING					
Instrument #	**Location and Position**	**Direction**	**Comments**	**Fixed Base**	**Shake Table**
			Accelerometers		
A01	top of bushing on plate	EW	Positive direction EAST perpendicular to bushing axis	x	x
A02	top of bushing on plate	NS	Positive direction NORTH	x	x
A03	top of bushing along bushing axis	AXIAL	Positive direction UP (or closes to UP)	x	x
A04	CG opper 85.22" from surface of adapter ring	EW	Positive direction EAST perpendicular to bushing axis		x
A05	CG opper 85.22" from surface of adapter ring	NS	Positive direction NORTH		x
A06	CG opper 54.75" from surface of adapter ring	EW	Positive direction EAST perpendicular to bushing axis	x	x
A07	CG opper 54.75" from surface of adapter ring	NS	Positive direction NORTH	x	x
A08	top of support structure - near lower lifting log	EW	Positive direction EAST perpendicular to bushing axis		x
A09	top of support structure - near center of plate	NS	Positive direction NORTH		x
A10	top of support structure - near lower lifting log	AXIAL	Axial Positive direction UP		x
A11	top of support structure - near lower lifting log	EW	Horizontal Positive direction EAST		x
A12	top of support structure - near lower lifting log	VERT	Vertical Positive direction UP		x
A13	bottom of bushing on plate	EW	Positive direction EAST perpendicular to bushing axis	x	x
A14	bottom of bushing on plate	NS	Positive direction NORTH	x	x
A15	extension platforrm	VERT	Center of base plate		x
A16	extension platforrm	EW	Center of base plate		x
A17	extension platforrm	NS	Center of base plate		x
A18	on frame's east leg to measure rotation	EW	Frame top		x
			Potentiomenters		
SP01	top of bushing on plate	EW	Positive direction EAST horizontal	x	x
SP02	top of bushing on plate	NS	Positive direction NORTH	x	x
SP03	top of support structure	EW	Short leg		x
SP04	top of support structure	NS	Mid Axis		x
SP05	bottom of bushing	EW	Positive direction EAST horizontal		x
SP06	bottom of bushing	NS	Positive direction NORTH		x
SP07	extension platforrm	EW-N	Connect to refrence frame		x
SP08	extension platforrm	EW-S	Connect to refrence frame		x
SP09	extension platforrm	NS	Connect to refrence frame		x
D1	potentiometer	D1	potentiometer between bushing and frame		x
			LED - KRYPTON		
LED01	West side on porcelain		As close as posible to the edge		x
LED02	West side on flange		As close as posible to the edge		x
LED03	Center on porcelain		As close as posible to the edge		x
LED04	Center on flange		As close as posible to the edge		x
LED05	East side on porcelain		As close as posible to the edge		x
LED06	East side on flange		As close as posible to the edge		x
			LoadCells		
LC01	250 lbs pull at top	EW/NS	For pull and quick release at top	x	
			Total Channels of instrumentation	10	34

Figure 96: Instrumentation Sketch for Bushing #8 – Laboratory Floor

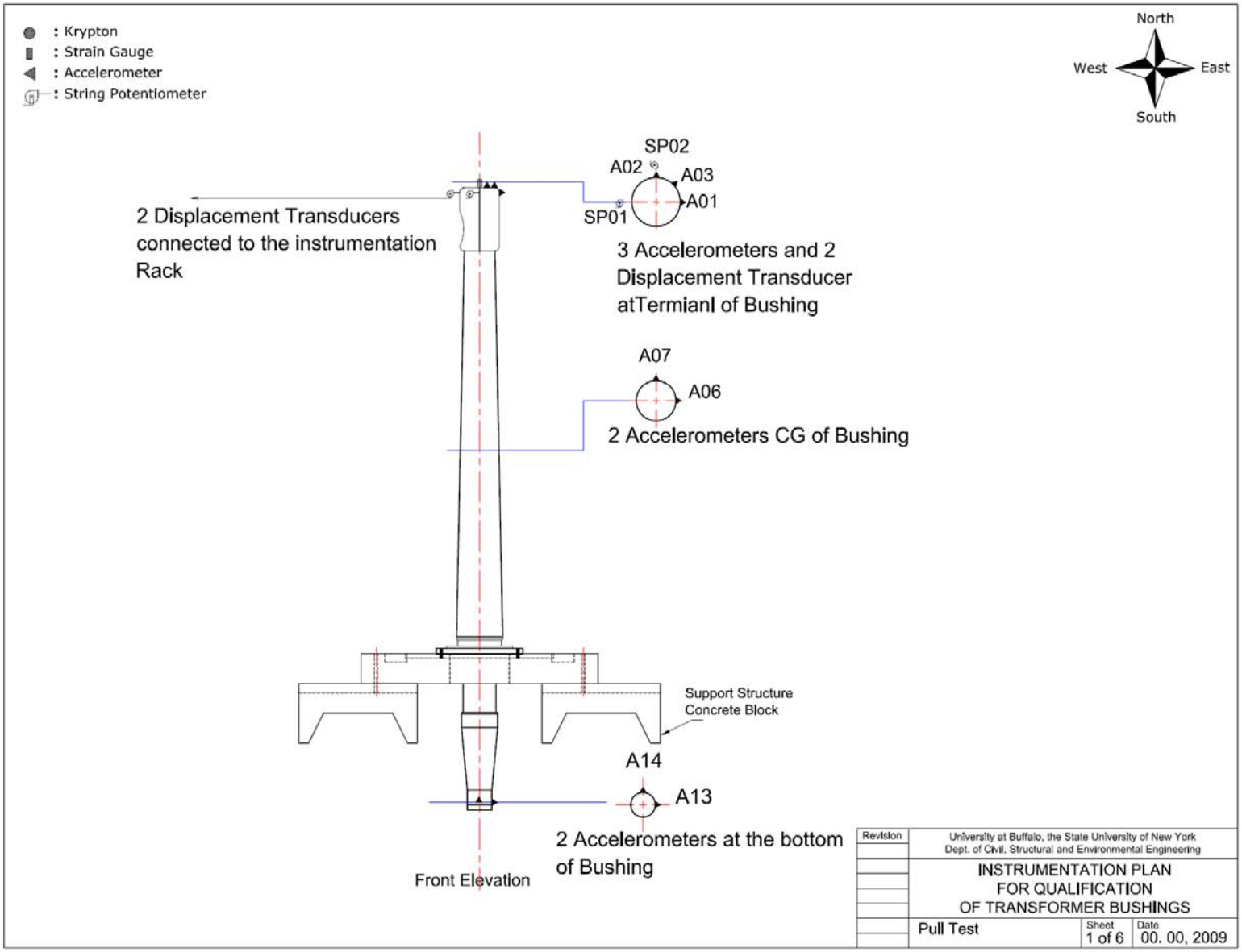

Figure 97: Instrumentation Sketch for Bushing #8 – Shake Table

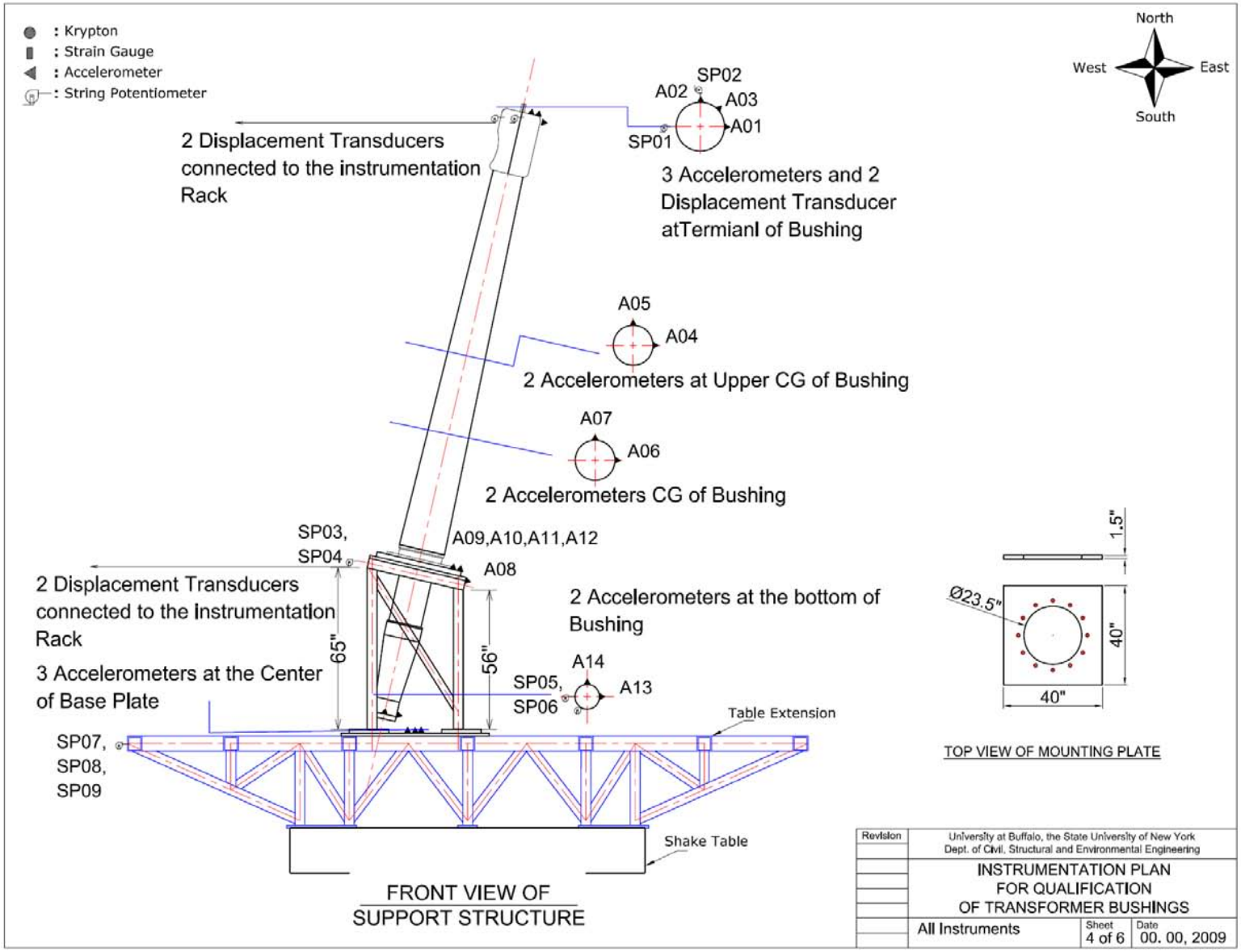

Figure 98: Instrumentation Sketch for Bushing #8 – LEDs for Krypton™ Camera

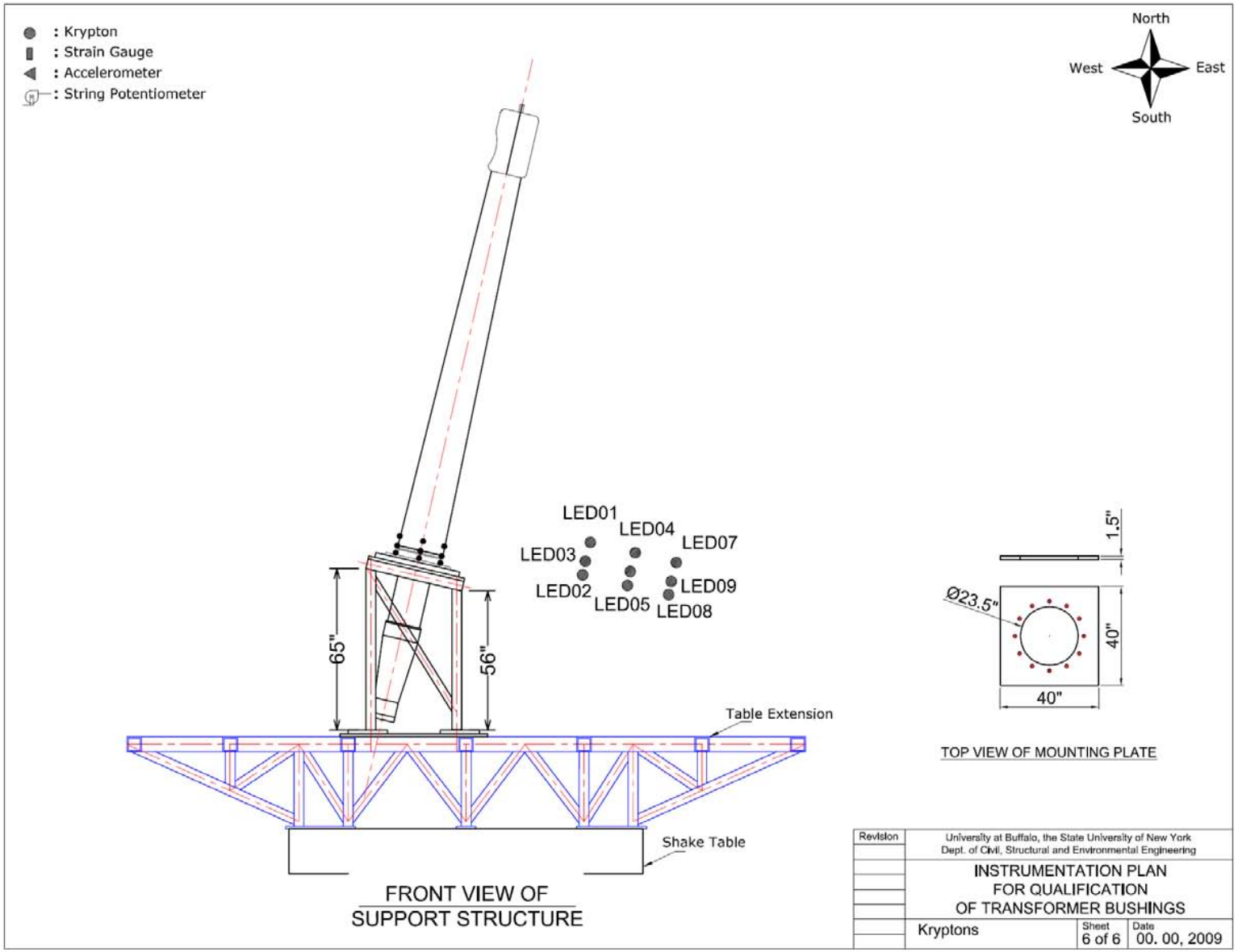

Table 24: First Part of Test Protocol – Static Testing (Bushing #5)

Seismic Evaluation and Qualification of Transformer Bushing 5									
Test No.			Location of Bushing	Test Direction	Test Description	Testing Setup	Test Date	File name in Repository	Remarks
25lb Weight is to be added at the top of the Bushing									
lifting hole in EW Direction									
1. Pre-Test Activities				500 kV Composite Bushing #5		CG Of Bushing =65.5" from Flange top			Upper Bushing CG=89"
TB-	01		N/A	N/A	Finding Weight of the Bushing		92909		1850 lbs
TB-	02		N/A	N/A	Finding Centre of Gravity of Bushing		92909		Check=83"
TB-	03	-NS-IH	Concrete Slab	NS	Impact Hammer Test		92909	tb03nsih.dat	
TB-	=B9	-NS-Ihmass	Concrete Slab	NS	Impact Hammer Test		92909	tb03nsihmass.dat	impact hammer on mass
TB-	04	-NE-IH	Concrete Slab	NE	Impact Hammer Test		92909	tb04neih.dat	
TB-	05	-EW-IH	Concrete Slab	EW	Impact Hammer Test		92909	tb05ew ih.dat	
TB-	06	-SE-IH	Concrete Slab	SE	Impact Hammer Test		92909	tb06seih.dat	
TB-	07	-PL-SG	Concrete Slab	NE	150 lb Pull Test for Caliberation of SG		92909	tb07plsg.dat	
TB-	7	-PL-SGb	Concrete Slab	EW	150 lb Pull Test for Caliberation of SG		92909	tb07plsgb.dat	
TB-	08	-PL-SG	Concrete Slab	SE	150 lb Pull Test for Caliberation of SG		92909	tb08plsg.dat	
TB-	09	-PL-200	Concrete Slab	EW	Pull Test of 200 lbs		92909	tb09pl200.dat	Quick release at 200 lbs
TB-	10	-NS-IH	Concrete Slab	NS	Impact Hammer Test		92909	tb10nsih.dat	5.1 Hz, 28.9 Hz
TB-	11	-EW-IH	Concrete Slab	EW	Impact Hammer Test		92909	tb11ew ih.dat	
TB-	12	-PL-300	Concrete Slab	EW	Pull Test of 300 lbs		92909	tb12pl300.dat	Quick released at 314 lbs
TB-	13	-NS-IH	Concrete Slab	NS	Impact Hammer Test		92909	tb13nsih.dat	
TB-	14	-EW-IH	Concrete Slab	EW	Impact Hammer Test		92909	tb14ew ih.dat	WE, 5.17Hz, 29.4 Hz
TB-	15	-PL-400	Concrete Slab	EW	Pull Test of 400 lbs		92909	tb15pl400.dat	Quick release at 400 lbs
TB-	16	-NS-IH	Concrete Slab	NS	Impact Hammer Test		92909	tb16nsih.dat	
TB-	17	-EW-IH	Concrete Slab	EW	Impact Hammer Test		92909	tb17ew ih.dat	WE, 5.19 Hz, 29.42 Hz
TB-	18	-PL-500	Concrete Slab	EW	Pull Test of 500 lbs		92909	tb18pl500.dat	Quick release at 500 lbs
TB-	19	-NS-IH	Concrete Slab	NS	Impact Hammer Test		92909	tb19nsih.dat	
TB-	20	-EW-IH	Concrete Slab	EW	Impact Hammer Test		92909	tb20ew ih.dat	
TB-	21	-PL-1000	Concrete Slab	EW	Pull Test of 1000 lbs		92909	tb21pl1000.dat	Quick release at 500 lbs
TB-	22	-NS-IH	Concrete Slab	NS	Impact Hammer Test		92909	tb22nsih.dat	
TB-	23	-EW-IH	Concrete Slab	EW	Impact Hammer Test		92909	tb23ew ih.dat	
TB-	24	-PL-1500	Concrete Slab	EW	Pull Test of 1500 lbs		92909	tb24pl1500.dat	1505 lbs, Quick release at 507 lbs, Freq, 5.07 Hz
TB-	25	-NS-IH	Concrete Slab	NS	Impact Hammer Test		92909	tb25nsih.dat	
TB-	26	-EW-IH	Concrete Slab	EW	Impact Hammer Test		92909	tb26ew ih.dat	
TB-	27	-PL-2000	Concrete Slab	EW	Pull Test of 2000 lbs		92909	tb27pl2000.dat	Quick release at 500 lbs
TB-	28	-NS-IH	Concrete Slab	NS	Impact Hammer Test		92909	tb28nsih.dat	
TB-	29	-EW-IH	Concrete Slab	EW	Impact Hammer Test		92909	tb29ew ih.dat	
TB-	30	PL-2800	Concrete Slab	EW	Pull Test of 2800 lbs		92909	tb30pl2800.dat	Quick release at 500lbs, Freq 5.03 Hz, 4.29 inch, 2.9% and 2.5% Damping
TB-	31	-NS-IH	Concrete Slab	NS	Impact Hammer Test		92909	tn31nsih.dat	
TB-	32	-EW-IH	Concrete Slab	EW	Pull Test of 2800 lbs		92909	tb32ew ih.dat	

Table 25: Second Part of Test Protocol – Dynamic Testing (Bushing #5)

2. Bushing Identification

Bushing at Center with no stiffneres/ no turret /on Shake Table

TB- 33 -WN	Center of Frame		WHITE NOISE TEST (0-50HZ, 0.1 g)		100109	tb33wn.dat	freq N 2.75 hz, 21 Hz, W 3.5, 21 Hz
TB- 34 -TBI	Center of Frame		Table Impulse test		100109	tb34tbl.dat	freq N 3.25 hz,19.5 Hz, W 3, 19.25 Hz, 42 Hz
TB- 35 -AH25	Center of Frame		ACCELERATION TIME HISTORY TEST (0.25g RRS)		100109	tb35ah25.dat	
TB- 36 -WN	Center of Frame		WHITE NOISE TEST (0-50HZ, 0.1 g)		100109	tb36wn.dat	
TB- 37 -TBI	Center of Frame		Table Impulse test		100109	tb37tbl.dat	
TB- 38 -AH50	Center of Frame		ACCELERATION TIME HISTORY TEST (0.5g RRS)		100109	tn38ah50.dat	RRS corrected for 1.4 factor
TB- 39 -WN	Center of Frame		WHITE NOISE TEST (0-50HZ, 0.1 g)		100109	tb39wn.dat	
TB- 40 -TBI	Center of Frame		Table Impulse test		100109	tb40tbl.dat	E: 2.85 Hz, 19.625 Hz
TB- 41 -AH100	Center of Frame		ACCELERATION TIME HISTORY TEST (1.0g RRS)		100109	tb41ah100.dat	E: 2.85 Hz, 19.625 Hz, N 1.81, 19.625
TB- 42 -NS-IH	Center of Frame	NS	Impact hammer NS		100109	tb42nsih.dat	Bottom of Bushing NS 38.8 Hz
TB- 43 -EW-IH	Center of Frame	EW	Impact hammer EW		100109	tb43ewih.dat	
TB- 42 -WN	Center of Frame		WHITE NOISE TEST (0-50HZ, 0.1 g)		100109	tb42wn.dat	
TB- 43 -TBI	Center of Frame		Table Impulse test		100109	tb43tbl.dat	
TB- 44 -AH150	Center of Frame		ACCELERATION TIME HISTORY TEST (1.5g RRS)		100109	tb44ah1.5.dat	2.o g rms achieved, so this is the run for 2.0 g rms
TB- 45 -WN	Center of Frame		WHITE NOISE TEST (0-50HZ, 0.1 g)		100109	tb45wn.dat	
TB- 46 -TBI	Center of Frame		Table Impulse test		100109	tb46tbl.dat	N 3.5 Hz, E 3.5 Hz
TB- 47 -AH225	Center of Frame		ACCELERATION TIME HISTORY TEST (2.25g RRS)		100109	tb47ah225.dat	GOOD FOR 2.5 G RRS
TB- 48 -WN	Center of Frame		WHITE NOISE TEST (0-50HZ, 0.1 g)		skipped	skipped	skipped
TB- 49 -TBI	Center of Frame		Table Impulse test		skipped	skipped	skipped
TB- 50 -AH250	Center of Frame		ACCELERATION TIME HISTORY TEST (2.5g RRS)		100109	TB47AH225.DAT	2.5 RRS, FREQ 1.75 Hz
TB- 51 -WN	Center of Frame		WHITE NOISE TEST (0-50HZ, 0.1 g)		100109	tb51tbl.dat	
TB- 51 -bWn	Center of Frame		WHITE NOISE TEST (0-50HZ, 0.1 g)		100109	tb51bWN.dat	3.26 Hz, 19.88
TB- 52 -TBI	Center of Frame		Table Impulse test		100109	tb52tbl.dat	E 3.25 Hz , 3.25
TB- 53 -AH300	Center of Frame		ACCELERATION TIME HISTORY TEST (3.0g RRS)		100109	tb53ah300.dat	
TB- 54 -WN	Center of Frame		WHITE NOISE TEST (0-50HZ, 0.1 g)		100109	tb54wn.dat	
TB- 55 -TBI	Center of Frame		Table Impulse test		100109	tb55tbl.dat	

3. Bushing Identification

Bushing at Center with no stiffneres/ no turret /on Shake Table

TB- 56 -PL-100	Center of Frame		Pull Test 100 lbs		93009	tb56pl100.dat	No Water in the tank
TB- 57 -PL-150	Center of Frame		Pull Test 150 lbs		93009	tb57pl150.dat	No water in the Tank
TB- 58 -PL-200	Center of Frame		Pull Test 200 Lbs		93009	tb58pl200.dat	No water in the tank
TB- 59 -PL-100	Center of Frame		Pull Test 100 lbs		93009	tb59pl100.dat	Filled with water
TB- 60 -PL-150	Center of Frame		Pull Test 150 lbs		93009	tb60pl150.dat	Filled with water
TB- 61 -PL-200	Center of Frame		Pull Test 200 lbs		93009	tb61pl200.dat	Filled with water

Table 26: Third Part of Test Protocol – Bushing #5

PAUSE FOR INSPECTION

4. Bushing Failure mode Identification

Check for max response during the test, mount the bushing accordingly, so that max response directin is EW

TB- 62 -NS-HH	Concrete Slab	NS	Hard Impact Hammer Test				
TB- 63 -WE-HH	Concrete Slab	WE	Hard Impact Hammer Test				
TB- 64 -PL	Concrete Slab	EW	Pull Test of 2800 lbs				Quick Release at 500 lbs
TB- 65 -NS-H	Concrete Slab	NS	Hard Impact Hammer Test				
TB- 66 -EW-IH	Concrete Slab	WE	Hard Impact Hammer Test				

Results of Bushing Tests

Test Results for Bushings #1, 2, and 3

Bushings #1, 2, and 3 were tested prior to the current study and the results of those investigations are reported in detail in Kong, 2010. The detailed description of methodical extraction of dynamic properties, effects of ground motions, failure modes and special effects of the location of the bushing can also be found in this paper. The relevant data that led to important information related to the evaluation of transformers is used in this report and is presented in various chapters. This section summarizes the key test results for Bushing #4A; all 6 bushings were tested in similar test protocols. The complete test results for Bushings #4A, 4B, 5, 6, 7 and 8, performed for this project, can be found in Appendix D.

Test Results for Bushing #4A

The test results for composite Bushing #4A are summarized in Table 27. The information processed from the testing is presented as the identified frequencies and damping from resonance searches.

Pull Test

A pull test is not required for qualification testing of composite bushings, according to IEEE 693. However, a pull test was performed on Bushing #4A to determine the reaction forces at the support structure connection and to quantify the stiffness of the condenser bushing in order to use the results for further academic investigations. A series of pull tests was performed in the EW direction with prescribed horizontal loadings from approximately 116 to 300 lb. The results of the pull tests are presented in Table 28 and Figure 99.

Frequency Searches

The frequency searches were performed using quick-release, impact hammer, white noise and impulse tests. The frequencies from all tests are usually consistent. The damping was determined from the time functions and from the frequency response functions. The half-power bandwidth method used to determine damping from frequency response functions is less accurate than the quick release, impact hammer or table impulse tests. The authors recommend that only damping values obtained from the quick release, impact hammer or table impulse tests be considered for use.

Quick Release Test – Bushing on Fixed Base

Quick release tests on Bushing #4A installed on the fixed base were performed after the static pull test; the frequencies and damping of the bushing were calculated from the measurements of the resulting oscillations. The results of the quick release tests for Bushing #4A are presented in Table 27 and in Figure 100.

Impact Hammer Test

Impact hammer tests were first performed with the composite bushing installed on the floor, and then with it installed on the support structure on the shake table. The results of the impact hammer tests are presented in Table 27 and Figure 101. The damping ratio is determined by the curve fitting method (Kong, 2010). The frequencies of the bushing mounted on the fixed base were 8.30 Hz and 8.28 Hz in the EW direction (aligned with the lifting lugs) and in the NS direction respectively; the damping ratios were 2.47% in both directions. The frequencies with the bushing

mounted on the support structure (simulating “as-installed” conditions) were 7.75 Hz in both the EW and NS directions, and the damping ratios were 2.69% and 2.11% in the EW and NS directions, respectively.

Table 27: Summary of Tests for Bushing #4A

Test No.	Frequency			Damping			Max Displacement	Force (lb)	Stiffness (lb/in)
Units	(Hz)			(%)			(in)	(lb)	(lb/in)
(1)	(3)	(4)	(5)	(6)	(7)	(8)	(9)	(10)	(11)
Direction	NS	EW	Vertical	NS	EW	Vertical			
Impact Hammer Test –Fixed base									
TB-U1-NSww05	8.32	-	-	4.35	-	-	-	-	-
TB-U1-WEww06	-	8.85	-	-	2.66	-	-	-	-
TB-U1-NS05	8.3	-	-	2.47	-	-	-	-	-
TB-U1-WE06	-	8.28	-	-	2.47	-	-	-	-
Quick Release Test - Fixed Base									
TB-U1-13	-	8.27	-	-	0.91	-	0.15	116.88	779.20
TB-U1-14		8.35			1.48		0.26	187.39	720.73
TB-U1-15		8.26			1.50		0.46	302.88	658.43
TB-U1-16	-	-	-	-	-	-	0.42	296.08	704.95
White Noise Test									
TBU1wn23	7.75	7.75	22.50	2.69	2.11	0.75	-	-	-
TBU1wn26	7.75	7.75	22.50	2.53	1.89	0.58	-	-	-
TBU1wn28	7.75	7.75	23.50	2.49	2.70	1.16	-	-	-
TBU1wn31	7.75	7.75	23.25	2.47	2.50	1.25	-	-	-
TBU1wn33	7.50	7.25	17.75	2.70	2.56	1.02	-	-	-
TBU1wn36	7.50	7.25	17.75	2.46	2.55	0.98	-	-	-
TBU1wn38	7.75	7.50	21.25	4.27	3.12	0.89	-	-	-
TBU1wn41	7.75	7.25	21.25	4.37	1.88	0.90	-	-	-
TBU1wn43	7.75	7.75	24.00	2.21	3.05	1.78	-	-	-
TBU1wn46	7.75	7.75	23.75	2.23	3.07	1.57	-	-	-
Table Impulse Test									
TBU1TBI24	7.70	7.78	-	0.70	0.70	-	-	-	-
TBU1TBI27	7.70	7.79	-	0.60	0.69	-	-	-	-
TBU1TBI29	7.79	7.79	-	0.53	0.61	-	-	-	-
TBU1TBI32	7.80	7.80	-	0.73	0.61	-	-	-	-
TBU1TBI34	7.59	7.12	-	0.97	0.52	-	-	-	-
TBU1TBI37	7.55	7.16	-	0.60	0.57	-	-	-	-
TBU1TBI39	7.80	7.37	-	0.49	0.84	-	-	-	-
TBU1TBI42	7.80	7.40	-	0.55	0.52	-	-	-	-
TBU1TBI44	7.86	7.80	-	0.50	0.63	-	-	-	-
TBU1TBI47	7.86	7.80	-	0.59	0.72	-	-	-	-
Final Pull Test									
TB-U1-PLB-50	-	-	-	-	-	-	0.72	297.14	412.69
TB-U1-PL-52	-	-	-	-	-	-	0.38	267.81	708.49
TB-U1-PL-54	-	-	-	-	-	-	0.80	534.03	670.89
TB-U1-PL-56	-	-	-	-	-	-	1.99	1220.32	613.23
TB-U1-PL-58	-	-	-	-	-	-	3.43	1959.59	571.98
TB-U1-PL-60	-	-	-	-	-	-	4.87	2632.16	540.83
TB-U1-PL-62	-	-	-	-	-	-	7.03	2855.60	406.49
TB-U1-PL-64	-	-	-	-	-	-	3.52	1251.28	355.48

Table 28: Results of Pull Tests for Bushing #4A

Test No.	Max Displacement	Force (lb)	Stiffness (lb/in)	Frequency	Damping	Testing Method
TB-U1-13	0.15	116.88	779.20	8.27	0.91	Quick Release
TB-U1-14	0.26	187.39	720.73	8.35	1.48	Quick Release
TB-U1-15	0.46	302.88	658.43	8.26	1.50	Quick Release
TB-U1-16	0.42	296.08	704.95	-	-	Pull Test

Figure 99: Results of Pull Tests for Bushing #4A

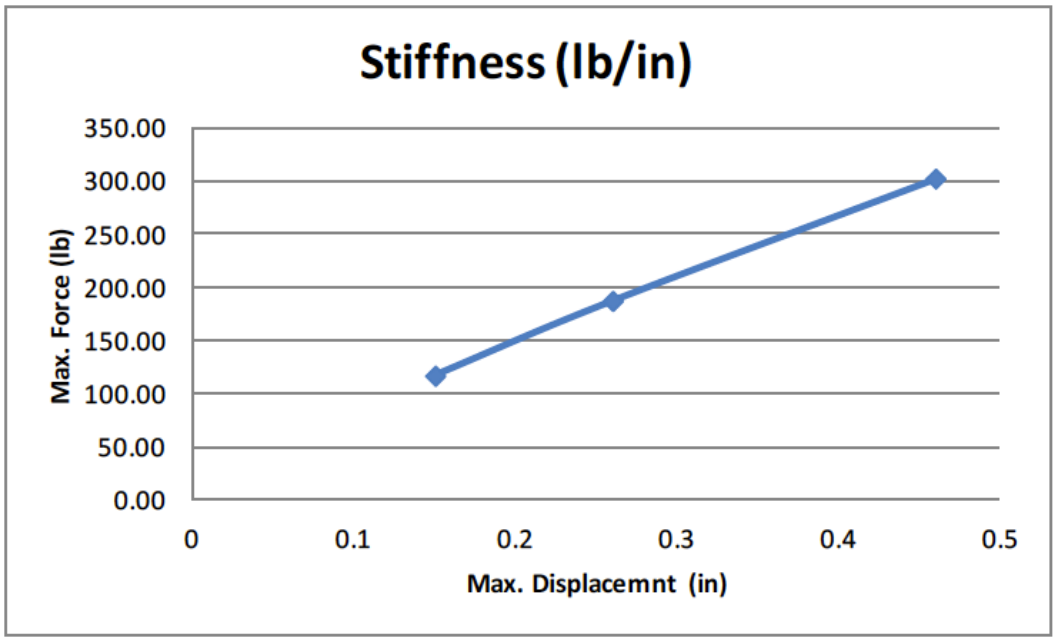

White Noise Test

The frequencies and damping ratio of the bushing were determined by transfer functions obtained from white noise tests. The peak of the transfer function is the fundamental frequency of the bushing and a half-power bandwidth method was used to determine the damping ratio. The summary of the frequencies is presented in Table 27. The frequencies from white noise tests were then used to develop "impulse tests" for the dominant frequencies of the bushing (see next section). The half-power bandwidth method used to determine damping is less accurate than a quick release, impact hammer or table impulse test; therefore the ratios are determined in the following section using impulse tests. The acceleration transfer function obtained in the white noise test is shown in Figure 102.

Table Impulse Test

The table impulse test identifies frequencies and damping of dominant frequencies using smoothed table acceleration impulse for control of a shake table by using a smoothing table impulse procedure developed by the SEESL at University at Buffalo. For the identification of system frequencies, a power spectral density (PSD) was calculated from output motion at the top

of the bushing and the system frequency is obtained by finding the frequency where the peak is located. For the identification of modal damping, a curve fitting method developed by the authors was used (Kong, 2010).

The acceleration history results of the table impulse tests are presented in Figure 103, and the dynamic characteristics are summarized in Table 27. The frequencies of the composite bushing are about 7.70 Hz (in test TBU1TBI24) before random motion tests and 7.86 Hz (in test TBU1TBI47), and the damping values of the bushing are 0.70% and 0.59% respectively.

Random Motion Tests

Random motion tests were performed for the seismic qualification of the condenser bushing. A summary of the accelerations recorded on various locations on the bushing is shown in Table 29 for the five levels of bushing locations.

Figure 100: Quick Release Test Response – Bushing #4A

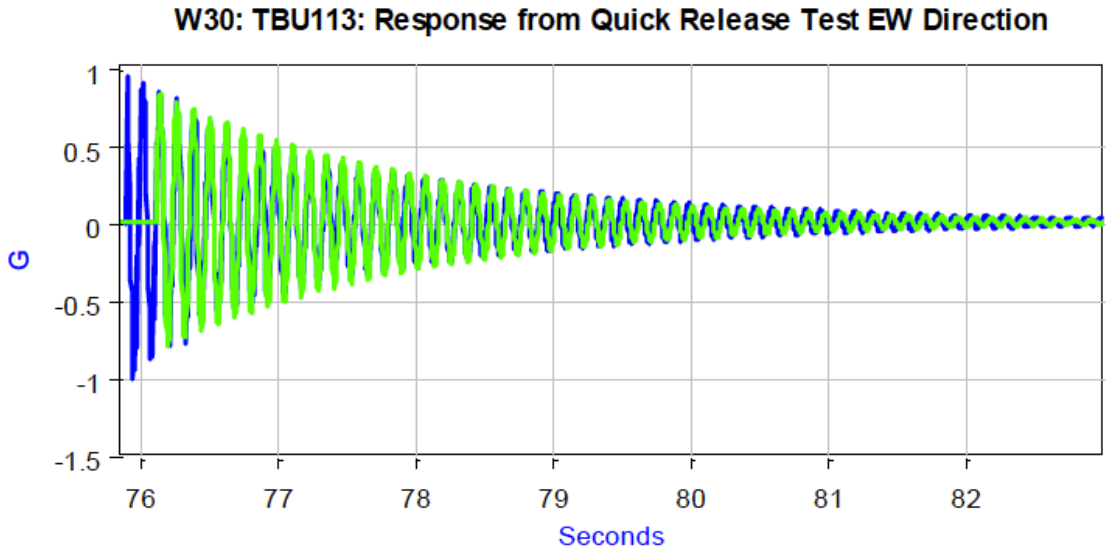

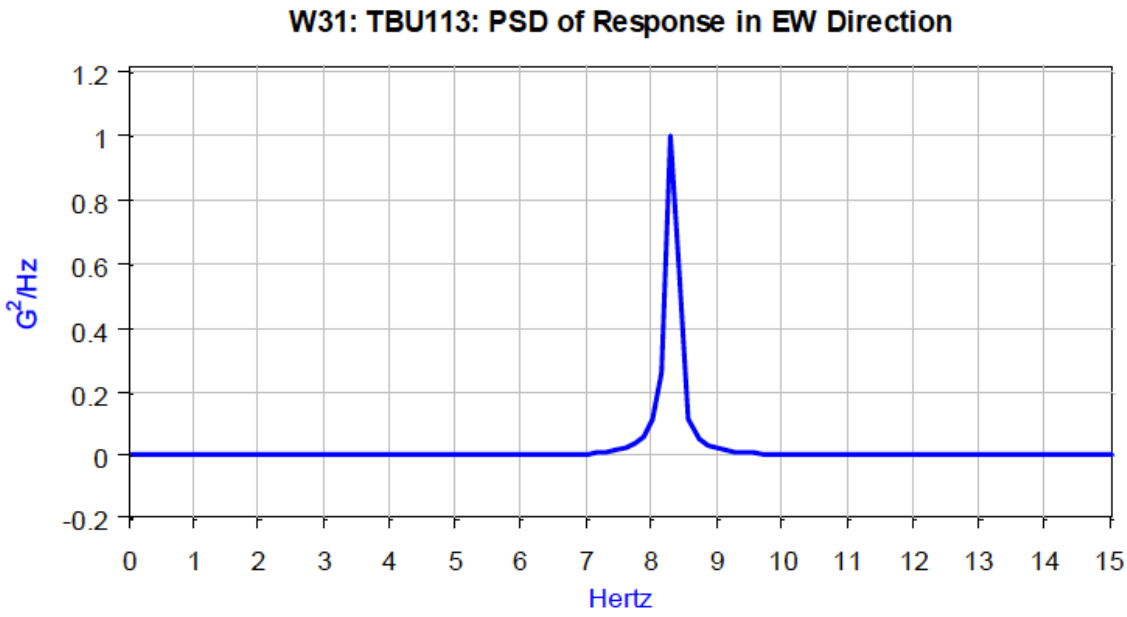

Figure 101: Impact Hammer Test Response – Bushing #4A

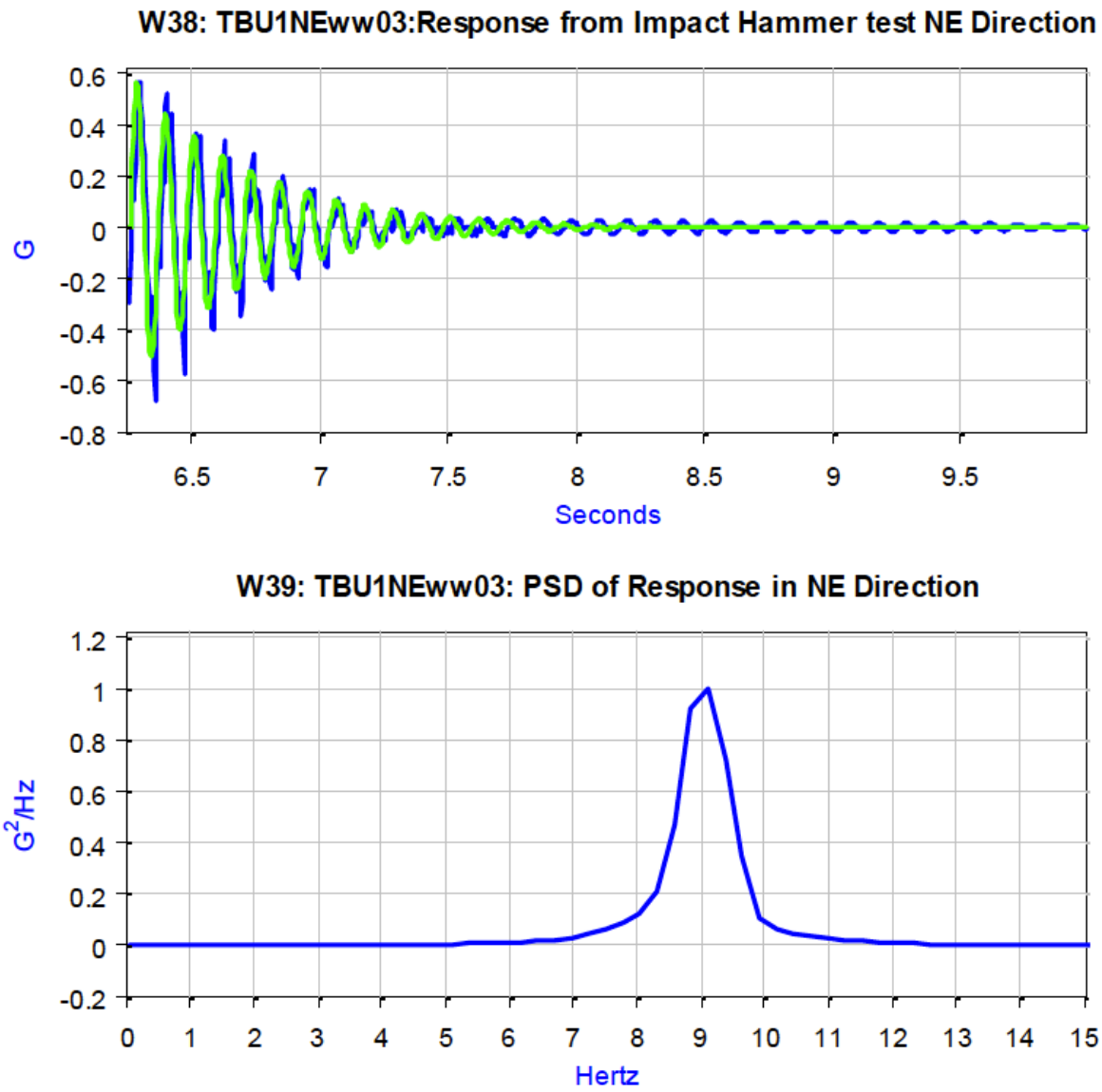

Figure 102: Transfer Functions – Bushing #4A

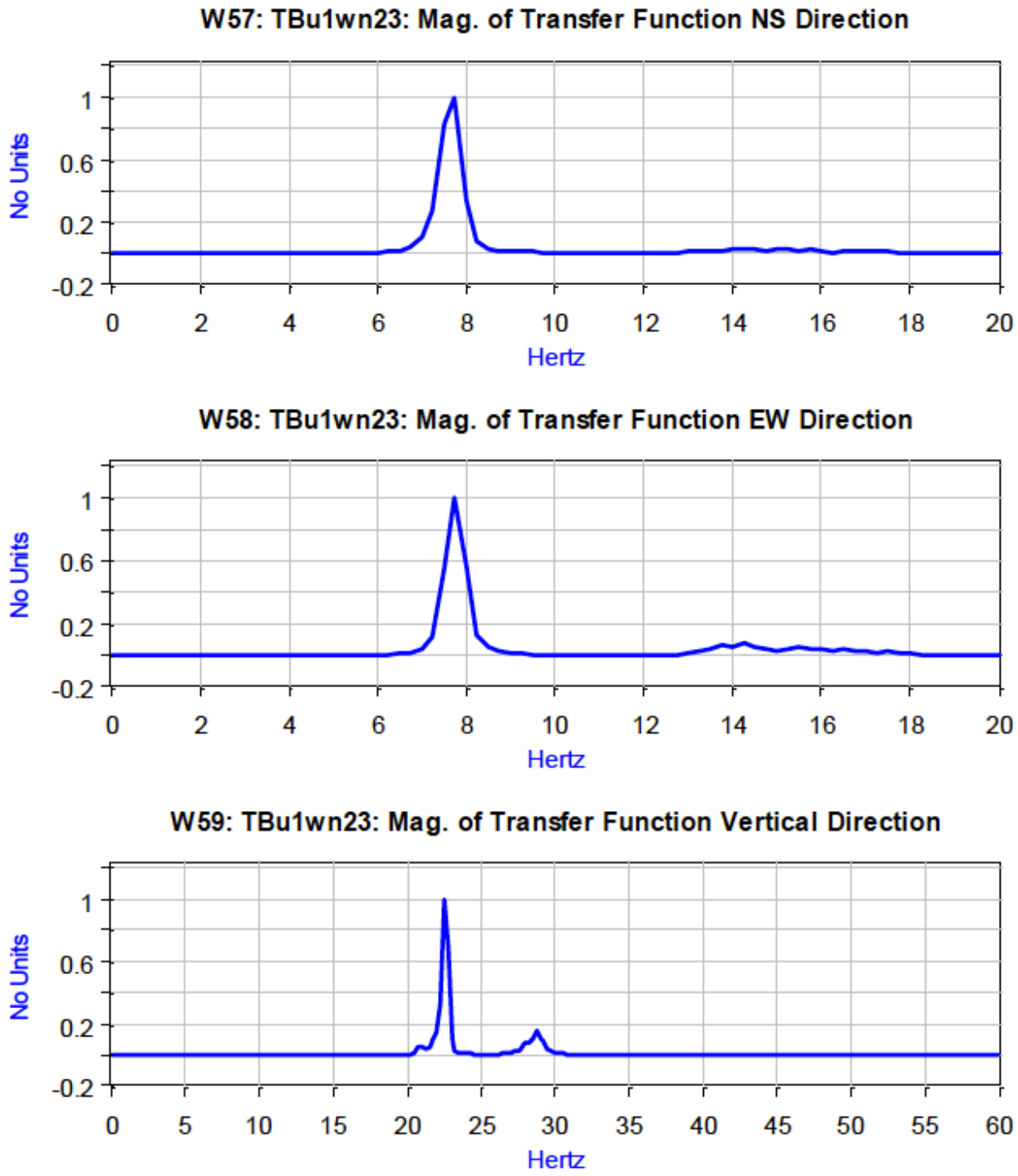

Figure 103: Table Impulse Test Response – Bushing #4A

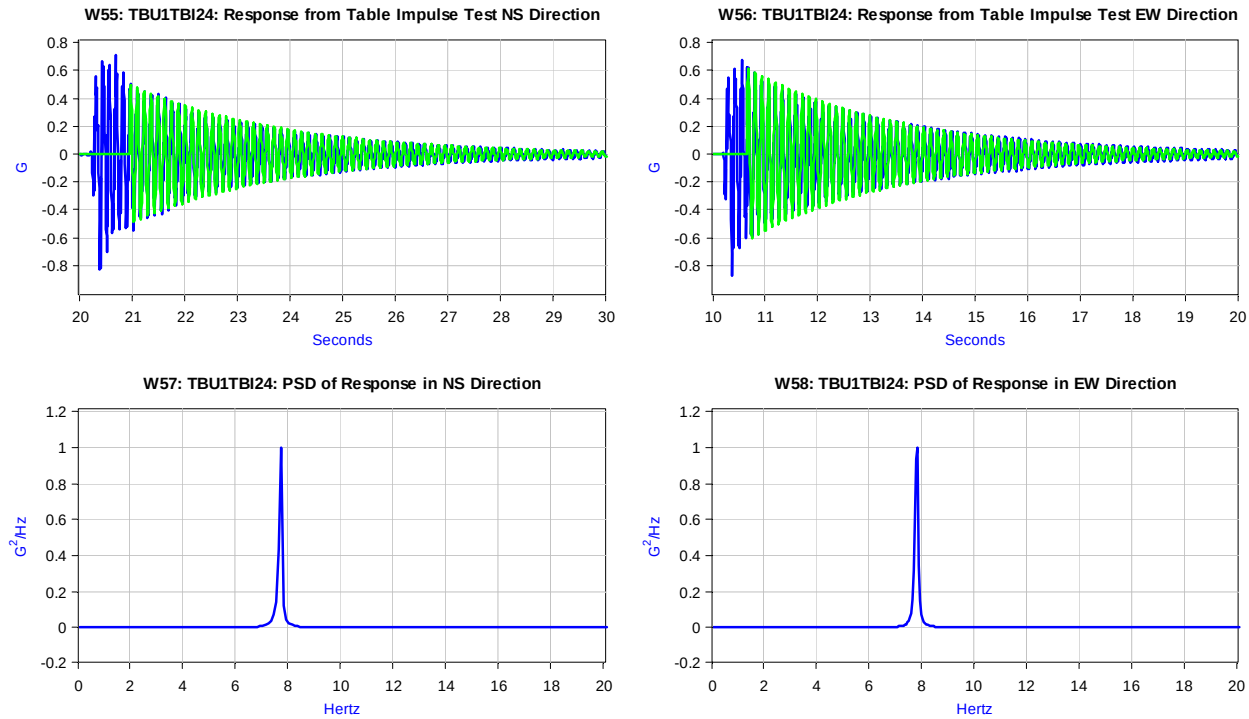

Figure 104: Acceleration Profile Along the Height of Bushing #4A – Rigid Frame

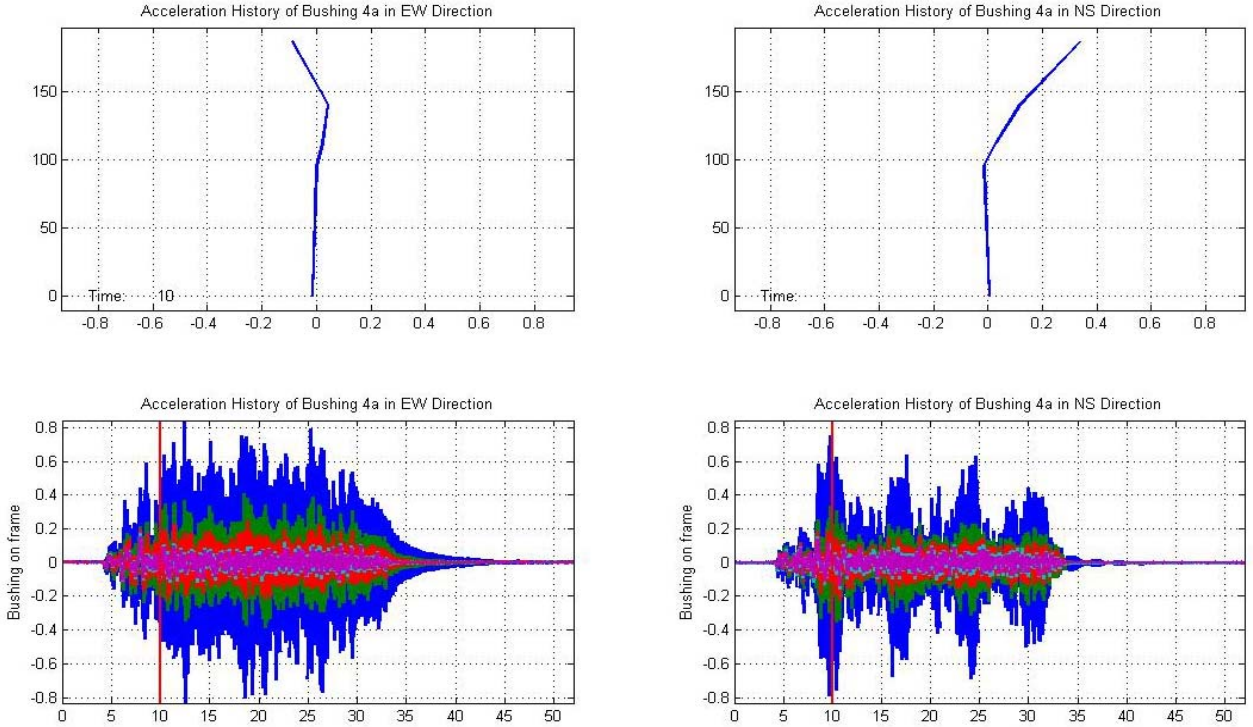

Table 29: Acceleration Distribution from Simulated Seismic Motion – Bushing #4A

Acceleration Distribution along the Height of Testing Setup																
Location	Units	0.125			0.125			0.125			0.125			0.125		
		TBU1AH12525			TBU1AH12530			TBU1AH12535			TBU1AH12545			TBU1AH12540		
(1)	(2)	(3)	(4)	(5)	(6)	(7)	(8)	(9)	(10)	(11)	(15)	(16)	(17)	(12)	(13)	(14)
Bushing Location on Frame																
		Center with 2 Stiffeners			Side with 2 Stiffeners			Side with no stiffeners			Corner with 1 Stiffeners			Corner with no Stiffeners		
Acceleration Distribution along the Height of Testing Setup																
Direction		NS	EW	Vertical	NS	EW	Vertical	NS	EW	Vertical	NS	EW	Vertical	NS	EW	Vertical
Top of Bushing	(g)	1.24	0.83	0.66	0.73	0.68	0.34	0.79	0.84	0.24	0.81	0.78	0.31	1.00	0.93	0.21
Upper CG Of Bushing	(g)	0.48	0.43	N/A	0.35	0.35	N/A	0.35	0.41	N/A	0.39	0.37	N/A	0.46	0.42	N/A
CG OF Bushing	(g)	0.30	0.26	N/A	0.21	0.20	N/A	0.23	0.25	N/A	0.21	0.21	N/A	0.25	0.23	N/A
Top of Frame/ Base of Bushing	(g)	0.21	0.19	0.61	0.14	0.17	0.25	0.16	0.17	0.18	0.15	0.18	0.25	0.16	0.18	0.18
Shake Table	(g)	0.18	0.17	0.12	0.12	0.15	0.10	0.14	0.16	0.11	0.14	0.16	0.11	0.15	0.16	0.11
Bending Moment at the Base of Bushing																
Moment from Strain Gauges	kip-in	11.28	8.00	N/A	7.39	6.67	N/A	7.20	8.20	N/A	7.85	7.67	N/A	9.24	9.91	N/A
Shear Force	Kip	N/A	N/A	N/A	N/A	N/A	N/A	N/A	N/A	N/A	N/A	N/A	N/A	N/A	N/A	N/A
Test Name.		TBU1AH12525			TBU1AH12530			TBU1AH12535			TBU1AH12545			TBU1AH12540		

Analytical Modeling of Installed Bushings

In parallel with the research to investigate the seismic performance of transformer/bushing systems by means of empirical testing of actual bushings in the laboratory, a parallel effort was also undertaken at SUNY-Buffalo to develop analytical models of bushings. The objective of this development work was to produce analytical (mathematical) models for the representation of transformer bushings that could be used in simulation studies, thereby allowing much more extensive, less costly and less time-consuming study of bushing response in as-installed conditions. It would, after all, be impractical to test every conceivable combination of bushing and transformer in use today, or contemplated for use, by utilities. But the development of accurate analytical models, validated with the empirical and experimental data available, and integrated with transformer analytical models, can potentially provide a valid means of analyzing transformer/bushing systems with reduced laboratory testing requirements.

The analytical background and simplified methods for evaluation of the dynamic properties and forces during bushing response and their incorporation into the needed bushing models are described in Appendix E. Formulations are done for one plane of behavior, assuming one principal direction of induced motion. Extension of the formulations to three-dimensional analysis would be relatively straightforward but much more involved mathematically, and is not included in the analysis.

CHAPTER 4:
Effects of Dynamic Response of Installed Bushings

This section analyses those specific effects that have been found to govern the dynamic behavior of as-installed bushings. First, an evaluation of the response of bushings installed on a rigid base versus the response of bushings on a flexible support is provided, in order to assess the sensitivity required in determining the bushings' properties. The evaluation is based on the numerical study with properties established in the experimental study.

Second, an evaluation of the impact of the location of bushings on the tank cover is developed based on experimental study and on the analytical understanding of the cover behavior.

Third, the effect of behavior on the base forces is presented while the evaluation of methods of measuring and calculating these forces provides a basis for further recommendations.

Fourth, this section explores the effects of rotational (rigid body) and vertical vibrations on the total response of the bushings.

Response of Bushings Installed on Flexible Cover Versus Installed on Rigid Cover

The response of a bushing when mounted on the transformer cover is depenent on its dynamic characteristics. However, if the bushing is installed on a rigid structure during the design-qualification process and then installed in the field on a flexible transformer cover, the response will be different. The responses and the amplifications in Figures 105 and 106 show the amplification of the roof cover of a 230 kV transformer and the response of the bushing tested (Bushing #6) if mounted on that transformer. (The orange lines represent the as-installed frequencies, or range of frequencies, of response, and the blue lines represent the fixed-base frequencies, or range of frequencies, of response.) The demand for one motion would be much below what the standard currently requires, but it would be much greater for the other motion. The factor of 2 required by the code will not be sufficiently conservative. The same situation would occur for the 500 kV transformer with a range of bushings (see Figure 107). If the whole set of bushings tested in this study is applied to the corresponding transformers, it is likely that many combinations of bushing and transformer will have frequencies in the larger amplification range.

If all bushings are subjected to the IEEE 693 spectral requirements, then most bushings installed on a flexible cover will have a larger demand than if mounted on a rigid base; see Figures 108–110, and Table 30.

Moreover, if mounted on a rigid structure and tested to the IEEE 693 requirements, the "stiffer" bushings, i.e., those having fixed base frequency larger than 8.0 Hz, will develop demands that will be lower than if they were mounted on a flexible cover, such as Bushings #6 and #7. All others will develop lateral demands in testing comparable to the lateral demands in the field

(those demands being in the higher portion of the spectrum). However, this is not a definitive result, as the rotational demands at the base of the bushing will be an additional variable.

Figure 105: Acceleration Spectra for 230 kV Transformer at HV Bushing

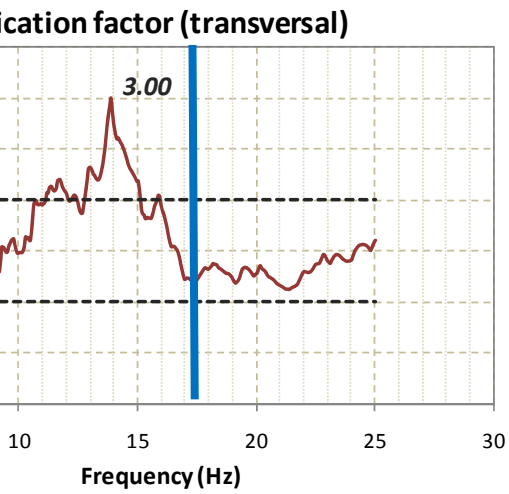

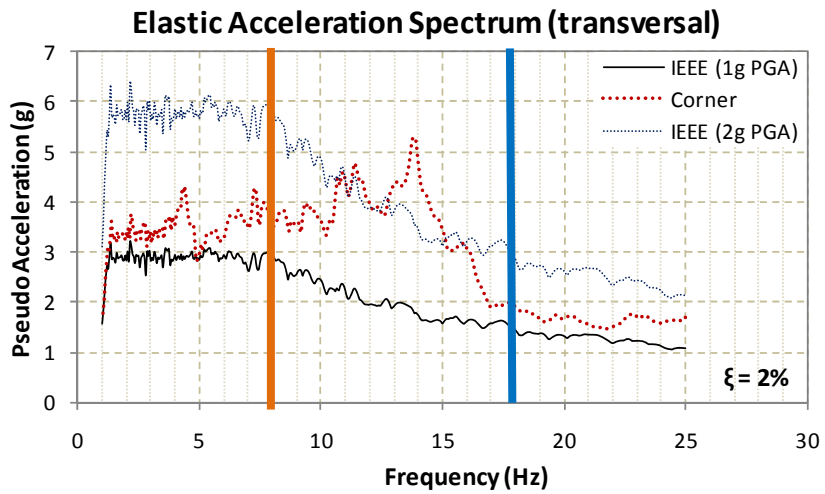

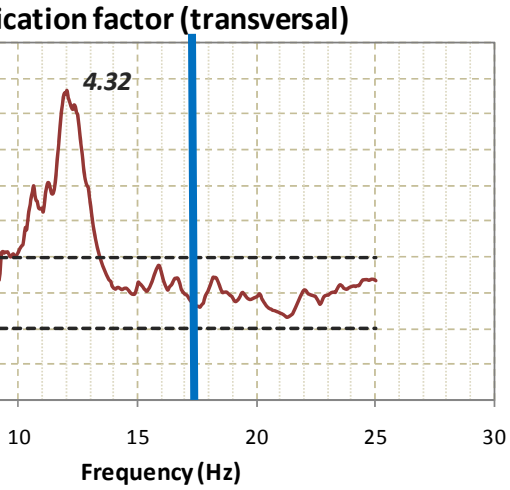

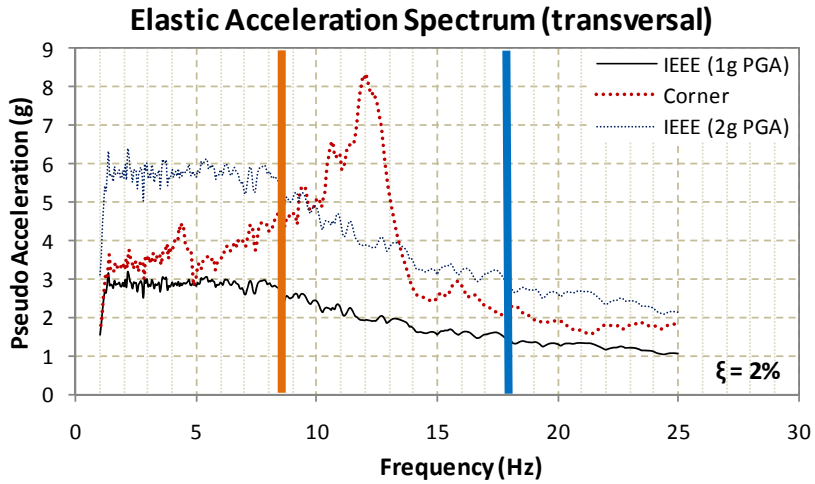

Reinhorn and Oikonomou, 2010

Figure 106: Acceleration Spectra for 230 kV Transformer at HV Bushing (cont'd.)

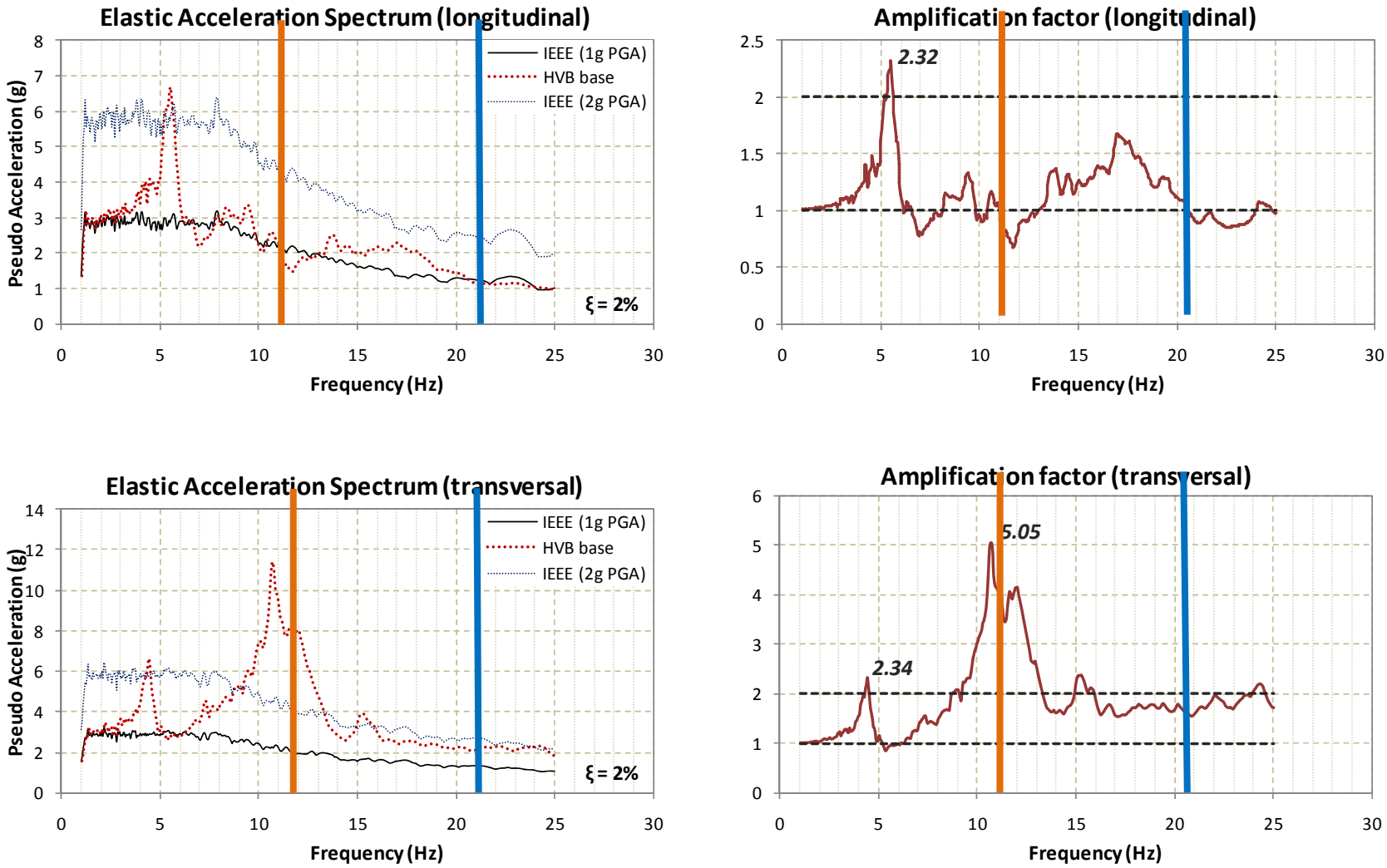

Reinhorn and Oikonomou, 2010

Figure 107: Acceleration Spectra for 500 kV Transformer at Bottom of HV Bushing

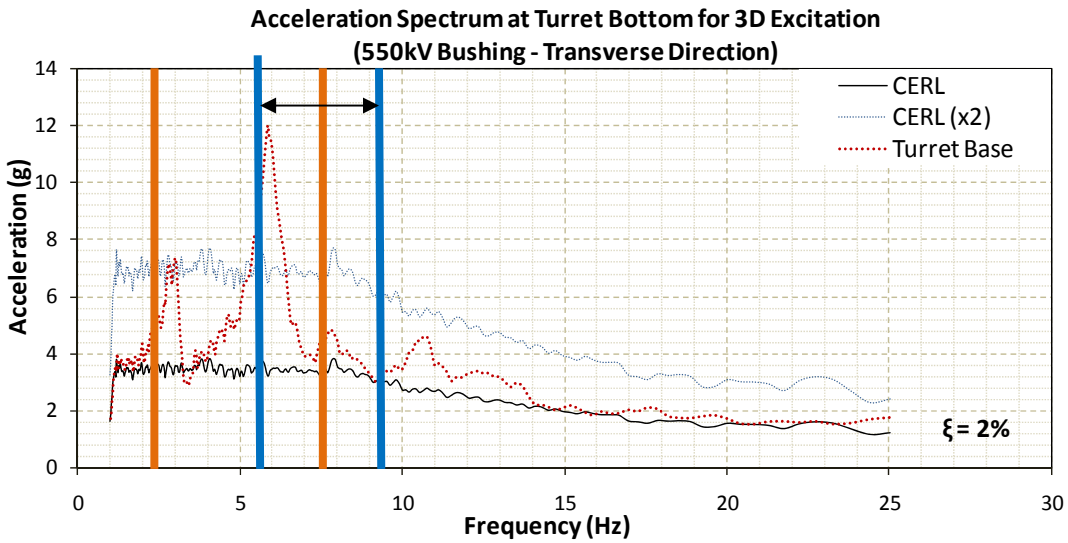

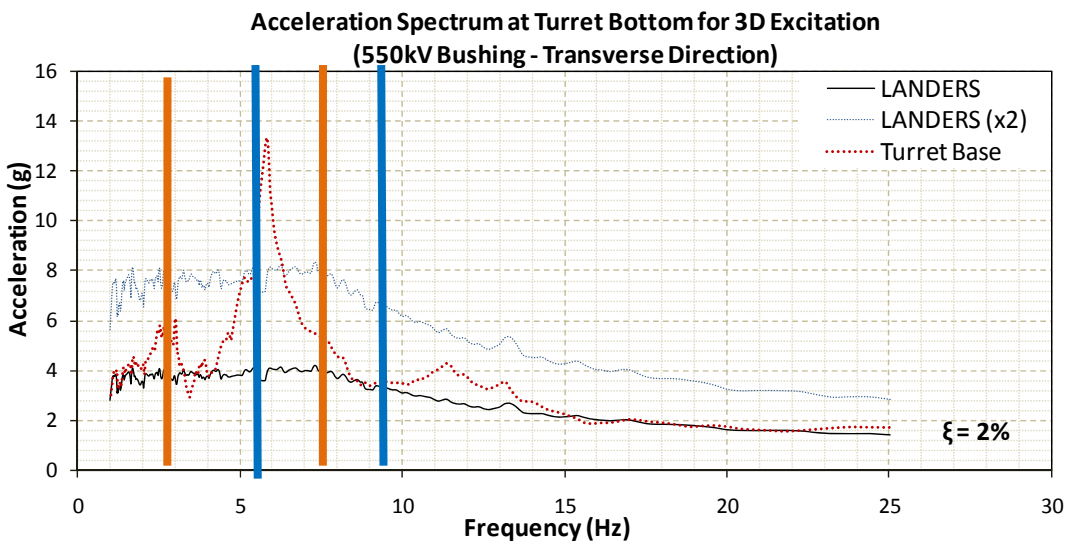

Reinhorn and Oikonomou, 2010

Figure 108: Spectral Amplification for 230 kV Transformer at Bottom of HV Bushing

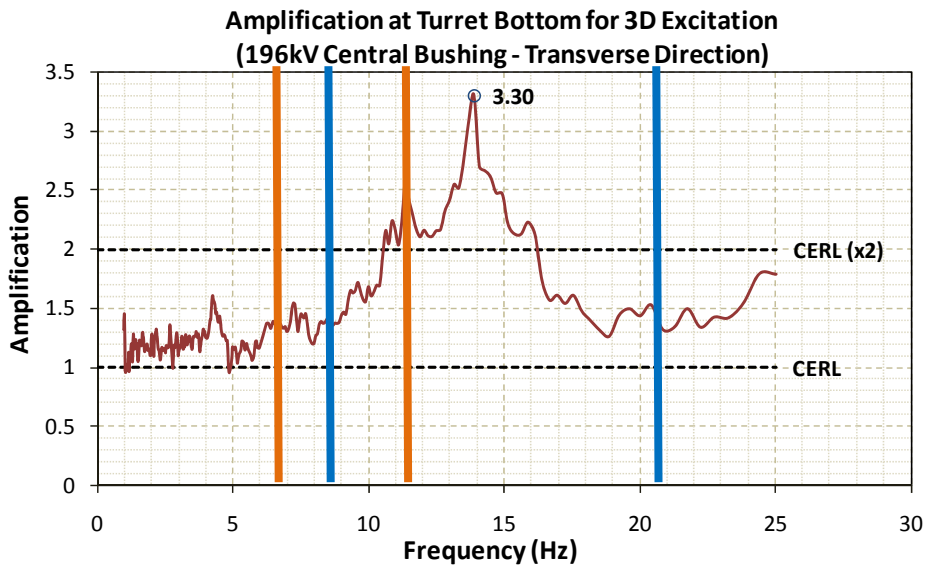

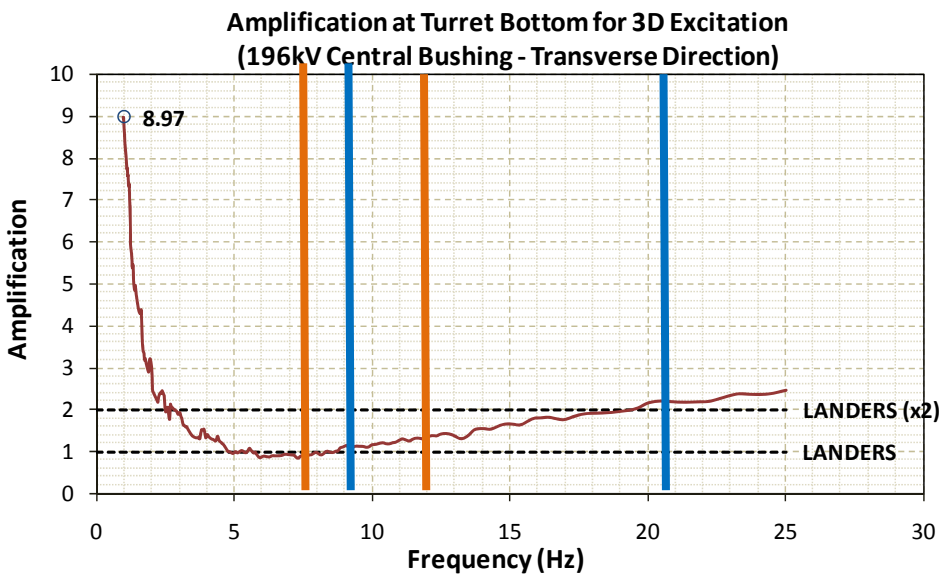

Reinhorn and Oikonomou, 2010

Figure 109: Acceleration Spectra and Expected Response of Bushings

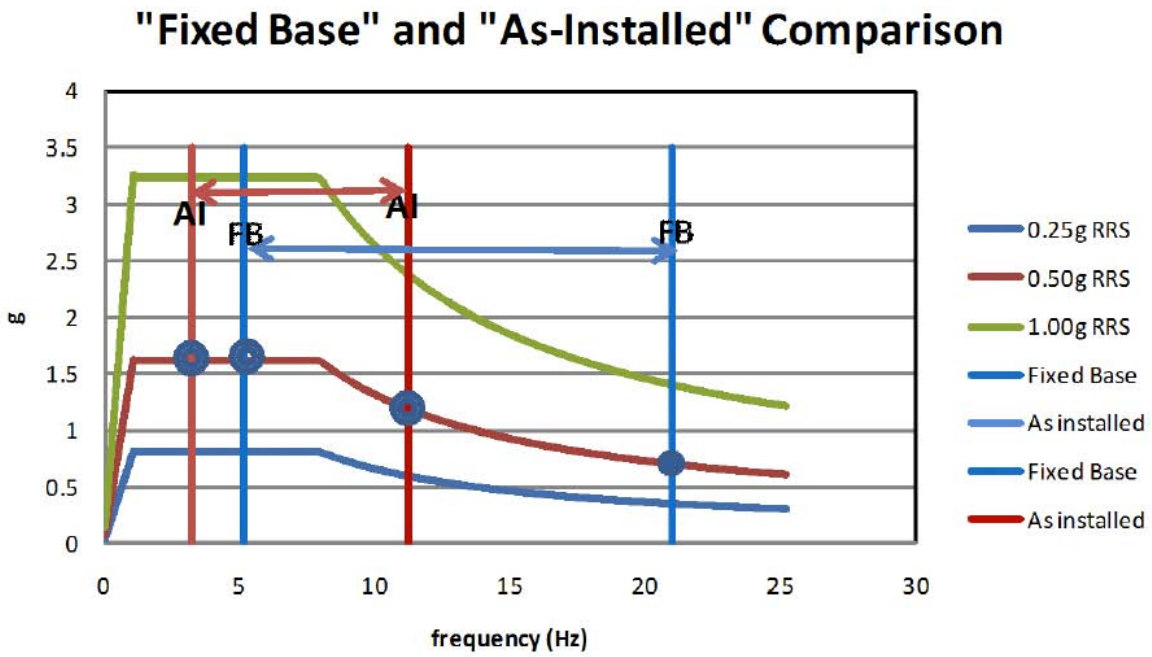

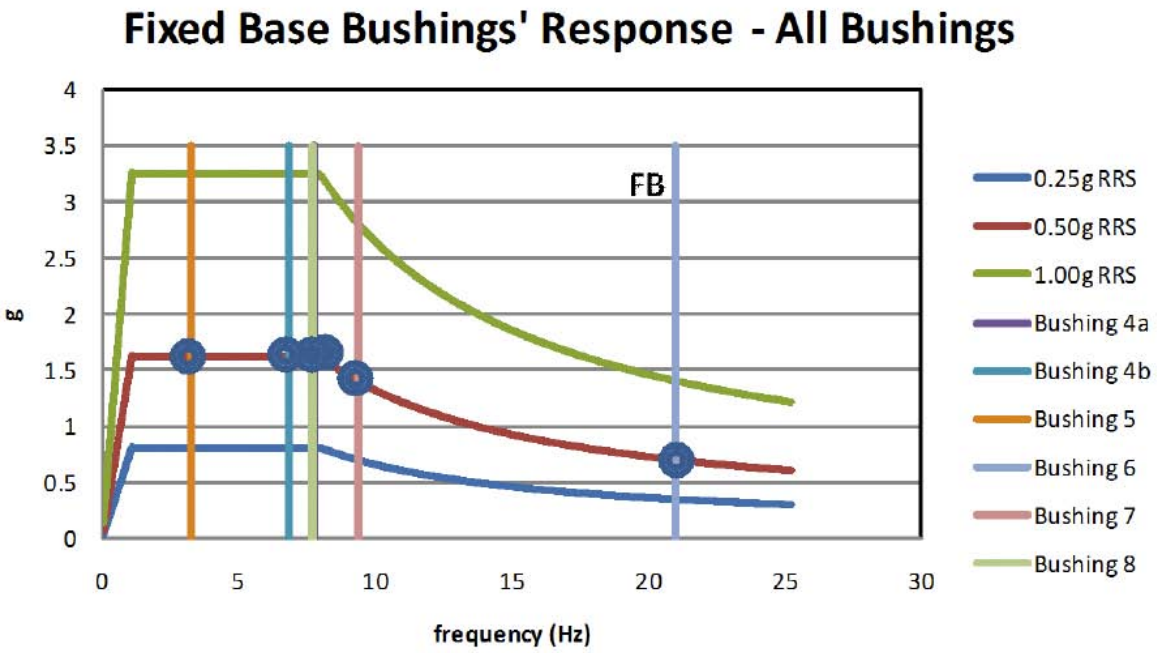

Figure 110: Acceleration Spectra and Expected Response of Bushings (cont'd.)

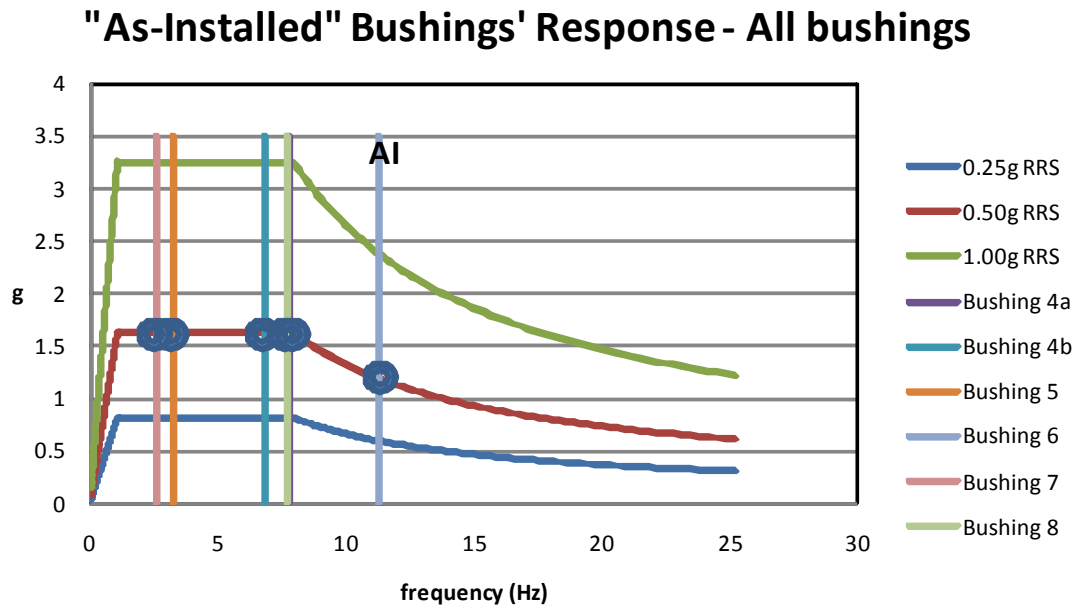

Table 30: Frequency (Hz) of Bushings in Analytical and Experimental Studies

Model Description	Rigid base	As Installed	Ratio A: Inst./Rigid (%)
(1)	(2)	(3)	(4)
Westinghouse 525 kV – mode 1	9.27	2.92	31.5
Siemens 230 kV – mode 1	16.85	9.14	54.2
Siemens 500 kV – mode 1	8.75	3.42	39.1
Ferranti-Packard 230 kV – mode 1	16.80	4.76	28.3
Bushing #1 – GE 500 kV	-	3.50	-
Bushing #2 – GE 550 kV	-	4.20	-
Bushing #3 – GE 550 kV	-	4.25	-
Bushing #4A – HSP 230 kV	8.55	7.50	87.7
Bushing #4B – HSP 230 kV	7.70	6.25	81.2
Bushing #5 – Trench 500 kV	5.20	3.25	62.5
Bushing #6 – ABB 196/230 kV	24.00	11.15	46.5
Bushing #7 – ABB 550 kV	9.10	2.50	27.5
Bushing #8 – ABB 550 kV	9.35	7.70	82.4
Minimum	5.20	2.50	27
Maximum	24.00	11.15	88

Effects of Location of Bushings on Transformer Cover

The frequencies for as-installed conditions, and their dependence on the location of bushings on the flexible base and on the use of a turret at the interface, are presented in Tables 31and 32; the frequency spectra show the same dependencies graphically in Figures 111 and 112. It should be noted that the transverse frequencies are strongly influenced by the corner mount that is changing the principal directions. Notable is the coupling of vertical and horizontal in the presence of a tilted bushing at a corner.

The location of the bushing near the edge changes the frequency in the direction perpendicular to the edge, increasing its value (see Figure 111, second row).

However, when the bushing is placed in the corner the frequency spectra measured in the longitudinal and transverse directions show two adjacent peaks (see Figure 111, third row). This is characteristic to principal directions not co-located with the longitudinal-transversal ones but positioned at 45° to those directions. The 45° directions are the principal directions of vibrations. In practice, these two frequencies are close together and lead to “beating,” or circular motion of bushings.

The vertical frequencies are also dependent on the location (see Figure 111, third column), which shows that the closer the bushing is to the edge, the higher the frequency; but if the bushing is in the center position, the frequency is lower and leads to larger vibrations and demands on the bushings.

With a tilted turret the vertical frequencies are affected, but in the corner position coupling appears between the vertical and horizontal frequencies (see Figure 112).

These influences in the magnification of response are significant, and must be considered in the qualification of bushings.

Table 31: Bushing Locations and Connection Interfaces on Flexible Transformer Cover

	No Turret	Vertical Turret	Tilted Turret
Bushing at Center	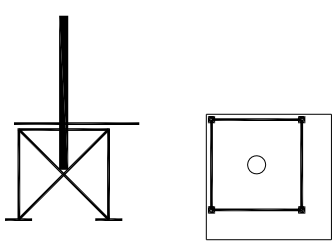	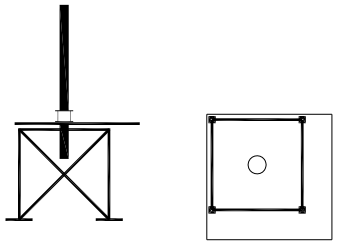	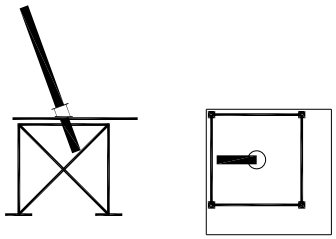
Bushing at Side	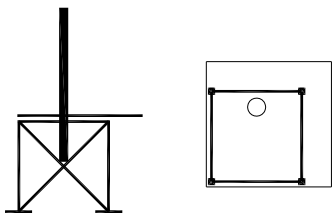	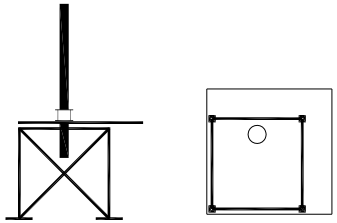	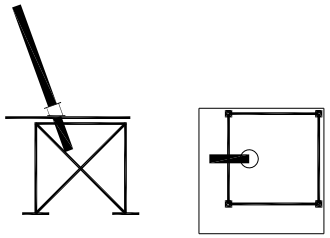
Bushing at Corner	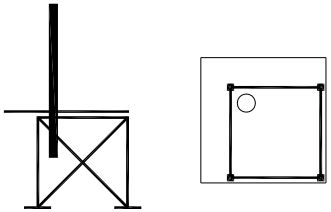	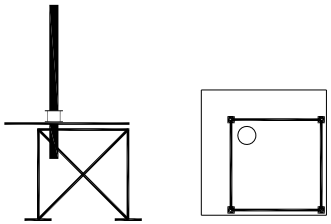	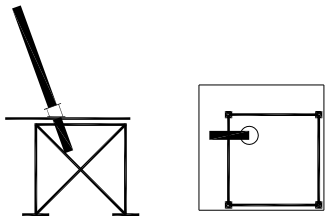

Kong, 2010

Table 32: As-Installed Frequencies of Different Bushings in Different Mounting Locations

Bushing location	No Turret			Vertical Turret			Tilted Turret		
	x	y	z	x	y	z	x	y	z
(1)	(2)	(3)	(4)	(5)	(6)	(7)	(8)	(9)	(10)
Bushing #2									
Bushing at center	2.7	2.7	8.2	-	-	-	2.9	2.8	8.6
Bushing at side	3.3	2.7	13.3	-	-	-	-	-	-
Bushing at corner	2.9 / 4.0	2.9 / 4.0	17.1	-	-	-	3.2 / 4.2	3.2./4.2	17.9
Bushing #3									
Bushing at center			8.6	4.0	4.0	8.6	4.2	4.0	9.3
Bushing at side			12.5	3.6	5.0	13.7	5.3	3.9	13.7
Bushing at corner			21.0	4.2	4.2	23.1	4.0 / 4.6	4.0 / 4.6	22.6

Figure 111: Frequency Dependence on Bushing Location – No Turret

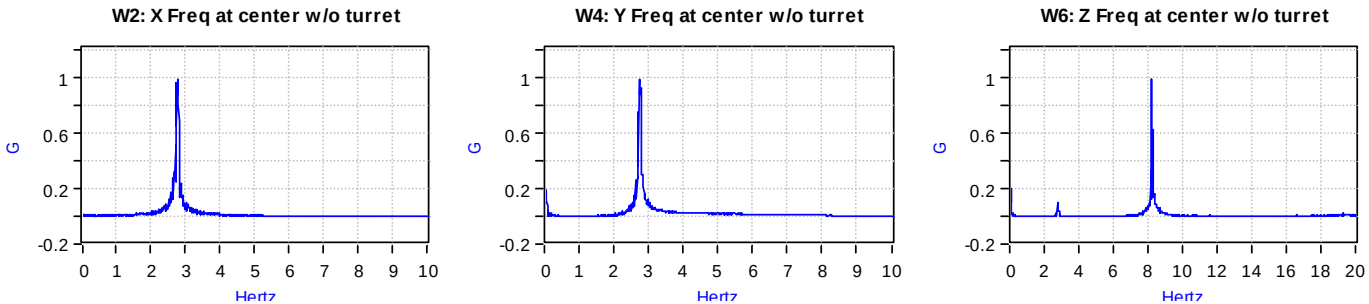

a) Bushing at center w/o turret

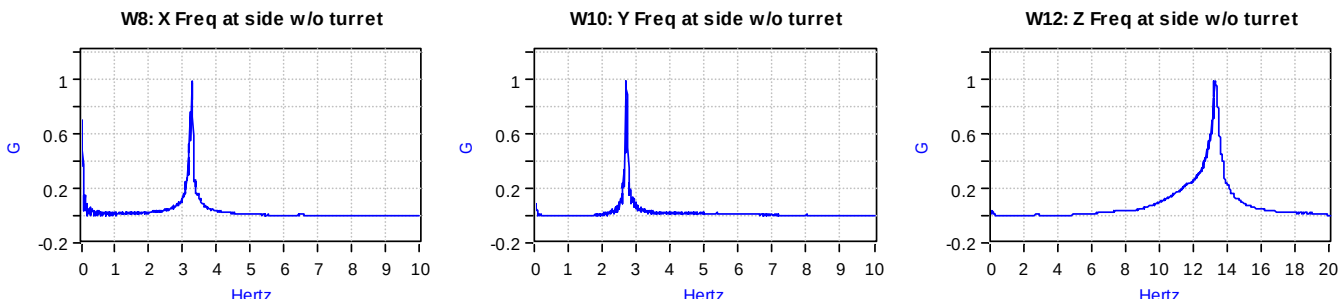

b) Bushing at side w/o turret

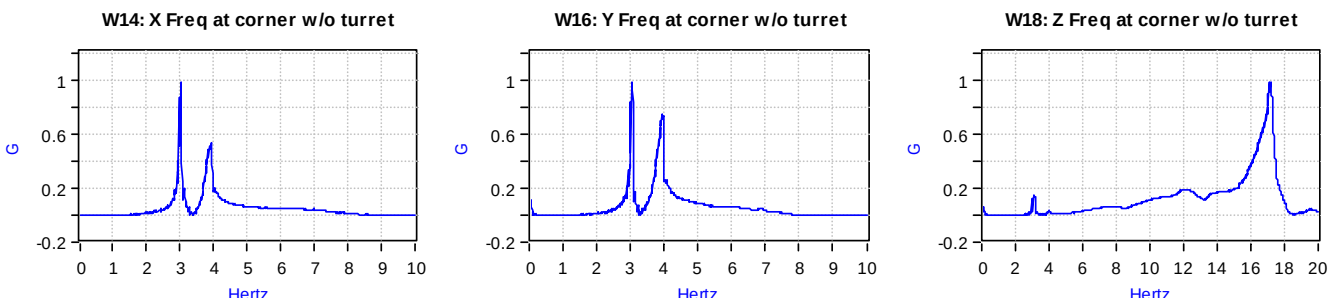

c) Bushing at corner w/o turret

Figure 112: Frequency Dependence on Bushing Location – Tilted Turret

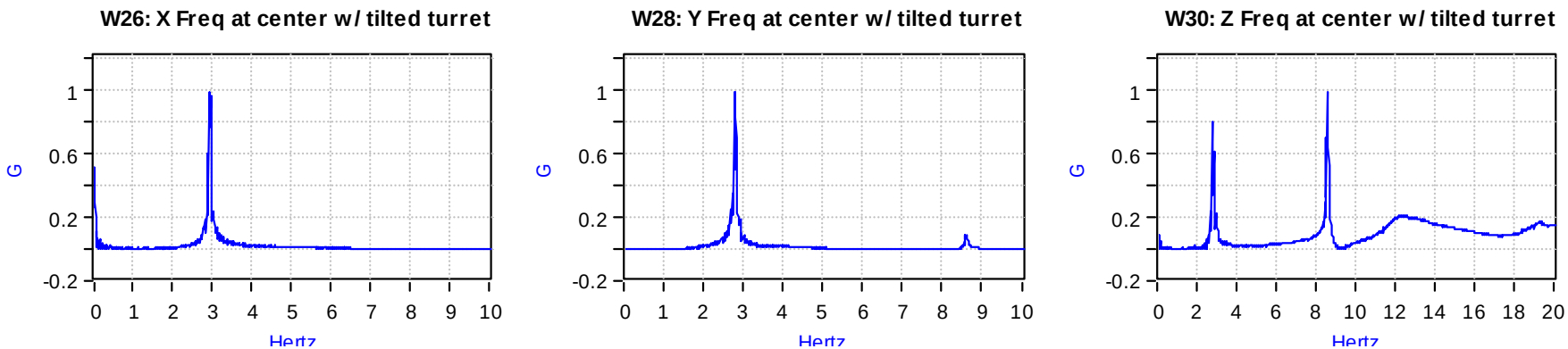

a) Bushing at center w/ tilted turret

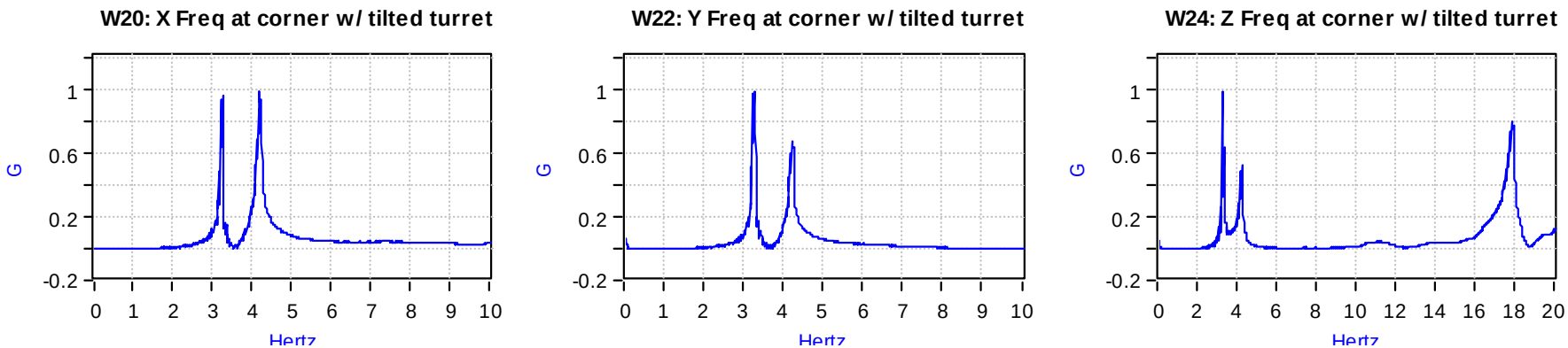

b) Bushing at corner w/ tilted turret

Forces at Bushings' Connections

Shear forces and moments at the base of the bushing, if they exceed the bushing's shear or moment capacity, can cause bushing slippage or damage, and bushing failure. The bushing's capacity is therefore defined as the amount of shear and/or moment forces at which failure occurs.

Forces and moments were determined through two methods: (a) direct measurement using strain gauges, calibrated either statically or electronically (shunt calibrations); and (b) using calculated values from acceleration measurements.

For the direct measurement methods, strain gauges were connected to the flanges of bushings and calibrated during pull tests.

However, IEEE 693 requires the calculation of forces from measured accelerations at the center of gravity multiplied by the total mass and by the height of the center of gravity above the mounting surface. This study shows that this formulation may not be the best way of calculating the moment demand on bushings.

As explained in Appendix E, the moment can be approximated if the acceleration and mass distributions can be assumed linear. In such a case it was shown that the moment can be calculated as:

$$M_B = \frac{m_b H^2 a_0}{12}\left[\left(a_b / a_0 + 1\right) + \frac{m_0}{m_b}\left(a_b / a_0 + 3\right)\right] \tag{117}$$

(NB: Equation numbers in this section correspond to those in Appendix E.) This equation can be simplified for different cases of mass and acceleration distribution. The cases are presented in Appendix E, and the formulae are presented here again along with the tables.

1) Case I: $a_b = a_o$ and $m_o = m_b$, constant acceleration and mass:

$$V_1 = m_b H a_0 \tag{118}$$

$$M_1 = \frac{m_b H^2 a_o}{2} \tag{119}$$

2) Case II: a_0 *and* $m_0 = m_b$, inverted triangular acceleration and constant mass:

$$V_2 = \frac{m_b H a_0}{2} = \frac{V_1}{2} = 0.50\, V_1 \tag{120}$$

$$M_2 = \frac{m_b H^2 a_o}{3} = \frac{M_1}{1.5} = 0.667 M_1 \tag{121}$$

3) Case III: $a_b = 0$ and $m_o = m_b /2$: inverted triangular acceleration and variable mass:

$$V_2 = \frac{m_b H a_0}{2} = \frac{V_1}{2} = 0.50\, V_1 \tag{122}$$

$$M_3 = \frac{m_b H^2 a_o}{4.8} = \frac{M_1}{2.4} = 0.417 M_1 \tag{123}$$

It should be noted that a_o is the acceleration at the top of bushing in the above formulations.

Assuming a uniform acceleration as in Case 1 above:

$$V = a_b \int_0^H m(z)\,dz = \frac{W}{g} a_b = \frac{W}{g} a_{CG} \tag{124}$$

where W is the weight of the structure above the flange section, and

$$M = a_b \int_0^H m(z)\,z\,dz = a_b \int_0^H m(z)\,dz \times \frac{\int_0^H m(z)\,z\,dz}{\int_0^H m(z)\,dz} = \frac{W}{g} a_b Z_{CG} = \frac{W}{g} a_{CG} Z_{CG} \tag{125}$$

Note that in this case the term Z_{CG} is dependent on the distribution of the mass *m(z)* only.

These last approximations are gross approximations, valid only for constant mass and acceleration distribution, which are not realistic.

Tables 33–38 show a comparison of directly measured forces and moments versus calculated values using the above relations.

The directly measured values and the values calculated by approximations do not match consistently. The most appropriate seems to be the inverted triangular acceleration distribution and constant mass (Eqs. (120) and (121)), in particular for Bushing #6. It should be mentioned that in all other bushing tests the calibration of strain gauges for direct measurement of forces were done for other purposes, with larger allowable errors. But the calibrations for Bushing #6 were carefully done and repeated; therefore, the direct measurements are most reliable.

In addition to measurements and calculations made for the original study, the shear forces and moments of Bushing #6 were obtained in an additional experimental study using direct measurements and the approximated formulation for Case 1 as shown by Eqs. (118) and (119), with data from Koliou et al., (2011).

Table 39 presents the moments, shears and elevations of the inertia centroid (IC) measured directly using strain gauges and calculated using Equation (116) with measured acceleration during testing. The inertia centroid (IC) is defined as the ratio of base moment to the shear force. Table 40 presents the ratios of the direct measurements to the calculated values.

Inspection of Tables 39 and 40 reveals that the calculated forces have better agreement with direct measurements than the calculated moments have with the direct measurements. The shear forces vary by up to 34% and the moments vary by up to 64%. Also, it is noticed that the centroids of inertia are elevated differently for bushings of different stiffness, and are usually larger than the position of center of gravity (CG), which was 14 inches for this bushing.

While the estimate of the shear forces by the simplest of the formulas is conservative, the base moments are not so conservative and may underestimate the actual values by as much as 50%.

Since the forces at the bases of bushings have a big role in the definition of strength capacity (forces and moments associated with failure) and in determining the seismic demand (forces that appear at various levels of excitations), the approximated calculations may not be suitable, while direct measurements can be reliable if calibrated properly.

Table 33: Acceleration and Strain Gauge Measurements of Bushing #4A

Bending moment Table						
g RRS		0.125	0.125	0.125	0.125	0.125
	Units	TBU1AH12525	TBU1AH12530	TBU1AH12535	TBU1AH12540	TBU1AH12545
(1)	(2)	(3)	(4)	(5)	(6)	(7)
Direct Measurement at the Base of Bushing						
NS	Kip-in	11.28	7.39	7.20	9.24	7.85
EW	Kip-in	8.00	6.67	8.20	9.91	7.67
Calculated Moment from M_{total} and a_{total}						
NS	Kip-in	2.60	1.84	1.95	2.17	1.82
EW	Kip-in	2.25	1.76	2.17	1.95	1.82
Calculated Moment from M_{UPPER} and a_{Upper}						
NS	Kip-in	5.36	3.85	3.91	5.13	4.35
EW	Kip-in	4.74	3.91	4.58	4.69	4.13
Calculated Moment from Equation 110						
NS	Kip-in	14.00	8.29	8.91	11.32	9.17
EW	Kip-in	9.35	7.70	9.51	10.53	8.83
Calculated Moment from Equation 112						
NS	Kip-in	9.34	5.53	5.95	7.55	6.12
EW	Kip-in	6.24	5.14	6.35	7.03	5.89
Calculated Moment from Equation 114						
NS	Kip-in	5.84	3.46	3.72	4.73	3.83
EW	Kip-in	3.90	3.21	3.97	4.40	3.69
Calculated Shear Force from Equation 109						
NS	Kip	0.33	0.19	0.21	0.26	0.21
EW	Kip	0.22	0.18	0.22	0.24	0.21
Calculated Shear Force from Equation 111						
NS	Kip	0.17	0.10	0.11	0.14	0.11
EW	Kip	0.11	0.09	0.12	0.13	0.11
Calculated Shear Force from Equation 113						
NS	Kip	0.12	0.07	0.08	0.10	0.08
EW	Kip	0.08	0.07	0.08	0.09	0.08

Ratio of Calculated to Measured Moments						
g RRS		0.125	0.125	0.125	0.125	0.125
	Units	TBU1AH12525	TBU1AH12530	TBU1AH12535	TBU1AH12540	TBU1AH12545
Calculated VS measured (M total) Moment						
NS	Kip-in	0.23	0.25	0.27	0.23	0.23
EW	Kip-in	0.28	0.26	0.26	0.20	0.24
Calculated VS measured (M Upper) Moment						
NS	Kip-in	0.47	0.52	0.54	0.56	0.55
EW	Kip-in	1.69	1.71	1.79	2.11	1.86
Calculated VS measured (Eq 110) Moment						
NS	Kip-in	1.24	1.12	1.24	1.23	1.17
EW	Kip-in	1.17	1.15	1.16	1.06	1.15
Calculated VS measured (Eq 112) Moment						
NS	Kip-in	0.83	0.75	0.83	0.82	0.78
EW	Kip-in	0.78	0.77	0.77	0.71	0.77
Calculated VS measured (Eq 114) Moment						
NS	Kip-in	0.52	0.47	0.52	0.51	0.49
EW	Kip-in	0.49	0.48	0.48	0.44	0.48

Table 34: Acceleration and Strain Gage Measurements of Bushing #4B

Bending moment Table							
g RRS		0.25	0.50	1.00	2.00	2.50	3.00
	Units	TBU2AH25	TBU2AH50	TBU2AH100	TBU2AH200	TBU2AH250	TBU2AH300
(1)	(2)	(3)	(4)	(5)	(6)	(7)	(8)
Direct Measurement at the Base of Bushing							
NS	Kip-in	13.50	25.71	46.92	100.28	N/A	N/A
EW	Kip-in	14.15	30.24	59.18	110.64	N/A	N/A
Calculated Moment from M_{total} and a_{total}							
NS	Kip-in	2.64	5.94	11.90	17.32	N/A	N/A
EW	Kip-in	2.74	5.75	11.38	18.52	N/A	N/A
Calculated Moment from M_{UPPER} and a_{Upper}							
NS	Kip-in	6.52	12.85	27.90	39.71	N/A	N/A
EW	Kip-in	5.64	11.04	21.64	45.97	N/A	N/A
Calculated Moment from Equation 110							
NS	Kip-in	11.87	23.57	50.96	80.70	N/A	N/A
EW	Kip-in	11.09	22.29	39.94	76.35	N/A	N/A
Calculated Moment from Equation 112							
NS	Kip-in	7.92	15.73	34.01	53.85	N/A	N/A
EW	Kip-in	7.40	14.87	26.65	50.95	N/A	N/A
Calculated Moment from Equation 114							
NS	Kip-in	4.96	9.85	21.29	33.71	N/A	N/A
EW	Kip-in	4.63	9.31	16.68	31.90	N/A	N/A
Calculated Shear Force from Equation 109							
NS	Kip	0.28	0.56	1.21	1.92	N/A	N/A
EW	Kip	0.26	0.53	0.95	1.82	N/A	N/A
Calculated Shear Force from Equation 111							
NS	Kip	0.15	0.30	0.66	1.04	N/A	N/A
EW	Kip	0.14	0.29	0.51	0.98	N/A	N/A
Calculated Shear Force from Equation 113							
NS	Kip	0.11	0.22	0.47	0.74	N/A	N/A
EW	Kip	0.10	0.21	0.37	0.70	N/A	N/A

Ratio of Calculated to Measured Moments							
g RRS		0.25	0.50	1.00	2.00	2.50	3.00
Test Name		TBU2AH25	TBU2AH50	TBU2AH100	TBU2AH200	TBU2AH250	TBU2AH300
Calculated VS measured (M total) Moment							
NS		0.20	0.23	0.25	0.17	N/A	N/A
EW		0.19	0.19	0.19	0.17	N/A	N/A
Calculated VS measured (M Upper) Moment							
NS		0.48	0.50	0.59	0.40	N/A	N/A
EW		0.40	0.37	0.37	0.42	N/A	N/A
Calculated VS measured (Eq 110) Moment							
NS		0.88	0.92	1.09	0.80	N/A	N/A
EW		0.78	0.74	0.67	0.69	N/A	N/A
Calculated VS measured (Eq 112) Moment							
NS		0.59	0.61	0.72	0.54	N/A	N/A
EW		0.52	0.49	0.45	0.46	N/A	N/A
Calculated VS measured (Eq 114) Moment							
NS		0.37	0.38	0.45	0.34	N/A	N/A
EW		0.33	0.31	0.28	0.29	N/A	N/A

Table 35: Acceleration and Strain Gauge Measurements of Bushing #5

Bending moment Table							
g RRS		0.25	0.50	1.00	2.00	2.50	3.00
	Units	TB35AH25	TB38AH50	TB41AH100	TB44AH150	TB47AH225	TN53AH300
(1)	(2)	(3)	(4)	(5)	(6)	(7)	(8)
Direct Measurement at the Base of Bushing							
NS	Kip-in	36.76	51.13	194.61	369.99	677.86	879.25
EW	Kip-in	68.26	107.50	353.45	604.03	1010.59	1036.89
Calculated Moment from M_{total} and a_{total}							
NS	Kip-in	56.59	71.98	213.66	332.87	562.01	690.58
EW	Kip-in	52.59	70.16	291.43	460.13	601.63	596.37
Calculated Moment from M_{UPPER} and a_{Upper}							
NS	Kip-in	60.73	76.91	262.24	425.98	N/A	N/A
EW	Kip-in	59.60	90.34	351.32	540.78	771.90	789.70
Calculated Moment from Equation 110							
NS	Kip-in	121.80	155.19	554.23	925.24	1554.07	1755.03
EW	Kip-in	127.67	195.61	743.32	1300.16	1934.99	1712.49
Calculated Moment from Equation 112							
NS	Kip-in	82.70	105.36	376.30	628.19	1055.13	1191.57
EW	Kip-in	86.68	132.81	504.68	882.75	1313.76	1162.69
Calculated Moment from Equation 114							
NS	Kip-in	53.37	68.00	242.84	405.40	680.93	768.98
EW	Kip-in	55.94	85.71	325.69	569.68	847.84	750.34
Calculated Shear Force from Equation 109							
NS	Kip	1.24	1.59	5.66	9.45	15.87	17.93
EW	Kip	1.30	2.00	7.59	13.28	19.76	17.49
Calculated Shear Force from Equation 111							
NS	Kip	0.63	0.81	2.88	4.81	8.09	9.13
EW	Kip	0.66	1.02	3.87	6.76	10.07	8.91
Calculated Shear Force from Equation 113							
NS	Kip	0.43	0.55	1.96	3.27	5.49	6.20
EW	Kip	0.45	0.69	2.63	4.59	6.84	6.05

Ratio of Calculated to Measured Moments						
g RRS	0.25	0.50	1.00	2.00	2.50	3.00
Test Name	TBU2AH25	TBU2AH50	TBU2AH100	TBU2AH200	TBU2AH250	TBU2AH300
Calculated VS measured (M total) Moment						
NS	1.54	1.41	1.10	0.90	0.83	0.79
EW	0.77	0.65	0.82	0.76	0.60	0.58
Calculated VS measured (M Upper) Moment						
NS	1.65	1.50	1.35	1.15	N/A	N/A
EW	0.87	0.84	0.99	0.90	0.76	0.76
Calculated VS measured (Eq 110) Moment						
NS	3.31	3.04	2.85	2.50	2.29	2.00
EW	1.87	1.82	2.10	2.15	1.91	1.65
Calculated VS measured (Eq 112) Moment						
NS	2.25	2.06	1.93	1.70	1.56	1.36
EW	1.27	1.24	1.43	1.46	1.30	1.12
Calculated VS measured (Eq 114) Moment						
NS	1.45	1.33	1.25	1.10	1.00	0.87
EW	0.82	0.80	0.92	0.94	0.84	0.72

Table 36: Acceleration and Strain Gauge Measurements of Bushing #6

Bending moment Table									
g RRS		0.25	0.25	0.50	0.75	1.00	1.25	1.50	1.75
	Units	TB21AH025	TB24AH025	TB27AH050	TB30AH075	TB33AH100	TB38AH125	TB41AH150	TB44AH175
(1)	(2)	(3)	(4)	(5)	(6)	(7)	(8)	(9)	(10)
Direct Measurement at the Base of Bushing									
NS	Kip-in	7.65	13.23	21.14	30.75	39.57	56.56	57.08	56.05
EW	Kip-in	10.54	19.95	33.57	56.63	72.70	92.18	97.08	107.52
Calculated Moment from M_{total} and a_{total}									
NS	Kip-in	2.63	5.33	10.21	11.73	16.28	21.94	25.68	30.06
EW	Kip-in	2.39	4.49	8.35	12.18	16.22	21.05	25.05	29.00
Calculated Moment from M_{UPPER} and a_{Upper}									
NS	Kip-in	4.39	9.01	17.65	23.78	32.24	43.64	45.90	52.48
EW	Kip-in	4.37	8.72	15.75	24.40	32.62	44.07	46.57	52.77
Calculated Moment from Equation 110									
NS	Kip-in	9.04	18.83	31.49	50.86	67.11	93.22	97.37	110.48
EW	Kip-in	9.42	18.21	32.21	51.49	65.80	83.18	93.39	107.12
Calculated Moment from Equation 112									
NS	Kip-in	6.22	12.95	21.65	34.98	46.15	64.10	66.95	75.97
EW	Kip-in	6.48	12.52	22.15	35.40	45.25	57.19	64.22	73.66
Calculated Moment from Equation 114									
NS	Kip-in	4.10	8.54	14.27	23.06	30.42	42.26	44.14	50.09
EW	Kip-in	4.27	8.26	14.60	23.34	29.83	37.71	42.34	48.56
Calculated Shear Force from Equation 109									
NS	Kip	0.24	0.49	0.82	1.32	1.74	2.42	2.53	2.87
EW	Kip	0.24	0.47	0.84	1.34	1.71	2.16	2.43	2.79
Calculated Shear Force from Equation 111									
NS	Kip	0.12	0.25	0.42	0.68	0.90	1.25	1.31	1.48
EW	Kip	0.13	0.24	0.43	0.69	0.88	1.12	1.25	1.44
Calculated Shear Force from Equation 113									
NS	Kip	0.08	0.17	0.29	0.47	0.62	0.86	0.90	1.02
EW	Kip	0.09	0.17	0.30	0.48	0.61	0.77	0.86	0.99

Ratio of Calculated to Measured Moments								
g RRS	0.25	0.25	0.50	0.75	1.00	1.25	1.50	1.75
Test Name	TB21AH025	TB24AH025	TB27AH050	TB30AH075	TB33AH100	TB38AH125	TB41AH150	TB44AH175
Calculated VS measured (M total) Moment								
NS	0.34	0.40	0.48	0.38	0.41	0.39	0.45	0.54
EW	0.23	0.23	0.25	0.22	0.22	0.23	0.26	0.27
Calculated VS measured (M Upper) Moment								
NS	0.57	0.68	0.83	0.77	0.81	0.77	0.80	0.94
EW	0.41	0.44	0.47	0.43	0.45	0.48	0.48	0.49
Calculated VS measured (Eq 110) Moment								
NS	1.18	1.42	1.49	1.65	1.70	1.65	1.71	1.97
EW	0.89	0.91	0.96	0.91	0.91	0.90	0.96	1.00
Calculated VS measured (Eq 112) Moment								
NS	0.81	0.98	1.02	1.14	1.17	1.13	1.17	1.36
EW	0.61	0.63	0.66	0.63	0.62	0.62	0.66	0.69
Calculated VS measured (Eq 114) Moment								
NS	0.54	0.65	0.68	0.75	0.77	0.75	0.77	0.89
EW	0.41	0.41	0.44	0.41	0.41	0.41	0.44	0.45

Table 37: Acceleration and Strain Gauge Measurements of Bushing #6 (cont'd.)

Bending moment Table										
g RRS		2.00	2.25	2.50	2.75	3.00	2.00	2.25	2.50	2.75
	Units	TB47AH200	TB50AH225	TB53AH250	TB56AH275	TB59AH300	TB62AH200	TB65AH225	TB68AH250	TB71AH275
(1)	(2)	(11)	(12)	(13)	(14)	(15)	(16)	(17)	(18)	(19)
Direct Measurement at the Base of Bushing										
NS	Kip-in	56.34	55.96	64.75	122.88	N/A	53.75	53.75	71.50	N/A
EW	Kip-in	116.82	128.48	167.97	133.27	N/A	138.19	187.75	286.41	N/A
Calculated Moment from M_{total} and a_{total}										
NS	Kip-in	34.55	34.68	39.13	39.40	47.30	33.57	37.66	42.08	40.69
EW	Kip-in	32.81	35.76	41.89	39.81	48.49	32.53	39.34	47.32	43.28
Calculated Moment from M_{UPPER} and a_{Upper}										
NS	Kip-in	59.50	56.96	64.29	113.80	124.32	58.23	59.86	55.62	N/A
EW	Kip-in	57.75	64.48	77.63	68.56	81.03	63.47	73.62	87.74	76.29
Calculated Moment from Equation 110										
NS	Kip-in	125.42	115.71	135.63	144.01	157.04	116.81	118.04	135.98	131.02
EW	Kip-in	120.98	139.27	155.35	138.06	154.67	126.04	133.54	144.46	148.49
Calculated Moment from Equation 112										
NS	Kip-in	86.24	79.56	93.27	99.03	107.98	80.32	81.17	93.51	90.10
EW	Kip-in	83.19	95.76	106.82	94.93	106.36	86.67	91.83	99.33	102.11
Calculated Moment from Equation 114										
NS	Kip-in	56.86	52.46	61.49	65.29	71.19	52.96	53.51	61.65	59.40
EW	Kip-in	54.85	63.14	70.43	62.59	70.12	57.14	60.54	65.49	67.32
Calculated Shear Force from Equation 109										
NS	Kip	3.26	3.01	3.53	3.74	4.08	3.04	3.07	3.54	3.41
EW	Kip	3.15	3.62	4.04	3.59	4.02	3.28	3.47	3.76	3.86
Calculated Shear Force from Equation 111										
NS	Kip	1.68	1.55	1.82	1.93	2.11	1.57	1.58	1.83	1.76
EW	Kip	1.62	1.87	2.09	1.85	2.08	1.69	1.79	1.94	1.99
Calculated Shear Force from Equation 113										
NS	Kip	1.16	1.07	1.25	1.33	1.45	1.08	1.09	1.26	1.21
EW	Kip	1.12	1.29	1.43	1.27	1.43	1.16	1.23	1.33	1.37

g RRS	2.00	2.25	2.50	2.75	3.00	2.00	2.25	2.50	2.75
Test Name	TB47AH200	TB50AH225	TB53AH250	TB56AH275	TB59AH300	TB62AH200	TB65AH225	TB68AH250	TB71AH275
Calculated VS measured (M total) Moment									
NS	0.61	0.62	0.60	0.32	N/A	0.62	0.70	0.59	N/A
EW	0.28	0.28	0.25	0.30	N/A	0.24	0.21	0.17	N/A
Calculated VS measured (M Upper) Moment									
NS	1.06	1.02	0.99	0.93	N/A	1.08	1.11	0.78	N/A
EW	0.49	0.50	0.46	0.51	N/A	0.46	0.39	0.31	N/A
Calculated VS measured (Eq 110) Moment									
NS	2.23	2.07	2.09	1.17	N/A	2.17	2.20	1.90	N/A
EW	1.04	1.08	0.92	1.04	N/A	0.91	0.71	0.50	N/A
Calculated VS measured (Eq 112) Moment									
NS	1.53	1.42	1.44	0.81	N/A	1.49	1.51	1.31	N/A
EW	0.71	0.75	0.64	0.71	N/A	0.63	0.49	0.35	N/A
Calculated VS measured (Eq 114) Moment									
NS	1.01	0.94	0.95	0.53	N/A	0.99	1.00	0.86	N/A
EW	0.47	0.49	0.42	0.47	N/A	0.41	0.32	0.23	N/A

Table 38: Acceleration and Strain Gauge Measurements of Bushing #7

Bending moment Table												
g RRS		0.15	0.20	0.25	0.30	0.35	0.40	0.45	0.50	0.55	0.65	0.80
	Units	TB47AH20	TB47AH20B	TB50AH25	TB53AH30	TB56AH35	TB59AH40	TB62AH45	TB66AH50	TB69AH55	TB72AH65	TB75AH80
(1)	(2)	(3)	(4)	(5)	(6)	(7)	(8)	(9)	(10)	(11)	(12)	(13)
Direct Measurement at the Base of Bushing												
NS	Kip-in	66.17	91.37	96.91	109.72	125.13	133.33	150.24	159.97	168.68	N/A	N/A
EW	Kip-in	88.34	116.83	119.90	142.91	149.09	161.93	166.50	171.52	194.48	N/A	N/A
Calculated Moment from Mtotal and atotal												
NS	Kip-in	57.29	64.31	82.01	93.59	107.05	122.11	131.26	127.15	138.79	297.53	297.53
EW	Kip-in	61.28	76.93	95.65	114.58	129.64	140.01	169.32	189.47	206.77	389.93	389.93
Calculated Moment from MUPPERand aUpper												
NS	Kip-in	85.39	107.35	135.54	154.24	178.64	216.86	222.04	223.37	240.72	338.31	338.31
EW	Kip-in	126.32	150.72	186.23	225.81	259.15	288.16	309.03	343.46	368.13	578.21	578.21
Calculated Moment from Equation 110												
NS	Kip-in	220.14	256.67	332.97	340.82	394.20	479.56	562.20	539.88	601.10	947.05	947.05
EW	Kip-in	297.69	322.12	379.72	443.36	502.02	548.92	558.27	627.34	732.91	1155.15	1155.15
Calculated Moment from Equation 112												
NS	Kip-in	147.96	172.51	223.80	229.07	264.95	322.31	377.86	362.86	404.01	636.52	636.52
EW	Kip-in	297.69	322.12	379.72	443.36	502.02	548.92	558.27	627.34	732.91	1155.15	1155.15
Calculated Moment from Equation 114												
NS	Kip-in	93.82	109.39	141.91	145.25	168.01	204.38	239.60	230.09	256.19	403.62	403.62
EW	Kip-in	126.87	137.28	161.84	188.96	213.96	233.95	237.93	267.37	312.36	492.32	492.32
Calculated Shear Force from Equation 109												
NS	Kip	2.22	2.58	3.35	3.43	3.97	4.83	5.66	5.44	6.05	9.54	9.54
EW	Kip	3.00	3.24	3.82	4.46	5.06	5.53	5.62	6.32	7.38	11.63	11.63
Calculated Shear Force from Equation 111												
NS	Kip	1.12	1.30	1.69	1.73	2.00	2.43	2.85	2.74	3.05	4.81	4.81
EW	Kip	1.51	1.64	1.93	2.25	2.55	2.79	2.83	3.18	3.72	5.86	5.86
Calculated Shear Force from Equation 113												
NS	Kip	0.75	0.88	1.14	1.16	1.34	1.64	1.92	1.84	2.05	3.23	3.23
EW	Kip	1.02	1.10	1.30	1.51	1.71	1.87	1.90	2.14	2.50	3.94	3.94

Ratio of Strain Gage Measurements to Acceleration Measurements											
g RRS	0.15	0.20	0.25	0.30	0.35	0.40	0.45	0.50	0.55	0.65	0.80
Test Name	TB47AH20	TB47AH20B	TB50AH25	TB53AH30	TB56AH35	TB59AH40	TB62AH45	TB66AH50	TB69AH55	TB72AH65	TB75AH80
Calculated VS measured (M total) Moment											
NS	0.87	0.70	0.85	0.85	0.86	0.92	0.87	0.79	0.82	N/A	N/A
EW	0.69	0.66	0.80	0.80	0.87	0.86	1.02	1.10	1.06	N/A	N/A
Calculated VS measured (M Upper) Moment											
NS	1.29	1.17	1.40	1.41	1.43	1.63	1.48	1.40	1.43	N/A	N/A
EW	1.43	1.29	1.55	1.58	1.74	1.78	1.86	2.00	1.89	N/A	N/A
Calculated VS measured (Eq 110) Moment											
NS	3.33	2.81	3.44	3.11	3.15	3.60	3.74	3.37	3.56	N/A	N/A
EW	3.37	2.76	3.17	3.10	3.37	3.39	3.35	3.66	3.77	N/A	N/A
Calculated VS measured (Eq 112) Moment											
NS	2.24	1.89	2.31	2.09	2.12	2.42	2.52	2.27	2.40	N/A	N/A
EW	3.37	2.76	3.17	3.10	3.37	3.39	3.35	3.66	3.77	N/A	N/A
Calculated VS measured (Eq 114) Moment											
NS	1.42	1.20	1.46	1.32	1.34	1.53	1.59	1.44	1.52	N/A	N/A
EW	1.44	1.18	1.35	1.32	1.44	1.44	1.43	1.56	1.61	N/A	N/A

Table 39: Moment-to-Shear Force Ratios and Elevation of the Inertia Centroid for Bushing #6

Calculated from Accelerometers Measurements						Direct From Strain Gauges Measurements					
	EQ1	EQ2	EQ3	EQ4	EQ5		EQ1	EQ2	EQ3	EQ4	EQ5
(1)	(2)	(3)	(4)	(5)	(6)	(7)	(8)	(9)	(10)	(11)	(12)
SHEAR FORCE AT THE BASE (kip)											
Bushing as Installed (f=10.35 Hz)											
NS	1.47	1.54	0.33	0.70	1.19	**NS**	1.30	1.32	0.37	0.64	0.75
EW	0.81	1.43	0.55	0.93	0.83	**EW**	0.70	0.85	0.50	0.54	0.69
SRSS	1.68	2.10	0.64	1.16	1.45	**SRSS**	1.48	1.57	0.63	0.84	1.02
Bushing with Stiffeners L6x4x1/2 on the plate (f=15.13 Hz)											
NS	0.93	1.07	0.24	0.57	0.61	**NS**	0.76	0.99	0.28	0.54	0.52
EW	0.57	1.16	0.24	0.42	0.53	**EW**	0.18	0.37	0.10	0.16	0.19
SRSS	1.09	1.58	0.34	0.71	0.81	**SRSS**	0.78	1.06	0.30	0.56	0.55
Bushing with Stiffeners L8x6x1/2 on the plate (f=16.14 Hz)											
NS	0.85	0.72	0.27	0.65	0.61	**NS**	0.79	1.05	0.21	0.47	0.50
EW	0.66	0.88	0.30	0.45	0.52	**EW**	0.34	0.44	0.18	0.28	0.41
SRSS	1.08	1.14	0.40	0.79	0.80	**SRSS**	0.86	1.14	0.28	0.55	0.64
MOMENTS AT THE BASE (kip-in)											
Bushing as Installed (f=10.35 Hz)											
NS	20.57	21.53	4.62	9.78	16.72	**NS**	28.15	27.97	4.87	10.00	19.21
EW	11.29	20.02	7.71	13.01	11.59	**EW**	13.79	25.55	8.43	15.07	12.58
SRSS	23.47	29.40	8.98	16.28	20.34	**SRSS**	31.35	37.88	9.74	18.09	22.96
Bushing with Stiffeners L6x4x1/2 on the plate (f=15.13 Hz)											
NS	13.06	14.98	3.37	8.01	8.53	**NS**	23.33	21.98	6.85	13.83	18.82
EW	8.01	16.24	3.34	5.84	7.40	**EW**	14.31	14.09	5.43	6.56	8.78
SRSS	15.32	22.09	4.74	9.91	11.29	**SRSS**	27.37	26.11	8.74	15.31	20.77
Bushing with Stiffeners L8x6x1/2 on the plate (f=16.14 Hz)											
NS	11.95	10.08	3.81	9.14	8.64	**NS**	22.44	11.99	4.56	10.01	10.89
EW	9.18	13.70	4.14	6.27	7.34	**EW**	13.57	16.88	6.50	7.15	10.60
SRSS	15.07	17.01	5.62	11.08	11.33	**SRSS**	26.23	20.70	7.94	12.30	15.20
MOMENT TO SHEAR FORCE RATIOS (in)											
Bushing as Installed (f=10.35 Hz)											
NS	14.00	14.00	13.97	14.00	14.01	**NS**	21.65	21.16	13.01	15.54	25.70
EW	14.00	14.00	14.00	14.00	14.00	**EW**	19.77	30.11	16.83	27.74	18.15
Bushing with Stiffeners L6x4x1/2 on the plate (f=15.13 Hz)											
NS	14.04	14.00	14.04	14.05	13.98	**NS**	30.70	22.20	24.46	25.61	36.19
EW	14.05	14.00	13.92	13.90	13.96	**EW**	79.50	38.08	54.30	41.00	46.21
Bushing with Stiffeners L8x6x1/2 on the plate (f=16.14 Hz)											
NS	14.00	14.00	14.00	13.98	14.16	**NS**	28.34	11.44	21.91	21.32	21.96
EW	14.00	15.58	14.00	14.00	14.00	**EW**	39.95	38.08	35.64	25.41	25.77

Table 40: Moment-to-Shear Force Ratios for Bushing #6

Ratios -"DIRECT" to "CALCULATED"							
	EQ1	EQ2	EQ3	EQ4	EQ5	AVG	1/AVG
(1)	(2)	(3)	(4)	(5)	(6)	(7)	(8)
SHEAR FORCE AT THE BASE (kip)							
Bushing as Installed (f=10.35 Hz)							
NS	0.88	0.86	1.13	0.92	0.63	0.88	1.13
EW	0.86	0.59	0.91	0.58	0.84	0.76	1.32
SRSS	0.88	0.75	0.97	0.72	0.70	0.81	1.24
Bushing as Installed (f=15.13 Hz)							
NS	0.82	0.93	1.17	0.95	0.85	0.94	1.06
EW	0.32	0.32	0.42	0.38	0.36	0.36	2.79
SRSS	0.72	0.67	0.88	0.80	0.69	0.75	1.34
Bushing as Installed (f=16.14 Hz)							
NS	0.93	1.45	0.76	0.72	0.81	0.94	1.07
EW	0.52	0.50	0.62	0.63	0.78	0.61	1.64
SRSS	0.80	1.00	0.69	0.69	0.80	0.80	1.26
MOMENTS AT THE BASE (kip-in)							
Bushing as Installed (f=10.35 Hz)							
NS	1.37	1.30	1.05	1.02	1.15	1.18	0.85
EW	1.22	1.28	1.09	1.16	1.09	1.17	0.86
SRSS	1.34	1.29	1.08	1.11	1.13	1.19	0.84
Bushing as Installed (f=15.13 Hz)							
NS	1.79	1.47	2.03	1.73	2.21	1.84	0.54
EW	1.79	0.87	1.63	1.12	1.19	1.32	0.76
SRSS	1.79	1.18	1.84	1.54	1.84	1.64	0.61
Bushing as Installed (f=16.14 Hz)							
NS	1.88	1.19	1.20	1.10	1.26	1.32	0.76
EW	1.48	1.23	1.57	1.14	1.44	1.37	0.73
SRSS	1.74	1.22	1.41	1.11	1.34	1.36	0.73
MOMENT TO SHEAR FORCE RATIOS (in)							
Bushing as Installed (f=10.35 Hz)							
NS	1.55	1.51	0.93	1.11	1.83	1.39	0.72
EW	1.41	2.15	1.20	1.98	1.30	1.61	0.62
Bushing as Installed (f=15.13 Hz)							
NS	2.19	1.59	1.74	1.82	2.59	1.98	0.50
EW	5.66	2.72	3.90	2.95	3.31	3.71	0.27
Bushing as Installed (f=16.14 Hz)							
NS	2.02	0.82	1.57	1.53	1.55	1.50	0.67
EW	2.85	2.44	2.55	1.82	1.84	2.30	0.43

Effects of Rotating Transformer Cover

As a result of bending of the cover plate of the transformer, the bushing develops a rigid body rotation as well as bending. The deflections at the tops of bushings (displacements relative to the displacements at the base) can be resolved to flexural deflections and rigid body rotations. Table 41, column (9), shows the contribution, in %, of rigid body rotations to the total relative displacements from the experimental study. For Bushing #5, a relatively flexible bushing, the rigid body rotation accounts for almost 40% of the total at various levels of testing. For Bushing #6 the rigid body rotation is almost 70% on average, while for Bushing#7, a tall, stiff bushing, the rigid body rotation approaches 85% on average.

The base rotation was measured from calculated displacements determined form accelerations, while assuming that the bottom stem of the bushing is infinitely rigid. The calculations may have a margin of error of up to 10%. However, even in the presence of such error the trend is clear and the base rotation cannot be neglected in determining the deformations and forces.

Table 41: Displacements Due to Bending and Rigid Body Rotations

Test No.	DISPLACEMENT							
Location	Measured Horizontal			Calculated Rotational			Calculated Flexural	Ratio
	Shake Table Extension	Top of Frame	Relative Trans. Top of Bushing	Rotation Shake Table Extension	Bushing Rigid Body Rotation	Max Top Relative Translation From Base Rotation	Absolute Flex. Displ. At top of Bushing	Max Ratio of Rigid vs Rel. Displacemnt
(1)	(2)	(3)	(4)	(5)	(6)	(7)	(8)	(9)
Units	(in)	(in)	(in)	(in/in)	(in/in)	(in)	(in)	(%)
Bushing #5								
TB35AH25	1.81	1.82	0.73	N/A	0.0019	0.34	0.56	68%
TB38AH50	3.09	3.11	1.19	N/A	0.0023	0.42	0.86	36%
TB41AH100	3.14	3.17	4.42	N/A	0.0093	1.73	3.11	42%
TB44AH150	4.47	4.62	8.07	N/A	0.0153	2.84	5.47	36%
TB47AH225	3.12	3.36	14.08	N/A	0.0268	4.95	9.49	35%
TN53AH300	3.82	4.17	22.29	N/A	0.0314	5.81	18.89	36%
Bushing#6								
TB24AH025	2.29	2.22	0.12	N/A	0.0013	0.11	0.14	21%
TB27AH050	4.19	4.02	0.23	N/A	0.0019	0.16	0.28	83%
TB30AH075	2.30	2.31	0.31	N/A	0.0019	0.16	0.19	91%
TB33AH100	3.11	3.28	0.42	N/A	0.0025	0.21	0.27	79%
TB38AH125	4.73	4.79	0.71	N/A	0.0043	0.35	0.47	65%
TB41AH150	1.92	1.96	0.57	N/A	0.0038	0.31	0.32	55%
TB44AH175	2.25	2.34	0.65	N/A	0.0046	0.37	0.40	65%
TB47AH200	2.65	2.77	0.72	N/A	0.0056	0.46	0.43	68%
TB50AH225	1.82	1.91	0.68	N/A	0.0054	0.44	0.43	78%
TB53AH250	2.09	2.20	0.79	N/A	0.0056	0.46	0.47	76%
TB56AH275	3.42	3.68	0.89	N/A	0.0070	0.57	0.66	70%
TB59AH300	4.30	4.63	1.25	N/A	0.0071	0.58	0.97	70%
Bushing#7								
TB47AH20B	1.55	1.57	1.18	N/A	0.0054	1.10	0.18	94%
TB50AH25	1.99	2.02	1.55	N/A	0.0073	1.51	0.21	99%
TB53AH30	2.42	2.45	1.77	N/A	0.0082	1.67	0.25	97%
TB56AH35	2.90	2.93	2.10	N/A	0.0096	1.96	0.28	95%
TB59AH40	3.38	3.42	2.46	N/A	0.0109	2.23	0.31	92%
TB62AH45	3.88	3.94	2.70	N/A	0.0121	2.49	0.34	93%
TB66AH50	2.62	2.70	2.78	N/A	0.0127	2.61	0.41	100%
TB69AH55	2.92	3.01	3.22	N/A	0.0145	2.97	0.49	92%
TB72AH65	3.46	3.55	4.29	N/A	0.0174	3.57	0.86	83%
TB75AH80	4.31	4.47	5.49	N/A	0.0186	3.82	1.90	70%
Instruments*	Potentiometer	Potentiometer	Potentiometer	N/A	Eq 1	Eq 2	Eq 3	Eq 4

The accelerations at the top of the bushings are also a combination of the flexural and base rotational accelerations (see Table 42). Column (12) shows that the rigid body accelerations may be larger than the total, since the flexural may be out of phase with the rigid body rotations. In any case, the rigid body rotations are comparable in size and larger than the flexural accelerations.

It should also be noted that the vertical accelerations at the top of the bushings are larger than the ground accelerations, but are mostly due to the plate cover vibrations (Table 42, columns (5), (6), and (7)).

Table 42: Accelerations Due to Bending and Rigid Body Rotations

Test No.	Acceleration										
Location	Measured Horizontal (Absolute)			Measured Vertical			Calculated Rotational			Calculated Flexural	Ratio
	Shake Table Extension	Top of Plate	Top of Bushing	Shake Table Extension	Top of Plate	Top of Bushing	Shake Table Extension	Rigid body Rotation	Top* Acceleration from Rigid Body Rotation	Flexural Top of Bushing	Ratio of col (10) to col (4)
(1)	(2)	(3)	(4)	(5)	(6)	(7)	(8)	(9)	(10)	(11)	(12)
Units	(g)	(g)	(g)	(g)	(g)	(g)	(g/in)	(g/in)	(g)	(g)	%
Bushiing 4b											
TBU1AH12525	0.18	0.21	1.24	0.12	0.61	0.66	N/A	0.0139	1.32	0.08	107%
TBU1AH12530	0.12	0.14	0.73	0.10	0.26	0.34	N/A	0.0013	1.17	0.43	159%
TBU1AH12535	0.14	0.16	0.79	0.11	0.18	0.24	N/A	0.0137	1.22	0.43	155%
TBU1AH12540	0.15	0.16	1.00	0.11	0.18	0.21	N/A	0.0111	0.99	0.01	99%
TBU1AH12545	0.14	0.15	0.81	0.11	0.25	0.31	N/A	0.0096	0.85	0.04	106%
Accelerometer	A04N	A12N	A19N	A06U	A14U	A21U	N/A	Formula	Formula	Col 4- Col 10	Col 10/Col 4
Bushiing 4b											
TBU2AH25	0.30	0.32	1.51	0.21	0.50	0.46	N/A	0.0169	1.54	0.03	102%
TBU2AH50	0.61	0.64	3.00	0.41	0.96	0.93	N/A	0.0301	2.68	0.32	89%
TBU2AH100	0.92	0.99	6.49	0.73	1.83	1.77	N/A	0.0467	3.95	2.54	61%
TBU2AH200	1.71	2.01	10.27	1.35	3.21	3.34	N/A	0.0908	7.09	3.18	69%
TBU2AH250	N/A	N/A	N/A	N/A	N/A	N/A	N/A	N/A	N/A	n/a	n/a
TBU2AH300	N/A	N/A	N/A	N/A	N/A	N/A	N/A	N/A	N/A	n/a	n/a
Accelerometer	A04N	A12N	A19N	A06U	A14U	A21U	N/A	Formula	Formula	Col 4- Col 10	Col 10/Col 4
Bushing 5											
TB35AH25	0.30	0.32	0.93	0.21	0.54	0.55	N/A	0.01	1.88	0.94	201%
TB38AH50	0.46	0.51	1.19	0.31	0.80	0.82	N/A	0.01	2.15	0.96	181%
TB41AH100	1.16	1.17	4.25	0.87	2.99	3.08	N/A	0.07	12.25	8.00	288%
TB44AH150	1.71	1.70	7.10	1.63	3.98	4.09	N/A	0.08	15.51	8.42	219%
TB47AH225	2.27	2.41	11.92	2.14	6.32	6.43	N/A	0.09	16.95	5.03	142%
TN53AH300	2.76	2.90	13.46	2.51	6.62	7.04	N/A	0.12	23.85	10.39	177%
Accelerometer	A04N	A15N	A22N	A06U	A17U	A24U	N/A	Formula	Formula	Col 4- Col 10	Col 10/Col 4
Bushing 6											
TB24AH025	0.34	0.38	1.06	0.35	0.45	0.49	N/A	0.0086	0.69	0.37	65%
TB27AH050	0.55	0.68	1.77	0.46	0.77	0.86	N/A	0.0013	1.16	0.61	65%
TB30AH075	0.77	0.79	2.86	0.59	1.79	1.75	N/A	0.0256	2.04	0.82	71%
TB33AH100	1.02	1.09	3.78	0.82	2.64	2.50	N/A	0.0333	2.78	1.00	74%
TB38AH125	1.35	1.54	5.25	1.75	4.10	3.96	N/A	0.0475	3.92	1.32	75%
TB41AH150	1.34	1.73	5.48	1.27	3.27	3.52	N/A	0.0462	3.77	1.71	69%
TB44AH175	1.55	2.00	6.22	1.50	3.90	4.23	N/A	0.0524	4.31	1.90	69%
TB47AH200	1.86	2.32	7.06	1.86	4.56	4.98	N/A	0.0609	5.32	1.74	75%
TB50AH225	2.35	2.94	6.51	2.15	5.25	5.75	N/A	0.0658	5.50	1.01	84%
TB53AH250	2.63	3.34	7.63	2.52	6.14	6.36	N/A	0.0749	6.17	1.46	81%
TB56AH275	2.44	2.81	8.11	2.43	5.46	6.12	N/A	0.1053	8.80	0.69	109%
TB59AH300	3.25	3.30	8.84	3.09	6.60	7.54	N/A	0.1048	7.56	1.28	85%
Accelerometer	A04N	A12N	A22N	A06U	A14U	A24U	N/A	Formula	Formula	Col 4- Col 10	Col 10/Col 4
Bushing 7											
TB47AH20B	0.27	0.30	0.85	0.19	0.69	0.99	N/A	0.0042	0.96	0.10	112%
TB50AH25	0.34	0.42	1.10	0.26	0.81	1.16	N/A	0.0063	1.37	0.27	124%
TB53AH30	0.41	0.44	1.13	0.32	0.92	1.32	N/A	0.0056	1.28	0.15	113%
TB56AH35	0.49	0.52	1.31	0.37	1.06	1.46	N/A	0.0062	1.37	0.07	105%
TB59AH40	0.49	0.59	1.59	0.43	1.16	1.60	N/A	0.0078	1.70	0.11	107%
TB62AH45	0.63	0.63	1.68	0.47	1.33	1.84	N/A	0.0080	1.76	0.08	105%
TB66AH50	0.74	0.76	1.79	0.56	1.44	2.02	N/A	0.0088	2.45	0.66	137%
TB69AH55	0.82	0.84	1.99	0.62	1.60	2.23	N/A	0.0101	2.75	0.76	138%
TB72AH65	0.98	0.99	2.41	0.75	2.02	2.41	N/A	0.0124	3.33	0.92	138%
TB75AH80	1.21	1.22	3.14	0.89	2.03	2.83	N/A	0.0177	3.64	0.50	116%
Instruments*	A01N	A09N	A22N	A03U	A14U	A24U	N/A	Eq 1	Eq 2	Col4-Col10	Col 10/Col 4

Summary of Effects of Dynamic Response of Installed Bushings

This section analyzed the specific effects that have been found to govern the seismic behavior of transformer bushings.

First, an evaluation of the response of bushings installed on a rigid base versus the response of bushings on a flexible support is provided, in order to assess the sensitivity required in determining the bushings' properties. The evaluation is based on the numerical study with properties established in the experimental study.

Second, an evaluation of the impact of the location of bushings on the tank cover is developed based on experimental study and on the analytical understanding of the cover behavior.

Third, the effect of behavior on the base forces is presented while the evaluation of methods of measuring and calculating these forces provides a basis for further recommendations.

Fourth, this section explored the effects of rotational (rigid body) and vertical vibrations on the total response of the bushings.

CHAPTER 5:
Critical Evaluation of Current Qualification Standards

The current practice of seismic qualification of transformer bushings, represented by the application of the requirements embodied in IEEE Standard 693-2005 (IEEE, 2005), has several shortcomings, as evidenced by the research described in this report. These shortcomings introduce challenges to the equipment qualified according to those requirements, including:

1) The qualification motion specified in IEEE 693 is amplified by a factor of two (2) in order to account for the flexibility of the tank and the cover plate. The testing performed for this research project indicated that a factor of 2 is not sufficient to account for the flexibility of the tank and cover plate in many instances of as-installed bushings. In other words, the influence of the dynamics of the transformer tank and cover is not properly considered in the current Standard. Moreover, the rotational excitation resulting from the distortions of the flexible cover of the transformer, and the vertical amplifications due to the cover flexibility, are not addressed by the Standard at all. Specifically, the research resulted in the following observations:

    a. Since the strength demand is a function of the correct description of the spectra of the lateral motion at the base of the bushing (i.e., at the top of the transformer tank), the dynamics of the tank, including the anchoring system, the core, coils, oil and tank cover, distort the horizontal motion transmitted to the bushing or turret, usually independent of the bushing size and location. The amplification factor of 2 is not conservative for many cases, as was observed in the testing of as-installed bushings in the laboratory.

    b. The cover of the transformer tank rotates in addition to its lateral translation, thereby introducing a rotational excitation to the base of the bushing (fulcrum) where it is connected to the tank. This rotational motion is not negligible and it is dependent on the location of the bushing on the transformer cover. This results in additional displacements and accelerations in all parts of the bushings.

    c. The dynamics of the transformer cover completely distort the vertical input in the bushing. The weight of the bushing (not its stiffness) changes the dynamics of the plate and the total amplification.

2) When the bushings are mounted on the transformer cover, their transverse and rotational dynamic properties change due to the flexibility of the transformer cover, which acts like a rotational spring. The current practice ignores these changes in the dynamics due to the bushing being mounted on the transformer cover, leading to these specific observations:

    a. The dynamic response of the bushing is dependent solely on the mounted (known also as “as-installed”) frequency.

    b. The variation of frequencies is dependent on the relative stiffness of the bushing and the transformer cover. The current practice does not recognize or require determination of such quantities for matching the bushing with the transformer.

c. Frequencies of vibration, when bushings are mounted on a rigid surface (such as a rigid tank cover), are substantially higher than the frequencies that result when the bushing is mounted on a flexible transformer cover.

d. The frequencies of vibration are also dependent on the location of the bushing with respect to the boundaries of the transformer cover, i.e., whether the bushing is mounted in the center, sides, corner, etc. In some transformers the as-installed frequencies are slightly influenced by the auxiliary equipment mounted on the cover.

3) The current acceptance criteria are based on the intensity of input measured in accelerations at zero period acceleration (ZPA, measured in g) frequencies; ZPA is approximately equal to the peak input acceleration (also known as PGA in seismology). Acceptance of a bushing is linked to lack of visible damage during the strongest shaking. Although this is a rational criterion, it is limited to the equipment tested during qualification, leaving very limited possibility to quantify the performance in mechanical terms for sufficient numbers of bushings relevant to design. Moreover, the quantities measured and calculated by the approximate methods, as suggested by the Standard, are gross approximations of inertia forces and moments, often neglecting the important special effects of translations, rotations, overturning and slippage. Specifically:

a. The qualification criteria are based on the visual appearance of various failure modes, such as slippage, oil leaks, or fractures, or major changes in the global flexibility of the bushings (for composites). However, these failures occur while the stresses exceed thresholds that can be determined by testing, or the stress resultants (shear forces and/or overturning or flexural moments) exceed similar thresholds. These thresholds are not known or specified by the manufacturer, and no such specifications are required as a description of the strength capacity of bushings. Without the specification of such quantities, it is impossible for manufacturers to design components or transformers that can accommodate the equipment.

b. When verifications are required by the standard, the stress resultants in connections or anchorage points (critical sections) are determined by multiplying the weights above the critical sections by the peak acceleration response at center of gravity (CG) determined from design spectra or from testing. This practice ignores the irregularity of the bushings and the dynamic behavior, which actually requires determining the resultants of maximum inertial forces and their centroid in order to calculate the demands in the critical sections.

c. The failure modes can be quantified in terms of stress resultants and prioritized according to the importance to the electrical functionality of the equipment. The lowest *unacceptable* failure mode should be defined as the *strength capacity.* This is not necessarily associated with the lowest failure mode, which may allow safe operation of the bushing; other, higher failure modes may be responsible for preventing safe operation. The strength associated with such mode can be determined by static testing and direct measurements, or perhaps directly by manufacturers. The *allowable strength*

capacity can then be established as a fraction of such forces, or moments, obtained using safety factors that account for uncertainties and for some of the dynamic effects.

d. The testing for qualifications must induce forces, or moments, in the critical sections at the performance levels required, which should be below the allowable strength capacity measured using the same engineering quantities. Engineering quantities such as forces, moments, stresses, and deformations should be measured during such qualifications to describe the *strength demands*. Although current practice recognizes some of the important quantities, it does not methodically identify the relevant quantities for most types of bushings.

CHAPTER 6:
Conclusions and Recommendations

Several recommendations for the standard are warranted by the studies identifying the current shortcomings in qualification of transformer bushings or of other equipment mounted on support structures

1. The acceptance criteria for performance qualification should be based on comparing the *demand for mechanical strength* expressed in the same engineering terms as the *specified strength capacity.* The equipment will be considered acceptable for a desired performance level if the *strength demand* for that performance level does not exceed the specified strength capacity. An under-capacity multiplier (e.g., 0.9) similar to that used in concrete or steel structures using the limit state design approach, can be considered here to account for uncertainties in determining the strength capacity.

2. Define the *strength capacity of equipment* (bushings) in terms of forces, moments, stresses and/or deformations associated with the lowest unacceptable failure modes which may not allow continuous operations of transformers. While there are data for most equipment, available from field observations and laboratory information, a database of failure modes and their priorities in defining interruption of operations can be developed.

3. Quantify the strength capacity of equipment (bushings) in terms of forces, moments, stresses and /or deformations associated to the lowest unacceptable failure mode by *"fragility testing"* either static or dynamic. A static testing is most cases conservative, unless the system is subjected to extremely large cycles of deterioration (fatigue). Therefore the manufacturer of the electrical component can test or define the strength capacity in terms of a *SPECIFIED (reliable) STRENGTH CAPACITY*, which can be derived from the forces that produce the failure, and reduced by safety factors accounting for uncertainties, dynamics, etc. The *SPECIFIED STRENGTH CAPACITY* should be then used in the acceptance criteria for performance qualification and in the design of all associated support equipment.

4. The *strength demand* expressed in the same engineering parameters as the *strength capacity* (i.e., forces, moments, stresses and or deformations*) should be determined based on the seismicity according to the current standard*, or according to any other more specific and documented requirement related to the local seismicity. The current Required Response Spectra scaled adequately for the performance levels for the ground motion, specified for the lateral and vertical effects, should be used as a minimum requirement. However, the stress demand for the bushings and other related equipment must consider (i) the *amplifications of those motions* and (ii) the additional *rotational motions of the support* (cover of the transformer) dependent on the cover construction and on the location of the bushings in respect to the walls of the transformer, as well as (iii) the *dynamic characteristics of the bushing as mounted on the transformer.*

5. Bushings can be qualified by testing in the laboratory to establish (i) *the reliable strength capacity* and (ii) *the seismic demand* for the desired performance level. In both cases shear

forces and moment and possibly deformations would have to be used to measure the mechanical strength. This objective could be accomplished by the following measures:

a. The *strength capacity* can be determined by a static pull test in the lateral direction. The reliable strength capacity can be a fraction of the total strength capacity and the specified manufacturer strength can serve as limit to the static test performed to that level. Strength capacity can be determined by mounting the bushing on a vibration table on a rigid stand and performing fragility testing to the lowest unacceptable failure mode.

b. The *seismic demand* should be determined by mounting the bushing on a support structure simulating the transformer cover with its flexible characteristics, in order to: (1) simulate the shift of frequency from the fixed to "as-mounted" conditions, and (2) modify the ground motion to the realistic motion at the base of bushing (as specified in 4., above).

c. Since the bushing can presumably be used with any arbitrary transformer, and the as-mounted properties may not be known, it is suggested that a stand with a flexible cover be used; the cover can shift the frequency to 8.0 Hz or below, such that the acceleration demand will be in the highest level of the spectrum.

d. The vertical motion should also be magnified, taking into consideration the flexibility of the cover of the transformer and the weight of the bushing, or the vertical frequency of the as-mounted bushing. The standard dynamic amplification factor should be used (e.g., Chopra, 1995).

e. The rotational motion is the most difficult to assess, since the location of the bushing plays a large role. However, by considering the asymmetric mode of the plate with the bushing placed in the center location, it is possible to find a conservative evaluation of the rotation (e.g., Chopra, 1995).

6. Additional notes resulting from the current research:

a. The direct measurement of forces and moments can be done by attaching strain measuring devices (strain gauges) to the porcelain nearest to the critical section, in the longitudinal direction of the bushing and at 45 degrees to that direction. The longitudinal gauges should be used to measure moments, while the inclined gauges should be used to measure shear. Strain rosettes (45°) can be used in diametrically opposed locations, in two orthogonal directions, one for each principal direction of the bushing. The strain gauges should be calibrated by pulling and releasing the bushing at its top, or at another desired location, up to the reliable strength capacity; pull tests should be repeated in the two orthogonal directions.

b. If the stiffness of the transformer cover is high, then rotational effects and vertical amplifications can be avoided, and the bushing dynamic characteristics will converge toward the fixed base mounting. In this case the bushing can be tested on the rigid stand according to the current guidelines.

c. The approximate formulations provided in Chapter 4 can serve as good approximations of the dynamic characteristics, if the transformer cover stiffness can be adequately estimated.

d. With proper measurements of structure response, $m(z)$, H, and "as-installed" frequency f_k , as well as the shape function $\varphi(z)$, it is possible to calculate the demand according to the formulations provided in Chapter 4. This can be done by designers of transformers and transformer bushings, or by utilities, and may significantly reduce the need for additional testing.

GLOSSARY

Table 43: Glossary of Terms and Acronyms

1D	one-dimensional
2D	two-dimensional
3D	three-dimensional
ABB	ASEA Brown Boveri, Inc.
AC	alternating current
AMP	dynamic amplification factor
AQR	acquisition rate
BPA	Bonneville Power Administration
CCD	charged-coupled device
CDF	cumulative distribution function
CEC	California Energy Commission (Energy Commission)
CERL	Construction Engineering Research Laboratory (Urbana, IL)
CG	center of gravity
Δ	delta (difference, differential, or change in a quantity)
DC	direct current
EERC	Earthquake Engineering Research Center (at UC-Berkeley)
EW	east-west
FEMA	Federal Emergency Management Agency
FFT	fast Fourier transform
f	frequency
ft	foot, feet
g	gravitational constant = 32 m/sec^2
GE	General Electric Co.
GF	gauge factor (or gage factor)
CG	center of gravity
h	height (vertical height above the bushing base)
HSL	high seismic level

HSP	Hochspannungsgerate Corp.
HV	high voltage, high-voltage
Hz	Hertz (unit of frequency = cycles per second)
IEEE	Institute of Electrical and Electronics Engineering
IFFT	inverse fast Fourier transform
in	inch, inches
kip	unit of force, equal to 1,000 lb
kV	kiloVolt (unit of voltage = 1,000 Volts)
LADWP	Los Angeles Department of Water & Power
lb	pound, pounds (unit of force)
LED	light-emitting diode
LV	low voltage, low-voltage
LVDT	linear variable differential transformer
LSL	low seismic level
m	meter
μ	micro ($=10^{-6}$)
MAF	moment amplification factor
MCEER	Multidisciplinary Center for Earthquake Engineering Research
MSL	medium seismic level
NCS	Non-structural Component Simulator
NS	north-south
Ω	ohm (unit of electrical resistance)
ω	angular frequency ($= 2\pi f$)
PEER	Pacific Earthquake Engineering Research (Laboratory)
PG&E	Pacific Gas & Electric Co.
PGA	peak ground acceleration
PIER	Public Interest Energy Research
PL	performance level
PoNE	probability of non-exceeding

PQL	performance qualification level
PSD	power spectral density
PTZ	pan/tilt/zoom (camera)
RD&D	research, development and demonstration
RRS	required response spectrum (or spectra)
RS	response spectrum (or spectra)
SEESL	Structural Engineering and Earthquake Simulation Laboratory
SQL	seismic qualification level
STEX	seismic test execution
SUNY	State University of New York
TDM	time domain modulation
TRS	test response spectrum
V	volt, voltage
ZPA	zero period acceleration

REFERENCES

Abacus 6.10, "U*ser's Manual and Theory Manual,"* Simulia, Chapter 4.

ASEA Brown Boveri (ABB) Inc., *Seismic Qualification of Transformer Bushing*, Report #1ZUA938501-ACA, Power Technology Products Division USA, Alamo, Tennessee, November 2004.

Abrahamson, N.: *Nonstationary Response-Spectrum Matching*, unpublished paper, 1996.

Anagnos, T.: *Development of an Electrical Substation Equipment Performance Database for Evaluation of Equipment Fragilities,* San Jose State University, PEER 2001/06, 1999.

Ashrafi, A.: *Issues of Seismic Response and Retrofit for Critical Substation Equipment*, Master of Science Thesis, New Jersey Institute of Technology, Newark, New Jersey, August 2003.

Ashrafi, A.; Feizi, B.; Saadeghvaziri, M. A.; Ersoy, S.: *Seismic Evaluation and Rehabilitation of Critical Components of Electrical Power Systems*, New Jersey Institute of Technology, Technical Report #PB2009-105546, Newark, New Jersey, March 2008.

Bellorini, S.; Bettinali, F.; Salvetti, M.; and Zafferani, G.: *Seismic Qualification of Transformer High Voltage Bushings*, IEEE Transactions on Power Delivery, 13(4), pp. 1208–1213, 1998.

Benassi, A. and Reinhorn, A. M.: *Modeling of Conductors in Electrical Equipment & Sensitivity Studies*, MCEER Task Report MCEER-TR-09-01, University at Buffalo – the State University of New York, Buffalo, New York, 2009.

Carmona, J. S.; Zabala, F.; Santalucia, J.; and Sisterna, C.: *Seismic Tests of High Voltage Equipment In Argentina,* A. A. Balkema Publishers, Rotterdam, Netherlands, vol. 5, pp. 2811-2815, 1992.

Chieh, S.; Chen, T.; Ch'eng, K.: *Seismic Reliability Analysis of High-Voltage Transformer*. World Information on Earthquake Engineering, Volume 17 (MCEER Collection), 2001.

Chopra, A. K.: *Dynamics of Structures: Theory and Applications to Earthquake Engineering, 2nd edition,* Prentice Hall International, 2000.

Earthquake Engineering Research Institute: *The Izmit (Kocaeli), Turkey Earthquake of August 17, 1999,* EERI Newsletter, 33(10), Oakland, California, 1999.

Earthquake Engineering Research Institute: *Northridge Earthquake Reconnaissance Report*, *Vol. 1: Earthquake Spectra*, Supplement C to EERI Newsletter Vol. 11, Oakland, California, April 1995.

Elder, L.: "*Seismic Qualification Report of XXX kV Bushing – Qualified to the High Level (0.5g ZPA of the RRS) of IEEE Std. 693-2005*, ABB Inc., Power Technology Products Division, USA, 2008.

Elliott, J. J.; O'Claire, D. E.; Mueller, W. H.; Kempner, L. Jr.: *Seismic Performance of 230kV Transformer Bushings,* Testing, Seismic Testing and Applied Research (STAR) Laboratory Report, Portland State University, Portland, Oregon, 2004.

Ersoy, S. and Saadeghvaziri, M. A.: *Seismic Response of Transformer-Bushing Systems*, IEEE Transactions on Power Delivery, 19(1), pp. 131-137, 2004.

Ersoy, S. and Saadeghvaziri, M. A.: *Seismic Response of Transformer-Bushing Systems*, Report to National Science Foundation, Award No. EEC-9701471, 2002.

Filiatrault, A. and Matt, H.: *Seismic Response of High-Voltage Transformer-Bushing Systems*, Earthquake Spectra, 21(4), pp. 1009-1026, 2005.

Filiatrault, A. and Matt, H.: *Seismic Response of High-Voltage Transformer-Bushing Systems*, Journal of Structural Engineering, 132(2), pp. 287-295, 2006.

Gasparini, D. A. and Vanmarcke, E.: *SIMQKE: A Program for Artificial Motion Generation*: *User's Manual and Documentation*, Massachusetts Institute of Technology, Department of Civil Engineering, Cambridge, Massachusetts, 1976.

Gilani, A. S. J.; Chavez, J. W.; Fenves, G. L.; and Whittaker, A. S.: *Seismic Evaluation of 196 kV Porcelain Transformer Bushings*, Pacific Earthquake Engineering Research (PEER) Center, Report No. PEER 98/02, University of California at Berkeley, Berkeley, California, 1998.

Gilani, A. S. J.; Whittaker, A. S.; and Fenves, G. L.: *Seismic Evaluation and Retrofit of Porcelain Transformer Bushings,* Earthquake Spectra, 17(4), pp. 597–616, 2001.

Gilani, A. S. J.; Whittaker, A. S.; Fenves, G. L.; and Fujisaki, E.: *Seismic Evaluation of 550 kV Porcelain Transformer Bushings*, Pacific Earthquake Engineering Research (PEER) Center, Report No. PEER 99/05, University of California at Berkeley, Berkeley, California, 1999.

Gilani, A. S. J.; Whittaker, A. S.; Fenves, G. L.; and Fujisaki, E.: *Seismic Evaluation and Retrofit of 230-kV Porcelain Transformer Bushings,* Pacific Earthquake Engineering Research (PEER) Center, Report No. PEER 99/14, University of California at Berkeley, Berkeley, California, 1999.

Gilani, A. S. J.; Whittaker, A. S.; Fenves, G. L.; Chen, C.H.; Ho, H.; and Fujisaki, E.: *Seismic Evaluation and Analysis of 230 kV Disconnect Switches,* Pacific Earthquake Engineering Research (PEER) Center, Report No. PEER 00/06, University of California at Berkeley, Berkeley, California, 2000.

Gundy, W.: *Seismic Qualification of a 230 kV Power Transformer*, Report 1018-54, W.E. Gundy & Associates, Inc., Hailey, Idaho, 2000.

Gundy, W.: *Seismic Qualification of a 500 kV Power Transformer*, Report 1018-58, W.E. Gundy & Associates, Inc., Hailey, Idaho, 2002.

Institute of Electrical and Electronics Engineers (IEEE): *IEEE Standard 693-2005, Recommended Practices for Seismic Design of Substations*, 2006.

Japanese Society of Civil Engineers (JSCE): *Dynamic Analysis and Earthquake Resistant Design (Volume 3)*, 2001.

Jonsson, L. and Johansson, R.: *Perpetual Pioneering – High-Voltage Bushings*, ABB Review, ABB Power Products, March 2009.

Kempner, L., Jr. (editor): *Substation Structure Design Guide – ASCE Manual of Practice No. 113*, Subcommittee on the Design of Substation Structures, Structural Engineering Institute, ASCE, 2007.

Kempner, L., Jr. and Watson, G.T.: A*SCE Substation Structure Design Guide*, in Electrical Transmission in a New Age (Jackman, D. E., ed.), Proceedings of the ASCE Conference, Sept. 9–12, Omaha, Nebraska, 2002.

Koliou, M.: *Seismic Protection of Electrical Transformer Bushing Systems by Stiffening Techniques,* Master of Science in Civil Engineering Thesis, University at Buffalo, The State University of New York, Buffalo, New York, 2010.

Koliou, M.; Filiatrault, A.; Reinhorn, A. M.; and Oliveto, N.: *Seismic Protection of Electrical Transformer Bushing Systems by Stiffening Techniques*, MCEER Technical Report MCEER-11-00xx (in review), University at Buffalo – the State University of New York, Buffalo, New York, 2011.

Kong, D.: *Evaluation and Protection of High Voltage Electrical Equipment Against Severe Shock and Vibrations,* Ph. D. Dissertation, University at Buffalo – the State University of New York, Buffalo, New York, 2010.

Matt, H. and Filiatrault, A.: *Seismic Qualification Requirements for Transformer Bushings*, Report No. SSRP - 2003/12, University of California at San Diego, San Diego, California, 2004.

Matt, H., and Filiatrault, A.: *Seismic Response of High Voltage Electrical Transformer–Bushing Systems*, ASCE Journal of Structural Engineering, 132(2), February 1, 2006.

Muhammad, F.: *Seismic Evaluation and Qualification of Transformer Bushings*, Ph. D. Dissertation, University at Buffalo – the State University of New York, Buffalo, New York (expected December 2011).

National Electrical Manufacturers Association (NEMA): *NEMA-ANSI Standard C29.9-1983 Wet-Process Porcelain Insulators (Apparatus, Post-Type),* American National Standards Institute (ANSI), 1983.

Pansini, A. J.: *Electrical Transformers and Power Equipment,* The Fairmont Press, Inc, 1999.

Pardoen, G.; Hamilton, C.; and Tavares, R.: *Improved Modeling of Electrical Substation Equipment for Seismic Loads*, presentation to BPA, University of California at Irvine, Irvine, California, Jan. 4, 2009.

Pierre, J.-R.: *Damage Caused by the Hanshin-Awaji (Kobe, Japan) Earthquake to the Electrical and Telecommunications Networks and Its Impact on the Implementation of Emergency Measures*, Hydro-Québec, Groupe Équipement, Report RE-GEN-95-40, 1995.

Reinhorn, A. M.; Filiatrault, A.; Muhammad, F.; Oliveto, N.; Oikonomou, K.; and Koliou, M.: *Evaluation of Transformer Bushings: Current and Recommended Practice,* MCEER Task Report MCEER-TR-11-01, University at Buffalo – the State University of New York, Buffalo, New York, 2011.

Reinhorn, A. M. and Oikonomou, K.: M*odeling of Transformers: 500 kV and 230 kV Cover Amplifications*, MCEER Task Report MCEER-TR-10-01, University at Buffalo – the State University of New York, Buffalo, New York, 2010.

Reinhorn, A. M.; Oikonomou, K.; Roh, H.; Schiff, A.; and Kempner, L., Jr.: *Modeling and Seismic Performance Evaluation of High Voltage Transformers and Bushings*, MCEER Technical Report MCEER-11-0004, University at Buffalo – the State University of New York, Buffalo, New York, 2011.

Reinhorn, A. M. (ed.): *Proceedings of the Workshop on Improving Earthquake Response of Substation Equipment,* MCEER Technical Report MCEER-11-0003, University at Buffalo – the State University of New York, Buffalo, New York, 2011.

Saadeghvaziri, M. A.; Feizi, B.; Kempner, L.; and Alston, D.: *On Seismic Response of Substation Equipment and Application of Base Isolation to Transformers*, IEEE Transactions on Power Delivery, 25(1), pp. 177-186, 2010.

Salvador, W. and Vandeleene, J. P.: *Seismic Design of Instrument Transformers,* GEC Alsthom Technical Review No. 7, pp. 55-66, 1991.

Schiff, A.: *Guide to the Improved Earthquake Performance of Electric Power Systems,* ASCE Manuals and Reports on Engineering Practice No. 96 (A. Schiff, editor), American Society of Civil Engineers, 1999.

Schiff, A.: *Response of the Imperial Valley Substation to the 7.2 Mw 4/4/10 Baja Earthquake (Draft),* Precision Measurement Instruments, December 21, 2010.

Schiff, A.: *Seismic Qualification of Transformer/Bushing Systems,* white paper and personal communication, March 4, 2007.

Schiff, A.: *Seismic Safety of Electrical Equipment,* National Science Foundation, 1977.

Schiff, A. and Kempner, L., Jr.: *Issues and Guidance for IEEE 693 Equipment Qualification Tests*, Precision Measurement Instruments, Los Altos Hills, California, 2003.

Schiff, A. (editor): *Northridge Earthquake Lifeline Performance and Post Earthquake Response,* Technical Council on Lifeline Earthquake Engineering (TCLEE), ASCE Monograph No. 8, Washington, DC, 1997.

Schiff, A. (editor): *Guide to Post-Earthquake Investigation of Lifelines*, Technical Council on Lifeline Earthquake Engineering (TCLEE), ASCE Monograph No. 11, Washington, DC, 1997.

Schiff, A. (editor): *Hyogoken Nabu (Kobe) Earthquake of January 17, 1995 Lifeline Performance,* American Society of Civil Engineers, Technical Council on Lifeline Earthquake Engineering (TCLEE), ASCE Monograph No. 14, Washington, DC, 1998.

Schiff, A. and Ostrom, D.: *Power Systems after the Northridge Earthquake: Emergency Operations and Changes in Seismic Equipment Specifications, Practice, and System Configuration*, ASCE Monograph No. 8, American Society of Civil Engineers, pp. 549-556, Washington, DC, August 1995.

Schiff, A. and Tang, A. K. (editors): *Chi-Chi, Taiwan, Earthquake of September 21, 1999 Lifeline Performance,* American Society of Civil Engineers, Technical Council on Lifeline Earthquake Engineering (TCLEE), ASCE Monograph No. 18, Washington, DC, 2000.

Sezen, H.; Elwood, K.; Whittaker, A. S.; Mosalam, K. M.; Wallace, J. W.; and Stanton, J. F.: *Structural Engineering Reconnaissance of the August 17, 1999 Earthquake: Kocaeli, Turkey,* Report No. PEER 00/09, Pacific Earthquake Engineering Research (PEER) Center, University of California at Berkeley, Berkeley, California, 2000.

Sezen, H. and Whittaker, A.: *Seismic Performance of Industrial Facilities Affected by the 1999 Turkey Earthquake,* Journal of Performance of Constructed facilities, American Society of Civil Engineers, February 2006.

Shames, I. H. and Dym, C. L.: *Energy and Finite Element Methods in Structural Mechanics,* Hemisphere Publishing Corporation, 1985.

Shinozuka, M. (editor): *The Hanshin-Awaji Earthquake of January 17, 1995: Performance of Lifelines,* Report No. NCEER-95-0015, National Center for Earthquake Engineering Research (NCEER), University at Buffalo – the State University of New York, Buffalo, New York, 1995.

Timoshenko, S. and Woinowsky-Krieger, S.: *Theory of Plates and Shells,* McGraw-Hill Book Co., Inc., 1959.

Tognazzini, R.: *Hector Mine Earthquake Damage Assessment Investigation*, private communication, Los Angeles Department of Water and Power, Los Angeles, California, 2002.

Villaverde, R.; Pardoen, G. C.; and Carnalla, S.: *Ground Motion Amplification at Base of Bushings Mounted on Electric Substation Transformers*, PEER/PG&E Award No. PGE-09566, University of California at Irvine, Irvine, California, 1999.

Villaverde, R.; Pardoen, G. C.; and Carnalla, S.: *Ground Motion Amplification at Flange Level of Bushings Mounted on Electric Substation Transformers*, Earthquake Engineering and Structural Dynamics, 30(5), pp. 621-632, 2001.

Wang, Y., and Gonzalez, J. R., *"Oregon Public Utilities Commission–Oregon Department of Geology and Mineral Industries Leadership Forum and Seismic Critical Energy Infrastructures Workshop,"* Oregon Department of Geology and Mineral Industries, O-08-10, April 2008.

Wilcoski, J. and Smith, S. J.: *Fragility Testing of a Power Transformer Bushing*, US Army Corps of Engineers, Construction Engineering Research Laboratories (CERL) Technical Report 97/57, 1997.

Wilcoski, J.; Gambil, J.; and Smith, S. J.: *The CERL Equipment Fragility and Protection Procedure (CEFAPP),* US Army Corps of Engineers, Construction Engineering Research Laboratories (CERL) Technical Report 97/58, 1997.

Wilcoski, J.: *Demonstration of CERL Equipment Fragility and Protection Procedure by Fragility Testing of a Power Transformer Bushing,* Proceedings of the Seminar on Seismic Design, Retrofit, and Performance of Nonstructural Components, San Francisco, California, 1998.

APPENDIX A:

TEST PROTOCOLS AND SEQUENCES

All nine bushings were tested according to the protocols (test sequences) listed in this section. The first three bushings were used to calibrate the test set-up and identify special mounting characteristics (Kong, 2010), while the last bushing was used to identify issues in the methods of direct measurements. The flexible support structure designed intentionally for this test series was first tested and its properties identified according to the protocol shown in Table A-1.

Table A-1: Test Protocol for Evaluation of Flexible Support Structure

(1)	(2)	(3)	(4)	(5)	(6)	(7)	(8)	(9)

column 1 :	Test No.	
column 2 :	Turret	N - no turret T - tilted turret V - vertical turret
column 3 :	Location of bushings	C - corner of the support structure S - side of the support structure O - center of the support structure
column 4 :	Test direction	
column 5 :	Test description	
column 6 :	Testing setup	
column 7 :	Test date	
column 8 :	Data file names in repository	
column 9 :	Remarks	

Frame Identification

* Two accelerometers should be attached to top of the support structure in the testing direction.
* Bushing hole should be at N-W corner

T01		EW	Static pull test ending with quick release in E-W dir.	2007.06.06	t01Run1.dat		
T01A		EW	Static pull test ending with quick release in E-W dir.	2007.06.06	t01Run2.dat		
T02		NS	Static pull test ending with quick release in N-Sdir.	Skipped	-		

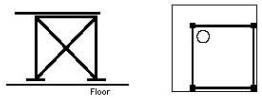

T03	L	EW	Static pull test ending with quick release in E-W dir.	2007.06.06	t03Run3.dat		

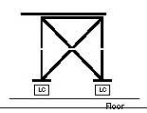

* Mount LADWP 500kV G.E. bushing on the mounting plate.

T04	L	SW	Static pull test ending with quick release in S-W dir.	2007.06.12	t04Run1.dat		
T04A	L	SW	Static pull test ending with quick release in S-W dir.	2007.06.12	t04bRun2.dat		

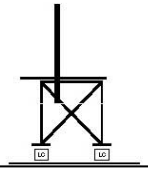

Test Protocol – Bushing #1

Bushing #1 was used for the calibration of the test frame and for understanding the influence of locating the bushing in various positions to determine the influence of boundary conditions on the as-installed frequencies.

The bushing was mounted in center, side and corner locations, both with and without a turret. The bushing was subjected to white noise and acceleration tests at various intensities. Table A-2 describes the complete test protocol for Bushing #1.

Table A-2: Test Protocol – Bushing #1

Bushing #1 : LADWP 500kV G.E. Bushing : Identify sensitivity of structural components

Bushing Identification **Bushing at corner / No turret**

TA01	N	C	NS	Static pull test ending with quick release in N-S dir.	2007.06.20	pullRun2.dat pull1_1.DAT
TA02	N	C	SW	Static pull test ending with quick release in S-W dir.	2007.06.20	pullRun3.dat pull2_2.DAT
TA02A	N	C	SW	Static pull test ending with quick release in S-W dir.	2007.06.20	pull3Run4.dat pull3_3.DAT
TA03	N	C		Table pulse test	2007.06.20	ta03pRun0.dat ta03k.txt ta03m_dat_1.DAT
TA04	N	C		White noise test (0-50Hz, 0.1g)	2007.06.20	ta04pRun1.dat ta04m.DAT

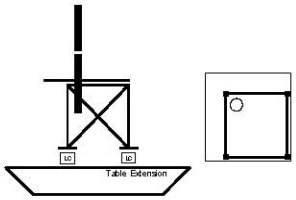

Seismic Evaluation

TA05	N	C		Acceleration time history test (0.1g RRS)	2007.06.21	ta05pRun5.dat ta05m_20070621_084210_0001_MD1.DAT ta05k.txt
TA06	N	C		White noise test	2007.06.21	ta06pRun1.dat ta06m_20070621_085432_0001_MD1.DAT
TA07	N	C		Acceleration time history test (0.25g RRS)	2007.06.21	ta07pRun1.dat ta07m_20070621_090249_0001_MD1.DAT ta07k.txt
TA08	N	C		White noise test	2007.06.21	ta08pRun1.dat ta08m_20070621_090758_0001_MD1.DAT

Bushing Identification **Bushing at side / No turret**

TA09	N	S	EW	Static pull test ending with quick release in E-W dir.	skipped	
TA10	N	S	NS	Static pull test ending with quick release in N-S dir.	skipped	
TA11	N	S		Table pulse test	2007.06.21	ta11pRun1.dat ta11m_20070621_145613_0001_MD1.DAT ta11k.txt
TA12	N	S		White noise test	2007.06.21	ta12pRun1.dat ta12m_20070621_150359_0001_MD1.DAT

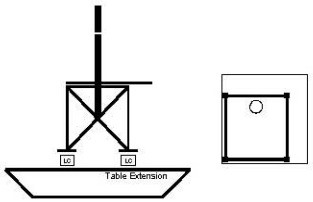

Table A-2: Test Protocol – Bushing #1 (cont'd.)

Seismic Evaluation							
TA13	N	S		Acceleration time history test (0.1g RRS)		2007.06.21	ta13pRun1.dat ta13m_20070621_151123_0001_MD1.DAT ta13k.txt
TA14	N	S		White noise test		2007.06.21	ta14pRun1.dat ta14m_20070621_151431_0001_MD1.DAT
TA15	N	S		Acceleration time history test (0.25g RRS)		skipped	
TA16	N	S		White noise test		skipped	
Bushing Identification			**Bushing at center / No turret**				
TA17	N	O	EW	Static pull test ending with quick release in E-W dir.	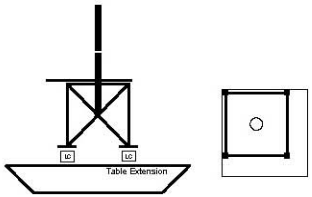	skipped	
TA18	N	O	NS	Static pull test ending with quick release in N-S dir.		skipped	
TA19	N	O		Table pulse test		2007.06.22	ta19pRun2.dat ta19m_20070622_110534_0002_MD1.DAT TA19.txt
TA20	N	O		White noise test		2007.06.22	ta20pRun1.dat ta20m_20070622_111253_0001_MD1.DAT
Seismic Evaluation							
TA21	N	O		Acceleration time history test (0.1g RRS)		2007.06.22	ta21pRun1.dat ta21m_20070622_111858_0001_MD1.DAT
TA22	N	O		White noise test		2007.06.22	ta22pRun1.dat ta22m_20070622_112347_0001_MD1.DAT
TA23	N	O		Acceleration time history test (0.25g RRS)		skipped	
TA24	N	O		White noise test		skipped	
Bushing Identification			**Bushing at center / No turret**				
TA25	N	O	SE	Static pull test ending with quick release in SE dir.	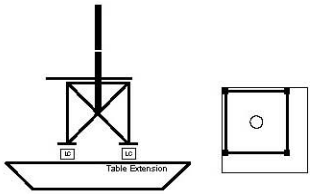	2007.07.16	ta-25Run12.dat
TA26	N	O	SW	Static pull test ending with quick release in SW dir.		2007.07.16	ta26Run14.dat
TA27	N	O		Table pulse test		2007.07.13	ta27bRun17.dat TA27B_20070713_155609_0001_MD1.DAT
TA28	N	O		Acceleration time history test (0.05g RRS)		2007.07.13	ta28cRun20.dat TA28c_20070713_163152_0001_MD1.DAT
TA29	N	O		Table pulse test		2007.07.13	ta29Run21.dat TA29_20070713_163552_0001_MD1.DAT

Table A-2: Test Protocol – Bushing #1 (cont'd.)

Bushing Identification **Bushing at side / No turret**

TA30	N	S	Table pulse test	2007.07.16	07-16-2007ta30Run9.dat TA30b_20070716_172539_0002_MD1.DAT	
TA31	N	S	Acceleration time history test (0.05g RRS)	2007.07.17	ta31dRun1.dat TA31d_20070717_094443_0001_MD1.DAT	
TA32	N	S	Table pulse test	2007.07.17	ta32aRun2.dat TA32a_20070717_095043_0001_MD1.DAT	

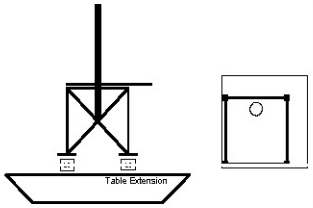

Bushing Identification **Bushing at corner / No turret**

TA33	N	C	Table pulse test	2007.07.18	ta33Run4.dat ta33_20070718_090851_0001_MD1.DAT	
TA34	N	C	Acceleration time history test (0.05g RRS)	2007.07.18	ta34bRun1.dat ta34b_20070718_094618_0001_MD1.DAT	
TA35	N	C	Table pulse test	2007.07.18	ta35Run2.dat ta35_20070718_095329_0001_MD1.DAT	

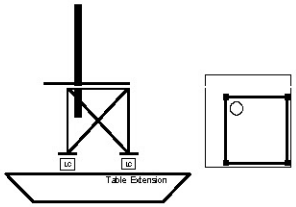

Bushing Identification **Bushing at corner / No turret / No load washer**

TA36	N	C	Table pulse test	2007.07.18	ta36Run4.dat ta36_20070718_141157_0001_MD1.DAT	
TA37	N	C	Acceleration time history test (0.05g RRS)	2007.07.18	ta37aRun1.dat ta37a_20070718_154445_0001_MD1.DAT	
TA38	N	C	Acceleration time history test (0.075g RRS)	2007.07.18	ta38cRun5.dat ta38c_20070718_151752_0001_MD1.DAT	
TA39	N	C	Table pulse test	2007.07.18	ta39Run1.dat ta39_20070718_152236_0001_MD1.DAT	

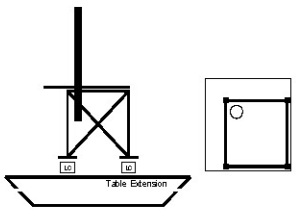

Bushing Identification **Bushing at corner / Tilted turret**

TA40	T	C	Table pulse test	2007.08.23	ta40Run3.dat	
TA41	T	C	Acceleration time history test (0.05g RRS)	2007.08.23	ta41dRun7.dat	
TA42	T	C	Table pulse test	2007.08.23	ta42Run8.dat	

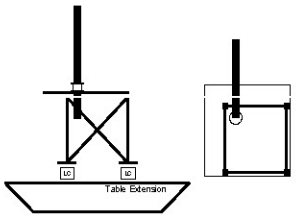

Table A-2: Test Protocol – Bushing #1 (cont'd.)

Bushing Identification **Bushing at center / Tilted turret**

TA43	T	O		Table pulse test	2007.08.23	ta43Run9.dat	
TA44	T	O		Acceleration time history test (0.05g RRS)	2007.08.23	ta44gRun16.dat	
TA45	T	O		Table pulse test	2007.08.23	ta45Run18.dat	

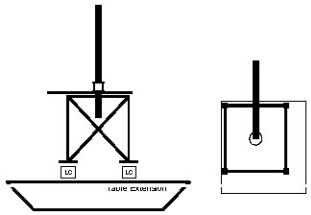

Bushing Identification **Bushing at side / Tilted turret**

TA46	T	S		Table pulse test	skipped		
TA47	T	S		Acceleration time history test (0.05g RRS)	skipped		
TA48	T	S		Table pulse test	skipped		

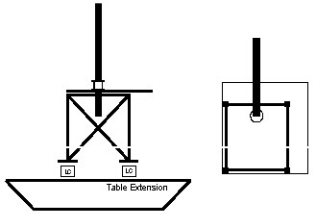

Property Evaluation **LADWP G.E. 550kV Bushing #1**

TA49				Finding the weight of the bushing			4000lb
TA50				Finding the center of the gravity of the bushing			
T05	L	C	EW	Static pull test ending with quick release in E-W dir.	skipped		
T06	L	C	NS	Static pull test ending with quick release in N-S dir.	skipped		

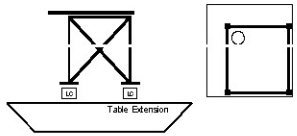

Test Protocol – Bushing #2

After measuring the total weight and center of gravity of Bushing #2, it was mounted on the corner of the testing frame and acceleration history tests were performed. The tests were performed from 0.1 g to 0.8 g RRS in intervals of 0.1 g.

Table A-3 describes the complete test protocol for Bushing #2.

Table A-3: Test Protocol – Bushing #2

Bushing #2 : CERL 550kV G.E. Bushing : Identify failure modes

* 25lb should be added to the top of bushing

Property Evaluation **CERL G.E. 550kV Bushing #2**

TB01		Finding the weight of the bushing	8/29/2007	2455lb	
TB02		Finding the center of the gravity of the bushing	8/29/2007	57.5" above mount plate	
TB03		Finding the weight of the bushing	8/29/2007	2800lb	
TB04		Finding the center of the gravity of the bushing	8/29/2007	57.5" above mount plate	
TB05	NS	Pull test to calibrate strain gages in NS dir	9/5/2007	tb05bRun11.dat	
TB06	EW	Pull test to calibrate strain gages in EW dir	9/5/2007	tb06Run12.dat	

Identify failure modes

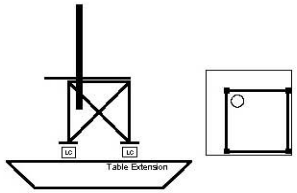

TB07	Table pulse test	9/5/2007	tb07Run1.dat	4.3Hz
TB08	White noise test	9/5/2007	tb08Run2.dat	4.1Hz
TB09	Acceleration time history test (PGA 0.1g)	9/5/2007	tb09Run3.dat	
TB10	Table pulse test	9/5/2007	tb10Run4.dat	4.3Hz
TB11	Acceleration time history test (PGA 0.2g)	9/5/2007	tb11Run5.dat	
TB12	Table pulse test	9/5/2007	tb12Run6.dat	4.3Hz
TB13	Acceleration time history test (PGA 0.3g)	9/5/2007	tb13Run7.dat	
TB14	Table pulse test	9/5/2007	tb14Run8.dat	4.3Hz
TB15	Acceleration time history test (PGA 0.4g)	9/5/2007	tb15bRun12.dat	
TB16	Table pulse test	9/5/2007	tb16Run11.dat	4.27Hz
TB17	Acceleration time history test (PGA 0.5g)	9/6/2007	tb17bRun1.dat	
TB18	Table pulse test	9/6/2007	tb18Run2.dat	
TB19	Acceleration time history test (PGA 0.6g)	9/6/2007	tb19Run3.dat	
TB20	Table pulse test	9/6/2007	tb20Run4.dat	
TB21	Acceleration time history test (PGA 0.7g)	9/6/2007	tb21Run5.dat	
TB22	Table pulse test	9/6/2007	tb22Run6.dat	
TB23	Acceleration time history test (PGA 0.8g)	9/6/2007	tb23Run7.dat	
TB24	Table pulse test	9/6/2007	tb24Run8.dat	

Test Protocol – Bushing #3

Bushing #3 was mounted on the corner of the frame. The input motion was modified to be the spectrum compatible sine sweep. Three tests were performed in each series, each test being in one principal direction. During the first series of tests, a sine sweep with acceleration amplitude of 0.25 g was used in both the NS and EW directions, and 80% of the 0.25 g was used in the vertical direction. After two such tests, the bushing was tested to 0.50 g using IEEE 693 spectrum compatible motion. Then the sine sweep tests were performed once again at 0.50 g RRS in two horizontal directions, and 80% of the motion was used in the vertical direction.

Table A-4 describes the complete test protocol for Bushing #3.

Table A-4: Test Protocol – Bushing #3

Bushing #3 : CERL 550kV G.E. Bushing : Qualification and Fragility test

Property Evaluation **CERL G.E. 550kV Bushing #3**

TC01		Finding the weight of the bushing	9/6/2007	2465lb	
TC02		Finding the center of the gravity of the bushing	9/6/2007	57.5" above mount plate	
TC03		Finding the weight of the bushing	9/6/2007	2810lb	
TC04		Finding the center of the gravity of the bushing	9/6/2007	57.5" above mount plate	
TC05	E	Pull test to calibrate strain gages toward East	9/13/2007	tc05bRun6.dat	
TC06	SE	Pull test to calibrate strain gages toward South-East	9/13/2007	tc06Run4.dat	
TC07	S	Pull test to calibrate strain gages toward South	9/13/2007	tc07Run3.dat	
TC08	SW	Pull test to calibrate strain gages toward South-West	9/13/2007	tc08bRun2.dat	

Identify failure modes

TC09		Table pulse test	9/13/2007	tc09Run8.dat	
TC10		White noise test	9/13/2007	tc10Run9.dat	
TC11		Qualification test to 0.25g RRS - IEEE 693	9/13/2007	tc11Run10.dat	
TC12		Table pulse test	9/13/2007	tc12Run12.dat	
TC13	EW	Qualification test to 0.25g RRS - Sine Sweep 100	9/13/2007	tc13Run13.dat	
TC14	NS	Qualification test to 0.25g RRS - Sine Sweep 100	9/13/2007	tc14Run14.dat	
TC15	V	Qualification test to 0.25g RRS - Sine Sweep 100 - 80%	9/13/2007	tc15Run15.dat	
TC16		Table pulse test	9/13/2007	tc16Run16.dat	
TC17	EW	Qualification test to 0.25g RRS - Sine Sweep 1200	9/13/2007	tc17Run17.dat	
TC18	NS	Qualification test to 0.25g RRS - Sine Sweep 1200	9/13/2007	tc18Run18.dat	
TC19	V	Qualification test to 0.25g RRS - Sine Sweep 1200 - 80%	9/13/2007	tc19Run19.dat	
TC20		Table pulse test	9/13/2007	tc20Run20.dat	
TC21		Qualification test to 0.5g RRS - IEEE 693	9/13/2007	tc21Run21.dat	
TC22		Table pulse test	9/13/2007	tc22Run22.dat	
TC23	EW	Qualification test to 0.5g RRS - Sine Sweep 100	9/13/2007	tc23Run24.dat	
TC24	NS	Qualification test to 0.5g RRS - Sine Sweep 100	9/13/2007	tc24Run27.dat	
TC25	V	Qualification test to 0.5g RRS - Sine Sweep 100 - 80%	9/13/2007	tc25Run31.dat	
TC26		Table pulse test	9/13/2007	tc26Run32.dat	
TC27	EW	Qualification test to 0.5g RRS - Sine Sweep 101	9/13/2007	tc27Run36.dat	
TC28	NS	Qualification test to 0.5g RRS - Sine Sweep 101	9/13/2007	tc28Run40.dat	

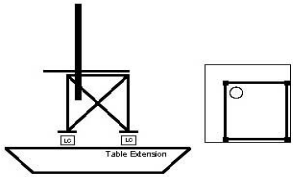

Test Protocol – Bushing #4A

For the first series of tests, Bushing #4A was mounted with different configurations of stiffeners. The main objective was to observe the change in frequency of bushings due to presence of stiffeners. The bushing when installed on the flexible plate had lower frequency of response due to the fact that the plate is more flexible without stiffeners.

For the first part of this protocol Bushing #4A was mounted on the rigid concrete block and impact hammer tests were performed to measure the fixed-base frequency and damping of the bushing. Also, the strain gauges on the mounting flange were calibrated with a small force applied at the top of the bushing. This calibration was necessary to find bending moments during dynamic testing.

After the fixed base tests, the bushing was then mounted at the center of the frame, and two L-shaped stiffeners were bolted on either side of the bushing to stiffen the plate. Frequency and damping ratio were measured in both principal direction (EW and NS). Then the bushing was moved to the side of the frame with the help of a re-locatable steel plate. Again two stiffeners were used and dynamic characteristics were measured for comparison purposes, the stiffeners were removed and acceleration history, white noise and table impulse tests were run. This sequence was important to observe the difference between the stiffened and un-stiffened plate when the bushing is located on the side of the frame. The bushing was then mounted in the corner location and was tested again with both stiffened and un-stiffened plate, using the aforementioned L-shaped stiffeners.

In the third sequence the bushing was once again mounted on the concrete block and impact hammer tests were performed to measure any change in frequency. Then the bushing was pulled in one direction only (EW Direction) with incremental loading. 100 lb. loading was applied in the first tests and 3,000 lb. in the last test, where a cracking sound was heard and the bushing was observed to have failed.

Table A-5 describes the complete test protocol for Bushing #4A.

Table A-5: Test Protocol – Bushing #4A

Seismic Evaluation and Qualification of Transformer Bushings

Test No.		Position of turret	Location of Bushing	Test Direction	Test Description	Testing Setup	Test Date	File name in Repository	Remarks
check if Weight is to be added at the top of the Bushing									
Check if water was added to the Bushings before testing									
1. Pre-Test Activities			HSP, LADWP 230 kV Composite Bushing #4a			CG Of Bushing =18.5" from Flange top			Upper Bushing CG=37.5"
TB-U1-	01	No Turret	N/A	N/A	Finding Weight of the Bushing	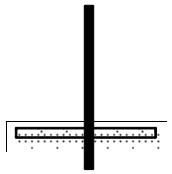	090726	TB-U1-01	510 lbs
TB-U1-	02	No Turret	N/A	N/A	Finding Centre of Gravity of Bushing		090726	TB-U1-02	CG-overall =18.5" form Flane; CG-upper= 37.5"
TB-U1-NE-w w -	03	No Turret	Concrete Slab	NE	Impact Hammer Test		090803	TB-U1-w w -03	w /o 15 lbs
TB-U1-SE--w w -	04	No Turret	Concrete Slab	SE	Impact Hammer Test		090803	TB-U1-w w -04	w /o 15 lbs
TB-U1-NS--w w -	05	No Turret	Concrete Slab	NS	Impact Hammer Test		090803	TB-U1-w w -05	w /o 15 lbs
TB-U1-WE-w w -	06	No Turret	Concrete Slab	EW	Impact Hammer Test		090803	TB-U1-w w -06	w /o 15 lbs
TB-U1-NE-	03	No Turret	Concrete Slab	NE	Impact Hammer Test		090803	TB-U1-03	w /15 lbs
TB-U1-SE-	04	No Turret	Concrete Slab	SE	Impact Hammer Test		090803	TB-U1-04	w /15 lbs
TB-U1-NS-	05	No Turret	Concrete Slab	NS	Impact Hammer Test		090803	TB-U1-05	w /15 lbs
TB-U1-EW-	06	No Turret	Concrete Slab	EW	Impact Hammer Test		090803	TB-U1-06	w /15 lbs
TB-U1-EW-lugs	07	No Turret	Concrete Slab	EW	Impact Hammer Test		090803	hammerlug	lugs direct
TB-U1-NS-cap	08	No Turret	Concrete Slab	NS	Impact Hammer Test		090803	hammercap	capacit dir
TB-U1-hvyh-NE-	09	No Turret	Concrete Slab	NE	Impact Hammer Test		090803	TBU1hvyhNE09	w /15 lbs-hardhit
TB-U1-hvyh-SE-	10	No Turret	Concrete Slab	SE	Impact Hammer Test		090803	TBU1hvyhSE10	w /15 lbs-hardhit
TB-U1-hvyh-NS-	11	No Turret	Concrete Slab	NS	Impact Hammer Test		090803	TBU1hvyhNS11	w /15 lbs-hardhit
TB-U1-hvyh-EW-	12	No Turret	Concrete Slab	EW	Impact Hammer Test	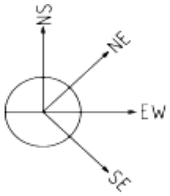	090803	TBU1hvyhEW12	w /15 lbs-hardhit
TB-U1-	13	No Turret	Concrete Slab	N/A	Pull Test 100 lb		090803	TB-U1-07	
TB-U1-	14	No Turret	Concrete Slab	N/A	Pull Test 200 lbs		090803	TB-U1-09	
TB-U1-	15	No Turret	Concrete Slab	N/A	Pull Test 300 lbs		090803	TB-U1-11	
TB-U1-	16	No Turret	Concrete Slab	N/A	Pul Test Continuous to 300lbs		090803	TB-U1-11b	stiffness test = k = 682.35 lbs/in
TB-U1-NE-	17	No Turret	Concrete Slab	EW	Impact Hammer Test		090804	TB-U1-w enoplate1	w /o 15 lbs 9.05Hz
TB-U1-EW-	18	No Turret	Concrete Slab	EW	Impact Hammer Test		090804	TB-U1-w eplate-18	w /15 lbs 8.32Hz

Note: The E direction is 15 degree (APPROXIMATELY) CW angle to the direction of lifting lug

Additional Data: Capacitance: 10.84 nF; Add Weeight: 15 lbs; Shakle Weight: 2.5 lbs

Table A-5: Test Protocol – Bushing #4A (cont'd.)

3. Bushing Identification

Note: Fill the Bushing with Water Bushing at Center/ no turret /on Shake Table

TB-U1-WN-	23		Center of Frame		WHITE NOISE TEST (0-50HZ, 0.1 g)	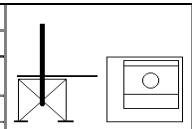	090805	tbu1w n23	freq = 7.5N, 7.75E,22.65V
TB-U1-TBI-	24		Center of Frame		Table Impulse test		090805	tbu1tbi24	freq = 7.5N, 7.75E,22.65V
TB-U1-AH125-	25		Center of Frame		ACCELERATION TIME HISTORY TEST (0.125g RRS)		090805	tbu1ah12525	freq=7.75N, 7.75E, 22Hz
TB-U1-WN-	26		Center of Frame		WHITE NOISE TEST (0-50HZ, 0.1 g)		090805	tbu1w n26	freq=7.75N, 7.75E, 22Hz
TB-U1-TBI-	27		Center of Frame		Table Impulse test		090805	tbu1tbi27	freq=7.75N, 7.75E, 22Hz

PAUSE FOR INSPECTION

4. Bushing Identification Bushing at Edge/ no turret /on Shake Table/with stiffenner

TB-U1-WN-	28		FRAME East EDGE		WHITE NOISE TEST (0-50 Hz, 0.1g)	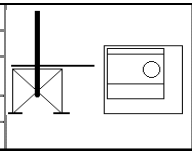	90806	tbu1w n28	freq=7.75 N, 7.75E, 21.75,23.75 V
TB-U1-TBI-	29		FRAME East EDGE		TABLE IMPULSE TEST		90806	tbu1tbi29	freq=7.75N, 7.75E
TB-U1-AH125-	30		FRAME East EDGE		ACCELERATION TIME HISTORY TEST (0.125g RRS)		90806	tbu1ah12530	freq=7.75N,7.75E, 21.75,22.125V
TB-U1-WN-	31		FRAME East EDGE		WHITE NOISE TEST (0-50 Hz, 0.1g)		90806	tbu1w n31	freq=7.75N,7.75E, 21.75,21.5V
TB-U1-TBI-	32		FRAME East EDGE		TABLE IMPULSE TEST		90806	tbu1tbi32	freq=7.75N,7.75E, 21.75,21.5V

PAUSE FOR INSPECTION

5. Bushing Identification Bushing at Edge/ no turret /on Shake Table

TB-U1-WN-	33		FRAME East EDGE		WHITE NOISE TEST (0-50 Hz, 0.1g)	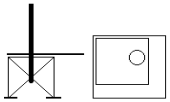	90806	tbu1w n33	
TB-U1-TBI-	34		FRAME East EDGE		TABLE IMPULSE TEST		90806	tbu1tbi34	freq=7.5N,7.1255E, 21.75,21.5V
TB-U1-AH125-	35		FRAME East EDGE		ACCELERATION TIME HISTORY TEST (0.125g RRS)		90806	tbu1ah12535	
TB-U1-WN-	36		FRAME East EDGE		WHITE NOISE TEST (0-50 Hz, 0.1g)		90806	tbu1w n36	freq=7.5N,7.125E, 21.75,21.5V
TB-U1-TBI-	37		FRAME East EDGE		TABLE IMPULSE TEST		90806	tbu1tbi37	freq=7.5N,7.125E, 21.75,21.5V

PAUSE FOR INSPECTION

6. Bushing Identification Bushing at corner/ no turret /on Shake Table

TB-U1-WN-	38		Frame NE Corner		WHITE NOISE TEST (0-50 Hz, 0.1g)	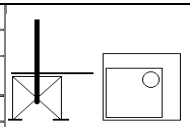	90806	tbu1w n38	freq=7.5N, 7.25 & 7.75E
TB-U1-TBI-	39		Frame NE Corner		TABLE IMPULSE TEST		90806	tbu1tbi39	
TB-U1-AH125-	40		Frame NE Corner		ACCELERATION TIME HISTORY TEST (0.125g RRS)		090806	tbu1ah12540	freq= 7.36N & 7.8N, 7.36E& 7.808E
TB-U1-WN-	41		Frame NE Corner		WHITE NOISE TEST (0-50 Hz, 0.1g)		090806	tbu1w n41	freq= 7.488N &7.744N, 7.23E,7.616E, 7.744E
TB-U1-TBI-	42		Frame NE Corner		TABLE IMPULSE TEST		090806	tbu1tbi42	

PAUSE FOR INSPECTION

Bushing at corner/ no turret /on Shake Table/with stiffenner

7. Bushing Identification

TB-U1-WN-	43		Frame NE Corner		WHITE NOISE TEST (0-50 Hz, 0.1g)	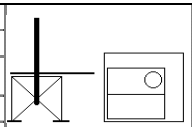	090806	tbu1w n43	
TB-U1-TBI-	44		Frame NE Corner		TABLE IMPULSE TEST		090806	tbu1tbi44	freq=7.8N, 7.8E
TB-U1-AH125-	45		Frame NE Corner		ACCELERATION TIME HISTORY TEST (0.125g RRS)		090806	tbu1ah12545	freq=7.625 N, 7.75E7.94E
TB-U1-WN-	46		Frame NE Corner		WHITE NOISE TEST (0-50 Hz, 0.1g)		090806	tbu1w n46	
TB-U1-TBI-	47		Frame NE Corner		TABLE IMPULSE TEST		090806	tbu1tbi47	freq= 7.8N, 7.8 E,7.8SE

Table A-5: Test Protocol – Bushing #4A (cont'd.)

PAUSE FOR INSPECTION

8. Bushing Failure mode Identification Started with 125 lbs

TB-U1-EW	48	No Turret	Concrete Slab	EW	Impact Hammer Test		090807	tbu1ew 45	freq=8.25 E
TB-U1-PL	49	No Turret	Concrete Slab	EW	Pull Test 100 lb		090807	tbu1pl46	100lb test due to slack in the cable
TB-U1-PL-B	50	No Turret	Concrete Slab	EW	Pull Test 300 lb		090807	tbu1pl46b	to get 300lb w e added 0.3in additional displacement for scaling
TB-U1-EW	51	No Turret	Concrete Slab	EW	Impact Hammer Test		090807	tbu1ew 51	hit tw ice during the test, freq=8.3125
TB-U1-PL	52	No Turret	Concrete Slab	EW	Pull Test 500 lbs		090807	tbu1pl52	tested to 372 lbs
TB-U1-EW	53	No Turret	Concrete Slab	EW	Impact Hammer Test		090807	tbu1ew 53	freq=8.3125 E
TB-U1-PL	54	No Turret	Concrete Slab	EW	Pull Test 1000 lbs		090807	tbu1pl54	tested to 635 lbs
TB-U1-EW	55	No Turret	Concrete Slab	EW	Impact Hammer Test		090807	tbu1ew 55	freq=8.3125 E
TB-U1-PL	56	No Turret	Concrete Slab	EW	Pull Test 1500 lbs		090807	tbu1pl56	tested to 1319 lbs
TB-U1-EW	57	No Turret	Concrete Slab	EW	Impact Hammer Test		090807	tbu1ew 57	freq=8.3125 E
TB-U1-PL	58	No Turret	Concrete Slab	EW	Pull Test 2000 lbs		090807	tbu1pl58	Tested to 2040 lbs
TB-U1-EW	59	No Turret	Concrete Slab	EW	Impact Hammer Test		090807	tbu1ew 59	freq=8.125E
TB-U1-PL	60	No Turret	Concrete Slab	EW	Pull Test 2500 lbs		090807	tbu1pl60	tested to 2700 lbs
TB-U1-EW	61	No Turret	Concrete Slab	EW	Impact Hammer Test		090807	tbu1ew 61	freq= 7.77 and 8.05 Hz
TB-U1-PL	62	No Turret	Concrete Slab	EW	Pull Test 3000 lbs		090807	tbu1pl62	test to 2900 lbs (Bushing Failed)
TB-U1-EW	63	No Turret	Concrete Slab	EW	Impact Hammer Test		090807	tbu1ew 63	freq=7.75, 7.93Hz
TB-U1-PL	64	No Turret	Concrete Slab	EW	Pull Test 1300 lbs		090807	tbu1pl64	tested to 1300 lbs
TB-U1-EW	65	No Turret	Concrete Slab	EW	Impact Hammer Test		090807	tbu1ew 65	Manual
TB-U1-PL	66	No Turret	Concrete Slab	EW	Pull Test 4000 lbs		N/A	N/A	Skipped
TB-U1-EW	67	No Turret	Concrete Slab	EW	Impact Hammer Test		N/A	N/A	Skipped
TB-U1-PL	68	No Turret	Concrete Slab	EW	Pull Test 4500 lbs		N/A	N/A	Skipped
TB-U1-EW	69	No Turret	Concrete Slab	EW	Impact Hammer Test		N/A	N/A	Skipped
TB-U1-PL	70	No Turret	Concrete Slab	EW	Pull Test 5000 lbs		N/A	N/A	Skipped
TB-U1-EW	71	No Turret	Concrete Slab	EW	Impact Hammer Test		N/A	N/A	Skipped
TB-U1-PL	72	No Turret	Concrete Slab	EW	Pull Test 5500 lbs		N/A	N/A	Skipped
TB-U1-EW	73	No Turret	Concrete Slab	EW	Impact Hammer Test		N/A	N/A	Skipped
TB-U1-PL	74	No Turret	Concrete Slab	EW	Pull Test 6000 lbs		N/A	N/A	Skipped
TB-U1-EW-	75	No Turret	Concrete Slab	EW	Impact Hammer Test		N/A	N/A	Skipped

Test Protocol – Bushing #4B

Bushing #4B was mounted on the fixed base to determine its physical properties. Impact hammer tests in principal directions (EW and NS) were used to find the fixed-base frequency and damping ratio. Pull tests in principal directions were performed to calibrate strain gauges, which were used later to determine the bending moment demand on the bushing. The bushing was then mounted on the frame in the center location for dynamic testing. White noise test and table impulse tests were followed by incremental acceleration history tests. The first test was performed at 0.25 g RRS and the final test was performed at 3.00 g RRS. Demand in terms of bending moment was measured in the bushing.

For the last sequence of testing, the bushing was once again mounted on the fixed base (concrete block) and pulled in the EW direction. The pull test was again divided into two components. During the first part the bushing was pulled from the top in the EW direction using the shake table, with each test composed of 10 cycles of equal force. The intent was to measure the stiffness and damping of the bushing. During the next sequence, the bushing was pulled in the EW direction with incremental loading to determine the capacity of bushing; a pre-determined force was applied at the top of bushing using the shake table and released at a certain lower level of force. The free vibration thus created was used to determine the change in the frequency and damping of the bushing.

Table A-6 describes the complete test protocol for Bushing #4B.

Table A-6: Test Protocol – Bushing #4B

Seismic Evaluation and Qualification of Transformer Bushings

Test No.		Position of turret	Location of Bushing	Test Direction	Test Description	Testing Setup	Test Date	File name in Repository	Remarks
check if Weight is to be added at the top of the Bushing									
Check if water was added to the Bushings before testing									
1. Pre-Test Activities			HSP, LADWP 230 kV Composite Bushing #4b			CG Of Bushing =_____"			Upper Bushing CG=_____"
TB-U2-	01	No Turret	N/A	N/A	Finding Weight of the Bushing	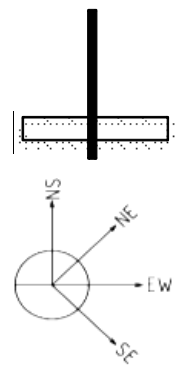	90810		350 lbs
TB-U2-	02	No Turret	N/A	N/A	Finding Centre of Gravity of Bushing		90810		
TB-U2-NE-	03	No Turret	Concrete Slab	NE	Impact Hammer Test		90810	tbu2ne03	light impact
TB-U2-SE-	04	No Turret	Concrete Slab	SE	Impact Hammer Test		90810	tbu2se04	light impact
TB-U2-NS-	05	No Turret	Concrete Slab	NS	Impact Hammer Test		90810	tbu2ns05	light impact
TB-U2-EW-	06	No Turret	Concrete Slab	EW	Impact Hammer Test		90810	tbu2ew 06	light impact
TB-U2-EW-lugs	07	No Turret	Concrete Slab	EW	Impact Hammer Test		90810	tbu2ew lugs07	
TB-U2-NS-cap	08	No Turret	Concrete Slab	NS	Impact Hammer Test		90810	tbu2nscap08	
TB-U2-	9.00	No Turret	Concrete Slab	NA	Pull Test 50 lbs w ith 400 lb LC		90810	tbu209	Release test at 50 lbs
TB-U2-	10.00	No Turret	Concrete Slab	NA	Pull Test 100 lbs release at 100 lbs		90810	tbu210	
TB-U2-	11.00	No Turret	Concrete Slab	N/A	Pull Test 200 lb		90810	tbu211	
TB-U2-	12.00	No Turret	Concrete Slab	N/A	Pull Test 725 lbs, Release at 580 lbs		90810	tbu212	
TB-U2-	13.00	No Turret	Concrete Slab	N/A	Pull Test 1250 lbs, Release at 1000 lbs		90810	tbu213	
TB-U2-	14.00	No Turret	Concrete Slab	N/A	Pul Test 1450lbs, Release at 1160 lbs		90810	tbu214	
TB-U2-	15.00	No Turret	Concrete Slab	N/A	Pull Test 1667 lbs, Release at 1160 lbs				SKIPPED
TB-U2-NE-	16.00	No Turret	Concrete Slab	EW	Impact Hammer Test				SKIPPED
TB-U2-EW-	17.00	No Turret	Concrete Slab	EW	Impact Hammer Test				SKIPPED

Table A-6: Test Protocol – Bushing #4B (cont'd.)

2. Bushing Identification

Note: Fill the Bushing with Water Bushing at Center/ no turret /on Shake Table

TB-U2-WN-	18		Center of Frame		WHITE NOISE TEST (0-50HZ, 0.1 g)		090810	tbu2w n18	
TB-U2-TBI-	19		Center of Frame		Table Impulse test		090810	tnu2tbi19	
TB-U2-AH25-	20		Center of Frame		ACCELERATION TIME HISTORY TEST (0.25g RRS)		090810	tbu2ah2520	
TB-U2-WN-	21		Center of Frame		WHITE NOISE TEST (0-50HZ, 0.1 g)		090810	tbu2w n21	
TB-U2-TBI-	22		Center of Frame		Table Impulse test		090810	tbu2tbi22	
TB-U2-AH50-	23		Center of Frame		ACCELERATION TIME HISTORY TEST (0.5g RRS)		090810	tbu2ah5023	
TB-U2-WN-	24		Center of Frame		WHITE NOISE TEST (0-50HZ, 0.1 g)		090810	tbu2w n24	
TB-U2-TBI-	25		Center of Frame		Table Impulse test		090810	tbu2tbi25	
TB-U2-AH100-	26		Center of Frame		ACCELERATION TIME HISTORY TEST (1.0g RRS)		090810	tbu2ah10026	
TB-U2-WN-	27		Center of Frame		WHITE NOISE TEST (0-50HZ, 0.1 g)		090810	tbu2w n27	
TB-U2-TBI-	28		Center of Frame		Table Impulse test		090810	tbu2tbi28	
TB-U2-AH200-	29		Center of Frame		ACCELERATION TIME HISTORY TEST (2.0g RRS)		090810	tbu2ah20029	
TB-U2-WN-	30		Center of Frame		WHITE NOISE TEST (0-50HZ, 0.1 g)		090810	tbu2w n30	
TB-U2-TBI-	31		Center of Frame		Table Impulse test		090810	tbu2tbi31	
TB-U2-AH250-	32		Center of Frame		ACCELERATION TIME HISTORY TEST (2.5g RRS)				SKIPPED
TB-U2-WN-	33		Center of Frame		WHITE NOISE TEST (0-50HZ, 0.1 g)		090811	tbu2w n33	
TB-U2-TBI-	34		Center of Frame		Table Impulse test		090811	tbu2tbi34	
TB-U2-AH300-	35		Center of Frame		ACCELERATION TIME HISTORY TEST (3.0g RRS)		090811	tbu2ah30035	Excessive Deformation w as noticed during the test and bolts w ere loose
TB-U2-WN-	36		Center of Frame		WHITE NOISE TEST (0-50HZ, 0.1 g)		090811	tbu2w n36	
TB-U2-TBI-	37		Center of Frame		Table Impulse test		090811	tbu2tbi37	

PAUSE FOR INSPECTION

Table A-6: Test Protocol – Bushing #4B (cont'd.)

3. Bushing Failure mode Identification

TB-U2-EW	38a	No Turret	Concrete Slab	EW	Impact Hammer Test		090811	tbu2ew 38a	Hammer Test With Loose Bolts
TB-U2-EW	38b	No Turret	Concrete Slab	EW	Impact Hammer Test		090811	tbu2ew 38b	Hammer Test w ith Tightened Bolts
TB-U2-PL	39	No Turret	Concrete Slab	EW	Pull Test 1450 lb		090812	tbu2pl39	Pull Test to 600 lbs, 2.55 in
TB-U2-EW	40	No Turret	Concrete Slab	EW	Impact Hammer Test		090812	tbu2ew 40	
TB-U2-PL	41a	No Turret	Concrete Slab	EW	Pull Test 1450 lb, 1 sec Test		090812	tbu2p41a	Pull Test to 1842 lbs
TB-U2-PL	41b	No Turret	Concrete Slab	EW	Caliberating the shake table		090812	tbu2p41b	Pull Test to 1469 lbs
TB-U2-PL	41c	No Turret	Concrete Slab	EW	Caliberating the shake table		090812	tbu2p41c	Pull Test To 1540 lbs
TB-U2-PL	41d	No Turret	Concrete Slab	EW	Caliberating the shake table		090812	tbu2p41d	Pull Test to 1159 lbs (3.8", 110 lb initial load)
TB-U2-PL	41	No Turret	Concrete Slab	EW	Caliberating the shake table		090812	tbu2p41	Pull Test To 609 lbs
TB-U2-EW	42	No Turret	Concrete Slab	EW	Impact Hammer Test		090812	tbu2ew 42	
TB-U2-EW	41a	No Turret	Concrete Slab	EW	Impact Hammer Test		090812	tbu2ew 42a	
TB-U2-EW	42b	No Turret	Concrete Slab	EW	Impact Hammer Test		090812	tbu2ew 42b	
TB-U2-PL	43	No Turret	Concrete Slab	EW	Pull Test 10 Cycles of 1 sec each		090812	tbu2pl43	
TB-U2-EW	44	No Turret	Concrete Slab	EW	Impact Hammer Test		090812	tbu2ew 44	
TB-U2-PL	45	No Turret	Concrete Slab	EW	Pull Test 10 Cycles of 1 sec each		090812	tbu2pl45	
TB-U2-EW	46	No Turret	Concrete Slab	EW	Impact Hammer Test		090812	tbu2ew 46	
TB-U2-PL	47	No Turret	Concrete Slab	EW	Pull Test 10 Cycles of 1 sec each		090812	tbu2pl47	2.7" snd 1655 lb load
TB-U2-EW	48	No Turret	Concrete Slab	EW	Impact Hammer Test		090812	tbu2ew 48	
TB-U2-PL	49	No Turret	Concrete Slab	EW	Pull Test 10 Cycles of 1 sec each		090812	tbu2pl49	intital load 261lb, 2.84", 1728lbs
TB-U2-EW	50	No Turret	Concrete Slab	EW	Impact Hammer Test		090812	tbu2ew 50	
TB-U2-PL	51	No Turret	Concrete Slab	EW	Pull Test 10 Cycles of 1 sec each		090812	tbu2pl51	initial load 261lbs, 2.8", 1708lbs
TB-U2-EW	52	No Turret	Concrete Slab	EW	Impact Hammer Test		090812	tbu2ew 52	
TB-U2-PL	53	No Turret	Concrete Slab	EW	Pull test 1700		090812	tbu2pl53	intial load …….2.07" 1267lb
TB-U2-EW	54	No Turret	Concrete Slab	EW	Impact Hammer Test		090812	tbu2ew 54	
TB-U2-PL	55	No Turret	Concrete Slab	EW	Pull Test 1950 lbs		090812	tbu2pl55	initial load=260, disp=3.26, 1983
TB-U2-EW	56	No Turret	Concrete Slab	EW	Impact Hammer Test		090812	tbu2ew 56	
TB-U2-PL	57	No Turret	Concrete Slab	EW	Pull Test 2200 lbs		090812	tbu2pl57	intial load=254lbs, 2189lbs
TB-U2-EW	58	No Turret	Concrete Slab	EW	Impact Hammer Test		090812	tbu2ew 58	
TB-U2-PL	59	No Turret	Concrete Slab	EW	Pull Test 2450 lbs		090812	tbu2pl59	intital load 250, 2467, 2.467 in
TB-U2-EW	60	No Turret	Concrete Slab	EW	Impact Hammer Test		090812	tbu2ew 60	
TB-U2-PL	61	No Turret	Concrete Slab	EW	Pull Test 2700 lbs		090812	tbu2pl61	initial load= 233lbs, 2744lbs , 4.74"
TB-U2-EW	62	No Turret	Concrete Slab	EW	Impact Hammer Test		090812	tbu2ew 62	
TB-U2-PL	63	No Turret	Concrete Slab	EW	Pull Test 2950 lbs		090812	tbu2pl63	initial load =255,5.4in, 3048 lbs
TB-U2-EW	64	No Turret	Concrete Slab	EW	Impact Hammer Test		090812	tbu2ew 64	
TB-U2-PL	65	No Turret	Concrete Slab	Ew	Pull Test 3200 lbs		090812	tbu2pl65	initial load=250lbs, 3405 lbs 6.255 in
TB-U2-EW	66	No Turret	Concrete Slab	EW	Impact Hammer Test		090812	tbu2ew 66	
TB-U2-PL	67	No Turret	Concrete Slab	EW	Pull Test 3450 lbs		090812	tbu2pl67	Pull Test to 3353 lbs (Cracking sound heard), initial load=250 llbs, 6.5"
TB-U2-EW	68	No Turret	Concrete Slab	EW	Impact Hammer Test		090812	tbu2ew 68	
TB-U2-PL	69	No Turret	Concrete Slab	EW	Pull Test 1500 lbs		090812	tbu2pl69	Pull Test to 1500 lbs
TB-U2-EW	70	No Turret	Concrete Slab	EW	Pull Test 1500 lbs		090812	tbu2pl70	Pull Test to 1462 lbs (full Failure) screw s tightened

Test Protocol – Bushing #5

In the first part of the testing the bushing was installed on the rigid base, and impact hammer test, pull test and sudden release tests were performed. In the second part of the testing the instruments were mounted on the flexible or rigid frame and then mounted on the shake table, and the bushing was subjected to a series of dynamic tests that included white noise tests, acceleration history test, and table impulse test. At this point it was necessary to measure the contribution of damping from oil in the transformer tank. The lower part of the bushing, while mounted on the frame, was immersed in a circular container filled with water. A sudden-release test was performed to measure the contribution of damping from the water, but the damping was not significant. In the last part of the testing, the bushing was once again installed on the fixed base and was tested either with impact hammer and simple pull test or pulled to failure to measure the capacity of bushing after going through major earthquake. The tests were stopped after every series of 3 tests to perform the visual inspection.

Table A-7 describes the complete test protocol for Bushing #5.

Table A-7: Test Protocol – Bushing #5

Seismic Evaluation and Qualification of Transformer Bushing 5

Test No		Location of Bushing	Test Direction	Test Description	Testing Setup	Test Date	File name in Repository	Remarks
25lb Weight is to be added at the top of the Bushing								
lifting hole in EW Direction								
1. Pre-Test Activities			500 kV Composite Bushing #5		CG Of Bushing =65.5" from Flange top			Upper Bushing CG=89"
TB- 01		N/A	N/A	Finding Weight of the Bushing		92909		1850 lbs
TB- 02		N/A	N/A	Finding Centre of Gravity of Bushing		92909		Check=83"
TB- 03	-NS-IH	Concrete Slab	NS	Impact Hammer Test		92909	tb03nsih.dat	
TB- =B9	-NS-Ihmass	Concrete Slab	NS	Impact Hammer Test		92909	tb03nsihmass.dat	impact hammer on mass
TB- 04	-NE-IH	Concrete Slab	NE	Impact Hammer Test		92909	tb04neih.dat	
TB- 05	-EW-IH	Concrete Slab	EW	Impact Hammer Test		92909	tb05ew ih.dat	
TB- 06	-SE-IH	Concrete Slab	SE	Impact Hammer Test		92909	tb06seih.dat	
TB- 07	-PL-SG	Concrete Slab	NE	150 lb Pull Test for Caliberation of SG		92909	tb07plsg.dat	
TB- 7	-PL-SGb	Concrete Slab	EW	150 lb Pull Test for Caliberation of SG		92909	tb07plsgb.dat	
TB- 08	-PL-SG	Concrete Slab	SE	150 lb Pull Test for Caliberation of SG		92909	tb08plsg.dat	
TB- 09	-PL-200	Concrete Slab	EW	Pull Test of 200 lbs		92909	tb09pl200.dat	Quick release at 200 lbs
TB- 10	-NS-IH	Concrete Slab	NS	Impact Hammer Test		92909	tb10nsih.dat	5.1 Hz, 28.9 Hz
TB- 11	-EW-IH	Concrete Slab	EW	Impact Hammer Test		92909	tb11ew ih.dat	
TB- 12	-PL-300	Concrete Slab	EW	Pull Test of 300 lbs		92909	tb12pl300.dat	Quick released at 314 lbs
TB- 13	-NS-IH	Concrete Slab	NS	Impact Hammer Test		92909	tb13nsih.dat	
TB- 14	-EW-IH	Concrete Slab	EW	Impact Hammer Test		92909	tb14ew ih.dat	WE, 5.17Hz, 29.4 Hz
TB- 15	-PL-400	Concrete Slab	EW	Pull Test of 400 lbs		92909	tb15pl400.dat	Quick release at 400 lbs
TB- 16	-NS-IH	Concrete Slab	NS	Impact Hammer Test		92909	tb16nsih.dat	
TB- 17	-EW-IH	Concrete Slab	EW	Impact Hammer Test		92909	tb17ew ih.dat	WE, 5.19 Hz, 29.42 Hz
TB- 18	-PL-500	Concrete Slab	EW	Pull Test of 500 lbs		92909	tb18pl500.dat	Quick release at 500 lbs
TB- 19	-NS-IH	Concrete Slab	NS	Impact Hammer Test		92909	tb19nsih.dat	
TB- 20	-EW-IH	Concrete Slab	EW	Impact Hammer Test		92909	tb20ew ih.dat	
TB- 21	-PL-1000	Concrete Slab	EW	Pull Test of 1000 lbs		92909	tb21pl1000.dat	Quick release at 500 lbs
TB- 22	-NS-IH	Concrete Slab	NS	Impact Hammer Test		92909	tb22nsih.dat	
TB- 23	-EW-IH	Concrete Slab	EW	Impact Hammer Test		92909	tb23ew ih.dat	
TB- 24	-PL-1500	Concrete Slab	EW	Pull Test of 1500 lbs		92909	tb24pl1500.dat	1505 lbs, Quick release at 507 lbs, Freq, 5.07 Hz
TB- 25	-NS-IH	Concrete Slab	NS	Impact Hammer Test		92909	tb25nsih.dat	
TB- 26	-EW-IH	Concrete Slab	EW	Impact Hammer Test		92909	tb26ew ih.dat	
TB- 27	-PL-2000	Concrete Slab	EW	Pull Test of 2000 lbs		92909	tb27pl2000.dat	Quick release at 500 lbs
TB- 28	-NS-IH	Concrete Slab	NS	Impact Hammer Test		92909	tb28nsih.dat	
TB- 29	-EW-IH	Concrete Slab	EW	Impact Hammer Test		92909	tb29ew ih.dat	
TB- 30	PL-2800	Concrete Slab	EW	Pull Test of 2800 lbs		92909	tb30pl2800.dat	Quick release at 500lbs, Freq 5.03 Hz, 4.29 inch, 2.9% and 2.5%
TB- 31	-NS-IH	Concrete Slab	NS	Impact Hammer Test		92909	tn31nsih.dat	
TB- 32	-EW-IH	Concrete Slab	EW	Pull Test of 2800 lbs		92909	tb32ew ih.dat	

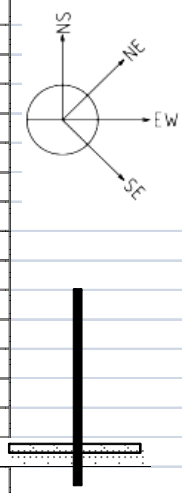

Table A-7: Test Protocol – Bushing #5 (cont'd.)

2. Bushing Identification

Bushing at Center with no stiffneres/ no turret /on Shake Table

TB-	33	-WN	Center of Frame		WHITE NOISE TEST (0-50HZ, 0.1 g)	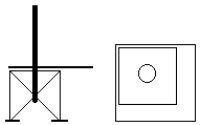	100109	tb33w n.dat	freq N 2.75 hz, 21 Hz, W 3.5, 21 Hz
TB-	34	-TBI	Center of Frame		Table Impulse test		100109	tb34tbi.dat	freq N 3.25 hz,19.5 Hz, W 3, 19.25 Hz, 42 Hz
TB-	35	-AH25	Center of Frame		ACCELERATION TIME HISTORY TEST (0.25g RRS)		100109	tb35ah25.dat	
TB-	36	-WN	Center of Frame		WHITE NOISE TEST (0-50HZ, 0.1 g)		100109	tb36w n.dat	
TB-	37	-TBI	Center of Frame		Table Impulse test		100109	tb37tbi.dat	
TB-	38	-AH50	Center of Frame		ACCELERATION TIME HISTORY TEST (0.5g RRS)		100109	tn38ah50.dat	RRS corrected for 1.4 factor
TB-	39	-WN	Center of Frame		WHITE NOISE TEST (0-50HZ, 0.1 g)		100109	tb39w n.dat	
TB-	40	-TBI	Center of Frame		Table Impulse test		100109	tb40tbi.dat	E: 2.85 Hz, 19.625 Hz
TB-	41	-AH100	Center of Frame		ACCELERATION TIME HISTORY TEST (1.0g RRS)		100109	tb41ah100.dat	E: 2.85 Hz, 19.625 Hz, N 1.81, 19.625
TB-	42	-NS-IH	Center of Frame	NS	Impact hammer NS		100109	tb42nsih.dat	Bottom of Bushing NS 38.8 Hz
TB-	43	-EW-IH	Center of Frame	EW	Impact hammer EW		100109	tb43ew ih.dat	
TB-	42	-WN	Center of Frame		WHITE NOISE TEST (0-50HZ, 0.1 g)		100109	tb42w n.dat	
TB-	43	-TBI	Center of Frame		Table Impulse test		100109	tb43tbi.dat	
TB-	44	-AH150	Center of Frame		ACCELERATION TIME HISTORY TEST (1.5g RRS)		100109	tb44ah150.dat	2.o g rrs achieved, so this is the run for 2.0 g rrs
TB-	45	-WN	Center of Frame		WHITE NOISE TEST (0-50HZ, 0.1 g)		100109	tb45w n.dat	
TB-	46	-TBI	Center of Frame		Table Impulse test		100109	tb46tbi.dat	N 3.5 Hz, E 3.5 Hz
TB-	47	-AH225	Center of Frame		ACCELERATION TIME HISTORY TEST (2.25g RRS)		100109	tb47ah225.dat	GOOD FOR 2.5 G RRS
TB-	48	-WN	Center of Frame		WHITE NOISE TEST (0-50HZ, 0.1 g)		skipped	skipped	skipped
TB-	49	-TBI	Center of Frame		Table Impulse test		skipped	skipped	skipped
TB-	50	-AH250	Center of Frame		ACCELERATION TIME HISTORY TEST (2.5g RRS)		100109	TB47AH225.DAT	2.5 RRS, FREQ 1.75 Hz
TB-	51	-WN	Center of Frame		WHITE NOISE TEST (0-50HZ, 0.1 g)		100109	tb51tbi.dat	
TB-	51	-bWn	Center of Frame		WHITE NOISE TEST (0-50HZ, 0.1 g)		100109	tb51bWN.dat	3.26 Hz, 19.88
TB-	52	-TBI	Center of Frame		Table Impulse test		100109	tb52tbi.dat	E 3.25 Hz, 3.25
TB-	53	-AH300	Center of Frame		ACCELERATION TIME HISTORY TEST (3.0g RRS)		100109	tb53ah300.dat	
TB-	54	-WN	Center of Frame		WHITE NOISE TEST (0-50HZ, 0.1 g)		100109	tb54w n.dat	
TB-	55	-TBI	Center of Frame		Table Impulse test		100109	tb55tbi.dat	

Table A-7: Test Protocol – Bushing #5 (cont'd.)

3. Bushing Identification

Bushing at Center with no stiffneres/ no turret /on Shake Table

TB-	56	-PL-100	Center of Frame		Pull Test 100 lbs	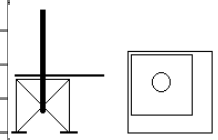	93009	tb56pl100.dat	No Water in the tank
TB-	57	-PL-150	Center of Frame		Pull Test 150 lbs		93009	tb57pl150.dat	No w ater in the Tank
TB-	58	-PL-200	Center of Frame		Pull Test 200 Lbs		93009	tb58pl200.dat	No w ater in the tank
TB-	59	-PL-100	Center of Frame		Pull Test 100 lbs		93009	tb59pl100.dat	Filled w ith w ater
TB-	60	-PL-150	Center of Frame		Pull Test 150 lbs		93009	tb60pl150.dat	Filled w ith w ater
TB-	61	-PL-200	Center of Frame		Pull Test 200 lbs		93009	tb61pl200.dat	Filled w ith w ater

PAUSE FOR INSPECTION

4. Bushing Failure mode Identification

Check for maxresponse during the test, mount the bushing accordingly, so that max response directin is EW

TB-	62	-NS-HIH	Concrete Slab	NS	Hard Impact Hammer Test	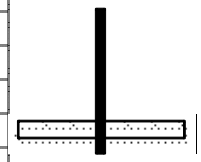	N/A	N/A	
TB-	63	-WE-HIH	Concrete Slab	WE	Hard Impact Hammer Test		N/A	N/A	
TB-	64	-PL	Concrete Slab	EW	Pull Test of 2800 lbs		N/A	N/A	Quick Release at 500 lbs
TB-	65	-NS-IH	Concrete Slab	NS	Hard Impact Hammer Test		N/A	N/A	
TB-U	66	-EW-IH	Concrete Slab	WE	Hard Impact Hammer Test		N/A	N/A	

Test Protocol – Bushing #6

The first porcelain bushing tested was Bushing #6. The bushing was anticipated to be rather rigid. As a first step the center of gravity and total weight of the bushing were measured in the SEESL laboratory. Then the bushing was mounted on the fixed base (concrete block) and impact hammer tests were conducted to measure the frequency and damping ratio of the bushing. A small force of 150 lb. was applied at the top of the bushing in both principal directions (EW and NS) to calibrate the strain gauges. The bushing was constructed of two porcelain segments. The lower segment was in contact with the metallic mounting flange. It was expected that the failure might occur by the slip of the porcelain component with respect to the metal mounting flange. A test retainer was fabricated and installed at that location to restrain lateral movement of the porcelain component. The bushing was then mounted on the flexible frame in the center location and tested with spectrum-compatible earthquake records, followed by random frequency search and table impulse tests. The first acceleration history test was performed at 0.25 g RRS and input was at 3.00 g RRS; at this acceleration input the failure of the bushing was observed.

Table A-8 describes the complete test protocol for Bushing #6.

Table A-8: Test Protocol – Bushing #6

Seismic Evaluation and Qualification of Transformer Bushing #6									
Test No.			**Location of Bushing**	**Test Direction**	**Test Description**	**Testing Setup**	**Test Date**	**File name in Repository**	**Remarks**
15lb Weight is to be added at the top of the Bushing									
lifting hole in EW Direction									
Measure Capacitance of the Bushing									
1. Pre-Test Activities				230 kV Porcelain Bushing #6		CG Of Bushing =14" from Flange top			Upper Bushing CG= 33 "
TB-	01		N/A	N/A	Finding Weight of the Bushing		92109	-	840 lbs
TB-	02		N/A	N/A	Finding Centre of Gravity of Bushing		92109	-	14" from mounting flange top
TB-	03	-PL-100	Center of Frame	EW	100 lbs Pull Test		92209	tb03pl100.dat	Container Not filled with Water
TB-	04	-PL-150	Center of Frame	EW	150 lbs Pull Test		92209	tb03pl150.dat	Container Not filled with Water
TB-	05	-PL-200	Center of Frame	EW	200 lbs Pull Test		92209	tb03pl200.dat	Container Not filled with Water
TB-	06	PL-100	Center of Frame	EW	100 lbs Pull Test		92209	tb06pl100.dat	Container Filled with Water
TB-	07	-PL-150	Center of Frame	EW	150 lbs Pull Test		92209	tb07pl150.dat	Container Filled with Water
TB-	08	-PL-200	Center of Frame	EW	200 lbs Pull Test		92209	tb08pl200.dat	Container Filled with Water
TB-	09	-NS-IH	Concrete Slab	NS	Impact Hammer Test (top pf bushing)		92309	tb09nsih.dat	
TB-	09	-NS-Ihb	Concrete Slab	NS	Impact Hammer Test (top pf bushing)		92309	tb09nsihb.dat	
TB-	10	-EW-IH	Concrete Slab	EW	Impact Hammer Test (top pf bushing)		92309	tb10ewih.dat	
TB-	10	-EW-Ihb	Concrete Slab	EW	Impact Hammer Test (top pf bushing)		92309	tb10ewihb.dat	
TB-	10	-EW-Ihc	Concrete Slab	EW	Impact Hammer Test (top pf bushing)		92309	tb10ewihc.dat	
TB-	11	NE-IH	Concrete Slab	NE	Impact Hammer Test (top pf bushing)		92309	tb11neih.dat	
TB-	12	SE-IH	Concrete Slab	SE	Impact Hammer Test (top pf bushing)		92309	tb12seih.dat	
TB-	13	NS-IH	Concrete Slab	NS	Impacthammer Test (Bottom of Bushing)		92309	tb13nsih.dat	
TB-	14	EW-IH	Concrete Slab	EW	Impacthammer Test (Bottom of Bushing)		92309	tb14ewih.dat	
TB-	15	NE-IH	Concrete Slab	NE	Impacthammer Test (Bottom of Bushing)		92309	tb15neih.dat	
TB-	16	SE-IH	Concrete Slab	SE	Impacthammer Test (Bottom of Bushing)		92309	tb16seih.dat	
TB-	17	-PL-SG	Concrete Slab	NS	150 lb Pull Test for Caliberation of SG		92309	tb17plns.dat	
TB-	18	-PL-SG	Concrete Slab	EW	150 lb Pull Test for Caliberation of SG		92309	tb18plew.dat	

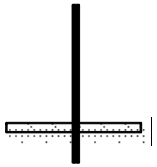

Table A-8: Test Protocol – Bushing #6 (cont'd.)

2. Bushing Identification

Bushing at Center with no stiffneres/ no turret /on Shake Table

TB-	19	-WN	Center of Frame		WHITE NOISE TEST (0-50HZ, 0.1 g)		92409	tb19w n.dat	
TB-	20	-TBI	Center of Frame		Table Impulse test		92409	tb20tbi.dat	
TB-	21	-AH25	Center of Frame		ACCELERATION TIME HISTORY TEST (0.25g RRS)		92409	tb21ah025.dat	max acceleration w as .13g
TB-	22	-WN	Center of Frame		WHITE NOISE TEST (0-50HZ, 0.1 g)		92409	tb22w n.dat	
TB-	23	-TBI	Center of Frame		Table Impulse test		92409	tb23tbi.dat	
TB-	24	-AH25	Center of Frame		ACCELERATION TIME HISTORY TEST (0.25g RRS)		92409	tb24ah25.dat	max acceleration Qa .25 g, freq N:13.75,11.125 Hz, E, 11.125
TB-	25	-WN	Center of Frame		WHITE NOISE TEST (0-50HZ, 0.1 g)		92409	tb25w n.dat	
TB-	26	-TBI	Center of Frame		Table Impulse test		92409	tb26tbi.dat	E 11.25 Hz, N-11, 20.25 Hz
TB-	27	-AH50	Center of Frame		ACCELERATION TIME HISTORY TEST (0.5g RRS)		92409	tb27ah050.dat	N 11 Hz, E
TB-	28	-WN	Center of Frame		WHITE NOISE TEST (0-50HZ, 0.1 g)		92409	tb28w n.dat	
TB-	29	-TBI	Center of Frame		Table Impulse test		92409	tb29tabi.dat	E 11.25 Hz, N-11
TB-	30	-AH75	Center of Frame		ACCELERATION TIME HISTORY TEST (0.75g RRS)		92409	tb30ah075.dat	
TB-	31	-WN	Center of Frame		WHITE NOISE TEST (0-50HZ, 0.1 g)		92409	tb31w n.dat	
TB-	32	-TBI	Center of Frame		Table Impulse test		92409	tb32tbi.dat	
TB-	33	-AH100	Center of Frame		ACCELERATION TIME HISTORY TEST (1.0g RRS)		92409	tb33ah100.dat	N: 11 hz, 13.75 Hz, E
TB-	34	-WN	Center of Frame		WHITE NOISE TEST (0-50HZ, 0.1 g)		92409	tb34w n.dat	N: 11 hz, 13.75 Hz, E
TB-	35	-TBI	Center of Frame		Table Impulse test		92409	tb35tbi.dat	N: 11hz, E 11.25
TB-	36	-WN	Center of Frame		WHITE NOISE TEST (0-50HZ, 0.1 g)		92509	tb36w n.dat	0.03125
TB-	37	-TBI	Center of Frame		Table Impulse test		92509	tb37tbi.dat	0.074074074
TB-	38	-AH125	Center of Frame		ACCELERATION TIME HISTORY TEST (1.25g RRS)		92509	tb38ah125.dat	
TB-	39	-WN	Center of Frame		WHITE NOISE TEST (0-50HZ, 0.1 g)		92509	tb39w n.dat	
TB-	40	-TBI	Center of Frame		Table Impulse test		92509	tb40tbi.dat	N:10.9375 Hz, E: 11.25 Hz
TB-	41	-AH150	Center of Frame		ACCELERATION TIME HISTORY TEST (1.5g RRS)		92509	tb41ah150.dat	
TB-	42	-WN	Center of Frame		WHITE NOISE TEST (0-50HZ, 0.1 g)		92509	tb42w n.dat	
TB-	43	-TBI	Center of Frame		Table Impulse test		92509	tb43tbi.dat	
TB-	44	-AH175	Center of Frame		ACCELERATION TIME HISTORY TEST (1.75g RRS)		92509	tb44ah175.dat	
TB-	45	-WN	Center of Frame		WHITE NOISE TEST (0-50HZ, 0.1 g)		92509	tb45w n.dat	
TB-	46	-TBI	Center of Frame		Table Impulse test		92509	tb46tbi.dat	N: 10.875 Hz, E 11.125
TB-	47	-AH200	Center of Frame		ACCELERATION TIME HISTORY TEST (2.0g RRS)		92509	tb47ah200.dat	

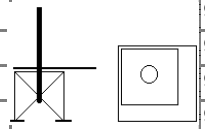

Table A-8: Test Protocol – Bushing #6 (cont'd.)

TB-	48	-WN	Center of Frame		WHITE NOISE TEST (0-50HZ, 0.1 g)	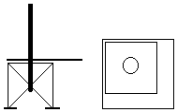	92509	tb48w n.dat	
TB-	49	-TBI	Center of Frame		Table Impulse test		92509	tb49tbi.dat	
TB-	50	-AH225	Center of Frame		ACCELERATION TIME HISTORY TEST (2.25g RRS)		92509	tb50ah225.dat	
TB-	51	-WN	Center of Frame		WHITE NOISE TEST (0-50HZ, 0.1 g)		92509	tb51w n.dat	
TB-	52	-TBI	Center of Frame		Table Impulse test		92509	tb52tbi.dat	
TB-	53	-AH250	Center of Frame		ACCELERATION TIME HISTORY TEST (2.5g RRS)		92509	tb53ah250.dat	
TB-	54	-WN	Center of Frame		WHITE NOISE TEST (0-50HZ, 0.1 g)		92509	tb54w n.dat	
TB-	55	-TBI	Center of Frame		Table Impulse test		92509	tb55tbi.dat	N: 10.875 Hz, E 11.125
TB-	56	-AH275	Center of Frame		ACCELERATION TIME HISTORY TEST (2.75g RRS)		92509	tb56ah275.dat	
TB-	57	-WN	Center of Frame		WHITE NOISE TEST (0-50HZ, 0.1 g)		92509	tb57w n.dat	
TB-	58	-TBI	Center of Frame		Table Impulse test		92509	tb58tbi.dat	
TB-	59	-AH300	Center of Frame		ACCELERATION TIME HISTORY TEST (3.0g RRS)		92509	tb59ah300.dat	
TB-	60	-WN	Center of Frame		WHITE NOISE TEST (0-50HZ, 0.1 g)		92509	tb60w n.dat	
TB-	61	-TBI	Center of Frame		Table Impulse test		92509	tb61tbi.dat	
TB-	62	-AH200	Center of Frame		ACCELERATION TIME HISTORY TEST (2.0g RRS)		92509	tb62ah200.dat	slip of porcelain.. 0.3 mm W & .3 mm S
TB-	63	-WN	Center of Frame		WHITE NOISE TEST (0-50HZ, 0.1 g)		92509	tb63w n.dat	
TB-	64	-TBI	Center of Frame		Table Impulse test		92509	tb64tbi.dat	
TB-	65	-AH225	Center of Frame		ACCELERATION TIME HISTORY TEST (2.25g RRS)		92509	tb65ah225.dat	.35 mm s and .78 mm W
TB-	66	-WN	Center of Frame		WHITE NOISE TEST (0-50HZ, 0.1 g)		92509	tb66w n.dat	
TB-	67	-TBI	Center of Frame		Table Impulse test		92509	tb67tbi.dat	
TB-	68	-AH250	Center of Frame		ACCELERATION TIME HISTORY TEST (2.5g RRS)		92509	tb68ah250.dat	.5mm W1.0 mm S
TB-	69	-WN	Center of Frame		WHITE NOISE TEST (0-50HZ, 0.1 g)		92509	tb69w n.dat	
TB-	70	-TBI	Center of Frame		Table Impulse test		92509	tb70tbi.dat	
TB-	71	-AH250	Center of Frame		ACCELERATION TIME HISTORY TEST (2.0g RRS)		92509	tb71ah275.dat	
TB-	72	-WN	Center of Frame		WHITE NOISE TEST (0-50HZ, 0.1 g)		92509	tb72w n.dat	
TB-	73	-TBI	Center of Frame		Table Impulse test		92509	tb73tbi.dat	

Test Protocol – Bushing #7

This bushing was anticipated to be rather rigid and heavier than Bushing #6. As a first step the center of gravity and total weight of bushing were measured in the SEESL laboratory. Then the bushing was mounted on the fixed base (concrete block) and impact hammer tests were conducted to measure the frequency and damping ratio of the bushing. A force of 100 lb. was applied at the top of the bushing in both principal directions (EW and NS) to calibrate the strain gauges. The bushing was then pulled with incremental force applied at the top of bushing, ranging from 100 lb., 300 lb., 450 lb., 600 lb. and finally to 900 lb. Impact hammer tests were performed, followed by the pull test to measure any shift of frequency due to pull tests. A retainer ring was designed and mounted on the bushing for dynamic testing; the bushing was then dynamically tested while mounted on the frame with a flexible plate. The input excitation varied from 0.20 g RRS to 0.65 g RRS, with increments of 0.05 g. The final test was run at 0.80 g RRS. Failure was observed at this level of input motion and tests were stopped.

Table A-9 describes the complete test protocol for Bushing #7.

Table A-9: Test Protocol – Bushing #7

Seismic Evaluation and Qualification of Transformer Bushings
Bushing # 7

Test No.	Location of Bushing	Test Direct.	Test Description	Testing Setup	Test Date	File name in Repository	Remarks
lifting hole in EW Direction							
1. Pre-Test Activities							
TB- 0 SAP	-	-	Analytical modeling and prediction		91202		
TB- 1	N/A	N/A	Finding Weight and CG of the Bushing		91202		W= 4330 CG= 47 " from top of flang
TB- 2	N/A	N/A	Finding Upper Weight and CG		91202		UW= 3012 UCG= 90 from top of flange
TB- 3	N/A	N/A	Measure the actual dimentions of bushings	61,52,40.5,17	91202		Measure and check draw ing. Fill attached table
TB- 4	N/A	N/A	Take picture of Identification plate		91202		Take Picture
TB- 5	Fix Base Concrete Slab	N/A	Install bushing on fix base		91202		
TB- 6	Fix Base Concrete Slab	N/A	Attach the 25Lb w eight at top		91202		
TB- 7	Fix Base Concrete Slab	N/A	Remove shipping ring and install retaining ring.		91202		Take Pictures
TB- 8	Fix Base Concrete Slab	N/A	Install Instrumentation acc to draw ing		91203		Take Pictures and Measure
TB- 9	N/A	NA	MEASURE the w eight of SST		91202		Frame structure w ith Plate
TB- 10	Fix Base Concrete Slab	NA	find the w asher position around the bushing		91202		E 9: NE 10: N 11: NW 6: w 10: sw 9: s 11: se 9
TB- 11 Cap	Fix Base Concrete Slab	NA	Measure Capacitance of Bushing				11nf

Table A-9: Test Protocol – Bushing #7 (cont'd.)

2. Fixed Base Testing of Bushing - Identification

TB- 12 PL100EW	Concrete Slab	EW	100 lb Pull Test at Top		91203	tb12pl100ew .dat	Use NCS, WE 9.37
TB- 13 PL100NS	Concrete Slab	NS	100 lb Pull Test at Top		91203	tb13pl100ns.dat	Use Cherry Picker
TB- 14 -NS-IH	Concrete Slab	NS	Impact Hammer Test		91203	tb14nsih.dat	Use NCS, WE 9.22 Hz, 30.7 Hz: NS 9.34 Hz, 32.91 Hz
TB- 14 =NS-Ihb	Concrete Slab	NS	Impact Hammer Test at the bottom of the bushing		91203	tb14nsihb.dat	EW : NS 9.38 Hz, 32.24 Hz (TOP),,,, EW 32.59 44.5 Hz
TB- 15 -NE-IH	Concrete Slab	NE	Impact Hammer Test		91203	tb15neih.dat	NE 9.24 Hz
TB- 16 -EW-IH	Concrete Slab	EW	Impact Hammer Test		91203	tb16ew ih.dat	Top of bushing EW 9.16 Hz, 19.49,30.32 Hz: Bottom of Bushing 9
TB- 16 ew -ihb	Concrete Slab	EW	Impact Hammer Test at the bottom of the bushing		91203	tb16ew inb.dat	
TB- 17 PL300EW	Concrete Slab	EW	300 lb Pull Test at Top		91203	tb17pl300ew .dat	Use NCS
TB- 18 -NS-IH	Concrete Slab	NS	Impact Hammer Test		-	skipped	
TB- 19 -NE-IH	Concrete Slab	NE	Impact Hammer Test		-	skipped	
TB- 20 -EW-IH	Concrete Slab	EW	Impact Hammer Test		-	skipped	
TB- 21 PL450EW	Concrete Slab	EW	450 lb Pull Testat Top		91203	tb21pl450ew .dat	Use NCS
TB- 22 -NS-IH	Concrete Slab	NS	Impact Hammer Test		-	skipped	
TB- 23 -NE-IH	Concrete Slab	NE	Impact Hammer Test		-	skipped	
TB- 24 -EW-IH	Concrete Slab	EW	Impact Hammer Test		-	skipped	
TB- 25 PL600EW	Concrete Slab	EW	600 lb Pull Test at Top	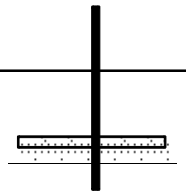	91203	th25pl600ew .dat	Use NCS
TB- 26 -NS-IH	Concrete Slab	NS	Impact Hammer Test		-	skipped	
TB- 27 -NE-IH	Concrete Slab	NE	Impact Hammer Test		-	skipped	
TB- 28 -EW-IH	Concrete Slab	EW	Impact Hammer Test		-	addw in(2)	
TB- 29 PL900EW	Concrete Slab	EW	900 lb Pull Test at Top		91203	tb29pl900ew .dat	Use NCS, stiffness 2.93 kip\in, EW 8.8 Hz
TB- 30 -NS-IH	Concrete Slab	NS	Impact Hammer Test		-	skipped	
TB- 31 -NE-IH	Concrete Slab	NE	Impact Hammer Test		-	skipped	
TB- 32 -EW-IH	Concrete Slab	EW	Impact Hammer Test		-	skipped	
TB- 33 PL900EW	Concrete Slab	EW	900 lb Pull Test at Upper CG		91203	tb33pl900ew .dat	Caliberate Strain Gauges and stiffness
TB- 34 PL900NS	Concrete Slab	NS	900 lb Pull Test at Upper CG		91203	tb34pl900ns.dat	Caliberate Strain Gauges and stiffness
TB- 35 -NS-IH	Concrete Slab	NS	Impact Hammer Test		91203	tb35nsih.dat	
TB- 36 -NE-IH	Concrete Slab	NE	Impact Hammer Test		91203	tb36neih.dat	
TB- 37 -EW-IH	Concrete Slab	EW	Impact Hammer Test		91203	tb37ew ih.dat	
TB- 38 -NS-IHB	Concrete Slab	NS	Impact Hammer Test		91203	tb38nsihb.dat	Imapct hammer at the bottom of Bushing
TB- 39 -EW-IHB	Concrete Slab	EW	Impact Hammer Test		91203	tb39ew ihb.dat	Imapct hammer at the bottom of Bushing

Table A-9: Test Protocol – Bushing #7 (cont'd.)

Check if stiffners are needed or not, after white noise test????, Install Oil Retaining Ring

TB- 40 PL300EW	Center of Frame	EW	300 lb Pull Test from measuring the Stiffnesss		91204	tb40pl300ew .dat	Caliberate Strain Gauges and stiffness
TB- 41 PL300NS	Center of Frame	NS	300 lb Pull Test from measuring the Stiffnesss		91204	tb41pl300ns.dat	Caliberate Strain Gauges and stiffness
TB- 42 -NS-IH	Center of Frame	NS	Impact Hammer Test		91204	tb42nsih.dat	
TB- 43 -NE-IH	Center of Frame	NE	Impact Hammer Test		91204	tb43neih.dat	
TB- 44 -EW-IH	Center of Frame	EW	Impact Hammer Test		91204	tb44ew ih.dat	
TB 45 -WN	Center of Frame		WHITE NOISE TEST (0-50HZ, 0.1 g)		91207	tb45w n.dat	w hite noise in 3 independent direction, E: 2.61 Hz, N:2.67 hz
TB 46 -TBI	Center of Frame		Table Impulse test		91207	tb46rbi.dat	table impulse generated at 8.3, 10.35, 11.56 Hz
TB 47 -AH20	Center of Frame		ACCELERATION TIME HISTORY TEST (0.20g RRS)		91207	tb47ah20.dat	0.15 g RRS
TB 47 -AH20b	Center of Frame		ACCELERATION TIME HISTORY TEST (0.20g RRS)		91207	tb67ah20b.dat	0.20 RRS
see if there is any seperation, 0.02 in may cause a leak, Discuss Stiffners							
TB 48 -WN	Center of Frame		WHITE NOISE TEST (0-50HZ, 0.1 g)		91207	tb48w n.dat	
TB 49 -TBI	Center of Frame		Table Impulse test		91207	tb49tbi.dat	N: 2.55 Hz, E: 2.6 Hz
TB 50 -AH25	Center of Frame		ACCELERATION TIME HISTORY TEST (0.25g RRS)		91207	tb50ah25.dat	N: 2.57 Hz, E: 2.57 Hz
TB 51 -WN	Center of Frame		WHITE NOISE TEST (0-50HZ, 0.1 g)		91207	tb51w n.dat	
TB 52 -TBI	Center of Frame		Table Impulse test		91207	tb52tbi.dat	N: 2.54Hz, E: 2.58 Hz
TB 53 -AH30	Center of Frame		ACCELERATION TIME HISTORY TEST (0.30g RRS)		91207	tb53ah30.dat	N: 2.57 Hz
TB 54 -WN	Center of Frame		WHITE NOISE TEST (0-50HZ, 0.1 g)		91207	tb54w n.dat	
TB 55 -TBI	Center of Frame		Table Impulse test		91207	tb55tbi.dat	NE:2.6 Hz, E: 2.52 Hz, 2.60 Hz
TB 56 -AH35	Center of Frame		ACCELERATION TIME HISTORY TEST (0.35g RRS)		91207	tb56ah35.dat	
TB 57 -WN	Center of Frame		WHITE NOISE TEST (0-50HZ, 0.1 g)		91207	tb57w n.dat	
TB 58 -TBI	Center of Frame		Table Impulse test		91207	tb58tbi.dat	
TB 59 -AH40	Center of Frame		ACCELERATION TIME HISTORY TEST (0.40g RRS)		91207	tb59ah40.dat	
TB 60 -WN	Center of Frame		WHITE NOISE TEST (0-50HZ, 0.1 g)		91207	tb60w n.dat	
TB 61 -TBI	Center of Frame		Table Impulse test		91207	tb61tbi.dat	
TB 62 -AH45	Center of Frame		ACCELERATION TIME HISTORY TEST (0.45g RRS)		91207	tb62ah45.dat	
TB 63 -WN	Center of Frame		WHITE NOISE TEST (0-50HZ, 0.1 g)		91207	tb63w n.dat	
TB- 64 -bWn	Center of Frame		WHITE NOISE TEST (0-50HZ, 0.1 g)		skipped	skiped	
TB 65 -TBI	Center of Frame		Table Impulse test		91207	tb65tbi.dat	
TB 66 -AH50	Center of Frame		ACCELERATION TIME HISTORY TEST (0.50g RRS)		91208	tb66ah50.dat	
TB 67 -WN	Center of Frame		WHITE NOISE TEST (0-50HZ, 0.1 g)		91208	tb67w n.dat	
TB 68 -TBI	Center of Frame		Table Impulse test		91208	tb68tbi.dat	
TB 69 -AH55	Center of Frame		ACCELERATION TIME HISTORY TEST (0.55g RRS)		91208	tb69ah55.dat	
TB 70 -WN	Center of Frame		WHITE NOISE TEST (0-50HZ, 0.1 g)		91208	tb70w n.dat	
TB 71 -TBI	Center of Frame		Table Impulse test		91208	tb71tbi.dat	
TB 72 -AH65	Center of Frame		ACCELERATION TIME HISTORY TEST (0.65g RRS)		91208	tb72ah65.dat	
TB 73 -WN	Center of Frame		WHITE NOISE TEST (0-50HZ, 0.1 g)		91208	tb73w n.dat	
TB 74 -TBI	Center of Frame		Table Impulse test		91208	tb74tbi.dat	
TB 75 -AH80	Center of Frame		ACCELERATION TIME HISTORY TEST (0.80g RRS)		91208	tb75ah80.dat	
TB 76 -WN	Center of Frame		WHITE NOISE TEST (0-50HZ, 0.1 g)		91208	tb76w n.dat	
TB 77 -TBI	Center of Frame		Table Impulse test		91208	tb77tbi.dat	

Test Protocol – Bushing #8

Bushing #8 was an ABB 550 kV lightweight porcelain bushing. The main objective of testing was to determine the seismic qualification of this particular type of bushing. The bushing was mounted on the fixed base (concrete block), strain gauges were calibrated, and frequencies in the principal directions (EW and NS) were measured. Then the bushing was mounted on the rigid frame, inclined at 20 degrees from horizontal and tested again for dynamic demand and capacity testing. The bushing was initially tested for 0.25 g RRS and then input acceleration was increased and the last test was performed at 170 g RRS.

Table A-10 describes the complete test protocol for Bushing #8.

Table A-10: Test Protocol – Bushing #8

Seismic Evaluation and Qualification of ABB 550kV Bushing									
Test No.			Location of Bushing	Test Direct.	Test Description	Testing Setup	Test Date	File name in Repository	Remarks
1. Pre-Test Activities									
BU	1		-		Measure CG of all bushing				Mark location of CG's w ith permanent marker
BU	2		-	-	Install 25 lb load on each terminal Pad				
BU	3		-	-	Measure Capacitance				Pin to flange housing
BU	4		-	-	Measure Capacitance				Pin to terminal pad at bottom
2. Fixed Base Testing of Bushing - Identification									
BU	5		Floor block		Install Bushing on floor				
BU	6		Floor block		Instrument bushing - accel + sp				
BU	7	PL-WE	Floor block	East	250 lbs Load for Pull Test at Top -Horizontally		12/18/2009	bu7plw e	Pull slow ly horizontally to 250# then release
BU	7	PL-We2	Floor block	East	250 lbs Load for Pull Test at Top -Horizontally		12/18/2009	bu7plw e2	Pull slow ly horizontally to 250# then release
BU	8	PL-NS	Floor block	South	250 lbs Load for Pull Test at Top -Horizontally		12/18/2009	bu8plns	Pull slow ly horizontally to 250# then release
BU	9	IH-WE	Floor block	East	Impact Hammer at Top		12/18/2009	bu9ihw e	Hit gently the top of bushing
BU	10	IH-NS	Floor block	South	Impact Hammer at Top		12/18/2009	bu10ihns	Hit gently the top of bushing
BU	11	PL-WE	Floor block	East	250 lbs Load for Pull Test at CG -Horizontally		12/18/2009	bu11plw e	Pull horizontally slow to 250# at CG bushing
BU	12	PL-NS	Floor block	South	250 lbs Load for Pull Test at CG -Horizontally		12/18/2009	bu12plns	Pull horizontally slow to 250# at CG bushing
3. Qualification Sequence on Shaking Table									
BU	13		Shake Table		Install on rigid frame		12/21/2009		
BU	14		Shake Table		Instrument bushing - accel + sp+LED		12/21/2009		
BU	15		Shake Table	-	Measure Capacitance		12/21/2009		Pin to flange housing
BU	16		Shake Table	-	Measure Capacitance		12/21/2009		Pin to terminal pad at bottom
Inspection of Specimen: interfaces, rubber seal, upper-lower bushing segments									
BU	17	IH-WE	Shake Table	East	Impact Hammer at Top		12/21/2009	bu17ihw e	Hit gently the top of bushing A01 EW, 7.78 Hz
BU	18	IH-NS	Shake Table	South	Impact Hammer at Top		12/21/2009	bu18ihns	Hit gently the top of bushing, A02 NS 7.5 Hz
BU	19	IH-WE	Shake Table	East	Impact Hammer at bottom		12/21/2009	bu19ihw e	Hit gently the bottom of bushing, A01 EW 7.8 Hz
BU	20	IH-NS	Shake Table	South	Impact Hammer at bottom		12/21/2009	bu20ihns	Hit gently the bottom of bushing, A02 NS 7.58 Hz
Inspection of Specimen: interfaces, rubber seal, upper-lower bushing segments									

Table A-10: Test Protocol – Bushing #8 (cont'd.)

BU	21	w n	Shake Table		WHITE NOISE TEST (0-50HZ, 0.1 g) 3D		12/21/2009	bu21w n.dat	Random Frequency Search - 3D
BU	22	tbi	Shake Table		Table Impulse test (function from Fahad)		12/21/2009	bu22tbi.dat	Values from White Noise test EW - 0.5Hz
BU	23	AH025	Shake Table		ACCELERATION TIME HISTORY TEST (0.25g RRS)		12/21/2009	bu23ah025.dat	Check TRS EW, NS, VERT
Inspection of Specimen: interfaces, rubber seal, upper-lower bushing segments									
BU	24	w n	Shake Table		WHITE NOISE TEST (0-50HZ, 0.1 g) 3D		12/22/2009	bu24en.dat	Random Frequency Search - 3D
BU	25	tbi	Shake Table		Table Impulse test (function from Fahad)		12/22/2009	bu25tbi.dat	Values from White Noise test EW - 0.5Hz
BU	26	AH100	Shake Table		ACCELERATION TIME HISTORY TEST (1.00g RRS)		12/22/2009	bu26ah100.dat	Check TRS EW, NS, VERT
Inspection of Specimen: interfaces, rubber seal, upper-lower bushing segments, No Visible damage at critical sections									
BU	27	w n	Shake Table		WHITE NOISE TEST (0-50HZ, 0.1 g) 3D		12/22/2009	bu27w n.dat	Random Frequency Search - 3D
BU	28	tbi	Shake Table		Table Impulse test (function from Fahad)		12/22/2009	bu28tbi.dat	Values from White Noise test EW - 0.5Hz
BU	29	AH120	Shake Table		ACCELERATION TIME HISTORY TEST (1.20g RRS)		12/22/2009	bu29ah120.dat	Check TRS EW, NS, VERT
Inspection of Specimen: interfaces, rubber seal, upper-lower bushing segments, No Visible damage at critical sections									
BU	30	w n	Shake Table		WHITE NOISE TEST (0-50HZ, 0.1 g) 3D		12/22/2009	bu30w n.dat	Random Frequency Search - 3D
BU	31	tbi	Shake Table		Table Impulse test (function from Fahad)		12/22/2009	bu31tbi.dat	Values from White Noise test EW - 0.5Hz
BU	32	AH140	Shake Table		ACCELERATION TIME HISTORY TEST (1.40g RRS)		12/22/2009	bu32ah140.dat	Check TRS EW, NS, VERT
Inspection of Specimen: interfaces, rubber seal, upper-lower bushing segments, No Visible damage at critical sections									
BU	33	w n	Shake Table		WHITE NOISE TEST (0-50HZ, 0.1 g) 3D		12/22/2009	bu33w n.dat	Random Frequency Search - 3D
BU	34	tbi	Shake Table		Table Impulse test (function from Fahad)		12/22/2009	bu34tbi.dat	Values from White Noise test EW - 0.5Hz
BU	35	AH160	Shake Table		ACCELERATION TIME HISTORY TEST (1.60g RRS)		12/22/2009	bu35ah160.dat	Check TRS EW, NS, VERT
Inspection of Specimen: interfaces, rubber seal, upper-lower bushing segments, No Visible damage at critical sections									
BU	36	w n	Shake Table		WHITE NOISE TEST (0-50HZ, 0.1 g) 3D		12/22/2009	bu36w n.dat	Random Frequency Search - 3D
BU	37	tbi	Shake Table		Table Impulse test (function from Fahad)		12/22/2009	bu37tbi.dat	Values from White Noise test EW - 0.5Hz
BU	38	AH170	Shake Table		ACCELERATION TIME HISTORY TEST (1.70g RRS)		12/22/2009	bu38ah170.dat	Check TRS EW, NS, VERT
es, rubber seal, upper-lower bushing segments, , upper part okay, Leakage on WWN side, Leakage on EES Control point, EN control p									
BU	39	w n	Shake Table		WHITE NOISE TEST (0-50HZ, 0.1 g) 3D		12/22/2009	bu39w n.dat	Random Frequency Search - 3D
BU	40	tbi	Shake Table		Table Impulse test (function from Fahad)		12/22/2009	bu40tbi.dat	Values from White Noise test EW - 0.5Hz

APPENDIX B:

INSTRUMENTATION OF BUSHINGS

Instrumentation of Bushing #4A

The instrumentation plan developed for Bushing #4A was designed to measure the demand on the bushing. Sixteen strain gauges were attached at the flange level to see the stress distribution along the circumference of the metallic housing, in which composite is glued. These strain gauges were calibrated for measuring the bending moments in dynamic testing. Acceleration is another very important parameter in testing of bushings, so 23 accelerometers were used at different critical locations to determine the acceleration distribution at these locations. These accelerations were used to measure the bending moment and shear force at the critical locations and then compared with those obtained from strain gauges. 8 string potentiometers were used to measure the deformation of the bushing along its length. Load cells rated at 400 lb. and 1000 lb. were used to pull the bushing at the top. Table B-1 shows the list of instruments used and Figures 1–5 show their locations on the testing setup.

Table B-1: Instrumentation List – Bushing #4A

Measurements List for Bushing 4

Instrument No. Unit 1		Measuments Position	Direction	Shake Table	on Floor	Comment
*** Strain Gauges**						
S01N		at flange near Top	N	x	x	
S02E		at flange near top	E	x	x	
S03S		at flange near top	S	x	x	
S04W		at flange near top	W	x	x	
S06N-1		at bottom of composite	N	x	x	
S06N		at bottom of composite	N	x	x	
S06N-2		at bottom of composite	N	x	x	
S07E-1		at bottom of composite	E	x	x	
S07E		at bottom of composite	e	x	x	
S07E-2		at bottom of composite	E	x	x	
S08S-1		at bottom of composite	S	x	x	
S08S		at bottom of composite	S	x	x	
S08S-2		at bottom of composite	S	x	x	
S09W-1		at bottom of composite	W	x	x	
S09W		at bottom of composite	W	x	x	
S09W-2		at bottom of composite	W	x	x	

*** Accelerometers**

A01N		at shake table	N	x		
A02E		at shake table	E	x		
A03U		at shake table	V	x		
A04N		at the table extension	N	x		
A05E		at the table extension	E	x		
A06U		at the table extension	V	x		
A07N		at the bottom of the Bushing	N	x		
A08E		at the bottom of the Bushing	E	x		
A09N		at the mounting plate of the support Frame	N	x		
A10E		at the mounting plate of the support Frame	E	x		
A12N		at the interface Ring	N	x		
A13E		at the interface Ring	E	x		
A14U		at the interface Ring	V	x		
A15N		at the CG of Bushing	N	x		
A16E		at the CG of Bushing	E	x		
A17N		at the CG of upper insulator	N	x		
A18E		at the CG of upper insulator	E	x		
A19N		at the terminal pad	N	x	x	
A20E		at the terminal pad	E	x	x	
A21U		at the terminal pad	V	x	x	
A22NE		at the terminal pad	NE	x	x	
A23SE		at the terminal pad	SE	x	x	

*** Potentiometers**

SP1E		at the table extension	E	x		connected at SE corner of Shake Table
SP2E		at the table extension	E	x		connected at NE corner of Shake Table
SP3N		at the table extension	N	x		connected at mid of Shake Table
SP6N		at the top of Frame	N	x		connected at NE corner of Frame
SP7N		at the top of Frame	N	x		connected at NE corner of Frame
SP10U		at the bottom of Bushing	V	x		Connected from Shake Table Extension
SP11E		at the Bushing Terminal	E	x	x	
SP12N		at the Bushing Terminal	N	x		

*** LED**

LED1E		at the interface Ring	E	x	x	
LED2N		at the interface Ring	N	x	x	
LED3E		At the composite interface	E	x	x	
LED4N		At the composite interface	N	x	x	
LED5E		Above the Flange	E	x	x	
LED6N		Above the Flange	N	x	x	
LED7E		at the CG of Bushing	E	x		
LED8N		at the CG of Bushing	N	x		
LED9E		at the CG of Upper Bushing	E	x		
LED10N		at the CG of Upper Bushing	N	x		

*** LOAD CELL**

LC		At the terminal Point	E		x	

Figure B-1: Instrumentation on Fixed Base – Bushing #4A

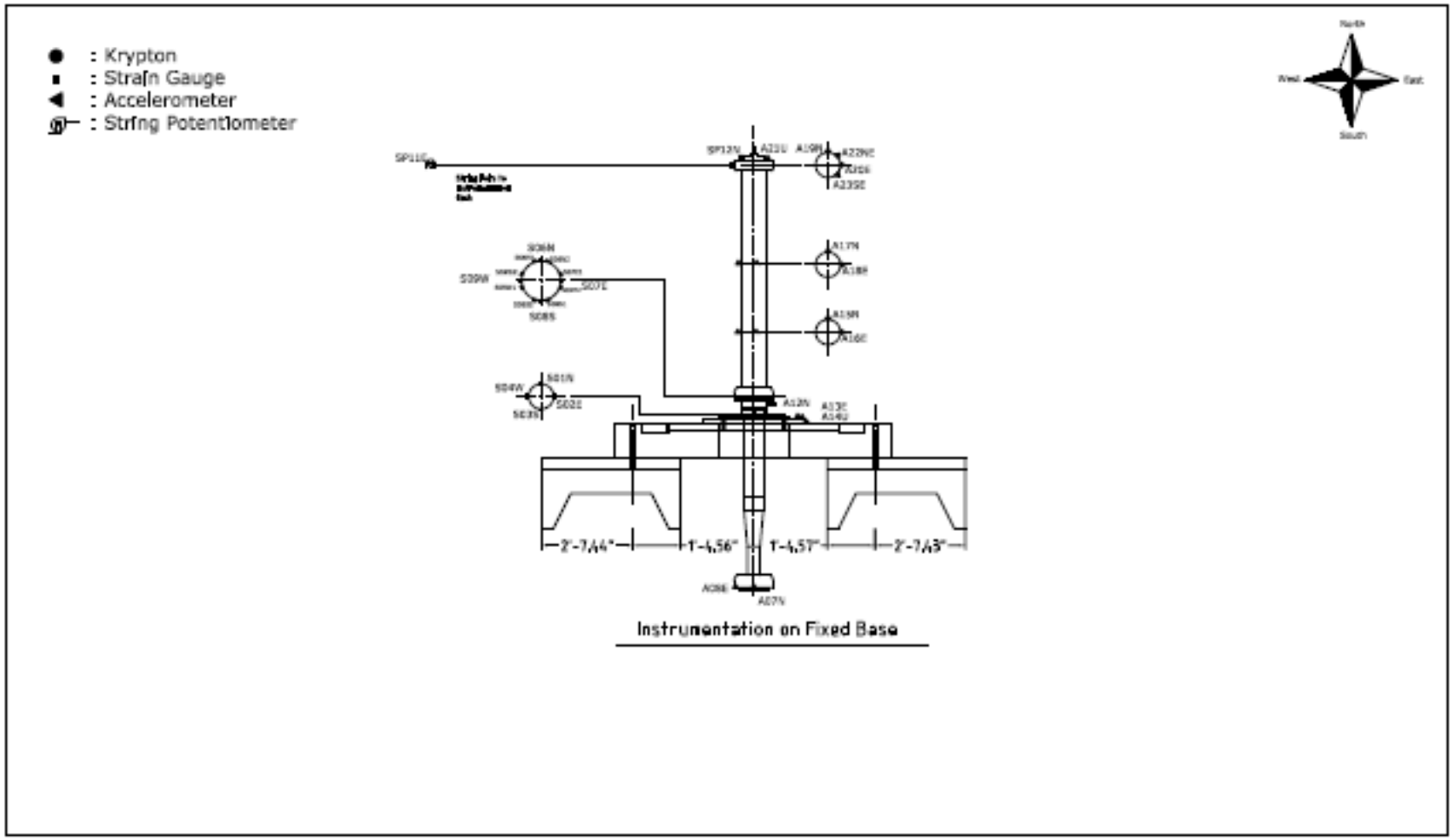

Figure B-2: Instrumentation on Shake Table Extension – Bushing #4A

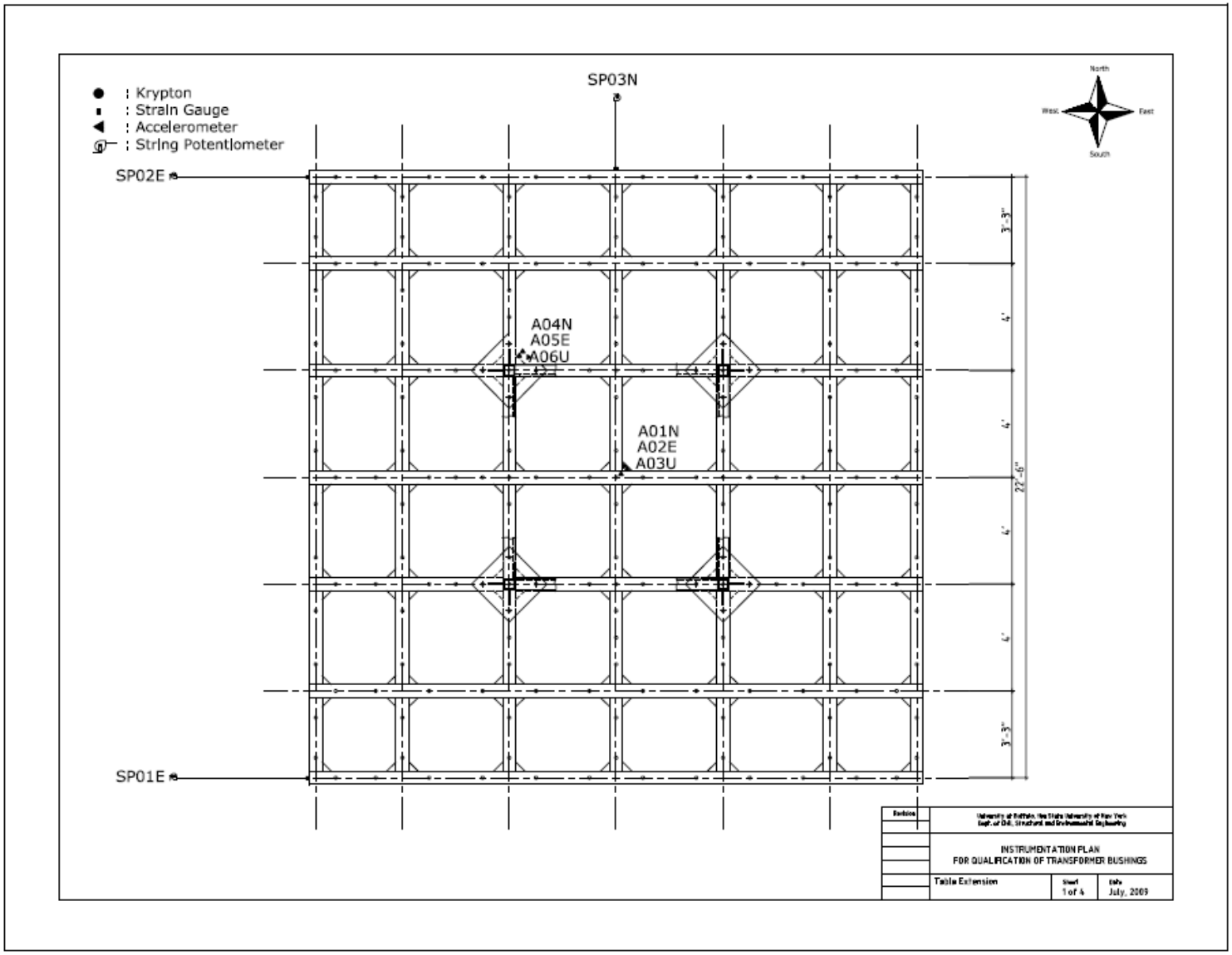

Figure B-3: Instrumentation on Frame and Flexible Top Plate – Bushing #4A

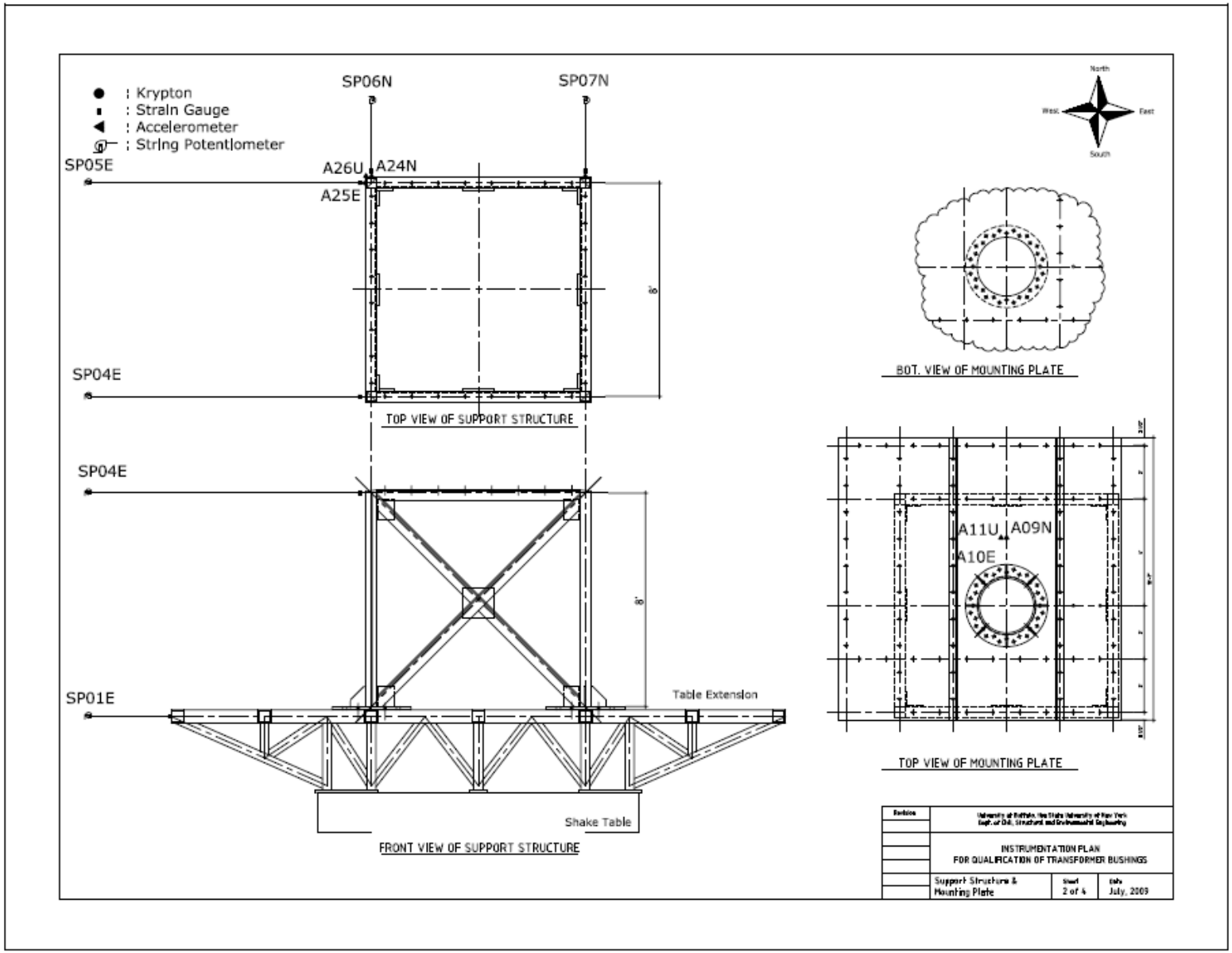

Figure B-4: Instrumentation on Frame – Bushing #4A

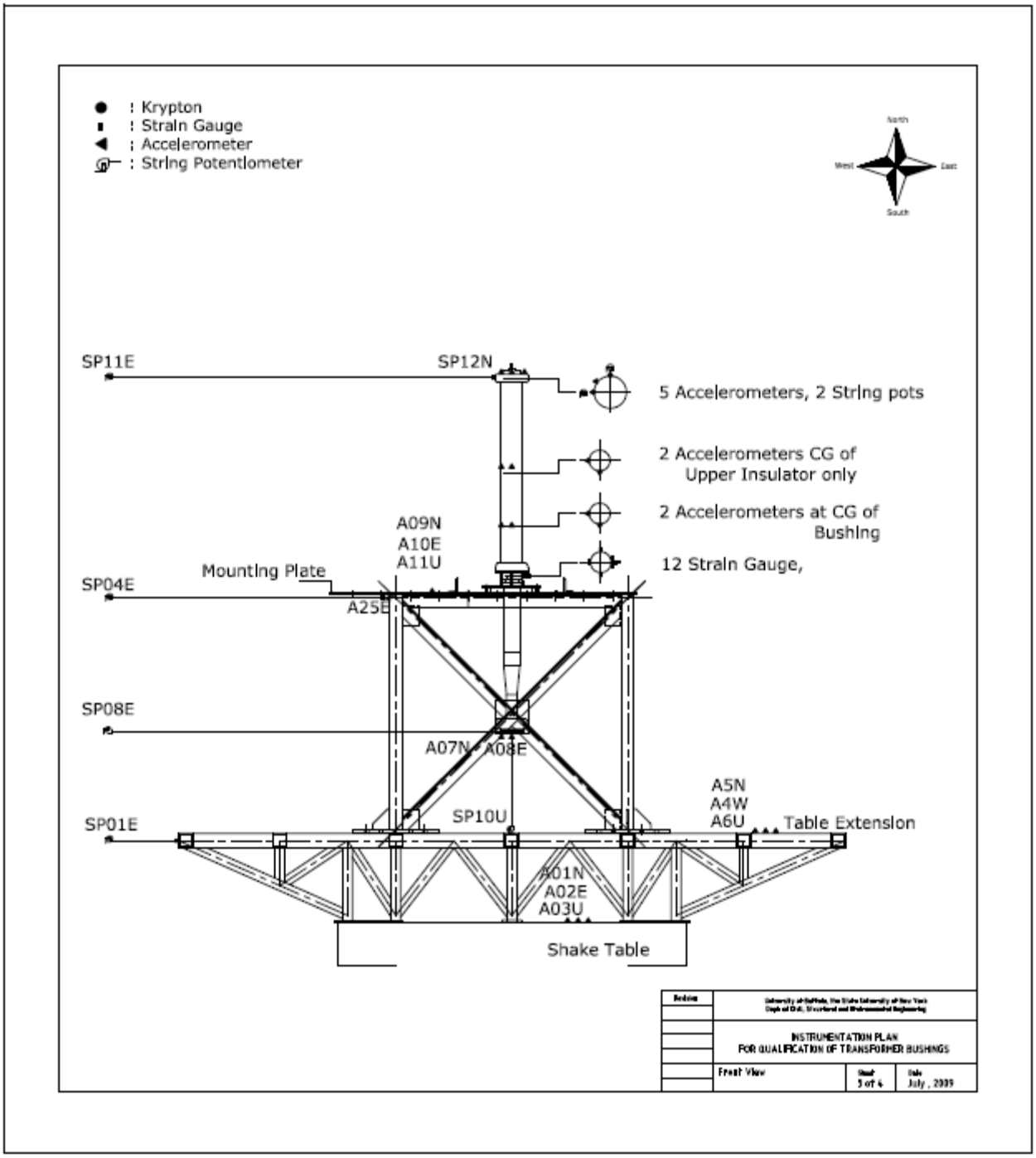

Figure B-5: Instrumentation Setup – Bushing #4A

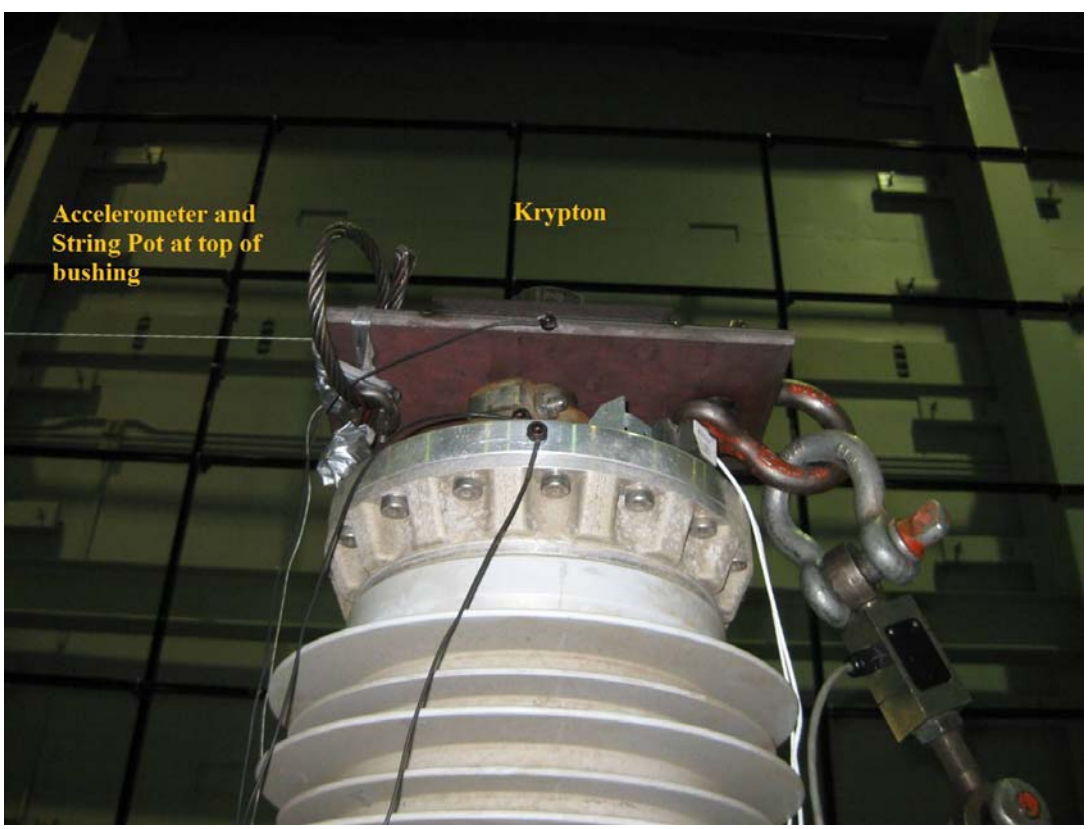

Instrumentation of Bushing #4B

Bushing #4B was tested in the laboratory in the same testing and instrumentation setup that was used for Bushing #4A. 21 strain gauges were attached at the flange level to measure the stress distribution along the circumference of the metallic housing, in which composite is glued. Of these strain gauges the ones in the NS and EW directions were calibrated for measuring bending moments in dynamic testing. 26 accelerometers were used at different critical locations to determine the acceleration distribution along the length of the bushing. These accelerations were used to measure the bending moment and shear force at the critical locations and then compared with those obtained from strain gauges. 12 string potentiometers were used to measure the deformation of the bushing. Load cells rated at 400 lb. and 1,000 lb. were used to pull the bushing at the top. Table B-2 shows the list of instruments and Figures B-6 through B-9 show their locations in the testing setup.

Table B-2: Instrumentation List – Bushing #4B

Measurements List for Bushing 4b

Instrument No. Unit 1		Measuments Position	Direction	Shake Table	on Floor	Comment
*** Strain Gauges**						
S01N		at flange near Top	N	x	x	
S02E		at flange near top	E	x	x	
S03S		at flange near top	S	x	x	
S04WN		at flange near top	W	x	x	
S05N		at flange near top	N	x	x	OPTIONAL
S06N-1		at bottom of composite	N	x	x	
S06N		at bottom of composite	N	x	x	
S06N-2		at bottom of composite	N	x	x	
S07E-1		at bottom of composite	E	x	x	
S07E		at bottom of composite	e	x	x	
S07E-2		at bottom of composite	E	x	x	
S08S-1		at bottom of composite	S	x	x	
S08S		at bottom of composite	S	x	x	
S08S-2		at bottom of composite	S	x	x	
S09W-1		at bottom of composite	W	x	x	
S09W		at bottom of composite	W	x	x	
S09W-2		at bottom of composite	W	x	x	
S10N-1		at bottom of composite	N	x	x	OPTIONAL
S10N		at bottom of composite	N	x	x	OPTIONAL
S10N-2		at bottom of composite	N	x	x	OPTIONAL
S04WS						

* Accelerometers						
A01N		at shake table	N	x		
A02E		at shake table	E	x		
A03U		at shake table	V	x		
A04N		at the table extension	N	x		
A05E		at the table extension	E	x		
A06U		at the table extension	V	x		
A07N		at the bottom of the Bushing	N	x		
A08E		at the bottom of the Bushing	E	x		
A09N		at the mounting plate of the support Frame	N	x		
A10E		at the mounting plate of the support Frame	E	x		
A11U		at the mounting plate of the support Frame	V	x		
A12N		at the interface Ring	N	x		
A13E		at the interface Ring	E	x		
A14U		at the interface Ring	V	x		
A15N		at the CG of Bushing	N	x		
A16E		at the CG of Bushing	E	x		
A17N		at the CG of upper insulator	N	x		
A18E		at the CG of upper insulator	E	x		
A19N		at the terminal pad	N	x	x	
A20E		at the terminal pad	E	x	x	
A21U		at the terminal pad	V	x	x	
A22NE		at the terminal pad	NE	x	x	
A23SE		at the terminal pad	SE	x	x	
A24N						
A25E						
A26U						

*** Potentiometers**

SP1E		at the table extension	E	x		connected at SE corner of Shake Table
SP2E		at the table extension	E	x		connected at NE corner of Shake Table
SP3N		at the table extension	N	x		connected at mid of Shake Table
SP4E		at the top of Frame	E	x	x	connected at SE corner of Frame
SP5E		at the top of Frame	E	x		connected at NE corner of Frame
SP6N		at the top of Frame	N	x		connected at NE corner of Frame
SP7N		at the top of Frame	N	x		connected at NE corner of Frame
SP8E		at the bottom of Bushing	E	x		connected to Eest side
SP9N		at the bottom of Bushing	N	x		connected to North side
SP10U		at the bottom of Bushing	V	x		Connected from Shake Table Extension
SP11E		at the Bushing Terminal	E	x	x	
SP12N		at the Bushing Terminal	N	x		

*** LED**

LED1E		at the interface Ring	E	x	x	
LED2N		at the interface Ring	N	x	x	
LED3E		At the composite interface	E	x	x	
LED4N		At the composite interface	N	x	x	
LED5E		Above the Flange	E	x	x	
LED6N		Above the Flange	N	x	x	
LED7E		at the CG of Bushing	E	x		
LED8N		at the CG of Bushing	N	x		
LED9E		at the CG of Upper Bushing	E	x		
LED10N		at the CG of Upper Bushing	N	x		

*** LOAD CELL**

LC		At the terminal Point	E		x	

Figure B-6: Instrumentation on Fixed Base – Bushing #4B

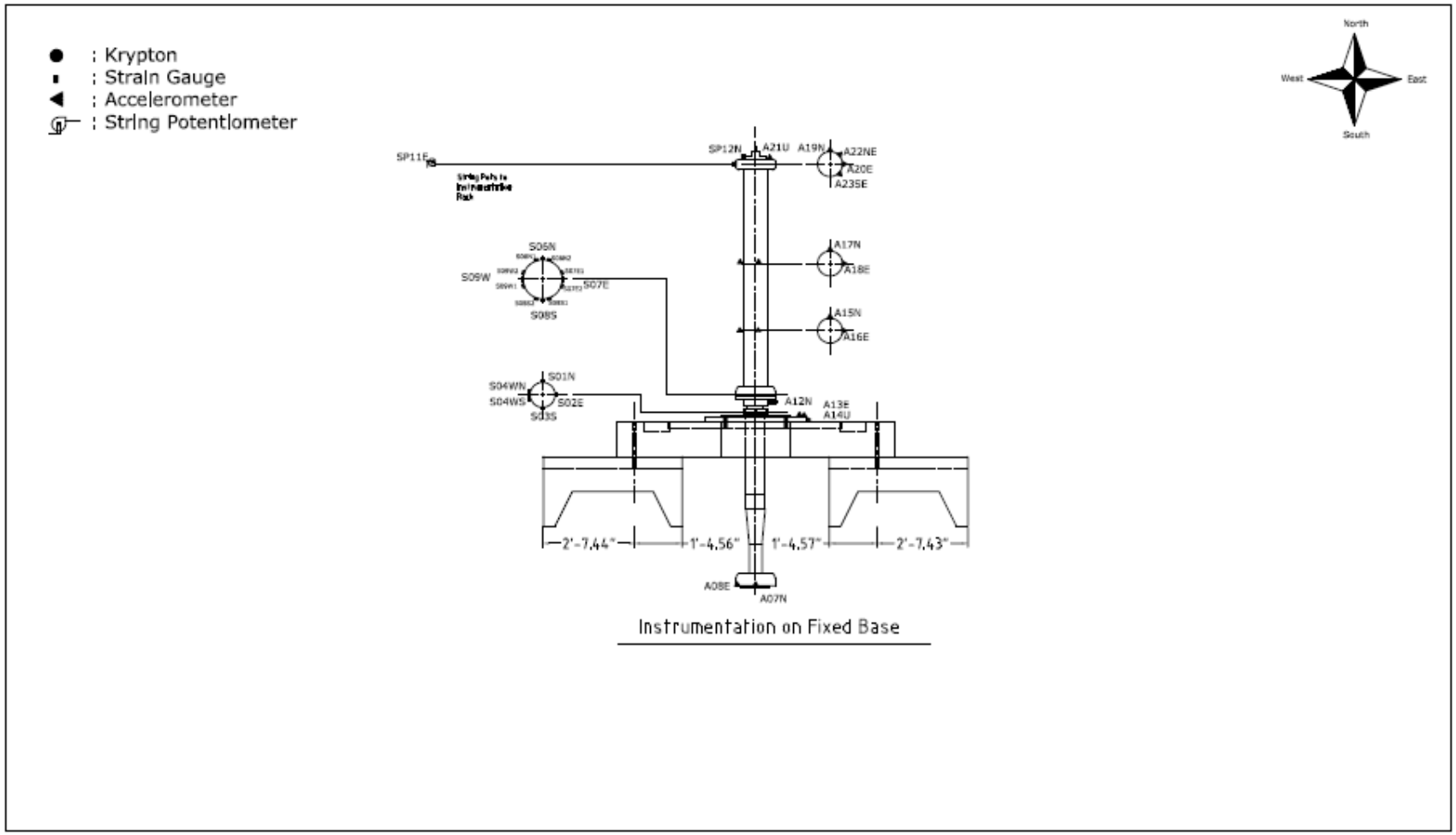

Figure B-7: Instrumentation on Shake Table Extension – Bushing #4B

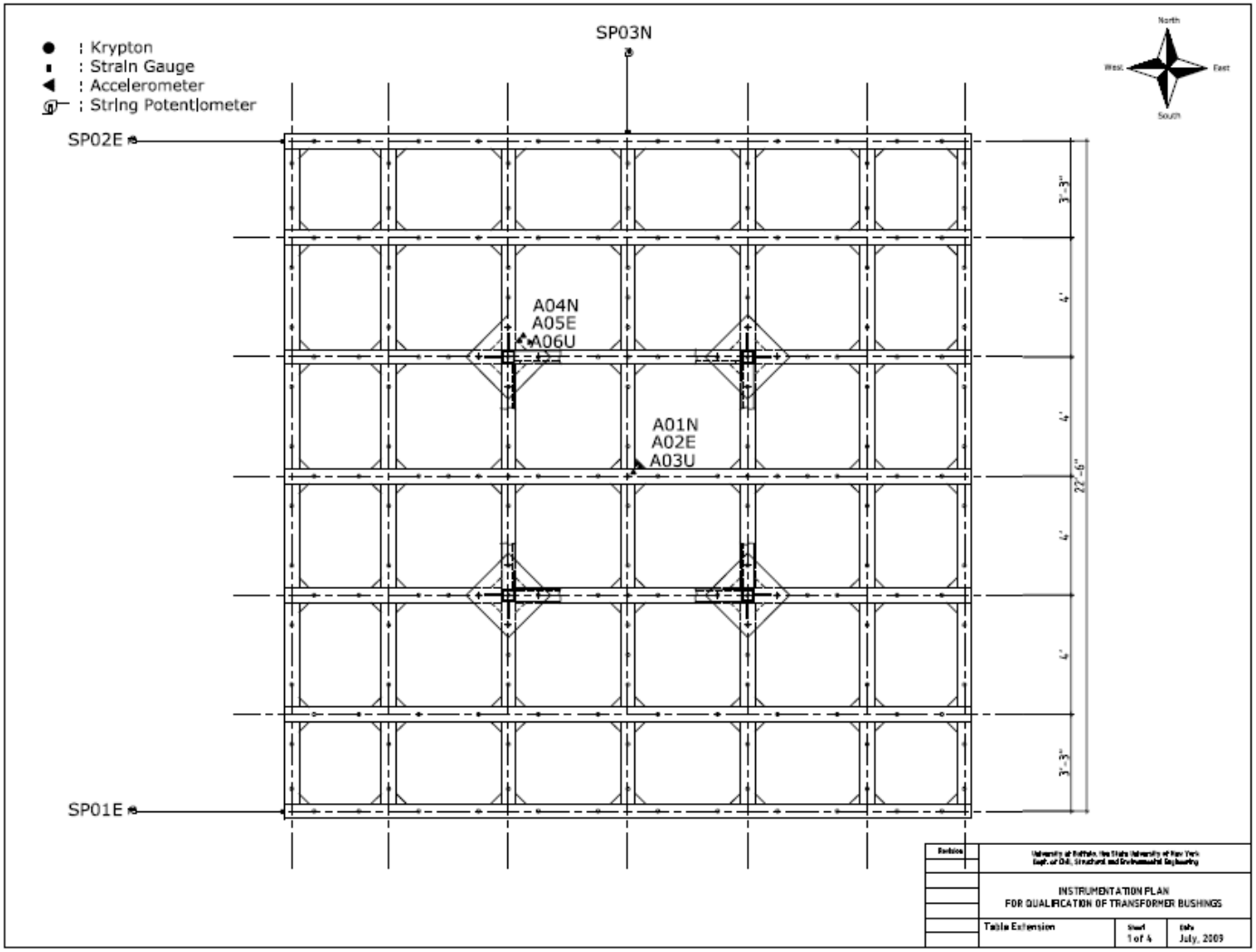

Figure B-8: Instrumentation on Frame and Flexible Top Plate – Bushing #4B

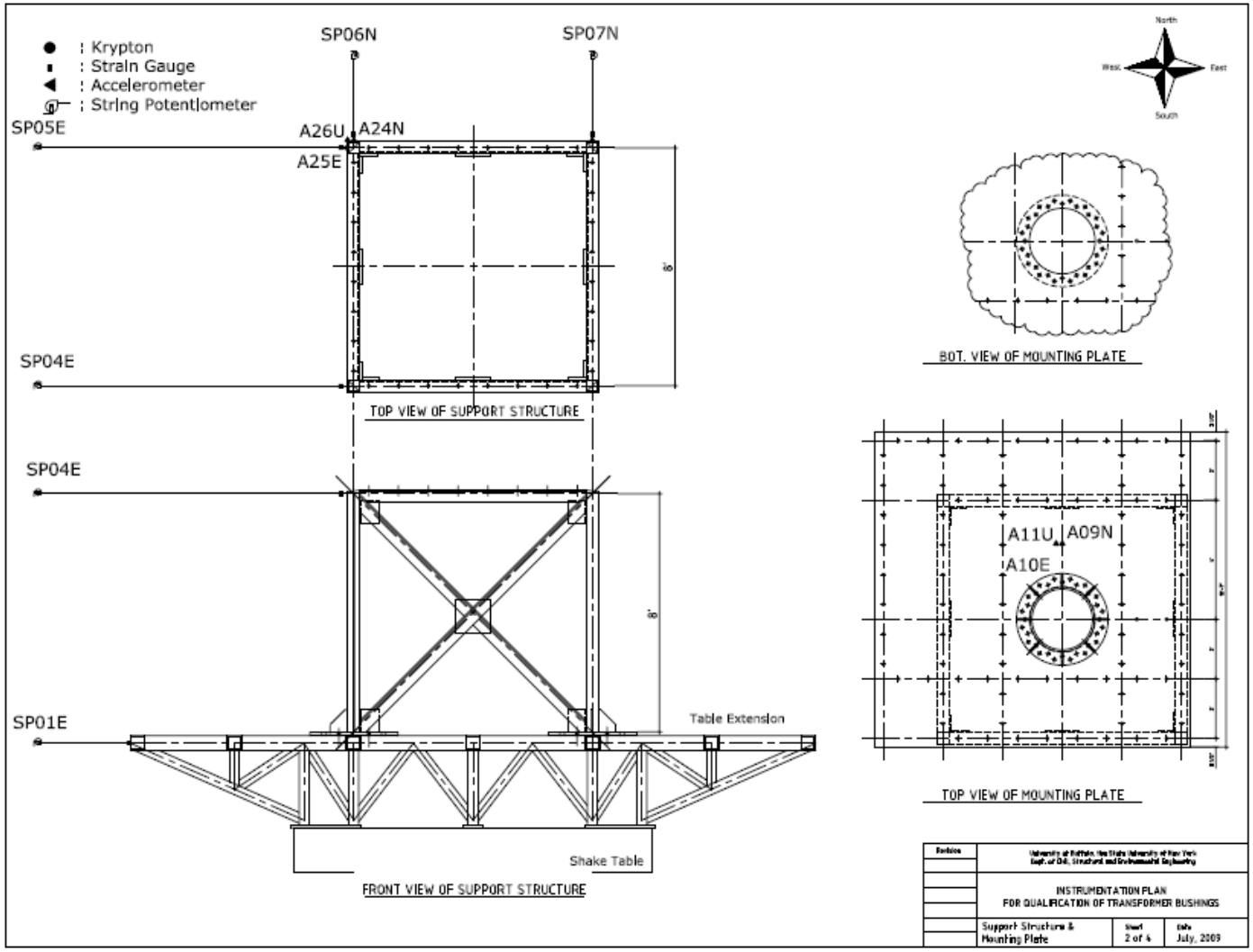

Figure B-9: Instrumentation on Frame – Bushing #4B

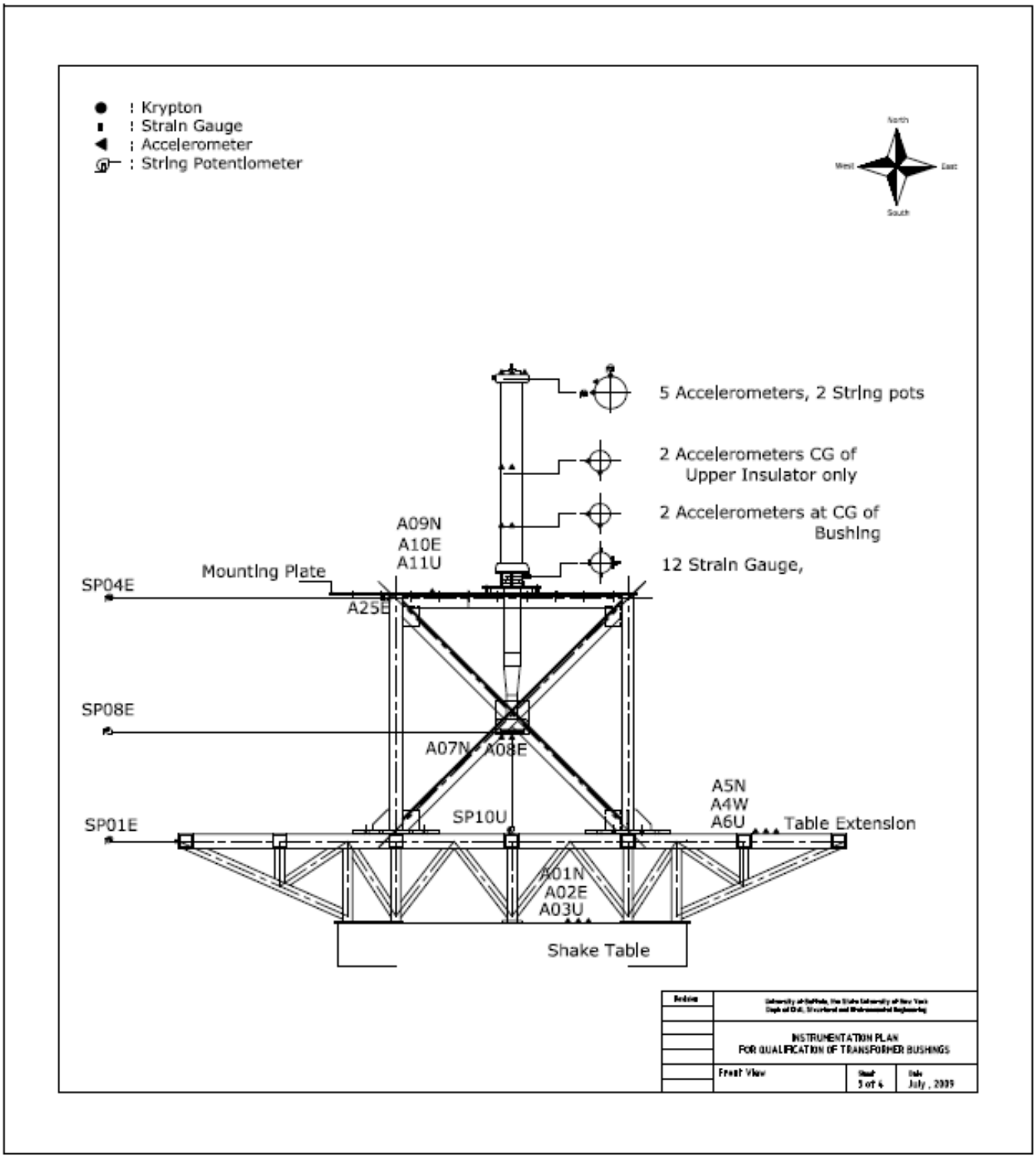

Instrumentation of Bushing #5

Bushing #5 instrumentation consisted of 18 strain gauges spread along the circumfrence of the mounting flange. 26 accelerometers were used in different locations. Response spectra were drawn using accelerometers on the shake table. 12 string potentiometers were used and 8 LEDs were used. Load cells rated at 400 lb. and 1,000 lb. were used to measure the force during the pull test. Table B-3 shows the list of instruments and Figures B-10 through B-15 show their locations on the bushing.

Table B-3: Instrumentation List – Bushing #5

Instrumentation List for Bushing 5

Instrument No.		Measuments	Direction	Shake	on	Comment
Unit 1		Position		Table	Floor	

*** Strain Gauges**

SNB		at flange near Bottom (Aluminum Flange)	N	x	x	
SNEB		at flange near Bottom (Aluminum Flange)	NE	x	x	
SEB		at flange near Bottom (Aluminum Flange)	E	x	x	
SSEB		at flange near Bottom (Aluminum Flange)	SE	x	x	
SSB		at flange near Bottom (Aluminum Flange)	S	x	x	
SSWB		at flange near Bottom (Aluminum Flange)	SW	x	x	
SNWB		at flange near Bottom (Aluminum Flange)	NW	x	x	
SNT		at flange near Top (on Insulator Flange)	N	x	x	
SNET		at flange near Top (on Insulator Flange)	NE	x	x	
SET		at flange near Top (on Insulator Flange)	E	x	x	
SSET		at flange near Top (on Insulator Flange)	SE	x	x	
SST		at flange near Top (on Insulator Flange)	S	x	x	
SSWT		at flange near Top (on Insulator Flange)	SW	x	x	
SWT		at flange near Top (on Insulator Flange)	W	x	x	
SNWT		at flange near Top (on Insulator Flange)	NW	x	x	
SWM		at flange near mid	W	x		added later on
SEM		at flange near mid	E	x		added later on
SSEM		at flange near mid	SE	x		added later on
SSM		at flange near mid	S	x		added later on
SSWM		at flange near mid	SW	x		added later on
SNWM		at flange near mid	NW	x		added later on
SNM		at flange near mid	N	x		added later on
SNEM		at flange near mid	NE	x		added later on
SEMT		At flange above mid and below top	E	x		added later on
SWMT		At flange above mid and below top	W	x		added later on

*** Accelerometers**

A01N		at shake table	N	x		
A02E		at shake table	E	x		
A03U		at shake table	V	x		
A04N		at the table extension	N	x		
A05E		at the table extension	E	x		
A06U		at the table extension	V	x		
A07N		at the bottom of the Bushing	N	x		
A08E		at the bottom of the Bushing	E	x		
A09N		On the Frame	N	x		
A10E		On the Frame	E	x		
A11U		On the Frame	V	x		
A12N		at the mounting plate of the support Frame	N	x		
A13E		at the mounting plate of the support Frame	E	x		
A14U		at the mounting plate of the support Frame	V	x		
A15N		at the interface Ring	N	x	x	
A16E		at the interface Ring	E	x	x	
A17U		at the interface Ring	V	x	x	
A18N		at the CG of Bushing	N	x	x	
A19E		at the CG of Bushing	E	x	x	
A20N		at the CG of upper insulator	N	x	x	
A21E		at the CG of upper insulator	E	x	x	
A22N		at the terminal pad	N	x	x	
A23E		at the terminal pad	E	x	x	
A24U		at the terminal pad	V	x	x	
A25NE		at the terminal pad	NE	x	x	
A26SE		at the terminal pad	SE	x	x	

*** Potentiometers**

SP1E		at the table extension	E	x		connected at SE corner of Shake Table
SP2E		at the table extension	E	x		connected at NE corner of Shake Table
SP3N		at the table extension	N	x		connected at mid of Shake Table
SP4E		at the top of Frame	E	x	x	connected at SE corner of Frame
SP5E		at the top of Frame	E	x		connected at NE corner of Frame
SP6N		at the top of Frame	N	x		connected at NE corner of Frame
SP7N		at the top of Frame	N	x		connected at NW corner of Frame
SP8E		at the bottom of Bushing	E	x		connected to Eest side
SP9N		at the bottom of Bushing	N	x		connected to North side
SP10U		at the bottom of Bushing	V	x		Connected from Shake Table Extension
SP11E		at the Bushing Terminal	E	x	x	
SP12N		at the Bushing Terminal	N	x	x	

*** LED**

LED1W		Bushing Flange	E		x	
LED2W		Bushing Flange	W		x	
LED3S		Hollow core composite Flange	E		x	
LED4S		Hollow core composite Flange	W		x	
LED5E		on Flange	W		x	
LED6E		on Flange	S		x	
LED7W		on Flange	W		x	
LED8W		Above the Flange	E		x	

*** LOAD CELL**

LC		At the terminal Point	E		x	

Figure B-10: Instrumentation on Fixed Base – Bushing #5

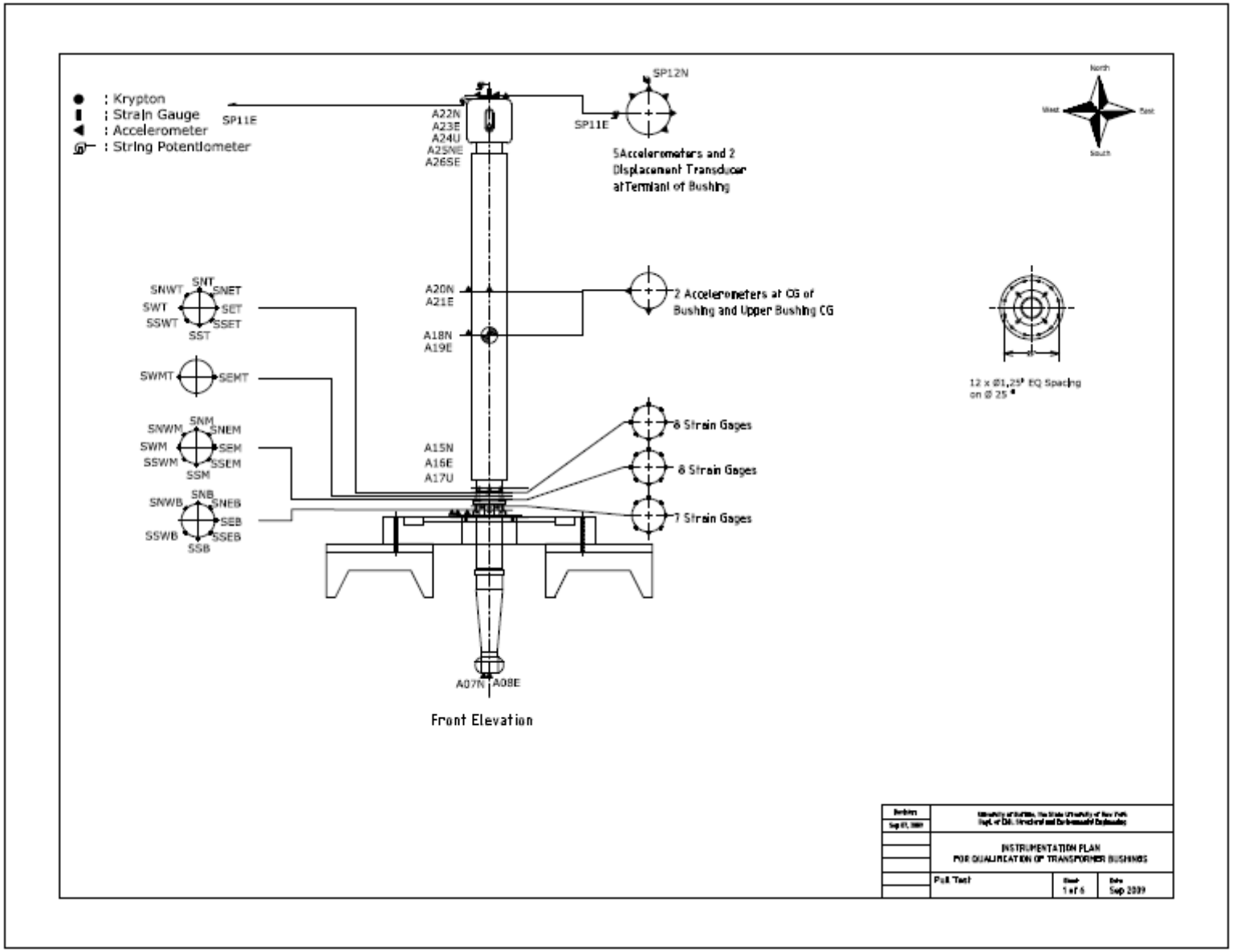

Figure B-11: Instrumentation on Shake Table Extension – Bushing #5

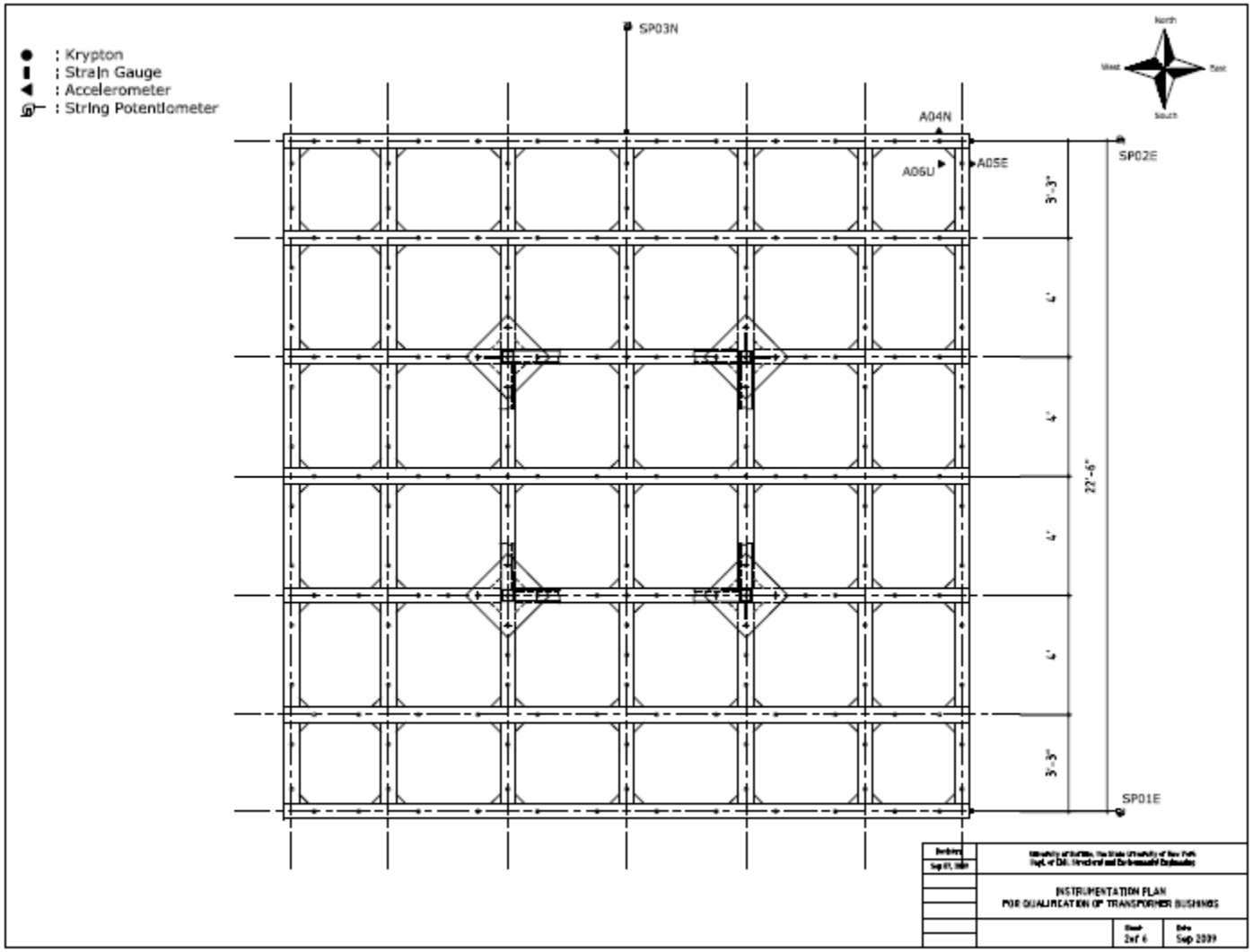

Figure B-12: Instrumentation on Frame and Flexible Top Plate – Bushing #5

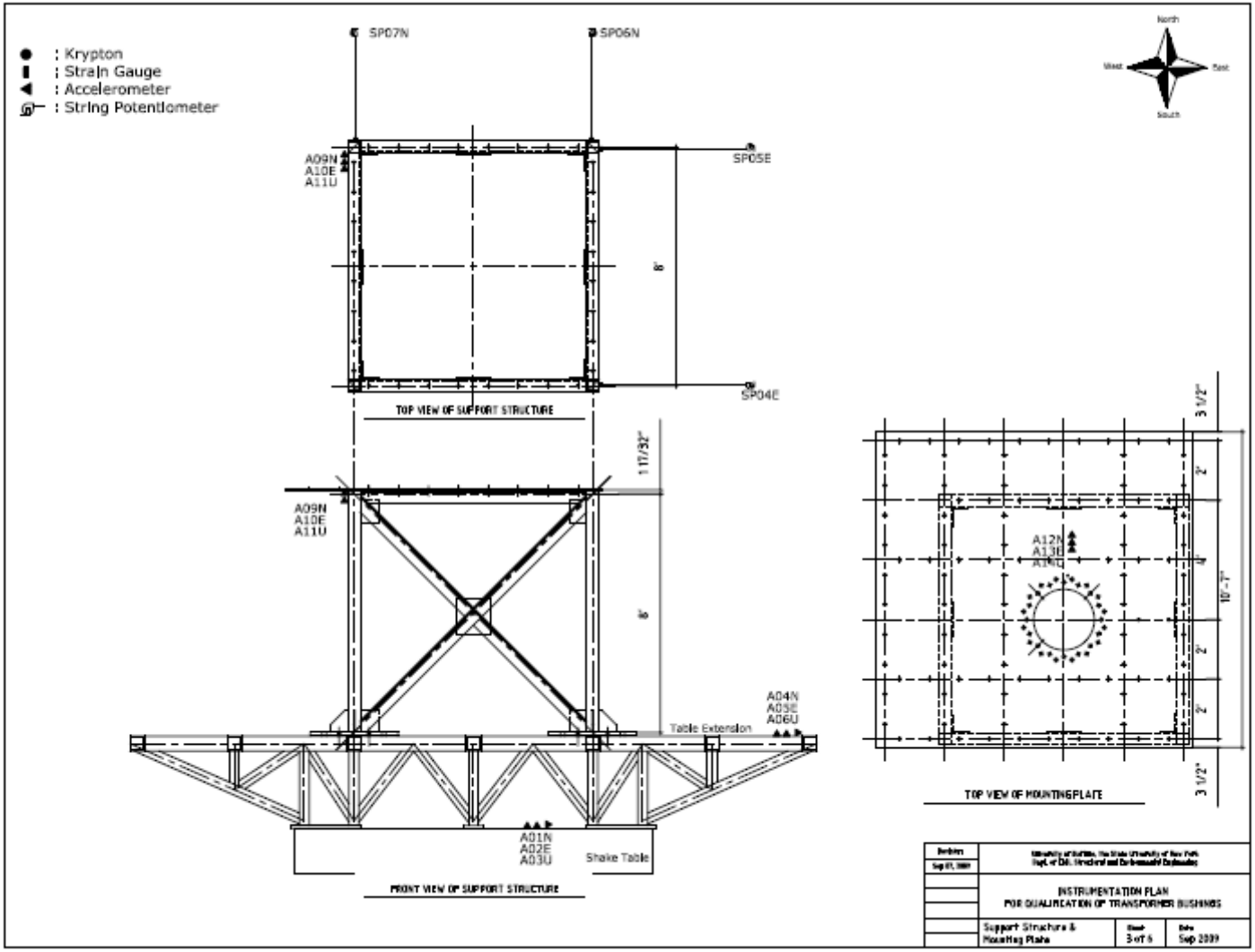

Figure B-13: Instrumentation on Frame and Flexible Top Plate – Bushing #5

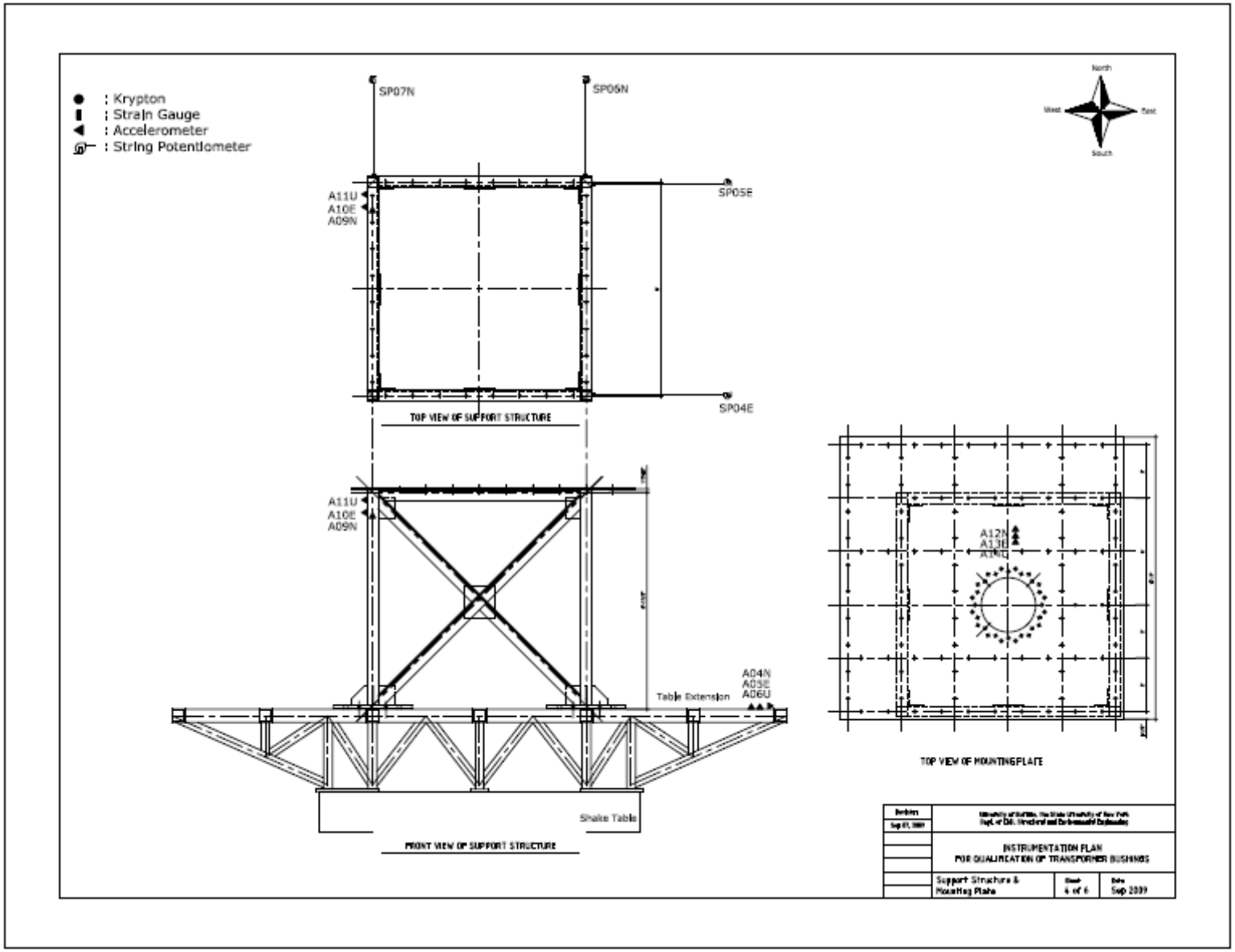

Figure B-14: Instrumentation on Frame – Bushing #5

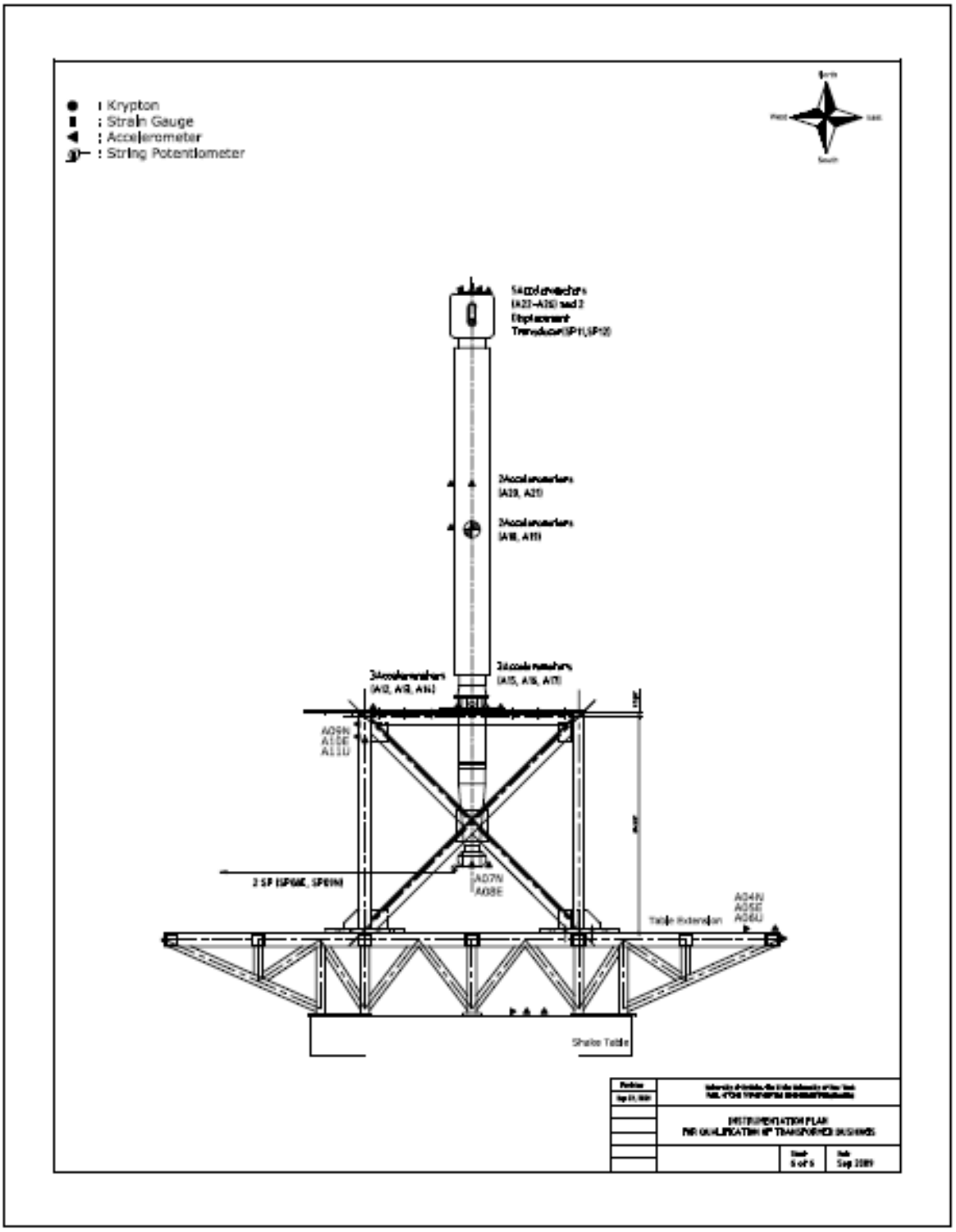

Figure B-15: Instrumentation Setup – Bushing #5

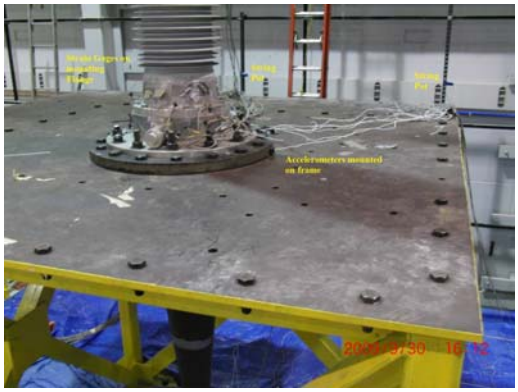

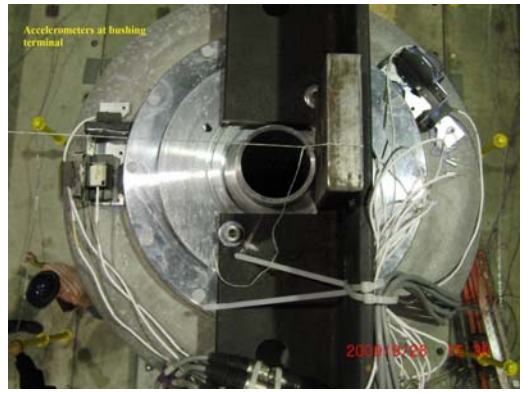

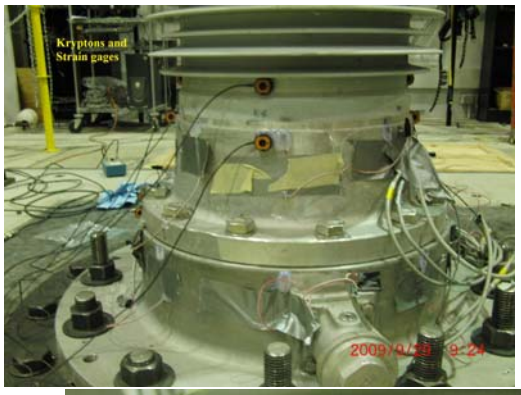

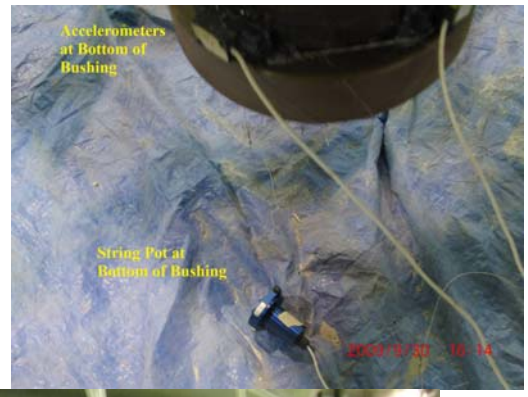

Instrumentation of Bushing #6

Bushing #6 instrumentation consisted of 16 strain gauges spread along the circumference of the mounting flange. 26 accelerometers were used in various locations. Response spectra were drawn using accelerometers on the shake table. 12 string potentiometers and 11 LEDs were used. Load cells rated at 400 lb. and 1,000 lb. were used to measure the force during the pull test. Table B-4 shows the list of instruments and Figures B-16 – B-22 show their locations on the bushing.

Table B-4: Instrumentation List – Bushing #6

Measurements List for Bushing 6

Instrument No.		Measuments	Direction	Shake Table (Container)	Shake	on	Comment
Unit 1		Position			Table	Floor	
*** Strain Gauges**							
SNT		at flange near Top (on Insulator Flange)	N		x	x	
SNET		at flange near Top (on Insulator Flange)	NE		x	x	
SET		at flange near Top (on Insulator Flange)	E		x	x	
SSET		at flange near Top (on Insulator Flange)	SE		x	x	
SST		at flange near lower (on Insulator Flange)	S		x	x	
SSWT		at flange near lower (on Insulator Flange)	SW		x	x	
SWT		at flange near lower (on Insulator Flange)	W		x	x	
SNWT		at flange near lower (on Insulator Flange)	NW		x	x	
SNB		At Bushing Flange Body	N		x	x	
SNEB		At Bushing Flange Body	NE		x	x	
SEB		At Bushing Flange Body	E		x	x	
SSEB		At Bushing Flange Body	SE		x	x	
SSB		At Bushing Flange Body	S		x	x	
SSWB		At Bushing Flange Body	SW		x	x	
SWB		At Bushing Flange Body	W		x	x	
SNWB		At Bushing Flange Body	NW		x	x	

*** Accelerometers**

A01N		at shake table	N		x		
A02E		at shake table	E		x		
A03U		at shake table	V		x		
A04N		at the table extension	N		x		
A05E		at the table extension	E		x		
A06U		at the table extension	V		x		
A07N		at the bottom of the Bushing	N		x		
A08E		at the bottom of the Bushing	E		x		
A09N		On the Frame	N		x		
A10E		On the Frame	E		x		
A11U		On the Frame	V		x		
A12N		at the mounting plate of the support Frame	N		x		
A13E		at the mounting plate of the support Frame	E		x		
A14U		at the mounting plate of the support Frame	V		x		
A15N		at the interface Ring	N		x	x	
A16E		at the interface Ring	E		x	x	
A17U		at the interface Ring	V		x	x	
A18N		at the CG of Bushing	N	x	x	x	
A19E		at the CG of Bushing	E	x	x	x	
A20N		at the CG of upper insulator	N		x	x	
A21E		at the CG of upper insulator	E		x	x	
A22N		at the terminal pad	N	x	x	x	
A23E		at the terminal pad	E	x	x	x	
A24U		at the terminal pad	V	x	x	x	
A25NE		at the terminal pad	NE	x	x	x	
A26SE		at the terminal pad	SE	x	x	x	

*** Potentiometers**

SP1E		at the table extension	E		x		connected at SE corner of Shake Table
SP2E		at the table extension	E		x		connected at NE corner of Shake Table
SP3N		at the table extension	N		x		connected at mid of Shake Table
SP4E		at the top of Frame	E		x	x	connected at SE corner of Frame
SP5E		at the top of Frame	E		x		connected at NE corner of Frame
SP6N		at the top of Frame	N		x		connected at NW corner of Frame
SP7N		at the top of Frame	N		x		connected at NE corner of Frame
SP8E		at the bottom of Bushing	E		x		connected to Eest side
SP9N		at the bottom of Bushing	N		x		connected to North side
SP10U		at the bottom of Bushing	V		x		Connected from Shake Table Extension
SP11E		at the Bushing Terminal	E	x	x	x	
SP12N		at the Bushing Terminal	N		x		

*** LED**

LED1		Bushing Flange West	W			x	
LED2		Bushing Flange South	S			x	
LED3		Bushing Flange East	E			x	
LED4		Porcelain West	W			x	
LED5		Porcelain South	S			x	
LED6		Porcelain East	E			x	
LED7		Porcelain south ___'	S			x	
LED8		Porcelain south ___'	S			x	
LED9		Porcelain south ___'	S			x	
LED10		Porcelain south ___'	S			x	
LED11		Porcelain south ___'	S			x	

*** LOAD CELL**

LC		At the terminal Point	E	x		x	

Figure B-16: Instrumentation on Fixed Base – Bushing #6

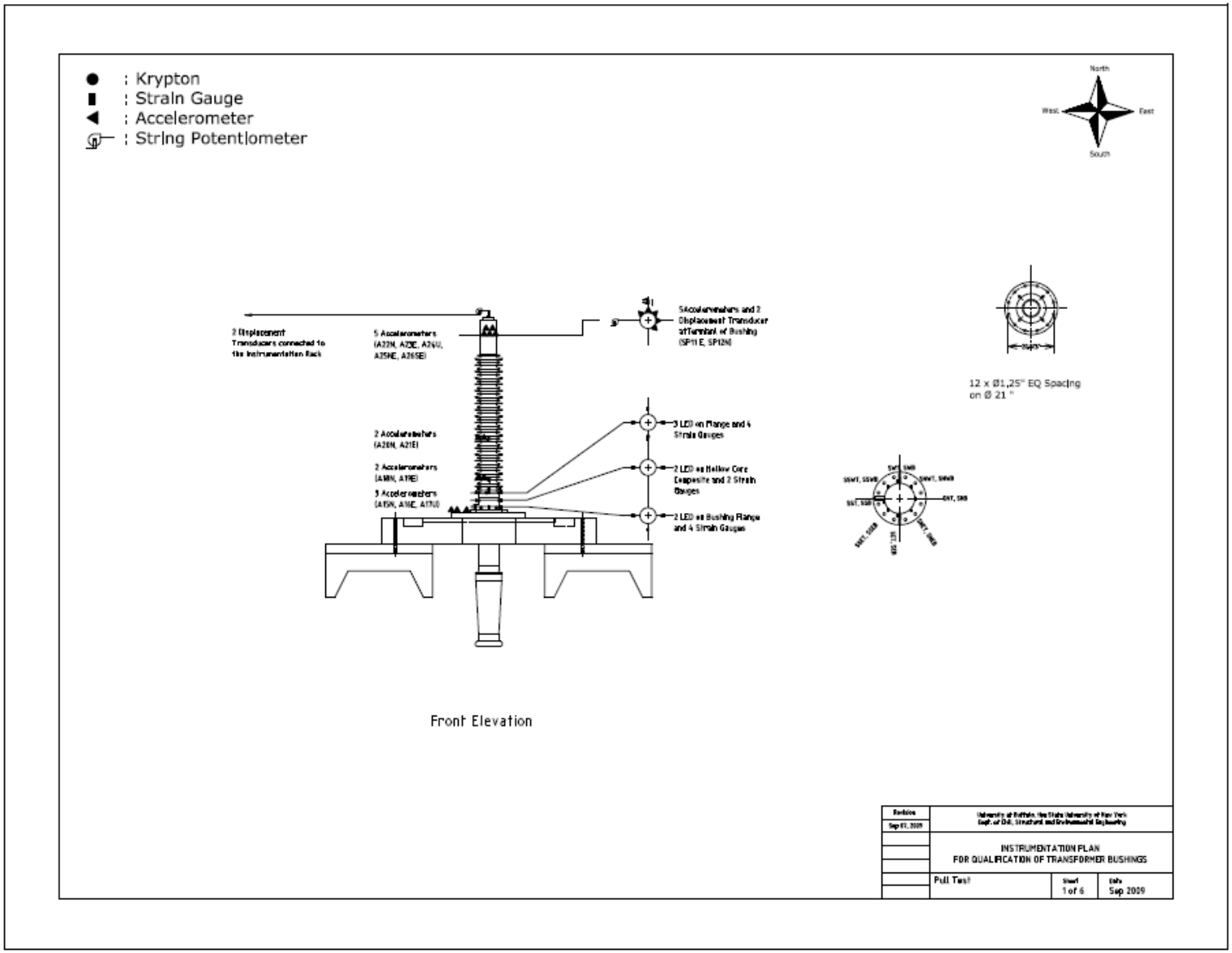

Figure B-17: Instrumentation on Shake Table Extension – Bushing #6

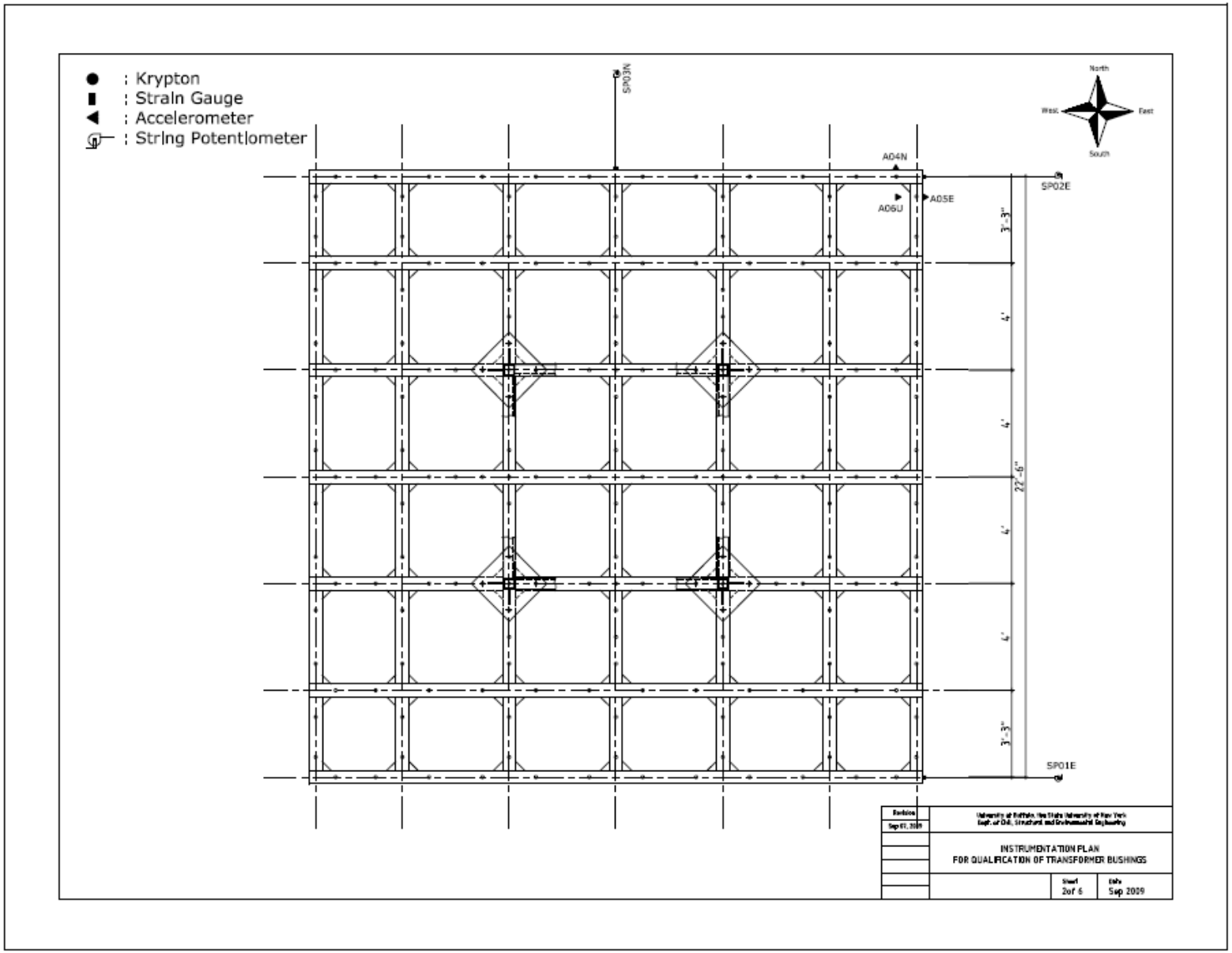

Figure B-18: Instrumentation on Frame and Flexible Top Plate – Bushing #6

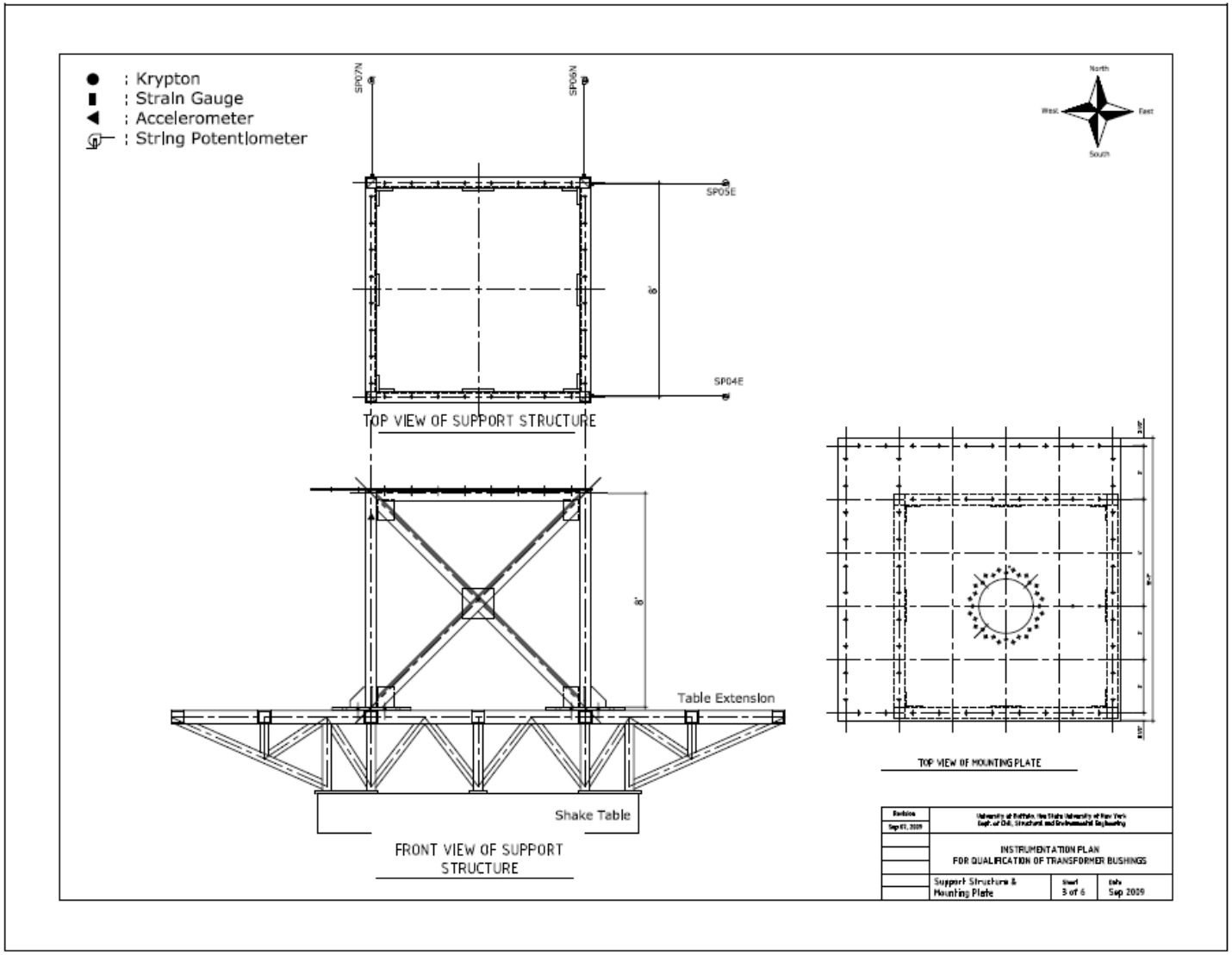

Figure B-19: String Pots on Frame and Flexible Top Plate – Bushing #6

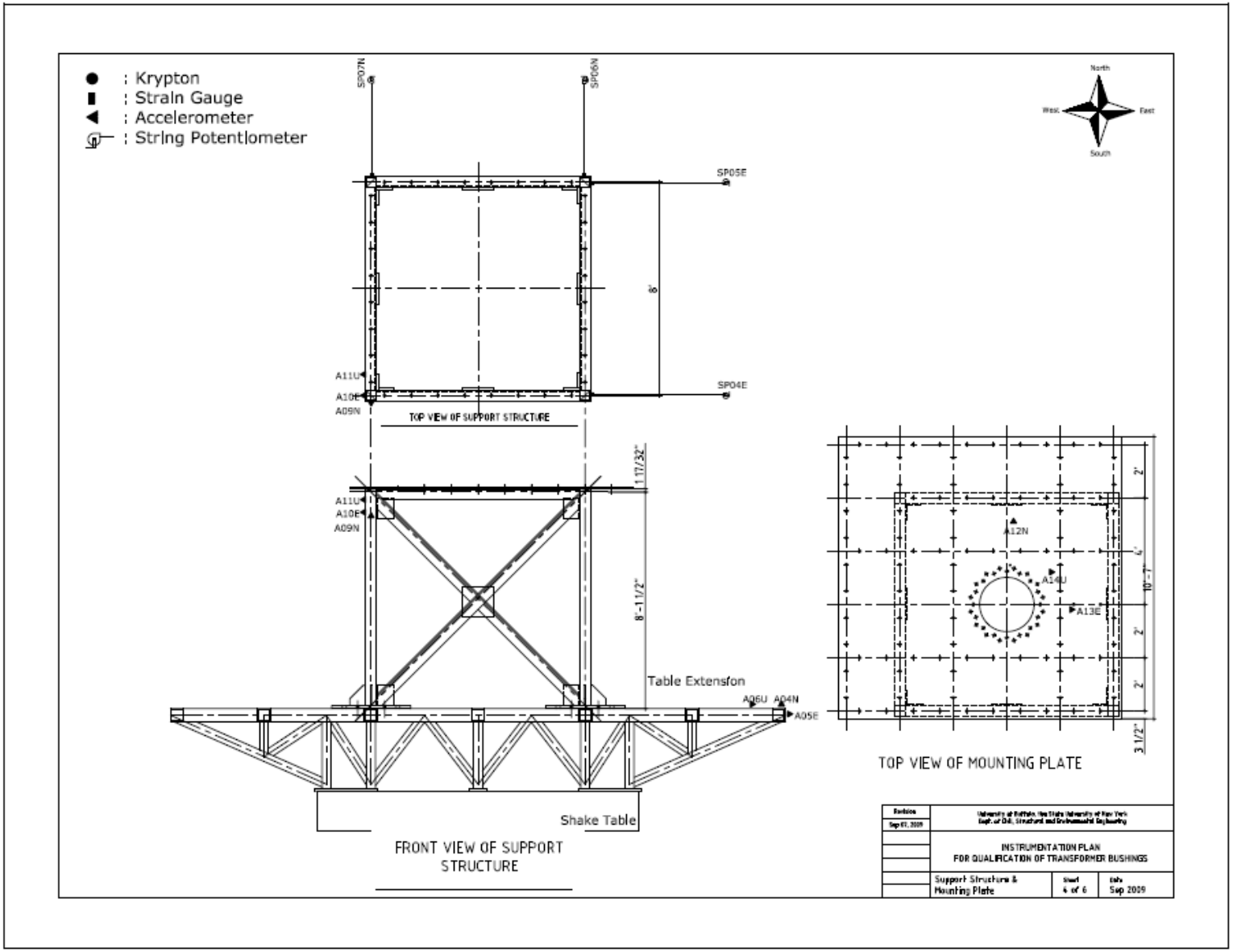

Figure B-20: Instrumentation on Frame – Bushing #6

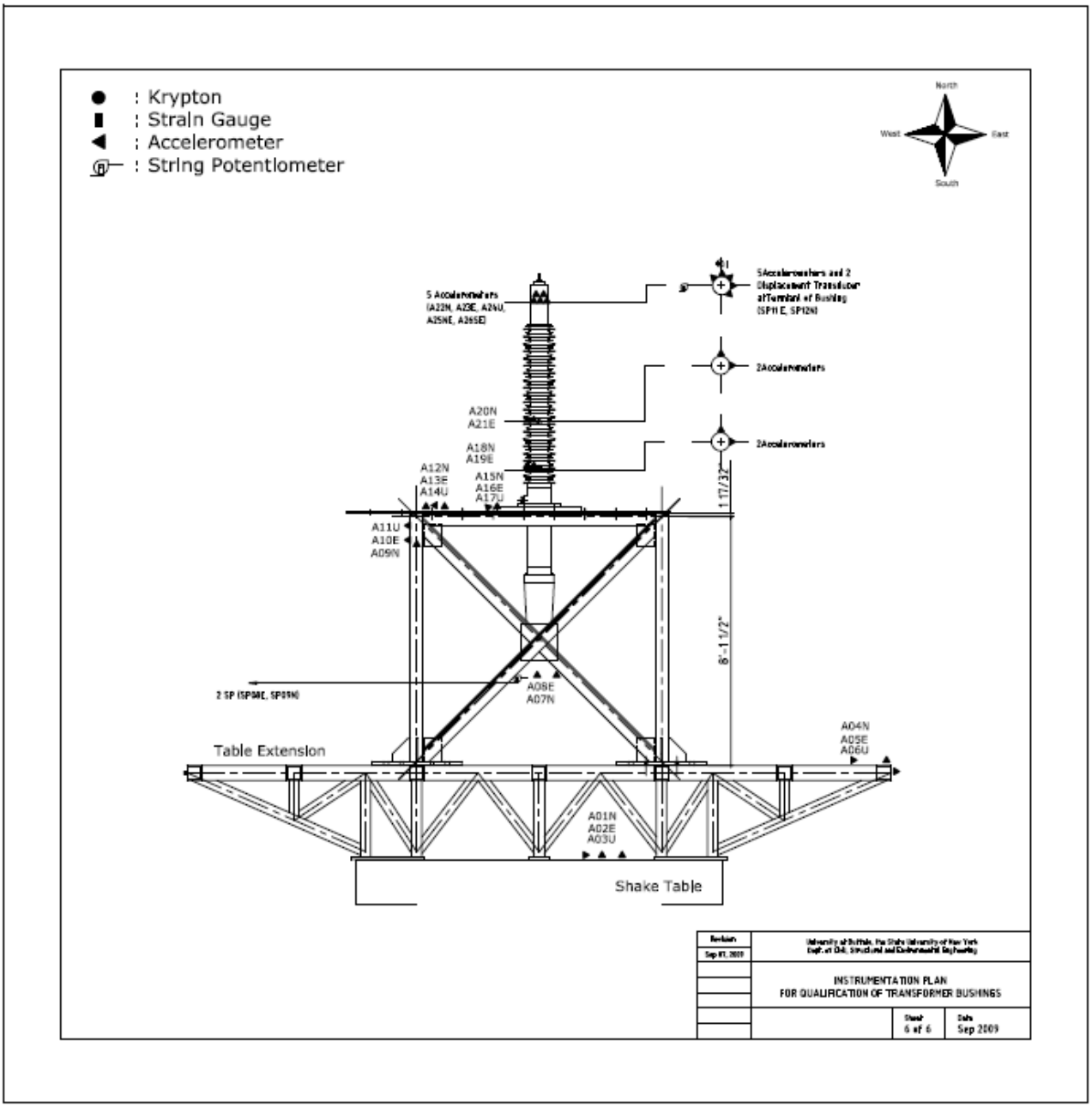

Figure B-21: Instrumentation Setup – Bushing #6

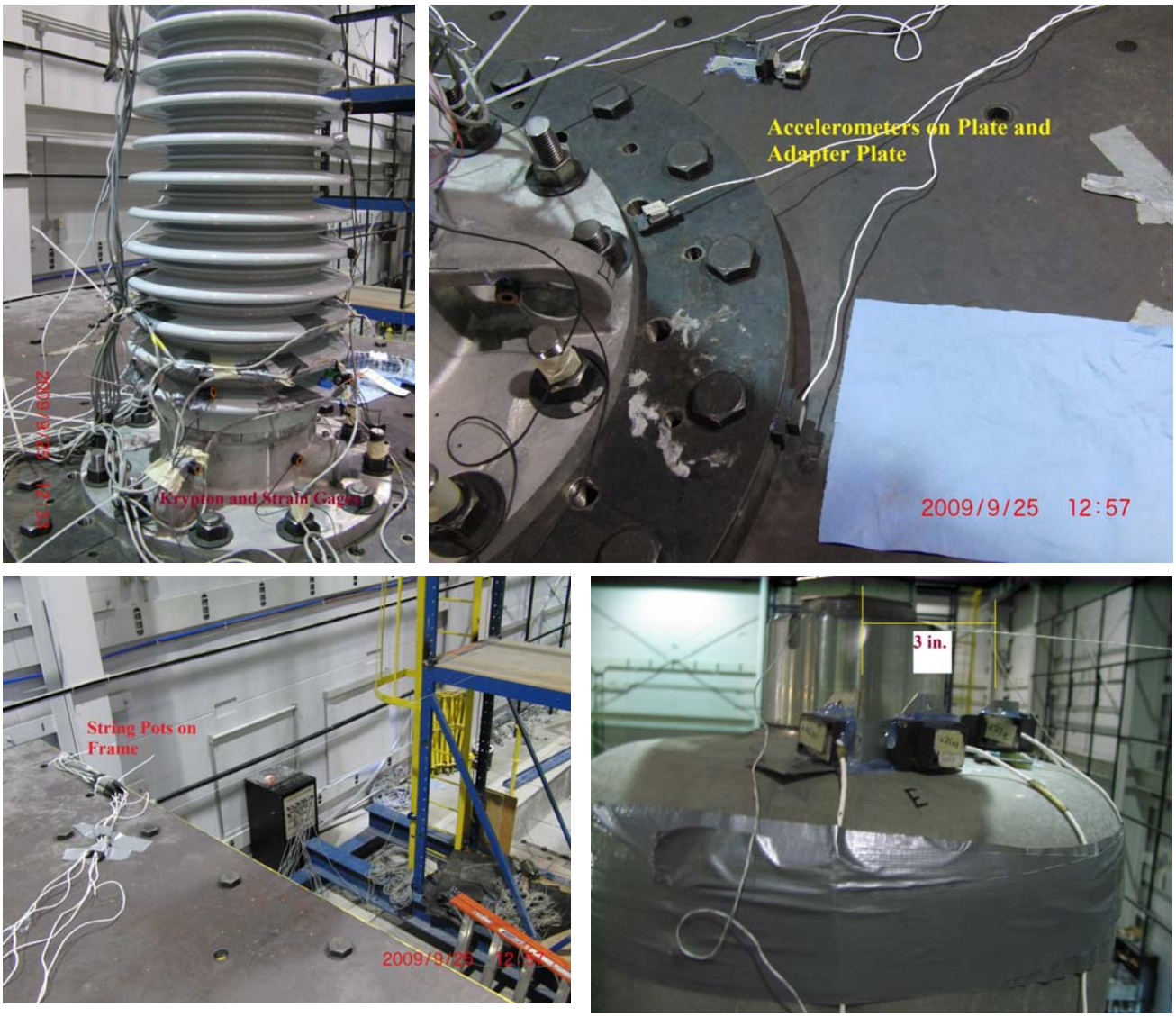

Figure B-22: Bushing #6 Mounted on Frame

Instrumentation of Bushing #7

Bushing #7 instrumentation consisted of 9 strain gauges spread along the circumfrence of the mounting flange. 26 accelerometers were used in various locations. Response spectra were drawn using accelerometers on the shake table. 16 string potentiometers and 8 LEDs were used. Load cells rated at 400 lb. and 1,000 lb. were used to measure the force during the pull test. Table B-5 shows the list of instruments and Figures B-23 – B-28 show their locations on the bushing.

Table B-5: Instrumentation List – Bushing #7

Measurements List for Bushing 7

Instrument No. Bushing 7	Measuments Position	Direction	Shake Table	on Floor	Comment
*** Strain Gauges**					
S01N	at flange near Top (1.5 " from Porcelain)	N	x	x	
S02NE	at flange near Top (1.5 " from Porcelain)	NE	x	x	
S03EEN	at flange near Top (1.5 " from Porcelain)	EEN	x	x	
S03EES	at flange near Top (1.5 " from Porcelain)	EES	x	x	
S04SE	at flange near Top (1.5 " from Porcelain)	SE	x	x	
S05SSE	at flange near Top (1.5 " from Porcelain)	SSE	x	x	
S05SSW	at flange near Top (1.5 " from Porcelain)	SSW	x	x	
S06SW	at flange near Top (1.5 " from Porcelain)	SW	x	x	
S07WWS	at flange near Top (1.5 " from Porcelain)	WWS	x	x	
S07WWN	at flange near Top (1.5 " from Porcelain)	WWN	x	x	
S08NW	at flange near Top (1.5 " from Porcelain)	NW	x	x	
S09					

*** Accelerometers**

A01N	at shake table	N	x		
A02E	at shake table	E	x		
A03U	at shake table	V	x		
A04N	at the table extension	N	x		
A05E	at the table extension	E	x		
A06U	at the table extension	V	x		
A07N	at the bottom of the Bushing	N	x		
A08E	at the bottom of the Bushing	E	x		
A09N	On the Frame	N	x		
A10E	On the Frame	E	x		
A11U	On the Frame	V	x		
A12N	at the mounting plate of the support Frame	N	x		
A13E	at the mounting plate of the support Frame	E	x		
A14U	at the mounting plate of the support Frame	V	x		
A15N	at the interface Ring	N	x	x	
A16E	at the interface Ring	E	x	x	
A17U	at the interface Ring	V	x	x	
A18N	at the CG of Bushing	N	x	x	
A19E	at the CG of Bushing	E	x	x	
A20N	at the CG of upper insulator	N	x	x	
A21E	at the CG of upper insulator	E	x	x	
A22N	at the terminal pad	N	x	x	
A23E	at the terminal pad	E	x	x	
A24U	at the terminal pad	V	x	x	
A25NE	at the terminal pad	NE	x	x	
A26SE	at the terminal pad	SE	x	x	

*** Potentiometers**

SP1E	at the table extension	E	x		connected at SE corner of Shake Table
SP2E	at the table extension	E	x		connected at NE corner of Shake Table
SP3N	at the table extension	N	x		connected at mid of Shake Table
SP4E	at the bottom of Bushing	E	x		connected to Eest side
SP5N	at the bottom of Bushing	N	x		connected to North side
SP6U	at the bottom of Bushing	V	x		Connected from Shake Table Extension
SP7E	at the top of Frame	E	x	x	connected at SE corner of Frame
SP8E	at the top of Frame	E	x		connected at NE corner of Frame
SP9N	at the top of Frame	N	x		connected at NE corner of Frame
SP10N	at the top of Frame	N	x		connected at NW corner of Frame
SP11E	at the CG of Bushing	E	x		
SP12N	at the CG of Bushing	N	x		
SP13E	at the Upper CG of Bushing	E	x		
SP14N	at the Upper CG of Bushing	N	x		
SP15E	at the Bushing Terminal	E	x	x	
SP16N	at the Bushing Terminal	N	x	x	

*** LED**

LED1W	Bushing Flange	E		x	
LED2W	Bushing Flange	W		x	
LED3S	Porcelain Flange	E		x	
LED4S	Porcelain Flange	W		x	
LED5E	on Flange	W		x	
LED6E	on Flange	S		x	
LED7W	on Flange	W		x	
LED8W	Above the Flange	E		x	

*** LOAD CELL**

LC	At the terminal Point	E	x	x	

Figure B-23: Instrumentation on Fixed Base – Bushing #7

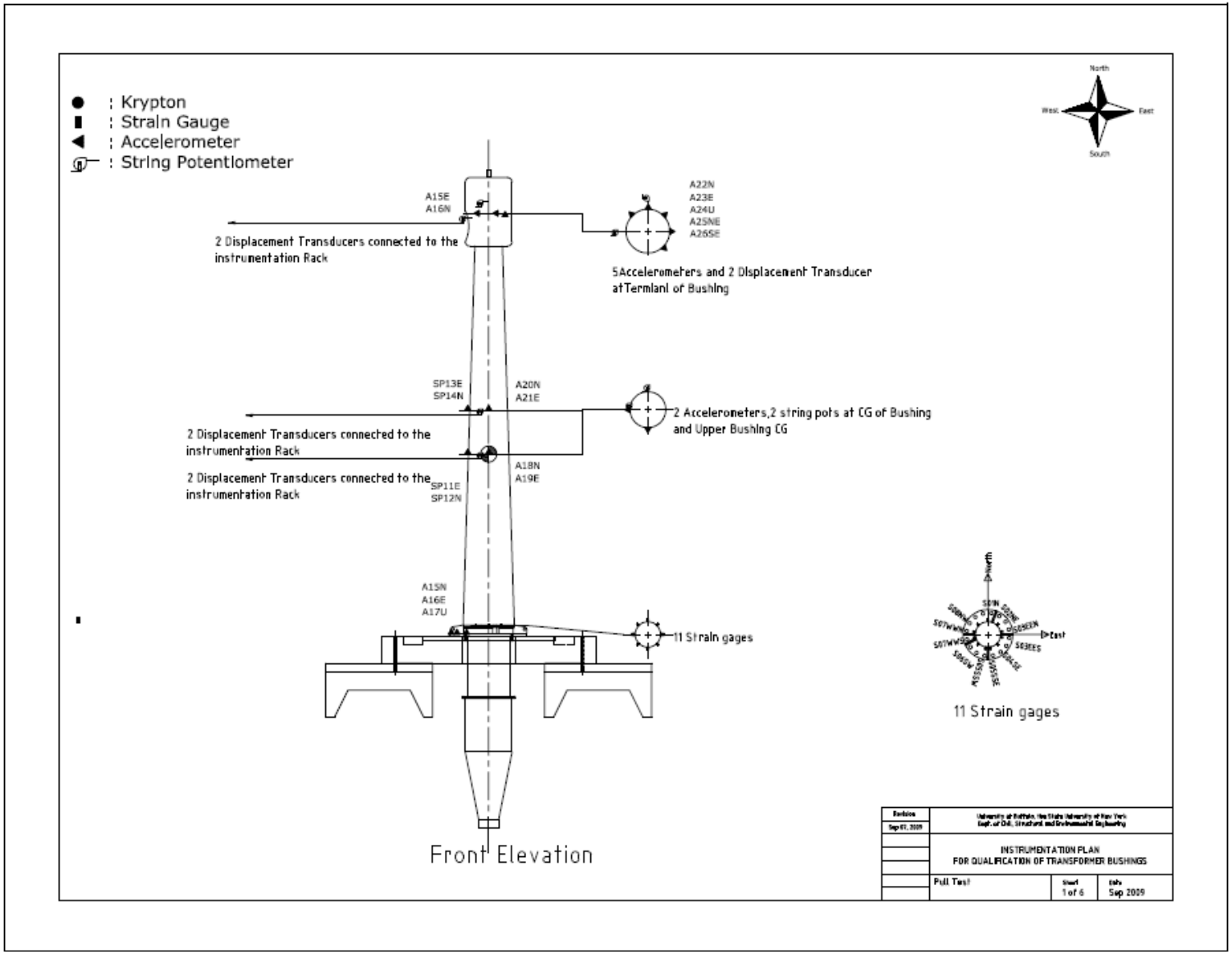

Figure B-24: Instrumentation on Shake Table Extension – Bushing #7

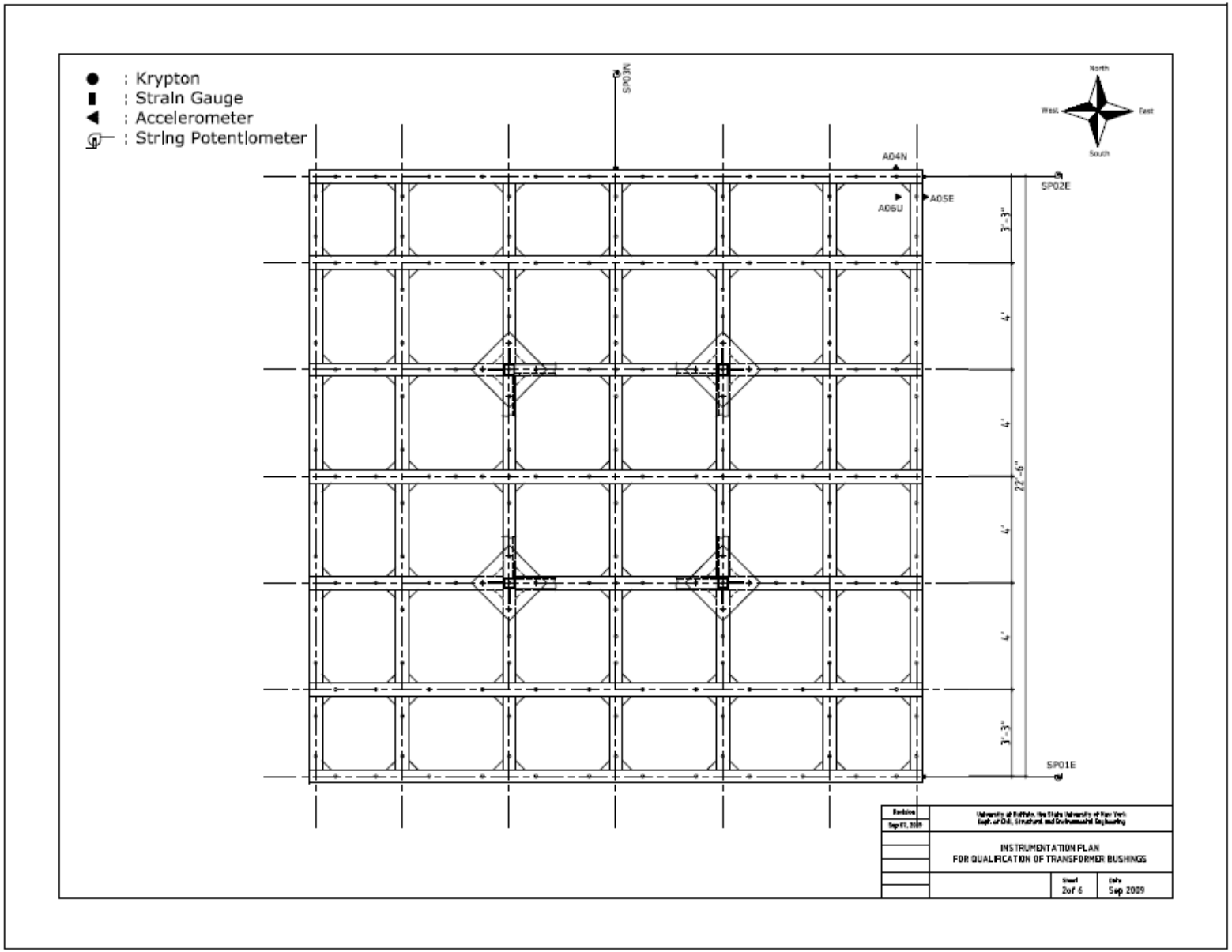

Figure B-25: Instrumentation on Frame and Flexible Top Plate – Bushing #7

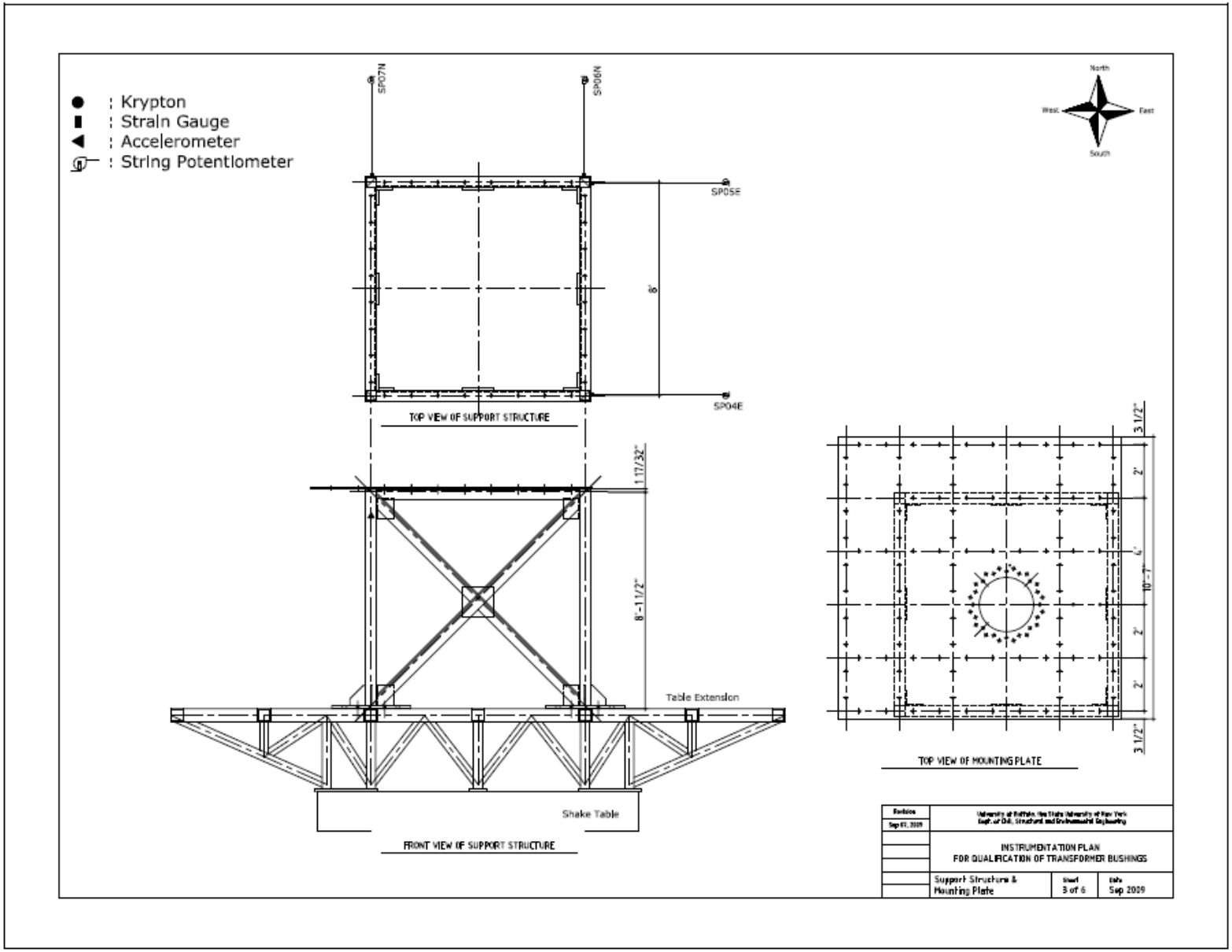

INSTRUMENTATION PLAN
FOR QUALIFICATION OF TRANSFORMER BUSHINGS
Sheet
2 of 6
Date
Sep 2009

Figure B-26: String Pots on Frame and Flexible Top Plate – Bushing #7

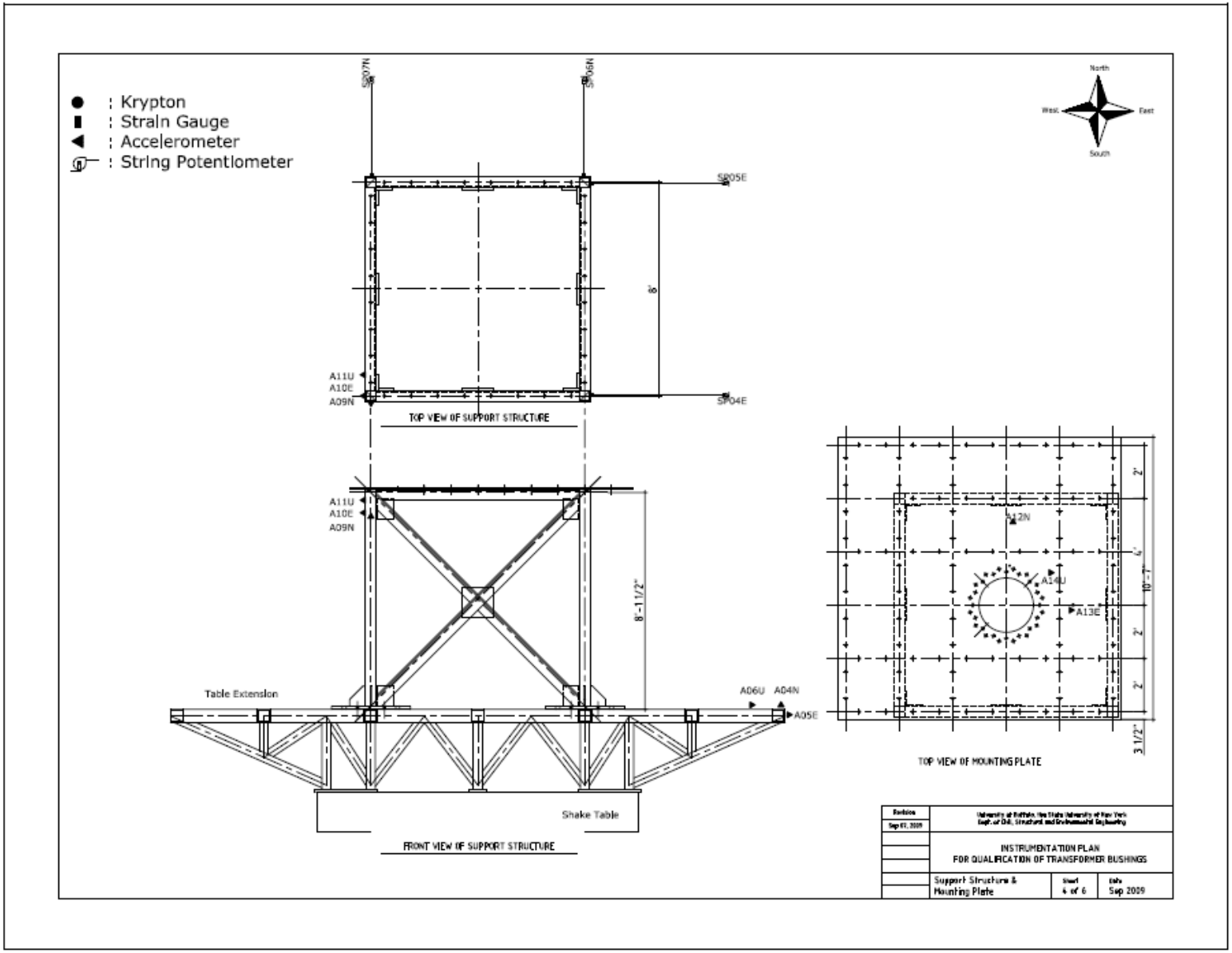

Figure B-27: Instrumentation on Frame – Bushing #7

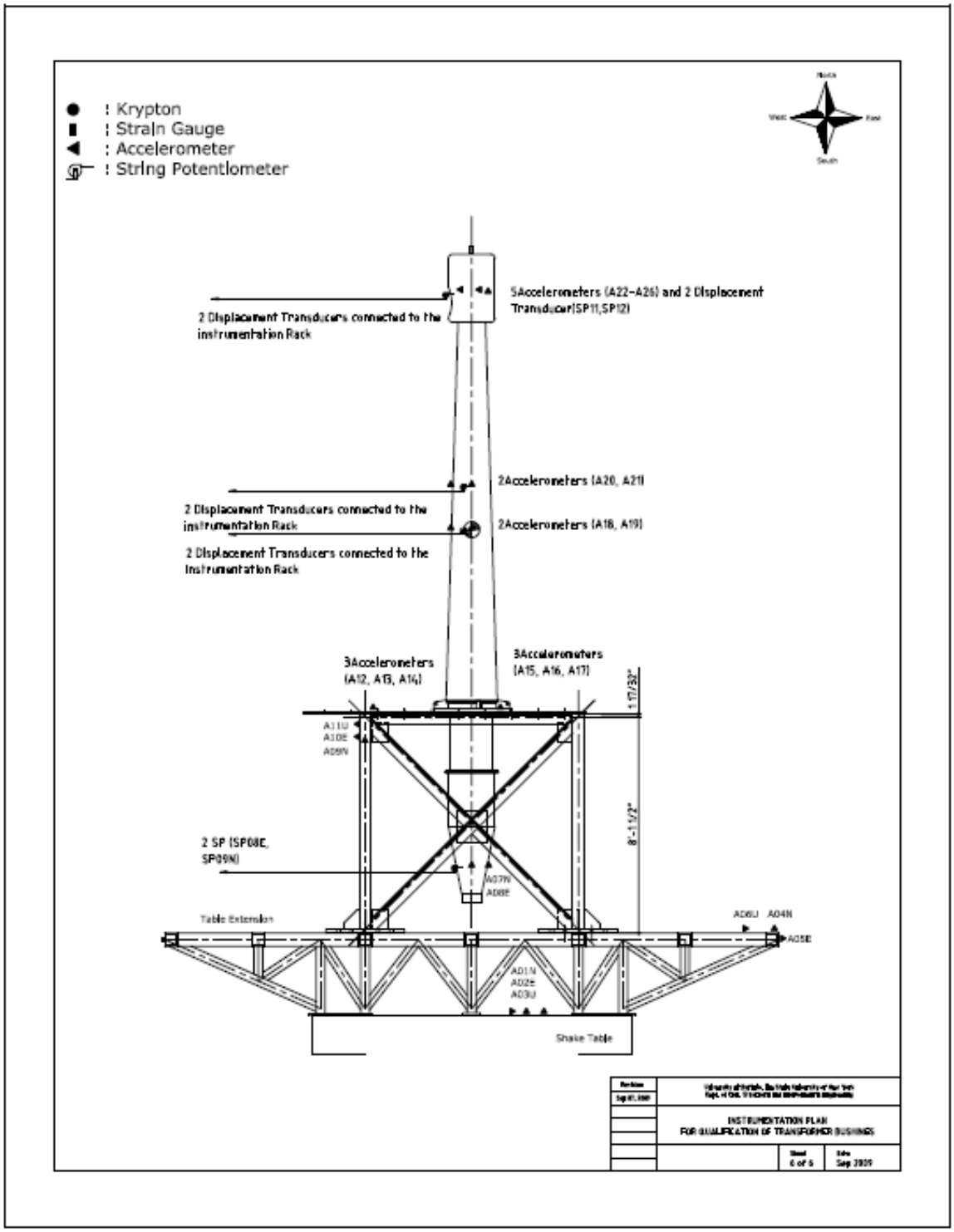

Figure B-28: Instrumentation Setup – Bushing #7

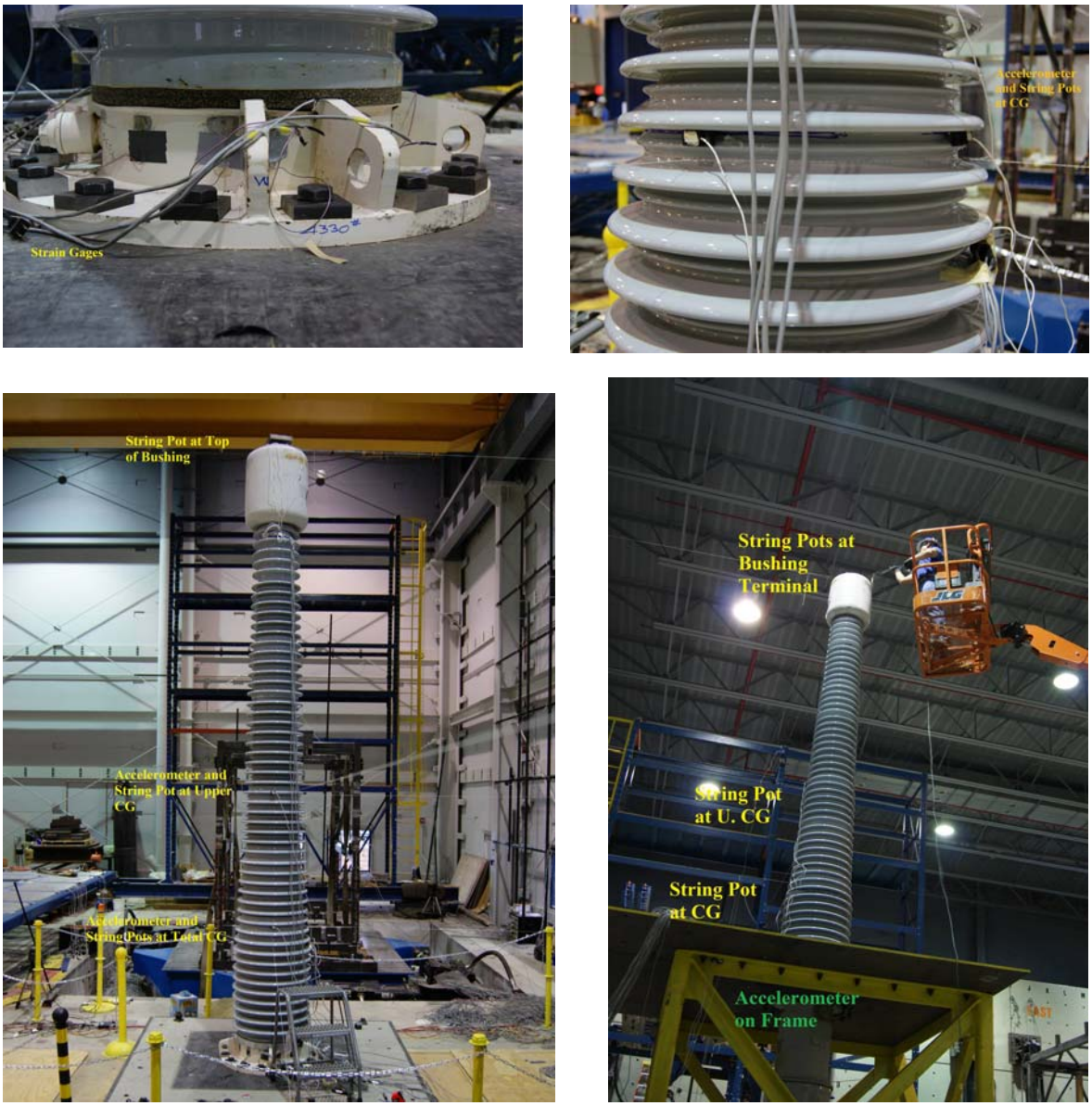

Instrumentation of Bushing #8

Bushing #8 instrumentation consisted of 18 accelerometers at various locations. Response spectra were drawn using accelerometers on the shake table. 9 string potentiometers, one linear potentiometer and 6 LEDs were used. Table B-6 shows the list of instruments and Figures B-29 – B-32 show their locations on the bushing.

Table B-6: Instrumentation List – Bushing #8

Instrumentation List for ABB 550Z3000SE BUSHING					
Instrument #	**Location and Position**	**Direction**	**Comments**	**Fixed Base**	**Shake Table**
Accelerometers					
A01	top of bushing on plate	EW	Positive direction EAST perpendicular to bushing axis	x	x
A02	top of bushing on plate	NS	Positive direction NORTH	x	x
A03	top of bushing along bushing axis	AXIAL	Positive direction UP (or closes to UP)	x	x
A04	CG opper 85.22" from surface of adapter ring	EW	Positive direction EAST perpendicular to bushing axis		x
A05	CG opper 85.22" from surface of adapter ring	NS	Positive direction NORTH		x
A06	CG opper 54.75" from surface of adapter ring	EW	Positive direction EAST perpendicular to bushing axis	x	x
A07	CG opper 54.75" from surface of adapter ring	NS	Positive direction NORTH	x	x
A08	top of support structure - near lower lifting log	EW	Positive direction EAST perpendicular to bushing axis		x
A09	top of support structure - near center of plate	NS	Positive direction NORTH		x
A10	top of support structure - near lower lifting log	AXIAL	Axial Positive direction UP		x
A11	top of support structure - near lower lifting log	EW	Horizontal Positive direction EAST		x
A12	top of support structure - near lower lifting log	VERT	Vertical Positive direction UP		x
A13	bottom of bushing on plate	EW	Positive direction EAST perpendicular to bushing axis	x	x
A14	bottom of bushing on plate	NS	Positive direction NORTH	x	x
A15	extension platforrm	VERT	Center of base plate		x
A16	extension platforrm	EW	Center of base plate		x
A17	extension platforrm	NS	Center of base plate		x
A18	on Frame leg (EAST) to measure rotation	EW	Frame top		x
Potentiomenters					
SP01	top of bushing on plate	EW	Positive direction EAST horizontal	x	x
SP02	top of bushing on plate	NS	Positive direction NORTH	x	x
SP03	top of support structure	EW	Short leg		x
SP04	top of support structure	NS	Mid Axis		x
SP05	bottom of bushing	EW	Positive direction EAST horizontal		x
SP06	bottom of bushing	NS	Positive direction NORTH		x
SP07	extension platforrm	EW-N	Connect to refrence frame		x
SP08	extension platforrm	EW-S	Connect to refrence frame		x
SP09	extension platforrm	NS	Connect to refrence frame		x
d1	potentio meter	d1	potentio meter between bushing and frame		x
LED - KRYPTON					
LED01	West side on porcelain		As close as posible to the edge		x
LED02	West side on flange		As close as posible to the edge		x
LED03	Center on porcelain		As close as posible to the edge		x
LED04	Center on flange		As close as posible to the edge		x
LED05	East side on porcelain		As close as posible to the edge		x
LED06	East side on flange		As close as posible to the edge		x
LoadCells					
LC01	250 lbs pull at top	EW/NS	For pull and quick release at top	x	
			Total Channels of instrumentation	11	33

Figure B-29: Instrumentation on Frame – Bushing #8

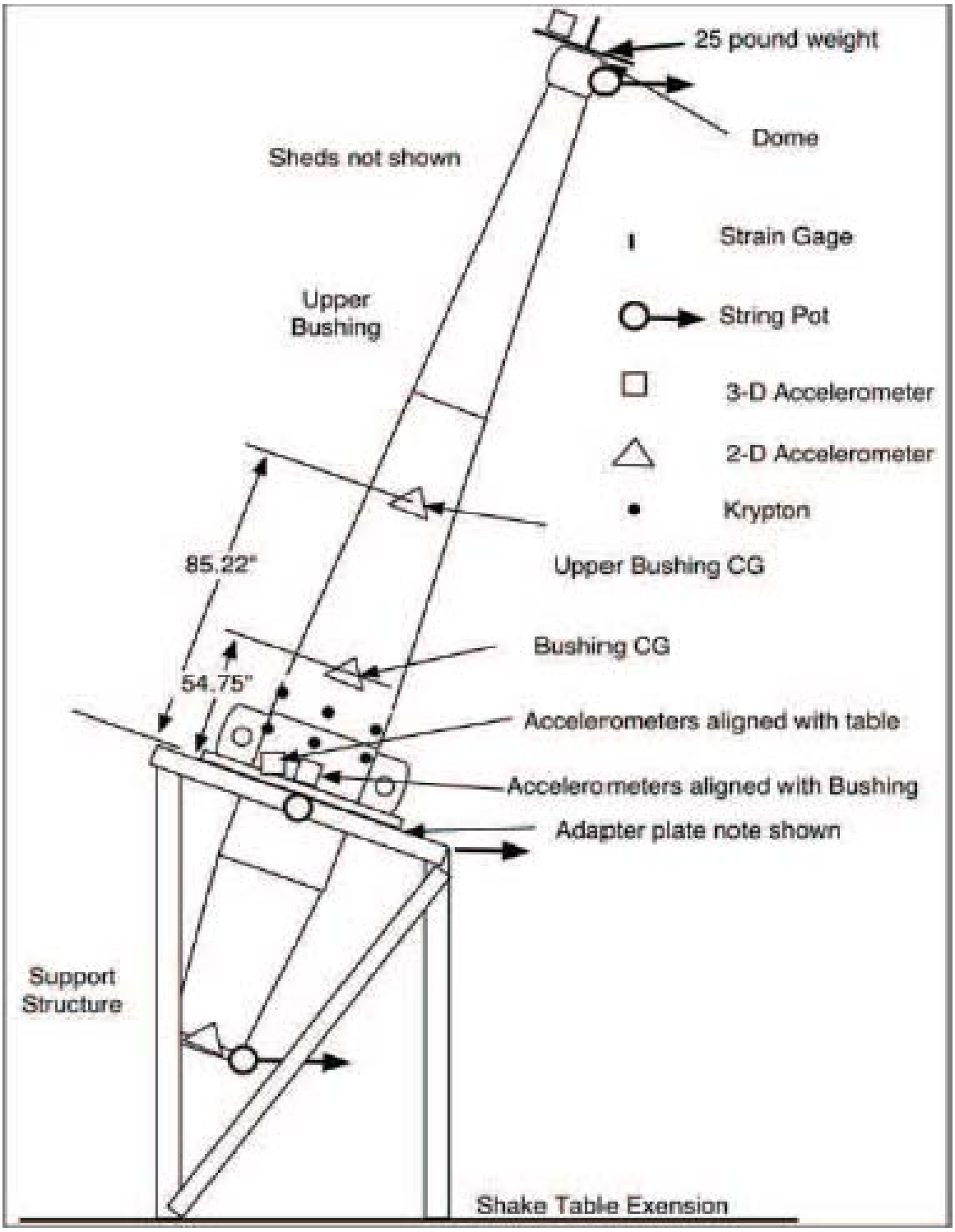

Figure B-30: Instrumentation on Fixed Base – Bushing #8

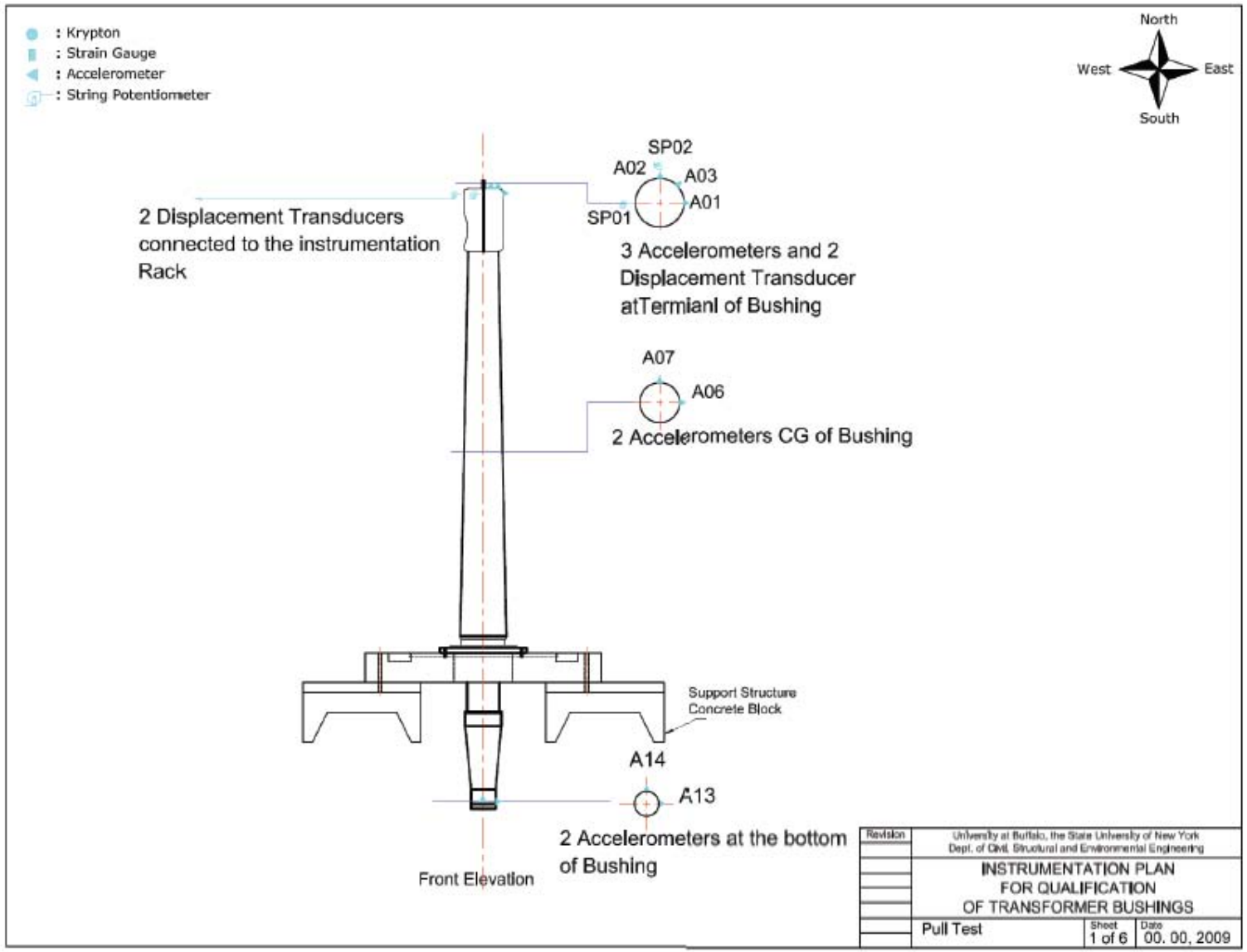

Figure B-31: Instrumentation on Frame – Bushing #8

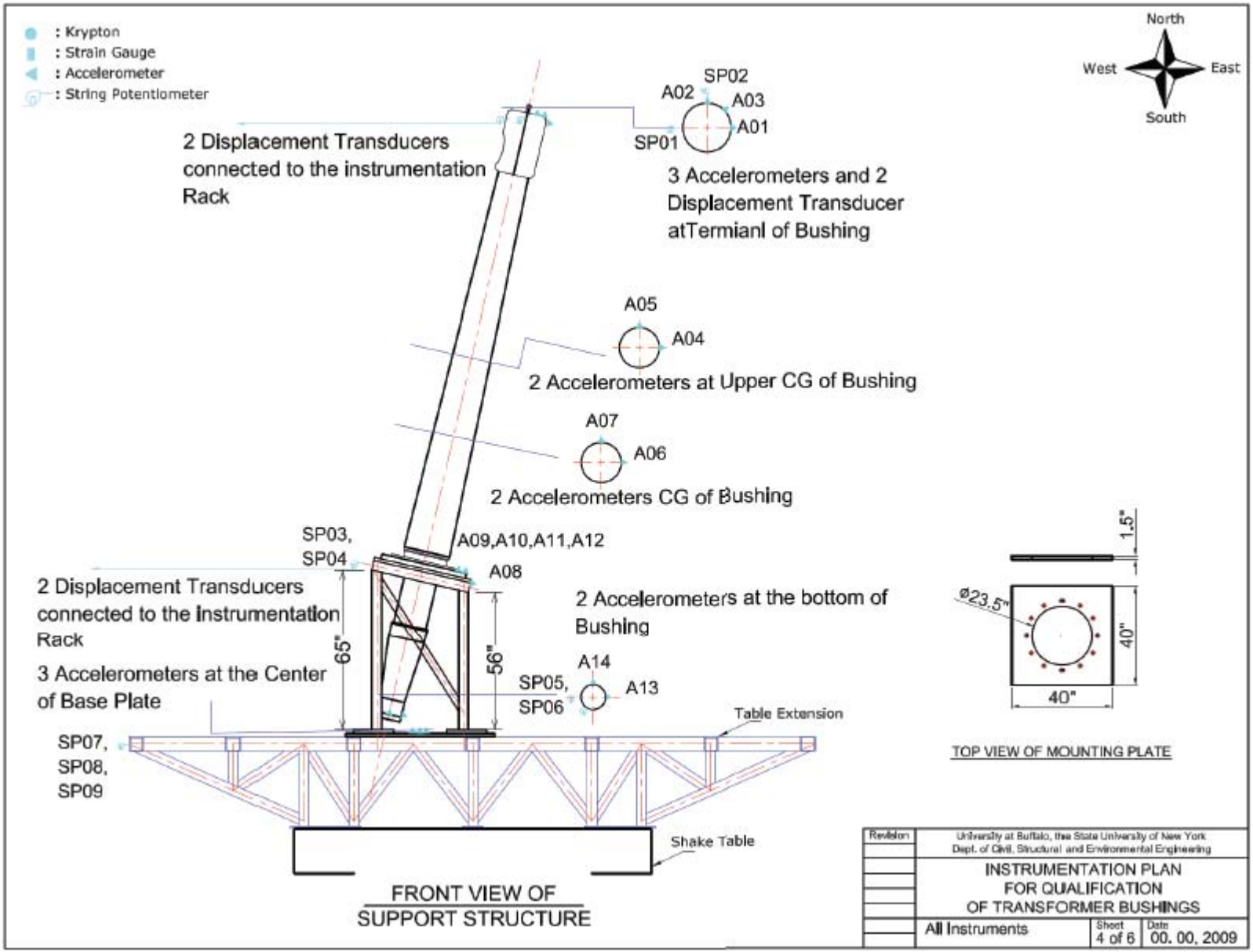

Figure B-32: Krypton™ Camera Setup – Bushing #8

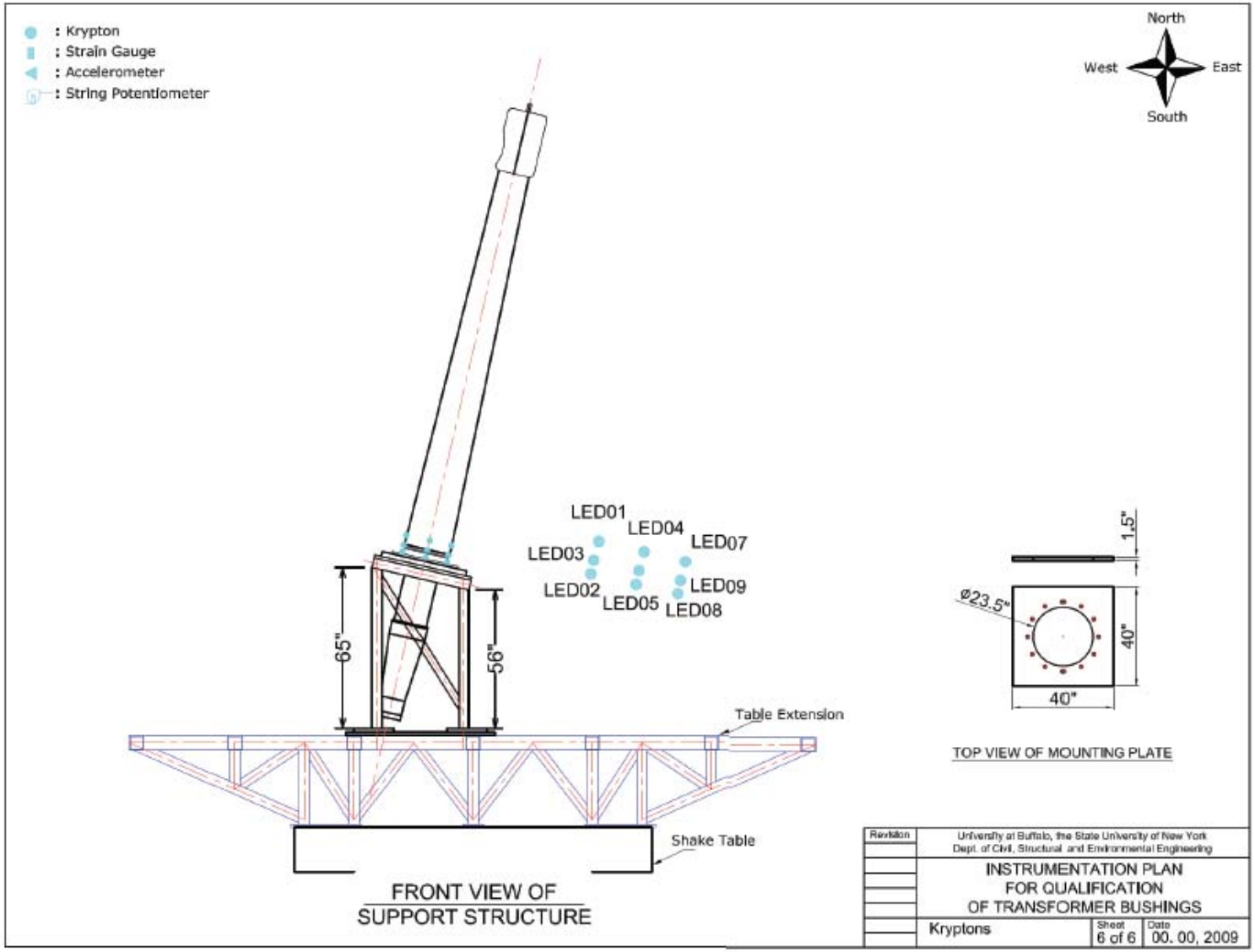

APPENDIX C:

INPUT HISTORY AND SPECTRA

This section describes the shake table motions used for testing of the various bushings. All the shake table motions were developed at SEESL at University at Buffalo to match the Required Response Spectrum (RRS) of IEEE 693-2005 using STEX with 24 lines per octave.

The acceleration history tests were named in the form of TBUxAH(xxx)(xx), in which:

1. TB stands for Transformer Bushing.
2. Ux stands for Unit Number of Bushing; some bushings had several units that were tested one after another, in same testing sequence.
3. AH(xxx) stands for Acceleration History at xxx intensity.
4. xx (the last set of numbers) is the test number in a sequence.

For example, the designation TBU1AH12525 means Transformer Bushing, Unit #1, Acceleration History Testing at the Peak Acceleration of 0.125 g, in the 25th test of the sequence.

In addition, the charts show the directions of motion N (North-South with North positive), E (East-West with East positive), and U (Vertical positive Upwards).

The spectral lines show the RRS and the range as –5% (lower line) to +30% (upper line).

The test protocols, including test sequences and test logs, shown in Appendix A, link the names of the tests with the test sequences and special conditions.

Test Response Spectra of Bushing #4A

Bushing #4A was a composite bushing. The main objective of the testing was to determine the changes in frequency and direction of free vibration when the bushing is mounted at different locations on the support frame. Furthermore, the effect of stiffening the base mount of the bushing was incorporated into the testing. Figures C-1 – C-5 show the acceleration histories and the Test Response Spectra (TRS) for Bushing #4A.

Figure C-1: Test Response Spectra of TBU1AH12525 – Bushing #4A Mounted at Center with 2 Stiffeners

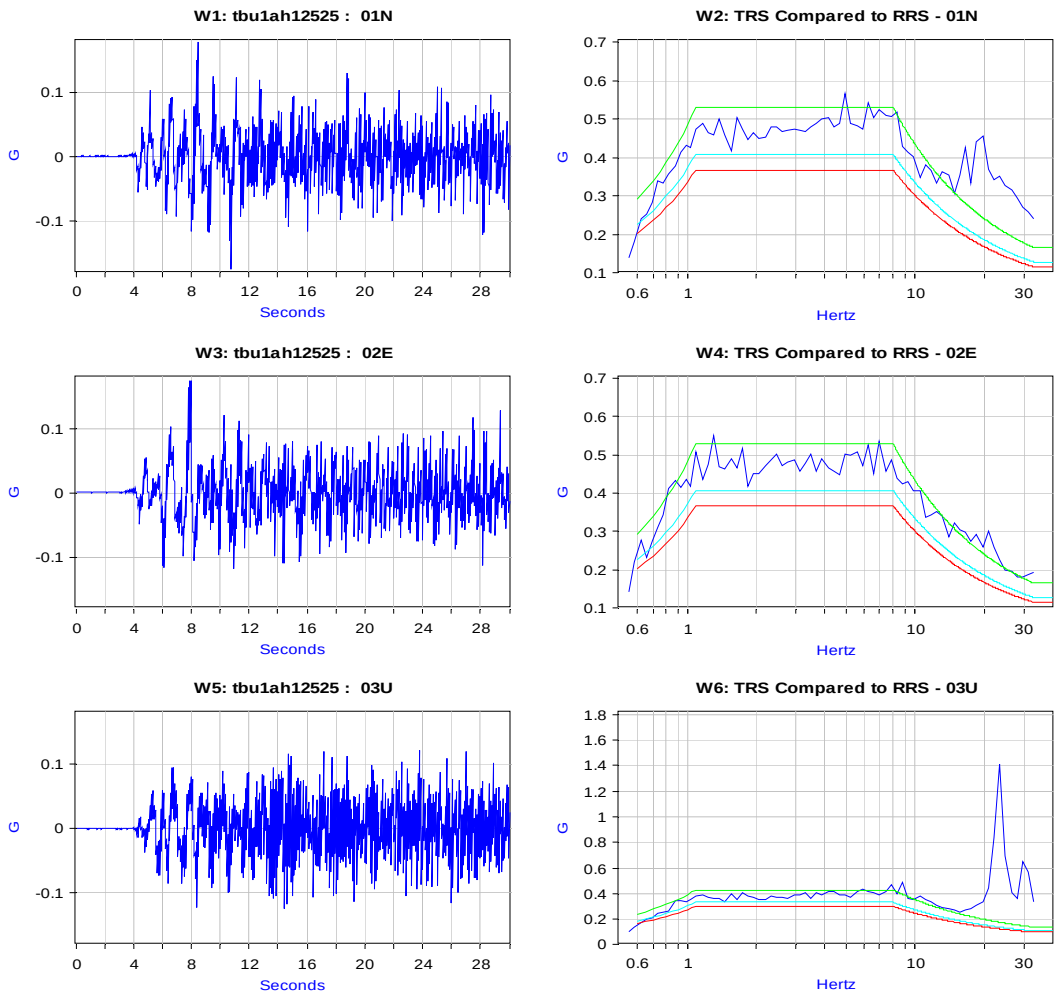

Figure C-2: Test Response Spectra of TBU1AH12530 – Bushing #4A Mounted at Side with 2 Stiffeners

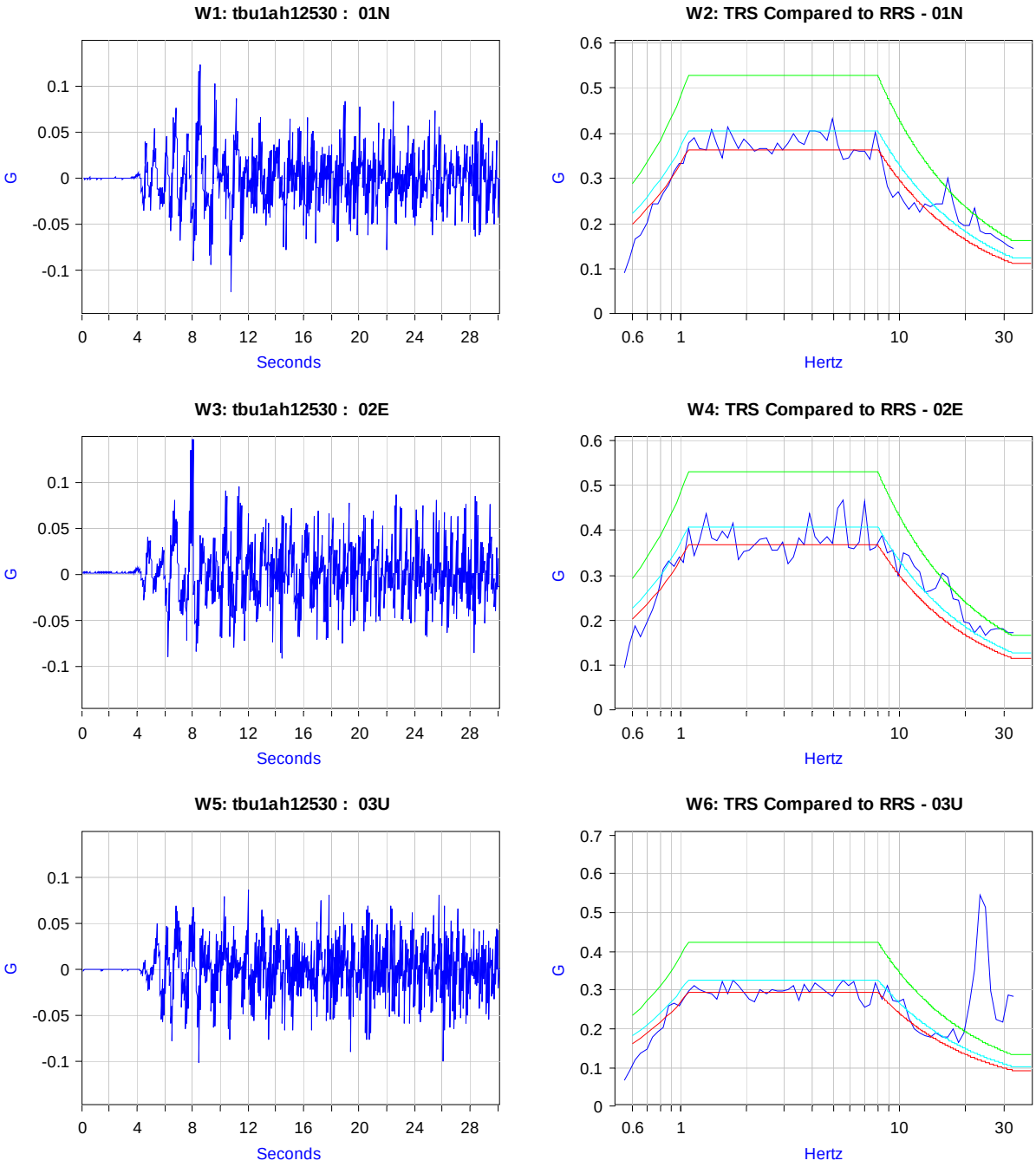

Figure C-3: Test Response Spectra of TBU1AH12535 – Bushing #4A Mounted at Side without Stiffeners

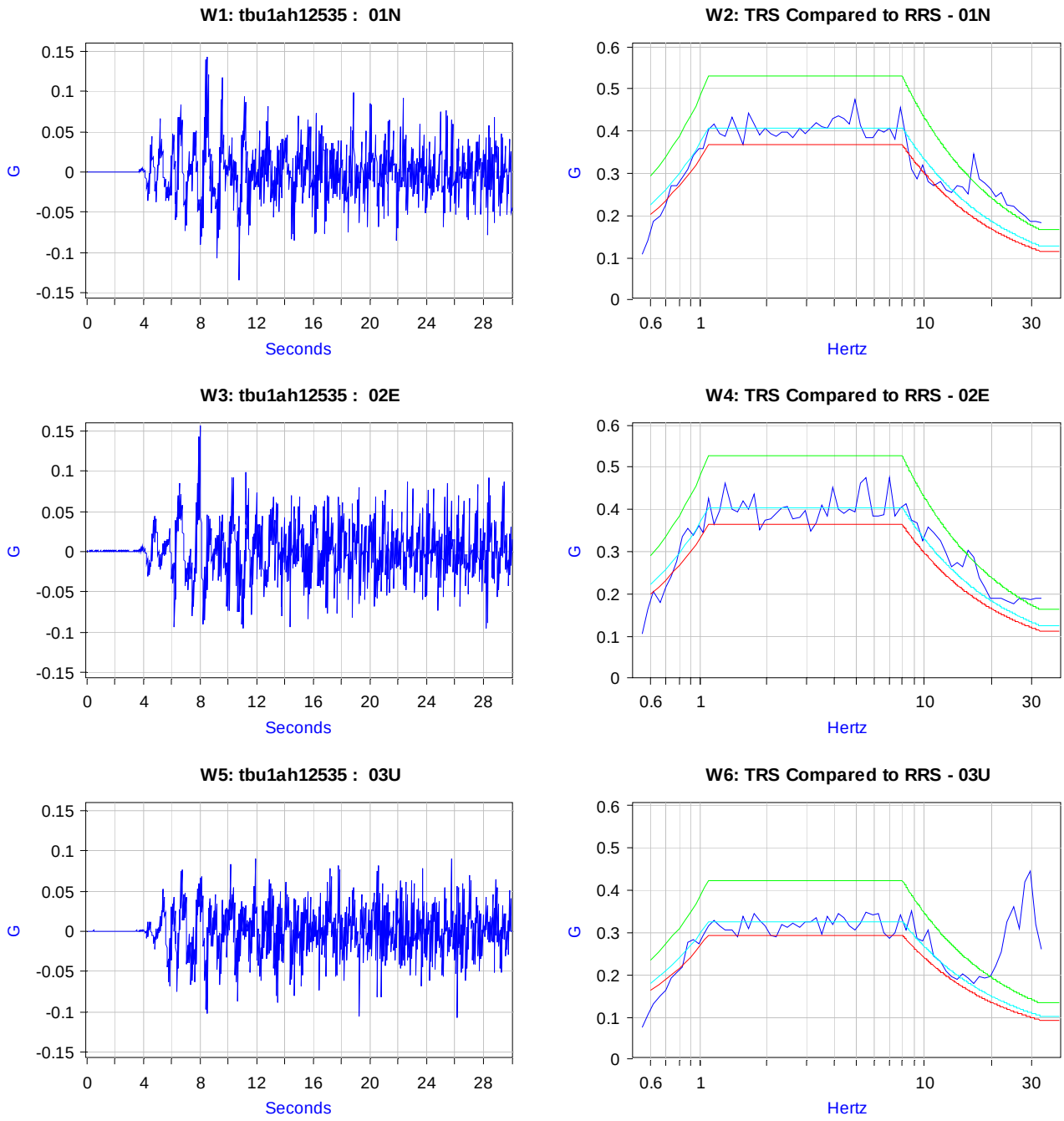

Figure C-4: Test Response Spectra of TBU1AH12540 – Bushing #4A Mounted at Corner without Stiffeners

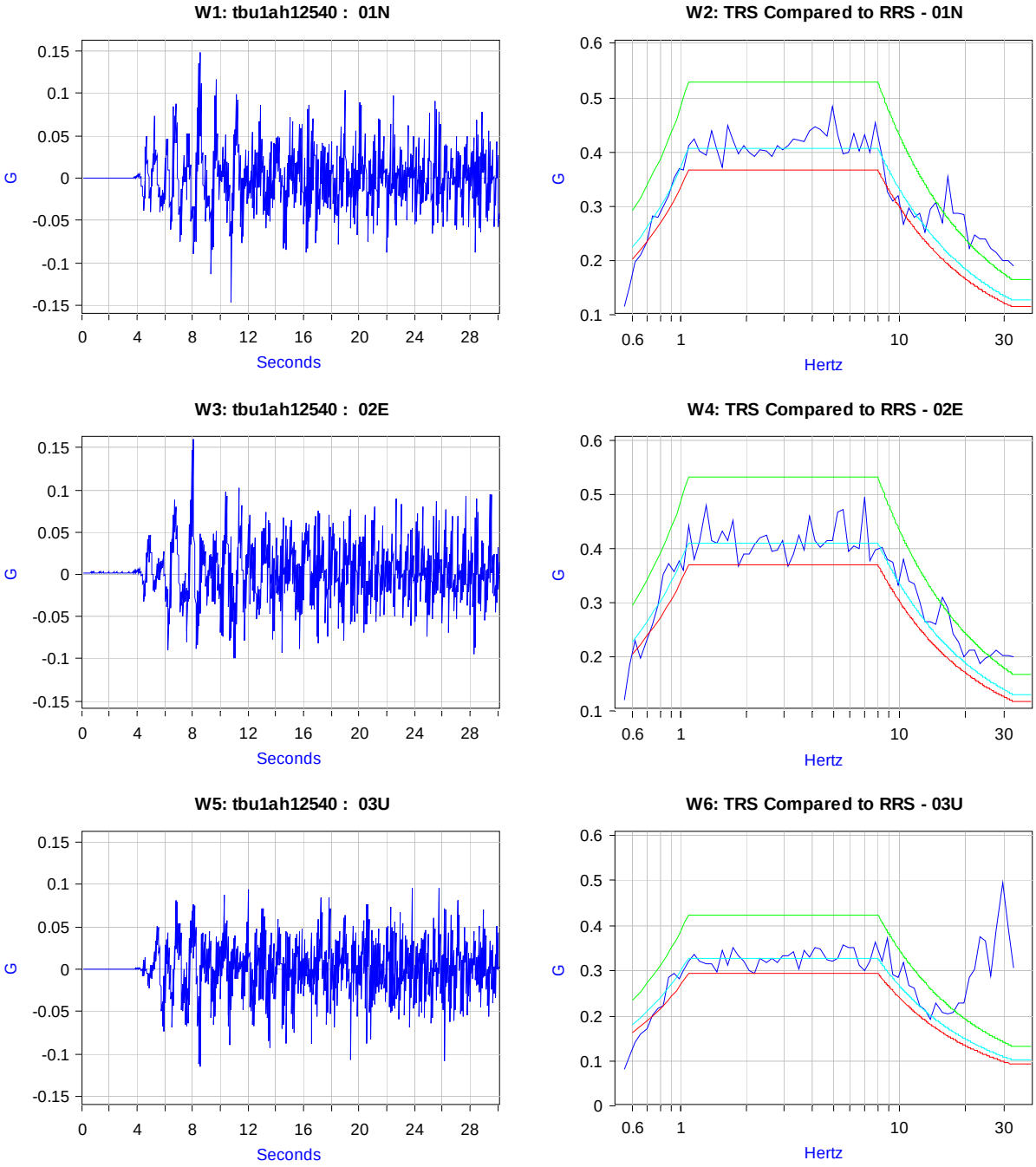

Figure C-5: Test Response Spectra of TBU1AH12545 – Bushing #4A mounted at corner with One Stiffener

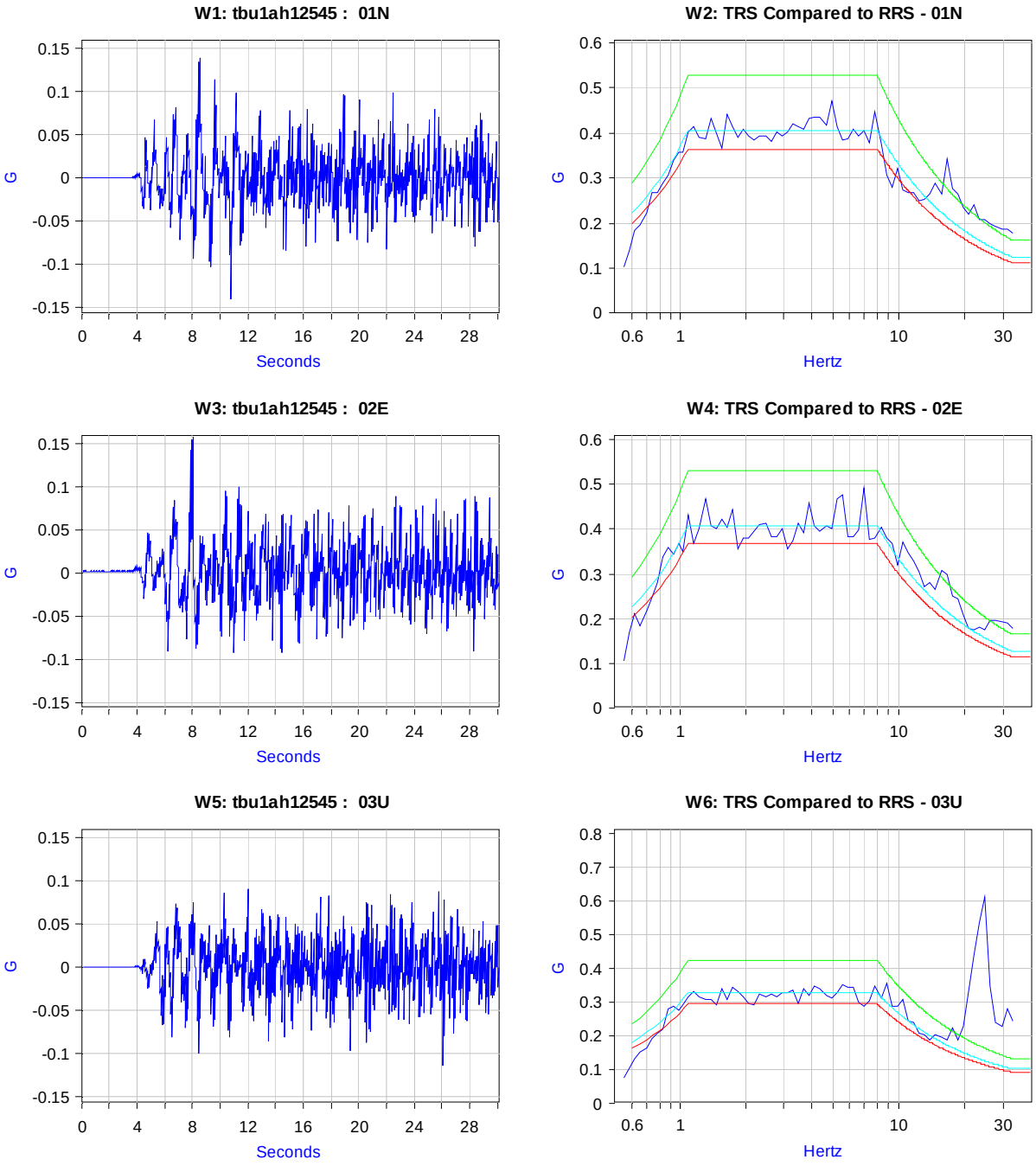

Test Response Spectra of Bushing #4B

Bushing #4B was also a composite bushing, with similar construction to but lighter in weight than Bushing #4A. The accelerations and the Test Response Spectra (TRS) for Bushing #4B are shown in Figures C-6 – C-9.

Figure C-6: Test Response Spectra of TBU2AH2520 – Bushing #4B Mounted in Center

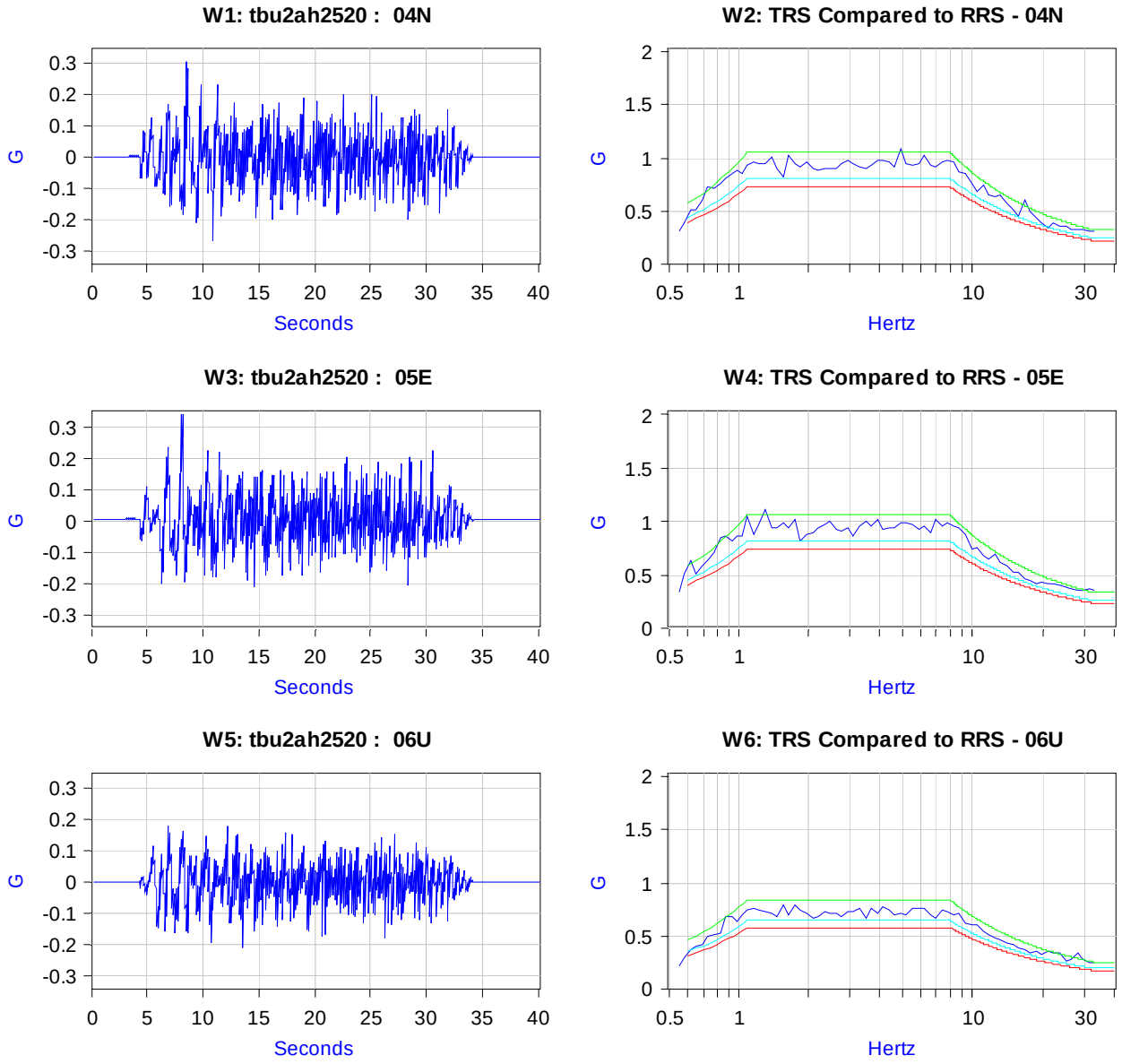

Figure C-7: Test Response Spectra of TBU2AH5023 – Bushing #4B Mounted in Center

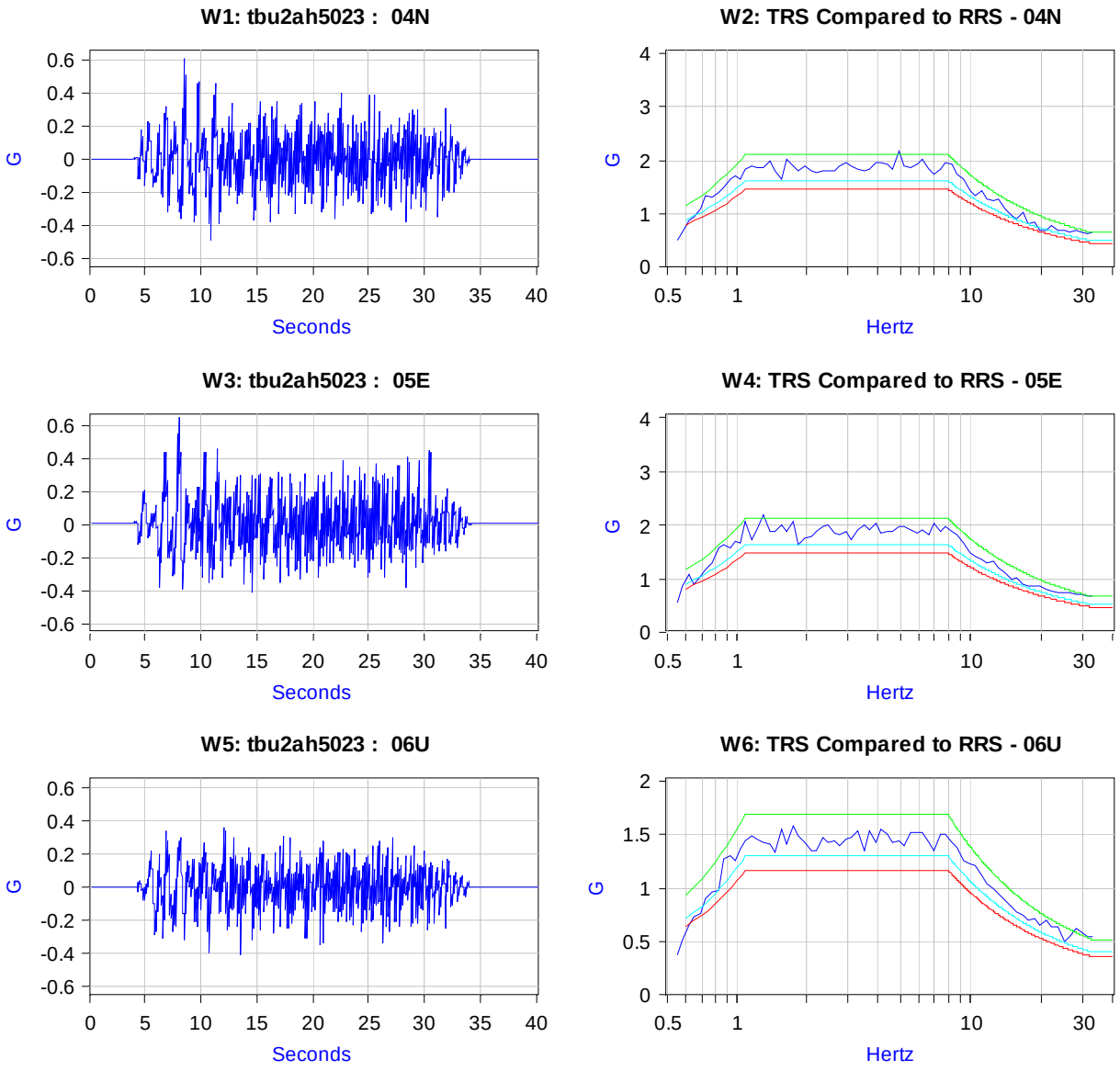

Figure C-8: Test Response Spectra of TBU2AH10026 – Bushing #4B Mounted in Center

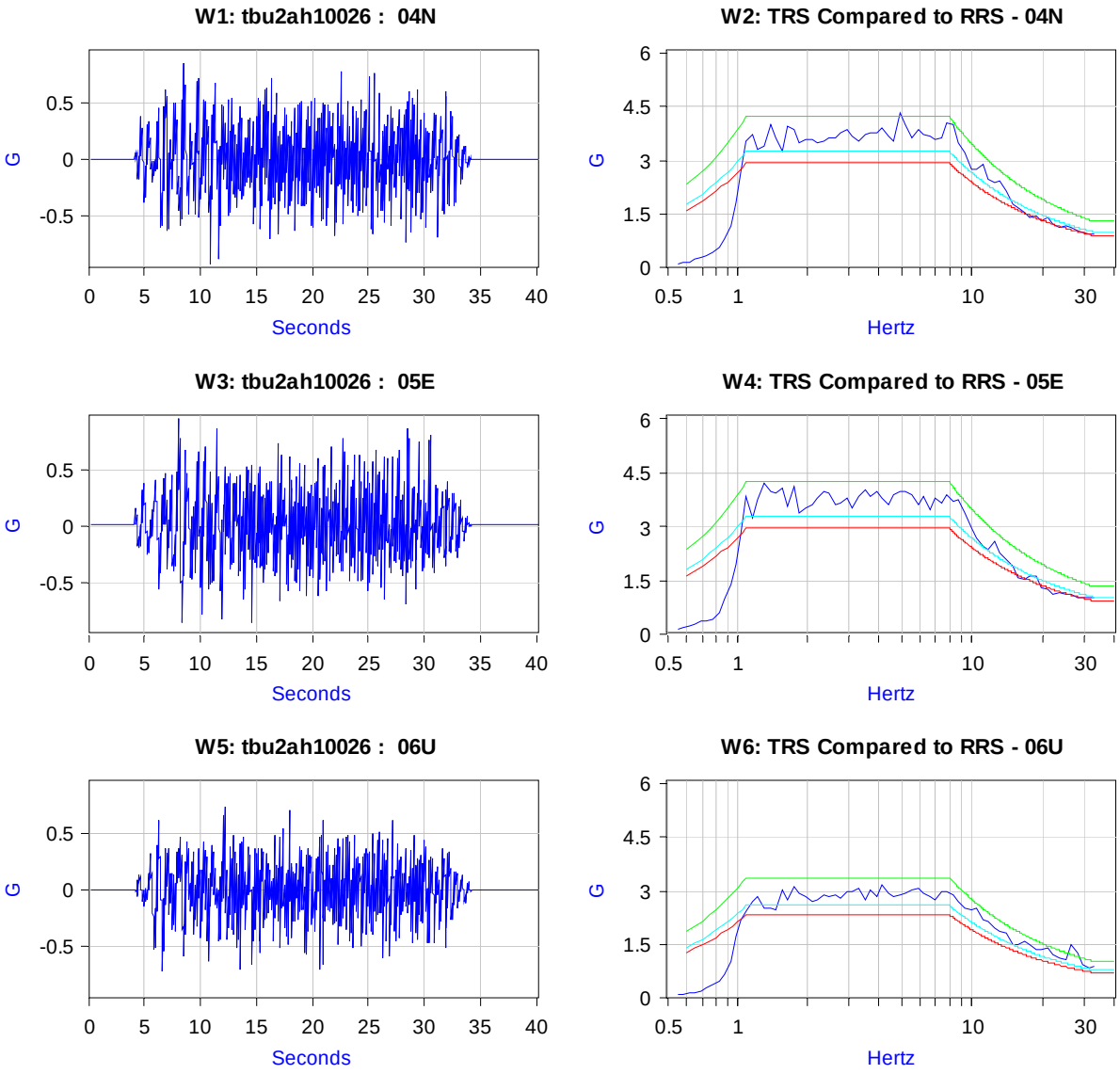

Figure C-9: Test Response Spectra of TBU2AH20029 – Bushing #4B Mounted in Center

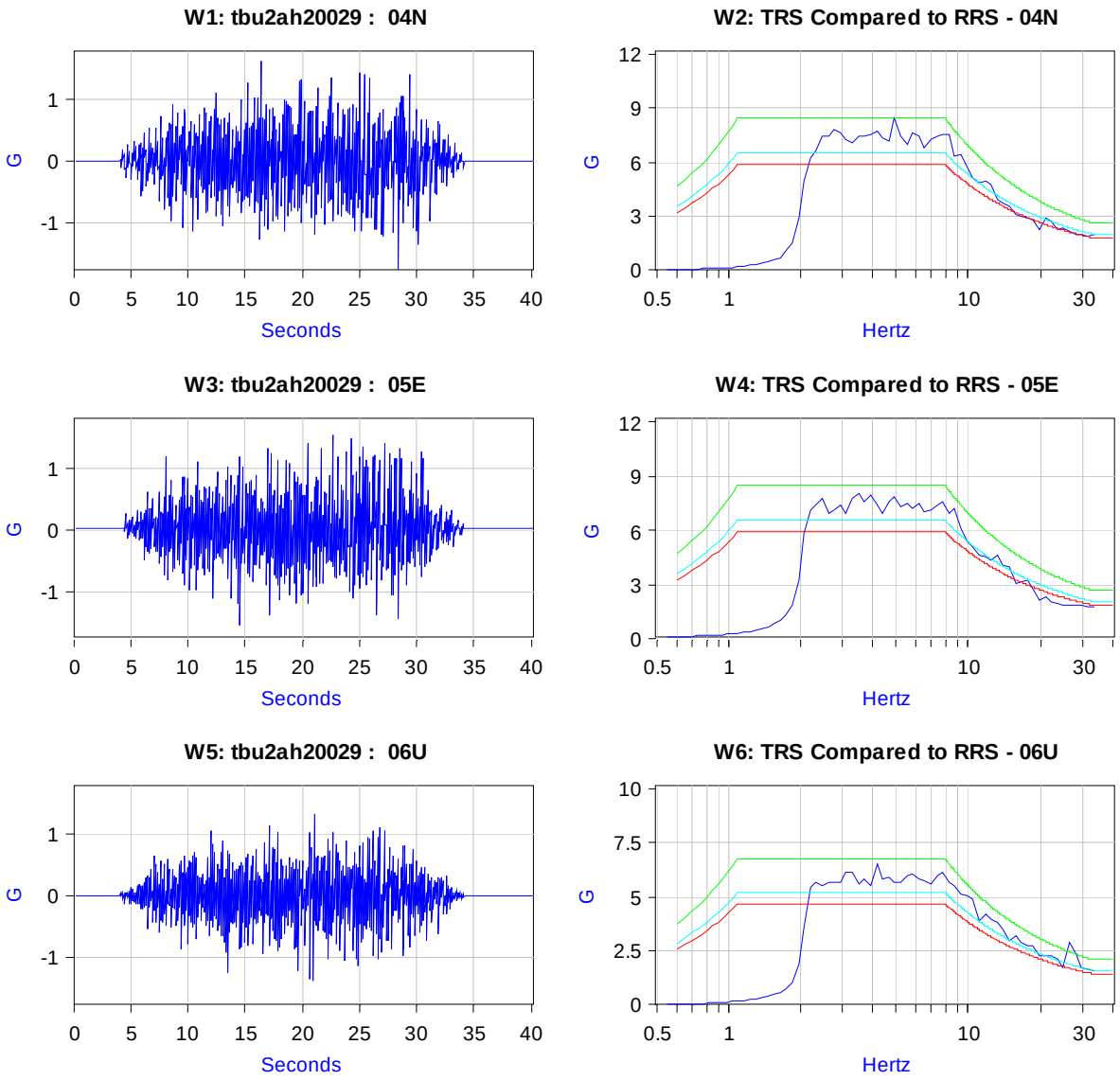

Test Response Spectra of Bushing #5

Bushing #5 is a 500 kV composite bushing. The bushing was tested at various locations on the support frame. The accelerations and the Test Response Spectra (TRS) for Bushing #5 are shown in Figures C-10 – C-15.

Figure C-10: Test Response Spectra of TB35AH025 – Bushing #5 Mounted in Center

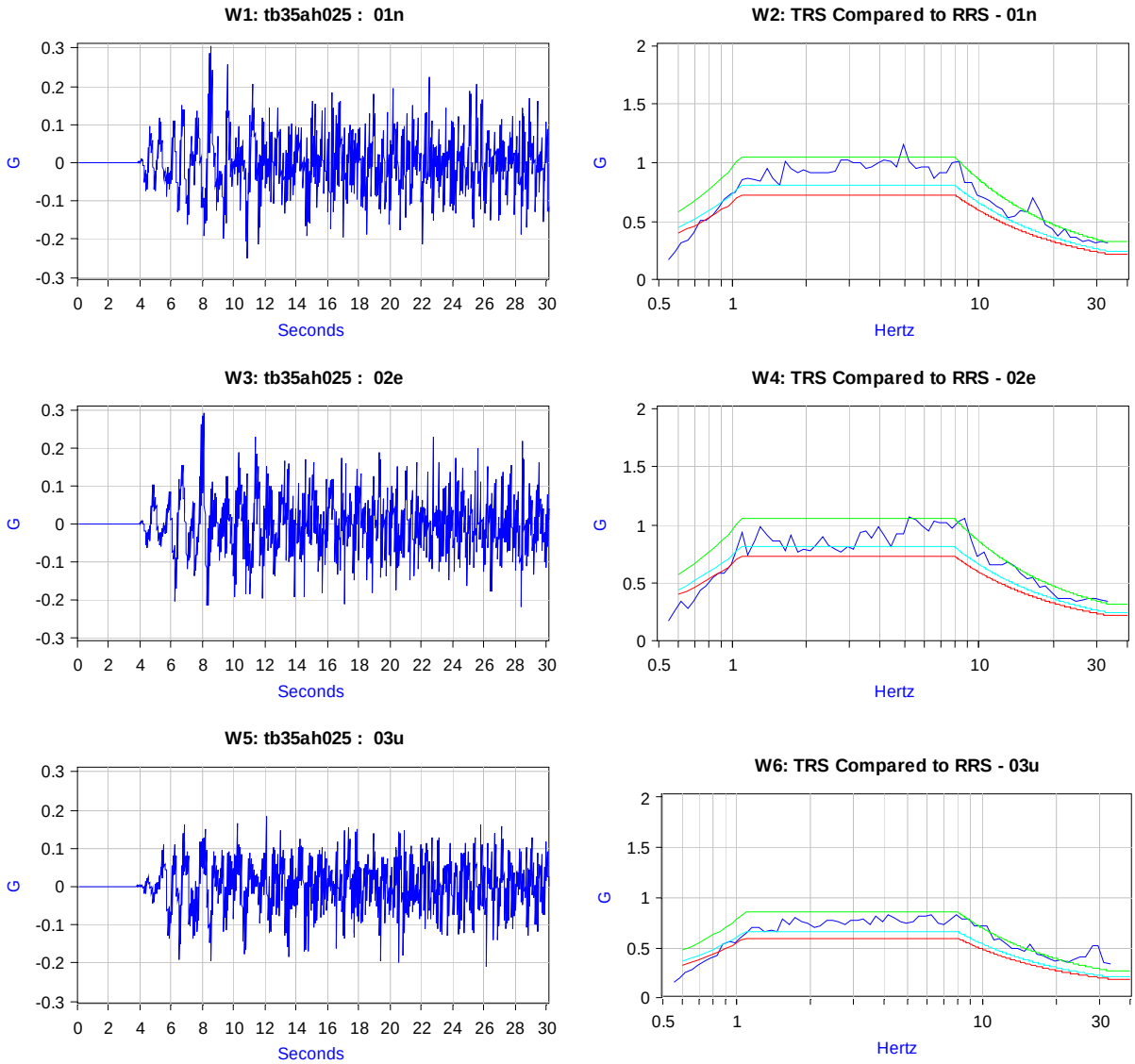

Figure C-11: Test Response Spectra of TB38AH050 – Bushing #5 Mounted in Center

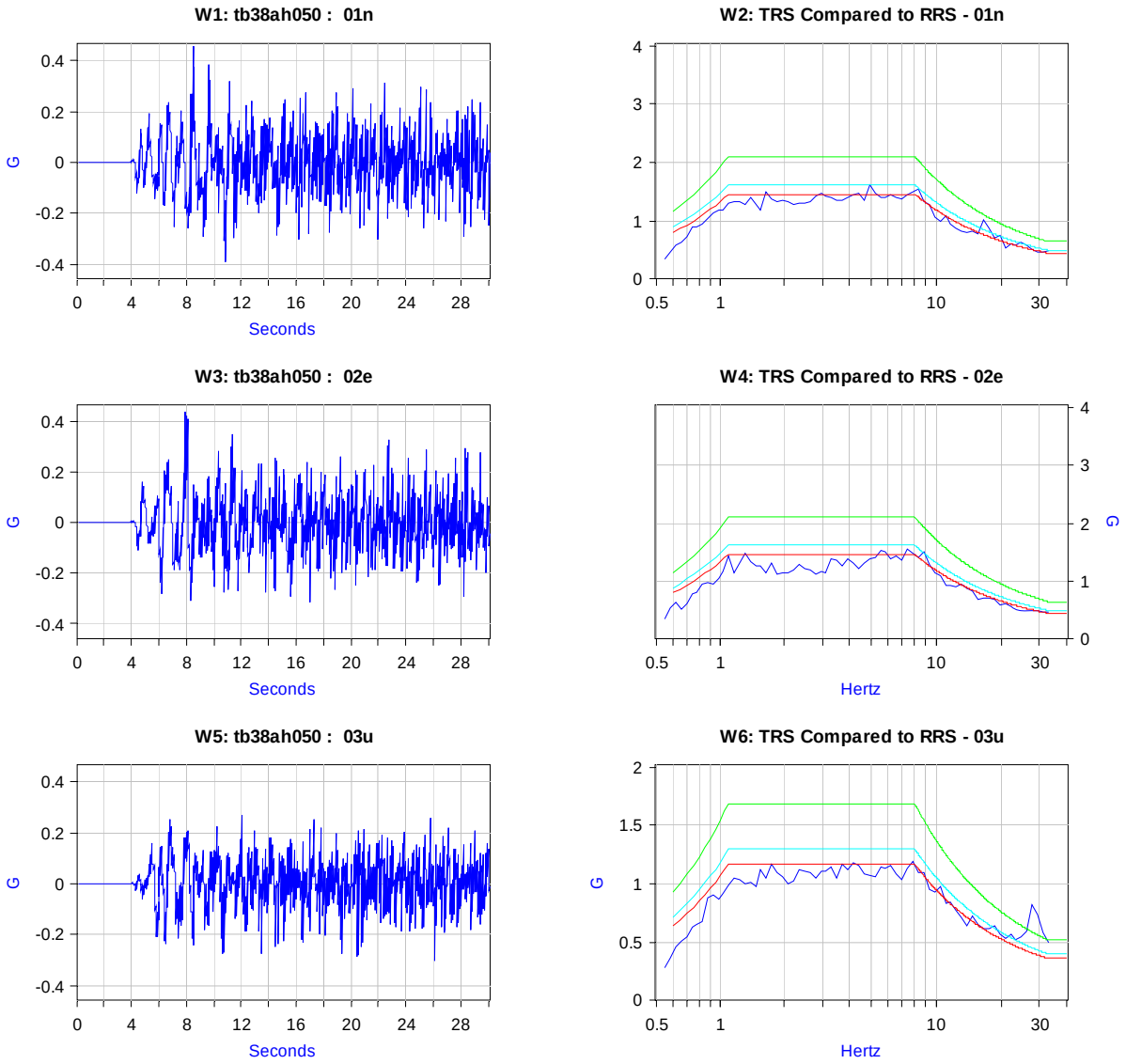

Figure C-12: Test Response Spectra of TB41AH100 – Bushing #5 Mounted in Center

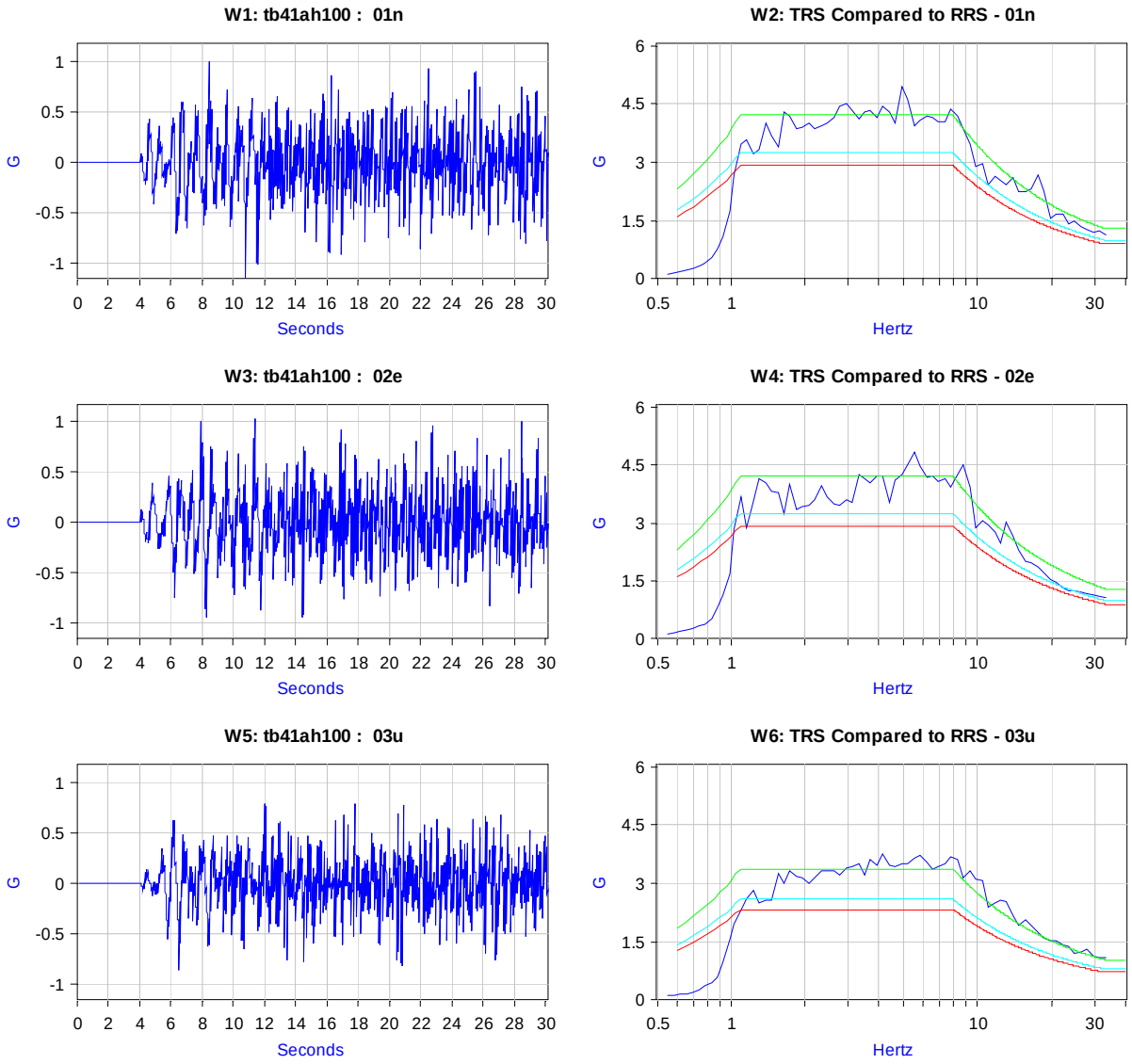

Figure C-13: Test Response Spectra of TB44AH200 – Bushing #5 Mounted in Center

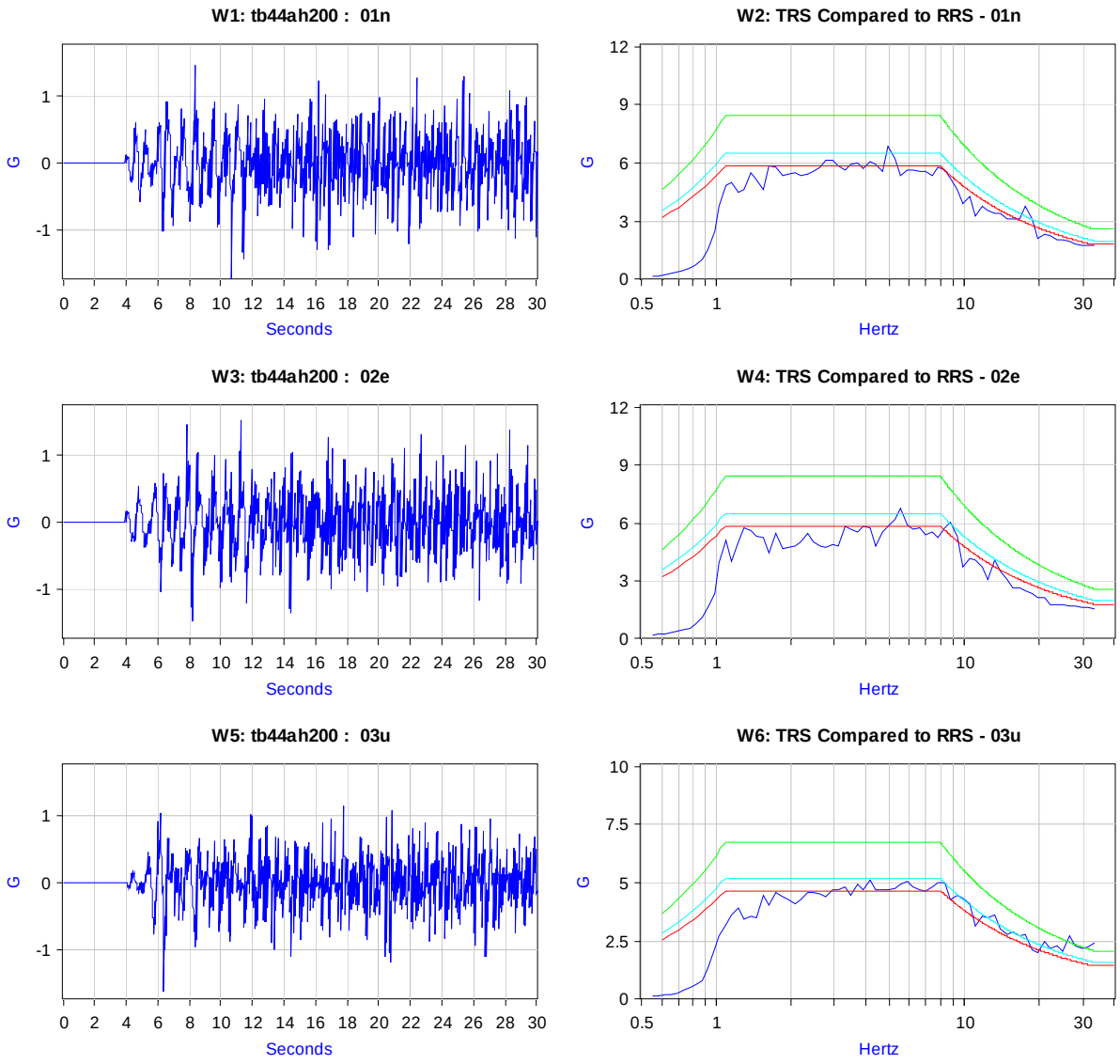

Figure C-14: Test Response Spectra of TB47AH250 – Bushing #5 Mounted in Center

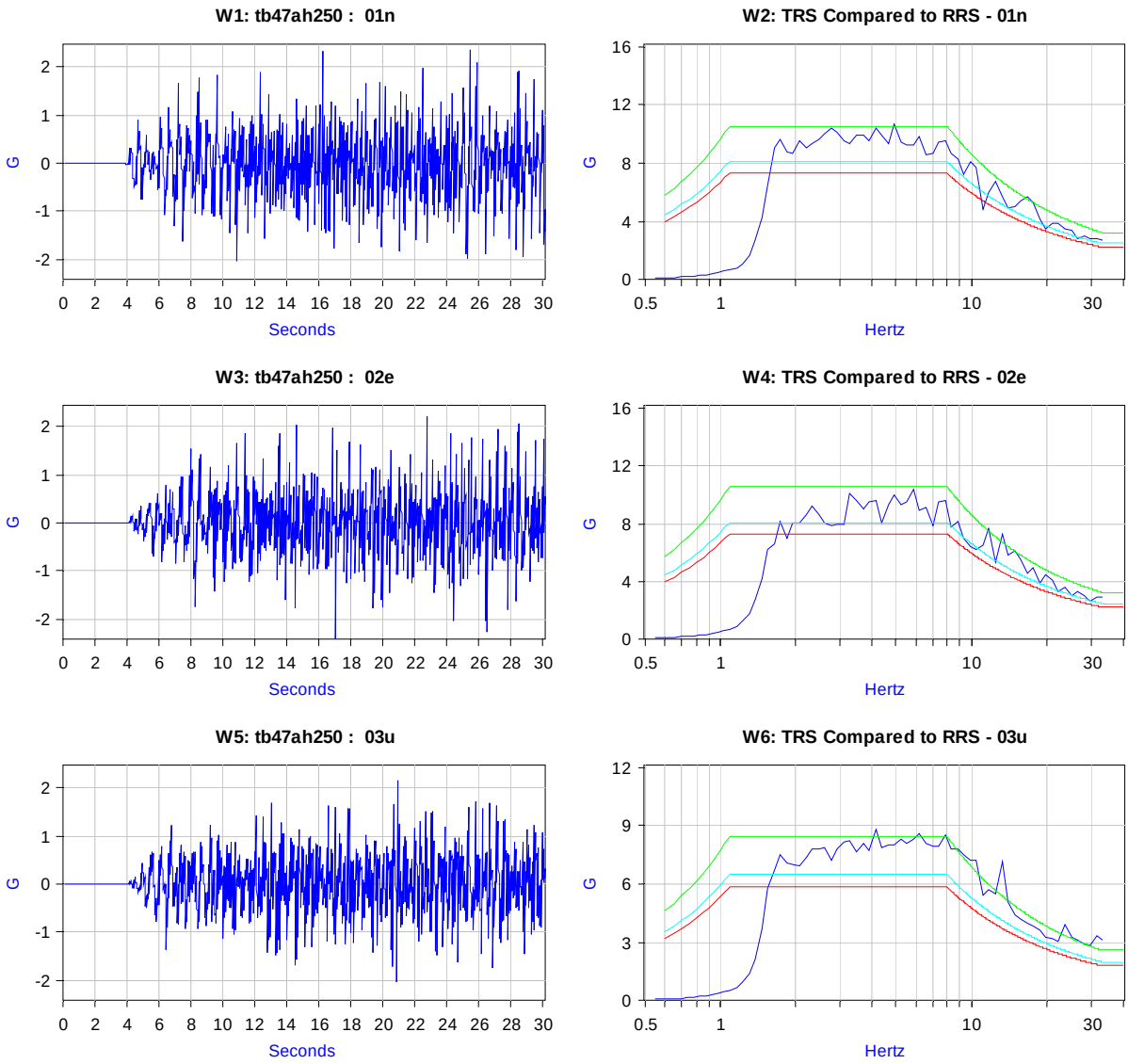

Figure C-15: Test Response Spectra of TB53AH300, Bushing #5 Mounted in Center

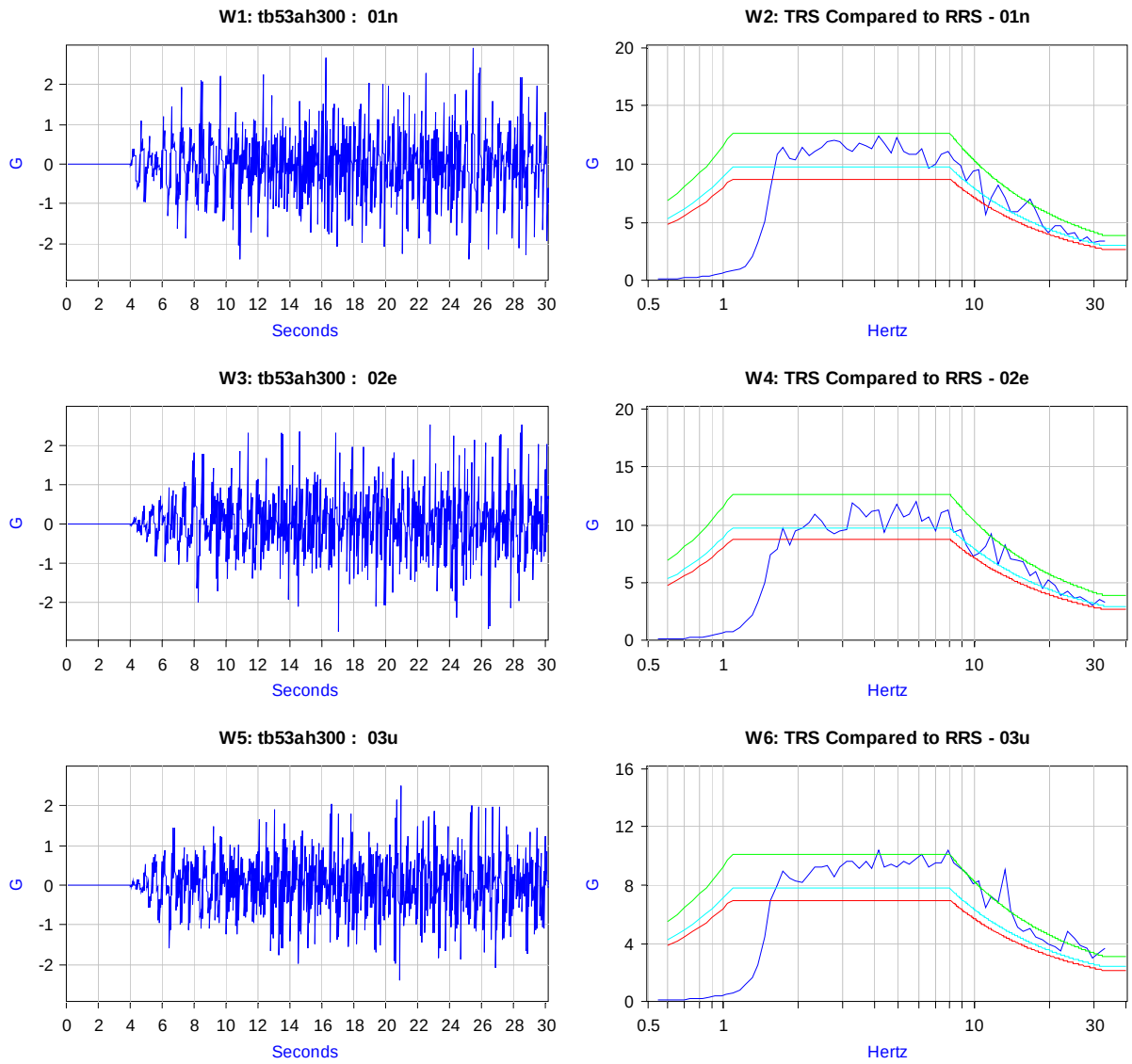

Test Response Spectra of Bushing #6

Bushing #6 is a porcelain bushing rated 230 kV. The magnitude of acceleration history was increased in successive tests. The response spectra obtained on the shake table extension are shown in Figures C-16 – C-33.

Figure C-16: Test Response Spectra of TB21AH025 – Bushing #6 Mounted in Center

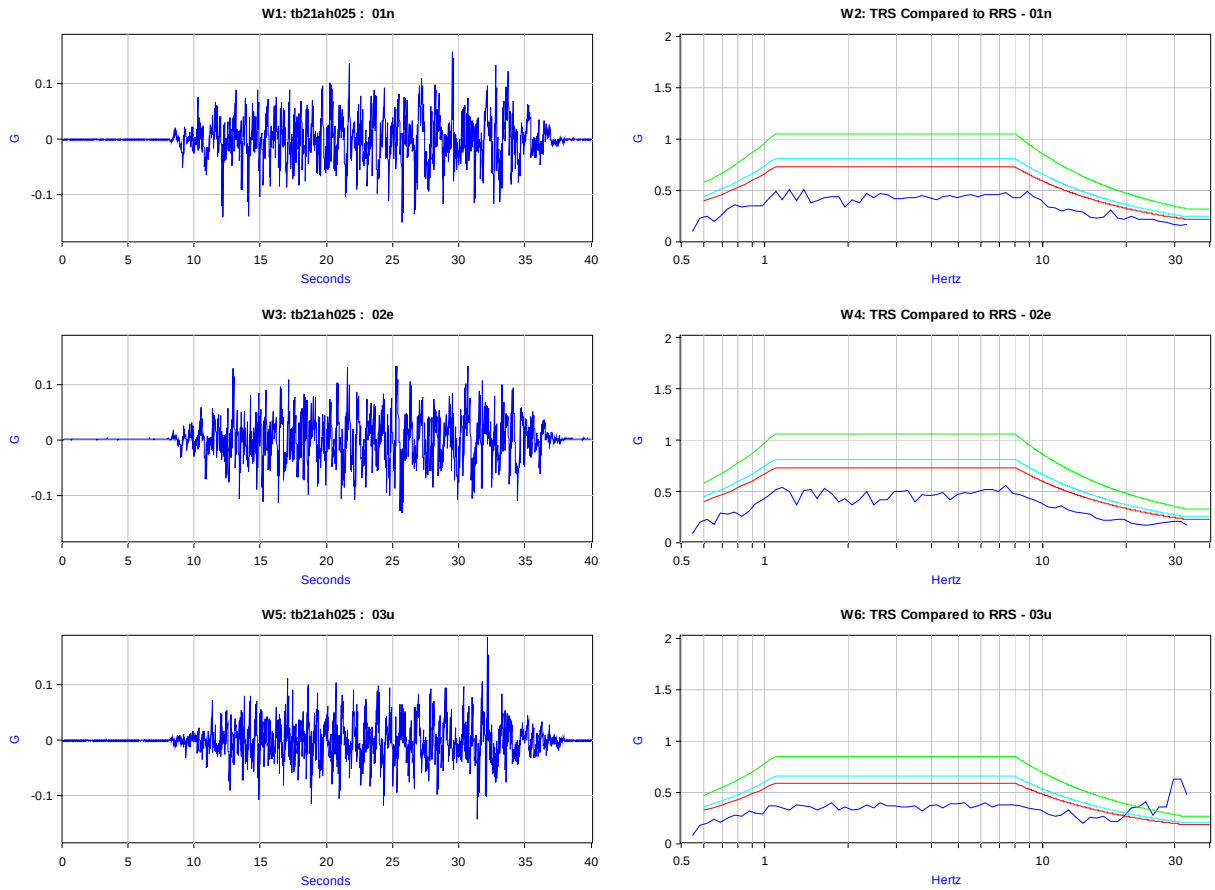

Figure C-17: Test Response Spectra of TB24AH025 – Bushing #6 Mounted in Center

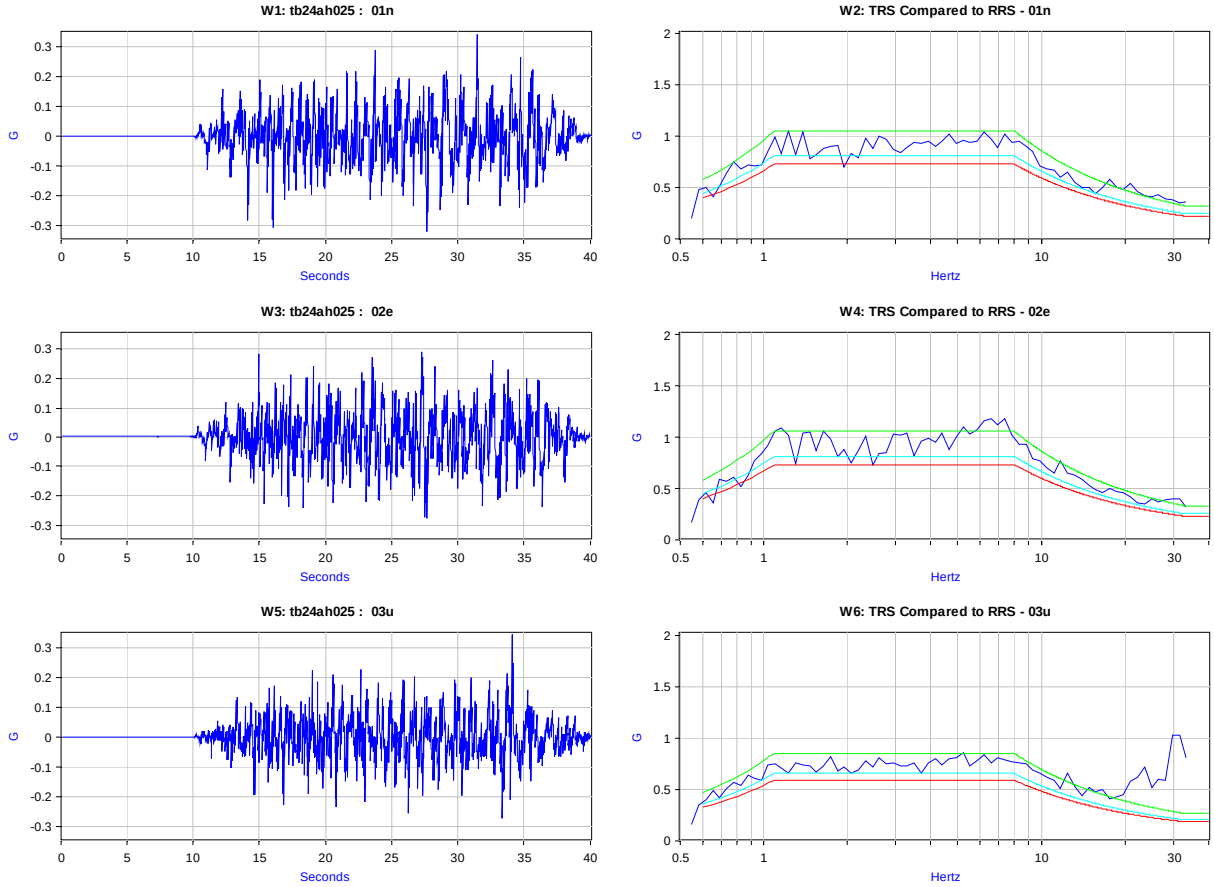

Figure C-18: Test Response Spectra of TB27AH050 – Bushing #6 Mounted in Center

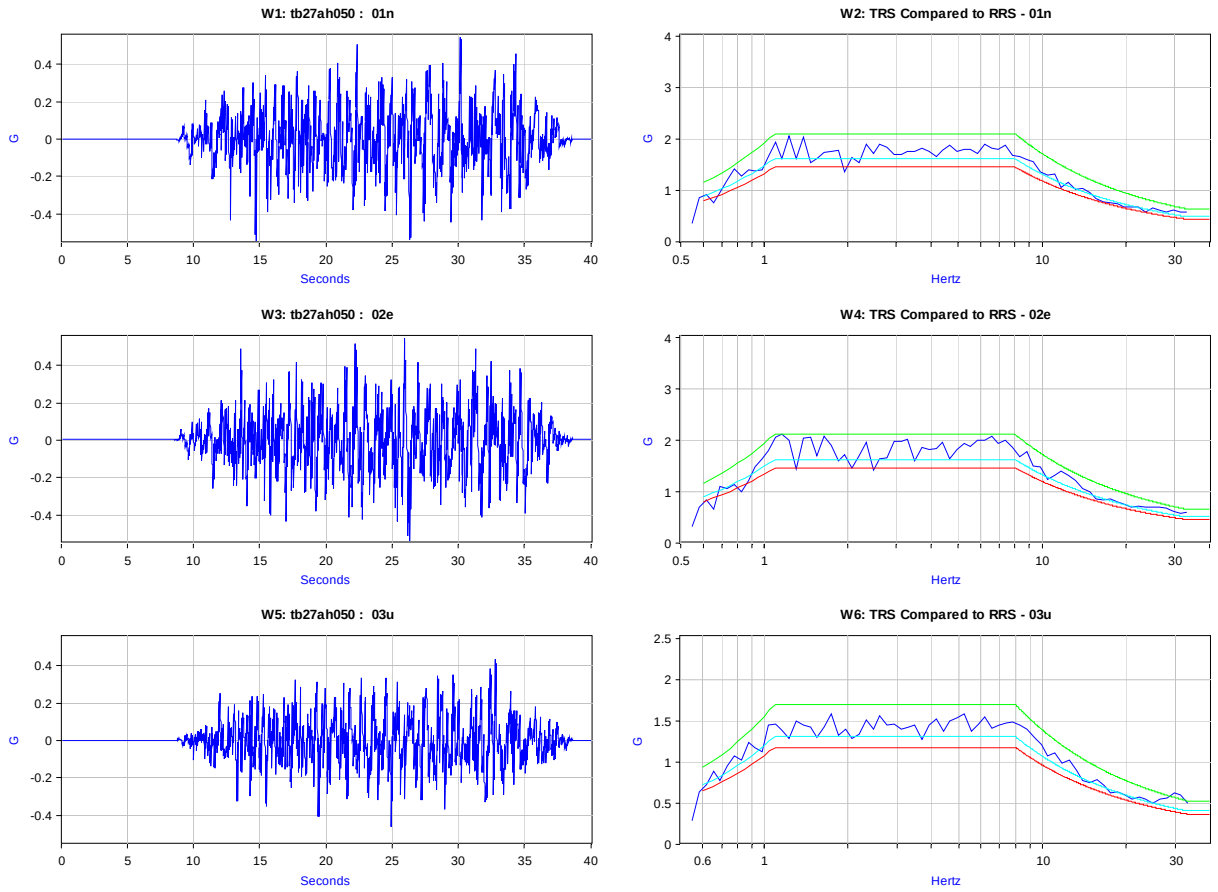

Figure C-19: Test Response Spectra of TB30AH075 – Bushing #6 Mounted in Center

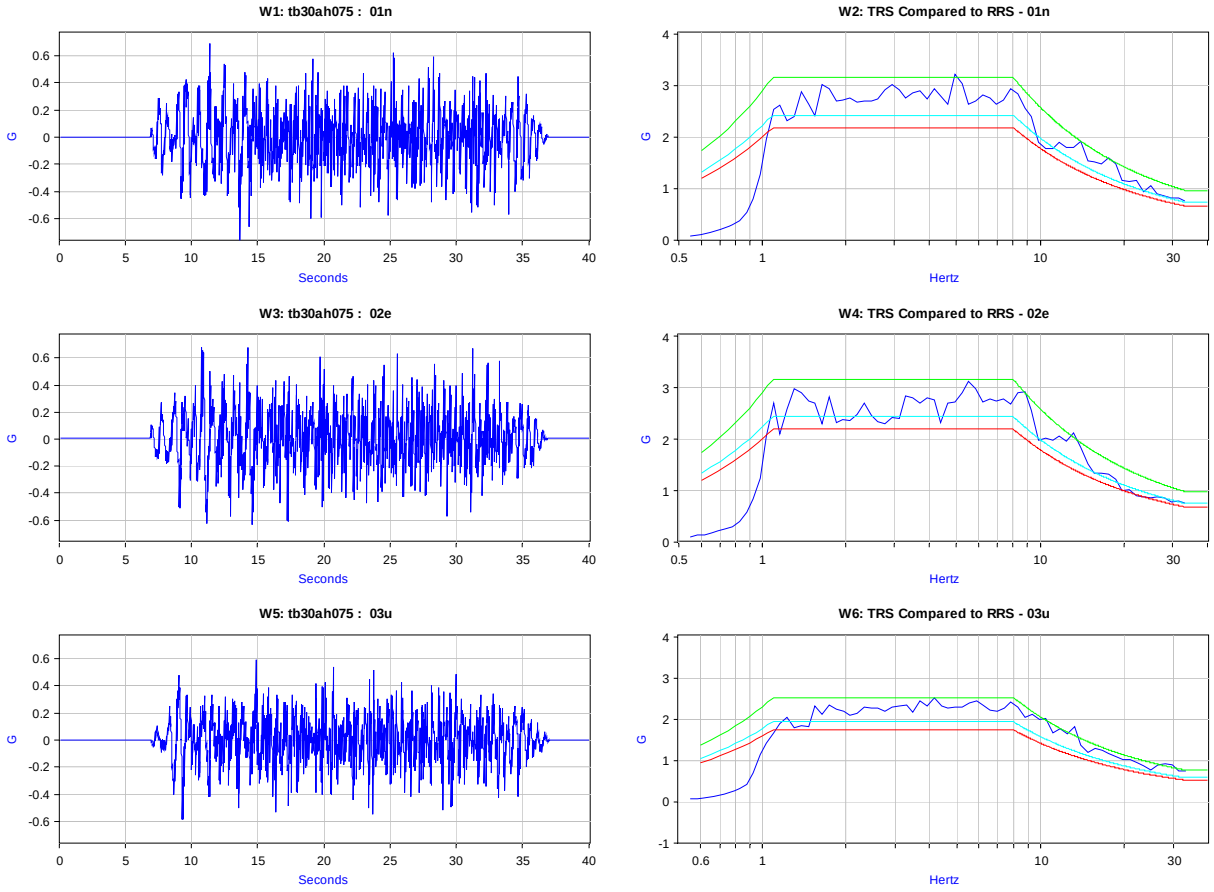

Figure C-20: Test Response Spectra of TB33AH100 – Bushing #6 Mounted in Center

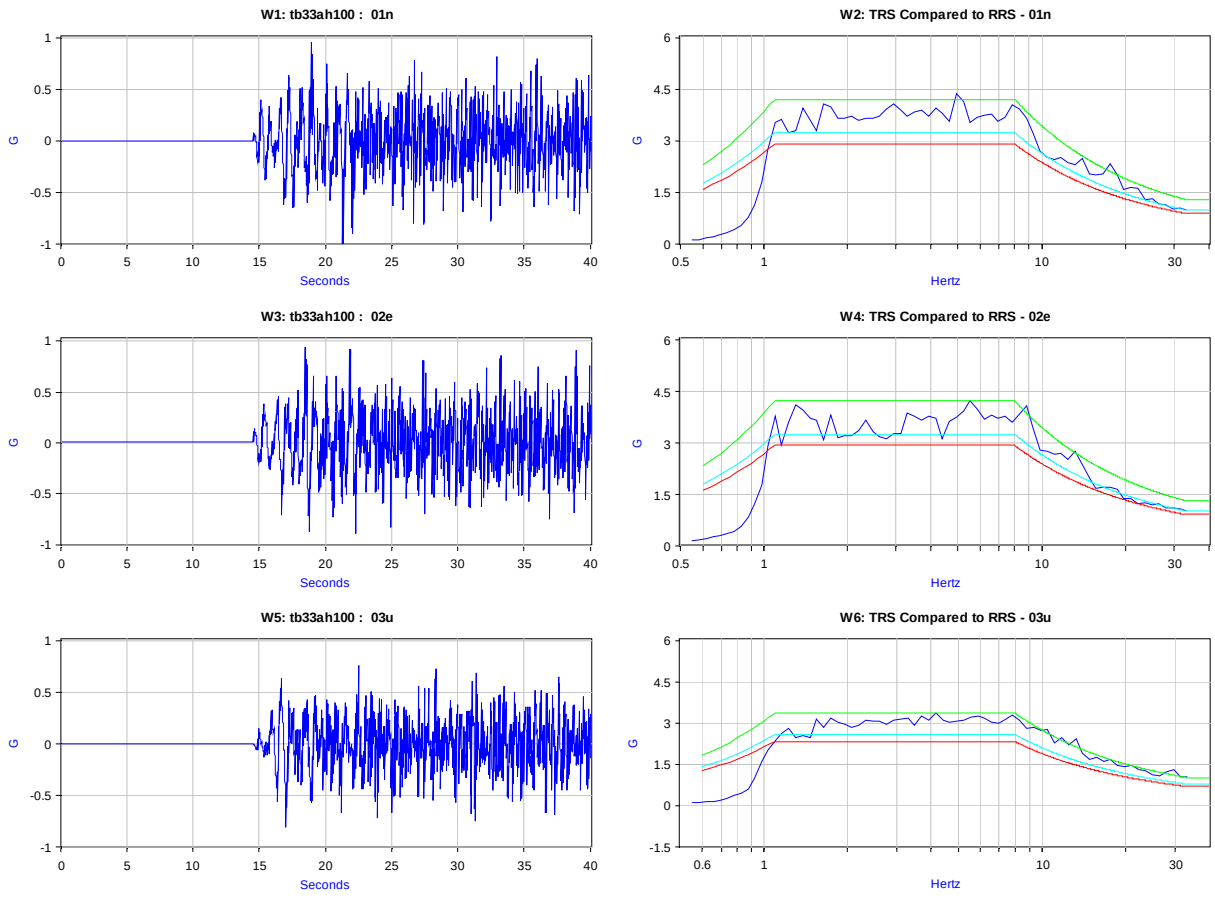

Figure C-21: Test Response Spectra of TB38AH125 – Bushing #6 Mounted in Center

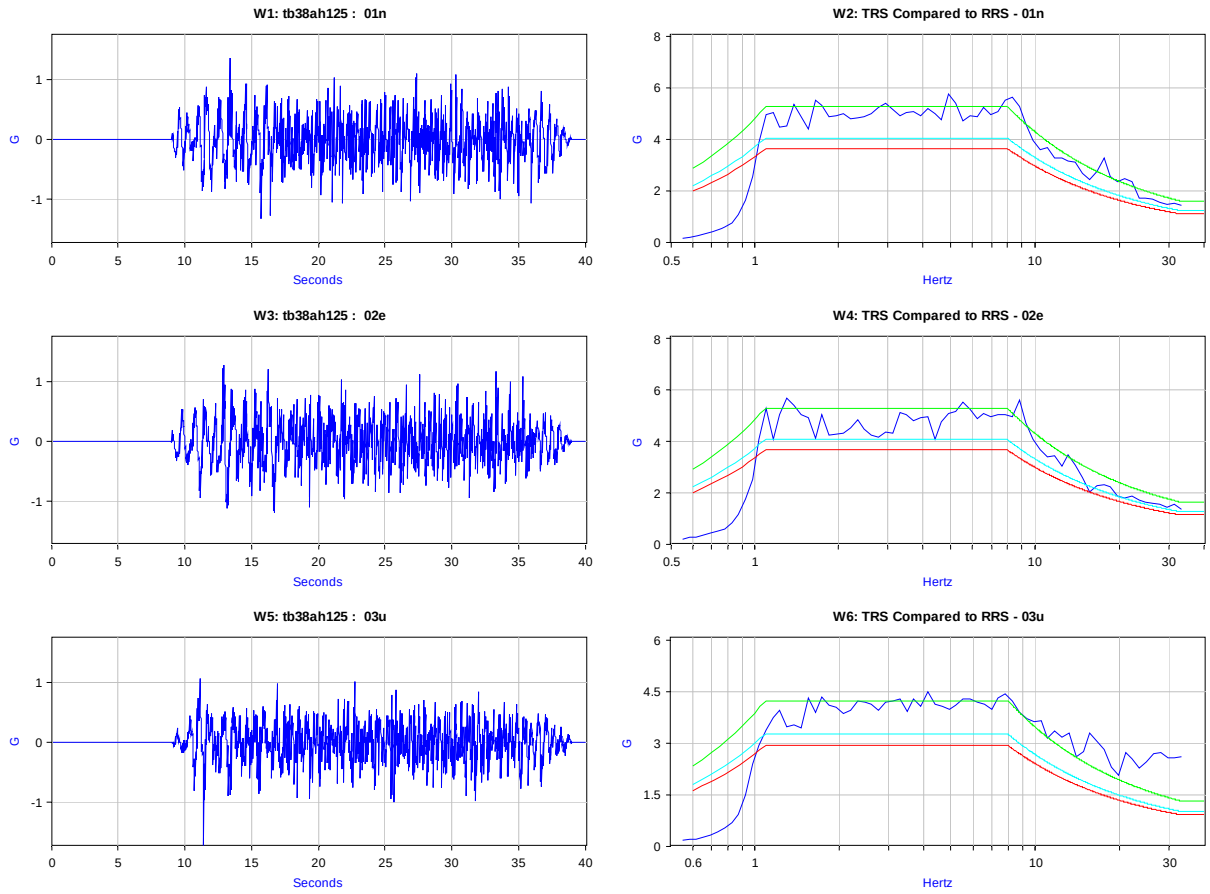

Figure C-22: Test Response Spectra of TB41AH150 – Bushing #6 Mounted in Center

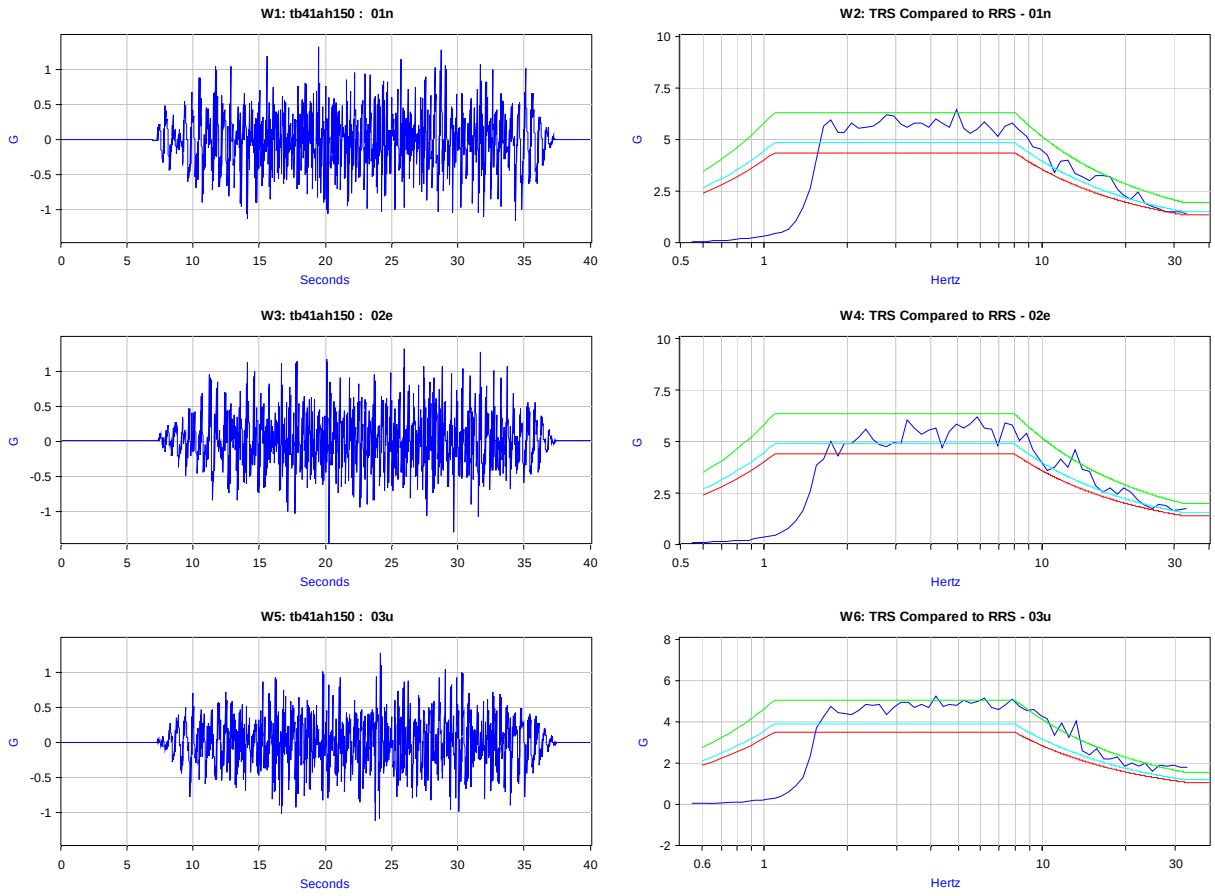

Figure C-23: Test Response Spectra of TB44AH175 – Bushing #6 Mounted in Center

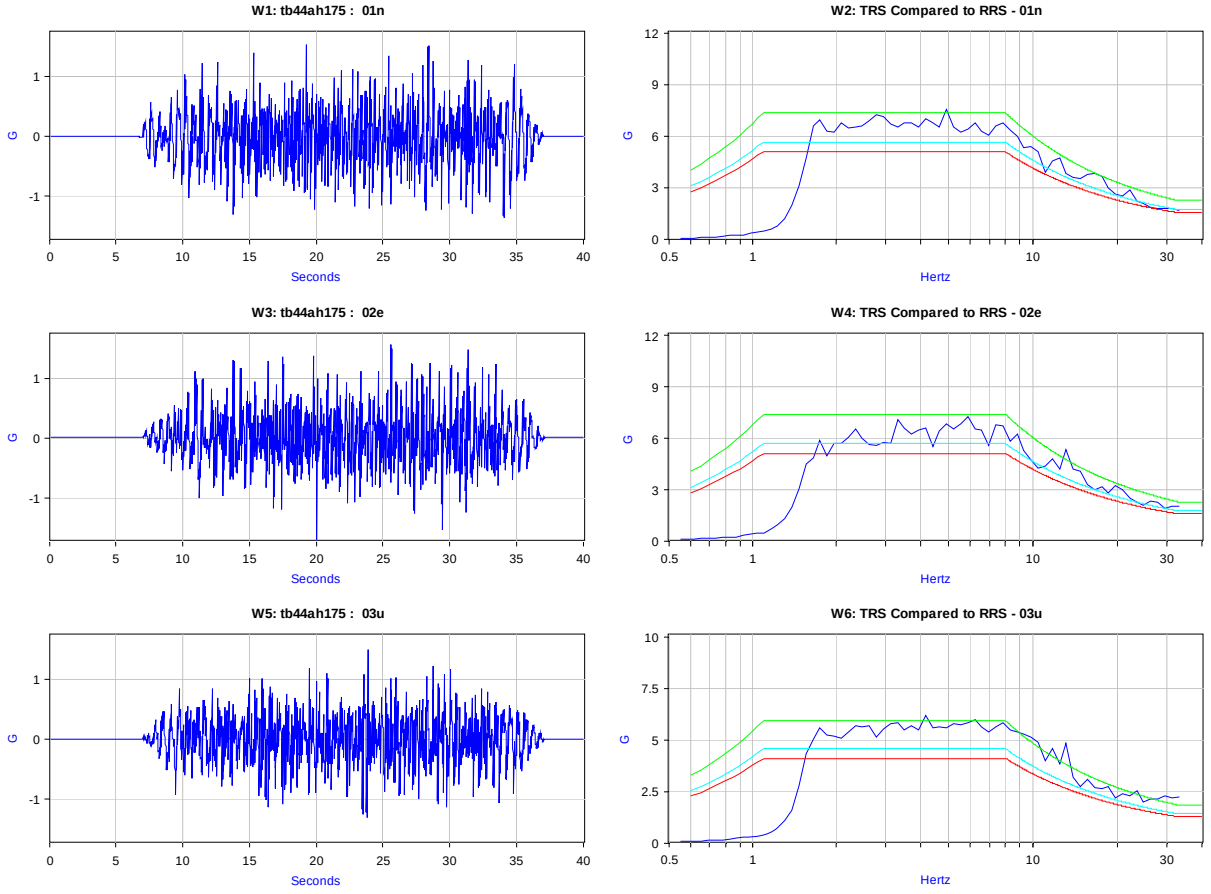

Figure C-24: Test Response Spectra of TB47AH200 – Bushing #6 Mounted in Center

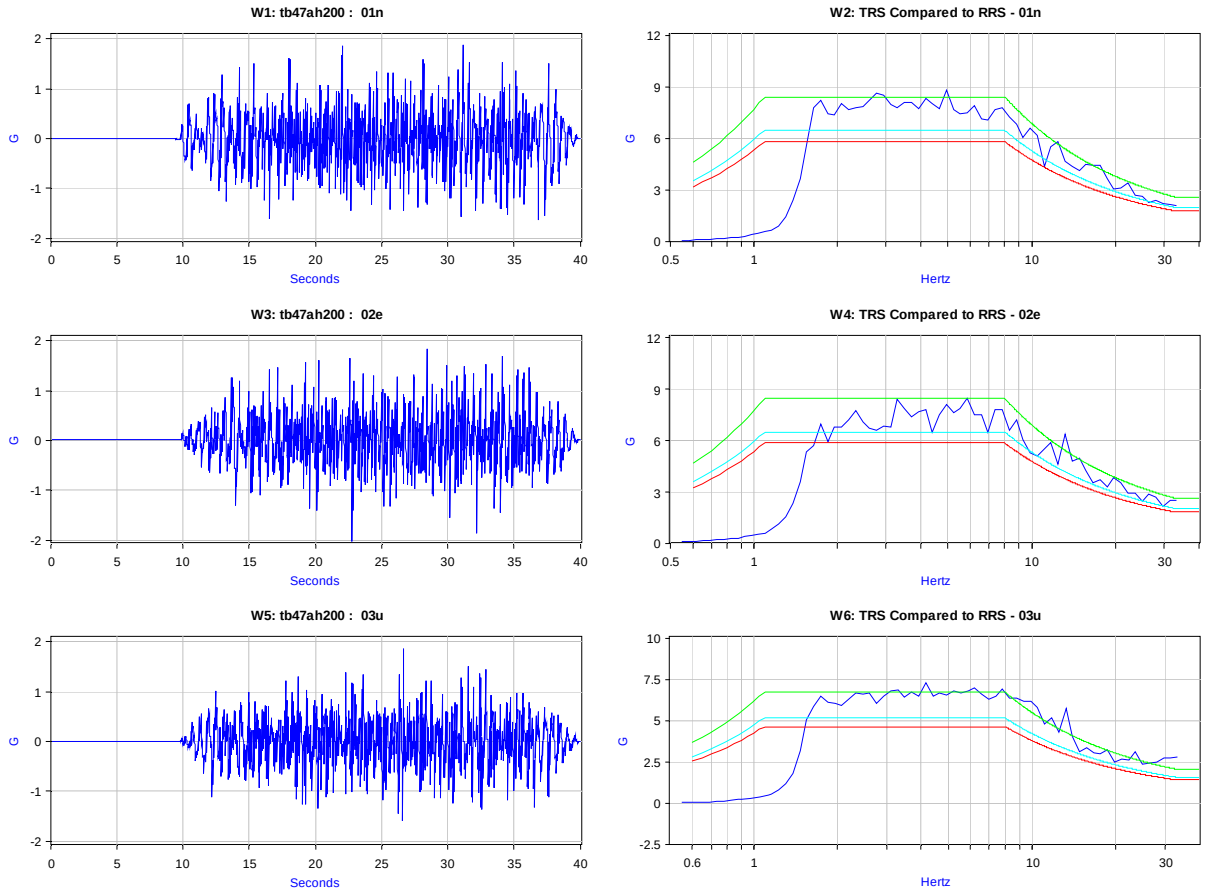

Figure C-25: Test Response Spectra of TB50AH225 – Bushing #6 Mounted in Center

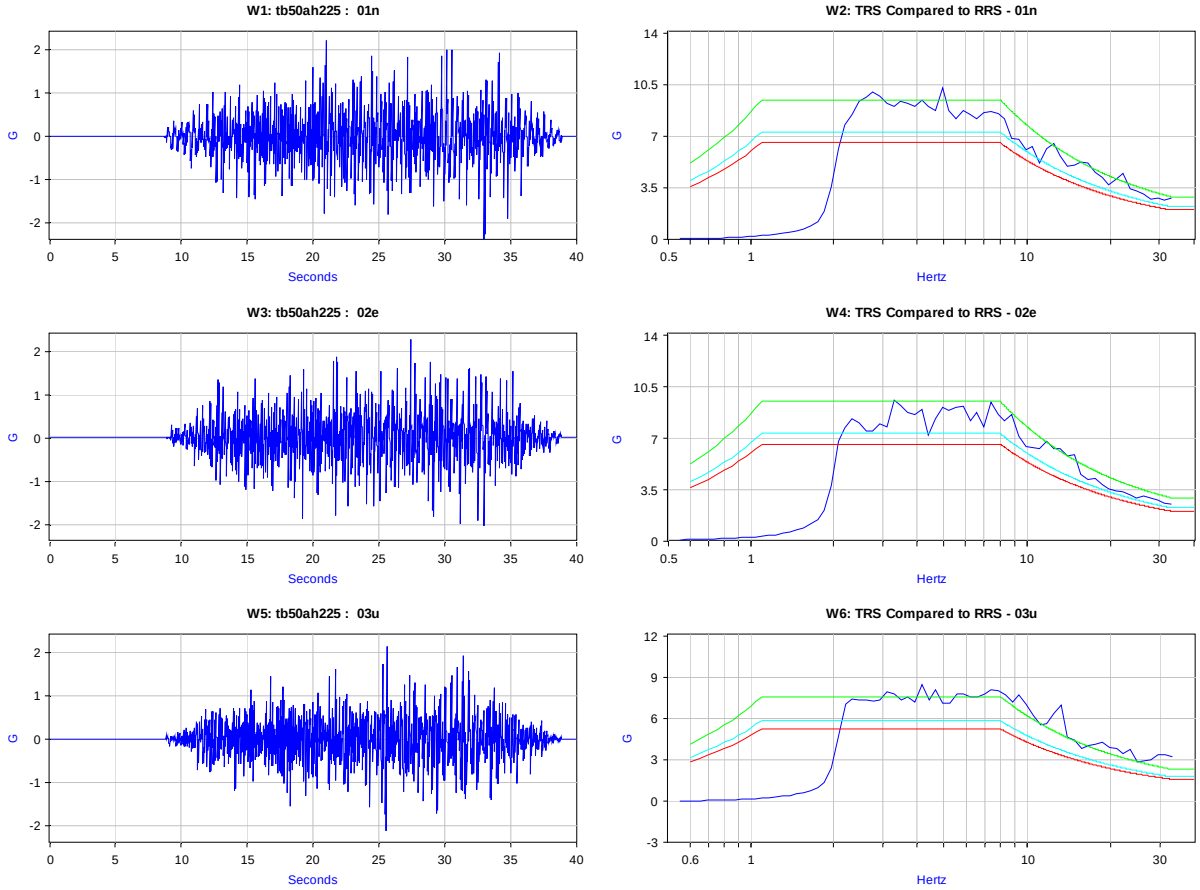

Figure C-26: Test Response Spectra of TB53AH250 – Bushing #6 Mounted in Center

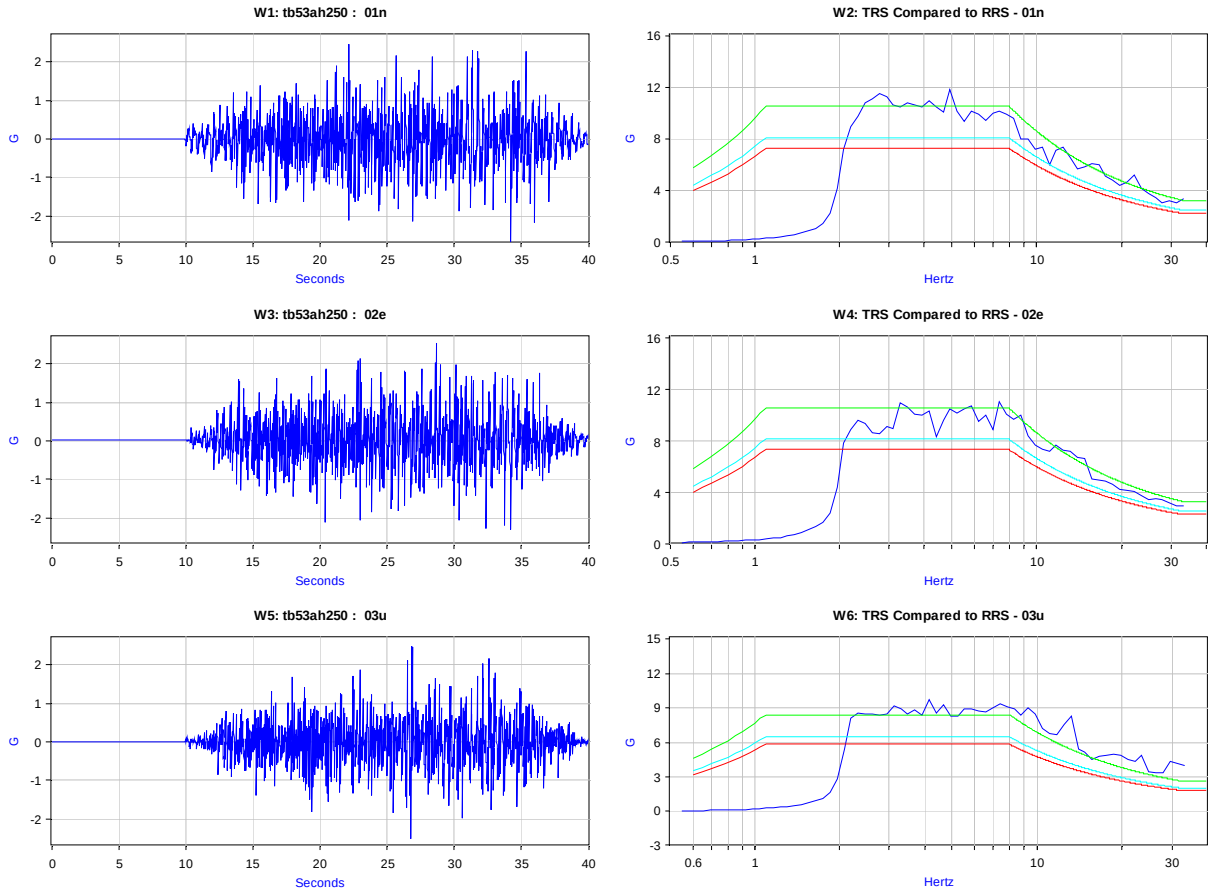

Figure C-27: Test Response Spectra of TB56AH275 – Bushing #6 Mounted in Center

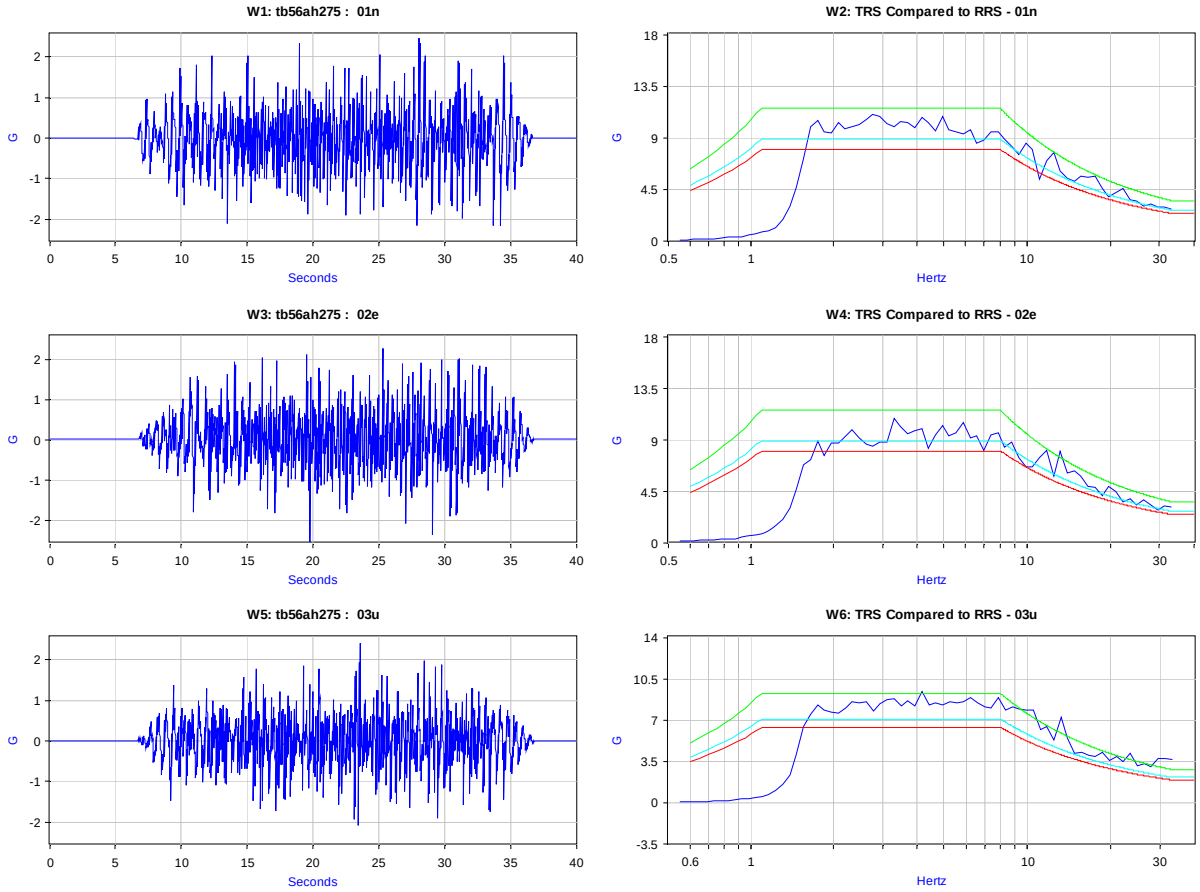

Figure C-28: Test Response Spectra of TB59AH300 – Bushing #6 Mounted in Center

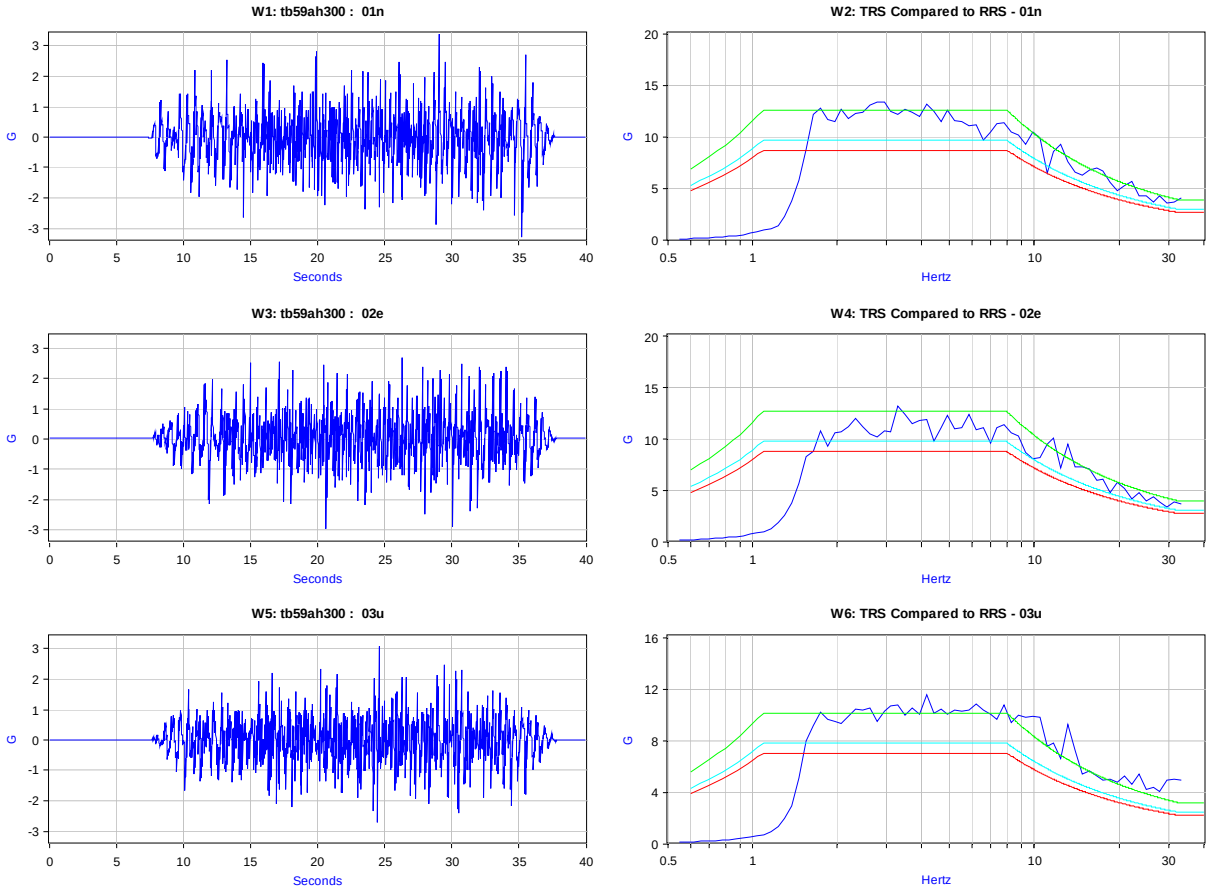

Figure C-29: Test Response Spectra of TB62AH200 – Bushing #6 Mounted in Center

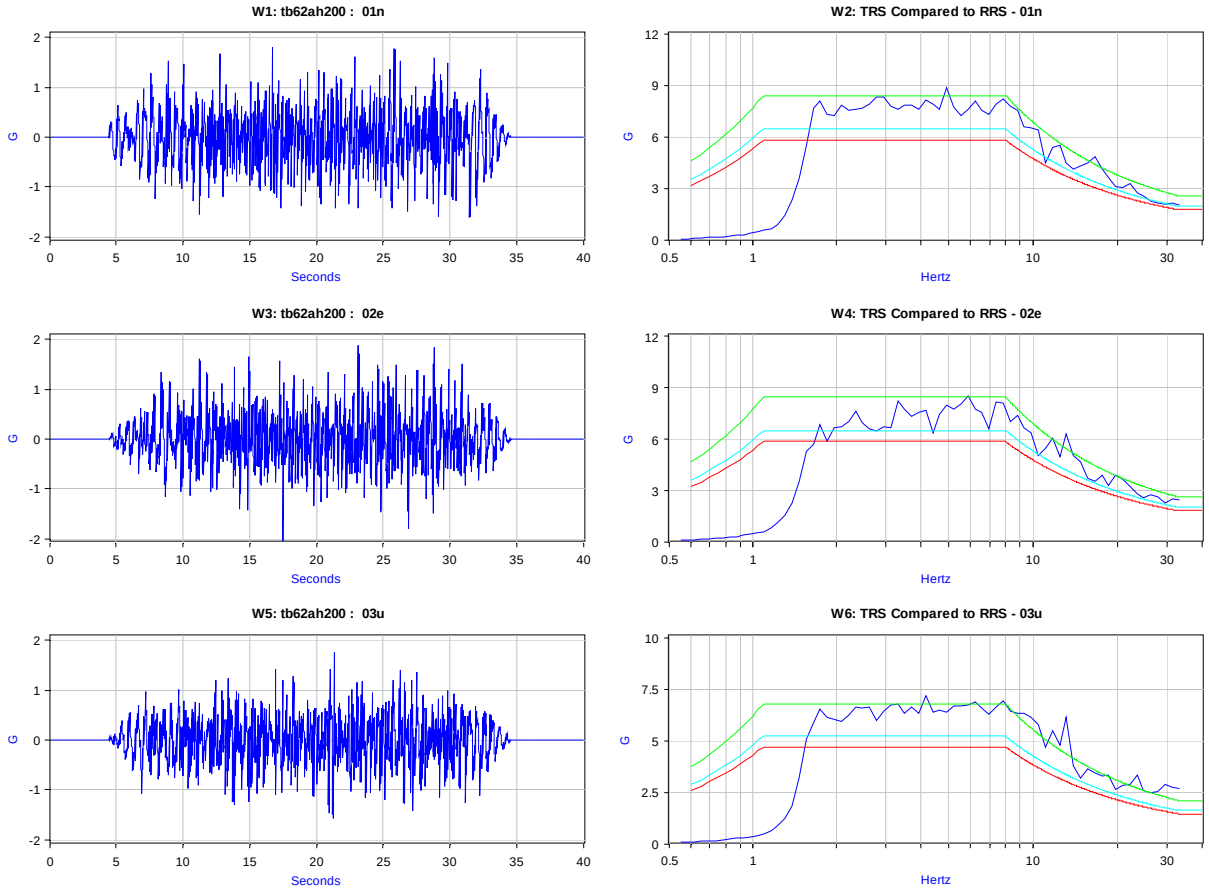

Figure C-30: Test Response Spectra of TB65AH225 – Bushing #6 Mounted in Center

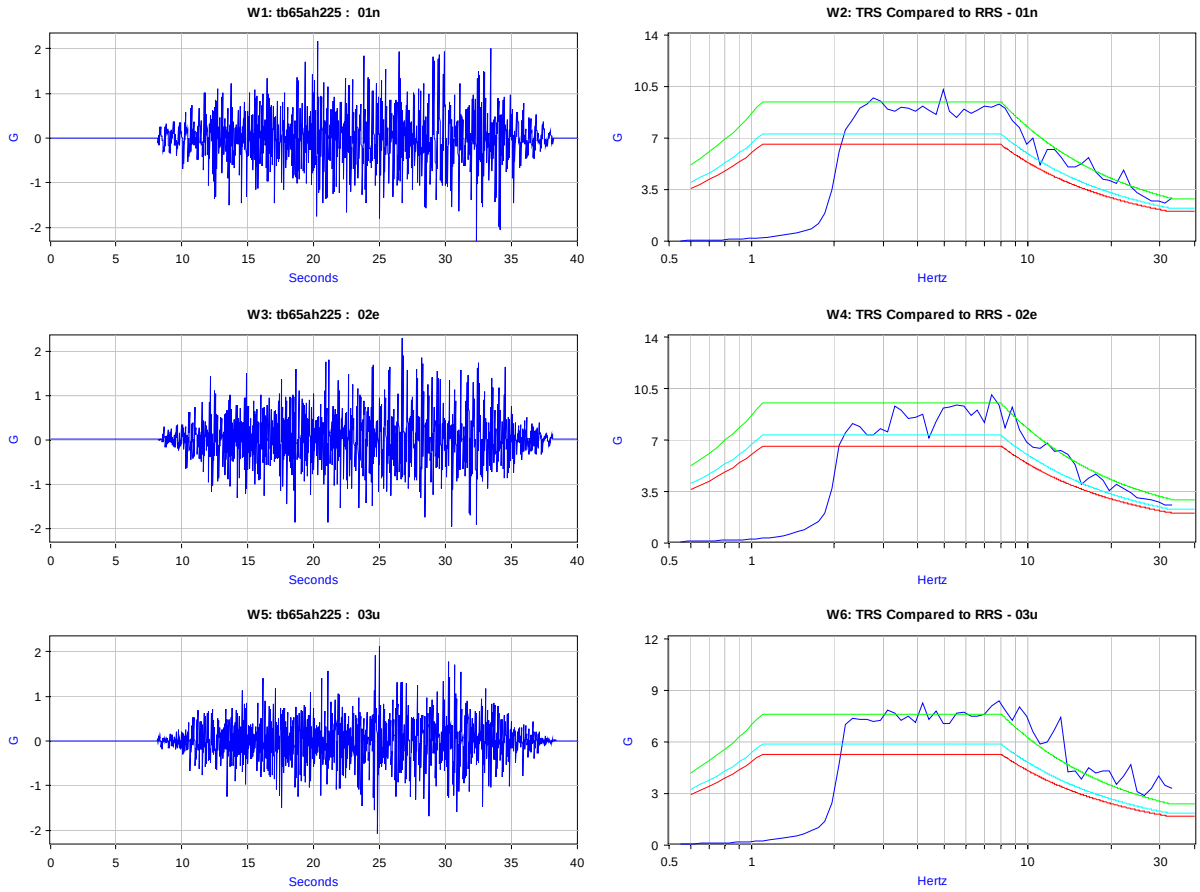

Figure C-31: Test Response Spectra of TB68AH250 – Bushing #6 Mounted in Center

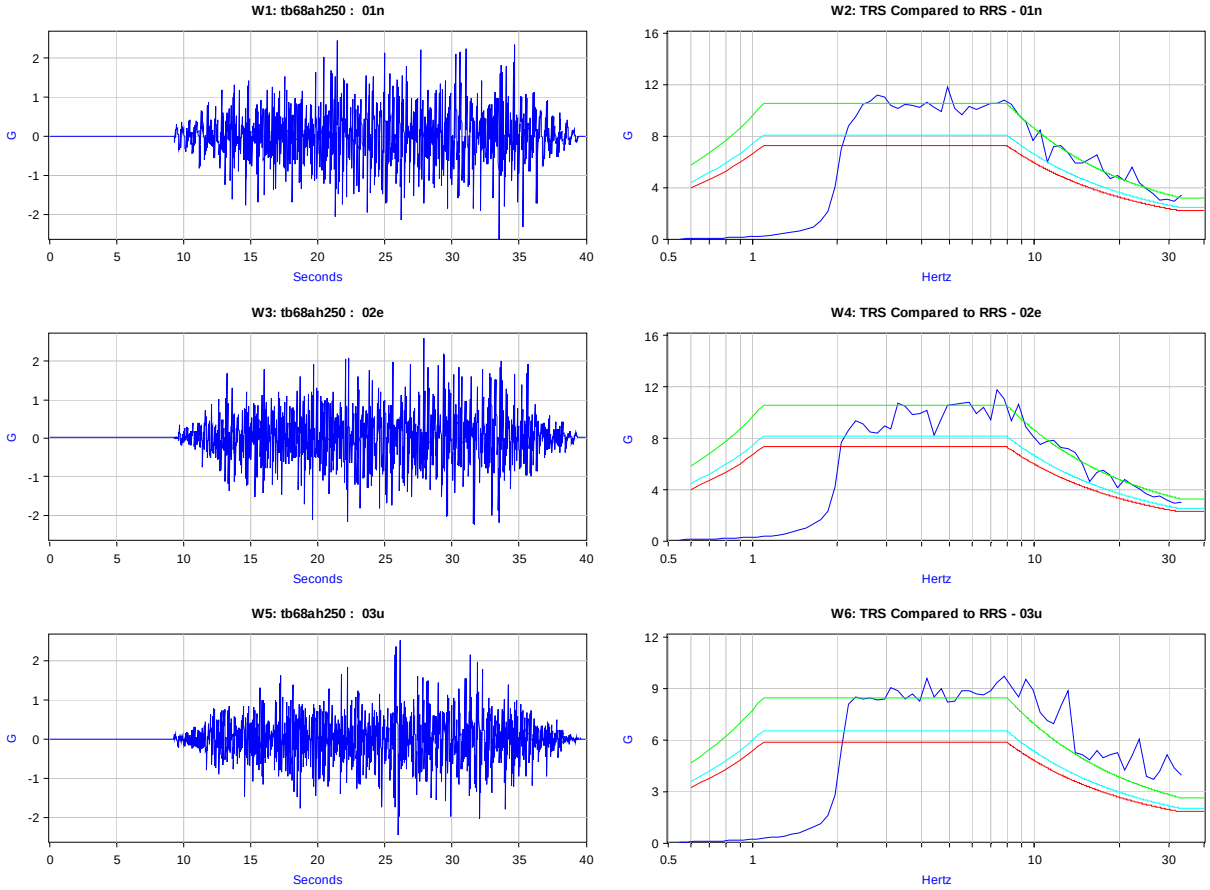

Figure C-32: Test Response Spectra of TB71AH275 – Bushing #6 Mounted in Center

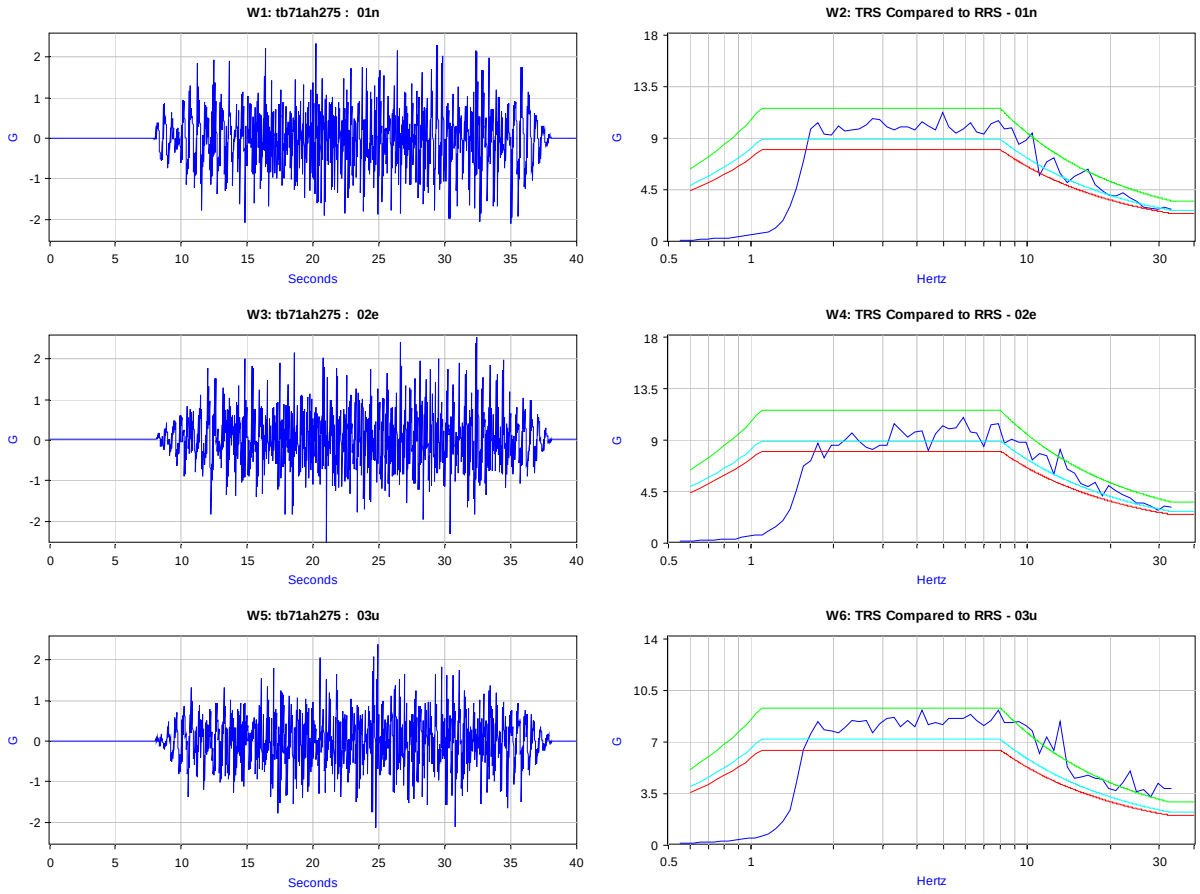

Figure C-33: Test Response Spectra of TB86AH225 – Bushing #6 Mounted in Center

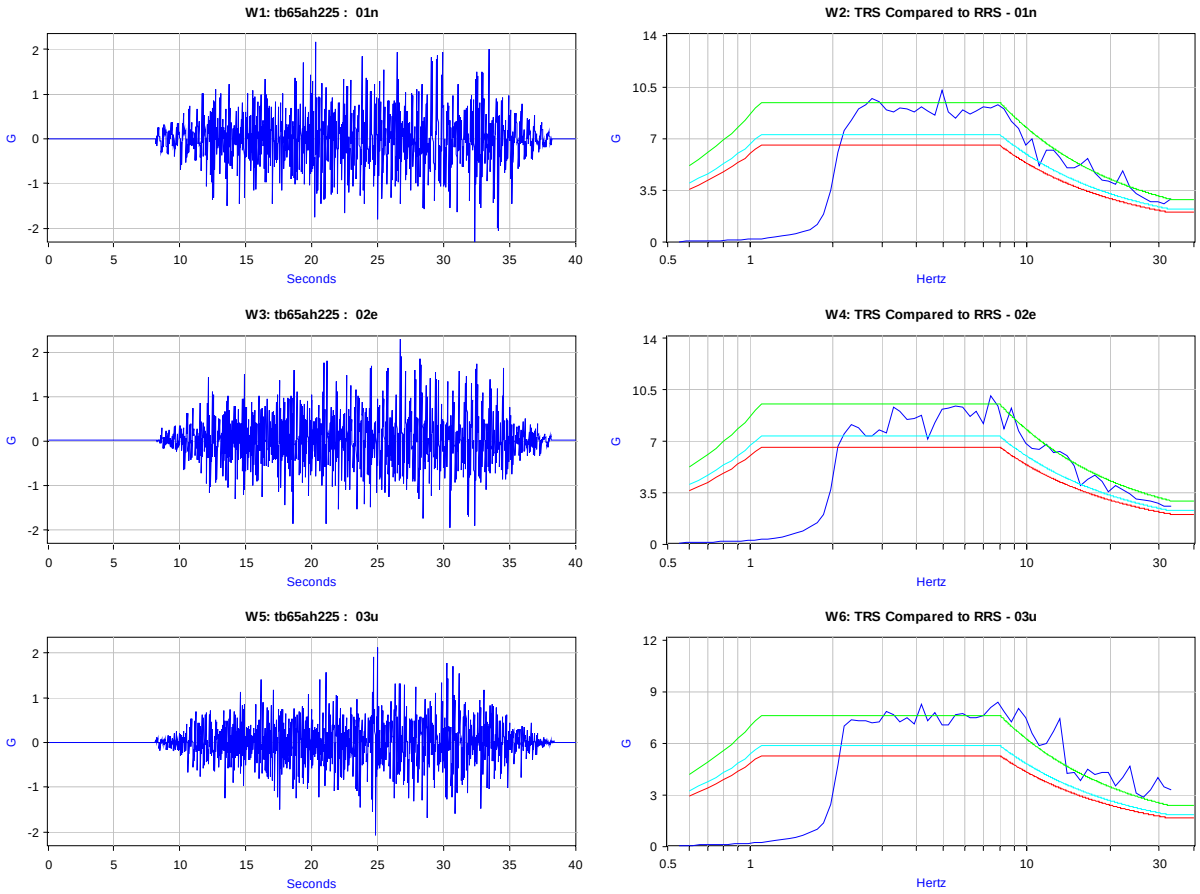

Test Response Spectra of Bushing #7

Bushing #7 is a 550 kV porcelain bushing. The magnitude of acceleration history was increased in successive tests. The response spectra obtained on the shake table extension are shown in Figures C-34 – C-42.

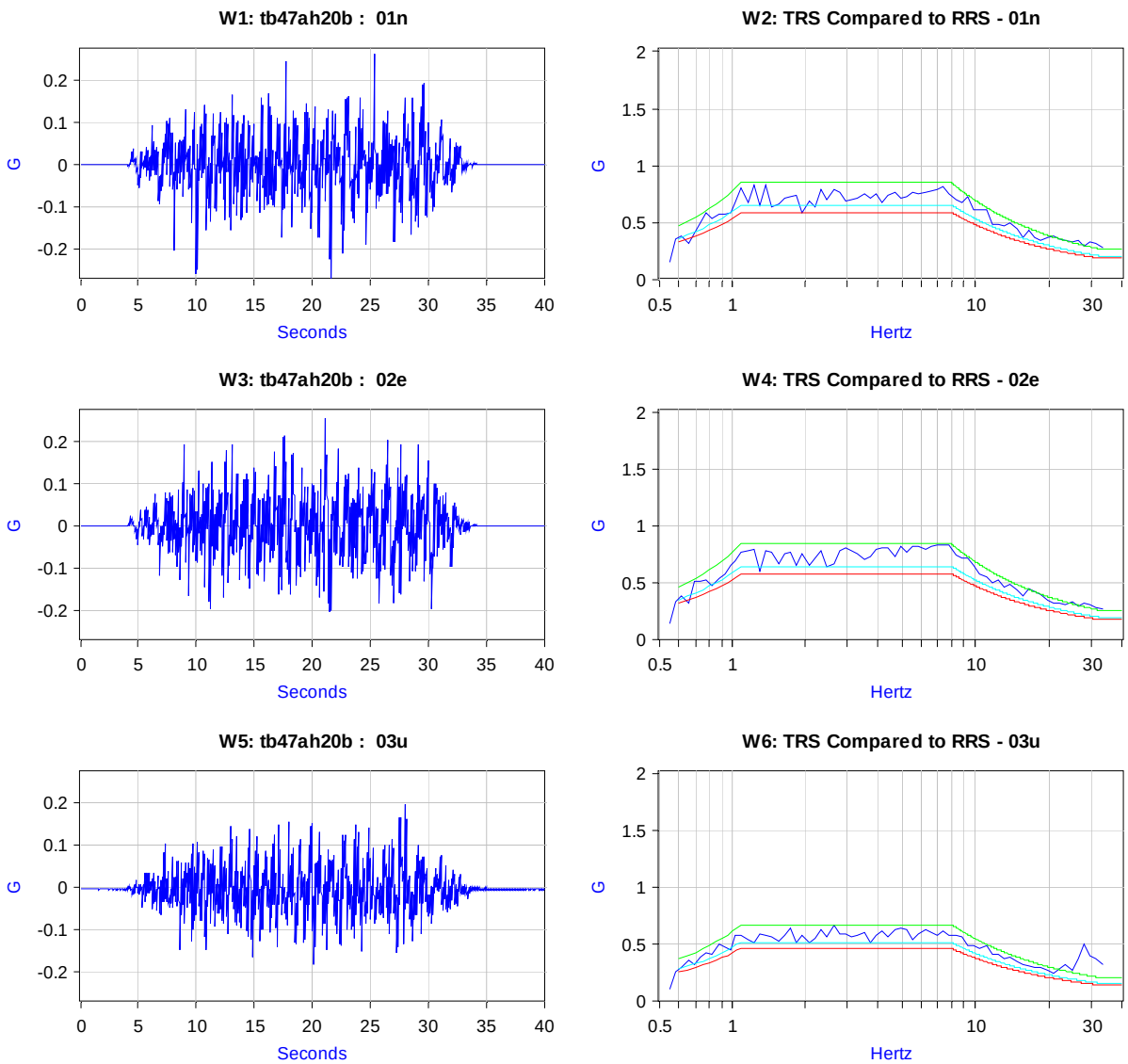

Figure C-34: Test Response Spectra of TB47AH20b – Bushing #7 Mounted in Center

Figure C-35: Test Response Spectra of TB50AH25 – Bushing #7 Mounted in Center

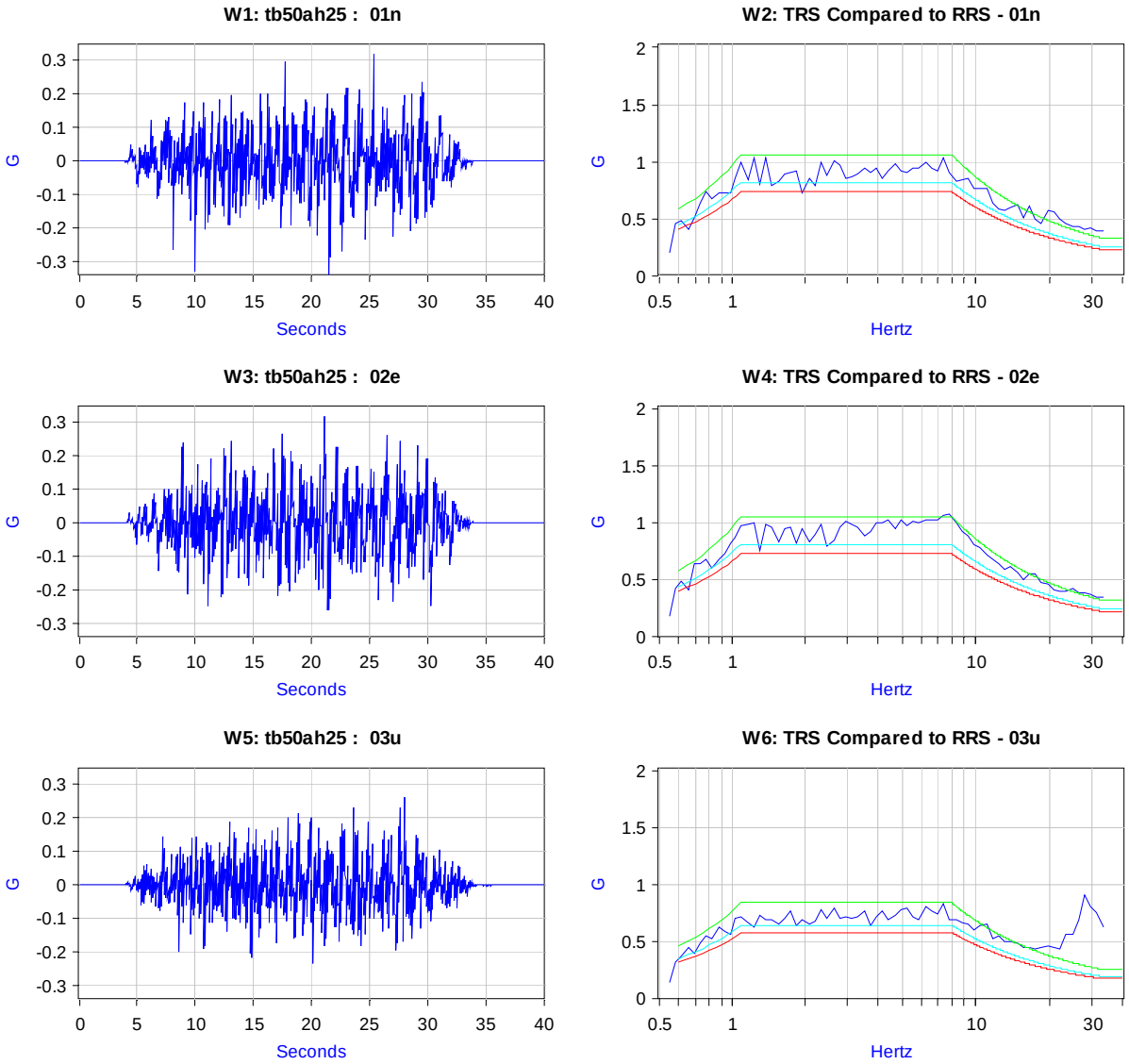

Figure C-36: Test Response Spectra of TB53AH30 – Bushing #7 Mounted in Center

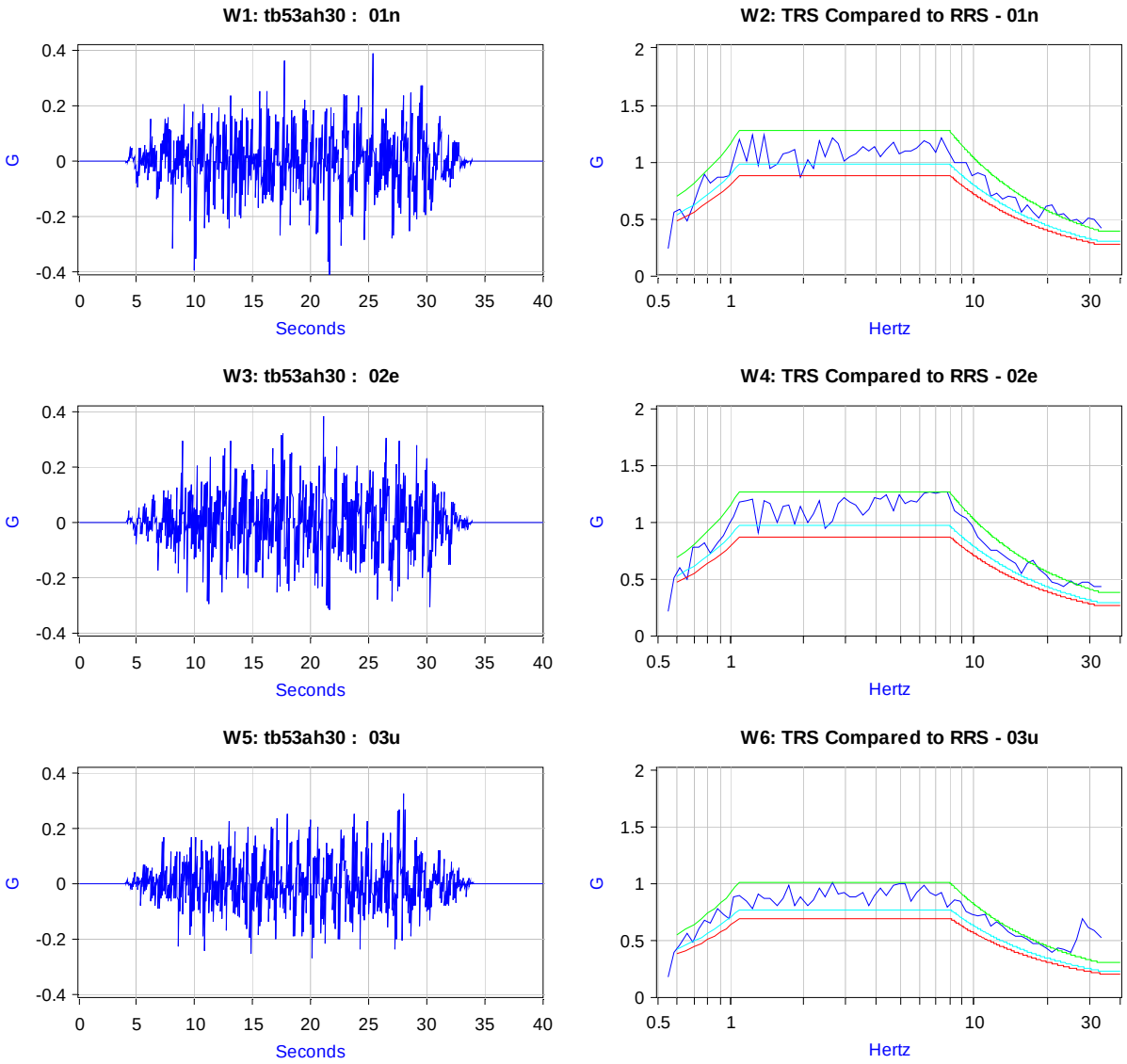

Figure C-37: Test Response Spectra of TB56AH35 – Bushing #7 Mounted in Center

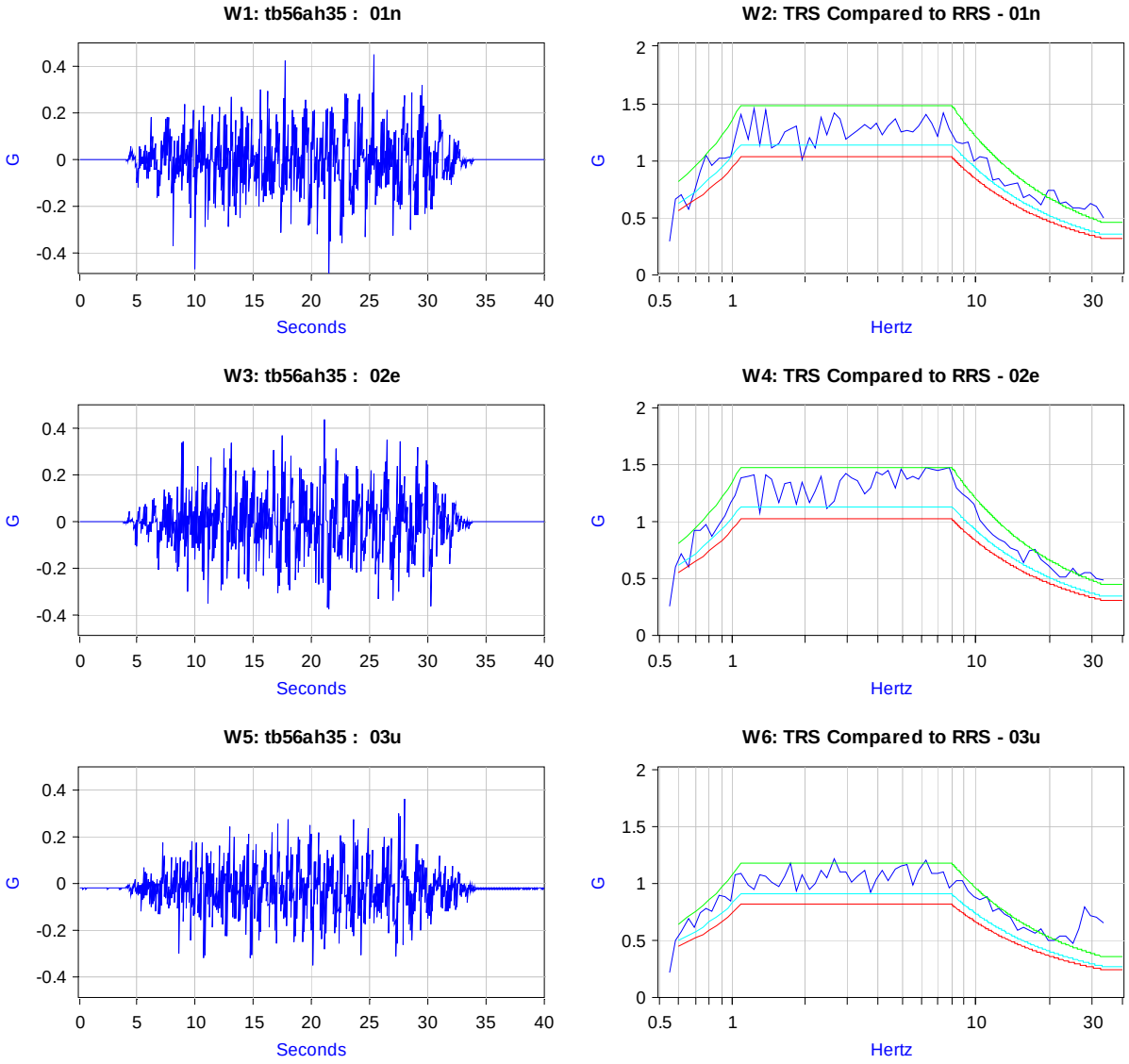

Figure C-38: Test Response Spectra of TB59AH40 – Bushing #7 Mounted in Center

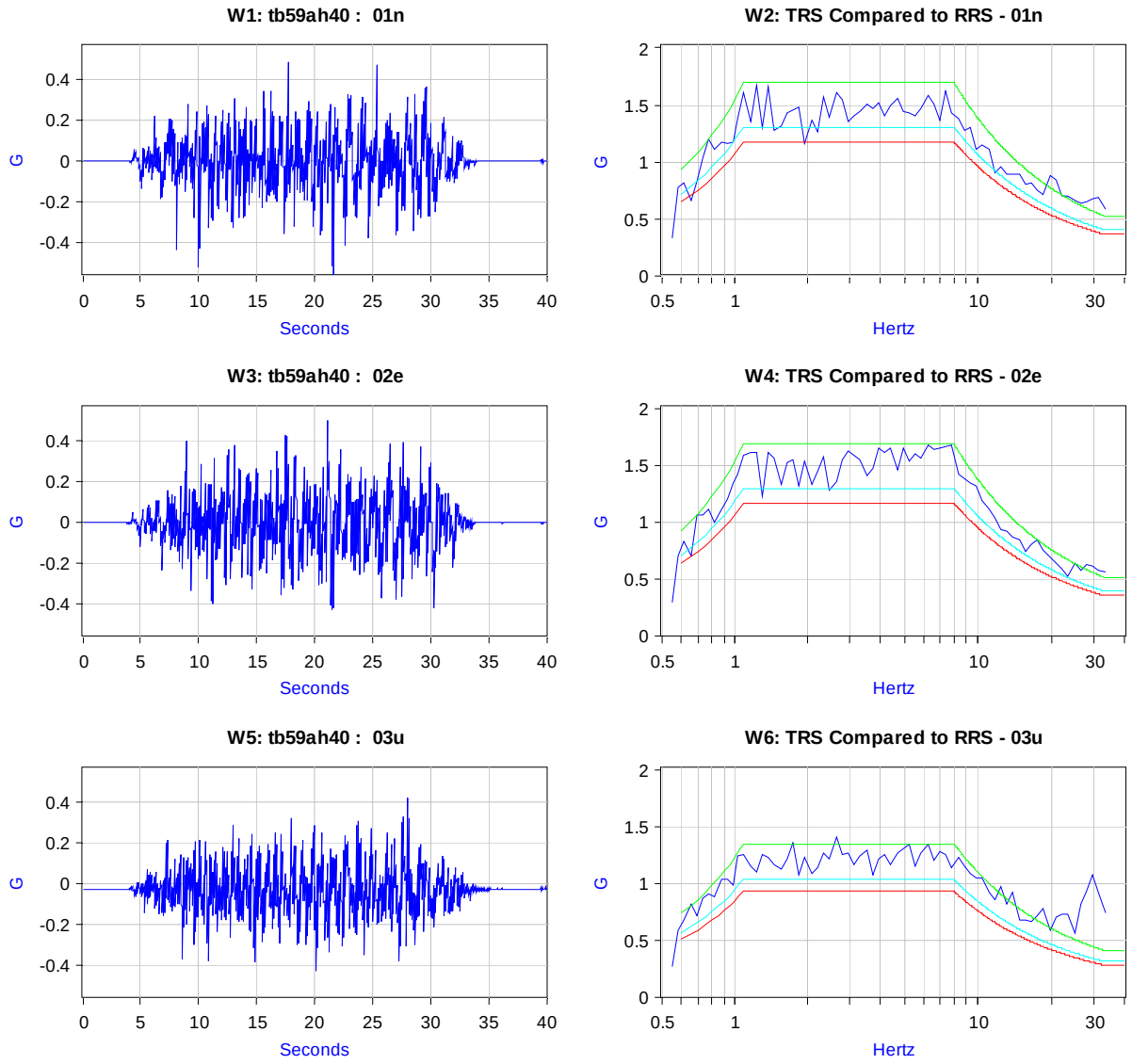

Figure C-39: Test Response Spectra of TB62AH45 – Bushing #7 Mounted in Center

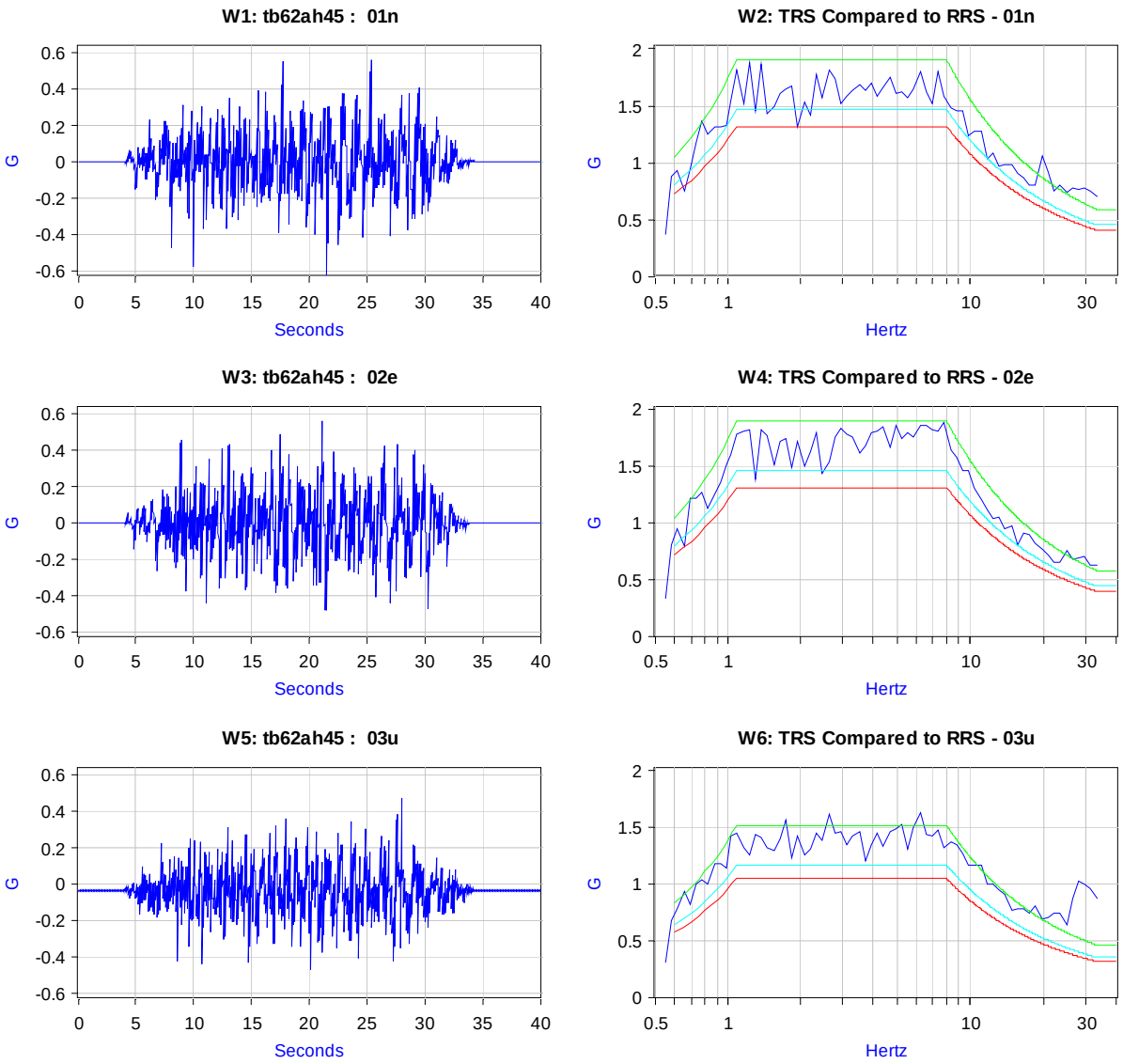

Figure C-40: Test Response Spectra of TB66AH50 – Bushing #7 Mounted in Center

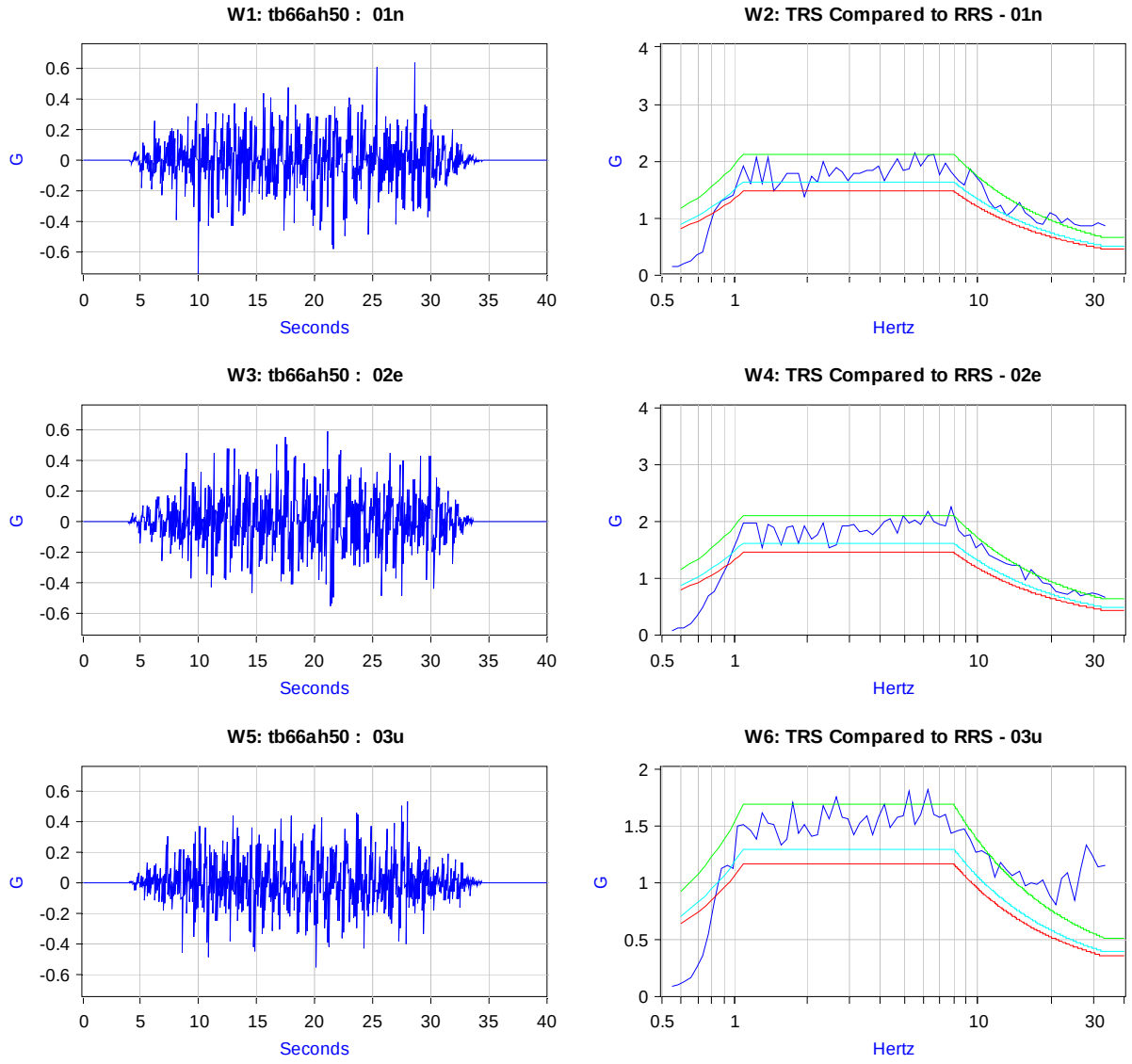

Figure C-41: Test Response Spectra of TB69AH55 – Bushing #7 Mounted in Center

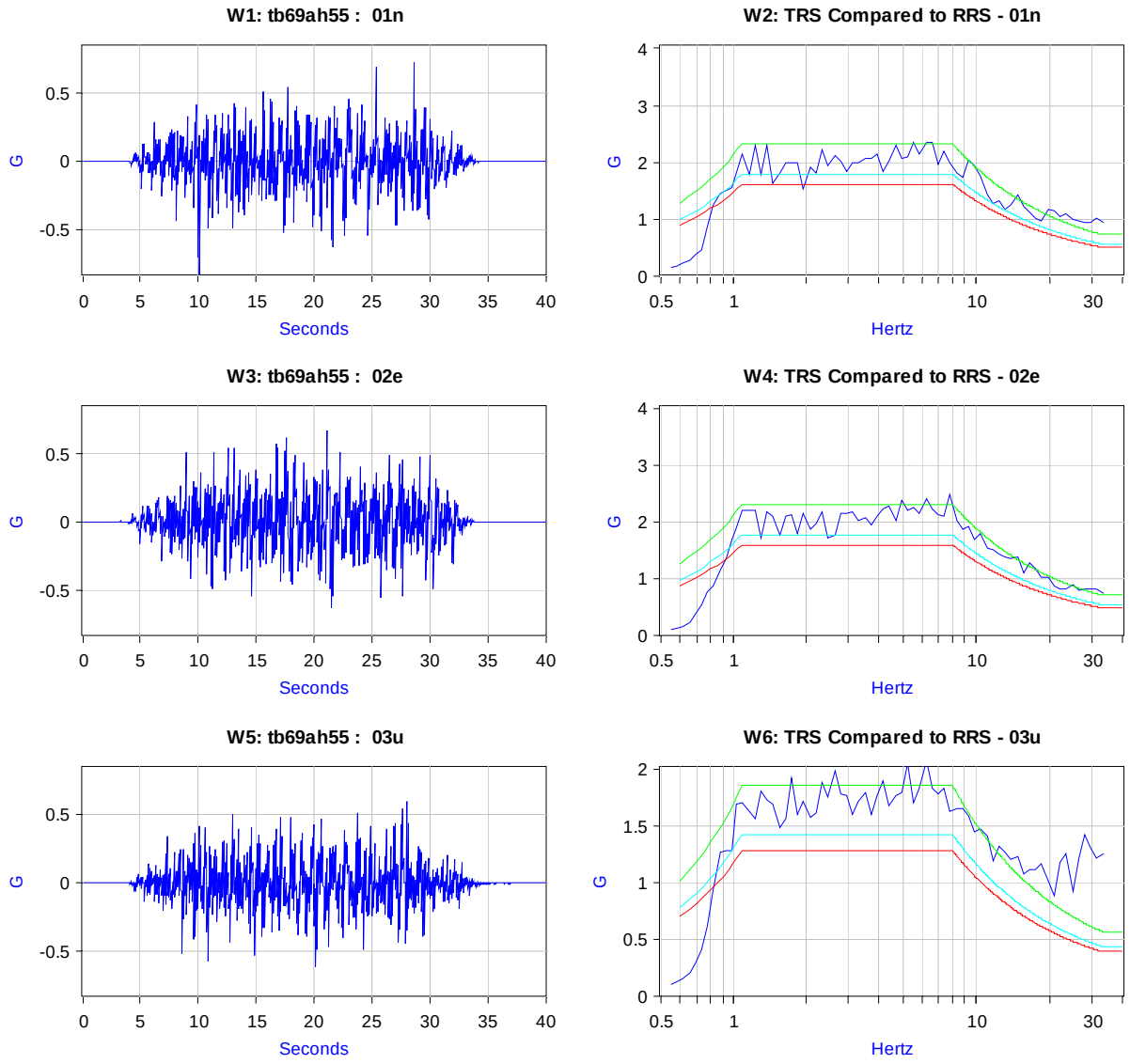

Figure C-42: Test Response Spectra of TB75AH80 – Bushing #7 Mounted in Center

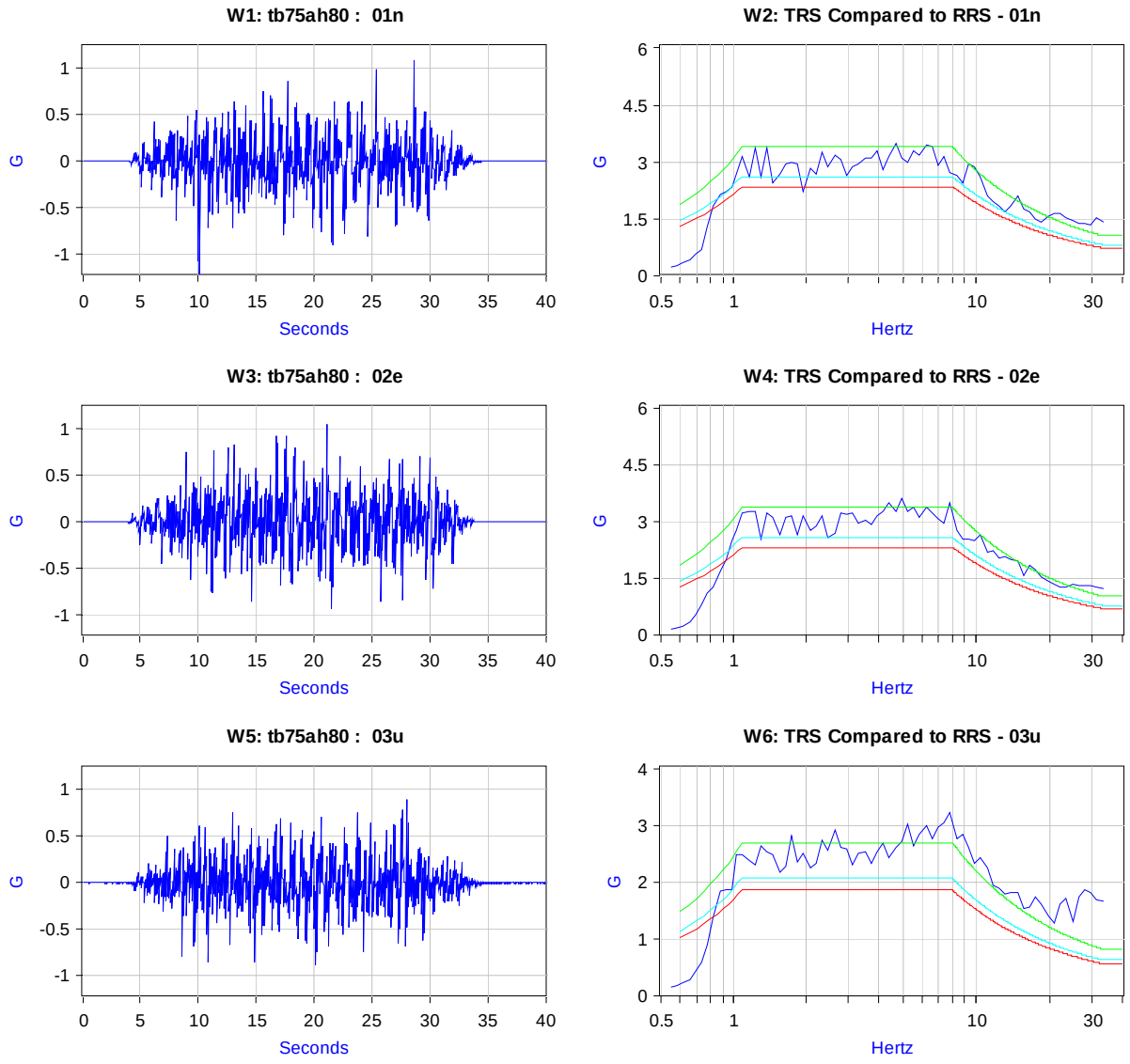

APPENDIX D:

BUSHING TEST RESULTS

This Appendix presents the testing results for individual bushings. All bushings were first mounted on the fixed base (a rigid concrete slab), and static testing was performed. Bushing frequencies, damping ratio and stiffness were measured. Second, each bushing was mounted on a flexible base support structure while a series of shake table tests were performed. Shake table tests included white noise tests followed by Acceleration History (AH) and Table Impulse (TI) tests.

The frequency of the Table Impulse test was obtained from the white noise test. The white noise test was used as system identification for possible damage to the bushing during the testing. The acceleration history tests were run to determine the level of demand on the bushings. A simple comparison between the demand (from the shake table tests) and capacity of the bushing (from the rigid base tests) was made to check the suitability of bushings to earthquake excitations. The earthquake records were generated at SEESL, State University of New York at Buffalo, to envelop the Required Response Spectra (RRS) defined by IEEE 693-2005, as shown in Appendix A.

Identification of Properties of Bushing #4A

This section is dedicated to Bushing #4A, which was tested according to the corresponding test protocol in Appendix A. A summary of the dynamic properties of Bushing #4A is presented in Table D-1.

Table D-1: Dynamic Properties of Bushing #4A from Various Tests

Test No.	Frequency			Damping			Max Displacement	Force (lb)	Stiffness (lb/in)
Units	(Hz)			(%)			(in)	(lb)	(lb/in)
(1)	(3)	(4)	(5)	(6)	(7)	(8)	(9)	(10)	(11)
Direction	NS	EW	Vertical	NS	EW	Vertical			
Impact Hammer Test –Fixed base									
TB-U1-NSww05	8.32	-	-	4.35	-	-	-	-	-
TB-U1-WEww06	-	8.85	-	-	2.66	-	-	-	-
TB-U1-NS05	8.3	-	-	2.47	-	-	-	-	-
TB-U1-WE06	-	8.28	-	-	2.47	-	-	-	-
Quick Release Test - Fixed Base									
TB-U1-13	-	8.27	-	-	0.91	-	0.15	116.88	779.20
TB-U1-14		8.35			1.48		0.26	187.39	720.73
TB-U1-15		8.26			1.50		0.46	302.88	658.43
TB-U1-16	-	-	-	-	-	-	0.42	296.08	704.95
White Noise Test									
TBU1wn23	7.75	7.75	22.50	2.69	2.11	0.75	-	-	-
TBU1wn26	7.75	7.75	22.50	2.53	1.89	0.58	-	-	-
TBU1wn28	7.75	7.75	23.50	2.49	2.70	1.16	-	-	-
TBU1wn31	7.75	7.75	23.25	2.47	2.50	1.25	-	-	-
TBU1wn33	7.50	7.25	17.75	2.70	2.56	1.02	-	-	-
TBU1wn36	7.50	7.25	17.75	2.46	2.55	0.98	-	-	-
TBU1wn38	7.75	7.50	21.25	4.27	3.12	0.89	-	-	-
TBU1wn41	7.75	7.25	21.25	4.37	1.88	0.90	-	-	-
TBU1wn43	7.75	7.75	24.00	2.21	3.05	1.78	-	-	-
TBU1wn46	7.75	7.75	23.75	2.23	3.07	1.57	-	-	-
Table Impulse Test									
TBU1TBI24	7.70	7.78	-	0.70	0.70	-	-	-	-
TBU1TBI27	7.70	7.79	-	0.60	0.69	-	-	-	-
TBU1TBI29	7.79	7.79	-	0.53	0.61	-	-	-	-
TBU1TBI32	7.80	7.80	-	0.73	0.61	-	-	-	-
TBU1TBI34	7.59	7.12	-	0.97	0.52	-	-	-	-
TBU1TBI37	7.55	7.16	-	0.60	0.57	-	-	-	-
TBU1TBI39	7.80	7.37	-	0.49	0.84	-	-	-	-
TBU1TBI42	7.80	7.40	-	0.55	0.52	-	-	-	-
TBU1TBI44	7.86	7.80	-	0.50	0.63	-	-	-	-
TBU1TBI47	7.86	7.80	-	0.59	0.72	-	-	-	-
Final Pull Test									
TB-U1-PLB-50	-	-	-	-	-	-	0.72	297.14	412.69
TB-U1-PL-52	-	-	-	-	-	-	0.38	267.81	708.49
TB-U1-PL-54	-	-	-	-	-	-	0.80	534.03	670.89
TB-U1-PL-56	-	-	-	-	-	-	1.99	1220.32	613.23
TB-U1-PL-58	-	-	-	-	-	-	3.43	1959.59	571.98
TB-U1-PL-60	-	-	-	-	-	-	4.87	2632.16	540.83
TB-U1-PL-62	-	-	-	-	-	-	7.03	2855.60	406.49
TB-U1-PL-64	-	-	-	-	-	-	3.52	1251.28	355.48

Identification of Dynamic Properties without Conductor Weight

Impact Hammer Testing

Impact hammer tests were used to find the frequency and damping ratio of Bushing #4A. Initially there was no mass at the top of bushing and frequencies were measured. Minimum frequency was observed in the NS direction of 8.32 Hz with maximum damping ratio of 4.35%; in the EW direction the frequency was 8.85 Hz and damping ratio was 2.66% (Table D-1). The frequency was derived from the Power Spectral Density (PSD) of the free vibration response, and the logarithmic decrement method was used to find the damping ratio. The results of the tests are shown in Figures D-1 through D-4.

Figure D-1: Acceleration Response of Bushing #4A, without Mass, in NE Direction

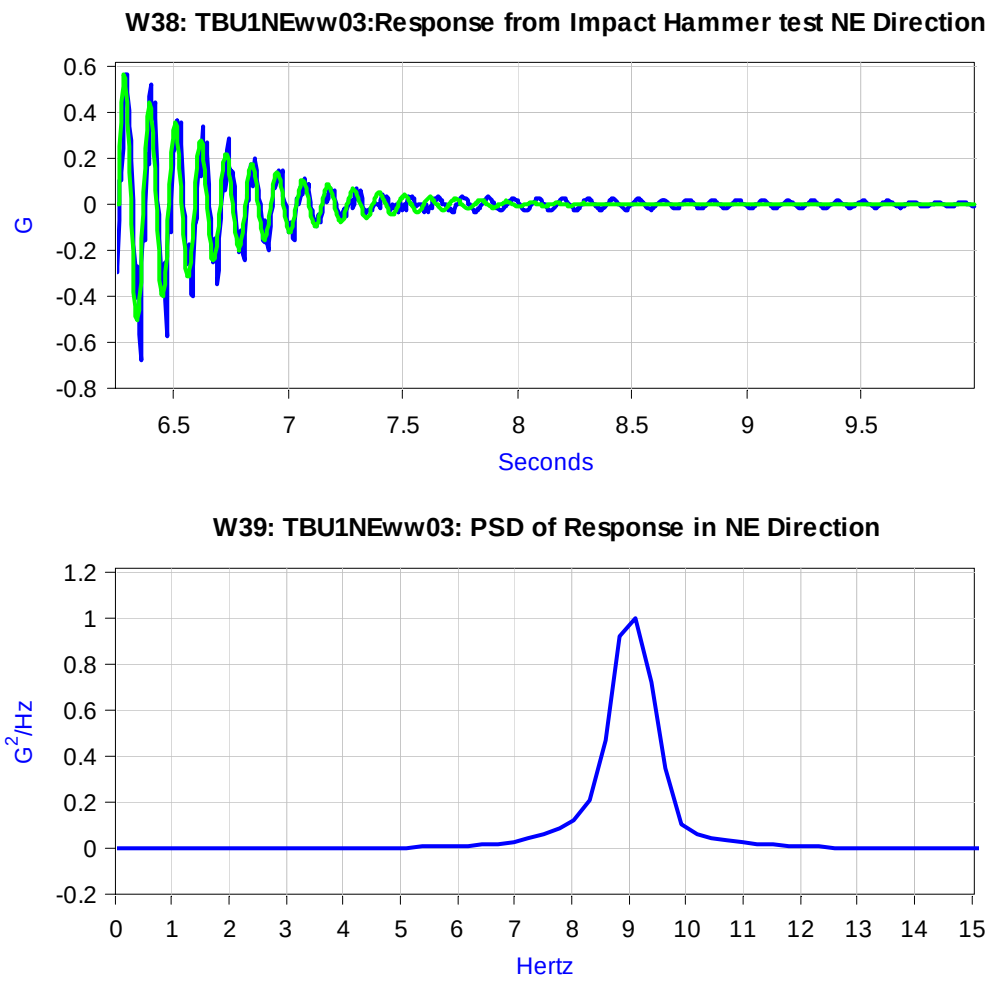

Figure D-2: Acceleration Response of Bushing #4A, without Mass, in SE Direction

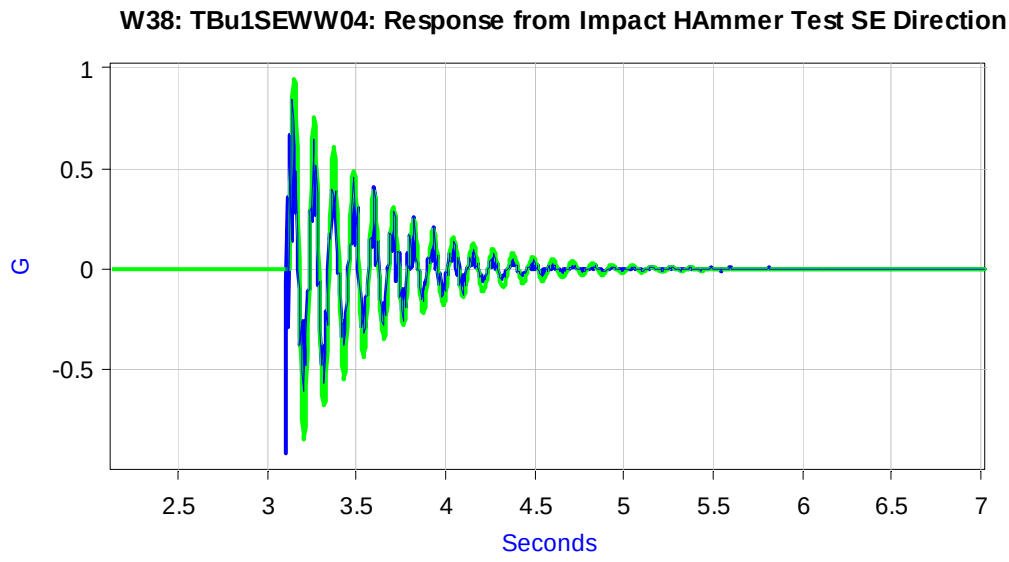

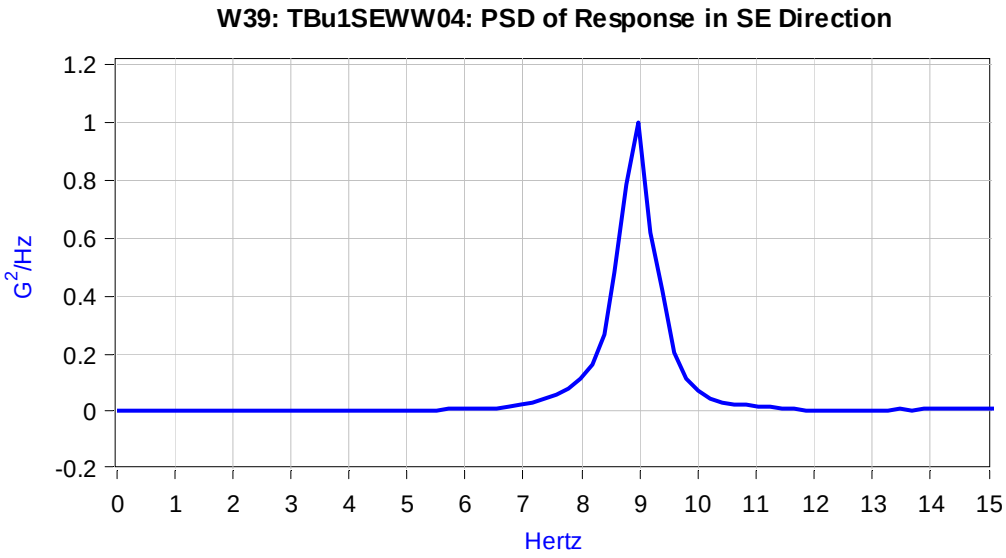

Figure D-3: Acceleration Response of Bushing #4A, without Mass, in NS Direction

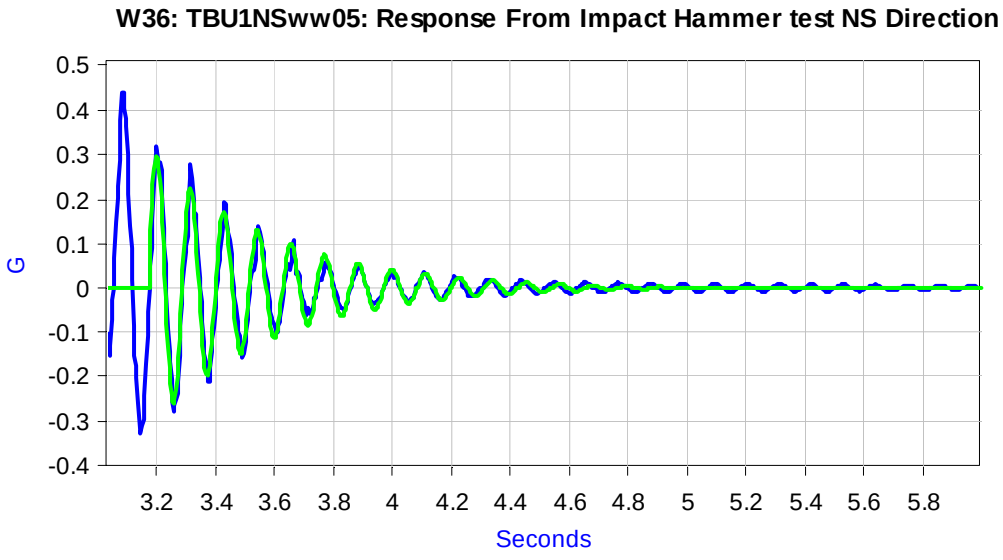

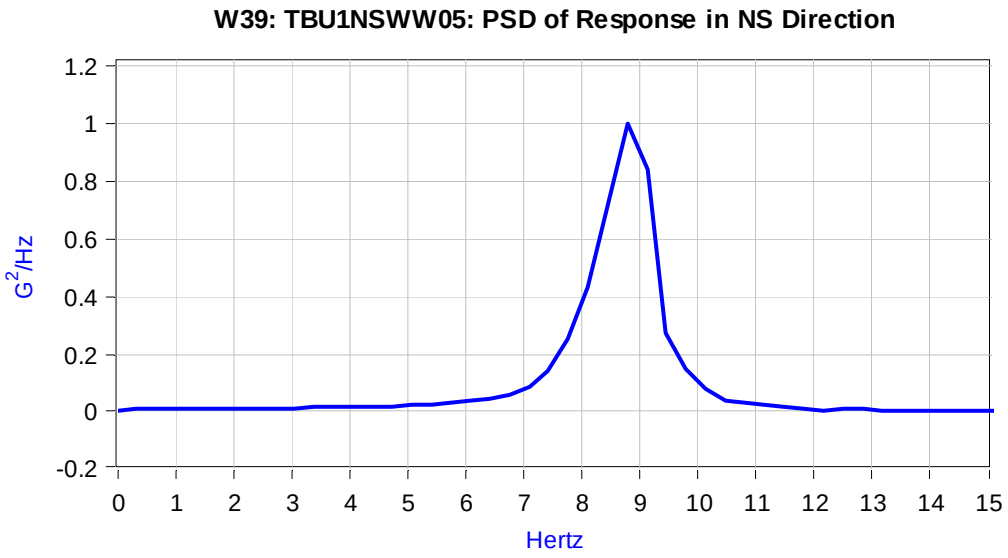

Figure D-4: Acceleration Response of Bushing #4A, without Mass, in NS Direction

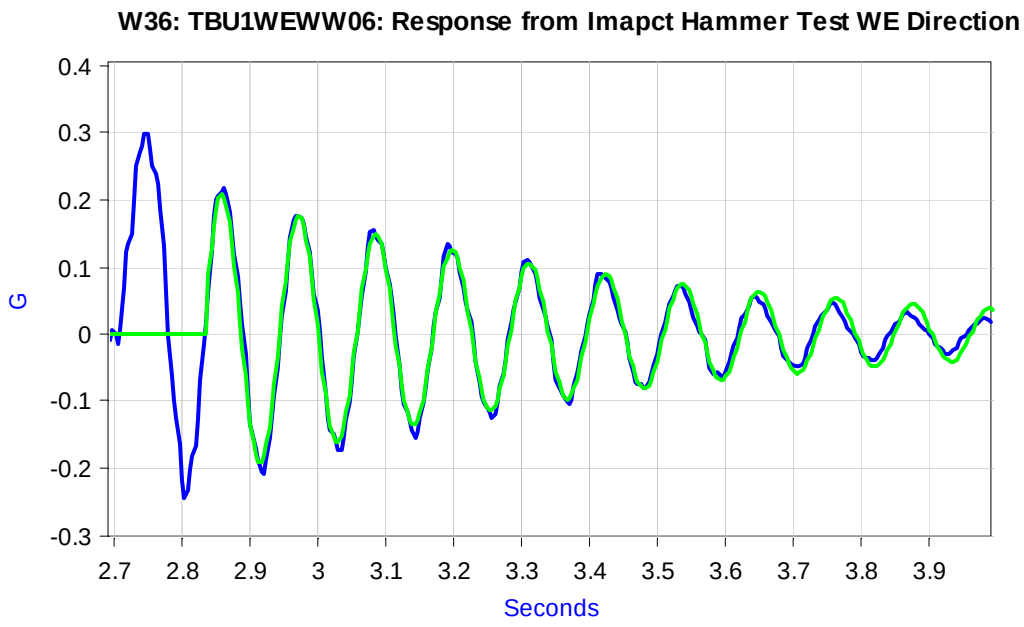

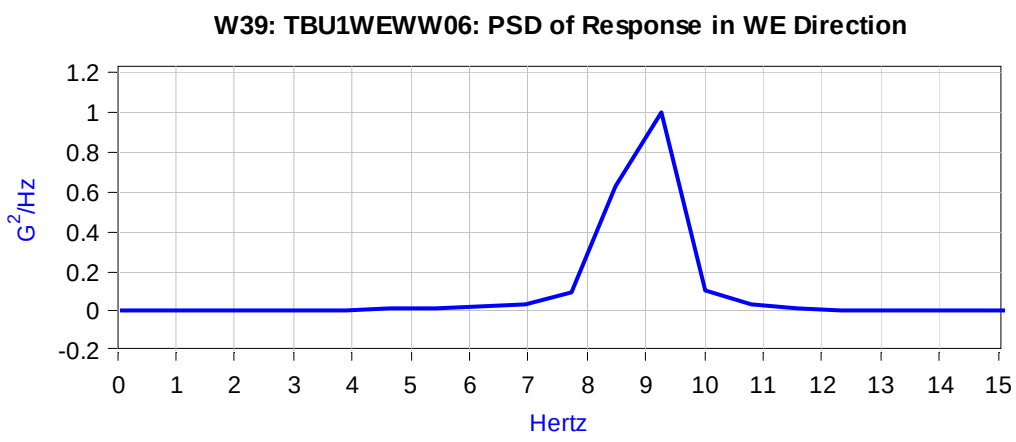

Identification of Dynamic Properties with Additional Conductor Weight

Impact Hammer Testing

A 15 lb. weight was attached at the top of the bushing and the impact hammer tests were run again. The weight simulated a portion of cable near the bushing top that might play a role in the bushing response. This time a maximum frequency of 8.3 Hz and a maximum damping ratio of 2.47% were observed in the NS direction, and 8.28 Hz max. frequency with 2.47% max. damping ratio in the EW direction (Table D-1). The acceleration response and the corresponding PSD in free vibration domain are shown in Figures D-5 – D-8.

Figure D-5: Acceleration Response of Bushing #4A, with 15 lb. Mass, in NE direction

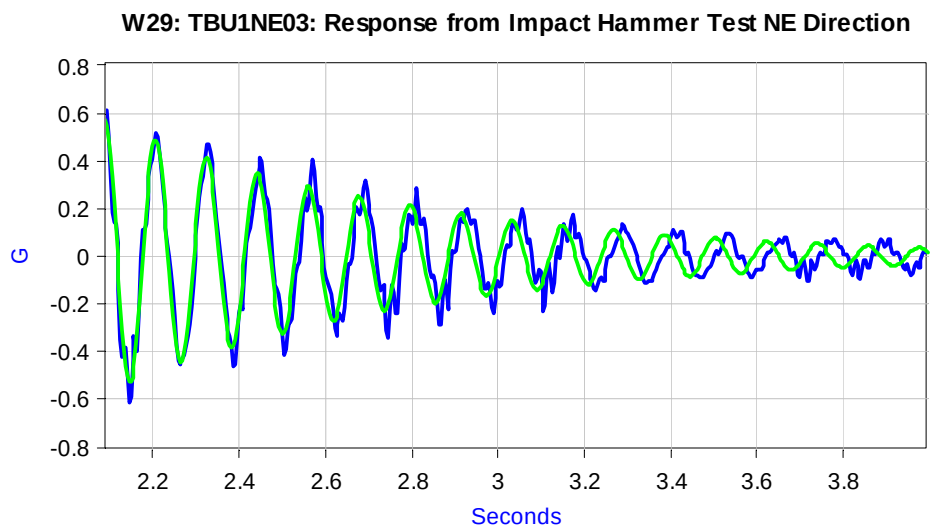

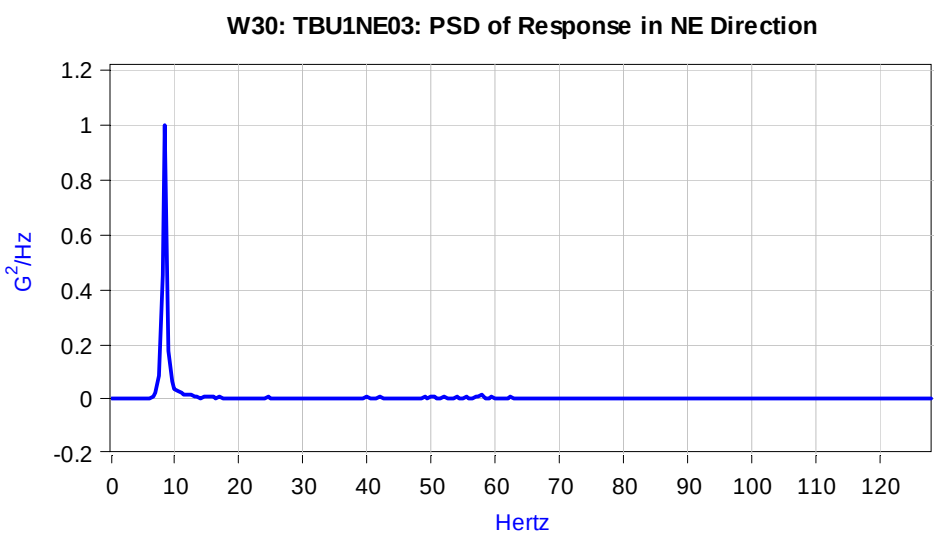

Figure D-6: Acceleration Response of Bushing #4A, with 15 lb. Mass, in SE direction

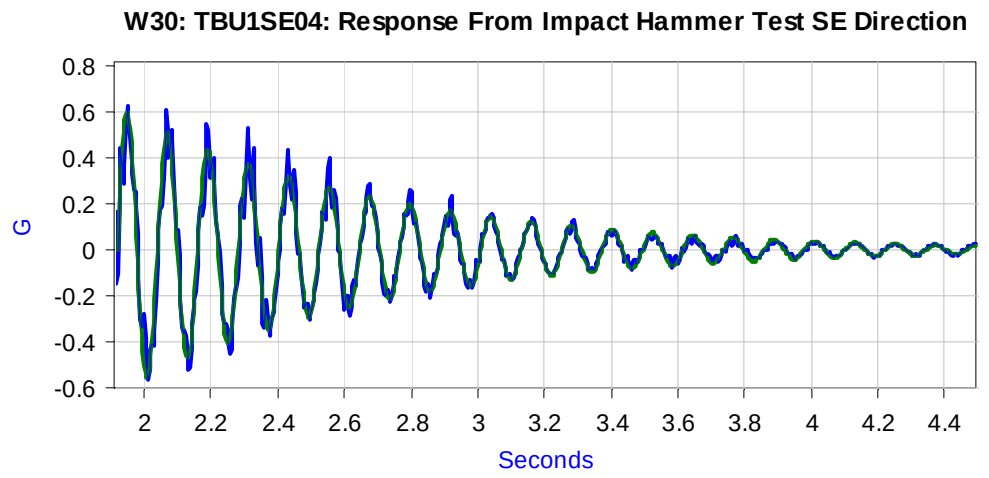

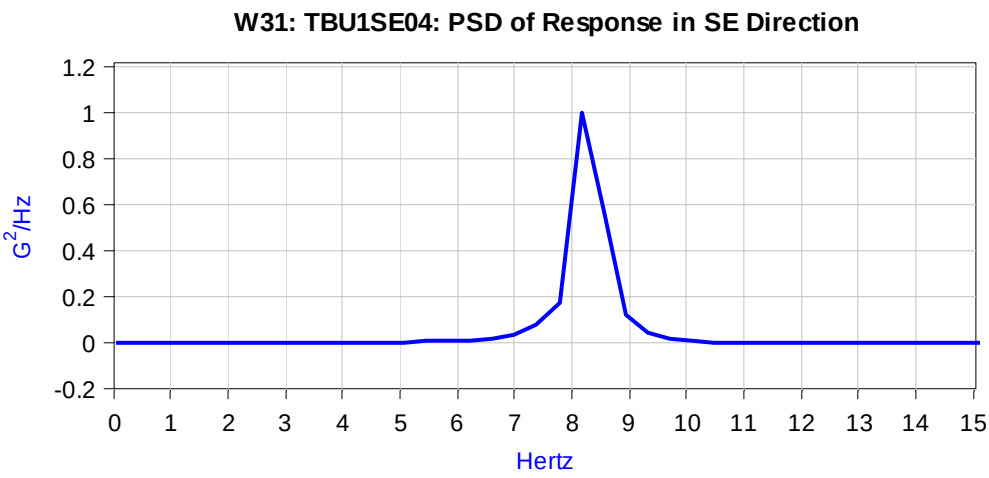

Figure D-7: Acceleration Response of Bushing #4A, with 15 lb. Mass, in NS direction

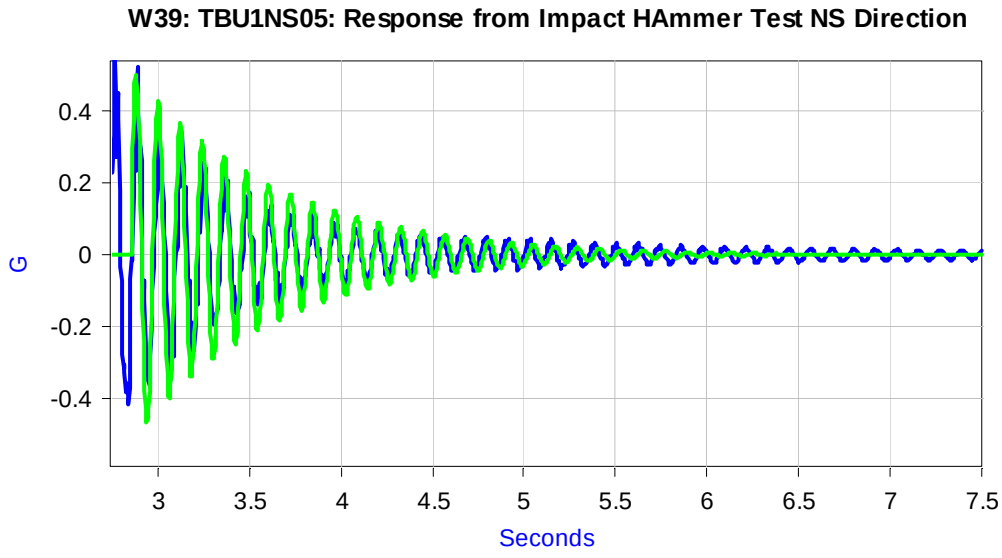

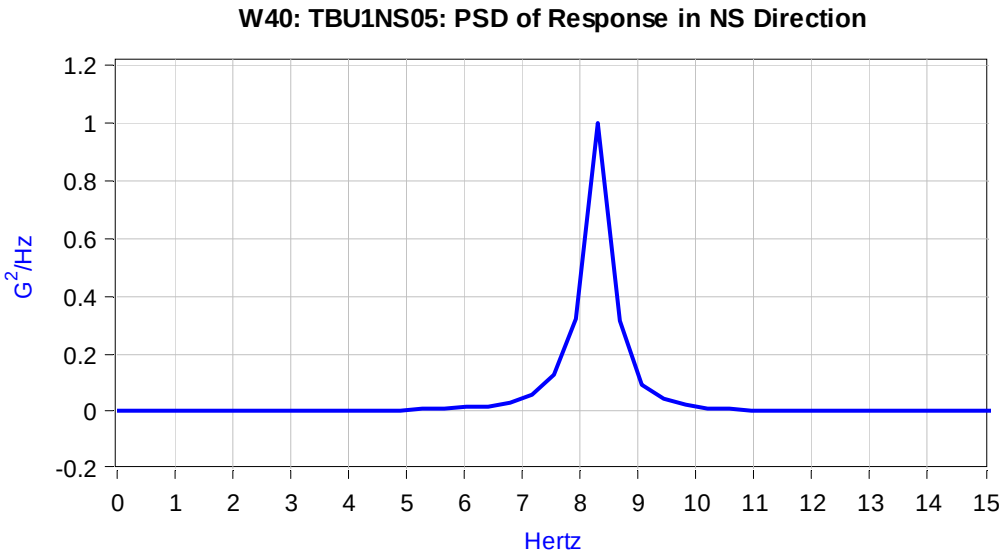

Figure D-8: Acceleration Response of Bushing #4A, with 15 lb. Mass, in WE direction

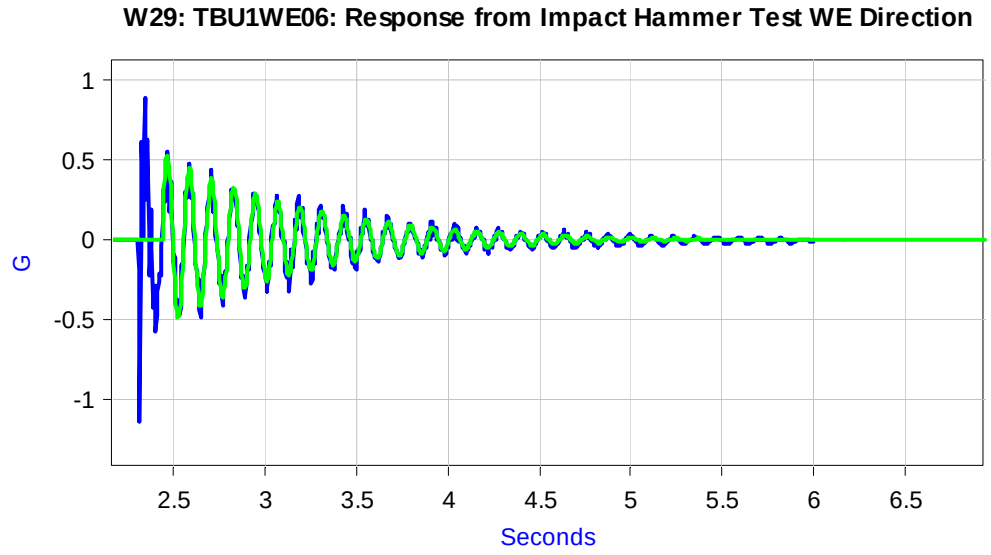

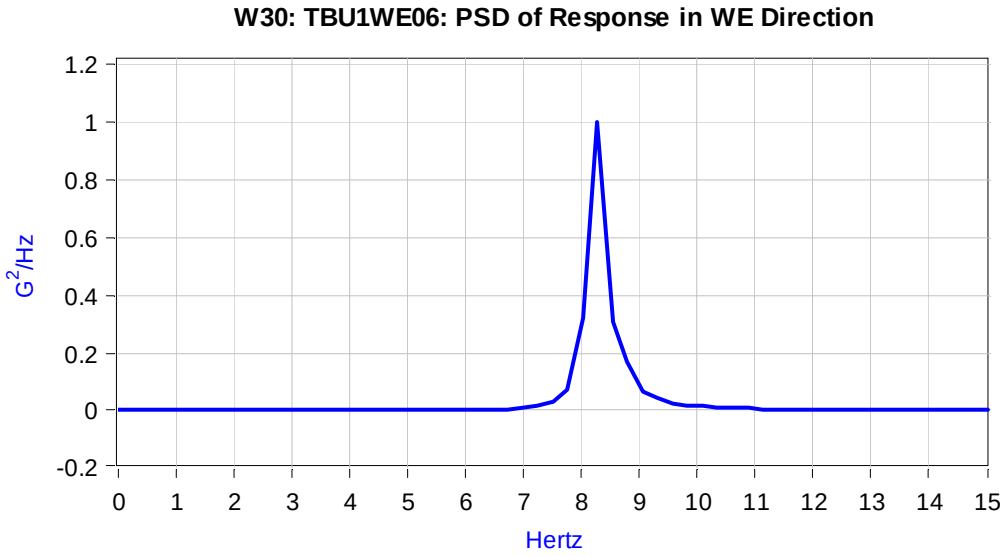

Pull and Sudden Release Tests

After the impact hammer tests, pull and sudden release tests were run on Bushing #4A; the bushing was pulled from the top and released suddenly, allowing the stiffness of the bushing and the frequency and damping ratio to be determined in a more detailed way. All the pull tests were run in the EW direction only. The stiffness varied between maximum values of 658 lb./in. to 779 lb./in. (Table D-1). Figures D-9 through D-11 show the frequencies and corresponding damping ratios for these tests. Figure D-12 shows the relationship between the initial force and displacement, representing the stiffness of the bushing.

Figure D-9: Acceleration Response from Quick Release Test TBU113 – Bushing #4A

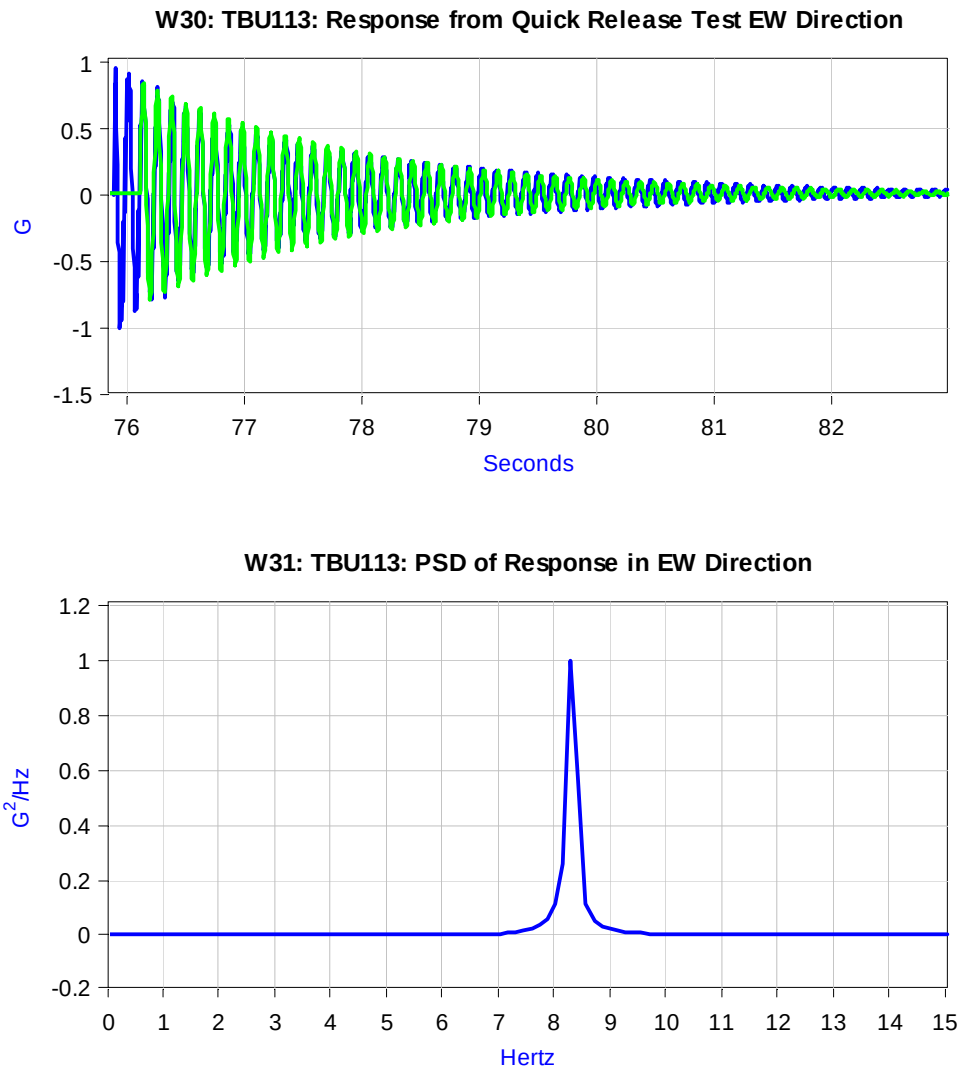

Figure D-10: Acceleration Response from Quick Release Test TBU114 – Bushing #4A

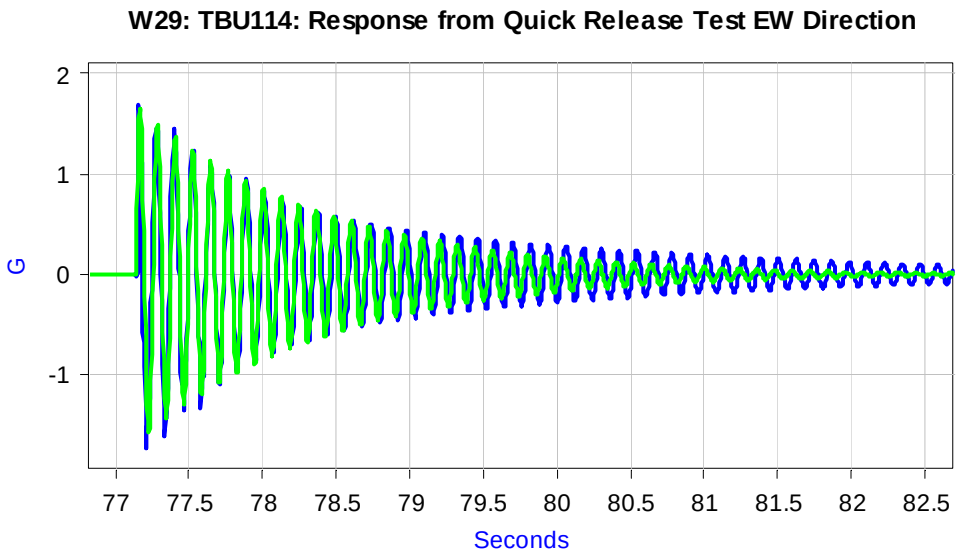

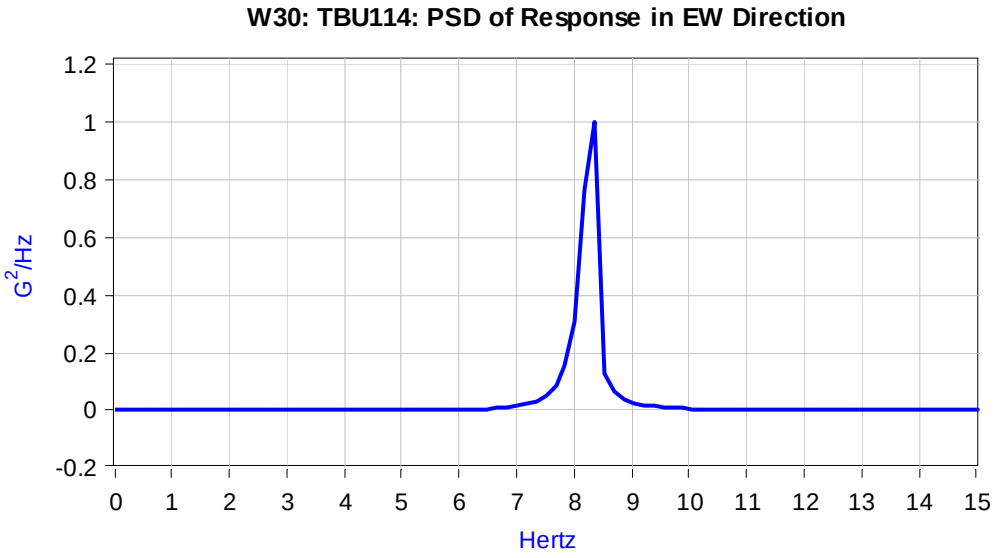

Figure D-11: Acceleration Response from Quick Release Test TBU115 – Bushing #4A

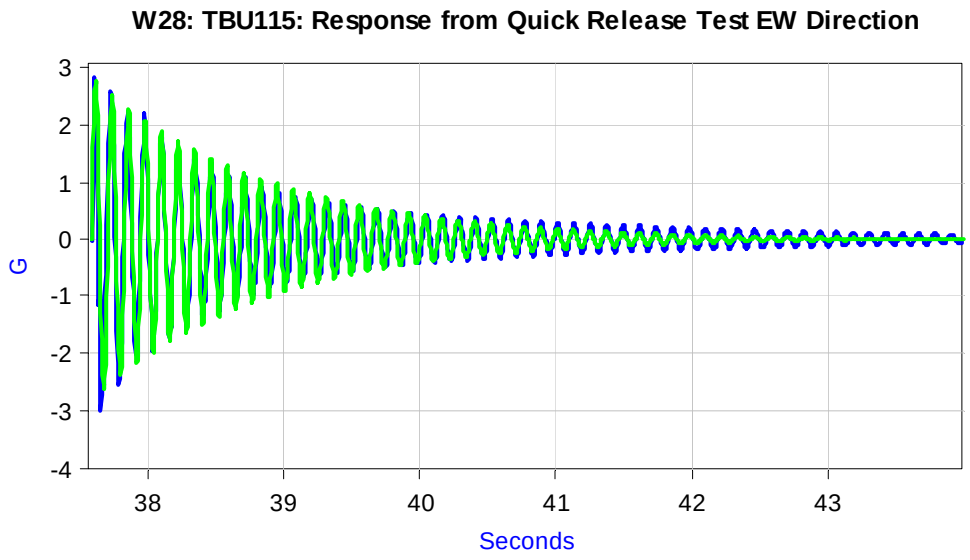

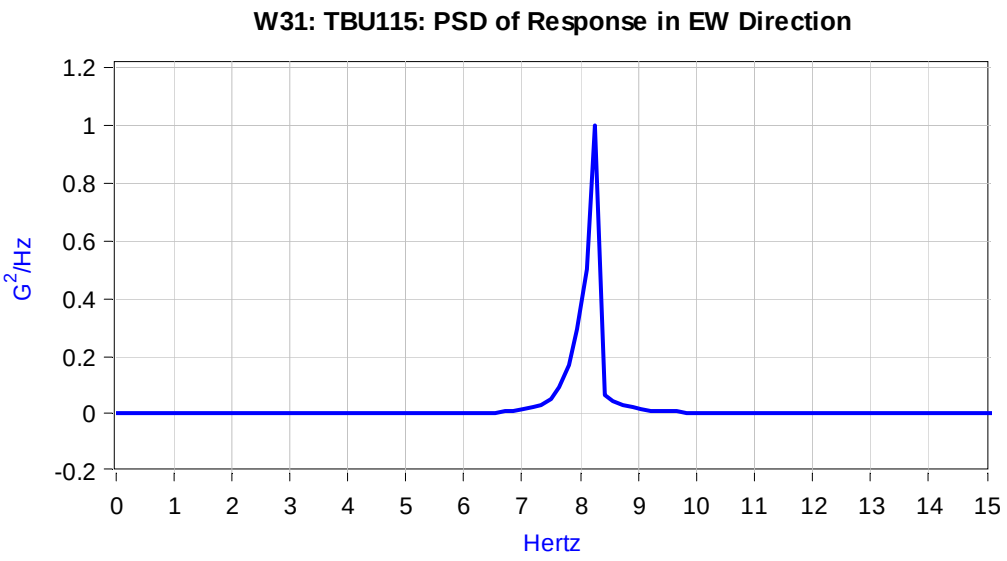

Figure D-12: Maximum Force vs. Maximum Displacement – Bushing #4A

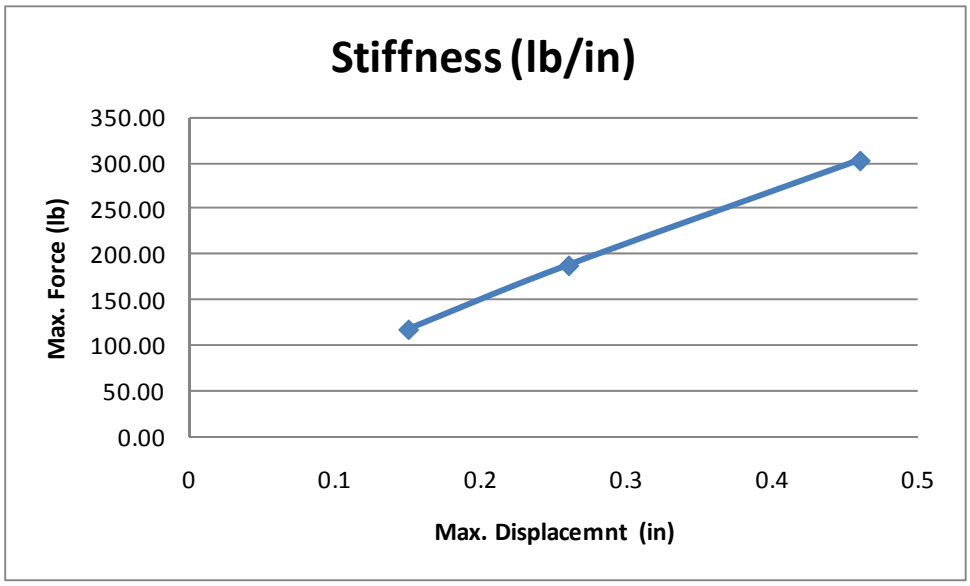

White Noise Tests

The frequencies and damping ratios of the bushing were determined by transfer functions obtained from white noise tests using the shake table. The peak of the transfer function is the fundamental frequency of the bushing and a half-power bandwidth method was used to determine the damping ratio. The summary of the frequencies is presented in Table D-1.

The frequencies from white noise tests were then used to develop "impulse tests" for the dominant frequencies of the bushing (see next section). The half-power bandwidth method used to determine damping is less accurate than a quick release, impact hammer or table impulse tests; therefore the ratios are re-determined in the following section using impulse tests. The acceleration transfer functions obtained in these tests are shown in Figures D-13 through D-22.

Figure D-13: Transfer Functions of Bushing #4A, Test TBU1wn23

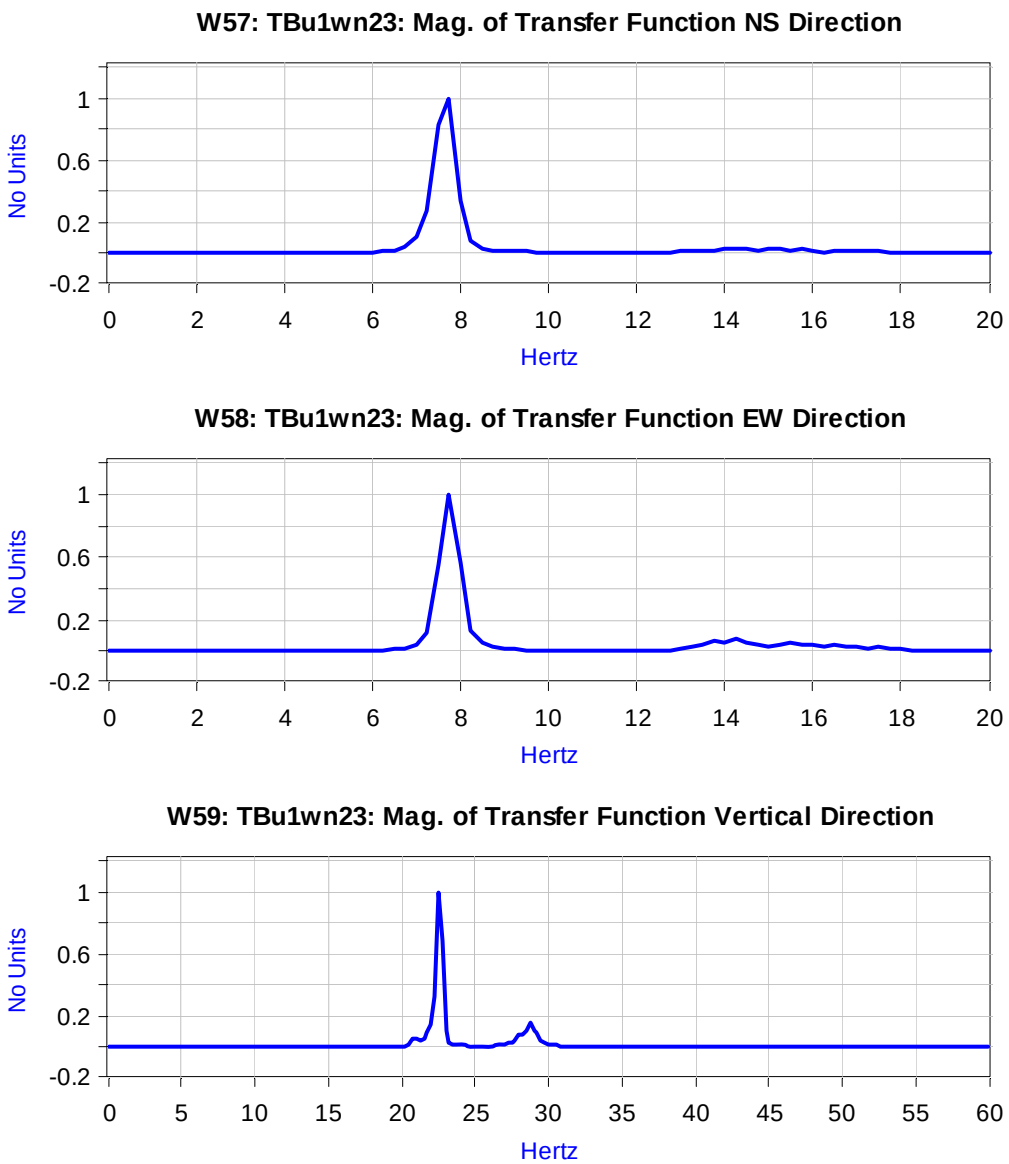

Figure D-14: Transfer Functions of Bushing #4A, Test TBU1wn26

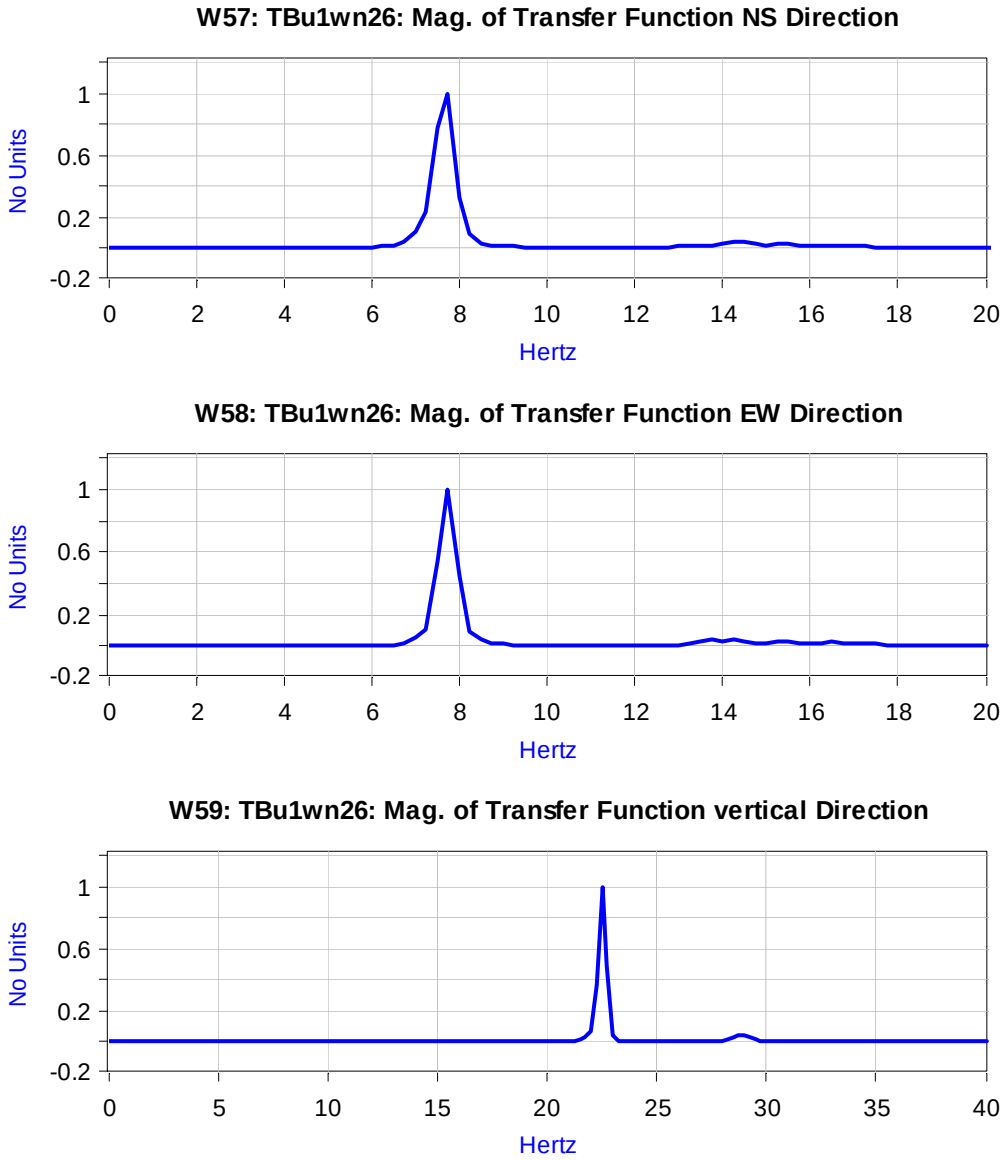

Figure D-15: Transfer Functions of Bushing #4A, Test TBU1wn28

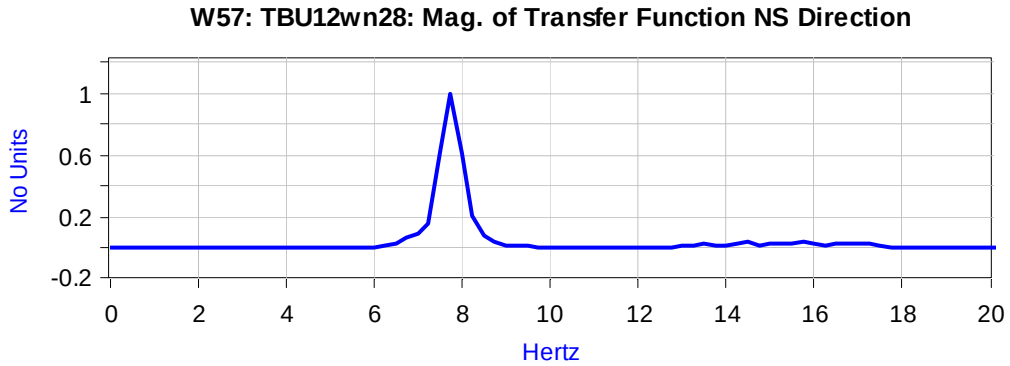

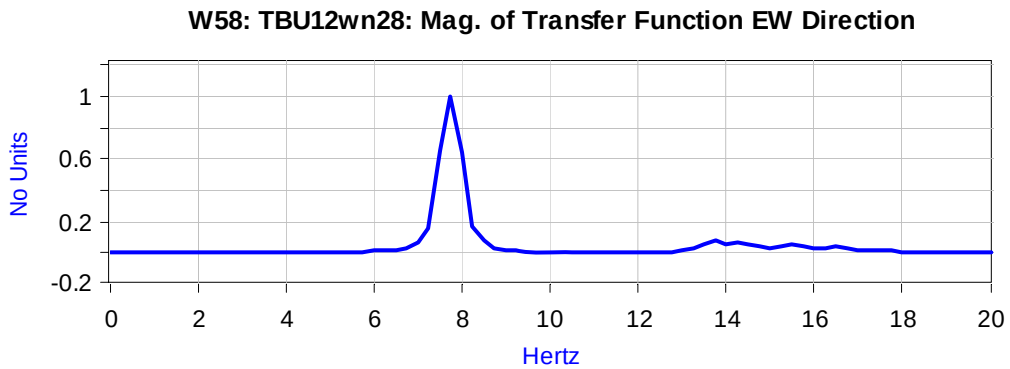

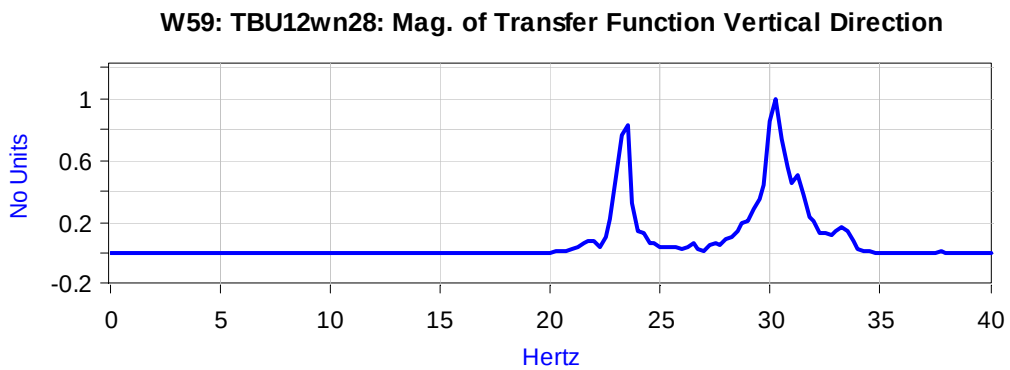

Figure D-16: Transfer Functions of Bushing #4A, Test TBU1wn31

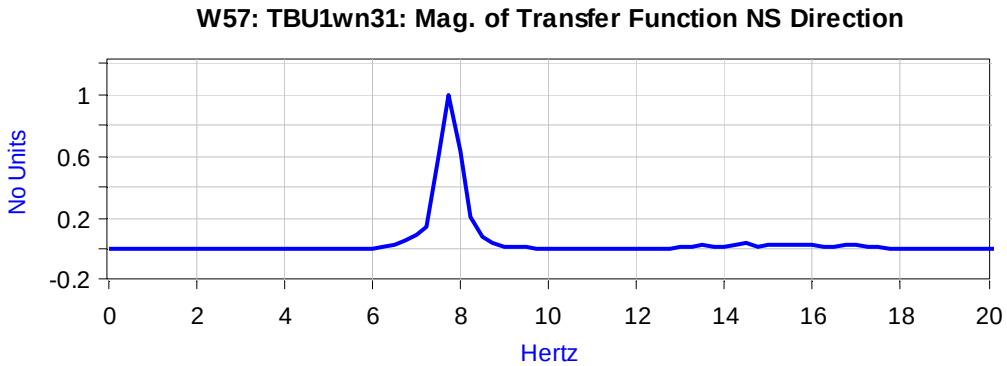

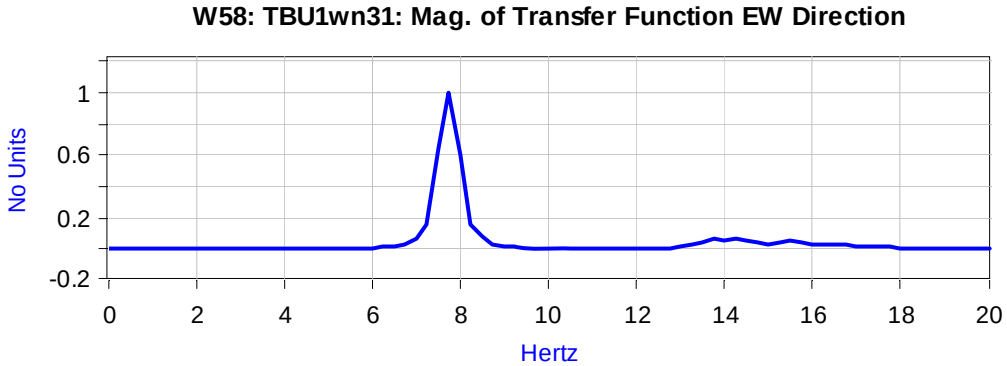

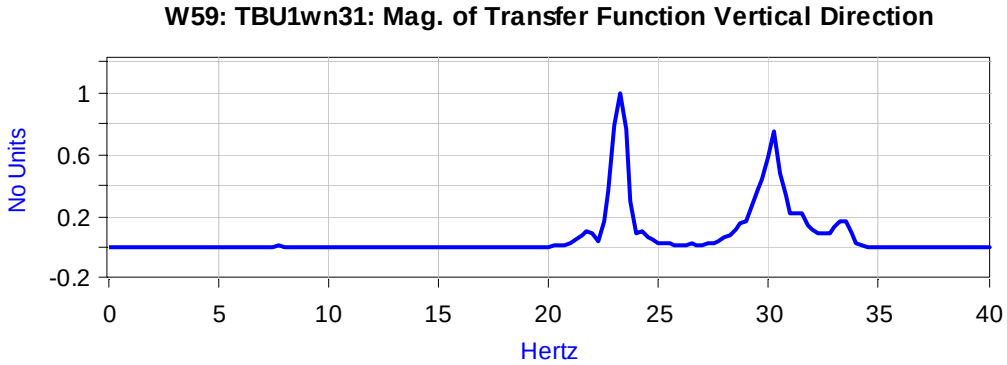

Figure D-17: Transfer Functions of Bushing #4A, Test TBU1wn33

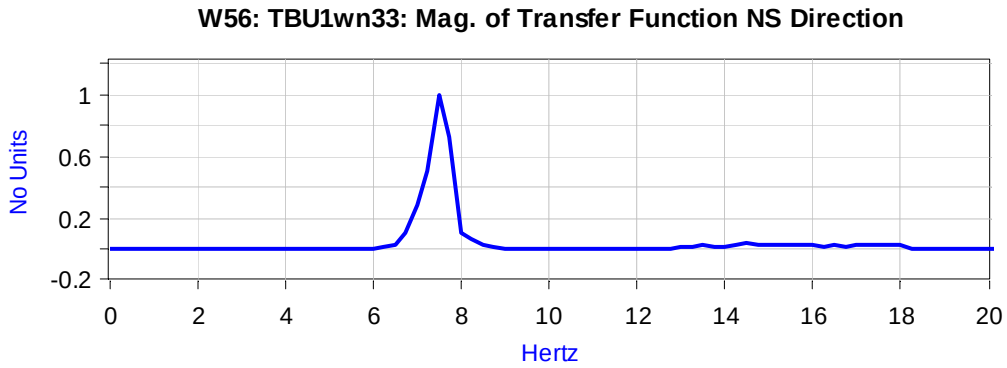

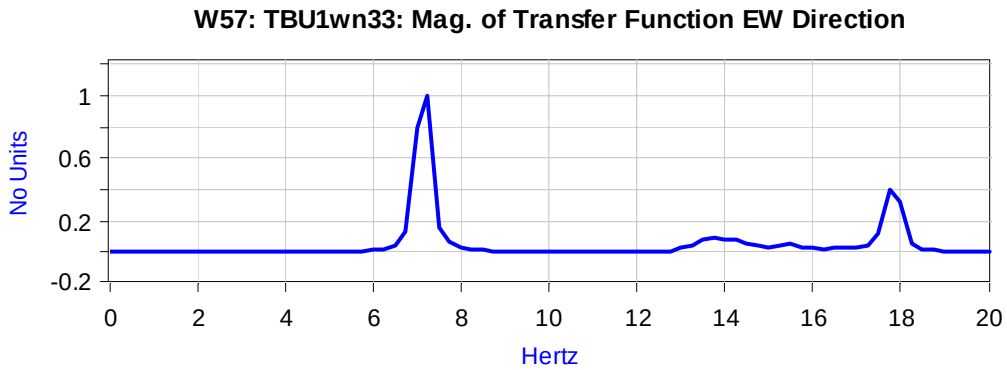

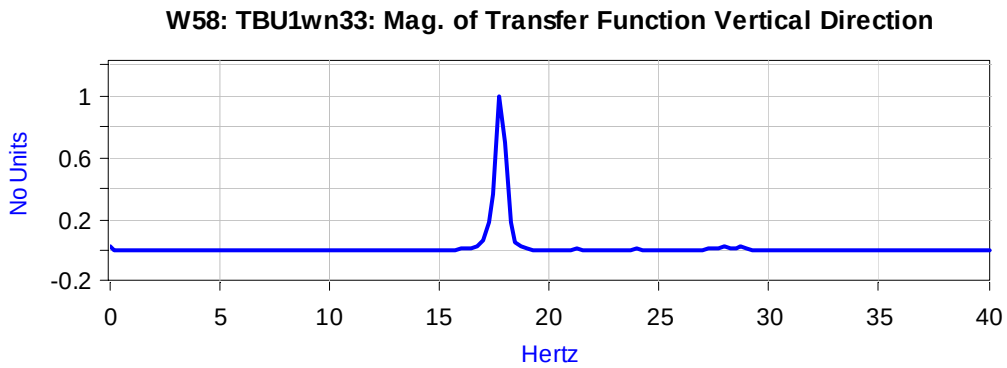

Figure D-18: Transfer Functions of Bushing #4A, Test TBU1wn36

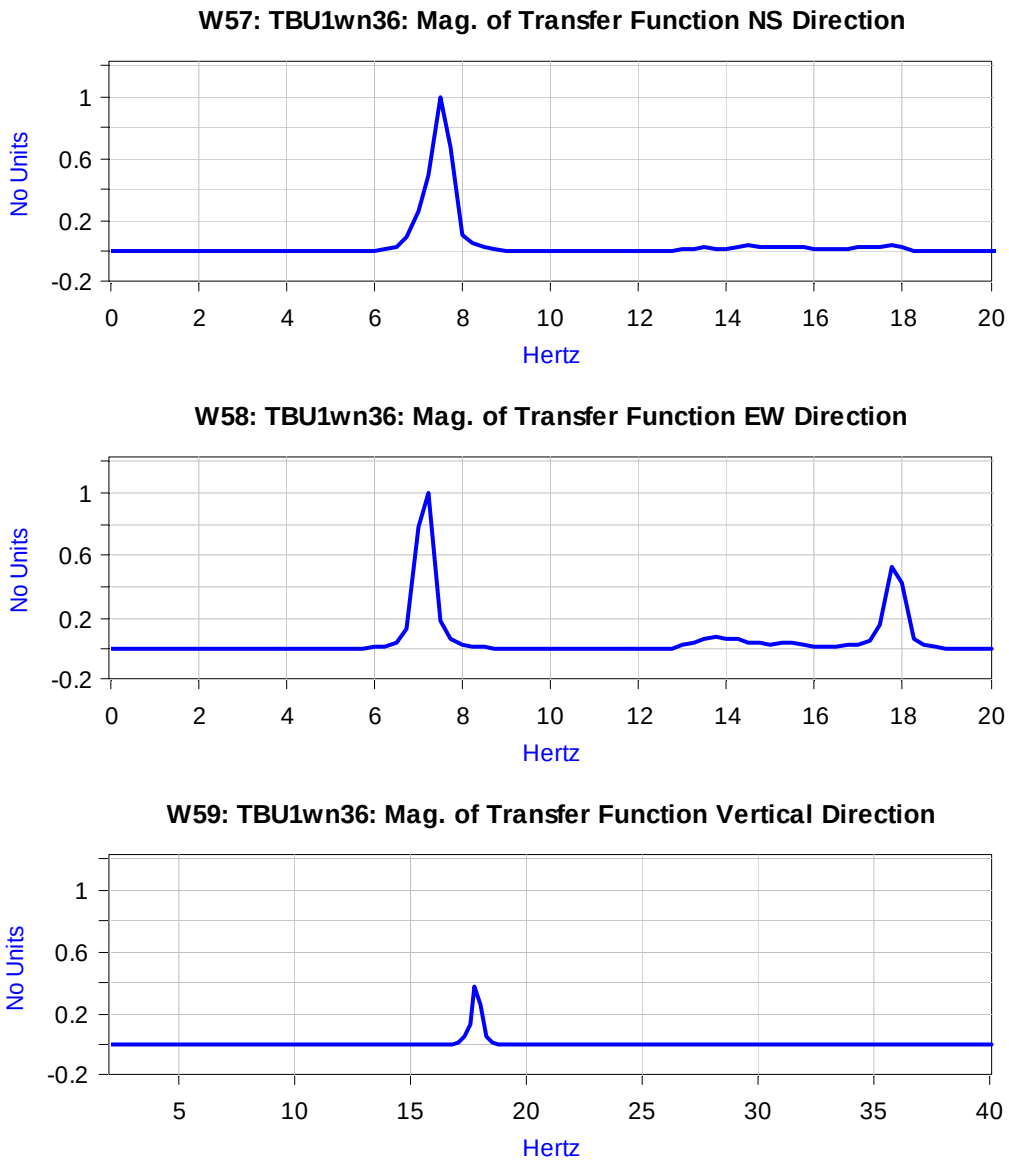

Figure D-19: Transfer Functions of Bushing #4A, Test TBU1wn38

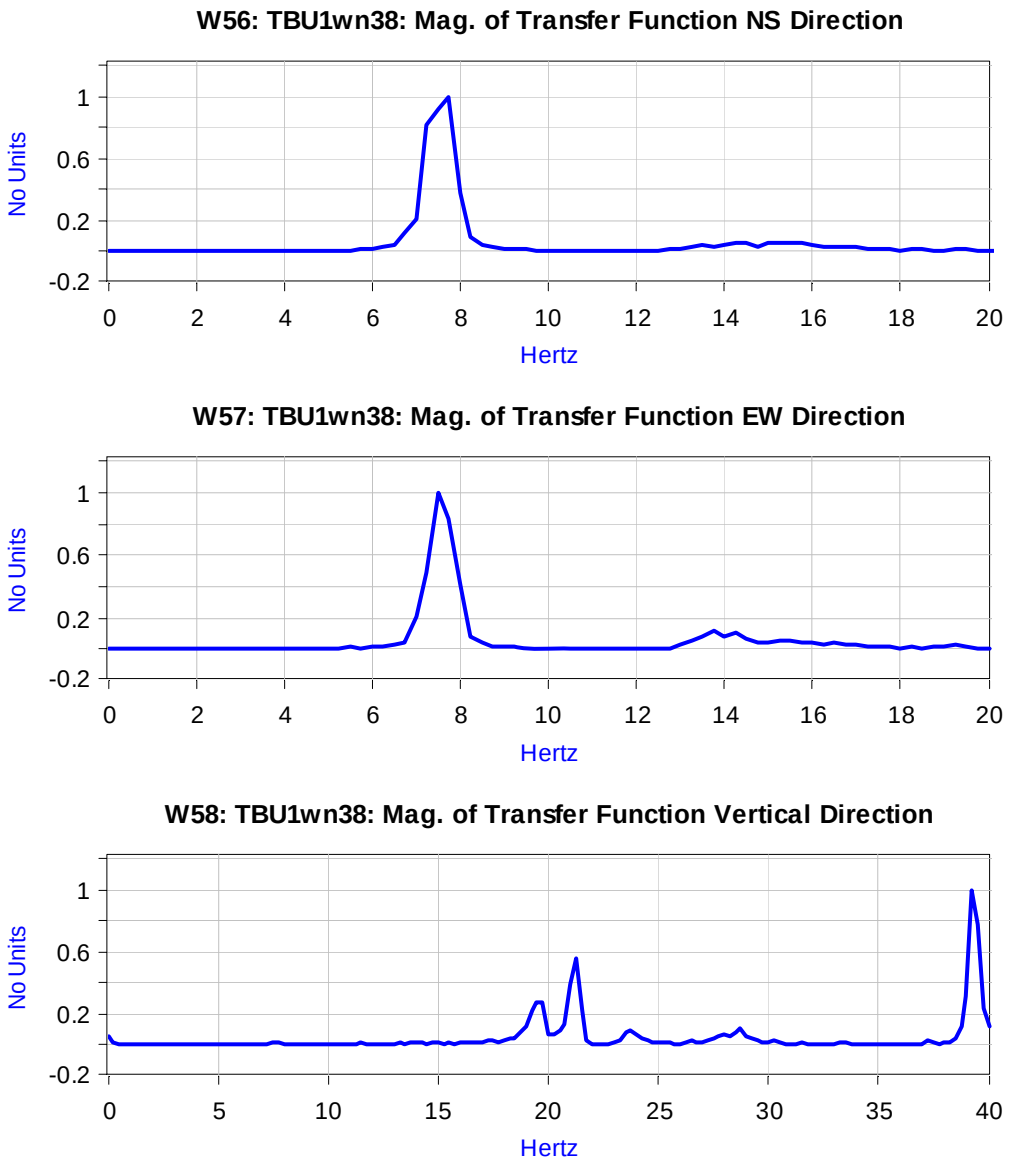

Figure D-20: Transfer Functions of Bushing #4A, Test TBU1wn41

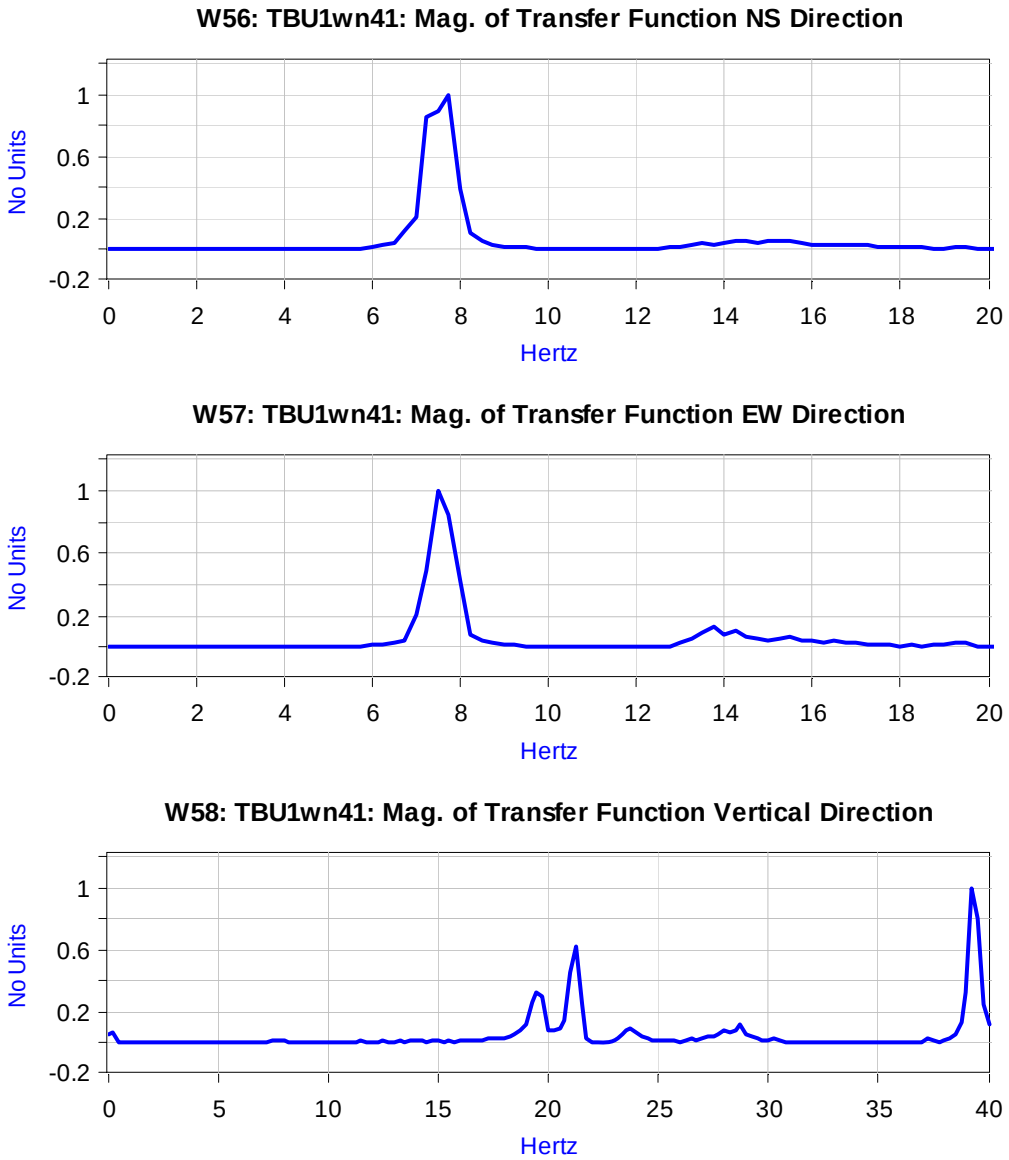

Figure D-21: Transfer Functions of Bushing #4A, Test TBU1wn43

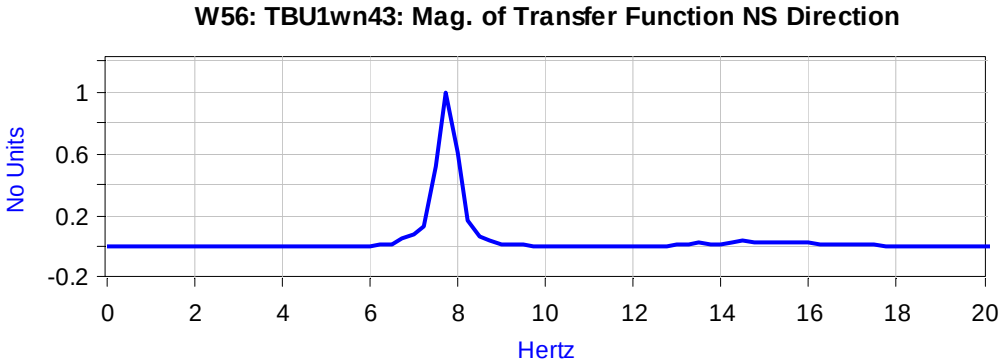

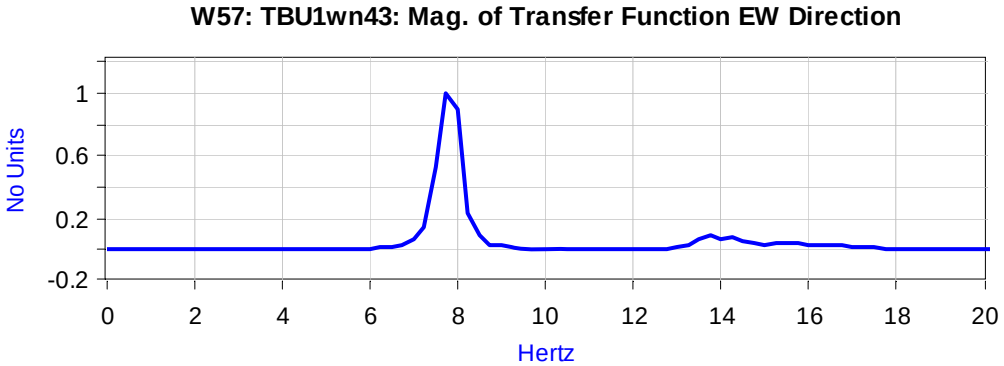

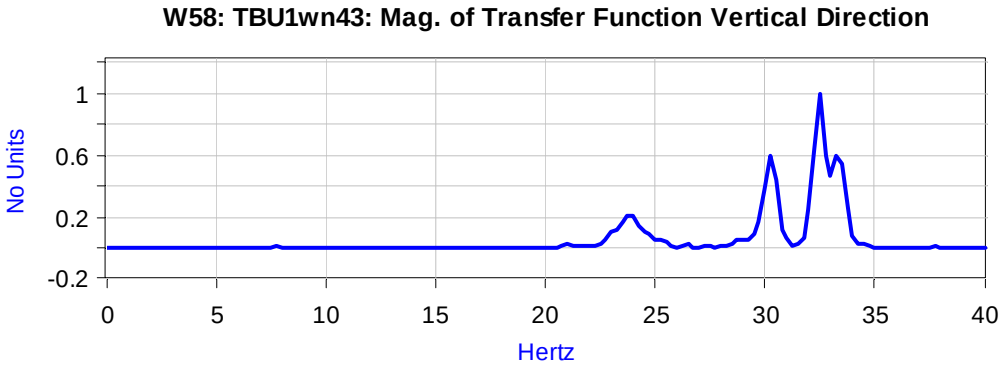

Figure D-22: Transfer Functions of Bushing #4A, Test TBU1wn46

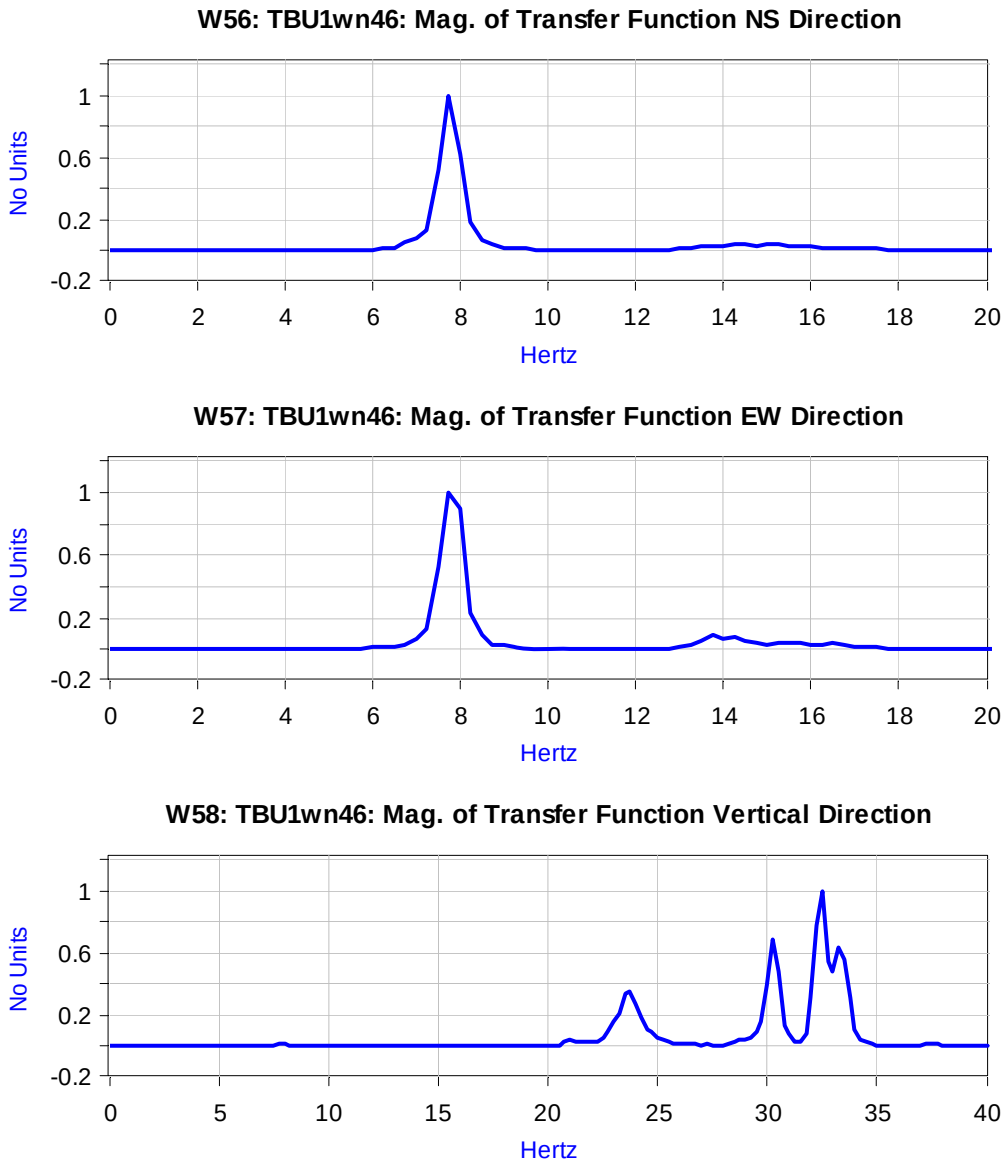

Table Impulse Tests

The table impulse test identifies frequencies and damping of dominant frequencies using smoothed table acceleration impulse for control of a shake table by using a smoothing table impulse procedure developed by the SEESL at University at Buffalo (Kong, 2010). For the identification of system frequencies, a power spectral density (PSD) was calculated from output motion at the top of the bushing and the system frequency is obtained by finding the frequency where the peak is located. For the identification of modal damping, a curve fitting method developed by the authors was used (Kong, 2010).

The acceleration history results of the table impulse tests are presented in Figures D-23 through D-32, and the dynamic characteristics are summarized in Table D-1. The frequencies of Bushing #4A in the NS direction are around 7.70 Hz in test TBU1TBI24 (before random motion tests), and 7.86 Hz in test TBU1TBI47; the damping values are 0.70% and 0.59%, respectively. The frequency in the EW direction is 7.78 Hz in test TBU1TBI24 (before random motion tests), and 7.80 Hz in test TBU1TBI47; the damping values are 0.70% and 0.72%, respectively.

Figure D-23: Table Impulse Test Response (Test TBU1TBI24) – Bushing #4A

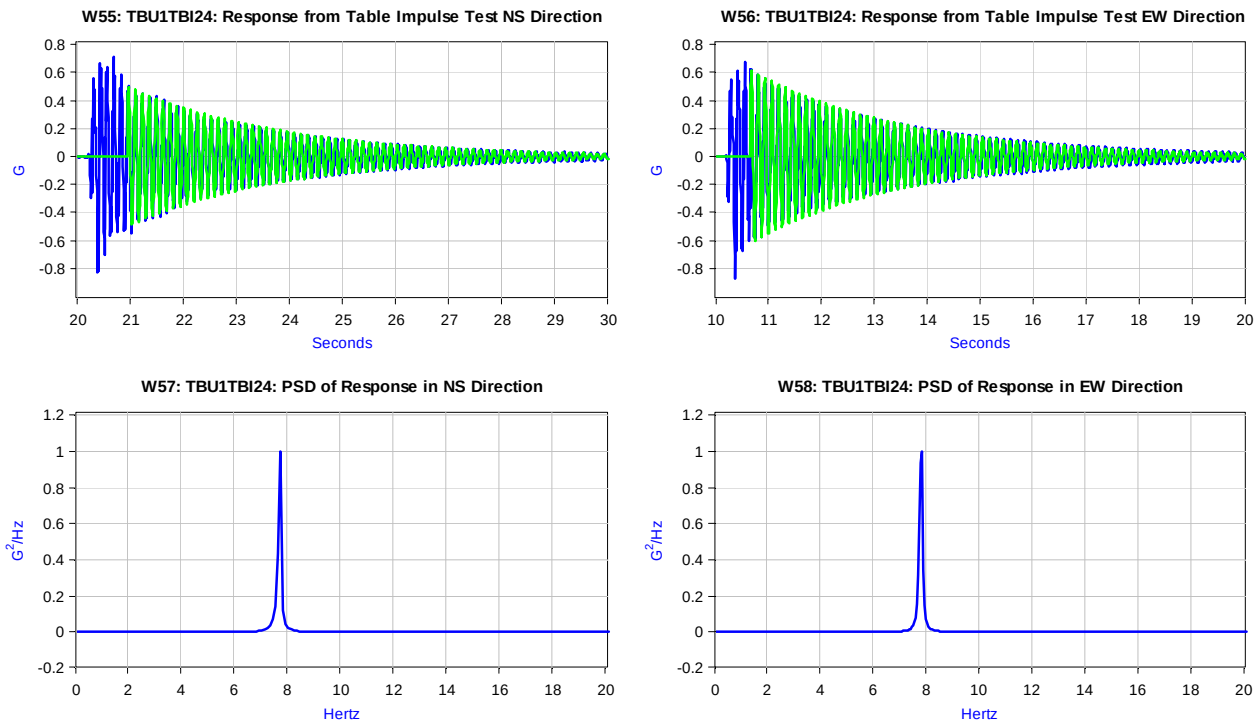

Figure D-24: Table Impulse Test Response (Test TBU1TBI27) – Bushing #4A

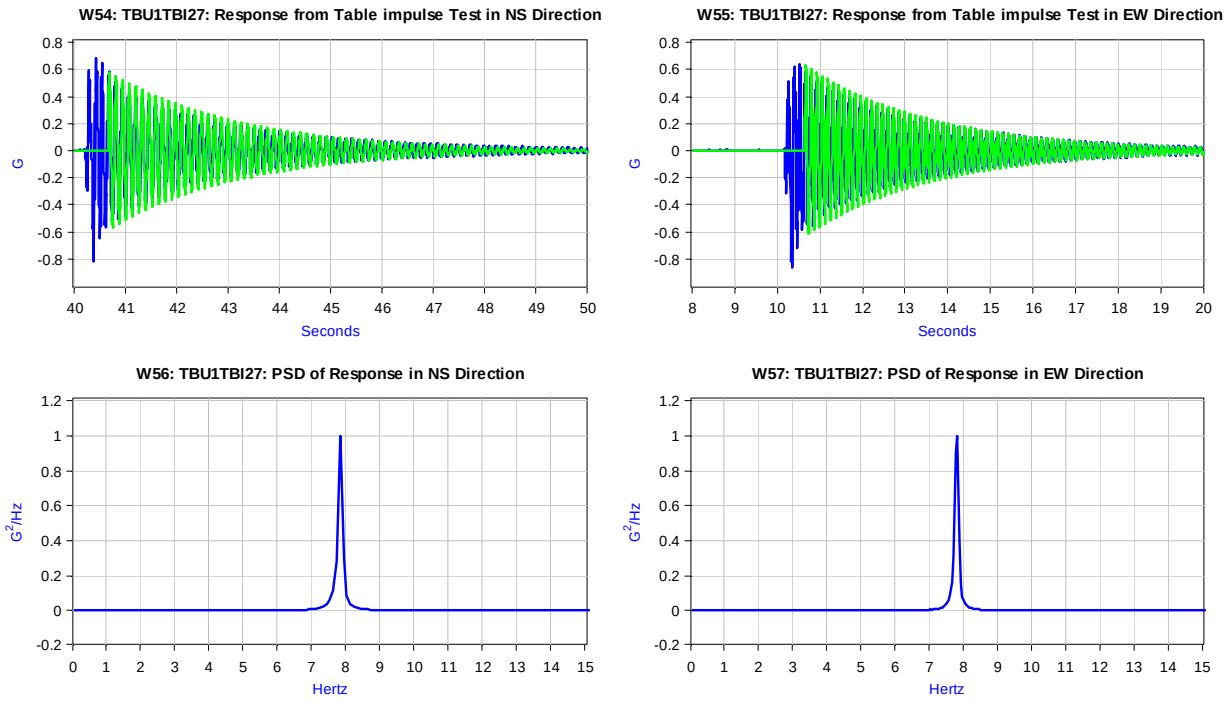

Figure D-25: Table Impulse Test Response (Test TBU1TBI29) – Bushing #4A

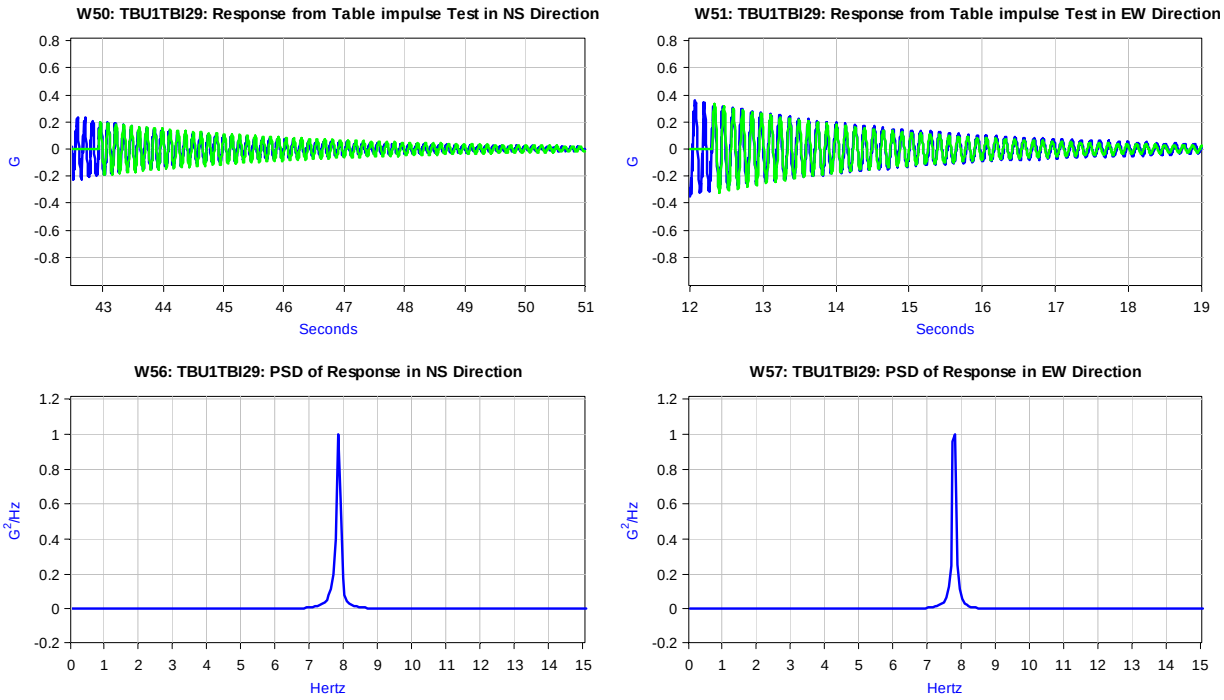

Figure D-26: Table Impulse Test Response (Test TBU1TBI32) – Bushing #4A

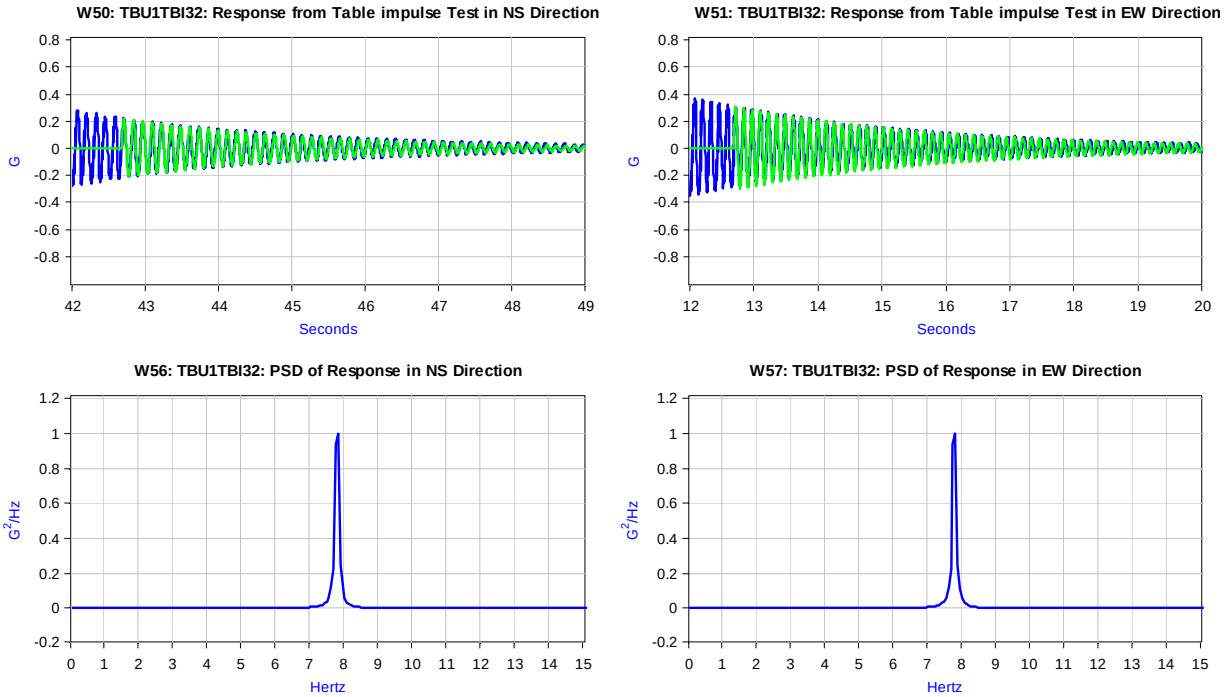

Figure D-27: Table Impulse Test Response (Test TBU1TBI34) – Bushing #4A

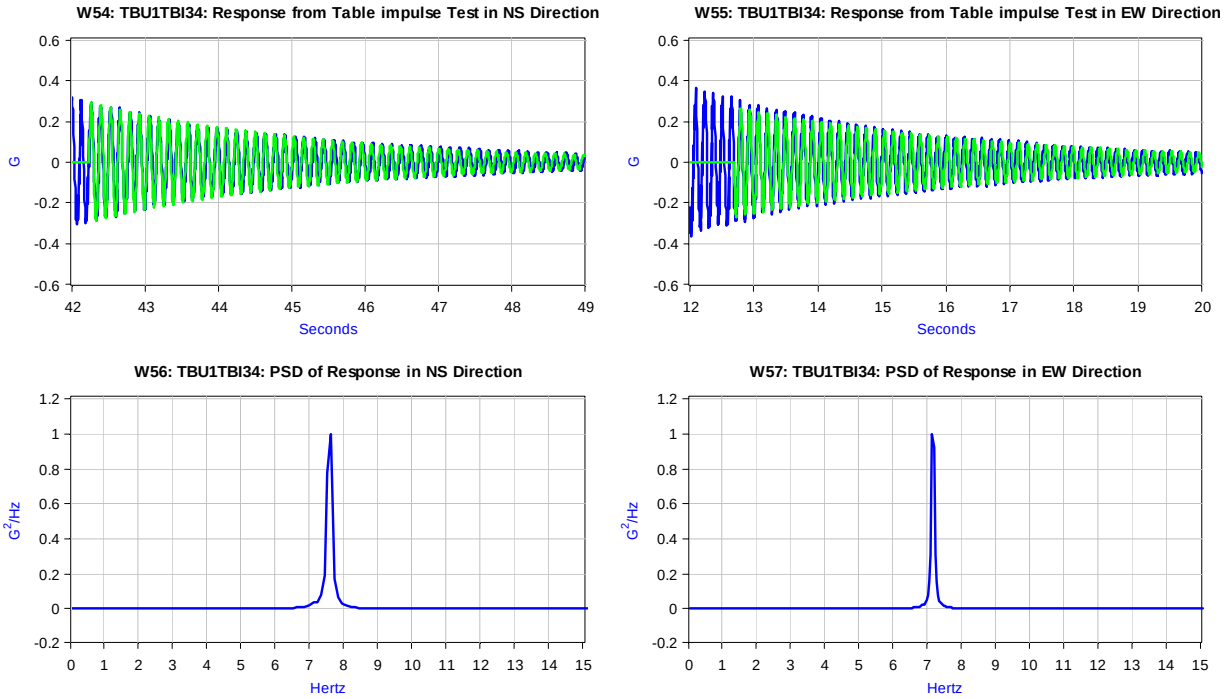

Figure D-28: Table Impulse Test Response (Test TBU1TBI37) – Bushing #4A

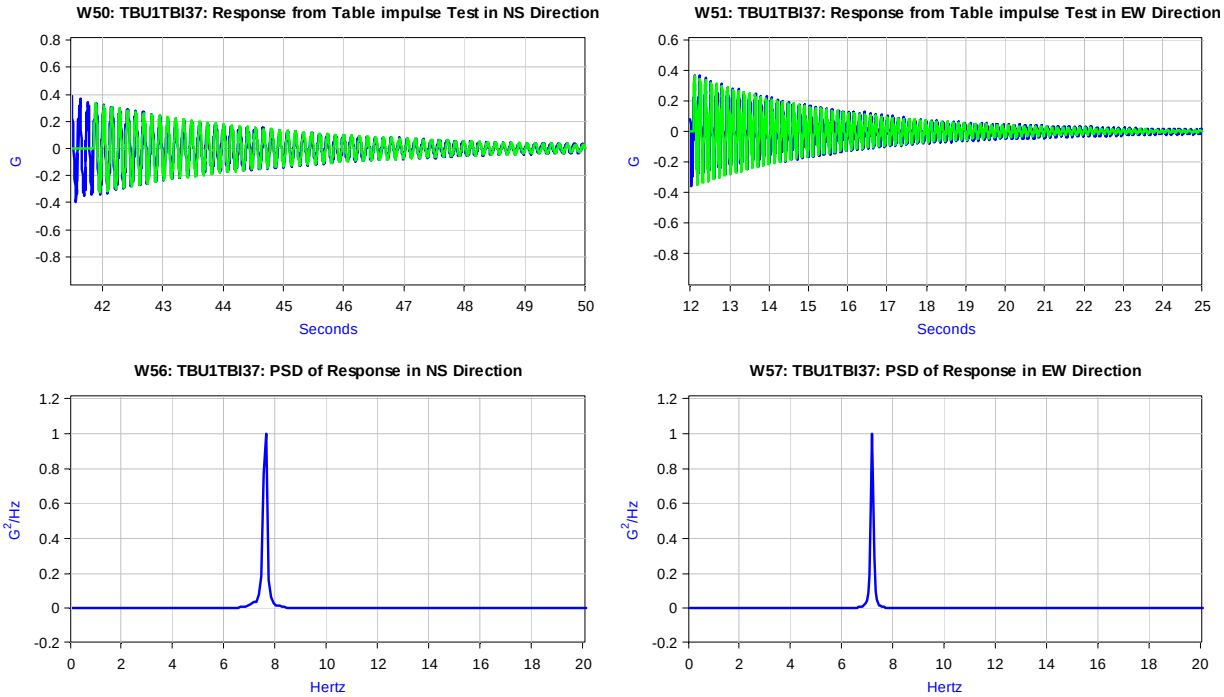

Figure D-29: Table Impulse Test Response (Test TBU1TBI39) – Bushing #4A

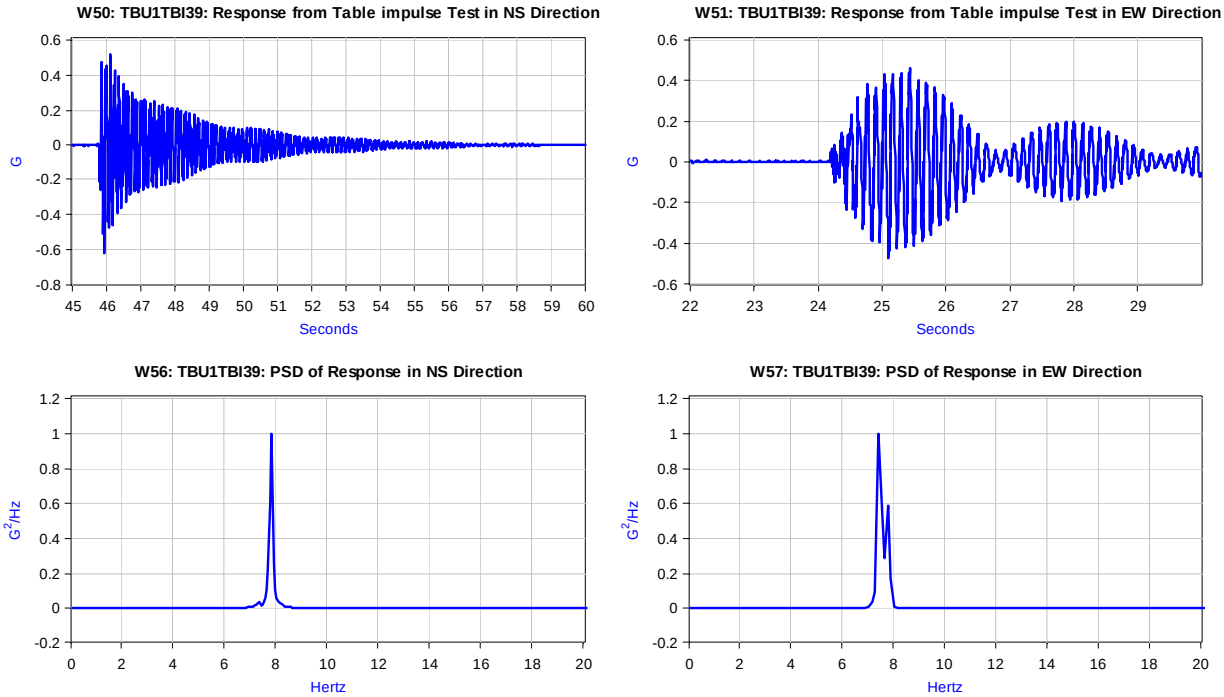

Figure D-30: Table Impulse Test Response (Test TBU1TBI42) – Bushing #4A

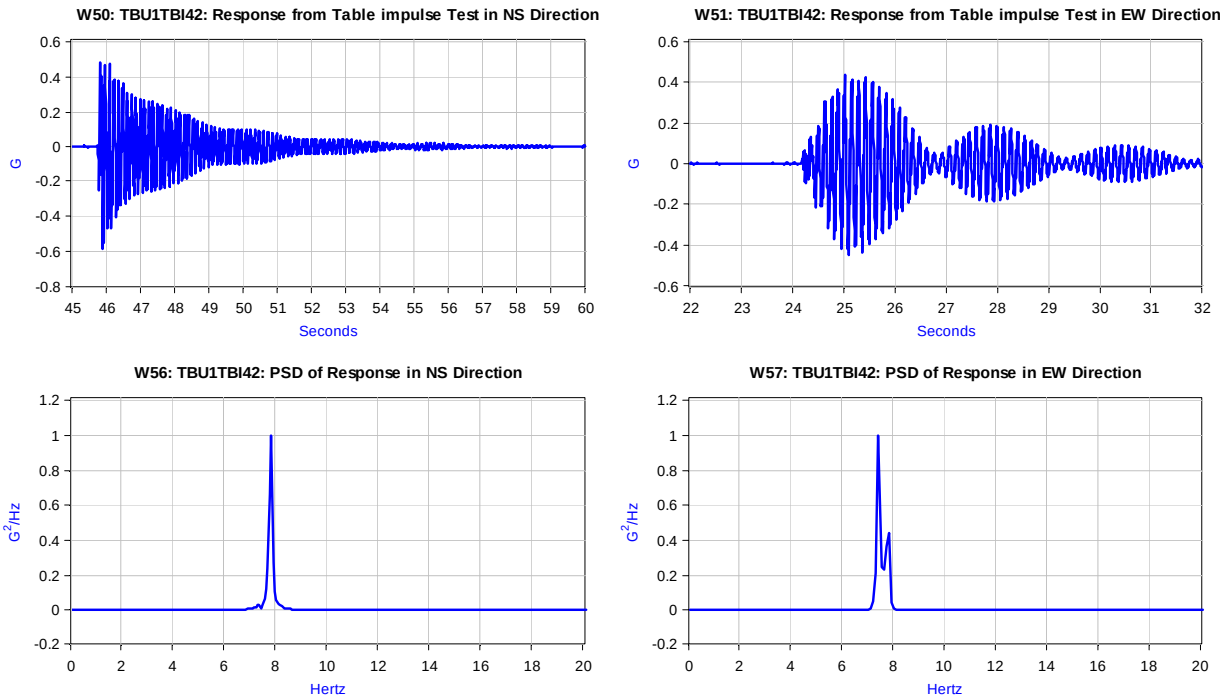

Figure D-31: Table Impulse Test Response (Test TBU1TBI44) – Bushing #4A

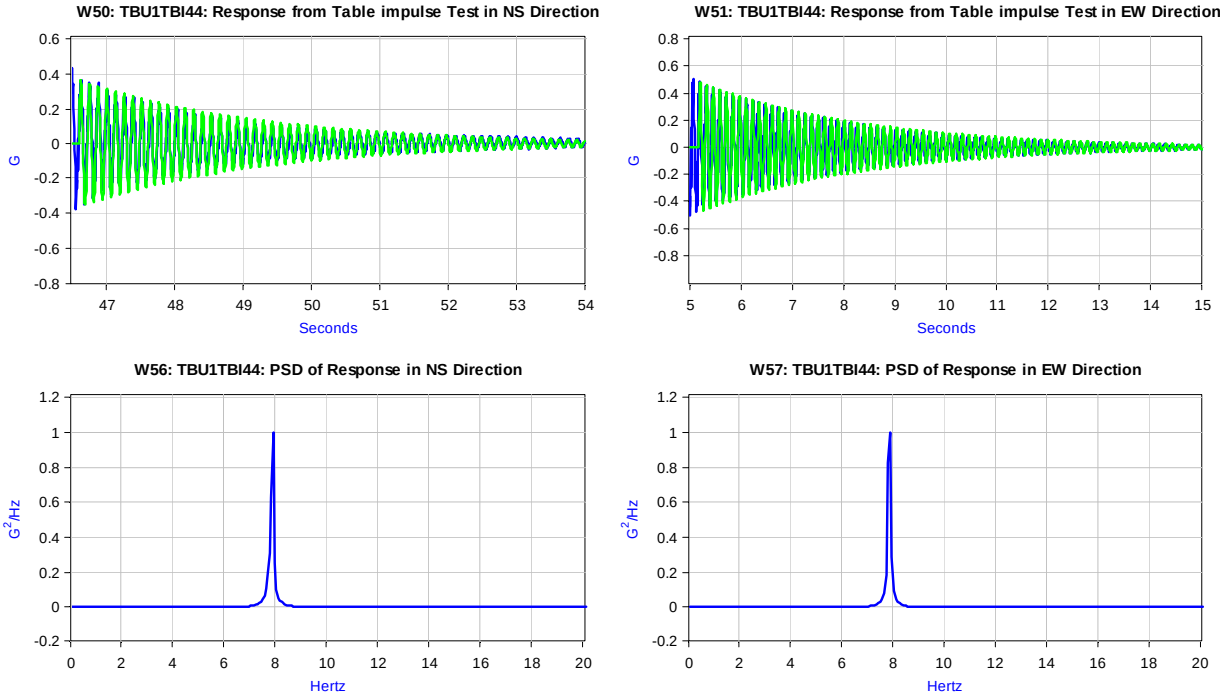

Figure D-32: Table Impulse Test Response (Test TBU1TBI47) – Bushing #4A

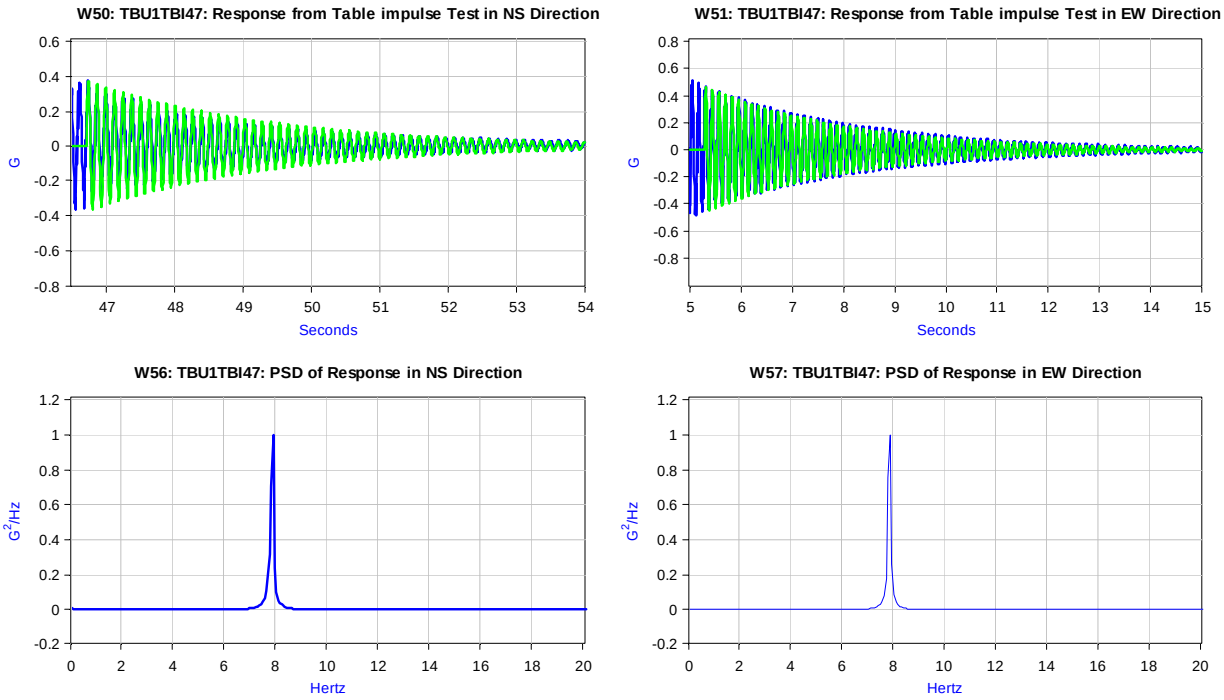

Acceleration History Tests

Acceleration history tests were performed for the seismic demand quantification of Bushing #4A. A summary of the accelerations recorded on various locations on the bushing is shown in Table D-2 for the five levels of test input motions.

This bushing was tested in all 3 locations on the frame: center, side and corner. These configurations were necessary to see if there was any change in the principal direction of motion. It was noticed that when the bushing is mounted on the corner, the principal axis of motion rotates by 45°. The effect of stiffeners was also part of the testing. Two L4X6X3/4 stiffeners were used to stiffen the plate. The main purpose of these tests was to eliminate any dynamic amplification of response due to plate flexibility. The stiffeners were first used when the bushing was mounted in the center location, and two stiffeners were used on either side of the bushing along the NS direction, in test TBU1AH12525. For the next test, TBU1AH12530, the bushing was moved to the side of the frame and two stiffeners were again used along the NS direction. For the last test the bushing was mounted on the corner and one stiffener was used. For all these tests, the frequency, damping ratio and moment demand were measured.

The acceleration history tests were used for calculations of the bending moment of the bushing at flange level. Strain gauges were used to measure the bending moment directly. A summary of bending moments is presented in Table D-2 and shown graphically in Figures D-33 through D-37.

Table D-2: Summary of Accelerations and Bending Moments – Bushing #4A

Location	Units	0.125 g RRS			0.125 g RRS			0.125 g RRS			0.125 g RRS			0.125 g RRS		
		TBU1AH12525			TBU1AH12530			TBU1AH12535			TBU1AH12540			TBU1AH12545		
(1)	(2)	(3)	(4)	(5)	(6)	(7)	(8)	(9)	(10)	(11)	(12)	(13)	(14)	(15)	(16)	(17)
Bushing Location on Frame																
Acceleration Distribution along the Height of Testing Setup																
Direction		NS	EW	Vertical	NS	EW	Vertical	NS	EW	Vertical	NS	EW	Vertical	NS	EW	Vertical
Top of Bushing	(g)	1.24	0.83	0.66	0.73	0.68	0.34	0.79	0.84	0.24	1.00	0.93	0.21	0.81	0.78	0.31
Upper CG Of Bushing	(g)	0.48	0.43	-	0.35	0.35	-	0.35	0.41	-	0.46	0.42	-	0.39	0.37	-
CG OF Bushing	(g)	0.30	0.26	-	0.21	0.20	-	0.23	0.25	-	0.25	0.23	-	0.21	0.21	-
Interface Ring	(g)	0.21	0.19	0.61	0.14	0.17	0.25	0.16	0.17	0.18	0.16	0.18	0.18	0.15	0.18	0.25
Shake Table	(g)	0.18	0.17	0.12	0.12	0.15	0.10	0.14	0.16	0.11	0.15	0.16	0.11	0.14	0.16	0.11
Bending Moment at the Base of Bushing																
Moment from Strain Gauges	kip-in	11.28	8.00	-	7.39	6.67	-	7.20	8.20	-	9.24	9.91	-	7.85	7.67	-

Figure D-33: Bending Moment of Bushing #4A in Horizontal Direction – Test TBU1AH12525

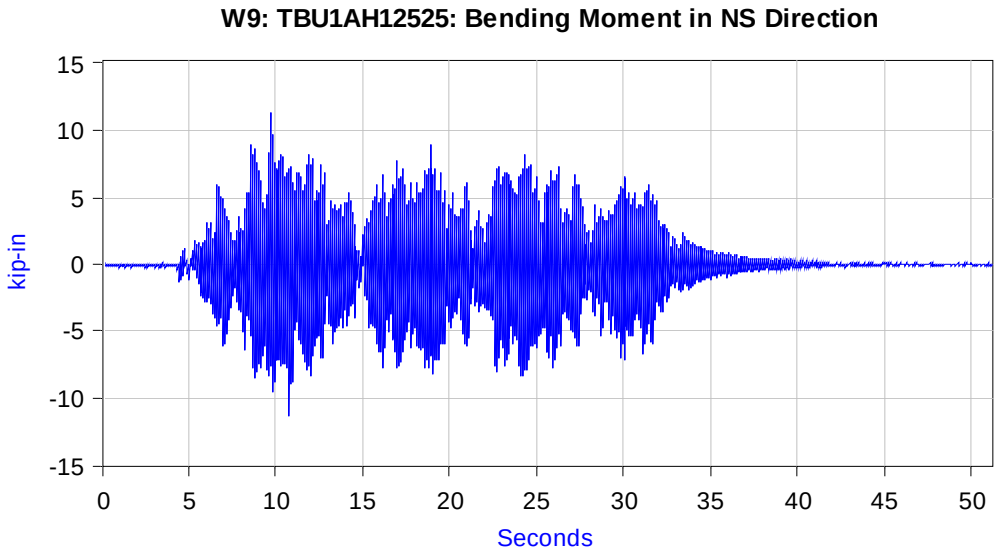

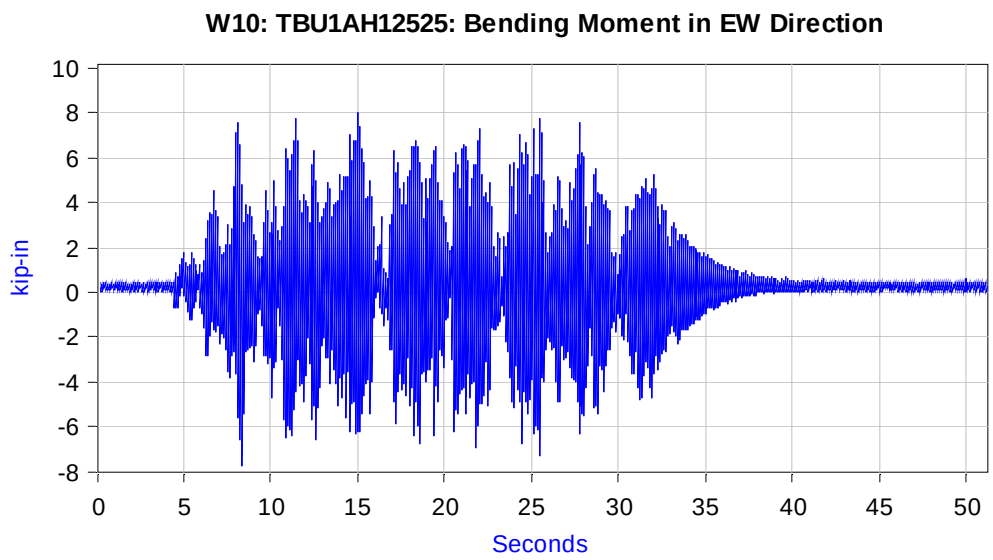

Figure D-34: Bending Moment of Bushing #4A in Horizontal Direction – Test TBU1AH12530

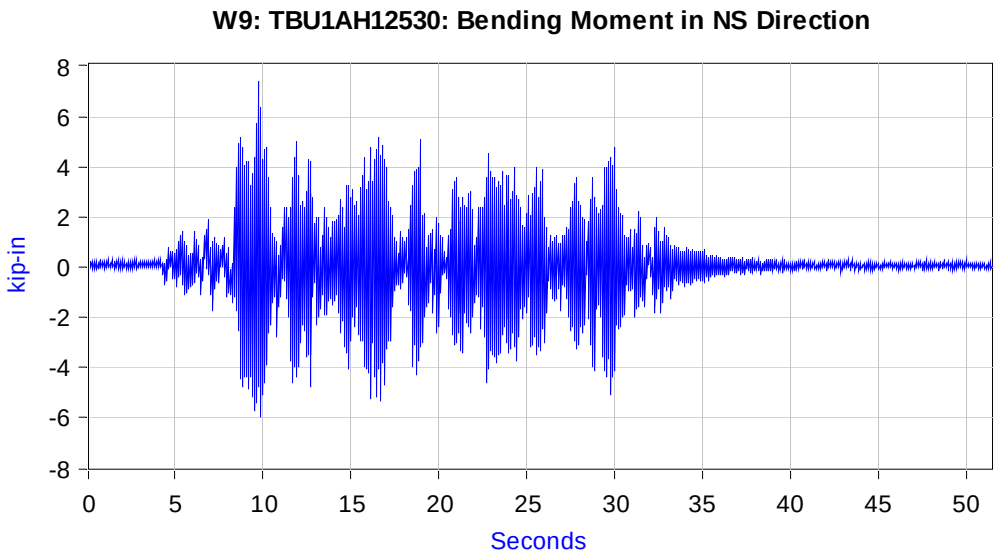

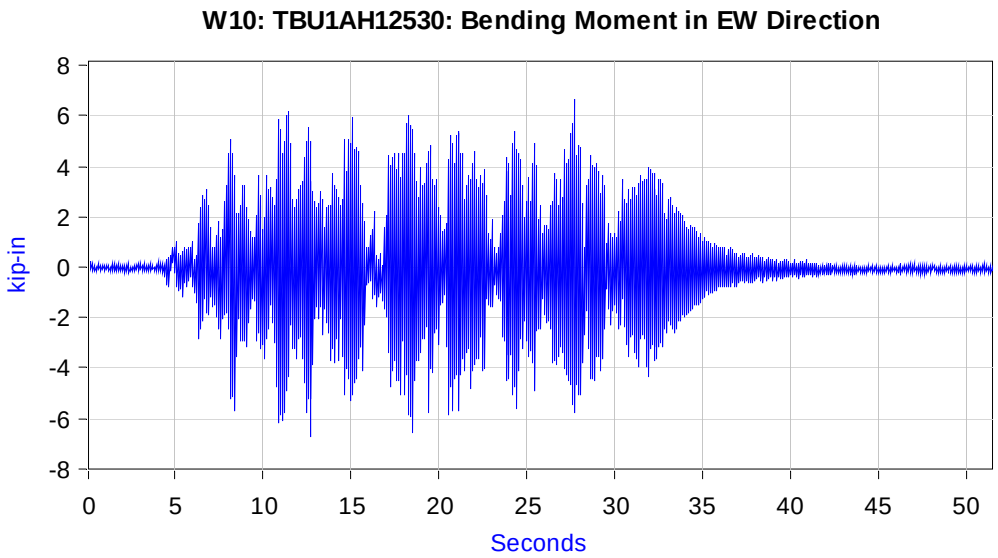

Figure D-35: Bending Moment of Bushing #4A in Horizontal Direction – Test TBU1AH12535

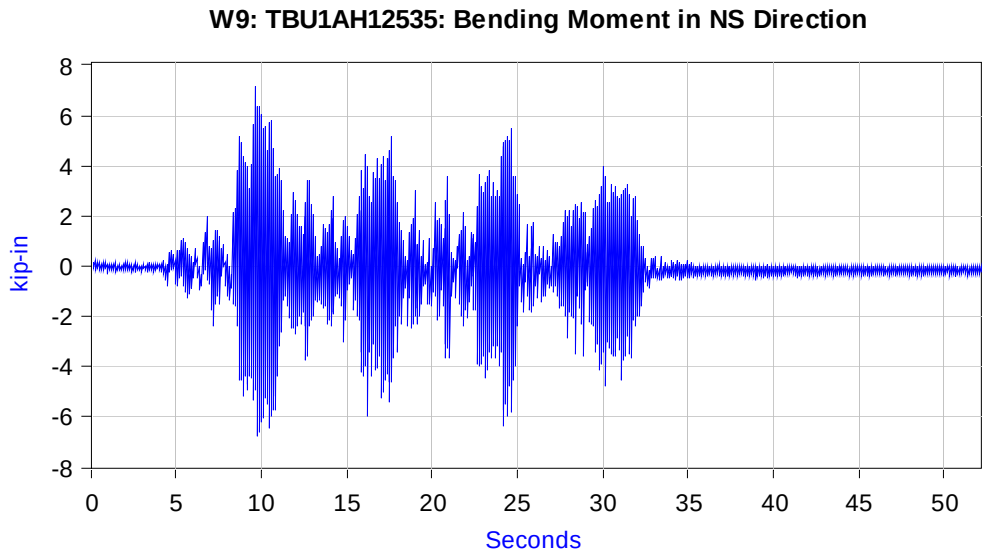

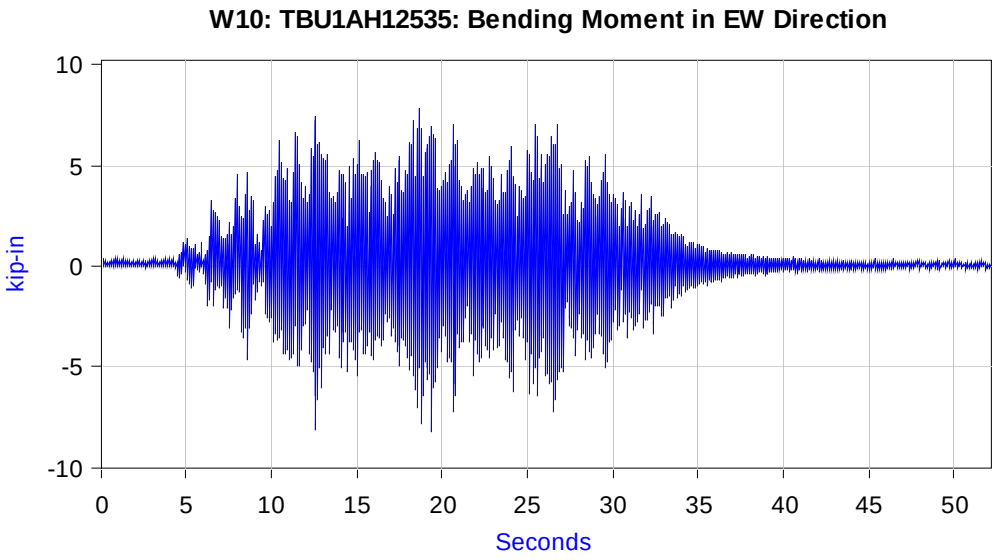

Figure D-36: Bending Moment of Bushing #4A in Horizontal Direction – Test TBU1AH12540

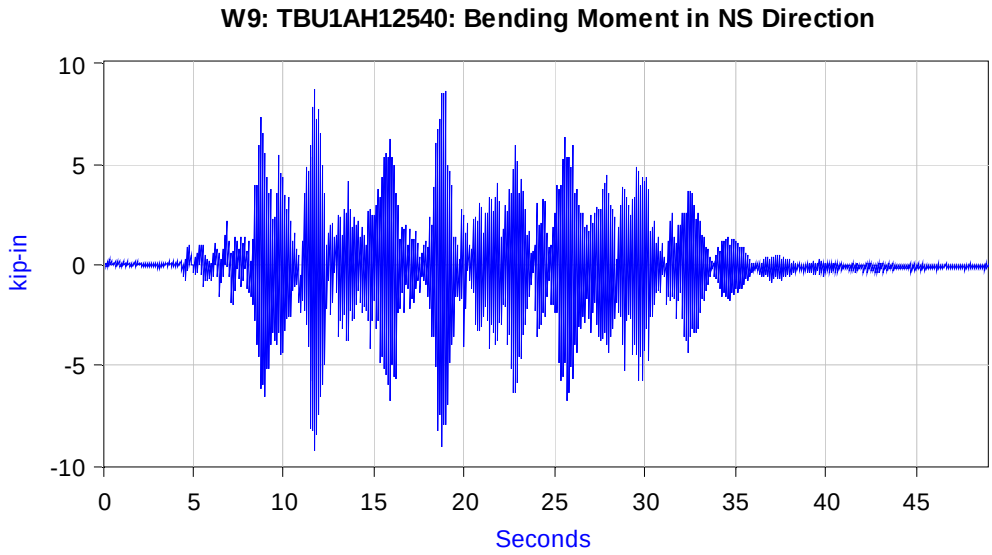

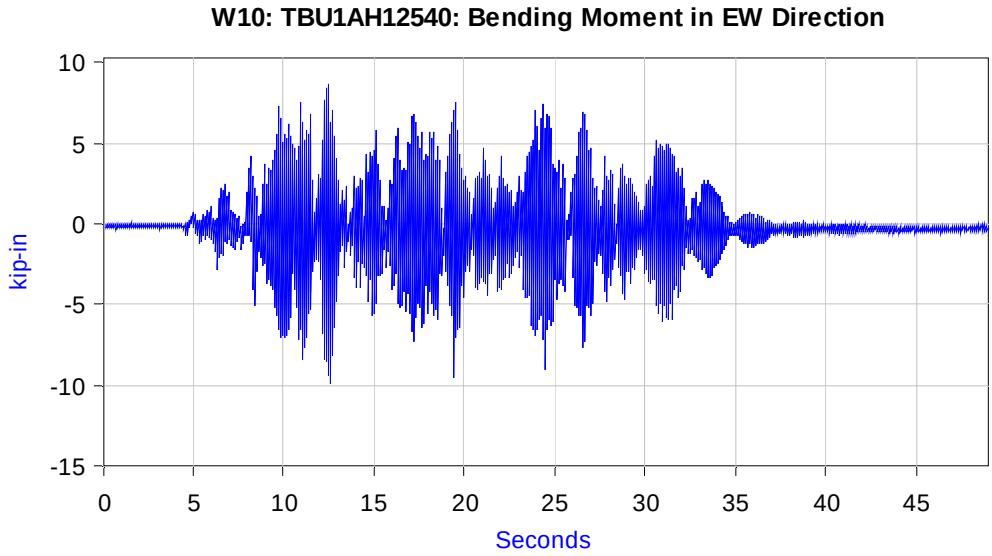

Figure D-37: Bending Moment of Bushing #4A in Horizontal Direction – Test TBU1AH12545

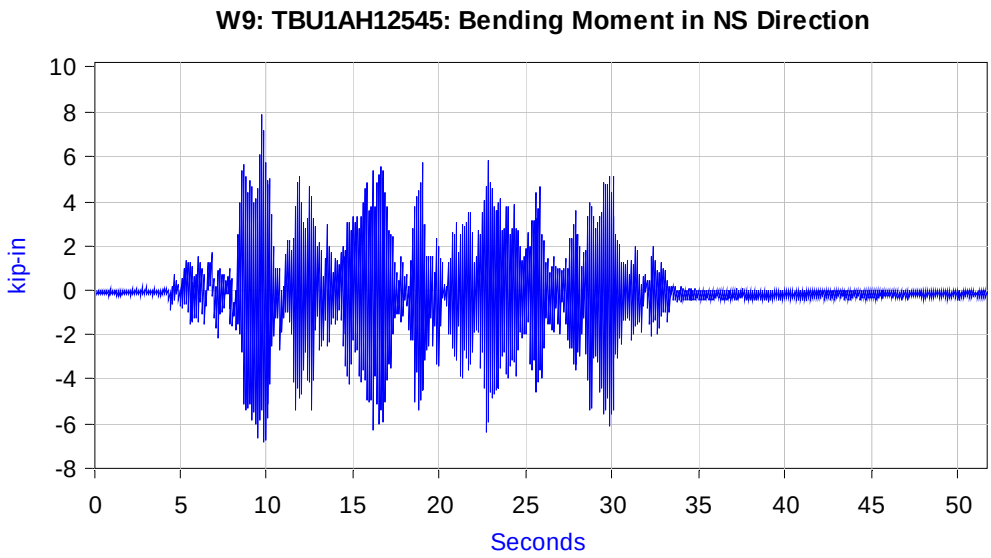

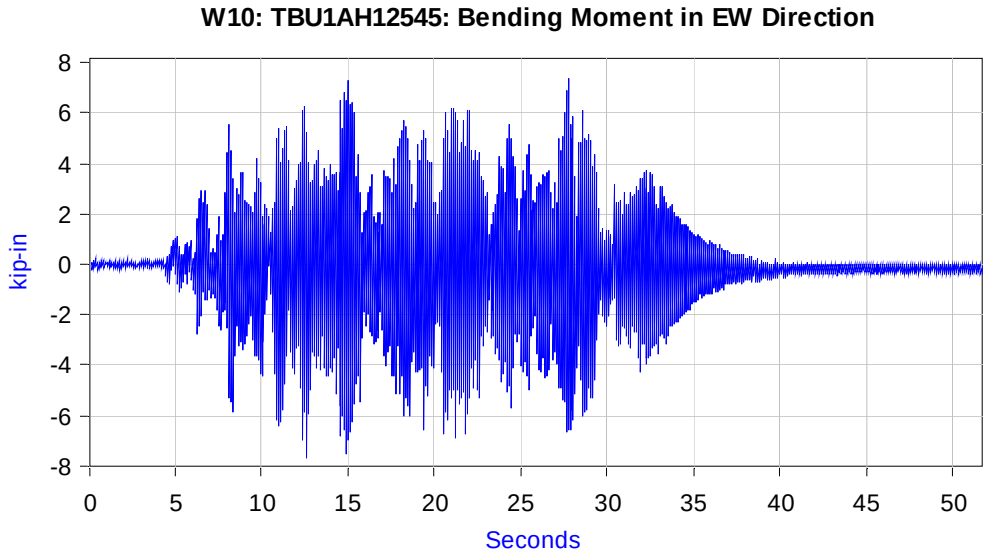

Residual Capacity Testing to Failure: Final Pull Test

Residual capacity testing of Bushing #4A was performed using static loading in a fixed-base configuration.

After the dynamic testing, Bushing #4A was installed on the fixed support and was pulled from the top. Figure D-38 shows the plots of all the tests. The force was increased in successive tests until a cracking sound was heard in test TBU1PL62. Cracks were not visible with the naked eye; however, the bushing was sawed longitudinally and cracks were visible in the capacitor material as shown in Figure D-39. The failure occurred at 2,855.6 lb., somewhat above expectation. Table D-1 shows the maximum displacement corresponding to the maximum force and bending moment observed at the critical section.

The test results also showed significant degradation of stiffness. A plot of maximum force vs. displacement is shown in Figure D-40. The stiffness reduction is also apparent from this graph, as shown by the dashed line between the last two points.

Figure D-38: Force vs. Displacement from Pull Tests – Bushing #4A

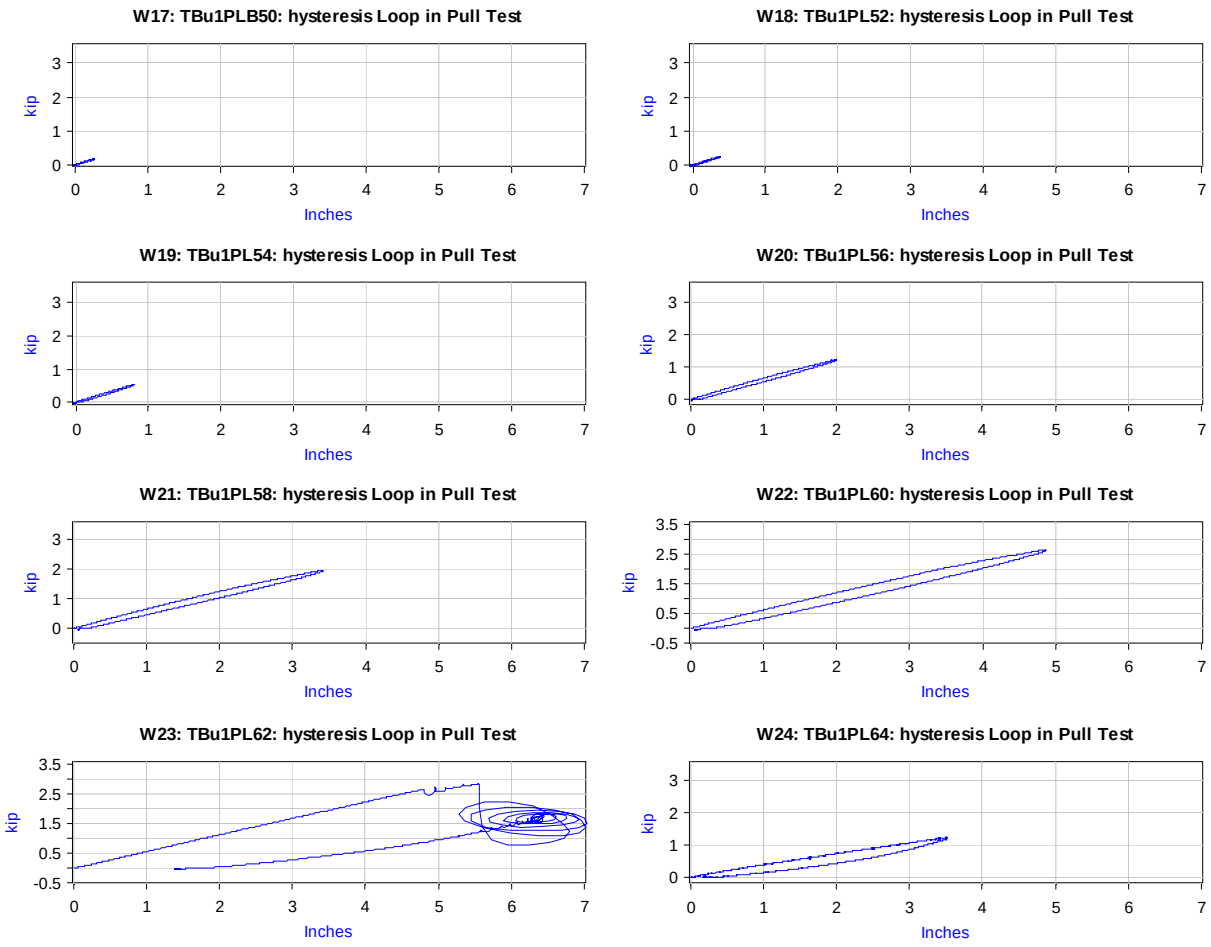

Figure D-39: Sectionalizing of Bushing #4A Showing the Visible Crack

Figure D-40: Maximum Force vs. Displacement from Pull Tests – Bushing #4A

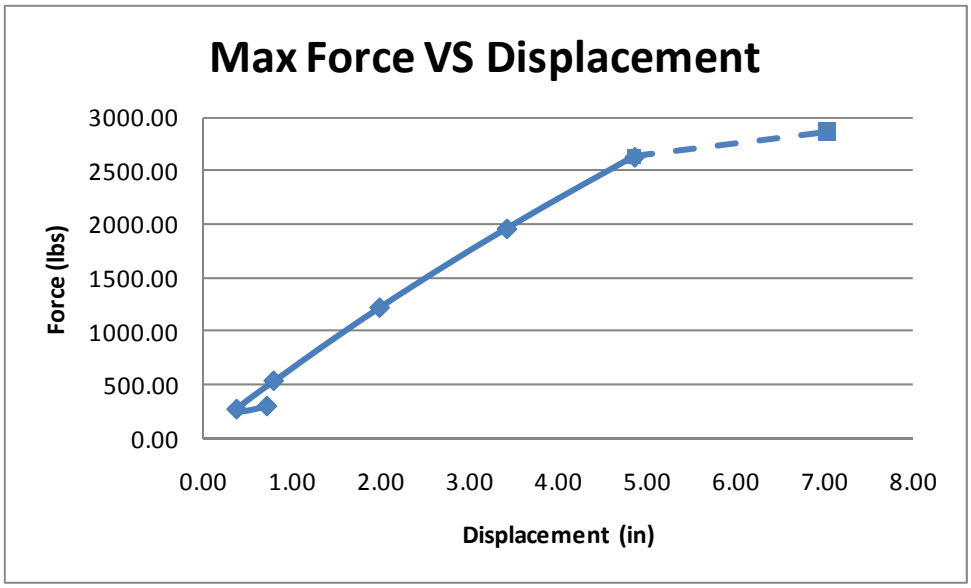

Identification of Properties of Bushing #4B

This section is dedicated to Bushing #4B, which was tested according to the corresponding test protocol in Appendix A. A summary for the dynamic properties is presented in Table D-3.

Identification of Properties with Additional Conductor Weight

Impact Hammer Testing

Impact hammer tests were used to find the frequency and damping ratio of Bushing #4B. A 15 lb. weight was mounted at the top of the bushing, which represented a portion of cable near the bushing top that might play a role in the bushing response. Minimum frequency was observed in the NS direction of 8.00 Hz with damping ratio of 1.20%; in the EW Direction the frequency was 8.15 Hz and damping ratio was 1.20%. Table D-3 shows detailed frequencies, damping ratio and the direction in which the tests were run. The Power Spectral Density (PSD) of the free vibration response gave the frequency of the bushing and the logarithmic decrement method was used to find the damping ratio. See Figures D-41 through D-44 for results of the tests.

Table D-3: Dynamic Properties of Bushing #4B from Various Tests

Test No.	Frequency			Damping			Max Displacement	Force	Stiffness
Units	(Hz)			(%)			(in)	(lb)	(lb/in)
(1)	(2)	(3)	(4)	(5)	(6)	(7)	(8)	(9)	(10)
Direction	NS	EW	Vertical	NS	EW	Vertical			
Impact Hammer Test –Fixed base									
TBU2NS05	8	-	-	1.2	-	-	-	-	-
TBU2EW06	-	8.15	-	-	1.2	-	-	-	-
Quick Release Test - Fixed Base									
TBU210	-	8.12	-	-	0.89	-	0.17	0.11	0.68
TBU211	-	7.99	-	-	1.80	-	0.23	0.19	0.82
TBU212	-	7.77	-	-	1.83	-	0.51	0.84	0.62
TBU213	-	7.45	-	-	2.65	-	1.70	1.00	0.59
TBU214	-	7.35	-	-	2.65	-	1.95	1.15	0.59
White Noise Test									
TBU2WN18	6.75	6.75	-	4.08	4.36	-	-	-	-
TBU2WN21	6.75	6.50	-	3.84	4.42	-	-	-	-
TBU2WN24	6.75	6.50	-	3.91	4.25	-	-	-	-
TBU2WN27	6.75	6.50	-	3.93	3.84	-	-	-	-
TBU2WN30	6.00	6.00	-	5.41	5.43	-	-	-	-
TBU2WN33	-	-	-	-	-	-	-	-	-
TBU2WN36	-	-	-	-	-	-	-	-	-
Table Impulse Test									
TBU2TBI19	6.80	6.60	-	1.43	1.35	-	-	-	-
TBU2TBI22	6.75	6.62	-	1.35	1.84	-	-	-	-
TBU2TBI25	6.75	6.50	-	0.92	1.55	-	-	-	-
TBU2TBI28	6.62	6.50	-	1.02	1.04	-	-	-	-
TBU2TBI31	5.87	6.00	-	2.19	2.77	-	-	-	-
TBU2TBI34	-	-	-	-	-	-	-	-	-
TBU2TBI37	-	-	-	-	-	-	-	-	-
Final Pull Test									
TB-U2-PL-43	-	-	-	-	-	-	2.25	1393.45	618.21
TB-U2-PL-45	-	-	-	-	-	-	2.33	1438.11	617.21
TB-U2-PL-47	-	-	-	-	-	-	2.29	1415.14	617.97
TB-U2-PL-49	-	-	-	-	-	-	2.38	1470.33	617.79
TB-U2-PL-51	-	-	-	-	-	-	2.34	1451.19	619.19
TB-U2-PL-53	-	-	-	-	-	-	1.62	1024.00	632.10
TB-U2-PL-55	-	-	-	-	-	-	2.81	1729.69	615.22
TB-U2-PL-57	-	-	-	-	-	-	3.20	1934.81	605.26
TB-U2-PL-59	-	-	-	-	-	-	3.72	2219.69	597.21
TB-U2-PL-61	-	-	-	-	-	-	4.24	2509.67	591.24
TB-U2-PL-63	-	-	-	-	-	-	4.79	2792.32	582.66
TB-U2-PL-65	-	-	-	-	-	-	5.50	3138.77	570.84
TB-U2-PL-67	-	-	-	-	-	-	5.49	3069.86	558.70
TB-U2-PL-69	-	-	-	-	-	-	4.43	1451.51	327.79
TB-U2-PL-70	-	-	-	-	-	-	4.03	1420.56	352.39

Figure D-41: Acceleration Response of Bushing #4B, with 15 lb. Mass, in NE Direction

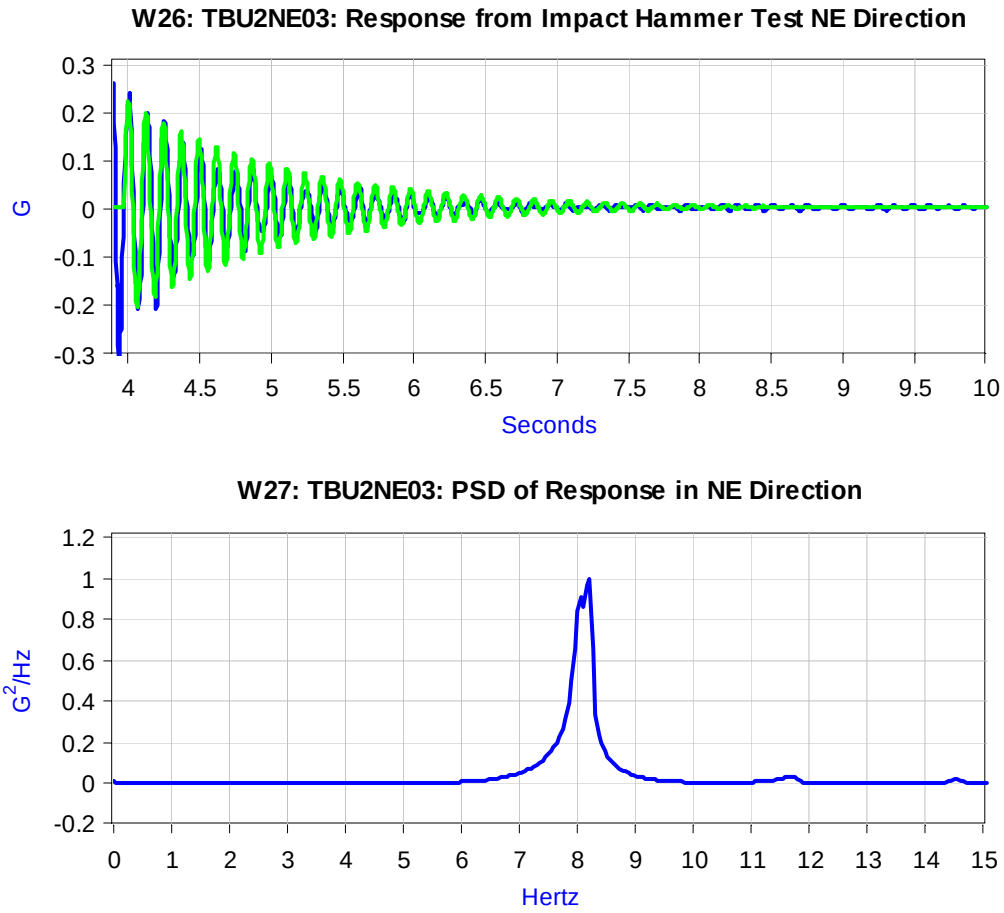

Figure D-42: Acceleration Response of Bushing #4B, with 15 lb. Mass, in SE Direction

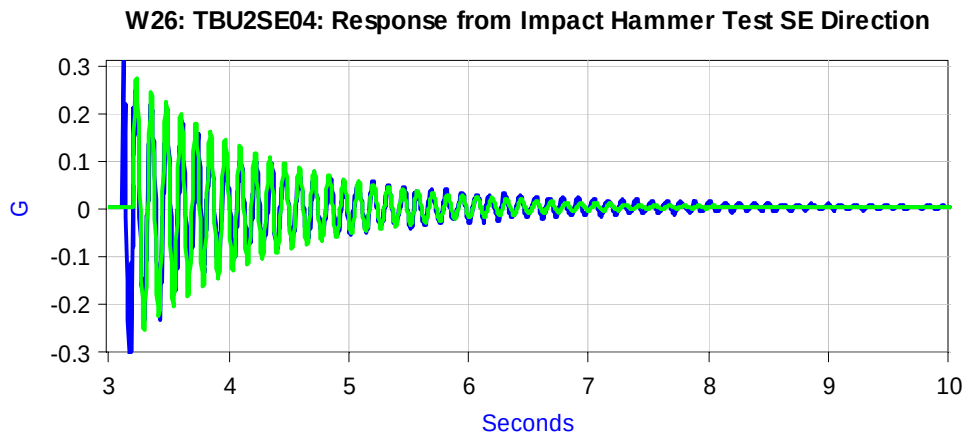

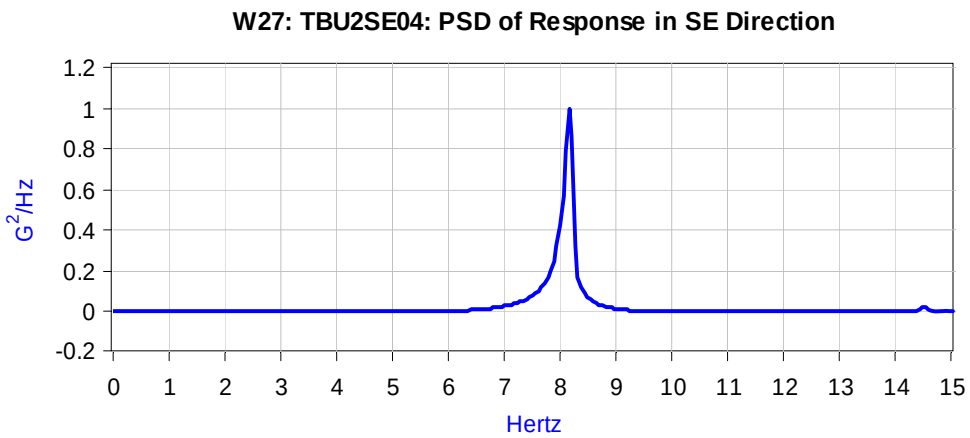

Figure D-43: Acceleration Response of Bushing #4B, with 15 lb. Mass, in NS Direction

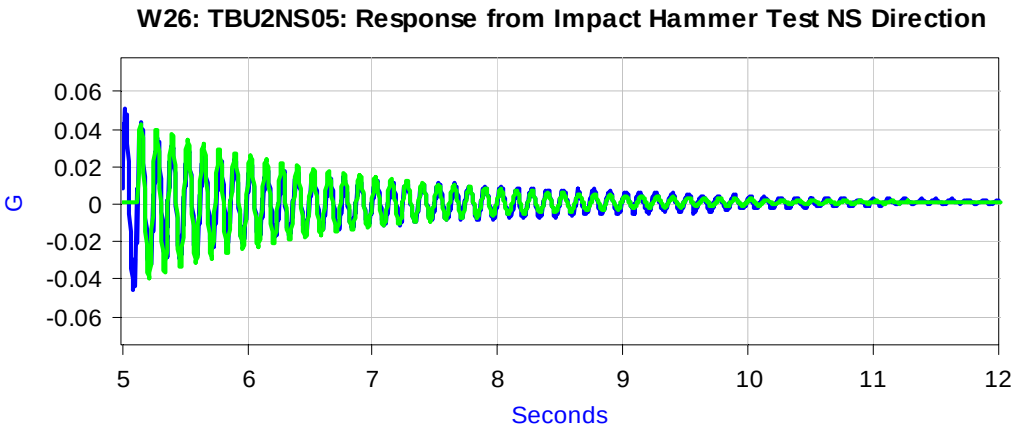

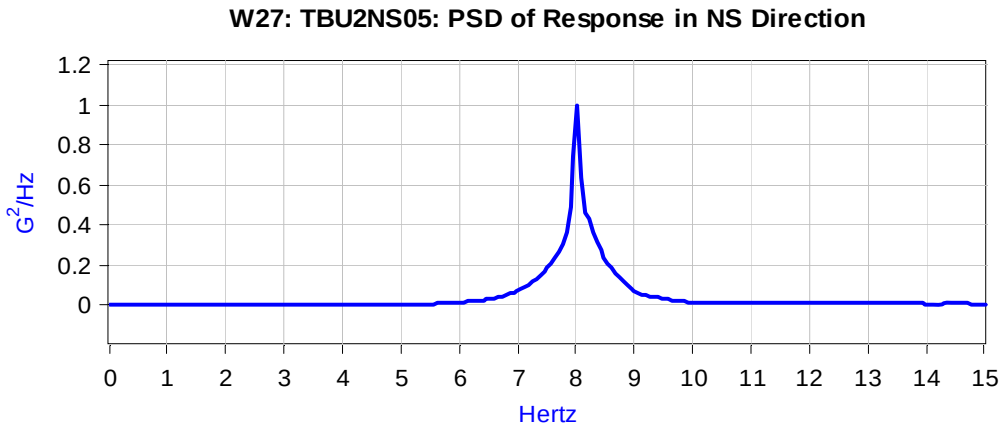

Figure D-44: Acceleration Response of Bushing #4B, with 15 lb. Mass, in EW Direction

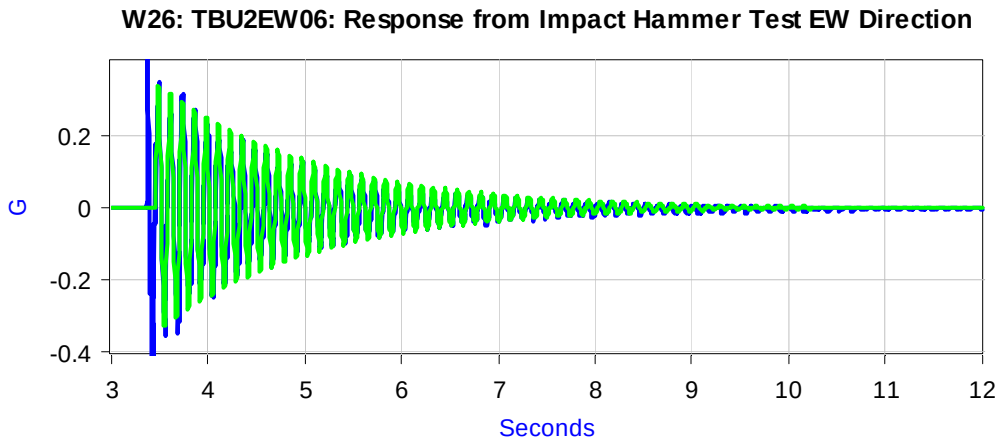

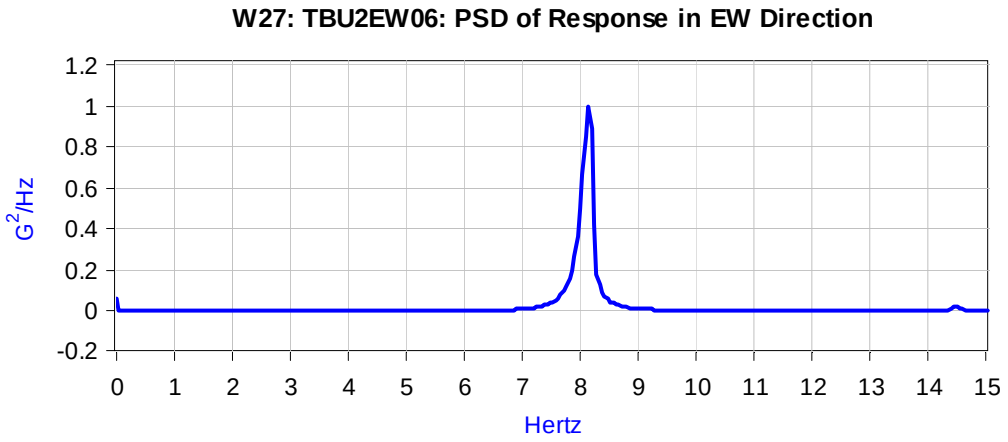

Pull and Sudden Release Tests

After impact hammer tests, the bushing was pulled from the top and released suddenly. All the pull tests were run in the EW direction only. This test showed the stiffness of the bushing, and the frequency and damping ratio were confirmed. The stiffness varied between maximum values of 658 lb./in. to 779 lb./in. (see Table D-3). Figures D-45 through D-49 show the frequencies and corresponding damping ratios for these tests. Figure D-50 shows the relationship between force and displacement.

Figure D-45: Acceleration Response from Quick Release Test TBU210 – Bushing #4B

W26: TBU210: Response from Pull Test EW Direction

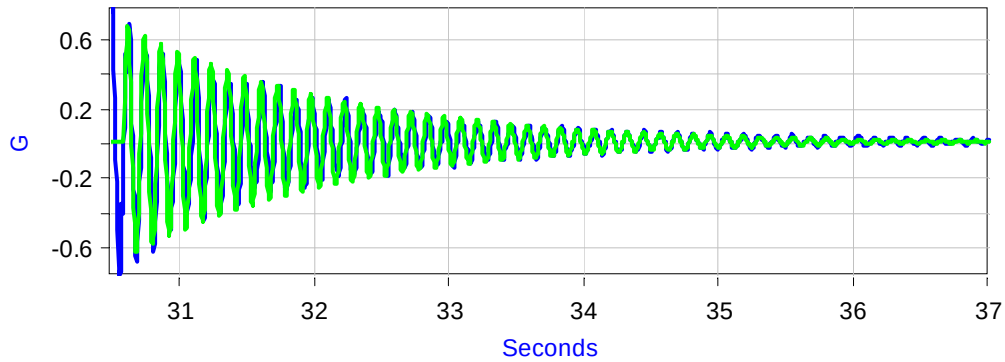

W27: TBU210:PSD of Response from Pull Test

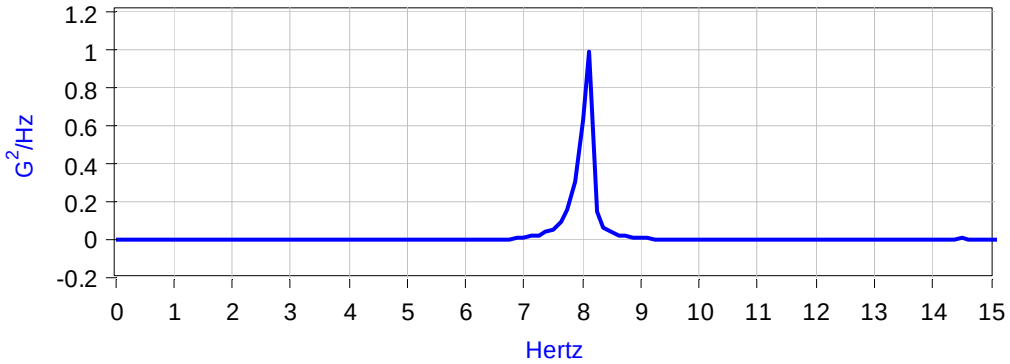

W29: TBU210: Bending Moment History Pull Test EW Direction

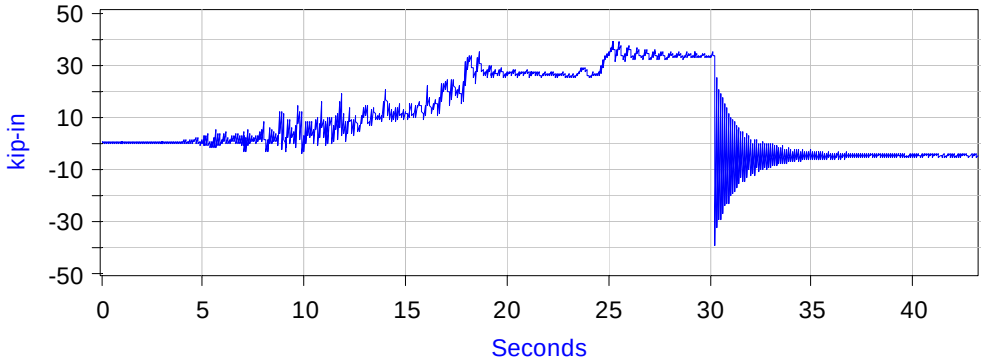

Figure D-46: Acceleration Response from Quick Release Test TBU211 – Bushing #4B

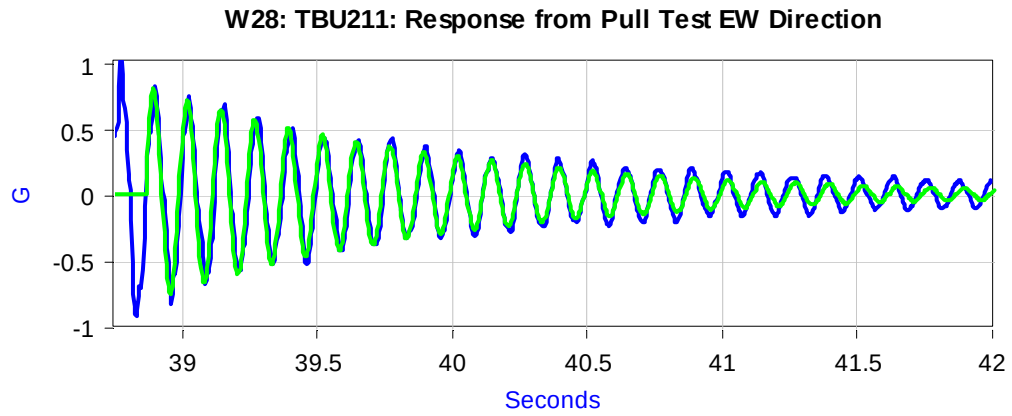

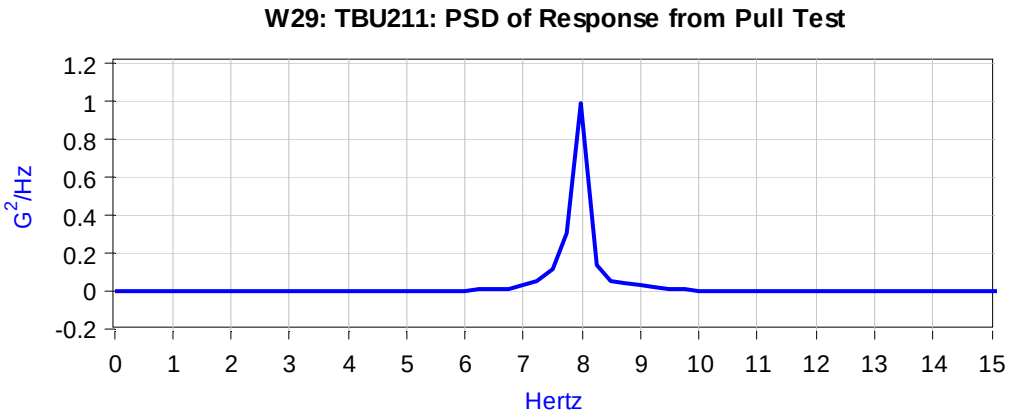

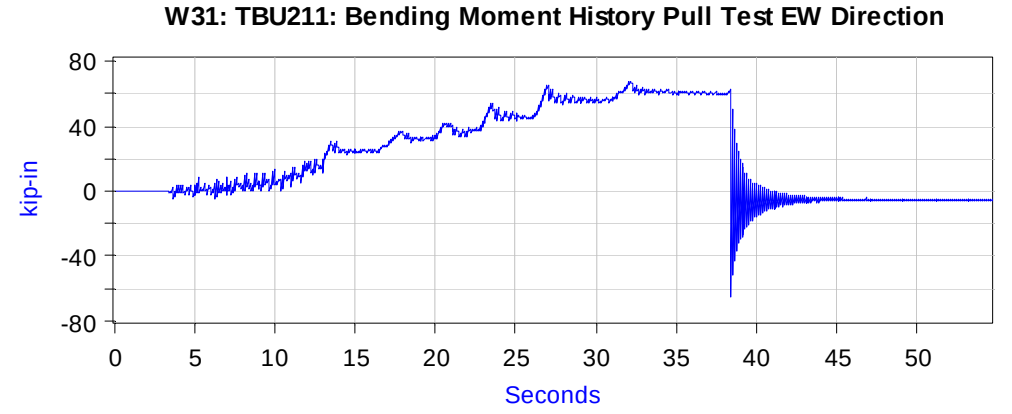

Figure D-47: Acceleration Response from Quick Release Test TBU212 – Bushing #4B

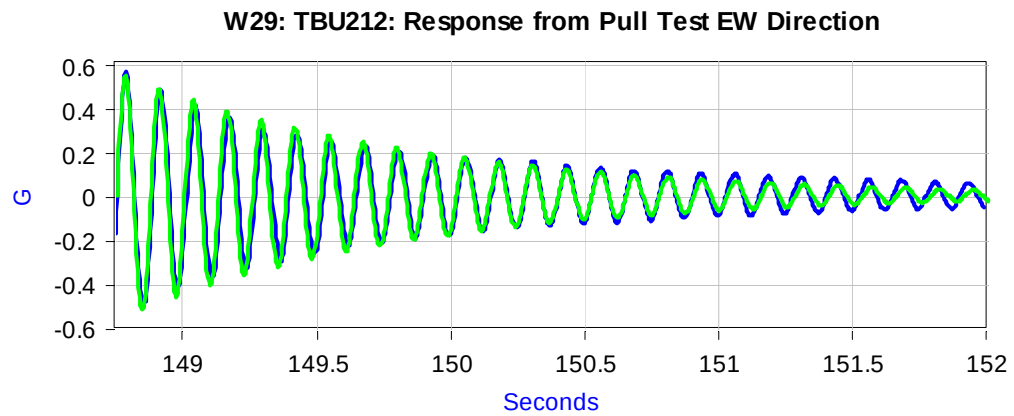

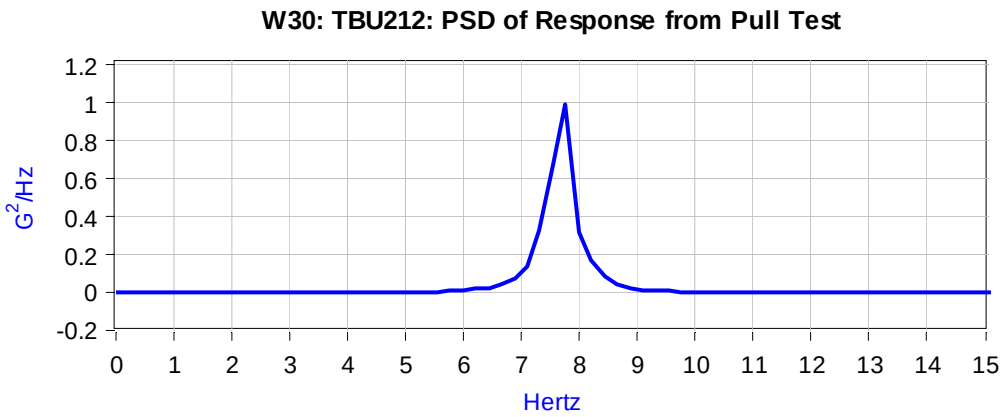

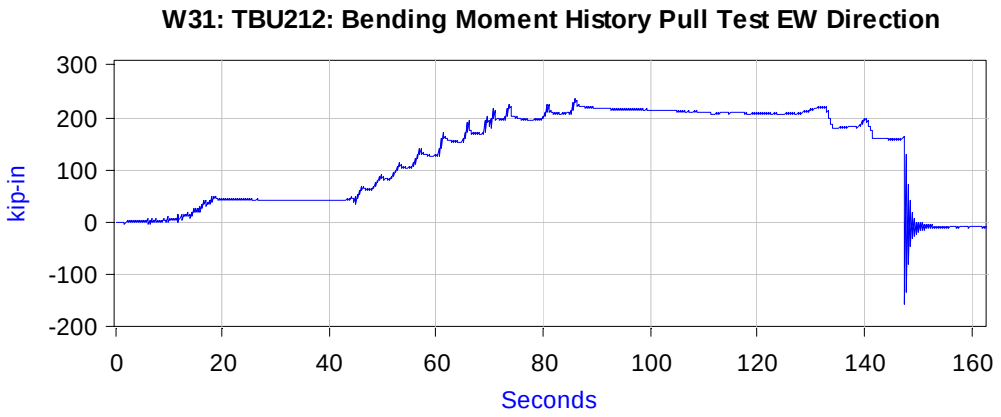

Figure D-48: Acceleration Response from Quick Release Test TBU213 – Bushing #4B

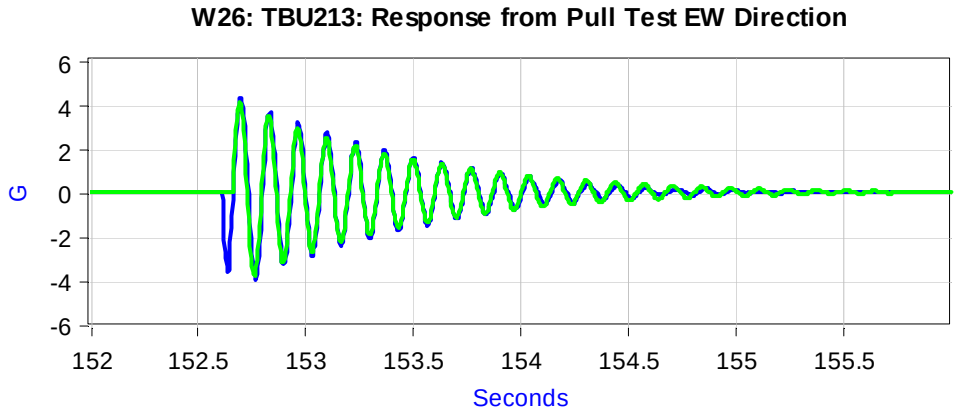

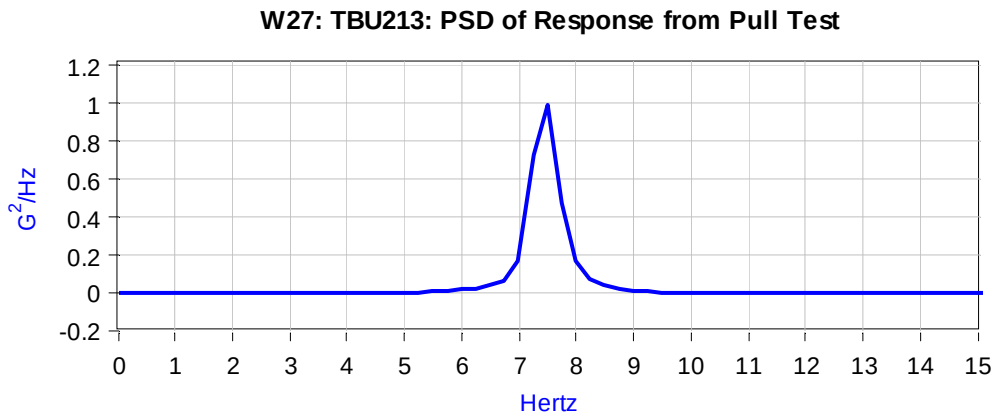

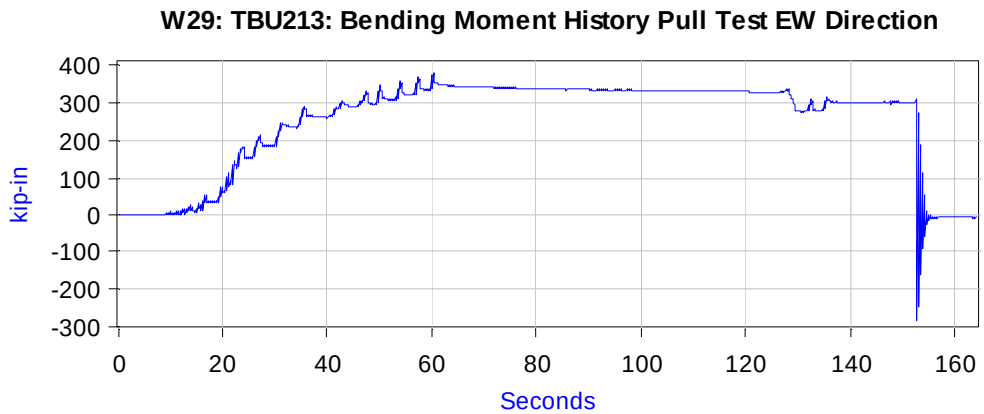

Figure D-49: Acceleration Response from Quick Release Test TBU214 – Bushing #4B

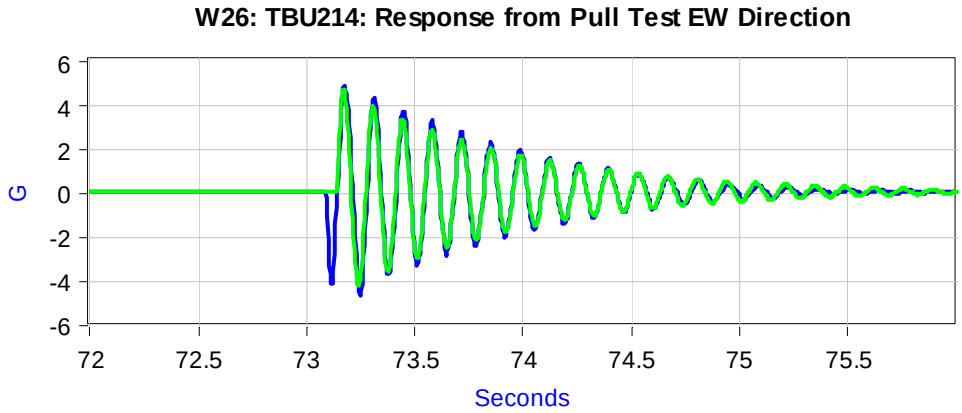

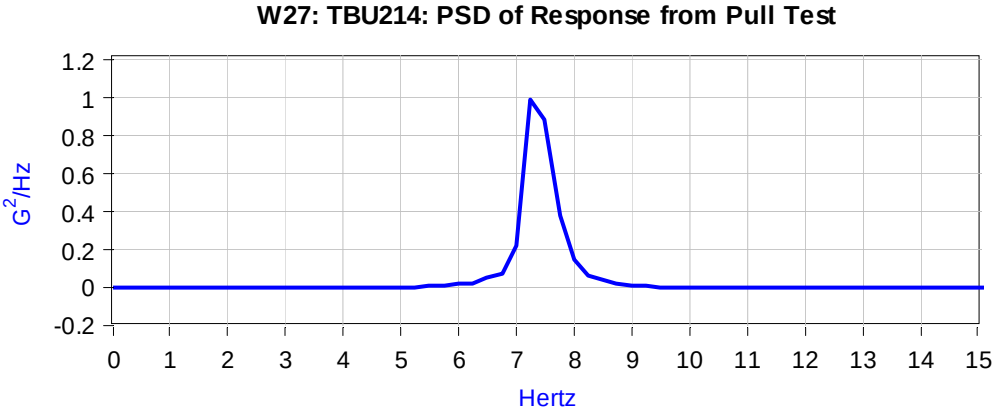

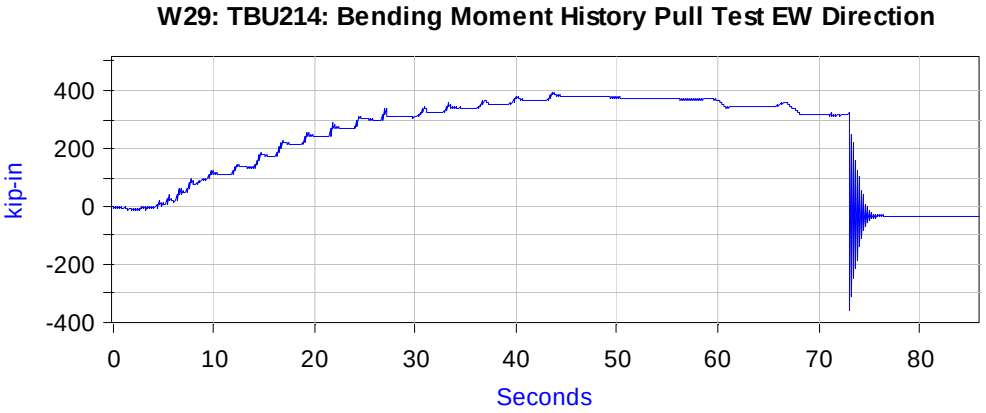

Figure D-50: Maximum Force vs. Maximum Displacement for Bushing #4B

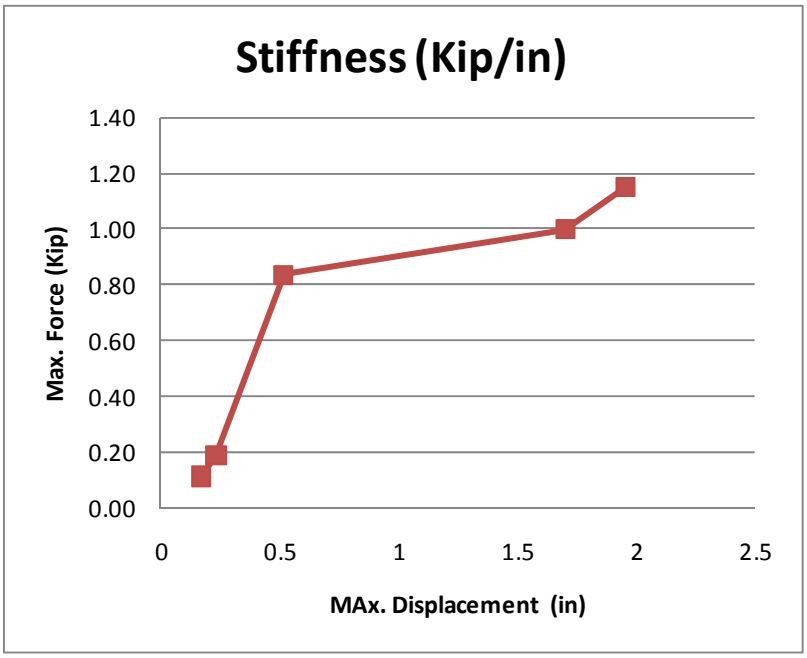

White Noise Tests

The frequencies and damping ratio of the bushing were determined by transfer functions obtained from white noise tests using the shake table. The peak of the transfer function is the fundamental frequency of the bushing and a half-power bandwidth method was used to determine the damping ratio. The summary of the frequencies is presented in Table D-3.

The frequencies from white noise tests were then used to develop "impulse tests" for the dominant frequencies of the bushing (see next section). The half-power bandwidth method used to determine damping is less accurate than a quick release, impact hammer or table impulse tests; therefore the ratios are re-determined in the following section using impulse tests. The acceleration transfer functions are shown in Figures D-51 through D-55.

Figure D-51: Transfer Functions of Bushing #4B, Test TBU2WN

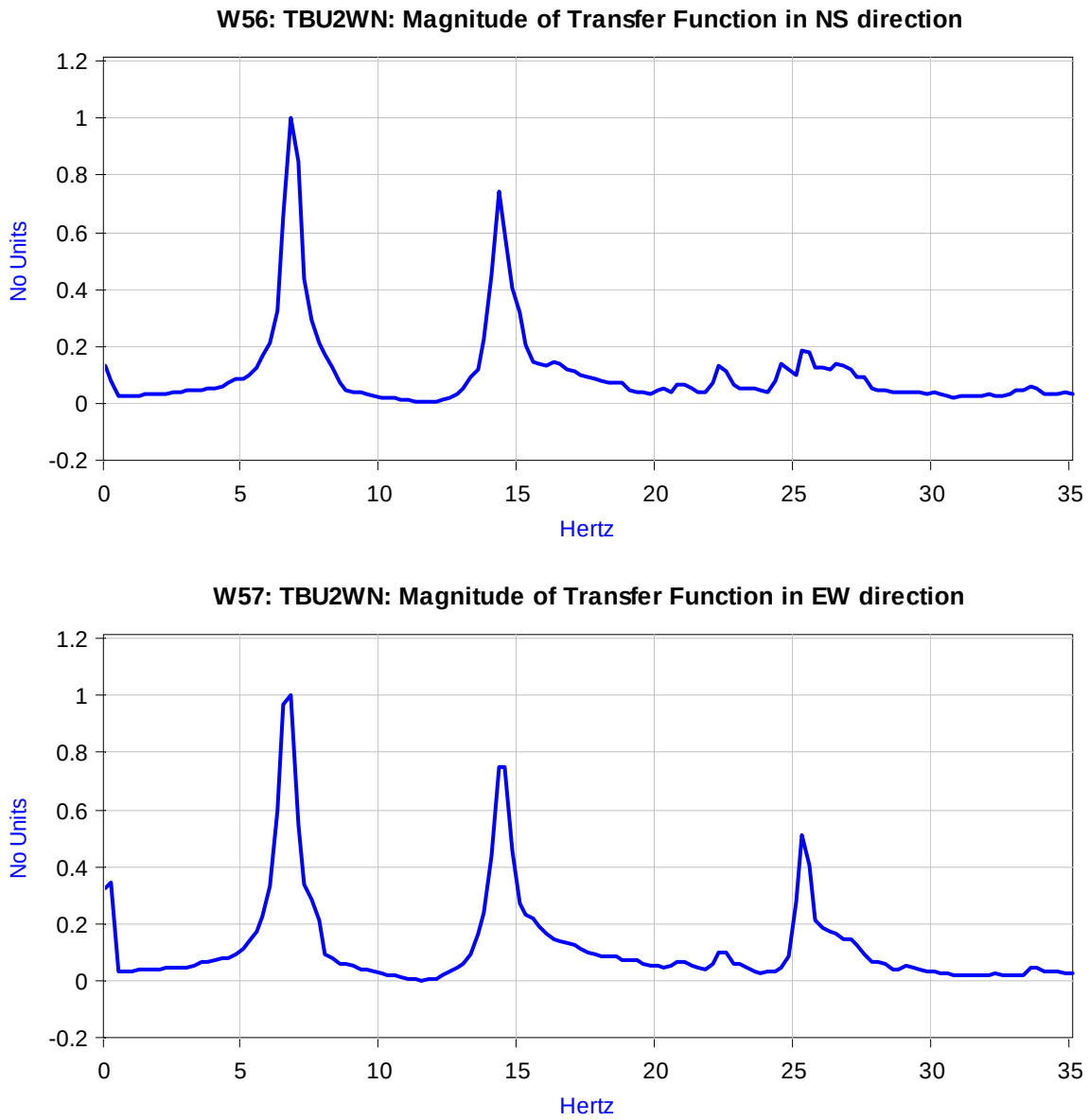

Figure D-52: Transfer Functions of Bushing #4B, Test TBU1WN21

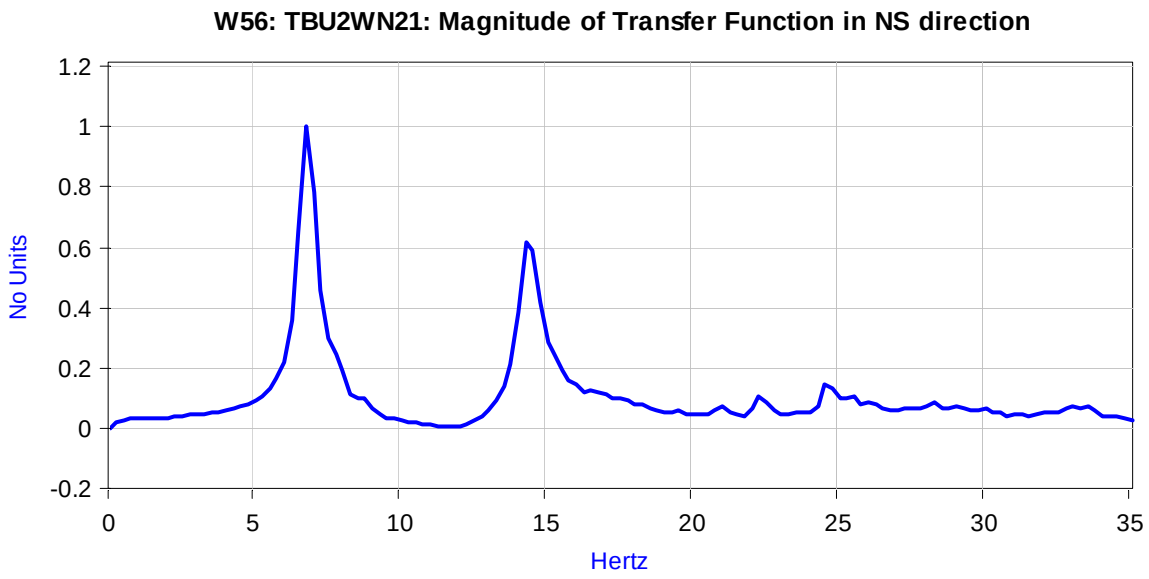

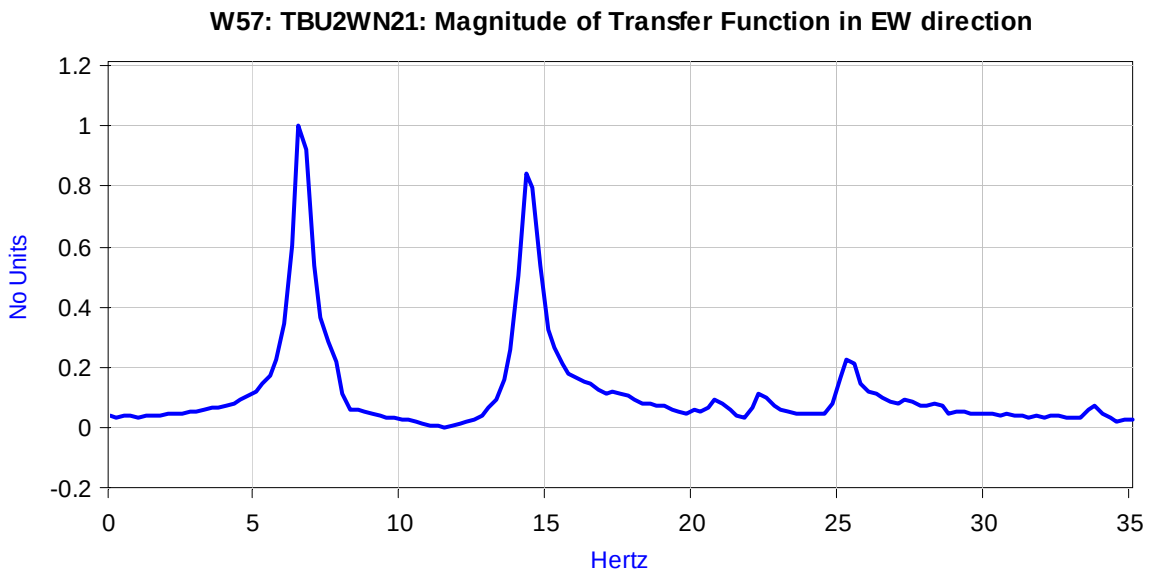

Figure D-53: Transfer Functions of Bushing #4B, Test TBU1WN24

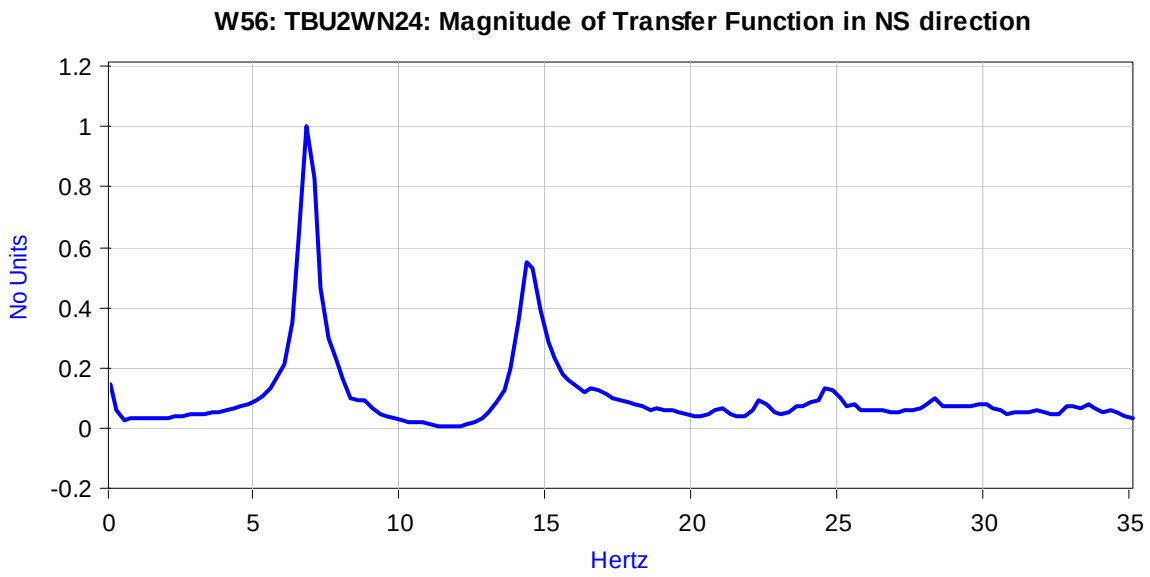

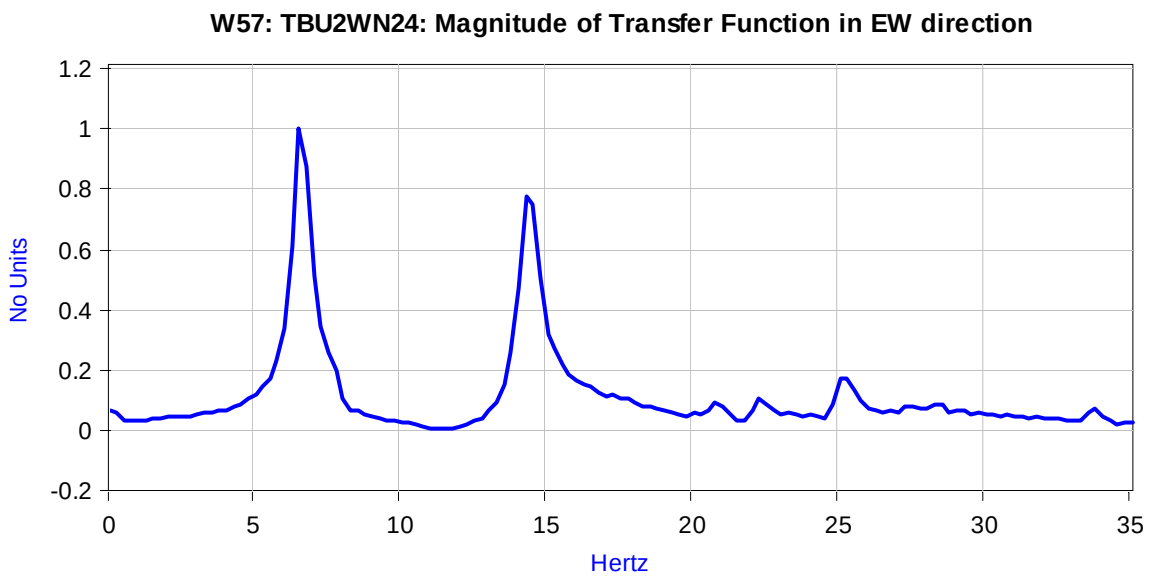

Figure D-54: Transfer Functions of Bushing #4B, Test TBU1WN27

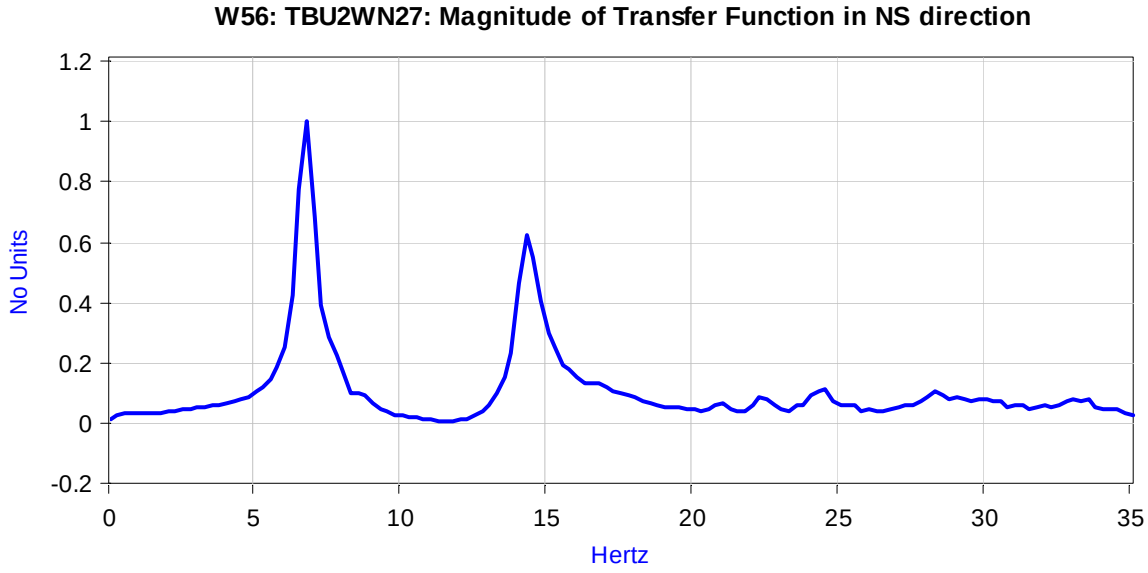

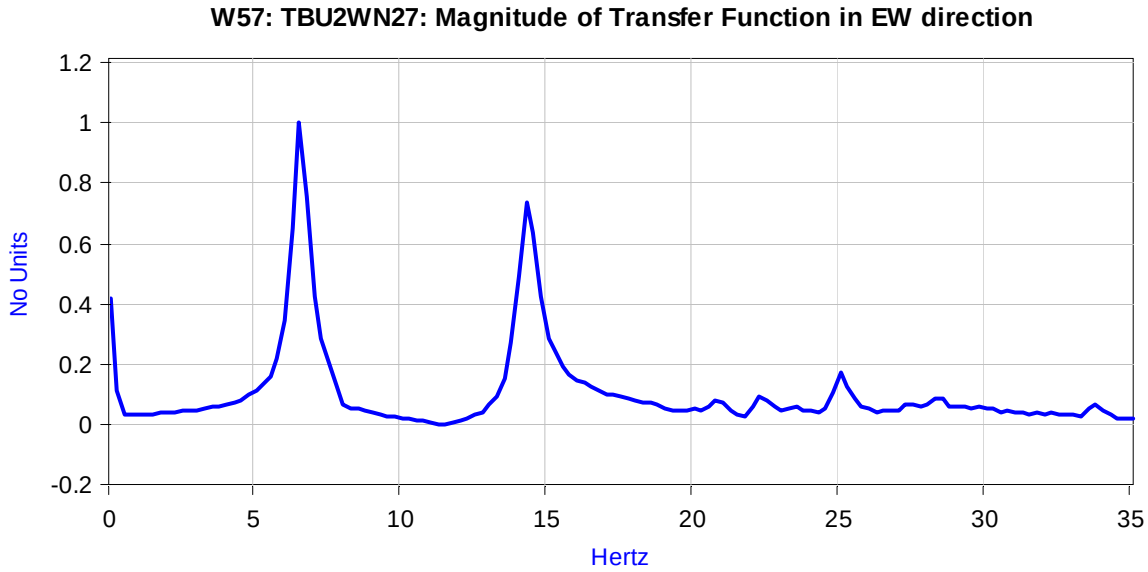

Figure D-55: Transfer Functions of Bushing #4B, Test TBU1WN30

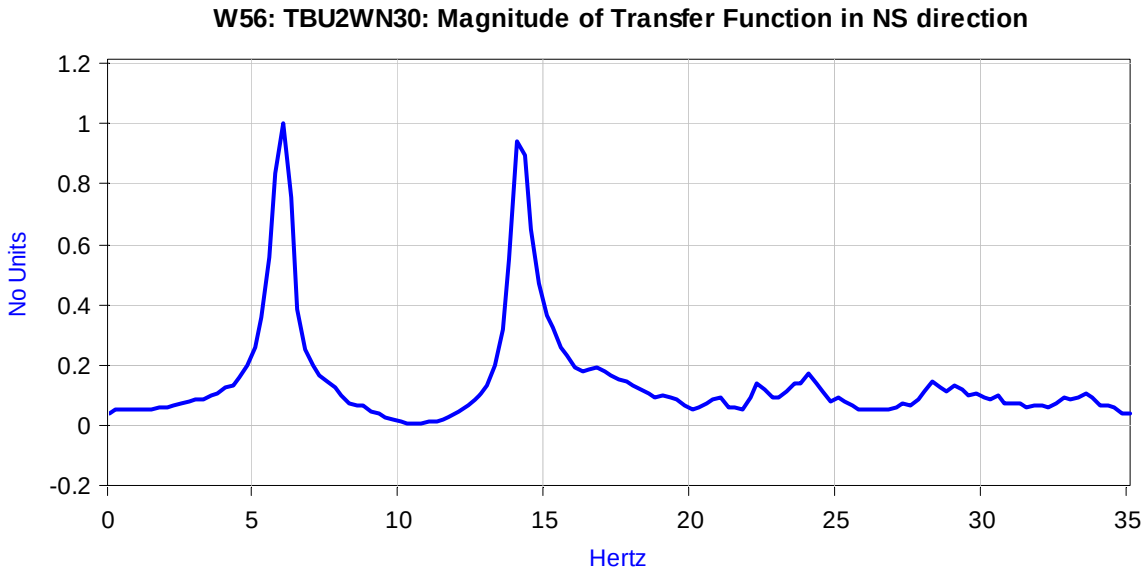

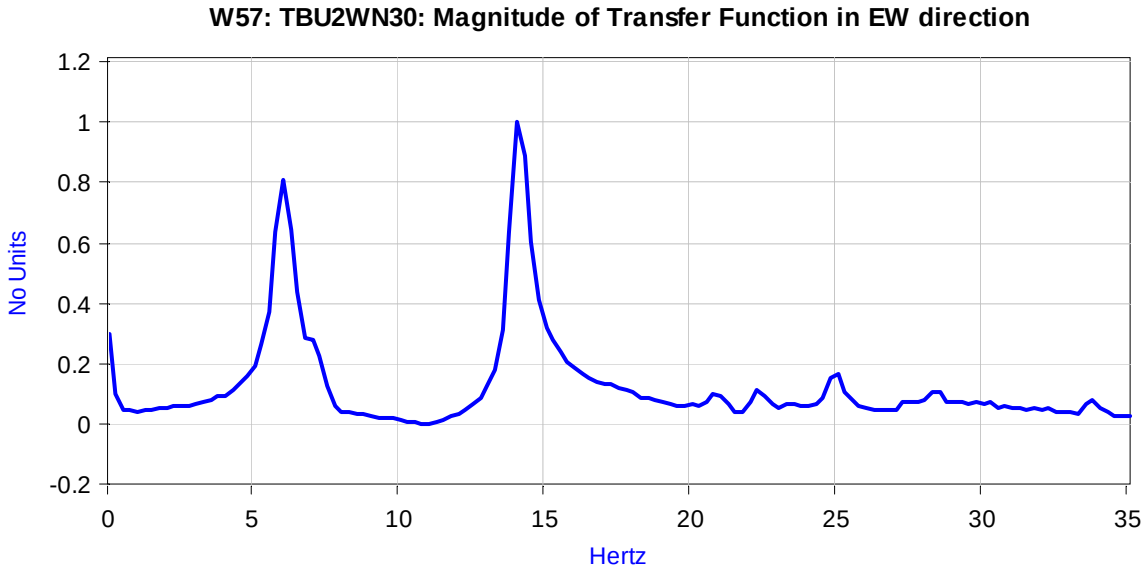

Table Impulse Tests

The table impulse test identifies frequencies and damping of dominant frequencies using smoothed table acceleration impulse for control of a shake table by using a smoothing table impulse procedure developed by the SEESL at University at Buffalo (Kong, 2010). For the identification of system frequencies, a power spectral density (PSD) was calculated from output motion at the top of the bushing and the system frequency is obtained by finding the frequency where the peak is located. For the identification of modal damping, a curve fitting method developed by the authors was used (Kong, 2010).

The acceleration history results of the table impulse tests are presented in Figures D-56 through D-60, and the dynamic characteristics are summarized in Table D-3. The frequencies of Bushing #4B in the NS direction are around 6.80 Hz in test TBU2TBI19 (before random motion tests), and 5.87 Hz in test TBU1TBI31; the damping values are 1.43% and 2.19%, respectively. The frequency in the EW Direction is 6.60 Hz in test TBU2TBI19 (before random motion tests), and 6.00 Hz in test TBU2TBI31; the damping values are 1.35% and 2.77%, respectively.

Figure D-56: Table Impulse Test Response (Test TBU2TBI19) – Bushing #4B

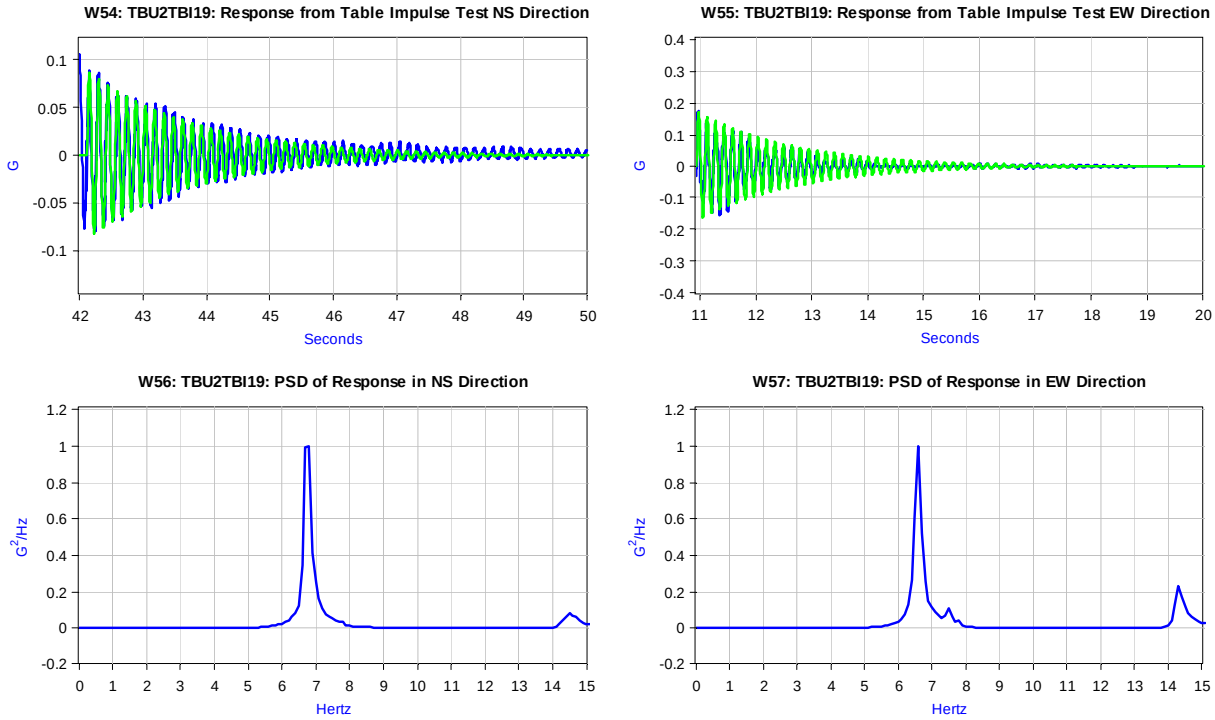

Figure D-57: Table Impulse Test Response (Test TBU2TBI22) – Bushing #4B

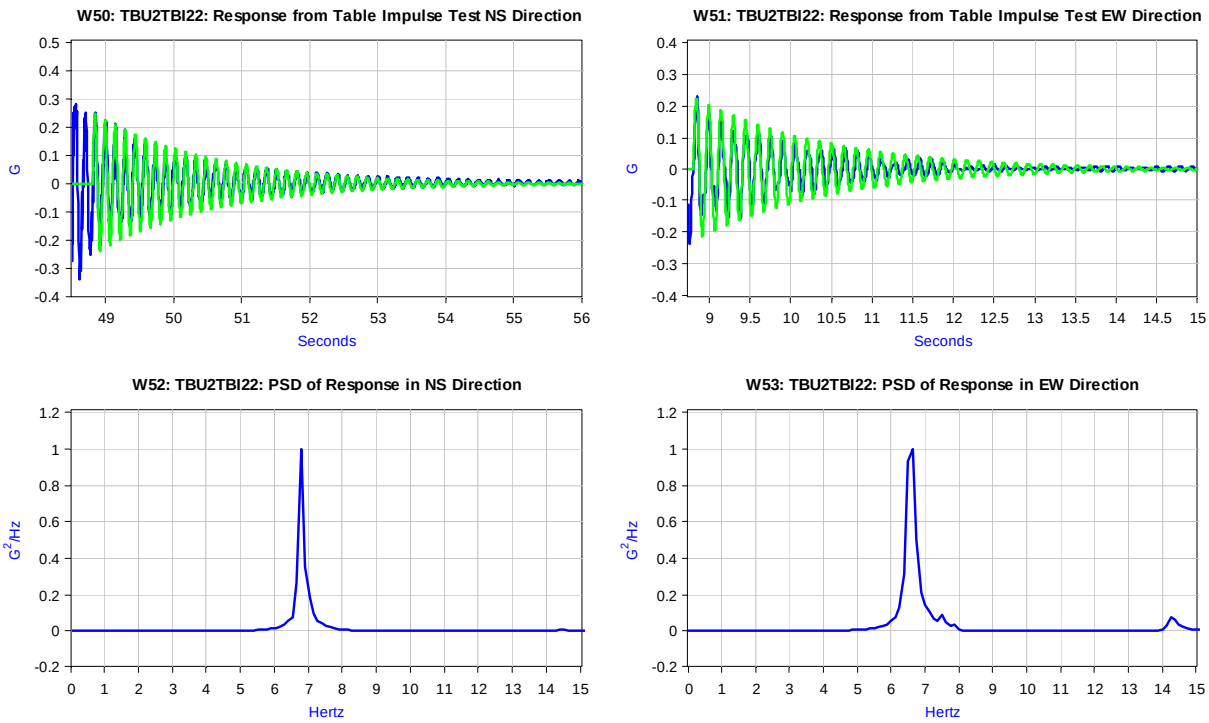

Figure D-58: Table Impulse Test Response (Test TBU2TBI25) – Bushing #4B

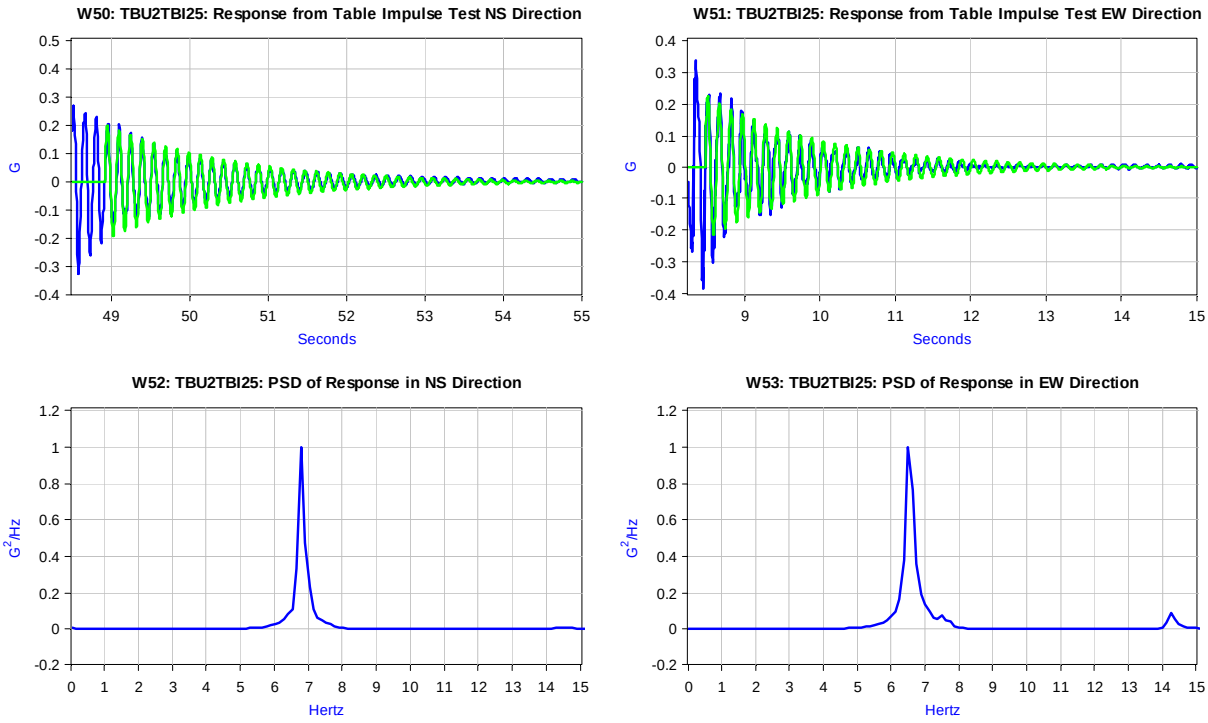

Figure D-59: Table Impulse Test Response (Test TBU2TBI28) – Bushing #4B

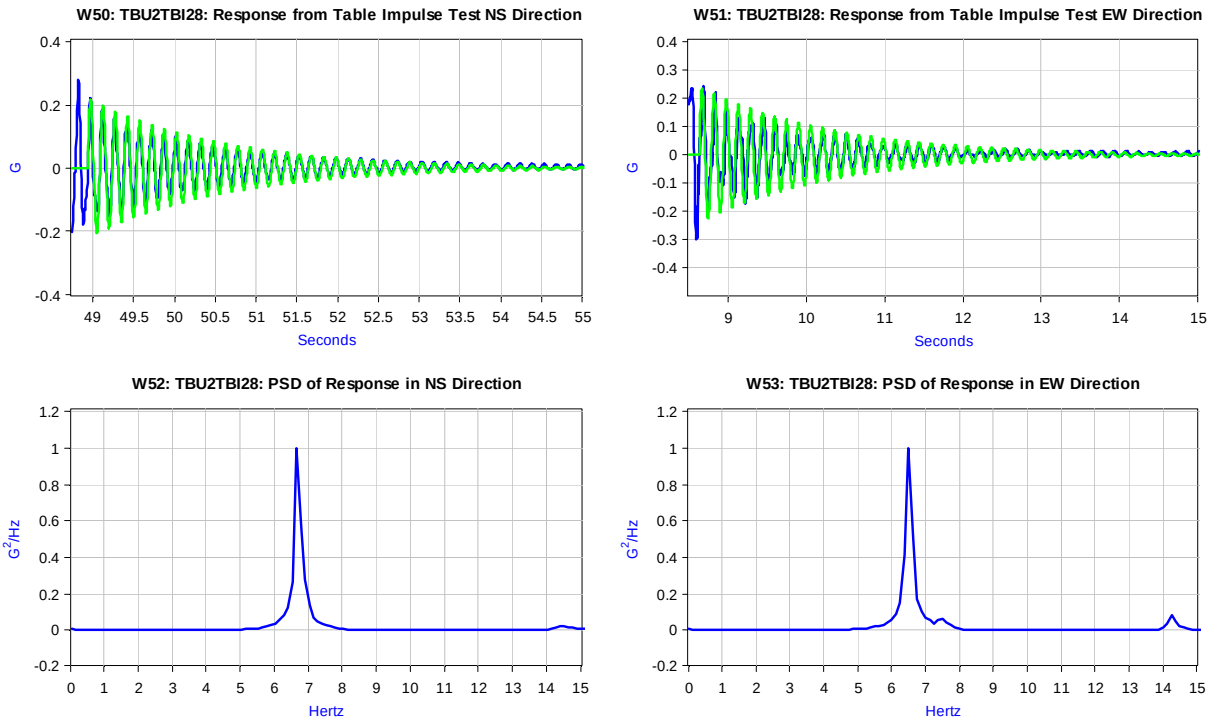

Figure D-60: Table Impulse Test Response (Test TBU2TBI31) – Bushing #4B

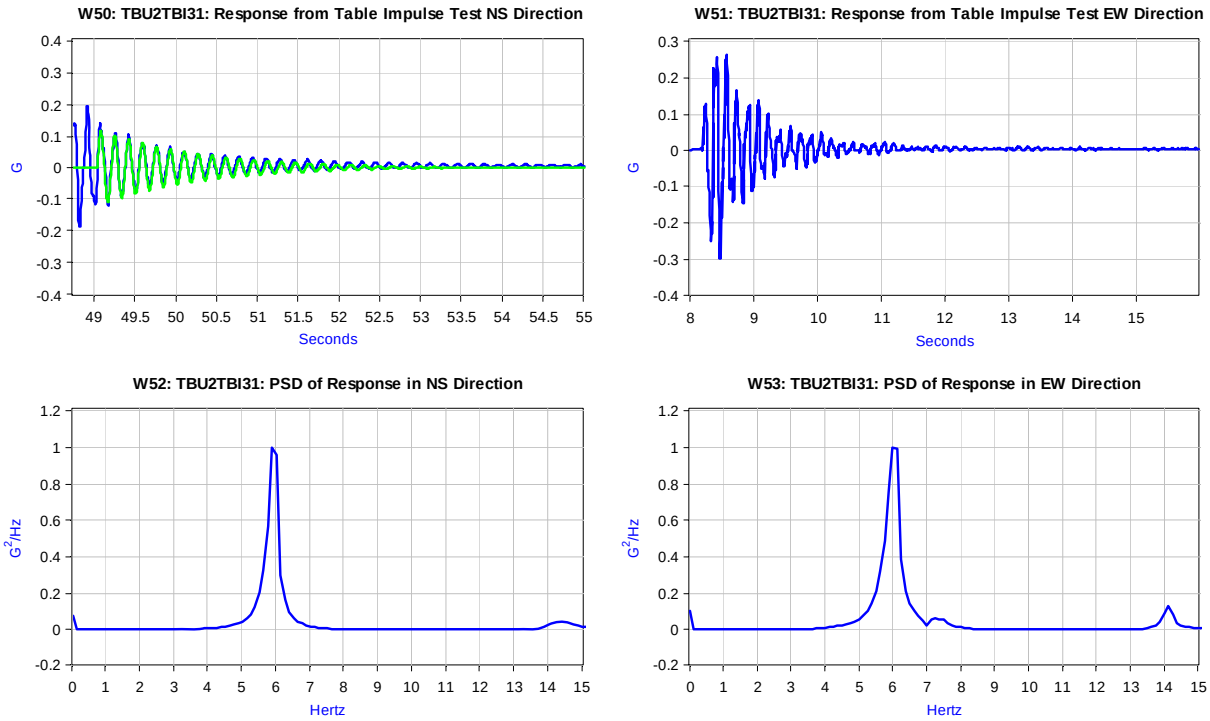

Acceleration History Tests

Acceleration history tests were performed for the seismic demand quantification of Bushing #4B. A summary of the accelerations recorded on various locations on the bushing are shown in Table D-4 for the six levels of test input motions. For electrical purposes Bushing #4B was similar to Bushing #4A, but structurally it was slightly different. The average value of stiffness of Bushing #4A is 715 lb./in., whereas the average value of stiffness for Bushing #4B is 660 lb./in., and the dead weight of Bushing #4A was also higher than Bushing #4B.

The acceleration history tests were used to measure the bending moment of Bushing #4B at flange level. Strain gauges were used to measure the bending moment. A summary of the bending moments is presented in Table D-4. Figures D-61 through D-64 show the bending moment history for various tests.

Table D-4: Summary of Accelerations and Bending Moments – Bushing #4B

Location	Units	0.25 g RRS			0.50 g RRS			1.00 g RRS			2.00 g RRS			2.50 g RRS			3.00 g RRS		
		TBU2AH25			TBU2AH50			TBU2AH100			TB44AH150			TB47AH225			TB53AH300		
(1)	(2)	(3)	(4)	(5)	(6)	(7)	(8)	(9)	(10)	(11)	(12)	(13)	(14)	(15)	(16)	(17)	(18)	(19)	(20)
Bushing Location on Frame																			
Acceleration Distribution along the Height of Testing Setup																			
Direction		NS	EW	Vertical	NS	EW	Vertical	NS	EW	Vertical	NS	EW	Vertical	NS	EW	Vertical	NS	EW	Vertical
Top of Bushing	(g)	1.51	1.41	0.46	3.00	2.84	0.93	6.49	5.08	1.77	10.27	9.72	3.34	-	-	-	-	-	-
Upper CG Of Bushing	(g)	0.84	0.73	-	1.66	1.43	-	3.61	2.80	-	5.13	5.94	-	-	-	-	-	-	-
CG OF Bushing	(g)	0.40	0.42	-	0.91	0.88	-	1.82	1.74	-	2.65	2.83	-	-	-	-	-	-	-
On Frame	(g)	0.32	0.38	0.50	0.64	0.71	0.96	0.99	1.05	1.83	2.00	1.80	3.21	-	-	-	-	-	-
Shake Table	(g)	0.30	0.34	0.21	0.61	0.64	0.41	0.92	0.93	0.73	1.71	1.55	1.35	-	-	-	-	-	-
Bending Moment at the Base of Bushing																			
Moment from Strain Gauges	kip-in	36.76	68.26	-	51.13	107.50	-	194.61	353.45	-	369.99	604.03	-	677.86	1010.59	-	879.25	1036.89	

Figure D-61: Bending Moment of Bushing #4A in Horizontal Direction – Test TBU2AH50)

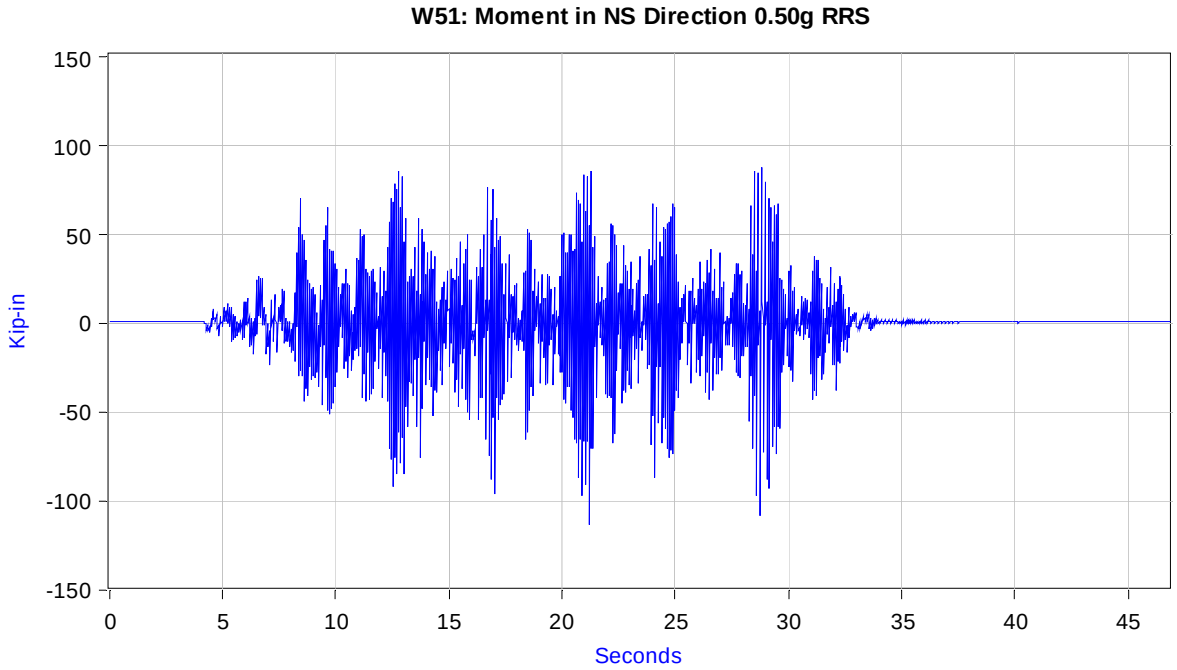

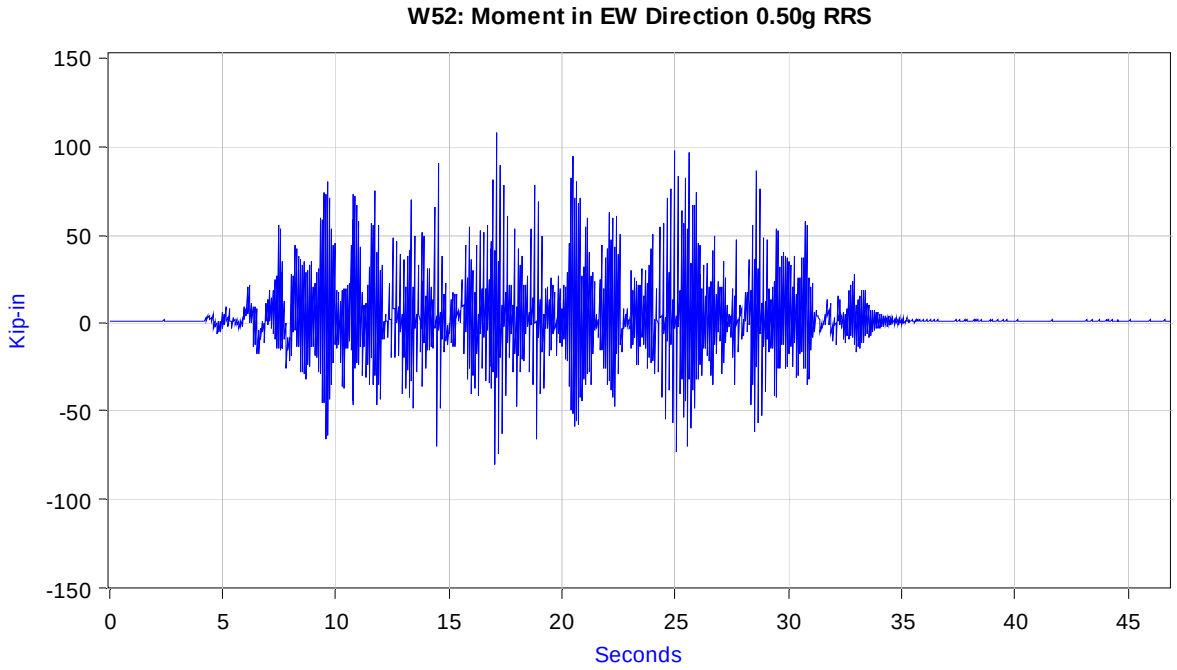

Figure D-62: Bending Moment of Bushing #4A in Horizontal Direction – Test TBU2AH100)

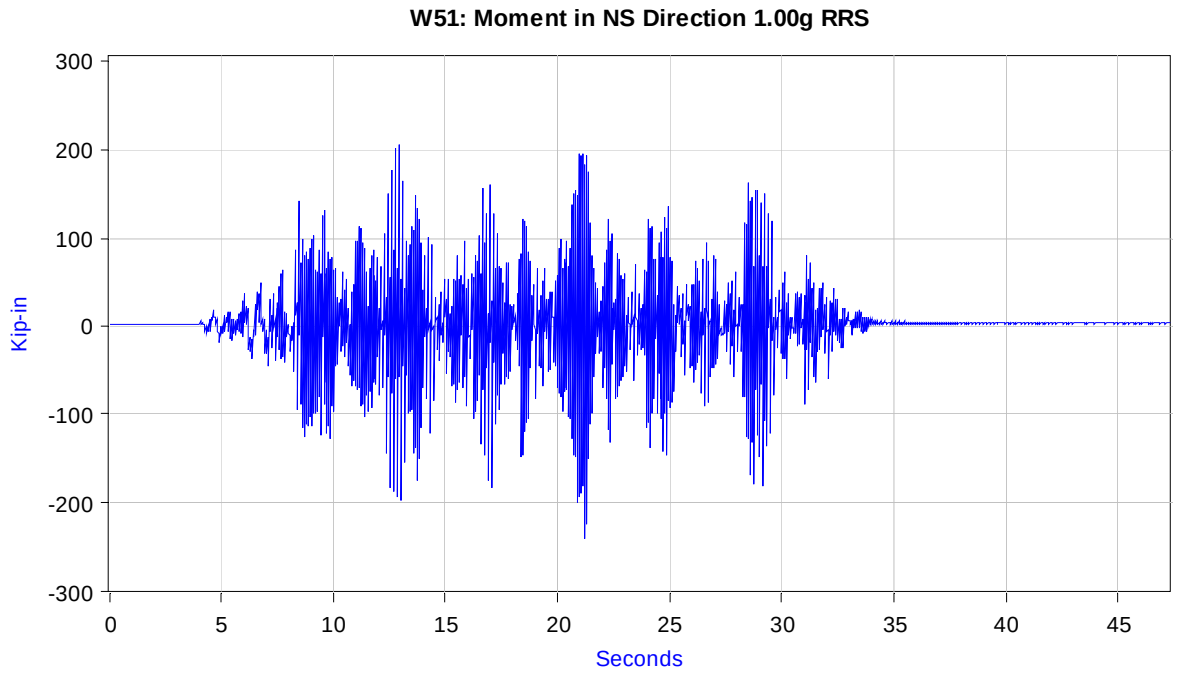

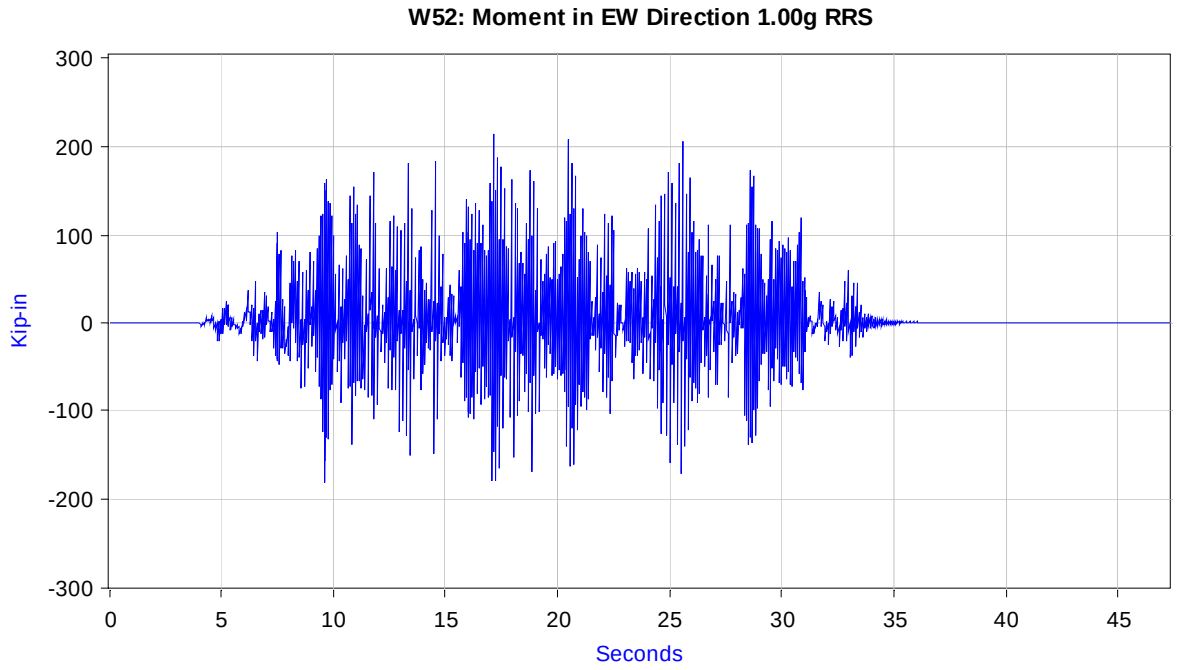

Figure D-63: Bending Moment of Bushing #4A in Horizontal Direction – Test TBU2AH200)

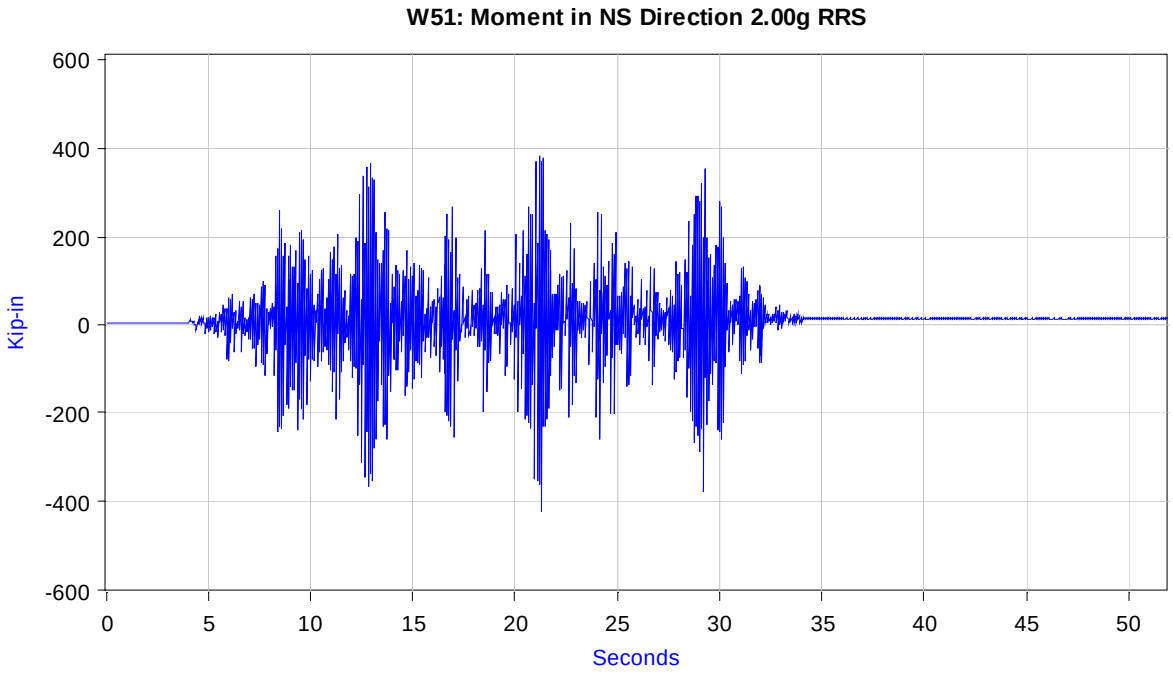

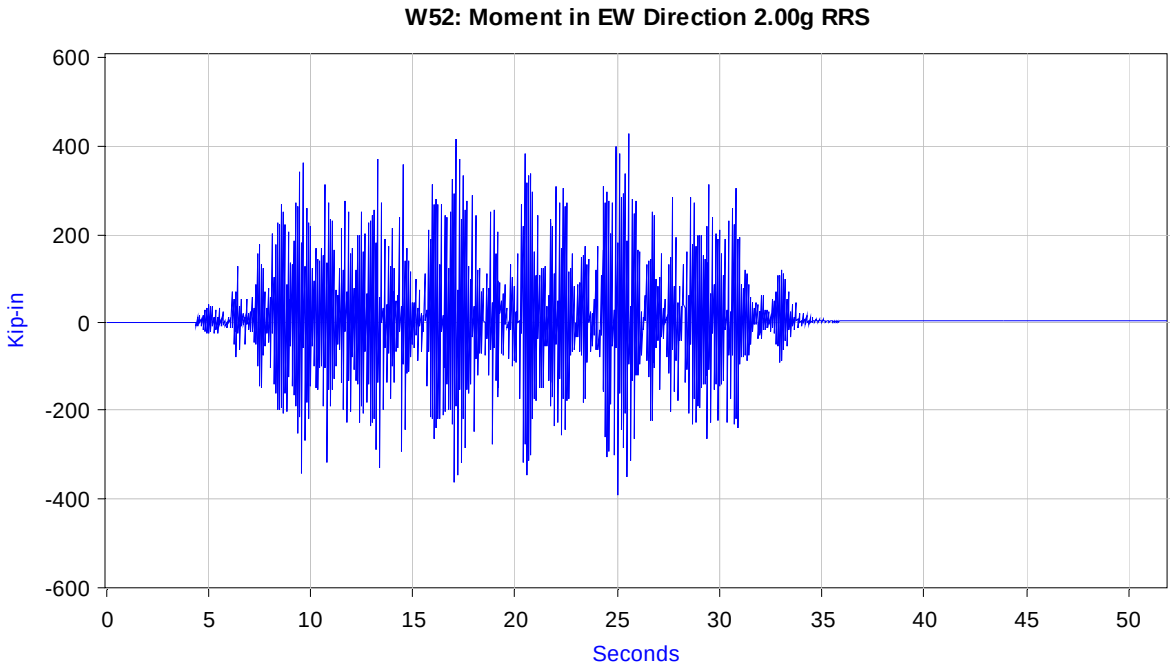

Figure D-64: Bending Moment of Bushing #4A in Horizontal Direction – Test TBU2AH300)

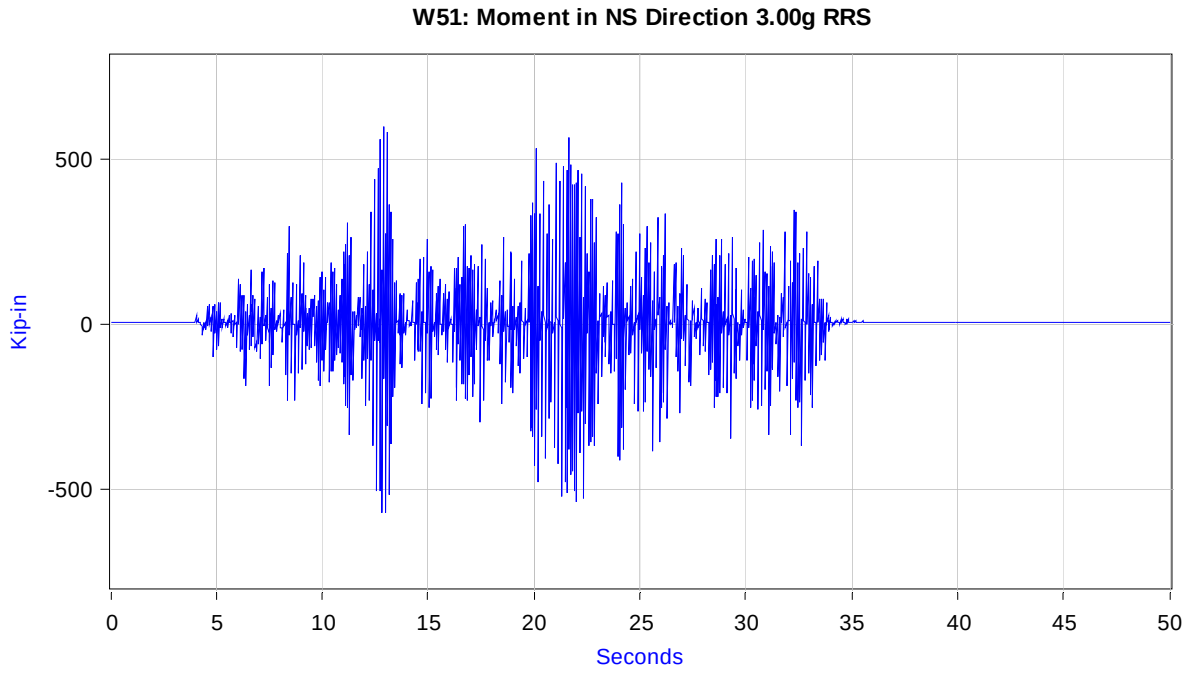

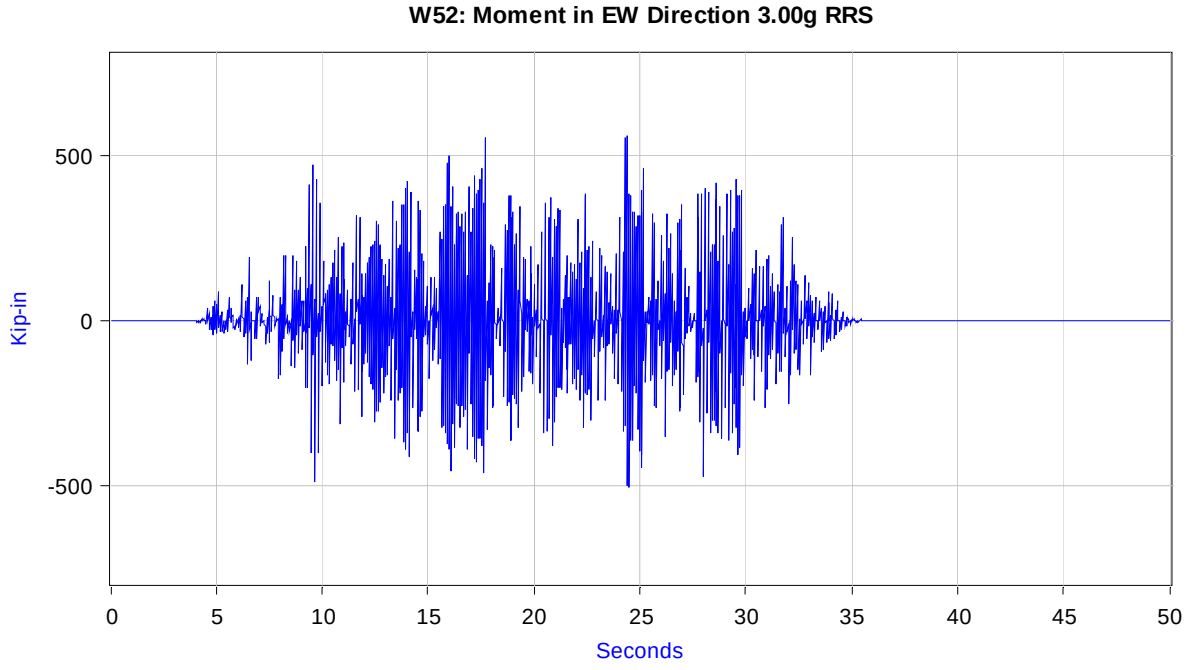

Final Pull Test

After dynamic testing, the bushing was mounted on the fixed base (concrete block) for final pull testing.

To perform these tests, the frame was mounted on the shake table extension and the top of the bushing was connected to the frame with straps and a load cell. The motion of the shake table in one direction applied the required force at the top of the bushing. Two types of pull tests were performed: during the first sequence of testing 10 cycles of constant amplitude motion was used, and for the second sequence the bushing was pulled at the top in an incremental loading pattern.

The results of the tests are shown in Figures D-65 through D-69.

Figure D-65: 10 Cycles of Pull Test in EW direction – Test TBU2PL43

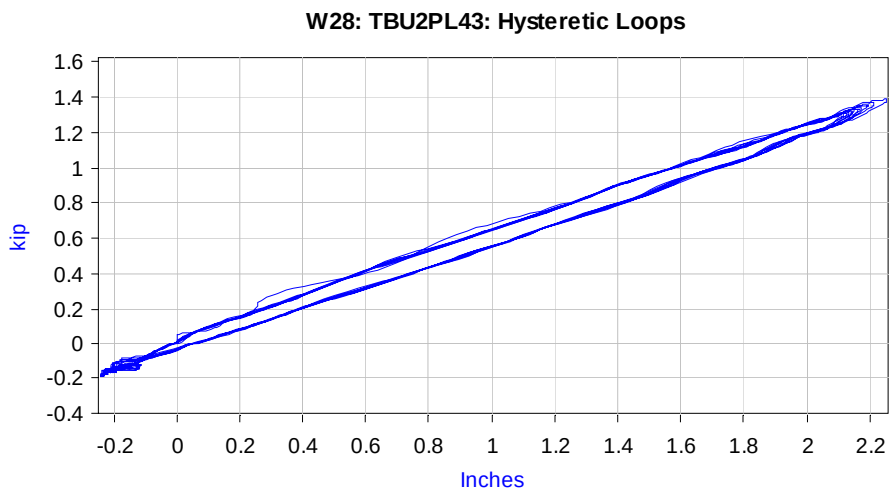

Figure D-66: 10 Cycles of Pull Test in EW direction – Test TBU2PL45

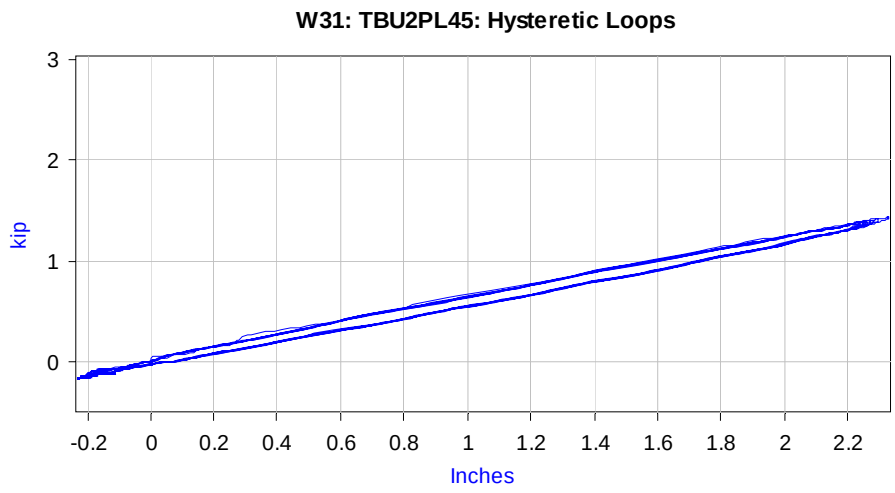
W31: TBU2PL45: Hysteretic Loops
kip
3
2
1
0
-0.2
0
0.2
0.4
0.6
0.8
1
1.2
1.4
1.6
1.8
2
2.2
Inches

Figure D-67: 10 Cycles of Pull Test in EW direction – Test TBU2PL47

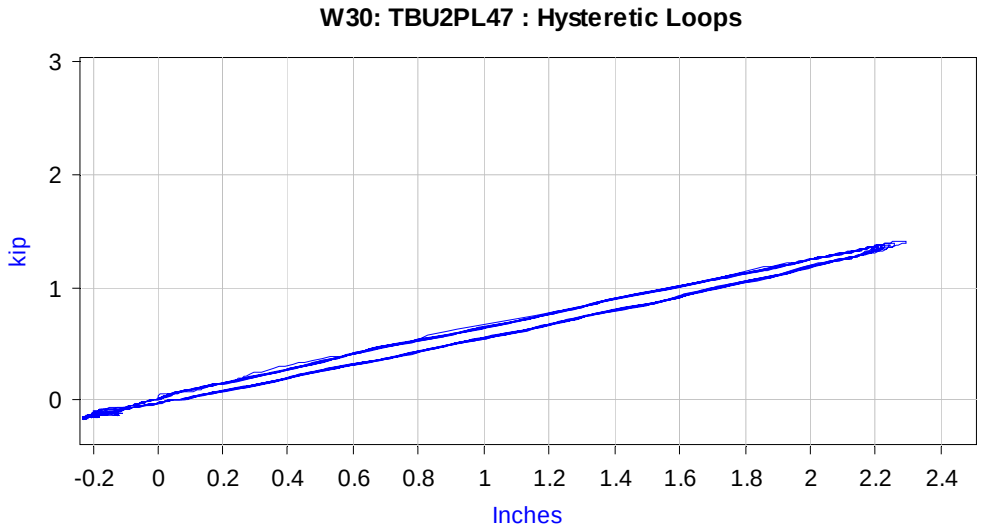

Figure D-68: 10 Cycles of Pull Test in EW direction – Test TBU2PL51

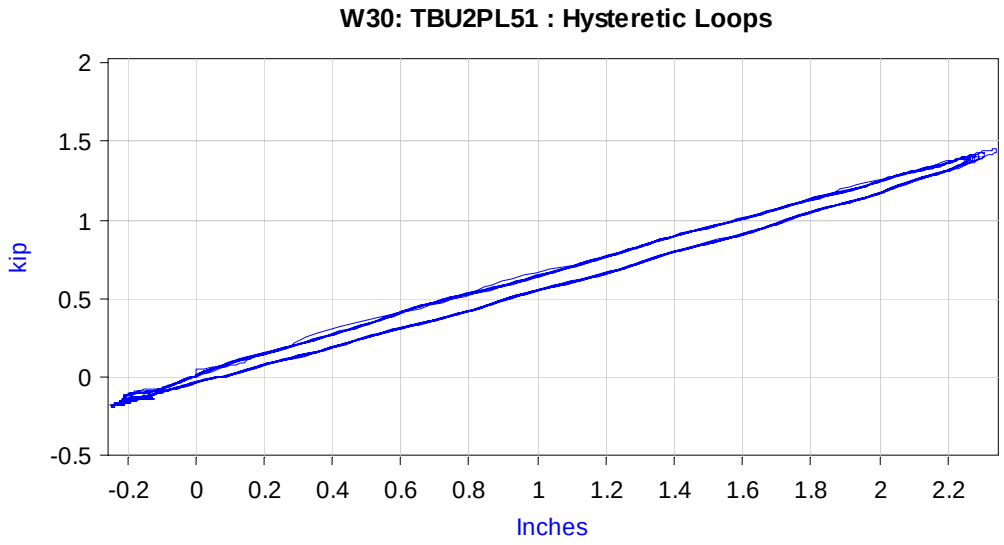

Figure D-69: Pull Test Data Until Bushing Failure – Test TBU2PL65

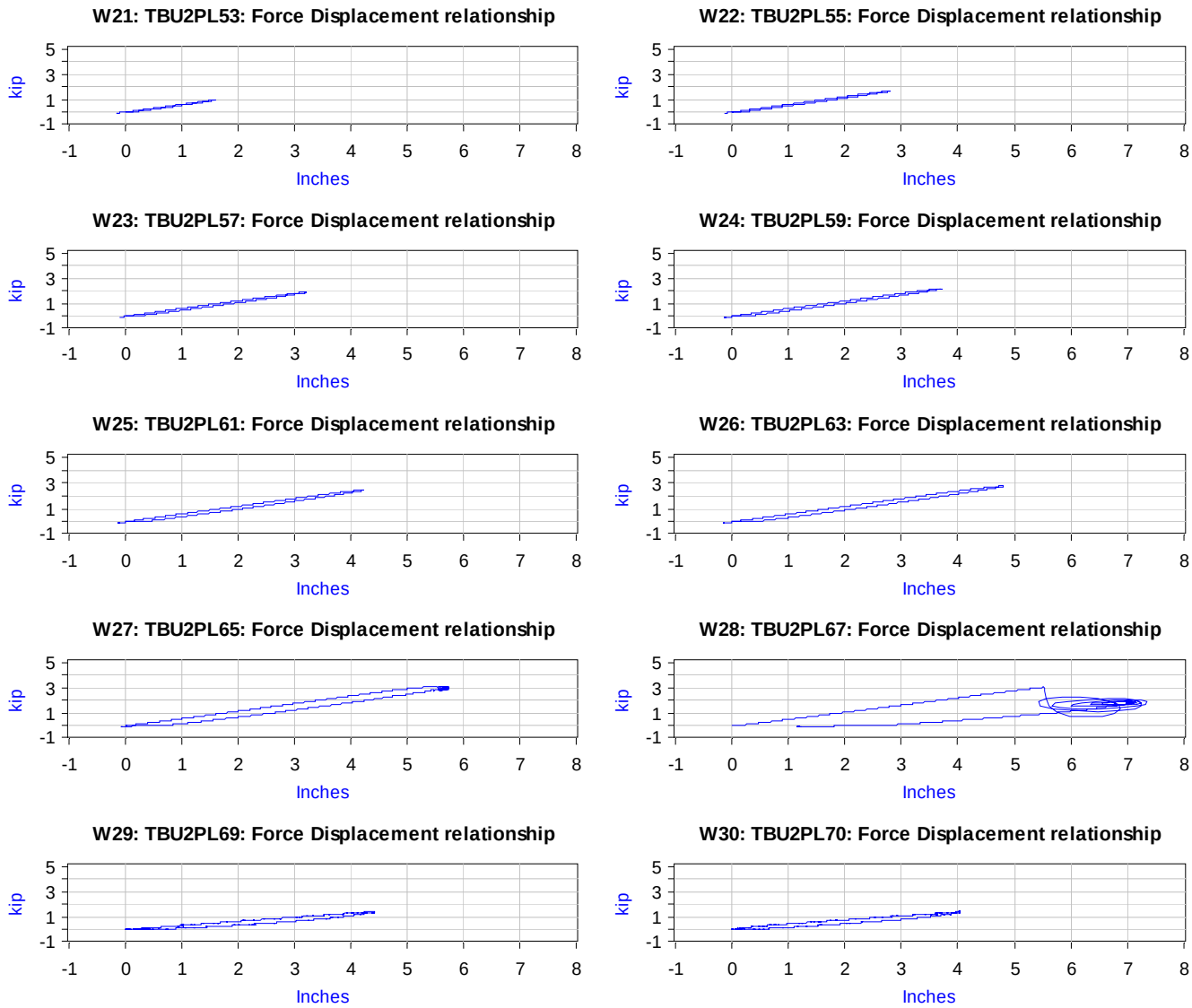

Identification of Properties of Bushing #5

This section is dedicated to Bushing #5, which was tested according to the corresponding test protocol in Appendix A. A summary of the dynamic properties of Bushing #5 is presented in Table D-5.

Identification of Dynamic Properties with Additional Conductor Weight

Impact Hammer Testing

Impact hammer tests were used to find the frequency and damping ratio of Bushing #5. A 25 lb. weight was mounted at the top of the bushing, which represented a portion of cable near the bushing top that might play a role in the dynamic response. Minimum frequency was observed in the NS direction of 5.08 Hz with a damping ratio of 2.00%; in the EW Direction the frequency was 5.27 Hz and damping ratio was 2.60%. The Power Spectral Density (PSD) of the free vibration response gave the frequency of the bushing, and the logarithmic decrement method was used to find the damping ratio. See Figures D-70 through D-87 for the results of these tests.

Table D-5: Dynamic Properties of Bushing #5 from Various Tests

Test No.	Frequency			Damping			Max Displacement	Force	Stiffness
Units	(Hz)			(%)			(in)	(lb)	(lb/in)
(1)	(2)	(3)	(4)	(5)	(6)	(7)	(8)	(9)	(10)
Direction	NS	EW	Vertical	NS	EW	Vertical			
Impact Hammer Test –Fixed base									
TB03NSIH	5.08	-	-	2.00	-	-	-	-	-
TB05EWIH	-	5.27	-	-	2.60	-	-	-	-
TB10NSIH	5.09	-	-	1.73	-	-	-	-	-
TB11EWIH	-	5.27	-	-	2.84	-	-	-	-
TB13NSIH	5.12	-	-	1.81	-	-	-	-	-
TB14EWIH	-	5.25	-	-	2.25	-	-	-	-
TB16NSIH	5.12	-	-	2.17	-	-	-	-	-
TB17EWIH	-	5.20	-	-	2.20	-	-	-	-
TB19NSIH	5.12	-	-	1.69	-	-	-	-	-
TB20EWIH	-	5.12	-	-	2.32	-	-	-	-
TB22NSIH	5.12	-	-	1.72	-	-	-	-	-
TB23EWIH	-	5.12	-	-	2.33	-	-	-	-
TB25NSIH	5.12	-	-	1.79	-	-	-	-	-
TB26EWIH	-	5.24	-	-	2.31	-	-	-	-
TB28NSIH	5.12	-	-	1.46	-	-	-	-	-
TB29EWIH	-	5.16	-	-	0.14	-	-	-	-
TB31NSIH	5.12	-	-	1.37	-	-	-	-	-
TB32EWIH	-	5.14	-	-	1.27	-	-	-	-
Quick Release Test - Fixed Base									
TB07PLSG	-	-	-	-	-	-	0.39	261.50	679.22
TB07PLSGB	-	-	-	-	-	-	0.21	152.60	713.75
TB09PL200	-	5.11	-	-	1.82	-	0.25	189.09	746.80
TB12PL300	-	5.08	-	-	1.92	-	0.42	283.00	676.22
TB15PL400	-	5.10	-	-	1.92	-	0.56	380.74	679.57
TB18PL500	-	5.10	-	-	1.92	-	0.74	517.76	695.96
TB21PL1000	-	5.07	-	-	1.88	-	1.45	979.31	673.63
TB24PL1500	-	5.06	-	-	1.94	-	2.19	1479.82	676.57
TB27PL2000	-	5.07	-	-	1.87	-	2.97	1985.76	669.07
TB30PL2800	-	5.05	-	-	1.64	-	4.27	2804.72	657.32
White Noise Test									
TB33WN	3.50	3.25	-	5.38	14.19	-	-	-	-
TB36WN	3.50	3.50	-	4.41	10.10	-	-	-	-
TB39WN	3.50	3.50	-	4.20	7.21	-	-	-	-
TB42WN	3.50	3.50	-	4.38	6.75	-	-	-	-
TB45WN	3.50	3.25	-	5.24	6.78	-	-	-	-
TB51WN	3.25	3.25	-	5.63	4.39	-	-	-	-
TB54WN	3.00	3.00	-	5.77	7.53	-	-	-	-
Table Impulse Test									
TB34TBI	3.32	3.00	-	8.46	2.08	-	-	-	-
TB37TBI	3.50	3.50	-	19.59	3.38	-	-	-	-
TB40TBI	3.50	3.50	-	1.73	2.02	-	-	-	-
TB43TBI	3.50	3.40	-	19.49	2.23	-	-	-	-
TB46TBI	3.50	3.40	-	2.49	1.61	-	-	-	-
TB52TBI	3.30	3.30	-	2.94	2.78	-	-	-	-
TB55TBI	3.10	3.10	-	3.22	2.94	-	-	-	-

Figure D-70: Acceleration Response of Bushing #5, with 25 lb. Mass, in NS Direction

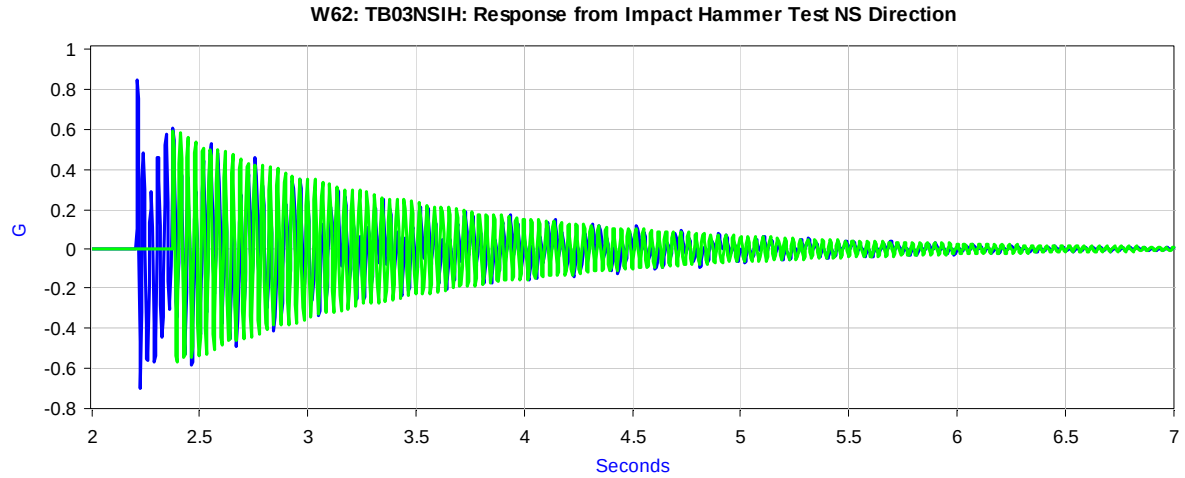

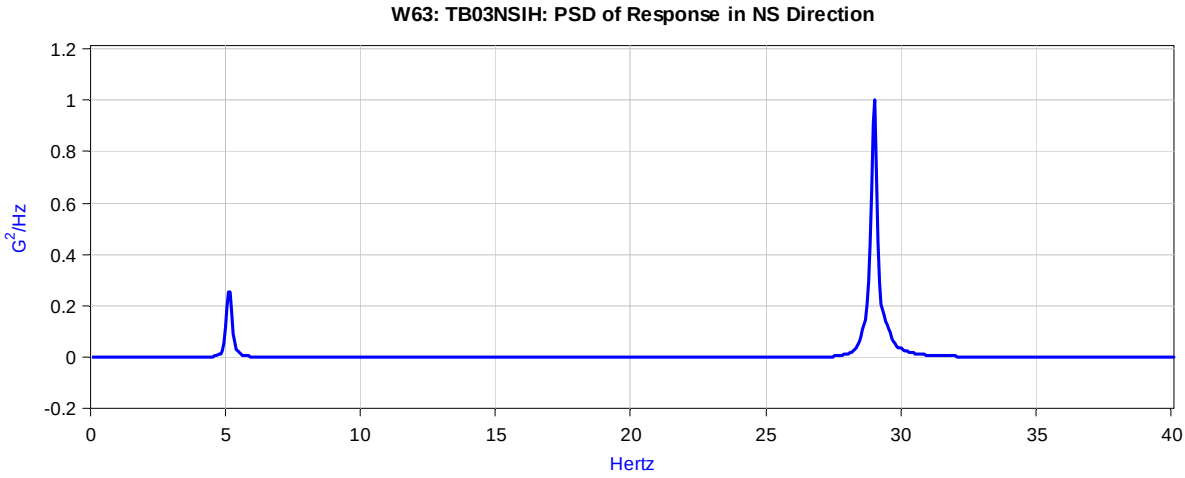

Figure D-71: Acceleration Response of Bushing #5, with 25 lb. Mass, in NE Direction

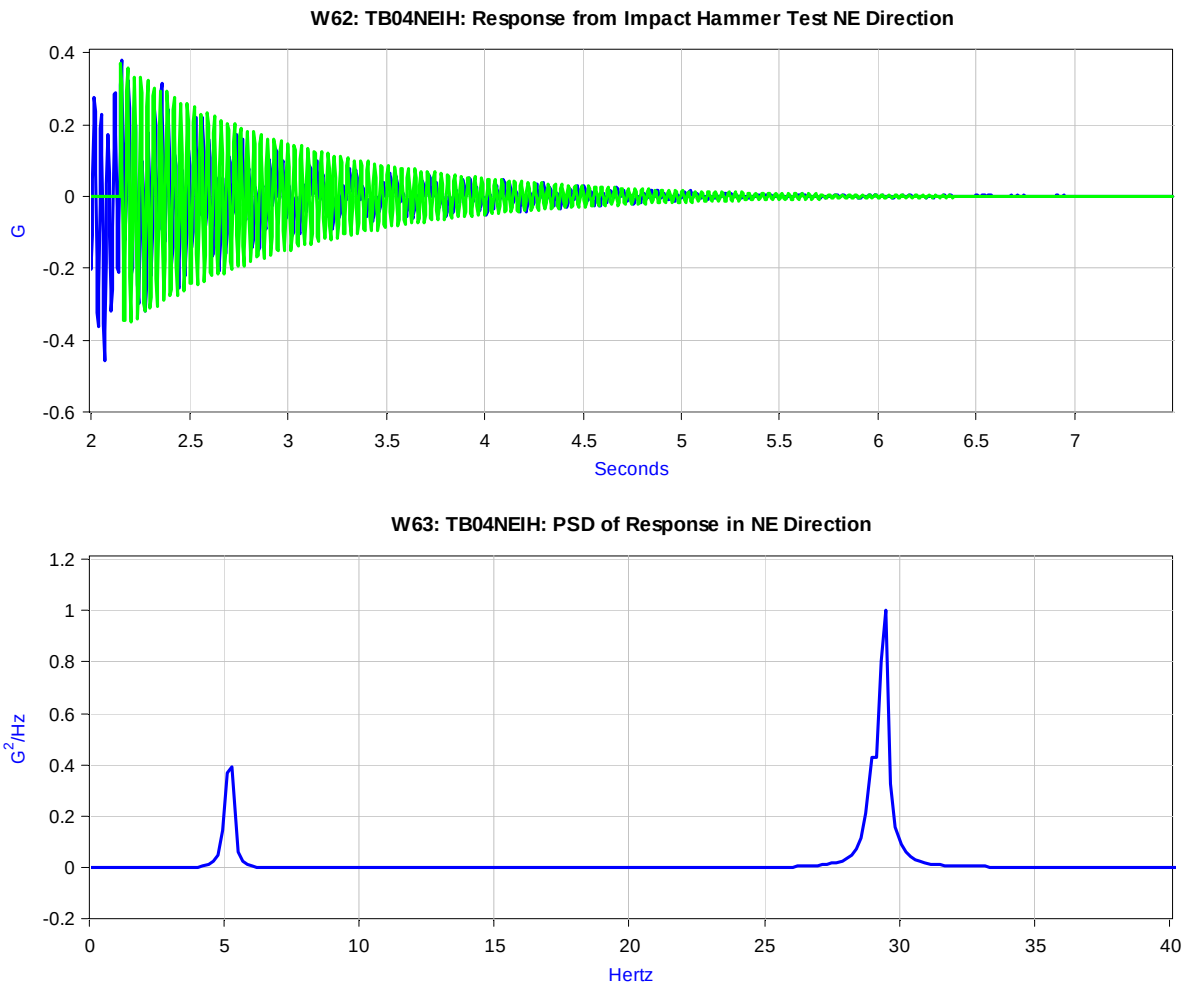

Figure D-72: Acceleration Response of Bushing #5, with 25 lb. Mass, in EW Direction

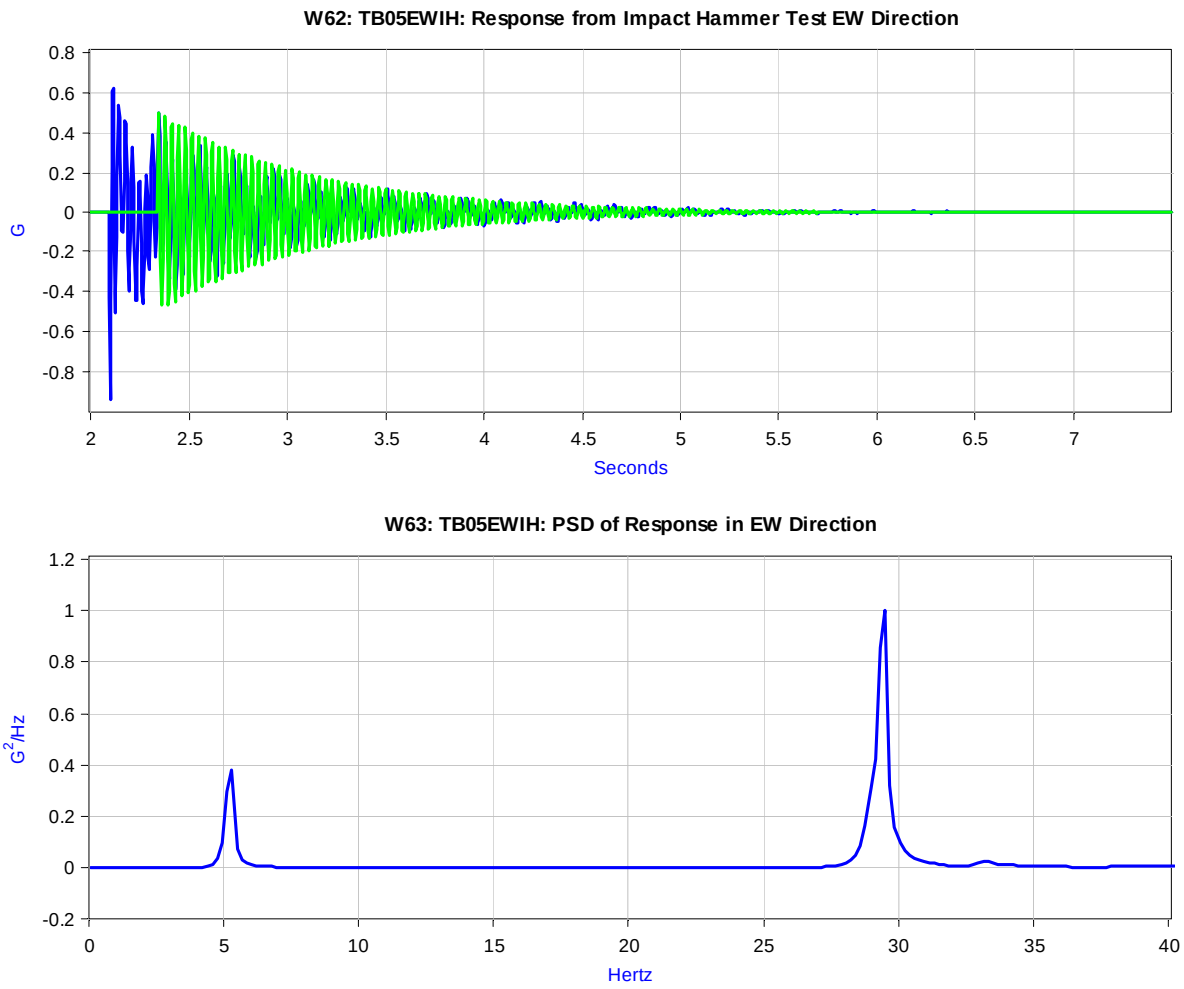

Figure D-73: Acceleration Response of Bushing #5, with 25 lb. Mass, in SE Direction

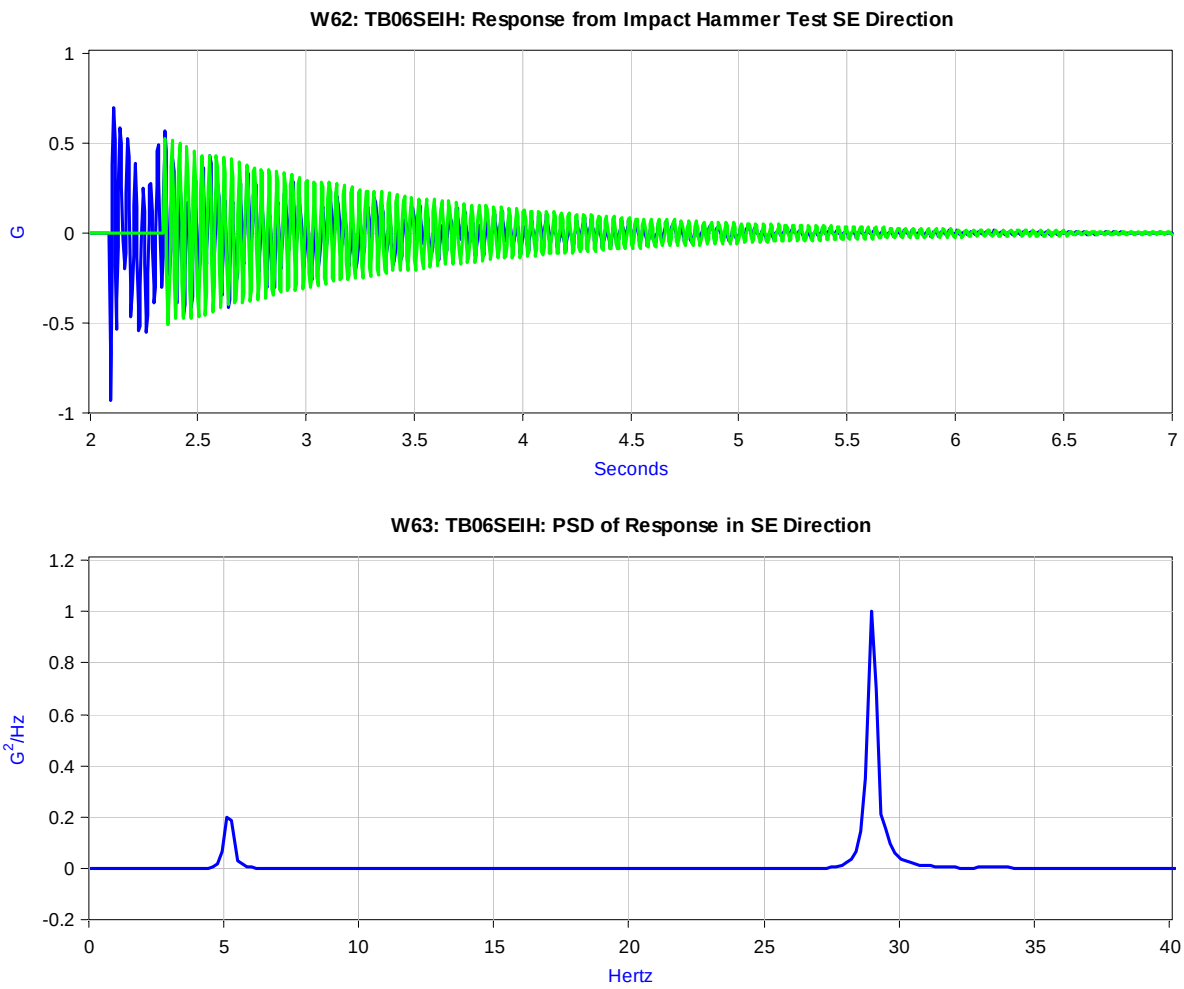

Figure D-74: Acceleration Response of Bushing #5, with 25 lb. Mass, in NS Direction

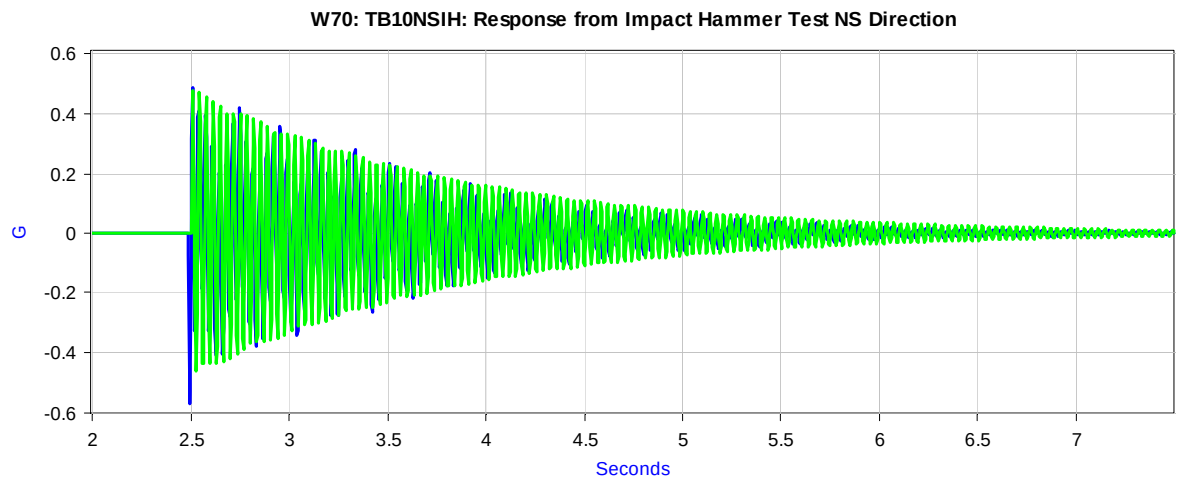

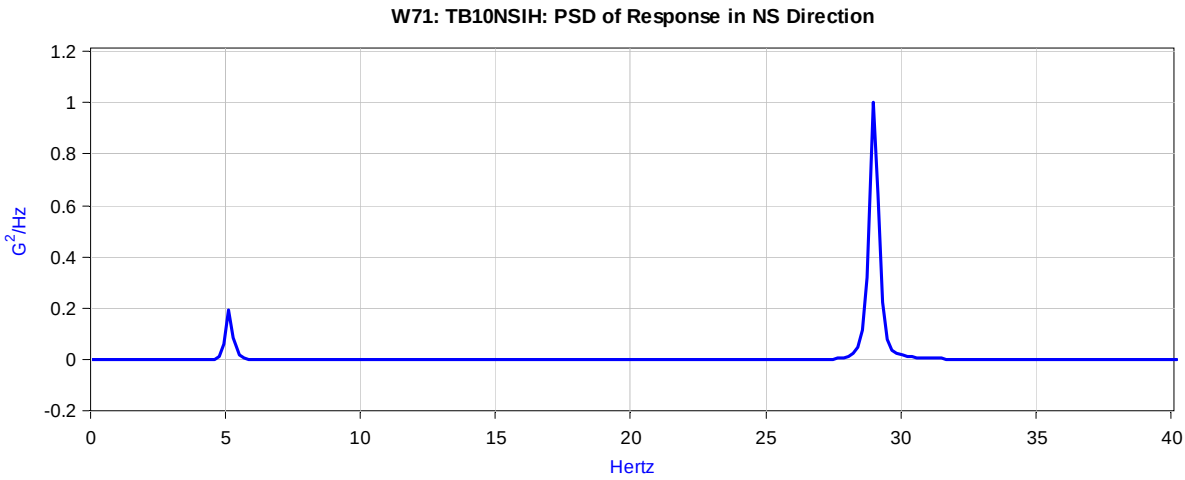

Figure D-75: Acceleration Response of Bushing #5, with 25 lb. Mass, in EW Direction

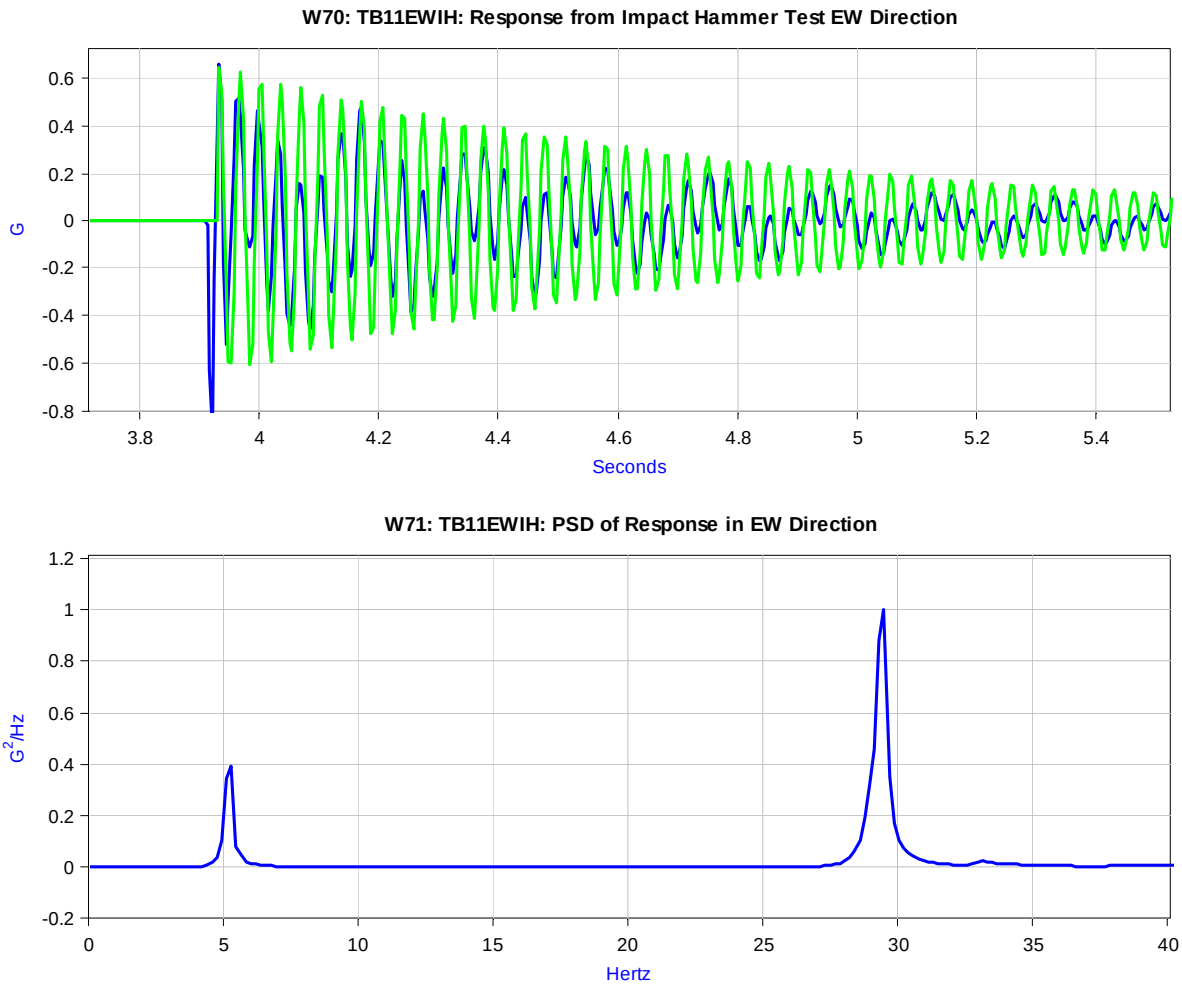

Figure D-76: Acceleration Response of Bushing #5, with 25 lb. Mass, in NS Direction

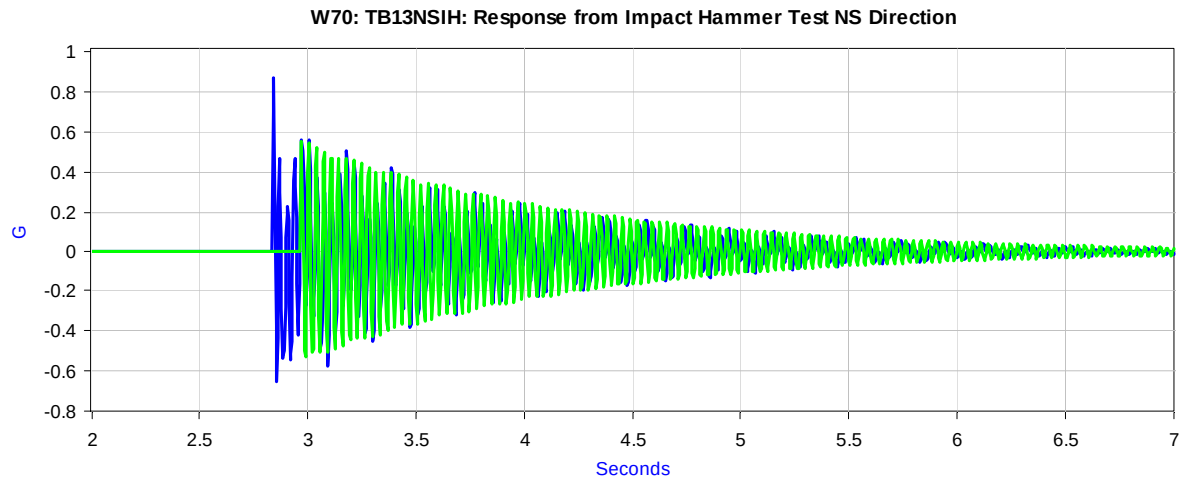

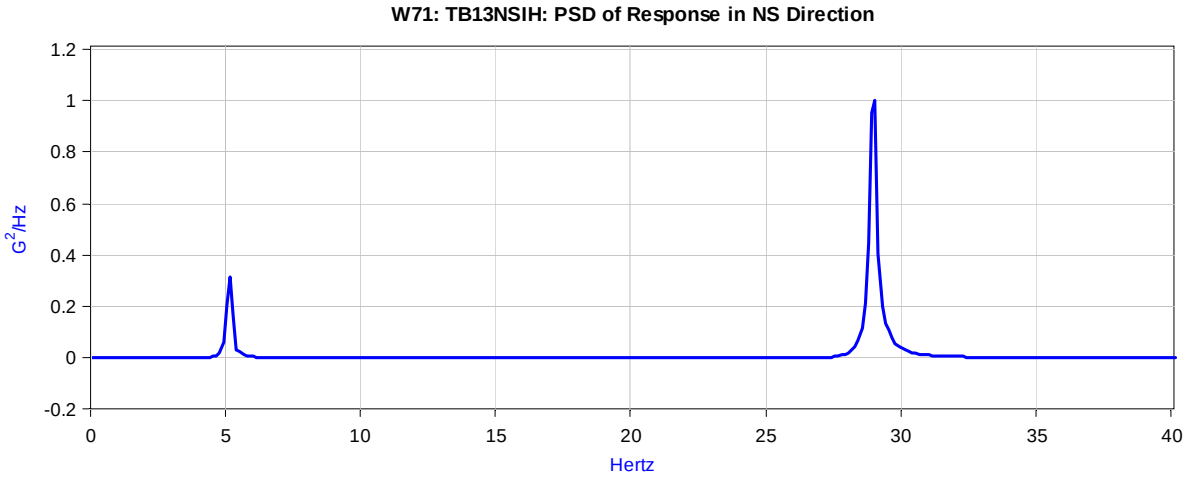

Figure D-77: Acceleration Response of Bushing #5, with 25 lb. Mass, in EW Direction

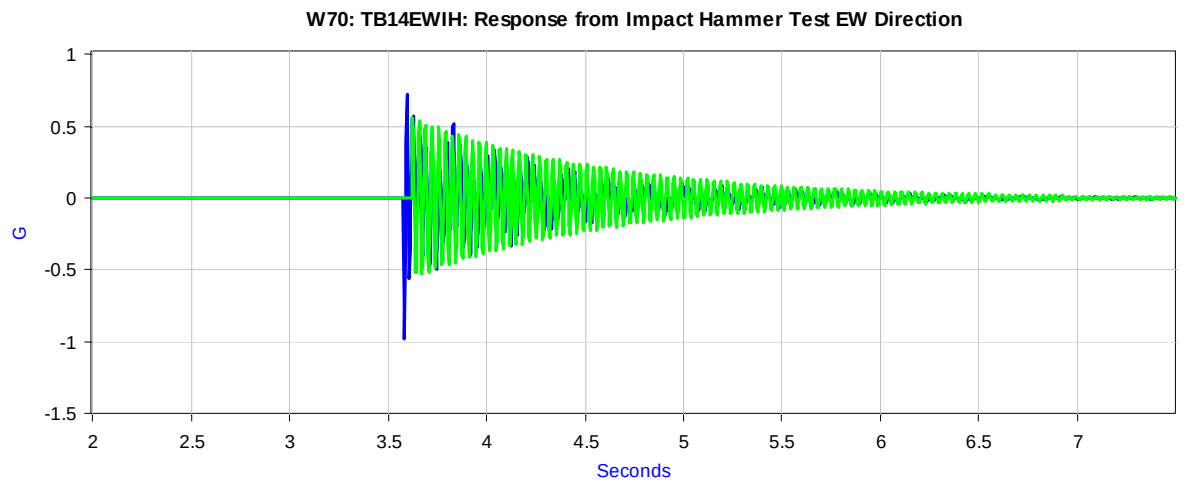

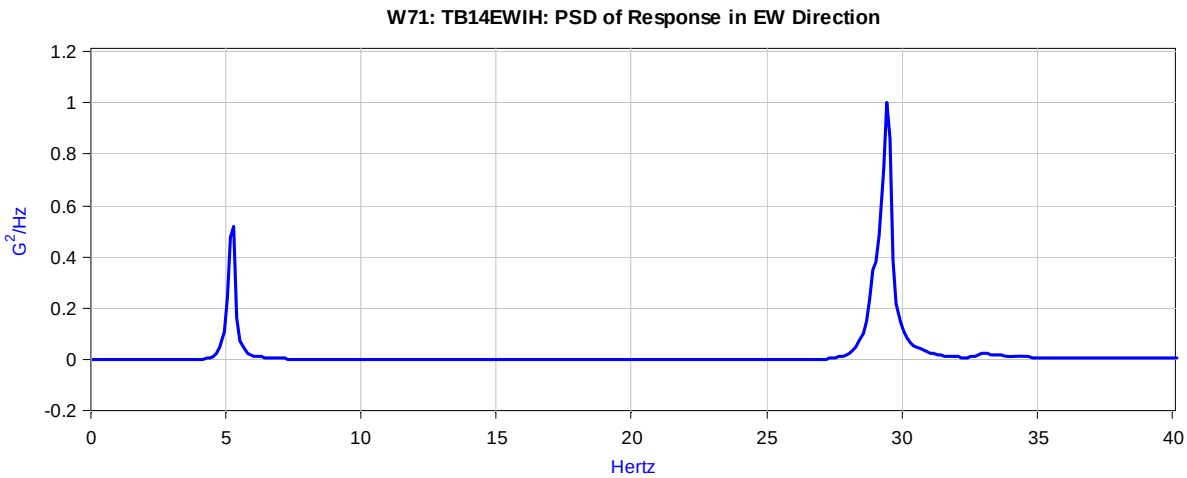

Figure D-78: Acceleration Response of Bushing #5, with 25 lb. Mass, in NS Direction

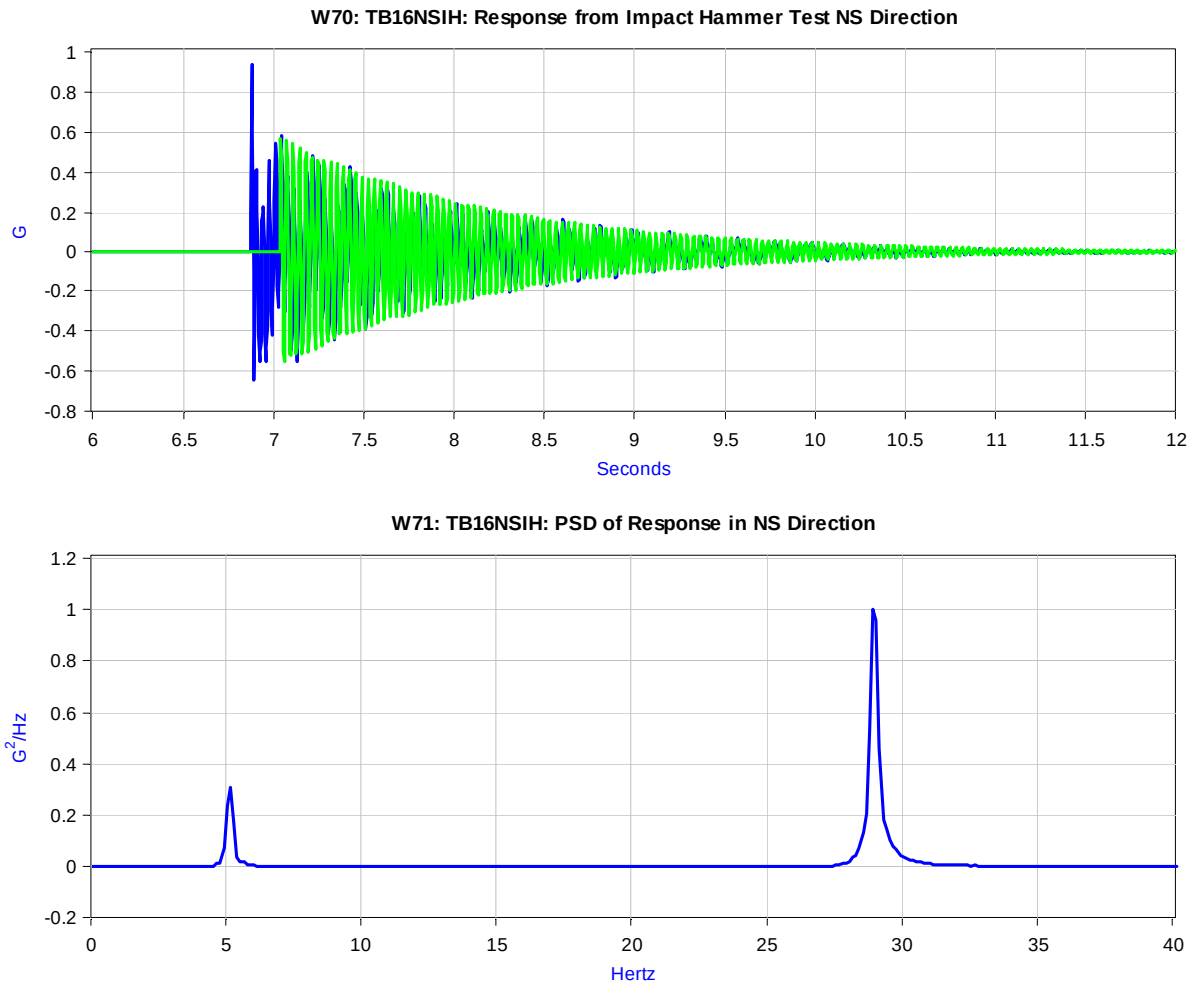

Figure D-79: Acceleration Response of Bushing #5, with 25 lb. Mass, in EW Direction

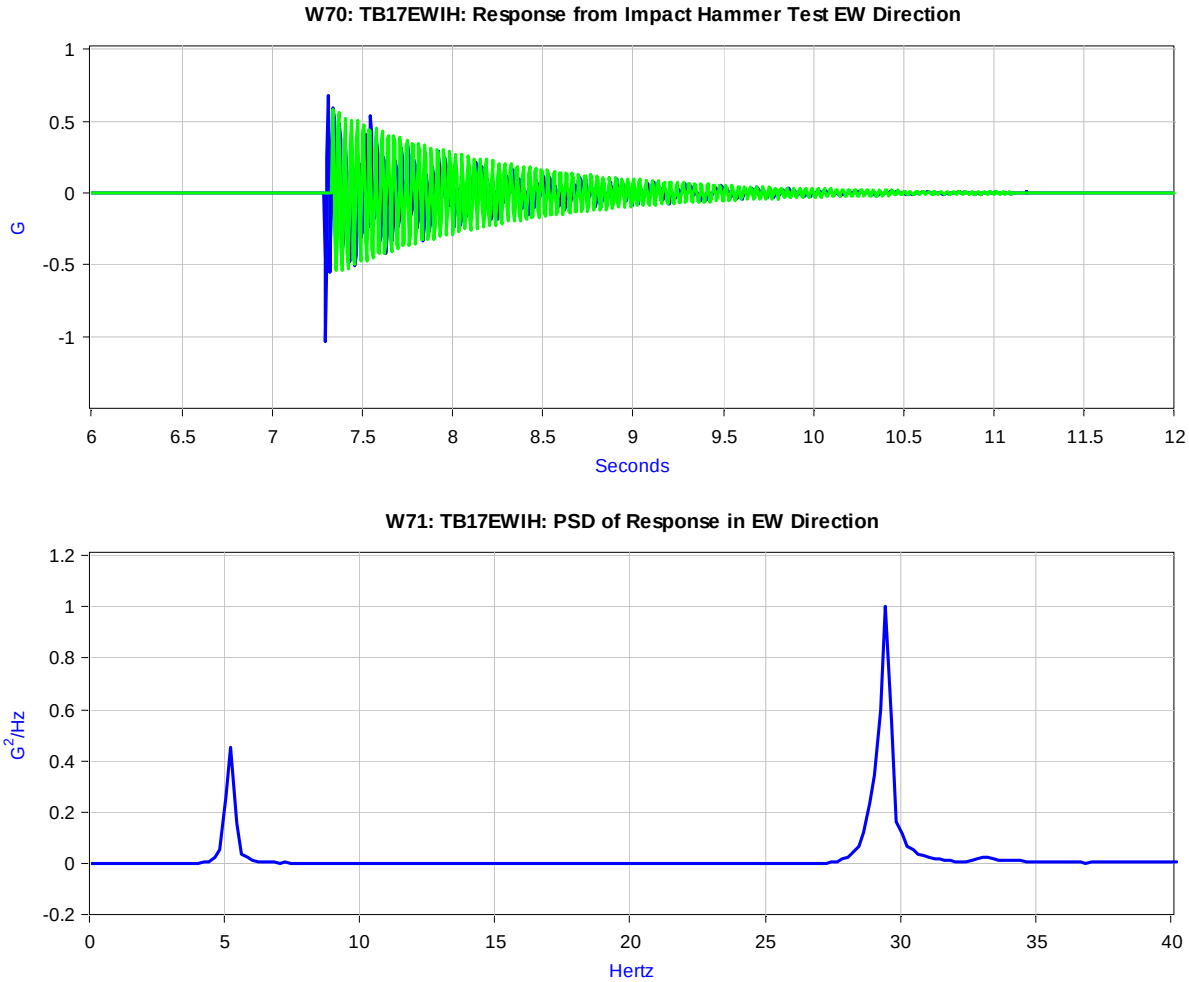

Figure D-80: Acceleration Response of Bushing #5, with 25 lb. Mass, in NS Direction

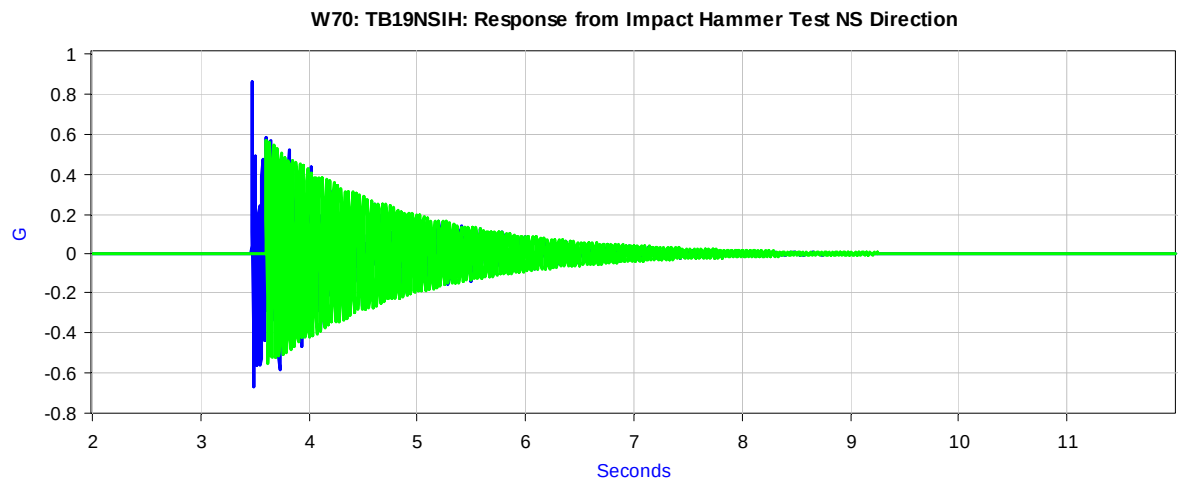

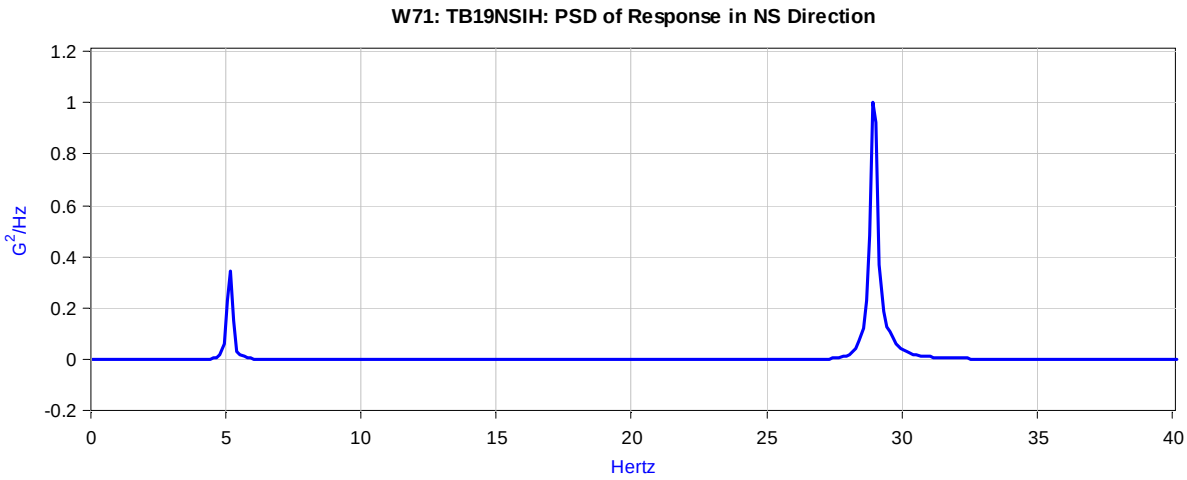

Figure D-81: Acceleration Response of Bushing #5, with 25 lb. Mass, in EW Direction

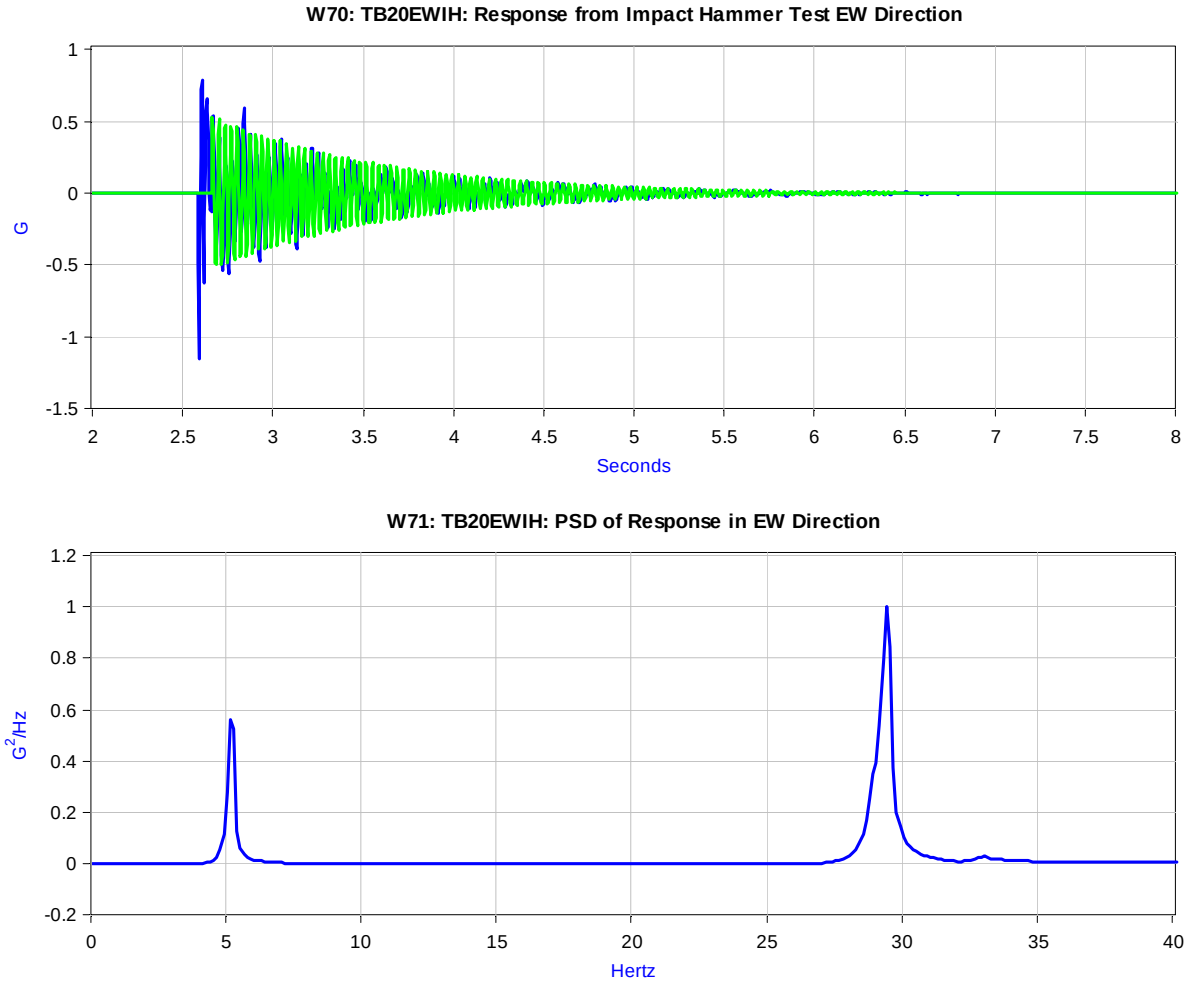

Figure D-82: Acceleration Response of Bushing #5, with 25 lb. Mass, in NS Direction

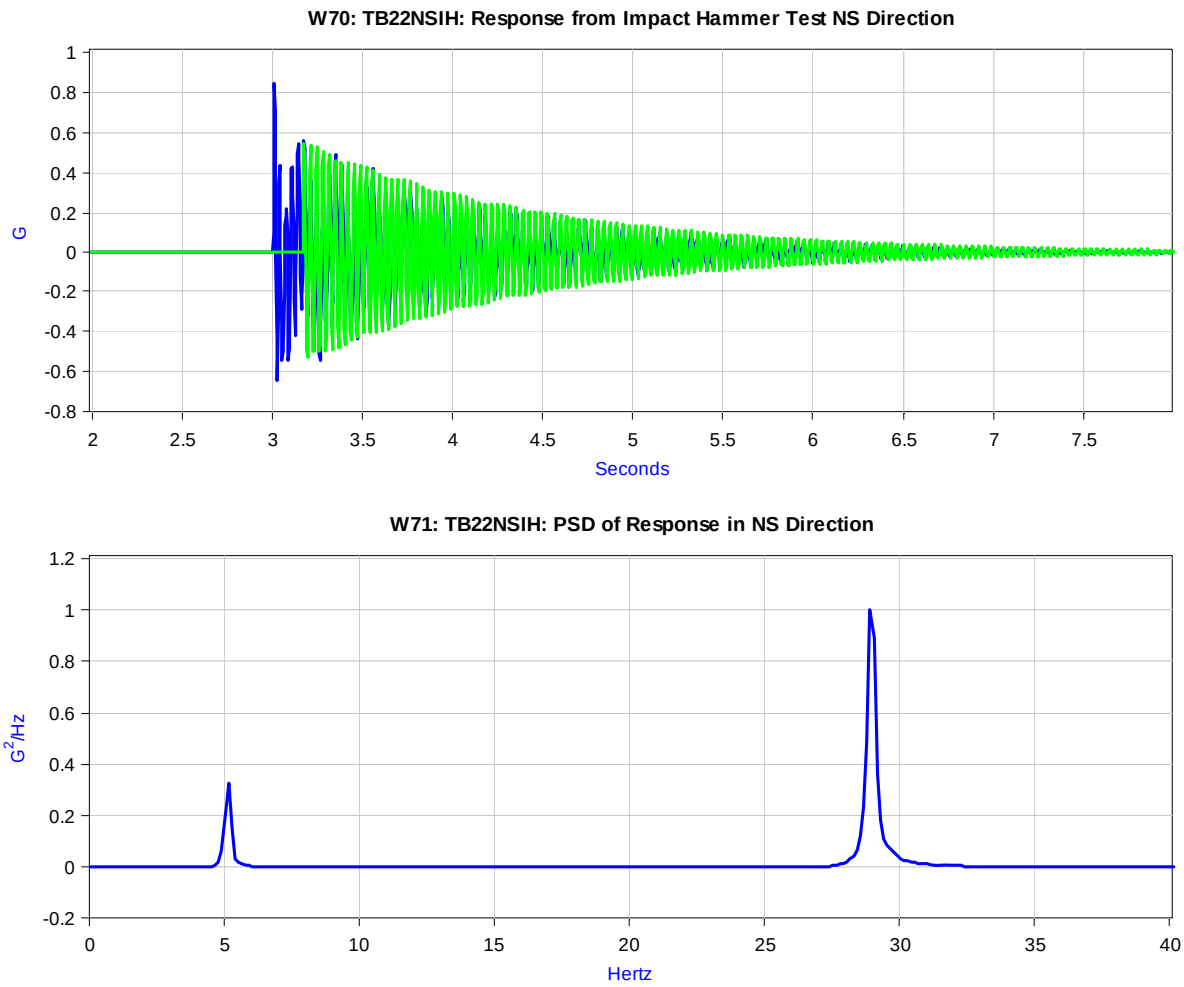

Figure D-81: Acceleration Response of Bushing #5, with 25 lb. Mass, in EW Direction

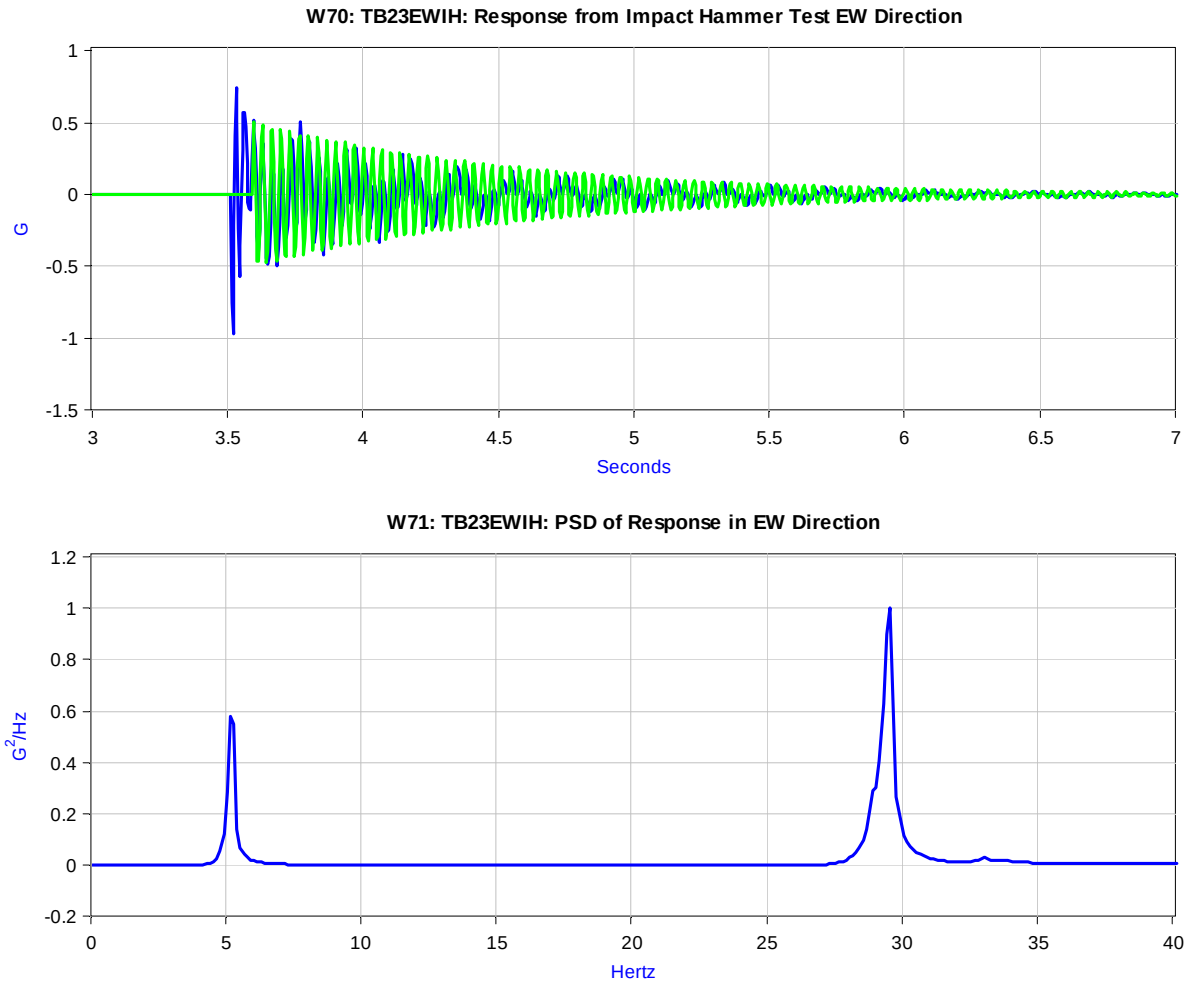

Figure D-82: Acceleration Response of Bushing #5, with 25 lb. Mass, in NS Direction

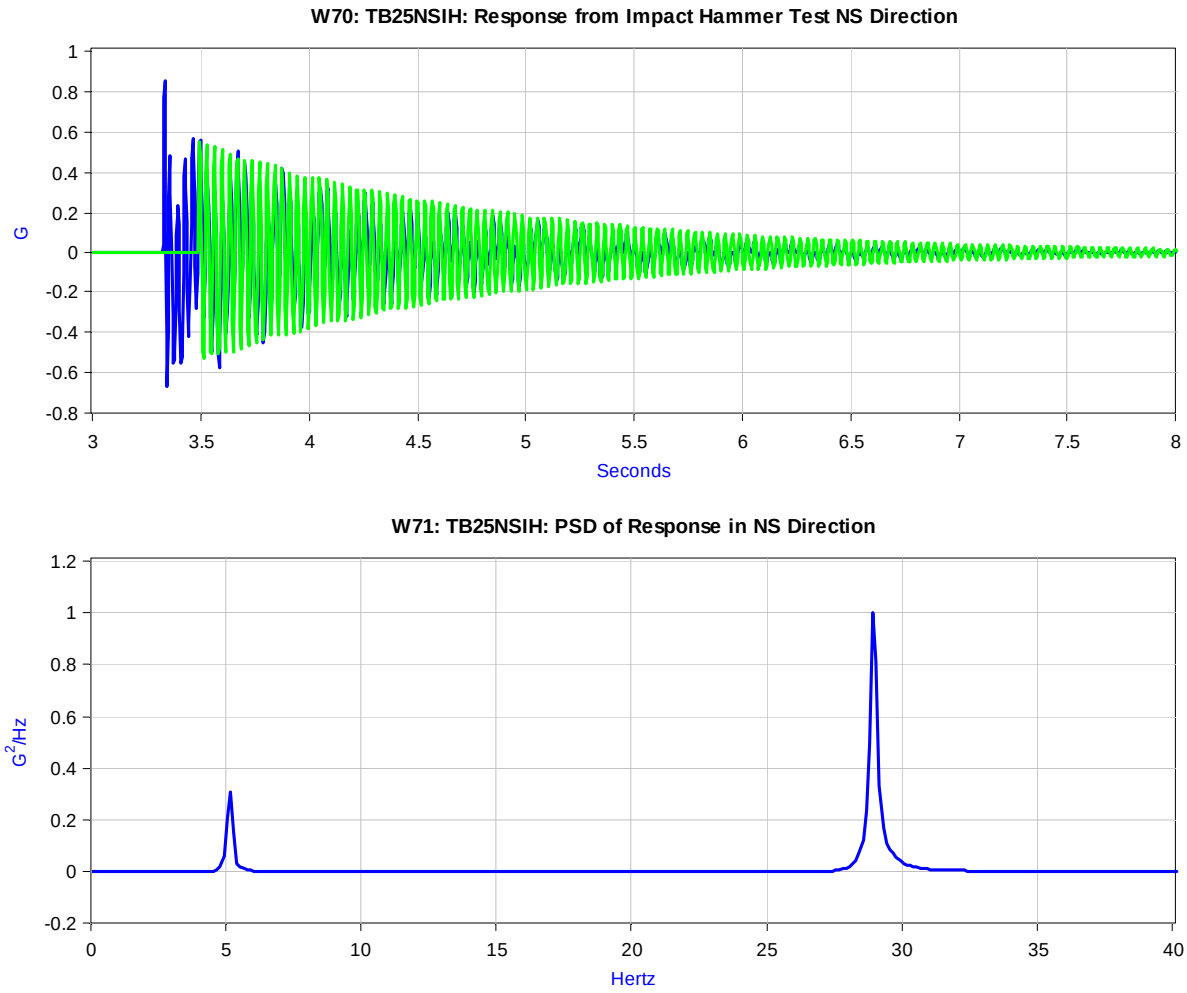

Figure D-83: Acceleration Response of Bushing #5, with 25 lb. Mass, in EW Direction

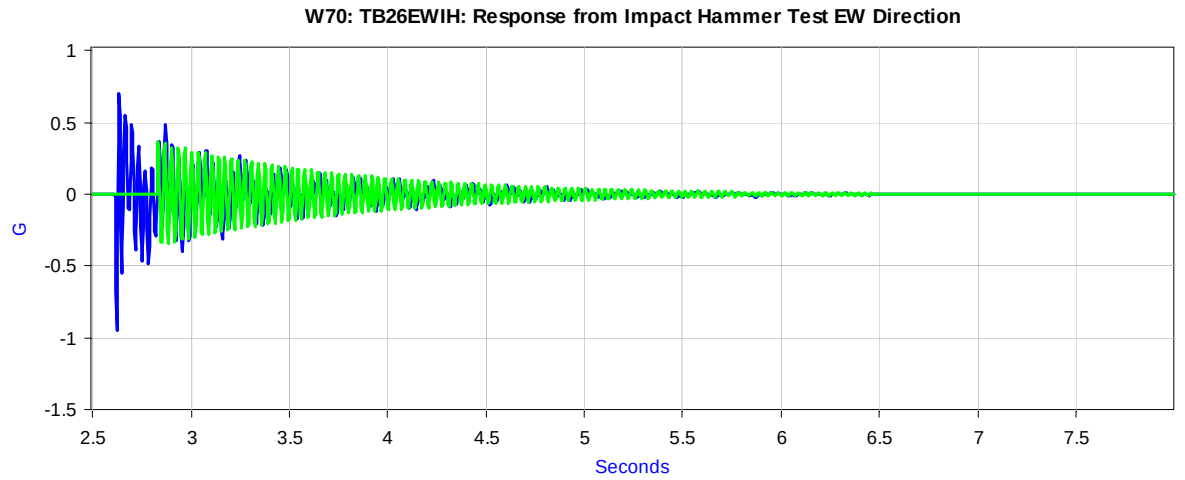

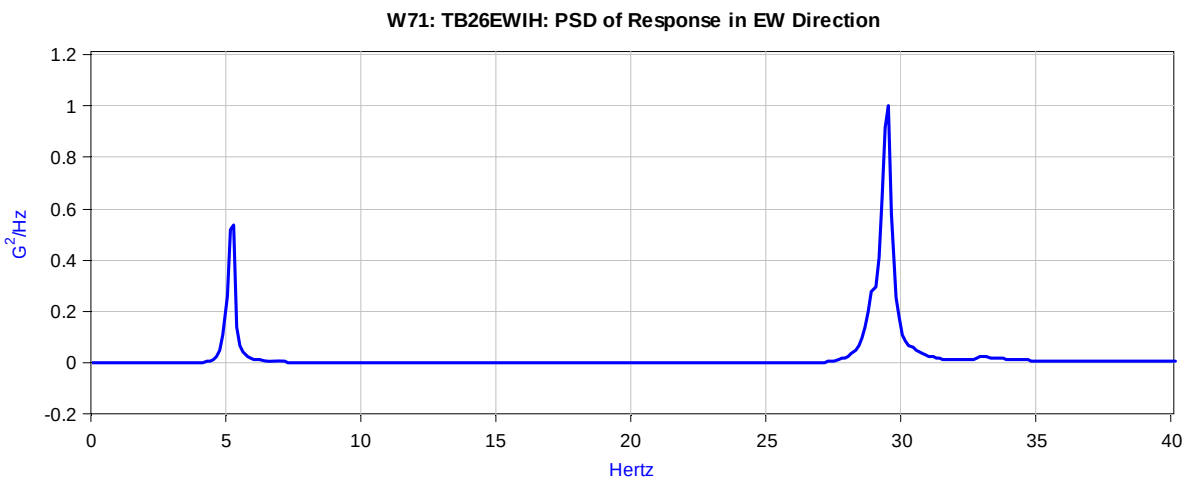

Figure D-84: Acceleration Response of Bushing #5, with 25 lb. Mass, in NS Direction

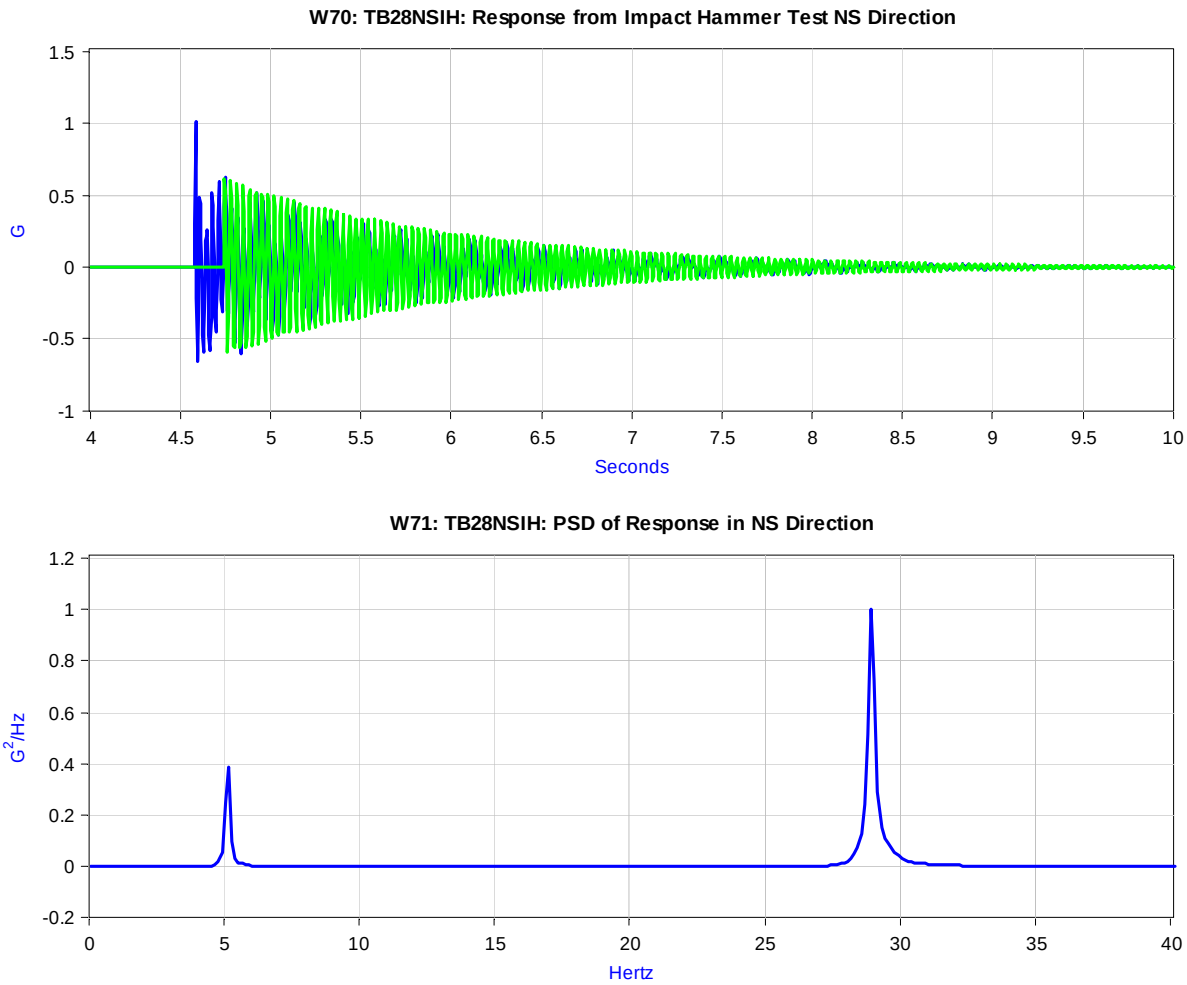

Figure D-85: Acceleration Response of Bushing #5, with 25 lb. Mass, in EW Direction

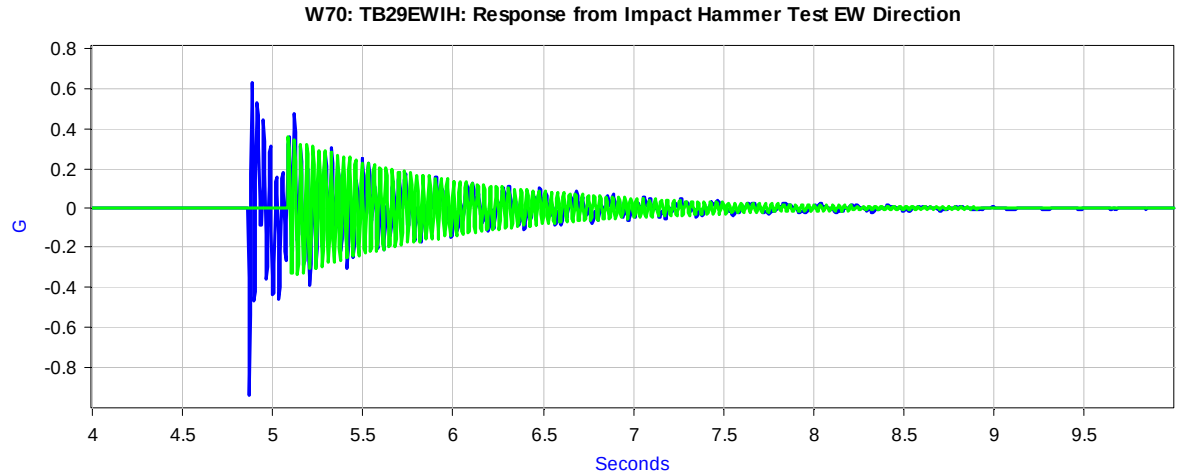

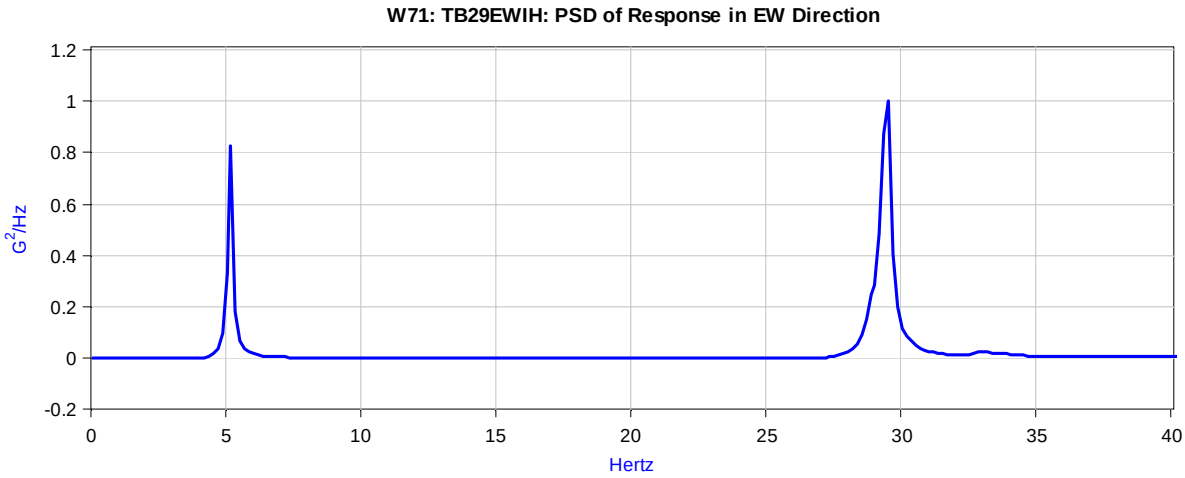

Figure D-86: Acceleration Response of Bushing #5, with 25 lb. Mass, in NS Direction

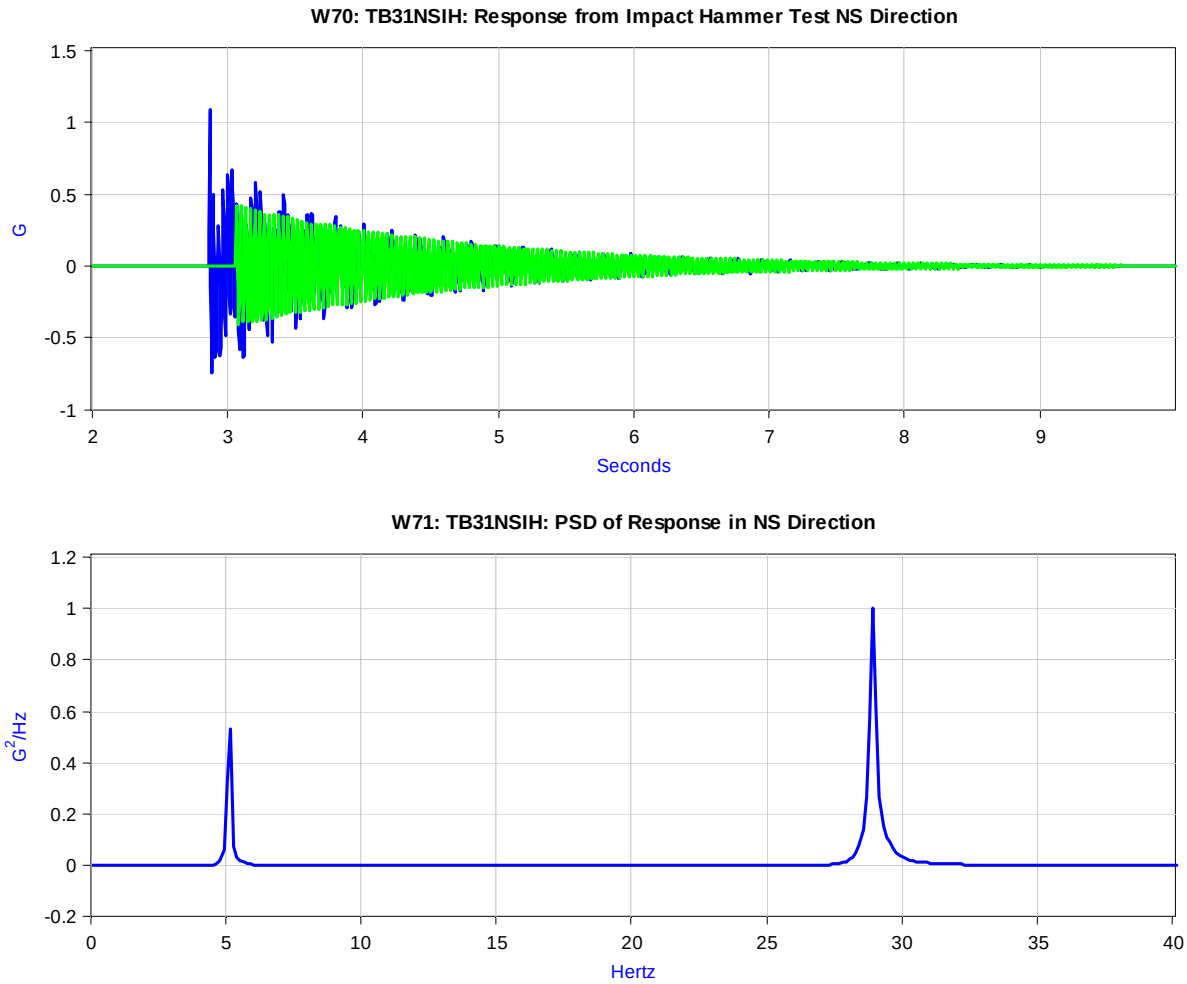

Figure D-87: Acceleration Response of Bushing #5, with 25 lb. Mass, in EW Direction

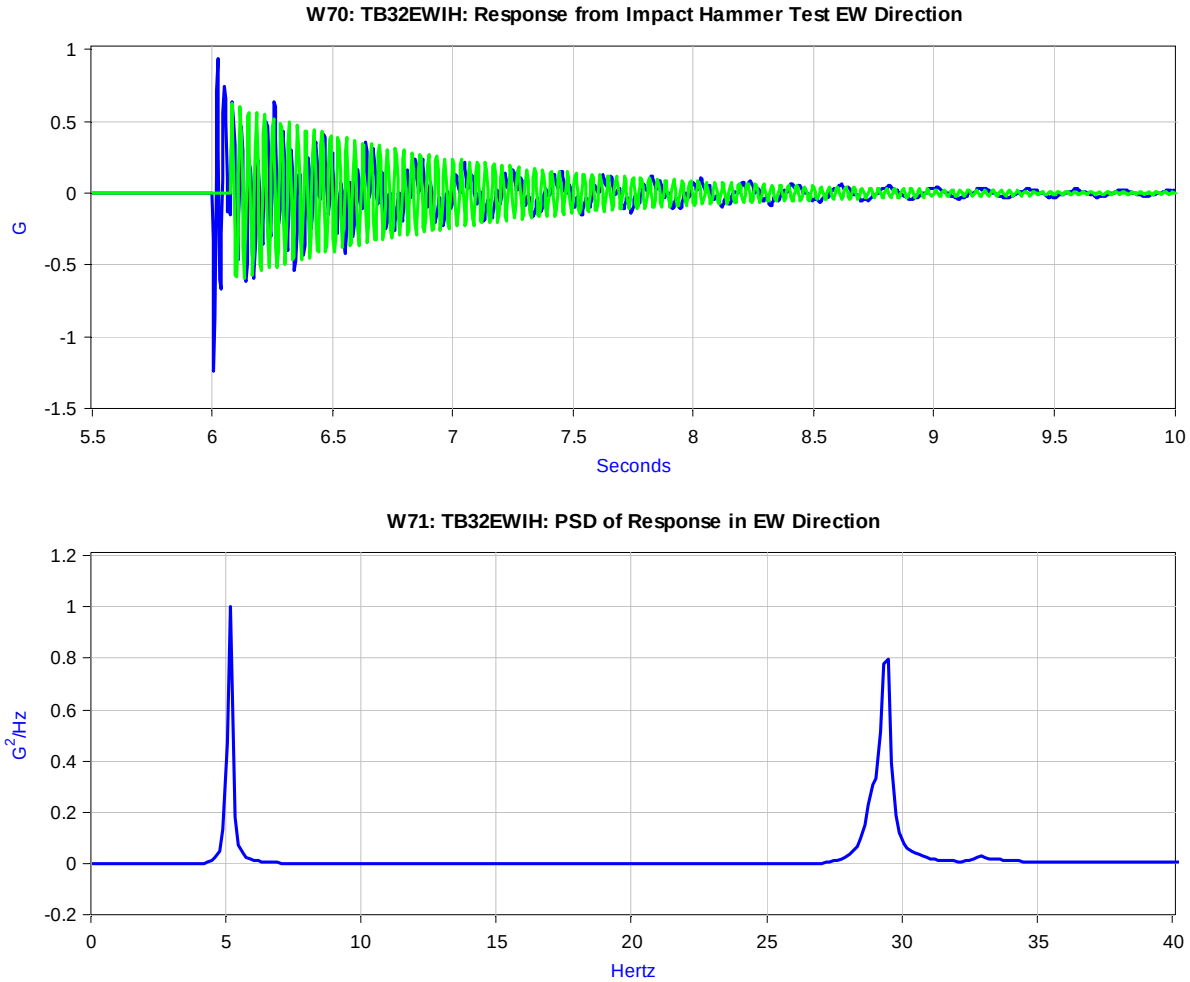

Pull and Sudden Release Tests

After the impact hammer tests, pull and sudden release tests were performed: the bushing was pulled from the top and released suddenly. This test showed the stiffness of the bushing and the frequency and damping ratio were confirmed. The stiffness varied between maximum values of 746.8 lb./in. to 657.3 lb./in. (Table D-5). All the pull tests were run in the EW direction only. See Figures D-88 through D-94 for the results of these tests. Figure D-95 shows the relationship between force and displacement, representing the stiffness of Bushing #5.

Figure D-88: Acceleration Response from Quick Release Test TB09PL200 – Bushing #5

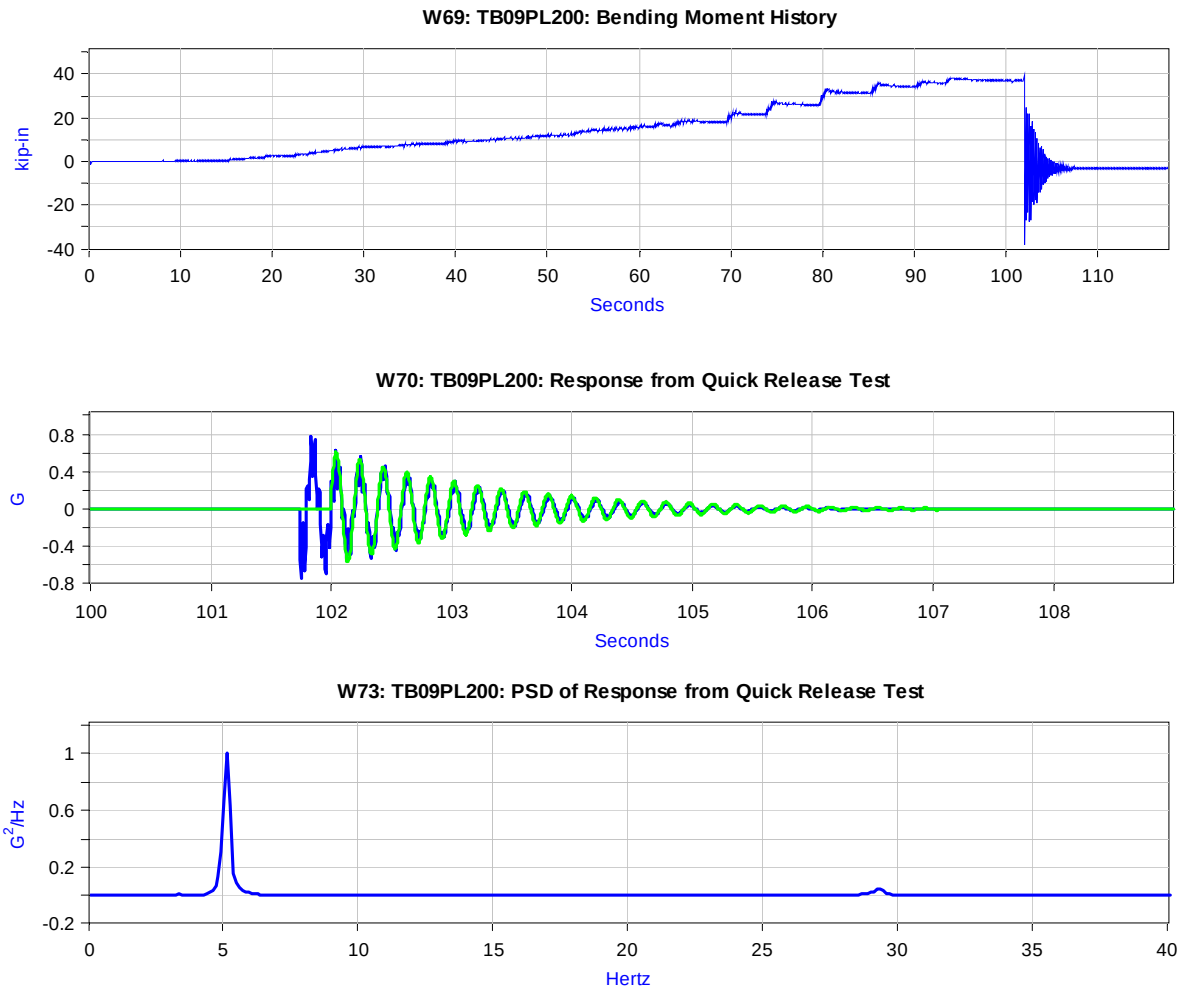

Figure D-89: Acceleration Response from Quick Release Test TB12PL300 – Bushing #5

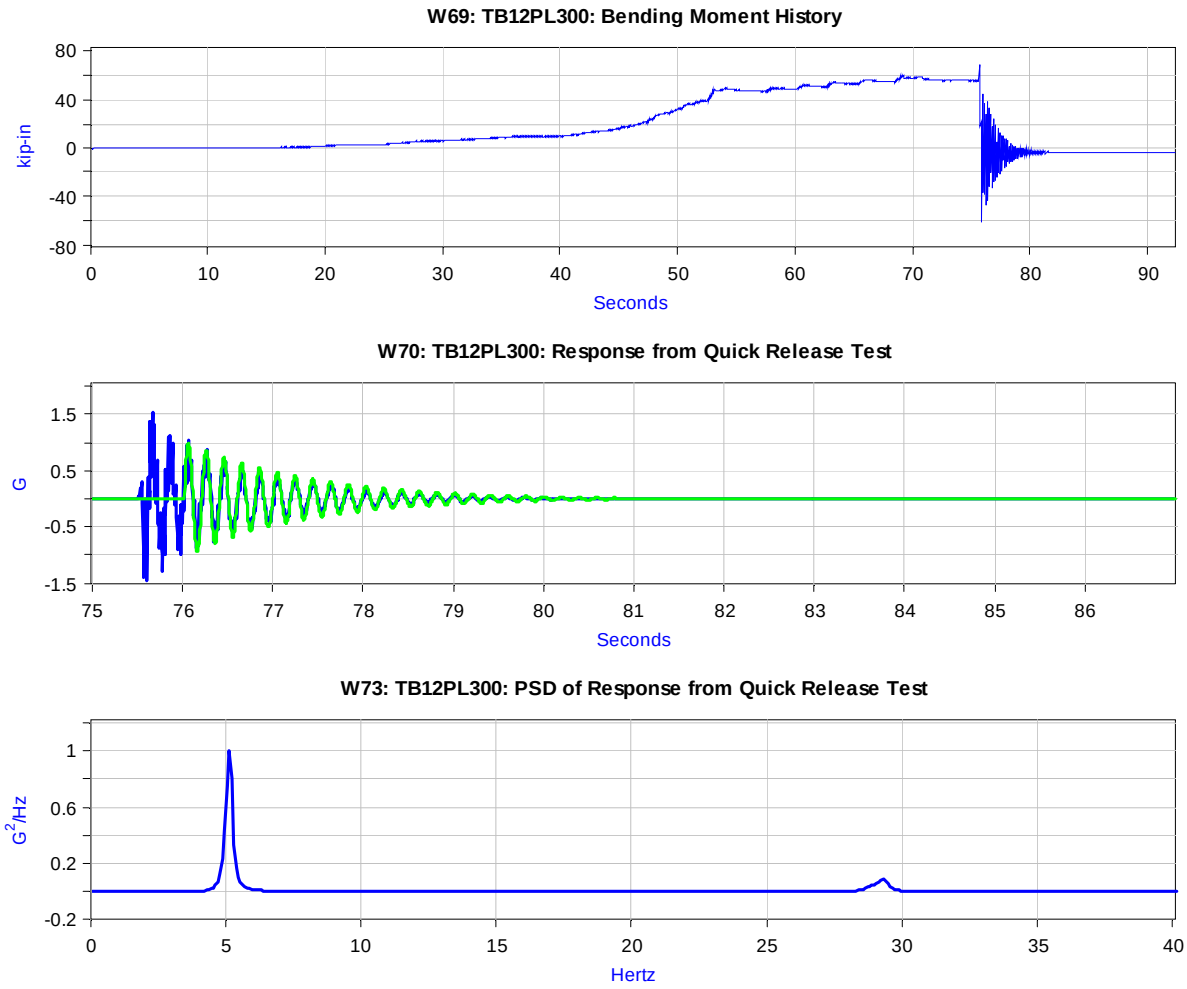

Figure D-90: Acceleration Response from Quick Release Test TB15PL400 – Bushing #5

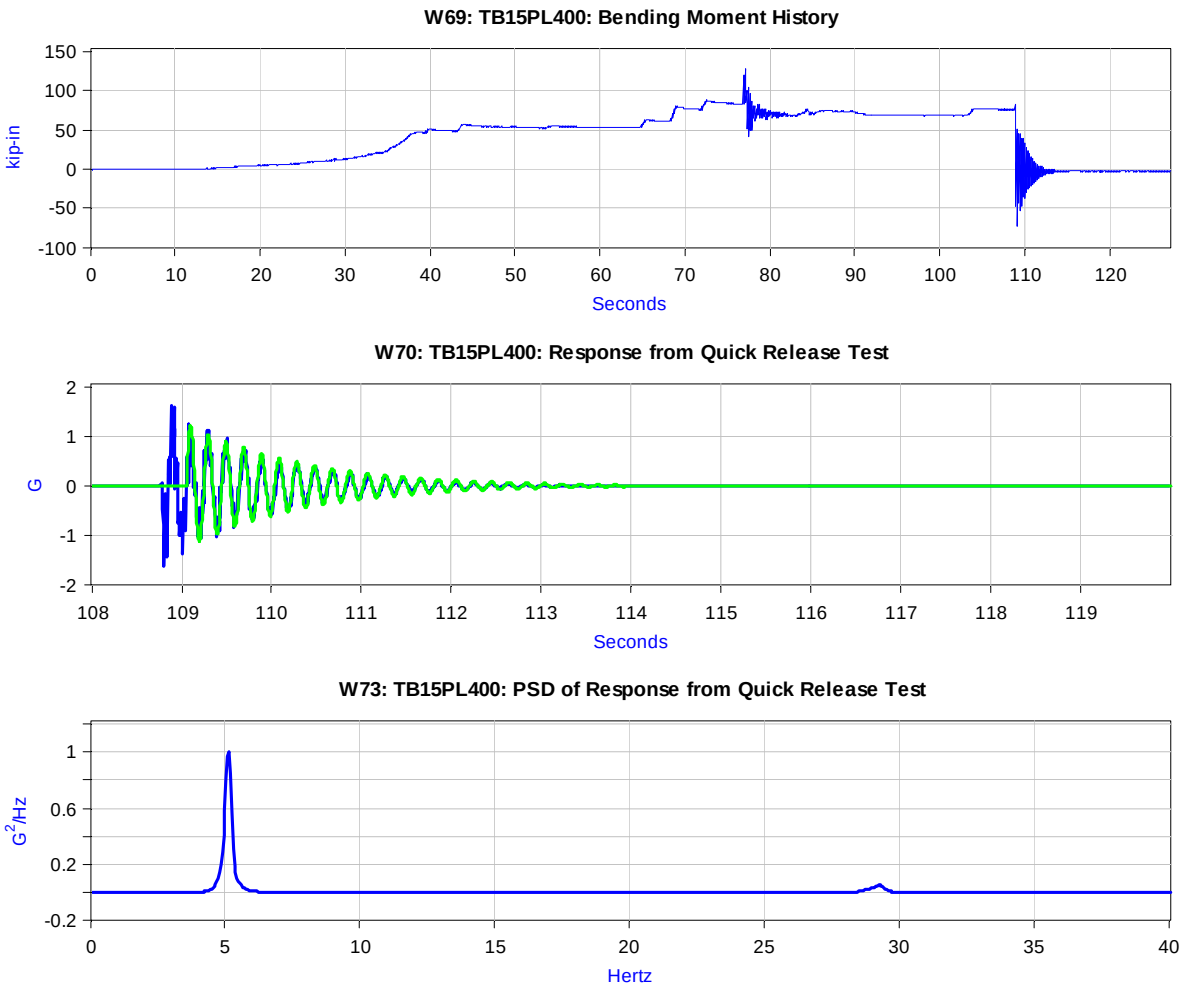

Figure D-91: Acceleration Response from Quick Release Test TB21PL1000 – Bushing #5

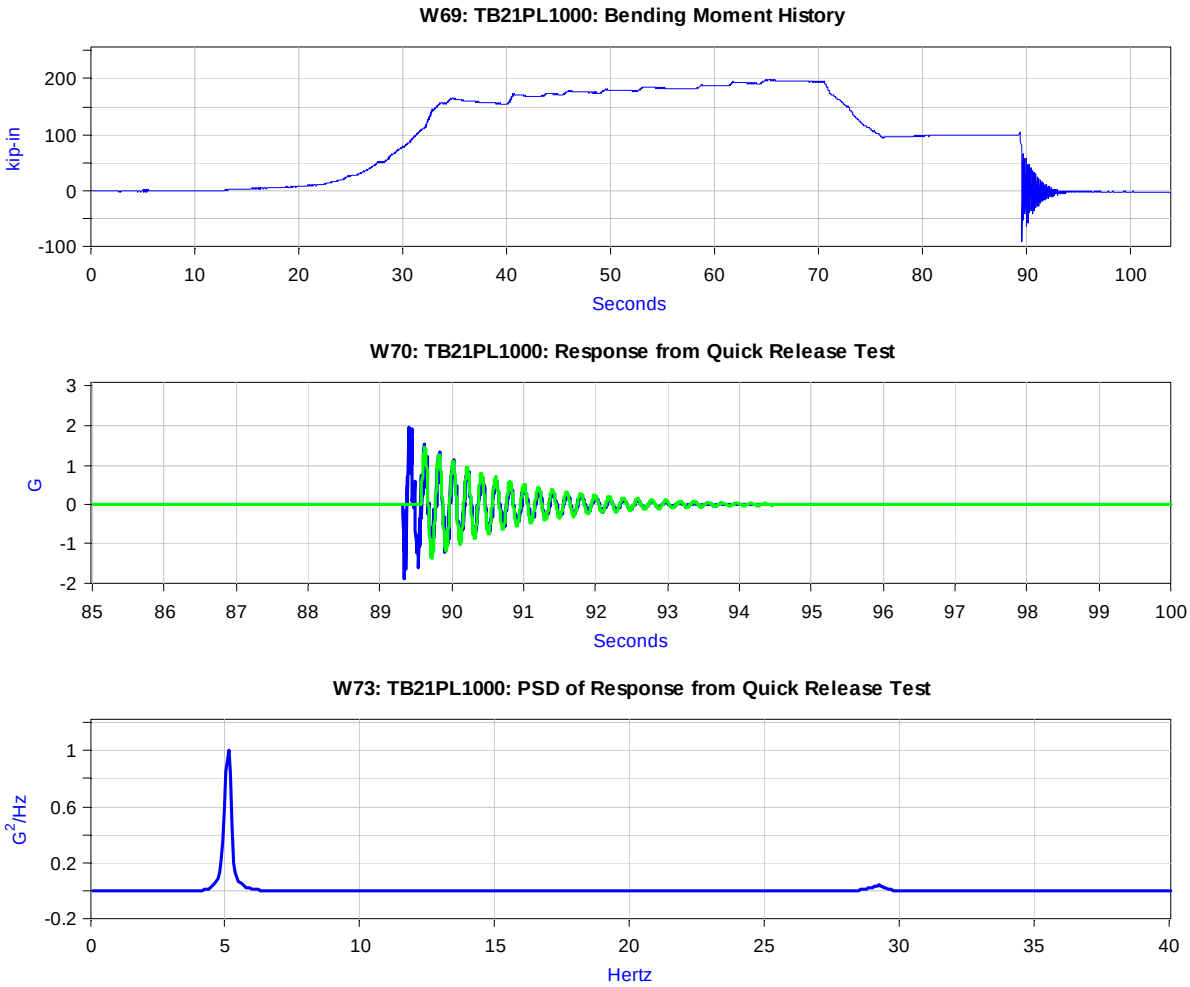

Figure D-92: Acceleration Response from Quick Release Test TB24PL1500 – Bushing #5

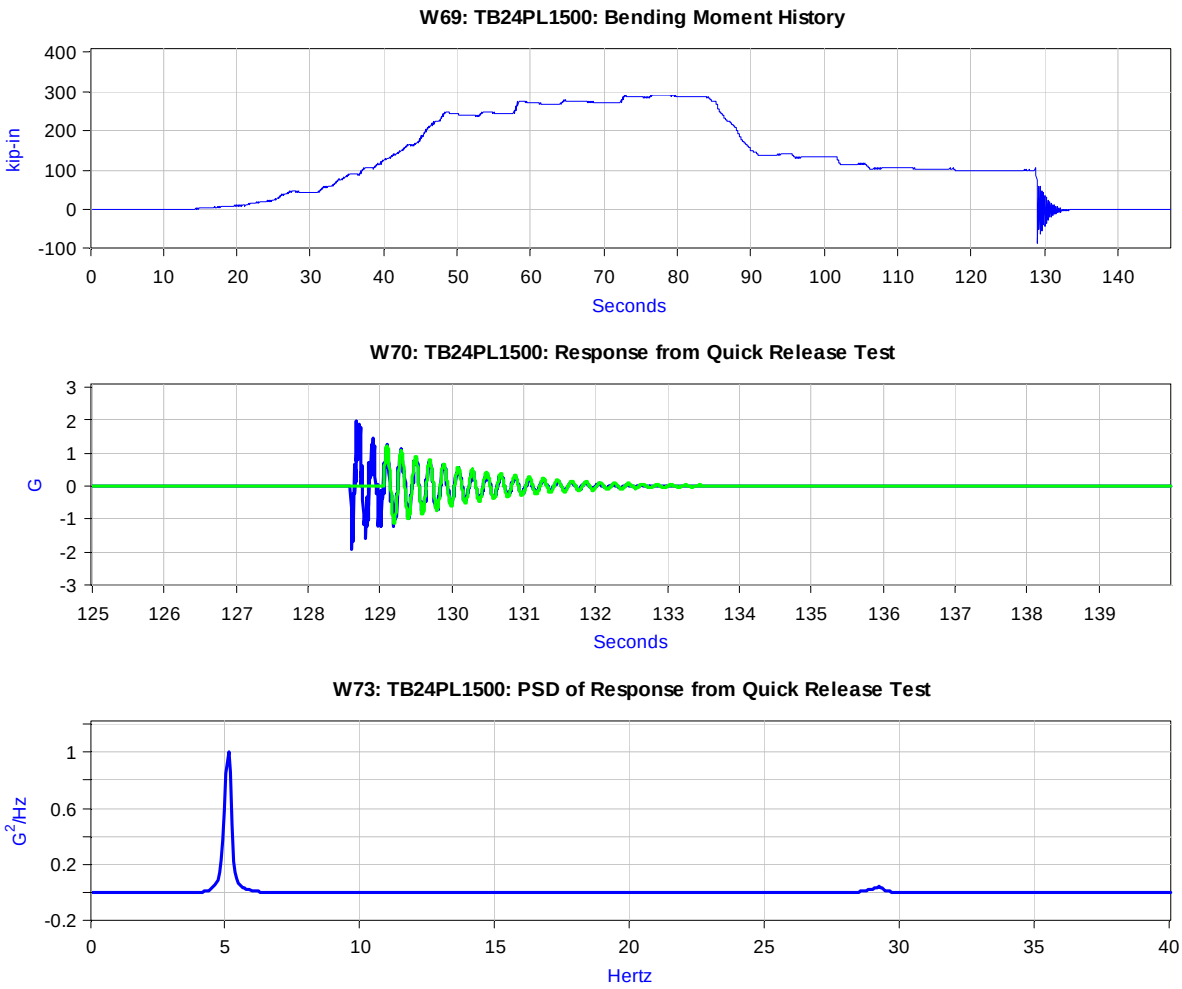

Figure D-93: Acceleration Response from Quick Release Test TB27PL2000 – Bushing #5

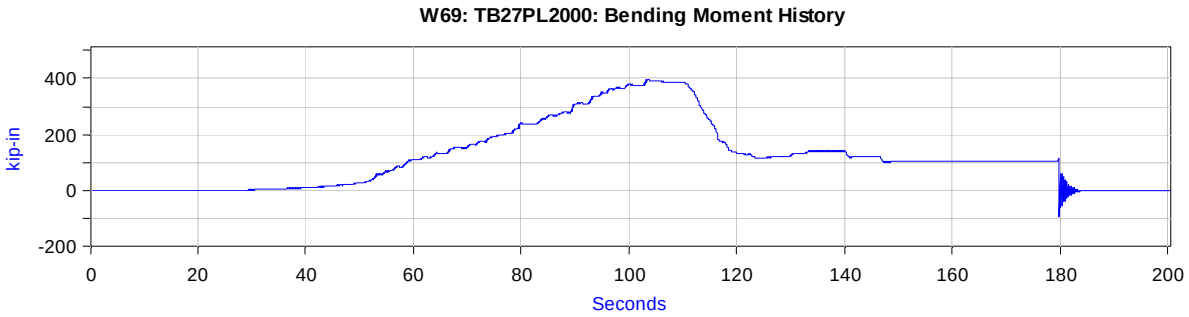

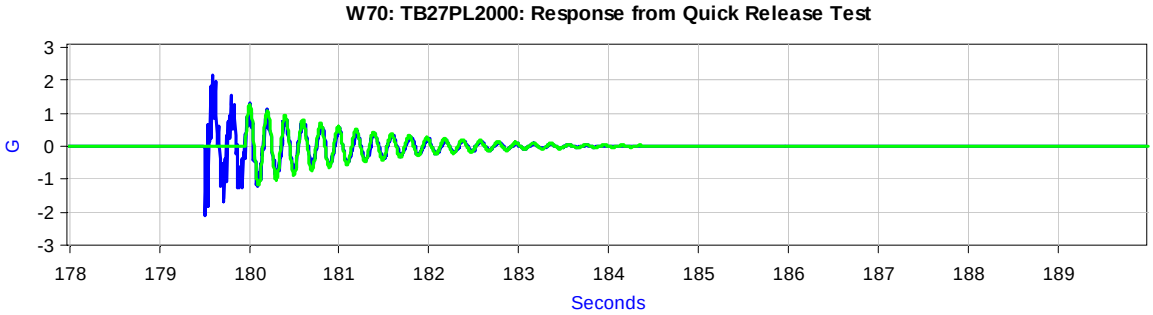

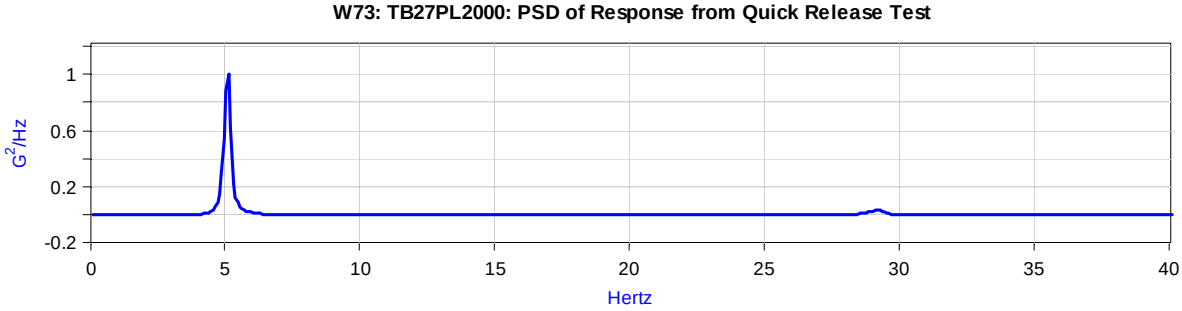

Figure D-94: Acceleration Response from Quick Release Test TB30PL2800 – Bushing #5

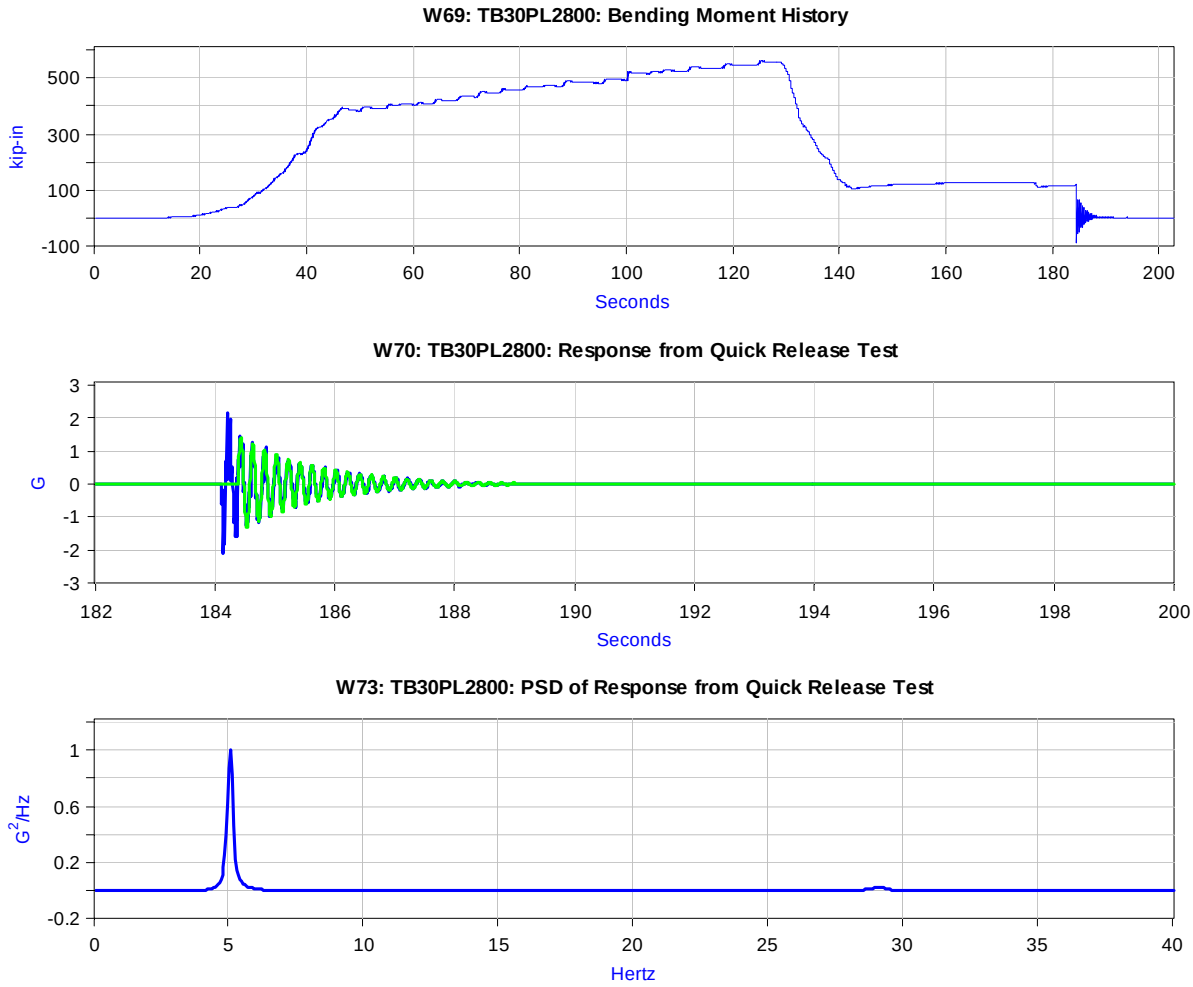

Figure D-95: Maximum Force vs. Maximum Displacement – Bushing #5

White Noise Tests

The frequencies and damping ratio of the bushing were determined by transfer functions obtained from white noise tests using the shake table. The peak of the transfer function is the fundamental frequency of the bushing and a half-power bandwidth method was used to determine the damping ratio. The summary of the frequencies is presented in Table D-5.

The frequencies from white noise tests were then used to develop "impulse tests" for the dominant frequencies of the bushing (see next section). The half-power bandwidth method used to determine damping is less accurate than a quick release, impact hammer or table impulse tests; therefore the ratios are re-determined in the following section using impulse tests. The acceleration transfer functions obtained in these tests are shown in Figures D-96 and D-97.

Figure D-96: Transfer Functions of Bushing #5, in NS Direction

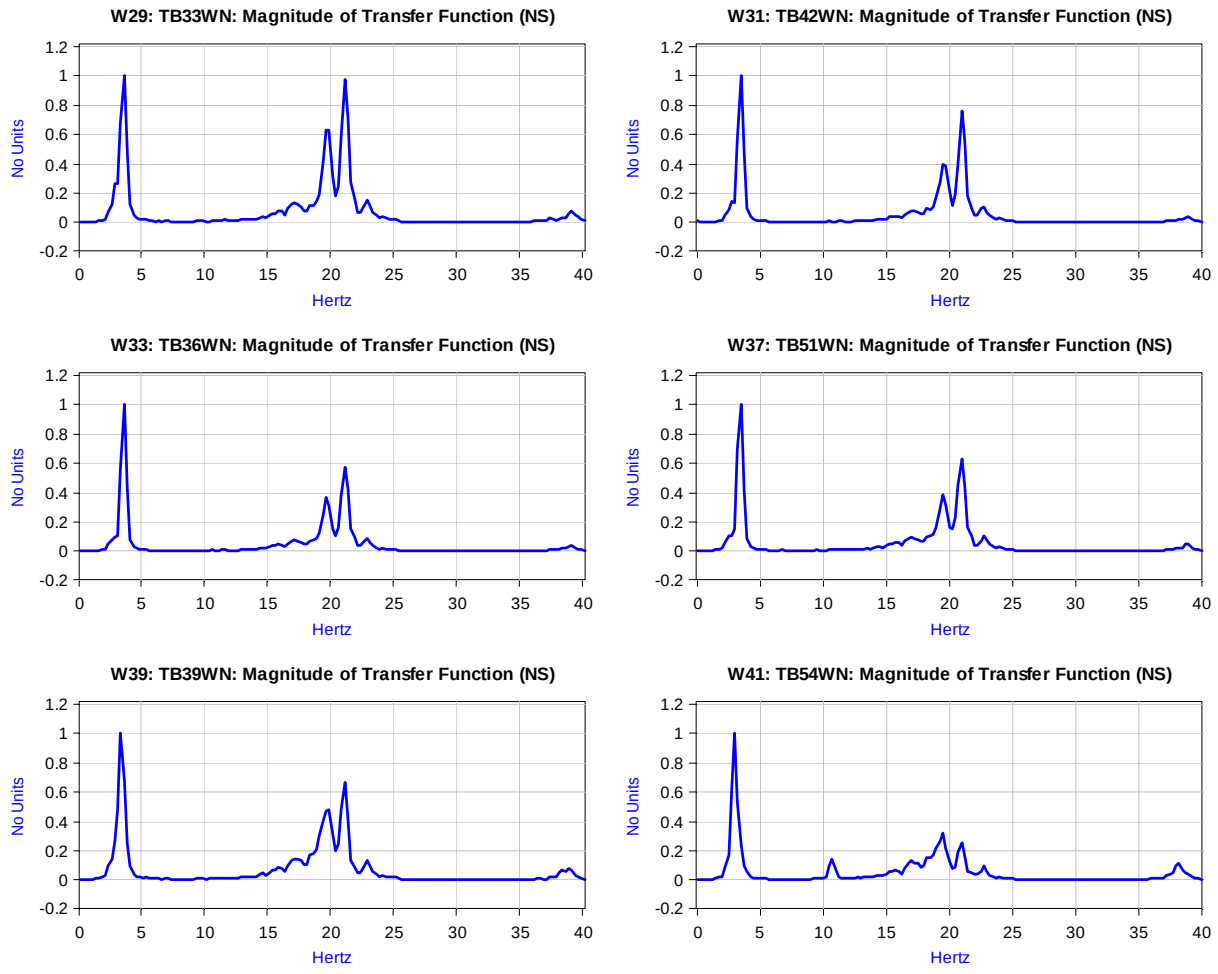

Figure D-97: Transfer Functions of Bushing 5, in EW Direction

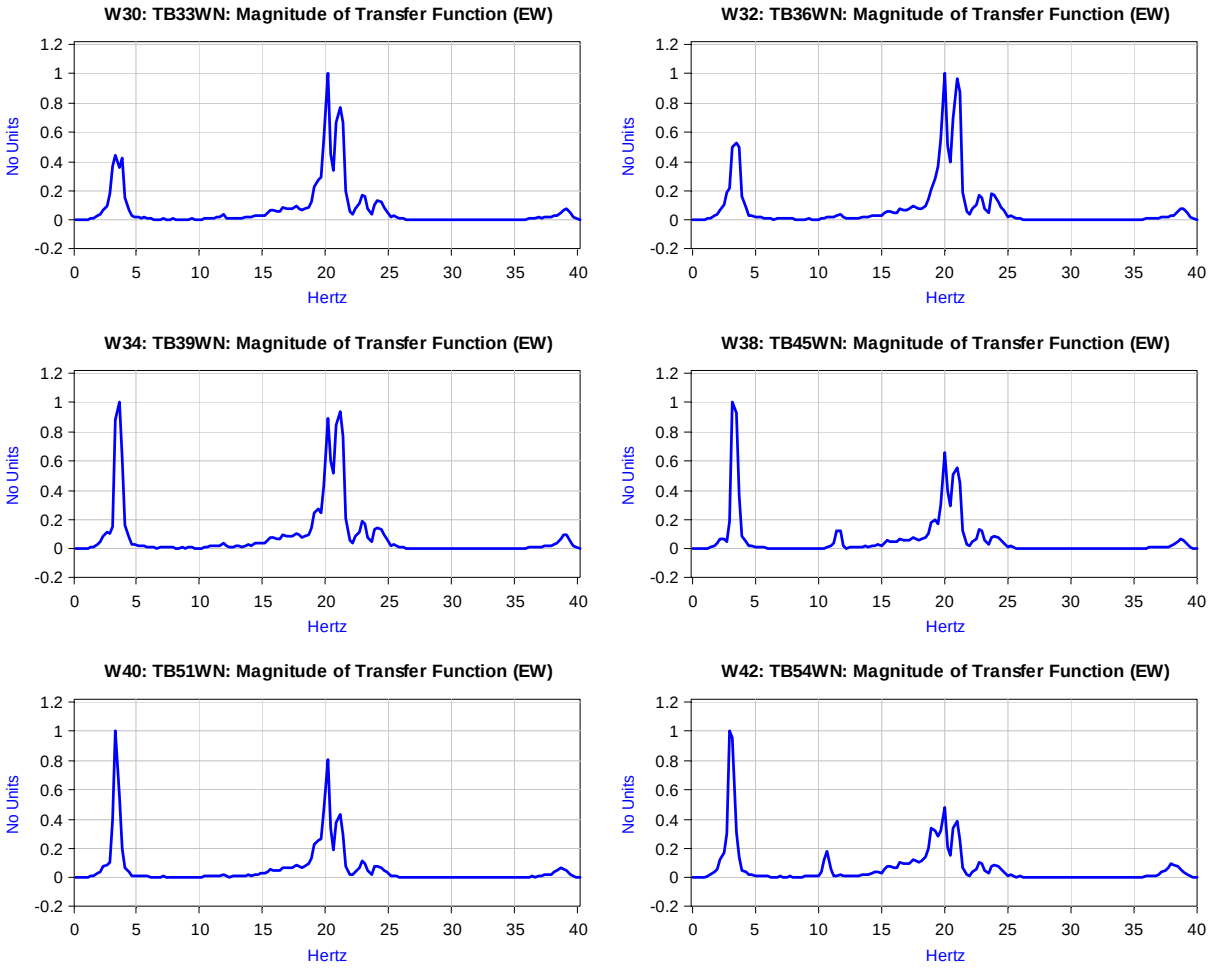

Table Impulse Tests

The table impulse test identifies frequencies and damping of dominant frequencies using smoothed table acceleration impulse for control of a shake table by using a smoothing table impulse procedure developed by the SEESL at University at Buffalo (Kong, 2010). For the identification of system frequencies, a power spectral density (PSD) was calculated from output motion at the top of the bushing and the system frequency is obtained by finding the frequency where the peak is located. For the identification of modal damping, a curve fitting method developed by the authors was used (Kong, 2010).

The acceleration history results of the table impulse tests are presented in Figure D-98, and the dynamic characteristics are summarized in Table D-5. The frequencies of Bushing #5 in the NS direction are around 3.32 Hz in test TB34TBI (before random motion tests), and 3.10 Hz in test TB55TBI; the damping values of the bushing are 8.45% and 3.22% respectively. The frequency of Bushing #5 in the EW Direction is 3.00 Hz in test TB34TBI (before random motion tests), and 3.10 Hz in test TB55TBI; the damping values of the bushing are 2.08% and 2.94%, respectively.

Figure D-98: Table Impulse Test Response (Tests TB34TBI to TB55TBI)

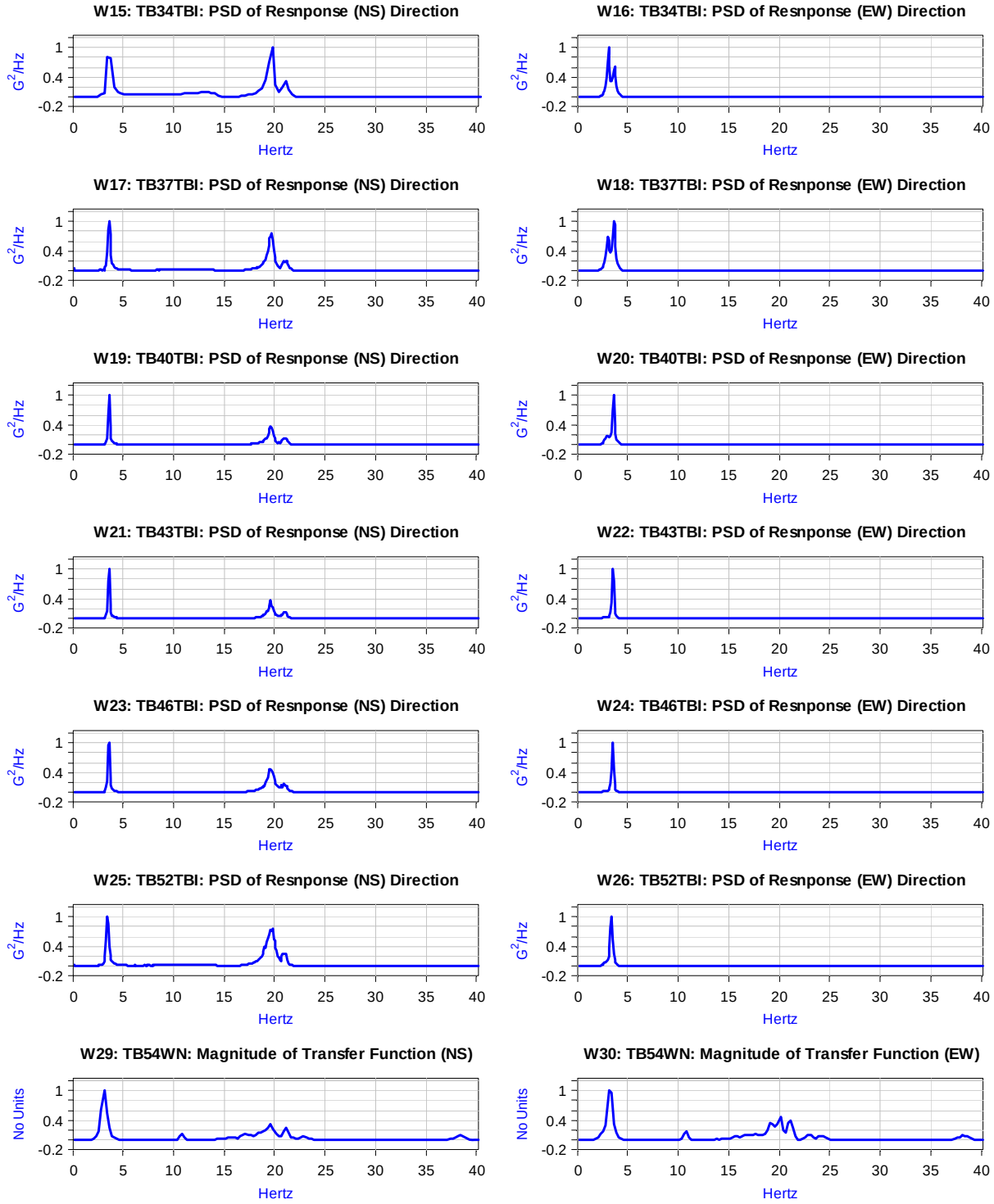

Acceleration History Tests

Acceleration history tests were performed to determine the seismic demand quantification of Bushing #5. A summary of the accelerations and bending moments recorded on various locations on the bushing are shown in Table D-7 for the six levels of test input motions. The average value of stiffness of Bushing #5 is 686 lb./in.

The acceleration history tests were used to measure the bending moment of the bushing at flange level. Strain gauges were used to measure the bending moments. A summary of bending moments is presented in Table D-6. The bending moment history is shown in Figures D-99 through D-103.

Table D-6: Acceleration Distribution and Bending Moments of Bushing #5 for Various Tests

Location	Units	0.25 g RRS			0.50 g RRS			1.00 g RRS			2.00 g RRS			2.50 g RRS			3.00 g RRS		
		TB35AH25			TB38AH50			TB41AH100			TB44AH150			TB47AH225			TB53AH300		
(1)	(2)	(3)	(4)	(5)	(6)	(7)	(8)	(9)	(10)	(11)	(12)	(13)	(14)	(15)	(16)	(17)	(18)	(19)	(20)
Bushing Location on Frame		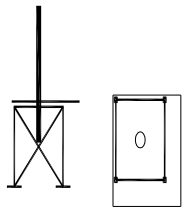			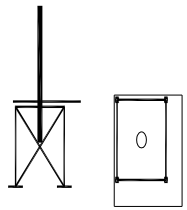			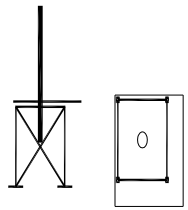			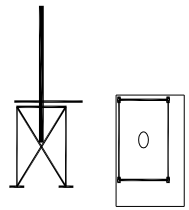			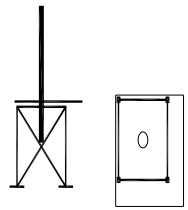			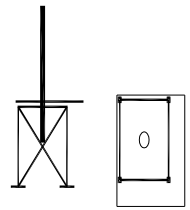		
Acceleration Distribution along the Height of Testing Setup																			
Direction		NS	EW	Vertical	NS	EW	Vertical	NS	EW	Vertical	NS	EW	Vertical	NS	EW	Vertical	NS	EW	Vertical
Top of Bushing	(g)	0.93	0.98	0.55	1.19	1.50	0.82	4.25	5.70	3.08	7.05	9.97	4.08	11.92	14.84	6.43	13.46	13.13	7.04
Upper CG Of Bushing	(g)	0.12	0.18	-	0.32	0.33	-	0.64	0.68	-	1.43	0.34	-	-	2.91	-	-	3.82	-
CG OF Bushing	(g)	0.04	0.09	-	0.22	0.15	-	0.18	0.76	-	1.09	0.54	-	4.64	2.31	-	5.70	2.55	-
On Frame	(g)	0.02	0.02	0.23	0.24	0.02	0.31	1.47	0.13	0.90	3.69	0.37	1.60	7.16	0.16	1.97	7.38	0.01	2.41
Shake Table	(g)	0.02	0.04	0.21	0.01	0.03	0.31	0.15	0.11	0.87	0.14	0.33	1.63	2.27	0.32	2.14	2.76	0.15	2.51
Bending Moment at the Base of Bushing																			
Moment from Strain Gauges	kip-in	36.76	68.26	-	51.13	107.50	-	194.61	353.45	-	369.99	604.03	-	677.86	1010.59	-	879.25	1036.89	

Figure D-99: Bending Moment of Bushing #5 in Horizontal Direction – Test TB35ah025

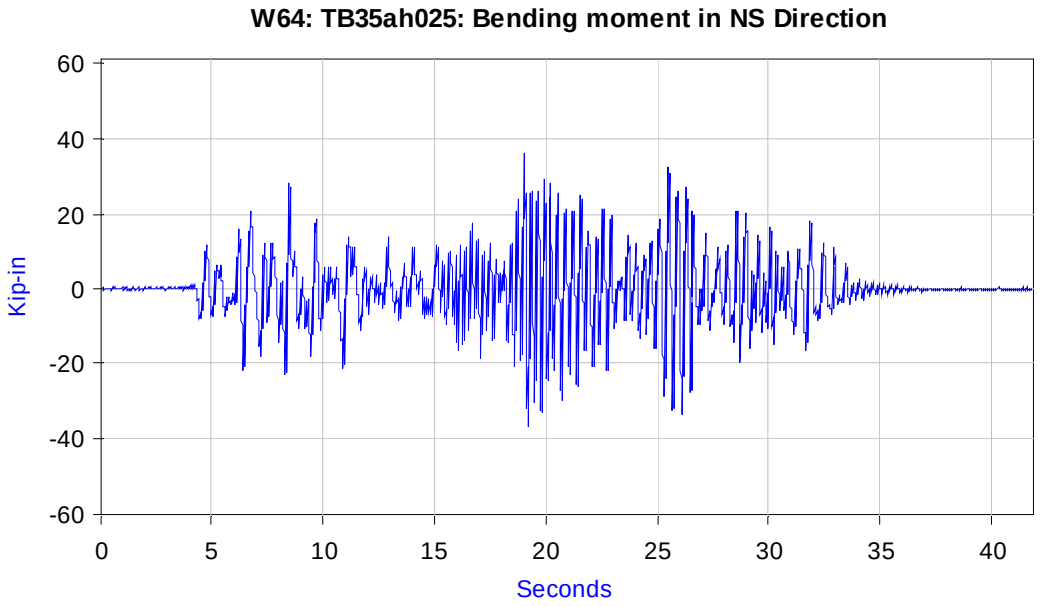

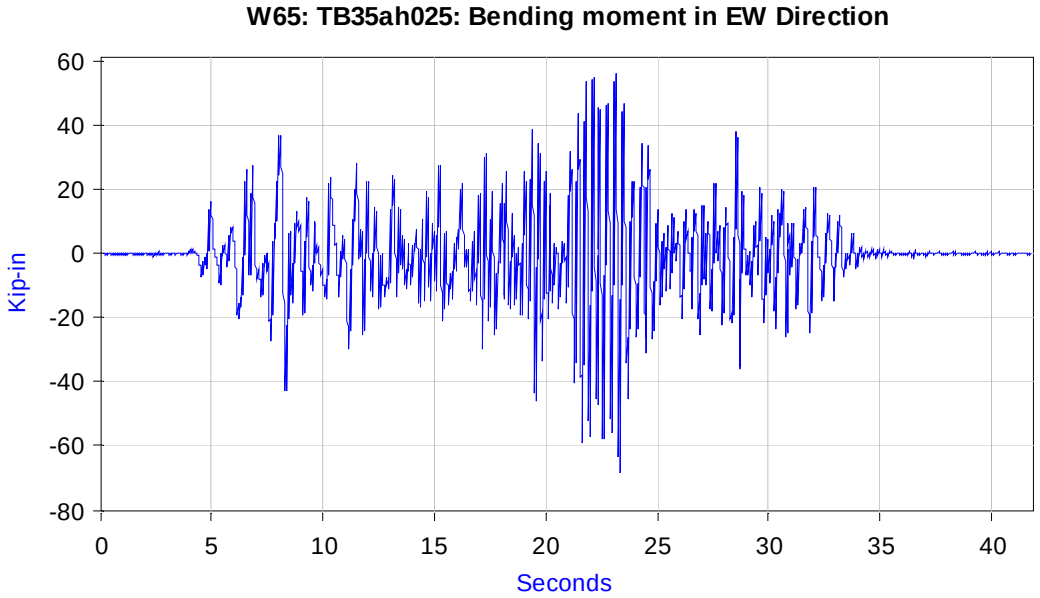

Figure D-100: Bending Moment of Bushing #5 in Horizontal Direction – Test TB38ah050

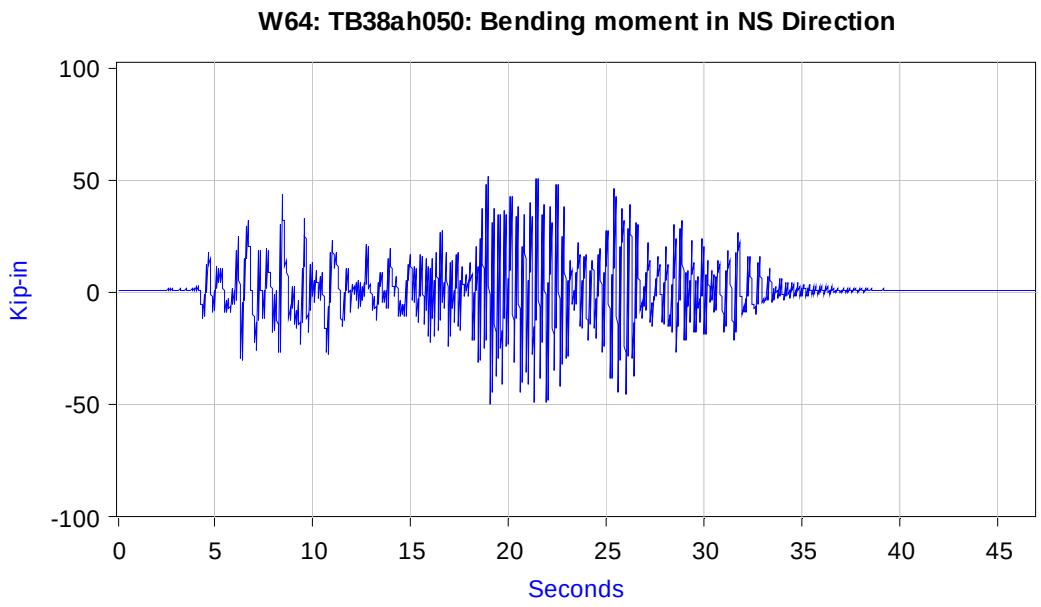

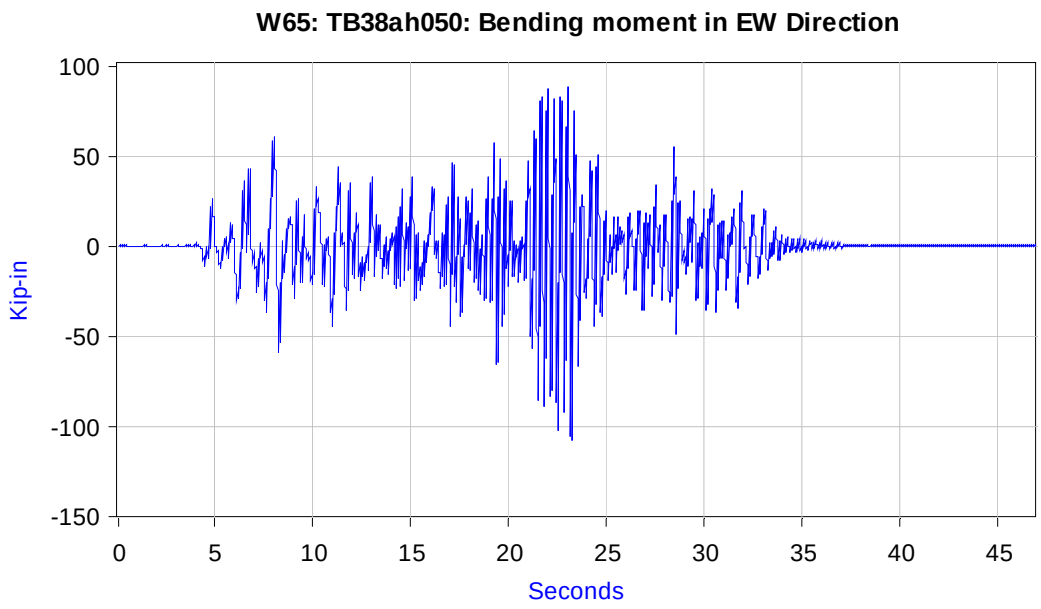

Figure D-101: Bending Moment of Bushing #5 in Horizontal Direction – Test TB41ah100

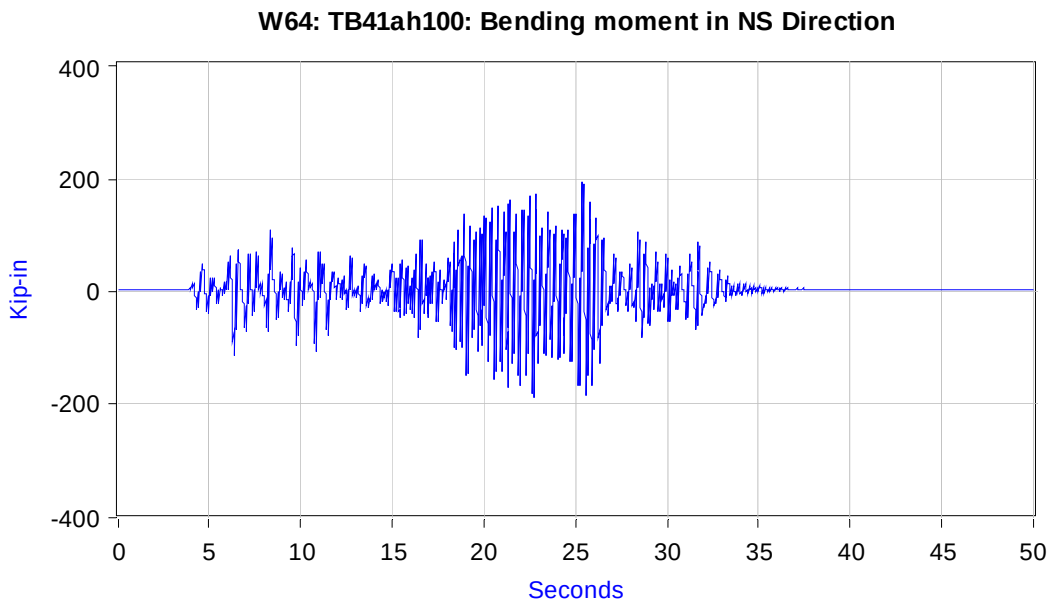

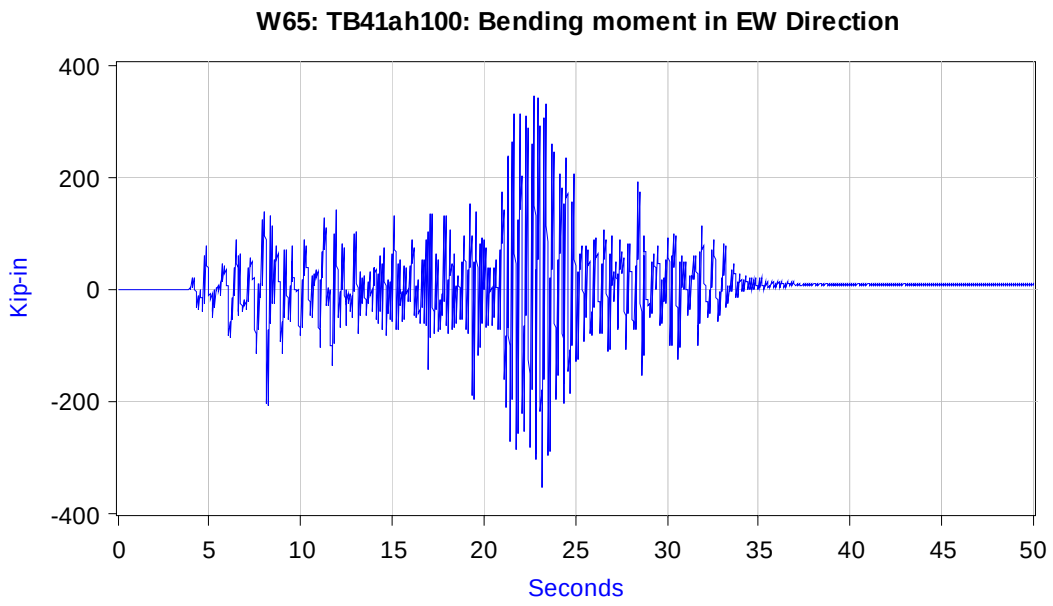

Figure D-102: Bending Moment of Bushing #5 in Horizontal Direction – Test TB44ah200

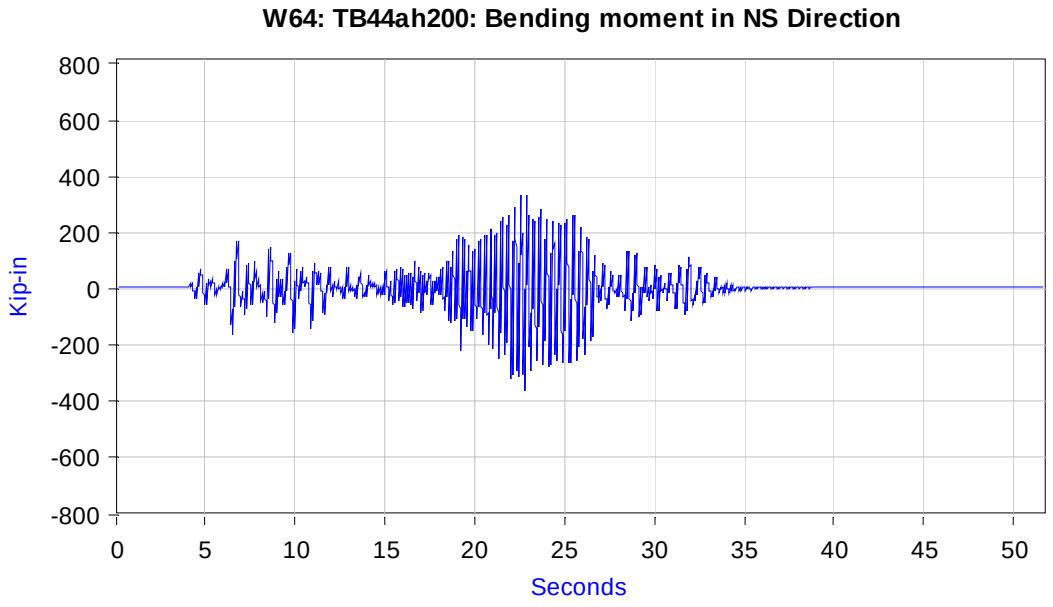

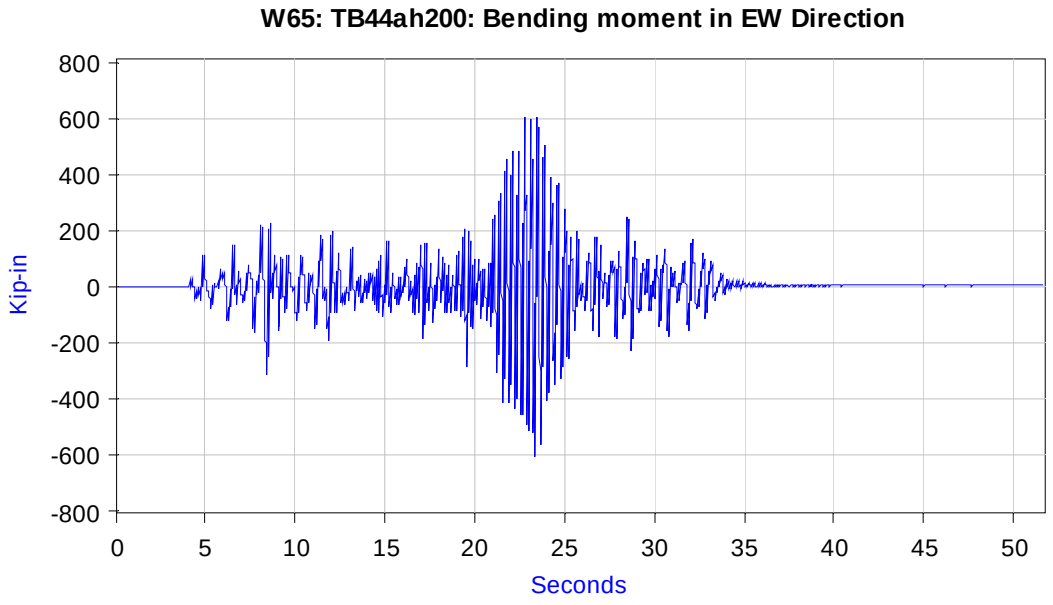

Figure D-103: Bending Moment of Bushing #5 in Horizontal Direction – Test TB53ah300

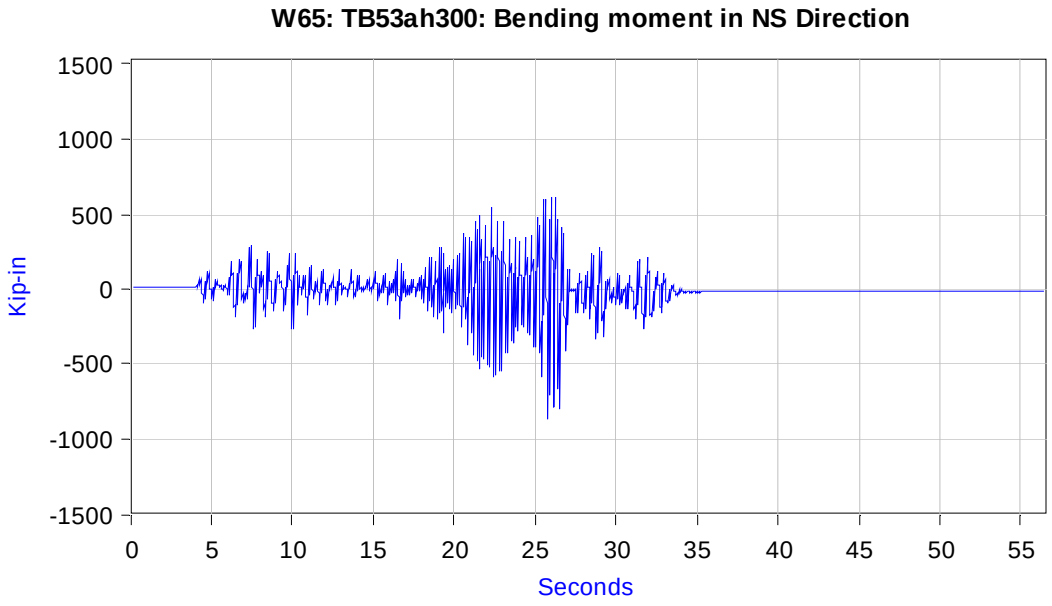

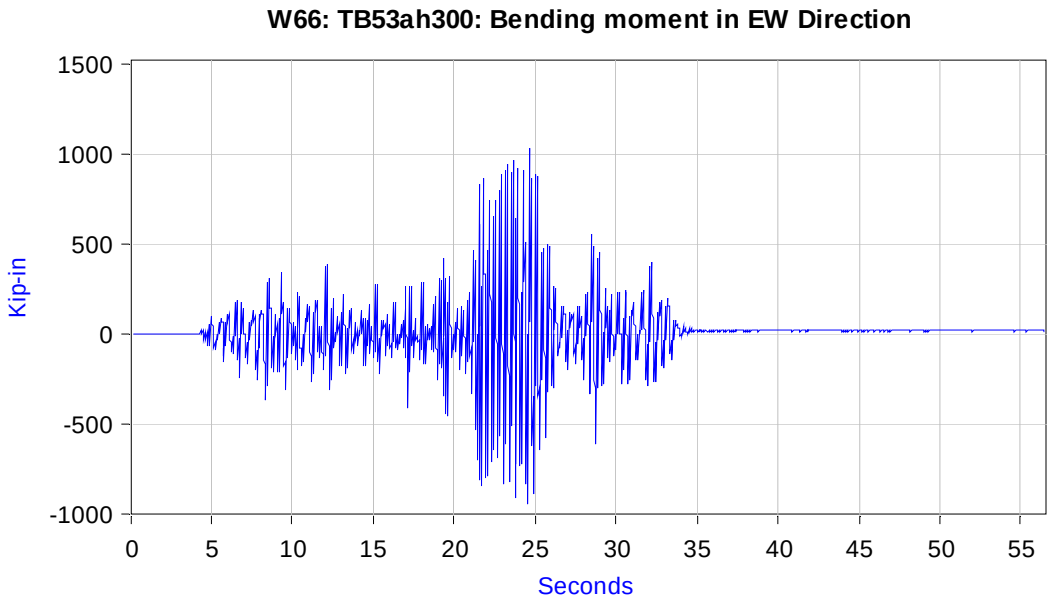

Identification of Properties of Bushing #6

Identification of Dynamic Properties with Additional Conductor Weight

Impact Hammer Testing

Impact hammer tests were used to find the frequency and damping ratio of Bushing #6. A 15 lb. weight was attached at the top of bushing, simulating a portion of cable near the bushing top that might play a role in the bushing response. Minimum frequency was observed in the NS direction of 23.63 Hz with damping ratio of 1.38%; in the EW direction the frequency was 25.94 Hz and damping ratio of 1.44%. Table D-7 shows the frequencies, damping ratios and the direction in which tests were run. The Power Spectral Density (PSD) of the free vibration response gave the frequency of the bushing and the logarithmic decrement method was used to find the damping ratio. Figures D-104 through D-110 show the results of the tests.

Table D-7: Dynamic Properties of Bushing #6 from Various Tests

Test No.	Frequency			Damping			Max Displacement	Force	Stiffness
Units	(Hz)			(%)			(in)	(lb)	(lb/in)
(1)	(2)	(3)	(4)	(5)	(6)	(7)	(8)	(9)	(10)
Direction	NS	EW	Vertical	NS	EW	Vertical			
Impact Hammer Test –Fixed base									
TB09NSIH	23.63	-	-	1.38	-	-	-	-	-
TB09NSIHB	23.75	-	-	1.01	-	-	-	-	-
TB10EWIH	-	25.94	-	-	1.44	-	-	-	-
TB10EWIHB	-	25.95	-	-	1.53	-	-	-	-
TB13NSIH	23.97	-	-	0.69	-	-	-	-	-
TB14EWIH	-	25.97	-	-	0.72	-	-	-	-
White Noise Test									
TB19WN	11.13	11.38	-	1.79	1.57	-	-	-	-
TB22WN	11.00	11.13	-	2.25	1.60	-	-	-	-
TB25WN	11.00	11.50	-	1.86	1.58	-	-	-	-
TB28WN	11.00	11.50	-	2.88	2.09	-	-	-	-
TB31WN	11.00	11.25	-	2.30	2.38	-	-	-	-
TB34WN	11.00	11.25	-	2.12	2.69	-	-	-	-
TB36WN	11.00	11.50	-	2.47	1.71	-	-	-	-
TB39WN	11.00	11.25	-	2.36	2.59	-	-	-	-
TB42WN	10.75	11.38	-	2.74	2.20	-	-	-	-
TB45WN	3.50	3.38	-	5.44	1.88	-	-	-	-
TB48WN	11.00	11.13	-	1.82	2.21	-	-	-	-
TB51WN	3.25	3.00	-	7.28	5.97	-	-	-	-
TB54WN	11.00	11.25	-	2.56	3.20	-	-	-	-
TB57WN	11.00	11.13	-	2.91	2.65	-	-	-	-
TB60WN	11.00	11.25	-	2.42	2.86	-	-	-	-
TB63WN	11.00	11.25	-	1.95	2.90	-	-	-	-
TB66WN	11.00	11.25	-	2.19	3.36	-	-	-	-
TB69WN	11.00	11.13	-	2.86	1.07	-	-	-	-
TB72WN	11.00	11.13	-	4.87	1.99	-	-	-	-
Table Impulse Test									
TB20TBI	11.00	11.20	-	1.05	0.75	-	-	-	-
TB23TBI	11.00	11.20	-	1.05	0.75	-	-	-	-
TB26TBI	10.85	11.19	-	1.15	0.88	-	-	-	-
tb29tbi	10.99	11.10	-	1.00	1.60	-	-	-	-
TB32TBI	10.88	11.19	-	1.36	1.28	-	-	-	-
TB35TBI	10.90	11.19	-	0.84	0.84	-	-	-	-
TB37TBI	10.90	11.24	-	0.84	0.80	-	-	-	-
TB40TBI	10.94	11.10	-	1.15	0.86	-	-	-	-
TB43TBI	10.90	11.19	-	1.15	0.65	-	-	-	-
TB46TBI	10.85	11.15	-	1.29	0.95	-	-	-	-
TB49TBI	10.90	11.15	-	0.96	0.95	-	-	-	-
TB52TBI	3.28	3.22	-	3.41	3.31	-	-	-	-
TB55TBI	10.92	11.10	-	0.58	0.92	-	-	-	-
TB58TBI	10.90	11.10	-	0.95	0.92	-	-	-	-
TB61TBI	10.99	11.10	-	0.95	0.92	-	-	-	-
TB64TBI	10.90	11.10	-	0.90	0.92	-	-	-	-
TB67TBI	10.87	11.08	-	1.00	0.66	-	-	-	-
TB70TBI	10.87	11.10	-	1.00	0.93	-	-	-	-
TB73TBI	10.87	11.05	-	1.18	0.75	-	-	-	-

Figure D-104: Acceleration Response of Bushing 6 in NS Direction

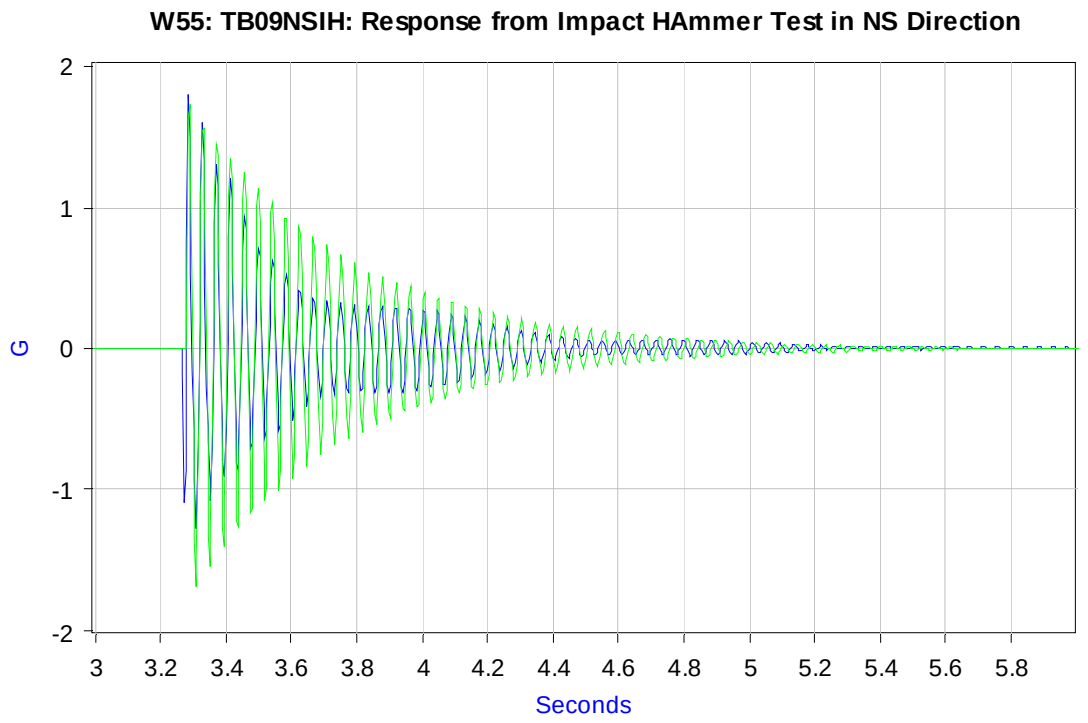

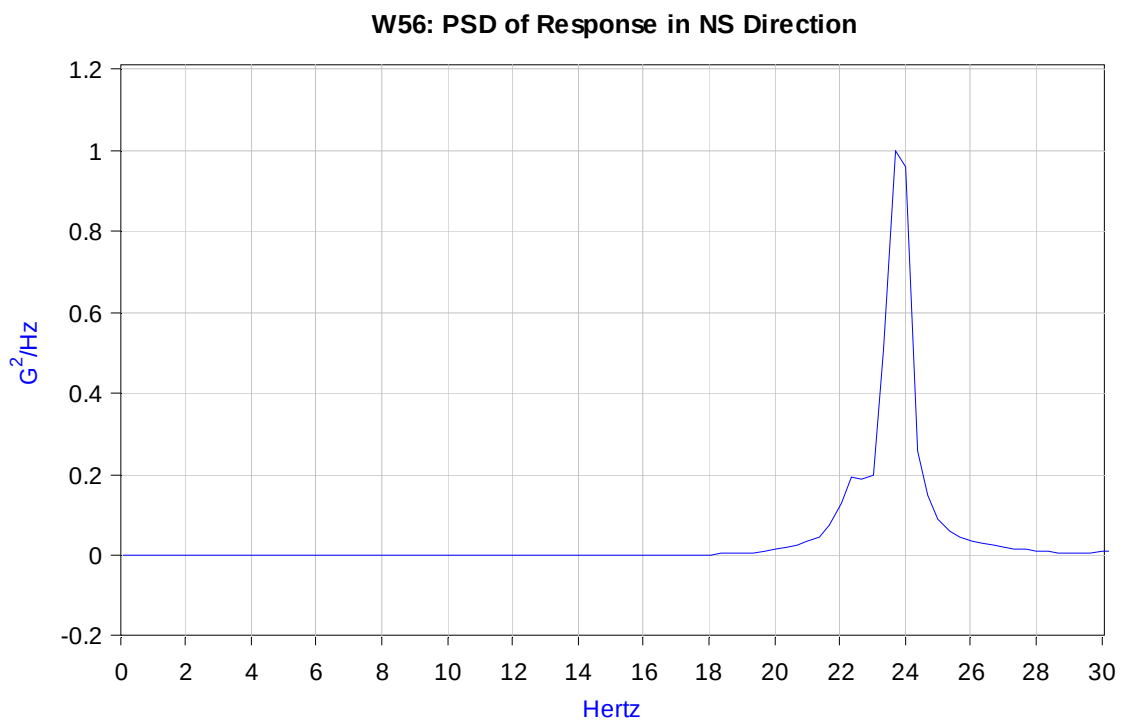

Figure D-105: Acceleration Response of Bushing 6 in NS Direction

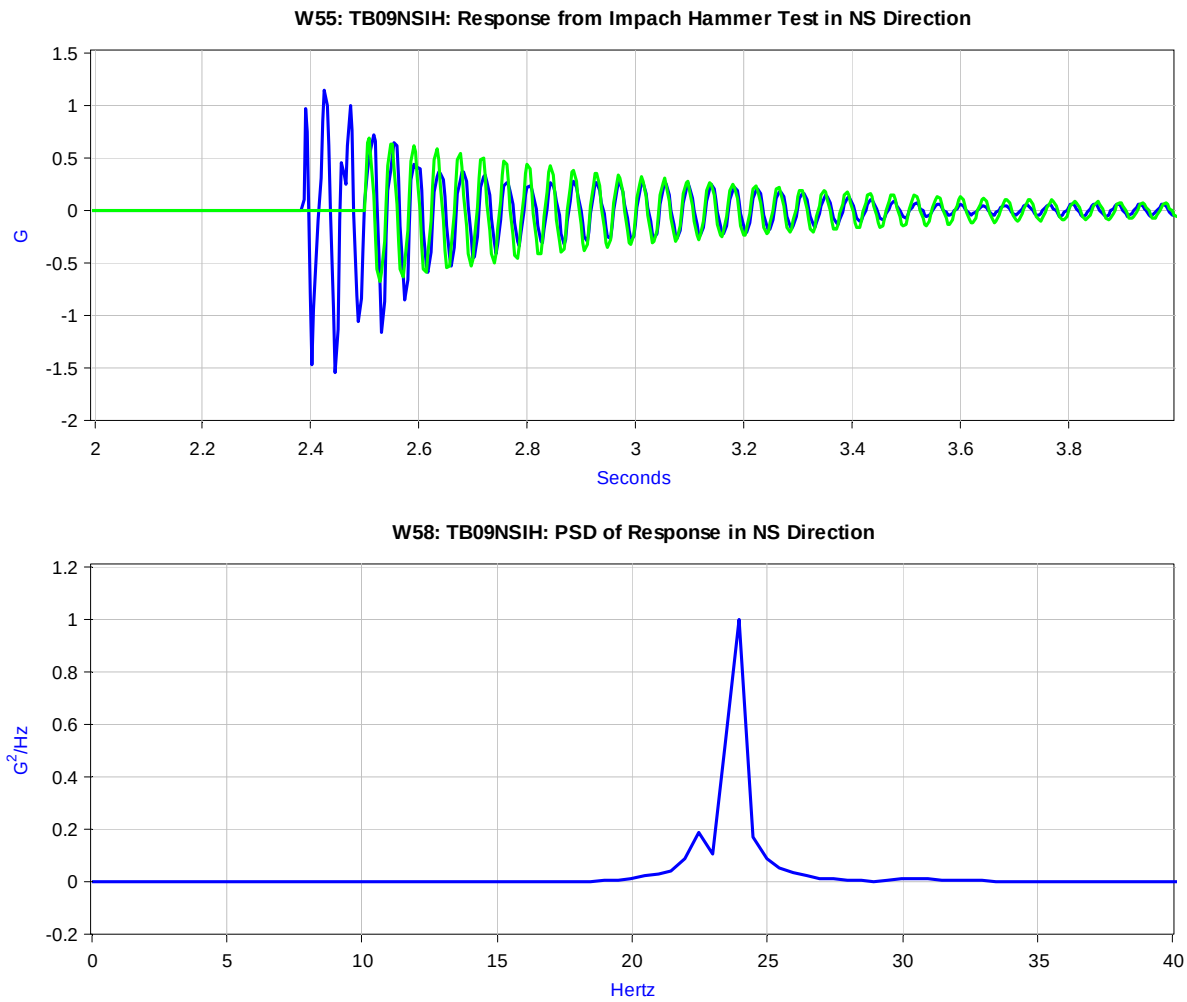

Figure D-106: Acceleration Response of Bushing 6 in EW Direction

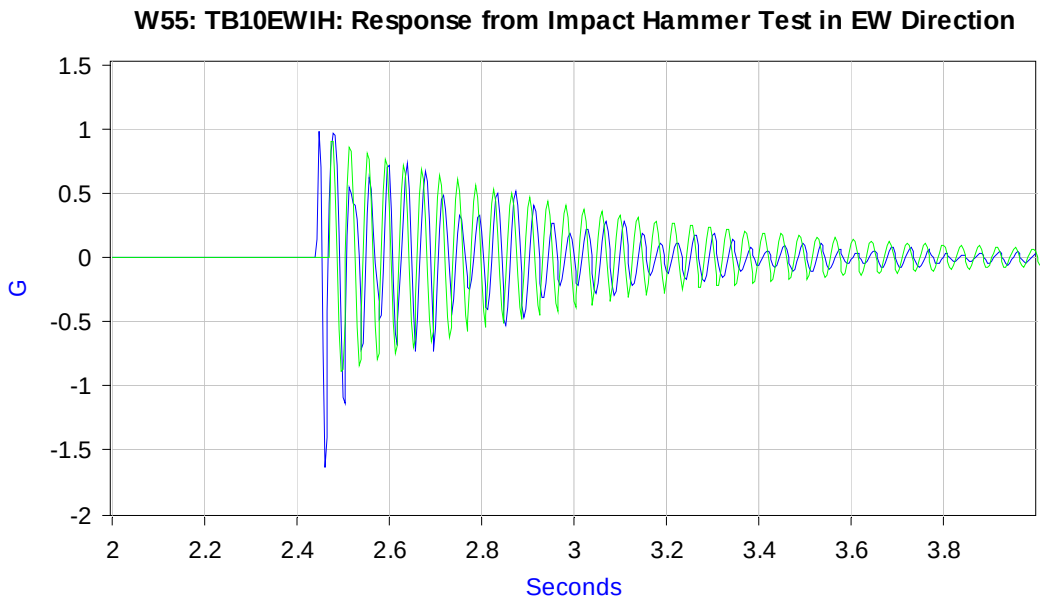

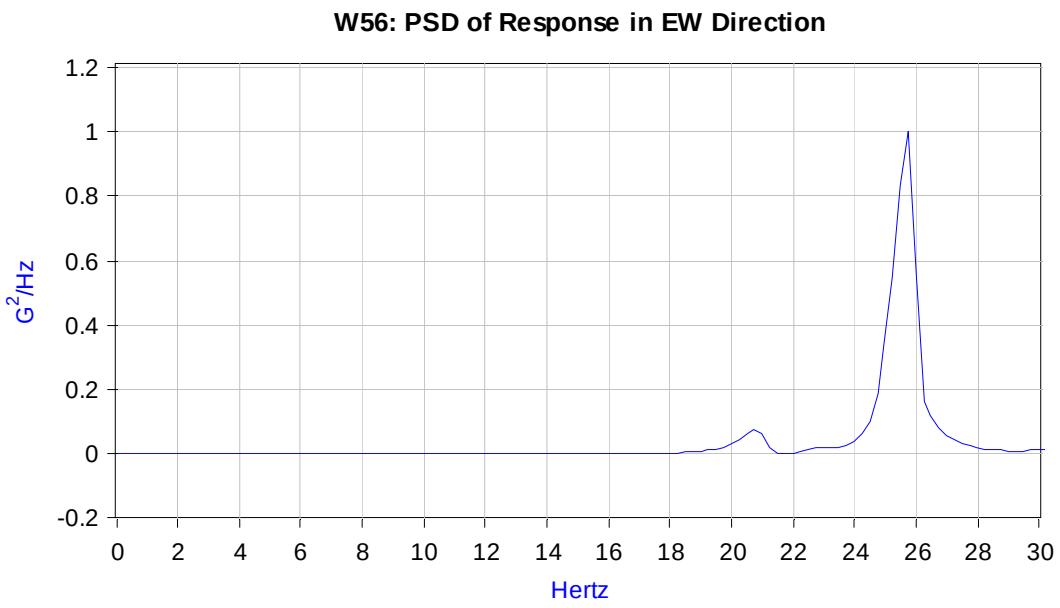

Figure D-107: Acceleration Response of Bushing 6 in EW Direction

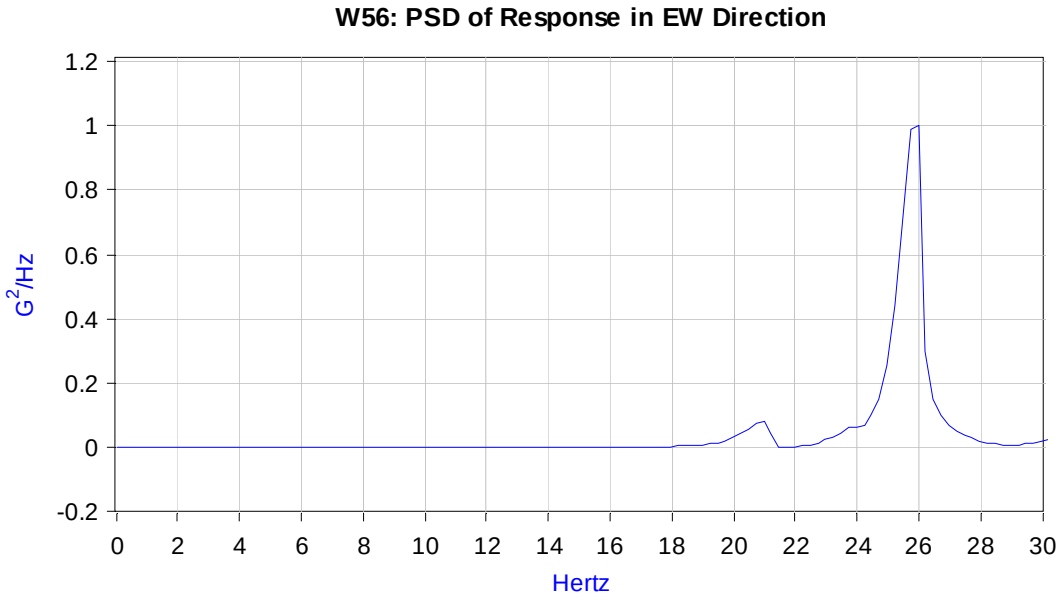

Figure D-108: Acceleration Response of Bushing 6 in EW Direction

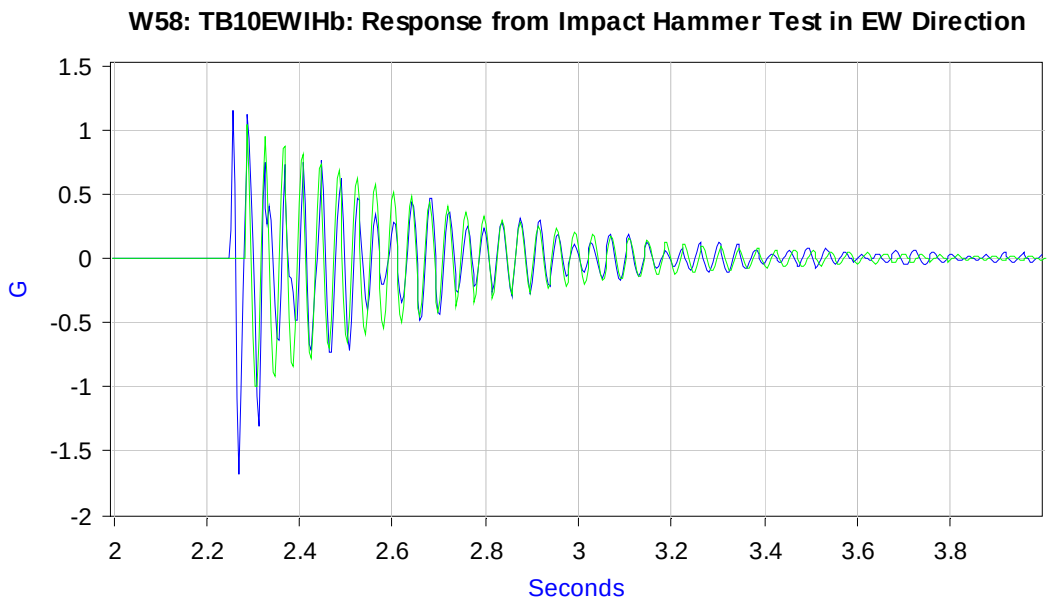

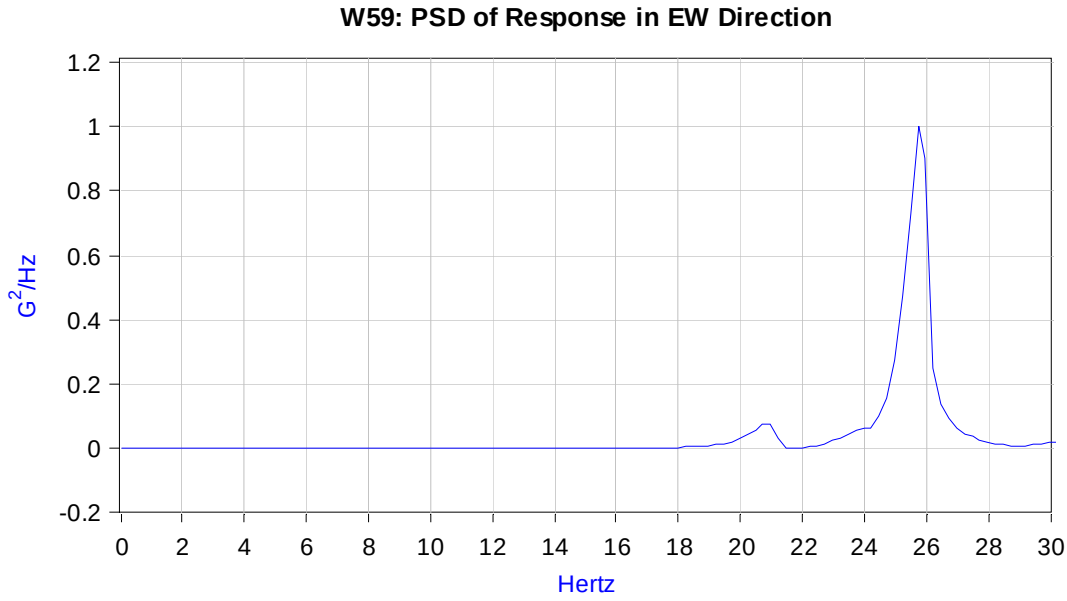

Figure D-109: Acceleration Response of Bushing 6 in EW Direction

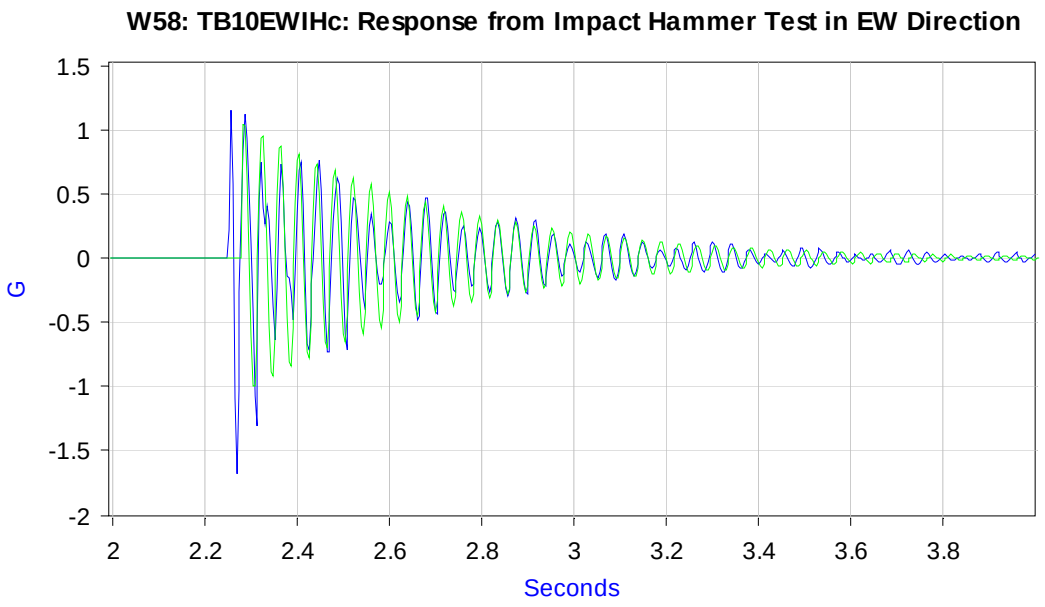

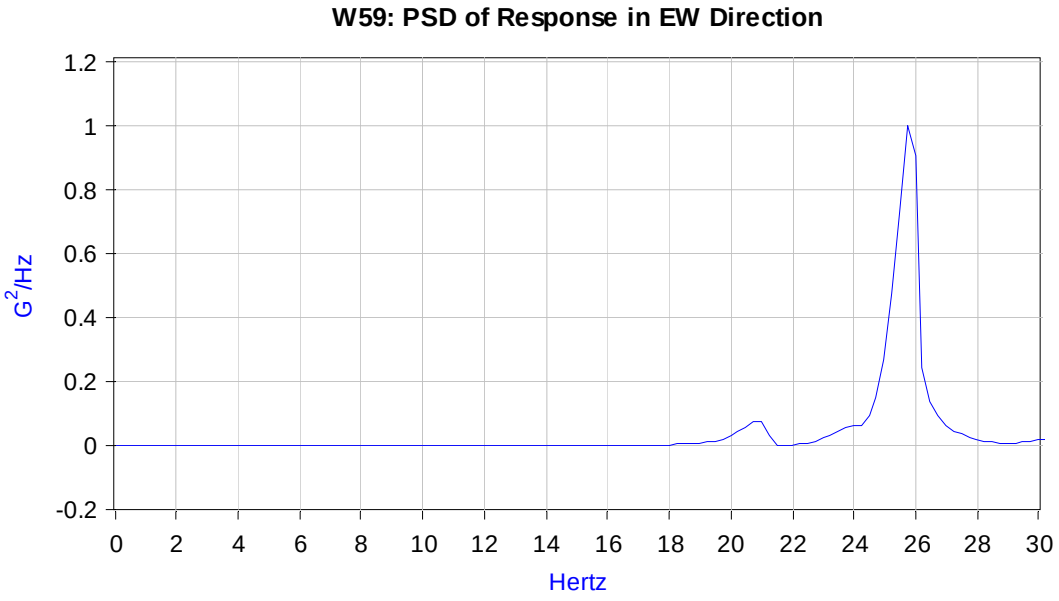

Figure D-110: Acceleration Response of Bushing 6 in EW Direction

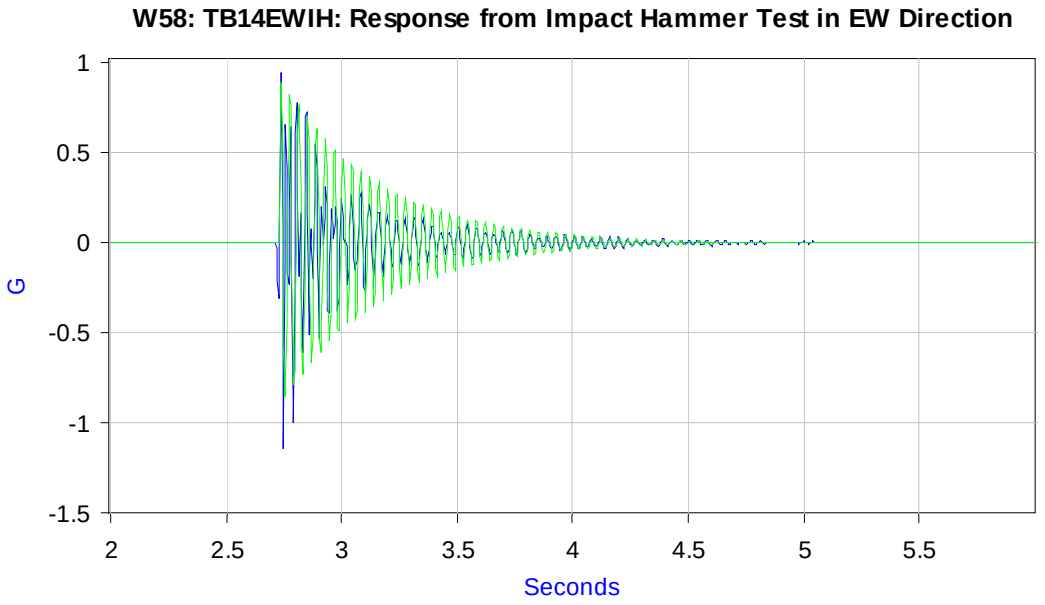

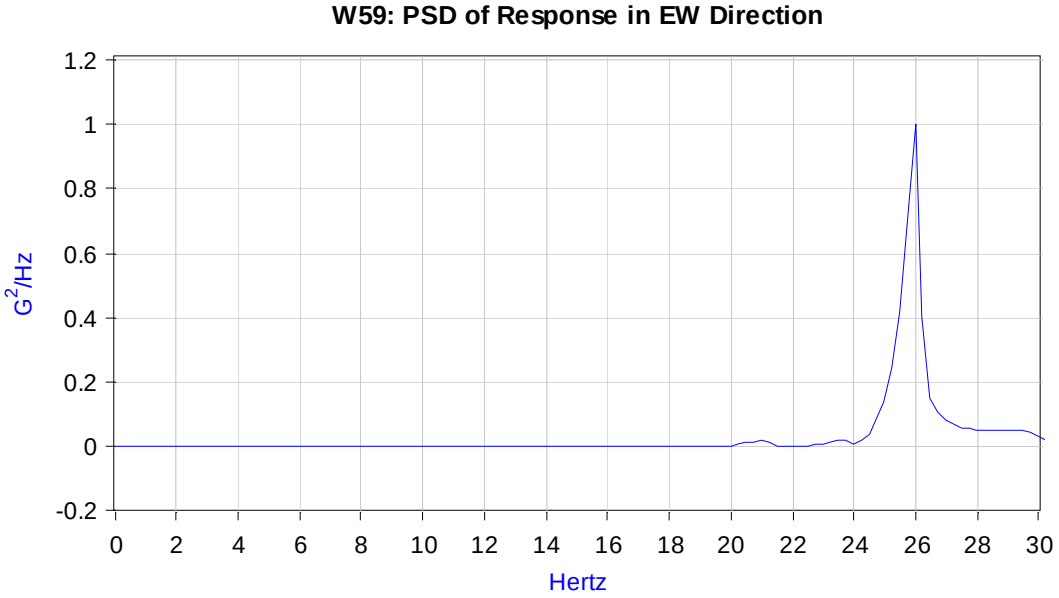

White Noise Tests

The frequencies and damping ratio of the bushing were determined by transfer functions obtained from white noise tests using the shake table. The peak of the transfer function is the fundamental frequency of the bushing and a half-power bandwidth method was used to determine the damping ratio. The summary of the frequencies is presented in Table D-7.

The frequencies from white noise tests were then used to develop "impulse tests" for the dominant frequencies of the bushing (see next section). The half-power bandwidth method used to determine damping is less accurate than a quick release, impact hammer or table impulse tests; therefore the ratios are re-determined in the following section using impulse tests. The acceleration transfer functions obtained in these tests are shown in Figures D-111 through D-129.

Figure D-111: Transfer Functions of Bushing #6, Test TB19WN

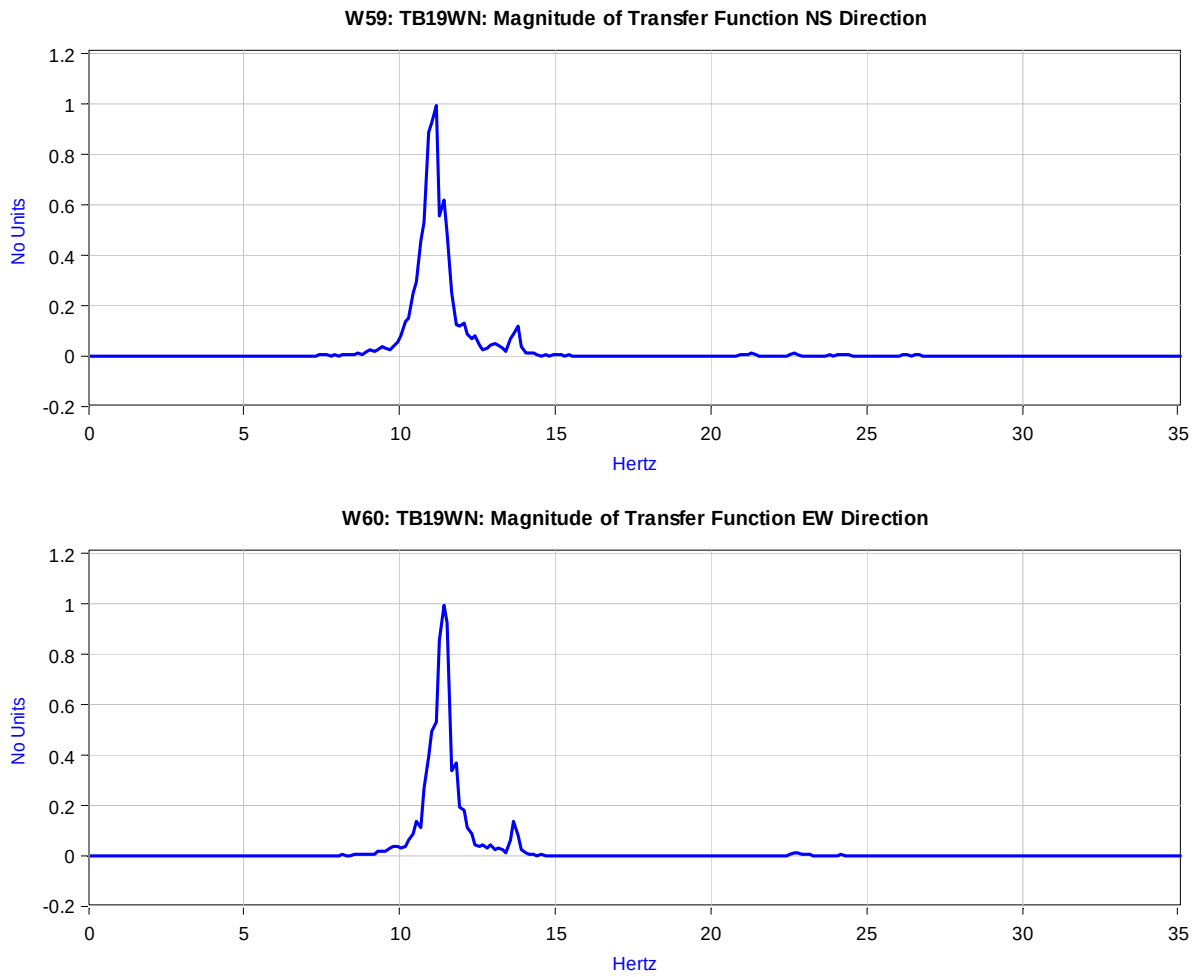

Figure D-112: Transfer Functions of Bushing #6, Test TB22WN

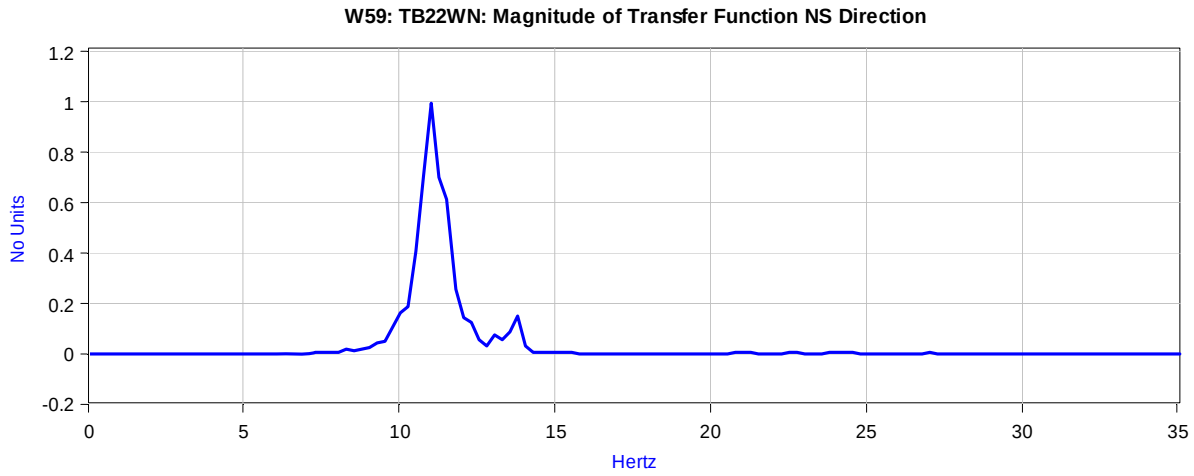

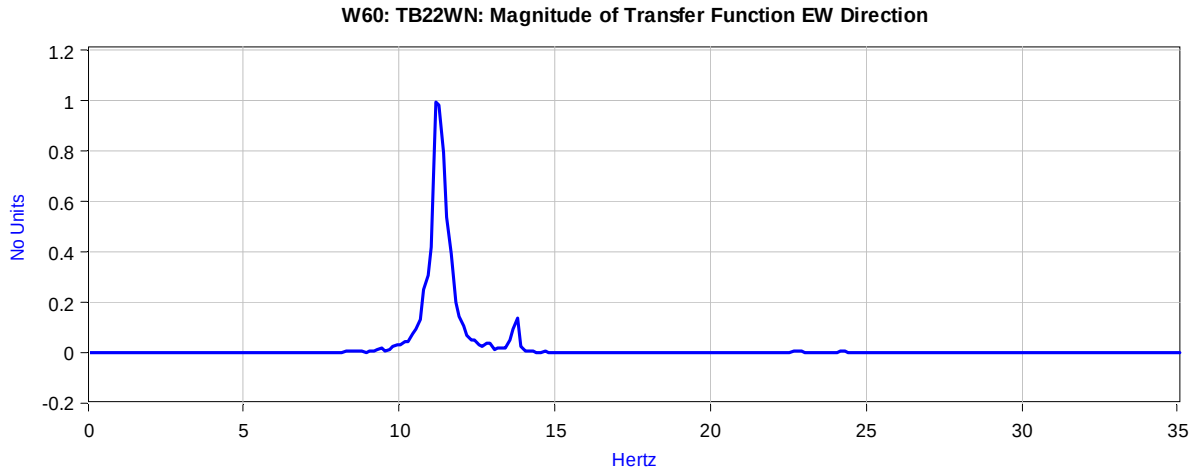

Figure D-113: Transfer Functions of Bushing #6, Test TB25WN

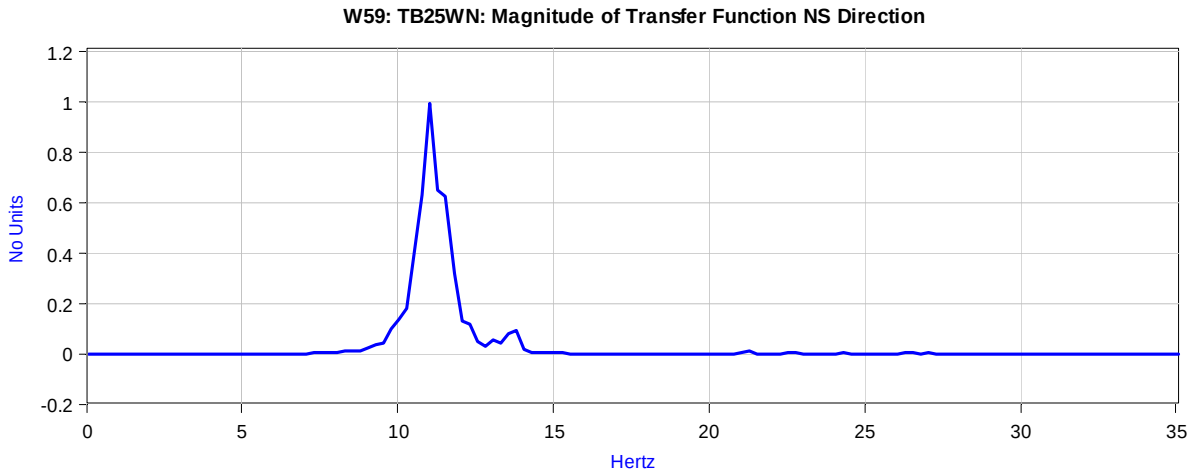

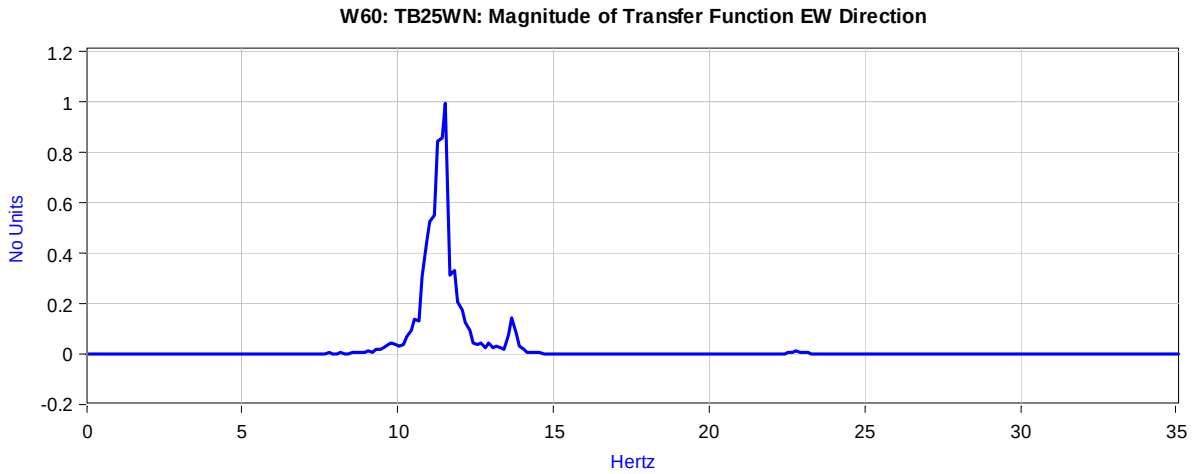

Figure D-114: Transfer Functions of Bushing #6, Test TB28WN

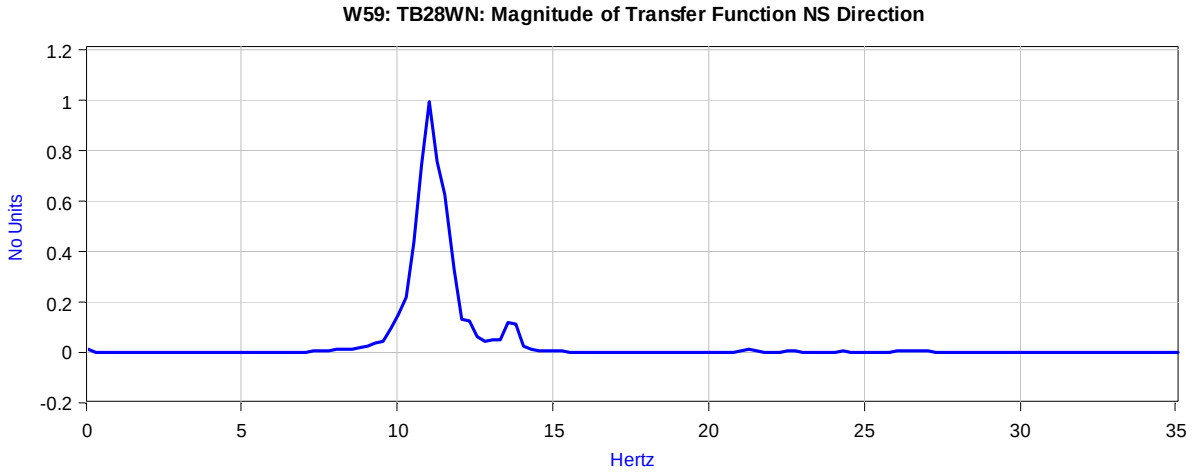

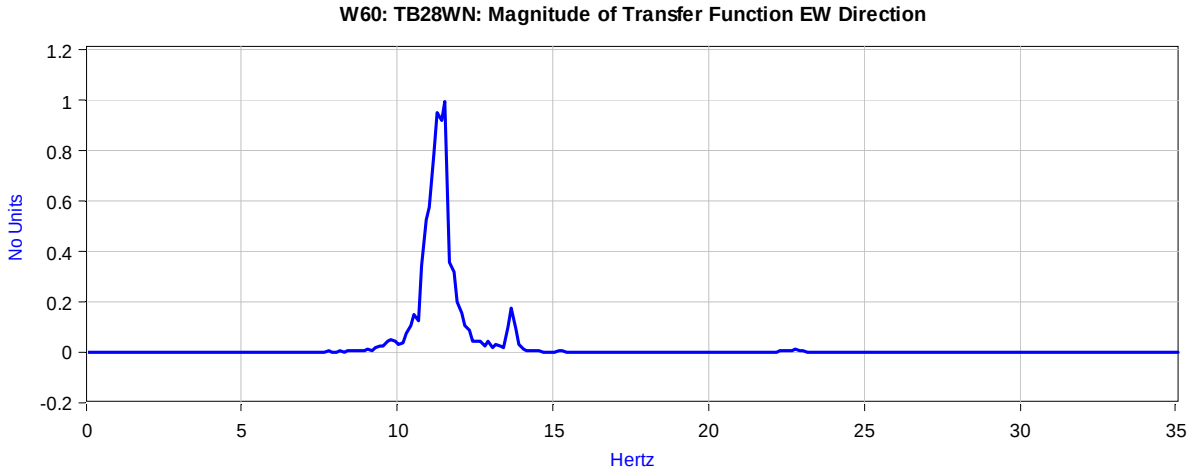

Figure D-115: Transfer Functions of Bushing #6, Test TB28WN

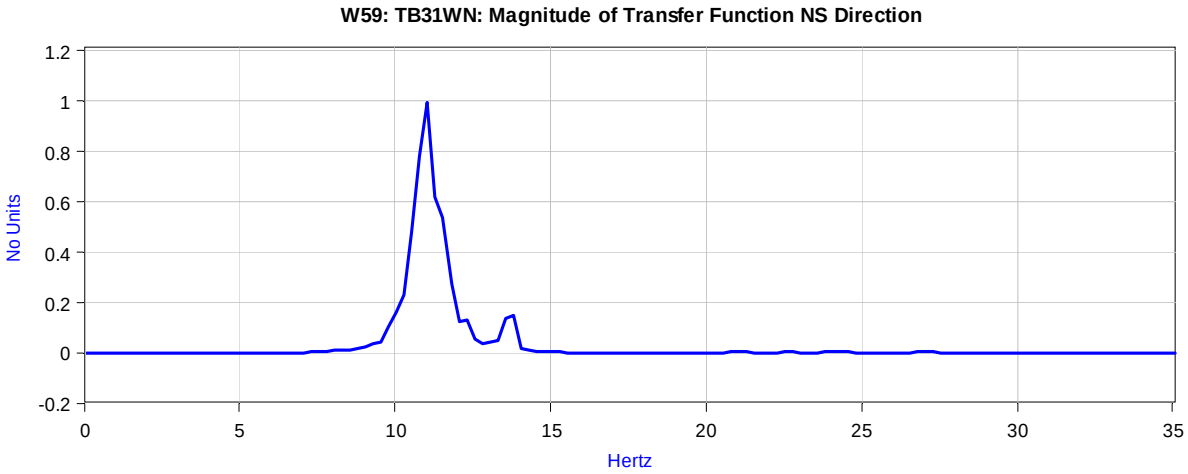

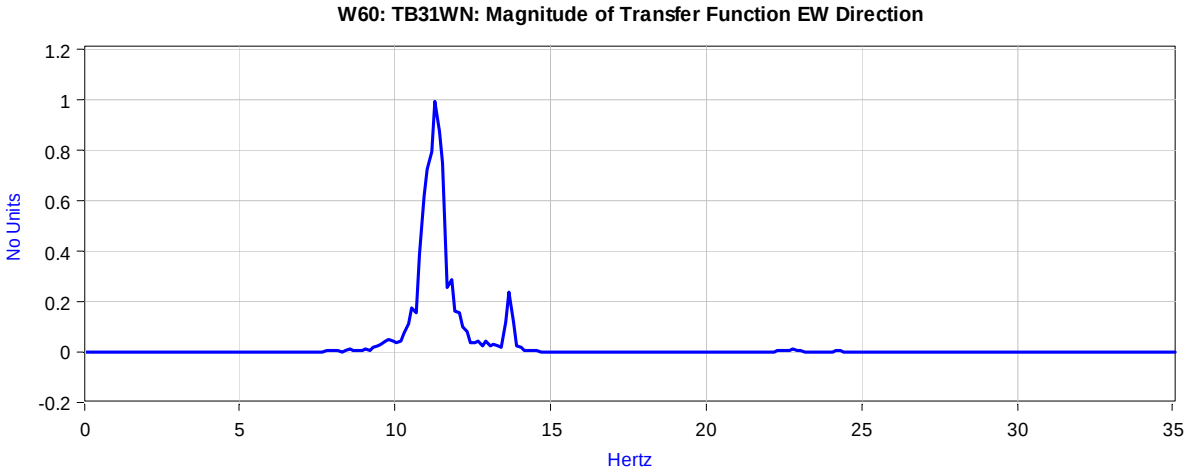

Figure D-116: Transfer Functions of Bushing #6, Test TB34WN

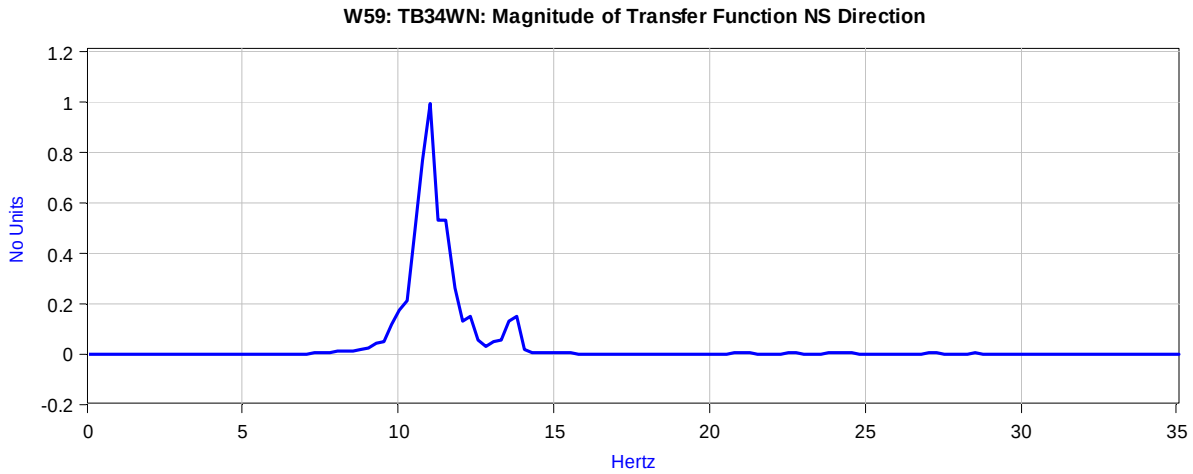

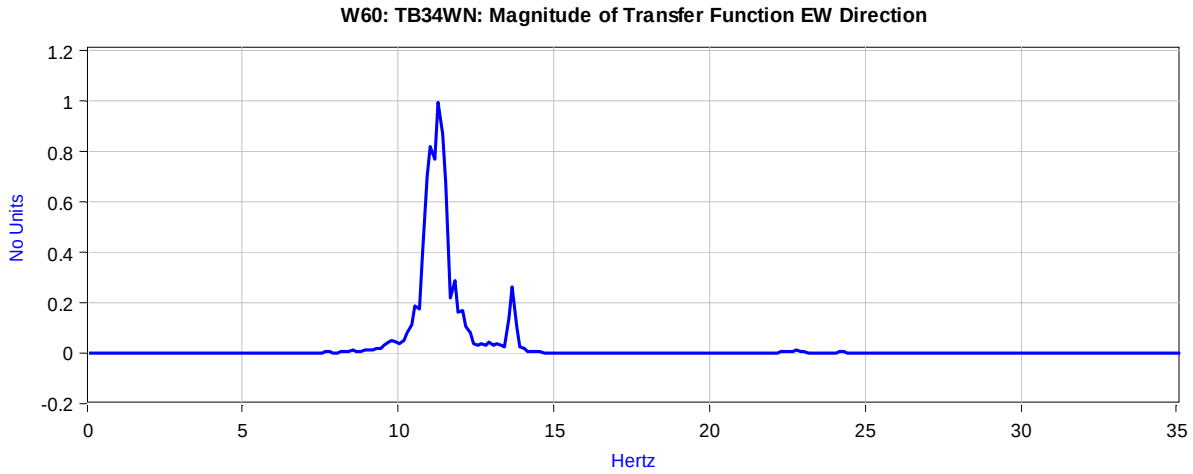

Figure D-117: Transfer Functions of Bushing #6, Test TB36WN

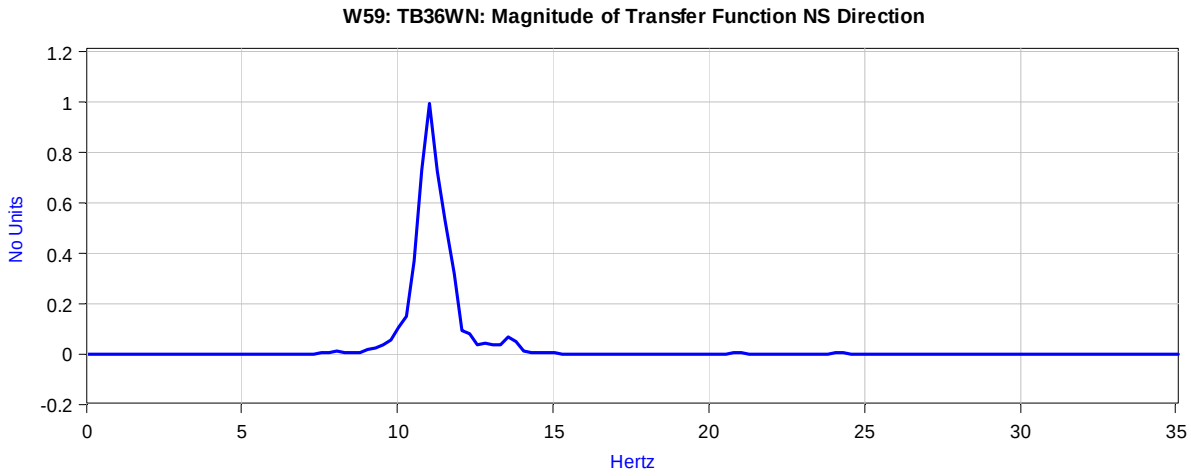

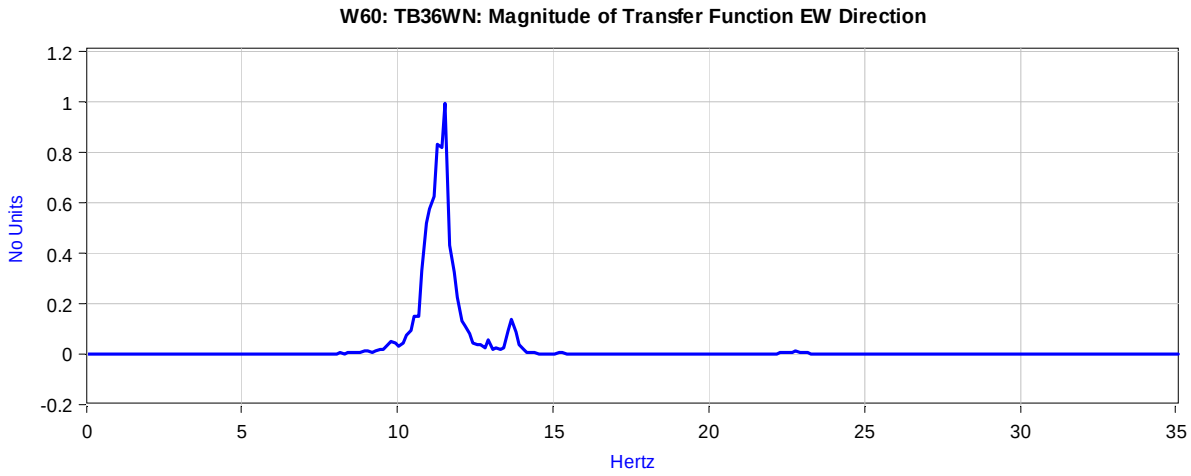

Figure D-118: Transfer Functions of Bushing #6, Test TB39WN

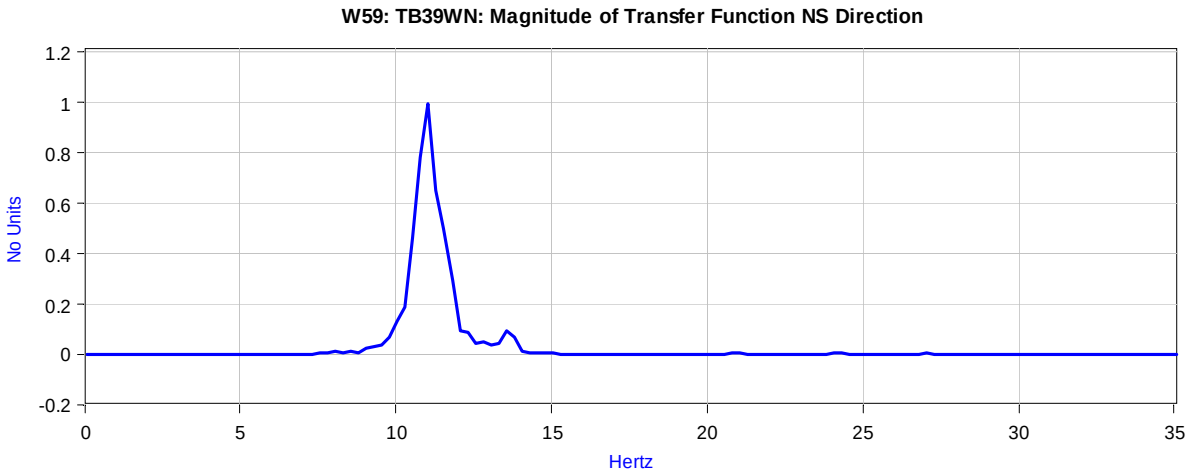

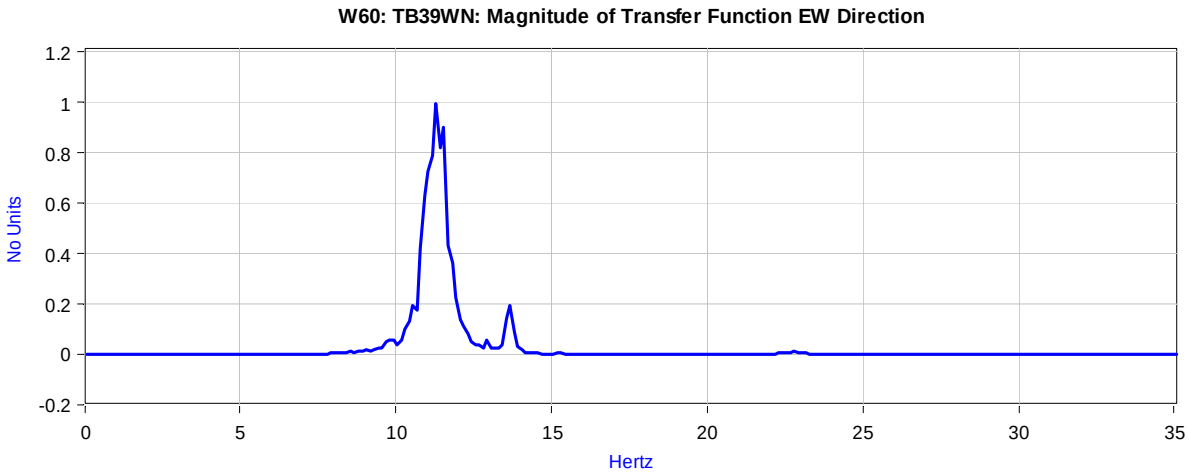

Figure D-119: Transfer Functions of Bushing #6, Test TB42WN

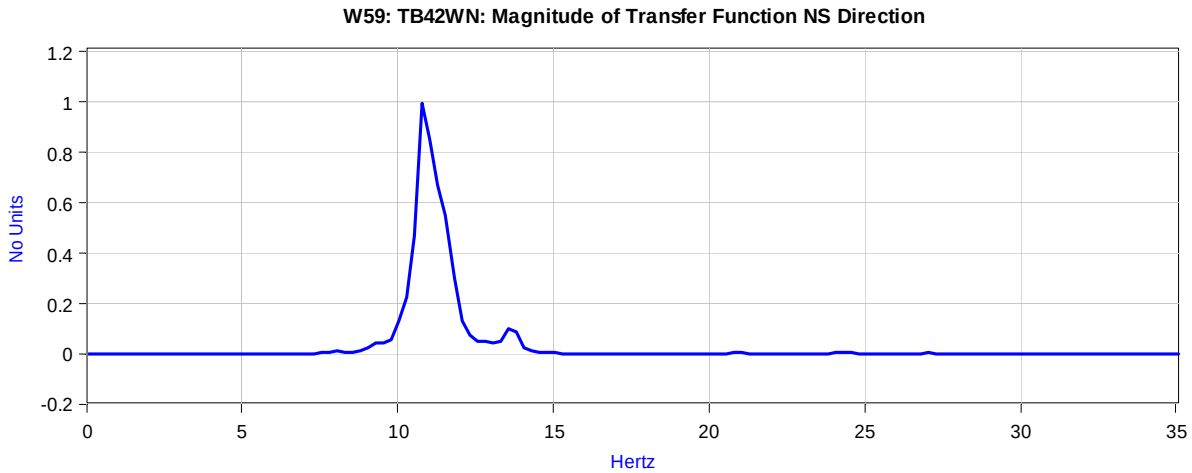

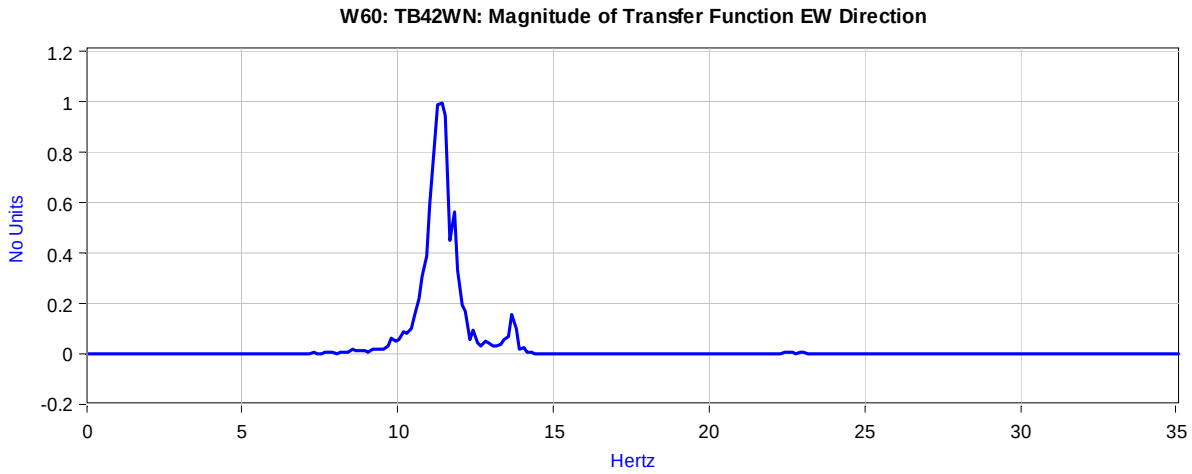

Figure D-120: Transfer Functions of Bushing #6, Test TB45WN

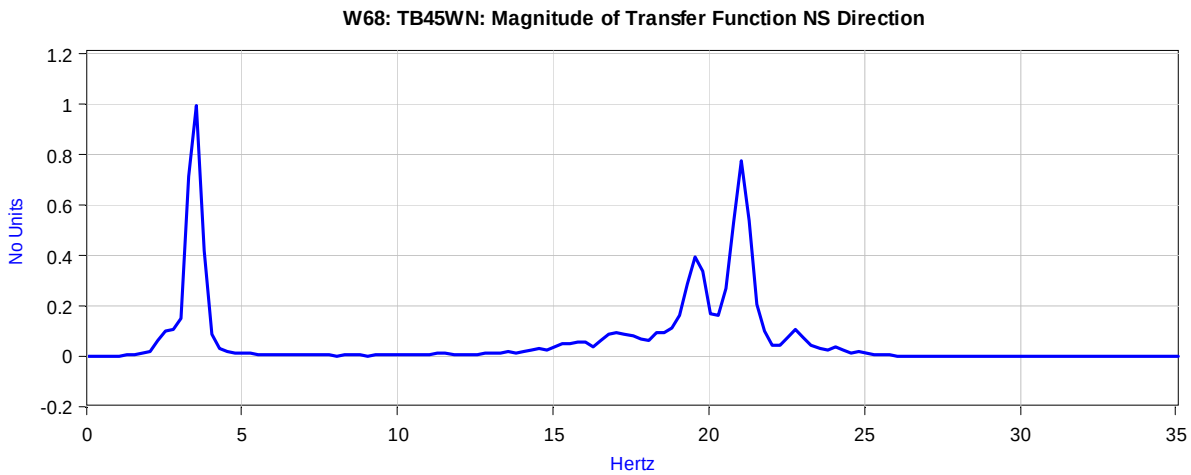

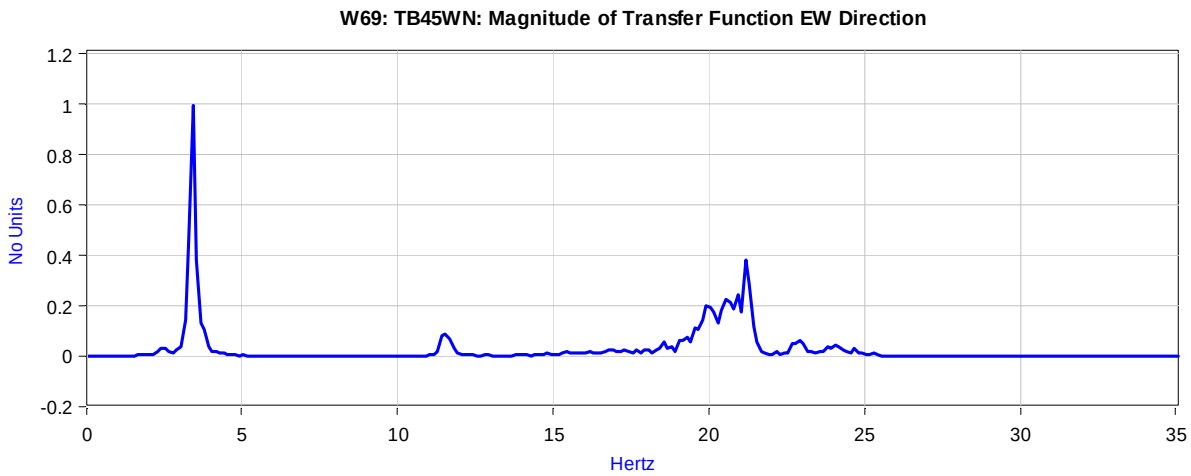

Figure D-121: Transfer Functions of Bushing #6, Test TB48WN

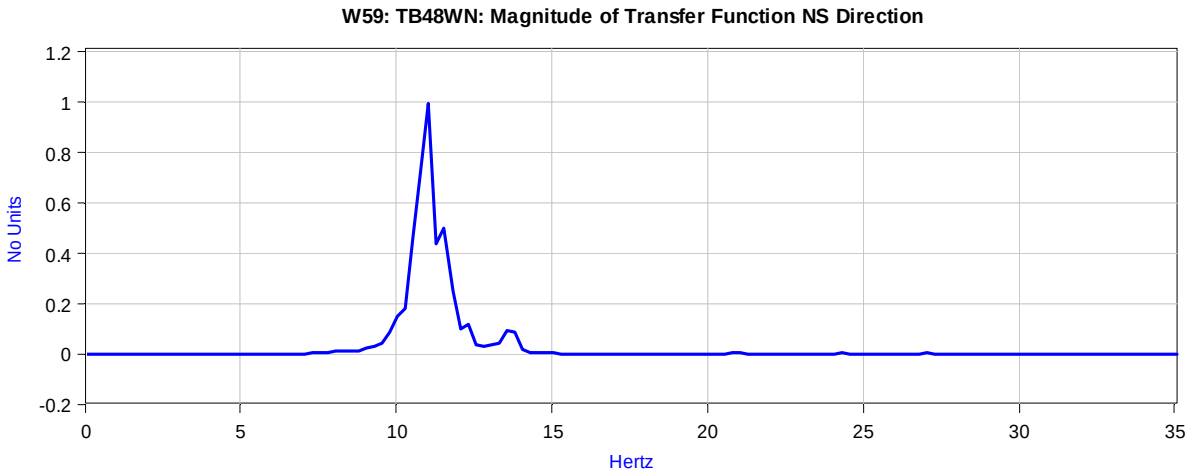

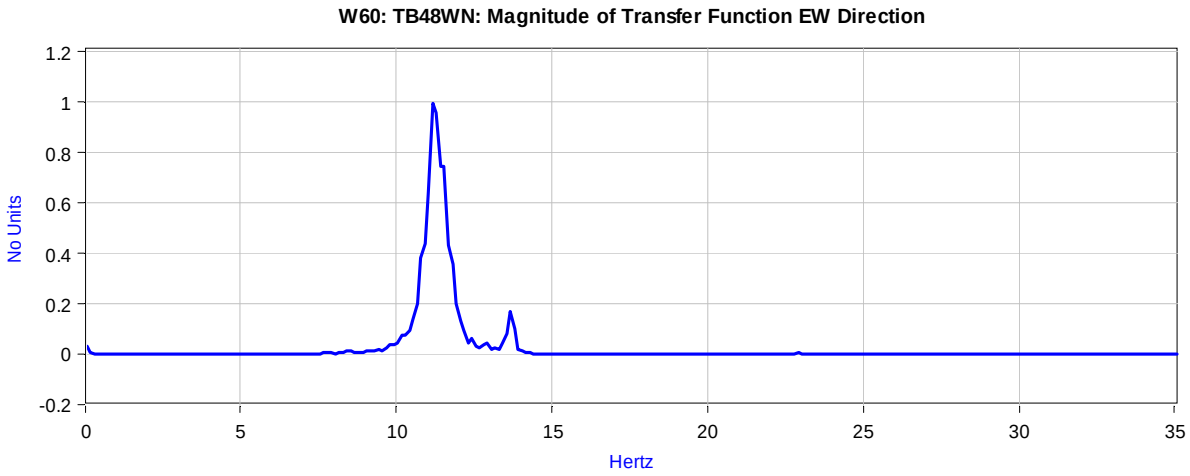

Figure D-122: Transfer Functions of Bushing #6, Test TB51WN

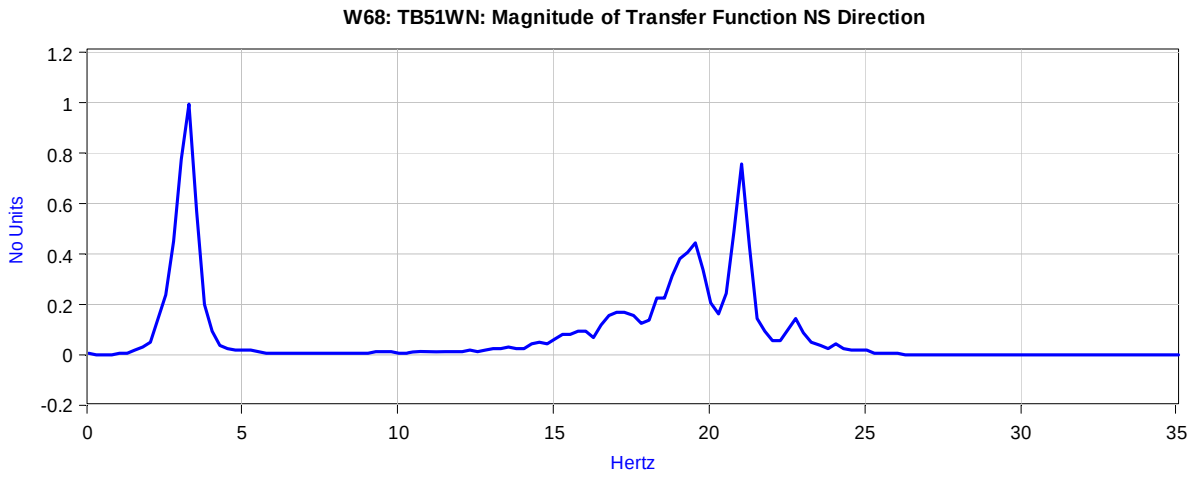

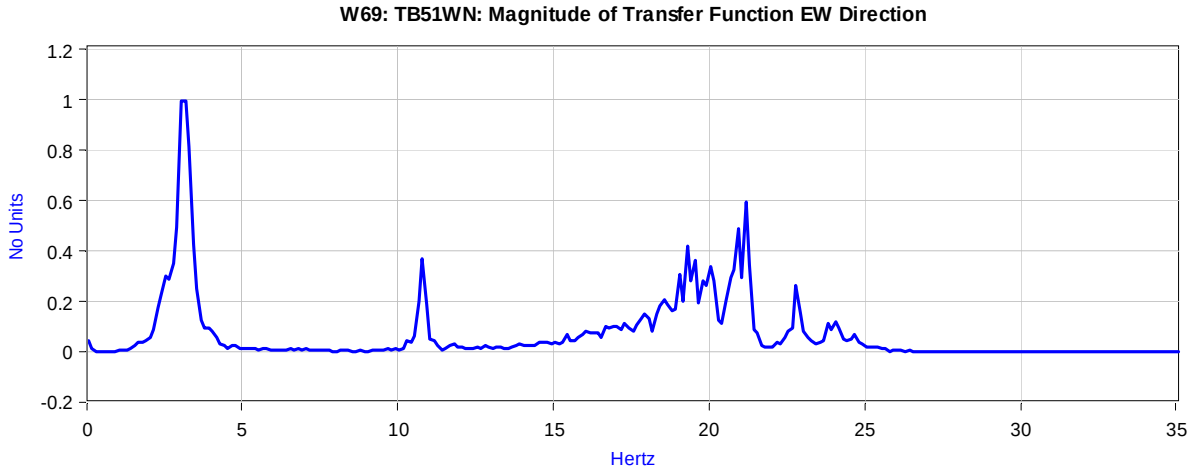

Figure D-123: Transfer Functions of Bushing #6, Test TB54WN

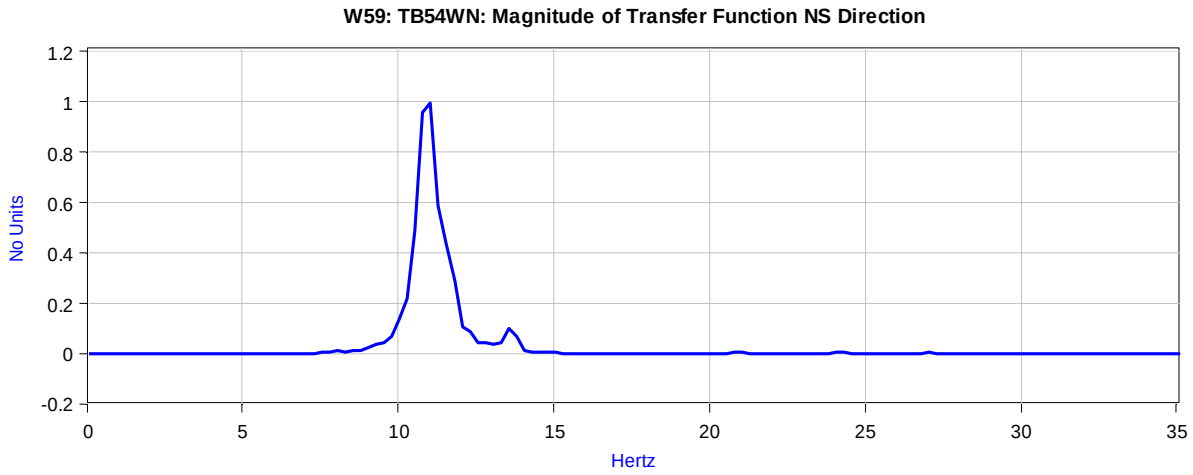

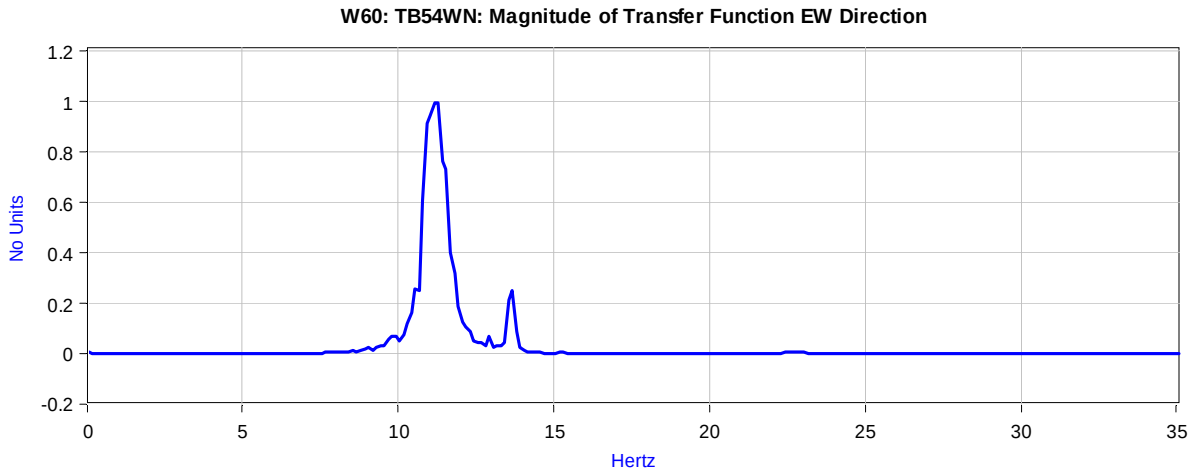

Figure D-124: Transfer Functions of Bushing #6, Test TB57WN

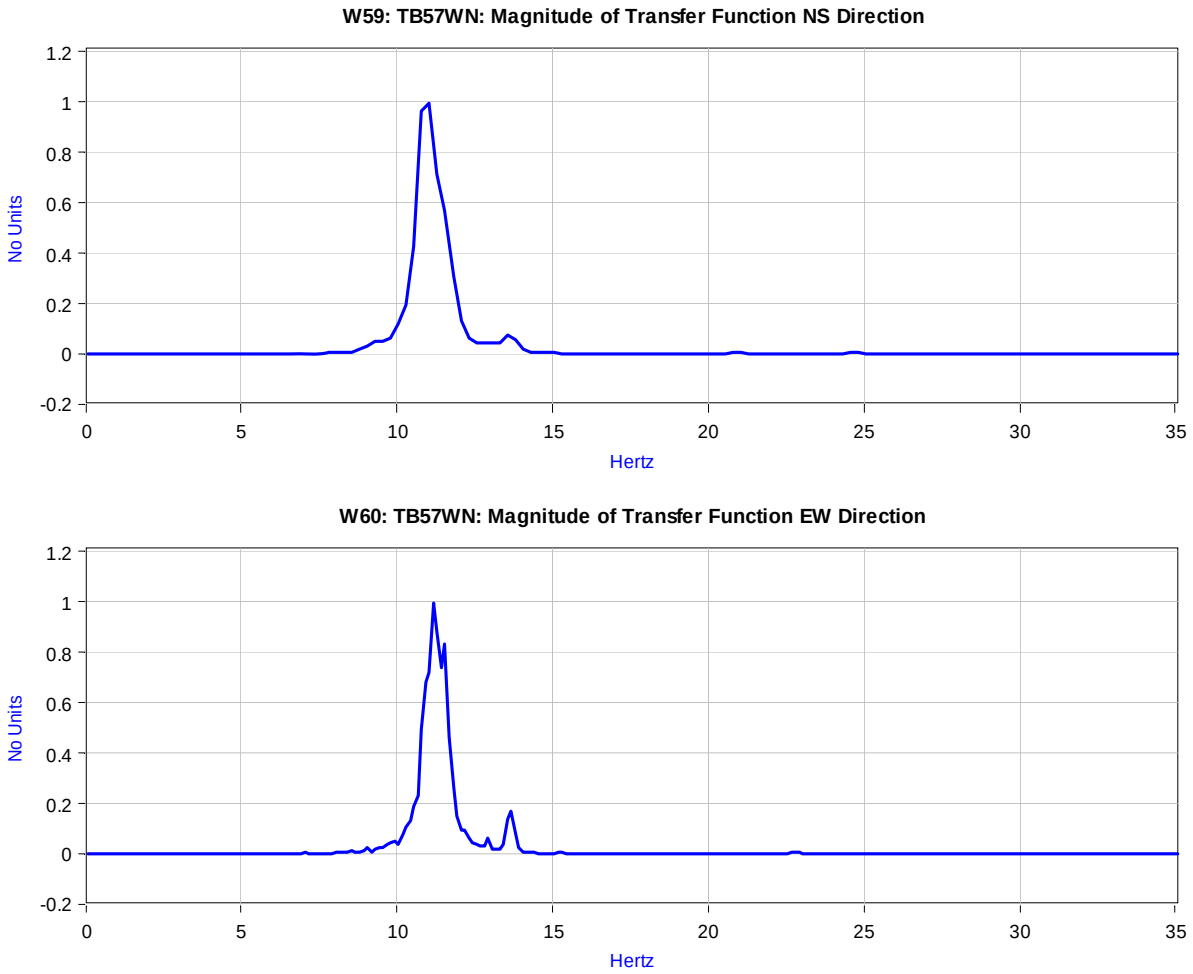

Figure D-125: Transfer Functions of Bushing #6, Test TB60WN

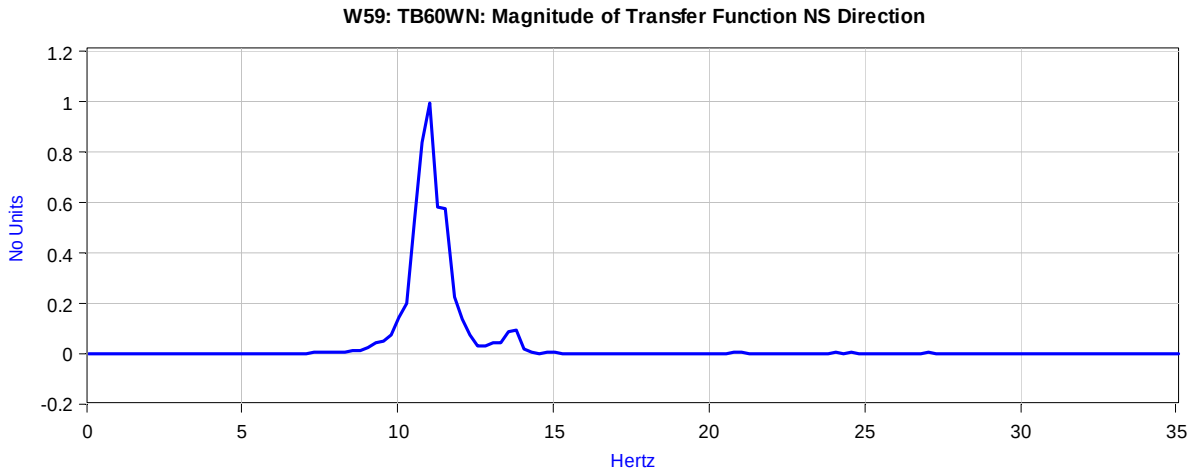

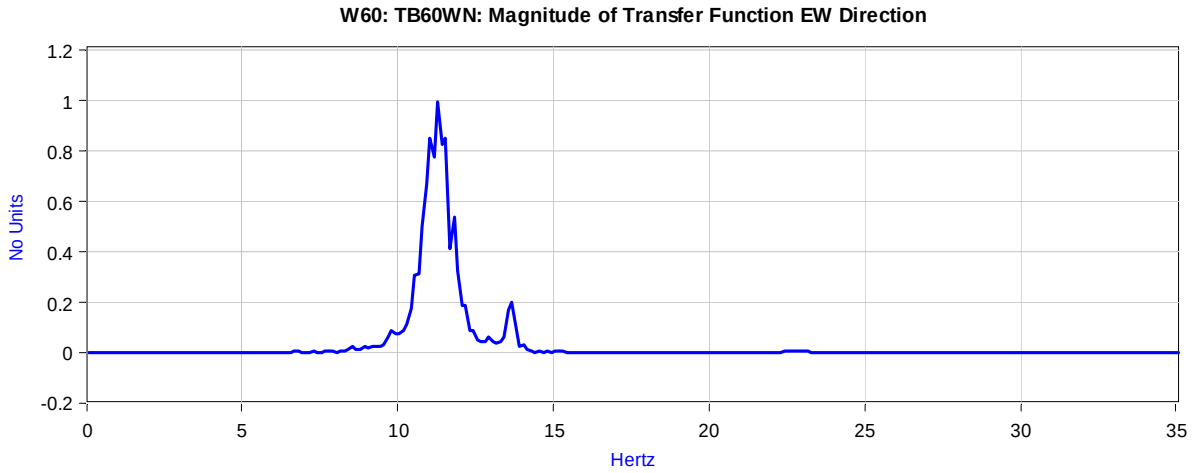

Figure D-126: Transfer Functions of Bushing #6, Test TB63WN

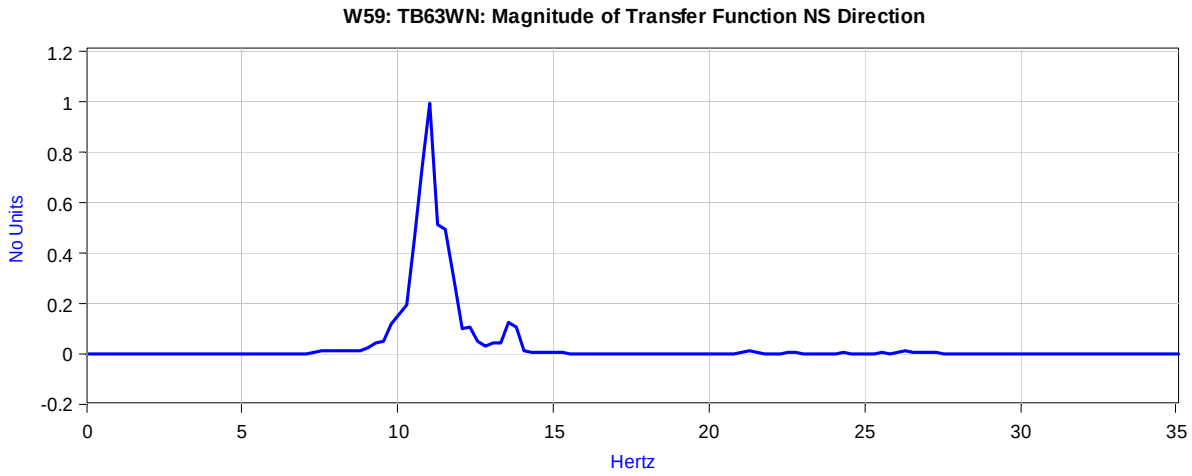

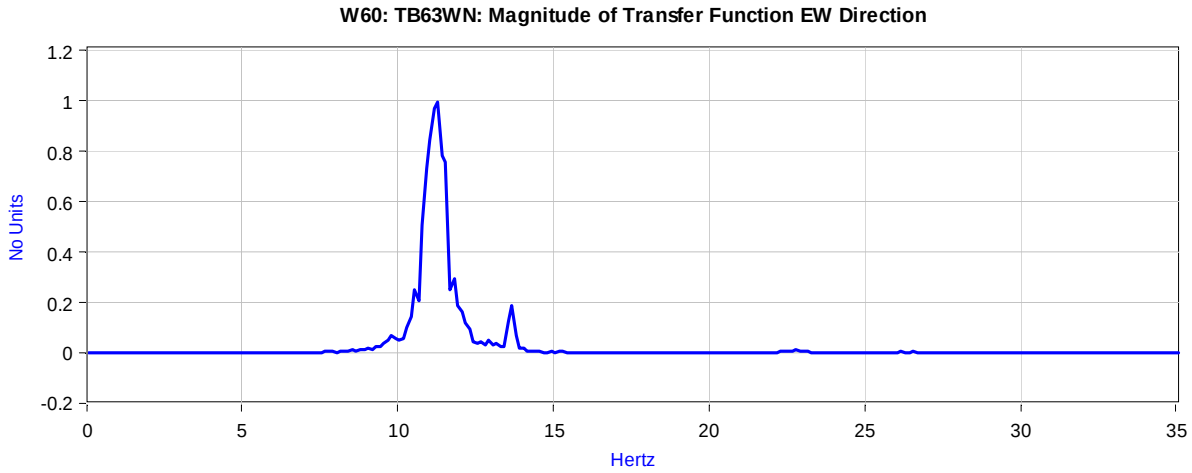

Figure D-127: Transfer Functions of Bushing #6, Test TB66WN

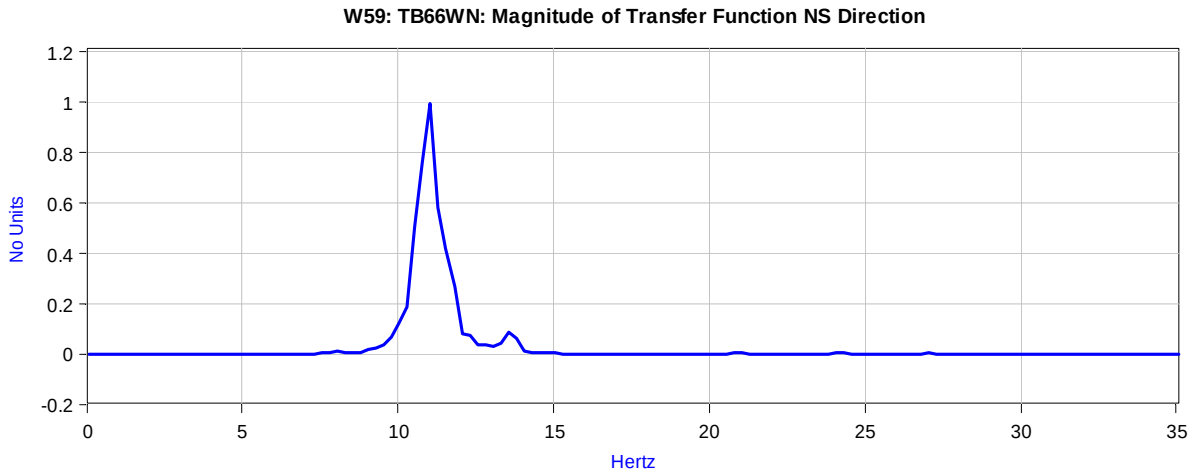

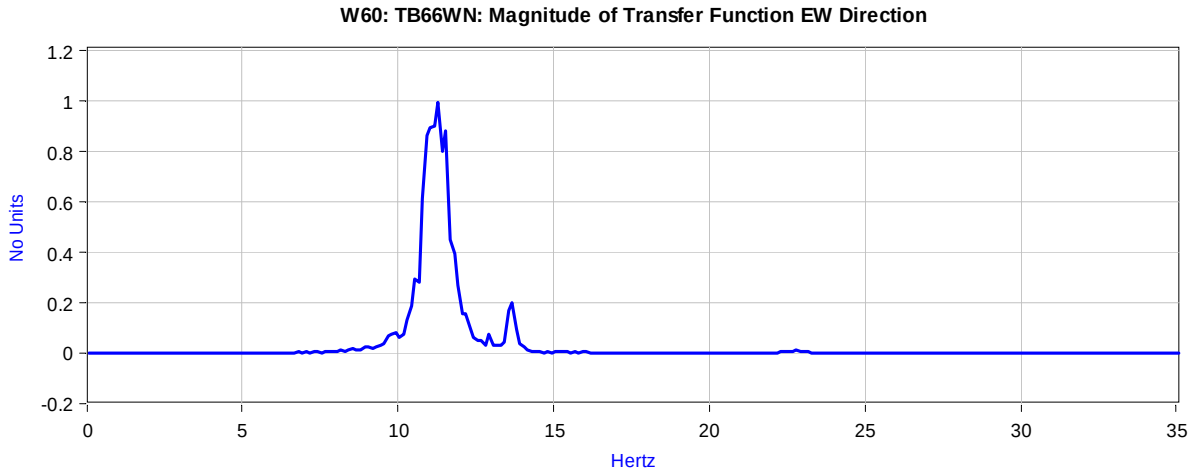

Figure D-128: Transfer Functions of Bushing #6, Test TB69WN

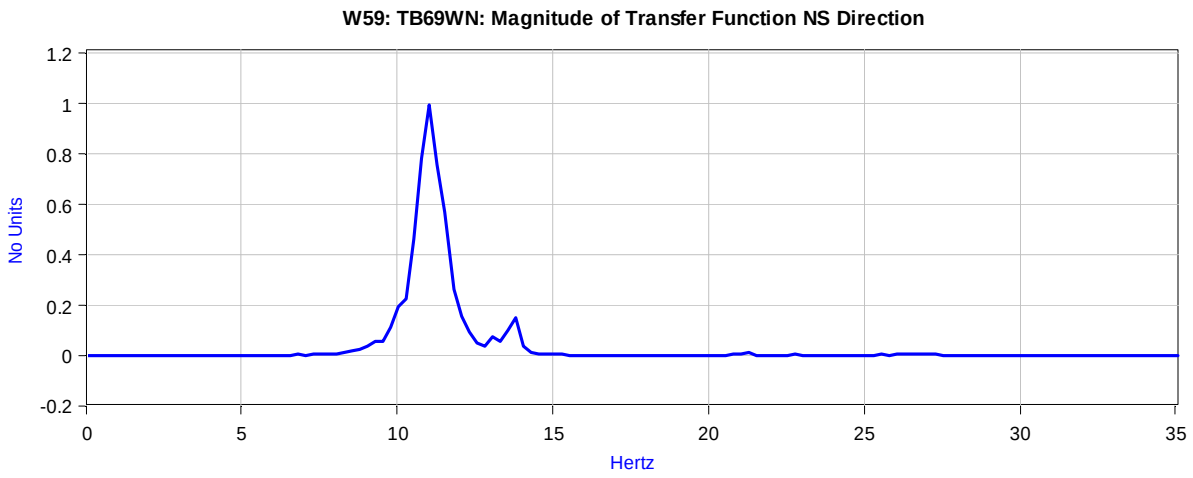

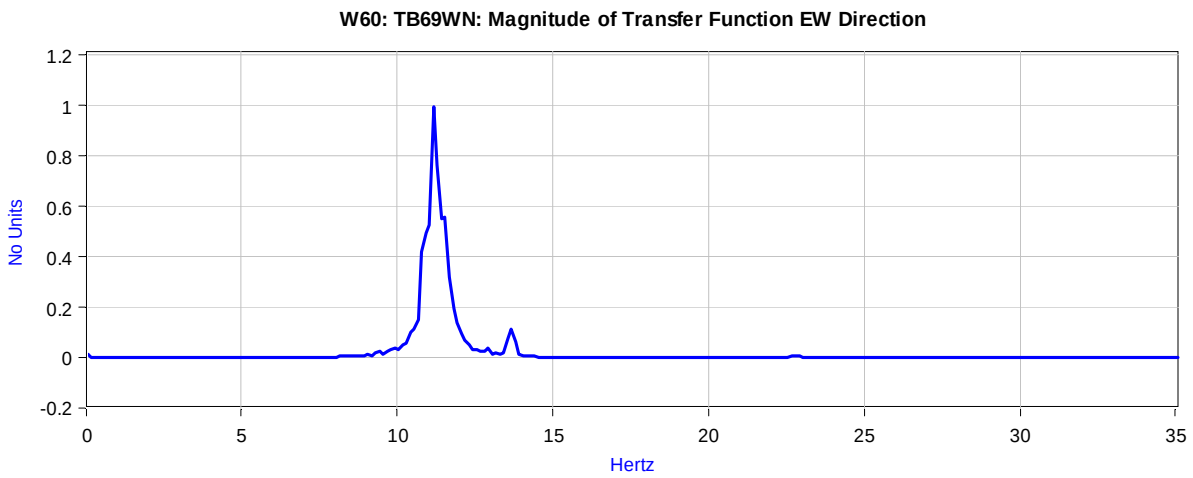

Figure D-129: Transfer Functions of Bushing #6, Test TB72WN

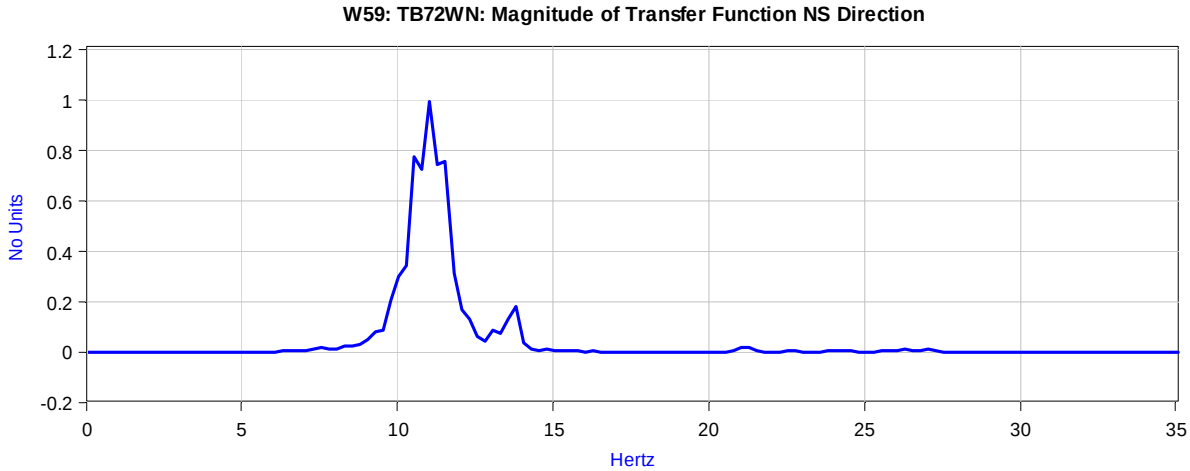

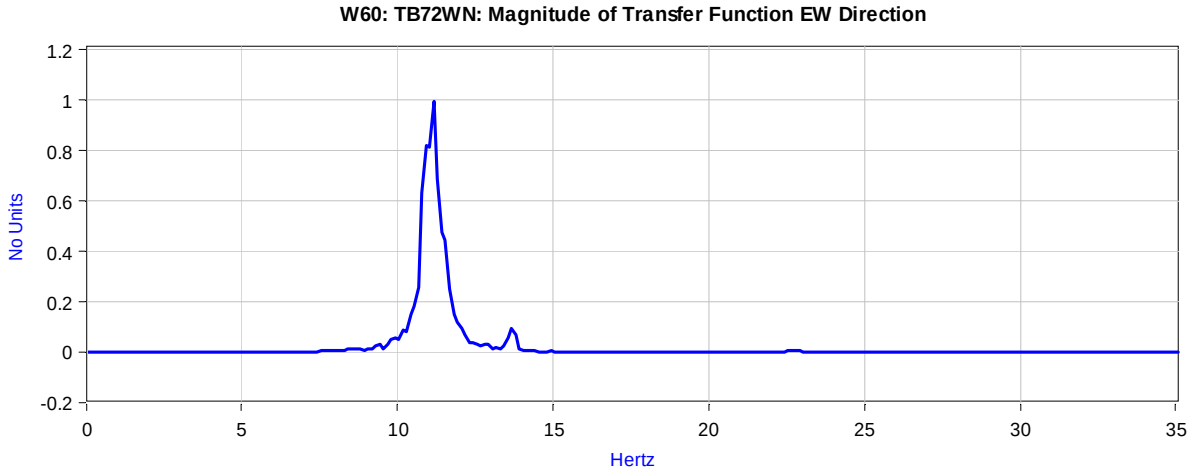

Table Impulse Tests

The table impulse test identifies frequencies and damping of dominant frequencies using smoothed table acceleration impulse for control of a shake table by using a smoothing table impulse procedure developed by the SEESL at University at Buffalo (Kong, 2010). For the identification of system frequencies, a power spectral density (PSD) was calculated from output motion at the top of the bushing and the system frequency is obtained by finding the frequency where the peak is located. For the identification of modal damping, a curve fitting method developed by the authors was used (Kong, 2010).

The acceleration history results of the table impulse tests are presented in Figures D-130 through D-147, and the dynamic characteristics are summarized in Table D-7. The frequencies of Bushing #6 in the NS direction are around 11 Hz in test TB20TBI (before random motion tests), and 10.87 Hz in test TB73TBI; the damping values are 1.05% and 1.18%, respectively. The frequency in the EW direction is 11.20 Hz in test TB20TBI (before random motion tests), and 11.05 Hz in test TB73TBI; the damping values are 0.75% and 0.75%, respectively.

Figure D-130: Table Impulse Test Response (Test TB20TBI) – Bushing #6

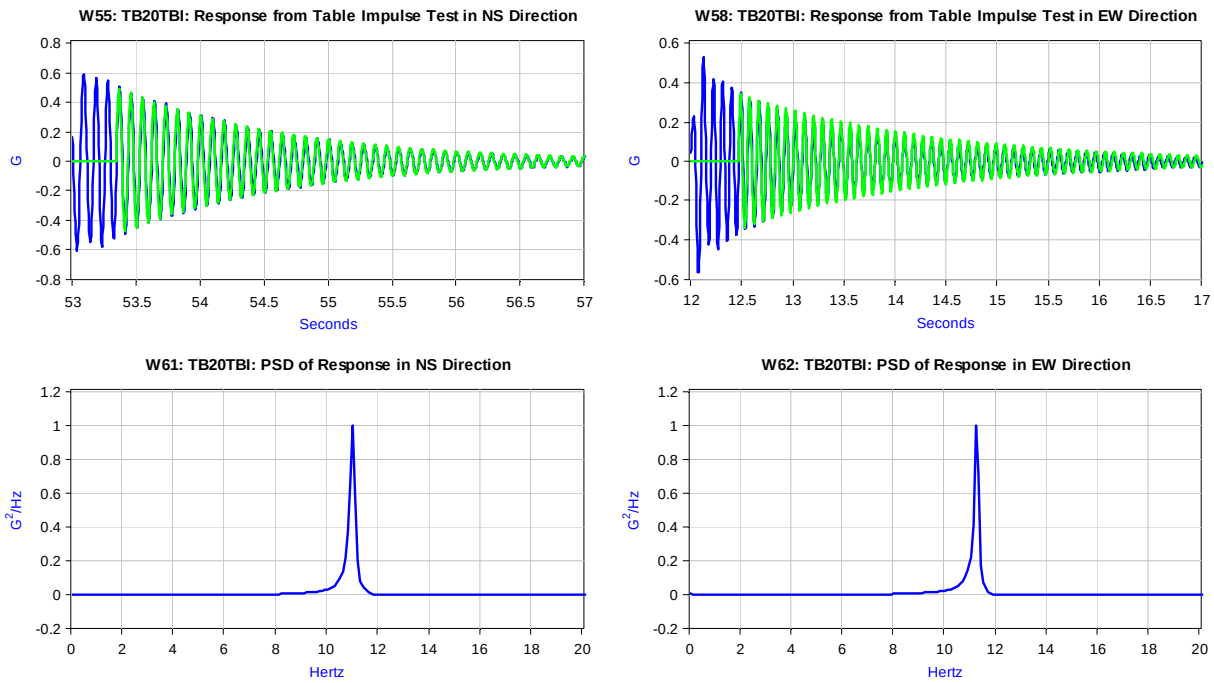

Figure D-131: Table Impulse Test Response (Test TB23TBI) – Bushing #6

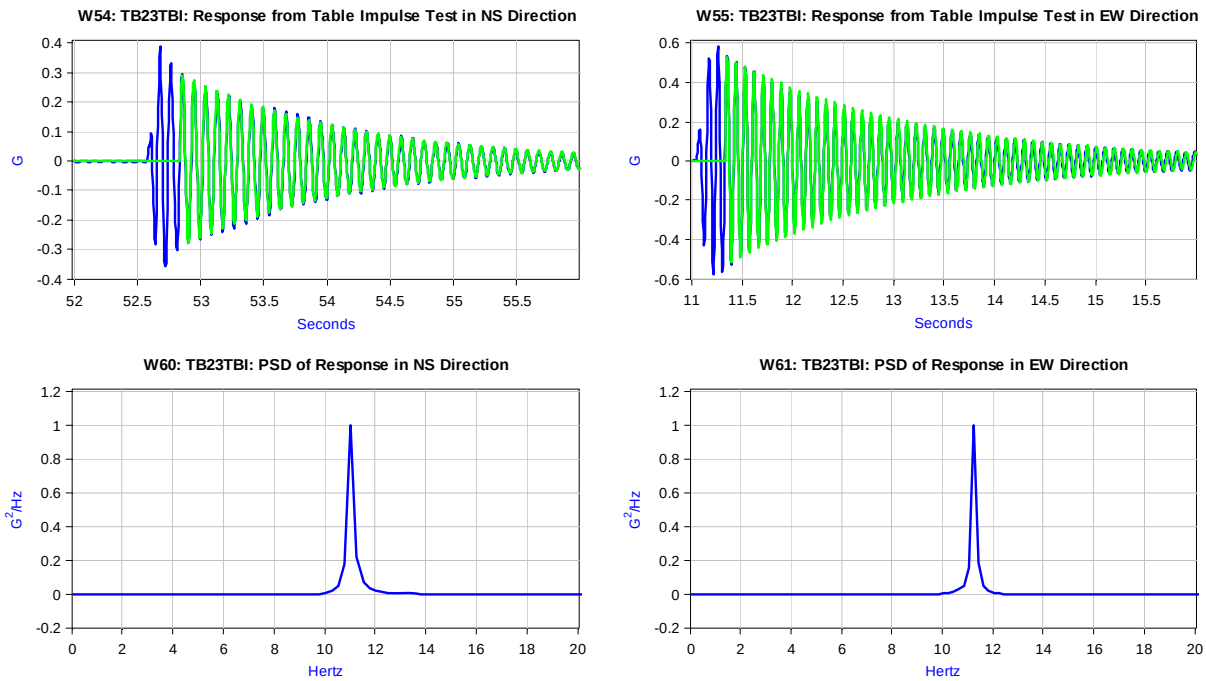

Figure D-132: Table Impulse Test Response (Test TB26TBI) – Bushing #6

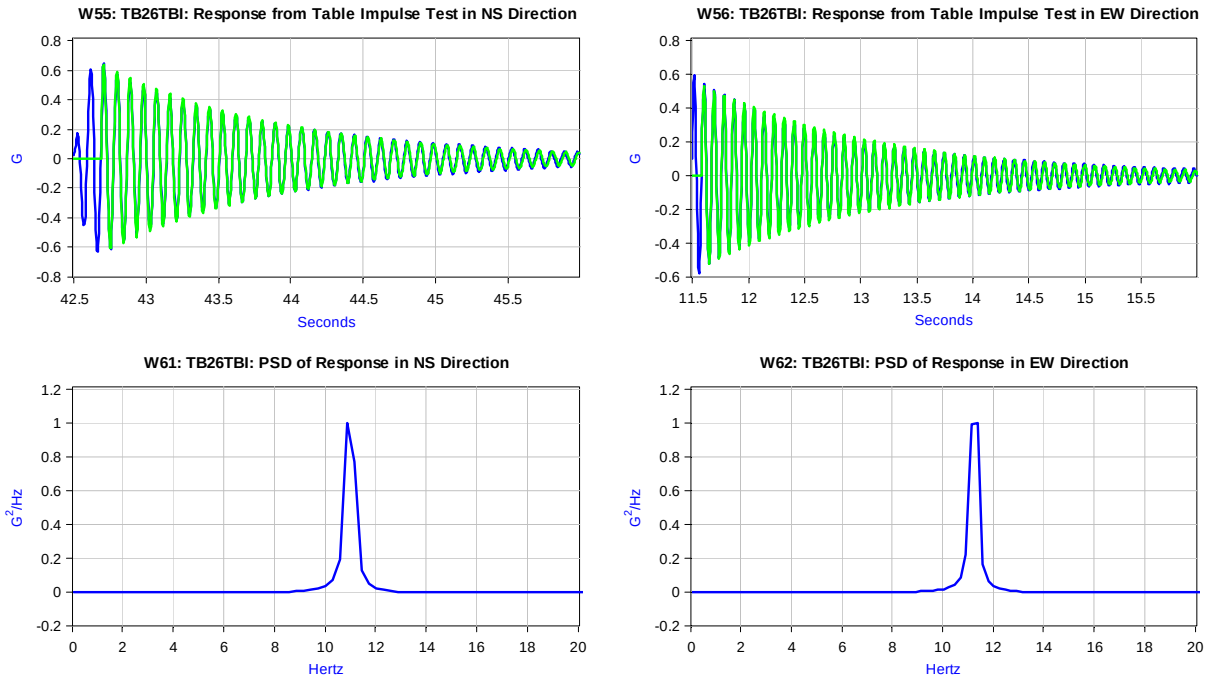

Figure D-133: Table Impulse Test Response (Test TB29TBI) – Bushing #6

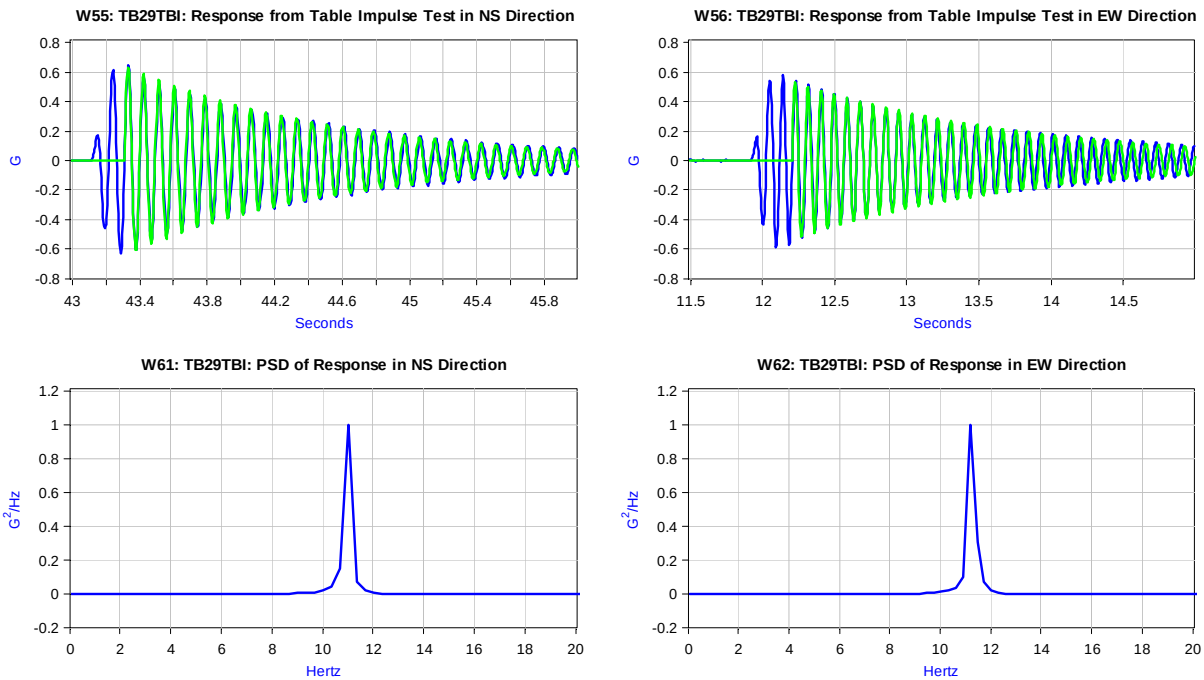

Figure D-134: Table Impulse Test Response (Test TB32TBI) – Bushing #6

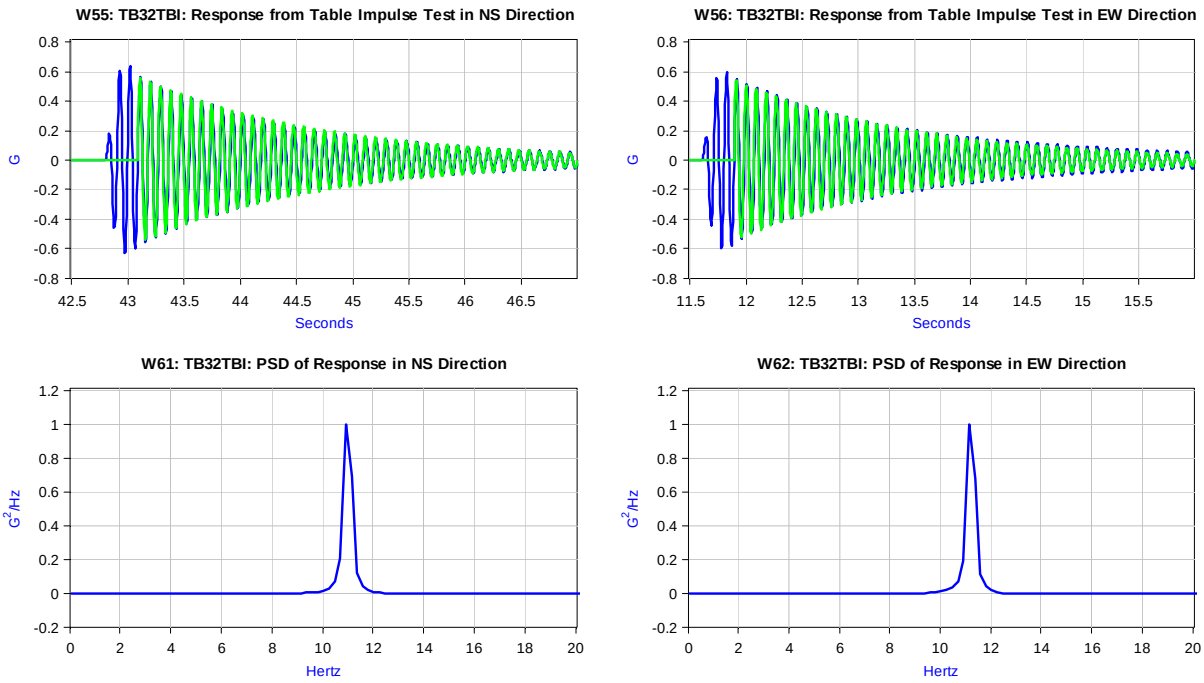

Figure D-135: Table Impulse Test Response (Test TB35TBI) – Bushing #6

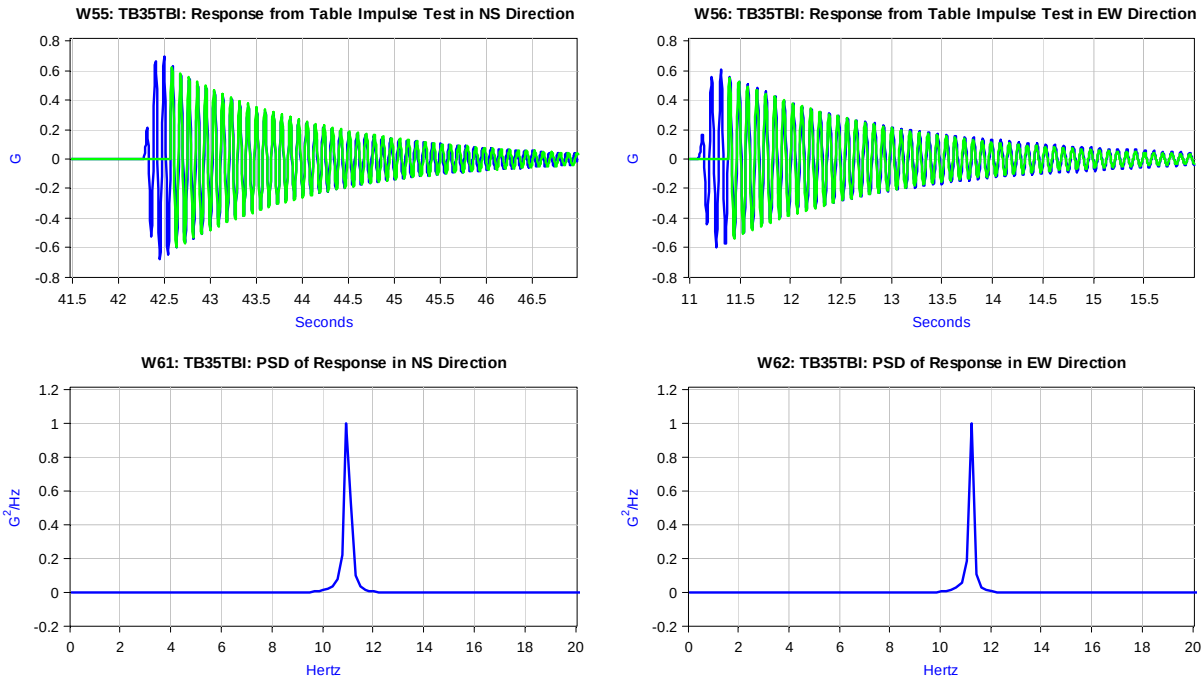

Figure D-136: Table Impulse Test Response (Test TB37TBI) – Bushing #6

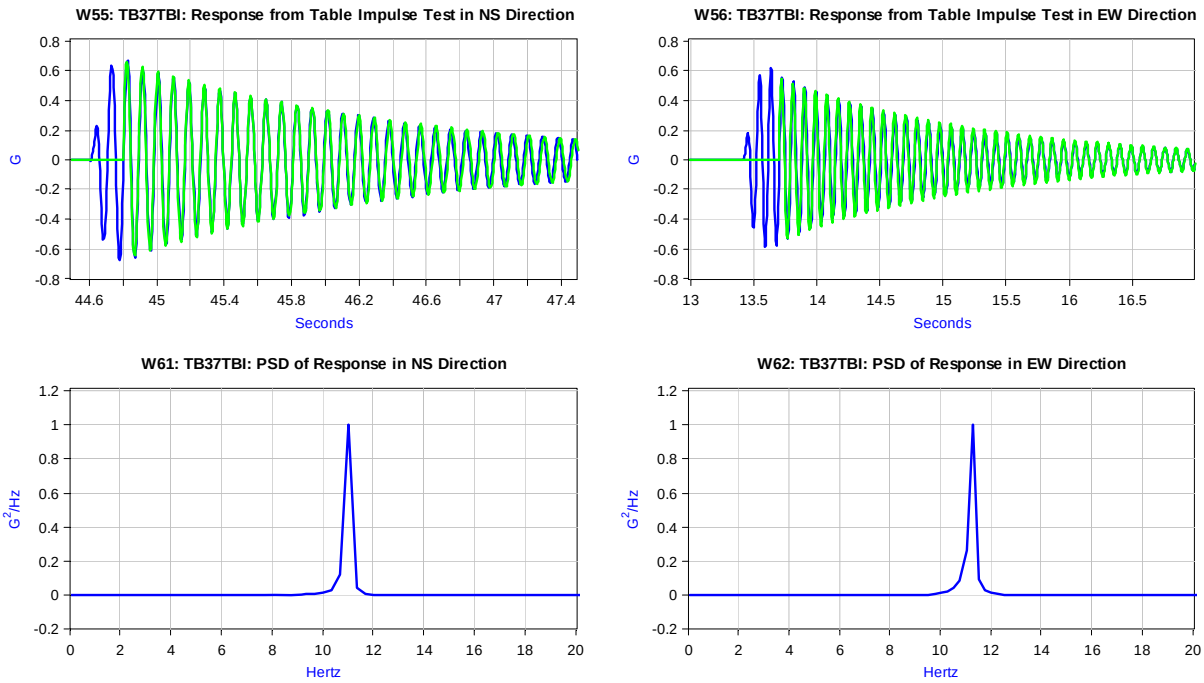

Figure D-137: Table Impulse Test Response (Test TB40TBI) – Bushing #6

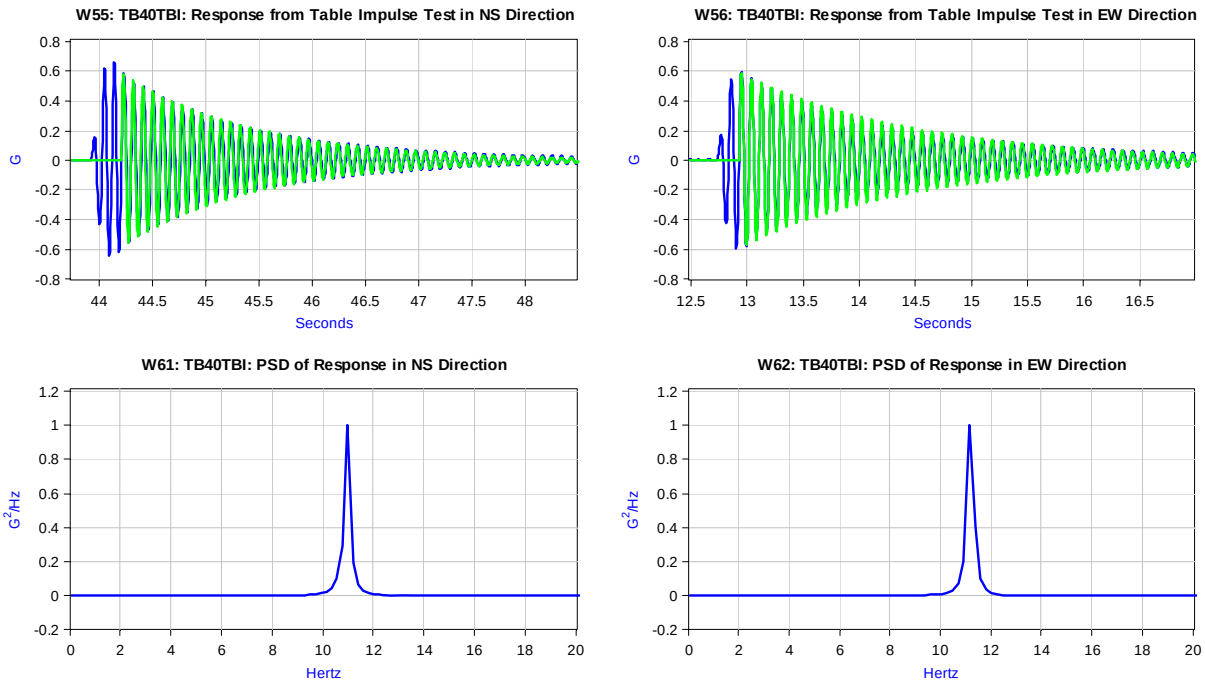

Figure D-138: Table Impulse Test Response (Test TB43TBI) – Bushing #6

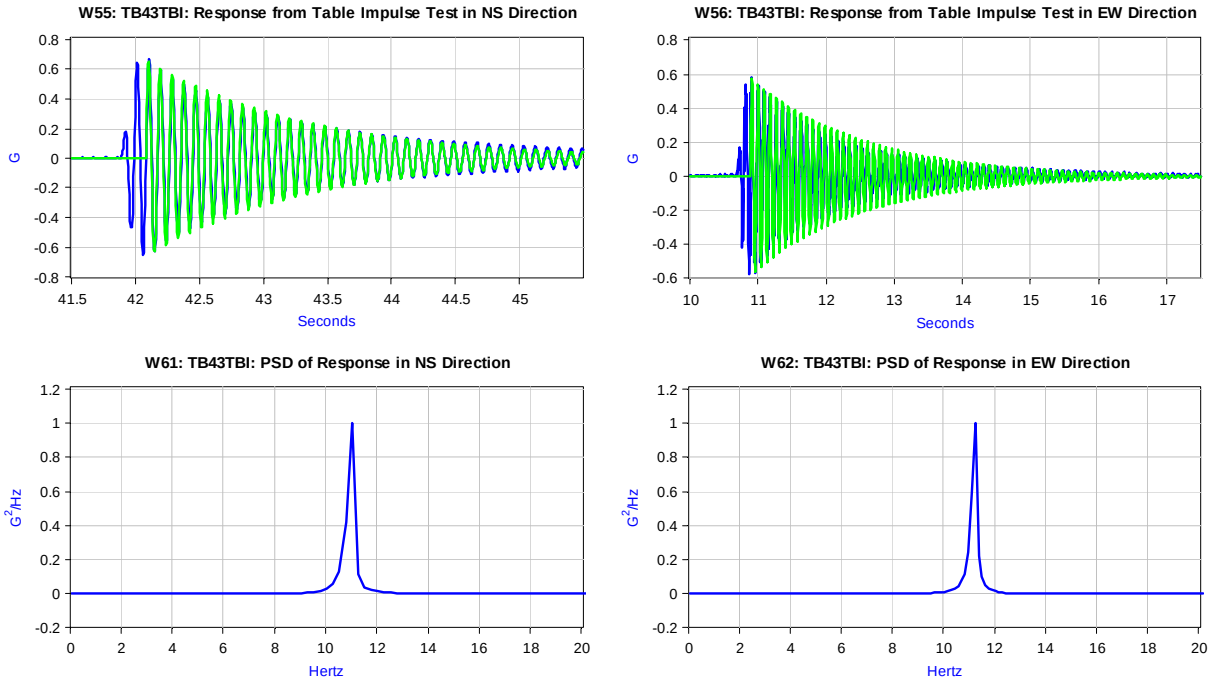

Figure D-139: Table Impulse Test Response (Test TB46TBI) – Bushing #6

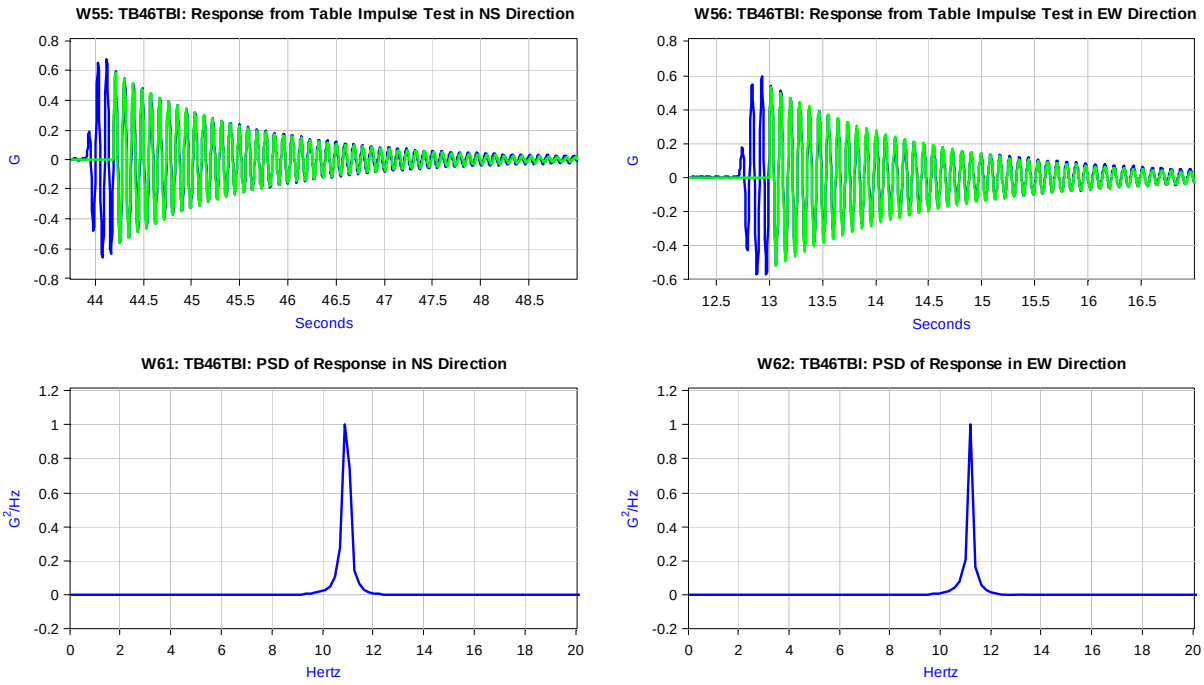

Figure D-140: Table Impulse Test Response (Test TB49TBI) – Bushing #6

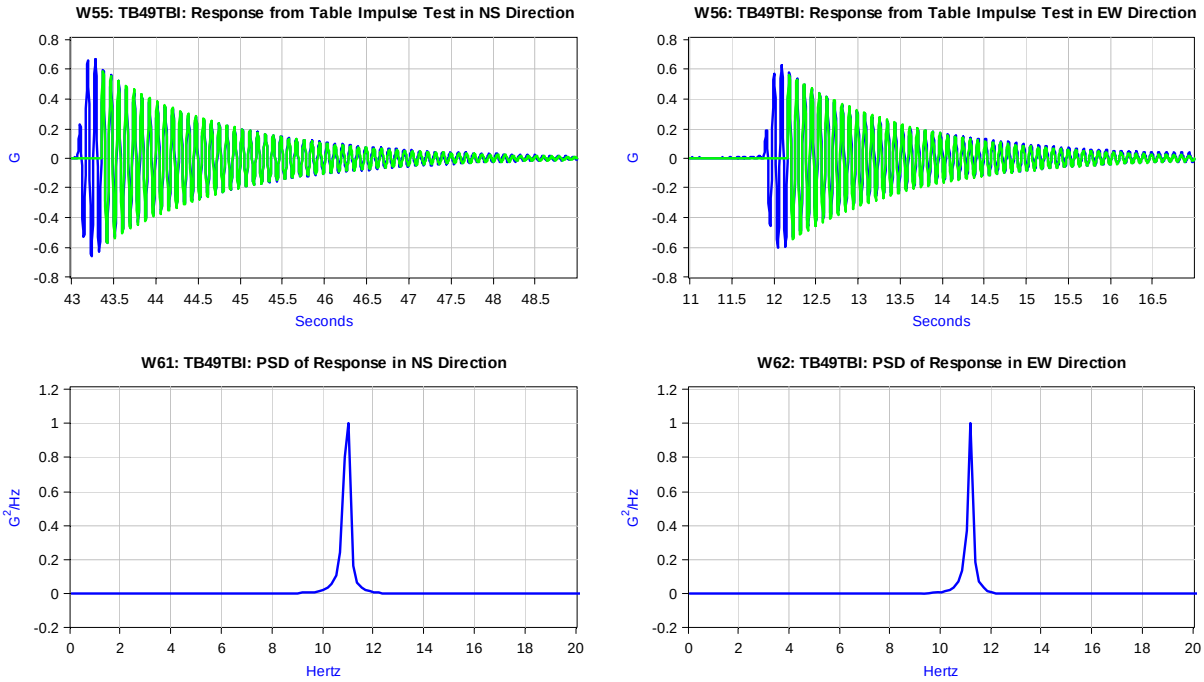

Figure D-141: Table Impulse Test Response (Test TB55TBI) – Bushing #6

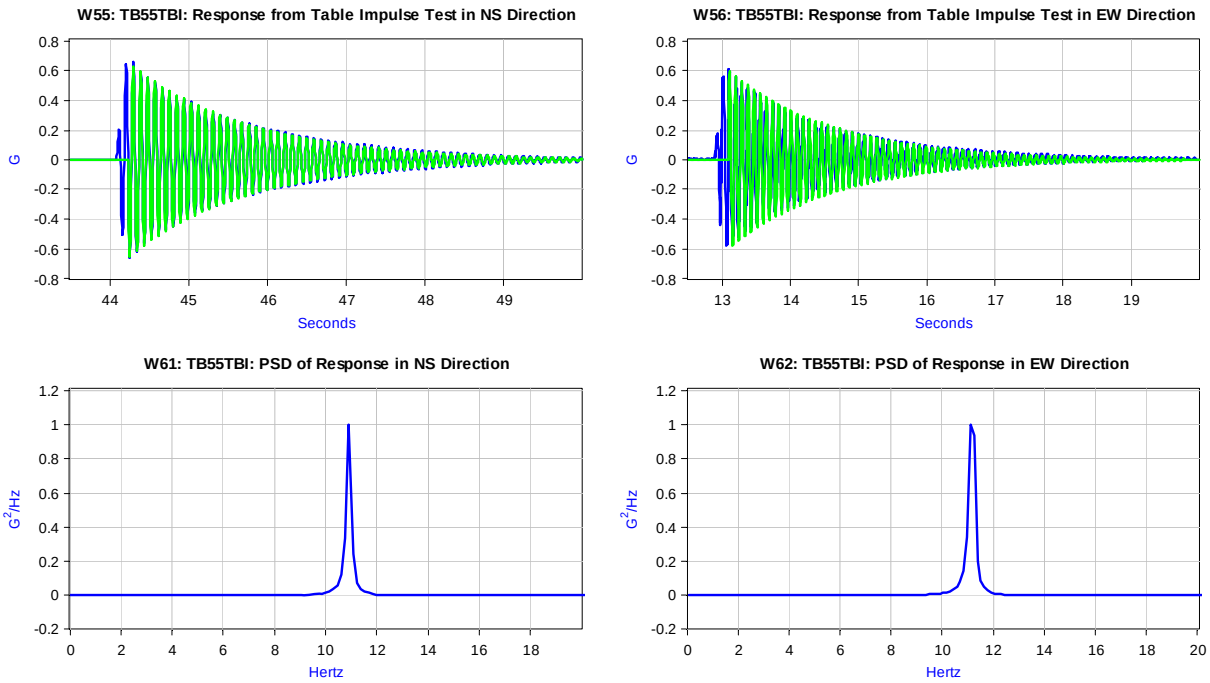

Figure D-142: Table Impulse Test Response (Test TB58TBI) – Bushing #6

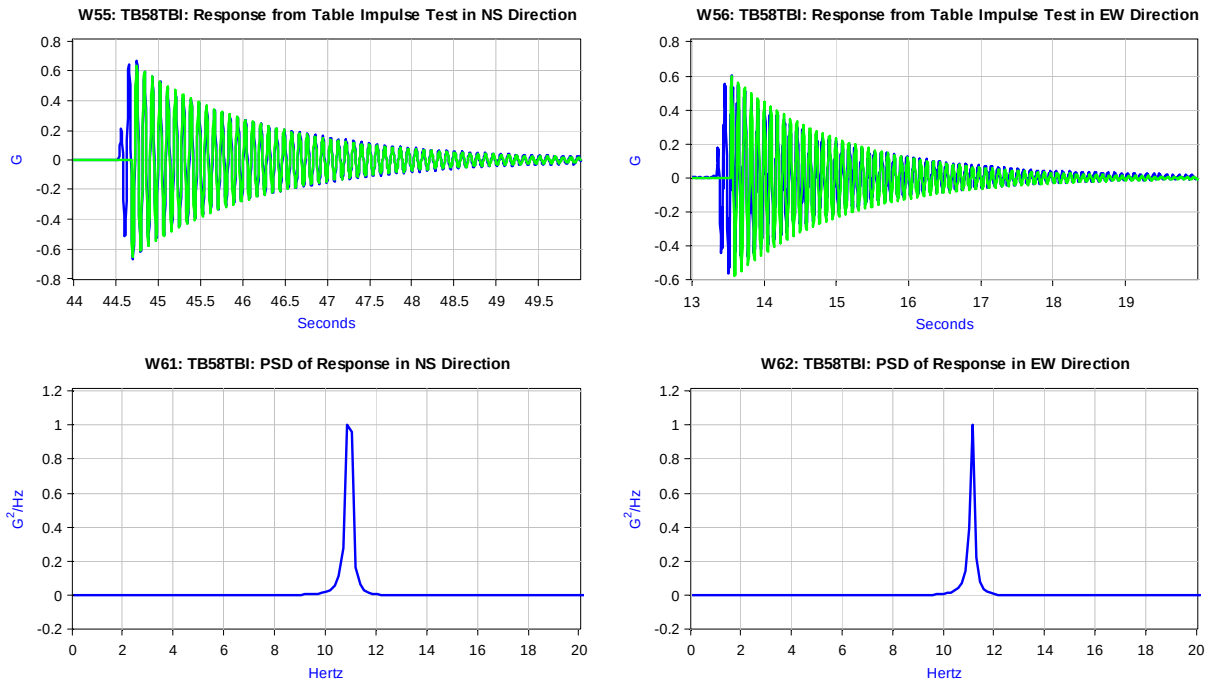

Figure D-143: Table Impulse Test Response (Test TB61TBI) – Bushing #6

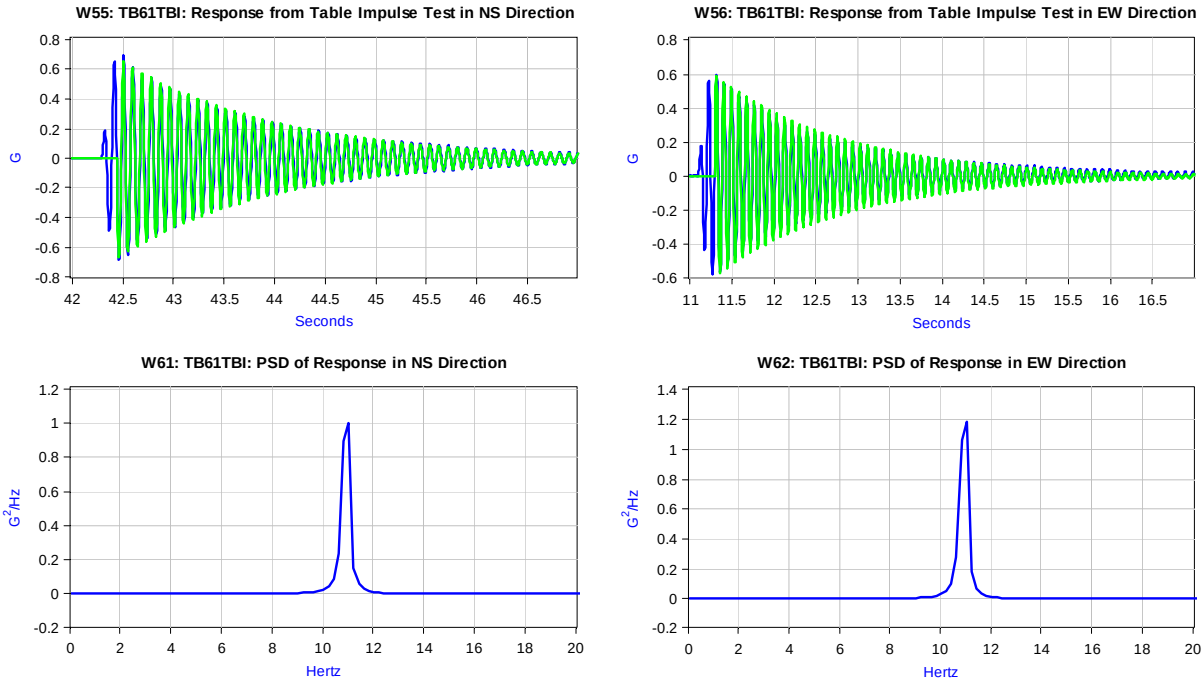

Figure D-144: Table Impulse Test Response (Test TB64TBI) – Bushing #6

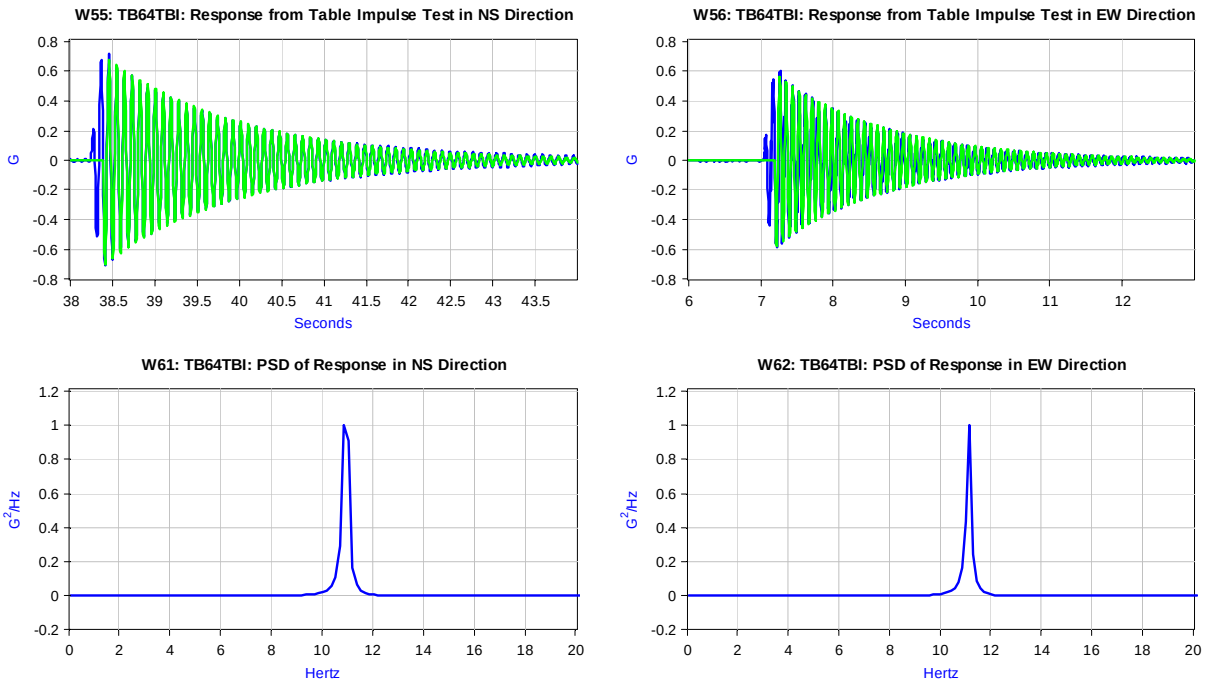

Figure D-145: Table Impulse Test Response (Test TB67TBI) – Bushing #6

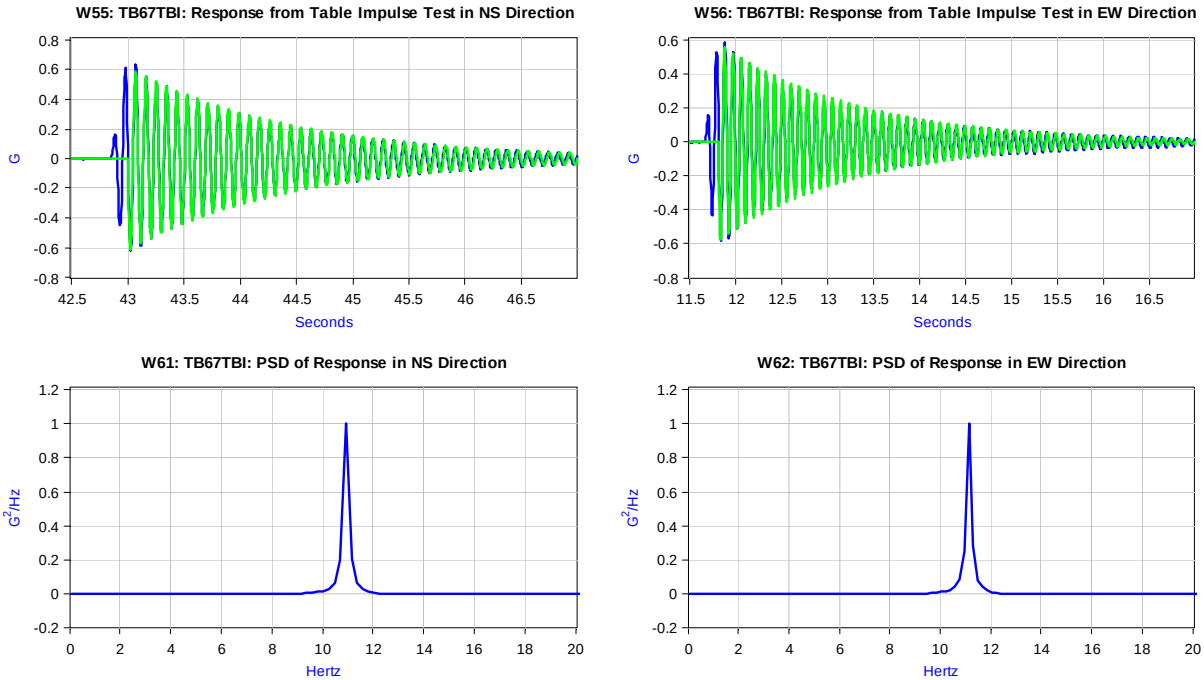

Figure D-146: Table Impulse Test Response (Test TB70TBI) – Bushing #6

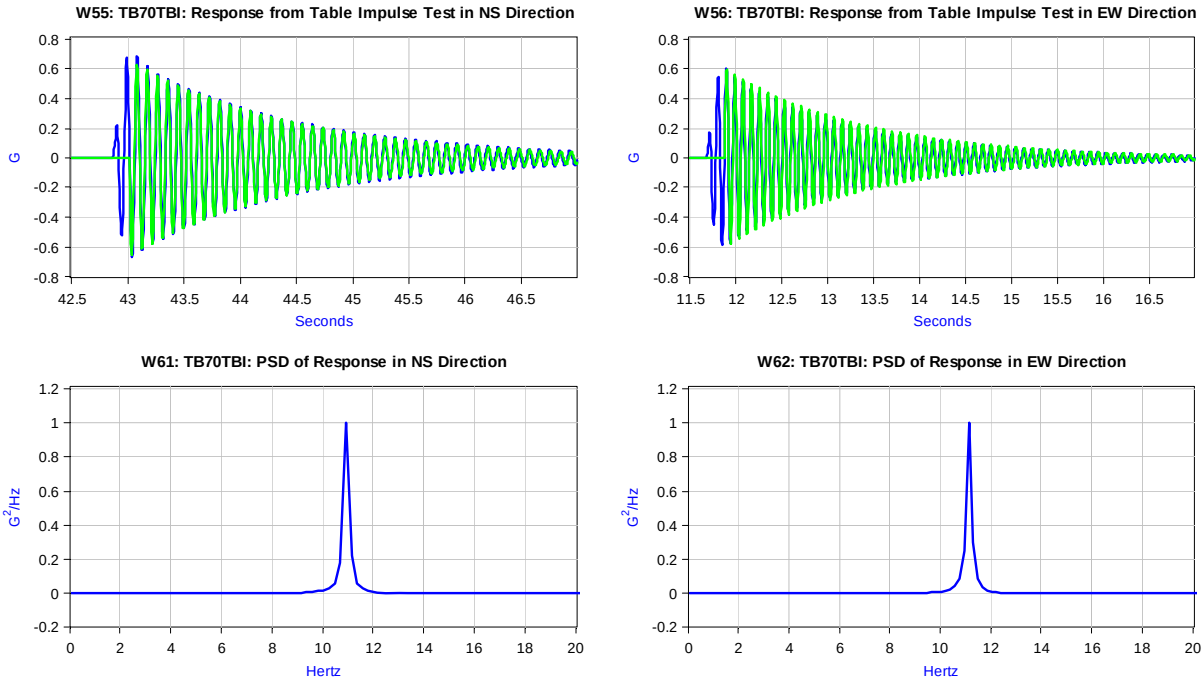

Figure D-147: Table Impulse Test Response (Test TB73TBI) – Bushing #6

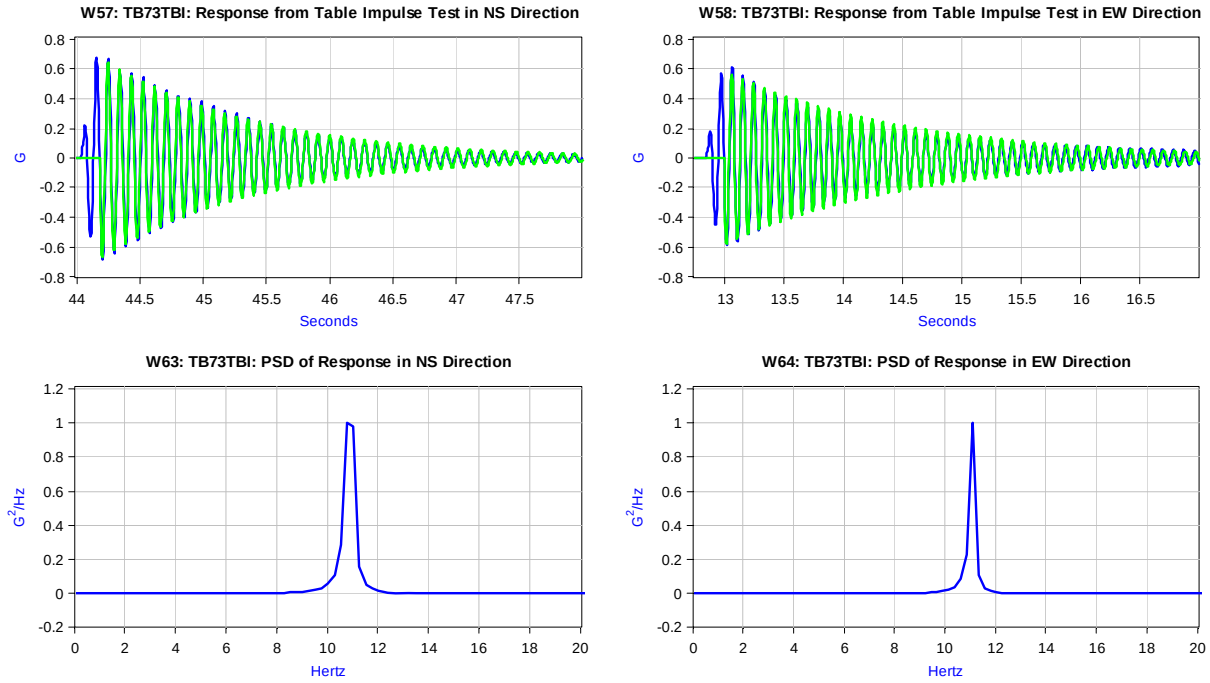

Acceleration History Tests

Acceleration history tests were performed for the seismic demand quantification of Bushing #6. A summary of the accelerations recorded on various locations on the bushing are shown in Table D-8 for the seventeen levels of test input motions.

The acceleration history tests were used to measure the bending moment of bushing at flange level. Strain gauges were used to measure the bending moments. A summary of bending moments is presented in Table D-8 and the results of the tests are shown in Figures D-148 through D-162.

Table D-8: Summary of Accelerations and Bending Moments – Bushing #6

Location	Units	0.25 g RRS			0.25 g RRS			0.50 g RRS			0.75 g RRS			1.00 g RRS			1.25 g RRS			1.50 g RRS			1.75 g RRS		
		TBU2AH25			TBU2AH50			TBU2AH100			TB44AH150			TB47AH225			TB53AH300			TBU2AH25			TBU2AH50		
(1)	(2)	(3)	(4)	(5)	(6)	(7)	(8)	(9)	(10)	(11)	(12)	(13)	(14)	(15)	(16)	(17)	(18)	(19)	(20)	(21)	(22)	(23)	(24)	(25)	(26)
Bushing Location on Frame																									
Acceleration Distribution along the Height of Testing Setup																									
Direction		NS	EW	Vertical	NS	EW	Vertical	NS	EW	Vertical	NS	EW	Vertical	NS	EW	Vertical	NS	EW	Vertical	NS	EW	Vertical	NS	EW	Vertical
Top of Bushing	(g)	0.51	0.53	0.25	1.06	1.03	0.49	1.77	1.81	0.86	2.86	2.90	1.75	3.78	3.70	2.50	5.25	4.68	3.96	5.48	5.26	3.52	6.22	6.03	4.23
Upper CG Of Bushing	(g)	0.29	0.29	-	0.59	0.57	-	1.16	1.04	-	1.56	1.61	-	2.12	2.15	-	2.87	2.90	-	3.02	3.06	-	3.45	3.47	-
CG OF Bushing	(g)	0.22	0.20	-	0.45	0.38	-	0.87	0.71	-	1.00	1.04	-	1.38	1.38	-	1.87	1.79	-	2.18	2.13	-	2.56	2.47	-
On Frame	(g)	0.31	0.16	0.19	0.61	0.32	0.35	1.09	0.59	0.49	1.89	0.81	0.60	2.44	1.13	0.78	3.24	1.54	1.72	3.28	1.61	1.28	3.83	1.92	1.47
Shake Table	(g)	0.16	0.14	0.19	0.34	0.29	0.35	0.55	0.56	0.46	0.77	0.73	0.59	1.02	0.99	0.82	1.35	1.36	1.75	1.33	1.42	1.27	1.55	1.65	1.50
Bending Moment at the Base of Bushing																									
Moment from Strain Gauges	kip-in	7.65	10.54	-	13.23	19.95	-	21.14	33.57	-	30.75	56.63	-	39.57	72.70	-	56.56	92.18	-	57.08	97.08	-	56.05	107.52	-

Location	Units	2.00 g RRS			2.25 g RRS			2.50 g RRS			2.75 g RRS			3.00 g RRS			2.00 g RRS			2.25 g RRS			2.50 g RRS			2.75 g RRS		
		TBU2AH100			TB44AH150			TB47AH225			TB53AH300			TB53AH300			TB53AH300			TB53AH300			TB53AH300			TB53AH300		
(1)	(2)	(3)	(4)	(5)	(6)	(7)	(8)	(9)	(10)	(11)	(12)	(13)	(14)	(15)	(16)	(17)	(18)	(19)	(20)	(21)	(22)	(23)	(24)	(25)	(26)	(27)	(28)	(29)
Bushing Location on Frame																												
Acceleration Distribution along the Height of Testing Setup																												
Direction		NS	EW	Vertical	NS	EW	Vertical	NS	EW	Vertical	NS	EW	Vertical	NS	EW	Vertical	NS	EW	Vertical	NS	EW	Vertical	NS	EW	Vertical	NS	EW	Vertical
Top of Bushing	(g)	7.06	6.81	4.98	6.51	7.84	5.75	7.63	8.74	6.36	8.11	7.77	6.12	8.84	8.71	7.54	6.57	7.09	5.22	6.64	7.52	6.06	7.65	8.13	7.14	7.37	8.36	6.42
Upper CG Of Bushing	(g)	3.92	3.80	-	3.75	4.24	-	4.23	5.11	-	7.49	4.51	-	8.18	5.33	-	3.83	4.18	-	3.94	4.84	-	3.66	5.77	-	LOST	5.02	-
CG OF Bushing	(g)	2.94	2.79	-	2.95	3.04	-	3.33	3.56	-	3.35	3.39	-	4.02	4.12	-	2.86	2.77	-	3.20	3.35	-	3.58	4.02	-	3.46	3.68	-
On Frame	(g)	4.38	2.35	1.80	5.60	2.67	2.09	6.17	3.07	2.44	7.18	3.10	2.31	5.74	3.94	2.93	4.29	2.32	1.65	5.28	2.76	2.01	5.91	3.29	2.52	5.44	3.14	2.21
Shake Table	(g)	1.86	1.88	1.86	2.35	2.10	2.15	2.63	2.34	2.52	2.44	2.30	2.43	3.25	2.88	3.09	1.80	2.07	1.76	2.33	2.08	2.13	2.60	2.49	2.55	2.28	2.77	2.39
Bending Moment at the Base of Bushing																												
Moment from Strain Gauges	kip-in	56.34	116.82	-	55.96	128.48	-	64.75	167.97	-	122.88	133.27	-	-	-	-	53.75	138.19	-	53.75	187.75	-	71.50	286.41	-	-	-	-

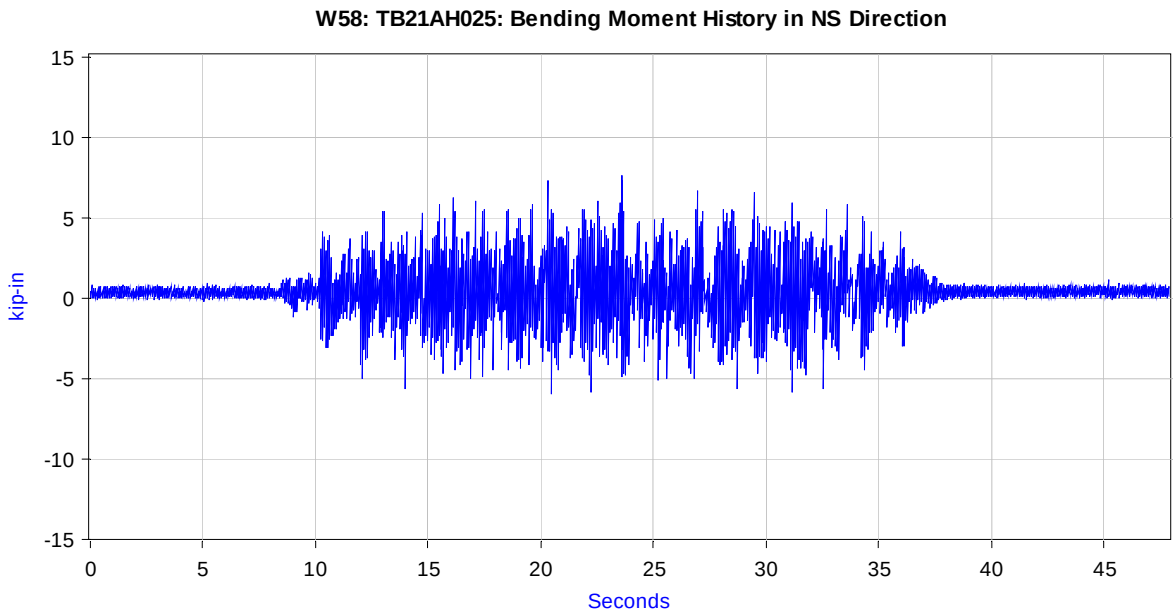

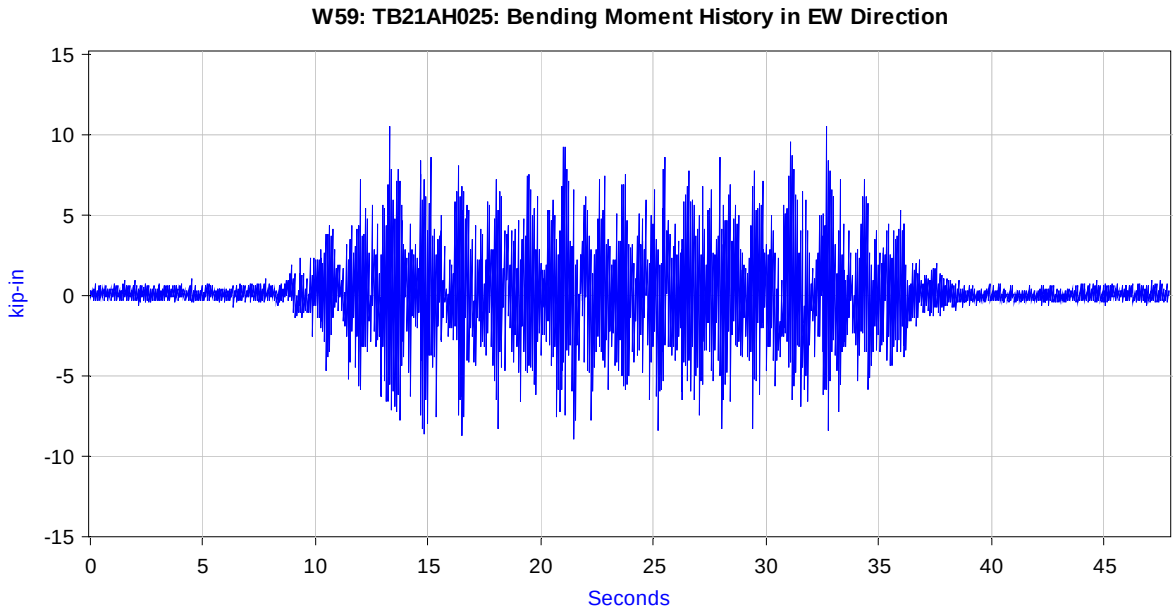

Figure D-148: Bending Moment of Bushing #6 in Horizontal Direction – Test TB21ah025

Figure D-149: Bending Moment of Bushing #6 in Horizontal Direction – Test TB24ah025

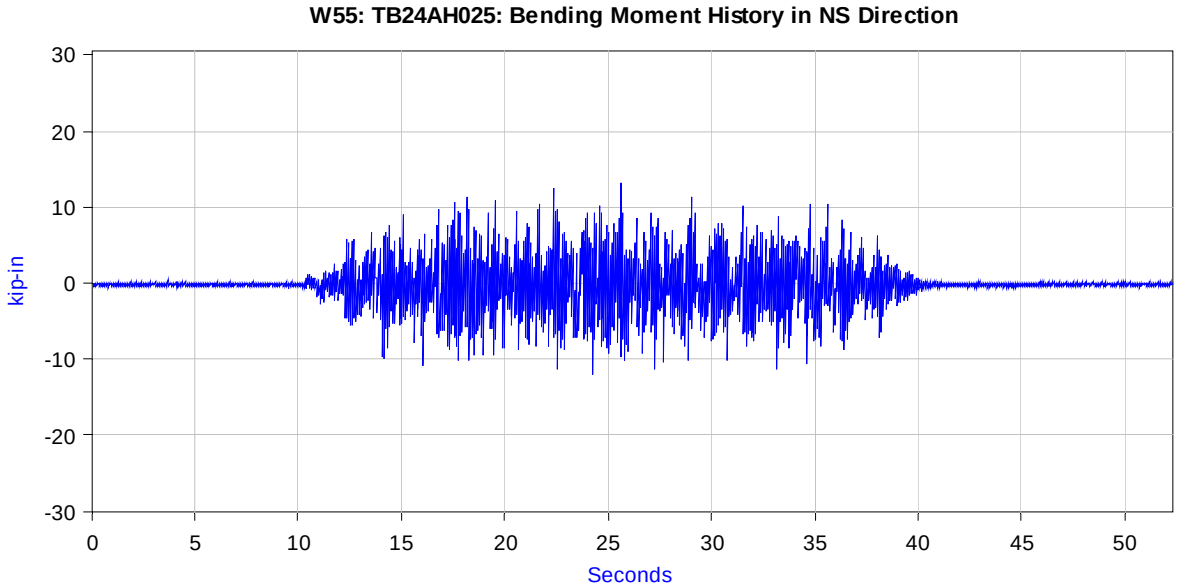

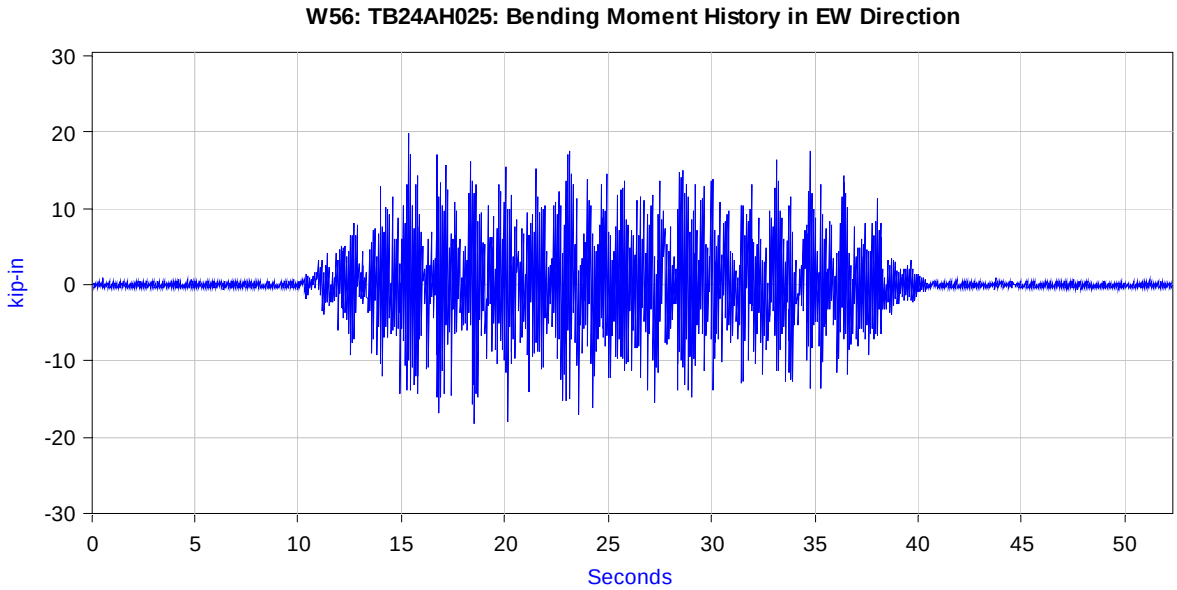

Figure D-150: Bending Moment of Bushing #6 in Horizontal Direction – Test TB27ah050

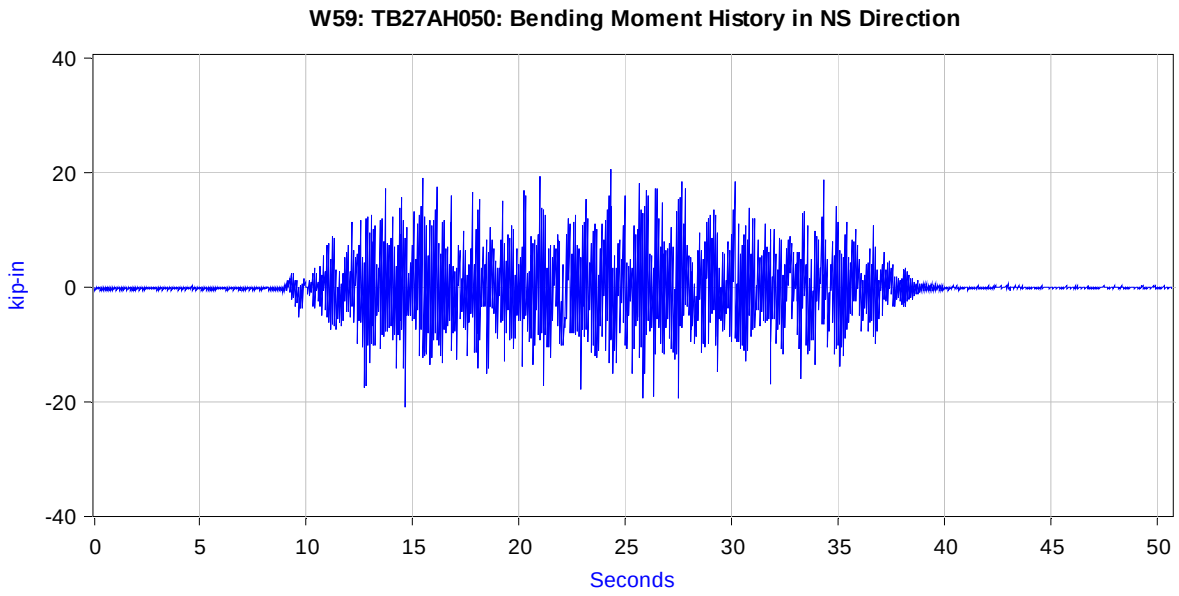

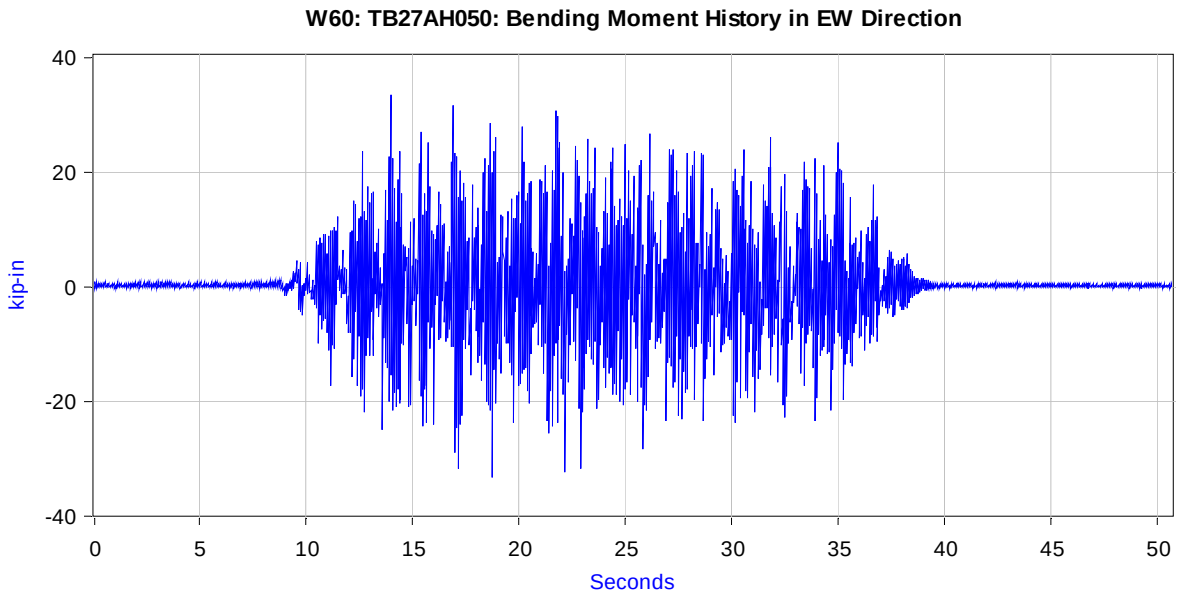

Figure D-150: Bending Moment of Bushing #6 in Horizontal Direction – Test TB30ah075

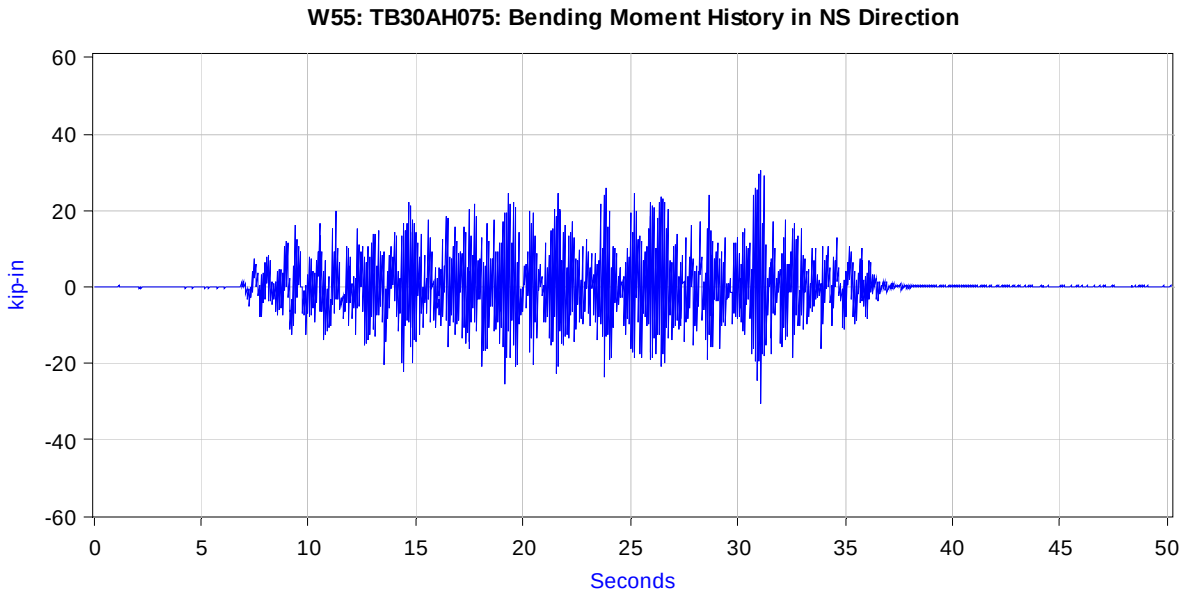

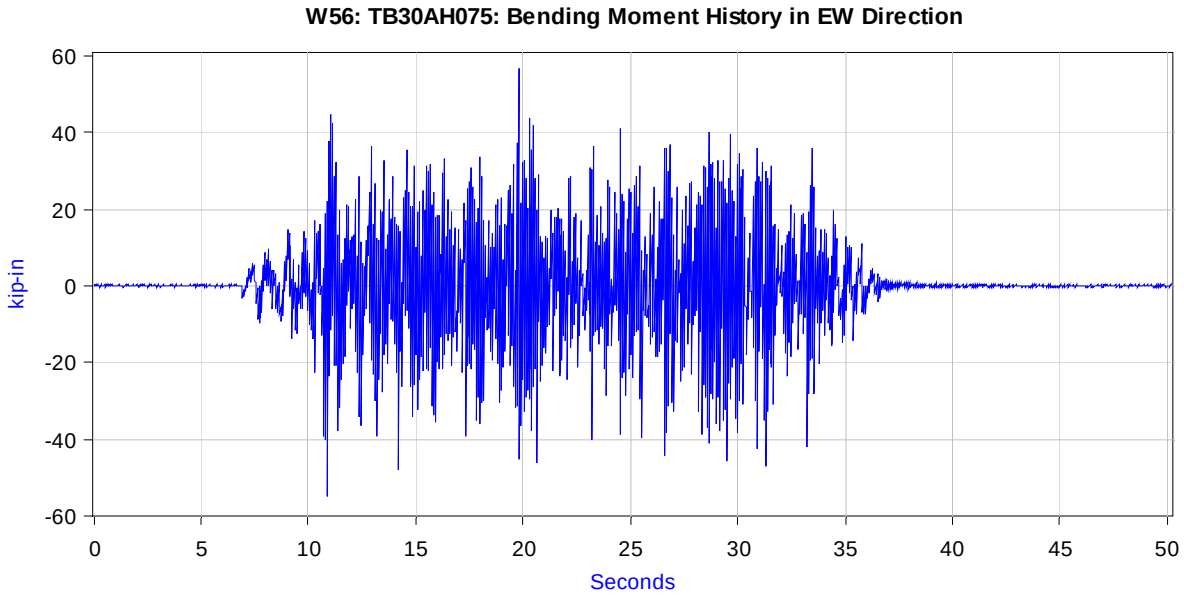

Figure D-151: Bending Moment of Bushing #6 in Horizontal Direction – Test TB33ah100

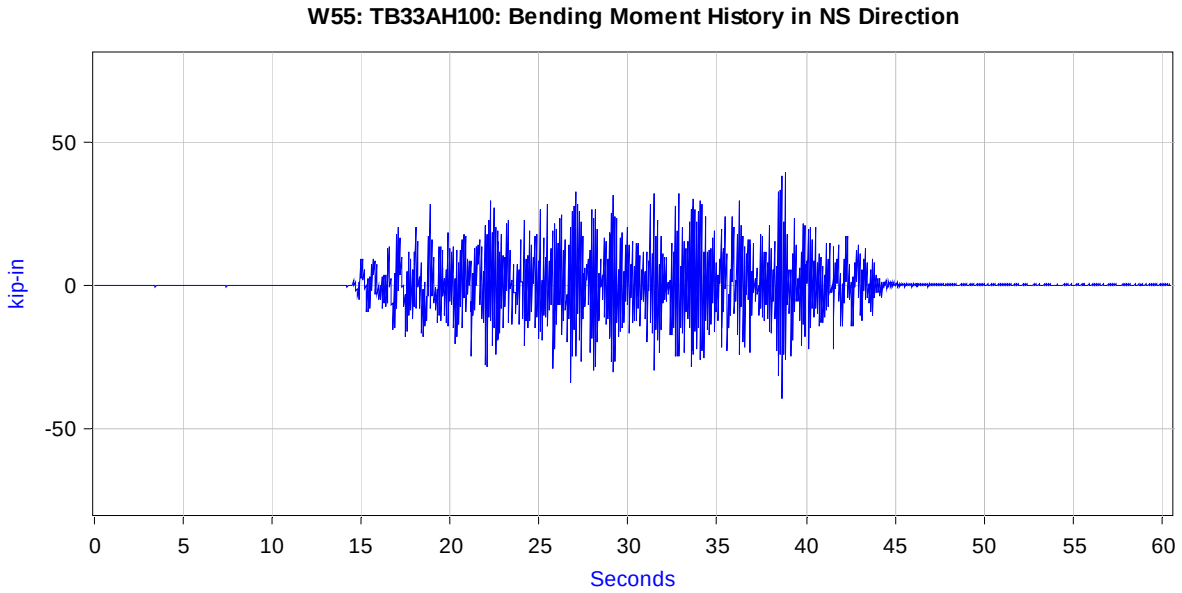

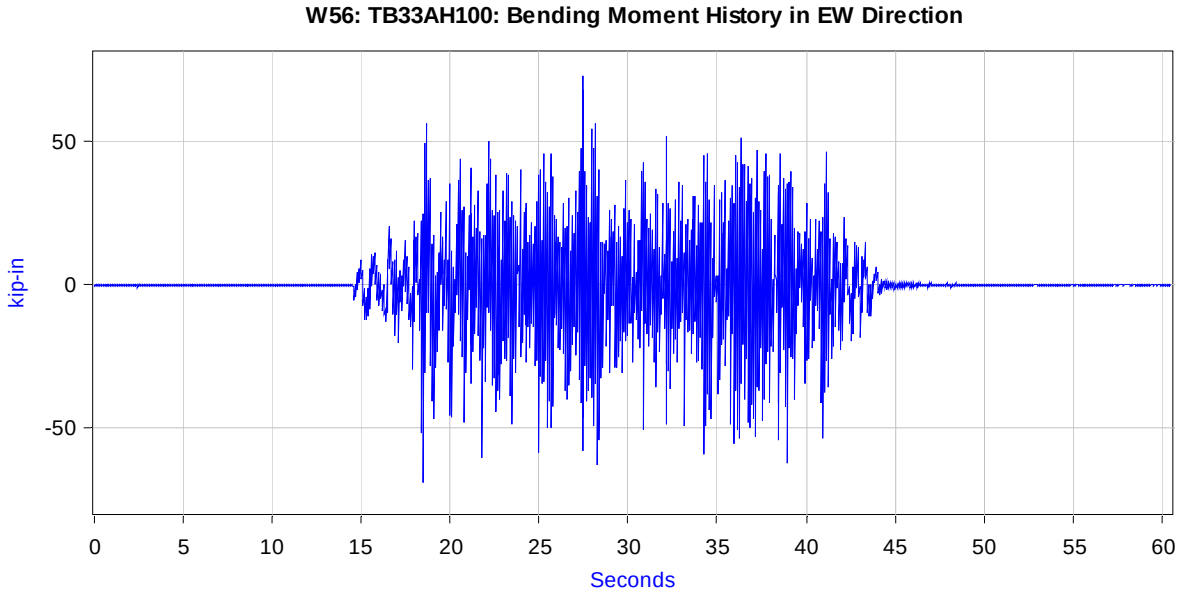

Figure D-152: Bending Moment of Bushing #6 in Horizontal Direction – Test TB38ah125

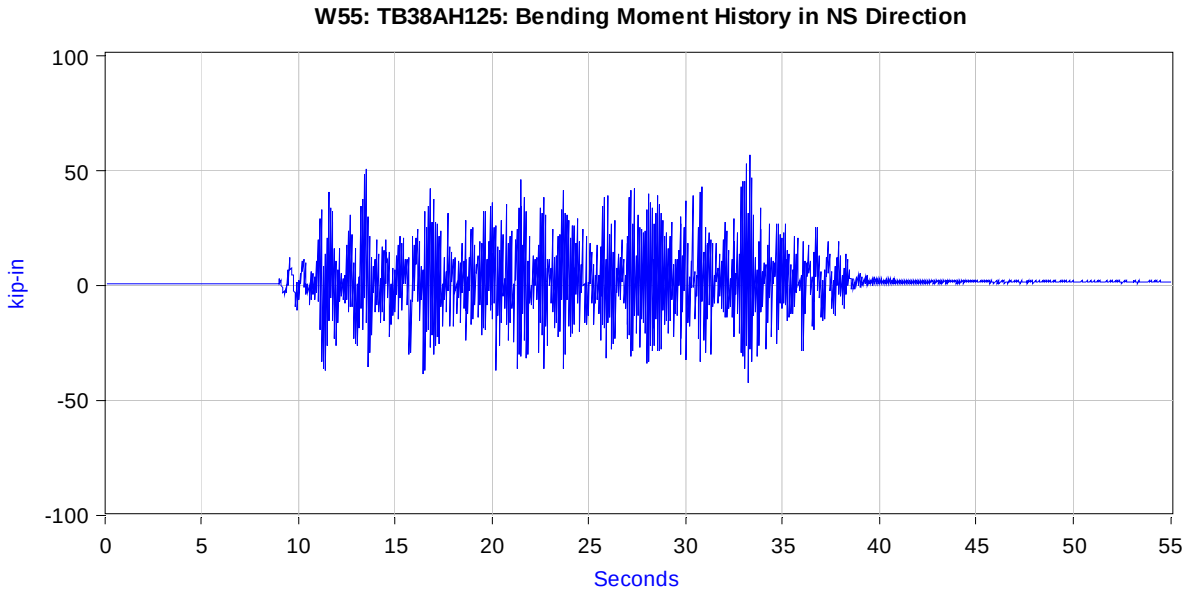

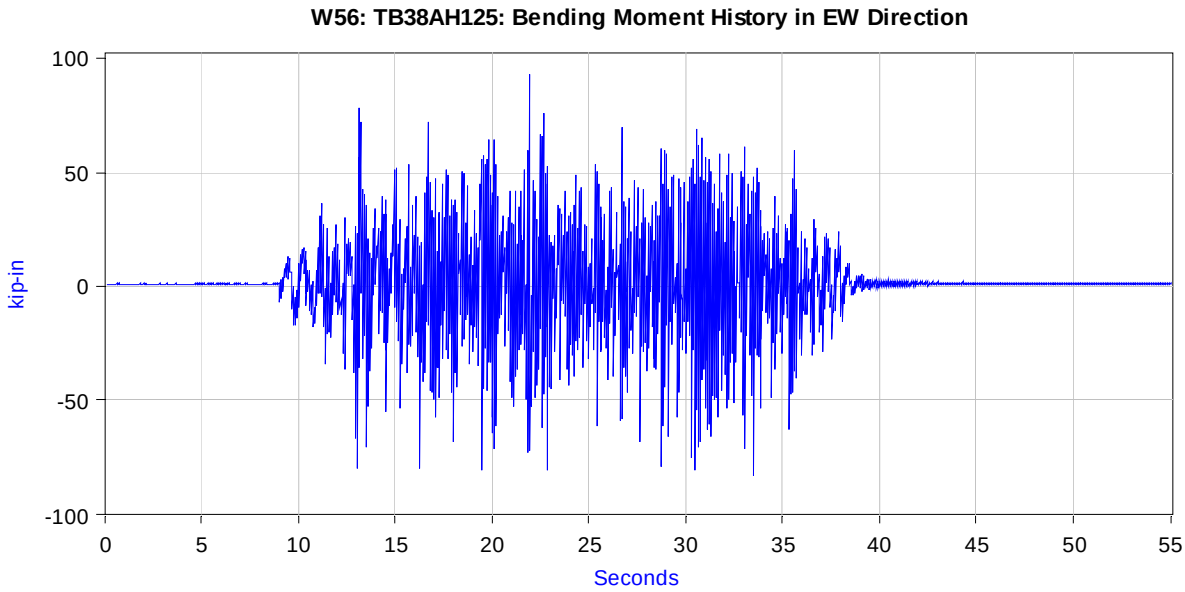

Figure D-153: Bending Moment of Bushing #6 in Horizontal Direction – Test TB41ah150

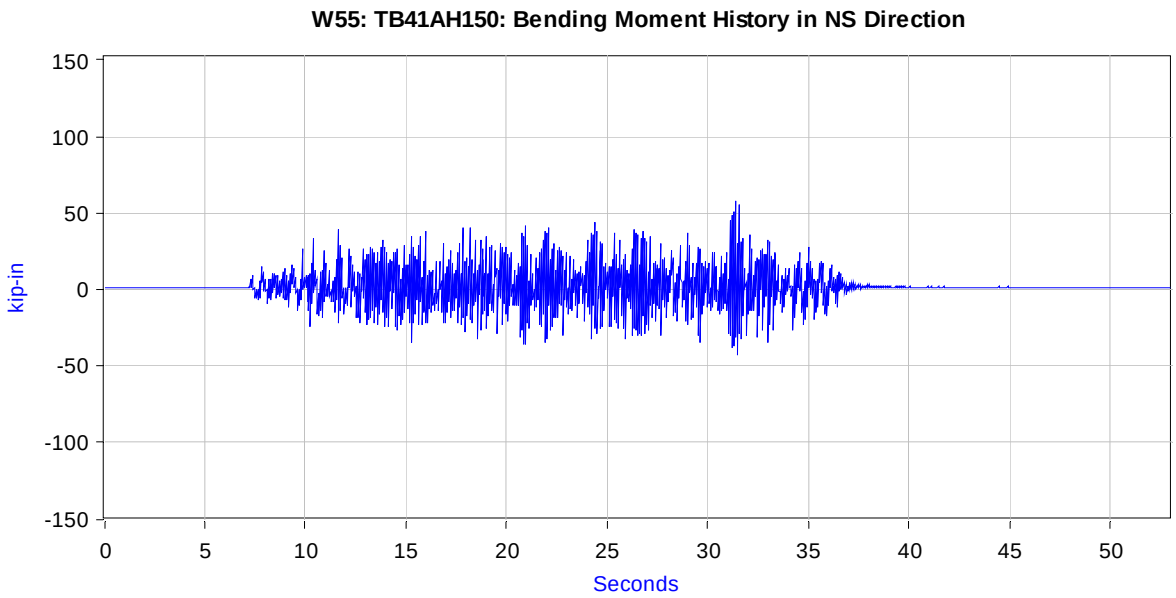

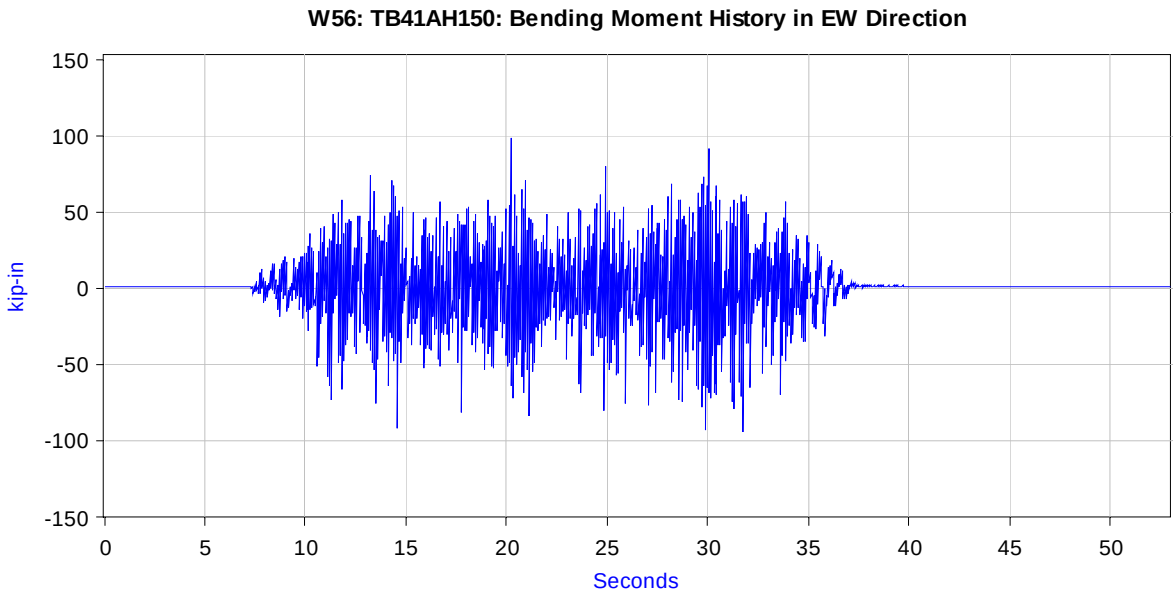

Figure D-154: Bending Moment of Bushing #6 in Horizontal Direction – Test TB44ah175

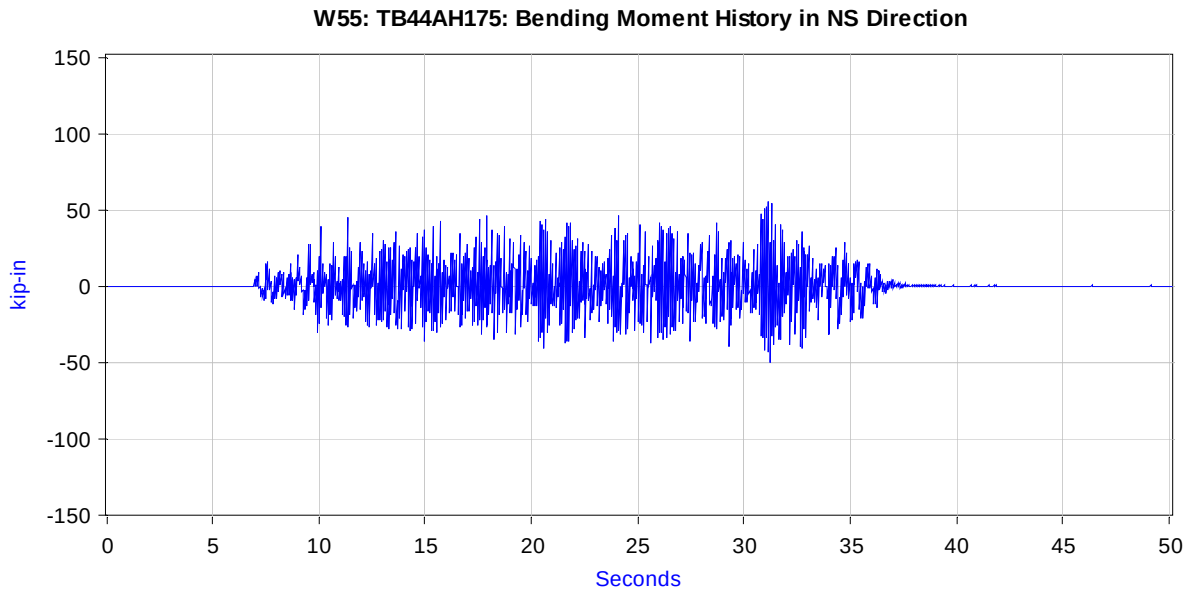

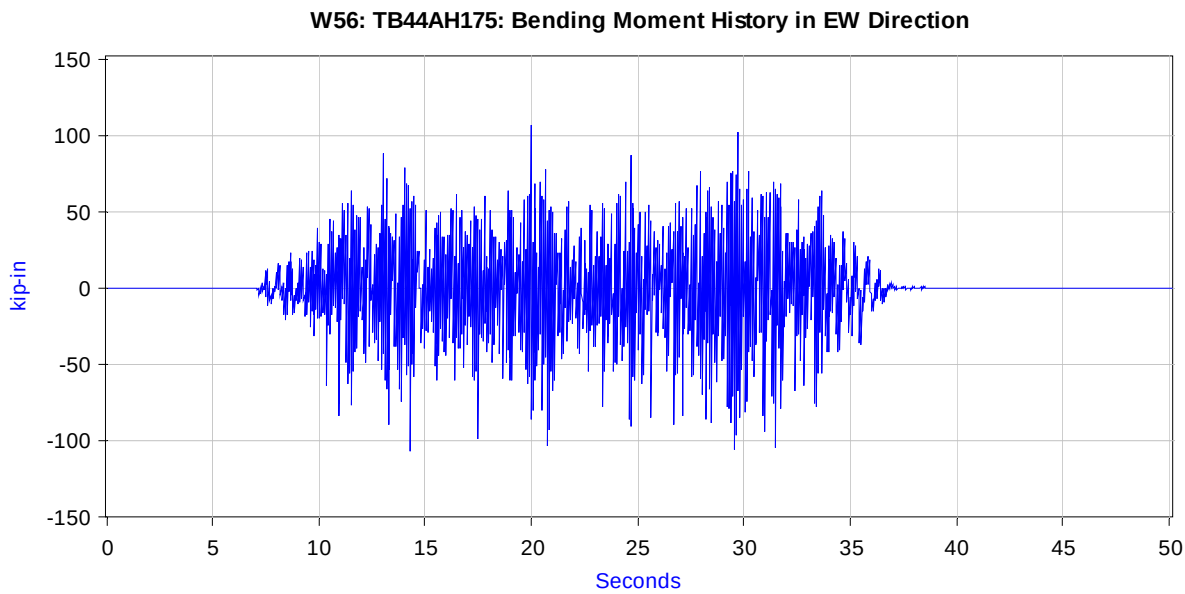

Figure D-155: Bending Moment of Bushing #6 in Horizontal Direction – Test TB47ah200

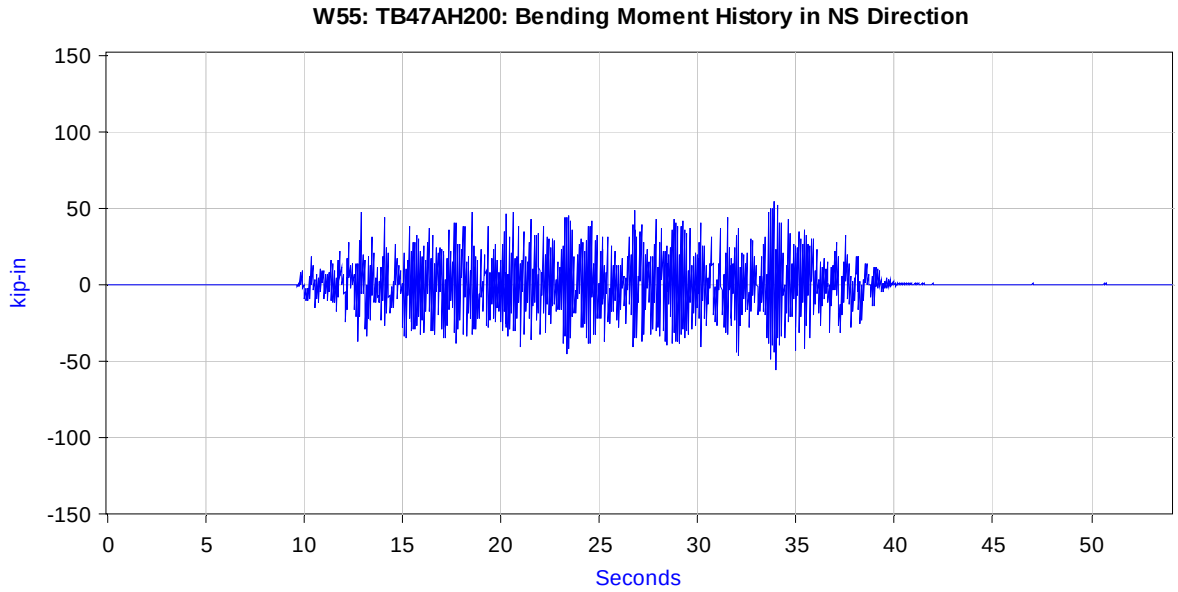

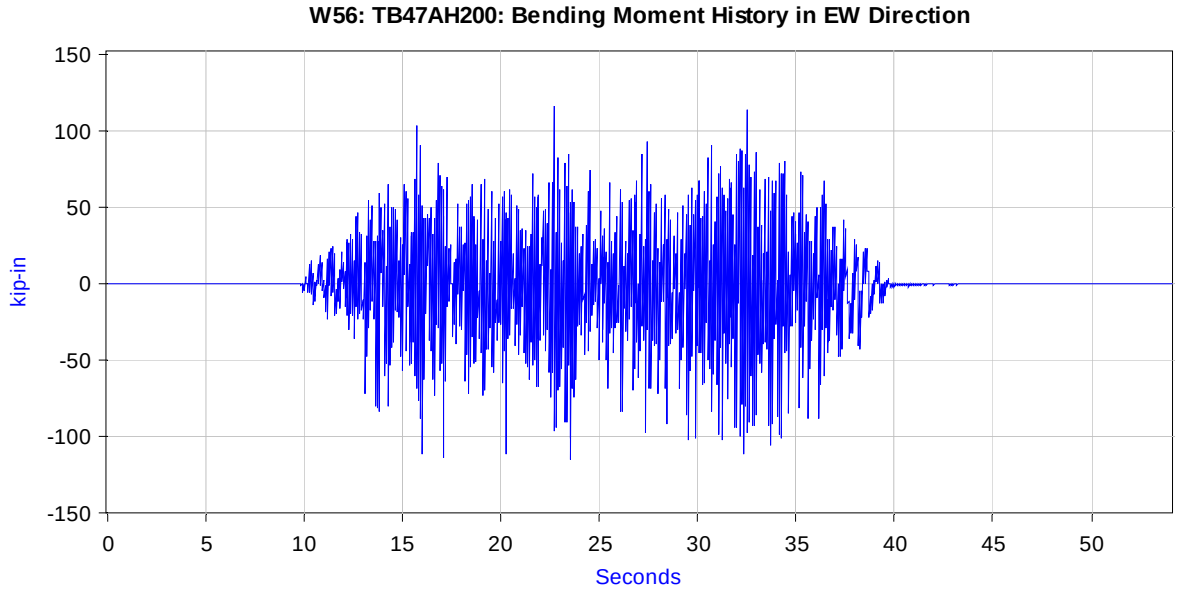

Figure D-156: Bending Moment of Bushing #6 in Horizontal Direction – Test TB50ah225

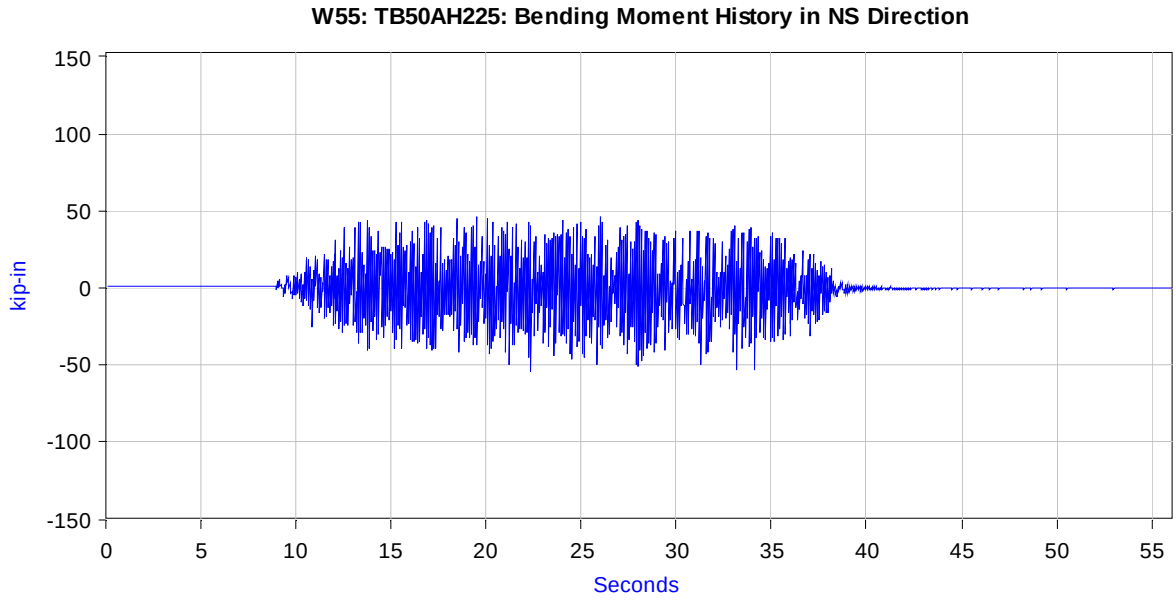

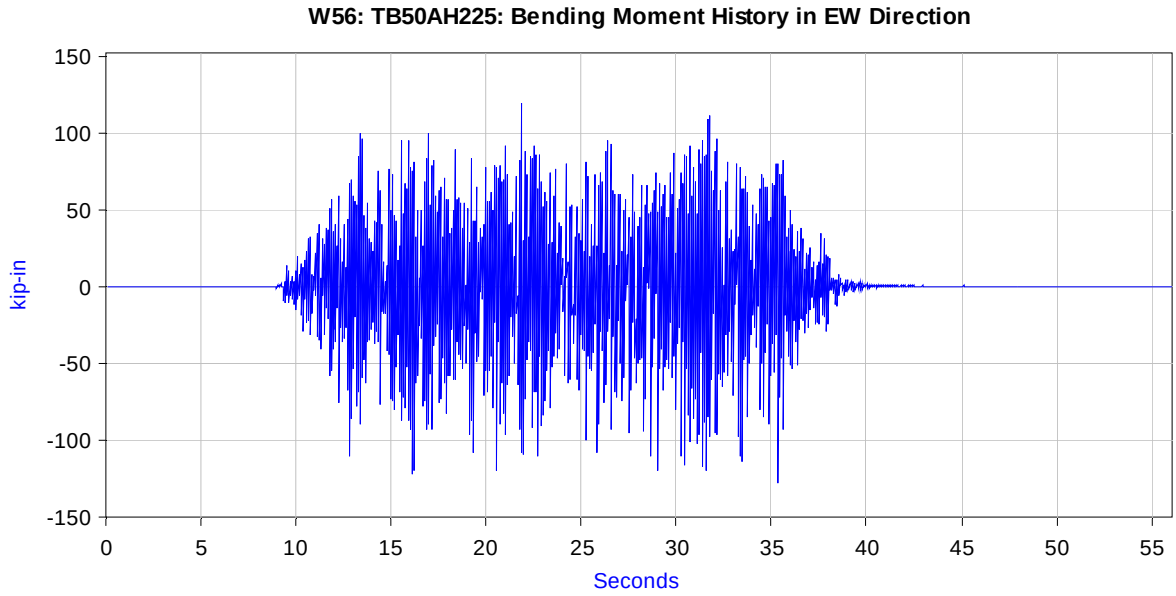

Figure D-157: Bending Moment of Bushing #6 in Horizontal Direction – Test TB30ah250

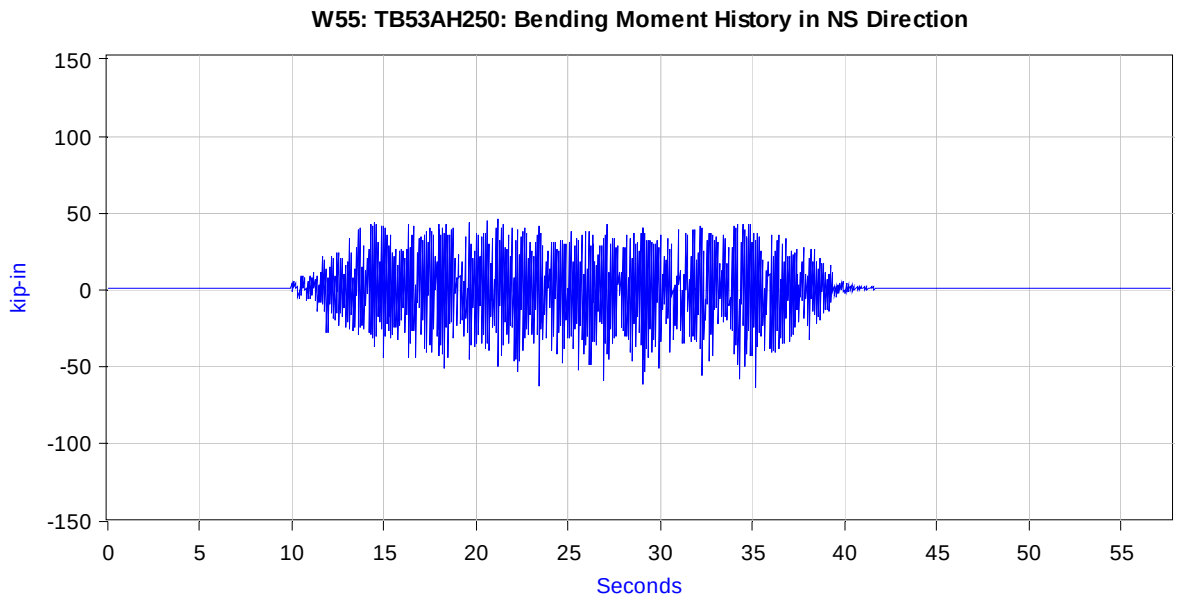

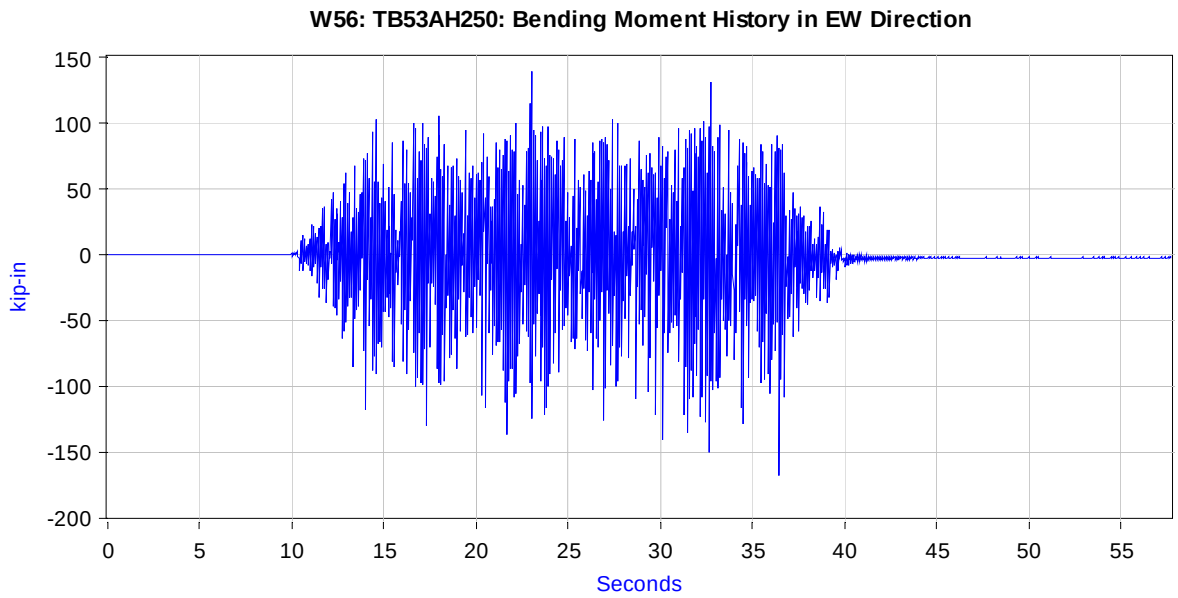

Figure D-158: Bending Moment of Bushing #6 in Horizontal Direction – Test TB56ah275

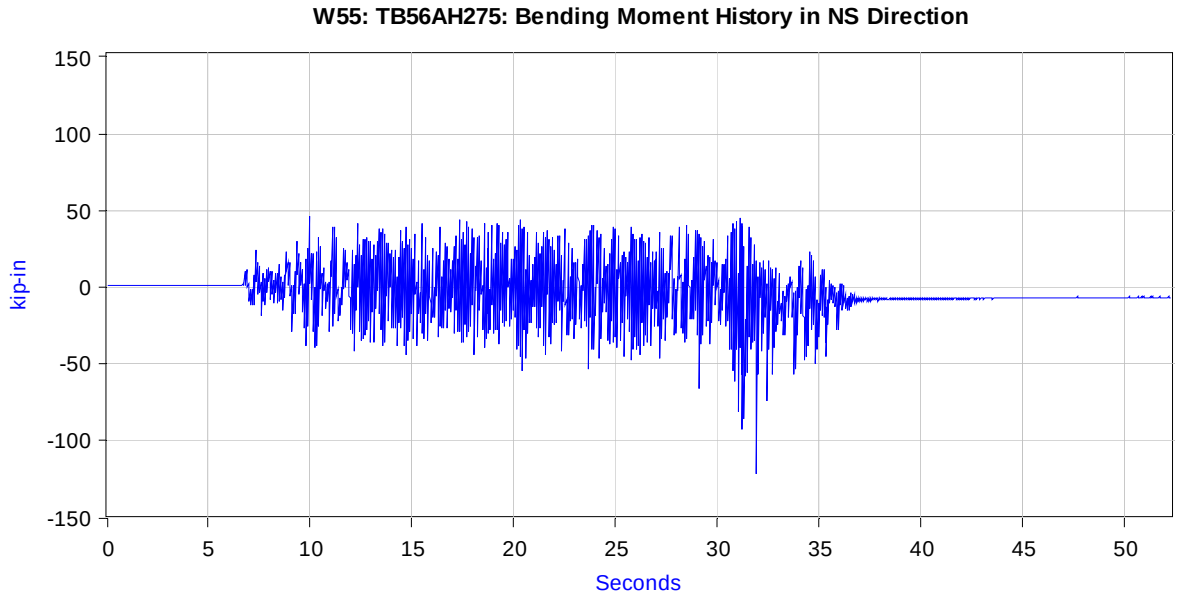

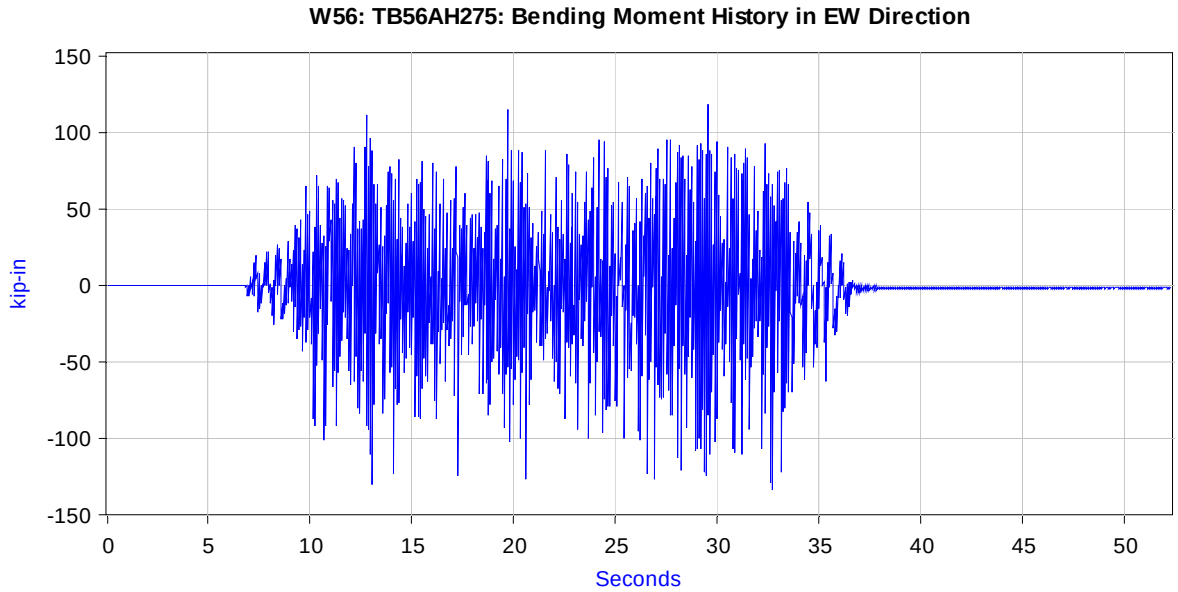

Figure D-159: Bending Moment of Bushing #6 in Horizontal Direction – Test TB62ah200

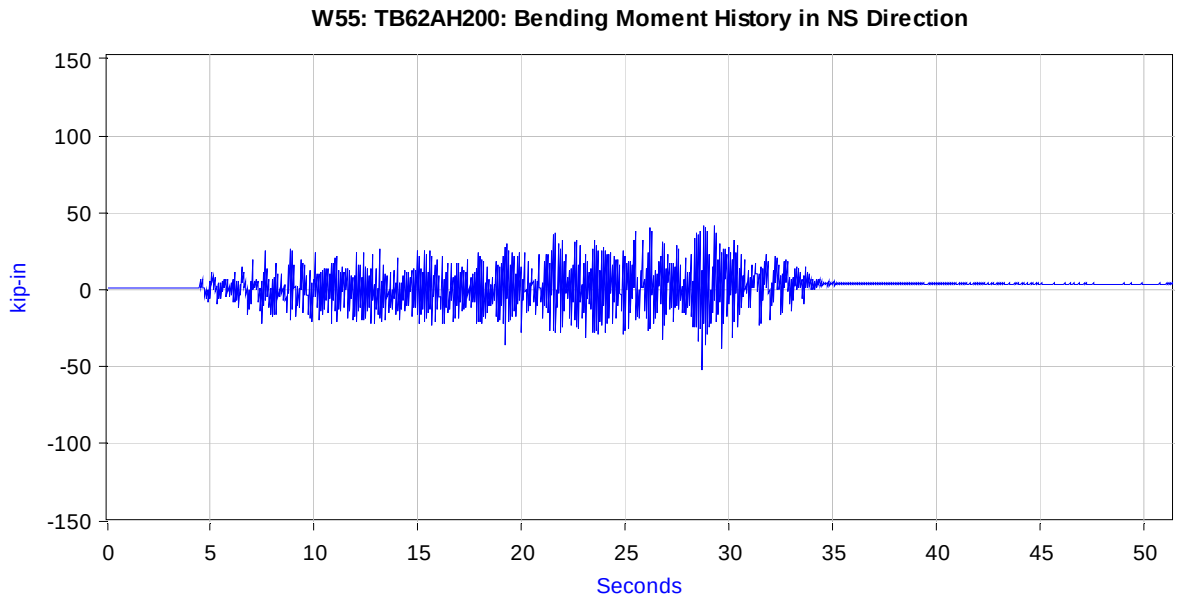

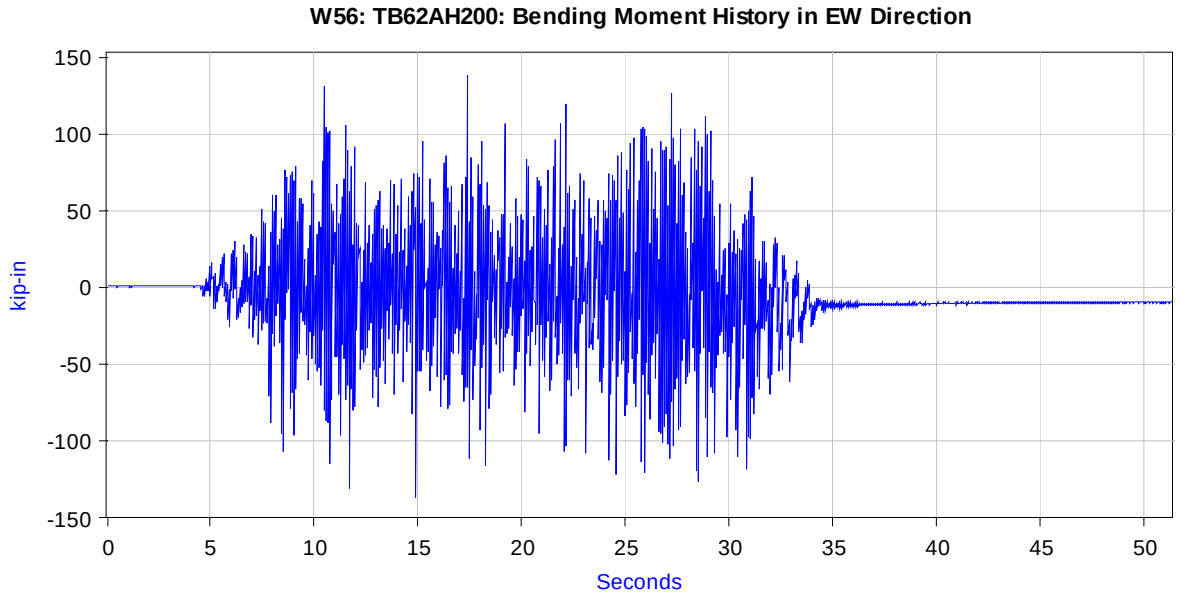

Figure D-160: Bending Moment of Bushing #6 in Horizontal Direction – Test TB65ah225

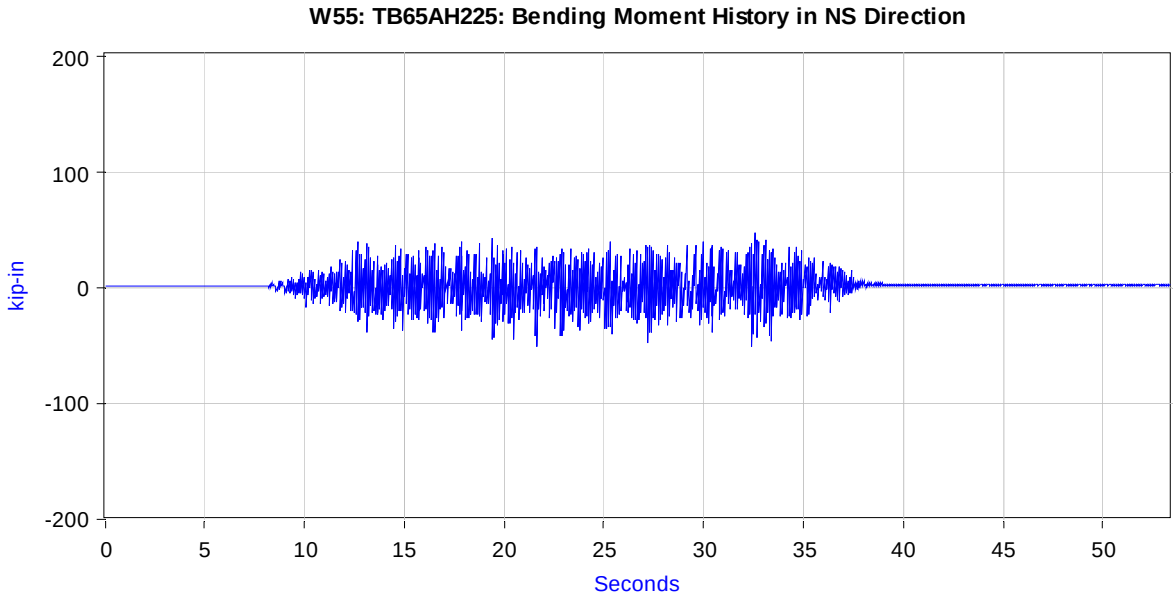

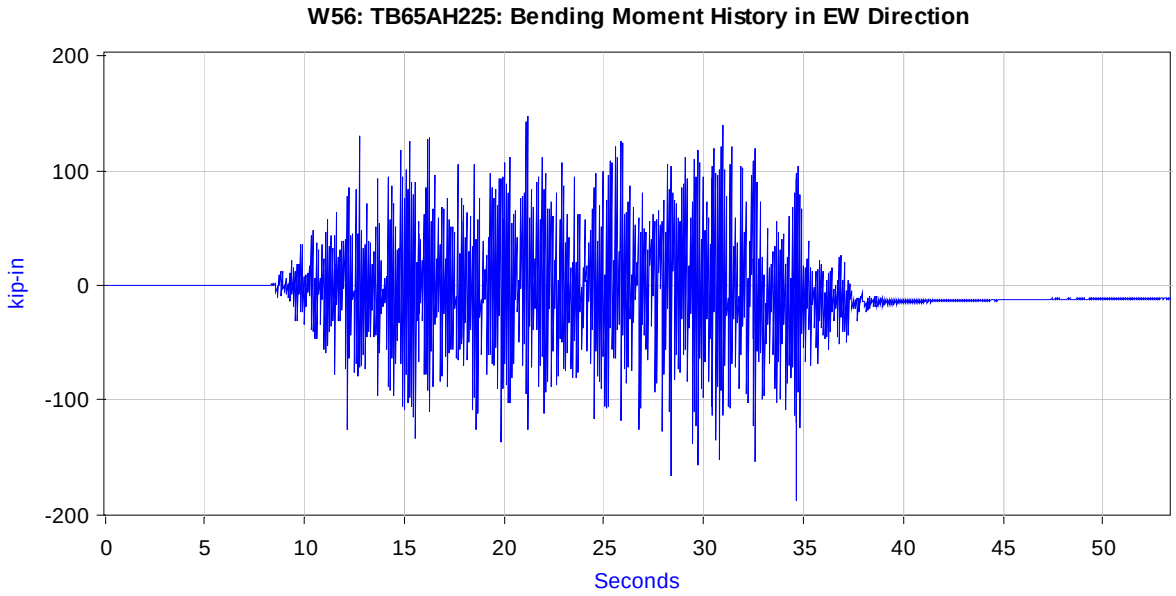

Figure D-161: Bending Moment of Bushing #6 in Horizontal Direction – Test TB68ah250

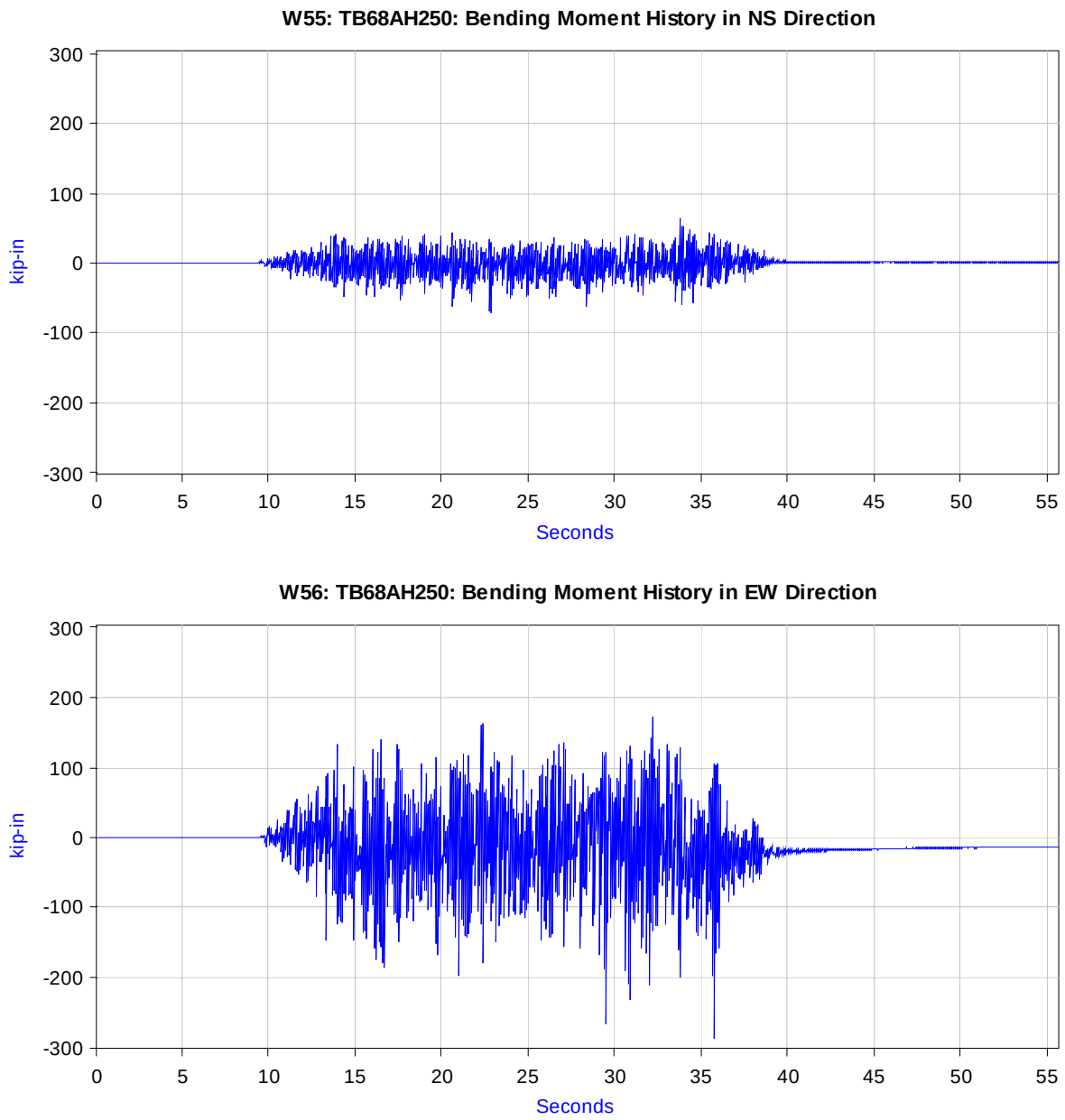

Figure D-162: Bending Moment of Bushing #6 in Horizontal Direction – Test TB71ah275

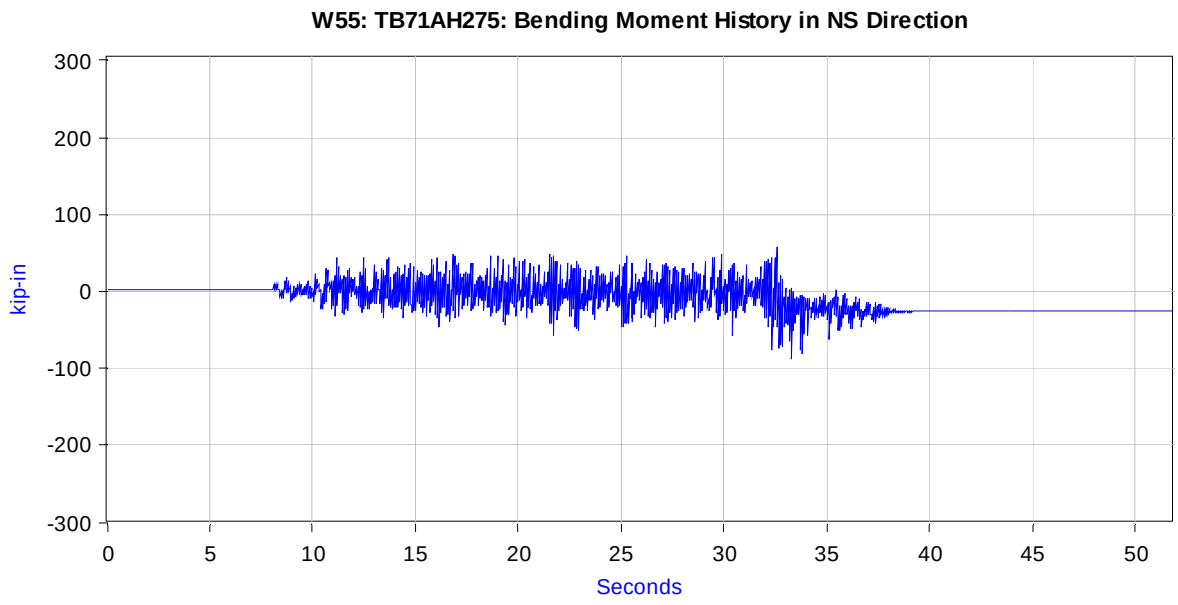

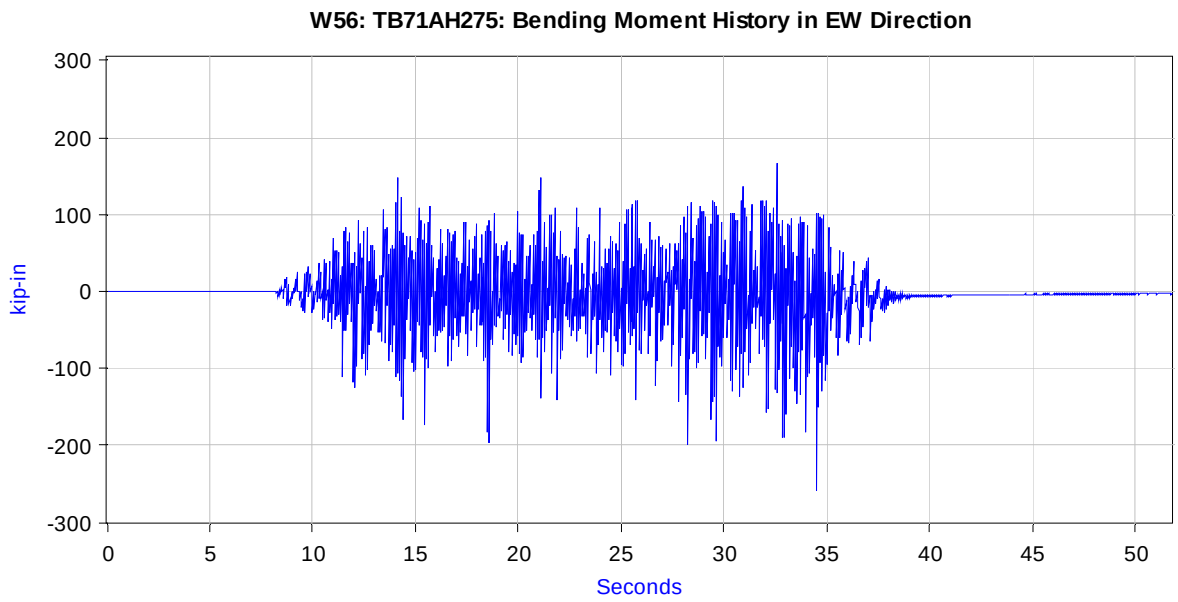

Failure Mode of Bushing #6

Bushing #6 was mounted on the center of the frame and excited to various earthquake intensities. The response of the bushing was measured for all tests and during the final test at 3.00 g RRS input motion, the bushing failed. The failure mode observed was the slipping of the porcelain unit with respect to the mounting flange accompanied with oil leakage (see Figures D-163 and D-164). The relative motion of the two parts was so great that the strain gauges could not record the actual strains and hence the demand for 3.00 g RRS could not be measured.

Figure D-163: Flange-Porcelain Interface Before Testing to 3.0 g RRS

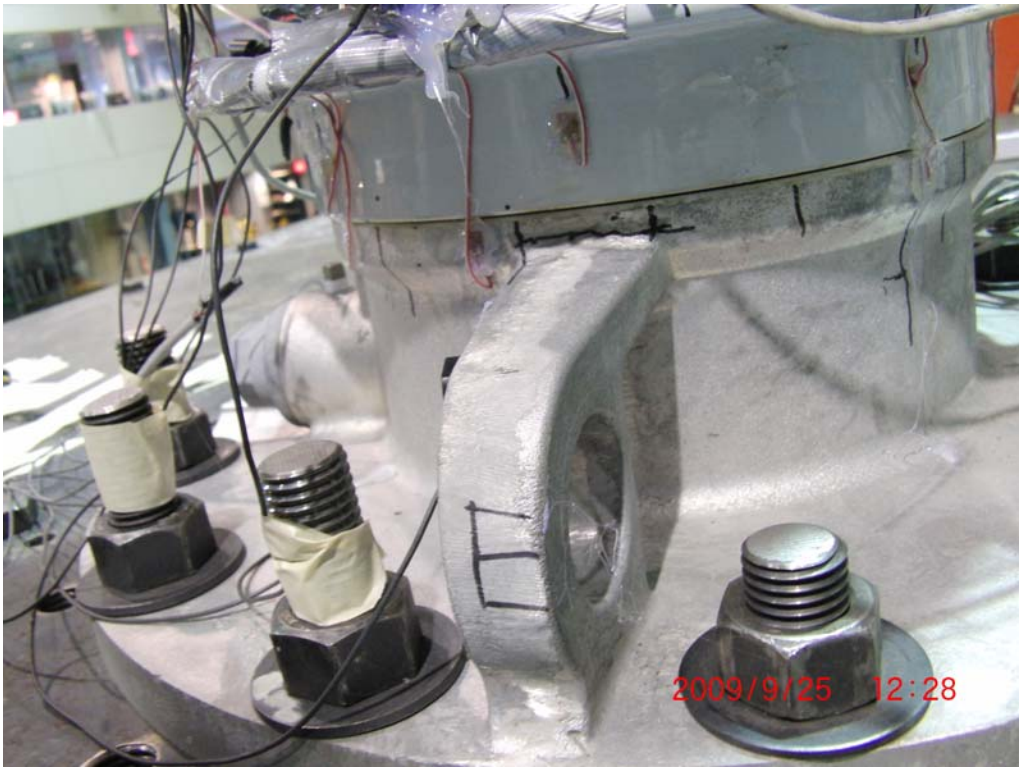

Figure D-164: Flange-Porcelain Interface After Testing to 3.0 g RRS

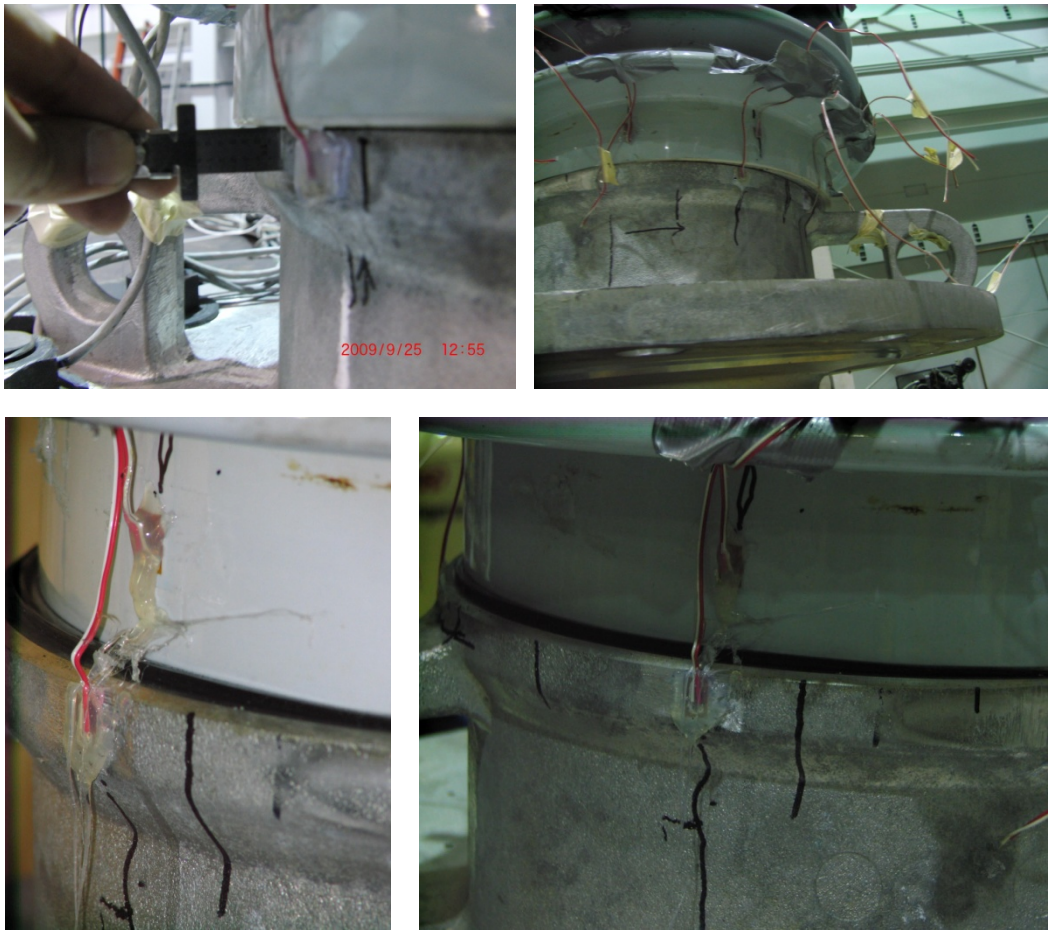

Identification of Properties of Bushing #7

Identification of Properties with Additional Conductor Weight

Impact Hammer Testing

Impact hammer tests were used to find the frequency and damping ratio of Bushing #7. A 25 lb. weight was mounted at the top of the bushing, simulating a portion of cable near the bushing top that might play a role in the bushing response. Minimum frequency was observed in the NS direction at 9.33 Hz with a damping ratio of 2.39%; in the EW Direction the frequency was 9.32 Hz with a damping ratio of 3.22%. Table D-9 shows detailed frequencies, damping ratios and the direction in which tests were run. A Power Spectral Density (PSD) of the free vibration response gave the frequency of the bushing, and the logarithmic decrement method was used to find the damping ratio. The results of the tests are shown in Figures D-165 through D-168.

Table D-10: Dynamic Properties of Bushing #7 from Various Tests

Test No.	Frequency			Damping			Max Displacement	Force	Stiffness
Units	(Hz)			(%)			(in)	(lb)	(lb/in)
(1)	(2)	(3)	(4)	(5)	(6)	(7)	(8)	(9)	(10)
Direction	NS	EW	Vertical	NS	EW	Vertical			
Impact Hammer Test –Fixed base									
TB14NSIH	9.33	-	-	2.39	-	-	-	-	-
TB16EWIH	-	9.32	-	-	3.22	-	-	-	-
TB35NSIH	9.48	-	-	4.18	-	-	-	-	-
TB37EWIH	-	8.99	-	-	2.58	-	-	-	-
Quick Release Test - Fixed Base									
TB12PL100EW	-	-	-	-	-	-	-	-	-
TB13PL100NS	-	-	-	-		-	0.04	0.13	3.05
TB17PL300EW	-	9.14	-	-	3.38	-	0.08	0.25	3.17
TB21PL450EW	-	9.13	-	-	3.66	-	0.13	0.46	3.42
TB25PL600EW	-	8.98	-	-	3.06	-	0.19	0.60	3.15
TB29PL900EW	-	8.74	-	-	3.91	-	0.33	0.93	2.81
TB33PL900EW	-	-	-	-		-	-	-	-
TB34PL900NS	-	-	-	-	-	-	0.09	0.92	10.19
White Noise Test									
TB45WN	2.50	2.50	-	7.66	8.79	-	-	-	-
TB48WN	2.50	2.50	-	6.59	5.19	-	-	-	-
TB51WN	2.50	2.50	-	5.39	4.88	-	-	-	-
TB54WN	2.50	2.50	-	6.73	4.93	-	-	-	-
TB57WN	2.50	2.50	-	7.80	4.85	-	-	-	-
TB60WN	2.50	2.50	-	7.52	4.79	-	-	-	-
TB63WN	2.50	2.50	-	6.07	4.81	-	-	-	-
TB67WN	2.50	2.50	-	6.58	4.78	-	-	-	-
TB70WN	2.50	2.50	-	6.02	4.83	-	-	-	-
TB73WN	2.50	2.50	-	6.20	4.83	-	-	-	-
TB76WN	2.50	2.50	-	5.78	4.95	-	-	-	-
Table Impulse Test									
TB46TBI	-	-	-	-	-	-	-	-	-
TB49TBI	-	-	-	-	-	-	-	-	-
TB52TBI	2.55	2.58	-	2.98	3.00	-	-	-	-
TB55TBI	2.54	2.56	-	2.98	3.00	-	-	-	-
TB58TBI	2.54	2.56	-	2.70	3.00	-	-	-	-
TB61TBI	2.52	2.55	-	2.70	3.42	-	-	-	-
TB65TBI	2.57	2.54	-	2.75	3.42	-	-	-	-
TB68TBI	2.52	2.57	-	2.57	3.00	-	-	-	-
TB71TBI	2.50	2.50	-	2.80	3.00	-	-	-	-
TB74TBI	2.50	2.50	-	2.80	2.50	-	-	-	-
TB77TBI	2.50	2.47	-	2.75	2.52	-	-	-	-

Figure D-165: Acceleration Response of Bushing 7, with 25 lb. Mass, in NS Direction

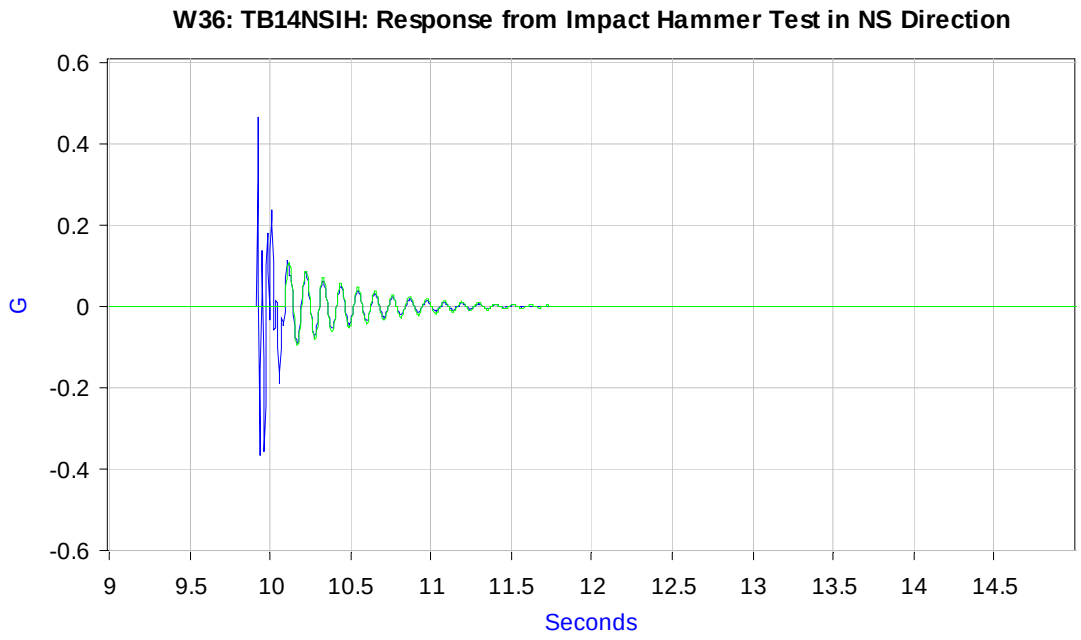

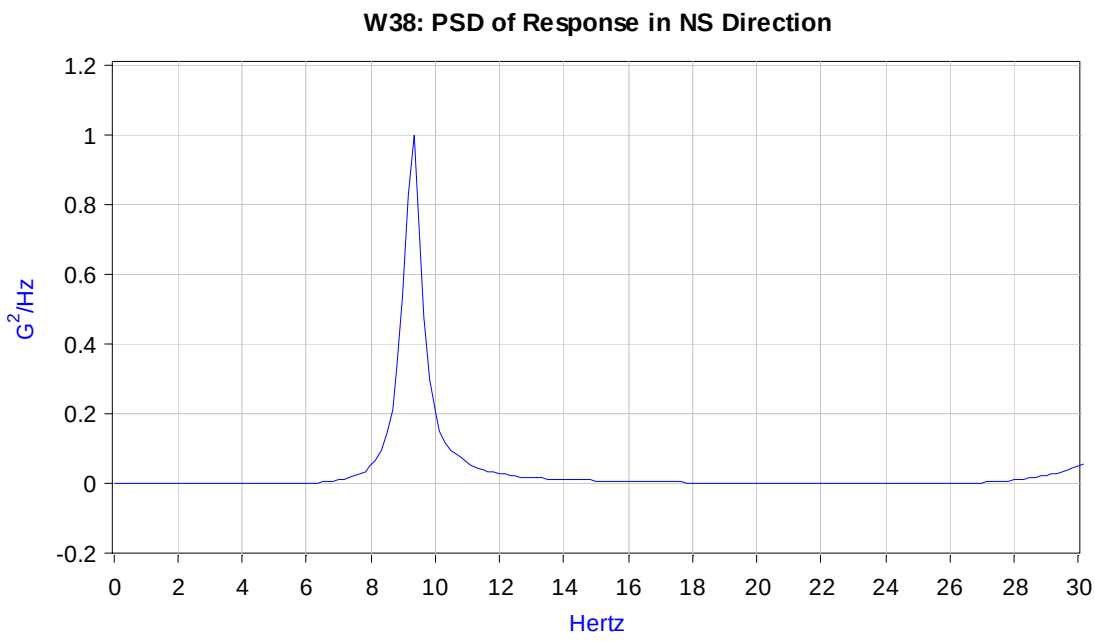

Figure D-166: Acceleration Response of Bushing 7, with 25 lb. Mass, in EW Direction

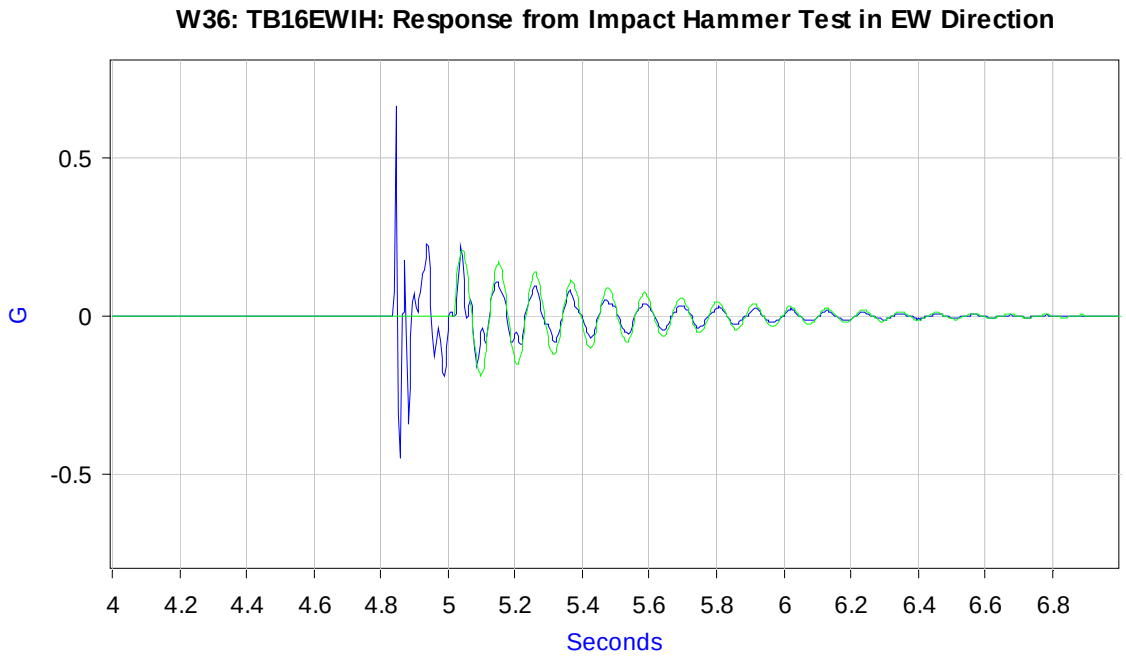

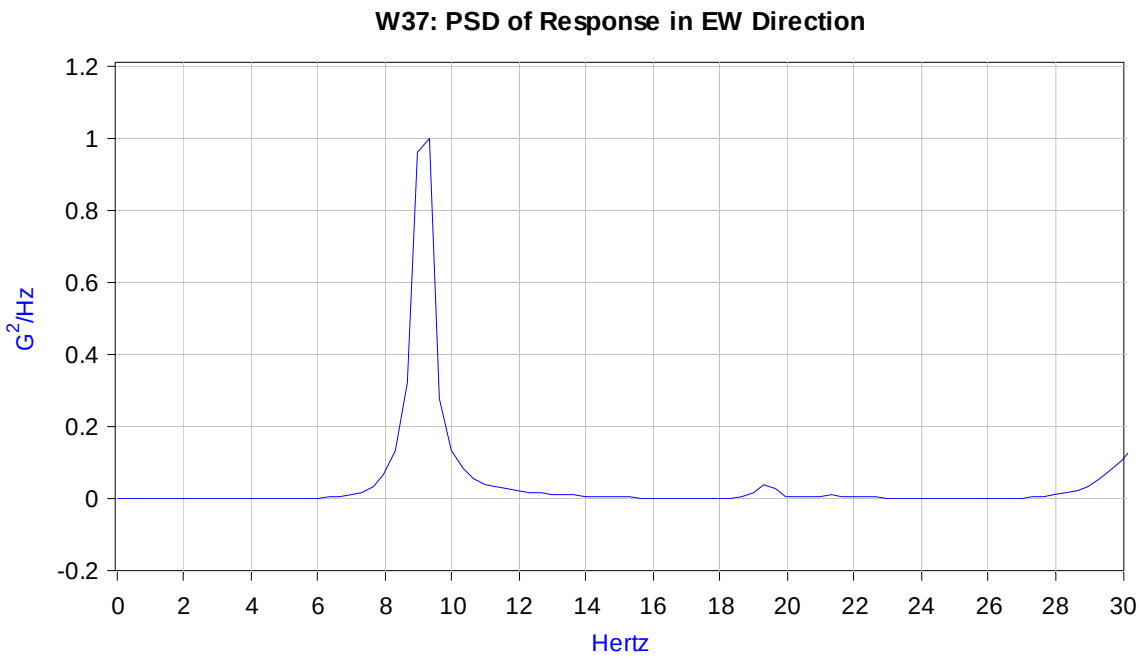

Figure D-167: Acceleration Response of Bushing 7, with 25 lb. Mass, in NS Direction

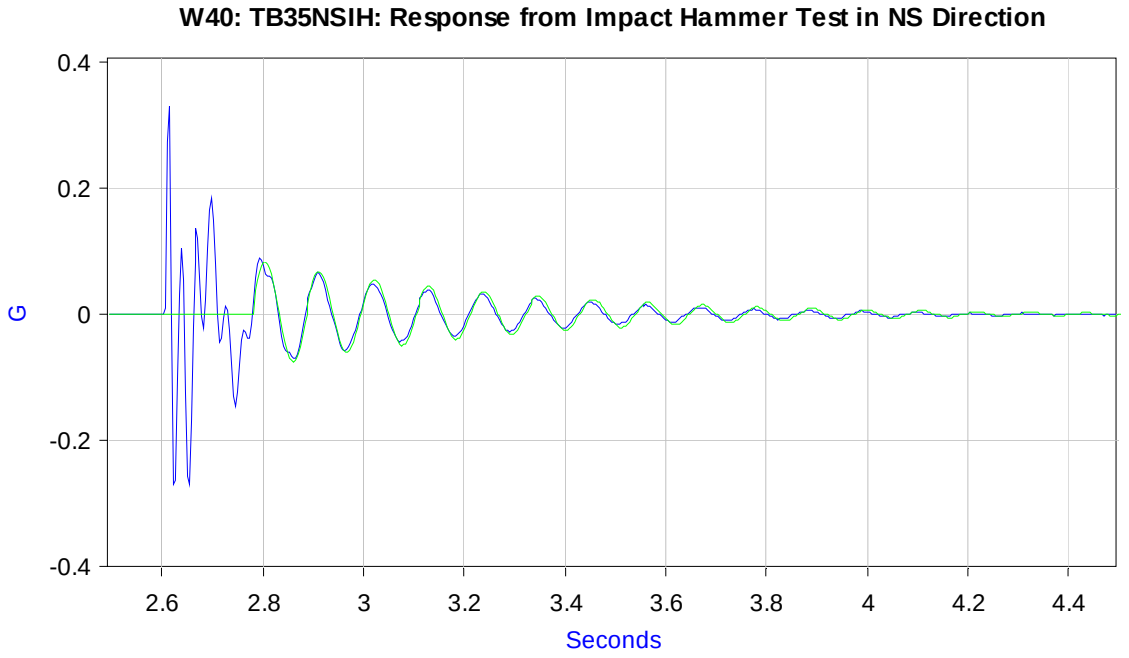

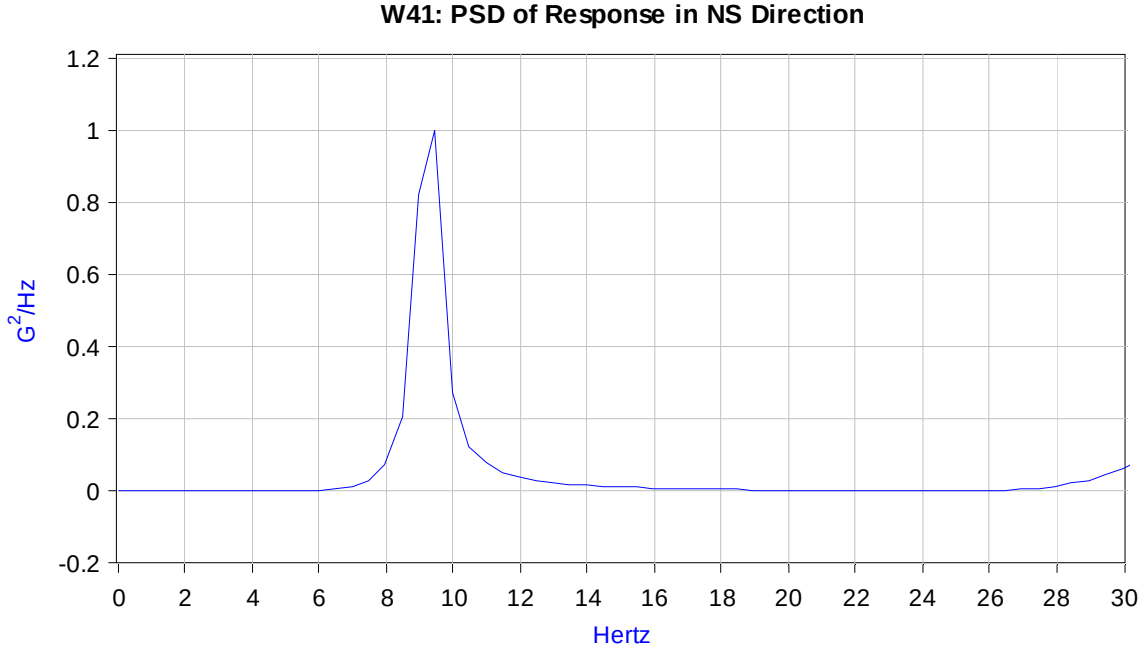

Figure D-168: Acceleration Response of Bushing 7, with 25 lb. Mass, in EW Direction

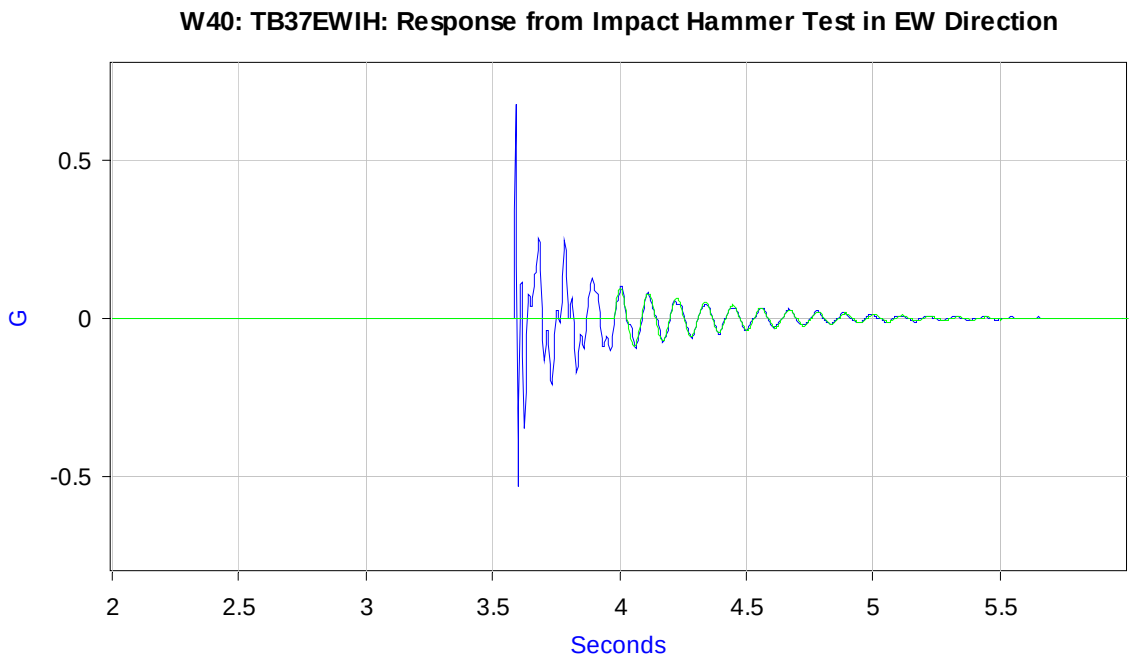

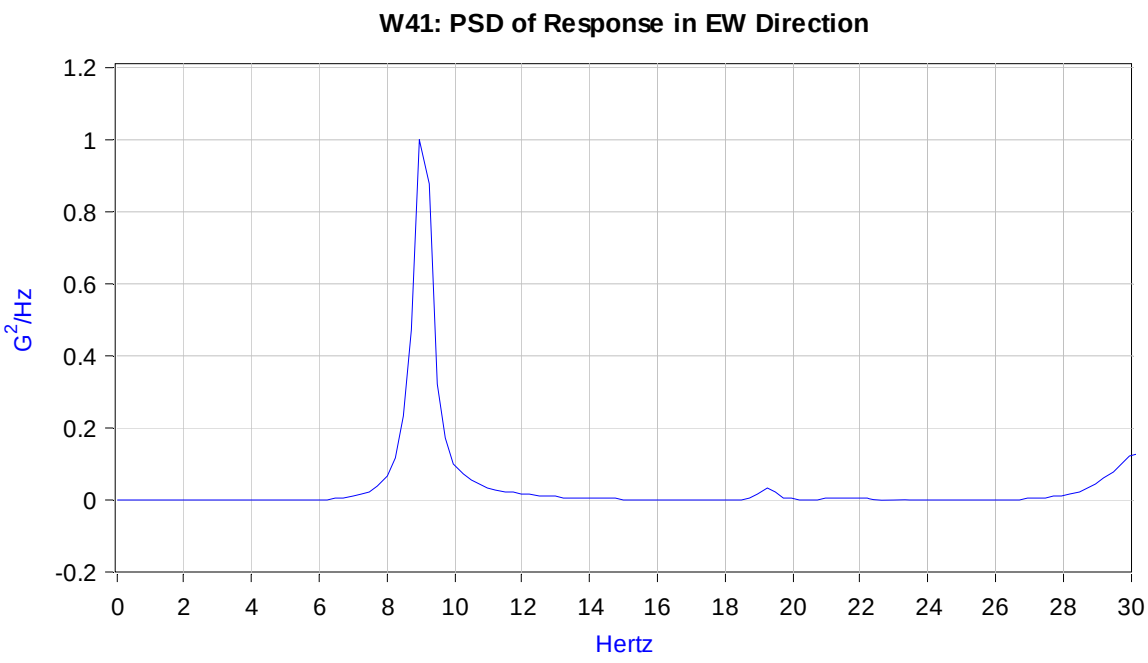

Pull and Sudden Release Tests

In these tests, Bushing #4A was pulled from the top and released suddenly, allowing the stiffness of the bushing and the frequency and damping ratio to be determined in a more detailed way. All the pull tests were run in the EW direction only. The stiffness varied between maximum values of 779 lb./in. to 658 lb./in. Table D-9 and Figures D-169 through D-172 show the acceleration responses, frequencies and corresponding damping ratios. Figure 173 shows the maximum displacement of the bushing as a function of the maximum force applied.

Figure D-169: Acceleration Response from Quick Release Test TB17pl300ew – Bushing #7

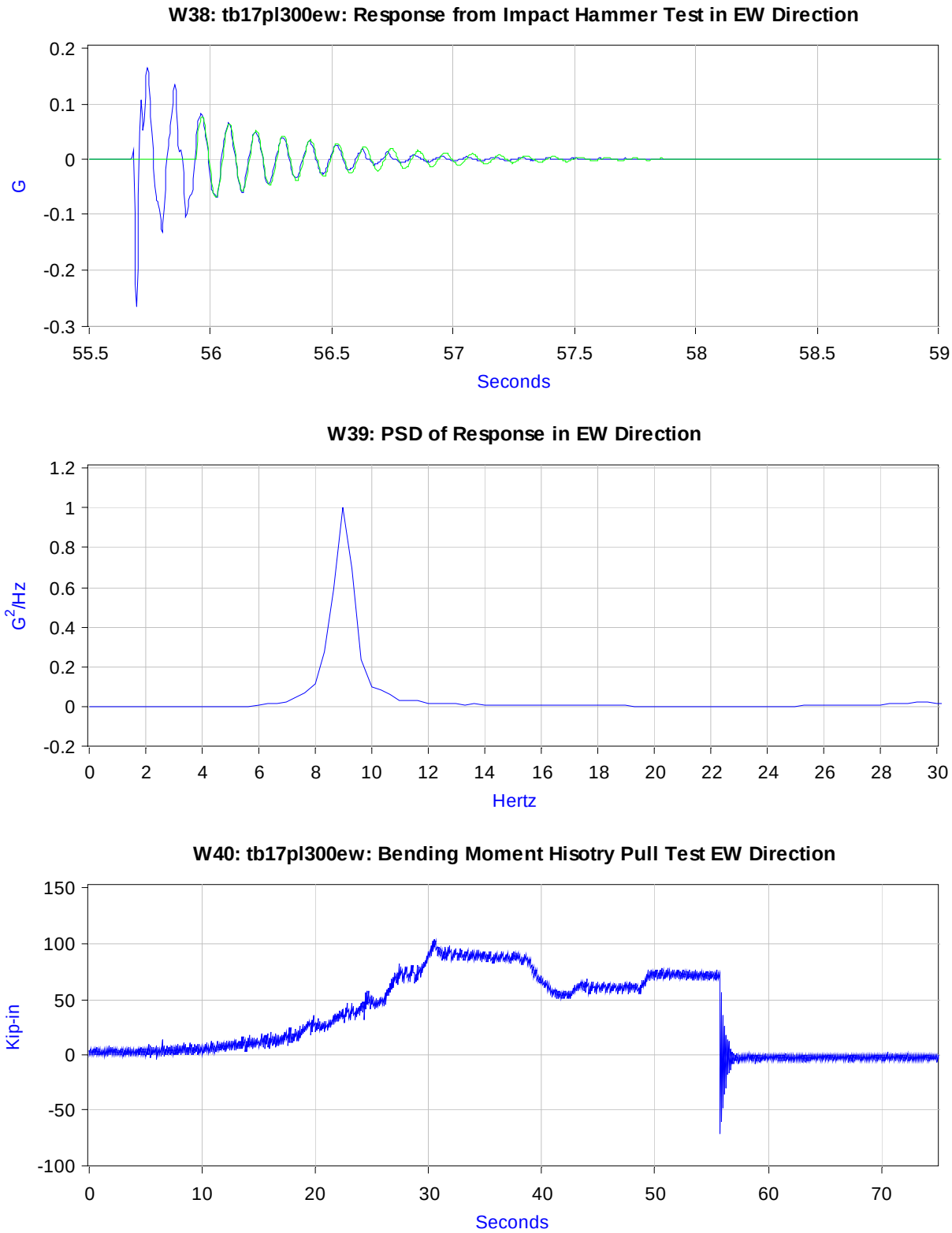

Figure D-170: Acceleration Response from Quick Release Test TB21pl450ew – Bushing #7

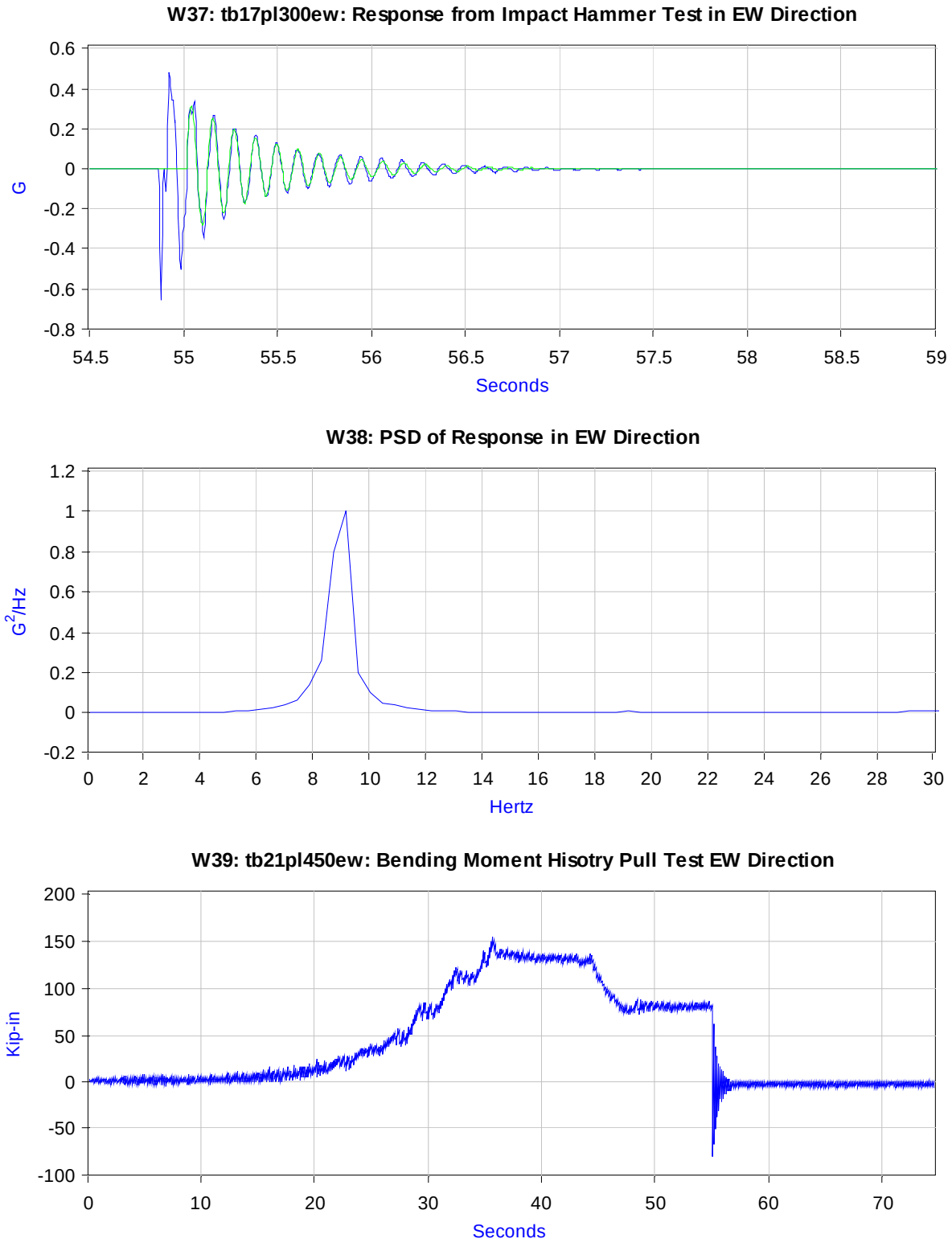

Figure D-171: Acceleration Response from Quick Release Test TB25pl600ew – Bushing #7

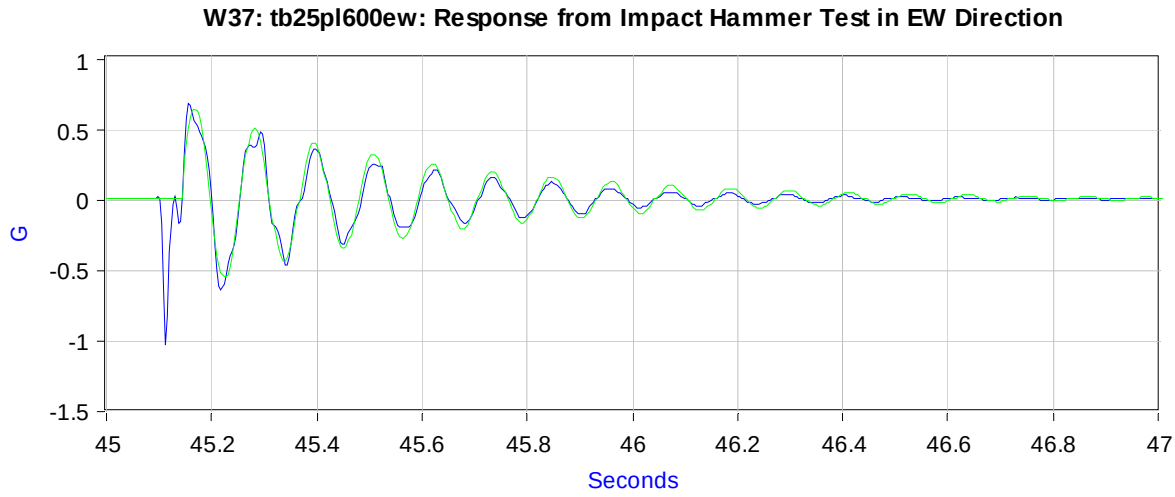

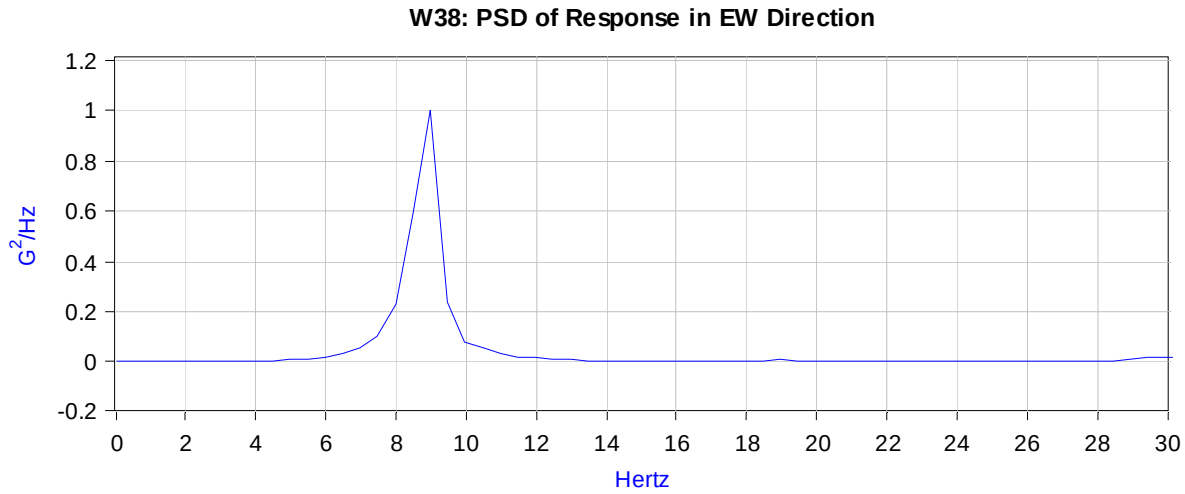

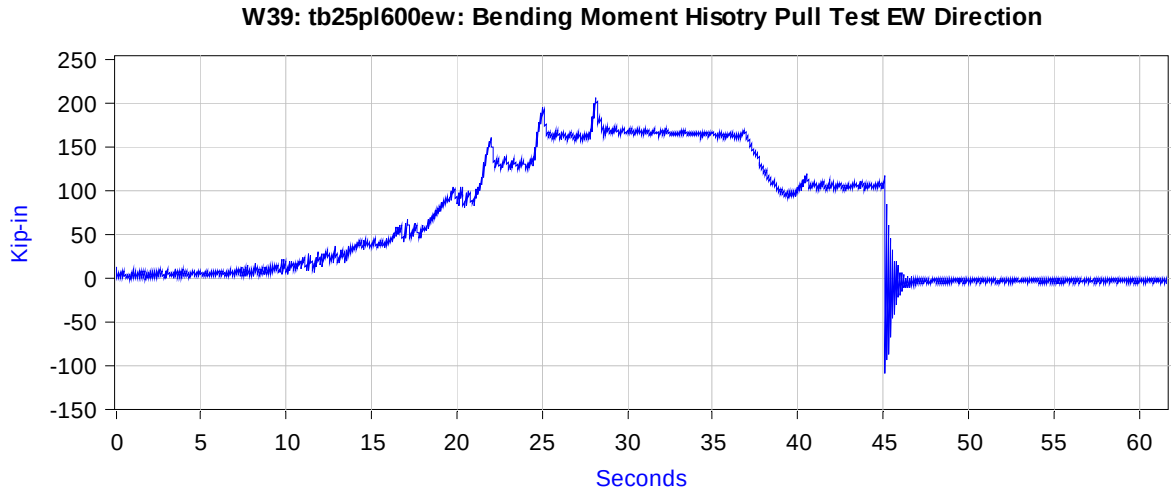

Figure D-172: Acceleration Response from Quick Release Test TB29pl900ew – Bushing #7

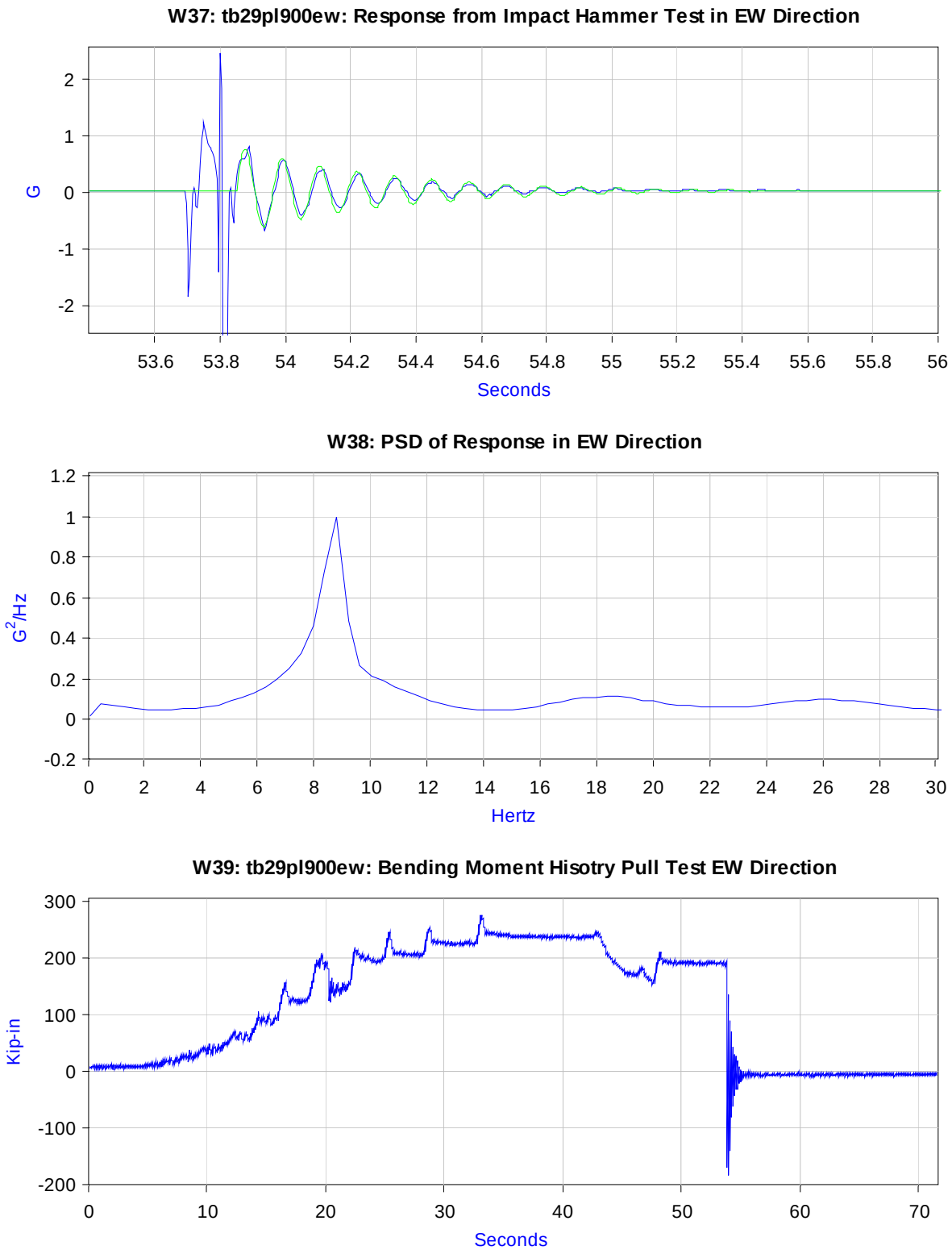

Figure D-173: Maximum Force vs. Maximum Displacement – Bushing #7

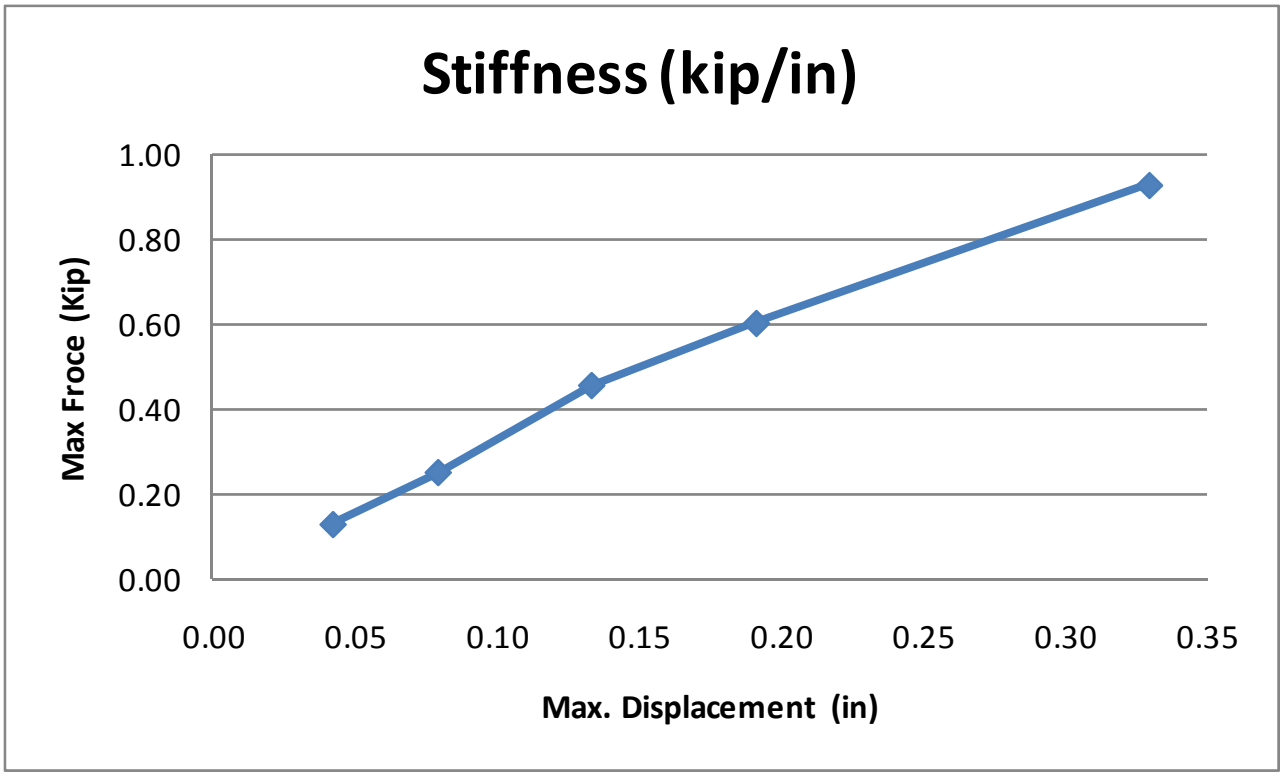

White Noise Tests

The frequencies and damping ratios of the bushing were determined by transfer functions obtained from white noise tests using the shake table. The peak of the transfer function is the fundamental frequency of the bushing and a half-power bandwidth method was used to determine the damping ratio. The summary of the frequencies is presented in Table D-9.

The frequencies from white noise tests were then used to develop "impulse tests" for the dominant frequencies of the bushing (see next section). The half-power bandwidth method used to determine damping is less accurate than a quick release, impact hammer or table impulse tests; therefore the ratios are re-determined in the following section using impulse tests. The acceleration transfer functions obtained from these tests are shown in Figures D-174 through D-180.

Figure D-174: Transfer Functions of Bushing #7, Test TB45WN

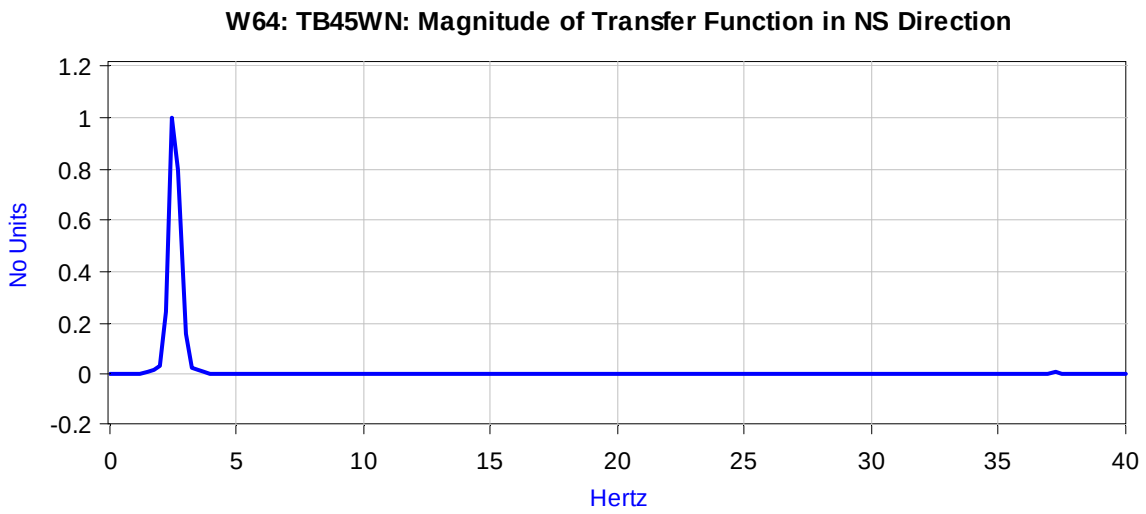

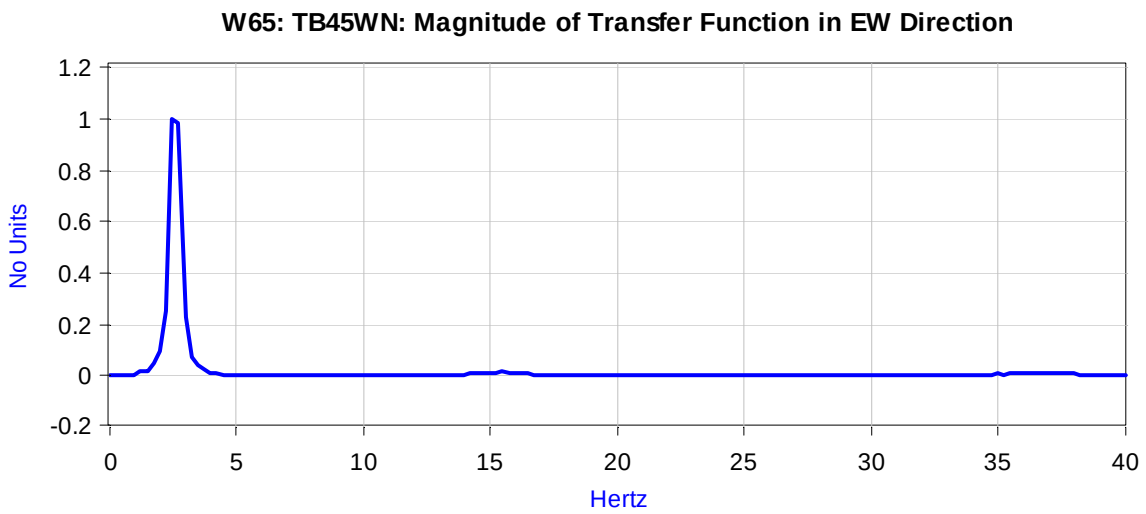

Figure D-175: Transfer Functions of Bushing #7, Test TB48WN

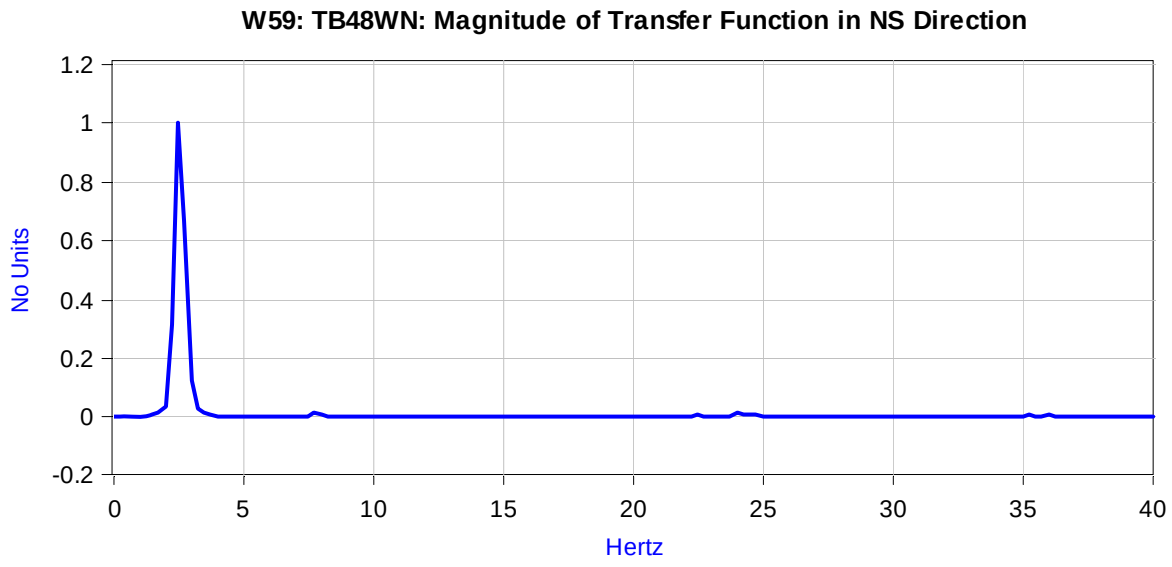

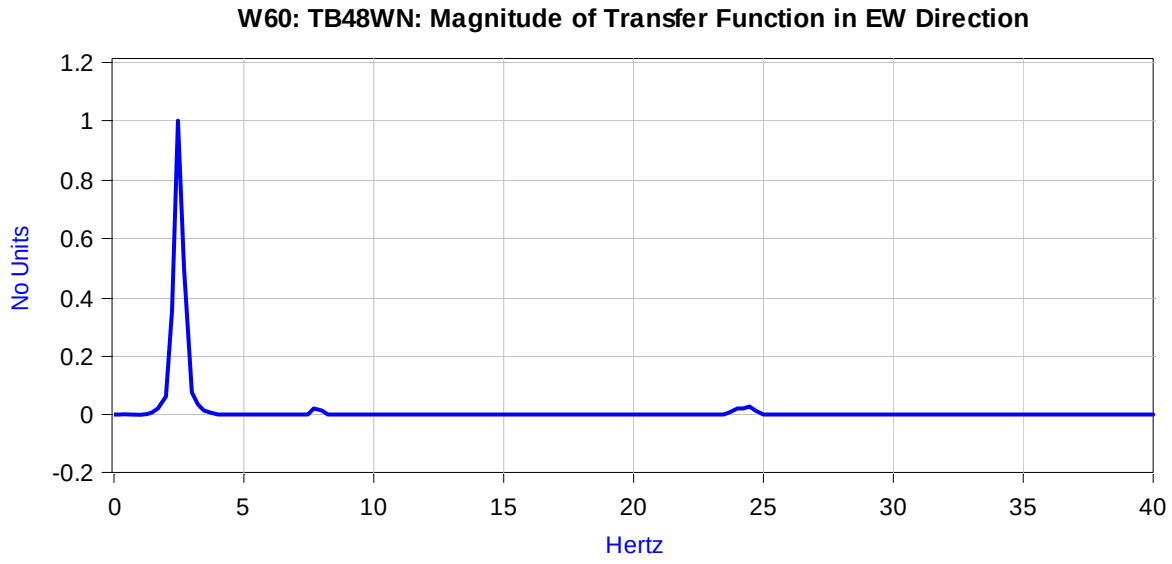

Figure D-176: Transfer Functions of Bushing #7, Test TB51WN

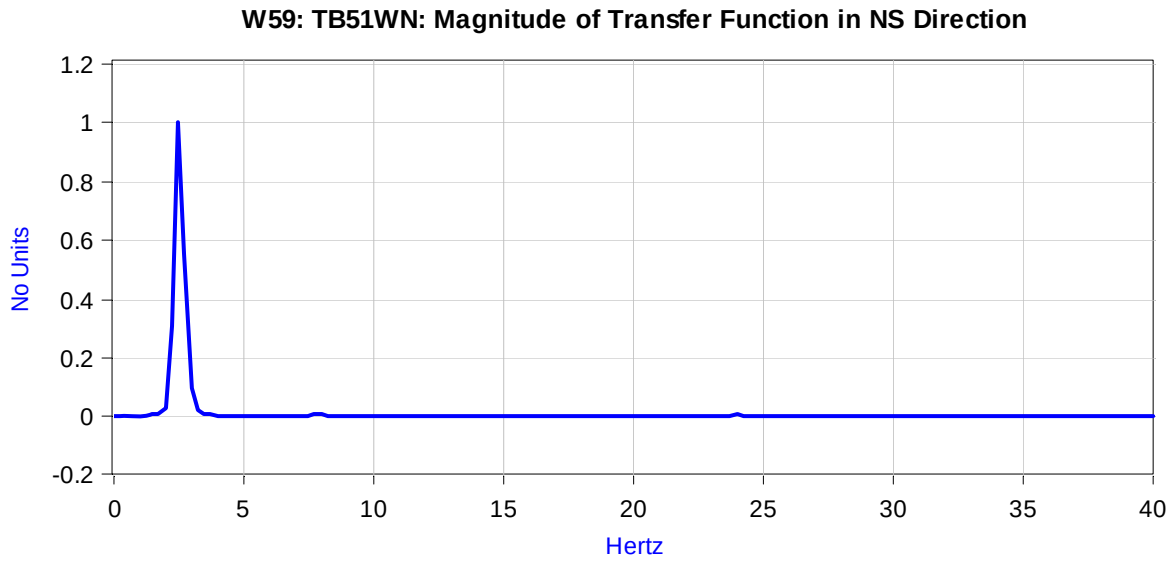

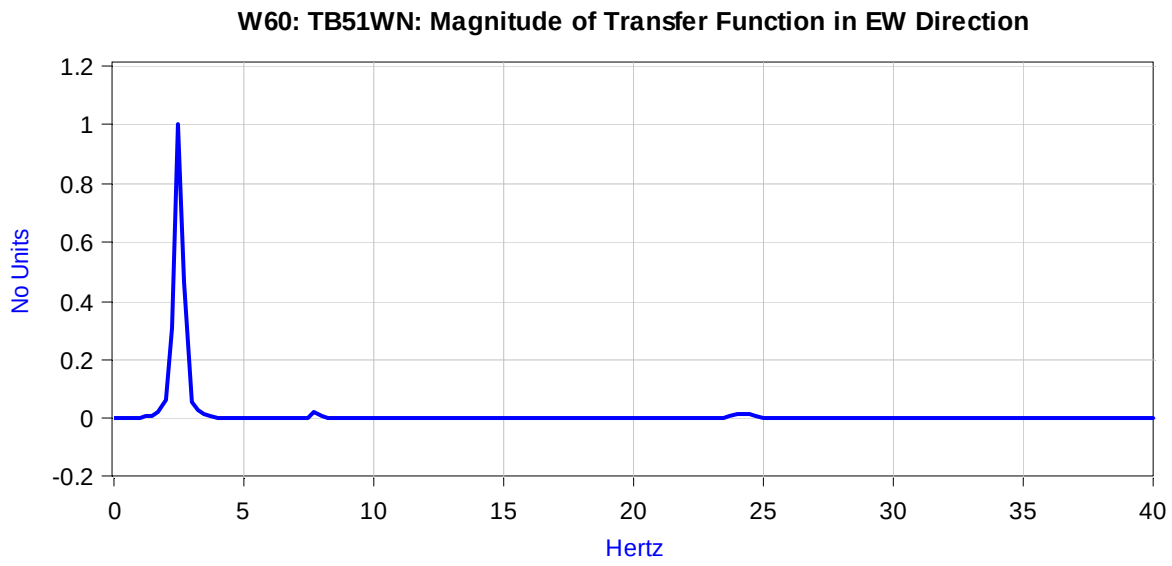

Figure D-177: Transfer Functions of Bushing #7, Test TB54WN

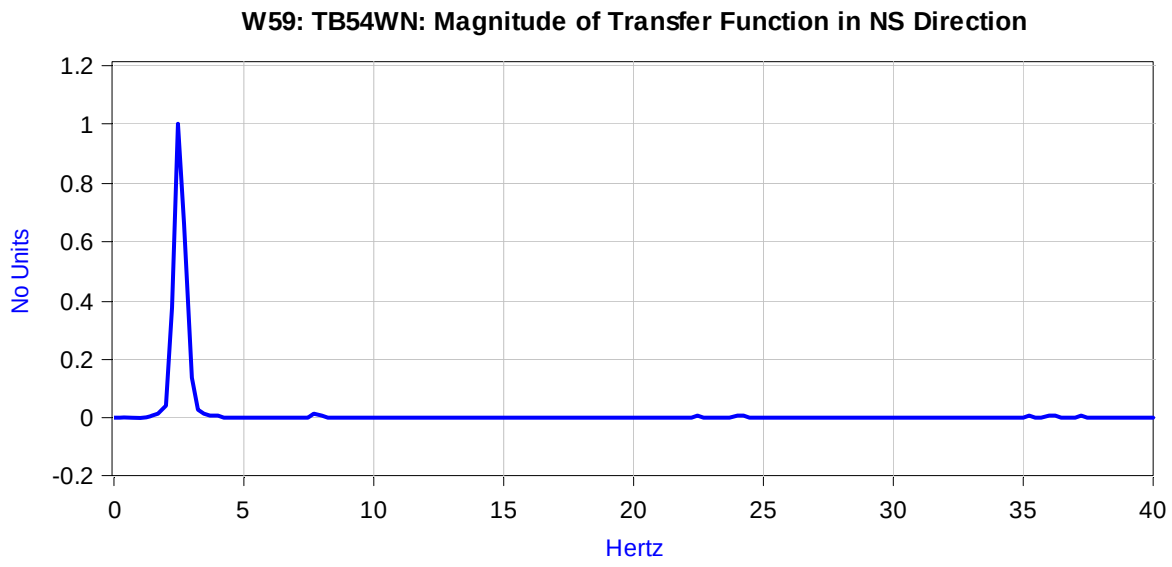

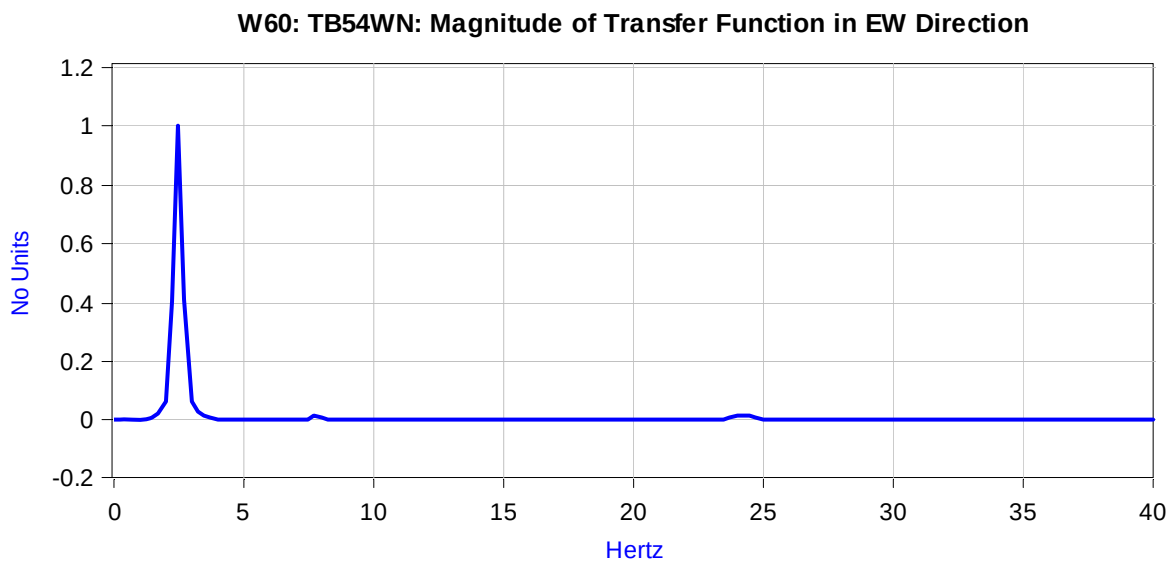

Figure D-178: Transfer Functions of Bushing #7, Test TB57WN

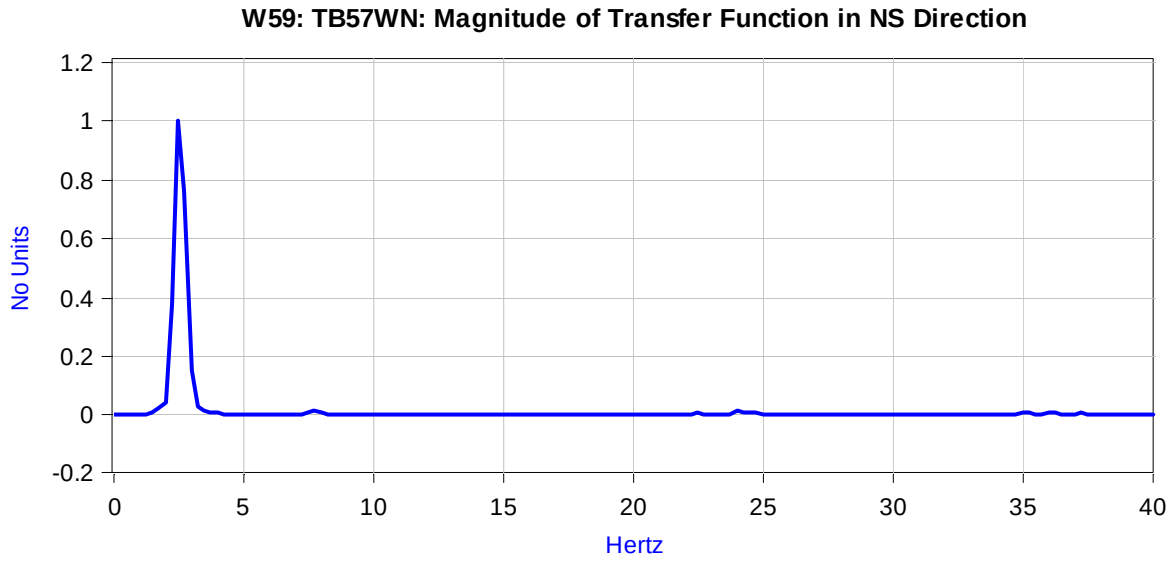

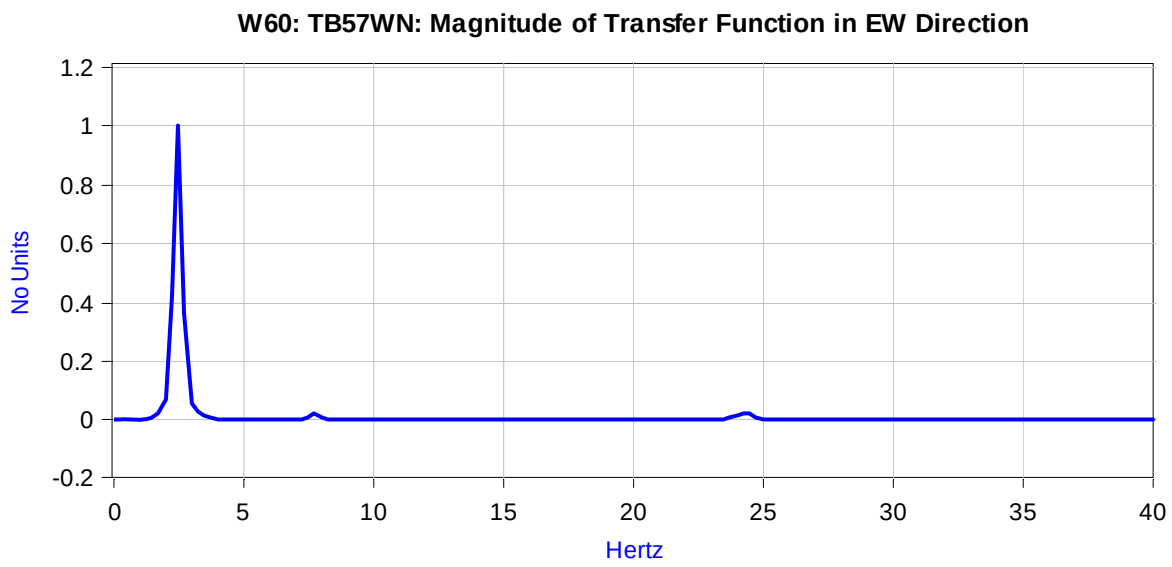

Figure D-179: Transfer Functions of Bushing #7, Test TB60WN

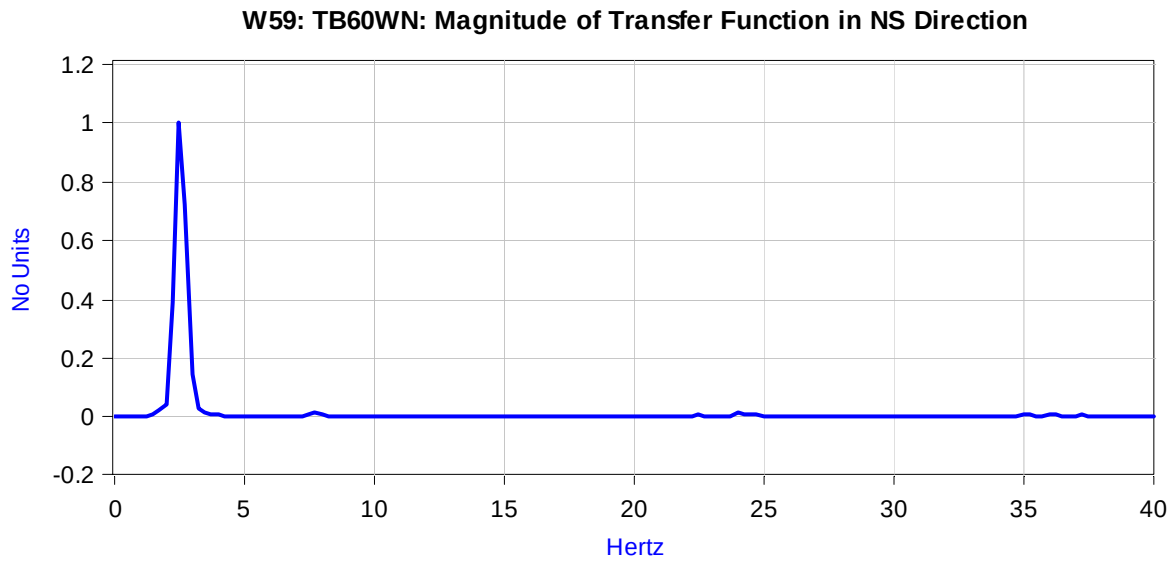

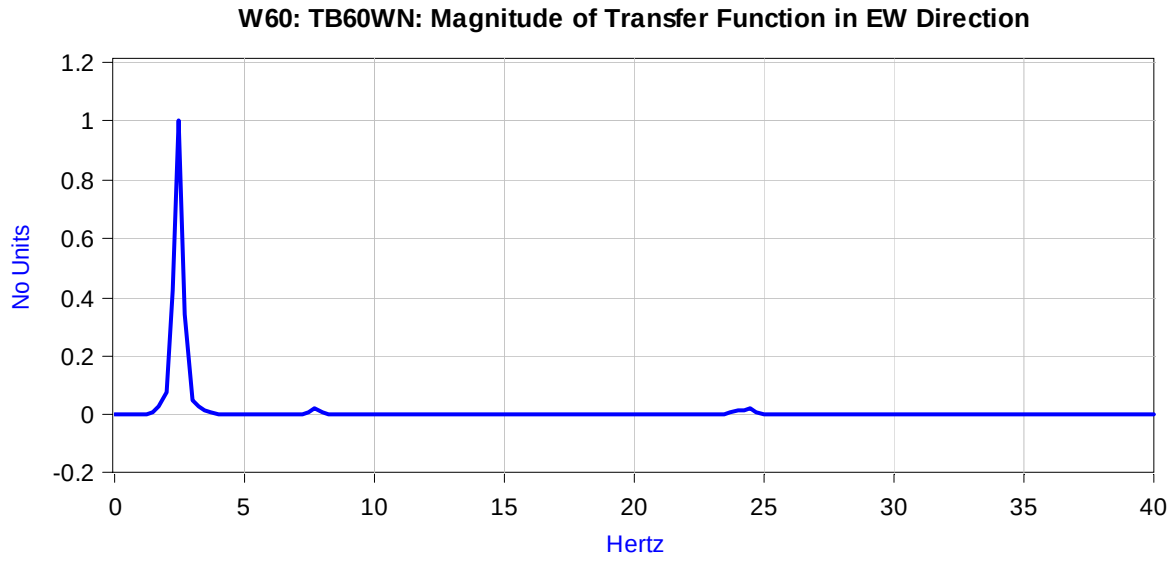

Figure D-180: Transfer Functions of Bushing #7, Test TB63WN

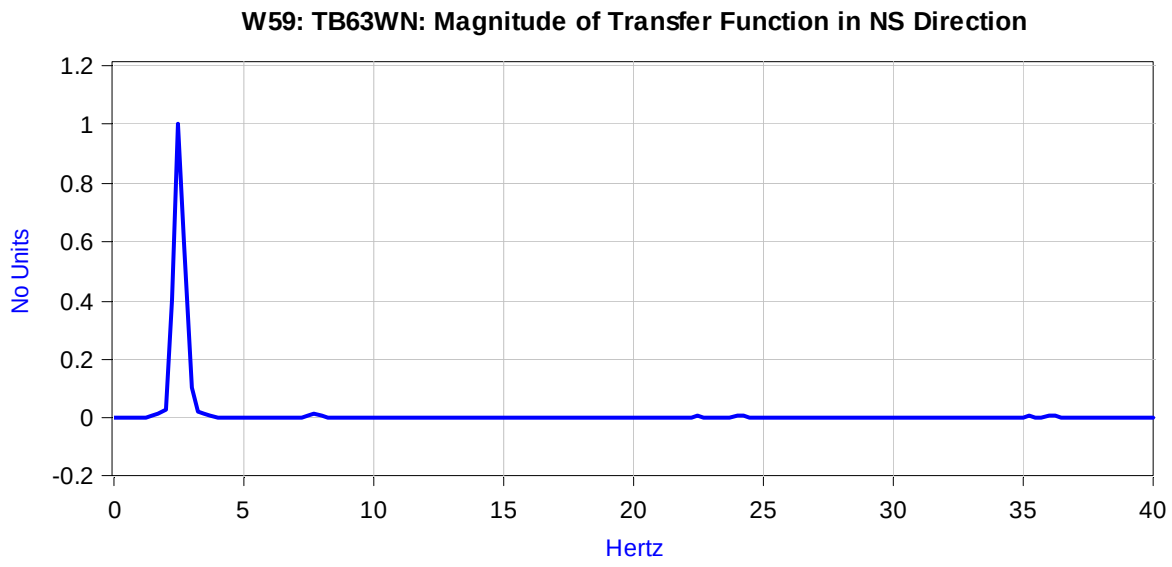

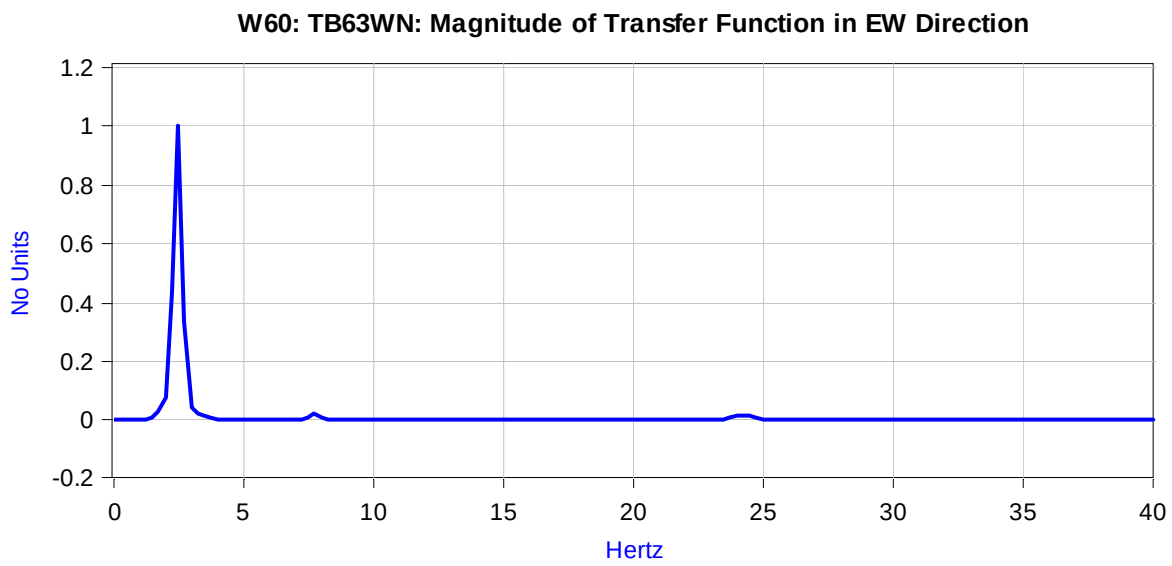

Table Impulse Tests

The table impulse test identifies frequencies and damping of dominant frequencies using smoothed table acceleration impulse for control of a shake table by using a smoothing table impulse procedure developed by the SEESL at University at Buffalo (Kong, 2010). For the identification of system frequencies, a power spectral density (PSD) was calculated from output motion at the top of the bushing and the system frequency is obtained by finding the frequency where the peak is located. For the identification of modal damping, a curve fitting method developed by the authors was used (Kong, 2010).

The acceleration history results of the table impulse tests are presented in Figures D-181 through D-189, and the dynamic characteristics are summarized in Table D-9. The frequencies of Bushing #7 in the NS direction are around 2.55 Hz in test TB52TBI (before random motion tests), and 2.50 Hz in test TB77TBI; the damping values are 2.98% and 2.75%, respectively. The frequency in the EW direction is 2.58 Hz in test TB52TBI (before random motion tests), and 2.47 Hz in test TB77TBI; the damping values are 3.00% and 2.52%, respectively.

Figure D-181: Table Impulse Test Response (Test TB52TBI) – Bushing #7

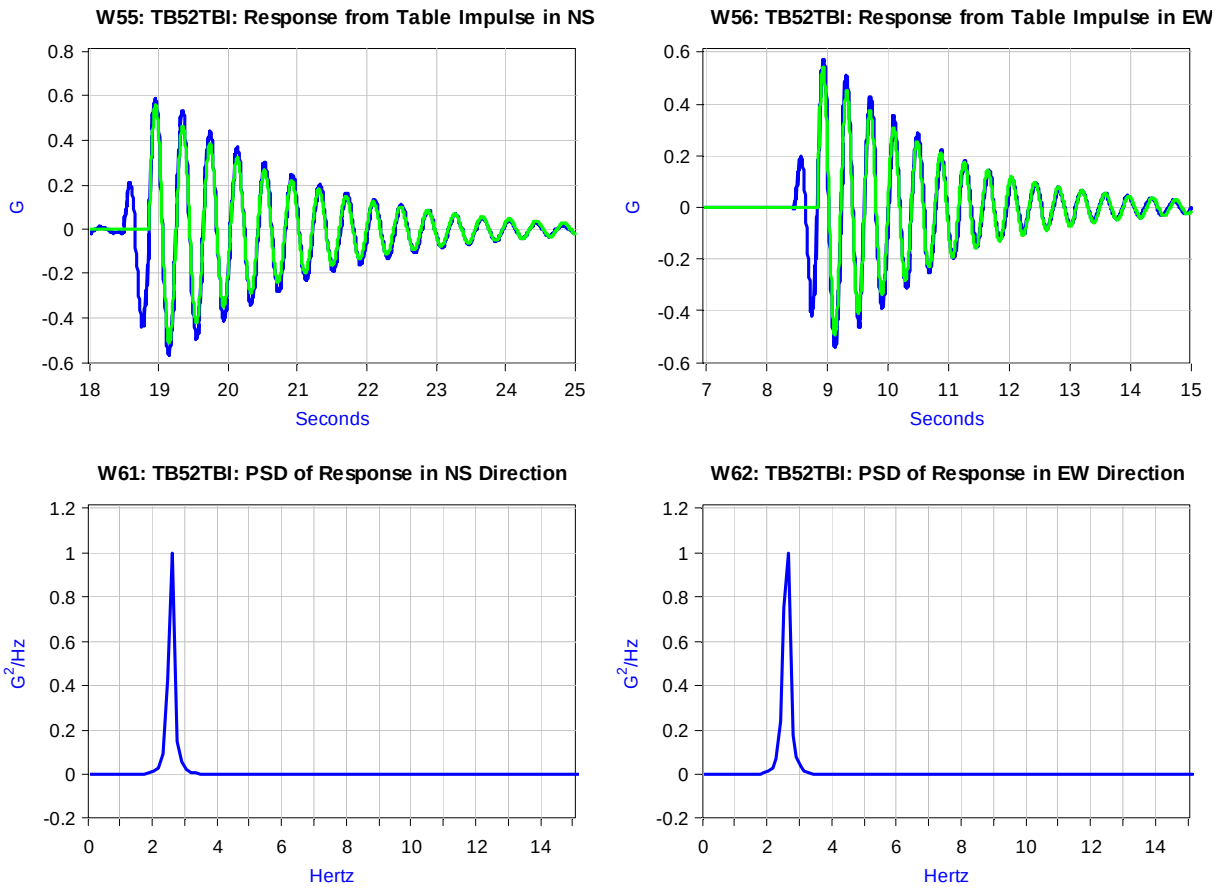

Figure D-182: Table Impulse Test Response (Test TB55TBI) – Bushing #7

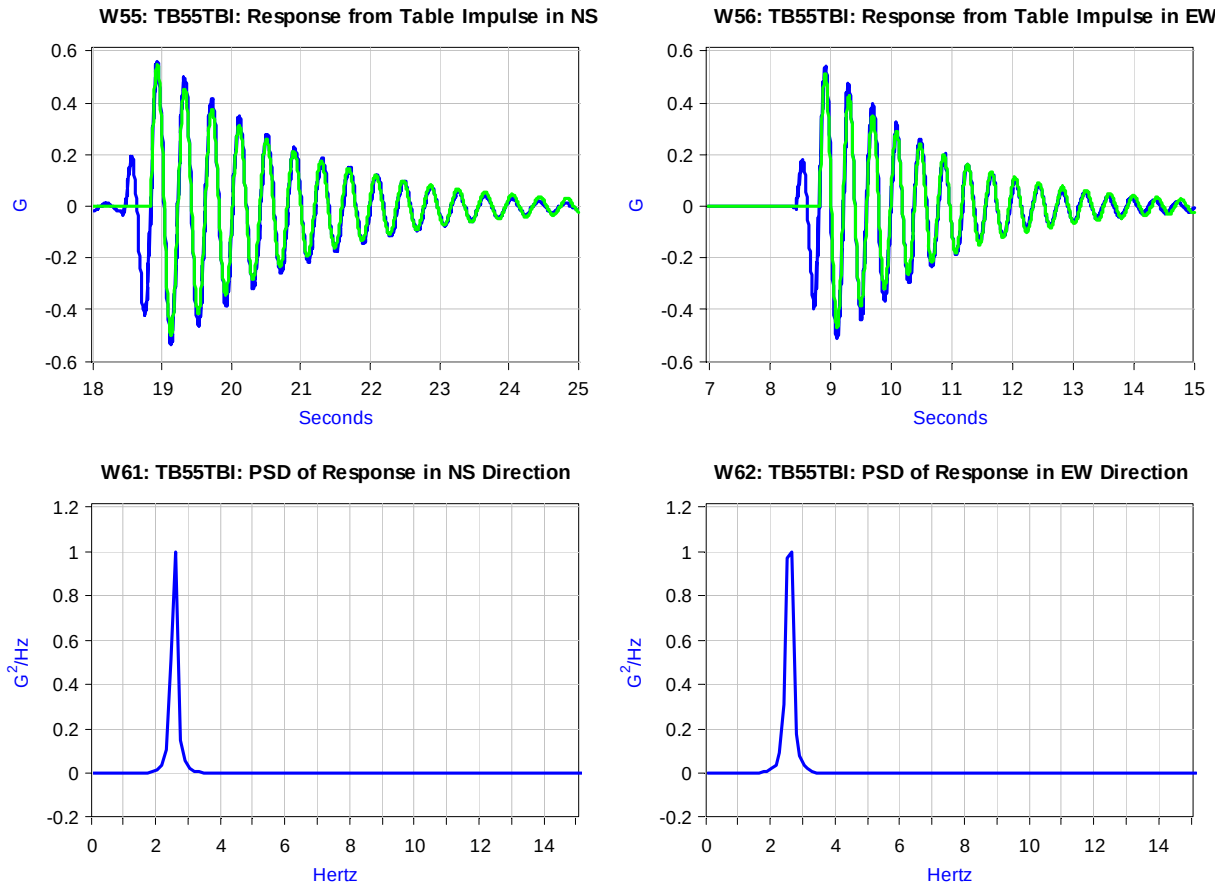

Figure D-183: Table Impulse Test Response (Test TB58TBI) – Bushing #7

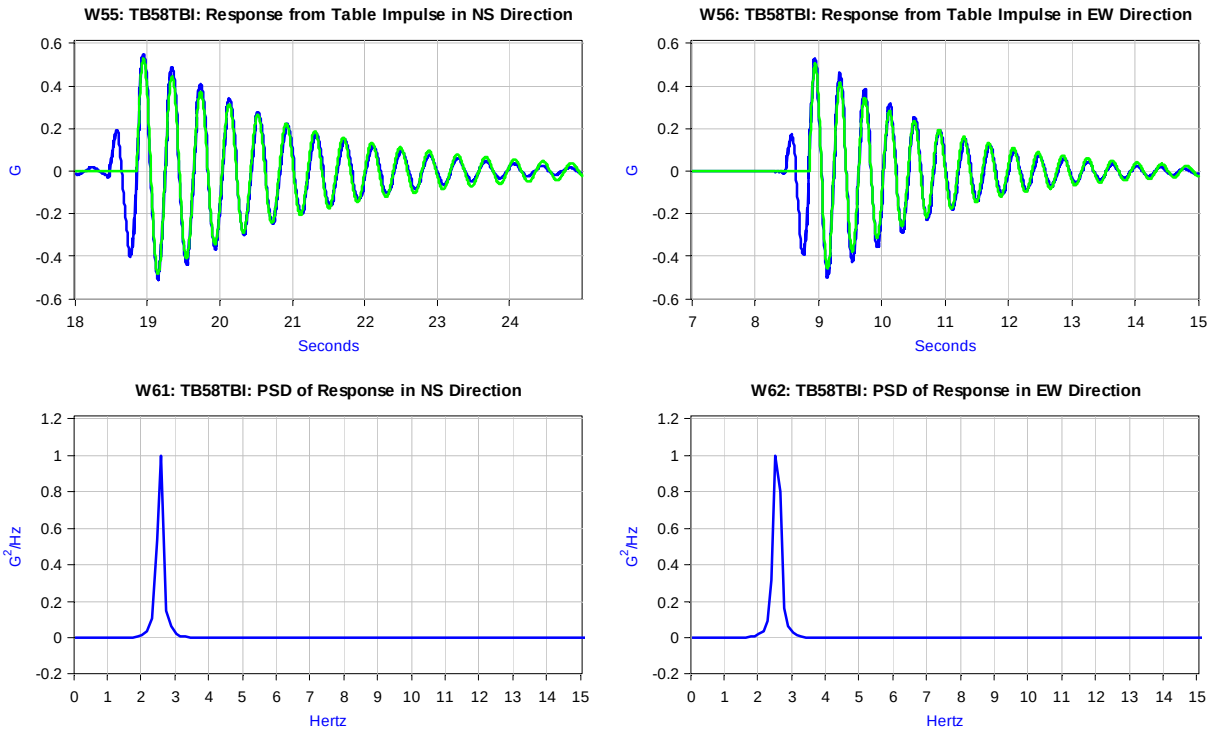

Figure D-184: Table Impulse Test Response (Test TB61TBI) – Bushing #7

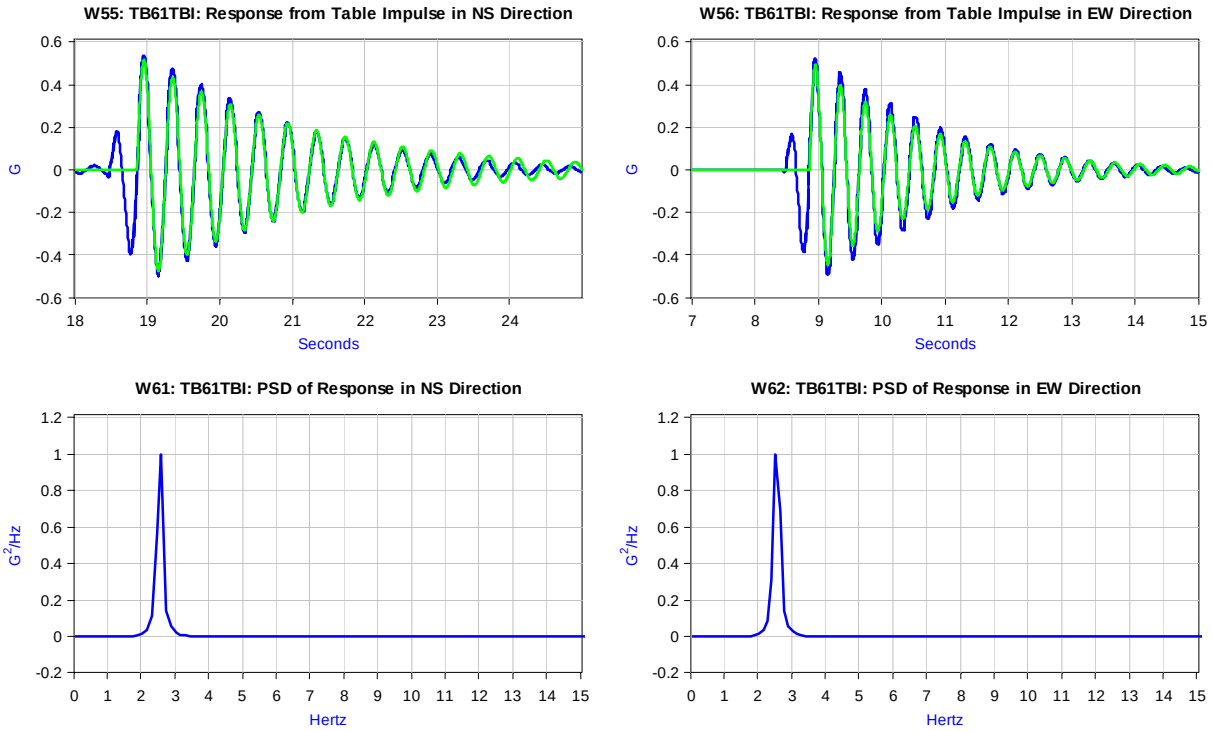

Figure D-185: Table Impulse Test Response (Test TB65TBI) – Bushing #7

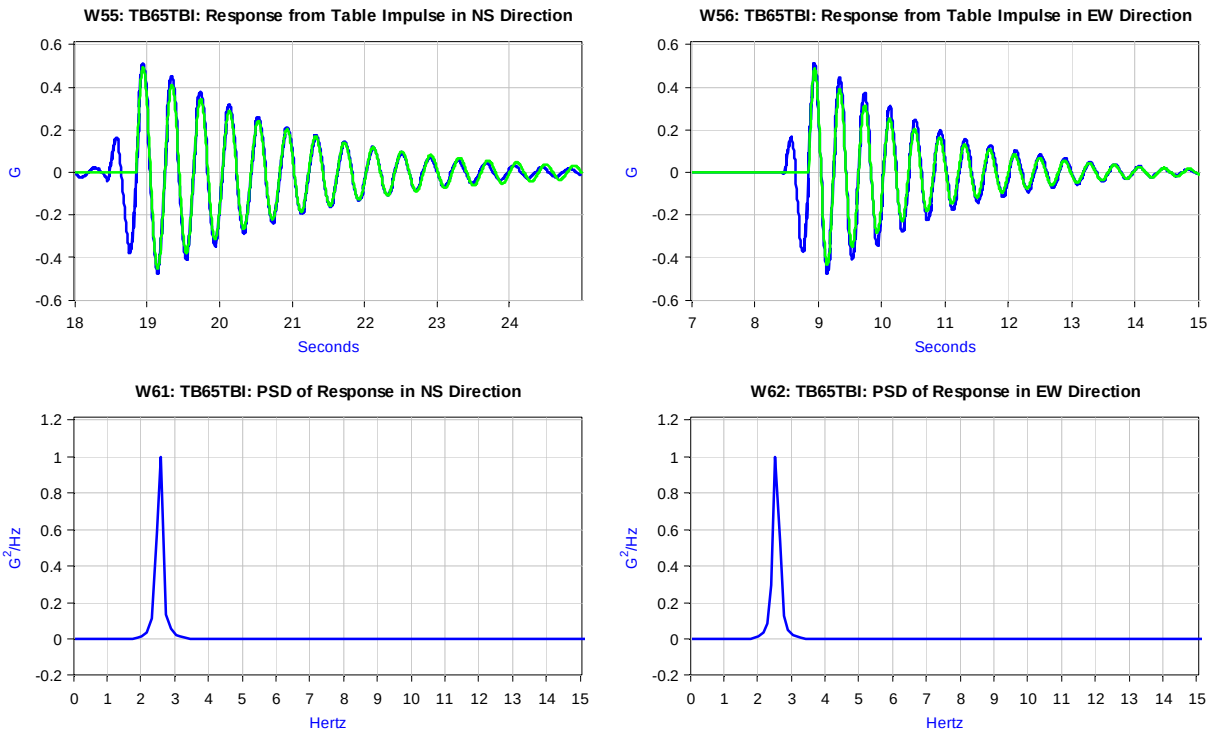

Figure D-186: Table Impulse Test Response (Test TB68TBI) – Bushing #7

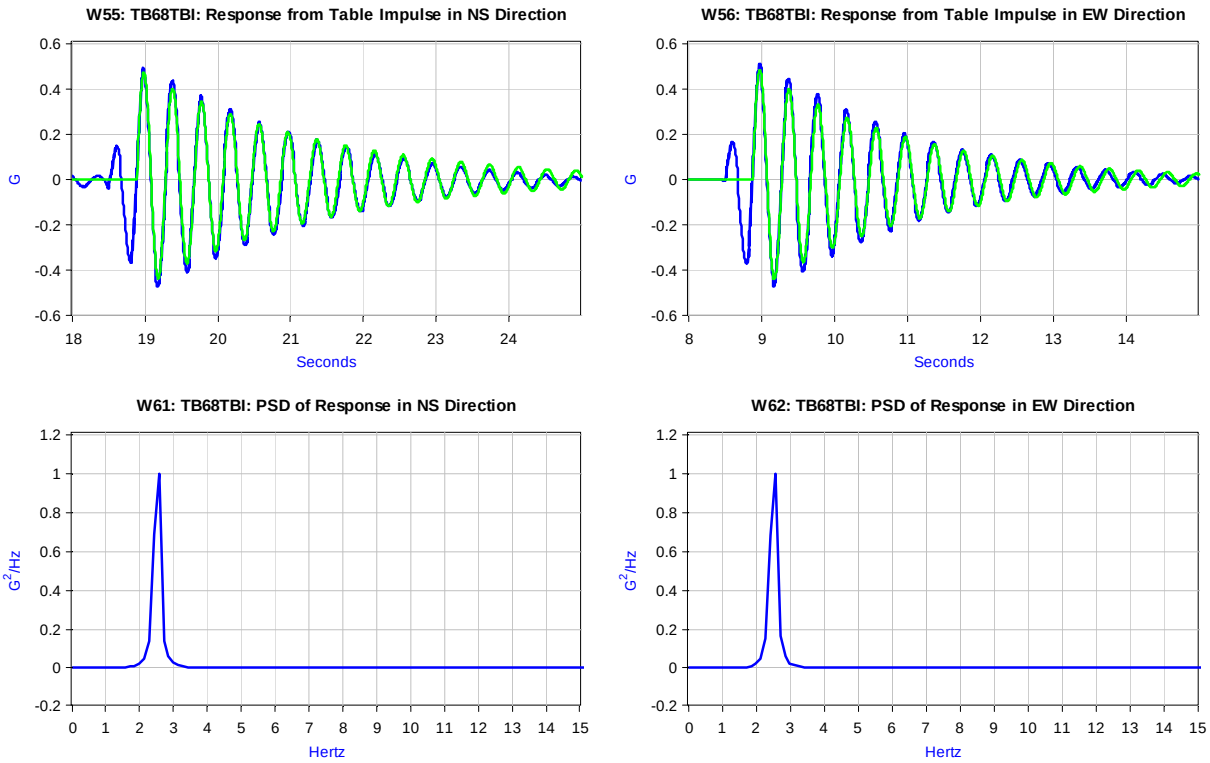

Figure D-187: Table Impulse Test Response (Test TB71TBI) – Bushing #7

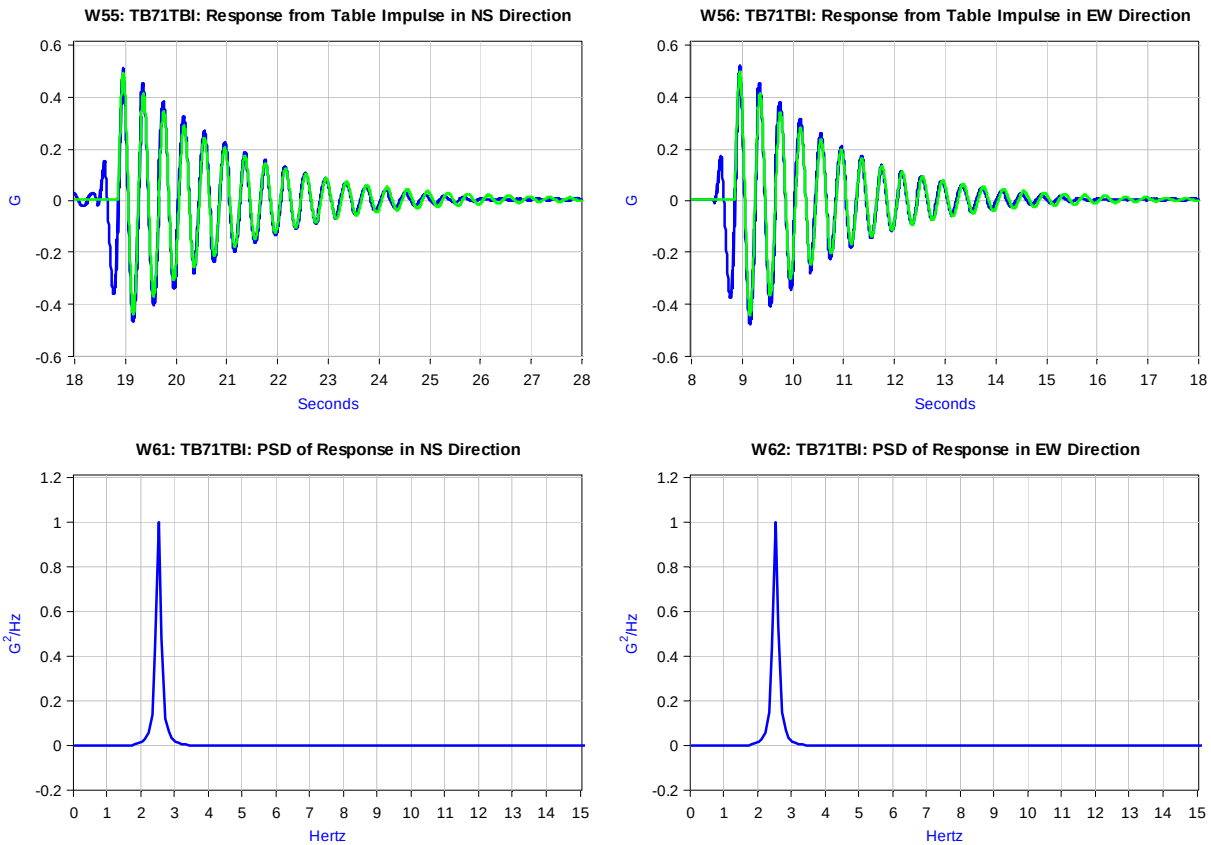

Figure D-188: Table Impulse Test Response (Test TB74TBI) – Bushing #7

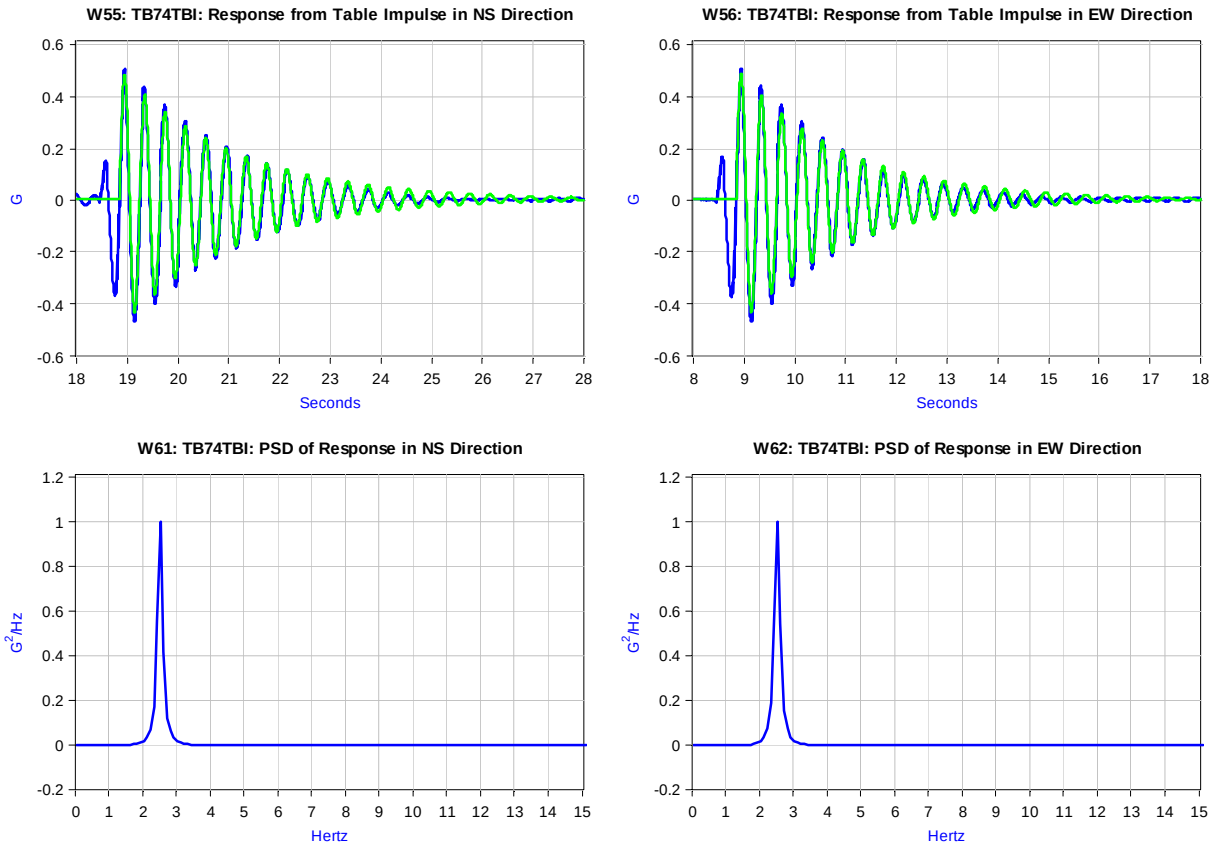

Figure D-189: Table Impulse Test Response (Test TB77TBI) – Bushing #7

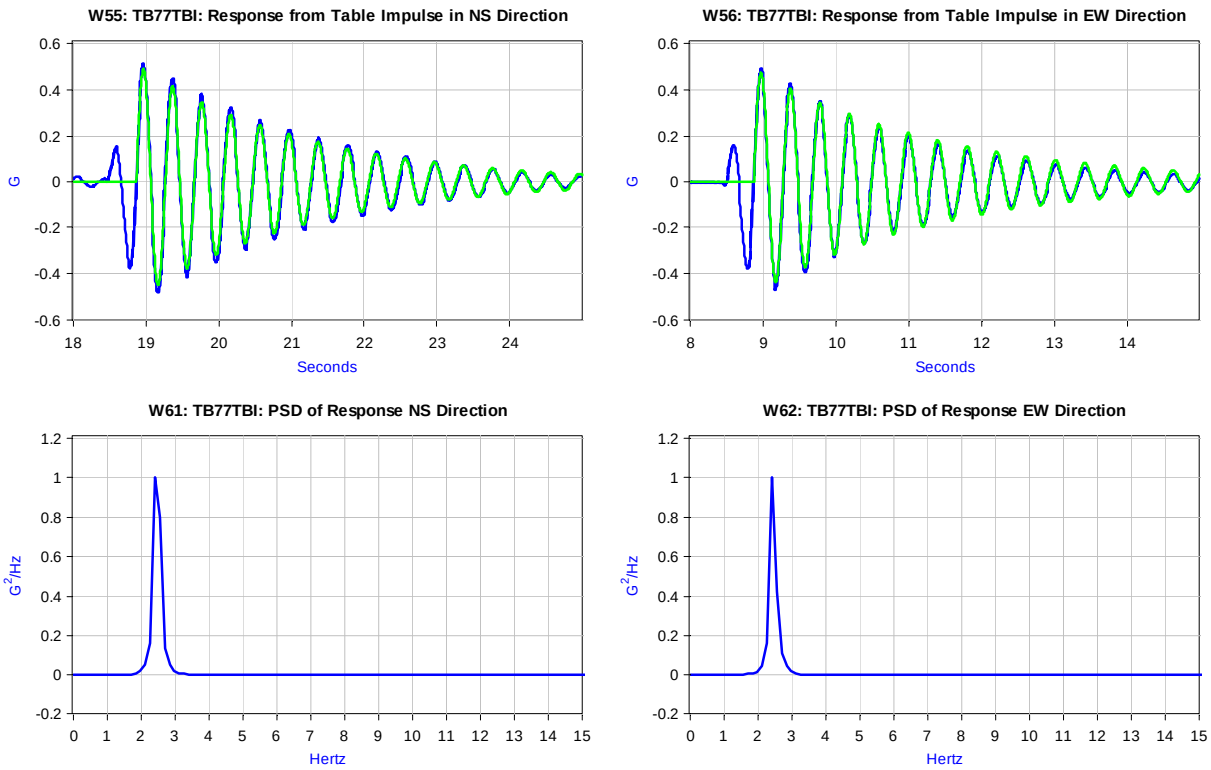

Acceleration History Tests

Acceleration history tests were performed for the seismic demand quantification of Bushing #7. A summary of the accelerations recorded on various locations on the bushing are shown in Table D-10 for the eleven levels of test input motions.

The acceleration history tests were used to measure the bending moment of the bushing at flange level. Strain gauges were used to measure the bending moments. A summary of bending moments is presented in Table D-10. Bending moment histories are shown in Figures D-190 through D-196.

Table D-10: Summary of Accelerations and Bending Moments – Bushing #7

Location	Units	0.15 g RRS			0.20 g RRS			0.25 g RRS			0.30 g RRS			0.35 g RRS		
		TB47AH20			TB47AH20B			TB50AH25			TB53AH30			TB56AH35		
(1)	(2)	(3)	(4)	(5)	(6)	(7)	(8)	(9)	(10)	(11)	(12)	(13)	(14)	(15)	(16)	(17)
Bushing Location on Frame																
Acceleration Distribution along the Height of Testing Setup																
Direction		NS	EW	Vertical	NS	EW	Vertical	NS	EW	Vertical	NS	EW	Vertical	NS	EW	Vertical
Top of Bushing	(g)	0.73	0.99	0.73	0.85	1.07	0.99	1.10	1.26	1.16	1.13	1.47	1.32	1.31	1.66	1.46
Upper CG Of Bushing	(g)	0.32	0.47	-	0.40	0.56	-	0.50	0.69	-	0.57	0.83	-	0.66	0.96	-
CG OF Bushing	(g)	0.28	0.30	-	0.32	0.38	-	0.40	0.47	-	0.46	0.56	-	0.53	0.64	-
On Frame	(g)	0.25	0.23	0.20	0.32	0.25	0.20	0.43	0.32	0.27	0.46	0.38	0.33	0.53	0.44	0.39
Shake Table	(g)	0.21	0.20	0.19	0.27	0.25	0.19	0.34	0.31	0.26	0.41	0.38	0.32	0.48	0.43	0.35
Bending Moment at the Base of Bushing																
Moment from Strain Gauges	kip-in	66.17	88.34	-	91.37	116.83	-	96.91	119.90	-	109.72	142.91	-	125.13	149.09	-

Location	Units	0.40 g RRS			0.45 g RRS			0.50 g RRS			0.55g RRS			0.65 g RRS			0.80 g RRS		
		TB59AH40			TB62AH45			TB66AH50			TB69AH55			TB72AH65			TB75AH80		
(1)	(2)	(9)	(10)	(11)	(12)	(13)	(14)	(15)	(16)	(17)	(9)	(10)	(11)	(12)	(13)	(14)	(15)	(16)	(17)
Bushing Location on Frame																			
Acceleration Distribution along the Height of Testing Setup																			
Direction		NS	EW	Vertical	NS	EW	Vertical	NS	EW	Vertical	NS	EW	Vertical	NS	EW	Vertical	NS	EW	Vertical
Top of Bushing	(g)	1.59	1.82	1.60	1.86	1.85	1.84	1.79	2.08	2.02	1.99	2.43	2.23	3.14	3.83	2.83	3.14	3.83	2.83
Upper CG Of Bushing	(g)	0.80	1.06	-	0.82	1.14	-	0.82	1.27	-	0.89	1.36	-	1.25	2.13	-	1.25	2.13	-
CG OF Bushing	(g)	0.60	0.69	-	0.65	0.83	-	0.62	0.93	-	0.68	1.02	-	1.46	1.92	-	1.46	1.92	-
On Frame	(g)	0.63	0.51	0.45	0.68	0.57	0.50	0.80	0.64	0.57	0.90	0.74	0.63	1.29	1.14	-	1.29	1.14	0.94
Shake Table	(g)	0.55	0.48	0.41	0.61	0.53	0.46	0.74	0.59	0.53	0.82	0.66	0.61	1.20	1.02	-	1.20	1.02	LOST
Bending Moment at the Base of Bushing																			
Moment from Strain Gauges	kip-in	133.33	161.93	-	150.24	166.50	-	159.97	171.52	-	168.68	194.48	-	-	-	-	-	-	-

Figure D-190: Bending Moment of Bushing #7 in Horizontal Direction – Test TB50ah025

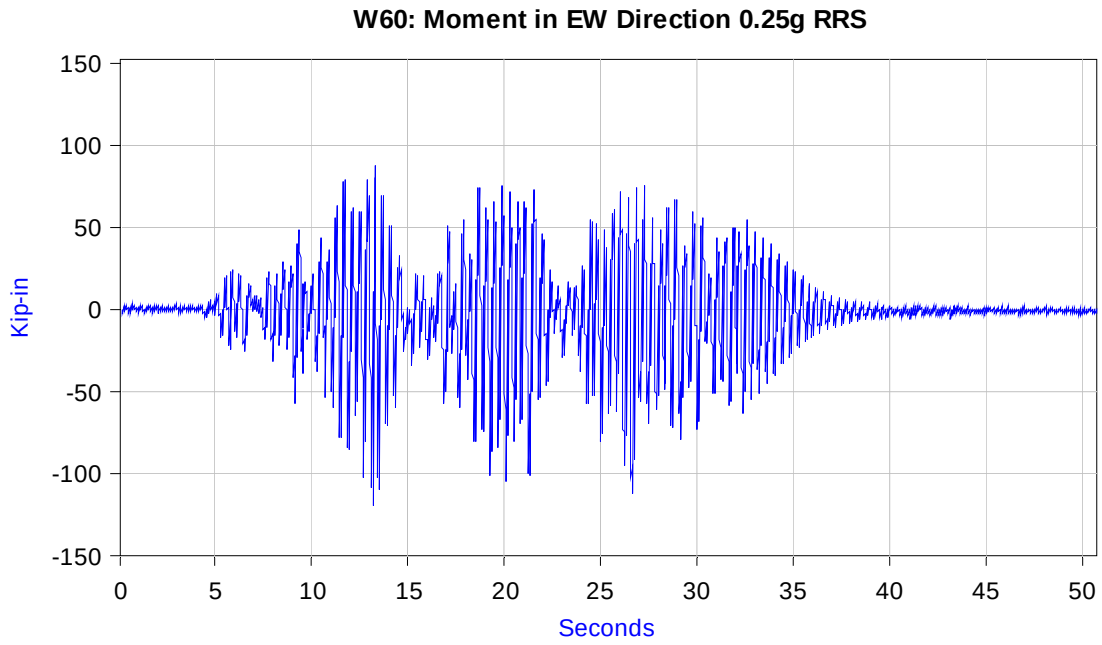

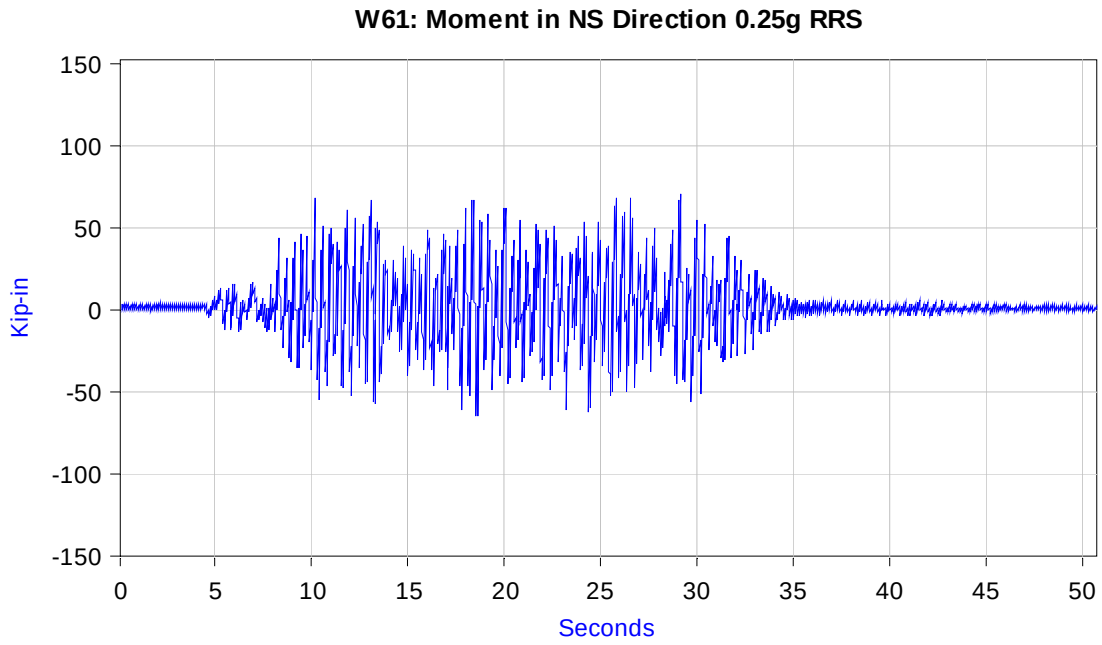

Figure D-191: Bending Moment of Bushing #7 in Horizontal Direction – Test TB53ah30

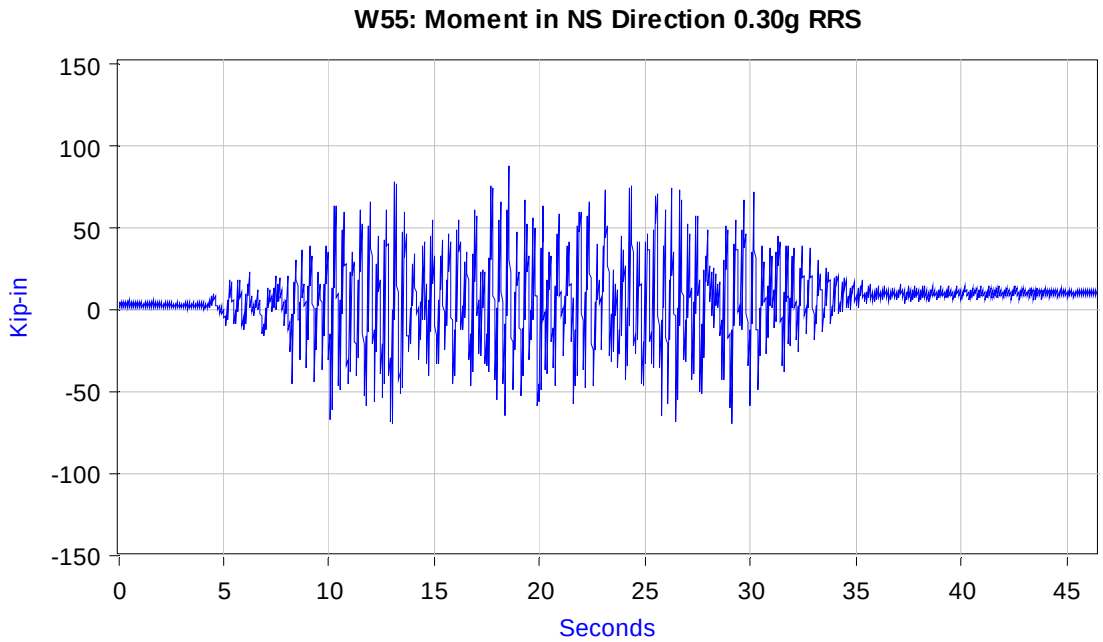

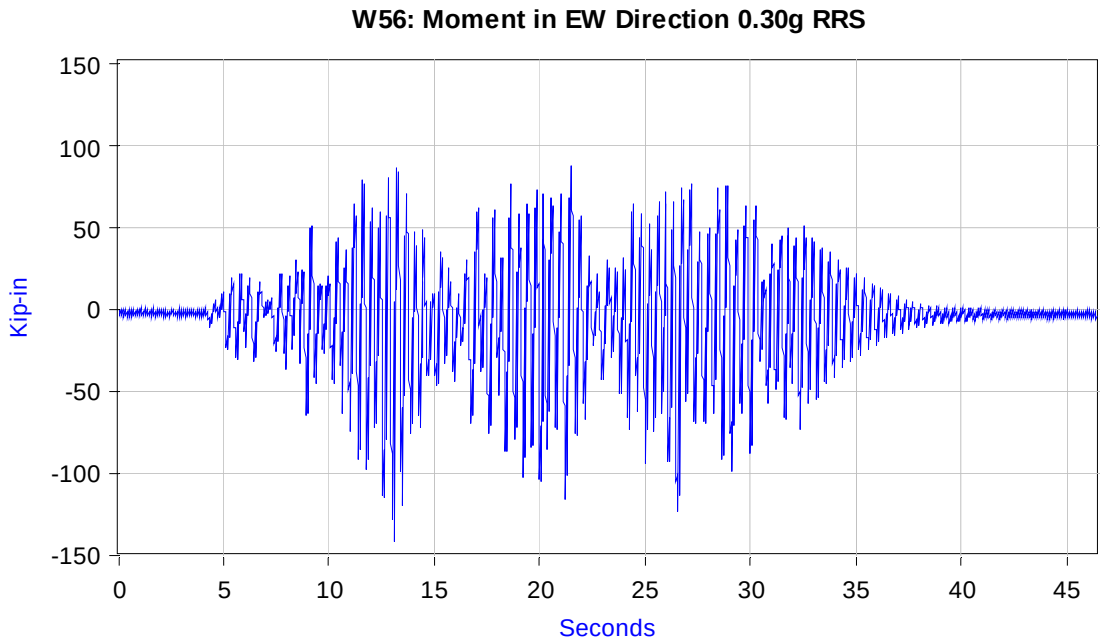

Figure D-192: Bending Moment of Bushing #7 in Horizontal Direction – Test TB56ah35

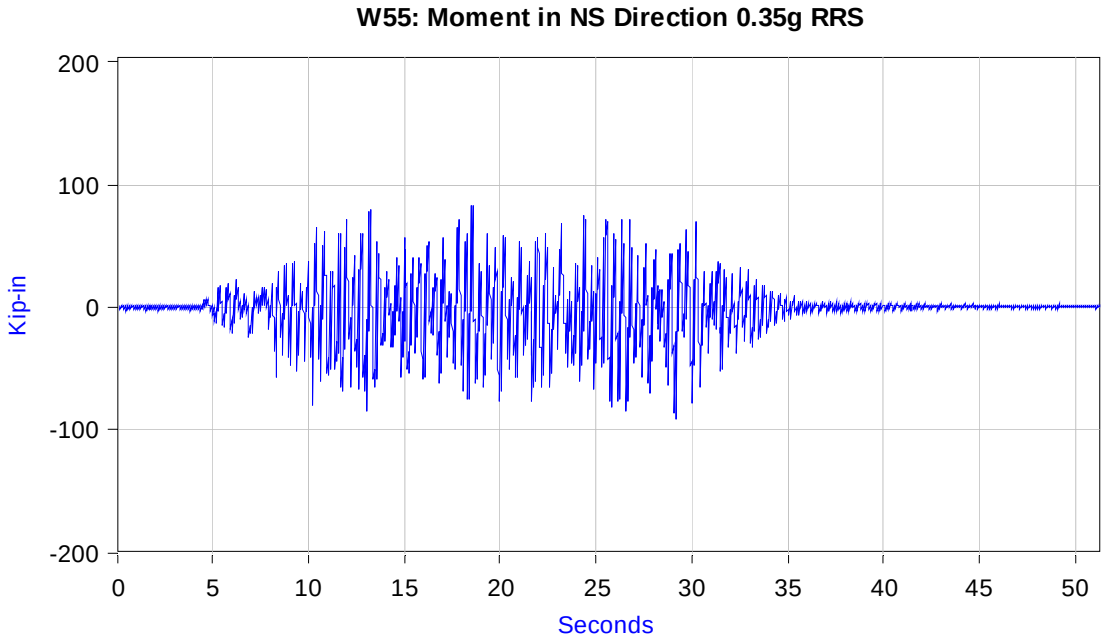

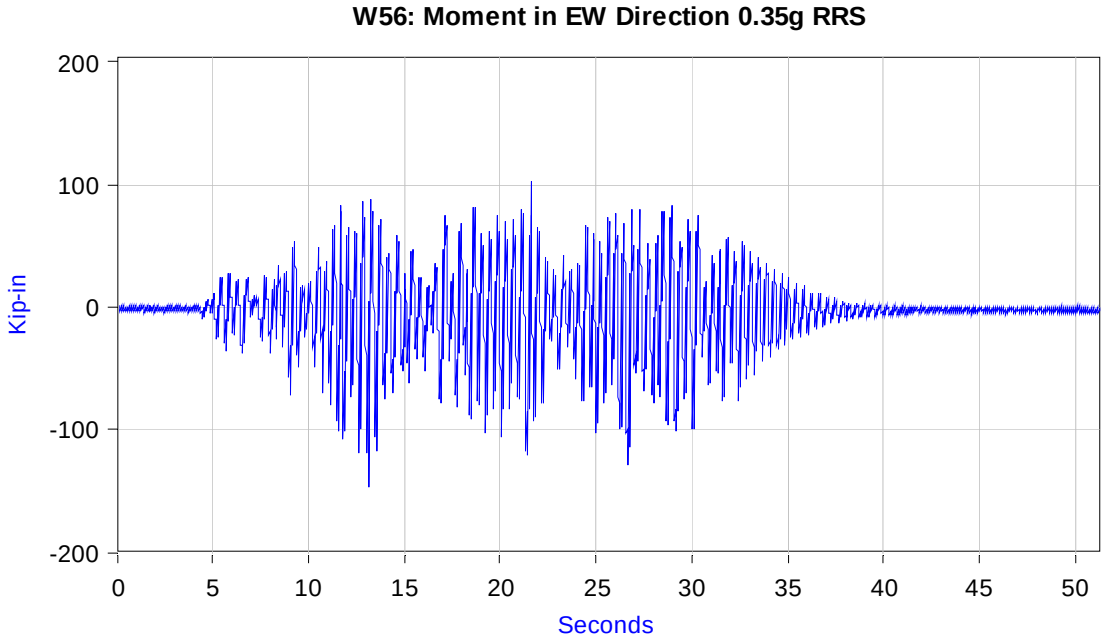

Figure D-193: Bending Moment of Bushing #7 in Horizontal Direction – Test TB59ah40

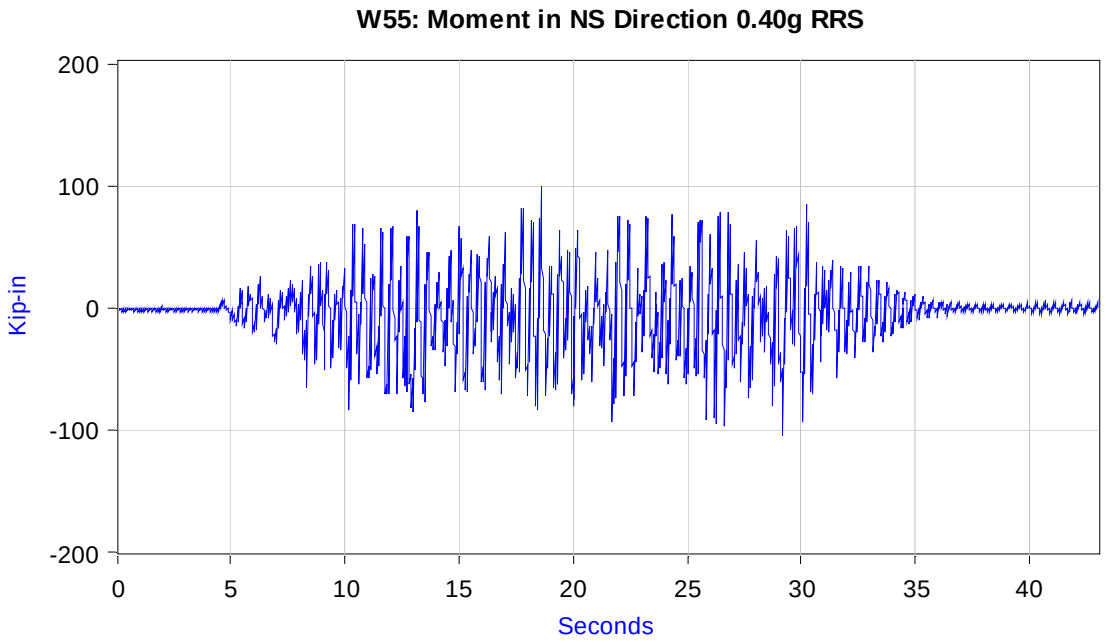

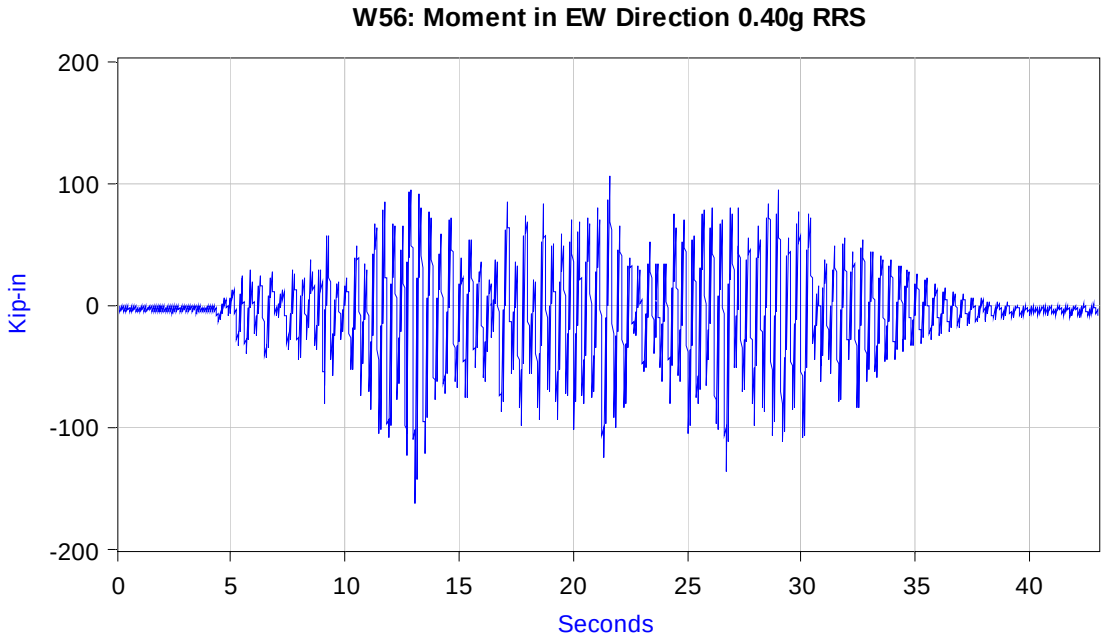

Figure D-194: Bending Moment of Bushing #7 in Horizontal Direction – Test TB62ah45

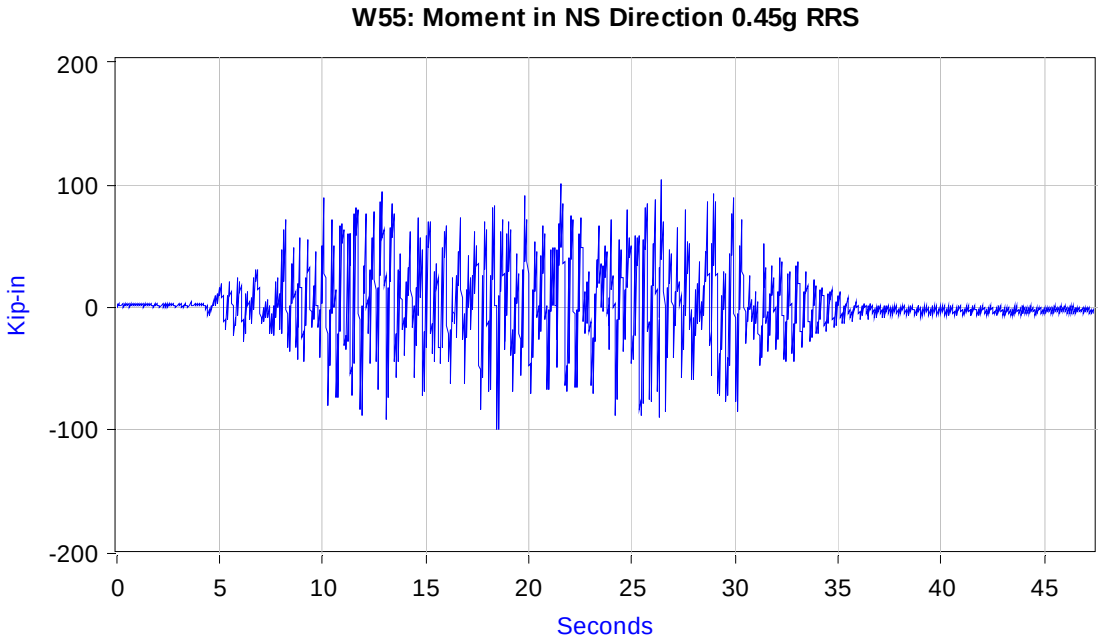

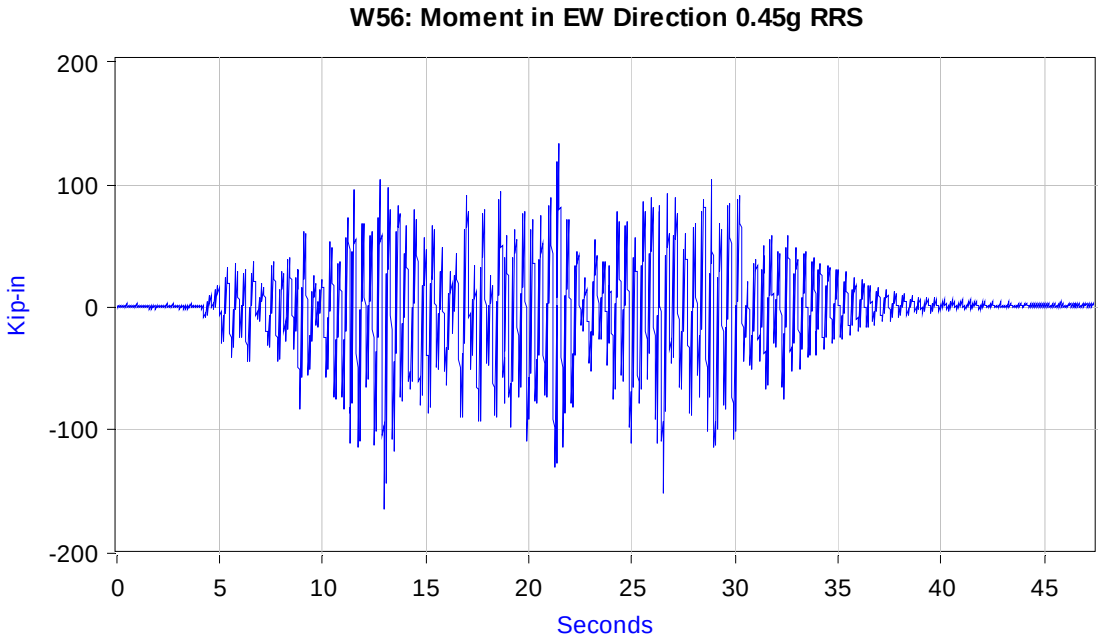

Figure D-195: Bending Moment of Bushing #7 in Horizontal Direction – Test TB66ah50

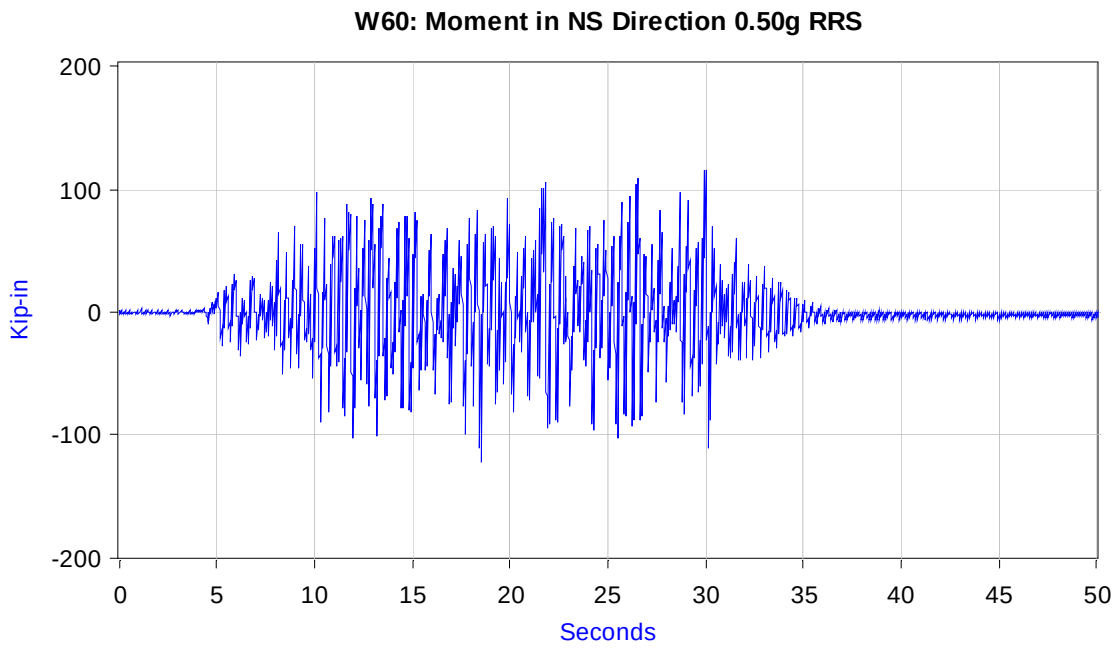

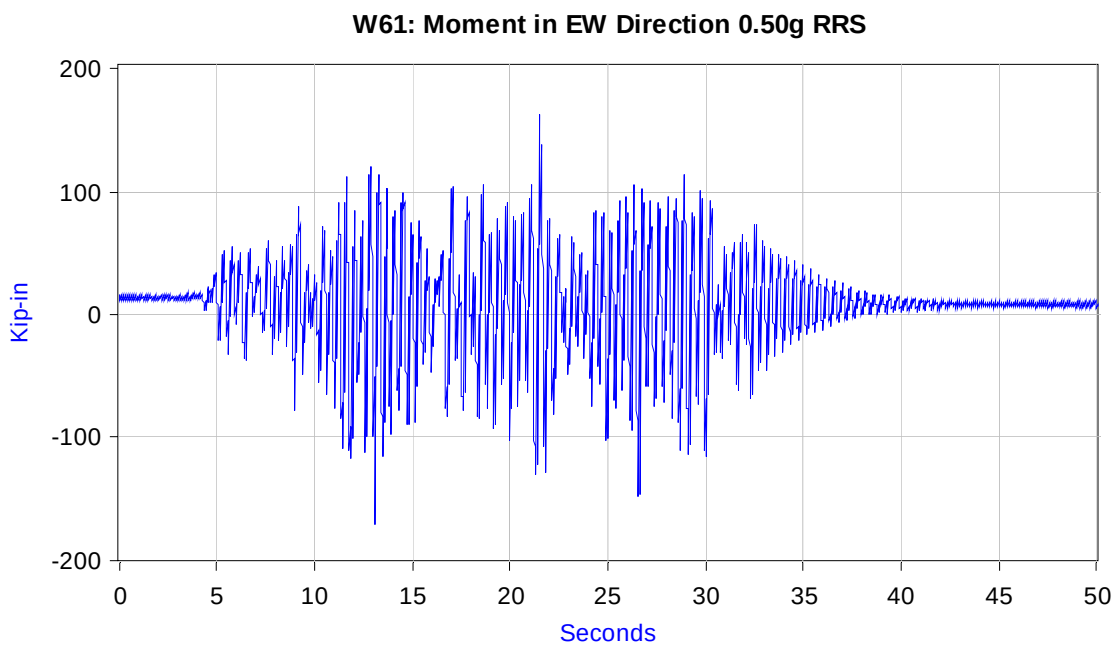

Figure D-196: Bending Moment of Bushing #7 in Horizontal Direction – Test TB69ah55

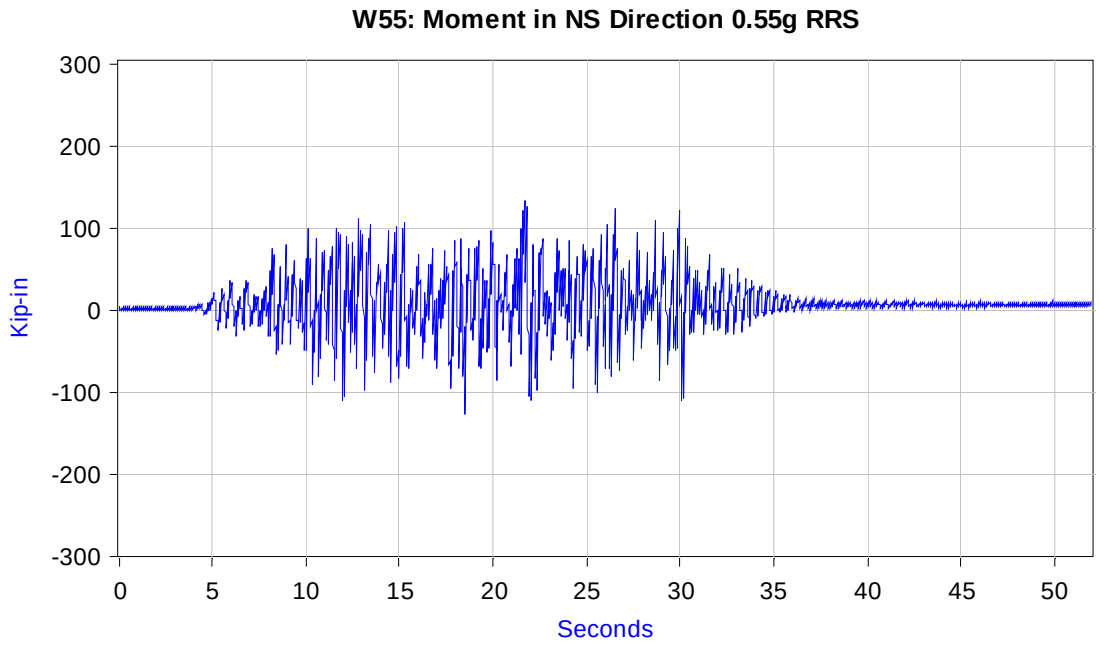

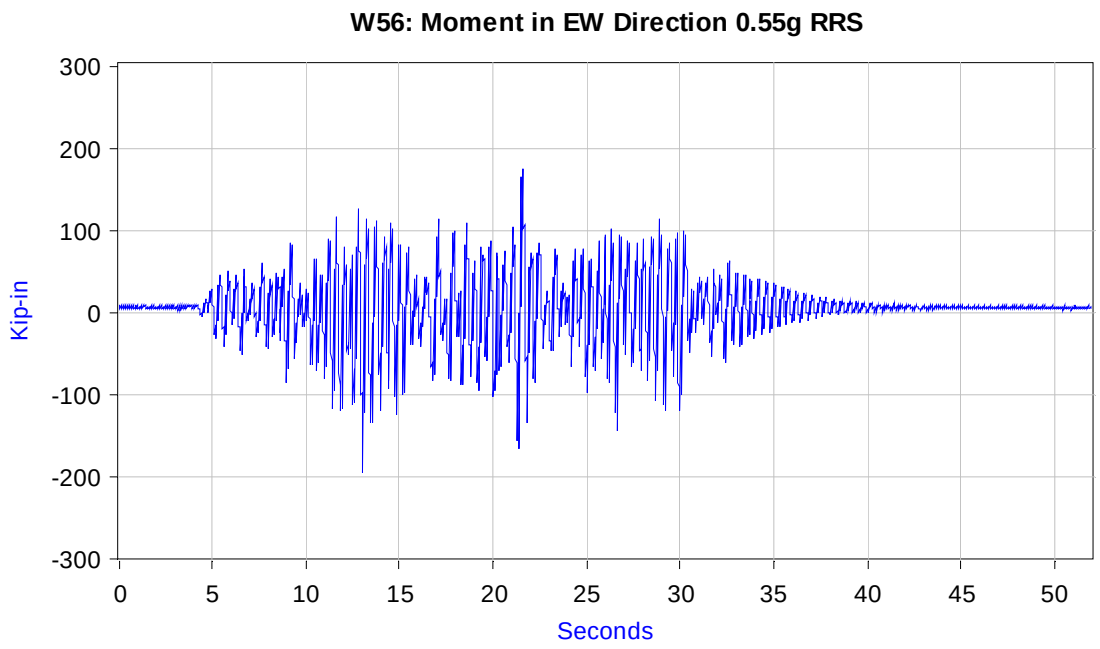

Failure Modes of Bushing #7

Bushing #7 was tested to failure using dynamic testing. The values of demand from this testing provide the strength capacity of the bushing. Bushing #7 was mounted in the center of the frame and excited to various earthquake intensities. The response of the bushing was measured for all tests and during the final test at 0.80 g RRS input motion the bushing failed. The failure mode observed was oil leakage from the unit, due to slip of the porcelain on the base flange (Figure D-197).

Figure D-197: Oil Leakage During the 0.80 g RRS Testing of Bushing #7

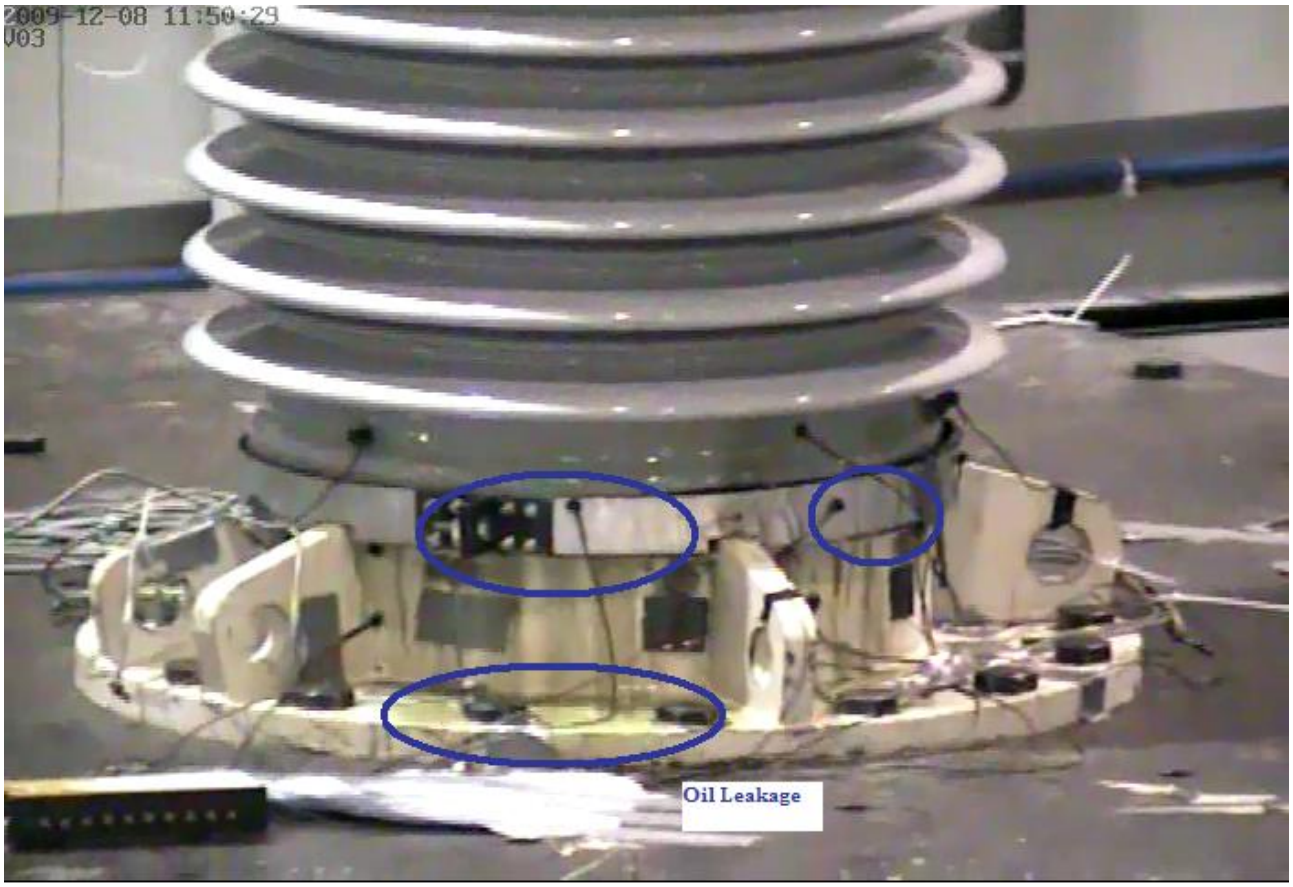

APPENDIX E:

DEVELOPMENT OF BUSHING MODELS

Introduction

The analytical background and simplified methods for the evaluation of dynamic properties and forces of transformer bushings during response to imparted motion are developed in this section. Formulations are done for one plane of behavior, assuming one principal direction. Extension to three-dimensional analytical modeling is straightforward, but requires a more lengthy extension of this analysis.

When the bushing is mounted on a transformer tank, either directly on the cover or on a turret, the bushing behaves like a cantilever with the mounting flange relatively rigid in respect to the rest of the body. However, when the bushing is mounted on a transformer cover that has vertical flexibility, while the tank has horizontal flexibility then the bushing can be installed on vertical and horizontal springs that represent the cover and the tank. It should be noted that the cover of the tank can also rotate due to its out-of-plane local rotational flexibility. This is best represented by the two vertical springs below the flange as shown in Figure E-1.

Figure E-1: Simplified Model of Bushing

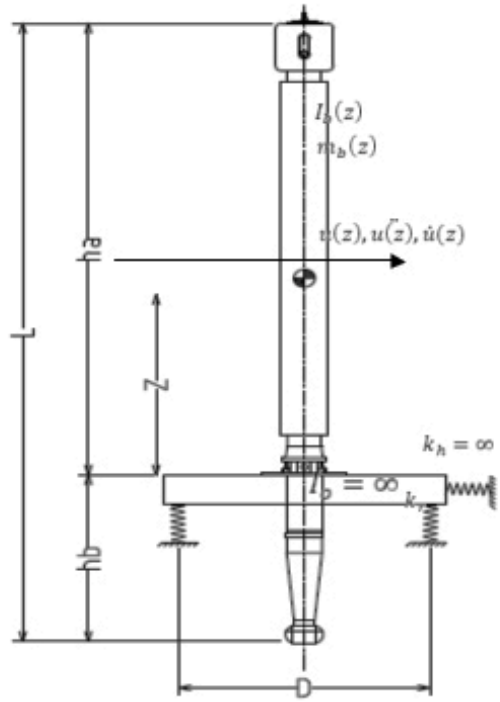

The stiffness and dynamic properties of bushings supported by the specified springs are determined analytically as a function of the assumed springs. These properties can be defined as the properties of the bushings "as-installed." Then, the properties of the springs that represent the cover and the tanks are determined analytically. Rigorous relations are determined first, followed by development of approximated but simpler formulations that could be used in the bushing design process.

The seismic response is also modeled analytically in order to understand the differences between the effects of the tank cover and its motions on the response of bushings and the forces leading to failure.

The results of the analytical and numerical analyses are compared where possible with the results of the laboratory testing.

Modeling Transformer Bushing Using Continuum

Referring to Figure E-1:

m(z) or $m_b(z)$	Distributed mass of bushing as a function of location above or below base plate
I(z) or $I_b(z)$	Moment of inertia of the bushing
Io $\rightarrow\infty$ -	Stiffness of base flange of bushing
k or k_θ	Stiffness of base, transformer cover, or turret and transformer cover

k_r	In-plane stiffness of transformer cover, which is assumed rigid in-plane
$\phi_r(z)$	r-th modal shape of bushing
$\ddot{u}(z,t), \dot{u}(z,t), u(z,t)$	Acceleration, velocity and displacement, respectively, at level z
$\ddot{u}_g(t);\ \ddot{\vartheta}_g(t)$	Horizontal and rotational acceleration at the base of bushing (excitations)
h_a	Vertical height above the connection base

Cantilever with distributed mass and elasticity

The bushing can be modeled by simple cantilevers connected through rotational springs, as shown in Figure E-2.

The equation of undamped motion of the system when excited by horizontal and rotational ground motion is:

$$m(z)\ddot{u}(z,t)+\left[EI(z)u''(z,t)\right]'' = -m(z)\ddot{u}_g(t)-m(z)z\ddot{\vartheta}_g(t) \tag{20}$$

The displacement *u(z,t)* can be written as a linear combination of the modes:

$$u(z,t)=\sum_{r=1}^{\infty}\phi_r(z)q_r(t) \tag{21}$$

Substituting Eq. (21) into Eq. (20) gives:

$$\sum_{r=1}^{\infty}m(z)\phi_r(z)\ddot{q}_r(t)+\sum_{r=1}^{\infty}\left[EI(z)\phi_r''(z)\right]'' q_r(t) = -m(z)\ddot{u}_g(t)-m(z)z\ddot{\vartheta}_g(t) \tag{22}$$

Figure E-2: Cantilever and Rotational Spring Model of Bushing

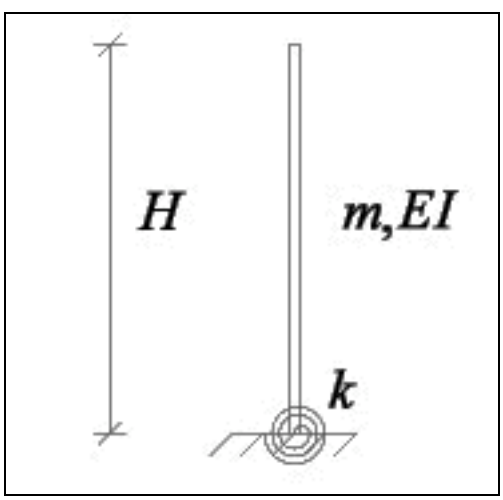

Multiplying each term of Eq. (22) by $\phi_n(z)$ and integrating over the height of the bushing leads to:

$$\sum_{r=1}^{\infty}\ddot{q}_r(t)\int_0^H m(z)\phi_r(z)\phi_n(z)dz+\sum_{r=1}^{\infty}q_r(t)\int_0^H\left[EI(z)\phi_r''(z)\right]''\phi_n(z)dz=$$
$$=-\ddot{u}_g(t)\int_0^H m(z)\phi_n(z)dz-\ddot{\vartheta}_g(t)\int_0^H m(z)z\phi_n(z)dz \tag{23}$$

For the orthogonality properties of modes, all the terms in the summations vanish except for the r = n term giving:

$$\ddot{q}_n(t)\int_0^H m(z)\left[\phi_n(z)\right]^2dz+q_n(t)\int_0^H\left[EI(z)\phi_n''(z)\right]''\phi_n(z)dz=$$
$$=-\ddot{u}_g(t)\int_0^H m(z)\phi_n(z)dz-\ddot{\vartheta}_g(t)\int_0^H m(z)z\phi_n(z)dz \tag{24}$$

Eq. (24) may be rewritten as:

$$M_n\ddot{q}_n(t)+K_nq_n(t)=-\mathrm{L}_n\ddot{u}_g(t)-\mathrm{L}_n^{\vartheta}\ddot{\vartheta}_g(t) \tag{25}$$

where

$$M_n=\int_0^H m(z)\left[\phi_n(z)\right]^2dz \qquad K_n=\int_0^H\left[EI(z)\phi_n''(z)\right]''\phi_n(z)dz$$
$$\mathrm{L}_n=\int_0^H m(z)\phi_n(z)dz \qquad \mathrm{L}_n^{\vartheta}=\int_0^H m(z)z\phi_n(z)dz \tag{26}$$

The expression of the generalized stiffness K_n in Eq. (26) can be integrated by parts twice as follows:

$$K_n=\int_0^H\left[EI(x)\phi_n''(z)\right]''\phi_n(z)dz=\left\{\left[EI(z)\phi_n''(z)\right]'\phi_n(z)\right\}_0^H-\left\{\left[EI(z)\phi_n''(z)\right]\phi_n'(z)\right\}_0^H+$$
$$+\int_0^H EI(z)\left[\phi_n''(z)\right]^2dz \tag{27}$$

For the cantilever with null moment and shear at the top H, and partially fixed (displacement) at the base 0, the first term vanishes at both ends and the second term vanishes at the top. In this particular case there is a rotational spring with stiffness k at the base (z = 0) and therefore

$$\left[EI(0)\phi_n''(0)\right]=k\left[\phi_n'(0)\right] \tag{28}$$

Eq. (27) assumes the following form:

$$K_n = \left[EI(0)\phi_n''(0)\right]\phi_n'(0) + \int_0^H EI(z)\left[\phi_n''(z)\right]^2 dz = k\left[\phi_n'(0)\right]^2 + \int_0^H EI(z)\left[\phi_n''(z)\right]^2 dz \tag{29}$$

The generalized stiffness K_n and the generalized mass M_n are related by:

$$K_n = \omega_n^2 M_n \quad or \quad f_n = 1/2\pi \cdot \sqrt{K_n / M_n} \tag{30}$$

The exact expression for the modal frequency (circular and direct) is:

$$\omega_n^2 = \frac{K_n}{M_n} = \frac{k\left[\phi_n'(0)\right]^2 + \int_0^H EI(z)\left[\phi_n''(z)\right]^2 dz}{\int_0^H m(z)\left[\phi_n(z)\right]^2 dz} \quad \text{or} \quad f_n = \frac{1}{2\pi}\sqrt{\frac{k\left[\phi_n'(0)\right]^2 + \int_0^H EI(z)\left[\phi_n''(z)\right]^2 dz}{\int_0^H m(z)\left[\phi_n(z)\right]^2 dz}} \tag{31}$$

Let us express the mode $\phi_n(z)$ as the sum of the fixed base mode shape $\phi_{n0}(z)$ and a linear mode shape due to the base rotation, that is:

$$\begin{aligned} \phi_n(z) &= \phi_{n0}(z) + \phi_n'(0)z \\ \phi_n'(z) &= \phi_{n0}'(z) + \phi_n'(0) \\ \phi_n''(z) &= \phi_{n0}''(z) \end{aligned} \tag{32}$$

Using Eq. (32) the expressions for the modal stiffness K_n and the modal mass M_n can be written as:

$$K_n = k\left[\phi_n'(0)\right]^2 + \int_0^H EI(z)\left[\phi_n''(z)\right]^2 dz = k\left[\phi_n'(0)\right]^2 + \int_0^H EI(z)\left[\phi_{n0}''(z)\right]^2 dz = k\left[\phi_n'(0)\right]^2 + K_{n0} \tag{33}$$

$$\begin{aligned} M_n &= \int_0^H m(z)\left[\phi_n(z)\right]^2 dz = \int_0^H m(z)\left[\phi_{n0}(z) + \phi_n'(0)z\right]^2 dz = \int_0^H m(z)\left[\phi_{n0}(z)\right]^2 dz \\ &+ \left[\phi_n'(0)\right]^2 \int_0^H m(z)z^2 dz + 2\phi_n'(0)\int_0^H m(z)\phi_{n0}(z)z dz = M_{n0} + \left[\phi_n'(0)\right]^2 M_1 + 2\phi_n'(0)M_{n01} \end{aligned} \tag{34}$$

where

$$\begin{aligned} K_{n0} &= \int_0^H EI(z)\left[\phi_{n0}''(z)\right]^2 dz \qquad & M_{n0} &= \int_0^H m(z)\left[\phi_{n0}(z)\right]^2 dz \\ M_1 &= \int_0^H m(z)z^2 dz & M_{n01} &= \int_0^H m(z)\phi_{n0}(z)z dz \end{aligned} \tag{35}$$

Substituting Eq. (33) and Eq. (34) into Eq. (31) we get:

$$\omega_n^2 = \left(4\pi f_n\right)^2 = \frac{K_n}{M_n} = \frac{k\left[\phi_n'(0)\right]^2 + K_{n0}}{M_{n0} + \left[\phi_n'(0)\right]^2 M_1 + 2\phi_n'(0) M_{n01}} \tag{36}$$

Eq. (36) can be written as:

$$f_n^2 = \frac{1}{4\pi^2}\frac{K_{n0}}{M_{n0}}\frac{\dfrac{k\left[\phi_n'(0)\right]^2}{K_{n0}}+1}{1+\left[\phi_n'(0)\right]^2\dfrac{M_1}{M_{n0}}+2\phi_n'(0)\dfrac{M_{n01}}{M_{n0}}} = f_{n0}^2\frac{1+\dfrac{k\left[\phi_n'(0)\right]^2}{K_{n0}}}{1+\phi_n'(0)\dfrac{\phi_n'(0)M_1+2M_{n01}}{M_{n0}}} =$$

$$= f_{n0}^2\frac{1+\dfrac{k\left[\phi_n'(0)\right]^2}{K_{n0}}}{1+\phi_n'(0)\dfrac{\phi_n'(0)\displaystyle\int_0^H m(z)z^2dz+2\int_0^H m(z)\phi_{n0}(z)zdz}{\displaystyle\int_0^H m(z)\left[\phi_{n0}(z)\right]^2dz}} \tag{37}$$

where:

$$f_{no} = \frac{1}{2\pi}\cdot\sqrt{\frac{\displaystyle\int_0^H EI(z)\left[\phi_{no}''(z)\right]^2dz}{\displaystyle\int_0^H m(z)\left[\phi_{no}(z)\right]^2dz}} \tag{38}$$

By using $\phi_n'(0)=M_n(0)/k$, where $M_n(0)$ is the moment at the base of the bushing, Eq. (37) may be written as:

$$f_n^2 = f_{n0}^2\frac{1+\dfrac{\left[M_n(0)\right]^2}{k}\dfrac{1}{K_{n0}}}{1+\dfrac{M_n(0)}{k}\dfrac{\dfrac{M_n(0)}{k}M_1+2M_{n01}}{M_{n0}}} = \frac{1+\dfrac{\left[M_n(0)\right]^2}{k}\dfrac{1}{\displaystyle\int_0^H EI(z)\left[\phi_{n0}''(z)\right]^2dz}}{1+\dfrac{M_n(0)}{k}\dfrac{\dfrac{M_n(0)}{k}\displaystyle\int_0^H m(z)z^2dz+2\int_0^H m(z)\phi_{n0}(z)zdz}{\displaystyle\int_0^H m(z)\left[\phi_{n0}(z)\right]^2dz}} \tag{39}$$

or simply:

$$f_n = f_{no} \cdot \sqrt{\frac{1+\frac{\left[M_n(0)\right]^2}{k}\frac{1}{\int_0^H EI(z)\left[\phi''_{n0}(z)\right]^2 dz}}{1+\frac{M_n(0)}{k}\frac{\frac{M_n(0)}{k}\int_0^H m(z)z^2dz+2\int_0^H m(z)\phi_{n0}(z)zdz}{\int_0^H m(z)\left[\phi_{n0}(z)\right]^2 dz}}} \tag{40}$$

Note that:

for k→∞ the frequency reduces to the fixed base frequency f_{no}, while

for k→0 the frequency gets close to zero depending on mass distribution, dynamic shape function, and magnitude of the base moment.

A clearer dependency can be obtained by solving accurately the dynamics of the system as shown next.

Exact Natural Mode Shapes and Frequencies

In the case of free vibration, Eq. (20) becomes:

$$m(z)\ddot{u}(z,t)+\left[EI(z)u''(z,t)\right]''=0 \tag{41}$$

A solution to Eq. (41) can be found of the form:

$$u(z,t)=\phi(z)q(t) \tag{42}$$

Substitution of Eq. (42) into Eq. (41) allows to transform the partial differential equation (41) into two ordinary differential equations, one governing the time function *q(t)*, that has the same form as the equation governing the free vibration of a single degree of freedom system, and the other governing the spatial function $\phi(z)$:

$$\ddot{q}(t)+\omega^2 q(t)=0 \tag{43}$$

$$\left[EI(z)\phi''(z)\right]''-\omega^2 m(z)\phi(z)=0 \tag{44}$$

For any given stiffness and mass distributions *EI(z)* and *m(z)* an infinite set of frequencies ω and mode shapes $\phi(z)$ exist that satisfy the eigenvalue problem defined by Eq. (44) and the boundary conditions for the beam. For the case of a uniform beam, that is, *EI(z)* = *EI* and *m(z)* = *m*, the equation governing the spatial function $\phi(z)$ becomes:

$$EI\phi^{IV}(z)-\omega^2 m\phi(z)=0 \text{ or } \phi^{IV}(z)-\beta^4\phi(z)=0 \tag{45}$$

Where:

$$\beta^4 = \frac{\omega^2 m}{EI} \tag{46}$$

The general solution to Eq. (45) is given by the following expressions:

$$\begin{aligned}
\phi(z) &= C_1 \sin\beta z + C_2 \cos\beta z + C_3 \sinh\beta z + C_4 \cosh\beta z \\
\phi'(z) &= \beta C_1 \cos\beta z - \beta C_2 \sin\beta z + \beta C_3 \cosh\beta z + \beta C_4 \sinh\beta z \\
\phi''(z) &= -\beta^2 C_1 \sin\beta z - \beta^2 C_2 \cos\beta z + \beta^2 C_3 \sinh\beta z + \beta^2 C_4 \cosh\beta z \\
\phi'''(z) &= -\beta^3 C_1 \cos\beta z + \beta^3 C_2 \sin\beta z + \beta^3 C_3 \cosh\beta z + \beta^3 C_4 \sinh\beta z
\end{aligned} \tag{47}$$

The solution given by Eq. (47) contains four unknown constants, C_1, C_2, C_3 and C_4, and the parameter β. Application of four boundary conditions, two at each end of the beam, allows for the evaluation of the eigenvalue parameter β, from which the natural frequency ω can be evaluated through Eq. (46), and provides a solution for three constants in terms of the fourth, resulting in the natural mode shape given by the first equation of Eq. (47).

In this particular case, at the base (z = 0) the displacement is zero and the bending moment is equal to the stiffness k of the rotational spring multiplied by the base rotation. Eq. (47) therefore gives:

$$\begin{aligned}
&u(0,t) = 0 \;\Rightarrow\; \phi(0) = 0 \;\Rightarrow\; C_2 + C_4 = 0 \;\Rightarrow\; C_4 = -C_2 \\
&M(0,t) = ku'(0,t) \;\Rightarrow\; EI\phi''(0) = k\phi'(0) \;\Rightarrow\; C_1 + \frac{2EI\beta}{k} C_2 + C_3 = 0
\end{aligned} \tag{48}$$

At the free end (z = H), the bending moment and shear are both zero. Therefore, after using Eq. (48), Eq. (47) gives:

$$\begin{aligned}
&M(H,t) = 0 \;\Rightarrow\; EI\phi''(0) = 0 \;\Rightarrow\; C_1 \sin\beta H + C_2(\cos\beta H + \cosh\beta H) - C_3 \sinh\beta H = 0 \\
&V(H,t) = 0 \;\Rightarrow\; EI\phi'''(0) = 0 \;\Rightarrow\; C_1 \cos\beta H + C_2(\sinh\beta H - \sin\beta H) - C_3 \cosh\beta H = 0
\end{aligned} \tag{49}$$

By defining an additional dimensionless parameter $\sigma = EI/kH$, Eq. (48) and Eq. (49) may be written in the following matrix form:

$$\begin{bmatrix} 1 & 2\sigma\beta H & 1 \\ s & c + C & -S \\ c & S - s & -C \end{bmatrix} \begin{bmatrix} C_1 \\ C_2 \\ C_3 \end{bmatrix} = \begin{bmatrix} 0 \\ 0 \\ 0 \end{bmatrix} \tag{50}$$

With:

$$s = \sin\beta H;\; c = \cos\beta H;\; S = \sinh\beta H;\; C = \cosh\beta H \tag{51}$$

Setting the determinant of the coefficient matrix of Eq. (50) to be zero yields the following frequency equation:

$$1 + cC - \beta H\sigma[sC - cS] = 0 \tag{52}$$

If we set $\sigma = 0$ in Eq. (52), meaning that the spring at the base has infinite stiffness, the frequency equation of a cantilever with fixed base is recovered.

Eq. (52) can be solved numerically for $\beta_n H$, where n = 1, 2, 3,… ∞. The natural frequencies ω_n can then be obtained from Eq. (46). The following procedure is adopted to obtain an expression for the natural mode off vibration corresponding to each value of $\beta_n H$. First the constant C_1 is condensed out of Eq. (50):

$$\begin{bmatrix} c+C & -S \\ S-s & -C \end{bmatrix} \begin{bmatrix} C_2 \\ C_3 \end{bmatrix} = \begin{bmatrix} -s \\ -c \end{bmatrix} C_1 \tag{53}$$

Then the constants C_2 and C_3 are expressed in terms of C_1 by inverting the coefficient matrix of Eq. (53):

$$\begin{bmatrix} C_2 \\ C_3 \end{bmatrix} = \frac{C_1}{Cc+Ss+1} \begin{bmatrix} Sc-Cs \\ Cc-Ss+1 \end{bmatrix} \tag{54}$$

Finally, using Eq. (54) and Eq. (48), the following expression is obtained for the natural modes of vibration:

$$\phi_n(z) = C_1 \left[\sin\beta_n z + \frac{Sc-Cs}{Cc+Ss+1}\cos\beta_n z + \frac{Cc-Ss+1}{Cc+Ss+1}\sinh\beta_n z + \frac{Cs-Sc}{Cc+Ss+1}\cosh\beta_n z \right] \tag{55}$$

C_1 is a parameter that depends on how the modes are normalized. It may be convenient to normalize the modes as to be unity at the top. In that case we have:

$$C_1 = 1 \Big/ \left[s + \frac{Sc-Cs}{Cc+Ss+1}c + \frac{Cc-Ss+1}{Cc+Ss+1}S + \frac{Cs-Sc}{Cc+Ss+1}C \right] \tag{56}$$

Influence of the Rotational Spring on the Fundamental Frequency

The fundamental frequency of a cantilever beam can be obtained by substituting the smallest root $\beta_n H$ of the frequency equation (52) into the following equation derived by using Eq. (46) to get:

$$f_{1,k} = \frac{1}{2\pi}\frac{(\beta_1 H)^2}{H^2}\sqrt{\frac{EI}{m}} \tag{57}$$

In the case of a fixed-base cantilever, $(\beta_n H)^2 = 3.516$. The influence of the rotational spring at the base on the fundamental frequency of a cantilever beam is shown in Figure E-3 by plotting $(\beta_1 H)^2$ as a function of the dimensionless parameter $\sigma = EI/kH$.

Figure E-4 shows the ratio of the fundamental frequency of the cantilever mounted on a semi-rigid base (represented by the base spring k) to that of the fixed base cantilever. Figure E-5 is a close up view of for $0 \le \sigma \le 1$, which is a range of more interest.

Figure E-3: $(\beta_1 H)^2$ as a Function of the Dimensionless Parameter σ = EI/kH

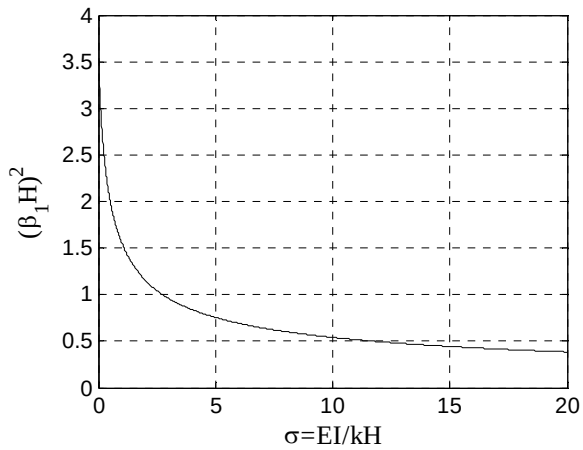

Figure E-4: Frequency Ratio for 0≤ σ ≤20

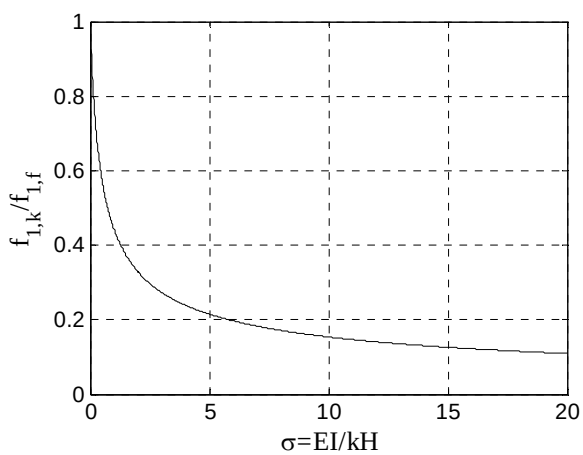

It should be noted that the reduction in frequency due to the flexible base is particularly important when σ becomes large and therefore for stiff bushings characterized by large *EI*, small *H* or both.

Approximate Evaluation of the Fundamental Frequency

An approximation to the frequency ratio curves plotted in Figures E-4 and E-5 may be obtained using the Southwell-Dunkerley method (Newmark and Rosenblueth, 1971[7]) as presented below. The cantilever bushing on flexible base is treated as the sum of a flexible system on fixed base and a rigid system on flexible base, both beams having the same uniform mass distribution. The decomposition of the system is shown in Figure E-6.

Figure E-5: Frequency Ratio for 0≤ σ ≤1

[7] Newmark, N.M. and Rosenblueth E., (1971), *Fundamentals of Earthquake Engineering*, Prentice Hall International, London

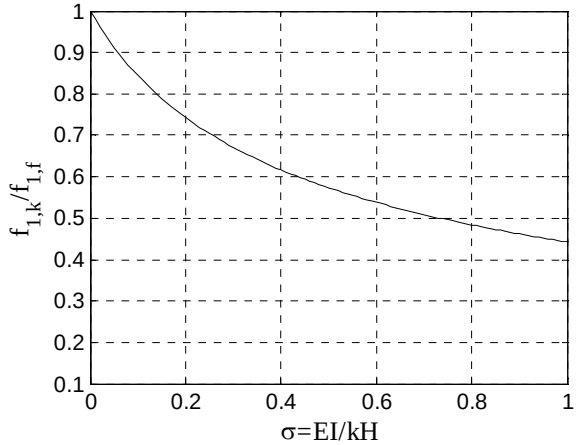

The fundamental frequency of the system on flexible base can then be evaluated as follows:

$$\frac{1}{f_{1,k}^2} = \frac{1}{f_{1,f}^2} + \frac{1}{f_r^2} \tag{58}$$

where $f_{1,k}$, $f_{1,f}$ and f_r are the fundamental frequencies of the systems shown in Figure E-6 (a), (b) and (c) respectively. Eq. (58) may be manipulated to yield:

$$f_{1,k} = f_{1,f}\sqrt{\frac{1}{1+\left(f_{1,f}/f_r\right)^2}} \tag{59}$$

Figure E-6: System Decomposition

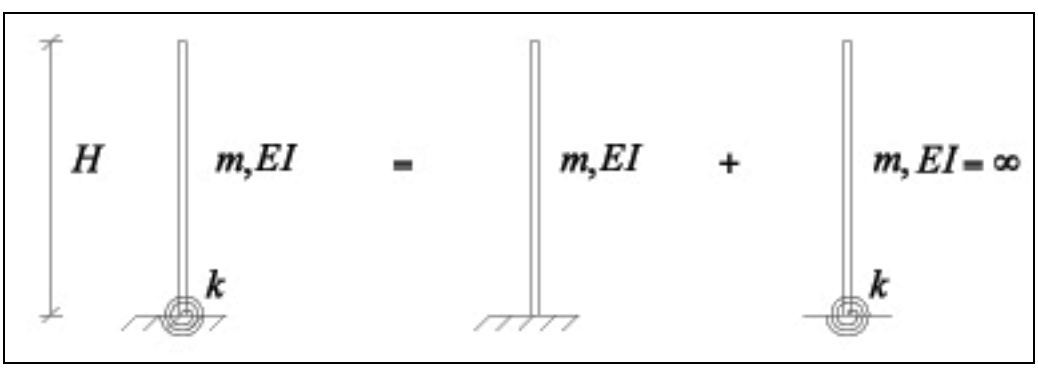

a) Flexible Base Cantilever; b) Fixed Base Cantilever; c) Rigid System on Flexible Base

The square of the first mode frequency of the cantilever beam on fixed base and that of the rigid beam with a spring at the base are easily evaluated as:

$$f_{1,f}^2 = \frac{(3.516)^2}{(2\pi)^2}\frac{EI}{mH^4}; \qquad f_r^2 = \frac{3}{(2\pi)^2}\frac{k}{mH^3} \tag{60}$$

Substituting Eq. (60) into Eq. (59) leads to the following expression for the frequency ratio:

$$f_{1,k} = f_{1,f}\sqrt{\frac{1}{1+\lambda\sigma}} \qquad \text{where} \qquad \lambda = \frac{(3.516)^2}{3} = 4.12; \qquad \sigma = \frac{EI}{kH} \tag{61}$$

Figure E-7 shows the frequency ratio based on the exact solution versus the approximation, Eq. (61), based on the Southwell-Dunkerley method. Since the differences are negligible, the latter may be used as an extremely good approximation for design purposes.

Figure E-7: Ratio of the Flexible to Fixed-base Frequency: Exact vs. Approximation

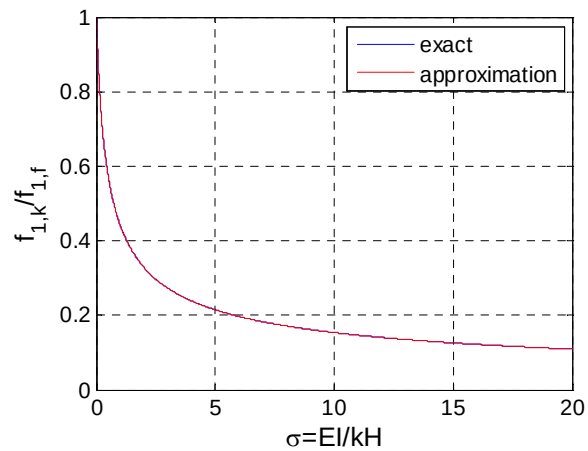

Cantilever with Distributed Mass and Additional Lumped Mass

The equation of undamped motion of the system excited by horizontal and rotational ground motion is derived from Eq. (20) adding the lumped mass M at the top (see Figure E-8):

$$\begin{aligned}\left[m(z)+\mathrm{M}\delta(z-H)\right]\ddot{u}(z,t)+\left[EI(z)u''(z,t)\right]'' = \\ -\left[m(z)+\mathrm{M}\delta(z-H)\right]\ddot{u}_g(t)-\left[m(z)+\mathrm{M}\delta(z-H)\right]z\ddot{\vartheta}_g(t)\end{aligned} \tag{62}$$

where $\delta(\cdot)$ represents the Dirac Delta function.

The displacement *u(z,t)* can be written as a linear combination of the modes:

$$u(z,t) = \sum_{r=1}^{\infty}\phi_r(z)q_r(t) \tag{21}$$

Substituting Eq. (21) into Eq. (62) gives:

$$\sum_{r=1}^{\infty}\left[m(z)+\mathrm{M}\delta(z-H)\right]\phi_r(z)\ddot{q}_r(t)+\sum_{r=1}^{\infty}\left[EI(z)\phi_r''(z)\right]''q_r(t)= \\ -\left[m(z)+\mathrm{M}\delta(z-H)\right]\ddot{u}_g(t)-\left[m(z)+\mathrm{M}\delta(z-H)\right]z\ddot{\vartheta}_g(t) \tag{63}$$

Figure E-8: Cantilever with Distributed Mass and Additional Lumped Mass

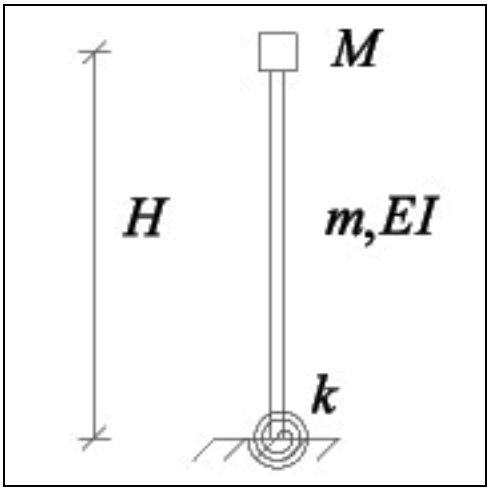

Multiplying each term of Eq. (62) by $\phi_n(z)$ and integrating over the height of the bushing leads to:

$$\sum_{r=1}^{\infty}\ddot{q}_r(t)\int_0^H\left[m(z)+\mathrm{M}\delta(z-H)\right]\phi_r(z)\phi_n(z)dz+\sum_{r=1}^{\infty}q_r(t)\int_0^H\left[EI(z)\phi_r''(z)\right]''\phi_n(z)dz= \\ =-\ddot{u}_g(t)\int_0^H\left[m(z)+\mathrm{M}\delta(z-H)\right]\phi_n(z)dz-\ddot{\vartheta}_g(t)\int_0^H\left[m(z)+\mathrm{M}\delta(z-H)\right]z\phi_n(z)dz \tag{64}$$

For the orthogonality properties of modes all the terms in the summations vanish except for the r = n term giving:

$$\sum_{r=1}^{\infty}\ddot{q}_r(t)\int_0^H\left[m(z)+\mathrm{M}\delta(z-H)\right]\left[\phi_n(z)\right]^2dz+\sum_{r=1}^{\infty}q_r(t)\int_0^H\left[EI(z)\phi_r''(z)\right]''\phi_n(z)dz= \\ =-\ddot{u}_g(t)\int_0^H\left[m(z)+\mathrm{M}\delta(z-H)\right]\phi_n(z)dz-\ddot{\vartheta}_g(t)\int_0^H\left[m(z)+\mathrm{M}\delta(z-H)\right]z\phi_n(z)dz \tag{65}$$

Exploiting the properties of the Dirac Delta function Eq. (65) becomes:

$$\ddot{q}_n(t)\left[\int_0^H m(z)\left[\phi_n(z)\right]^2 dz + \mathrm{M}\left[\phi_n(H)\right]^2\right] + q_n(t)\int_0^H \left[EI(z)\phi_n''(z)\right]''\phi_n(z)dz =$$
$$= -\ddot{u}_g(t)\left[\int_0^H m(z)\phi_n(z)dz + \mathrm{M}\phi_n(H)\right] - \ddot{\vartheta}_g(t)\left[\int_0^H m(z)z\phi_n(z)dz + \mathrm{M}H\phi_n(H)\right] \tag{66}$$

Eq. (66) may be rewritten as:

$$M_n\ddot{q}_n(t) + K_n q_n(t) = -\mathrm{L}_n\ddot{u}_g(t) - \mathrm{L}_n^{\vartheta}\ddot{\vartheta}_g(t) \tag{67}$$

Where:

$$M_n = \int_0^H m(z)\left[\phi_n(z)\right]^2 dz + \mathrm{M}\left[\phi_n(H)\right]^2 \qquad K_n = \int_0^H \left[EI(z)\phi_n''(z)\right]''\phi_n(z)dz$$
$$\mathrm{L}_n = \int_0^H m(z)\phi_n(z)dz + \mathrm{M}\phi_n(H) \qquad \mathrm{L}_n^{\vartheta} = \int_0^H m(z)z\phi_n(z)dz + \mathrm{M}H\phi_n(H) \tag{68}$$

The expression of the generalized stiffness K_n in Eq. (68) can be integrated by parts twice as follows:

$$K_n = \int_0^H \left[EI(x)\phi_n''(z)\right]''\phi_n(z)dz = \left\{\left[EI(z)\phi_n''(z)\right]'\phi_n(z)\right\}_0^H - \left\{\left[EI(z)\phi_n''(z)\right]\phi_n'(z)\right\}_0^H +$$
$$+\int_0^H EI(z)\left[\phi_n''(z)\right]^2 dz \tag{69}$$

For the cantilever with null moment and shear at the top H, and partially fixed (displacement) at the base 0, the first term vanishes at both ends and the second term vanishes at the top. In this particular case there is a rotational spring with stiffness k at the base (z = 0) and therefore:

$$\left[EI(0)\phi_n''(0)\right] = k\left[\phi_n'(0)\right] \tag{70}$$

Eq. (69) assumes the following form:

$$K_n = \left[EI(0)\phi_n''(0)\right]\phi_n'(0) + \int_0^H EI(z)\left[\phi_n''(z)\right]^2 dz = k\left[\phi_n'(0)\right]^2 + \int_0^H EI(z)\left[\phi_n''(z)\right]^2 dz \tag{71}$$

The generalized stiffness K_n and the generalized mass M_n are related by:

$$K_n = \omega_n^2 M_n \tag{72}$$

Exact Natural Mode Shapes and Frequencies

At the base the displacement is zero and the bending moment is equal to the stiffness k of the rotational spring multiplied by the base rotation. Eq. (47) therefore gives:

$$u(0,t)=0 \;\Rightarrow\; \phi(0)=0 \;\Rightarrow\; C_2+C_4=0 \;\Rightarrow\; C_4=-C_2$$
$$M(0,t)=ku'(0,t) \;\Rightarrow\; EI\phi''(0)=k\phi'(0) \;\Rightarrow\; C_1+\frac{2EI\beta}{k}C_2+C_3=0 \tag{73}$$

At the free end the bending moment is zero while the shear force is equal to the inertia force acting on the lumped mass M. Therefore, after using Eq. (73), Eq. (47) gives:

$$M(H,t)=0 \;\Rightarrow\; EI\phi''(H)=0 \;\Rightarrow\; C_1\sin\beta H+C_2(\cos\beta H+\cosh\beta H)-C_3\sinh\beta H=0$$
$$V(H,t)=M\ddot{u}(H,t)=-\omega^2\mathrm{M}\,u(H,t) \;\Rightarrow\; EI\phi'''(H)+\omega^2\mathrm{M}\phi(H)=0$$
$$\Rightarrow\; \phi'''(H)+\frac{\omega^2\mathrm{M}}{EI}\phi(H)=0 \;\Rightarrow\; C_1(\sin\beta H-\alpha\cos\beta H)$$
$$+C_2(\alpha\sin\beta H-\alpha\sinh\beta H+\cos\beta H-\cosh\beta H)+C_3(\cosh\beta H+\sinh\beta H)=0 \tag{74}$$

where:

$=1/\rho\beta H$ and $\rho=\mathrm{M}/mH$ are dimensionless parameters.

By defining an additional dimensionless parameter $\sigma=EI/H$, Eq. (73) and Eq. (74) may be written in the following matrix form:

$$\begin{bmatrix} 1 & 2\sigma\beta H & 1 \\ s & c+C & -S \\ s-\alpha c & \alpha(s-S)+c-C & \alpha C+S \end{bmatrix}\begin{bmatrix} C_1 \\ C_2 \\ C_3 \end{bmatrix}=\begin{bmatrix} 0 \\ 0 \\ 0 \end{bmatrix} \tag{75}$$

With:

$$s=\sin\beta H;\; c=\cos\beta H;\; S=\sinh\beta H;\; C=\cosh\beta H \tag{76}$$

Setting the determinant of the coefficient matrix of Eq. (75) to be zero yields the following frequency equation**:**

$$\alpha(1+\cos\beta H\cosh\beta H+\sigma\beta H\sin\beta H\cosh\beta H+\sigma\beta H\cos\beta H\sinh\beta H)+\cos\beta H\sinh\beta H$$
$$-\sin\beta H\cosh\beta H-2\sigma\beta H\sin\beta H\sinh\beta H=0 \tag{77}$$

If we set $\sigma=0$ in Eq. (77), meaning that the spring at the base has infinite stiffness, the frequency equation of the same system with fixed base is recovered.

It should be noted that α in Eq. (77) is a function of βH. Eq. (77) can be solved numerically for $\beta_n H$, where n = 1, 2, 3,…∞. The natural frequencies ω_n can then be obtained from Eq. (46). The following procedure is adopted to obtain an expression for the natural mode of vibration corresponding to each value of $\beta_n H$. First the constant C_1 is condensed out of Eq. (75):

$$\begin{bmatrix} c+C & -S \\ \alpha(s-S)+c-C & \alpha C+S \end{bmatrix}\begin{bmatrix} C_2 \\ C_3 \end{bmatrix}=\begin{bmatrix} -s \\ \alpha c-s \end{bmatrix}C_1 \tag{78}$$

Then the constants C_2 and C_3 are expressed in terms of C_1 by inverting the coefficient matrix of Eq. (78):

$$\begin{bmatrix} C_2 \\ C_3 \end{bmatrix} = \frac{C_1}{\alpha(1+cC+sS)+2cS} \begin{bmatrix} \alpha(cS-sC)-2sS \\ \alpha(1+cC-sS)-2sC \end{bmatrix} \tag{79}$$

Finally using Eq. (79) and Eq. (73) the following expression is obtained for the natural modes of vibration:

$$\begin{aligned} \phi_n(z) = C_1 \Bigg[& \sin\beta_n z + \frac{\alpha(cS-sC)-2sS}{\alpha(1+cC+sS)+2cS}\cos\beta_n z + \\ & + \frac{\alpha(1+cC-sS)-2sC}{\alpha(1+cC+sS)+2cS}\sinh\beta_n z + \frac{2sS-\alpha(cS-sC)}{\alpha(1+cC+sS)+2cS}\cosh\beta_n z \Bigg] \end{aligned} \tag{80}$$

C_1 is a parameter that depends on how the modes are normalized. It may be convenient to normalize the modes as to be unity at the top. In that case:

$$\begin{aligned} C_1 = 1 \Bigg/ \Bigg[& \sin\beta_n H + \frac{\alpha(cS-sC)-2sS}{\alpha(1+cC+sS)+2cS}\cos\beta_n H + \\ & + \frac{\alpha(1+cC-sS)-2sC}{\alpha(1+cC+sS)+2cS}\sinh\beta_n H + \frac{2sS-\alpha(cS-sC)}{\alpha(1+cC+sS)+2cS}\cosh\beta_n H \Bigg] \end{aligned} \tag{81}$$

Influence of the Rotational Spring on the Fundamental Frequency

The fundamental frequency can be obtained by substituting the smallest root $\beta_n H$ of the frequency in Eq. (77) into the following equation, derived by using Eq. (46), to get:

$$f_{1,k} = \frac{1}{2\pi}\frac{(\beta_1 H)^2}{H^2}\sqrt{\frac{EI}{m}} \tag{82}$$

The influence of the base rotational spring on the fundamental frequency of a cantilever beam is shown in Figure E-9 by plotting the ratio of the frequency of the cantilever with the base spring to that of the fixed base cantilever for different values of the mass parameter $\rho = M/mH$.

Approximate Evaluation of the Fundamental Frequency

An approximation to the frequency ratio curves plotted in Figure E-9 may again be obtained by using the Southwell-Dunkerley method. The cantilever bushing on flexible base is treated as the sum of a flexible system on fixed base and a rigid system on flexible base, both systems having the same uniform mass distribution m and the same lumped mass ρmH at the top. The decomposition is shown in Figure E-10.

Figure E-9: Frequency Ratio for 0≤ σ ≤1 and different values of ρ

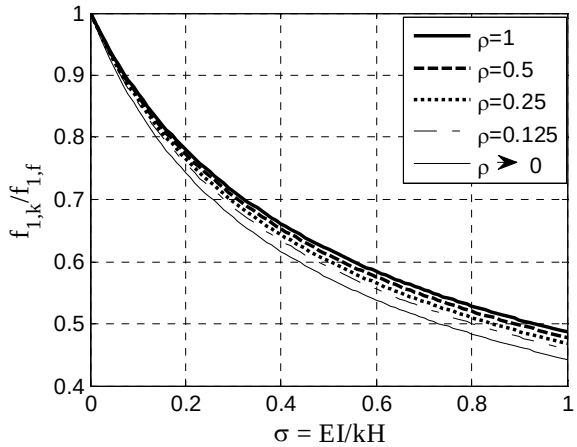

Figure E-10: Flexible Base System Decomposition

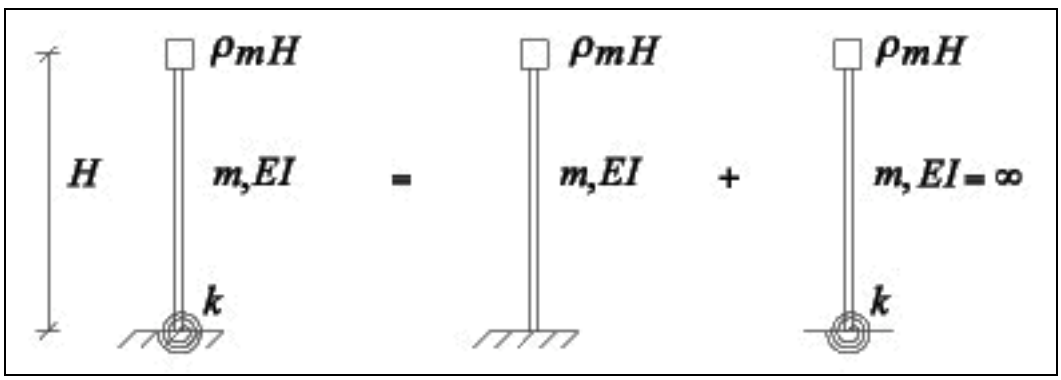

(a) Flexible Base Cantilever (b) Fixed Base Cantilever (c) Rigid System on Flexible Base

The frequency of the system on flexible base can then be evaluated as follows:

$$\frac{1}{f_{1,k}^2} = \frac{1}{f_{1,f}^2} + \frac{1}{f_r^2} \tag{83}$$

where $f_{1,k}$, $f_{1,f}$ and f_r are the fundamental frequencies of the systems shown in Figure E-10(a), (b) and (c) respectively. Eq. (83) may be manipulated to yield:

$$f_{1,k} = f_{1,f}\sqrt{\frac{1}{1+\left(f_{1,f}/f_r\right)^2}} \tag{84}$$

The square of the frequency of the rigid system shown in Figure E-10(c) is evaluated as:

$$f_r^2 = \frac{1}{(2\pi)^2}\frac{3}{(3\rho+1)}\frac{k}{mH^3} \tag{85}$$

The square of the first mode frequency of the cantilever beam with a lumped mass at the top and on fixed base may be evaluated itself using the Southwell-Dunkerley method. For this purpose the system of Figure E-10(b) is decomposed as the sum of a cantilever with uniformly distributed mass m and one with a lumped mass ρmH at the top, both systems having the same stiffness. The decomposition is shown in Figure E-11.

Figure E-11: Fixed Base System Decomposition

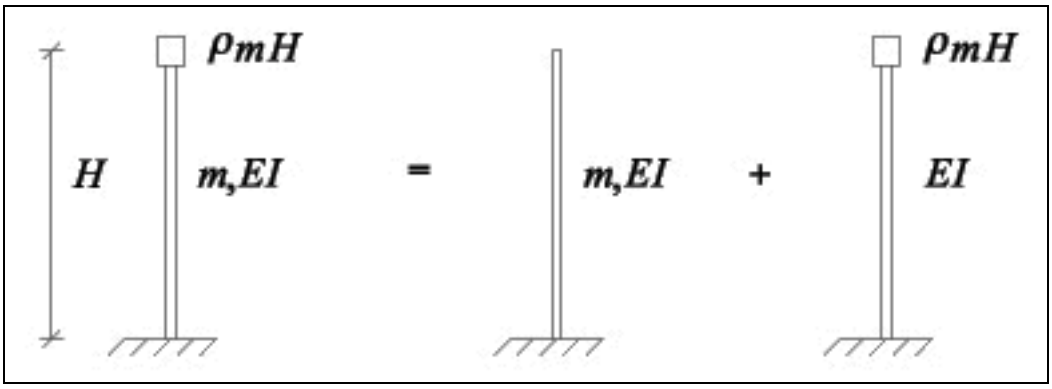

(a) Uniform and Lumped Mass (b) Uniform Mass Only (c) Lumped Mass Only

The frequency of the combined system can then be evaluated as follows:

$$\frac{1}{f_{1,\mathrm{f}}^2} = \frac{1}{f_{\mathrm{distributed}}^2} + \frac{1}{f_{\mathrm{lumped}}^2} \tag{86}$$

where $f_{1,f}$, $f_{\mathrm{distributed}}$ and f_{lumped} are the frequencies of the systems shown in Figure E-11(a), (b) and (c) respectively. Eq. (86) may be solved for the square of the fixed base frequency giving:

$$f_{1,f}^2 = \frac{f_{\mathrm{distributed}}^2 \, f_{\mathrm{lumped}}^2}{f_{\mathrm{distributed}}^2 + f_{\mathrm{lumped}}^2} \tag{87}$$

The square of the frequencies of the systems shown in Figure E-11(b) and (c) are evaluated as:

$$f_{\mathrm{distributed}}^2 = \frac{(3.516)^2}{(2\pi)^2}\frac{EI}{mH^4} \qquad f_{\mathrm{lumped}}^2 = \frac{1}{(2\pi)^2}\frac{3}{\rho}\frac{EI}{mH^4} \tag{88}$$

Substituting Eq. (88) into Eq. (87) gives:

$$f_{1,f}^2 = \frac{1}{(2\pi)^2}\frac{3}{\rho + \frac{1}{\lambda}}\frac{EI}{mH^4} \qquad \text{where} \qquad \lambda = \frac{(3.516)^2}{3} \approx 4.12 \tag{89}$$

Eq. (85) and Eq. (89) can then be substituted into Eq. (84) to give the following expression for the frequency ratio:

$$f_{1,k} = f_{1,f}\sqrt{\frac{1}{1+\chi\sigma}} \quad \text{where} \quad \chi(\rho) = \frac{3\rho+1}{\rho+(1/\lambda)}, \quad \rho = \mathrm{M}/mH \quad \text{and} \quad \lambda = 4.12 \tag{90}$$

Figure E-12 shows the exact variation of frequency ratio versus that obtained by using Eq. (90) in the case of a mass parameter $\rho = \mathrm{M}/mH$. In this case the coefficient χ in Eq. (90) is approximately equal to 3.2.

Figure E-12: Ratio of the Flexible to Fixed Base Frequency: Exact Solution vs. Approximation ρ=1

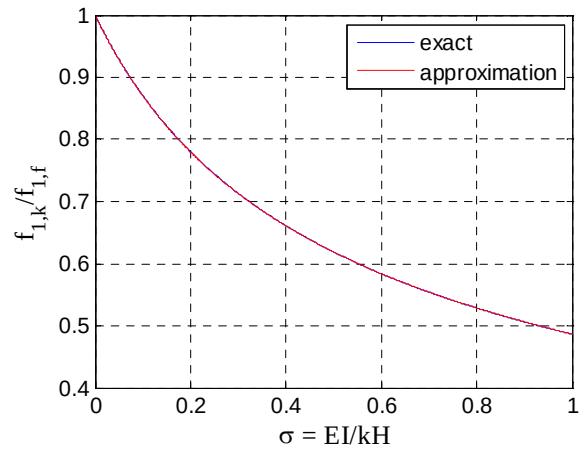

It is seen from Eq. (90) that when $\rho = 0$, meaning that there is no lumped mass at the top of the cantilever, $\chi = \lambda$ 4.12 and as expected Eq. (90) coincides with Eq. (61). When ρ becomes very large, the effect of the distributed mass is negligible compared to that of the lumped mass at the top and $\chi \to 3$. The exact solution for the case of a lumped mass is described next.

Cantilever with an Additional Lumped Mass at the Top

Let us define $k_f = 3EI/H^3$ as the lateral bending stiffness of the fixed base cantilever, and $k_\theta = k/H^2$ as the lateral stiffness due to the rotational spring at the base (see Figure E-13). The two act in series to give:

$$k_t = \frac{k_\theta k_f}{k_\theta + k_f} = k_f \frac{1}{1+k_f/k_\theta} \tag{91}$$

The frequency of the fixed base cantilever is:

$$f_f = \frac{1}{2\pi}\sqrt{\frac{k_f}{\mathrm{M}}} \tag{92}$$

The frequency of the system on a flexible base is:

$$f_k = \frac{1}{2\pi}\sqrt{\frac{k_t}{\mathrm{M}}} = f_f\sqrt{\frac{1}{1+k_f/k_\theta}} = f_f\sqrt{\frac{1}{1+3EI/kH}} = f_f\sqrt{\frac{1}{1+3\sigma}} \tag{93}$$

or more simply:

$$f_k = f_f \sqrt{\frac{1}{1+3\sigma}} \qquad \text{where} \qquad \sigma = EI / kH \tag{94}$$

Figure E-13: System Considered

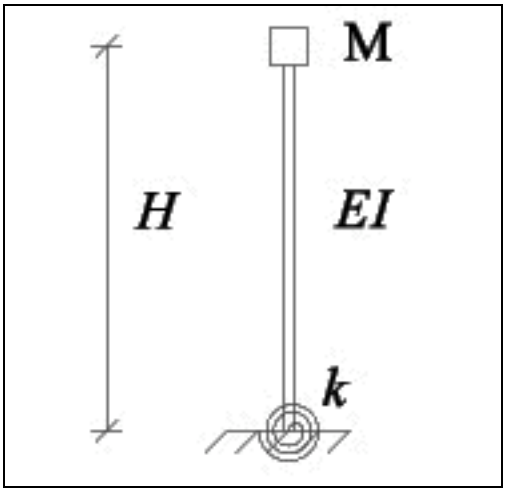

From Eq. (93) it can be noticed that for a structure on a very flexible support ($k_\theta \to 0$) the actual frequency f_k tends to zero. If the base stiffness is very high ($k_\theta \to \infty$), then the as-installed frequency f_k is very close to the fixed base one f_f.

Summary of Fundamental Frequencies of Bushings Mounted on a Flexible Base

In the following a series of formulas to evaluate the as installed frequencies of bushings are presented.

Lumped Mass

$$f_k = f_f \sqrt{\frac{1}{1+3\sigma}}$$

Where (see Figure 6(a)):

$$\sigma = \frac{EI}{kH} \qquad f_f = \frac{1}{2\pi}\sqrt{\frac{3EI/H^3}{M}}$$

Uniformly Distributed Mass

$$f_{1,k} = f_{1,f} \sqrt{\frac{1}{1+\lambda\sigma}}$$

Where (see Figure 8):

$$\lambda = \frac{(3.516)^2}{3} \approx 4.12 \qquad f_{1,f} = \frac{3.516}{2\pi}\sqrt{\frac{EI}{mH^4}}$$

Combined Uniformly Distributed Mass and Lumped Mass at the Top

$$f_{1,k} = f_{1,f}\sqrt{\frac{1}{1+\chi\sigma}}$$

Where (see Figure E-10(a)):

$$\chi(\rho) = \frac{3\rho+1}{\rho+(1/\lambda)} \qquad \rho = \mathrm{M}/mH \qquad f_{1,f} = \frac{1}{2\pi}\sqrt{\frac{3\lambda}{1+\rho\lambda}\,\frac{EI}{mH^4}}$$

The formulas assume that the rotation spring represents the local rotational stiffness of the plate cover system. Methods of calculating the rotational stiffness are presented in the next section.

Evaluation of the Stiffness k of the Base Cover Plate

In both the exact formulations and the approximations presented above a key parameter is the *rotational stiffness* ***k*** of the cover plate to which the bushings are connected. In the following sections the evaluation of the rotational stiffness of the cover plate is addressed using both a beam approach and the theory of plates.

Evaluation of k Using Beam Approach

The rotational base stiffness k is herein evaluated by considering the base plate as an equivalent beam having length *L*, width b_{eff} (estimated from experience and/or engineering judgment) and depth *h*. Three cases are considered based on different end conditions. For all cases *E* represents the modulus of elasticity and $I=b_{eff}h^3/12$ is the second moment of inertia of the cross section of the equivalent beam representing the cover plate.

Simply Supported Beam

In the case of a simply supported beam (Figure E-14), the base rotational stiffness can be evaluated as:

$$k = \frac{EI_c}{L}\frac{1}{1/3-a-a^2} = \alpha\frac{EI_c}{L} \qquad where \quad a = \frac{x}{L} \quad \text{and} \quad \alpha = \frac{1}{1/3-a-a^2} \tag{95}$$

Figure E-14: Simply Supported Equivalent Beam

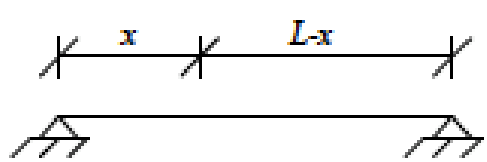

Figure E-15 shows the variation of α with the position of the bushing on the simply supported base plate.

Beam Fixed at Both Ends

In the case of a beam fixed at both ends (see Figure E-16), the base rotational stiffness can be evaluated as:

$$k = \frac{EI_c}{L}\frac{1}{a - 4a^2 + 6a^3 - 3a^4} = \beta\frac{EI_c}{L} \qquad where \quad a = \frac{x}{L} \quad \text{and} \quad \beta = \frac{1}{a - 4a^2 + 6a^3 - 3a^4} \tag{96}$$

Figure E-17 shows the variation of β with the position of the bushing on the fixed-fixed base plate.

Figure E-15: Variation of α with the Position of the Bushing

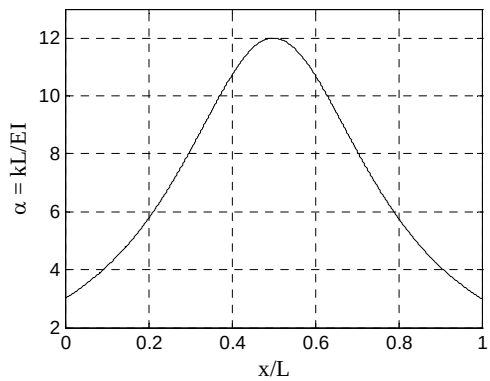

Figure E-16: Equivalent Beam Fixed at Both Ends

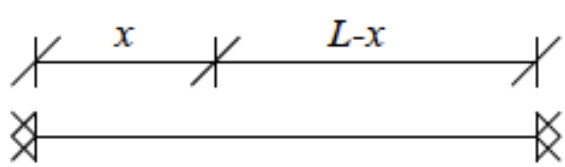

Figure E-17: Variation of β with the Position of the Bushing

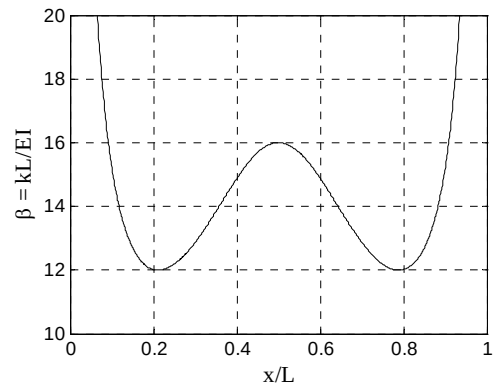

Fixed Simply Supported Beam

In the case of a beam fixed at one end and simply supported at the other (see Figure E-18), the base rotational stiffness can be evaluated as:

$$k = \frac{EI_c}{L}\frac{1}{a - 3a^2 + 3a^3 - 3/4a^4} = \gamma\frac{EI_c}{L} \quad where\ \ a = \frac{x}{L} \quad \text{and} \quad \gamma = \frac{1}{a - 3a^2 + 3a^3 - 3/4a^4} \tag{97}$$

Figure E-19 shows the variation of γ with the position of the bushing on the fixed-simply supported base plate. Figure E-20 shows a comparison of the variation of α with the position of the bushing for the previous three cases.

Figure E-18: Fixed-Simply Supported Equivalent Beam

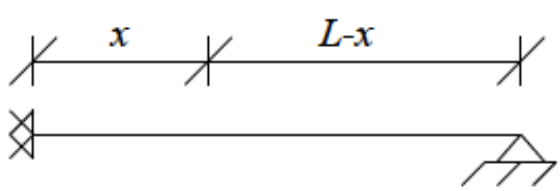

Figure E-19: Variation of γ with the Position of the Bushing

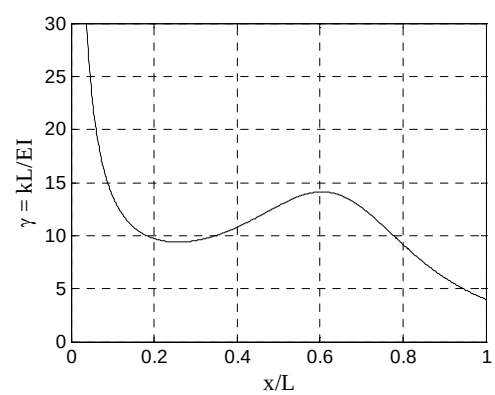

Figure E-20: Variation of α with the Position of the Bushing

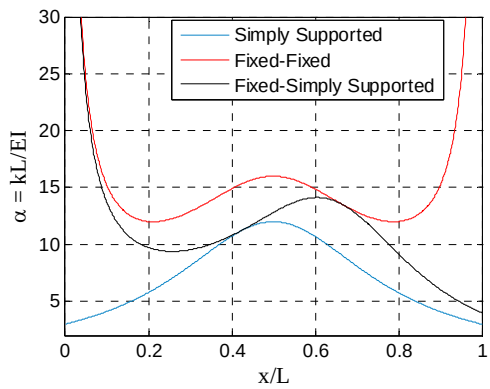

Evaluation of k Using Classical Theory of Plates

The rotational stiffness of the cover plate of the transformer, denoted by k, is an essential ingredient in the computation of the as-installed frequency of bushings. Its evaluation is described herein by using the classical theory of plates. The assumption of plane stress in the plate is employed and therefore transverse shear is neglected and set equal to zero. It is important to stress at this point that such theory is consistent, and gives accurate results, only if applied to thin plates, that is plates where the thickness to width ratio is much smaller than 0.1.

This section is organized as follows. First an exact analytical solution is presented for simply supported and clamped circular plates. Then the exact solution for the simply supported circular plates is replicated by means of a finite element model in ABAQUS. This is done to check on the accuracy of the finite element model to be used later to evaluate the stiffness of square and rectangular plates, for which an exact analytical solution is not available.

Exact Analytical Solutions for Circular Plates

An exact analytical solution for circular thin plates, loaded by a moment M at the center, is available in Timoshenko and Woinowsky-Krieger [ ]. The system therein considered is shown in Figure E-21. To avoid infinitely large rotations φ at the center of the plate, the central portion of radius b is considered absolutely rigid. The interested reader can find the details of the derivation in the above reference. Herein we present results in terms of the rotational stiffness k only.

Figure E-21: Circular Plate Assumption

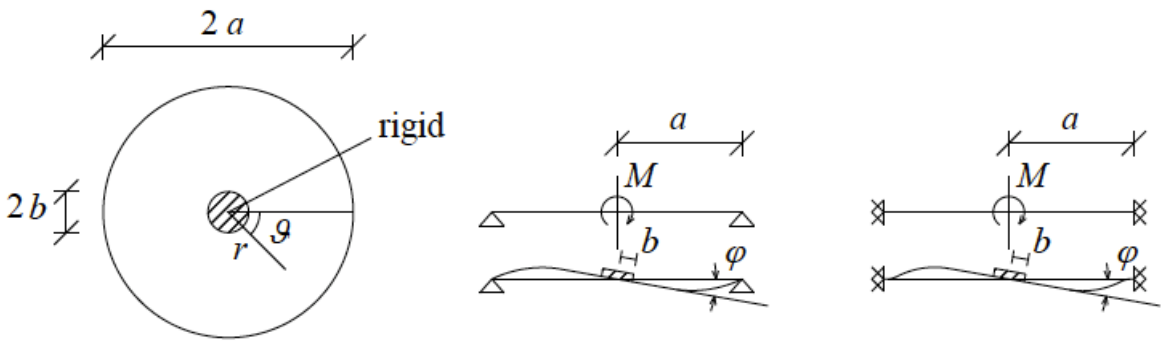

a) Plane View b) Simply Supported Outer Edge c) Clamped Outer Edge

The rotational stiffness can be expressed as:

$$k = \frac{M}{\varphi} = \alpha E h^3 \tag{98}$$

where E is the longitudinal modulus of elasticity and h is the thickness of the plate.

The parameter α, which is function of the Poisson ratio ν and of the geometric ratio $\beta = b/a$, is evaluated by different expressions depending on the boundary conditions. For circular plates in which the outer boundary is simply supported, the following expression holds:

$$\begin{aligned} &\alpha = \frac{\pi}{3d\left(1-\nu^2\right)}\left[(\nu-1)\beta^2 - (3+\nu)\beta^{-2}\right] \qquad \textit{where} \\ &d = \log\beta\left[(1-\nu)\beta^2 + (3+\nu)\beta^{-2}\right] - \left[2(1+\nu) - \nu\beta^2 - (2+\nu)\beta^{-2}\right] \end{aligned} \tag{99}$$

For circular plates in which the outer boundary is clamped, the expressions that holds is instead:

$$\alpha = \frac{\pi}{3d\left(1-\nu^2\right)}\left[\beta^{-2} - \beta^2\right] \qquad \textit{where} \qquad d = \log\beta\left(\beta^2 - \beta^{-2}\right) + \left(\beta^2 - 1\right)\left(\beta^{-2} - 1\right) \tag{100}$$

Figure E-22(a) shows the variation of the stiffness parameter α for both simply supported and clamped circular plates having a Poisson ratio equal to 0.3.

Figure E-22: Variation of α for circular plates

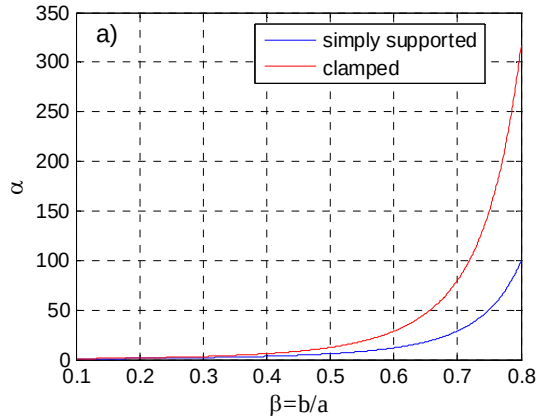

a) Simply supported and clamped plates

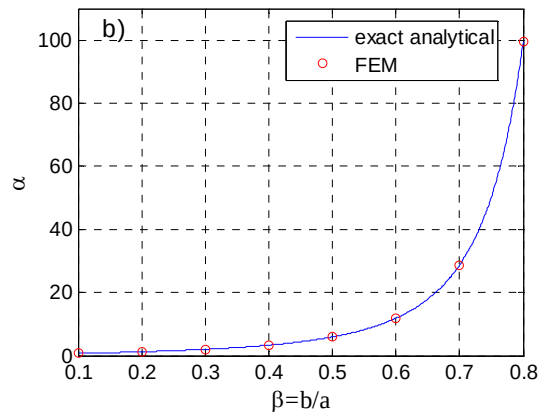

b) Numerical vs. Exact Solution – simply supported

The results for the simply supported plate shown in Figure E-22(a), and obtained by means of Eq. (99), were replicated for discrete values of β using a finite element model (FEM) in ABAQUS. In order to simulate the behavior described by the classical theory of plates, elements with no shear deformation were used. In particular the plate was modeled by STRI3 triangular shell elements with 6 degrees of freedom per node. Figure E-22(b) shows how the FEM solution converges to the exact analytical solution. The finite element analysis was performed on the circular plates merely to investigate its convergence properties and assess its reliability. Once the results proved to be more than satisfactory, the analyses were extended to the evaluation of the rotational stiffness of square and rectangular plates. No exact analytical solutions are available in these cases. The attempt to develop an exact solution leads to a computationally inefficient procedure that requires a large number of Fourier series terms to account for the conditions on the external boundary. Moreover the resulting system of equations happens to be numerically ill-conditioned. Therefore a semi-empirical-numerical procedure is suggested below for square and rectangular plates.

Numerical (FEM) Solutions for Square Plates

In this section the results of finite element analyses performed on simply supported square plates are presented. As in the case of the circular plates, the FEM consists of STRI3 shell elements available in the ABAQUS element library. These are linear triangular elements with no shear deformation, suitable to describe the behavior of the classical plate theory. A series of analyses up to convergence was performed for discrete values of $\beta=b/a$ between 0.1 and 0.8 (a is in this case the semi-width of the plate).

The rotational stiffness can still be expressed by Eq. (98). The results in terms of the parameter α are shown, in Figure E-23(a), for plates with ν=0.3. Altering the exact solution for the circular plate, Eq. (99), by introducing the parameters c_1 to c_7, the FEM results are fitted in Figure E-23(a) using the following expression:

$$\alpha = \frac{\pi}{3d\left(1-\nu^2\right)}\left[\left(\nu-1\right)\beta^2 c_1 - \left(3+\nu\right)\beta^{-2} c_2\right] \qquad where$$
$$d = \log\beta\left[\left(1-\nu\right)\beta^2 c_3 + \left(3+\nu\right)\beta^{-2} c_4\right] - \left[2\left(1+\nu\right)c_5 - \nu\beta^2 c_6 - \left(2+\nu\right)\beta^{-2} c_7\right] \tag{101}$$

The coefficients in Eq. (101) and Eq. (101) are: c_1=-0.2274, c_2=0.5375, c_3=-0.0349, c_4=0.5367, c_5=0.5716, c_6=1, c_7=0.5155. These were obtained using a nonlinear least squares optimization method available in the *Curve Fitting Toolbox* in MATLAB. The accuracy of the fitted function is shown in Figure E-23(b), where the error is defined as follows:

$$error = \frac{\left|\alpha_{fitted} - \alpha_{FEM}\right|}{\alpha_{FEM}} \tag{102}$$

If the coefficients are all set equal to 1, Eq. (99) for simply supported circular plates is recovered. It is worth pointing out at this time that the value of ν in Eq. (101) is set equal to 0.3. If a different value of the Poisson ratio were to be assumed, another set of finite element analysis would have to be performed to determine a new set of coefficients.

It is interesting to see how the solution expressed by Eq. (101) compares to those for the inscribed and circumscribed circular plates. This comparison is shown in Figure E-24.

Figure E-23: FEM Solution for Simply Supported Square Plates

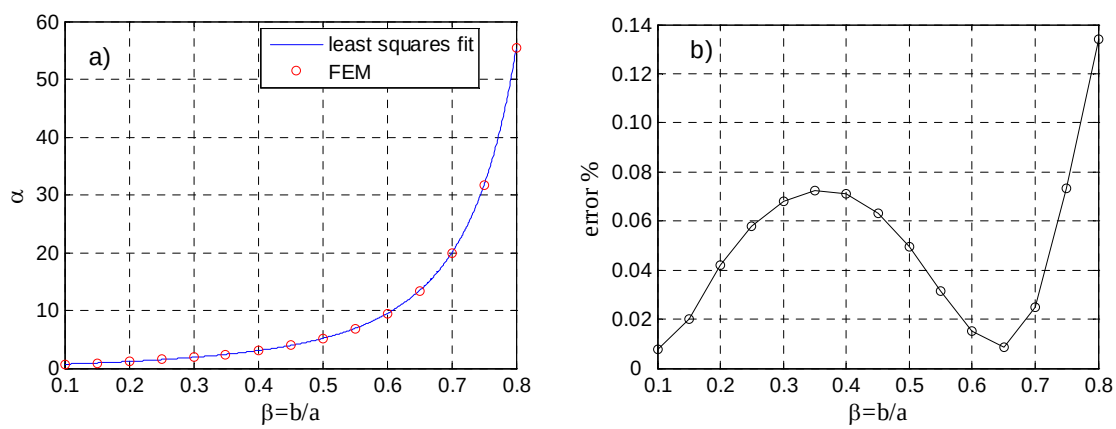

a) Variation of α

b) Percent Error of Fit

As expected, the square plate is stiffer than its corresponding circumscribed plate but less stiff than its corresponding inscribed plate. Moreover, the stiffness of the square plate is very close to that of the inscribed circular plate for small values of β but the difference increases as β becomes larger.

Figure E-25 shows the error that would be committed if the stiffness of a square plate were to be evaluated by using the expression for the inscribed circular plate.

Figure E-24: Comparison of α for Square Plates and Corresponding Inscribed and Circumscribed Plates

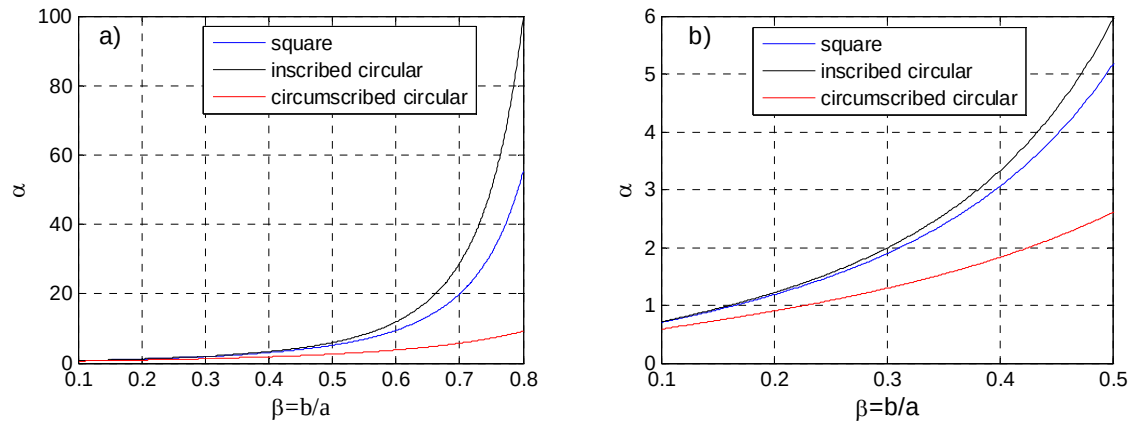

a) 0.1≪β≪0.8 b) close up view for 0.1≪β≪0.5

Figure E-25: Error in Using the Stiffness of Inscribed Circular Plates to Evaluate the Stiffness of Square Plates

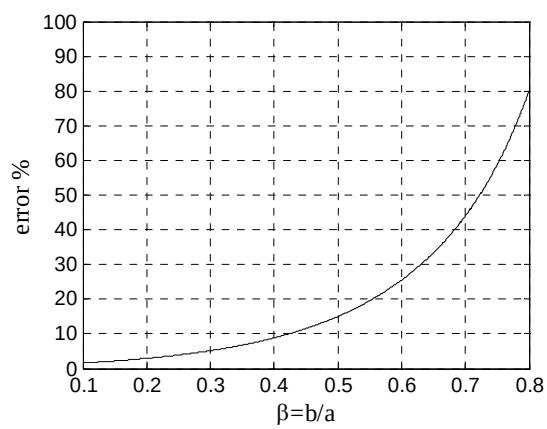

Numerical (FEM) solutions for rectangular plates

In the previous section, an expression for the evaluation of the rotational stiffness of simply supported square plates was presented. This has the same form as the exact analytical solution for simply supported circular plates and was derived using a least squares optimization method. The expression found gives results that are in extremely good agreement with the numerical ones obtained by finite element analysis using ABAQUS. Therefore, it seems

reasonable to extend the same approach to the evaluation of the rotational stiffness of rectangular plates.

Plates with different length to width ratio L/a were considered, and a series of finite element analyses performed for discrete values of $\beta=b/a$ between 0.1 and 0.8. The numerical results are fitted using the same optimization procedure developed for the square plates. The coefficients for Eq. (101) are presented in Table E-1, along with the maximum and mean error of the fitted curves plotted in Figure E-26.

The results in terms of error in Table E-1 indicate that, given the length to width ratio L/a, Eq. (101) may be used together with a least squares optimization procedure to provide a very accurate expression for the rotational stiffness parameter α as a function of β From a practical point of view, it would be ideal if an expression could be obtained for each coefficient, in terms of the length to width ratio L/a. Unfortunately though, the coefficients presented in Table E-1 appear to vary in random fashion with L/a.

Figure E-26: Variation of α for Rectangular Plates

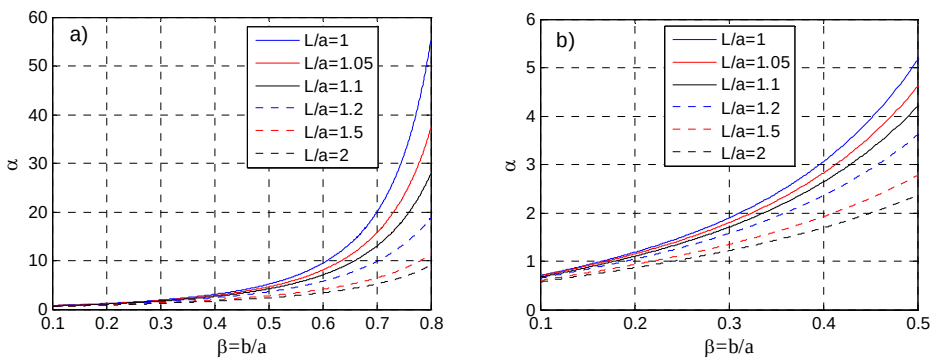

a) 0.1≪β≪0.8 (b) 0.1≪β≪0.5

Table E-1: Fitting Coefficients and Error to Numerical Results for Rectangular Plates

L/a	c_1	c_2	c_3	c_4	c_5	c_6	c_7	max error %	mean error %
1	-0.2274	0.5375	-0.0349	0.5367	0.5716	1.0000	0.5155	0.13	0.05
1.05	0.8502	1.0000	0.7228	0.9687	0.8258	0.8018	0.8372	1.57	0.38
1.1	-0.4073	0.7219	-0.0184	0.7216	0.6597	1.0000	0.6137	0.12	0.04
1.2	0.8362	1.0000	0.6756	0.9861	0.7275	0.7582	0.7261	0.58	0.14
1.5	1.0000	0.6840	0.5100	0.6808	0.4131	0.7355	0.3790	0.14	0.04
2	0.7173	1.0000	0.7361	0.9932	0.4159	0.8203	0.4028	0.21	0.09

However, the problem of finding an expression for the stiffness parameter α in terms of both β and L/a, may be further approximated as follows. In Figure E-27, the numerical results in terms of stiffness parameter α are plotted against L/a, for values of β within the range [0.1, 0.6]. In the same figure these are fitted using the following function:

$$\alpha = a_1 \exp\left\{a_2 \frac{L}{a}\right\} + a_3 \exp\left\{a_4 \frac{L}{a}\right\} \tag{103}$$

Figure E-27: Stiffness parameter α against L/a for 0.1≪β≪0.6: Numerical Values and Least Squares Fit Using Eq. (103)

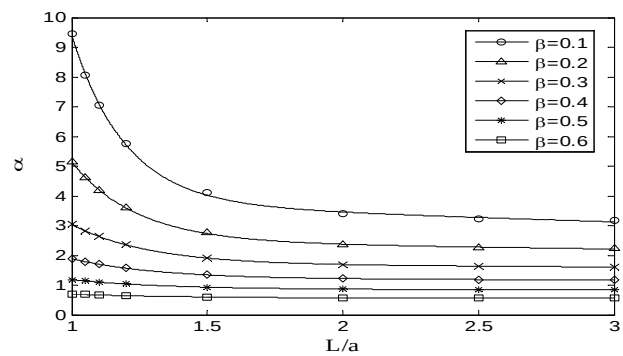

The values of the coefficients that appear in Eq. (103), and that were used to obtain the curves shown in Figure E-27, are plotted in Figure E-28, where they are fitted using the following expressions:

$$\begin{aligned} a_1 &= 0.000344 \exp\{23.99\beta\} + 0.695 \exp\{10.19\beta\} \\ a_2 &= -2.277 \exp\{0.8622\beta\} - 0.02043 \exp\{6.898\beta\} \\ a_3 &= (1.14E-06) \exp\{21.33\beta\} + 0.4003 \exp\{3.708\beta\} \\ a_4 &= -0.0159 \exp\{3.792\beta\} + 0.01923 \exp\{1.98\beta\} \end{aligned} \tag{104}$$

The use of the empirical Equations 84 and 85 for the evaluation of the stiffness parameter α leads to the errors shown in Table E-2. The maximum and mean errors are seen to be equal to 4.59% and 1.42% respectively. It is important to point out that the above empirical expressions were derived, and therefore give the errors shown in Table E-2, for values of beta in the range [0.1, 0.6]. However, for larger values of β a separate set of empirical equations can be derived if needed. A 3-dimensional plot of α, as a function of both β and L/a, is shown in Figure E-29.

Figure E-28: Variation with β of Least Squares Coefficients in Eq. (103)

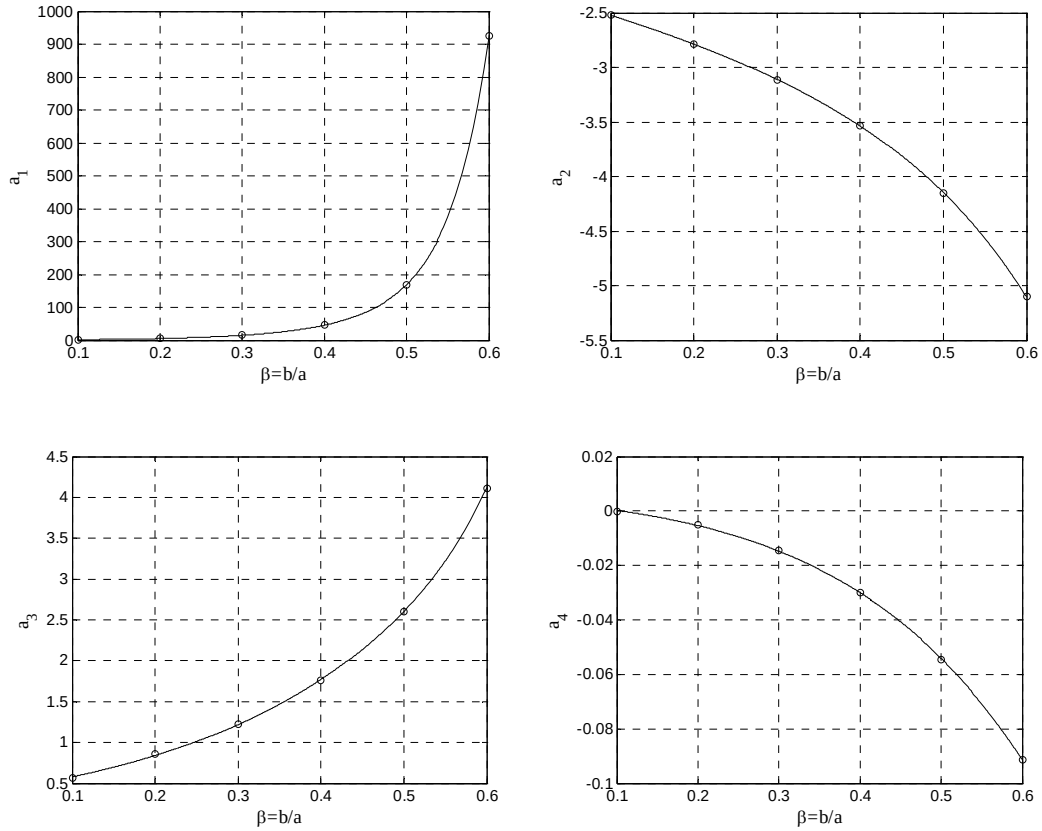

Table E-2: Percent Error as a Function of β and L/a

L/a \ β	0.1	0.2	0.3	0.4	0.5	0.6
1.0	4.69	1.45	0.76	0.02	0.31	0.44
1.05	4.58	1.38	0.54	0.45	0.44	0.77
1.1	4.46	1.37	0.48	0.59	0.57	0.81
1.2	4.23	1.46	0.60	0.41	0.01	0.47
1.5	3.73	1.74	1.02	0.19	1.18	1.92
2.0	3.45	1.68	0.67	0.82	0.79	1.98
2.5	3.37	1.66	0.56	1.05	0.96	1.59
3.0	3.33	1.82	0.95	0.20	0.75	1.69

Figure E-29: Stiffness Parameter α as a Function of β and L/a

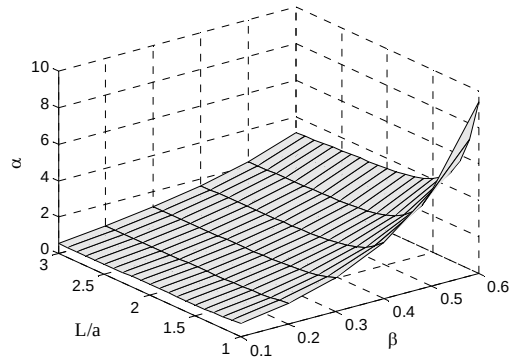

Dynamic Response of Bushings: Forces at Base Mounting

The shear and bending moment of bushings with distributed mass can be obtained exactly by solving the following modal equations:

$$M_n \ddot{q}_n(t) + K_n q_n(t) = -\mathrm{L}_n \ddot{u}_g(t) - \mathrm{L}_n^{\vartheta} \ddot{\vartheta}_g(t) \tag{105}$$

Where:

$$\begin{aligned} M_n &= \int_0^H m(z)\left[\phi_n(z)\right]^2 dz \qquad & K_n &= \int_0^H \left[EI(z)\phi_n''(z)\right]'' \phi_n(z)\, dz \\ \mathrm{L}_n &= \int_0^H m(z)\phi_n(z)\, dz \qquad & \mathrm{L}_n^{\vartheta} &= \int_0^H m(z) z \phi_n(z)\, dz \end{aligned} \tag{106}$$

The mode shapes $\phi_n(z)$ can be evaluated by the procedures presented in Section 2.1. The modal shear forces and bending moments at any level of the bushing are given by:

$$V_n(z,t) = \frac{\partial(EI(z)\phi_n''(z))}{\partial z} q_n(t) \tag{107}$$

$$M_n(z,t) = EI(z)\phi_n''(z)\; q_n(t) \tag{108}$$

It can be shown that the shear force and the moment can be simply defined as:

$$V(z,t) = \sum_1^N V_n(z,t) = \sum_1^N \int_z^H \omega_n^2 m(\zeta)\phi_n(\zeta) q_n(t) d\zeta \tag{109}$$

$$M(z,t) = \sum_1^N M_n(z,t) = \sum_1^N \int_z^H \omega_n^2 m(\zeta)\phi_n(\zeta) q_n(t) \zeta d\zeta \tag{110}$$

The shear at the base and the bending moment are:

$$V_B(t) = \sum_1^N V_{B,n}(t) = \sum_1^N \omega_n^2 \, q_n(t) \int_0^H m(z)\phi_n(z)\,dz \tag{111}$$

$$M_B(t) = \sum_1^N M_{B,n}(t) = \sum_1^N \omega_n^2 \, q_n(t) \int_0^H z \; m(z)\phi_n(z) \; dz \tag{112}$$

where N is the number of modes considered.

Using a spectral approach, the maximum response can be approximated as:

$$\omega_n^2 q_{\max,n} = \left[\Gamma_n S_a(f_n) + \Gamma_n^{\vartheta} S_{\ddot{\theta}}(f_n) \right] \tag{113}$$

where $\Gamma_n = \dfrac{\mathrm{L}_n}{M_n}$ and $\Gamma_n^{\vartheta} = \dfrac{\mathrm{L}_n^{\vartheta}}{M_n}$ are participation factors obtained by the expressions in Eq. (26).

Therefore the maximum base modal shear and moments can be simply specified as:

$$V_{Bn,\max} = \left[\Gamma_n S_a(f_n) + \Gamma_n^{\vartheta} S_{\ddot{\theta}}(f_n) \right] \int_0^H m(z)\phi_n(z)\,dz = \left[\Gamma_n S_a(f_n) + \Gamma_n^{\vartheta} S_{\ddot{\theta}}(f_n) \right] \mathrm{L}_n \tag{114}$$

$$M_{Bn,\max} = \left[\Gamma_n S_a(f_n) + \Gamma_n^{\vartheta} S_{\ddot{\theta}}(f_n) \right] \int_0^H z \; m(z)\phi_r(z)\,dz = \left[\Gamma_n S_a(f_n) + \Gamma_n^{\vartheta} S_{\ddot{\theta}}(f_n) \right] \mathrm{L}_n^{\vartheta} \tag{115}$$

It should be noted that both the base moment and the shear are function of the base motion that includes the influence of the base translation u_g and the rotation θ of the cover of the transformer supporting the bushing. The total forces due to the contribution of all the modes considered should be obtained from an SRSS rather than a simple addition since the modal maxima are in general not synchronous.

Note also that the spectral accelerations are function of the "as-installed frequency" f_k, which may influence substantially the forces in the lower frequency ranges.

The position of the resultant inertia force (Center of Inertia) producing the maximum shear and moment is:

$$z_{IC} = \frac{\int_0^H z \; m(z)\phi_n(z)\,dz}{\int_0^H m(z)\phi_n(z)\,dz} \tag{116}$$

The acceleration at the center of inertia is therefore:

$$a(z_{CI}) = \left[\Gamma_n S_a(f_n) + \Gamma_n^{\vartheta} S_{\ddot{\theta}}(f_n) \right] \phi_n(z_{CI}) \tag{117}$$

The acceleration at the top of the bushing is then:

$$a(z_{TOP}) = \left[\Gamma_n S_a(f_n) + \Gamma_n^{\vartheta} S_{\ddot{\theta}}(f_n)\right]\phi_n(z_{TOP}) \tag{118}$$

The ratio of accelerations at the top and at the Center of Inertia depends on the position of this center:

$$\frac{a(z_{TOP})}{a(z_{CI})} = \frac{\phi_n(z_{TOP})}{\phi_n(z_{CI})} \tag{119}$$

Approximation of Forces for Particular Cases

Constant Mode Shape Throughout the Height

Assuming $\phi_n(z) = \phi_0$, which is not typical for bushings, then the Center of Inertia coincides with the Center of Gravity (or Center of Mass):

$$z_{IC} = \frac{\int_0^H z\, m(z)\phi_n(z)\,dz}{\int_0^H m(z)\phi_n(z)\,dz} = \frac{\phi_o \int_0^H z\, m(z)\, dz}{\phi_o \int_0^H m(z)\, dz} = z_{CG} \tag{120}$$

In such case the maximum shear force and the moment for the arbitrary and uniform mass distributions are:

$$V_{Bn,\max} = \left[\Gamma_n S_a(f_n) + \Gamma_n^{\vartheta} S_{\ddot{\theta}}(f_n)\right] \int_0^H m(z)\, dz = \left[\Gamma_n S_a(f_n) + \Gamma_n^{\vartheta} S_{\ddot{\theta}}(f_n)\right] m_0 H \tag{121}$$

$$M_{Bn,\max} = \left[\Gamma_n S_a(f_n) + \Gamma_n^{\vartheta} S_{\ddot{\theta}}(f_n)\right] \int_0^H z\, m(z)\,dz = \left[\Gamma_n S_a(f_n) + \Gamma_n^{\vartheta} S_{\ddot{\theta}}(f_n)\right] m_o \frac{H^2}{2} \tag{122}$$

Since the Center of Inertia is the same as the Center of Mass and the mode shape constant, the acceleration at the above named centers and at the top are equal.

$$z_{IC} = \frac{H}{2} = z_{CG} \quad \textit{and} \quad \frac{a(z_{TOP})}{a(z_{CI})} = 1 \tag{123}$$

This is a gross assumption for cases where mode shapes and mass distribution are not constant.

Linear Mode Shape

Assuming a linear mode shape $\phi_n(z) = z/H$ gives:

$$z_{IC} = \frac{\int_0^H z\, m(z)\frac{z}{H}\,dz}{\int_0^H m(z)\frac{z}{H}\, dz} = \frac{\int_0^H z^2\, m(z)\, dz}{\int_0^H z\, m(z)\, dz} \neq z_{CG} \tag{124}$$

For a uniformly distributed mass $m(z) = m_0$ then:

$$z_{IC} = \frac{2H}{3} \neq z_{CG} \tag{125}$$

$$\frac{a(z_{TOP})}{a(z_{CI})} = \frac{3}{2} \tag{126}$$

In such case the maximum shear force and the moment for the arbitrary and uniform mass distributions are:

$$V_{Bn,\max} = \left[\Gamma_n S_a(f_n) + \Gamma_n^{\vartheta} S_{\ddot{\theta}}(f_n)\right] \int_0^H m(z)\frac{z}{H}dz = \left[\Gamma_n S_a(f_n) + \Gamma_n^{\vartheta} S_{\ddot{\theta}}(f_n)\right] m_0 \frac{H}{2} \tag{127}$$

$$M_{Bn,\max} = \left[\Gamma_n S_a(f_n) + \Gamma_n^{\vartheta} S_{\ddot{\theta}}(f_n)\right] \int_0^H z\, m(z)\frac{z}{H}dz = \left[\Gamma_n S_a(f_n) + \Gamma_n^{\vartheta} S_{\ddot{\theta}}(f_n)\right] m_0 \frac{H^2}{3} \tag{128}$$

Note that if the mass is lumped at the center of gravity (CG), multiplication of the mass by the acceleration at the center of gravity is suitable only in the case of constant mode shape. This may happen when the bushing is infinitely rigid, is mounted on a rigid base and the base translates without rotation. While this may be the case for some very stiff construction, all other cases should be treated more accurately.

Base shear and base moment by approximations

Usually the transverse acceleration at the base of the bushing and at the top are proportional to the overall shape of the tank and the bushing. These accelerations can be obtained from Eq. (96), using spectral values, or directly from measurements in the field or lab. Using the notation in Figure E-30, the acceleration distribution can be formulated approximately as:

$$a(z) = a_b + (a_0 - a_b)\left(\frac{z}{H}\right) \tag{129}$$

Assuming that the mass is also varying linearly along length, it can be expressed as:

$$m(z) = m_b - (m_b - m_0)\left(\frac{z}{H}\right) \tag{130}$$

Figure E-30: Approximated Distribution of Acceleration and Mass of Bushings

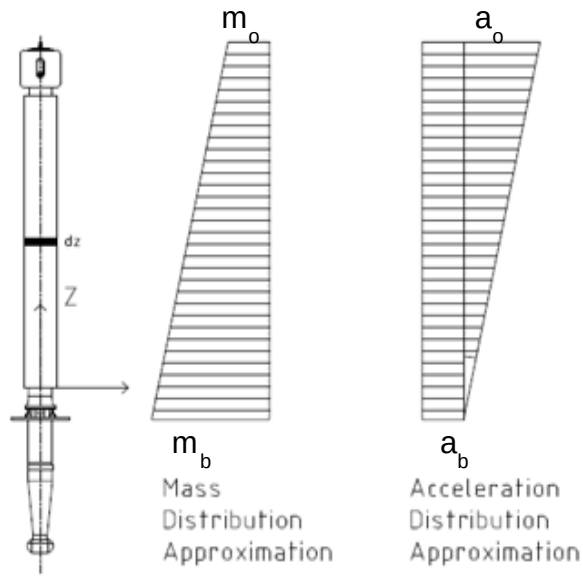

Neglecting damping, the shear force and bending moment at the base of the bushings are given by:

$$V_B = \int_0^H m(z)a(z)dz \tag{131}$$

$$M_B = \int_0^H m(z)a(z)z\,dz \tag{132}$$

Assuming that the acceleration and mass have the distribution given by Eq. **Error! Reference source not found.** and Eq. **Error! Reference source not found.**, the shear force at the base becomes:

$$V_B = \int_0^H \left[m_b - (m_b - m_0)\left(\frac{z}{H}\right)\right]\left[a_b + (a_0 - a_b)\left(\frac{z}{H}\right)\right]dz \tag{133}$$

After evaluation:

$$V_B = \frac{m_b H a_0}{6}\left[(2a_b / a_0 + 1) + \frac{m_0}{m_b}(a_b / a_0 + 2)\right] \tag{134}$$

The base moment is obtained similarly:

$$M_B = \int_0^H \left[m_b - (m_b - m_0)\left(\frac{z}{H}\right)\right]\left[a_b + (a_0 - a_b)\left(\frac{z}{H}\right)\right]zdz \tag{135}$$

After evaluation we get:

$$M_B = \frac{m_b H^2 a_0}{12}\left[\left(a_b / a_0 + 1\right) + \frac{m_0}{m_b}\left(a_b / a_0 + 3\right)\right] \tag{136}$$

Several simple cases are considered below.

Case I: Constant Acceleration and Mass ($a_b = a_0$ and $m_b = m_0$)

$$V_1 = m_b H a_0 \tag{137}$$

$$M_1 = \frac{m_b H^2 a_0}{2} \tag{138}$$

Case II: Inverted Triangular Acceleration and Constant Mass ($a_b = 0$ and $m_b = m_0$)

$$V_2 = \frac{m_b H a_0}{2} = \frac{V_1}{2} = 0.50\, V_1 \tag{139}$$

$$M_2 = \frac{m_b H^2 a_0}{3} = \frac{M_1}{1.5} = 0.667 M_1 \tag{140}$$

Case III: Inverted Triangular Acceleration and Variable Mass ($a_b = 0$ and $m_b = 2m_0$)

$$V_3 = \frac{m_b H a_0}{3} = \frac{V_1}{3} = 0.33\, V_1 \tag{141}$$

$$M_3 = \frac{m_b H^2 a_0}{4.8} = \frac{M_1}{2.4} = 0.417 M_1 \tag{142}$$

It should be noted that a_0 is the acceleration at the top of the bushing.

Assuming a uniform acceleration as in Case I above:

$$V = a_b \int_0^H m(z)\,dz = \frac{W}{g} a_b = \frac{W}{g} a_{CG} \tag{143}$$

$$M = a_b \int_0^H m(z)\,z\,dz = a_b \int_0^H m(z)\,dz \times \frac{\int_0^H m(z)\,z\,dz}{\int_0^H m(z)\,dz} = \frac{W}{g} a_b Z_{CG} = \frac{W}{g} a_{CG} Z_{CG} \tag{144}$$

where W is the weight of the structure above the flange section.

Note that in this case the variable Z_{CG} is dependent on the distribution of the mass *m(z)* only.

The current practice recommends multiplying the weight of the structure by the acceleration at the center of gravity (CG) - to calculate the shear force - and then to multiply by the elevation of the center of gravity Z_{CG} - to calculate the base moment. This is valid only for a constant acceleration response along the height of the structure (Case 1). However, for more realistic distributions of acceleration the shear and moments calculated that way are erroneous.

Summary of Dynamic Response Calculations

Lumped Mass

The frequency of vibration is evaluated as:

$$f_k = f_f \sqrt{\frac{1}{1+3\sigma}} \qquad \text{where} \qquad \sigma = EI / kH \tag{145}$$

The fixed base frequency f_f is given by Eq. (92), or can be determined by experiments.

The center of inertia is located at the top of the bushing, that is:

$$z_{IC} = H \tag{146}$$

The maximum base shear is and the associated bending moment can be evaluated as follows:

$$V_{B,\max} = \left[S_a(f) + HS_{\ddot{\theta}}(f) \right] \mathrm{M} \tag{147}$$

$$M_{B,\max} = V_{B,\max} \cdot z_{IC} = \left[S_a(f) + HS_{\ddot{\theta}}(f) \right] \mathrm{M}\, H \tag{148}$$

Uniformly Distributed Mass

The frequencies of vibration can be evaluated exactly as:

$$f_{n,k} = \frac{1}{2\pi} \frac{(\beta_n H)^2}{H^2} \sqrt{\frac{EI}{m}} \tag{149}$$

where $\beta_n H$ is the nth root of the frequency in Eq. (52). Mode shapes are given by Eq. (55).

The frequency of the first mode of vibration may be evaluated approximately, but very accurately, as:

$$f_{1,k} = f_{1,f} \sqrt{\frac{1}{1+\lambda\sigma}} \qquad \text{where} \qquad \lambda = \frac{(3.516)^2}{3} = 4.12; \qquad \sigma = \frac{EI}{kH} \tag{150}$$

The fixed base frequency $f_{1,f}$ is determined by experiments or as:

$$f_{1,f} = \frac{3.516}{2\pi} \sqrt{\frac{EI}{mH^4}} \tag{151}$$

The frequency $f_{1,k}$ evaluated by Eq. (61) can be used in Eq. **Error! Reference source not found.** to calculate β_1 which can then be substituted into Eq. (55) to evaluate the first mode shape $\phi_1(z)$.

The center of inertia is evaluated with the following expression:

$$z_{IC} = \frac{\int_0^H z\, m(z) \phi_n(z)\, dz}{\int_0^H m(z) \phi_n(z)\, dz} = \frac{\mathrm{L}_n^{\vartheta}}{\mathrm{L}_n} \tag{152}$$

where L_n and L_n^{ϑ} are defined in Eq. (26).

The maximum modal base shear and the associated base bending moment can be evaluated as:

$$:V_{Bn,\max} = \left[\Gamma_n S_a(f) + \Gamma_n^{\vartheta} S_{\ddot{\theta}}(f)\right] \int_0^H m(z)\phi_n(z)dz \tag{153}$$

$$M_{Bn,\max} = \left[\Gamma_n S_a(f) + \Gamma_n^{\vartheta} S_{\ddot{\theta}}(f)\right] \int_0^H z\, m(z)\phi_n(z)dz = V_{Bn,\max} \cdot z_{IC} \tag{154}$$

where and $\Gamma_n^{\vartheta} = \mathrm{L}_n^{\vartheta} / M_n$ are modal participation factors obtained from Eq. (26).

Combined Uniformly Distributed Mass and Lumped Mass at the Top

The frequencies of vibration can be evaluated exactly as:

$$f_{n,k} = \frac{1}{2\pi} \frac{(\beta_n H)^2}{H^2} \sqrt{\frac{EI}{m}} \tag{155}$$

where $\beta_n H$ is the nth root of the frequency in Eq. (77). The corresponding mode shapes are given by Eq. (80).

The frequency of the first mode of vibration may be evaluated approximately, but still very accurately, as:

$$f_{1,k} = f_{1,f} \sqrt{\frac{1}{1+\chi\sigma}} \quad \text{where} \quad \chi(\rho) = \frac{3\rho+1}{\rho+(1/\lambda)}, \quad \rho = \mathrm{M}/mH \quad \text{and} \quad \lambda = 4.12 \tag{156}$$

The fixed base frequency $f_{1,f}$ is determined by experiments or as:

$$f_{1,f} = \frac{1}{2\pi} \sqrt{\frac{3\lambda}{1+\rho\lambda} \frac{EI}{mH^4}} \tag{157}$$

The frequency $f_{1,k}$ evaluated by Eq. (90) can be used in Eq. **Error! Reference source not found.** to calculate β_1 which can then be substituted into Eq. (80) to evaluate the first mode shape $\phi_1(z)$.

The center of inertia is evaluated with the following expression:

$$z_{IC} = \frac{\int_0^H z\, m(z)\phi_n(z)dz}{\int_0^H m(z)\phi_n(z)dz} = \frac{\mathrm{L}_n^{\vartheta}}{\mathrm{L}_n} \tag{158}$$

where L_n and L_n^{ϑ} are defined in Eq. (68).

The maximum modal base shear and the associated base bending moment can be evaluated as:

$$V_{Bn,\max} = \left[\Gamma_n S_a(f) + \Gamma_n^{\vartheta} S_{\ddot{\theta}}(f)\right]\left[\int_0^H m(z)\phi_n(z)dz + \mathrm{M}\phi_n(H)\right] \tag{159}$$

$$M_{Bn,\max} = \left[\Gamma_n S_a(f) + \Gamma_n^{\vartheta} S_{\ddot{\theta}}(f)\right]\left[\int_0^H z\,m(z)\phi_n(z)dz + H\mathrm{M}\phi_n(H)\right] = V_{Bn,\max} \cdot z_{IC} \tag{160}$$

where and $\Gamma_n^{\vartheta} = \mathrm{L}_n^{\vartheta} / M_n$ are modal participation factors obtained from Eq. (68).

Comparison of Analytical and Experimental Properties

The analytical development was evaluated using the experimental data collected for Bushings #4A, 4B, 5, 6 and 7. The data for the other Bushing #8 was not completed for this task.

The frequencies measured for the bushings mounted on the rigid block (fixed base) were used to calibrate the computational parameter of distributed stiffness EI. This was done both analytically and numerically using a bushing model developed in SAP2000 computer program (Finite Element Program). The stiffness k of the support plate simulating the transformer cover is calculated using Eq. (98) with the parameter α derived from Eq. (101), which gives α = 2.4439. The stiffness is obtained as $k = \alpha E h^3$ = 2.99E+04 kip in.

The value of the parameter σ is obtained from Eq. (94) and is displayed for each of the bushings in Table E-3. The analytical frequency is calculated using Eq. (94) and is displayed in Table E-3 along with the measured fixed base frequency and with the frequency obtained from a simulated numerical model based on SAP. The errors in calculations are small (in most cases below 2%, and in some cases reach maximum of 18%). The larger errors may be due to inadequate measurements or misunderstanding of the stiffness-mass distribution.

The amplification frequency ratio (see Figure E-31) is dependent on both plate cover and bushing stiffness, and cannot be attributed only to voltage capacity, length or other properties. The parameters influencing such ratios were established in this section.

Table E-3: Comparison of Simplified Analytical Model and Experiments

Source	Properties	Units	Bushing 4a	Bushing 4b	Bushing 5	Bushing 6	Bushing 7
(1)	(2)	(3)	(4)	(5)	(6)	(7)	(8)
Physical Properties of Bushings	Material of Insulator		Composite	Composite	Composite	Porcelain	Porcelain
	Voltage Capacity	kV	230.00	230.00	500.00	196/230	550.00
	Height above the flange	in	91.20	91.20	192.20	91.40	208.30
	Height Below the Flange	in	59.50	59.50	65.00	60.00	86.70
	Total Height of Bushing	in	150.70	150.70	251.72	151.40	295.00
	Upper Bushing Weight	lbs	248.06	172.37	1306.96	446.95	3012.00
	Lower Bushing Weight	lbs	161.94	112.63	443.04	293.05	1218.00
	Total Bushing Weight	lbs	510.00	385.00	1850.00	840.00	4330.00
	Total Mass	$kip/in/sec^2$	6.43E-04	4.47E-04	3.39E-03	1.16E-03	7.80E-03
Data from Identificatiion**	σ	Kip/in^2	0.0395	0.0256	0.3557	0.651	3.0941
	Bending rigidity EI	$kip\text{-}in^2$	1.08E+05	6.99E+04	2.04E+06	1.78E+06	1.93E+07
Frequencies Measured and Estimated	Measured Fixed Base	Hz	8.32	8.04	5.16	25.10	9.25
	Estimated Fixed Base Analytically	Hz	8.32	8.04	5.16	25.10	9.25
	Estimated Fixed Base Numerically (SAP)	Hz	8.32	8.04	5.16	25.10	9.25
	Measured As-Installed	Hz	7.75	6.30	3.25	11.17	2.53
	Estimated As-Installed Analytically	Hz	7.72	7.65	3.29	13.08	2.49
	Estimated As-Installed Numerically (SAP)*	Hz	8.00*	7.62	3.23	11.56	2.40
Error	Error experiemnt vs analysis	%	0.4%	17.6%	1.2%	14.6%	1.6%

* Two stiffeners were used in the test and SAP models which might explain higher frequency in analytical model

** EI calculated from the fixed base frequency

Figure E-31: Ratio of As-installed vs. Fixed-base Frequencies of Bushings

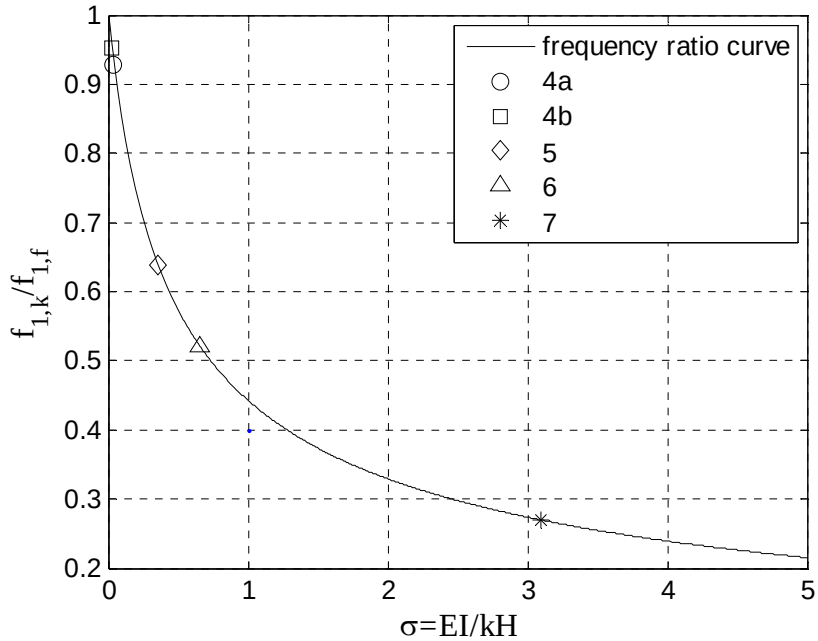

Summary of Analytical Modeling of Installed Bushings

The analytical study revealed several properties already observed in the numerical and in the experimental study. These observations can be summarized as follows:

1) The dynamic properties of the bushings when installed on the transformer cover are dependent on the stifness *k* of the cover, in paticular on the rotational (out-of-plane) stiffness of the cover assembly.

2) The stiffness is dependent not only on the material and structural propertiees of the cover, but also on the boundary conditions of the cover and the location of the bushing in respect to those boundary conditions (the edges of the cover).

3) The stiffness of the cover can be estimated from simplified formulations and parameters developed in this section.

4) The base forces and moments are dependent on the mass and stiffness distribution of the bushings as well as on the dynamic properties of the as-installed bushings, which dictate the level of excitation (spectral demands) both laterally and rotationally.

5) Finally, most of the issues developed due to the cover frequency can be eliminated by rigidizing the transformer cover. When the stiffness *k* takes large values, the as-installed frequency tends to be equal to the fixed base frequency, while the rotational motion at the base of the bushing becomes negligible. Moreover, the lateral acceleration may take its lowest value in the spectral response. Methods for stiffening of the transformer cover have been addressed by Koliou et al. (2011).